NEWCASTLE UNIVERSITY LIBRARY
087 07053 5

STRUCTURAL ENGINEERING DIVISION
DEPARTMENT OF CIVIL ENGINEERING
UNIVERSITY OF NEWCASTLE UPON TYNE

JUNE, 1970

THE STRESS DISTRIBUTION IN, AND STABILITY OF, SPACE FRAMES WITH PARTICULAR REFERENCE TO RADIAL RIBBED DOMES

VOLUME I

by

F. A. AULD, B.Sc., C. Eng., M.I.C.E.

Thesis submitted for the Degree of Doctor of Philosophy

ERRATA

SUMMARY (1st Page).	Penultimate line - "indluence" should read "influence".
P.4	6th line from the bottom of the page - "lintol" should read "lintel".
P.87	Equation (6.36). Expression for δy_2 is: $\left[\int_0^L (s^2/EI)ds\right] py2 + \left[\int_0^L (s/EI)ds\right] m_2$
P.91.	Line above Equation (6.45) should read: "Equations (6.40), (6.42) and (6.44), when combined give:"
P.124	2nd line after Equation (7.57) - "meridonal" should read "meridional."
P.130	11th line down - "is" should read "are".
P.133	5th line down - "effects" should read "affects".
P.139	10th line down - "equation (8.15)" should read "equation (8.14)".
P.158	7th line down - Reference "(29)" should read "(28)".
P.182	Line after Equation (10.6) should read: "where w = load per unit run carried by each ring member span;"
P.201	9th line from the bottom of the page - "slope" should read "slopes".
P.207	Last sentence should read: "Although axial force values can be obtained easily for the horizontal purlins under symmetrical loads and the diagonal bracing under unsymmetrical loads, to obtain similar results analytically for a general system of loads would be extremely difficult".
P.215	Last line should read: "IV it can be seen that, under unsymmetrical loading conditions, a segment of the dome roof area with an angle".
P.216	5th line down should read: "For the theoretical maximum vertical reaction to occur, under unsymmetrical loading conditions, a segment".

UNIV. NEWCASTLE UPON TYNE

P.226 — 10th line from the bottom of the page should read:
"member system under unsymmetrical loading conditions, a segment of the dome roof area with an angle of 270°,"

P.226 — 5th line from the bottom of the page should read:
"member system under unsymmetrical loading conditions, a segment of the radial ribbed dome with an angle of"

P.228 — Add to end of text:
"23. Symmetrical loading conditions on the primary member system of a radial ribbed dome produce the maximum horizontal and vertical reactions".

FRONTISPIECE - THE LIGHTFOOT SPORTS CENTRE,

NEWCASTLE UPON TYNE.

A Radial Ribbed Dome Space Frame

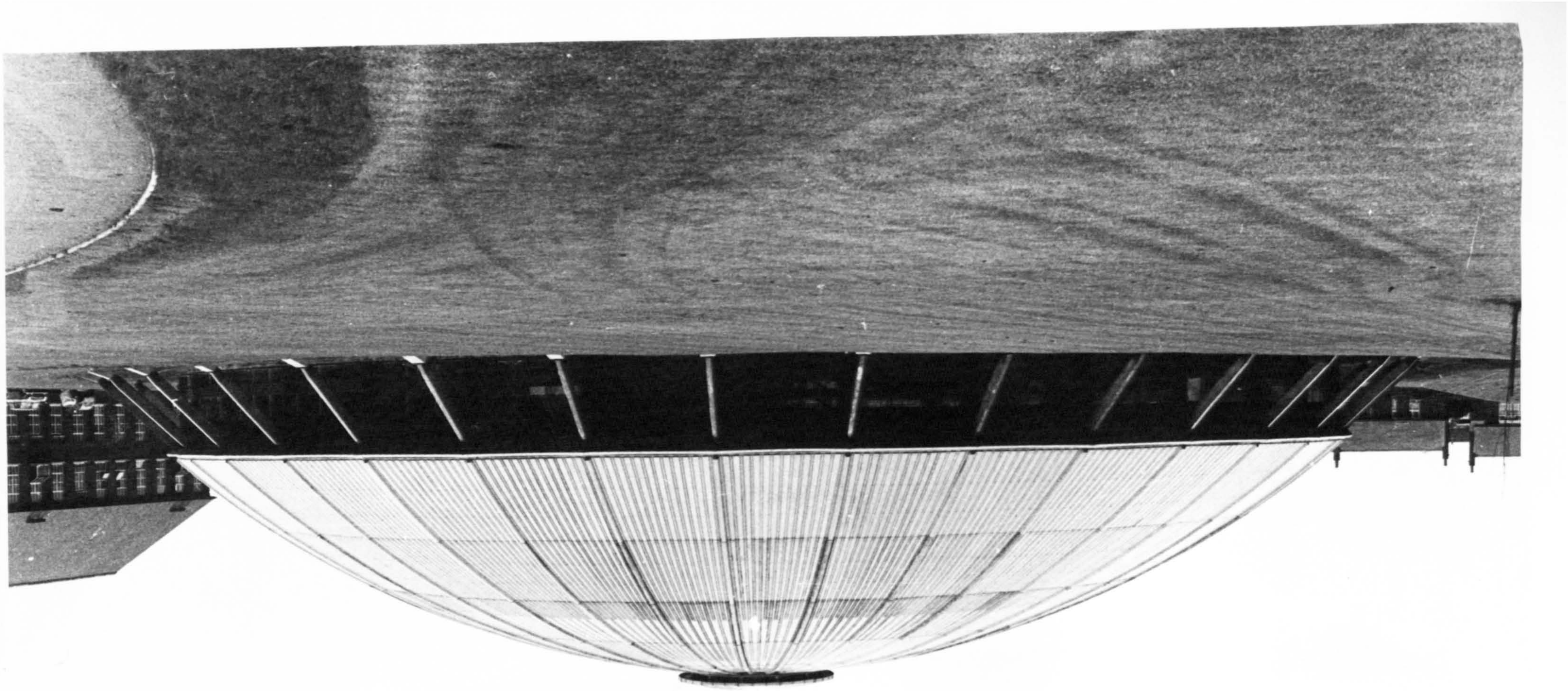

SUMMARY

Tho research project is concerned with the stress distribution in, and stability of, space frames. Tarticular emphasis is placed on the study of radial ribbed domes.

The development and classification of the main types of space frame are discussed and a brief history of dome construction is included. Braced dome systems are detailed comprehensively.

Methods for determining the stresses in space frames are given. These include analysis procedures for statically determinate and statically indeterminate pin-jointed structures. The solution of statically indeterminate space frames without pin-joints is also considered. Specific methods for analysing the stresses in braced domes are reviewed.

Radial ribbed dome stress analysis methods are discussed in detail. In particular, the analysis of three-pinned unstiffened semi-circular radial ribbed domes, by the method of Makowski and Gogate, is reproduced. The method has been modified to simplify the analysis of low rise-to-span domes with three-pinned unstiffened circular arc radial ribs. A computer program, based on this method, has also been developed.

Literature relating to loads on domes is reviewed. Special reference is made to snow loading and wind pressure distribution.

To compare radial ribbed dome theoretical stress analysis values with results obtained experimentally, a model dome has been constructed. Calculations and design drawings for the prototype structure are included along with details of the model. Results of tests on the materials employed in the construction of the model dome are also presented.

By using a displacement technique on the model, indluence line diagrams of force have been obtained with, and without, bracing. Rib

strains and apex ring deflections are tabulated.

An assessment of the analysis methods for space frames is given and comments on dome loading are included. The test results are discussed and conclusions are drawn. Suggestions are also made for further research.

ACKNOWLEDGEMENTS

The author wishes to thank Professor W. F. Cassie and Professor P. C. G. Isaac for the opportunity to carry out research in the Department of Civil Engineering at the University of Newcastle upon Tyne. Thanks are also due to Mr. D. W. Cooper, Reader in Structural Design, for his guidance and encouragement throughout the research project.

A special mention needs to be made of the help received from Mr. G. Carter, in the Structural Engineering Division, whose ideas and technical skill enabled the author to complete his experimental work.

Further thanks are extended to Mrs. N. Trayling for her patience in typing the thesis, to Mrs. L. Osborn for tracing many of the graphs and to Mr. G. Finch for his excellent photography work.

The author is also indebted to the Science Research Council for financial support, without which the project would not have been undertaken.

Plywood for the model dome was supplied by the Finnish Plywood Development Association, glue by C.I.B.A. (A.R.L.) Ltd., and steel angle by Dexion Ltd.

Interest in the project originated from the construction of a laminated timber radial ribbed dome at Newcastle upon Tyne, the Lightfoot Sports Centre, which is the only structure of its type in England.

VOLUME I

CONTENTS

Chapter		Page
1.	INTRODUCTION	
	1.1 The Development of Space Structures.	1
	1.2 Classification of the Main Types of Space Frame Roof Structures Composed of Prefabricated Units.	2
2.	A BRIEF HISTORY OF VAULT AND DOME CONSTRUCTION	
	2.1 Early Aegean, Egyptian and Western Asiatic Vault and Dome Construction.	4
	2.2 Roman and Byzantine Vault and Dome Construction.	7
	2.3 Moslem and Indian Vault and Dome Construction.	10
	2.4 Dome and Vault Construction in the Middle Ages.	13
	2.5 Dome and Vault Construction Between the Middle Ages and the Present Day.	13
3.	BRACED DOMES	
	3.1 Classification of the Main Types of Braced Domes.	17
	3.2 Schwedler Domes.	18
	3.3 Network Domes.	19
	3.4 Plate-type Domes.	20
	3.5 Zimmermann Domes.	20
	3.6 Stiffly-jointed Framed Domes.	21
	3.7 Lamella Domes.	21
	3.8 Kiewitt Domes.	22
	3.9 Two- and Three-way Grid Domes.	22
	3.10 Geodesic Domes.	23
	3.11 Ribbed Domes and Reasons for the Research Project.	24
4.	THE STRESS ANALYSIS OF STATICALLY DETERMINATE PIN-JOINTED SPACE FRAMES	
	4.1 The Equilibrium of Concurrent Forces in Space.	28
	4.2 The Method of Joints Applied to Simple Space Trusses.	30
	4.3 The Statically Determinate Constraint of a Rigid Body in Space.	32
	4.4 The Method of Sections Applied to Compound Space Trusses.	36
	4.5 General Conditions for the Assembly of Statically Determinate Space Trusses.	37
	4.6 The Analysis of Complex Space Trusses.	43
	4.7 Henneberg's Method.	47
	4.8 The Tension Coefficients Method.	48
	4.9 The Method of Conjugate Forces.	50
5.	THE STRESS ANALYSIS OF STATICALLY INDETERMINATE PIN-JOINTED SPACE FRAMES	
	5.1 Elastic Deformation and Strain Energy.	53
	5.2 The Theorem of Least Work.	54
	5.3 Application of the Theorem of Least Work to the Stress Analysis of Statically Indeterminate Pin-Jointed Space Frames.	55

Chapter			Page
5.	5.4	The Maxwell-Mohr Method.	56
	5.5	Temperature and Error Effects.	57
	5.6	The Gap Reduction Method.	57
	5.7	The Influence Coefficients Method.	59
6.	THE STRESS ANALYSIS OF STATICALLY INDETERMINATE SPACE FRAMES WITHOUT PIN-JOINTS		
	6.1	The Influence Coefficients Method.	64
	6.2	Matrix Methods.	72
7.	THE STRESS ANALYSIS OF BRACED DOMES		
	7.1	The Schwedler Dome.	99
	7.2	The Stiff-jointed Framed Dome.	
		7.2(a) El-Sayed El-Schasly's Method.	101
		7.2(b) Kaufmann's Method.	103
		7.2(c) The Influence Coefficients Method.	105
	7.3	The Shell Analogy.	
		7.3(a) Principles of the Shell Analogy Method.	113
		7.3(b) The Shell Analogy Applied to Schwedler and Stiff-jointed Framed Domes.	116
		7.3(c) Application to Pin-connected Domes.	119
		7.3(d) Application to Stiff-jointed Domes.	125
		7.3(e) The Shell Analogy as a Design Method.	128
	7.4	Miscellaneous Domes.	
		7.4(a) The Grid Dome.	128
		7.4(b) Network, Flate-type, Zimmermann and Geodesic Domes.	131
8.	THE STRESS ANALYSIS OF RADIAL RIBBED DOMES		
	8.1	Design Assumptions.	132
	8.2	Three-pinned Unstiffened Radial Ribbed Domes.	133
	8.3	The Analysis of Three-pinned Unstiffened Semi-circular Radial Ribbed Domes by the Method of Makowski and Gogate.	
		8.3(a) Notation.	134
		8.3(b) General Expressions of the Apex Displacements.	135
		8.3(c) General Expressions of the Reaction Components at Any Support of the Dome.	137
	8.4	The Analysis of Three-pinned Unstiffened Circular Arc Radial Ribbed Domes.	140
	8.5	Two-hinged Unstiffened Radial Ribbed Domes.	142
		8.5(a) Vertex Point Rotation Effect.	143
		8.5(b) Vertex Point Translation Effect.	147
	8.6	Two-hinged Unstiffened Radial Ribbed Dome With Apex Ring.	150
	8.7	Two-hinged Stiffened Radial Ribbed Domes.	151
		8.7(a) Symmetrical Loading.	152
		8.7(b) Skew-symmetrical Loading	154
9.	LOADS ON DOMES		
	9.1	Dead Load.	157
	9.2	Live Load.	157
	9.3	Snow Load.	158

Chapter		Page
9.	9.4 Wind Load.	
	9.4(a) Basic Considerations.	161
	9.4(b) Factors Influencing the Choice of a Design Wind Speed.	164
	9.4(c) Recommended Procedures for Determining the Design Wind Speed.	165
	9.4(d) Pressure and Shape Coefficients.	169
	9.4(e) Wind Tunnel Test Values	171
	9.4(f) Formulae for Use With the Shell Analogy	174
10.	DESIGN, CONSTRUCTION AND TESTING OF THE MODEL RADIAL RIBBED DOME	
	10.1 Design of the Model Dome.	
	10.1(a) General Considerations.	177
	10.1(b) American Institute of Timber Construction General Design Procedure for Radial Ribbed Domes.	180
	10.1(c) Prototype Dome Design.	183
	10.1(d) Model Dome Component Sizes.	187
	10.2 Construction of the Model Dome.	
	10.2(a) Base Ring Erection.	188
	10.2(b) Rib Manufacture.	191
	10.2(c) Fabrication of Base and Crown Connectors.	193
	10.2(d) Apex Ring Fabrication.	194
	10.2(e) Horizontal Purlin Ring Construction.	194
	10.2(f) Diagonal Bracing Attachment.	196
	10.3 Testing of the Model Dome Construction Materials.	
	10.3(a) Radial Rib Timber.	196
	10.3(b) Adhesive Employed in Radial Rib Laminating Process.	198
	10.4 Testing of the Model Dome.	
	10.4(a) Direct and Indirect Test Methods.	198
	10.4(b) Application of Direct and Indirect Test Methods to Model Dome.	199
11.	ANALYSIS OF TEST RESULTS AND CONCLUSIONS	
	11.1 Assessment of Analysis Methods.	
	11.1(a) Statically Determinate Pin-jointed Space Frames.	203
	11.1(b) Statically Indeterminate Pin-jointed Space Frames.	204
	11.1(c) Statically Indeterminate Space Frames Without Pin-joints.	204
	11.1(d) Braced Domes.	206
	11.1(e) Continuous Radial Ribbed Domes.	207
	11.2 Comments on Dome Loading.	209
	11.3 Base Reactions.	
	11.3(a) 6 Ribs in Dome.	210
	11.3(b) 36 Ribs in Dome.	214
	11.3(c) 36 Ribs in Dome With Horizontal Purlin Rings.	216
	11.4 Apex Ring Forces.	
	11.4(a) 6 Ribs in Dome.	217
	11.4(b) 36 Ribs in Dome.	218
	11.4(c) 36 Ribs in Dome With Horizontal Purlin Rings.	220
	11.5 Rib Bending Moments.	221
	11.6 Apex Ring Deflections.	222
	11.7 Further Research.	223

Chapter		Page
11.	11.8 Summary of Conclusions.	225
	REFERENCES	229
	ADDITIONAL REFERENCES	232

APPENDIX I
Tests on Model Radial Ribbed Dome Materials - Results.

APPENDIX II
Tests on Model Radial Ribbed Dome - Test Results.
Tests 1 - 22.

APPENDIX III
Design of Prototype Laminated Timber Radial Ribbed Dome.
Calculation Sheet Nos. 1 - 25.

APPENDIX IV
Analysis of Test Results. Table Nos. 1 - 16.

LIST OF FIGURES

		Between Pages
1.	A Double-Layer Space Grid.	3, 4
2.	A Braced Barrel Vault.	3, 4
3.	A Braced Dome.	3, 4
4.	A Folded Plate Structure.	3, 4
5.	A Suspended Cable Roof.	3, 4
6.	Early Vault and Dome Construction. Sheet No. 1.	5, 6
7.	Early Vault and Dome Construction. Sheet No. 2.	6, 7
8.	Early Vault and Dome Construction. Sheet No. 3.	8, 9
9.	Early Vault and Dome Construction. Sheet No. 4.	10, 11
10.	Schwedler and Network Domes.	19, 20
11.	Plate-type and Zimmermann Domes.	20, 21
12.	Stiffly-jointed and Lamella Domes.	21, 22
13.	Kiewitt and Two-way Grid Domes.	22, 23
14.	Three-way Grid and Geodesic Domes.	23, 24
15.	The Equilibrium of Concurrent Forces in Space.	28, 29
16.	Simple Space Trusses.	31, 32
17.	Statically Determinate Constraint of a Rigid Body in Space	32, 33
18.	Compound Space Trusses.	36, 37
19.	General Conditions for the Assembly of Statically Determinate Space Trusses.	37, 38
20.	The Analysis of Complex Space Trusses. Sheet No. 1.	43, 44
21.	The Analysis of Complex Space Trusses. Sheet No. 2.	44, 45
22.	Henneberg's Method.	47, 48
23.	The Method of Conjugate Forces.	50, 51
24.	The Elastic Deformation of Statically Indeterminate Pin-jointed Space Frames.	53, 54
25.	The Gap Reduction Method.	57, 58
26.	Matrix Methods. Sheet No. 1.	77, 78
27.	Matrix Methods. Sheet No. 2.	84, 85
28.	Matrix Methods. Sheet No. 3.	96, 97
29.	Schwedler's Analytical Method.	99, 100
30.	The Integration of Diagrams for the Determination of Influence Coefficients.	107, 108
31.	Easy Determination of Influence Coefficients (Makowski). Sheet No. 1.	109, 110
32.	Easy Determination of Influence Coefficients (Makowski). Sheet No. 2.	109, 110
33.	Easy Determination of Influence Coefficients (Makowski). Sheet No. 3.	109, 110
34.	Stiff-jointed Framed Domes.	110, 111
35.	The Shell Analogy. Sheet No. 1.	116, 117
36.	The Shell Analogy. Sheet No. 2.	124, 125
37.	Grid Dome Analysis.	129, 130
38.	Stress Analysis of Three-pinned Unstiffened Semi-circular Arch-ribbed Domes (Makowski and Gogate). Sheet No. 1.	134, 135
39.	Deflections of the Apex of a Semi-circular Three-pinned Arch (Makowski and Gogate).	136, 137
40.	Stress Analysis of Three-pinned Unstiffened Semi-circular Arch-ribbed Domes (Makowski and Gogate). Sheet No. 2.	137, 138

		Between Pages
41.	Deflections of the Apex of a Circular Three-pinned Arch	140, 141
42.	Reactions and Forces Acting on a Circular Three-pinned Arch.	141, 142
43.	Reaction Components for Unit Load on a Circular Arc Radial Ribbed Dome.	142, 143
44.	Two-hinged Unstiffened Radial Ribbed Domes. Sheet No. 1.	143, 144
45.	Two-hinged Unstiffened Radial Ribbed Domes. Sheet No. 2.	145, 146
46.	Two-hinged Unstiffened Radial Ribbed Domes. Sheet No. 3.	147, 148
47.	Two-hinged Unstiffened Radial Ribbed Dome With Apex Ring	150, 151
48.	Two-hinged Stiffened Radial Ribbed Domes. Sheet No. 1.	151, 152
49.	Two-hinged Stiffened Radial Ribbed Domes. Sheet No. 2.	154, 155
50.	Snow Loading on Domes.	160, 161
51.	Wind Loads on Domes. Sheet No. 1.	170, 171
52.	Wind Loads on Domes. Sheet No. 2.	174, 175
53.	American Institute of Timber Construction Radial Ribbed Dome Notation.	180, 181
54.	Details of Jig Used in Laminating Process for Timber Dome Ribs (Model).	191, 192
55.	Base Horizontal Deformeter.	199, 200
56.	Base Vertical Deformeter.	199, 200
57.	Apex Ring Displacement Apparatus.	200, 201

LIST OF PLATES

The Lightfoot Sports Centre, Newcastle upon Tyne. A Radial Ribbed Dome Space Frame.		Frontispiece
		Between Pages
1.	The Lightfoot Sports Centre Apex Ring.	26, 27
2.	The Lightfoot Sports Centre Linned Base.	26, 27
3.	The Lightfoot Sports Centre Diagonal Bracing.	26, 27
4.	The Model Radial Ribbed Dome Base Ring.	188, 189
5.	Model Dome Rib Laminating Process - Laminates Ready for Glue Application.	191, 192
6.	Model Dome Rib Laminating Process - Glue Being Applied to Laminates.	191, 192
7.	Model Dome Rib Laminating Process - Laminates Glued and Clamped in Jig.	191, 192
8.	Model Dome Rib Laminating Process - Curved Rib Blocks Removed from Jig.	191, 192
9.	Model Dome - Finished Ribs Erected on Base Ring.	192, 193
10.	Drilling of Model Dome Rib Purlin Connection Bolt Holes from Plywood Template.	193, 194
11.	Model Dome Bases and Crown Connector With Fabrication Jigs.	193, 194
12.	Model Dome Apex Ring.	194, 195
13.	Model Dome Purlin Jigs A, B and C, Load Hangers D and Plywood Rib Template Drill Guide E.	194, 195
14.	Model Dome - Ribs and Purlins in Position.	196, 197
15.	Tensometer Testing Apparatus.	197, 198
16.	2 in. Standard Beam Testing Apparatus.	197, 198
17.	Avery Compression Testing Apparatus With 2 in. Standard Compression Parallel to Grain Test Specimen.	197, 198
18.	2 cm. Standard Static Bending Test to B.S. 373 : 1957 in Tensometer Apparatus.	197, 198
19.	2 cm. Standard Shear Parallel to Grain Test to B.S. 373:1957 in Tensometer Apparatus.	197, 198
20.	Tension Parallel to Grain Test to B.S. 373:1957 in Tensometer Apparatus.	197, 198
21.	2 in. Standard Compression Perpendicular to Grain Test to B.S. 373:1957 in Tensometer Apparatus.	197, 198
22.	2 cm. and 2 in. Standard Static Bending Test Specimens (European Redwood).	197, 198
23.	2 cm. Standard Shear Parallel to Grain and Tension Parallel to Grain Specimens (European Redwood).	197, 198
24.	2 in. Standard Compression Parallel to Grain and Compression Perpendicular to Grain Specimens (European Redwood).	197, 198
25.	Base Horizontal Deformeter and Node Point Loading.	199, 200
26.	Base Vertical Deformeter.	199, 200
27.	Apex Ring Vertical Displacement.	201, 202
28.	Apex Ring Tangential Displacement.	201, 202

LIST OF FIGURES IN APPENDIX I

1. Moisture Content and Specific Gravity Determination of Rib Timber.
2. Static Bending Test to B.S. 373:1957 on Rib Timber, Specimen No. 1. (2 cm.)
3. Static Bending Test to B.S. 373:1957 on Rib Timber, Specimen No. 2. (2 cm.)
4. Static Bending Test to B.S. 373:1957 on Rib Timber, Specimen No. 3. (2 cm.)
5. Static Bending Test to B.S. 373:1957 on Rib Timber, Specimen No. 4. (2 cm.)
6. Static Bending Test to B.S. 373:1957 on Rib Timber, Specimen No. 5. (2 cm.)
7. Static Bending Test to B.S. 373:1957 on Rib Timber, Specimen No. 6. (2 cm.)
8. Static Bending Tests to B.S. 373:1957 on Rib Timber, Specimen Nos. 1 - 6. (2 cm.)
9. Shear Parallel to Grain Test to B.S. 373:1957 on Rib Timber, Specimen No. 1.
10. Shear Parallel to Grain Test to B.S. 373:1957 on Rib Timber, Specimen No. 2.
11. Shear Parallel to Grain Test to B.S. 373:1957 on Rib Timber, Specimen No. 3.
12. Shear Parallel to Grain Test to B.S. 373:1957 on Rib Timber, Specimen No. 4.
13. Shear Parallel to Grain Test to B.S. 373:1957 on Rib Timber, Specimen No. 5.
14. Shear Parallel to Grain Test to B.S. 373:1957 on Rib Timber, Specimen No. 6.
15. Tension Parallel to Grain Test to B.S. 373:1957 on Rib Timber, Specimen No. 1.
16. Tension Parallel to Grain Test to B.S. 373:1957 on Rib Timber, Specimen No. 2.
17. Tension Parallel to Grain Test to B.S. 373:1957 on Rib Timber, Specimen No. 3.
18. Tension Parallel to Grain Test to B.S. 373:1957 on Rib Timber, Specimen No. 4.
19. Tension Parallel to Grain Test to B.S. 373:1957 on Rib Timber, Specimen No. 5.
20. Tension Parallel to Grain Test to B.S. 373:1957 on Rib Timber, Specimen No. 6.
21. Tension Parallel to Grain Tests to B.S. 373:1957 on Rib Timber, Specimen Nos. 1 - 6.
22. Compression Perpendicular to Grain Test to B.S. 373:1957 on Rib Timber, Specimen No. 1.
23. Compression Perpendicular to Grain Test to B.S. 373:1957 on Rib Timber, Specimen No. 2.
24. Compression Perpendicular to Grain Test to B.S. 373:1957 on Rib Timber, Specimen No. 3.
25. Compression Perpendicular to Grain Test to B.S. 373:1957 on Rib Timber, Specimen No. 4.
26. Compression Parallel to Grain Test to B.S. 373:1957 on Rib Timber, Specimen No. 1.
27. Compression Parallel to Grain Test to B.S. 373:1957 on Rib Timber, Specimen No. 1.
28. Compression Parallel to Grain Test to B.S. 373:1957 on Rib Timber, Specimen No. 2.
29. Compression Parallel to Grain Test to B.S. 373:1957 on Rib Timber, Specimen No. 2.

30. Compression Parallel to Grain Test to B.S. 373:1957 on Rib Timber, Specimen No. 3.
31. Compression Parallel to Grain Test to B.S. 373:1957 on Rib Timber, Specimen No. 3.
32. Compression Parallel to Grain Test to B.S. 373:1957 on Rib Timber, Specimen No. 4.
33. Compression Parallel to Grain Test to B.S. 373:1957 on Rib Timber, Specimen No. 4.
34. Compression Parallel to Grain Tests to B.S. 373:1957 on Rib Timber, Specimen Nos. 1 - 4.
35. Static Bending Test to B.S. 373:1957 on Rib Timber, Specimen No. 1 (2in.).
36. Static Bending Test to B.S. 373:1957 on Rib Timber, Specimen No. 1 (2in.).
37. Static Bending Test to B.S. 373:1957 on Rib Timber, Specimen No. 2 (2in.).
38. Static Bending Test to B.S. 373:1957 on Rib Timber, Specimen No. 2 (2in.).
39. Static Bending Test to B.S. 373:1957 on Rib Timber, Specimen No. 3 (2in.).
40. Static Bending Test to B.S. 373:1957 on Rib Timber, Specimen No. 3 (2in.).
41. Static Bending Test to B.S. 373:1957 on Rib Timber, Specimen No. 4 (2in.).
42. Static Bending Test to B.S. 373:1957 on Rib Timber, Specimen No. 4 (2in.)
43. Static Bending Tests to B.S. 373:1957 on Rib Timber, Specimen Nos. 1 - 4 (2in.)
44. (a) Measurement of the Loss in Weight With Time of Adhesive Employed in the Construction of the Dome Ribs.
44. (b) Measurement of the Loss in Weight With Time of Adhesive Employed in the Construction of the Dome Ribs.
45. Graphs of Loss in Weight With Time of Adhesive Employed in the Construction of the Dome Ribs.

LIST OF TABLES AND SHEETS IN APPENDIX II

Test No.

1. Experimental Determination of Horizontal Reaction Influence Coefficients. Table Nos. 1 - 3.
1. Measurement of Rib Strains Using Huggenberger Tensometer Gauges. Table Nos. 4, 5.
1. Measurement of Apex Ring Displacements at Rib No. 36. Table No. 6.
1. Experimental Determination of Horizontal Reaction Influence Coefficients. Sheet Nos. 1 - 5.
2. Experimental Determination of Vertical Reaction Influence Coefficients. Table Nos. 1 - 3, Sheet Nos. 1 - 5.
3. Experimental Determination of Apex Ring Vertical Force Influence Coefficients. Table Nos. 1 - 3, Sheet Nos. 1 - 5.
4. Experimental Determination of Apex Ring Radial Force Influence Coefficients. Table Nos. 1 - 3, Sheet Nos. 1 - 5.
5. Experimental Determination of Apex Ring Tangential Force Influence Coefficients. Table Nos. 1 - 3, Sheet Nos. 1 - 4.
6. Experimental Determination of Horizontal Reaction Influence Coefficients. Table Nos. 1, 2, Sheet Nos. 1 - 5.
7. Experimental Determination of Vertical Reaction Influence Coefficients. Table Nos. 1, 2, Sheet Nos. 1 - 5.
8. Experimental Determination of Apex Ring Vertical Force Influence Coefficients. Table Nos. 1, 2, Sheet Nos. 1 - 5.
9. Experimental Determination of Apex Ring Radial Force Influence Coefficients. Table Nos. 1, 2, Sheet Nos. 1 - 5.
10. Experimental Determination of Apex Ring Tangential Force Influence Coefficients. Table Nos. 1 - 3, Sheet Nos. 1 - 4.
11. Measurement of Rib Strains Using Huggenberger Tensometer Gauges. Table Nos. 1, 2.
11. Measurement of Apex Ring Displacements at Rib No. 36. Table No.3.
12. Experimental Determination of Horizontal Reaction Influence Coefficients. Table Nos. 1 - 10. Sheet Nos. 1 - 8.
13. Experimental Determination of Vertical Reaction Influence Coefficients. Table Nos. 1 - 10. Sheet Nos. 1 - 6.
14. Experimental Determination of Apex Ring Vertical Force Influence Coefficients. Table Nos. 1 - 10. Sheet Nos. 1 - 4.
15. Experimental Determination of Apex Ring Radial Force Influence Coefficients. Table Nos. 1 - 10. Sheet Nos. 1 - 4.
16. Experimental Determination of Apex Ring Tangential Force Influence Coefficients. Table Nos. 1 - 18. Sheet Nos. 1 - 7.
17. Measurement of Apex Ring Displacements at Rib No. 36. Table Nos. 1 - 4.
17. Measurement of Rib Strains Using Huggenberger Tensometer Gauges. Table No. 5.
18. Experimental Determination of Horizontal Reaction Influence Coefficients. Table No. 1.
19. Experimental Determination of Vertical Reaction Influence Coefficients. Table No. 1.
20. Experimental Determination of Apex Ring Vertical Force Influence Coefficients. Table No. 1.
21. Experimental Determination of Apex Ring Radial Force Influence Coefficients. Table No. 1.
22. Measurement of Rib Strains Using Huggenberger Tensometer Gauges. Table No. 1.
22. Measurement of Apex Ring Displacements at Rib No. 36. Table No. 2.

LIST OF TABLES IN APPENDIX IV

1. Theoretical Force Influence Coefficients for Three-pinned and Two-pinned Arches (Plane Frames).
2. Theoretical Force Influence Coefficients for Radial Ribbed Dome (Space Frame - Makowski and Gogate Method Modified by Author). 6 No. Ribs in Dome.
3. Experimental Force Influence Coefficients for Model Radial Ribbed Dome (6 No. Ribs of Constant I).
4. Experimental Force Influence Coefficients for Model Radial Ribbed Dome (6 No. Ribs of Constant I).
5. Experimental Force Influence Coefficients for Model Radial Ribbed Dome (6 No. Ribs of Constant I).
6. Experimental Force Influence Coefficients for Model Radial Ribbed Dome (6 No. Ribs of varying I).
7. Experimental Force Influence Coefficients for Model Radial Ribbed Dome (6 No. Ribs of varying I).
8. Experimental Force Influence Coefficients for Model Radial Ribbed Dome (6 No. Ribs of varying I).
9. Theoretical Horizontal Reaction Influence Coefficients for Radial Ribbed Dome (Space Frame - Makowski and Gogate Method Modified by Author) 36 No. Ribs in Dome.
10. Theoretical Vertical Reaction Influence Coefficients for Radial Ribbed Dome (Space Frame - Makowski and Gogate Method Modified by Author) 36 No. Ribs in Dome.
11. Experimental Horizontal Reaction Influence Coefficients for Model Radial Ribbed Dome (36 No. Ribs of varying I without bracing).
12. Experimental Vertical Reaction Influence Coefficients for Model Radial Ribbed Dome (36 No. Ribs of varying I without bracing).
13. Experimental Apex Ring Vertical Force Influence Coefficients for Model Radial Ribbed Dome (36 No. Ribs of varying I without bracing).
14. Experimental Apex Ring Radial Force Influence Coefficients for Model Radial Ribbed Dome (36 No. Ribs of varying I without bracing).
15. Experimental Apex Ring Tangential Force Influence Coefficients for Model Radial Ribbed Dome (36 No. Ribs of varying I without bracing).
16. Experimental Force Influence Coefficients for Model Radial Ribbed Dome (36 No. Ribs of varying I with horizontal bracing).

VOLUME II

CONTENTS

Dwg. No. Ph.D. Thesis No. 1.	Principal Dimensions of Prototype and Model Domes.
Dwg. No. Ph.D. Thesis No. 2.	Design of Prototype Dome. Three-pinned Arch Method. Sheet No. 1.
Dwg. No. Ph.D. Thesis No. 3.	Design of Prototype Dome. Three-pinned Arch Method. Sheet No. 2.
Dwg. No. Ph.D. Thesis No. 4.	Design of Prototype Dome. Three-pinned Arch Method. Sheet No. 3.
Dwg. No. Ph.D. Thesis No. 5.	Design of Prototype Dome. Three-pinned Arch Method. Sheet No. 4.
Dwg. No. Ph.D. Thesis No. 6.	Design of Prototype Dome. Two-pinned Arch Method. Sheet No. 1.
Dwg. No. Ph.D. Thesis No. 7.	Design of Prototype Dome. Two-pinned Arch Method. Sheet No. 2.
Dwg. No. Ph.D. Thesis No. 8.	Design of Prototype Dome. Two-pinned Arch Method. Sheet No. 3.
Dwg. No. Ph.D. Thesis No. 9.	Dimensions of Prototype Dome Components.
Dwg. No. Ph.D. Thesis No. 10.	Model Dome Base Ring Details and Rib Setting Out Plan.
Dwg. No. Ph.D. Thesis No. 11.	Details of Model Radial Ribbed Dome.

Electronic Computer Determination of the Theoretical Reaction Components and Bending Moments Induced in a Circular Arc Radial Ribbed Dome by a Unit Vertical Load.

Contents Sheet.

Computer Program Notation.

Program User Notes (Sheet Nos. A, B, C.)

	Sheet Nos.
Program	1 - 6
Input Data (n = 3 = No. of arches)	7
Output Data (n = 3)	8 - 14
Input Data (n = 18)	15
Output Data (n = 18)	16 - 52

CHAPTER I

INTRODUCTION

1.1 THE DEVELOPMENT OF SPACE STRUCTURES

The design of structural frameworks in a two-dimensional form is commonplace. This type of structure can only resist forces applied in its own plane. Frameworks which extend into three dimensions are known as space structures and result in a spreading of forces throughout the system. Stresses in directly loaded members are reduced while stresses in members not directly loaded are increased. The ability of space structures to distribute loads in this manner increases their design efficiency as less material with less weight is required for their construction.

At the present time, the demand for buildings with large, clear spans has created a greater need for light construction with economy in materials. To reduce weight in a structure, each individual component must possess the smallest allowable section size and building materials should be stressed to their design limits. As the distribution of loads, the spreading of forces and the reduction of bending moments are characteristics of space frameworks and lead to the utilization of material to its limits, the development of this form of structure for the purpose of covering large areas has been very rapid in recent years.

The design of lightweight buildings with large, clear, internal spans presents the architect and engineer with severe design problems. Stress analysis of such structures has become more critical and more accurate methods of design are required to cope with the problems involved. In recent years, the traditional two-dimensional methods of design have been superseded in some cases by space framework techniques

involving three dimensions. The effect of adding a third dimension to design analysis increases the amount of calculating work required, but the advent of the electronic computer has removed some of the tedium from the engineer's task.

Advances in the design of space frameworks have also been aided by the availability of improved building materials. A vast amount of research work, over the past few years, has been directed towards the provision of construction materials possessing higher strength-to-weight ratios and investigations in this field have produced some valuable results. At one time, construction in reinforced concrete, steel, timber and brickwork was carried out mainly with beam and column arrangements of structural members which imposed restrictions on architectural imagination. Nowadays, the development of aluminium, plastics and laminated timber for constructional purposes has enlarged the creative scope of the architect and engineer to such an extent that large, clear-span, aesthetically beautiful structures can now be erected with very little restriction on shape. Aided by improved welding techniques, the recent developments in steel have produced a constructional material which cannot be matched for strength, reliability adaptability and economy. Steel, aluminium, plastics and laminated timber are ideally suited to space frame methods of construction employing prefabricated units and it is in this field that major technical advances have been made over the last few years.

1.2 CLASSIFICATION OF THE MAIN TYPES OF SPACE FRAME ROOF STRUCTURES COMPOSED OF PREFABRICATED UNITS

Although it is almost impossible to classify completely all space frame roof structures, many can be listed under three general groups.[1]

1. Skeleton Frameworks

The first group consists of skeleton frameworks in which the members are all interconnected at nodes. Double-layer grid frameworks, braced barrel vaults and braced domes are included in this category.

Figures 1, 2 and 3 show typical examples of these three types of space structure.

2. Stressed Skin Systems

The second main classification group is composed of stressed skin systems in which the covering acts as an integral part of the structure. Folded plate systems belong to this group. Figure 4 illustrates such a structure.

3. Suspended Structures

The remaining principal category for classifying space structures is concerned with suspended systems. Cable roofs are examples of this form of structure and Figure 5 shows a suspended cable roof with a shape similar to that of a bicycle wheel.

This review of the main types of prefabricated space frame roof structures indicates clearly that variations in structural form at the present time are almost limitless and the architectural and engineering scope in the field of space structures is enormous. Research work can only be directed along narrow paths and it is with dome structures that this thesis is mainly concerned.

Structural Engineering Division
Department of Civil Engineering
University of Newcastle upon Tyne

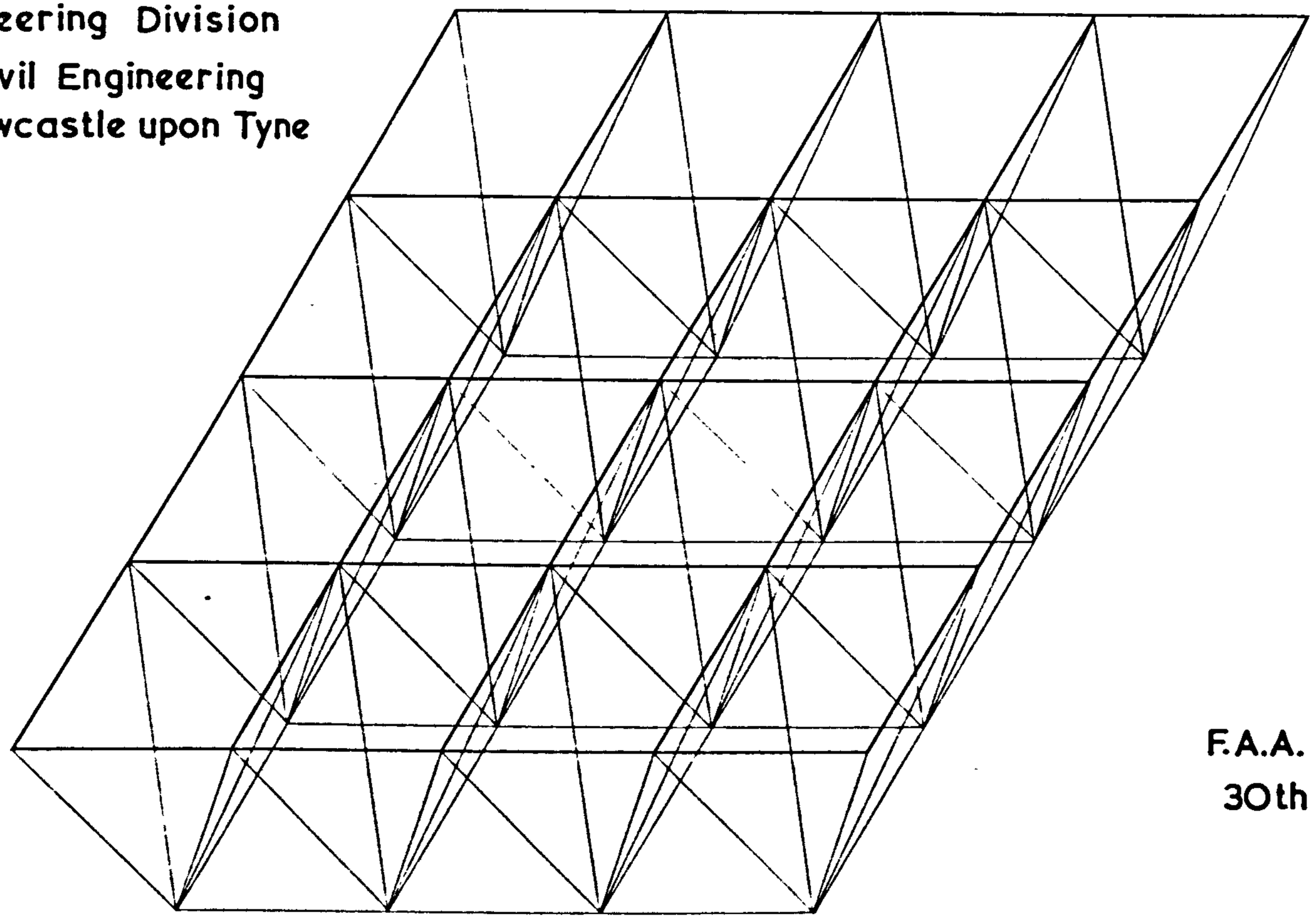

F.A.A. Ph.D. Thesis
30th Oct., 1968

FIG. 1 A DOUBLE-LAYER SPACE GRID

Structural Engineering Division
Department of Civil Engineering
University of Newcastle upon Tyne

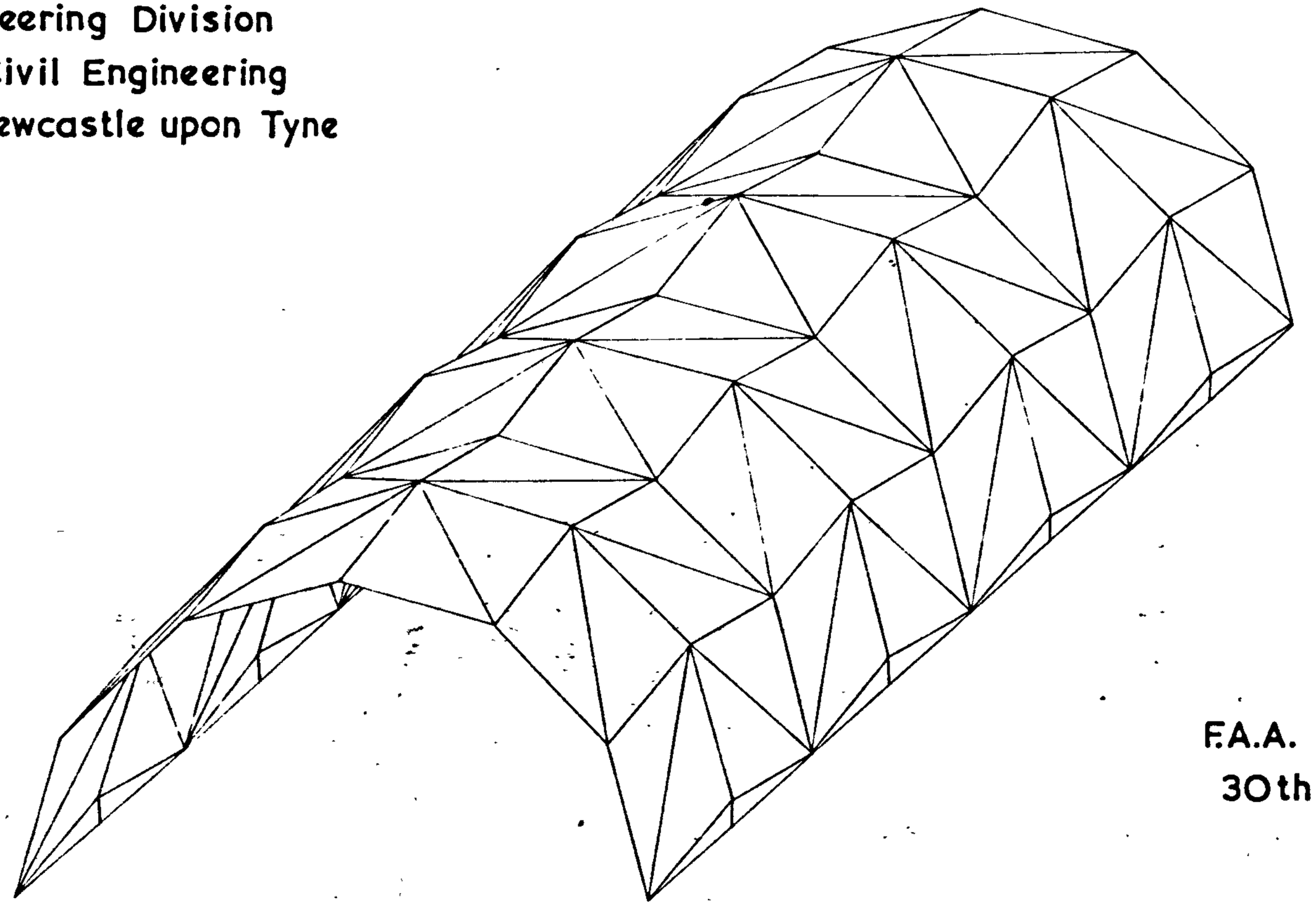

F.A.A. Ph.D. Thesis
30th Oct., 1968

FIG. 2 A BRACED BARREL VAULT

Structural Engineering Division
Department of Civil Engineering
University of Newcastle upon Tyne

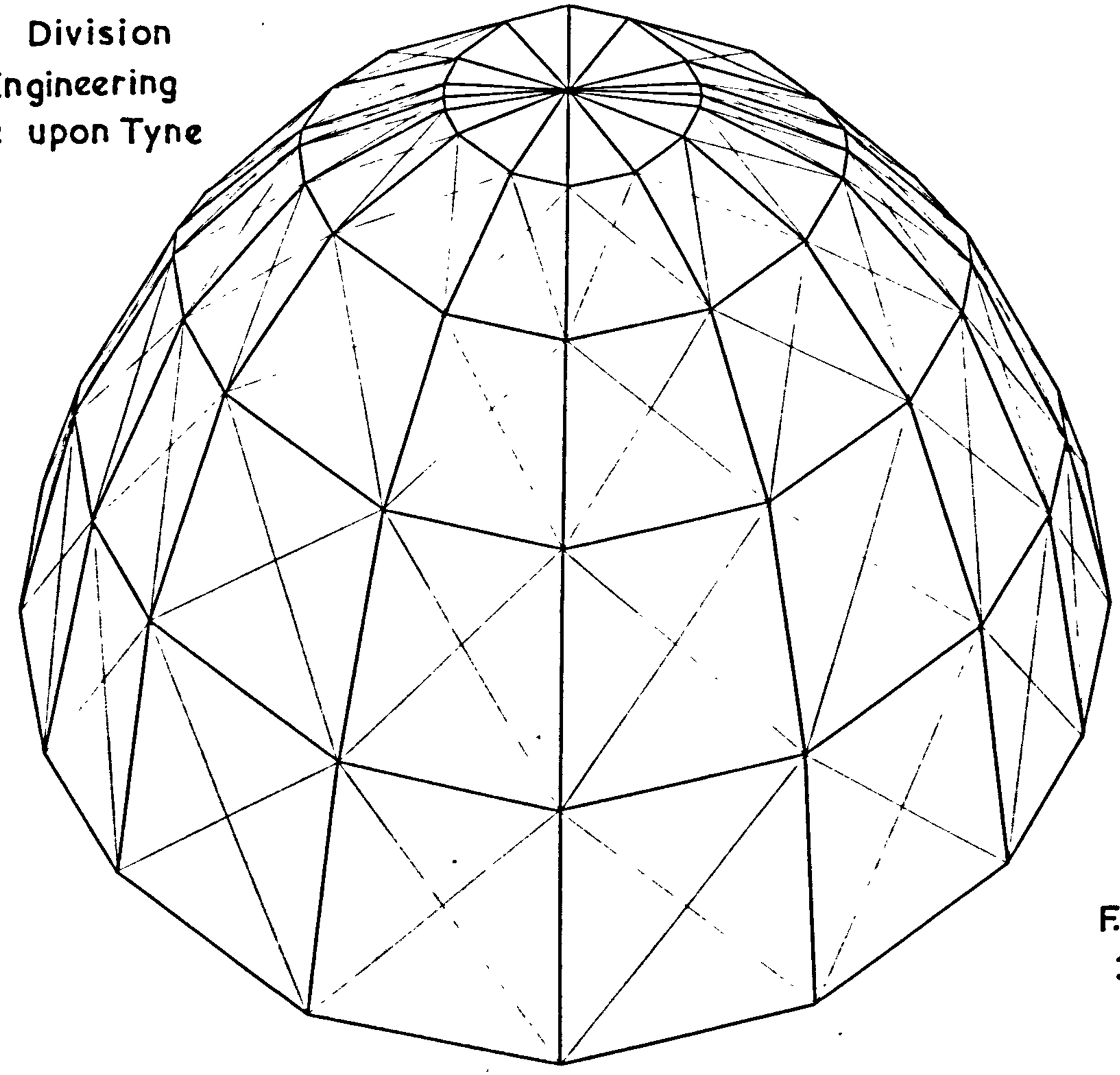

F.A.A. Ph.D. Thesis
30th Oct., 1968

FIG. 3 A BRACED DOME

Structural Engineering Division
Department of Civil Engineering
University of Newcastle upon Tyne

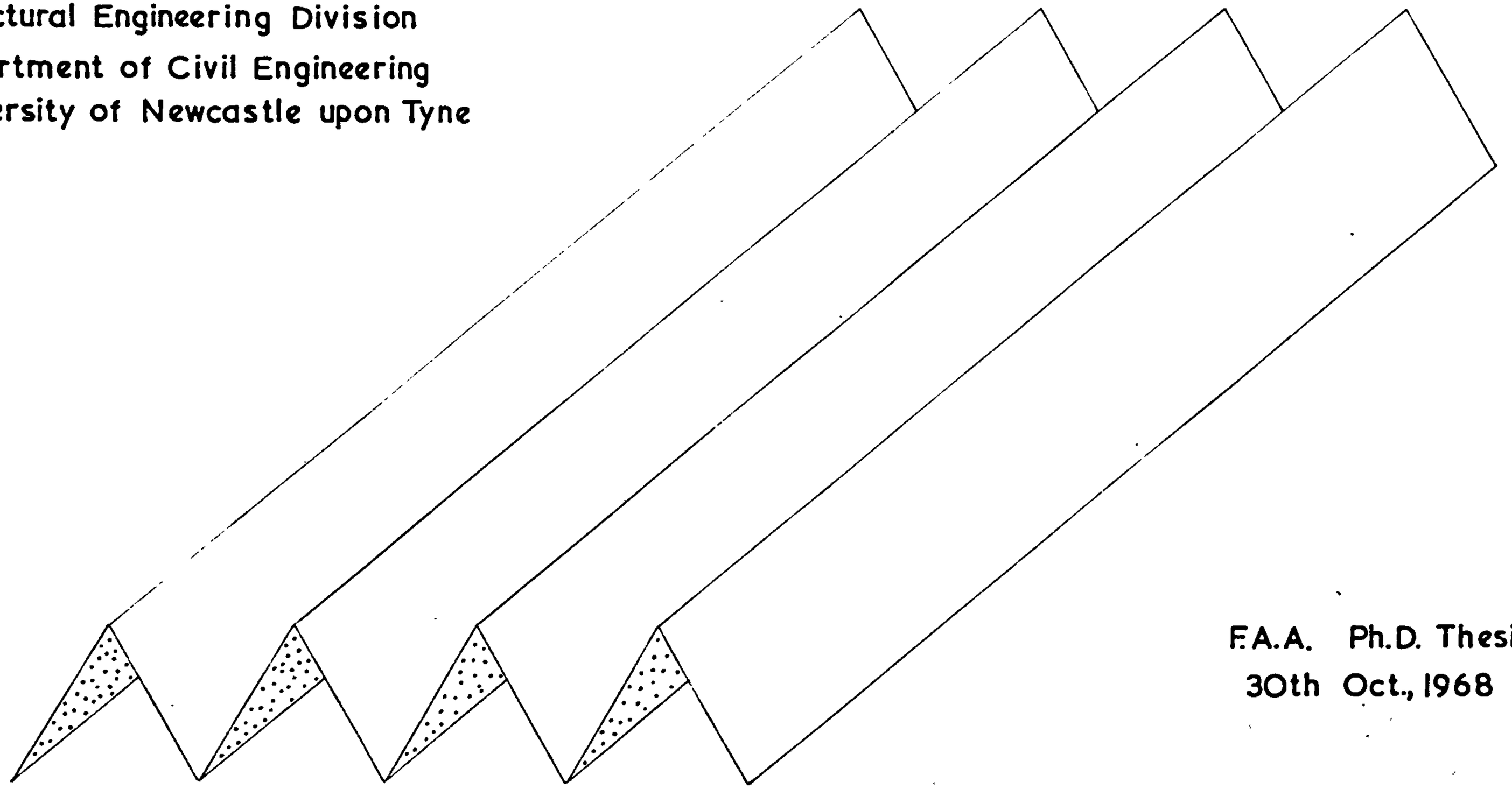

F.A.A. Ph.D. Thesis
30th Oct., 1968

FIG. 4 A FOLDED PLATE STRUCTURE

Structural Engineering Division
Department of Civil Engineering
University of Newcastle upon Tyne

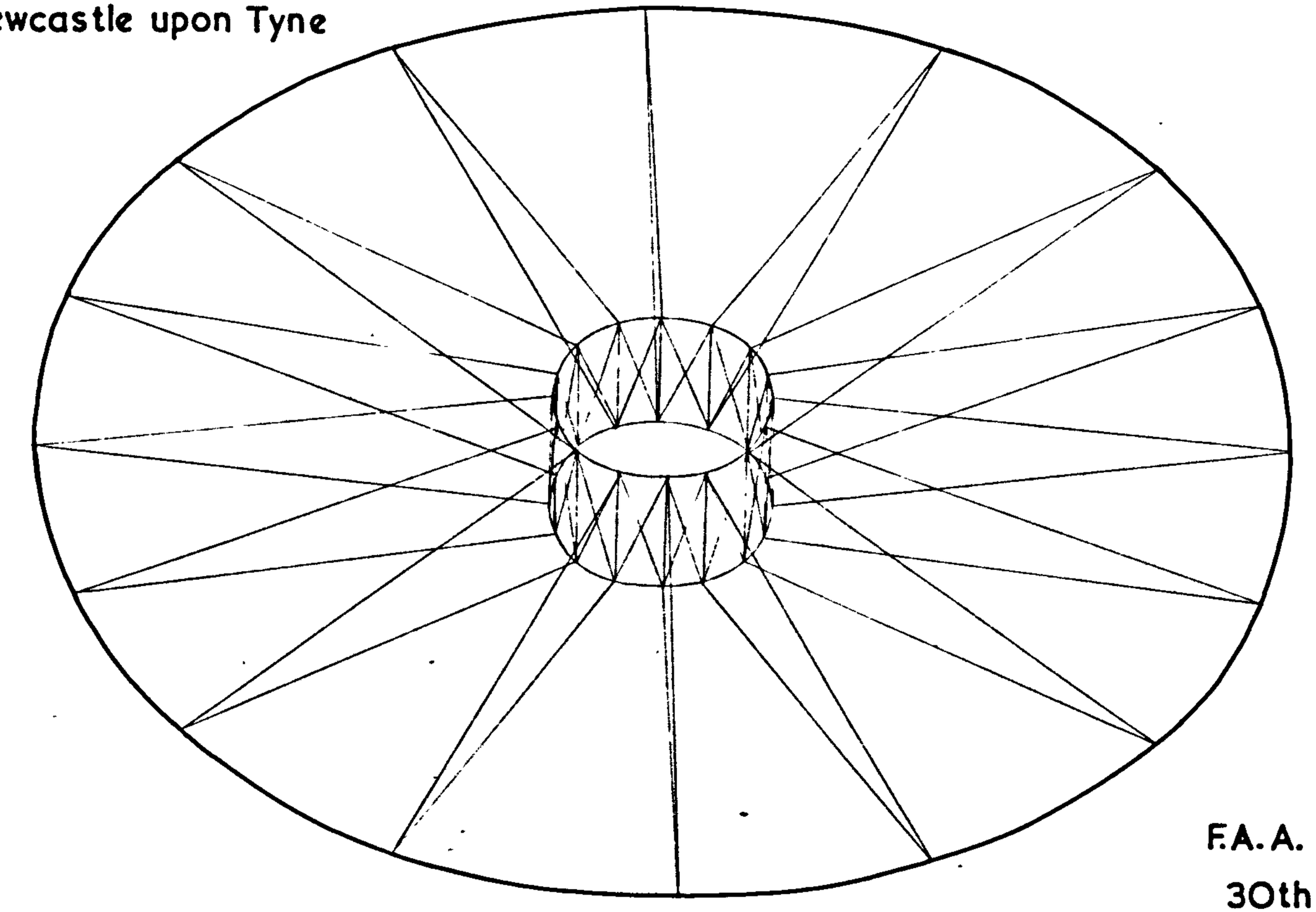

F.A.A. Ph.D. Thesis
30th Oct., 1968

FIG. 5 A SUSPENDED CABLE ROOF

CHAPTER II

A BRIEF HISTORY OF VAULT AND DOME CONSTRUCTION

2.1 EARLY AEGEAN, EGYPTIAN AND WESTERN ASIATIC VAULT AND DOME CONSTRUCTION

A vault is described as an arched roof, continuous arch, set or series of arches whose joints radiate from a central point or line.(2) The dome represents a specific form of this structural concept, having a rounded vault as a roof and a circular, elliptical or polygonal base. Being curved in two directions, the dome is theoretically the most efficient shape for covering large areas as it encloses the maximum amount of space with the minimum surface area. Dome and vault construction have been practised for thousands of years, the various forms being dictated by the availability and development of building materials.

The first known dome structures were built in the sixth or fifth millennium B.C.(3) Excavations at Arpachiyah, about four miles east of the ancient Assyrian capital of Nineveh, revealed domical shaped buildings constructed with pisé, a mixture of clay and earth rammed together with gravel. Similar buildings were found at the Neolithic site of Khirokitia in Cyprus and burial chambers, with stone domical roofs, appeared in Crete about 2,700 B.C.

Although early Egyptian buildings consisted mainly of heavy post and lintol forms of construction, in some instances arches were employed in connection with sun dried bricks. Arch construction was employed over nearly every opening by the ancient western Asiatic peoples of Babylonia, Assyria and Persia as, in these areas, the only available building material consisted of sun dried bricks.(4) Two methods of sun dried brick construction were employed over openings by

these ancient peoples.(5) The first was the corbelling method in which bricks were laid in horizontal courses. Where an opening occurred, each brick in the course above protruded slightly beyond the one in the course below until the bricks eventually met together again at the crown of the arch after a number of courses had been laid. The second method, voussoir arch construction, employed bricks on edge over the opening in a radiating pattern.

In early dome construction a conical shaped dome was normally obtained as a direct result of corbelling successive courses of building material. This shape was determined by the need to maintain structural stability and because it was extremely difficult to close a true hemispherical dome using the corbelling method of construction.

Figure 6(a) shows an ingenious method of forming a small dome roof over a pit which was discovered at Khafaje, in Eshnunna, about 2,000 B.C. The first course of bricks was raised up on pieces of rubble at two diametrically opposite points on the pit wall. As each successive course of bricks was added, the structure gradually attained a domical shape and the dome was completed when the brick courses met at the crown.

An early example of a vaulted roof, constructed by the corbelling technique, is shown in Figure 6(b). This tomb was discovered at Ur, the ancient Chaldean capital, and was constructed with sun baked brick in the third millennium B.C. Another example, built with the same material, is the roof of the Sanctuary in the Temple of Seti I at Abydos, in Egypt, which was constructed about 1,350 B.C. In this roof the corbelled brickwork was chiselled smooth to form a round vault.

Although these two examples of the corbelling technique were constructed in sun baked brick, this method reached perfection in the beehive shaped, stone tombs of the Greeks in the Mycenaen period. Two such tombs were those of Agamemnon and his wife, Clytaemnestra. This

EARLY VAULT AND DOME CONSTRUCTION. SHEET NO. I

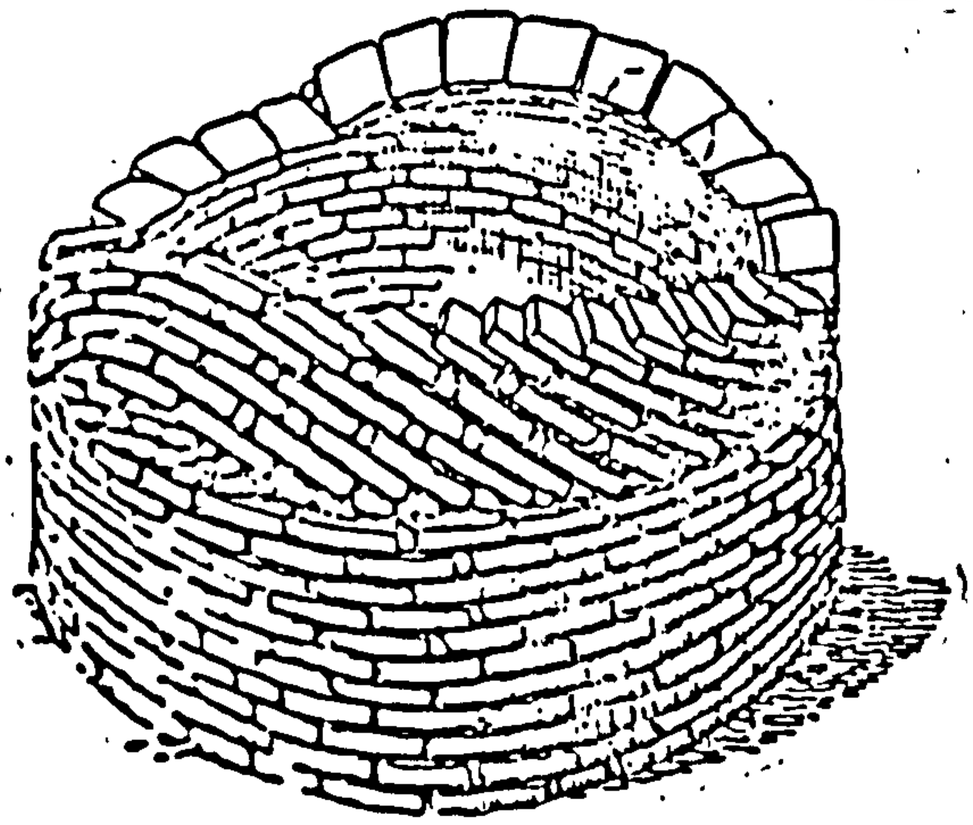

a) Domed roof to a pit excavated at Khafaje, in Eshnunna; *c.* 2000 B.C.



b) Corbel-vaulted tomb at Ur; third millennium B.C.

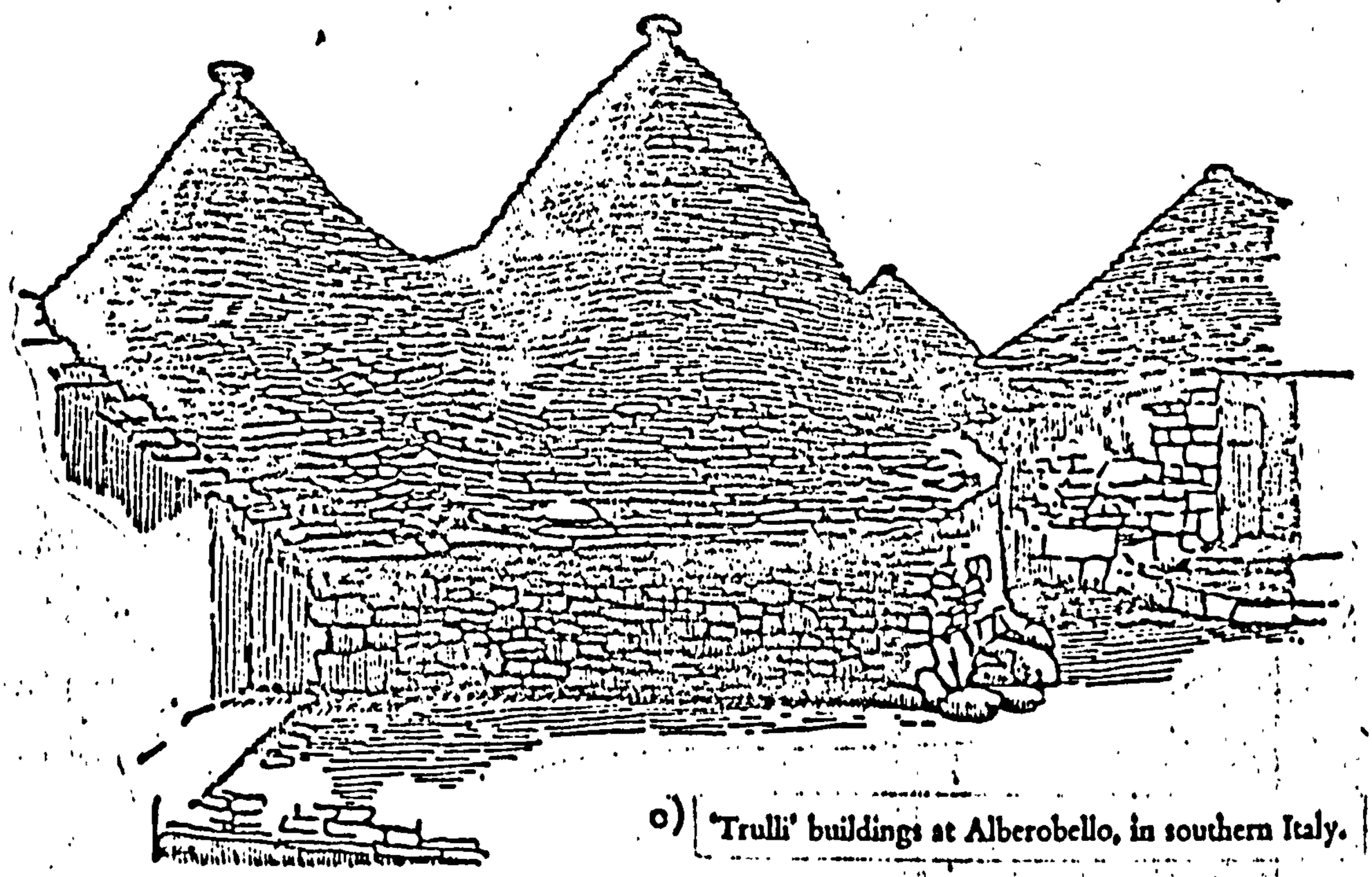

c) 'Trulli' buildings at Alberobello, in southern Italy.

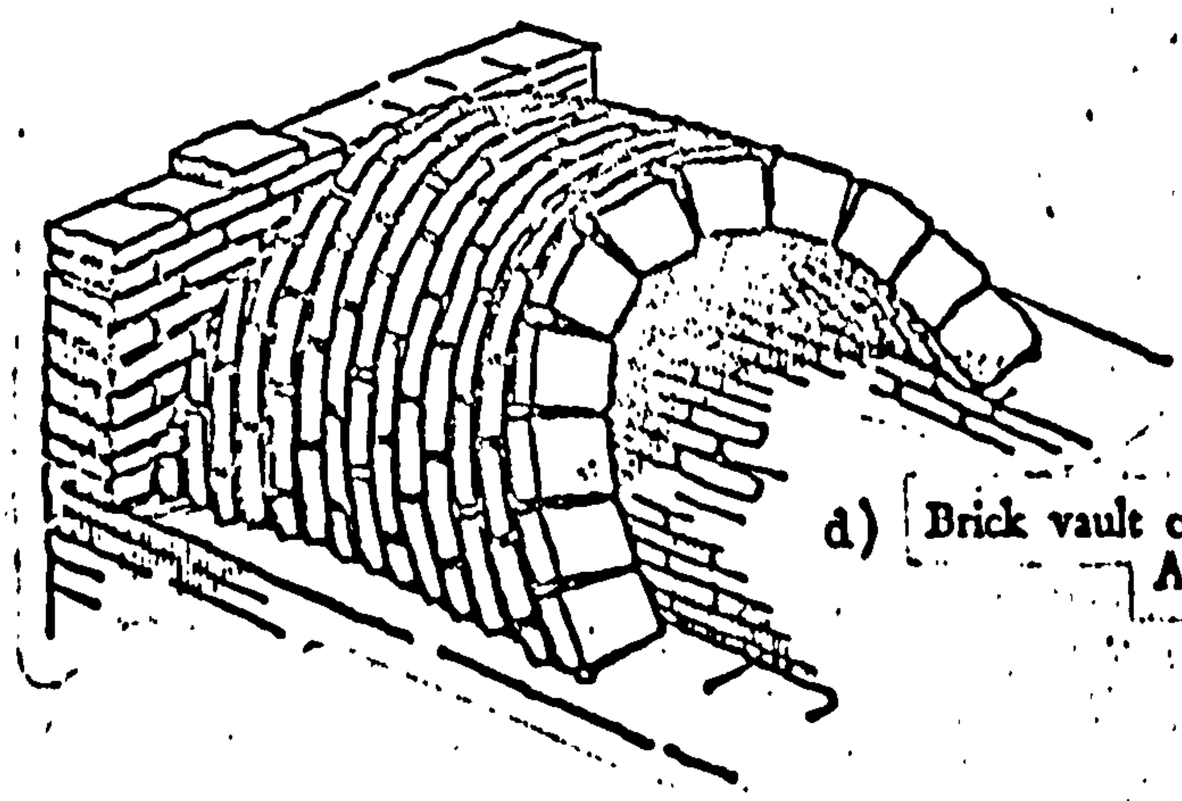

d) Brick vault of the type excavated at Khorsabad, Assyria; 722 B.C.

FIG. 6

F.A.A. Ph.D. Thesis.
31st Oct., 1968.

Structural Engineering Division,
Department of Civil Engineering,
University of Newcastle upon Tyne.

technique can also be seen in existing buildings at Alberobello in southern Italy, Figure 6(c). Many of them are modern but the original forms were extremely ancient.

Although the corbelled roof is ideally suited to circular buildings, the shape was not restricted to this form alone. Rectangular and other shaped buildings were also constructed by this method.

Where inclement climates were experienced, a watertight building was desirable. A weatherproof shelter could be constructed by filling gaps in the corbelled roof with stones and clay or by completely covering the structure with mounds of earth.

Arch construction, employing vertical courses of bricks, required wooden centreing for support while building work was in progress. In countries which were virtually timberless, the use of this material was impracticable and a method of arch construction was devised which needed no centreing. Each successive course of bricks forming the arch rested on the previous ring at an angle and was held in position partly by friction and partly by the adhesive nature of the mortar used. Figure 6(d) illustrates this method of construction. The example shown dates from the first quarter of the eighth century B.C. and was a brick vault over a culvert in the great palace of Sargon at Khorsabad in Assyria. This method of construction was also employed in Mesopotamia and Persia, and much later by Byzantine builders who thoroughly understood the principles of dome construction and built such masterpieces as Santa Sophia and SS. Sergius and Bacchus at Constantinople.

Figure 7(a) shows a cleverly contrived method of building a centreless vault over a rectangular area which is used in southern Persia to this day. An excellent example of an arched vault, constructed by this technique, is to be found at Baghdad in the Palace of Chosroes I (A.D. 531 - 579) at Ctesiphon. The vault is parabolic in

EARLY VAULT AND DOME CONSTRUCTION. SHEET NO. 2

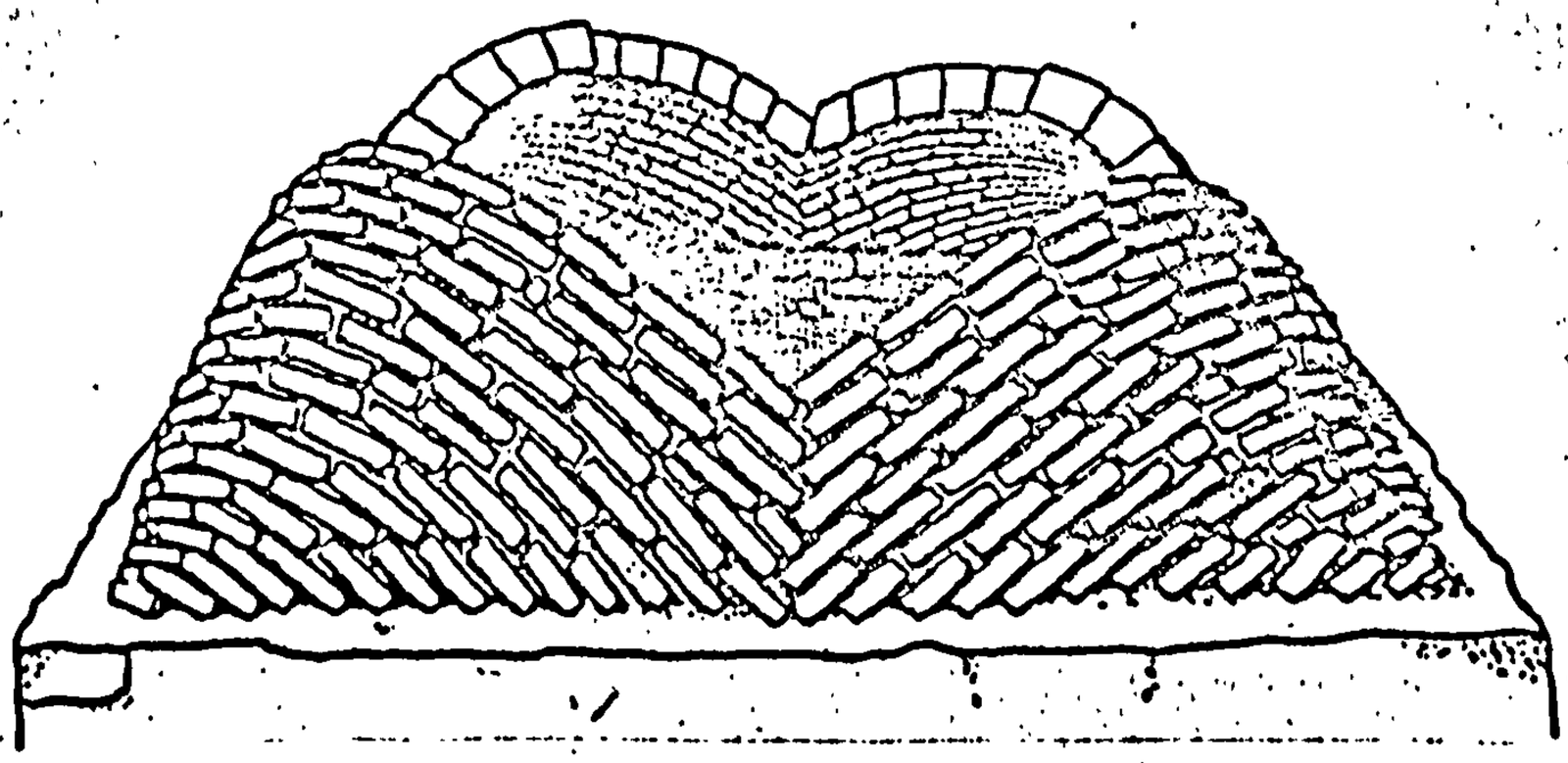

a) Centreless vault to a modern rectangular building in southern Persia.

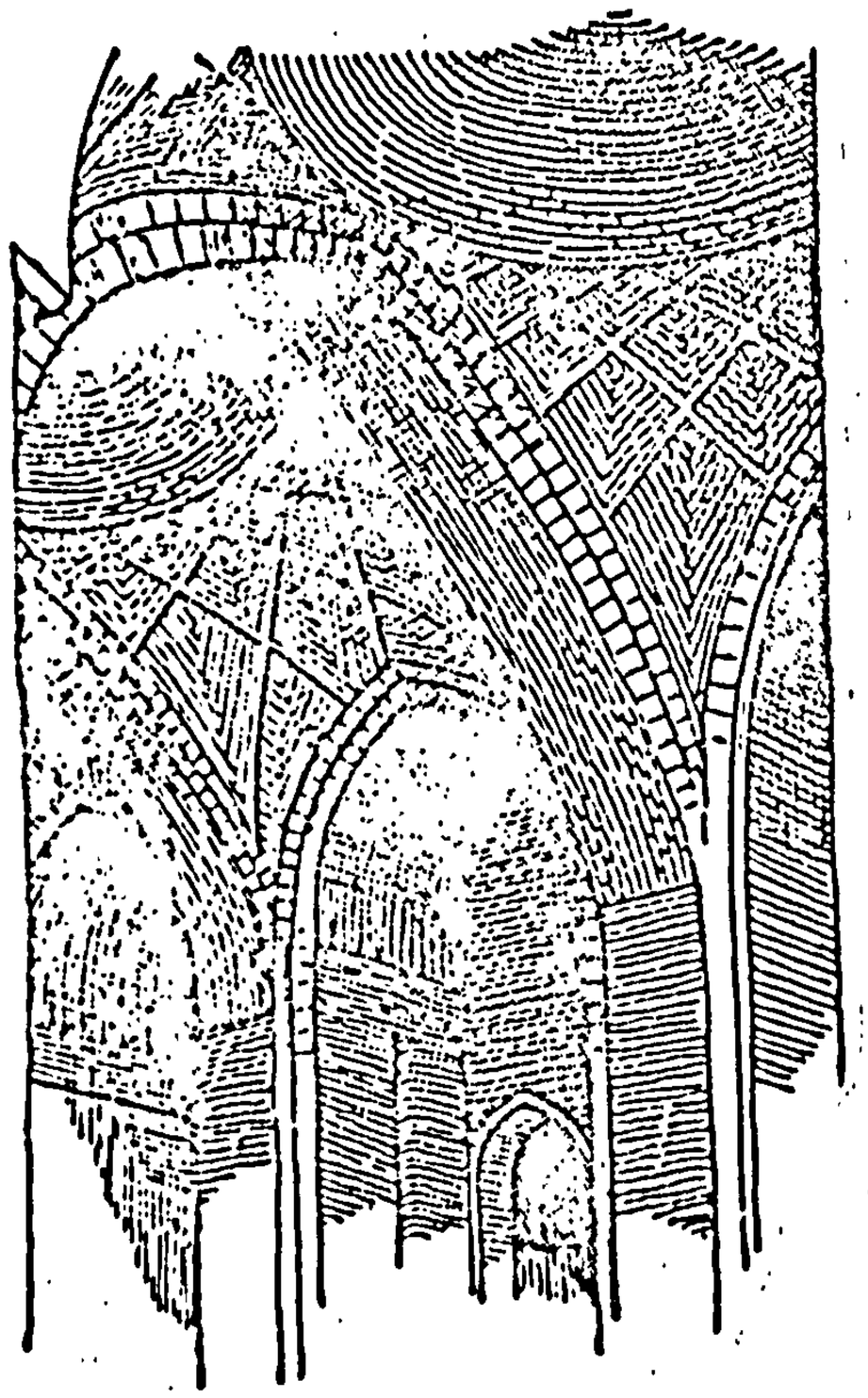

b) Masjid-i-Jami, Isfahan. The arches and vaults on the south-east side of the Great Dome Chamber.

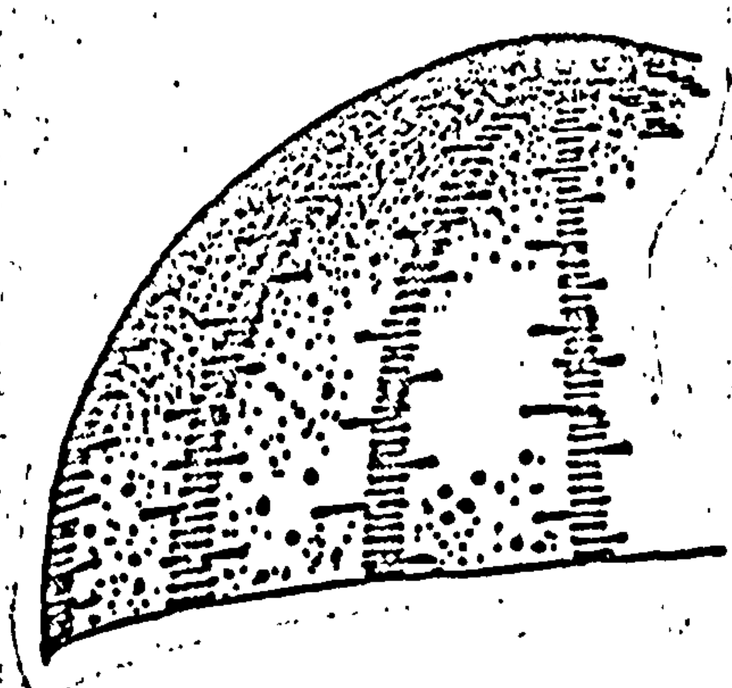

c) Brick ribs in Roman vault construction.

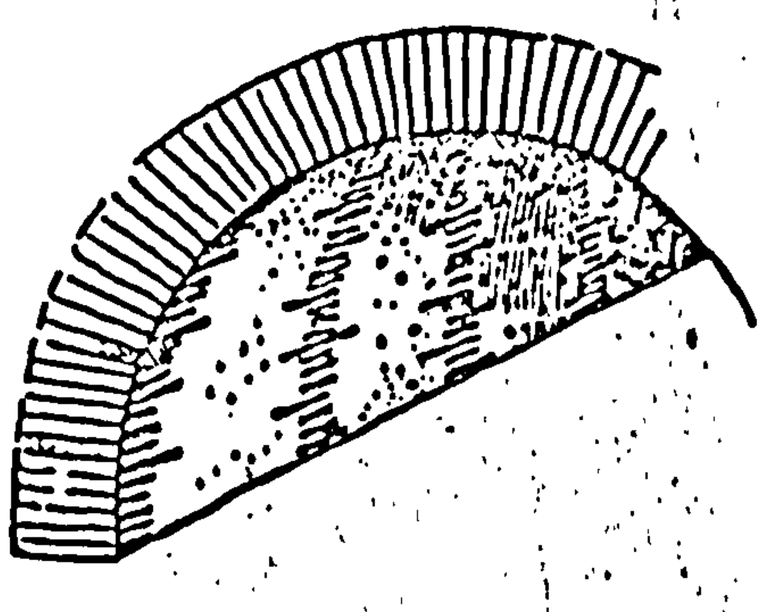

FIG. 7

F.A.A. Ph.D. Thesis.
31st Oct., 1968.

Structural Engineering Division,
Department of Civil Engineering,
University of Newcastle upon Tyne.

shape, about 83 feet in span and over 100 feet in height. It forms the largest unreinforced brick vault in the world and was constructed in A.D. 550. The building techniques employed in the construction of this vault were similar to those which had been practised in Iraq since Babylonian times. In contrast to these techniques was a later development in Persian work where arches and vaults were built using bricks on edge. This method of construction can be observed in parts of the interior of Masjid-i-Jami, at Isfahan, Figure 7(b).

2.2 ROMAN AND BYZANTINE VAULT AND DOME CONSTRUCTION

Roman vault and dome construction is characterized by the employment of the voussoir technique for arch construction and by the use of concrete. The arch was known to the Greeks and other ancient civilizations but the Roman achievement was in developing, for the first time, an architecture based upon the structural principles of the arch. Heavy buttresses were required to support these vaults and domes.

Timber formwork was needed for support in the construction of Roman vaults and domes from concrete or mortared rubble. Impressions of the shuttering can still be seen on many of the surviving buildings in Rome and elsewhere. A fair finish could be obtained, at exposed ends of the structure, by casting a layer of bricks into the concrete, as in the vaults at the Golden House of Nero. Tiled soffits were also popular because rendering and decoration could be carried out, if desired, after the form-work was struck. Examples of this type of construction can be seen in the Colosseum at Rome, at Hadrian's Villa near Tivoli and in the Baths of Caracalla.

The employment of concrete, for dome and vault construction, produced extremely heavy loads on formwork. In an effort to relieve formwork of excessive pressures the technique was developed of incorporating brick ribs into the structure. The ribs were constructed at intervals along the transverse centre line of vaults, Figure 7(c)

bottom, as at Hadrian's Villa. By using this method part of the imposed load was carried by the brick ribs and part by the formwork. Once the concrete had set, the ribs formed a monolithic structure with the hardened concrete and became of secondary importance. Brick ribs were also constructed along the diagonal lines of intersection of crossing vaults, as in the Baths of Diocletian, and they were formed along the meridians in cupolas and apses, Figure 7(c) top, as in the Sibylline Temple at Tivoli, in the Temple of Minerva Medica, and in the Baths of Agrippa in Rome. Interlaced ribs were employed in the apses of the Temple of Venus and Roma.

By using the technique of casting brick ribs into concrete structures, loads on formwork could be decreased to a limited extent. For large spans it was necessary to lighten the overall weight of the structure and various methods were employed by the Romans to achieve this objective. A system of coffering was devised which was incorporated in several buildings at Rome. Recessed squares can be observed in the soffit of the dome of the Pantheon, Figure 8(a), and recessed octagonal vaults are to be seen in the Basilica of Constantine or Maxentius, Figure 8(b). Lozenge shaped recesses were constructed in the roof of the apses of the Temple of Venus and Roma, Figure 8(c).

Hollow terracotta tubes, specially made for the purpose, were also employed as a device for decreasing the weight of a structure. The tubes, usually about 8 to 10 inches long and $2\frac{1}{2}$ to $3\frac{1}{2}$ inches in diameter, were embedded in the concrete or mortared rubble. One end of the tube remained open while the other was closed and tapered so that lines of tubes could be connected together. These tubes are illustrated in Figure 8(d). This form of construction was employed in the tomb of Scipios on the Via Appia, Rome, and in the Golden House of Nero.

Several examples of domes, constructed with terracotta tubes and

EARLY VAULT AND DOME CONSTRUCTION. SHEET NO.3

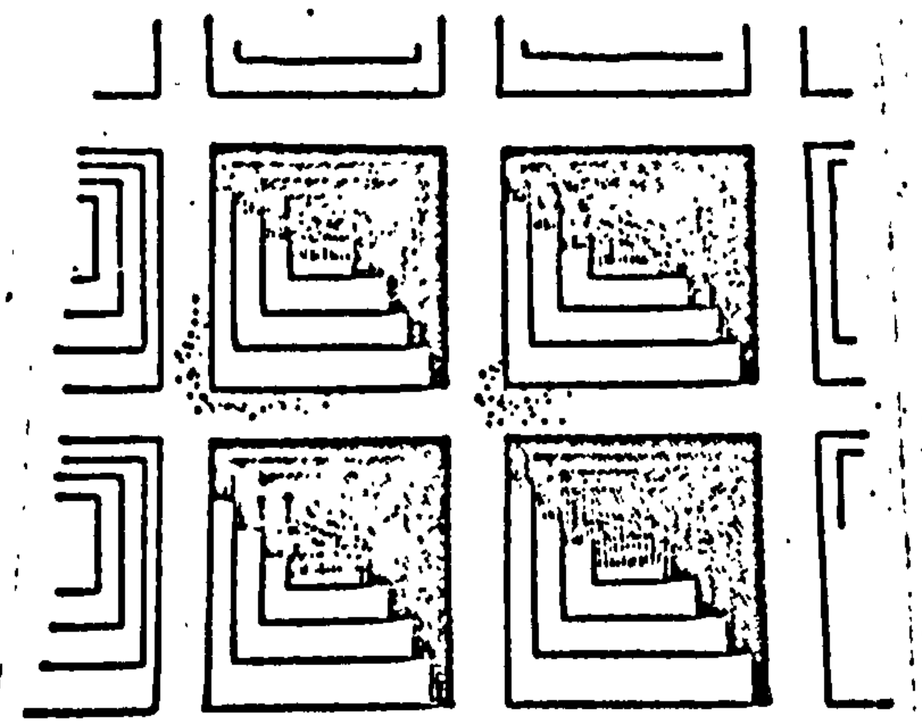

a) Coffering on the dome of the Pantheon, Rome.

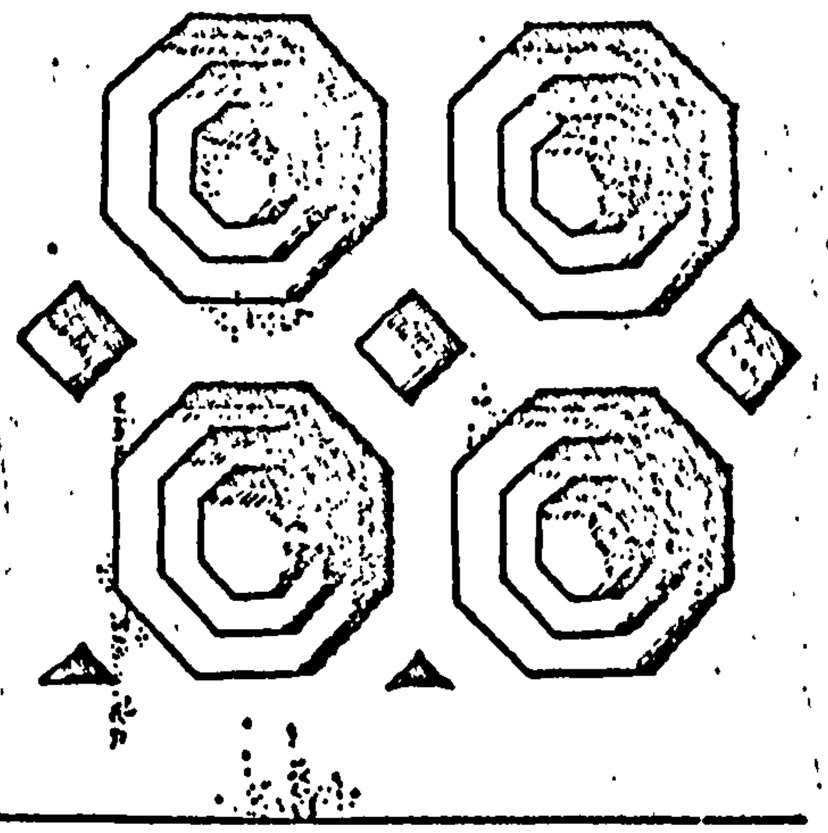

b) Coffering on the vault of the Basilica of Constantine or Maxentius, Rome.

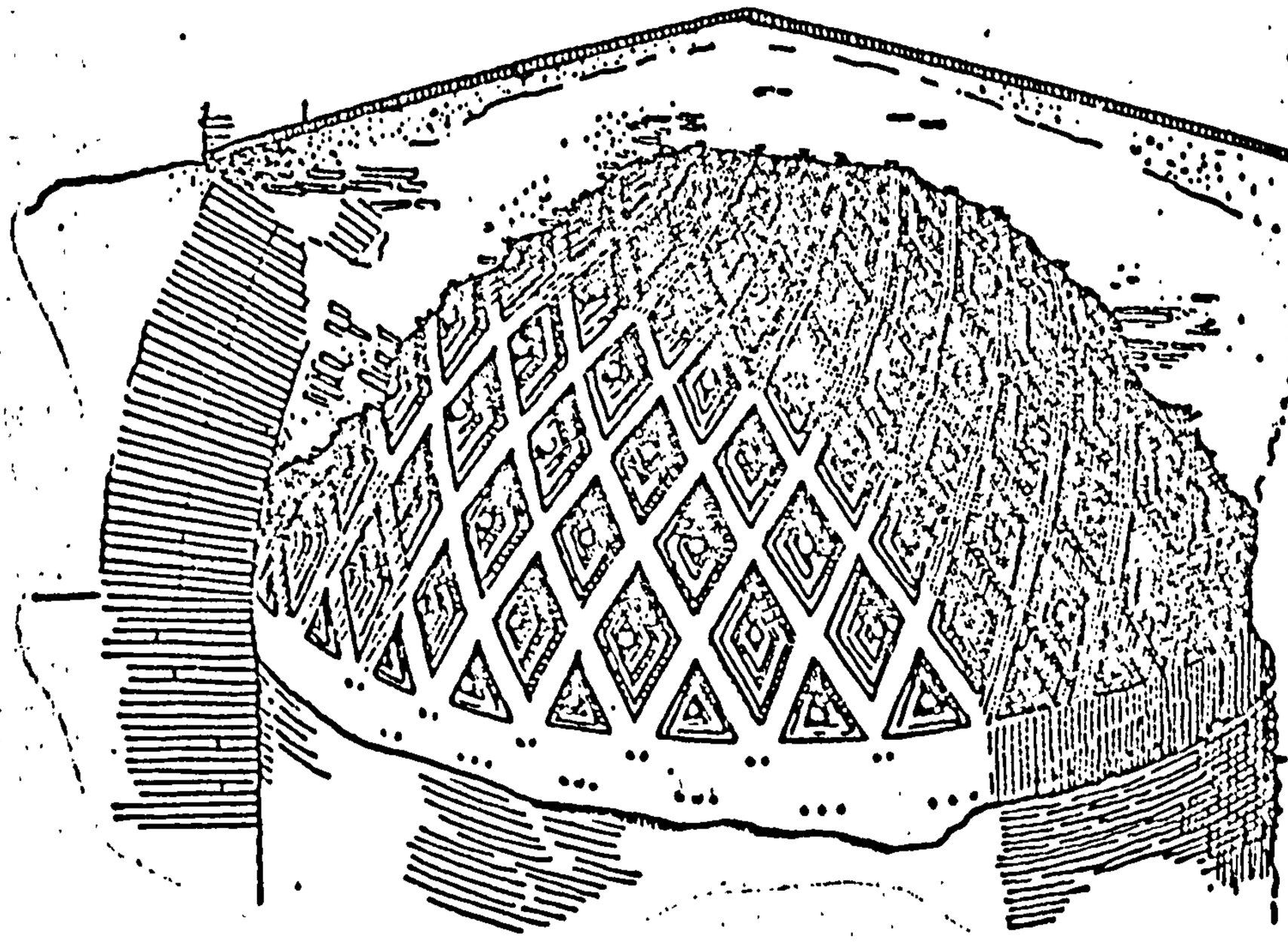

c) Coffered apse of the Temple of Venus and Roma, Rome.

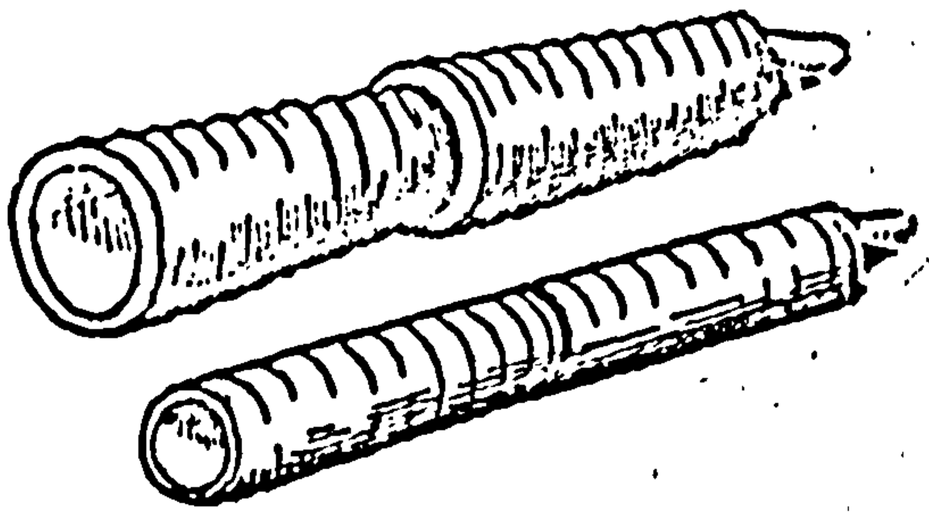

d) Hollow tubes used in ancient domes and ceilings.

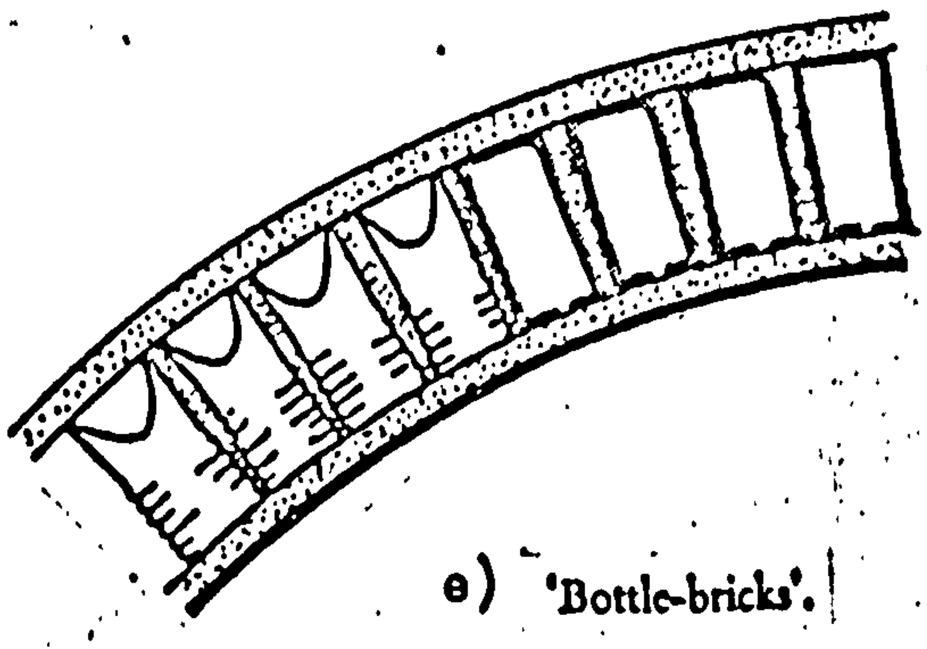

e) 'Bottle-bricks'.

FIG. 8

F.A.A. Ph.D. Thesis.
31st Oct.,1968.

Structural Engineering Division,
Department of Civil Engineering,
University of Newcastle upon Tyne.

wine jars, can be seen at Ravenna. Superimposed rings of small tubes are contained in the dome of the Baptistery of Neone, constructed in 449 - 452 A.D. Terracotta wine jars and amphorae are to be found in the dome and four barrel vaults of the Mausoleum of Galla Placidia, also built in the middle of the fifth century A.D. In this last structure, roofing tiles were laid on small amounts of mortar placed between the jars.

Adjacent to the Mausoleum of Galla Placidia stands the Roman Byzantine church of Santa Vitale. This church, ordered by Bishop Ecclesius and built by Guiliano Argentario, was consecrated in A.D. 547 by Archbishop Massimian. The drum wall of the church, below the dome roof, contained jars about 2 feet high, 5½ inches in diameter, standing upright. Small red terracotta tubes, about 7 inches long and 2¾ inches in diameter, were embedded in the concrete of the dome itself.

The Romans employed special hollow terracotta blocks in the construction of vaults over baths. Hot air could be circulated throughout the walls and ceilings to provide warmth and prevent condensation. Hollow vaults were not used again until a thousand years after this period.

A gradual decline in the fortunes of the Roman Empire commenced shortly after the year A.D. 100. After losing Central and Western Europe, Rome no longer held a central position geographically and in A.D. 324 Constantine transferred the capital to what is now Istanbul. Until a few years ago, Istanbul was known as Constantinople, after Constantine, but originally it was called Byzantium.

The Byzantine building techniques were similar to those of the eastern world and vaults were built, without centreing, by laying bricks at an angle.(6) Two magnificent structures erected at Istanbul, in the Byzantine period, were the Santa Sophia and SS. Sergius and Bacchus. These two buildings were constructed in the fifth and sixth

centuries employing the corbelling technique of dome construction whereas, during the same period, Roman builders favoured vertical brickwork construction which required the use of wooden centreing while work was in progress.

Another improvement on Roman dome construction, developed by Byzantine builders, was the employment of pendentives, Figure 9(a), to support domes over areas square in plan. Although pendentives had been used by the Romans, their domes were only erected over circular or polygonal shaped areas.

In A.D. 540, a mission was sent by Empress Theodora from Constantinople to Nubia. Egyptian architecture was greatly influenced by this mission and during the succeeding hundred years, until the invasion of the Mohammedans in A.D. 640, much dome and vault construction was carried out similar to the type found at Constantinople. Vaults, built in the same manner as those at Khorsabad, in Assyria, are to be found in the Nubian Christian churches and the method of construction has survived in Egypt to modern times.

2.3 MOSLEM AND INDIAN VAULT AND DOME CONSTRUCTION

In the seventh century A.D., the Moslem religion was founded by Mohammed. The Mohammedans were a warlike race of people and their empire eventually stretched from Spain to India. Despite the vast extent of the Mohammedan Empire and the diverse character of its conquered peoples, Islamic architecture had a similarity throughout its entire area because of the power of the established autocracy.

The Byzantine style of dome construction was modified to make domes easier to construct and several kinds of arch were developed, particularly the pointed arch and the horse-shoe arch. Corbels, which had been so predominant in early Aegean construction, were developed as elements of architectural design. Finally the ribs known to Roman builders and employed by them in brick in some of their concrete

EARLY VAULT AND DOME CONSTRUCTION. SHEET NO. 4

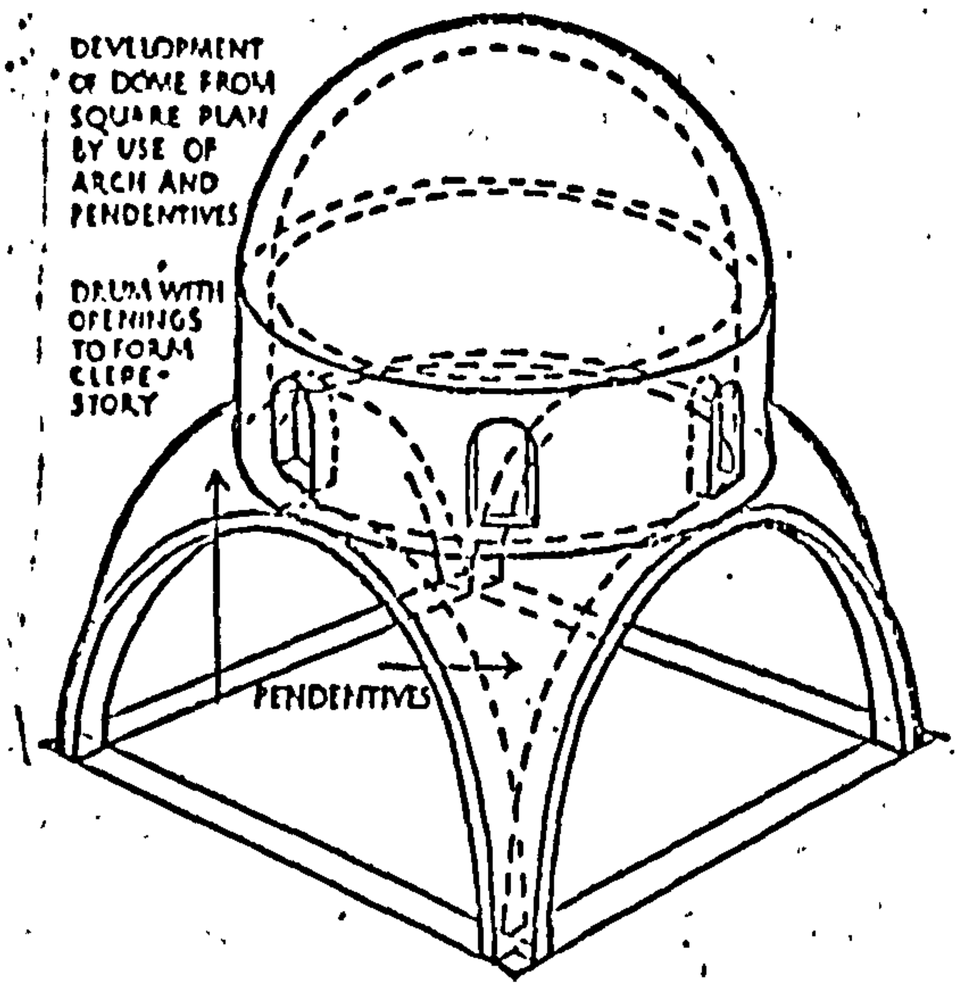

a) Byzantine Dome

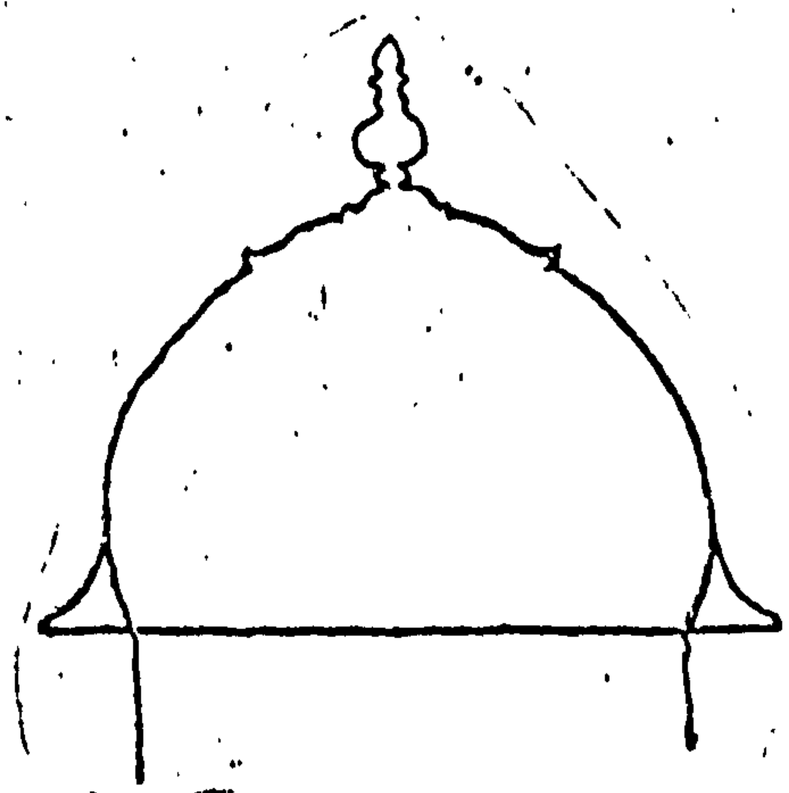

b) Diagram of Bell-shaped Dome.

Indian

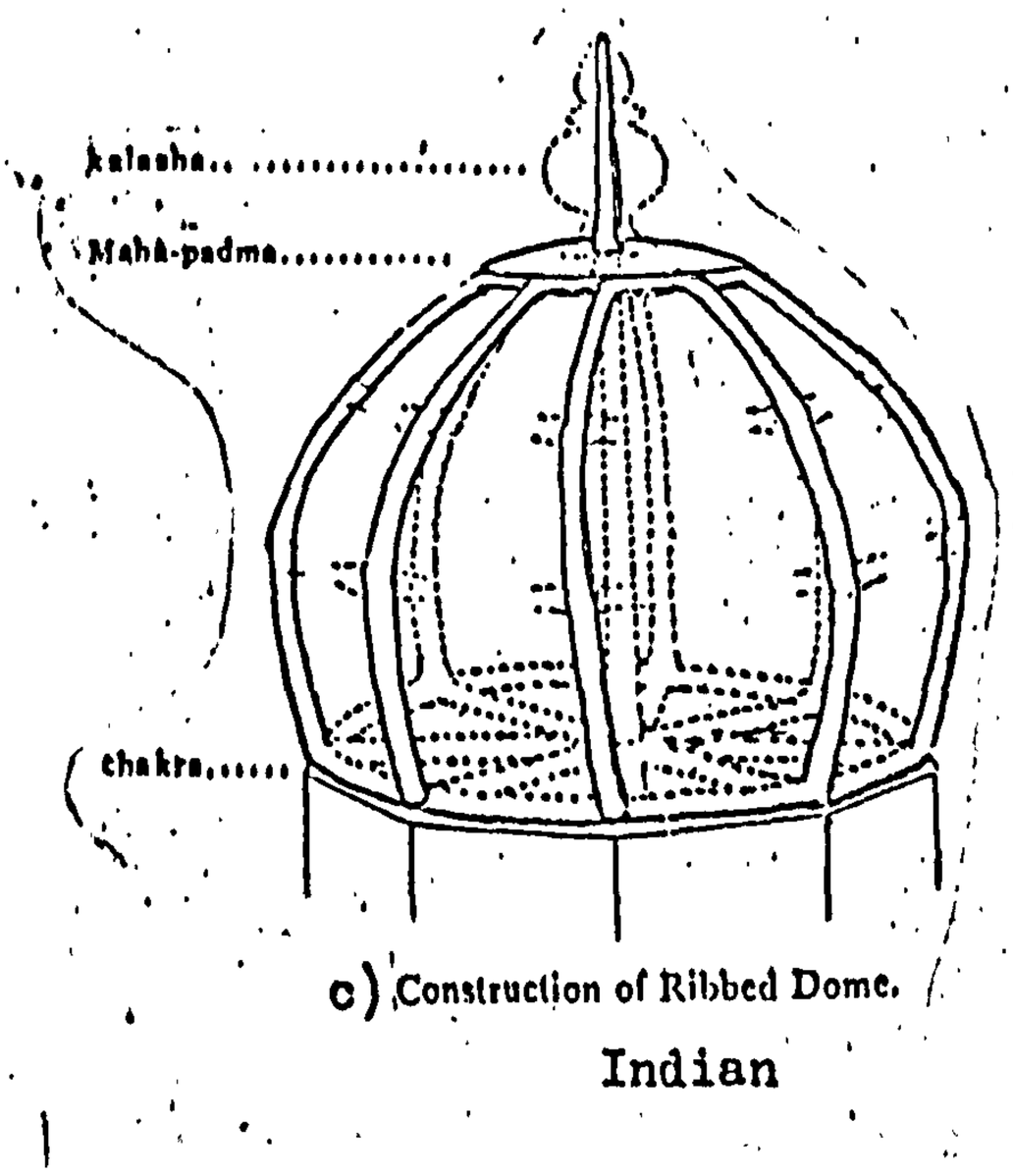

c) Construction of Ribbed Dome.

Indian

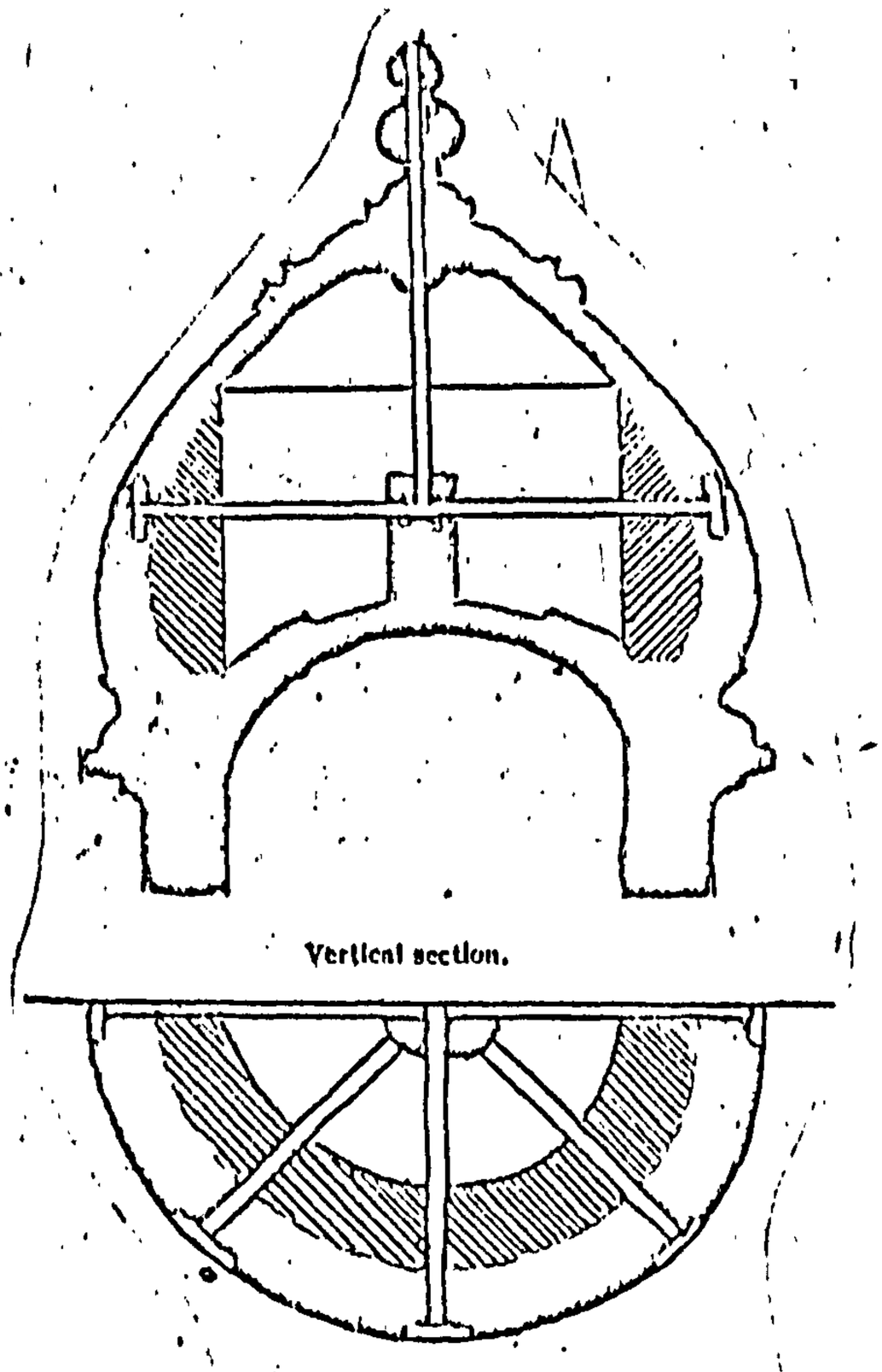

Vertical section.

Half-sectional plan.

d) Dome similar to fig. c) constructed of Permanent Materials.

FIG. 9

F.A.A. Ph.D. Thesis.
31st Oct., 1968.

Structural Engineering Division,
Department of Civil Engineering,
University of Newcastle upon Tyne.

vaults, was at last picked out from the mass of heavy concrete in which it was normally embedded. Hence the first skeleton forms of building appeared and the control of forces in lines began.

The practice was adopted, in Palestine, of using timber for cupolas of large size, probably due to the frequency and severity of earthquakes in those regions.(7) Two such dome structures, constructed in timber, were the Dome of the Rock, at Jerusalem, and the Congregational Mosque of Damascus.

The Dome of the Rock was built by Abd al-Malik and the works were completed in A.D. 691. A double cupola construction was employed, the internal dome being divided into ornamental compartments and the external dome being simply constructed of timber covered with sheets of gilt metal. There was a free space between the two domes, which were kept in place by iron rods crossing one another. This dome was destroyed twice, once by earthquake in 1016 and once by fire in 1448. After each disaster the dome was replaced in a similar fashion. The Congregational Mosque of Damascus was also constructed in a similar manner to the Dome of the Rock, but after being destroyed by fire in 1400 the dome was replaced in masonry.

Two methods of domical construction can be found in early Moslem mosques in India.(8) In the first method, peculiar to India, the dome is built up of horizontal courses of stone. The second method employs stone ribs, resting upon an octagonal base, to form the structural framework and the intervals between the ribs are filled up with horizontal masonry. Of these two types of domical construction, the ribbed dome was the earliest form as it was directly derived from primitive or temporary domes built with a framework of bamboo or of wood.

The principal Indian building styles may be roughly divided into three main periods according to roof construction. Firstly, there was

a period in which roofs were built with a framework of bamboo. In the second period the bamboo construction was reproduced more permanently in timber carpentry. The third period of building developed from the first and second periods when the original wooden forms of construction were adapted for use with brick and stone. In all three periods brick and stone were used to some extent in the substructure of the buildings.

The lotus flower was adopted as the symbol for all Buddhism and Hinduism. Early Buddhist horse-shoe arches, constructed from bent bamboo, resembled the lotus leaf in shape. Buddhist and Hindu domes constructed from bamboo also imitated the bell-shaped lotus fruit, Figure 9(b). The lotus leaf or bent bamboo arch became the structural basis of the distinctive bulbous Indian domes which differed slightly in shape from the more pointed and smoother curved Arab domes.

In primitive Indian ribbed domes, made with a bamboo or wooden framework, there were four essential parts which ensured the stability of the whole, Figure 9(c):

(1) the pole or axis, which was firmly fixed either in the ground or upon a stable base, such as an inner roof or dome;

(2) the bamboo or wooden ribs;

(3) the ties by which the ribs were secured to the pole at the springing of the dome;

(4) the cap which secured the ribs at the crown of the dome.

With the exception of the central pole and the horizontal ties, this form of construction is very similar to the larger scale radial ribbed domes of the present day. The spike, or finial, which protruded from the top of Arab domes was only ornamental, whereas in Indian domes it was an important member forming an integral part of the dome itself.

The primitive lotus dome, translated into permanent materials, Figure 9(d), had many practical recommendations, for the form was one

in which the outward thrust was reduced to a minimum. Although in later years stone construction replaced the lighter wooden forms and massive domes were built over Indian temples by the horizontal course method, the earlier system continued in vogue in Persia and Central Asia where stone construction on a large scale never became general.

With the need for large span construction in modern times, the heavier dome forms are impracticable. Hence the present day erection techniques have reverted once more, in radial ribbed dome construction, to similar methods employed by the primitive Buddhists.

2.4 DOME AND VAULT CONSTRUCTION IN THE MIDDLE AGES

Very few major developments in dome design and construction occurred in the Middle Ages. Round arches, barrel-vaults, cross-vaults, ribbed-vaults and domes were all employed as architectural and structural features during this period but only small improvements were made in erection techniques. Although many builders of the time had an understanding of the control of forces in directions, most domes were still constructed in stone or masonry in the massive form.

A few timber domes still exist from this period in France, Germany and Scandinavia but they were mainly employed as an external protective cover over the masonry dome proper. The frameworks of these structures were very complex and consisted of many bracing members.

2.5 DOME AND VAULT CONSTRUCTION BETWEEN THE MIDDLE AGES AND THE PRESENT DAY

Again, during this period of time, few major developments in dome and vault construction occurred until the eighteenth and nineteenth centuries. Hollow block arch construction was revived in the latter half of the eighteenth and beginning of the nineteenth centuries. This technique was employed by J. D. Antoine, in 1778, to build the Palais de Justice in Paris.

In 1785 special hollow pots, about 7 inches long and 7 inches wide,

were incorporated in the floor panels, arches and domes of several buildings in Paris. The pots, usually set in plaster of Paris, possessed one hexagonal end, the other being round. Both ends were closed. These bottle shaped bricks were embodied in buildings such as the Palais Royal, the Bourse, the Madeleine, the Chambre des Deputies, the Archives de la Cour des Comptes and elsewhere in Paris.

The trend of employing bottle shaped bricks for constructional purposes spread rapidly to England at this period. Variations in size and shape were numerous. Pots, square at one end and resembling those shown in Figure 8(e), were used by Henry Holland in the construction of the domed portico for Prince Frederick, Duke of York and Albany, at Dover House, Whitehall. Sir John Soane, who constructed the dome and arches of the Stock Office at the Bank of England in 1792 and 1793 employed a similar form of construction. In 1803 and 1804 William Strutt incorporated cylindrical pots, about 4½ inches in diameter, in the arched floors of a mill at Belper. Approximately half a century later, the great ceiling of St. George's Hall, Liverpool, completed in 1849, was erected using 140,000 hollow blocks, each block being 12 inches long and 4 inches square.

Vaults and domes are no longer built using the hollow block form of construction. This building technique is mainly employed, at the present time, in flat floor systems.

The advent of the eighteenth and nineteenth centuries saw possibly the most important developments so far experienced in dome construction. It was at this time that braced domes gained rapidly in popularity, especially in Germany and France. The imagination of architects and engineers was greatly stirred by the capabilities of such structures for covering large spans with the result that several large exhibition buildings were covered by domes in this period.

A major contribution to the increased popularity of braced dome

construction was the introduction of a new structural material at this time, iron. Architects and structural engineers were quick to realize the potentialities and advantages of this high strength and comparatively light in weight material.

Iron was employed for the first time in dome construction in 1811 by Bellangé and Brunet who erected a 127 feet diameter iron dome over the central part of the Corn Market in Paris. Although much interest was shown by architects and engineers in this dome, the building methods employed consisted only of adapting timber forms of construction to wrought ironwork. Nevertheless, a start had been made and soon many churches in France and Germany were roofed by iron braced domes.

Most of the early domes were constructed from a number of latticed half-trusses which were connected to a latticed ring girder at the centre. The lower boom of each half-truss was normally straight, the upper one being curved, and the dome roof was simply supported on circular walls. With smaller domes the central ring and lantern were omitted and the half-trusses were directly connected to each other at the centre. This form of construction produces no horizontal thrusts at the supports despite the external appearance having the shape of a dome. However, in most cases a horizontal base ring of a polygonal shape was normally provided to increase the stiffness of the structure. Domes of this form were also employed to cover areas square or octagonal in shape and, with larger spans, the lower booms of the trusses were also curved forming latticed ribbed domes.

The shape of earlier braced domes was hemispherical, producing no horizontal thrusts at the supports. Later domes employed a shallower form of construction resulting in high thrusts at the base and several cases are known where collapses occurred due to insufficient restraint at the edge. This led engineers to consider, in more detail, the problems involved in braced dome analysis and soon several eminent

civil engineers, realizing the advantages of space systems, took a great interest in this form of construction.

The second half of the eighteenth century saw many developments in various forms of braced iron domes. In Germany the leading authorities at the time were Schwedler (popularly known as "the father of domed structures"), Henneberg, Mohr, Ritter, Müller-Breslau, Scharowsky and Zimmermann, each of whom contributed greatly to the development of the three-dimensional systems.

In more recent years, the need for large, clear-span structures has further increased the popularity of braced domes and space structures in general. Although, until recent years, improvements were hampered by the lack of suitable lightweight structural materials, nowadays research and development work has provided materials with increased strength-to-weight ratios and hence many three-dimensional systems of construction are being built today.

Reinforced concrete is still employed in the erection of shell domes but this form of construction has limitations in spite of the fact that the flexibility and ease of moulding of concrete make it possible to construct any shape. The necessity for complicated and expensive formwork, not normally required when using prefabricated components, for supporting the reinforced concrete shells during the casting and curing periods makes this type of construction uneconomical for large spans. Thus, it is with the braced dome form of construction involving prefabricated parts, made from materials such as steel, aluminium, plastics and laminated timber, that the interest of the architect and engineer is mainly directed today.

CHAPTER III

BRACED DOMES

3.1 CLASSIFICATION OF THE MAIN TYPES OF BRACED DOMES

Braced dome systems of construction have a special importance in engineering practice and many large span structures of this type have been erected in recent years. The members of such building forms are either curved and lie on a surface of revolution, or they are straight and have their connecting points lying on such a surface. No obstruction is imposed on the inner space of buildings employing this arrangement of component parts.

Braced domes can be subdivided into four general categories:[9]

(1) frame or skeleton type (single-layer dome);

(2) truss type (or double-layer dome), extremely rigid and suitable for very large spans;

(3) stressed skin type (in which the covering forms an integral part of the structural system);

(4) formed surface type (in which sheets are bent and interconnected along their edges to form the main skeleton of the dome).

Braced domes consist largely of prefabricated units which are joined together at suitable points, called nodes, by simple connectors. The number of different sized members is kept to a minimum to reduce production costs and standard connectors are employed to speed up erection techniques.

Structures of the braced dome type possess great stiffness. Their weight compares favourably with more orthodox forms of construction for short spans and, for large spans, domes provide the only logical

solution to the problem of enclosing such areas.

In the past, braced domes have been constructed over exhibition and concert halls, stadiums and planetariums, water reservoirs, gas and oil storage tanks. Nowadays, domes are being erected over dance halls, skating rinks, supermarkets, restaurants, banks, summer houses, stores, warehouses and workshops. Swimming pools and greenhouses are also popular types of buildings for which domical shaped coverings are employed and rigid radomes are now used to house delicate radar equipment.

Although four general braced dome categories have been mentioned previously, it is possible to subdivide these groups further into several specific dome types:

(1) Schwedler domes;

(2) Network domes;

(3) Plate-type domes;

(4) Zimmermann domes;

(5) Stiffly-jointed framed domes;

(6) Lamella domes;

(7) Kiewitt domes;

(8) Two- and three-way grid domes;

(9) Geodesic domes;

(10) Ribbed domes.

The number of different component systems is almost limitless in braced dome construction and therefore it is not possible to produce a complete classification of the various forms. However, the majority of braced domes can be identified with one of the ten types listed.

3.2 SCHWEDLER DOMES

One of the simplest forms of braced dome construction was first developed by J. W. Schwedler in the 19th century. Schwedler domes, as they are called, consist of ribs or curved meridional bars connected

together by a number of horizontal polygonal rings. If the members are pin-connected they form a system of quadrilaterals which can only resist symmetrical loading. To stiffen the structure so that it will also carry unsymmetrical loading, these quadrilaterals are subdivided into two triangles by the addition of a diagonal member. No stresses are produced in the diagonals of a pin-connected dome if symmetrical loading occurs, but if the loading is unsymmetrical then tension or compression stresses develop. Compression in long members must be avoided or large sectional areas will be required to resist buckling and lead to uneconomical design. Therefore, it is normal practice, in Schwedler type domes, to provide each quadrilateral with two slender diagonals; when one diagonal is under tension, the other is subjected to compression and yields taking virtually no load. This method is known as counter-bracing.

On certain assumptions, Schwedler domes can be regarded as statically determinate structures and they can be analyzed accordingly. It is this fact which has been responsible, to a large extent, for the popularity of Schwedler domes over the past years. The layout of a typical Schwedler dome is shown in Figure 10(a).

An early attempt to increase the stability of braced domes consisted of erecting two simple Schwedler domes, one above the other, to form a multiple dome. This produced one of the first types of double-layer dome structure.

3.3 NETWORK DOMES

If each polygonal ring of a Schwedler dome is rotated through an angle of $\frac{\pi}{n}$ with respect to the ring below, where n = number of sides, then a network dome is formed. This rotation results in each trapezium of the Schwedler dome being transformed into two triangles which lie in different planes. The marked difference between meridional rib bars and the diagonals, which is present in the Schwedler dome, disappears

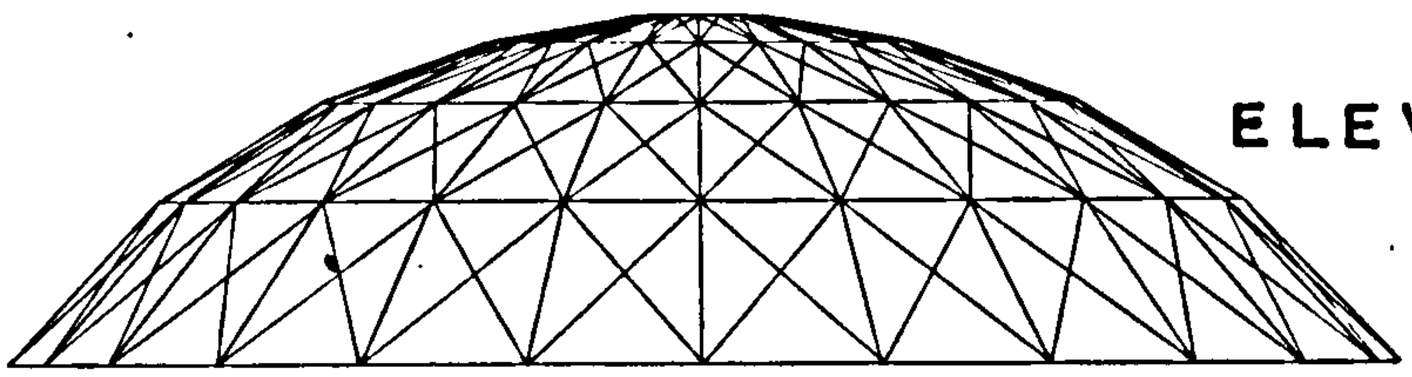

ELEVATION

SCHWEDLER DOME

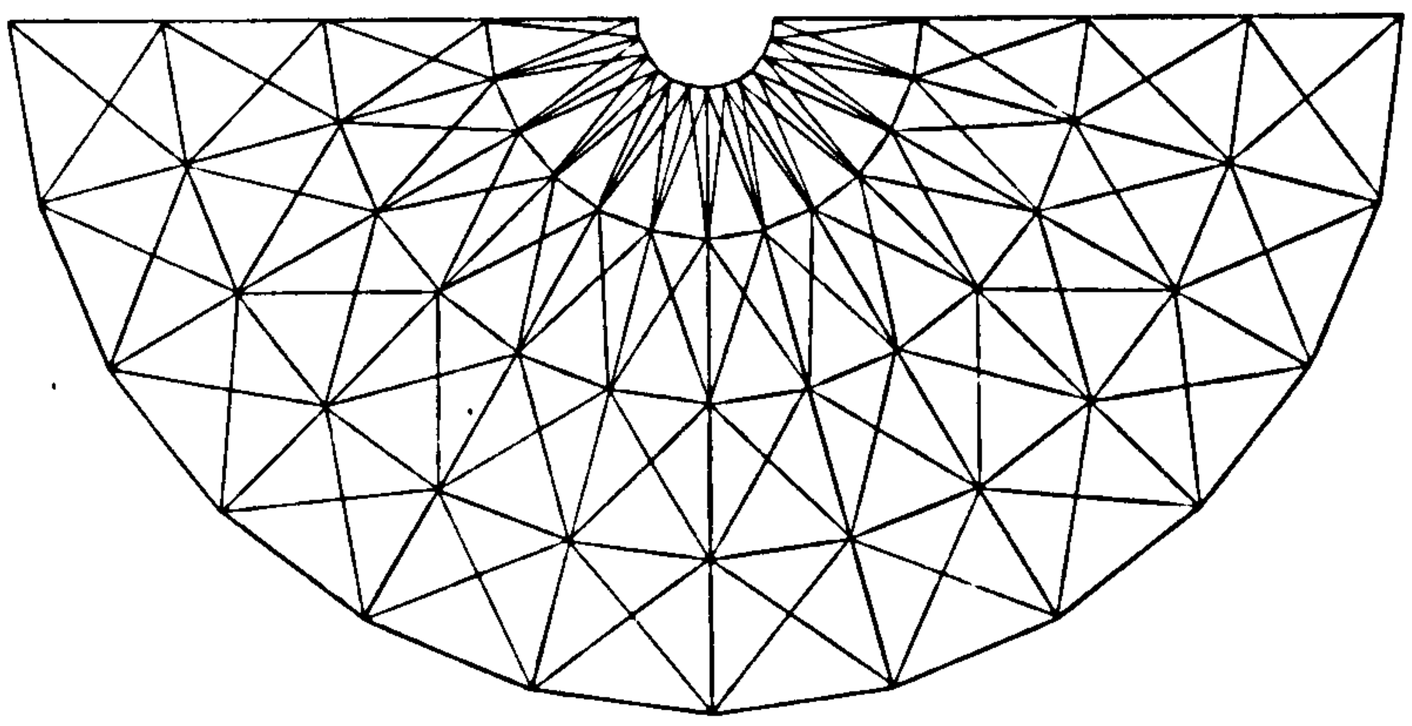

PLAN

A

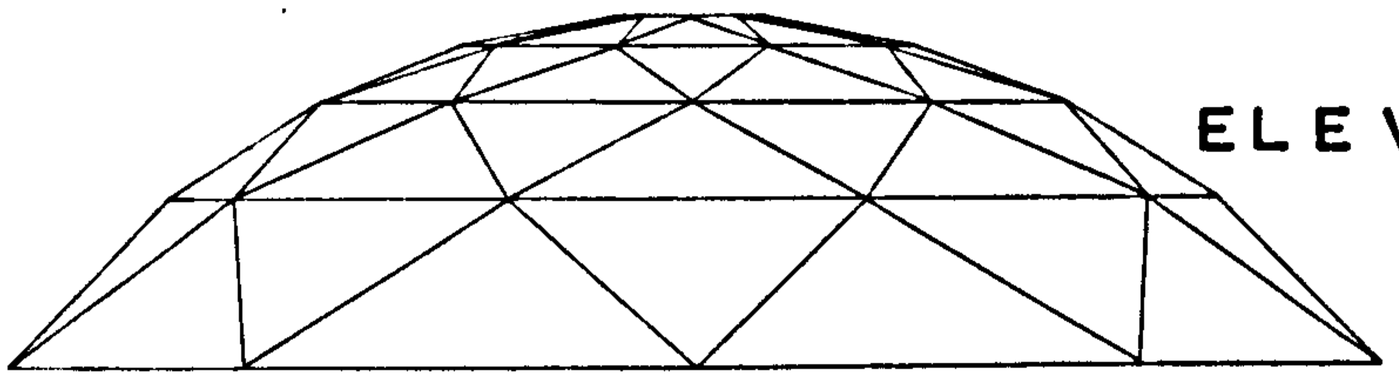

ELEVATION

NETWORK DOME

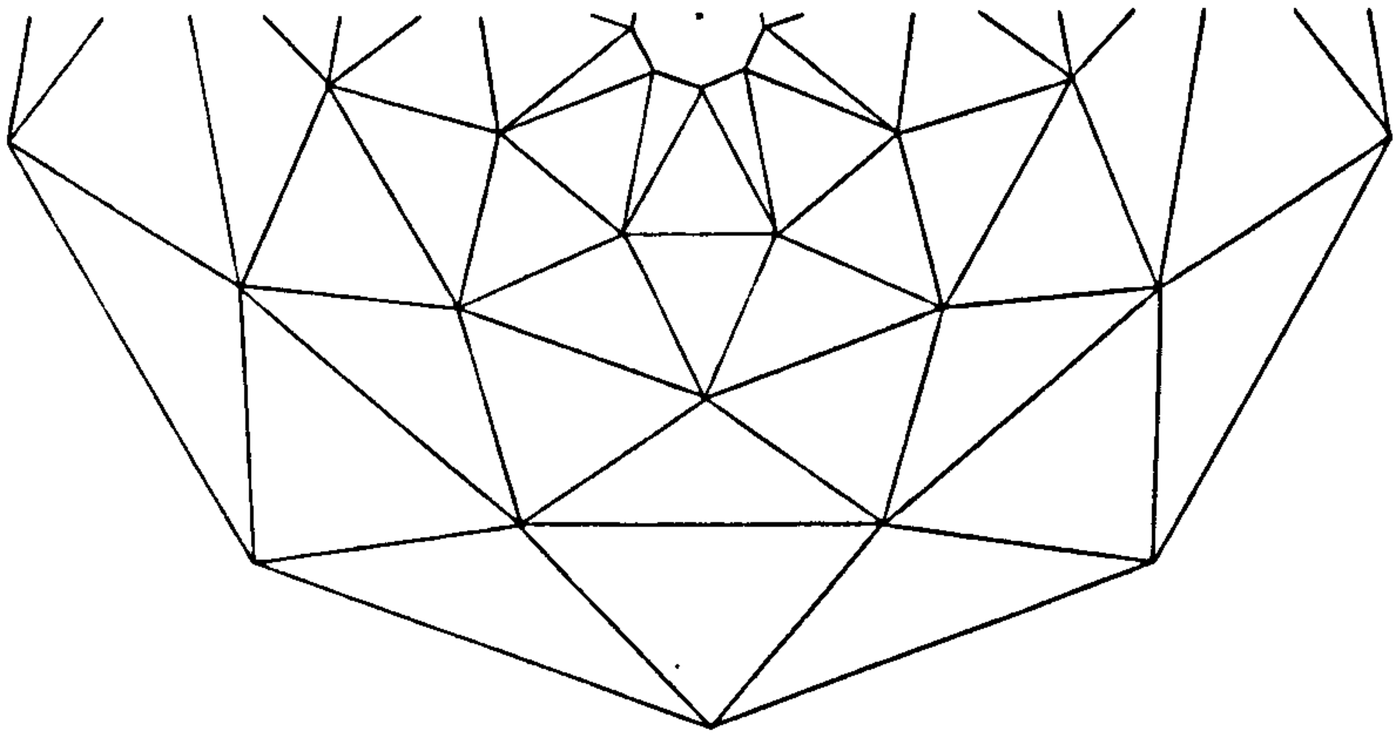

PLAN

B

FIG. 10

F.A.A. Ph.D. Thesis
4th Nov., 1968

Structural Engineering Division
Department of Civil Engineering
University of Newcastle upon Tyne

in the network dome.

Regular pin-connected network domes are statically determinate and stable only if they possess an odd number of sides otherwise, with an even number of sides, the structure becomes critical. A network dome is illustrated in Figure 10(b).

3.4 PLATE-TYPE DOMES

Plate-type domes are suitable for erecting over square or rectangular areas. They can be derived from Schwedler domes which are composed of a small number of sides. The sides are filled in with several bars, all lying in the same plane, forming a triangulated bracing network. An example of this type of dome can be seen in Figure 11(a). Plate-type domes are also statically determinate if pin-jointed.

3.5 ZIMMERMANN DOMES

Although outdated by modern day construction techniques, the braced domes developed by Zimmermann in Germany, before the First World War, provided an interesting solution to overcome the high horizontal thrusts obtained in shallow domes. Zimmermann domes are statically determinate if the members are pin-connected and half the supports consist of "ball bearings". In other words, the supports possess complete freedom of movement in the horizontal plane and exert only vertical reactions. The other supports have their horizontal reactions fixed in a pre-determined line along the direction of the base members as shown in Figure 11(b). This form of construction entirely removes the need for lateral restraint and hence it is possible to support even the shallowest of domes on slender walls.

One other main feature of Zimmermann domes is that each ring has twice as many sides as the ring above. They are also suitable for any layout and give a pleasing regular arrangement of bars.

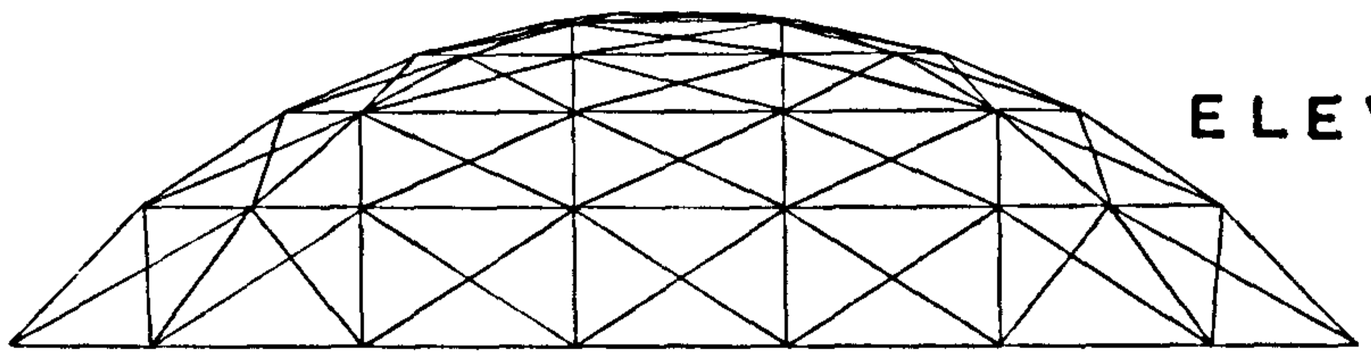

ELEVATION

PLATE-TYPE DOME

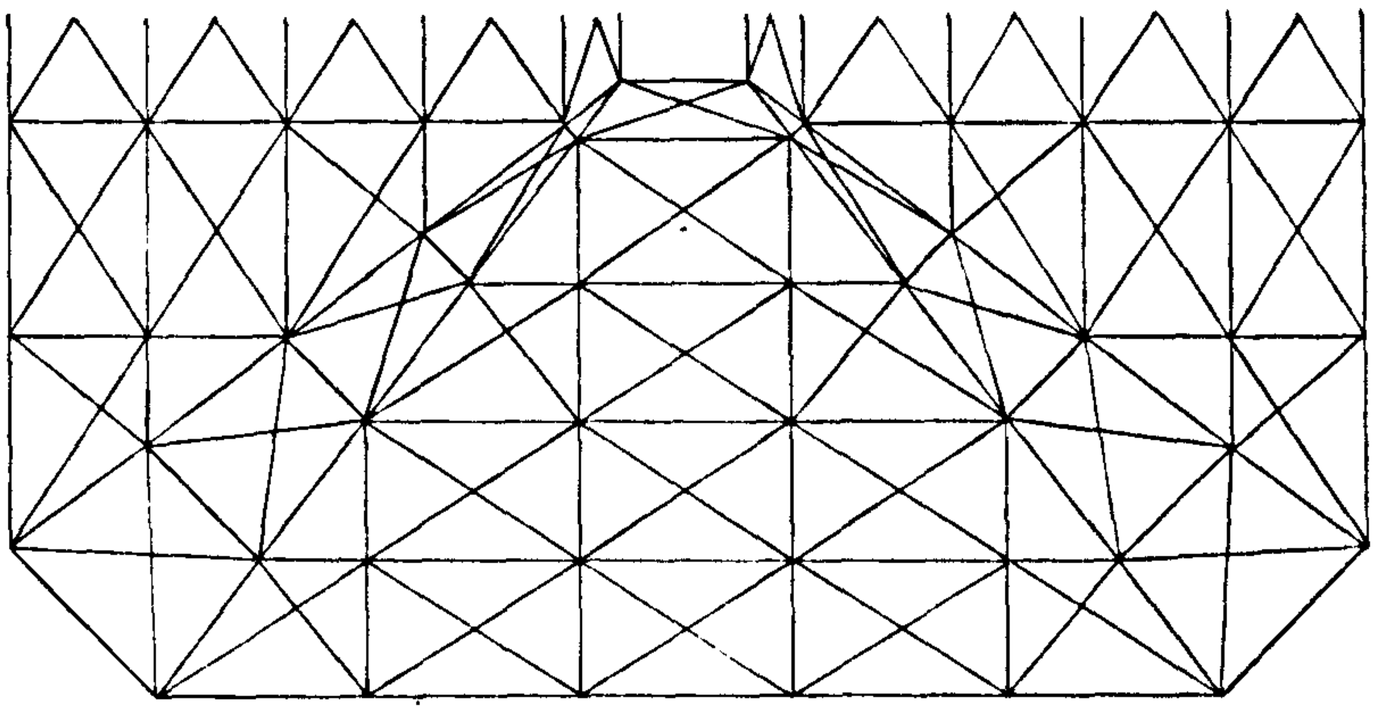

PLAN

A

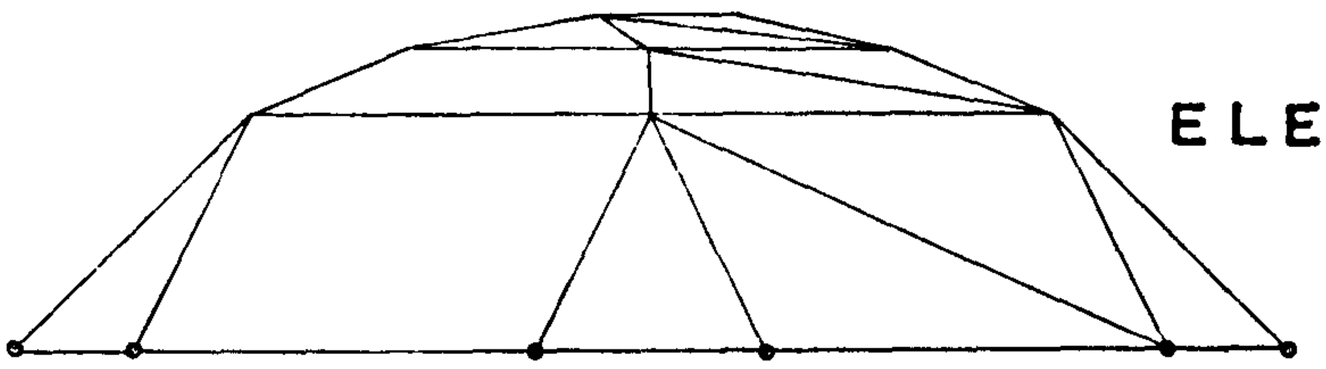

ELEVATION

ZIMMERMANN DOME

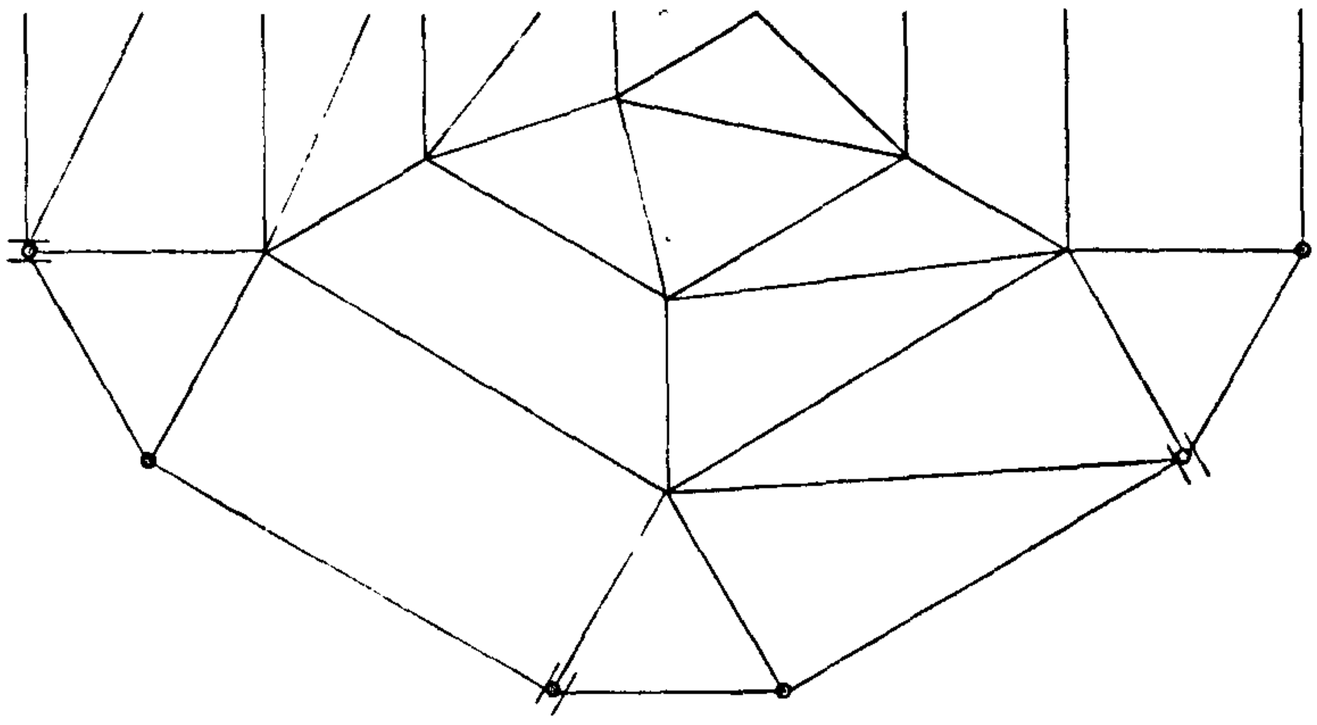

PLAN

B

FIG. 11

F.A.A. Ph.D. Thesis
4th Nov., 1968

Structural Engineering Division
Department of Civil Engineering
University of Newcastle upon Tyne

3.6 STIFFLY-JOINTED FRAMED DOMES

If the diagonal members of a Schwedler dome are removed and the joints of the remaining continuous meridional ribs and horizontal polygonal rings are made rigid, then a stiffly-jointed framed dome is obtained. Although these two types of dome are identical in layout and form their behaviour is radically different.

Schwedler domes carry external loads by means of axial stresses in the members with a complete absence of moments. In stiffly-jointed framed domes, bending moments are present as well as axial forces.

Without diagonals and under unsymmetrical loading the Schwedler dome is unstable and forms a mechanism whereas the stiffly-jointed framed dome is stable under these conditions. Stiffly-jointed framed domes are highly redundant structures and diagonals only add to their redundancy.

The methods of analysis available for Schwedler domes are completely inadequate for applying to stiffly-jointed framed domes. Whereas the solution of Schwedler domes is quite straightforward, the solution of stiffly-jointed framed domes can be very complicated.

Several domes have been erected in the U.S.A. employing the stiffly-jointed frame technique but their components have been extremely heavy. These structures are not amenable to modern day prefabrication techniques and many of them require substantial connections as illustrated in Figure 12(a).

3.7 LAMELLA DOMES

Lamella domes consist of a large number of interconnecting units, called lamellas, which form a lozenge-shaped pattern. The units are normally composed of steel, aluminium or timber and each lamella is twice the length of the side of a diamond. Figure 12(b) illustrates the lamella system of braced dome construction.

In timber lamella domes, complete stability of the structure is

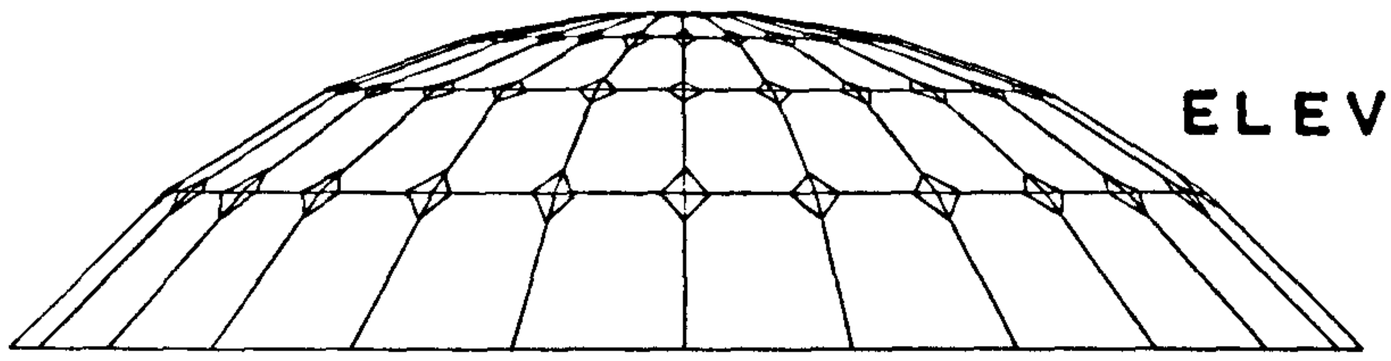

ELEVATION

STIFFLY-JOINTED DOME

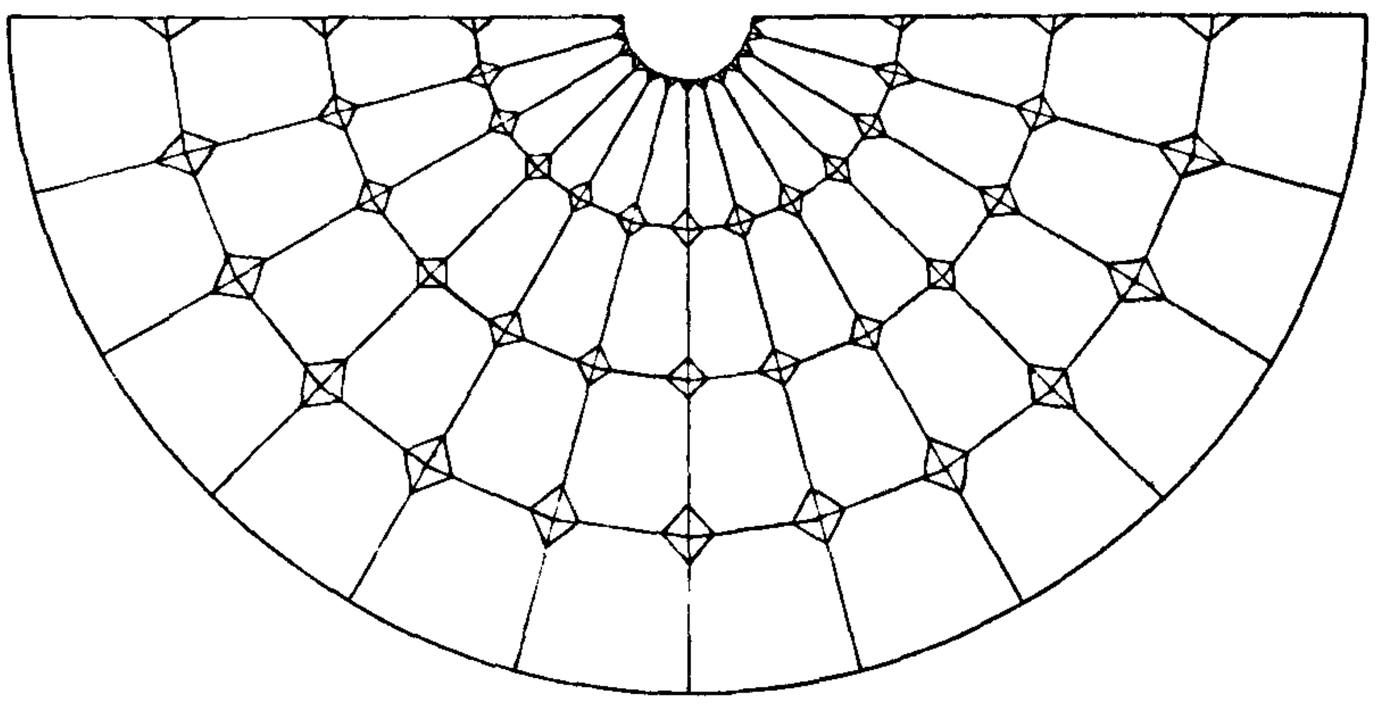

PLAN

A

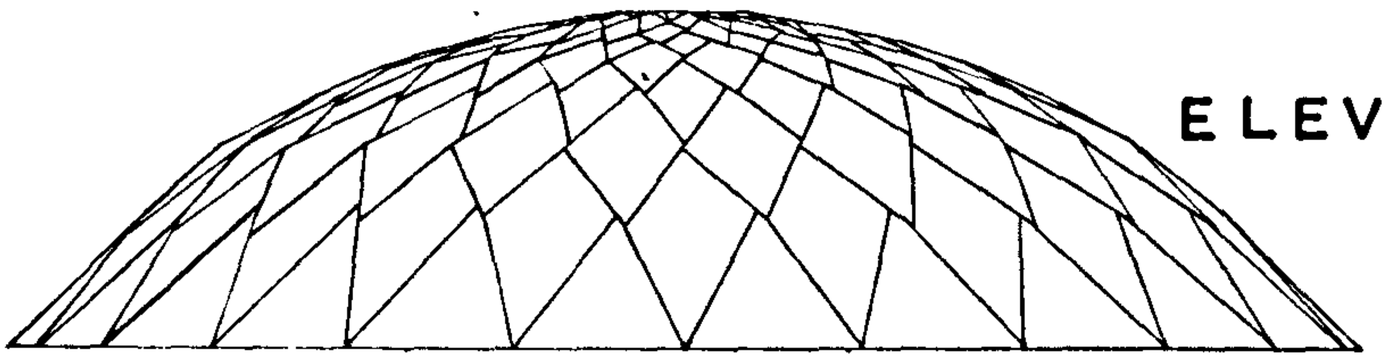

ELEVATION

LAMELLA DOME

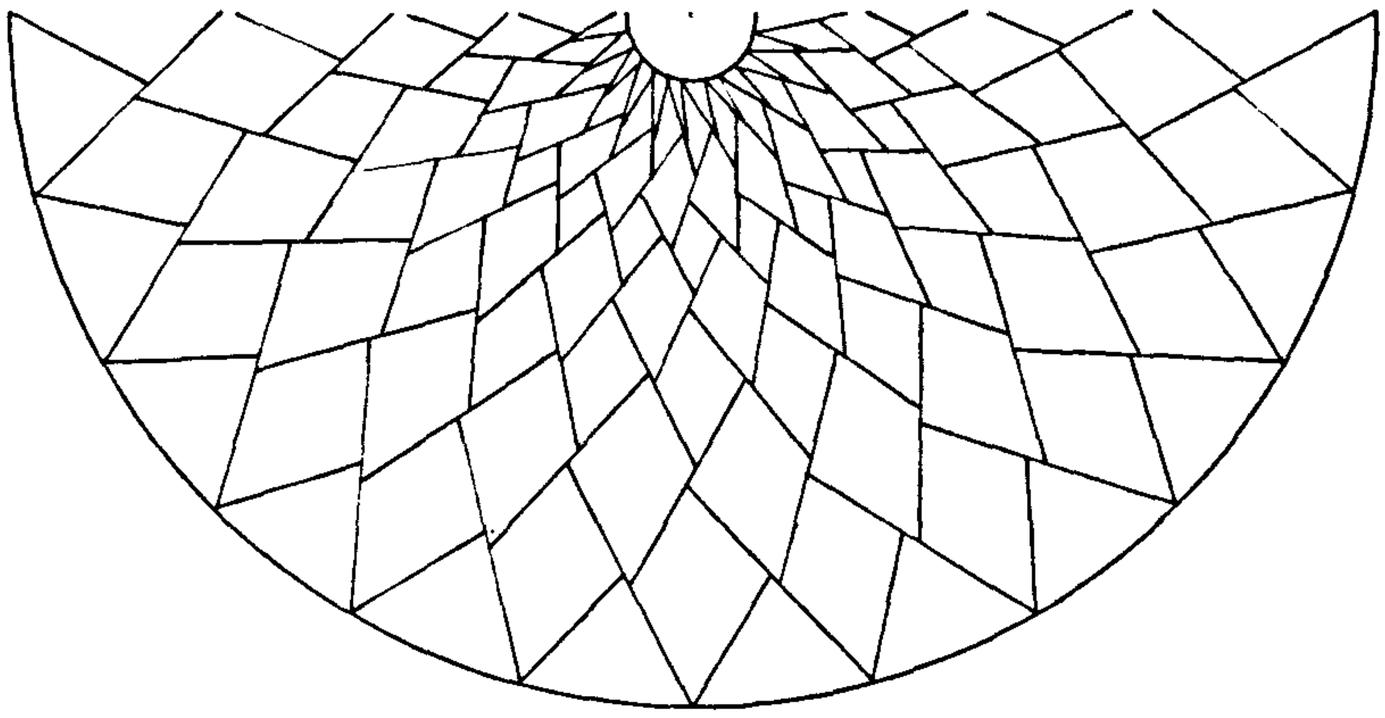

PLAN

B

FIG. 12

Structural Engineering Division
Department of Civil Engineering
University of Newcastle upon Tyne

F.A.A. Ph.D. Thesis
4th Nov., 1968

produced by the decking which stiffens each diamond shape in the direction of its surface. Timber lamellas are assembled on site by means of bolts and plates and where each joint occurs, one lamella unit runs continuously through with the adjacent intersecting members connecting at its midpoint. This frequent bracing of the lamella units produces a most efficient structure for resisting compressive forces and results in an even stress distribution throughout the dome. Large concentrated or live loads are distributed throughout the framework producing mainly axial forces in the lamella units and this leads to a saving in material.

3.8 KIEWITT DOMES

A special type of lamella dome has been developed in the U.S.A. by Dr. Kiewitt and is normally employed in steelwork construction. Kiewitt domes, as they are called, consist of a "parallel lamella" system in which the dome is divided into a number of sectors of equal size braced by two sets of lamella members, each parallel to one of the main radial ribs. A Kiewitt dome is illustrated in Figure 13(a).

Engineers believe that the lamella system of construction is practicable for spans of 40 - 1200 feet. At present, the largest steel dome in the world is the 642 feet diameter Harris County Sports Stadium at Houston, Texas, U.S.A., and this structure is a Kiewitt dome of the parallel lamella form.

3.9 TWO- AND THREE-WAY GRID DOMES

Grid domes consist of a network of intersecting ribs as shown in Figures 13(b) and 14(a). Figure 13(b) illustrates a two-way grid dome and the layout of a three-way grid dome can be seen in Figure 14(a).

Grid domes are usually shallow in form and, as such, their analysis is very complicated. Appreciable bending moments exist in the members together with the axial forces. The roof covering adds greatly to the stability of this type of structure and hence most grid domes belong to

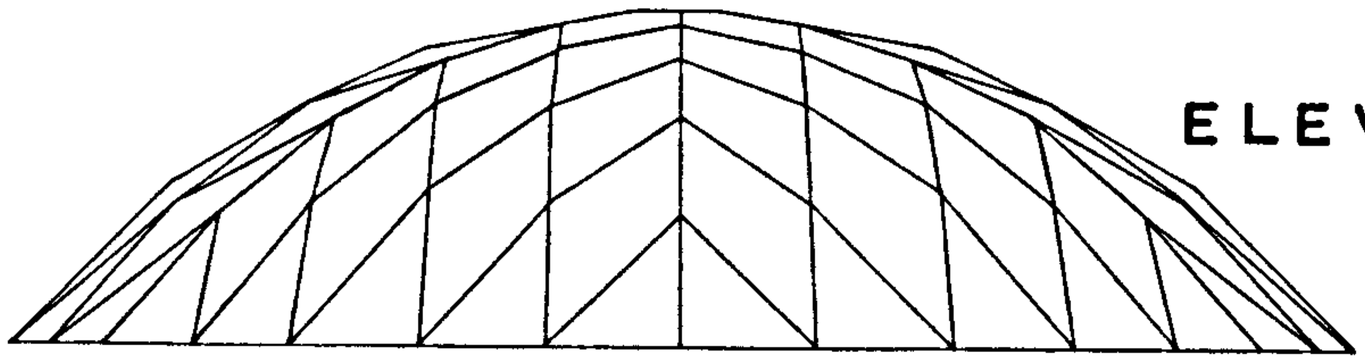

ELEVATION

KIEWITT DOME

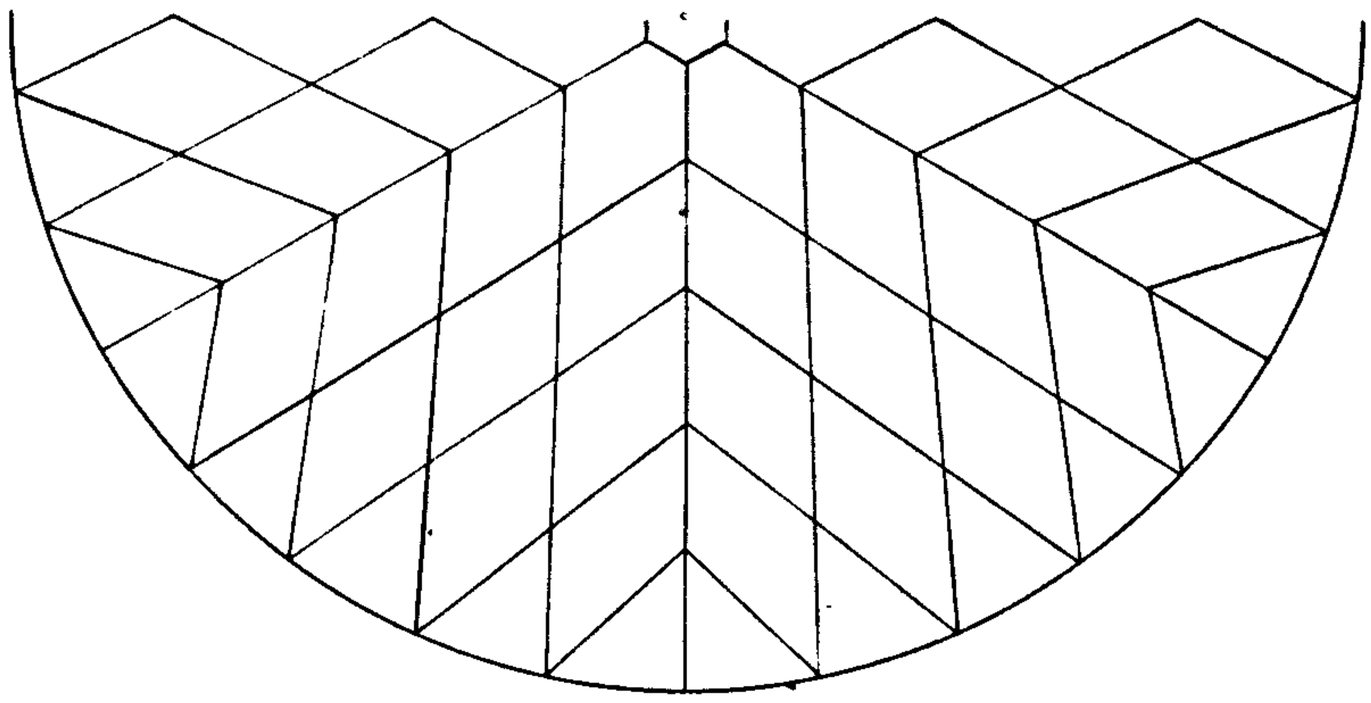

PLAN

A

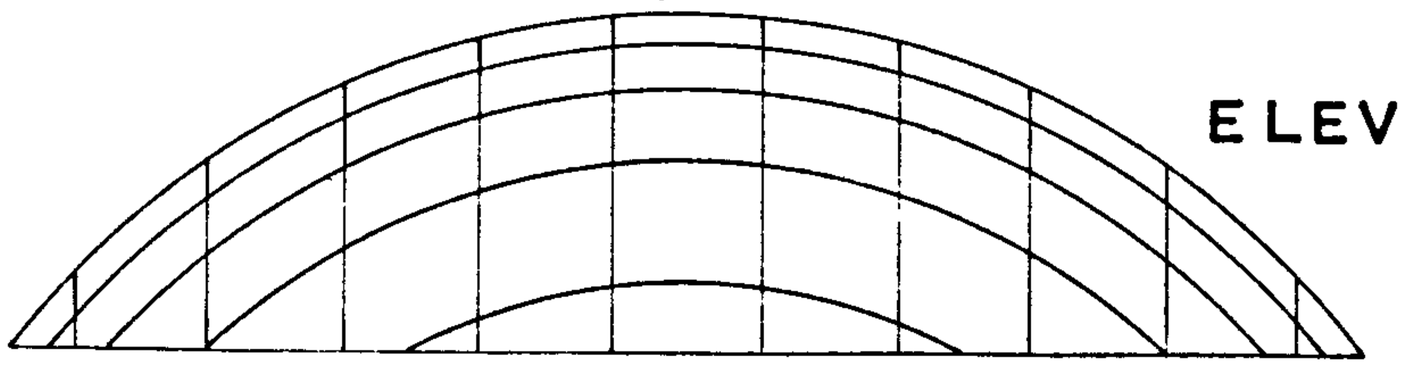

ELEVATION

TWO-WAY GRID DOME

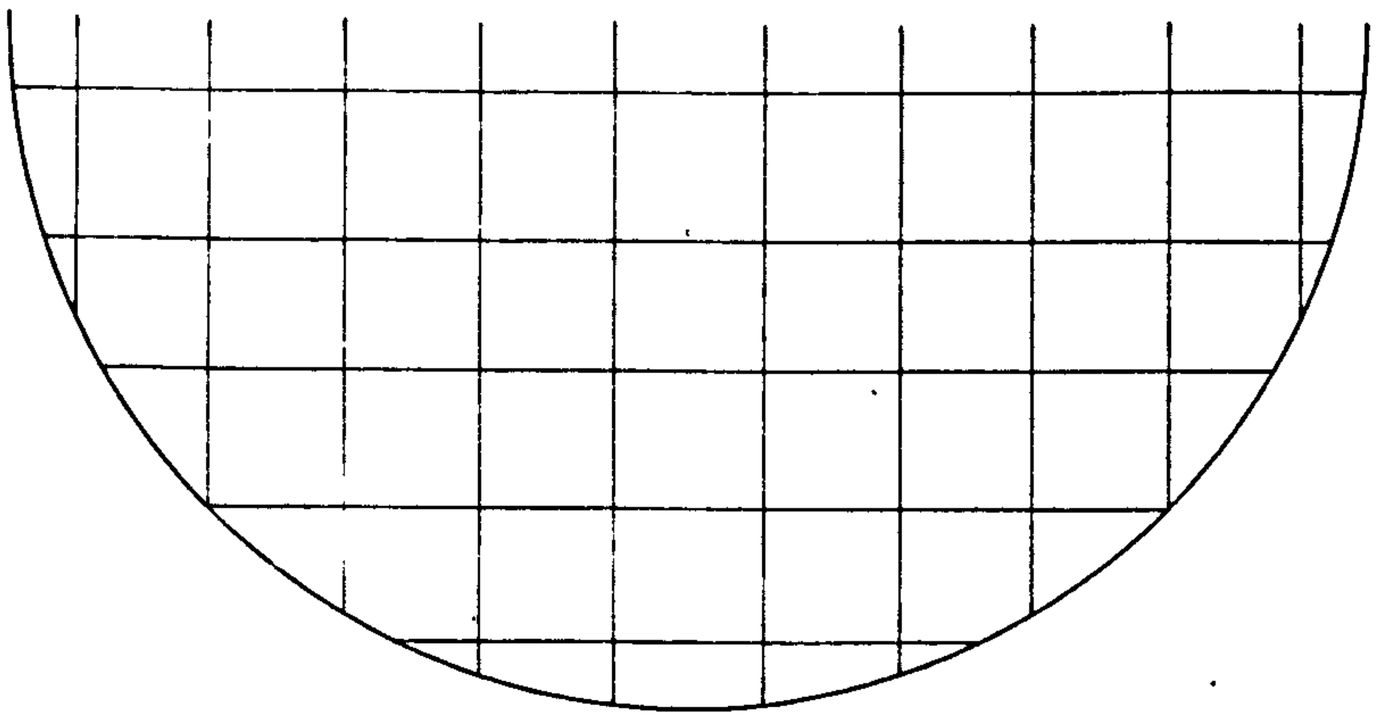

PLAN

B

FIG. 13

Structural Engineering Division
Department of Civil Engineering
University of Newcastle upon Tyne

F.A.A. Ph.D. Thesis
4th Nov., 1968

the stressed skin category. Grid systems of construction are very rigid, light in weight and highly economical and the stress distribution produced under both symmetrical and unsymmetrical loading is remarkably uniform.

For very large span domes a greater structural depth is required than for shorter spans and therefore grids of the double-layer type are often employed. Steel and aluminium are especially suited to this form of construction.

Previous to recent years, it was impracticable to join together many members of a framework at one point. At present, with the availability of improved materials and advanced welding techniques, a number of space frame systems are available which employ multi-member connections. Although these systems are normally employed in the flat double-layer structures, as shown in Figure 1, several types can be employed, without much modification, in the erection of large span double-layer grid domes.

3.10 GEODESIC DOMES

Braced domes normally consist of prefabricated members which vary in length and are joined by suitable connectors. To overcome the problem of different sized individual components an attempt was made, in America by Buckminster Fuller, to produce dome construction units which were all of identical shape. In this way all units could be mass produced and completely interchangeable. The result was the development of the geodesic dome.

Geodesic domes are another form of triangulated dome in which the elements forming the skeleton of the structure are curved and lie on the great circles of a true sphere. The framework of the intersecting elements forms a three-way grid of equilateral spherical triangles.

A sphere can be divided, around its surface, into 20 equilateral spherical triangles and the resulting space framework is known as an

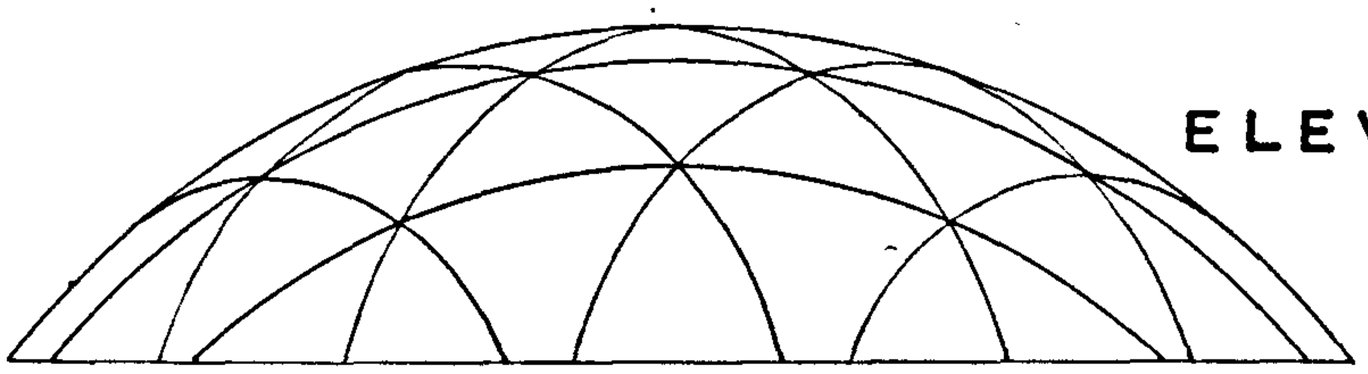

ELEVATION

THREE–WAY GRID DOME

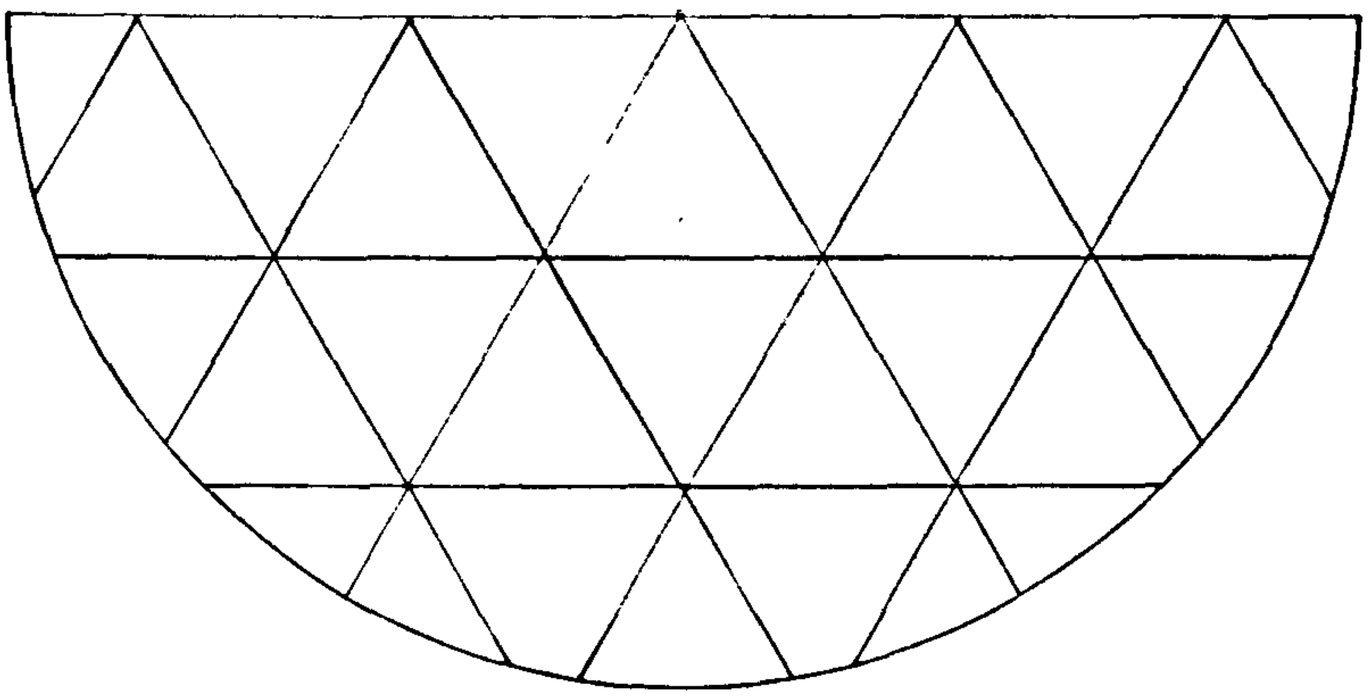

PLAN

A

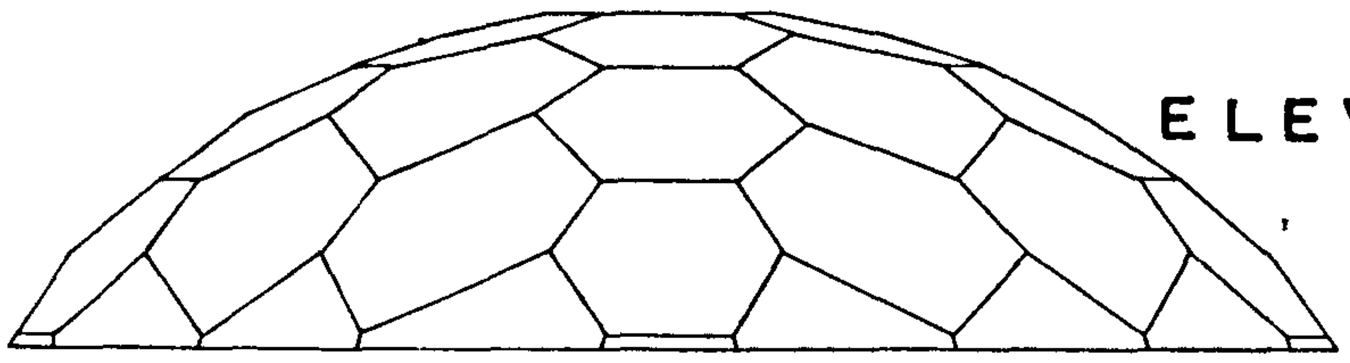

ELEVATION

GEODESIC DOME

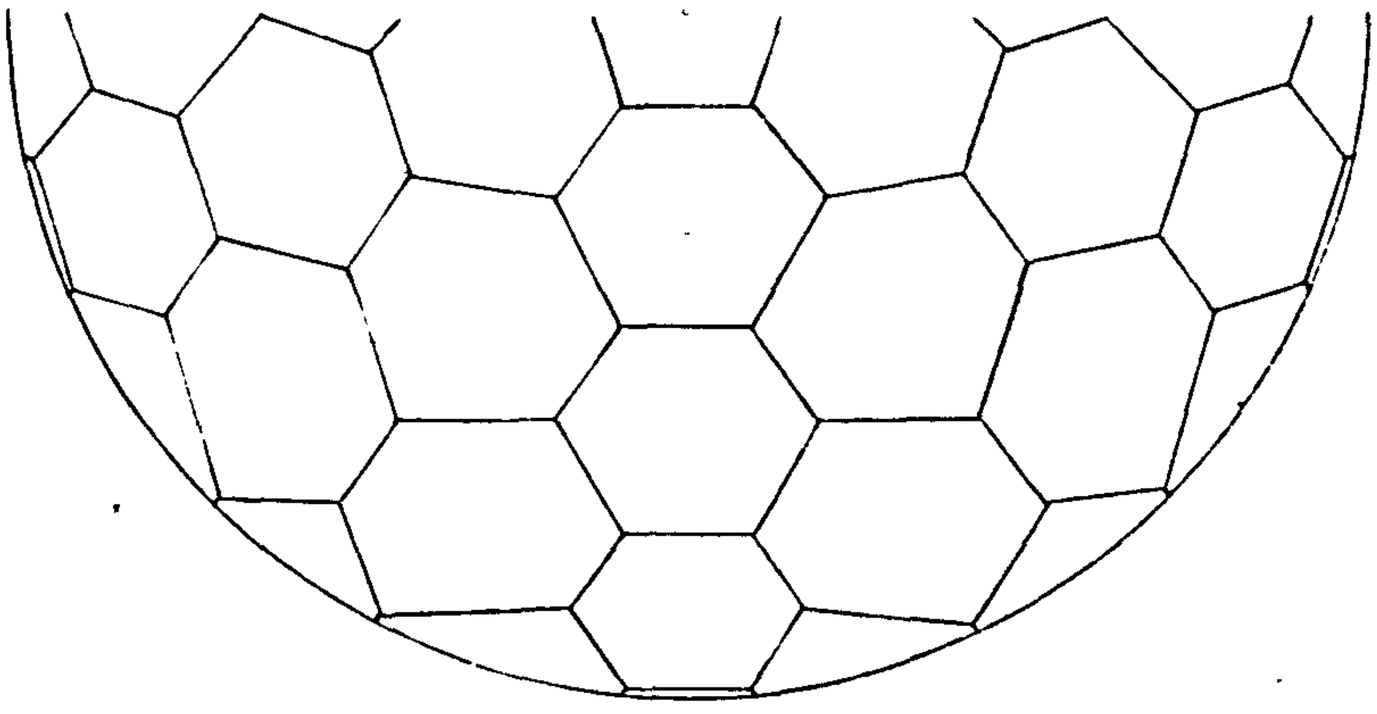

PLAN

B

FIG. 14

Structural Engineering Division
Department of Civil Engineering
University of Newcastle upon Tyne

F.A.A. Ph.D. Thesis
4th Nov., 1968

icosahedron.. In early Buckminster Fuller domes the members followed the arrangement of an icosahedron but further developments in dome construction have resulted in the equilateral spherical triangles being divided into smaller units, as shown in Figure 14(b). These component arrangements result in a regular network of members and produce an even stress distribution under applied loading. Again, as with many of the previously mentioned types of braced domes, the roof covering in geodesic domes can be employed to stiffen the structure and in some cases the roofing is employed as part of the structural unit.

Double-layer geodesic domes are employed for covering areas of large span in order to reduce the possibility of node buckling which would occur in single-layer domes under concentrated loads. One disadvantage of the geodesic dome is the irregular pattern obtained around its base due to the geodesic subdivision and the architectural appearance of such structures depends upon correct treatment of the surrounding areas. Geodesic domes possess good acoustic properties and are highly fire resistant if treated with a protective covering.

3.11 RIBBED DOMES AND REASONS FOR THE RESEARCH PROJECT

So far in this thesis the main types of prefabricated space structures have been reviewed and details of the various forms of braced dome construction have been discussed. To complete the survey of space frame systems, the last type of braced dome mentioned on the list, the ribbed dome, will now be considered. Structures of the ribbed dome form are of principal interest to the author and he has chosen to concentrate his research in this field of space frameworks.

Ribbed domes were employed in very early forms of construction and they are still very popular today, mainly because of the possibility of prefabrication. These domes consist of a number of identical radial ribs, solid or latticed, which are connected together at the crown and

supported in an adequate way at the base.

Domes which have their radial ribs pin-connected to foundation blocks are of the "unstiffened" type whereas those which are connected to a base ring are of the "stiffened" type. The latter form exerts only vertical reactions on its supports as horizontal forces are resisted by the base ring.

At the apex, the rigidity of the joint depends on the method of construction. If the apex joint is made fully rigid, then fixing moments occur and the stress analysis of such a dome becomes tedious. It is normal practice, with ribbed domes, to provide a lantern ring at the apex and when the ribs are loaded, depending upon the stiffness of this ring, a hinge action occurs.

Ribbed domes are normally pinned at their foundations as it is often impossible, and nearly always uneconomical, to provide footings which would completely fix the ribs against rotation at the supports. A dome with the ribs pin-connected to the ground, but rigidly fixed at the apex, can resist a perfectly general system of loading whereas, if a spherical hinge is introduced at the apex, the resulting three-pinned ribbed dome can only resist loads applied in the vertical planes and passing through the neutral axis of the ribs. Normal practice employs horizontal polygonal purlin rings and diagonal bracing in order to stabilize the structure.

The Frontispiece is a photograph of a typical ribbed dome structure composed of laminated timber radial ribs, horizontal timber purlin rings and mild steel diagonal bracing rods. This dome covers the Lightfoot Sports Centre, in Newcastle upon Tyne, and inspired the author's research project. Although the Lightfoot Sports Centre dome has mainly a timber framework, similar buildings could also be erected quite easily in steel or other materials.

Plates 1, 2 and 3 show some of the structural features of the

Lightfoot Sports Centre which are typical of ribbed dome construction in general. Plate 1 is a view of the apex ring with the radial ribs, horizontal purlin rings and diagonal bracing clearly visible. In Plate 2 the pinned base of the dome is illustrated and a close-up of the diagonal bracing can be seen in Plate 3.

At first sight, it must appear that analysis techniques are already well established for evaluating the stresses in braced domes and the behaviour of these structures under load can be determined with a great amount of accuracy. To a certain extent this is true but, unfortunately, very little published information is available on the subject. Although Makowski[10] and Benjamin[11],[12] have produced excellent works with respect to the analysis of braced domes, in order to produce workable methods of design much of the theory has been considerably simplified by assuming ideal conditions.

In practice, for large span radial ribbed domes, the number of ribs is dictated by the cross-sectional dimensions required for the purlins spanning between adjacent members. For a dome with a diameter of approximately 200 feet the number of ribs required can be as many as 36. Again, the position of the purlin rings along the radial ribs is governed by the permissible span of the roof covering and hence as many as 20 rings could be employed in a 200 feet diameter dome. Together with the apex ring and the diagonal bracing, which provides lateral stability, the radial ribs and horizontal purlin rings form a complex structural system for which the stress distribution cannot be obtained by tests on simplified models with a small number of components. The author feels that even though the work of Makowski and Benjamin has been verified by experiments on simple small scale models the application of their techniques, along with those of other research workers, to a scale model of larger dimensions, consisting of many members as employed in actual practice, would be a worth-while project.

PLATE 1 - THE LIGHTFOOT SPORTS CENTRE

APEX RING

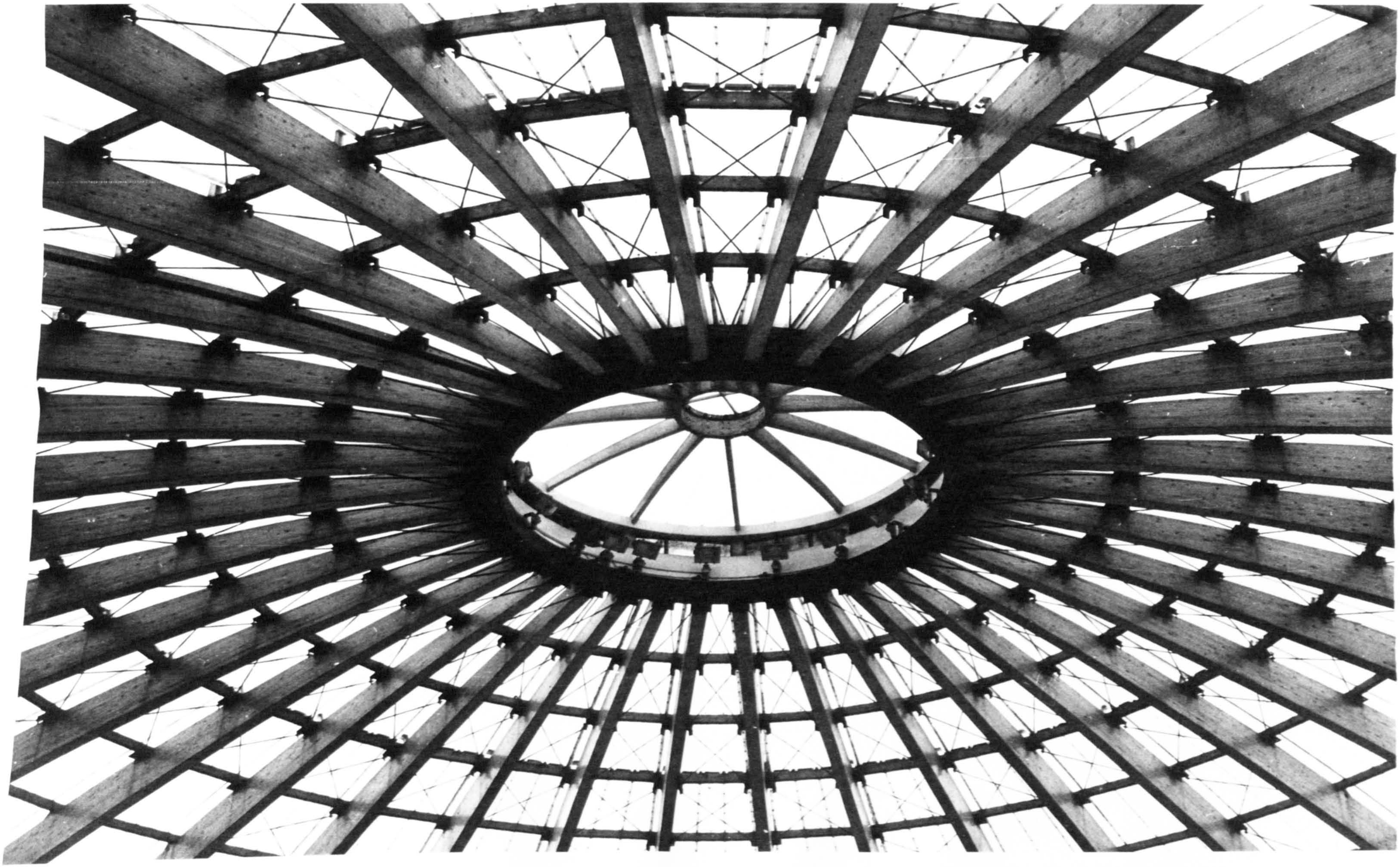

PLATE 2 - THE LIGHTFOOT SPORTS CENTRE

PINNED BASE

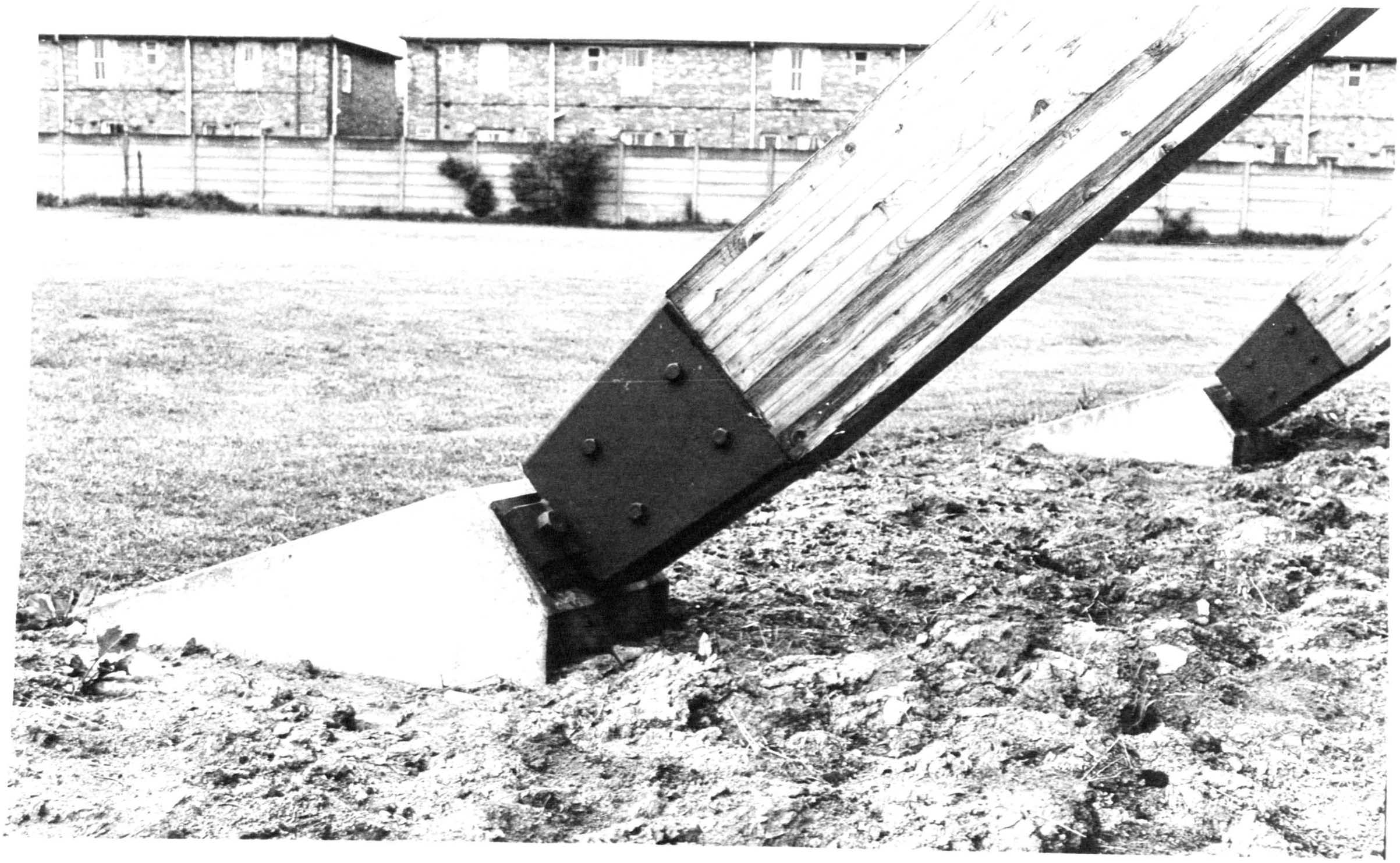

PLATE 3 - THE LIGHTFOOT SPORTS CENTRE

DIAGONAL BRACING

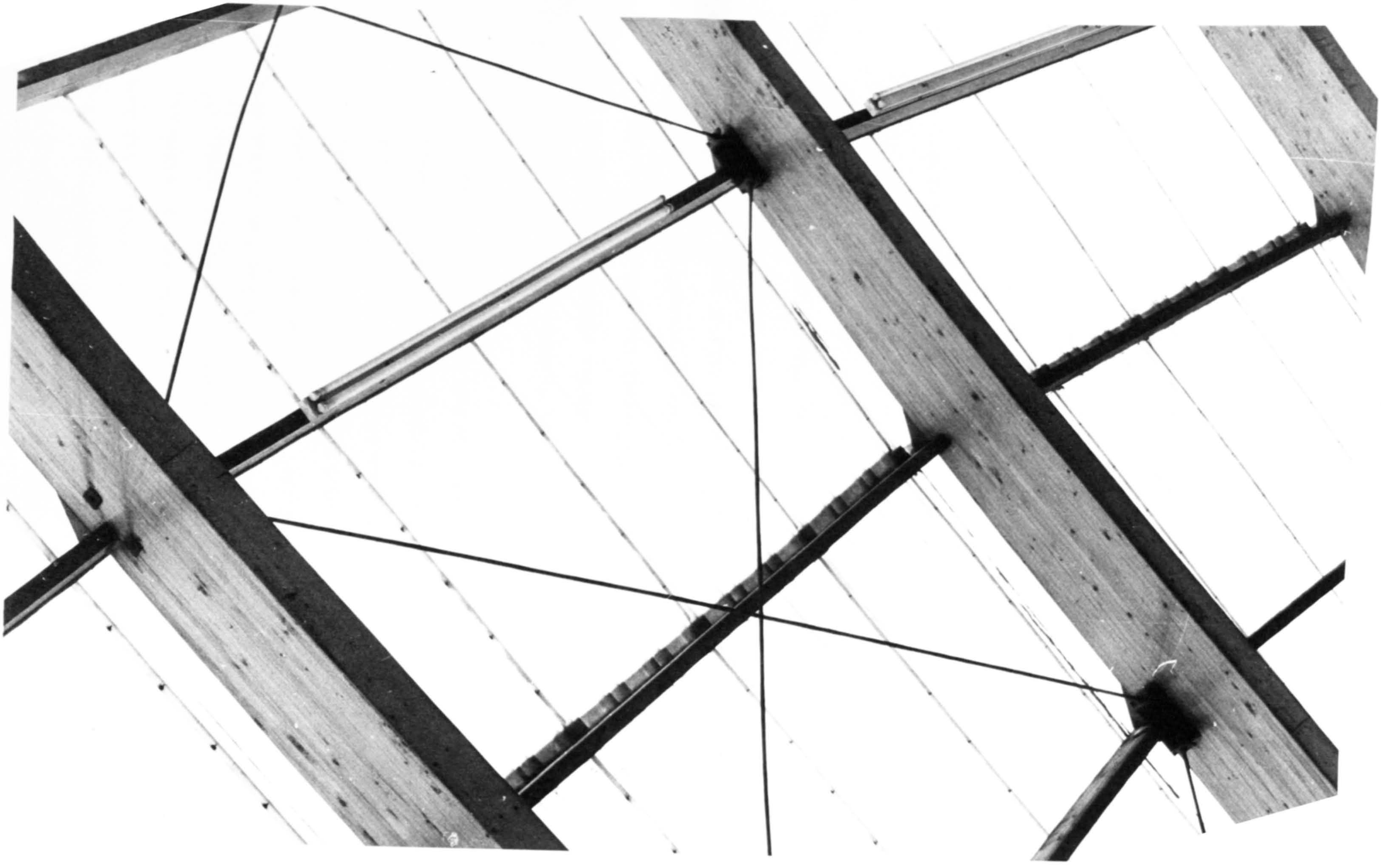

Tests on a small sized scale model of the Lightfoot Sports Centre have also led the author to believe that much additional information could be gained by experimenting with a large scale model. With such a model the work of Makowski and Benjamin could be greatly extended, especially in the field of low rise-to-span radial ribbed domes.

Effects of the most important factors in braced dome design, snow and wind, on the stability of, and stress distribution in, braced domes, which are at present debatable, could also be investigated if a sufficiently large scale model was constructed. The model could be erected first in the laboratory for initial testing of the structure and then dismantled and re-erected in the field for actual snow and wind load observations.

The author has decided, therefore, to summarize briefly the methods available for determining the stress distribution in space frames generally, to discuss in more detail the methods employed for braced domes and to review the literature at present available on the subject of radial ribbed domes. With the help of tests on a scale model an attempt will be made to produce more accurate design information for radial ribbed domes. The apex ring stiffness, the horizontal purlin rings, the diagonal bracing and the roof covering all play their part in the stability characteristics of domes with radial ribs and it is the effects of these components, on stress distribution, with which the author's research project will be concerned.

For the analysis of large diameter dome structures the use of a digital computer is indispensable and a program will also be developed to calculate theoretical stresses in radial ribbed domes. A comparison between theoretical and experimental results can then be made on completion of the test schedule.

CHAPTER IV

THE STRESS ANALYSIS OF STATICALLY DETERMINATE PIN-JOINTED SPACE FRAMES[13]

4.1 THE EQUILIBRIUM OF CONCURRENT FORCES IN SPACE

The law of the parallelogram of forces states that two forces P_1 and P_2, as represented by the vectors $\overline{OA}$ and $\overline{OB}$ in Figure 15(a), are equivalent in action to a single resultant force R obtained as the diagonal $\overline{OC}$ of the parallelogram formed on the given vectors as shown. This principle can also be employed to find the resultant of a number of forces in space which have a common point of application.

Consider the three concurrent forces F_1, F_2 and F_3, represented by the vectors $\overline{OA}$, $\overline{OB}$ and $\overline{OD}$ in Figure 15(b). Applying the principle of the parallelogram of forces to the vectors $\overline{OA}$ and $\overline{OB}$ first, the resultant $\overline{OC}$ is obtained as shown. Again, by applying this principle to the partial resultant just obtained and the force F_3 represented by $\overline{OD}$, the resultant R of the complete system can be deduced. This method can be extended to find the resultant of any number of concurrent forces in space. The magnitude of the resultant of such a system is equal to the geometric sum of the given forces and its line of action passes through the point of concurrence of these forces.

It can easily be seen from the foregoing discussion that the orthogonal projection of the resultant of a system of concurrent forces in space on any plane will be equal to the algebraic sum of the projections of the forces on the same plane. For equilibrium, the algebraic sums of the projections must disappear and hence the following equations of equilibrium are arrived at:

$$\Sigma X_i = 0 \; ; \; \Sigma Y_i = 0 \; ; \; \Sigma Z_i = 0 \quad \ldots\ldots\ldots \quad (4.1)$$

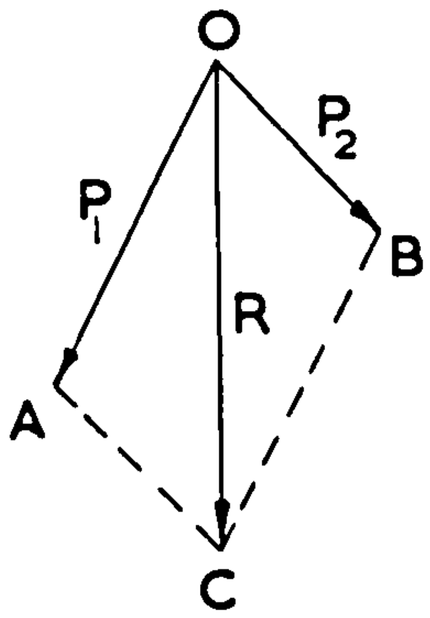

(a)

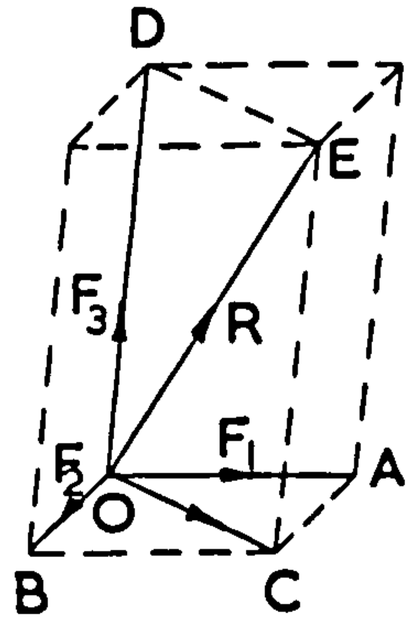

(b)

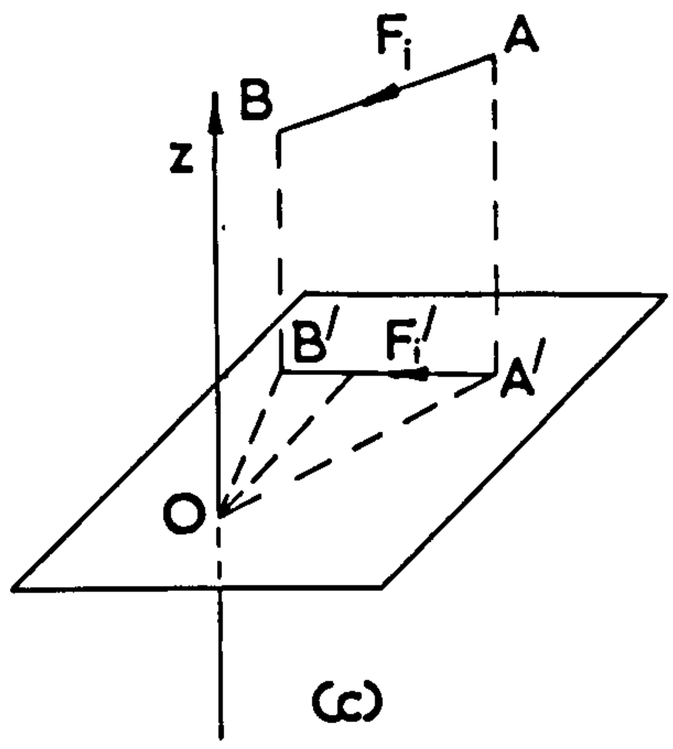

(c)

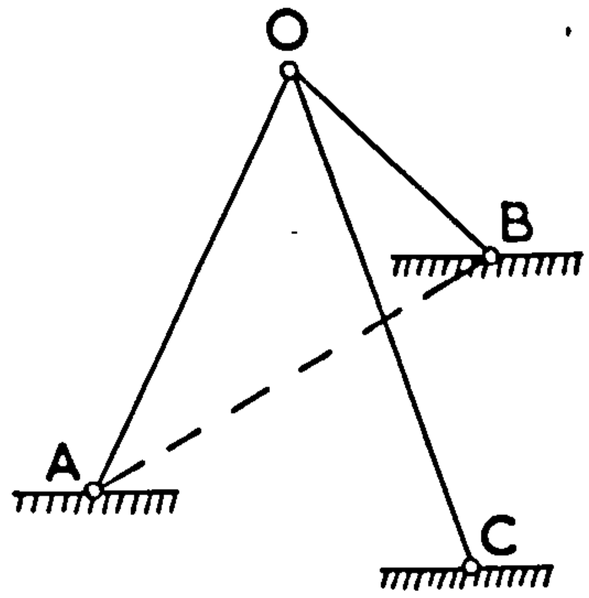

(d)

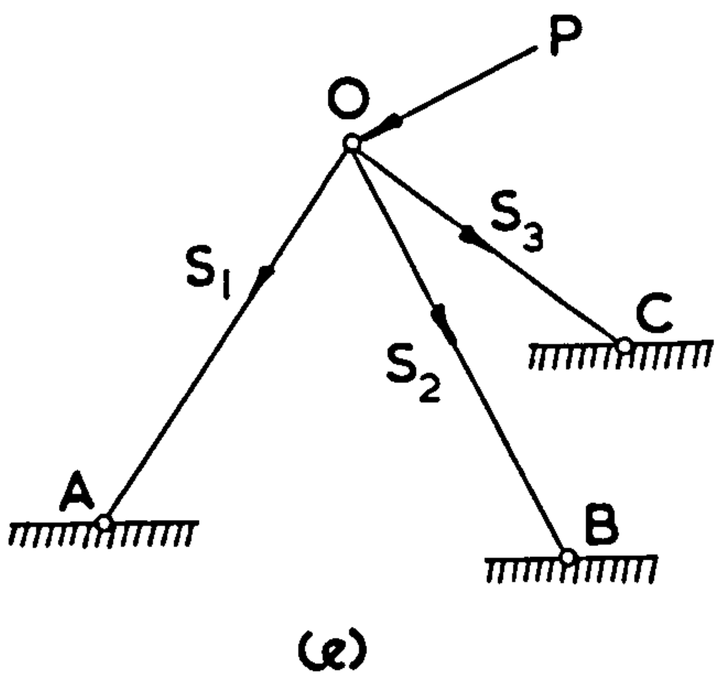

(e)

FIG. 15
THE EQUILIBRIUM OF CONCURRENT FORCES IN SPACE

F.A.A. Ph.D. Thesis
4th June, 1969

Structural Engineering Division
Department of Civil Engineering
University of Newcastle upon Tyne

where X_i, Y_i and Z_i are the orthogonal projections of any force F_i and the summations are understood to include all forces in the system.

The moment of a force about an axis is a notion which is often useful when determining stresses in space frames. Considering Figure 15(c), the force F_i, represented by $\overline{AB}$, can be projected on a plane which lies at right angles to an axis Z. The plane meets the axis Z at point O and the moment of the projected force can then be obtained about this point. By the theorem of moments,[14] the algebraic sum of the moments of a system of concurrent forces about any axis is equal to the moment of their resultant force about the same axis. Hence, for any system of concurrent forces in space to be in equilibrium, the algebraic sum of their moments about any axis must be zero because the resultant disappears.

Consider now the problem of completely constraining a point in space. Looking at Figure 15(d) it can be seen that to fully fix the point O in space, three bars are required. If the third point C were to lie in the plane of O and the other two points A and B, then complete constraint would not be realized. Hence for complete and satisfactory constraint of a point in space it must be attached to a foundation by three bars the axes of which do not lie in one plane.

Referring to Figure 15(e), when a force P is applied at the point O, which is fully constrained, axial forces will be induced in the three supporting bars. At O we have a system of four concurrent forces, one of which is known. By applying the three equations (4·1) the unknown forces can be obtained. This system is, therefore, statically determinate. If the point O had been attached to a foundation by more than three bars, other unknown forces would be present which could not be solved by applying equations (4·1). The structure would then be statically indeterminate. A system where there were less than three supporting bars, or three supporting bars

in one plane, would be unstable and could not remain in equilibrium under the application of an applied force P that did not coincide with the plane of the bars.

There are various ways of applying the conditions of equilibrium, represented by equations (4·1), to statically determinate space frames. The forces in the system can be projected on to orthogonal axes x, y and z and their algebraic sums equated to zero. A plane of the structure could also be used for projecting the forces on or moments could be taken with respect to an axis and their summation carried out and equated to zero. Where difficulty is encountered in determining analytically the projections or moments of the forces with respect to various axes, a graphical method can be employed. Triangles of forces are produced from plan and elevation scale drawings of the space framework and the unknown forces are determined from these.

4.2 THE METHOD OF JOINTS APPLIED TO SIMPLE SPACE TRUSSES

An assembly of bars in space, connected together at their ends to form a rigid structure, is known as a space truss. This type of framework is employed in engineering for many purposes. Radar telescopes, transmission-line towers and cranes are some of the structures normally constructed in the form of a space truss. In practice the joints in such systems are made rigid and hence the adjustment of forces, which would occur in a pin-jointed arrangement, is not obtained and secondary bending moments are produced. However, in a number of types of space truss, the primary action of the structure is not altered to a large extent by the introduction of secondary bending and sufficiently accurate values of the axial forces are obtained for design purposes by considering a pin-jointed system. Hence, in many instances of space frame analysis, ideal spherical hinges are assumed to exist at the joints and the effect of secondary bending can be considered, if required, after a pin-jointed analysis has been carried out. In some

structures bending and torsional stresses are predominant and, in these cases, exact methods of analysis must be employed.

Previously in this Chapter, it was established that for complete constraint in space a point must be attached to a foundation by three bars the axes of which do not lie in one plane. Referring to Figure 16(a), this principle can be extended to form a rigid structure in space from any system of bars. Considering first the point E which is constrained by three bars AE, BE and CE. The two points F and G are further constrained by three bars each and hence a rigid structure is obtained. From these observations it can be seen that any rigid space truss can be constructed by first attaching a joint to a foundation by three bars that do not lie in one plane and then establishing each further joint by three bars which also do not lie in one plane. Any space frame constructed according to this principle is known as a simple space truss and an example of such a truss is shown in Figure 16(b).

If the space frame in Figure 16(b) is subjected to the action of several applied loads, then internal forces will be induced in the members. The evaluation of these internal forces constitutes the analysis of the truss. In order to simplify the analysis procedure, certain assumptions must first be made. These are:

(1) the bars are weightless;

(2) the bars are connected by spherical hinges;

(3) the external forces are only applied at the joints.

Assumptions of this nature appertain to ideal frame systems but produce, in the main, a sufficiently accurate stress analysis. Under these conditions the frame members will only be loaded in tension or compression along their axes. At each joint, therefore, we have a system of concurrent forces to which the equations of (4·1) can be applied. This method is known as the method of joints.

To analize space frames by the method of joints it is necessary to

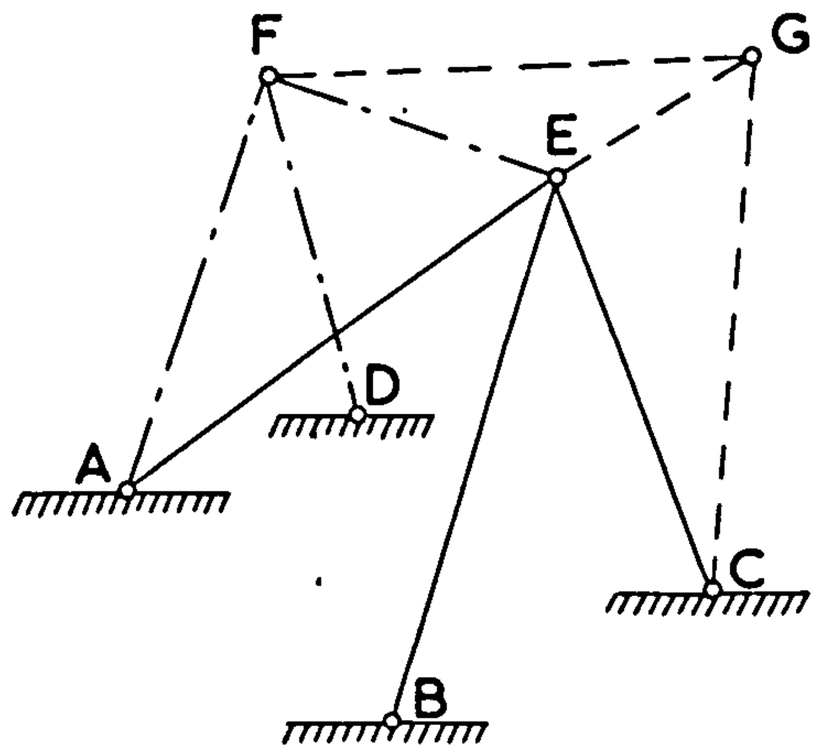

(a)

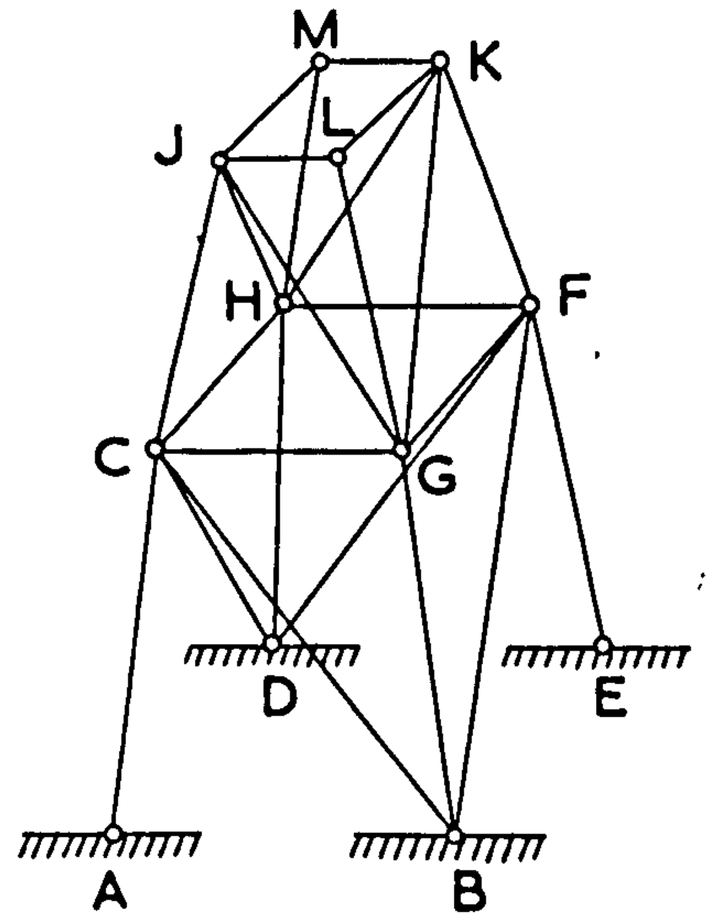

(b)

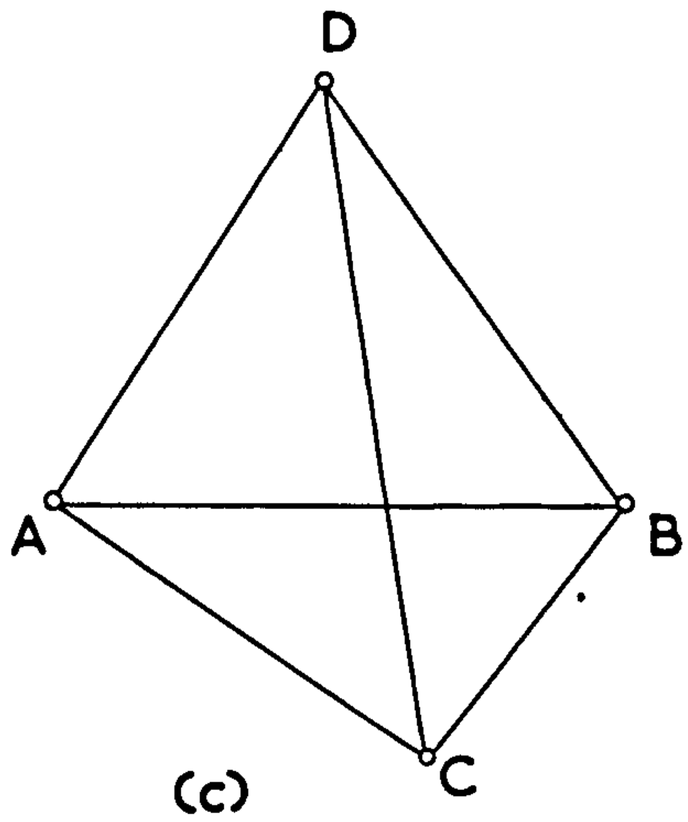

(c)

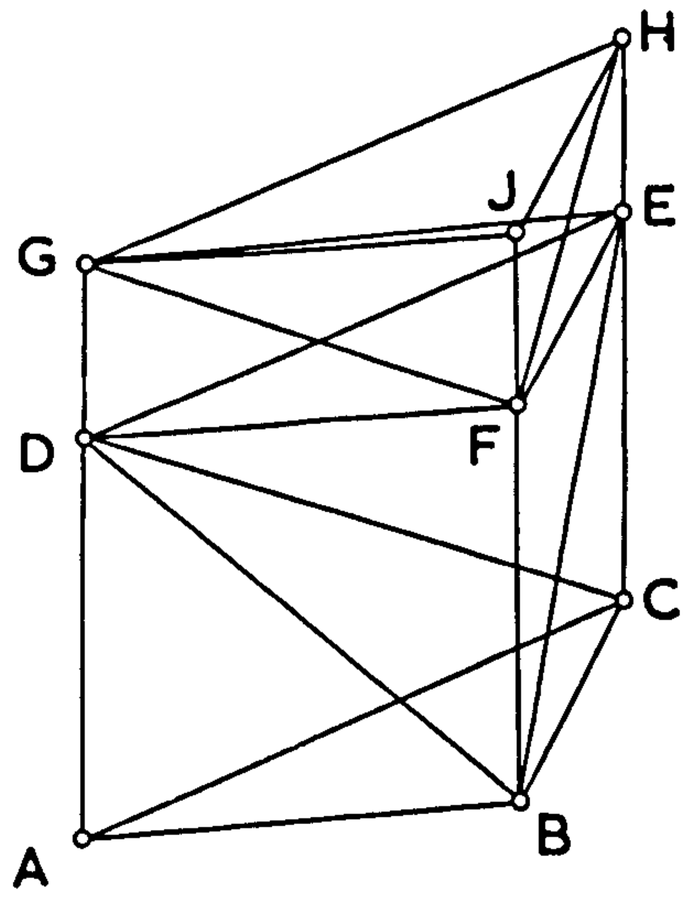

(d)

FIG. 16 SIMPLE SPACE TRUSSES

F.A.A. Ph.D. Thesis
6th June, 1969

Structural Engineering Division
Department of Civil Engineering
University of Newcastle upon Tyne

find first a joint of the truss to which only three bars not in one plane are attached. The forces in these bars can then be found from the conditions of equilibrium (4·1). Each subsequent joint must also have only three unknown bar forces not in one plane for solution by equations (4·1), or the method of joints breaks down. From a consideration of the way in which a simple space truss is formed, as mentioned previously, it can be seen that all simple space trusses can be solved by the method of joints. By analysing first the last joint formed in such a structure and then solving for each subsequent joint a complete stress determination can be carried out.

The simple space trusses so far discussed have all been dependent, for rigidity, upon their attachment to a foundation. In some cases a structure is required which is completely independent of a foundation. For the basis of this type of space frame a triangle of bars AB, BC and CA is needed, as shown in Figure 16(c), to which is added three more bars AD, BD and CD not in one plane and rigidly constraining the joint D in space. This arrangement of bars in space forms a rigid tetrahedron which will not be distorted by applied loads at its joints provided the small elastic deformations of the bars under axial load are neglected. By adding consecutive joints, each constrained by only three bars not in one plane, any rigid structure can be obtained which is independent of a foundation. Structures formed in this way are also known as simple space trusses and can be solved by the method of joints. Typical of this type of frame is the truss shown in Figure 16(d).

4.3 THE STATICALLY DETERMINATE CONSTRAINT OF A RIGID BODY IN SPACE

Under normal conditions, a system of forces acting on a rigid body in space will not be concurrent or coplanar. However, in all cases a resultant force or a resultant couple can be obtained.

Considering Figure 17(a), any force F_i acting at a point A on a rigid body can be replaced by an equal force F_i', acting at O, and a

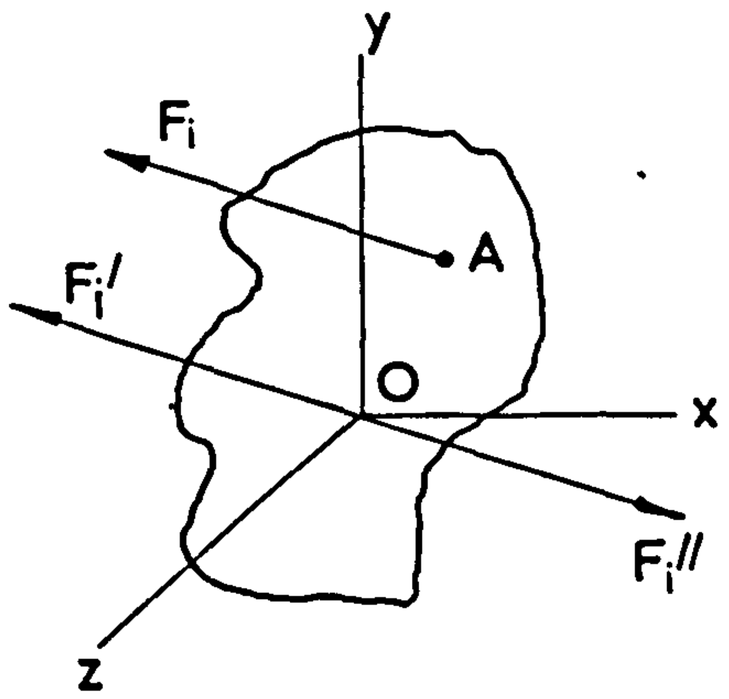

(a)

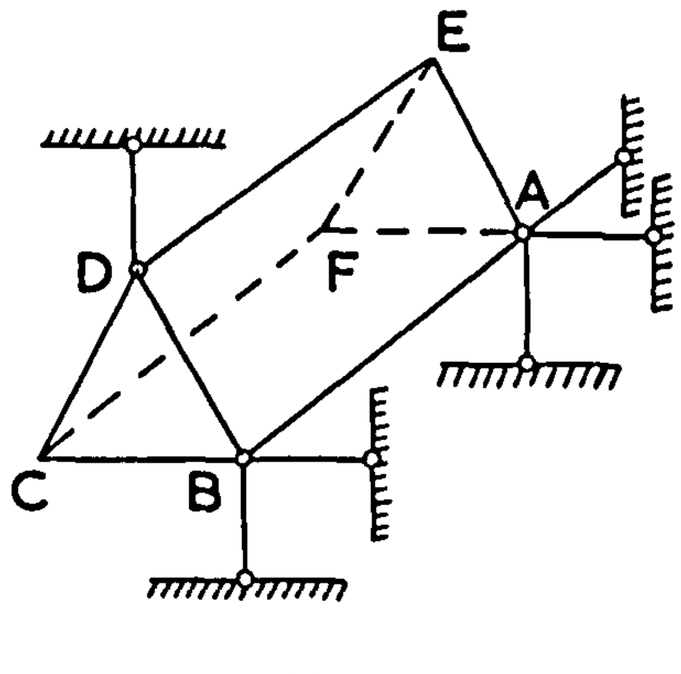

(b)

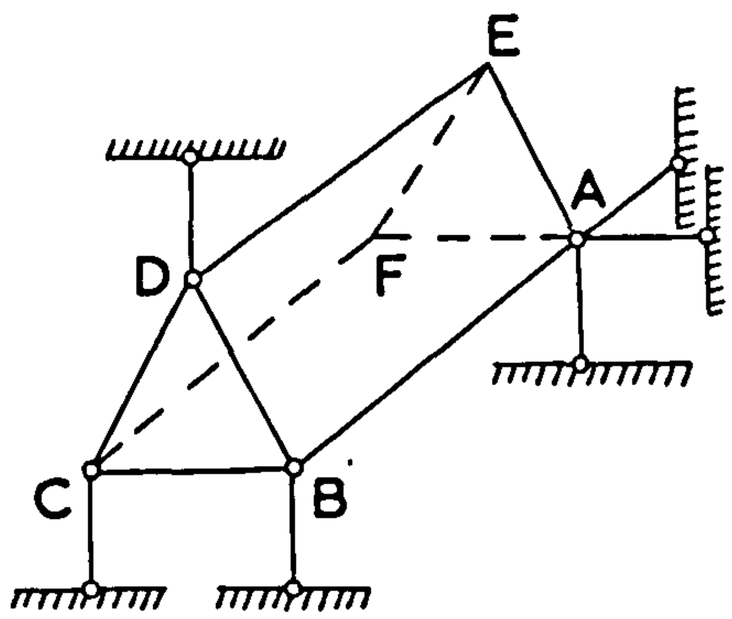

(c)

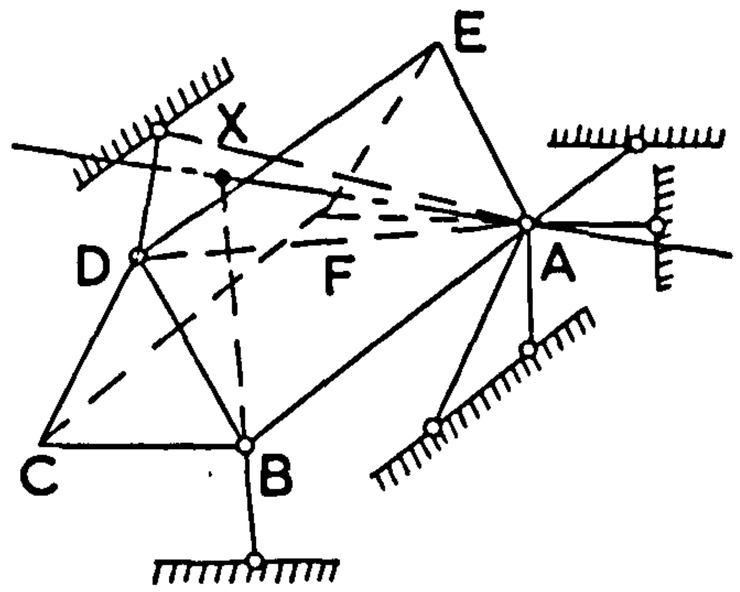

(d)

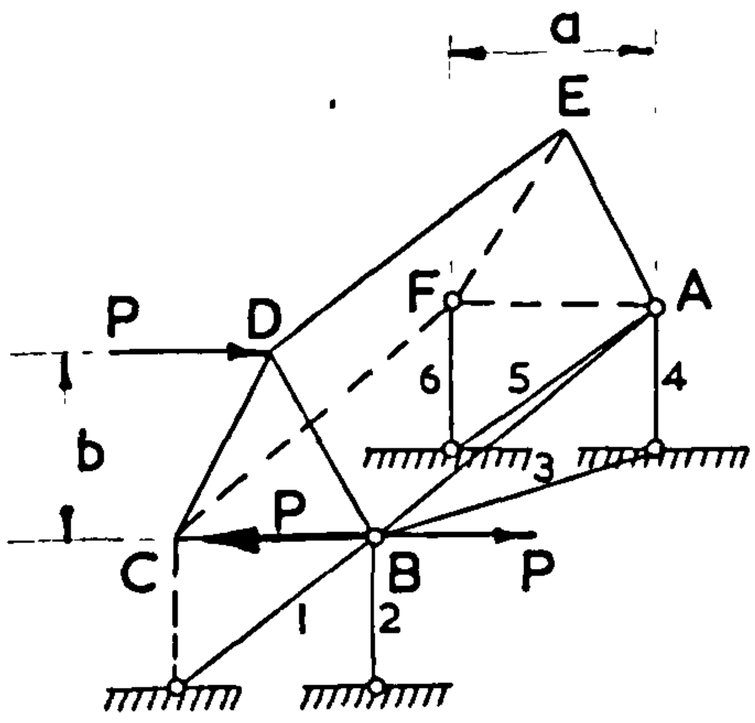

(e)

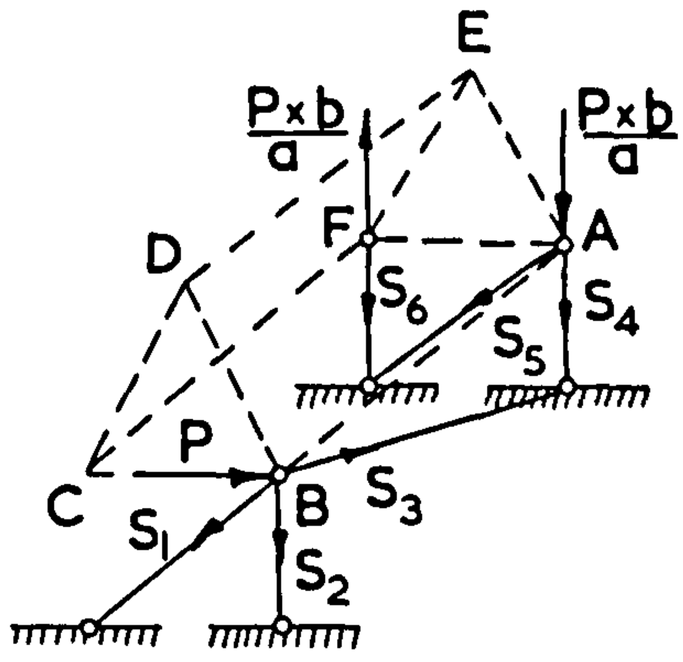

(f)

FIG. 17 STATICALLY DETERMINATE CONSTRAINT OF A RIGID BODY · IN SPACE

F.A.A. Ph.D. Thesis
10th June, 1969

Structural Engineering Division
Department of Civil Engineering
University of Newcastle upon Tyne

couple formed by the forces F_i and F_i''. The procedure involves the application of two equal and opposite forces F_i' and F_i'' at O which, being themselves in equilibrium, do not alter the action of the given Force F_i at A. For any general system of forces, therefore, a concurrent set of forces can be produced at any point O together with a series of couples the moments of which are given by the moments of the forces about this same point. For equilibrium to occur the resultant force and the resultant couple must vanish. Hence the algebraic sums of the projections of the given forces on the coordinate axes x, y and z must be zero and the algebraic sums of the moments of the given forces with respect to these axes must also be zero. Thus the general conditions of equilibrium for any system of forces in space can be expressed by:

$$\Sigma X_i = 0 \quad ; \quad \Sigma Y_i = 0 \quad ; \quad \Sigma Z_i = 0 \quad ;$$

$$\Sigma M_x = 0 \quad ; \quad \Sigma M_y = 0 \quad ; \quad \Sigma M_z = 0 \quad \ldots\ldots\ldots (4\cdot2)$$

From these equations any six unknown elements can be solved.

Consider now the problem of constraining completely any rigid body in space. Referring to Figure 17(b), the point A can be completely constrained, as discussed in Art. 4·1, by attaching it to a foundation by means of three bars not lying in one plane. Any point on the rigid body ABCDEF would then be free to rotate around the surface of a sphere. This sphere would have its origin at A and a radius equal to the distance between A and the point being rotated. Two bars only are now required to constrain the point B in a plane which forms a tangent to the sphere but rotation of the body about the axis AB is still possible. Another bar is therefore needed at one of the points C, D, E or F to completely constrain the rigid body in space. The axis of this sixth bar also must not intersect AB or complete constraint will not be obtained. From these observations it can be concluded that at least six bars are necessary for the complete constraint of a rigid body in

space.

It must not be assumed that six bars will always produce complete constraint. In Figure 17(c) the three bars attached to the points B, C and D are parallel to each other and hence any external force system will produce appreciable changes in length of these members. Again, in Figure 17(d), with four bars attached at A and two other bars connected at the points shown, the bar joined to D forms a plane with the point A. The axis of the bar at B meets this plane at some point X and hence all six bars intersect the axis AX. If a system of external forces is now applied to this body and a moment is formed about the axis AX, the six supporting bars will be unable to develop a balancing moment and the body will rotate to a new position. We can conclude, from the foregoing discussions, that for complete constraint of a rigid body in space six supporting bars are always required and the bars must be arranged so that their axes cannot all be intersected by a straight line. This condition is usually sufficient but in exceptional circumstances, even though the axes of the supporting six bars cannot be intersected by a straight line, the determinant of the six equations (4.2) vanishes and indicates incomplete constraint.

If external forces are applied to the rigid body shown in Figure 17(b), internal axial forces will be induced in the supporting bars i.e. reactions, which are directed along the axes of the supporting bars, will occur at the joints. Both external and reactive forces form a general system which is in equilibrium. The forces are not concurrent, coplanar or parallel but the six equations (4.2), which represent the conditions of equilibrium, are sufficient to determine the six unknown supporting bar reactions. Thus the six bars which are required for the complete constraint of a rigid body in space also form a statically determinate system of supports. With more supports the system becomes statically indeterminate. In the special case where the

axes of the six supports intersect a straight line the determinant of the six equilibrium equations (4.2) vanishes and this system of supports is also statically indeterminate.

When analysing a statically determinate system of supports for a rigid body in space the supporting bars are first replaced by the reactive forces which act along the axes of the bars and have a known direction. This produces a free-body diagram. In general, by applying next the conditions of equilibrium (4.2), the six unknown reactions can be obtained. However, in most cases, it is more useful to employ different axes to those represented by the coordinate axes x, y and z. Since the body is in equilibrium it follows that the algebraic sum of the moments of all forces about any axis must be zero and the algebraic sum of the projections of all forces on any axis is also equal to zero. Hence, by inspection, it is possible to employ the conditions of equilibrium (4.2) in such a way as to obtain equations with less than the six bar force unknowns present.

A general system of forces in space may sometimes be solved by introducing an equivalent loading. Considering Figure 17(e), the force P acting at D on the rigid body ABCDEF can be replaced by an equivalent force P at B and a couple which has a moment equal to P x b. This technique was discussed at the beginning of Art. 4.3, and involves the application of two equal and opposite forces, of magnitude P, at the joint B. The two forces at B are in equilibrium and do not alter the action of the force P at D. Thus, as can be seen in Figure 17(f), the equivalent loading system consists of a force P acting at B and a couple applied at the end AEF giving forces of $\frac{P \times b}{a}$ in opposite directions at A and F. The three applied loads in Figure 17(f) are equivalent to the single force system in Figure 17(e) but the problem is now reduced to a series of concurrent forces which can be analysed by the most elementary procedures.

4.4 THE METHOD OF SECTIONS APPLIED TO COMPOUND SPACE TRUSSES

In Art. 4.3 we saw how a rigid body could be constrained completely in space by six supporting bars provided their axes could not be intersected by a straight line. It is easy to conclude from this fact that any self-contained simple space truss, such as that shown in Figure 16(d), may be attached to a foundation in a similar manner. Referring to Figure 18(a), the simple space truss ABCDEFGH is attached to a foundation by six supporting bars. This arrangement of bars and joints produces a rigid statically determinate structure which can remain in equilibrium under any system of external forces as shown. The framework under consideration is now classed as a compound space truss!

To carry out an analysis of compound space trusses the method of joints is not normally adequate by itself. Looking at Figure 18(a) it can be seen that no joints have been formed with less than four bars. Hence the unknown bar forces cannot be solved by the method of joints. However, it is possible to obtain the unknown supporting bar forces by considering the whole of the space truss ABCDEFGH as a free body. By applying the equations of equilibrium (4•2) to the free body, the values of the reactions which act along the axes of the supporting bars can be determined. After this procedure has been carried out it is then easy to analyse the remaining simple space truss by the method of joints. The method just mentioned for the solution of compound space trusses is known as the method of sections.

Compound space trusses can themselves be self-contained. Figure 18(b) illustrates a structure of this type. Two simple space trusses ABCDEFGH and IJKLMNOP are connected together by six bars in a manner which satisfies the conditions for complete constraint of a rigid body in space. This arrangement of bars produces a rigid statically determinate structure but it is impossible to obtain the member forces,

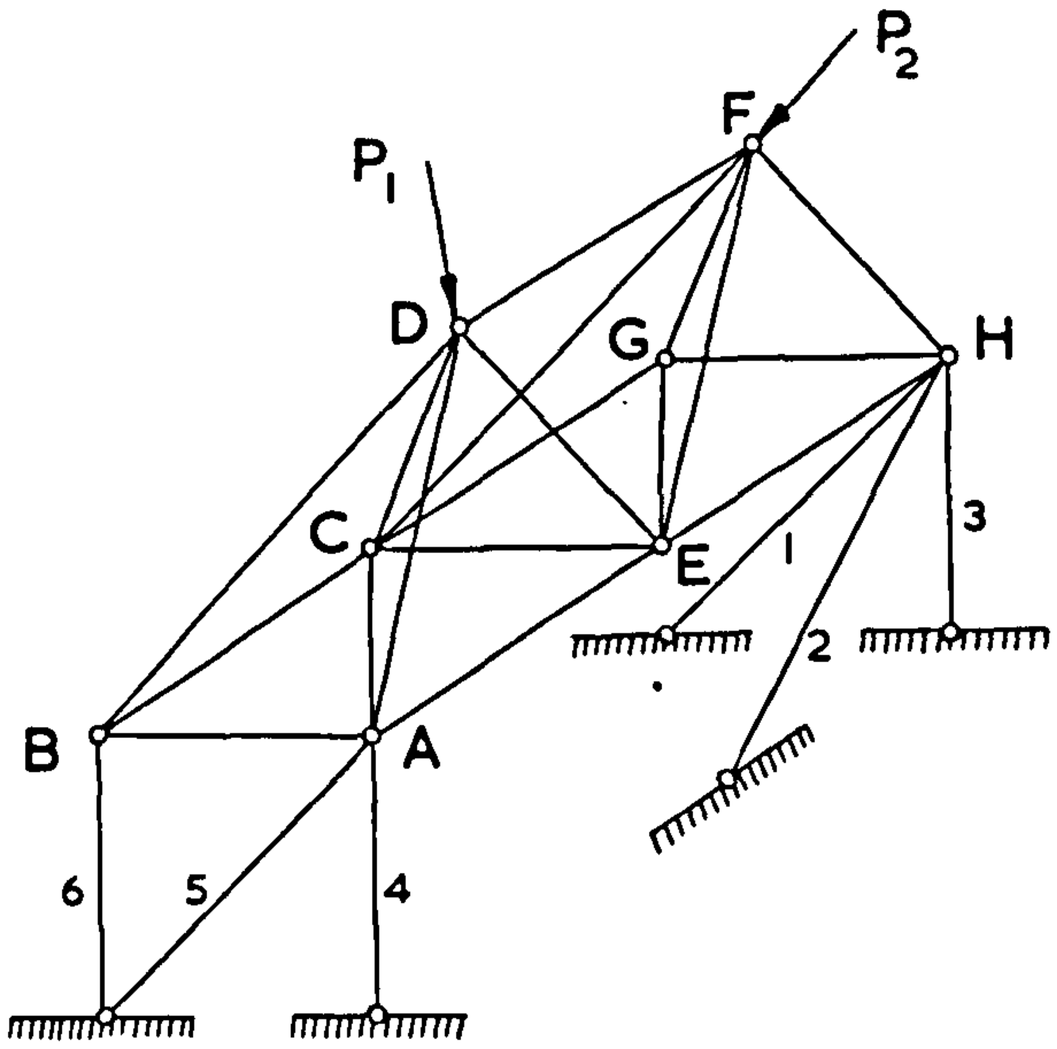

(a)

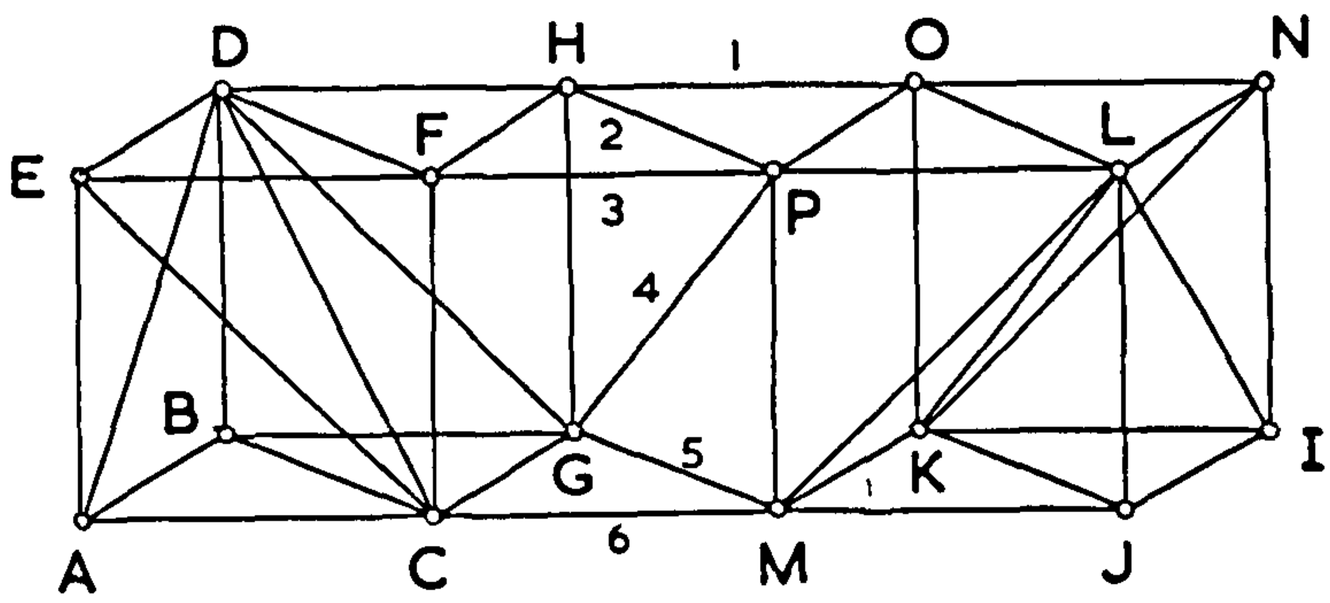

(b)

FIG. 18 COMPOUND SPACE TRUSSES

F.A.A. Ph.D. Thesis
11th June, 1969

Structural Engineering Division
Department of Civil Engineering
University of Newcastle upon Tyne

induced by an external system of loading, by the method of joints. Instead, a section must be taken through the six bars which connect the simple space trusses together. Two free body diagrams are therefore formed to which the six equilibrium equations (4.2) can be applied and the six unknown bar forces evaluated. Once the method of sections procedure has been employed and the reactions acting on the simple space trusses are known the analysis can be completed by the method of joints.

4.5 GENERAL CONDITIONS FOR THE ASSEMBLY OF STATICALLY DETERMINATE SPACE TRUSSES

In this section of Chapter IV the general conditions required for the statically determinate assembly of a number of bars in space to form a rigid truss will be discussed. Art. 4.2 showed how a simple space truss could be constructed by attaching a joint to a foundation by means of three bars not lying in one plane and then establishing further joints each supported by a similar arrangement of bars. The simple space truss illustrated in Figure 19(a) is assembled in this manner. From the general principle employed in the formation of simple space trusses we obtain the relationship:

$$m = 3j \quad \ldots\ldots\ldots \quad (4.3)$$

where m is the number of members in the structure and j is the number of joints.

While the rule for the assembly of simple space trusses is straightforward it does not constitute the only method of assembling bars in space to form rigid trusses. If bars BF and DG are removed from the simple space truss shown in Figure 19(a) and added at the positions FH and IK, as illustrated in Figure 19(b), a compound space truss is obtained. The portion EFGHIJKL forms, in itself, a simple space truss which is attached to a foundation by six bars the axes of

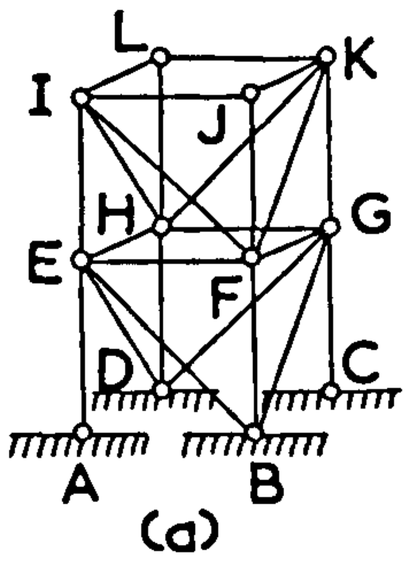

(a)

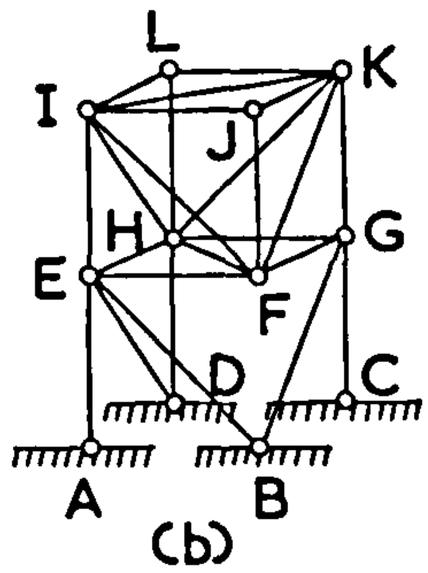

(b)

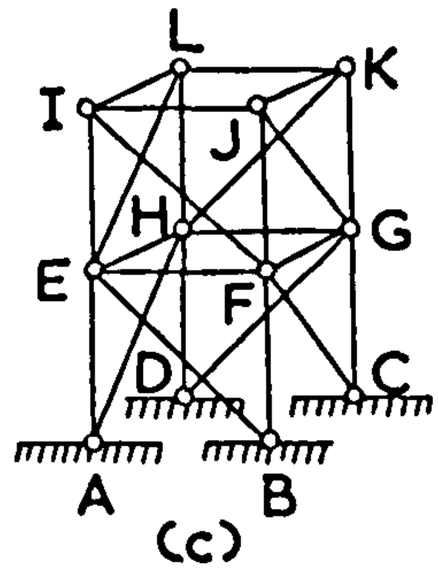

(c)

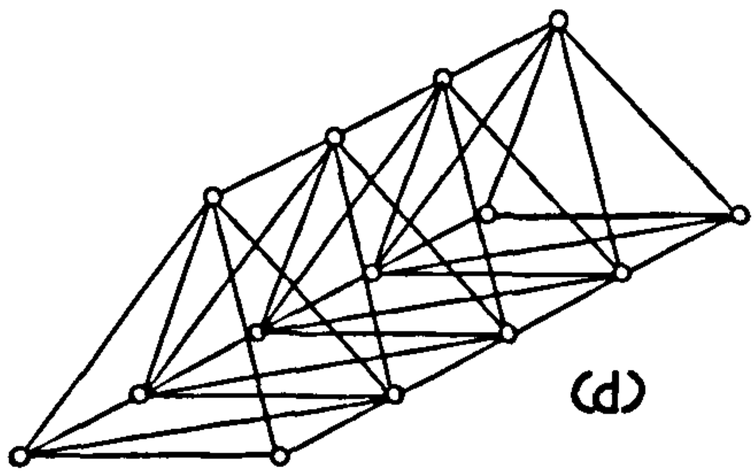

(d)

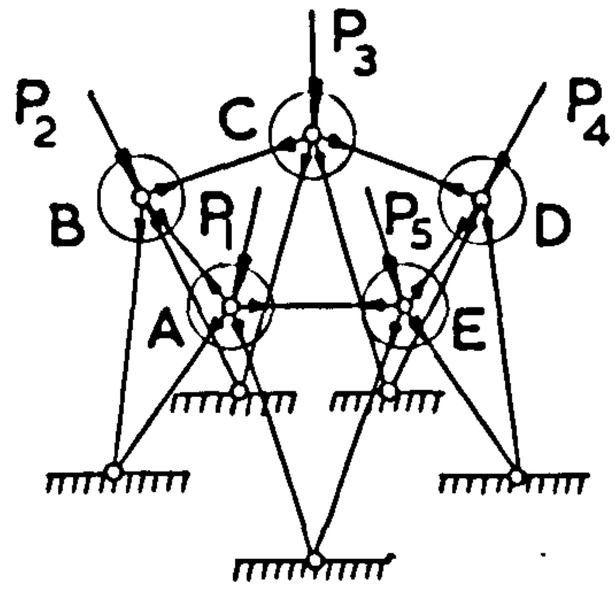

(e)

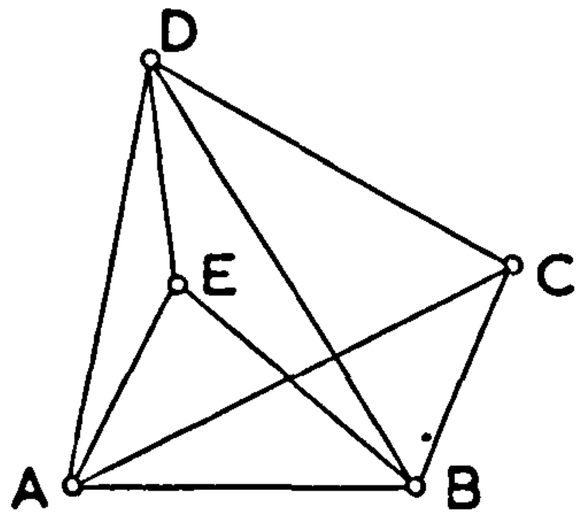

(f)

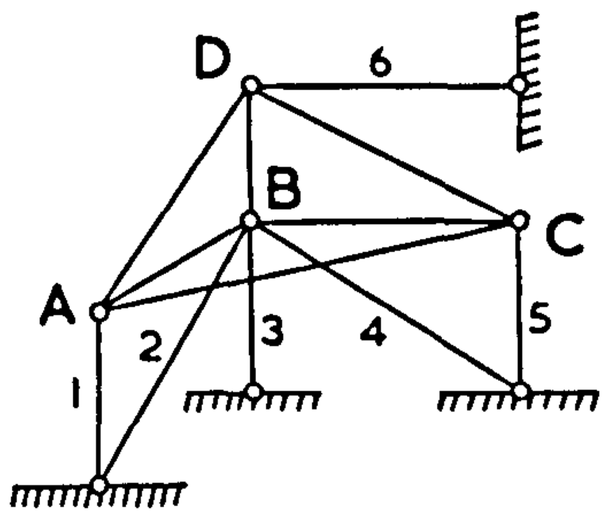

(g)

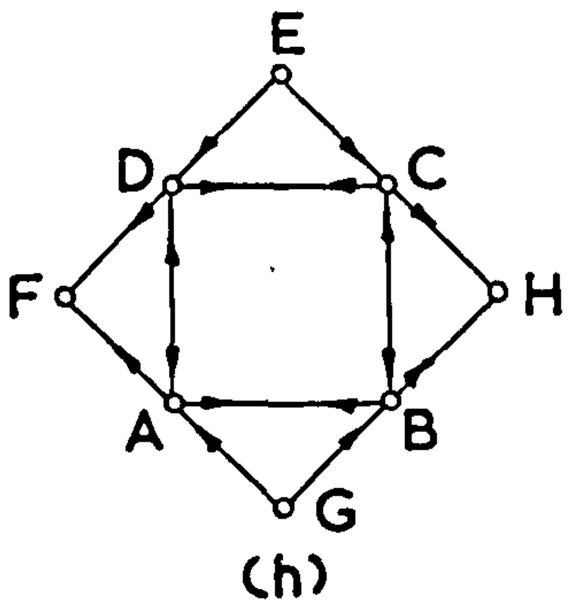

(h)

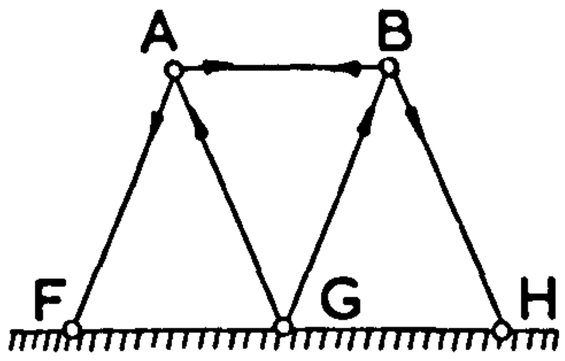

(i)

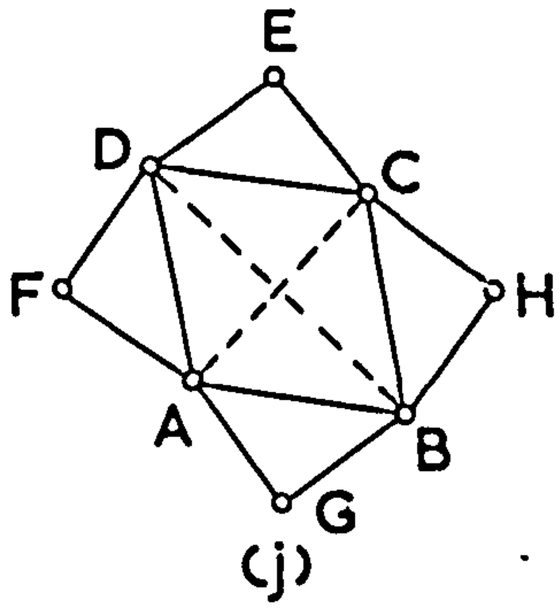

(j)

FIG. 19 GENERAL CONDITIONS FOR THE ASSEMBLY OF STATICALLY DETERMINATE SPACE TRUSSES

F.A.A. Ph.D. Thesis
16th June, 1969

Structural Engineering Division
Department of Civil Engineering
University of Newcastle upon Tyne

which cannot all be intersected by a straight line. Although the structure classification has been altered the relationship (4.3) still holds true for the compound space truss since the number of joints and bars is the same as for the simple space truss. Another arrangement of members is shown in Figure 19(c). This space truss, which is also rigid, is neither of the simple type nor of the compound form and is classed as a complex space truss. Many engineering structures exist in the latter form and they also satisfy the relationship (4.3).

From the preceding examples it can be concluded that 3j members are always required and usually sufficient, when properly arranged, for the rigid interconnection between themselves and a foundation of j joints in space. This observation also holds true for any self-contained space truss which is attached to a foundation by six bars arranged according to the principles required for the complete constraint of a rigid body in space. In Art. 4.2 the rules for the formation of a self-contained simple space truss were discussed and showed how a triangle of bars was first required to form a base upon which further joints, each constrained by three bars not in one plane, could be attached. Hence, apart from the first three bars which need three joints, the relationship between the number of members and the number of joints is given by equation (4.3). Therefore, for a complete self-contained simple space truss including the first three bars and joints, the member-joint relationship is given by:

$$m = 3(j-3) + 3 = 3j - 6 \quad \ldots\ldots\ldots \quad (4.4)$$

If now six bars are added to completely constrain the self-contained truss in space, the relationship given by equation (4.3), i.e. $m = 3j$, is again obtained.

When constructing space frames it is often necessary, for the sake of utility, to avoid the use of members which would obstruct the internal space. Considering any self-contained space truss without internal

diagonals, it can be proved that the relationship (4.4) still holds true if the truss is in the form of a closed polyhedron with triangular plane faces or if the faces are divided into triangles. The truss will also constitute a rigid body if its members are arranged in this manner. To prove these facts it is necessary to begin with a theorem that is credited ~~by~~ to Euler and which deduces the relationship between the number of faces, edges and apices of any closed polyhedron.

Starting with one face, represented by any closed polygon, it can be seen that the number of edges is equal to the number of apices. Proceeding to the next face, one edge and two apices are present from the first face. Next, for the third face, two edges and three apices are already in existence. Thus, on proceeding, one more edge has to be added to each face than the number of apices and the number of edges gains on the number of apices at a rate equal to the number of faces which have been added to the first face at the time of consideration. It can be concluded, therefore, that neglecting the last face added in the formation of a closed polyhedron the number of edges is equal to the number of apices plus the number of faces added to the first face. The last face is formed entirely from existing edges and apices and hence a second extra face is obtained. The relationship between faces, edges and apices of a closed polyhedron can, therefore, be written in the form:

$$m = j + (f - 2) \quad \ldots\ldots\ldots \quad (4.5)$$

where m is the number of edges, j is the number of apices and f is the number of faces. This equation expresses the Euler theorem mentioned previously and can be applied generally to any closed polyhedron.

In the case of a closed polyhedron with triangular sides or with sides divided into triangles, a further relationship between faces, f, and edges, m, can be determined. Each edge is common to two faces and each face has three edges. Hence it follows that:

$$m = \frac{3}{2}f \quad \ldots\ldots\ldots \quad (4\cdot6)$$

Introducing this relationship into equation (4·5), a solution of m = 3j - 6 is obtained which is expressed by equation (4.4). This proves that any self-contained space truss in the form of a closed polyhedron without internal diagonals and having triangular sides satisfies the condition represented by equation (4.4). A typical truss of this type is illustrated in Figure 19(d) and is classed as a complex truss.

Space trusses, as it has been shown, can be classed under three general groups:

(1) simple space trusses;

(2) compound space trusses;

(3) complex space trusses.

For each type the relationship m = 3j holds true and is a general requirement of rigidity and complete constraint. This relationship is also significant in another way which will be discussed now. Referring to Figure 19(e), this structure is a completely constrained space truss consisting of m members and j joints upon which external forces are applied at the joints. Under the system of loading shown only axial forces will be present in the members and the determination of these unknown forces constitutes the analysis of the truss. If the space truss had been of the simple variety, or of the compound form, then the unknown axial forces could have been obtained by the method of joints for the former type and the method of sections for the latter. However, the space truss in Figure 19(e) is a complex truss and when applied to such a truss the two methods of solution just mentioned may fail. Four bars are connected at each joint of Figure 19(e) so that the method of joints cannot be applied. A section through six bars, the axes of which cannot be intersected by a straight line, is not available for use with the method of sections and hence a more general approach to the problem must be considered. The bars are first replaced by two

equal and opposite forces which represent the reactions at the ends of the bars and act in the direction of their axes. Thus j systems of concurrent forces in equilibrium are obtained. By applying the equations of statics (4·1), i.e. $\Sigma X_i = 0$; $\Sigma Y_i = 0$; $\Sigma Z_i = 0$, 3j simultaneous equations with m unknowns are obtained. For the condition where m = 3j there are sufficient equations to solve all the unknowns and therefore in all but exceptional cases, where the determinant of the 3j simultaneous equations of statics vanishes, a unique solution will be obtained.

From the preceding discussion it can be concluded that if any completely constrained space truss satisfies the condition m = 3j then it is statically determinate and the unknown internal forces, which result from any external system of applied loads, can be found by the equations of statics alone. If $m > 3j$ then the structure is statically indeterminate and a study of the elastic deformations in the bars is required to account for the way in which the internal bar forces adjust themselves to maintain equilibrium. If $m < 3j$ the structure will be unstable and may collapse under applied loads.

Returning now to the condition where m = 3j, in some exceptional circumstances the determinant of the 3j system of simultaneous equations, obtained by statics for a complex truss, has a zero value. Hence a definite solution cannot be obtained for the axial forces. If a zero value is obtained it is an indication that the truss is unstable under the action of external loads and this condition is termed as a critical form.

Considering the simple space truss in Figure 19(f), it can be seen that a critical form occurs if the point E lies in the plane of ABD. The rule for the formation of simple space trusses by the addition of joints completely constrained by three members not lying in one plane would then have been ignored, and it would be possible for the joint E

to move under applied loads. Similarly the compound space truss in Figure 19(g) is a critical form because the axes of the six supporting bars which attach the simple space truss ABCD to its foundation, can all be intersected by the axis of the member BD or are parallel to it. Hence a limited amount of rotation about this axis is possible.

The visual detection of critical forms is easy in the cases of simple and compound space trusses and can be avoided by adhering to the rules for their formulation. However, in the case of complex trusses, critical forms sometimes cannot be observed by inspection and an indication of instability may be gained from a consideration of the determinant of the 3j equations of statics obtained for the j joints of the system. If the determinant is different from zero the structure is statically determinate; if not it is statically indeterminate and critical.

The evaluation of determinants is impracticable, however, and another method of determining whether a complex space truss is rigid or not needs to be employed in most cases. Since a critical form depends only on the member arrangement and not upon the applied loads it follows that if, under any load system, the axial forces in the members of the structure can be obtained without ambiguity then the determinant will not be zero and the structure will be rigid. If, however, ambiguity does occur a critical form is present and the determinant will be zero. The simplest method of carrying out such an investigation is to apply a zero load at each joint. One obvious solution for equilibrium at the joints is that zero axial forces are present in the members. If no other values different from zero can be found which satisfy the equilibrium conditions at the joints, the truss is statically determinate and rigid. However, if a set of axial forces different from zero can be obtained, under zero loading, which satisfy the conditions of equilibrium at the joints then ambiguity has

occurred and the truss has a critical form. The analysis of a truss under zero load conditions in order to detect a critical form is known as the zero load test.

The zero load test will now be applied to the complex space truss illustrated in Figures 19(h) and (i). This structure satisfies the relationship m = 3j and consists of a square frame ABCD supported in a horizontal plane by eight members attached to a foundation. With zero load at the joints, an arbitrary tension is assumed to exist in AF while, at the same time, an equal compression occurs in AG. The resultant of these two forces acts in the plane of ABCD at right angles to the line of AC. This resultant can be balanced by tension in AB and compression in AD and hence the conditions of equilibrium can be satisfied. Similarly equilibrium can be maintained at the joints B, C and D. From this it can be concluded that, under zero load, a set of axial forces different from zero can exist in the truss members and consequently the truss has a critical form because of its ambiguous solution. In this case it is easy to see from Figure 19(j) that the points A, B, C and D are free to move along the diagonals of the square ABCD and hence the structure is unstable.

4.6 THE ANALYSIS OF COMPLEX SPACE TRUSSES

The general problems involved in the formation of space trusses were considered in Art. 4.5 and a method was established to detect critical types. This article is concerned with the analysis of complex trusses which have been proved to be statically determinate and rigid.

Although the method of joints can only be applied in general to simple trusses, as discussed in Art. 4.2, it can also be employed, in certain circumstances, for the solution of complex trusses. Figure 20(a) shows a complex truss which satisfies the relationship m = 3j and is therefore statically determinate. It is also rigid. Starting at the joint J, the forces in the bars 1, 2 and 3 can easily be

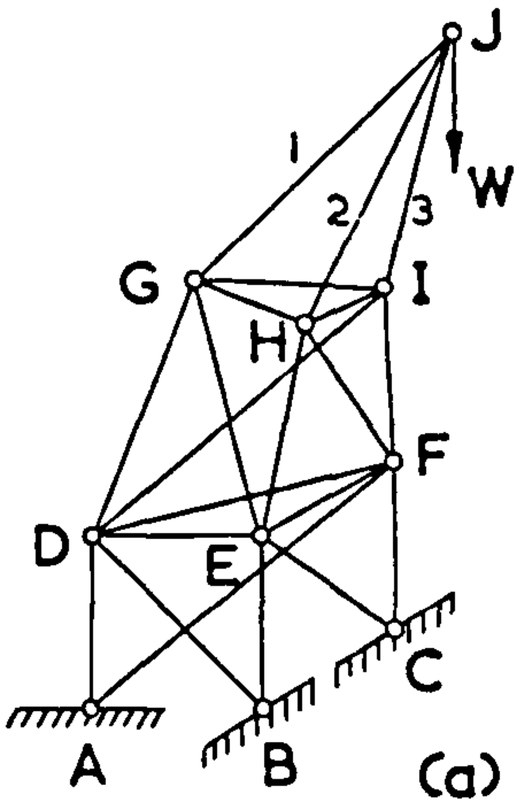

(a)

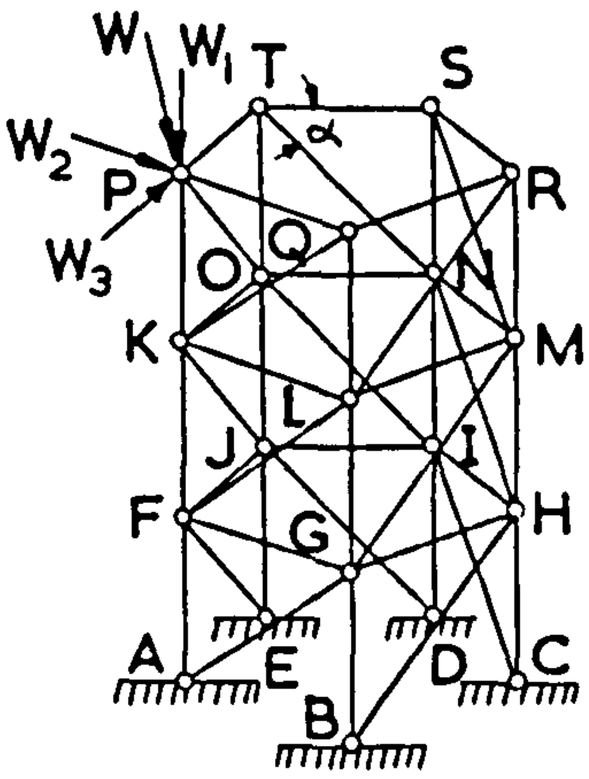

(b)

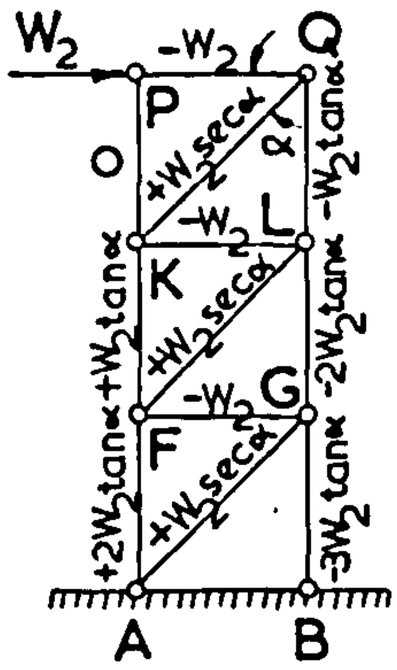

(c)

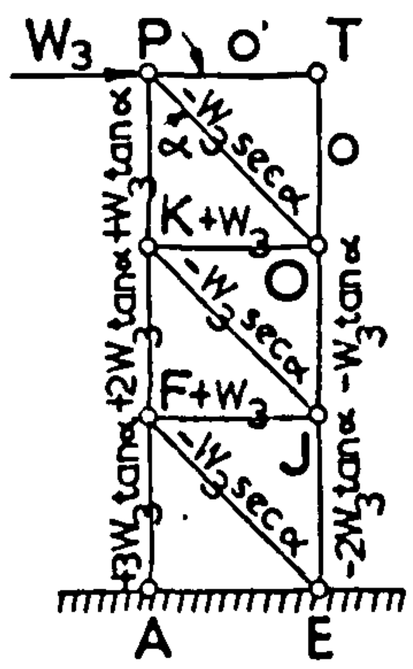

(d)

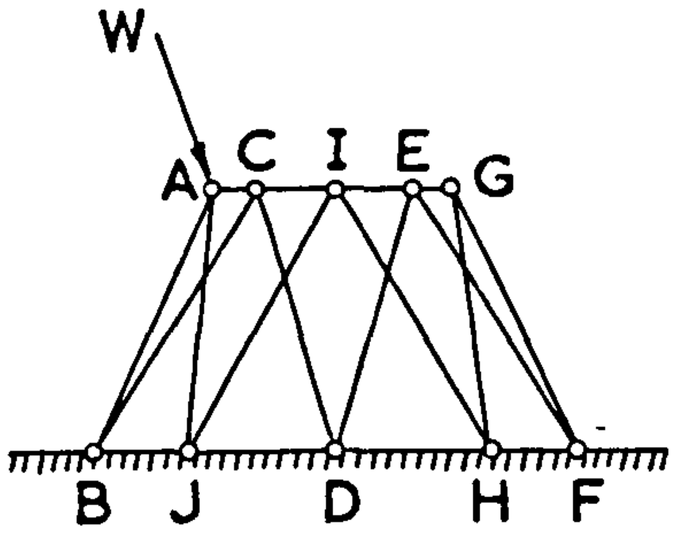

(e)

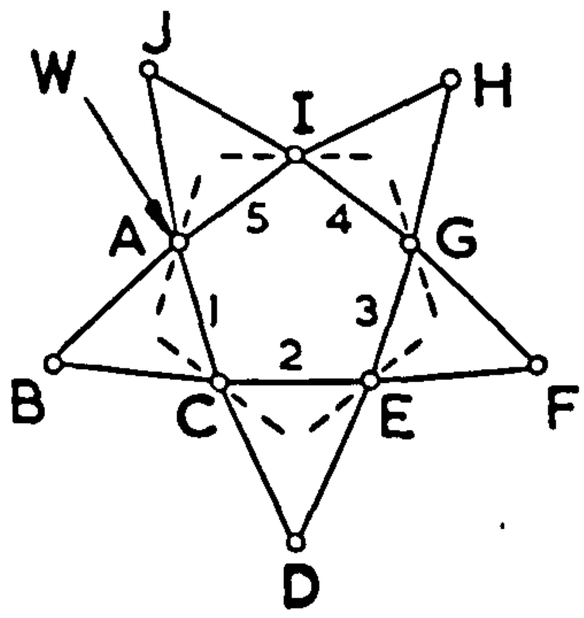

(f)

FIG. 20 THE ANALYSIS OF COMPLEX SPACE TRUSSES SHEET NO. 1

F.A.A. Ph.D. Thesis
23rd June, 1969

Structural Engineering Division
Department of Civil Engineering
University of Newcastle upon Tyne

determined. These forces act as reactions at the joints G, H and I to which the conditions of equilibrium (4•1) can then be applied. At each of the joints G, H and I it can be seen that four bars are present together with the known reaction force. Since there are only three equations of statics (4•1) it appears at first sight that a solution for the unknown forces cannot be obtained. However, at each of the joints being considered, there are three bars which lie in one plane. If the forces at the joint are projected onto a plane which is normal to the co-planar forces the remaining unknown force value is obtained immediately. Having found two of the forces at each joint the other forces can easily be obtained and the truss solved by repeated application of this principle.

Where symmetrical arrangements of members occur in space frames the problems of analysis are greatly simplified. Consider the radial ribbed dome illustrated in Figure 21. At all joints a vertical point load has been applied and these loads have equal values around the horizontal rings. The zero load test is first employed to test the rigidity of the structure. Four bars are attached at the joints in the top ring and three of the bars at each joint lie in one plane. If, under zero load conditions, the equilibrium of these joints is considered, then an assumed axial force in the bar not lying in the plane of the co-planar bar forces cannot be balanced by any other member force if projections are taken on a plane at right angles to the plane of the co-planar forces. Hence under zero load conditions no axial forces other than zero forces can be present in the top ring members. If the top ring bars are removed, two bars are left at each joint which also can only contain zero axial forces under zero load conditions. Therefore it can be seen that if all the other joints in the system are considered in a similar manner, a structural system exists in which the members can only contain zero axial forces under zero load con-

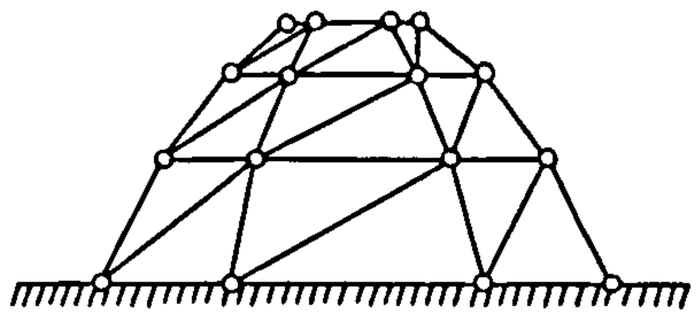

(a)

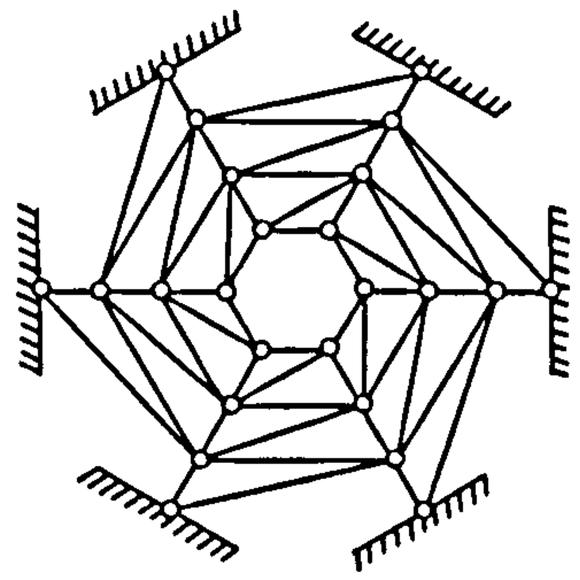

(b)

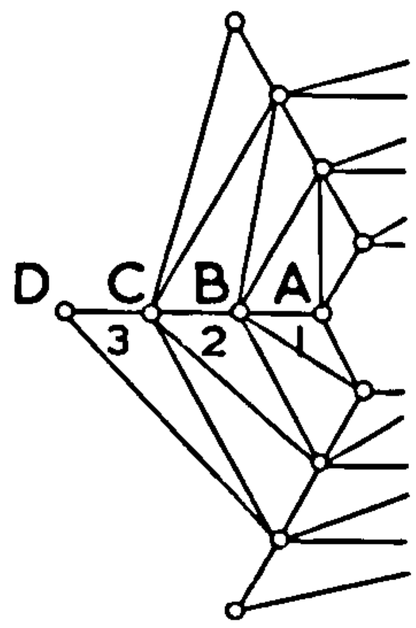

(c)

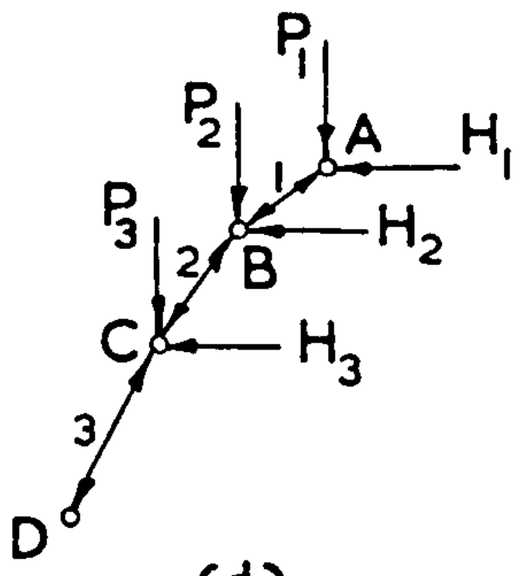

(d)

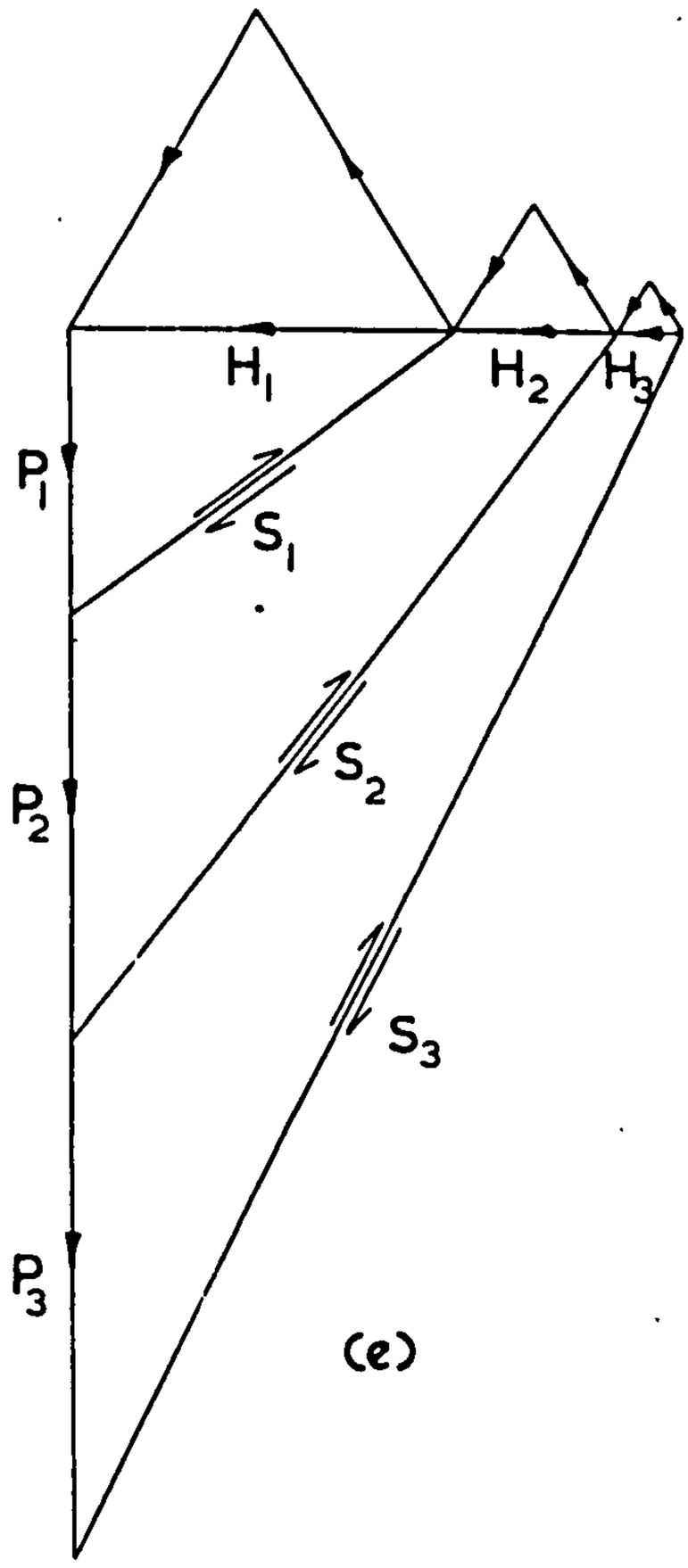

(e)

FIG. 21 THE ANALYSIS OF COMPLEX SPACE TRUSSES SHEET NO. 2

F.A.A. Ph.D. Thesis
23rd June, 1969

Structural Engineering Division
Department of Civil Engineering
University of Newcastle upon Tyne

ditions and the framework must be rigid and statically determinate. From these observations we conclude that if, under any system of loads which are not equal to zero, a solution can be obtained for the axial forces in the space frame system which satisfies the conditions of equilibrium then it must be the true solution.

Having first established that the dome in Figure 21 is rigid and statically determinate, it is now possible to proceed to the analysis of the system. Figures 21(c) and (d) show a meridian of the dome upon which vertical loads P_1, P_2 and P_3 act at the joints. Since the loads act in the plane of the meridian the horizontal rings must exert resultant forces H_1, H_2 and H_3, also in the plane of the meridian, in order to maintain equilibrium. The diagonal members under these conditions are inactive and the axial bar forces are equal throughout each horizontal ring. Beginning with the joint A, a polygon of forces can be constructed for each of the meridian rib joints in turn. From the force polygons the axial forces S_1, S_2 and S_3 can be determined along with the resultants H_1, H_2 and H_3 of the two equal horizontal ring bar forces at each joint. The corresponding ring bar forces are easily obtained by resolving the resultants H_1, H_2 and H_3 into components parallel to the axes of the ring bars as shown by the equilateral triangles. Since the conditions along each meridian are identical the force diagram represents a complete analysis of the dome.

The analysis of statically determinate space trusses can frequently be simplified by reducing the problem to a series of plane trusses. Figure 20(b) illustrates a complex space truss which can be solved in this manner. It satisfies the relationship $m = 3j$ for statically determinate conditions and can easily be proved rigid by the zero load test. Therefore it can be concluded that under any system of loads different from zero there will be only one set of axial forces at the joints which can satisfy the conditions of equilibrium

and any procedure employed to find these forces will be a valid one. The load at joint F, W in Figure 20(b), is first resolved into three components W_1, W_2 and W_3 which act in the plane of the individual trusses illustrated by Figures 20(c) and (d). These trusses can now be analysed separately. Considering the force W_1, it can be seen that only the bars FK, KF and FA will be active and these bars contain compressive forces equal to W_1. The values for the forces in the plane trusses ABFGKLPQ, under load W_2, and AEFJKOPT, under load W_3, are given in Figure 20(c) and Figure 20(d) respectively and to complete the analysis for the original loading system W, the bar forces in each separate system are added algebraically.

When a system of concurrent forces in space is such that the forces all lie in two intersecting planes, the resultant of the forces in either plane must lie along the line of intersection of the two planes. This follows from the conditions of equilibrium whereby the resultant of the forces in one plane must be equal, opposite and collinear with the forces in the other plane. In general this principle is very useful when employed in the analysis of complex space trusses and greatly simplifies the force determination. Figures 20(e) and (f) show a complex space truss which is rigid and statically determinate. The load W is applied at A. Considering first the unloaded joint C, it can be seen that the supporting bars BC and CD form a plane which intersects the plane of the pentagon AIGEC along a horizontal line shown dotted. It follows, therefore, that the resultant force at the joint C acts along the horizontal dotted line. By projecting all the forces at C on a horizontal axis normal to this line it can be seen that $S_1 = -S_2$. Similar conclusions can be drawn for the joints E, G and I and hence $S_1 = -S_2 = S_3 = -S_4 = S_5$. Having found $S_1 = S_5$ it is then a simple operation to solve for these forces by projecting all the forces at A onto an axis which is normal to the

plane formed by the supporting bars AB and AJ. The analysis for the remainder of the structure can then be completed by the method of joints.

4.7 HENNEBERG'S METHOD

Another method of analysis which can sometimes be employed for complex statically determinate space trusses, not solvable by the procedures discussed in Art. 4.6, is Henneberg's method. The complex truss in Figure 22(a) is in equilibrium under the given load system W which acts along the axis BD. If the bar AD, denoted by x, is removed and another bar, a, inserted between joints B and D, as in Figure 22(b), a simple self-contained space truss is formed which can be analysed rapidly by the method of joints. The forces in the simple system due to unit loads applied at the joints A and D along the line of AD, Figure 22(c), can also be obtained easily by the method of joints. To obtain the forces in the original complex system the effects of the two simple space truss loading conditions must be added together.

Let S_i' be the axial force in any bar of the simplified system, Figure 22(b), under the load W and let s_i' be the force in the same bar under the unit load conditions, Figure 22(c). If the unit forces in Figure 22(c) are replaced by forces of magnitude X then the axial force in any bar will become $s_i'X$. Adding the effects of the two loading conditions together, it follows that for the simple space truss:

$$S_i = S_i' + s_i'X \quad \ldots\ldots\ldots \quad (4.7)$$

where S_i is the axial force in any bar of the system under both sets of loads. Hence for any bar, a, the relationship is:

$$S_a = S_a' + s_a'X \quad \ldots\ldots\ldots \quad (4.8)$$

If, now, the axial force in bar, a, is taken as zero the value of X is found from:

$$S_a' + s_a'X = 0 \quad \ldots\ldots\ldots \quad (4.9)$$

i.e.
$$X = \frac{S_a'}{s_a'} \quad \ldots\ldots\ldots \quad (4.10)$$

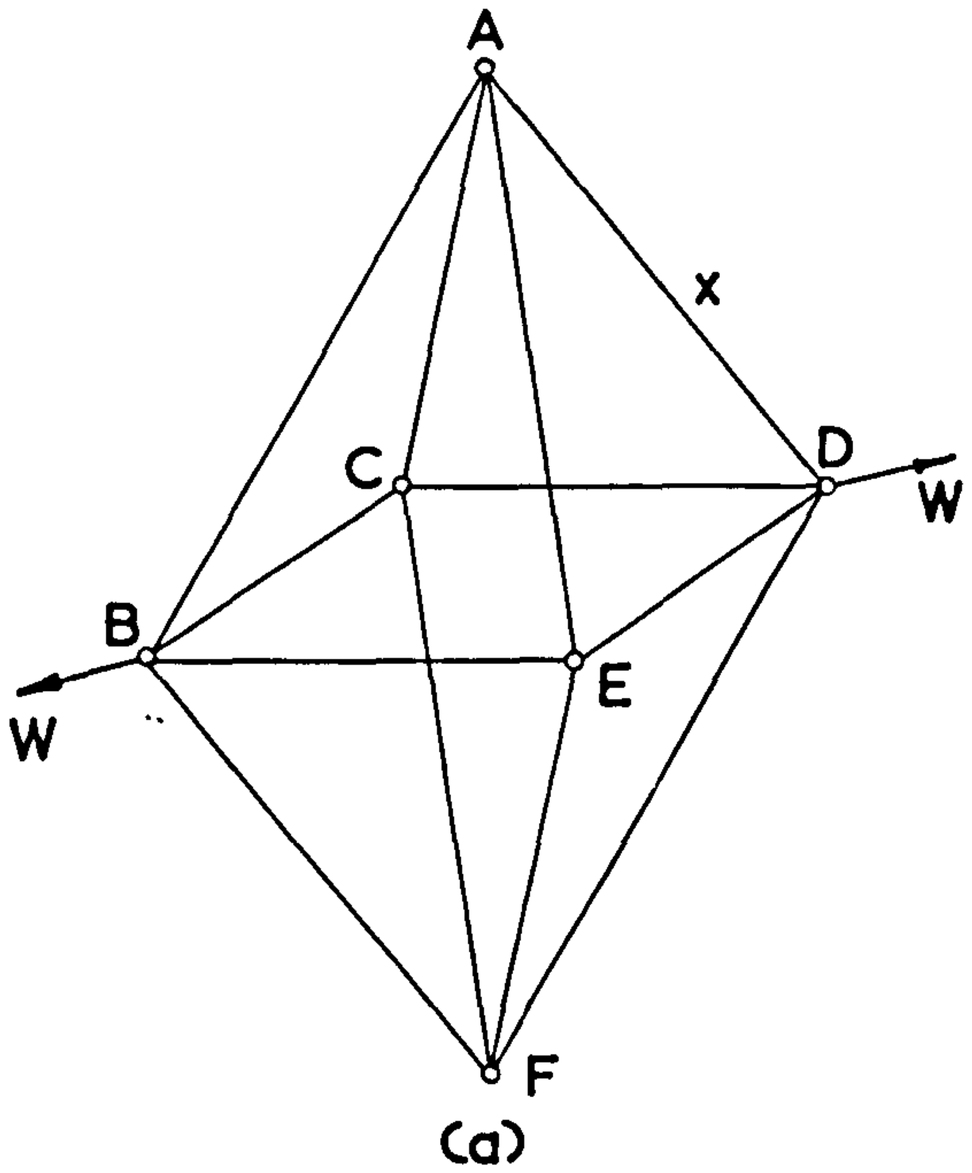

(a)

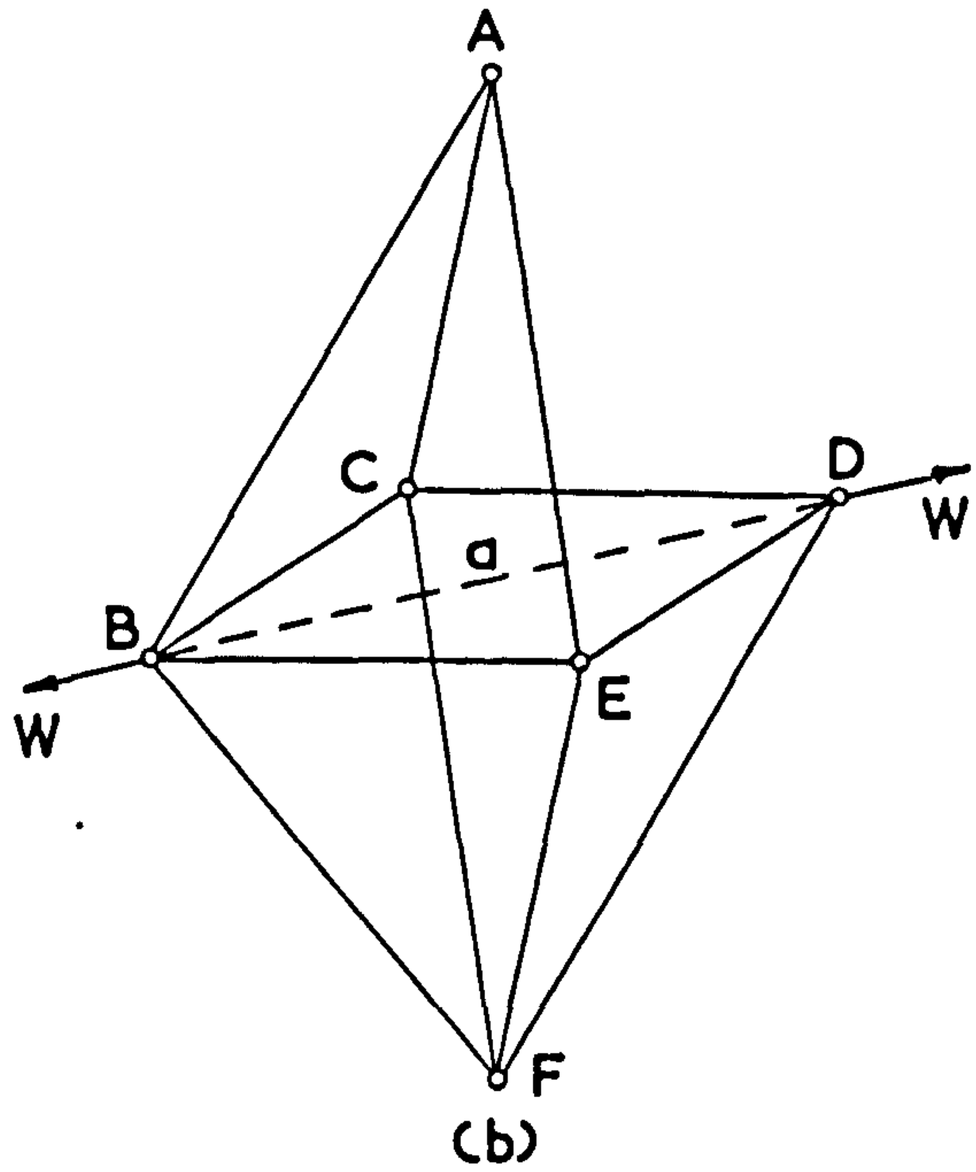

(b)

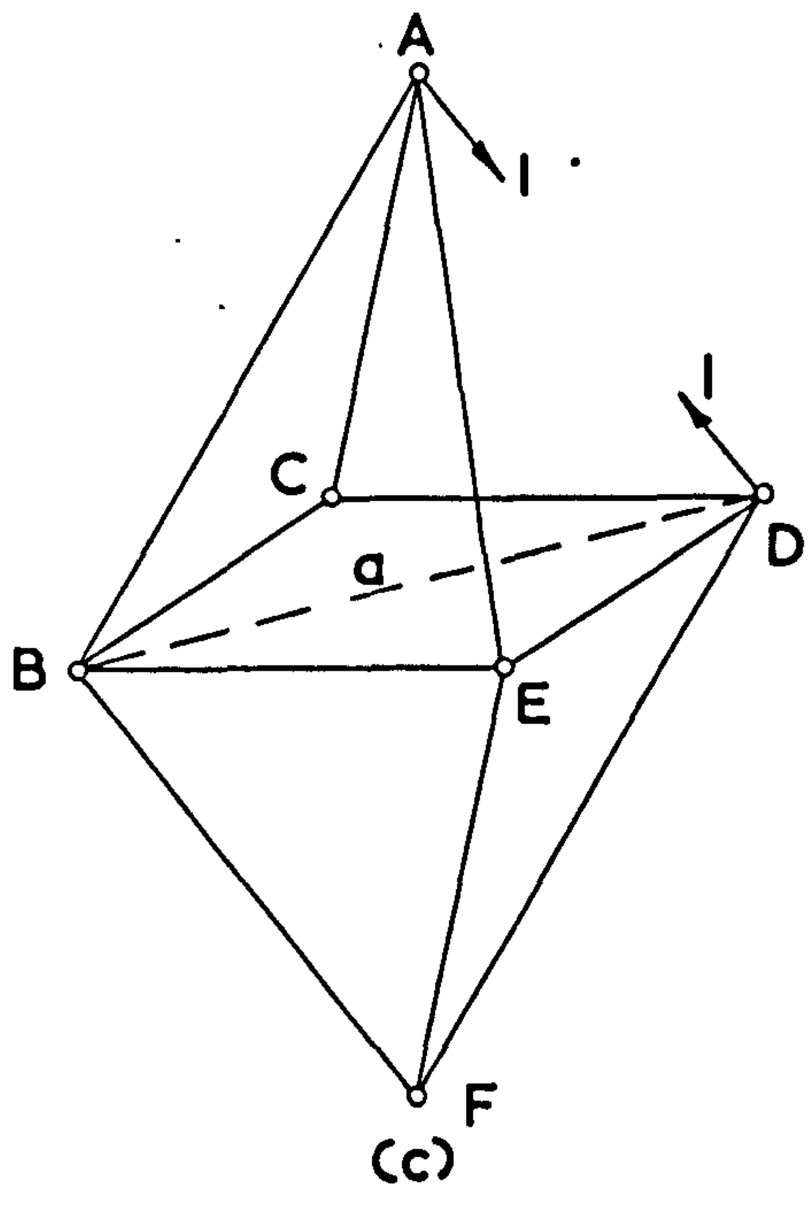

(c)

FIG. 22 HENNEBERG'S METHOD

F.A.A. Ph.D. Thesis
26th June, 1969

Structural Engineering Division
Department of Civil Engineering
University of Newcastle upon Tyne

and the bar, a, can be removed from the space truss to give the original complex system. Having found the value of X which makes S_a = 0 the remaining forces in the system can be found from equation (4·7). If, in equation (4·10), the value of s_a' is zero when employing Henneberg's method for the solution of complex trusses, then an indeterminate structure has been formed. Therefore this method can also be used as a test for critical forms.

Since the removal of a bar of the structure is necessary in the application of Henneberg's method, there arises the problem of choosing which bar. Actually any bar can be removed provided the bar which is added in its place, to simplify the structure, also restores the rigidity of the system otherwise statically indeterminate conditions will occur. The choice of removal and restoration is then a matter of which system will give the easiest analysis. In some cases it is necessary to remove more than one bar to obtain a system which can be analysed in a simple manner. This requires the addition of the same number of bars as those removed but arranged in a more suitable fashion. If S_i' is the axial force in any bar due to the W loading and s_i' , s_i'' ....., represent the forces due to each pair of unit loads added in place of the bars removed then:

$$S_i = S_i' + s_i' X_1 + s_i'' X_2 + \ldots\ldots\ldots \quad (4\cdot11)$$

where X_1, X_2, ..., are chosen to satisfy the following equations:

$$\left.\begin{aligned} S_{a_1} &= S_{a_1}' + s_{a_1}' X_1 + s_{a_1}'' X_2 + \ldots\ldots = 0 \\ S_{a_2} &= S_{a_2}' + s_{a_2}' X_1 + s_{a_2}'' X_2 + \ldots\ldots = 0 \\ &\ldots\ldots\ldots\ldots\ldots\ldots\ldots\ldots \end{aligned}\right\} \ldots\ldots \quad (4\cdot12)$$

From equation (4·11) a complete analysis can be made after finding the values of X_1, X_2 .....

4.8 THE TENSION COEFFICIENTS METHOD[10],[12],[15]

This analytical method of force calculation was devised by Southwell[16] and can easily be applied to statically determinate pin-jointed space frames. If the tension coefficient for any bar in such

a system is represented by t, then:

$$t = \frac{\text{Load in the bar, T}}{\text{Length of the bar, l}}$$

Denoting the projections of the bar along three mutually perpendicular axes by a, b and c, it follows that:

$$\cos\alpha = \frac{a}{l} \; ; \; \cos\beta = \frac{b}{l} \; ; \; \cos\gamma = \frac{c}{l}$$

By applying the laws of statics at any joint, it can be seen that:

$$\sum_{i}^{n} \frac{Ta}{l} + X = 0$$

$$\sum_{i}^{n} \frac{Tb}{l} + Y = 0 \qquad \ldots\ldots (4{\cdot}13)$$

$$\sum_{i}^{n} \frac{Tc}{l} + Z = 0$$

where X, Y, Z are the components of the joint external load resolved along the three mutually perpendicular axes. In order to obtain a direct solution, i.e. three simultaneous equations with only three unknowns, there must only be three bars connected at the joint. The equations (4·13) then reduce to:

$$X + t_1a_1 + t_2a_2 + t_3a_3 = 0$$

$$Y + t_1b_1 + t_2b_2 + t_3b_3 = 0 \qquad \ldots\ldots (4{\cdot}14)$$

$$Z + t_1c_1 + t_2c_2 + t_3c_3 = 0$$

from which

$$t_1 = - \frac{\begin{vmatrix} Xa_2 & a_3 \\ Yb_2 & b_3 \\ Zc_2 & c_3 \end{vmatrix}}{\Delta}$$

where

$$\Delta = + \begin{vmatrix} a_1 & a_2 & a_3 \\ b_1 & b_2 & b_3 \\ c_1 & c_2 & c_3 \end{vmatrix}$$

The values of t_2 and t_3 are obtained in a similar way and the forces in the bars are given by:

$$T_1 = t_1l_1 \; ; \; T_2 = t_2l_2 \; ; \; T_3 = t_3l_3$$

Although the method of analysis employing tension coefficients is an

elegant one, it has certain limitations. For a space frame system which is composed of many members the work involved becomes very tedious when applying equations (4·14) to every joint. Each joint solution also depends on the solution of a previous joint and hence errors in the calculation of forces at one joint may be carried over into other joints producing an incorrect stress distribution.

4.9 THE METHOD OF CONJUGATE FORCES[10],[12]

Of the several graphical methods which are available for the determination of stresses in statically determinate pin-jointed space frames, the best one is that which employs conjugate forces. Professor Benjamin Mayor[17] first put forward this method in 1926 and a modified form was published by Constant[18] in 1934. By employing conjugate forces the normal difficulties encountered when working in three-dimensional systems are overcome as the problem is reduced to a system of equivalent co-planar forces which can be more readily analysed. Having obtained the values for the co-planar forces, the three-dimensional analysis can then be carried out without much effort.

If the force in any bar of a space framework is denoted by F, Figure 23(a), then it can be resolved into vertical and horizontal components which are given by:

$$R = F \sin \phi \quad \ldots\ldots\ldots \quad (4\cdot15)$$

$$F' = F \cos \phi \quad \ldots\ldots\ldots \quad (4\cdot16)$$

The component F' lies in the horizontal plane ABCD and R is perpendicular to it. At any point N, lying in the plane ABCD, conjugate forces $F'' = F'$ can be applied. The system is in equilibrium because $\Sigma R = 0$ and $\Sigma F' = 0$ and therefore the force F' may be transferred to N thus introducing a moment Mo which is given by:

$$Mo = F'b = F''b \quad \ldots\ldots\ldots \quad (4\cdot17)$$

From equations (4·15), (4·16) and (4·17) it can be seen that:

$$b = \frac{Mo}{F'} = \frac{Mo}{F\cos\phi} = \frac{Mo}{R}\tan\phi = a\tan\phi \quad \ldots\ldots \quad (4\cdot18)$$

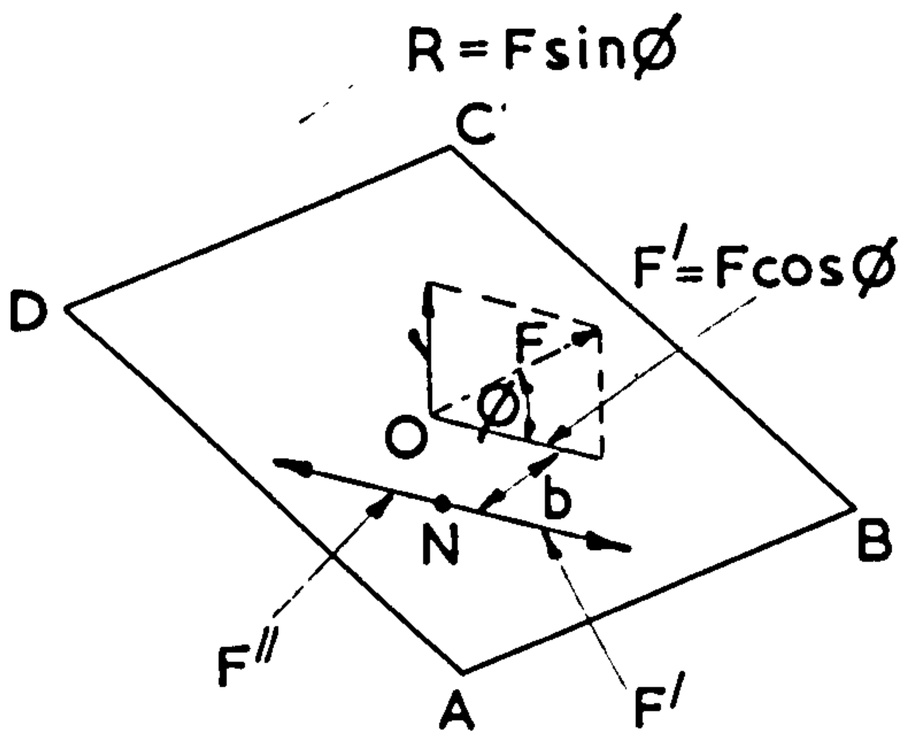

(a)

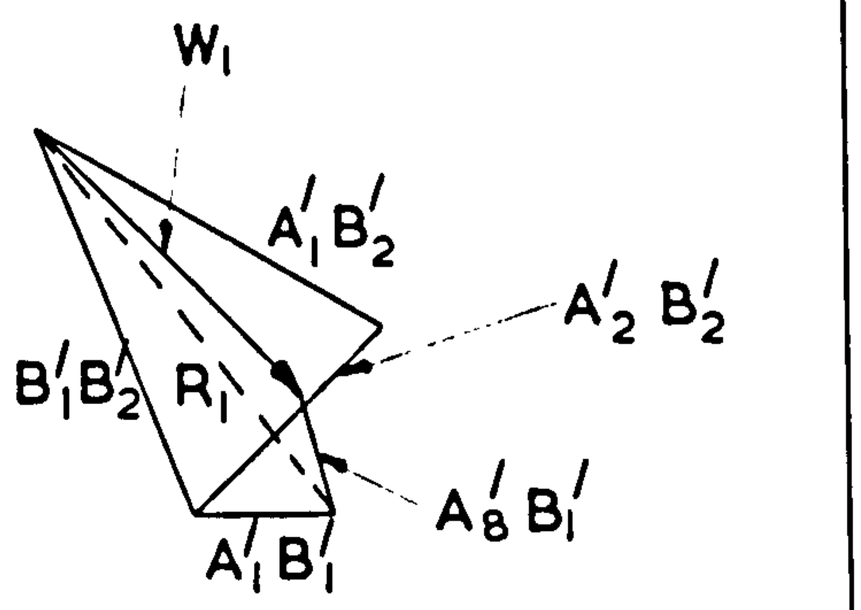

(b)

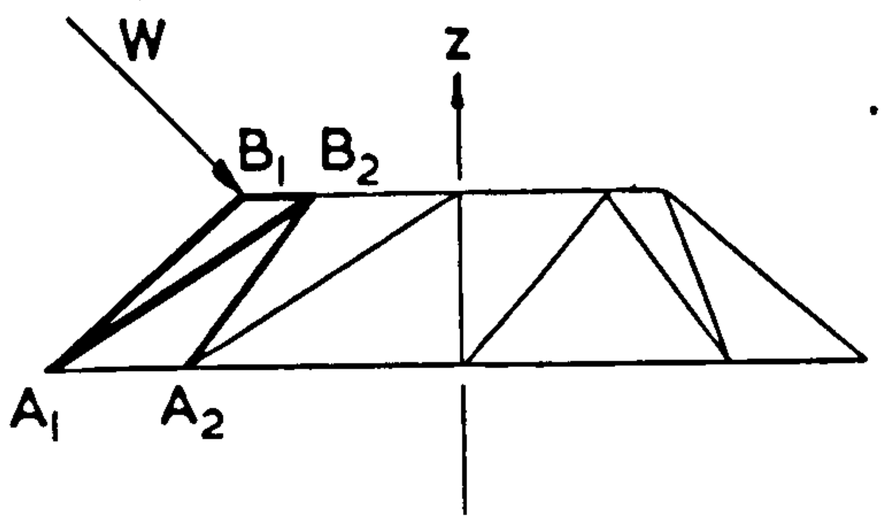

(c)

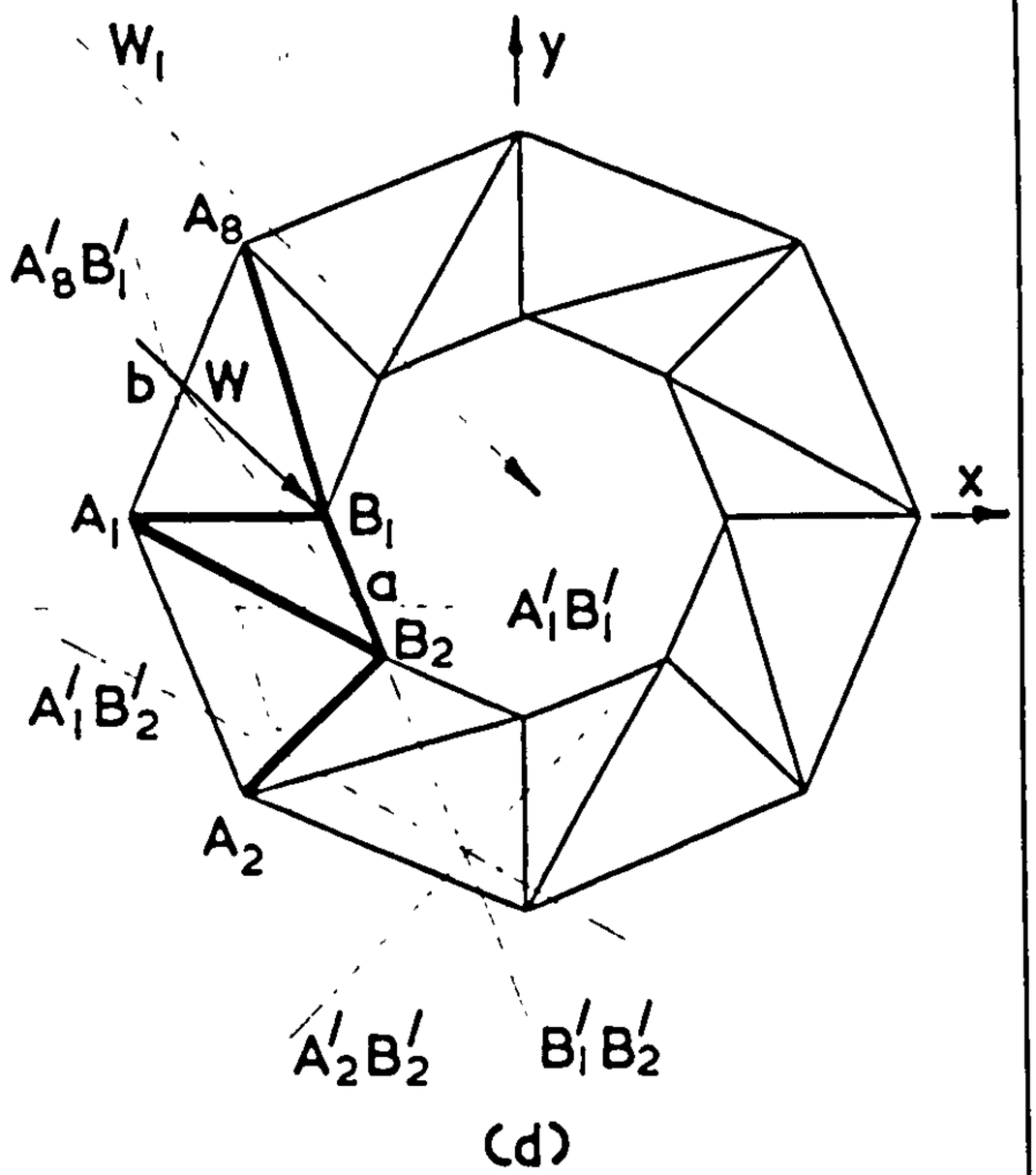

(d)

FIG. 23 THE METHOD OF CONJUGATE FORCES

F.A.A. Ph.D. Thesis
8th Oct., 1969

Structural Engineering Division
Department of Civil Engineering
University of Newcastle upon Tyne

where

$$a = \frac{Mo}{R} \quad \ldots\ldots\ldots (4\cdot19)$$

The value of a is constant for all forces in the system. It is a simple process at this stage to prove that the system of conjugate forces is in rotational equilibrium:

$$\Sigma Mo = \Sigma F' b = \Sigma F' \, a\tan\phi = a\Sigma F' \tan\phi$$

$$= a\Sigma F \cos\phi \tan\phi = a\Sigma F \sin\phi$$

$$= a\Sigma R = 0$$

The application of the method of conjugate forces is demonstrated in Figures 23(b), (c) and (d). Figure 23(d) is a plan view of a statically determinate pin-jointed space frame which can be analysed easily by the graphical method employing conjugate forces. An elevation of the structure is shown in Figure 23(c) and the force diagram is produced in Figure 23(b). By inspection the active members can be located and are shown as heavy lines.

A value of a is first chosen arbitrarily and this value is maintained throughout the problem. The position of the conjugate force for each member is calculated using equation (4·18), i.e. $b = a \tan\phi$. Where a bar in the system is horizontal, $\phi = 0$ and therefore $\tan\phi = 0$. The value of b is also zero and the line of action of the conjugate force corresponds to the member axis. Where ϕ is not equal to zero various values for b will be obtained and the lines of action of the conjugate forces will be those shown as broken lines in Figure 23(d).

A simple rule can be stated as to which side of the member plan to draw the conjugate force line. For the force system shown in Figure 23(a), with R positive and a clockwise couple of Mo, if the observer ascends along the line of action of the force F, from O, the conjugate force F' lies on his right. If the observer descends from O then the conjugate force lies to his left.

Having produced the conjugate force lines on a plan of the space system it is then an easy matter to obtain a conjugate force diagram as illustrated in Figure 23(b). First consider the joint B_1. The conjugate force lines for the members A_1B_1 and B_1B_2 meet at a. For bar A_8B_1, its conjugate force meets the line of action of the external load W, acting on the joint B_1, at b. The graphical solution to this problem depends upon the fact that the conjugate forces must have a common resultant, R_1, acting along the axis ab. To complete the stress diagram the conjugate force W_1, for the external load, is first drawn to scale and from the known directions of R_1 and the other conjugate force lines the solution can be obtained. When several members meeting at a joint lie in one plane the conjugate force lines intersect at a common point. This is illustrated by the joint B_2 in Figure 23(d). The actual forces in the space system are found from equation (4·16) once the complete conjugate force diagram has been obtained.

The advantages of this method of analysis, which employs conjugate forces, increases with the complexity of the system. Member conjugate force lines have only to be drawn once and when solutions are required for various external load systems the necessary force lines need only be added when required.

CHAPTER V

THE STRESS ANALYSIS OF STATICALLY INDETERMINATE PIN-JOINTED SPACE FRAMES

5.1 ELASTIC DEFORMATION AND STRAIN ENERGY

Under the action of applied loads space frameworks undergo a small amount of deformation. If the structure is statically determinate, this deformation has little effect on the internal stress distribution produced in the system and the loaded configuration can be assumed to be the same as the unloaded configuration. However, with statically indeterminate space frames, small deformations have a significant effect on the stress distribution induced in the system and need to be studied before a complete analysis can be obtained.

Most materials, within certain limits, can be regarded as elastic i.e. they regain their original form and dimensions after the load has been removed. Such materials obey Hooke's Law which states that, within the elastic limit, a strain is proportional to the stress producing it. In the case of a bar under tension, Figure 24(a), a straight line relationship between load and deflection is obtained as shown in Figure 24(b). When the load P is increased the bar elongates and work is done which is stored in the bar in the form of strain energy.

To calculate the amount of strain energy produced in a bar the effect of the load P_1, as seen in Figure 24(b), is first considered. The load P_1 creates an elongation δ_1 in the bar. Any further increase of load dP_1 produces an additional elongation $d\delta_1$ and the work done is given by $P_1 d\delta_1$. This work is represented by the area bcde. Neglecting the area of bcf, which is a small quantity of second order, the total

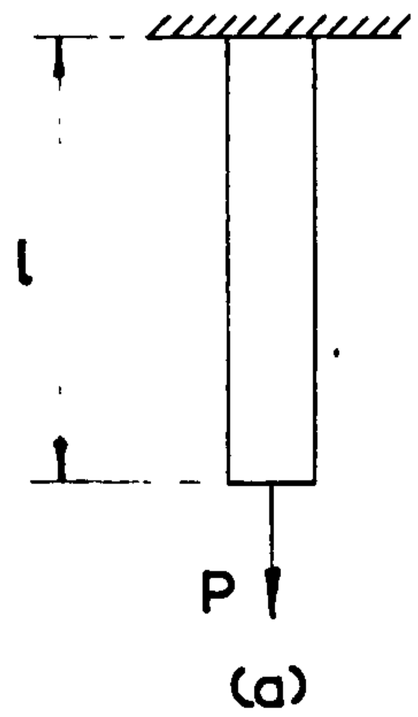

(a)

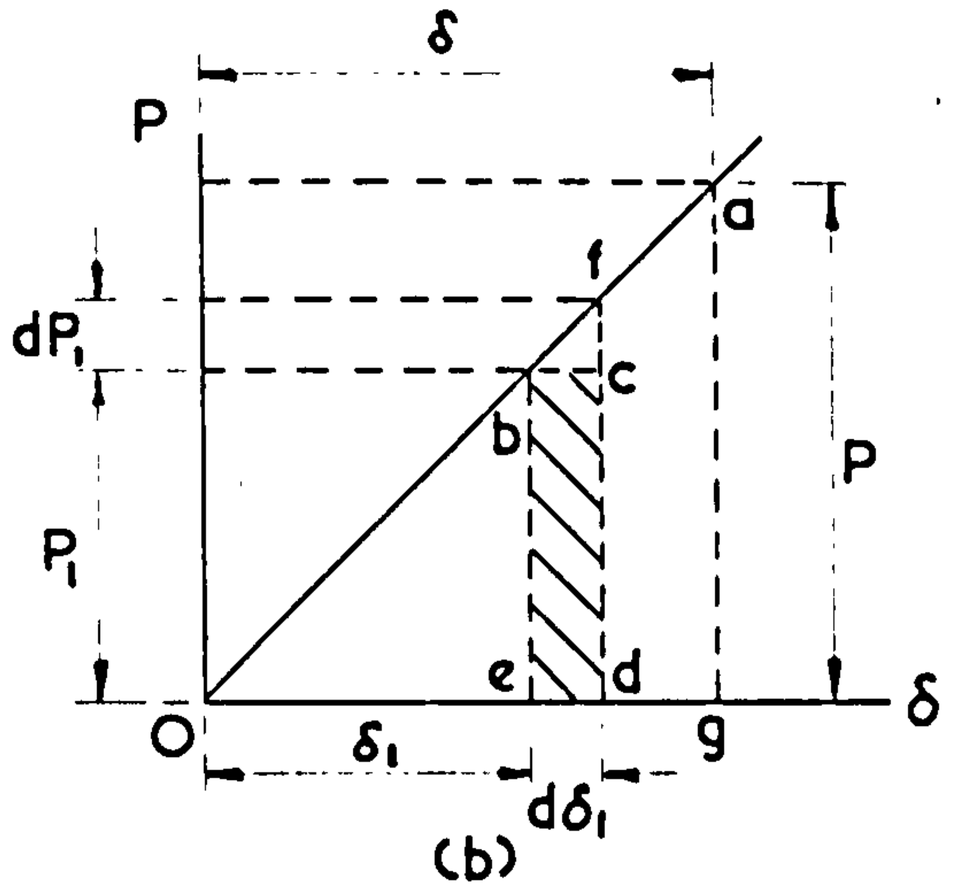

(b)

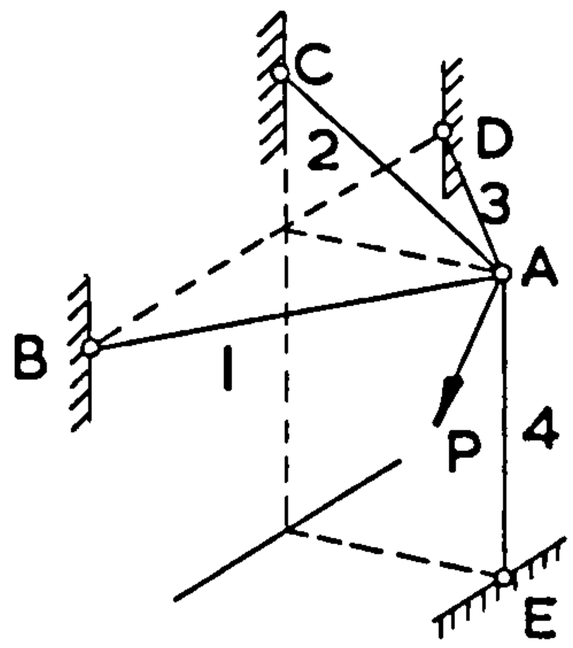

(c)

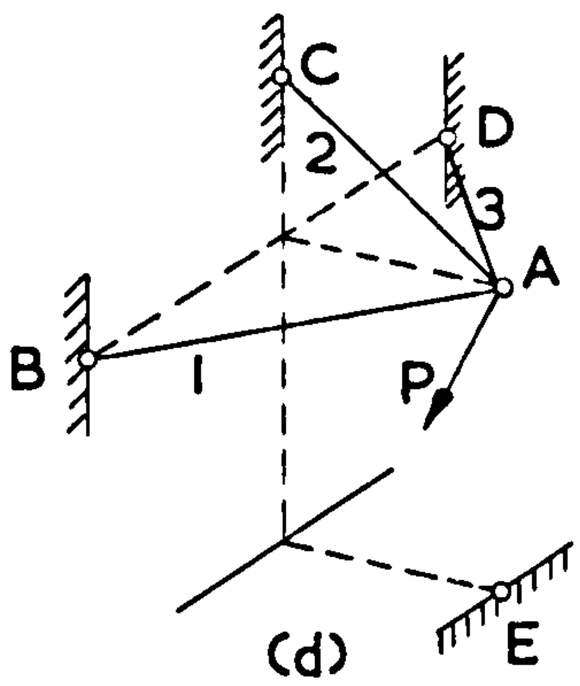

(d)

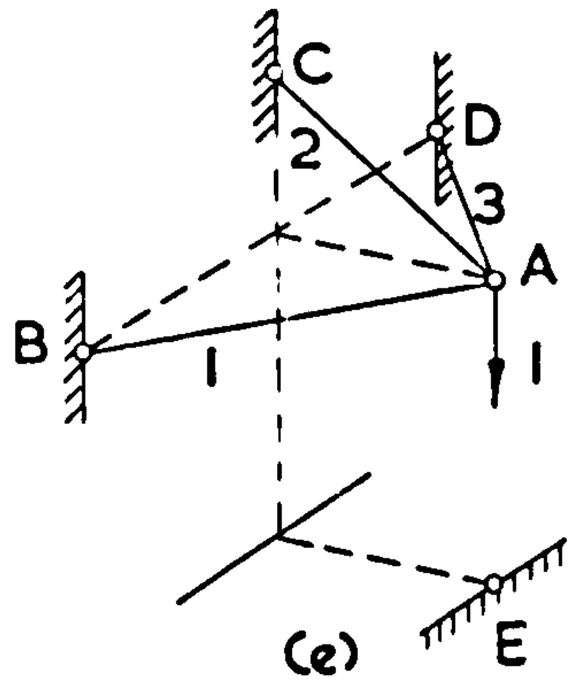

(e)

FIG. 24 THE ELASTIC DEFORMATION OF STATICALLY INDETERMINATE PIN-JOINTED SPACE FRAMES

F.A.A. Ph.D. Thesis
7th July, 1969

Structural Engineering Division
Department of Civil Engineering
University of Newcastle upon Tyne

work done due to any load P is given by the summation of all elements, similar to bcde, under the load-deflection curve. Hence the total strain energy stored in the bar is obtained from the expression:

$$U = \frac{P\delta}{2} \quad \ldots\ldots\ldots (5\cdot1)$$

where U is the total strain energy. Since the Elastic Modulus, E, of the bar is defined as the ratio of the stress on the cross-section to its longitudinal strain there exists the relationship:

$$E = \frac{Pl}{A\delta} \quad \ldots\ldots\ldots (5\cdot2)$$

where A is the area of the cross-section. Substituting for δ in equation (5·1) the strain energy in the bar can be denoted by:

$$U = \frac{P^2 l}{2AE} \quad \ldots\ldots\ldots (5\cdot3)$$

5.2 THE THEOREM OF LEAST WORK

The second theorem of Castigliano is represented by the relationship[19]:

$$\Delta = \frac{\delta U}{\delta W} \quad \ldots\ldots\ldots (5\cdot4)$$

where Δ is the displacement of any point in the structure due to the corresponding load W. In statically indeterminate structures the redundant members are restrained and have no displacements, hence, if X, Y, Z ..... represent the redundant forces, the following equations are obtained:

$$\frac{\delta U}{\delta X} = 0 \; ; \; \frac{\delta U}{\delta Y} = 0 \; ; \; \frac{\delta U}{\delta Z} = 0 \text{ etc. } \ldots\ldots (5\cdot5)$$

where U is a second-degree function of X, Y, Z, ... By differentiating twice with respect to the redundant forces and seeing that they are positive it can be determined that the strain energy function, U, is a minimum. This means the structure willdeform in such a way as to keep its strain energy, or work done by the external forces, to a minimum. The statement just iterated is known as the theorem of least work and is very useful for analysing statically indeterminate frames. From equations (5·5) the values of the redundant reactions are easily obtained as there are always as many equations as the unknown forces.

5.3 APPLICATION OF THE THEOREM OF LEAST WORK TO THE STRESS ANALYSIS OF STATICALLY INDETERMINATE PIN-JOINTED SPACE FRAMES[13]

The space frame in Figure 24(c) consists of four bars AB, AC, AD and AE which attach the joint A to a foundation as shown. AB and AD lie in a horizontal plane whereas AC and AE lie in a vertical plane. Considering the conditions m = 3j for a statically determinate system of bars in space attached to a foundation, it can be seen that the frame has one redundant member which will be taken as bar AE. When a load P is applied at the joint A the internal force in the redundant member AE will have a value of X. The forces in the other members are then given by the expression:

$$S_i = S_i' + s_i' X \quad \ldots\ldots\ldots \quad (5.6)$$

where S_i is the force in any member i, S_i' is the force in the same member when the load P is applied to the primary frame with AE removed, Figure 24(d), and s_i' is the influence number for the member i. These influence numbers are obtained by applying a unit load in place of the redundant member, Figure 24(e), in order to calculate the corresponding axial forces in the primary frame system.

To obtain the redundant force by the theorem of least work, the strain energy expression (5·3) becomes:

$$U = \sum \frac{S_i^2 l_i}{2A_i E} + \frac{X^2 l_o'}{2A_o E} = \frac{1}{2}\left(\sum S_i^2 \rho_i + X^2 \rho_o\right) \quad \ldots\ldots \quad (5.7)$$

for the complete space frame. Setting $\frac{\delta U}{\delta X} = 0$ this expression is reduced to:

$$\frac{\delta U}{\delta X} = \sum S_i s_i' \rho_i + X \rho_o = 0 \quad \ldots\ldots \quad (5.8)$$

If ρi is the same for all members then, on substituting for S_i from equation (5·6), X is given from :

$$X = -\frac{\sum S_i' s_i'}{\sum (s_i')^2 + 1} \quad \ldots\ldots \quad (5.9)$$

Once X has been evaluated the forces in the members can be obtained

from equation (5·6).

When solving for X it is best to set out all the forces in a tabular form so that the summation of the various forces can be carried out without much difficulty. Since the strain energy methods of solution require a consideration of all individual members in a structure their use is limited to systems which contain only a few bars.

5.4 THE MAXWELL-MOHR METHOD[13]

The Maxwell-Mohr method of calculating the deflections of joints in a space truss may be employed to find the stress distribution in such a system. A joint will deflect under the action of any change in length of individual members and the total deflection can be obtained by summating these separate effects.

Considering the space frame illustrated in Figure 24(c) without the load P. If the bar AE is removed and a unit load applied at A in place of P, then to ensure equilibrium of the system a force of s_i' must be added in the direction of AE. In other words the unit load would produce a force of s_i' in bar AE. The small deflection of the joint A under the action of the unit load in the direction of P will be $\Delta\delta$ whereas the small deflection of member AE under the force s_i' is Δl_i. Applying the principle of virtual displacements to the system, which is in equilibrium, the relationship:

$$1.\ \Delta\delta - s_i'.\ \Delta l_i = 0 \quad \ldots\ldots (5\cdot10)$$

is obtained since the work done on the small displacements must vanish. Transforming equation (5·10) gives:

$$\Delta\delta = \Delta l_i . s_i' \quad \ldots\ldots (5\cdot11)$$

Thus it can be seen that the deflection at joint A is obtained by multiplying the change in length of the bar AE by the ratio s_i'. Having found this factor the actual loading system can now be investigated.

The deflection in any member i along its axis and under load S_i

is $\frac{S_i l_i}{A_i E}$ so that the deflection of joint A in Figure 24(c), due to the elongation in the bar i, will be given by:

$$\Delta\delta = \frac{S_i l_i}{A_i E} \cdot s_i' = S_i \rho_i s_i' \quad \ldots\ldots (5\cdot12)$$

Summating for all the bars in the system and assuming the principle of superposition holds true for small displacements the total deflection is obtained from:

$$\delta = \sum S_i \rho_i s_i' + X\rho_o \quad \ldots\ldots (5\cdot13)$$

where X is the force in the redundant bar AL of the complete framework under load P. Since it is the function of a redundant force to prevent any displacement at its point of application δ is zero and hence equation (5·13) is the same as equation (5·8).

5.5 TEMPERATURE AND ERROR EFFECTS

Changes in length due to temperature and the effect of errors in bar lengths can be accommodated very easily when applying equation (5·8) in the analysis of statically indeterminate space frames.

Instead of $S_i\rho_i$ and $X\rho_o$ the expressions $S_i\rho_i + \alpha t_i l_i + \Delta_i$ and $X\rho_o + \alpha t_o l_o + \Delta_o$ can be employed where Δi represents the error in any bar and $\alpha t_i l_i$ is the change in length of any bar due to a variation in temperature. Equation (5·8) becomes:

$$\sum(S_i\rho_i + \alpha t_i l_i + \Delta_i)s_i' + X\rho_o + \alpha t_o l_o + \Delta_o = 0 \quad \ldots\ldots (5\cdot14)$$

from which

$$X = -\frac{\sum(S_i'\rho_i + \alpha t_i l_i + \Delta_i)s_i' + \alpha t_o l_o + \Delta_o}{\sum(s_i')^2\rho_i + \rho_o} \quad \ldots\ldots (5\cdot15)$$

This expression applies to any pin-connected space framework with one redundant member.

5.6 THE GAP REDUCTION METHOD

This approach to the solution of forces induced in loaded, highly redundant, pin-jointed space frames is a very powerful one. The method

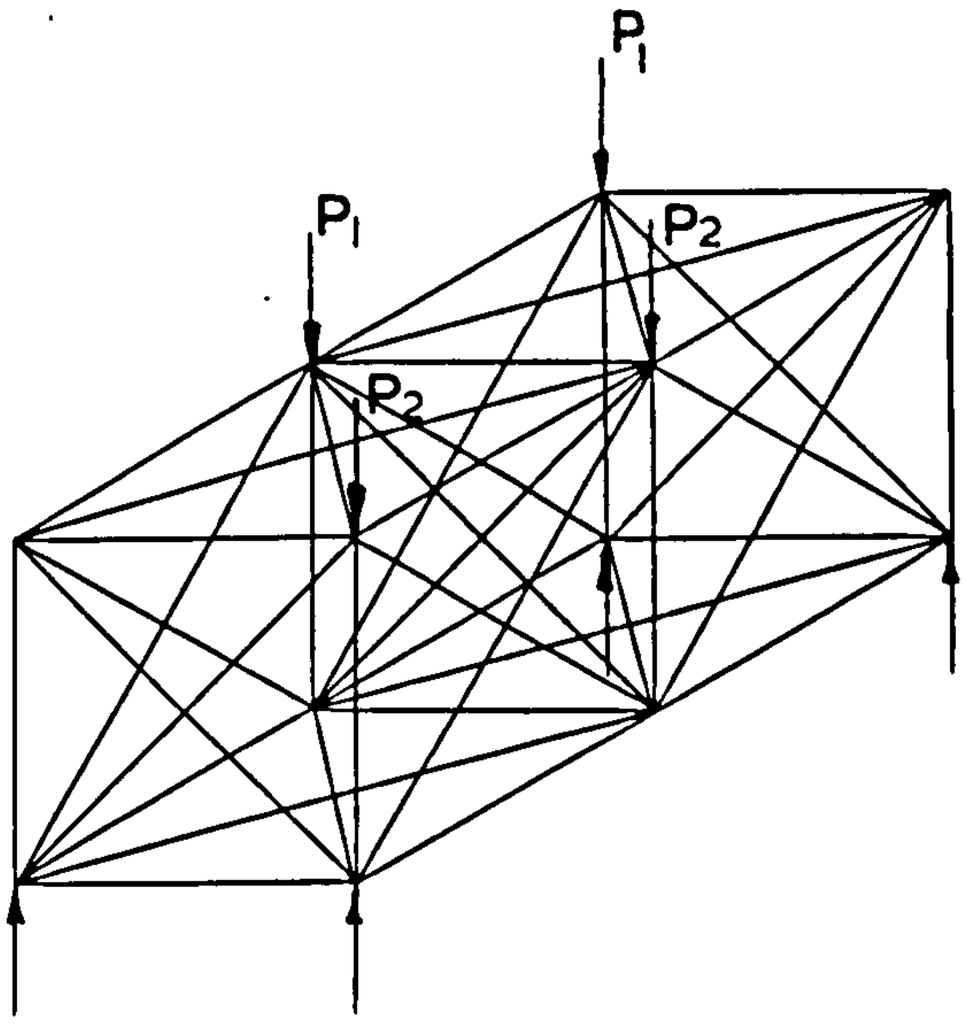

(a)

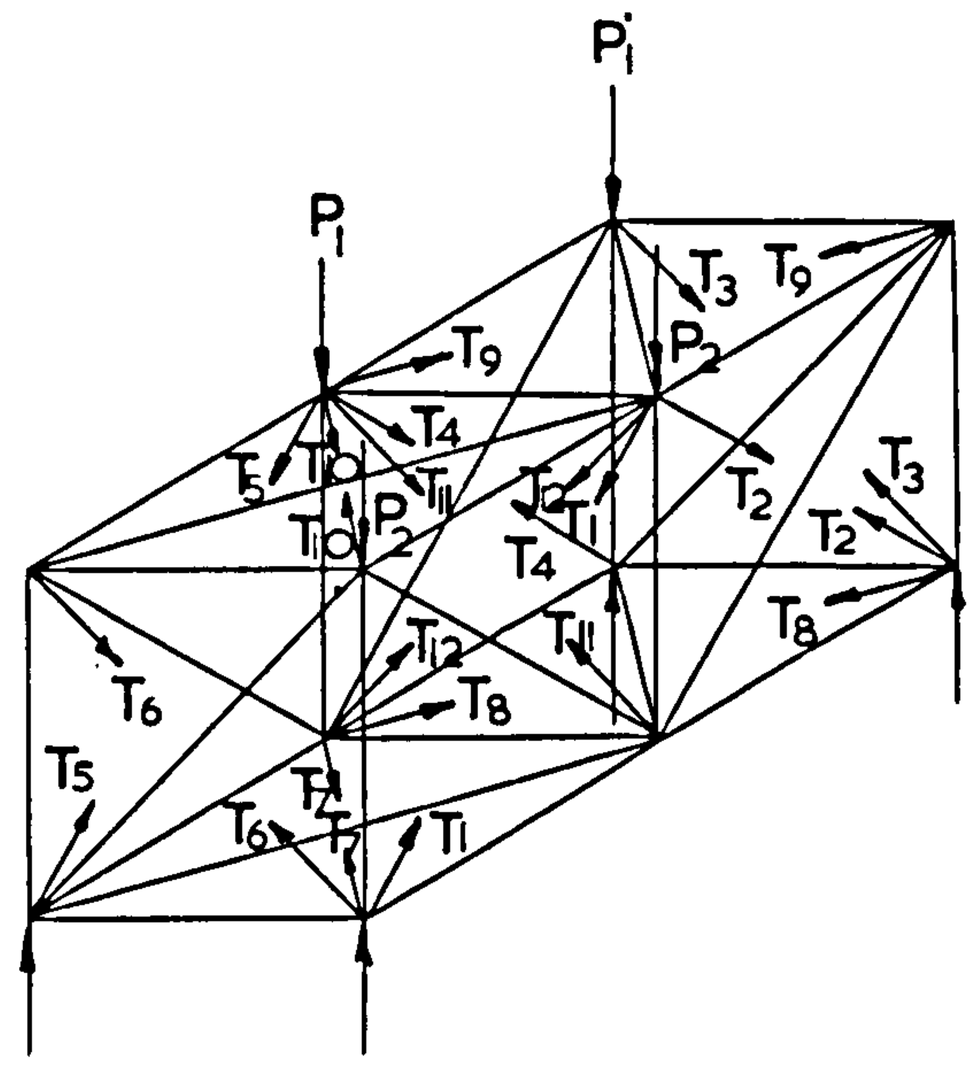

(b)

FIG. 25 THE GAP REDUCTION METHOD

F.A.A. Ph.D. Thesis
13th Oct., 1969

Structural Engineering Division
Department of Civil Engineering
University of Newcastle upon Tyne

was first put forward by Wright[20] for the analysis of plane frames and was extended to space systems by Byrne.[21]

Consider the loaded framework illustrated in Figure 25(a). The number of members, m, in the structure is 42. With j = 12 joints, a statically determinate self-contained system would require 3j - 6 members i.e. 30. Hence the redundancy is 12 and therefore twelve members must theoretically be cut to produce the statically determinate space frame which is shown in Figure 25(b). The forces W in the determinate frame, under the loads shown, can easily be calculated by inspection or by tension coefficients and are best set out in a tabular form to aid subsequent working out.

The next stage of the analysis consists of applying unit loads T_1, T_2 ....., along the axes of the cut bars and each series of forces, U_1 for T_1, U_2 for T_2, ..., which is induced in the space system by these loads, is tabulated alongside the determinate frame forces. Every member in the redundant frame extends an amount, e, under unit load and these extension values are calculated and tabulated from a knowledge of the cross-section size, member length and Elastic Modulus of the constituent material. The gaps in the cut members are determined from the expressions $\Sigma U_1 We$ for gap 1, $\Sigma U_2 We$ for gap 2, ...

In order to solve the problem it is necessary to find out what loads need to be applied to the cut members to close the gaps. Thus the effect of applying a unit load at one gap has to be considered for that gap and all the other gaps. The effect of applying a unit load at gap 1 produces $\Sigma U_1 U_1 e$ on gap 1, $\Sigma U_1 U_2 e$ on gap 2, ... Similarly a unit load applied at gap 2 produces $\Sigma U_2 U_1 e$ on gap 1, $\Sigma U_2 U_2 e$ on gap 2, ... These values, which are again best set out in a tabulated form, are known as operators. Having now obtained sufficient information regarding the interaction between gaps, the gap reduction process can begin.

The values of the original gaps, given by $\Sigma U_1 We$, $\Sigma U_2 We$ ....., are first written down and then reduced systematically until negligible by using the operators. To obtain the forces required to close the gaps, a simple summation of the T values is all that is necessary and the forces in the other members can easily be deduced from the original table containing the series of forces W,T and U. Although the technique, which is employed in the method just described, is a relaxational one involving the liquidation of unbalanced forces, the physical concept of reducing gaps is quite different to that involved in orthodox solutions by relaxation methods.

5.7 THE INFLUENCE COEFFICIENTS METHOD[10]

Influence coefficients can be employed to calculate stresses in redundant pin-jointed frameworks. An influence coefficient is the value of the force which occurs at a joint when it, or some adjacent joint, undergoes a unit displacement in a known direction. The basis of this method of analysis is a relaxation process which involves the liquidation of unbalanced forces. Simultaneous equations are not encountered and the method is primarily concerned with the determination of the deformation in a structure. The relaxation approach to structural analysis involving influence coefficients is attributed to Southwell.[22]

First of all when analysing a structure, using influence coefficients, it is necessary to determine the stresses caused by a unit displacement of any joint in the framework assuming all other joints are fixed. This is known as the "unit problem". Once the interaction between all the joints is known, any specified load system can be dealt with.

Initially all joints in the framework are assumed to be fixed in position such that all the members are unstrained and all applied loads are taken directly by the imaginary joint constraints. On displacing

a joint in some specified direction the force developed from this joint is transferred, in part or as a whole, to the rigidly held adjacent constraints. If now these constraints are relaxed and the joints allowed to move, then forces will again be transmitted to the next constraints. When this process is repeated many times loads appear again on constraints which previously have been relieved of load. Although this occurs, the forces which are transmitted to the constraints tend to decrease so that eventually the structure takes all the forces and negligible forces remain in the constraints. The remaining small constraint forces are known as residuals and can be brought below any defined limit by successive relaxation.

Stress determination involving relaxation methods does not give exact results by mathematical standards but it is sufficiently accurate for most design purposes. After the required standard of accuracy has been reached, the total displacements are obtained by summating the deflections imposed during the relaxation process and the forces in the members are found from these known distortion characteristics.

When analysing pin-jointed space frameworks using influence coefficients and the relaxation process, the constraints at any joint have only to control its three component displacements. To obtain a solution for the "unit problem" involved here it is necessary to consider a member MF, connecting two joints, M and F, which have any position relative to each other. Joint F is fixed and displacements of u, v, w are imposed on M. It is now required to find the forces which are imposed by the member on F and M and these forces are obtained from the following equations:

$$
\begin{aligned}
-X_M = X_F &= \Omega_{MF}(\Delta x^2 u + \Delta x.\Delta y.v + \Delta x.\Delta z.w) \\
-Y_M = Y_F &= \Omega_{MF}(\Delta y.\Delta x.u + \Delta y^2 v + \Delta y.\Delta z.w) \qquad \ldots\ldots (5.16 \\
-Z_M = Z_F &= \Omega_{MF}(\Delta z.\Delta x.u + \Delta z.\Delta y.v + \Delta z^2.w)
\end{aligned}
$$

where $\Omega_{MF} = \frac{EA}{L^3}$ A = cross-sectional area of bar MF
L = Length
E = Modulus of Elasticity of bar material

and Δx, Δy, Δz represent $(x_M - x_F)$, $(y_M - y_F)$, $(z_M - z_F)$ respectively. Equations (5·16) can be expressed more concisely in terms of influence coefficients as follows:

$$X_F = \widehat{xx}_F.u + \widehat{xy}_F.v + \widehat{xz}_F.w$$
$$Y_F = \widehat{yx}_F.u + \widehat{yy}_F.v + \widehat{yz}_F.w \qquad \ldots\ldots (5·17)$$
$$Z_F = \widehat{zx}_F.u + \widehat{zy}_F.v + \widehat{zz}_F.w$$

where:

$$\begin{aligned}
-\widehat{xx}_M &= \widehat{xx}_F = \Omega_{MF}(\Delta x)^2 \\
-\widehat{yy}_M &= \widehat{yy}_F = \Omega_{MF}(\Delta y)^2 \\
-\widehat{zz}_M &= \widehat{zz}_F = \Omega_{MF}(\Delta z)^2 \\
-\widehat{xy}_M &= \widehat{xy}_F = \Omega_{MF}(\Delta x.\Delta y) = \widehat{yx}_F = -\widehat{yx}_M \\
-\widehat{yz}_M &= \widehat{yz}_F = \Omega_{MF}(\Delta y.\Delta z) = \widehat{zy}_F = -\widehat{zy}_M \\
-\widehat{zx}_M &= \widehat{zx}_F = \Omega_{MF}(\Delta z.\Delta x) = \widehat{xz}_F = -\widehat{xz}_M
\end{aligned} \qquad \ldots\ldots (5.18)$$

The terms $\widehat{xx}$, $\widehat{xy}$, $\widehat{xz}$, ..., are the influence coefficients and for any joint A, say, $\widehat{xx}_A$, $\widehat{xy}_A$, $\widehat{xz}_A$, represent the forces in the x-direction which come on A as a result of unit displacements in the directions of x, y and z respectively. Influence coefficient values depend upon the properties of the member whose joints are being displaced; these values should be determined for each member in a structure and set out in a table. Once this table has been prepared, a displacement can be caused at any joint and the forces which are imposed by the framework on the constraints, as a result of this process, can be obtained.

From equations (5·17), the forces developed by applying a unit displacement, i.e. u = 1, along the X - X axis with no displacements in the directions of the other axes, can be determined. For this case the values of the influence coefficients will be as follows:

$$X_M = -\widehat{xx}_F$$
$$Y_M = -\widehat{yx}_F$$

$$Z_M = - \widehat{zx}_F$$

For any number of bars attached at joint M it can be seen that, by superposition, the forces become:

$$X_M = - \sum \widehat{xx}_F$$

$$Y_M = - \sum \widehat{yx}_F$$

$$Z_M = - \sum \widehat{zx}_F$$

Unit displacements in the directions of the Y-Y and Z-Z axes produce:

$$X_M = - \sum \widehat{xy}_F \qquad X_M = - \sum \widehat{xz}_F$$

$$Y_M = - \sum \widehat{yy}_F \qquad Y_M = - \sum \widehat{yz}_F$$

$$Z_M = - \sum \widehat{zy}_F \qquad Z_M = - \sum \widehat{zz}_F$$

These summations are carried out for all members attached to M.

An "operations table" can now be prepared which contains all the unit displacement effects. This table requires two lines for each joint displacement, the first of which gives the forces resulting from unit displacement. In the second line the largest of these forces is reduced to some convenient value while, at the same time, the remaining forces and deflections are reduced in proportion. The second line also shows directly the deflection of any joint which is required to remove the residuals acting on this joint.

After completing the "operations table" the relaxation process can commence. A displacement is applied at each joint such that the residuals at the joints are reduced until they reach a negligible value. Summation of the individual displacements at each joint gives the total deflection employed and the bar forces are obtained from the known equation:

$$T_{MF} = (L.\Omega\epsilon)_{MF} = \Omega_{MF} \left(\Delta x.u + \Delta y.v + \Delta z.w \right)$$

$$= \Omega_{MF} \left[(x_M - x_F)(u_M - u_F) + (y_M - y_F)(v_M - v_F) + (z_M - z_F)(w_M - w_F) \right] \quad \ldots (5.19)$$

In this equation ϵ is the total extension of the member MF due to strain.

The labour involved in working out a solution for tho stress distribution in pin-jointed space frameworks, using influence coefficients, depends entirely upon the number of joints present. Hence redundancy is not so important as it is in the more classical methods.

CHAPTER VI

THE STRESS ANALYSIS OF STATICALLY INDETERMINATE SPACE FRAMES WITHOUT PIN-JOINTS

6.1 THE INFLUENCE COEFFICIENTS METHOD

The classical methods of analysis, by strain energy, slope deflection or moment distribution, can be applied to rigidly jointed space frameworks but are limited to structures of low redundancy. Where high redundancies occur, relaxation methods can sometimes be employed and the process of employing influence coefficients, which was first discussed in Art. 5.7, will now be discussed with reference to rigid frames.

To define a configuration completely for a rigidly jointed space structure, the directions of the ends of each member must be specified as well as the joint positions. This means that three components of rotation must also be controlled along with the three displacement components. Residual forces only are sustained in the constraints of pin-jointed structures whereas, in rigid frameworks, residual forces and residual moments are sustained by the constraints. This is due to the fact that in rigid frames the joint rotation transmits couples to adjacent joints by shearing and torsion actions. The "unit problem", involving a study of the forces and couples produced by terminal displacements in any member, is more complicated for rigid frames than it is for pin-jointed structures because of the necessity to resist the joint rotations.

Referring to any arbitrarily orientated member MF, which is straight and uniform, the central line of the member is taken as the direction Ox and the principal axes of inertia of the cross-section

have the directions Oy, Oz respectively. A relationship exists between x, y, z and the fixed directions x', y', z' which is given by the orthogonal scheme:

	x'	y'	z'
x	l	m	n
y	l_1	m_1	n_1
z	l_2	m_2	n_2

where l, m, n, etc., are the direction-cosines and satisfy the condition that:

$$\begin{vmatrix} l & m & n \\ l_1 & m_1 & n_1 \\ l_2 & m_2 & n_2 \end{vmatrix} = +1$$

If u_M, v_M, w_M are the component displacements of the moved joint M in the directions Ox', Oy', Oz' respectively and p_M, q_M, r_M are the component rotations of M about axes parallel to Ox', Oy', Oz' respectively, then the forces and couples acting on the end M can be expressed in terms of influence coefficients as follows:

$$\begin{aligned}
X &= \widehat{xx}.u_M + \widehat{xy}.v_M + \widehat{xz}.w_M + \widehat{xp}.p_M + \widehat{xq}.q_M + \widehat{xr}.r_M \\
Y &= \widehat{yx}.u_M + \widehat{yy}.v_M + \widehat{yz}.w_M + \widehat{yp}.p_M + \widehat{yq}.q_M + \widehat{yr}.r_M \\
Z &= \widehat{zx}.u_M + \widehat{zy}.v_M + \widehat{zz}.w_M + \widehat{zp}.p_M + \widehat{zq}.q_M + \widehat{zr}.r_M \\
M_x &= \widehat{px}.u_M + \widehat{py}.v_M + \widehat{pz}.w_M + \widehat{pp}.p_M + \widehat{pq}.q_M + \widehat{pr}.r_M \\
M_y &= \widehat{qx}.u_M + \widehat{qy}.v_M + \widehat{qz}.w_M + \widehat{qp}.p_M + \widehat{qq}.q_M + \widehat{qr}.r_M \\
M_z &= \widehat{rx}.u_M + \widehat{ry}.v_M + \widehat{rz}.w_M + \widehat{rp}.p_M + \widehat{rq}.q_M + \widehat{rr}.r_M
\end{aligned} \quad \ldots\ldots (6.1)$$

The values of the influence coefficients depend upon the fixity of the connections at the ends M and F, Two systems may be encountered in practice, one in which both ends are rigidly fixed and the other having one end fixed while the opposite end is freely jointed. Cases also occur where no resistance is offered to one, two or three components of joint connection. The values of the influence coefficients are

given as follows:[10]

(a) Member MF having both ends stiffly jointed

$$\widehat{xx} = \frac{EA}{L}.l^2 + \frac{12}{L^3}(B_2 l_1^2 + B_1 l_2^2)$$

$$\widehat{yy} = \frac{EA}{L}.m^2 + \frac{12}{L^3}(B_2 m_1^2 + B_1 m_2^2)$$

$$\widehat{zz} = \frac{EA}{L}.n^2 + \frac{12}{L^3}(B_2 n_1^2 + B_1 n_2^2)$$

$$\widehat{zy} = \widehat{yz} = \frac{EA}{L}.mn + \frac{12}{L^3}(B_2 m_1 n_1 + B_1 m_2 n_2)$$

$$\widehat{xz} = \widehat{zx} = \frac{EA}{L}.nl + \frac{12}{L^3}(B_2 n_1 l_1 + B_1 n_2 l_2)$$

$$\widehat{yx} = \widehat{xy} = \frac{EA}{L}.lm + \frac{12}{L^3}(B_2 l_1 m_1 + B_1 l_2 m_2)$$

$$\widehat{pp} = \frac{C}{L}.l^2 + \frac{4}{L}(B_1 l_1^2 + B_2 l_2^2)$$

$$\widehat{qq} = \frac{C}{L}.m^2 + \frac{4}{L}(B_1 m_1^2 + B_2 m_2^2)$$

$$\widehat{rr} = \frac{C}{L}.n^2 + \frac{4}{L}(B_1 n_1^2 + B_2 n_2^2)$$

$$\widehat{rq} = \widehat{qr} = \frac{C}{L}.m.n + \frac{4}{L}(B_1 m_1 n_1 + B_2 m_2 n_2)$$

$$\widehat{pr} = \widehat{rp} = \frac{C}{L}.n.l + \frac{4}{L}(B_1 n_1 l_1 + B_2 n_2 l_2) \qquad \ldots\ldots (6.2)$$

$$\widehat{qp} = \widehat{pq} = \frac{C}{L}.l.m + \frac{4}{L}(B_1 l_1 m_1 + B_2 l_2 m_2)$$

$$\widehat{px} = \widehat{xp} = \frac{6}{L^2}(B_2 - B_1)\, l_1.l_2$$

$$\widehat{qx} = \widehat{xq} = \frac{6}{L^2}(B_2 l_1 m_2 - B_1 l_2 m_1)$$

$$\widehat{rx} = \widehat{xr} = \frac{6}{L^2}(B_2 l_1 n_2 - B_1 l_2 n_1)$$

$$\widehat{py} = \widehat{yp} = \frac{6}{L^2}(B_2 m_1 l_2 - B_1 m_2 l_1)$$

$$\widehat{qy} = \widehat{yq} = \frac{6}{L^2}(B_2 - B_1)\, m_1.m_2$$

$$\widehat{ry} = \widehat{yr} = \frac{6}{L^2}(B_2 m_1 n_2 - B_1 m_2 n_1)$$

$$\widehat{pz} = \widehat{zp} = \frac{6}{L^2}(B_2 n_1 l_2 - B_1 n_2 l_1)$$

$$\widehat{qz} = \widehat{zq} = \frac{6}{L^2}(B_2 n_1 m_2 - B_1 n_2 m_1)$$

$$\widehat{rz} = \widehat{zr} = \frac{6}{L^2}(B_2 - B_1)\, n_1.n_2$$

In these expressions:

E denotes the Modulus of Elasticity for the material;

L is the length;

A is the cross-sectional area of the member;

B_1 (= EAk_1^2) is its flexural rigidity about an axis parallel to Oy;

B_2 (= EAk_2^2) is its flexural rigidity about an axis parallel to Oz;

C is the torsional rigidity of the cross-section.

(a) <u>Member MF in which end M is stiffly jointed and end F is freely jointed</u>

Since the end F of the member MF is pin-jointed, p_F, q_F, r_F are unresisted. Hence the influence coefficient values are:

$$\widehat{xx} = \frac{EA}{L}.l^2 + \frac{3}{L^3}(B_2l_1^2 + B_1l_2^2)$$

$$\widehat{yy} = \frac{EA}{L}.m^2 + \frac{3}{L^3}(B_2m_1^2 + B_1m_2^2)$$

$$\widehat{zz} = \frac{EA}{L}.n^2 + \frac{3}{L^3}(B_2n_1^2 + B_1n_2^2)$$

$$\widehat{zy} = \widehat{yz} = \frac{EA}{L}.m.n. + \frac{3}{L^3}(B_2m_1n_1 + B_1m_2n_2)$$

$$\widehat{xz} = \widehat{zx} = \frac{EA}{L}.n.l + \frac{3}{L^3}(B_2n_1l_1 + B_1n_2l_2)$$

$$\widehat{yx} = \widehat{xy} = \frac{EA}{L}.l.m + \frac{3}{L^3}(B_2l_1m_1 + B_1l_2m_2)$$

$$\widehat{pp} = \frac{3}{L}(B_1l_1^2 + B_2l_2^2)$$

$$\widehat{qq} = \frac{3}{L}(B_1m_1^2 + B_2m_2^2) \qquad \ldots\ldots (6.3)$$

$$\widehat{rr} = \frac{3}{L}(B_1n_1^2 + B_2n_2^2)$$

$$\widehat{rq} = \widehat{qr} = \frac{3}{L}(B_1m_1n_1 + B_2m_2n_2)$$

$$\widehat{pr} = \widehat{rp} = \frac{3}{L}(B_1n_1l_1 + B_2n_2l_2)$$

$$\widehat{qp} = \widehat{pq} = \frac{3}{L}(B_1l_1m_1 + B_2l_2m_2)$$

$$\widehat{px} = \widehat{xp} = \frac{3}{L^2}(B_2 - B_1)\,l_1.l_2$$

$$\widehat{qx} = \widehat{xq} = \frac{3}{L^2}(B_2l_1m_2 - B_1l_2m_1) \qquad \text{(cont.,)}$$

$$\widehat{rx} = \widehat{xr} = \frac{3}{L^2}(B_2 l_1 n_2 - B_1 l_2 n_1)$$

$$\widehat{py} = \widehat{yp} = \frac{3}{L^2}(B_2 m_1 l_2 - B_1 m_2 l_1)$$

$$\widehat{qy} = \widehat{yq} = \frac{3}{L^2}(B_2 - B_1)\, m_1 . m_2 \qquad \ldots\ldots (6\cdot3)$$

$$\widehat{ry} = \widehat{yr} = \frac{3}{L^2}(B_2 m_1 n_2 - B_1 m_2 n_1)$$

$$\widehat{pz} = \widehat{zp} = \frac{3}{L^2}(B_2 n_1 l_2 - B_1 n_2 l_1)$$

$$\widehat{qz} = \widehat{zq} = \frac{3}{L^2}(B_2 n_1 m_2 - B_1 n_2 m_1)$$

$$\widehat{rz} = \widehat{zr} = \frac{3}{L^2}(B_2 - B_1)\, n_1 . n_2$$

(c) Member MF in which end M is freely jointed and F is stiffly jointed

For this case, since M is the moved joint, p_M, q_M, r_M are unresisted and only u_M, v_M, w_M appear in equations (6.1) which are reduced to:

$$X = \widehat{xx}.u_M + \widehat{xy}.v_M + \widehat{xz}.w_M$$

$$Y = \widehat{yx}.u_M + \widehat{yy}.v_M + \widehat{yz}.w_M \qquad \ldots\ldots (6.4)$$

$$Z = \widehat{zx}.u_M + \widehat{zy}.v_M + \widehat{zz}.w_M$$

The values of the influence coefficients are:

$$\widehat{xx} = \frac{EA}{L}.l^2 + \frac{3}{L^3}(B_2 l_1^2 + B_1 l_2^2)$$

$$\widehat{yy} = \frac{EA}{L}.m^2 + \frac{3}{L^3}(B_2 m_1^2 + B_1 m_2^2)$$

$$\widehat{zz} = \frac{EA}{L}.n^2 + \frac{3}{L^3}(B_2 n_1^2 + B_1 n_2^2)$$

$$\widehat{zy} = \widehat{yz} = \frac{EA}{L}.m.n + \frac{3}{L^3}(B_2 m_1 n_1 + B_1 m_2 n_2) \qquad \ldots\ldots (6\cdot5)$$

$$\widehat{xz} = \widehat{zx} = \frac{EA}{L}.n.l + \frac{3}{L^3}(B_2 n_1 l_1 + B_1 n_2 l_2)$$

$$\widehat{yx} = \widehat{xy} = \frac{EA}{L}.l.m + \frac{3}{L^3}(B_2 l_1 m_1 + B_1 l_2 m_2)$$

The quantities X, Y, Z, M_x, M_y, M_z, in equations (6·1), are the forces and moments which come upon the member at its end M which moves. In consequence of this, the forces and moments which are exerted by the member on constraints are as follows:

(1) at the joint which is moved in the relaxation:

$$X_M,\ Y_M,\ Z_M,\ (M_x)_M,\ (M_y)_M,\ (M_z)_M = -\ (X,\ Y,\ Z,\ M_x,\ M_y,\ M_z)$$

(2) at the joint which is not moved:

$$\begin{aligned} X_F,\ Y_F,\ Z_F &= X,\ Y,\ Z \\ (M_x)_F &= M_x + L\ (nY - mZ) \\ (M_y)_F &= M_y + L\ (lZ - nX) \\ (M_z)_F &= M_z + L\ (mX - lY) \end{aligned} \qquad \ldots\ldots (6.6)$$

The forces X, Y, Z acting upon the moved and fixed joints can be seen to be equal in value, but opposite in sign. However the couples appearing at the fixed end, due to the movement of the other end, are completely different from the couples applied at the moved end. Equations (6·6) are not normally employed in this form as, in calculating moments by them, much additional work is required. It is much easier to modify the values of the influence coefficients which are used with equations (6·1) to give directly the forces and moments on the fixed and the moving joints. These are rather complicated in the general case but can be simplified by assuming the member has the same flexural rigidity against bending in all planes, i.e. $B_1 = B_2 = B$. The values of the influence coefficients are now given, under this assumption, as follows:

(a) Member MF having both ends stiffly jointed

For the moved joint	For the unmoved joint
$\widehat{xx}_M = -\ 12\ \frac{B}{L^3} - Fl^2$	$\widehat{xx}_F = 12\ \frac{B}{L^3} + Fl^2$
$\widehat{yy}_M = -\ 12\ \frac{B}{L^3} - Fm^2$	$\widehat{yy}_F = 12\ \frac{B}{L^3} + Fm^2$
$\widehat{zz}_M = -\ 12\ \frac{B}{L^3} - Fn^2$	$\widehat{zz}_F = 12\ \frac{B}{L^3} + Fn^2$
$\widehat{zy}_M = \widehat{yz}_M = -\ Fmn$	$\widehat{zy}_F = \widehat{yz}_F = Fmn$
$\widehat{xz}_M = \widehat{zx}_M = -\ Fnl$	$\widehat{xz}_F = \widehat{zx}_F = Fnl$
$\widehat{yx}_M = \widehat{xy}_M = -\ Flm$	$\widehat{yx}_F = \widehat{xy}_F = Flm$
$\widehat{pp}_M = -\ \frac{4B}{L} - G.l^2$	$\widehat{pp}_F = -\ 2\ \frac{B}{L} + H.l^2$

For the moved joint	For the unmoved joint
$\widehat{qq}_M = -4\frac{B}{L} - G.m^2$	$\widehat{qq}_F = -2\frac{B}{L} + H.m^2$
$\widehat{rr}_M = -4\frac{B}{L} - G.n^2$	$\widehat{rr}_F = -2\frac{B}{L} + H.n^2$
$\widehat{rq}_M = \widehat{qr}_M = -G.m.n$	$\widehat{rq}_F = \widehat{qr}_F = H.m.n$
$\widehat{pr}_M = \widehat{rp}_M = -G.n.l$	$\widehat{pr}_F = \widehat{rp}_F = H.n.l$
$\widehat{qp}_M = \widehat{pq}_M = -G.l.m$	$\widehat{qp}_F = \widehat{pq}_F = H.l.m$
$\widehat{px}_M = \widehat{xp}_M = \widehat{qy}_M = \widehat{yq}_M = \widehat{rz}_M = \widehat{zr}_M = 0$	$\widehat{px}_F = \widehat{xp}_F = \widehat{qy}_F = \widehat{yq}_F = \widehat{rz}_F = \widehat{zr}_F = 0$
$\widehat{qz}_M = \widehat{zq}_M = -\widehat{ry}_M = -\widehat{yr}_M = \frac{6B.l}{L^2}$	$\widehat{qz}_F = -\widehat{zq}_F = -\widehat{ry}_F = \widehat{yr}_F = \frac{6B.l}{L^2}$
$\widehat{rx}_M = \widehat{xr}_M = -\widehat{pz}_M = -\widehat{zp}_M = \frac{6B.m}{L^2}$	$\widehat{rx}_F = -\widehat{xr}_F = -\widehat{pz}_F = \widehat{zp}_F = \frac{6B.m}{L^2}$
$\widehat{py}_M = \widehat{yp}_M = -\widehat{qx}_M = -\widehat{xq}_M = \frac{6B.n}{L^2}$	$\widehat{py}_F = -\widehat{yp}_F = -\widehat{qx}_F = \widehat{xq}_F = \frac{6B.n}{L^2}$
(6.7)	(6.8)

In the above expressions, $F = \frac{EA}{L} - \frac{12B}{L^3}$, $G = \frac{C - 4B}{L}$ and $H = \frac{C + 2B}{L}$

(b) Member MF having one end stiffly jointed and the other end freely jointed

For the moved joint (stiffly jointed end)	For the unmoved joint (freely jointed end)
$\widehat{xx}_M = -3\frac{B}{L^3} - F_1 l^2$	$\widehat{xx}_F = 3\frac{B}{L^3} + F_1 l^2$
$\widehat{yy}_M = -3\frac{B}{L^3} - F_1 m^2$	$\widehat{yy}_F = 3\frac{B}{L^3} + F_1 m^2$
$\widehat{zz}_M = -3\frac{B}{L^3} - F_1 n^2$	$\widehat{zz}_F = 3\frac{B}{L^3} + F_1 n^2$
$\widehat{zy}_M = \widehat{yz}_M = -F_1 m.n$	$\widehat{zy}_F = \widehat{yz}_F = F_1 m.n$
$\widehat{xz}_M = \widehat{zx}_M = -F_1 n.l$	$\widehat{xz}_F = \widehat{zx}_F = F_1 n.l$
$\widehat{yx}_M = \widehat{xy}_M = -F_1 l.m$	$\widehat{yx}_F = \widehat{xy}_F = F_1 l.m$
$\widehat{pp}_M = -3\frac{B}{L} + 3\frac{B}{L}.l^2$	(6.10)
$\widehat{qq}_M = -3\frac{B}{L} + 3\frac{B}{L}.m^2$	All other coefficients for the unmoved joint are equal to zero and the final formulae are:
$\widehat{rr}_M = -3\frac{B}{L} + 3\frac{B}{L}.n^2$	

$$\widehat{rq}_M = \widehat{qr}_M = 3\,\frac{B}{L}.m.n$$

$$\widehat{pr}_M = \widehat{rp}_M = 3\,\frac{B}{L}.n.l$$

$$\widehat{qp}_M = \widehat{pq}_M = 3\,\frac{B}{L}.l.m$$

$$\widehat{px}_M = \widehat{xp}_M = \widehat{qy}_M = \widehat{yq}_M = \widehat{rz}_M = \widehat{zr}_M = 0$$

$$-\widehat{qz}_M = -\widehat{zq}_M = \widehat{ry}_M = \widehat{yr}_M = -3\,\frac{B}{L^2}.l$$

$$-\widehat{rx}_M = -\widehat{xr}_M = \widehat{pz}_M = \widehat{zp}_M = -3\,\frac{B}{L^2}.m$$

$$-\widehat{py}_M = -\widehat{yp}_M = \widehat{qx}_M = \widehat{xq}_M = -3\,\frac{B}{L^2}.n$$

(6·9)

$$X_F = \widehat{xx}_F.u_M + \widehat{xy}_F.v_M + \widehat{xz}_F.w_M$$

$$Y_F = \widehat{yx}_F.u_M + \widehat{yy}_F.v_M + \widehat{yz}_F.w_M$$

$$Z_F = \widehat{zx}_F.u_M + \widehat{zy}_F.v_M + \widehat{zz}_F.w_M$$

$$(M_x)_F = 0$$

$$(M_y)_F = 0$$

$$(M_z)_F = 0$$

because F is pin-jointed.

$F_1 = \frac{EA}{L} - 3\,\frac{B}{L^3}$ in the above equations.

The influence coefficient values, set out above, need to be determined for all members in a structure. Extreme care must be taken when calculating these values as errors will not be observed until the final structural analysis is complete. Hence, if errors are present at the beginning of the analysis, all work carried out in the subsequent relaxation process will be wasted.

Once the influence coefficient values are known the effect which any joint displacement has on a member, or group of members, connected at a particular joint can be deduced and an "operations table" drawn up. The relaxation process from this point onwards in the analysis is the same as that discussed in Art. 5·7. By successive approximations the residual forces X, Y, Z and the residual moments M_x, M_y, M_z are liquidated to negligible values. The total distortions are noted after completing the process of relaxation and the resulting stresses in the bars are then easily determined.

The main advantage of the relaxation method, which employs influence coefficients, is that redundancy has only a small effect on the time required to obtain a solution. In carrying out such an

analysis, the amount of work involved depends mainly upon the number of joints to be moved. The number of members in a structure governs only the time required for determining the influence coefficient values and preparing the "operations table". Once the tabulation is completed, the relaxation process, which involves the liquidation of residual forces, does not depend upon the number of redundant members present as the analysis involves only a study of the deflections of the joints. Thus the relaxation method of analysis provides not only the stresses in the bars of a framework but also the distorted shape under applied loads.

When using relaxation techniques, speed of convergence in the liquidation of the residual forces is very important. Block and group relaxation can be employed very effectively to achieve this end. Their application reduces the total number of separate operations in the liquidation process and therefore reduces the time required to solve particular problems. The groups and blocks, if properly chosen, simplify considerably the relaxation process and permit more rapid approximation to the result.

For complicated rigidly jointed space structures, the amount of calculation necessary to carry out a relaxation analysis will be enormous. With ordinary desk computers such an analysis will require several assistants working under the guidance of experienced relaxation people for several months. However for many highly redundant space structures, having rigid connections, the relaxation process offers the only possible means of analytical solution.

6.2 MATRIX METHODS[23]

An analysis of the stresses in a large, complex, statically indeterminate space frame by traditional manual methods requires an enormous amount of human effort. With the development of automatic computers in recent years a practical approach to structural analysis

has evolved which employs matrix algebra. Although matrix methods involve a large amount of systematic calculation, from the theoretical point of view they express the analysis in a compact and precise manner which is at the same time quite general. Thus the structural theory can be treated as a unified whole without the fundamental principles being obscured by computational devices on the one hand or physical differences between structures on the other. From a practical point of view the systematic approach to the analysis of structures, which matrix algebra provides, presents a suitable basis for the development of computer programs and has stimulated a large amount of research in this field.

Methods of structural analysis for linear space frameworks require that three sets of conditions are satisfied by the loads and displacements induced in the members and joints due to some external force system. These conditions are:

(1) The loads acting on the ends of each member and the displacements of those ends must satisfy equations derived from the stress-strain relationship of the material of the member.

(2) The displacements of the ends of each member must be compatible with the displacements of the joints to which the member is attached. These are termed the conditions of compatibility.

(3) The loads acting on the ends of each member must be such as will keep the member in equilibrium. Furthermore, the sum of the loads acting on the ends of the members meeting at any joint must equal the external load applied at the joint. These are termed the conditions of equilibrium.

Broadly speaking, it is possible to classify methods of structural analysis according to the order in which the conditions of equilibrium

and compatibility are applied. Methods in which the compatibility conditions are used first give rise to equations of joint equilibrium and are called equilibrium or displacement methods. Methods in which the equilibrium conditions are satisfied first lead to equations of displacement compatibility and are called compatibility or force methods.

The basis of the equilibrium approach to the analysis of space frameworks is that joint displacements are considered to be the fundamental unknowns. When applying this method, the first step consists of expressing the member end-loads in terms of the corresponding end-displacements. The member end-load expressions are, in general, integrals of the appropriate differential equations of extension, flexure or torsion associated with the member. They can be determined either by direct integration of the differential equations or by differentiating the appropriate strain energy expressions with respect to the end-displacements. For linear structures the member end-loads are linear functions of the end-displacements, the coefficients of the end displacements being functions of the dimensions and material properties of the members.

The next stage in the analysis consists of employing the conditions of compatibility to express the member end-displacements in terms of the joint displacements. In this manner expressions are obtained for the loads acting on the ends of the members in terms of the unknown joint displacements which satisfy the stress-strain conditions (1) and the compatibility conditions (2). These expressions for the member end-loads are now substituted into the equations of joint equilibrium. The result is a set of equations, the load-displacement equations of the structure, which relates the known joint loads to the unknown joint displacements. Each component of joint displacement contributes one equation to this set, the constant term in the equation being the corresponding component of the applied loading. The solution of the

set of equations gives the unknown joint displacements and the expressions already employed in setting up the equilibrium equations can be used to find the member end-loads. When carrying out an analysis by the equilibrium approach, the number of equations which have to be solved is equal to the total number of independent displacement variables, or degrees of freedom, of the structure and is not affected by whether the structure is statically determinate or not.

The compatibility approach to structural analysis employs, as its first step, expressions which contain the deformations in terms of member end-loads. These expressions are in the inverted form compared with the equilibrium approach which uses the stress-strain relations for the members to express end-loads in terms of end-displacements. After the deformations have been obtained in terms of member end-loads, the end-loads are expressed in terms of the redundant forces and moments, and the known external loads, by means of the conditions of equilibrium. Hence all the member deformations are obtained as functions of the external loads and the unknown redundants.

The next step consists of applying the compatibility conditions to these deformations and the result is a set of equations which, in effect, states that the structure is continuous at the points at which the redundant forces and moments act. Values for the redundant forces and moments are obtained by solving the set of equations. The member end loads can then be determined and the expressions for the member deformations in terms of the applied loads may be used to find the joint displacements.

A comparison of the equilibrium and compatibility approaches should be based on the amount of work which has to be done in setting up the equations and the ease with which the work can be systematized. With regard to these points, for space frameworks, the basic unknowns of the equilibrium approach, the joint displacements, are obvious physical

quantities associated with the structure. On the other hand, the basic unknowns of the compatibility approach are a certain number of forces and moments which must be chosen according to certain rules. Any general computer program based on the compatibility approach to structural analysis must include a systematic process for determining the number and location of these forces and moments.

In an analysis of space frameworks, as previously stated, use is made of the three basic sets of conditions involving the stress-strain relationships of the members, the compatibility conditions satisfied by the member end-displacements and the equilibrium conditions satisfied by the member end-loads. Before these equations can be expressed in general matrix form it is necessary to define a notation which is precise but general. When considering a general space frame, joints are donoted by capital letters A, B, ..., N, (or numbers 1, 2, ...,). Points at which the structure is attached to a rigid foundation are referred to as O and members in the framework are identified by lower case letters a, b, ..., n. In considering the properties of individual members, the suffixes 1 and 2 refer to the two ends with end 1 corresponding to the joint which has its identifying letter nearest the beginning of the alphabet. To define the orientation of a member in space it is necessary to specify the angle which it makes with the coordinate axes and the direction of the member is defined as the line running from end 1 to end 2.

Displacement vectors, in subsequent analysis procedures, are denoted by the symbol d, with appropriate suffixes to indicate the joint or member referred to. The displacement vectors include joint translations and rotations. They also refer to the corresponding group of quantities associated with member end-displacements. Each displacement vector for a general three-dimensional space frame has six components of which three are translations and three are rotations.

Similarly, the symbol p is used to denote the load vectors which consist of all the force and moment components acting on a joint or on the end of a member. For each component in a displacement vector there is a component in the corresponding load vector, forces being associated with translations and moments with rotations. Thus, in a general space frame with coordinate axes x, y, z, the displacement and load vectors have the general form:

$$d = \begin{bmatrix} \delta_x \\ \delta_y \\ \delta_z \\ \theta_x \\ \theta_y \\ \theta_z \end{bmatrix} \qquad p = \begin{bmatrix} p_x \\ p_y \\ p_z \\ m_x \\ m_y \\ m_z \end{bmatrix}$$

where δ , θ , p and m indicate translation, rotation, force and moment components respectively. Throughout the analysis procedure, a right-handed system of coordinate axes, as shown in Figure 26(a), is employed. Where a number of p's or d's are combined to form vectors representing the complete set of joint loads or joint displacements of a structure, such vectors are denoted by the symbols F and D.

When deriving the load-displacement relations for a particular member of a structure it is normal to consider a coordinate system which is best suited to the member. This is known as the member coordinate system. Since the structure is normally formed by connecting a number of members together, it is also necessary to have a common coordinate system for all the member end-loads and end-displacements. A set of coordinates used for defining the joint displacements of a structure, or the loading applied to it, is called a set of frame or system coordinates.

In some types of structure, such as continuous beams, the member and system coordinates are the same. However, in most cases, they are different and this necessitates a change from one to the other. This transformation can be carried out quite easily by matrix notation.

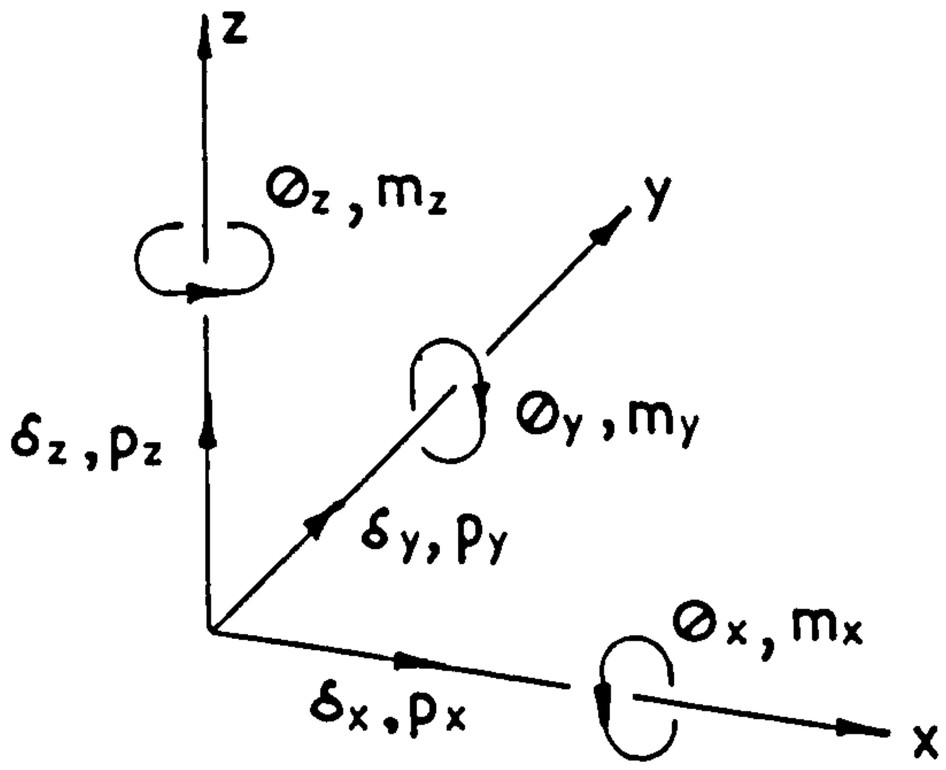

(a) Coordinate Axes

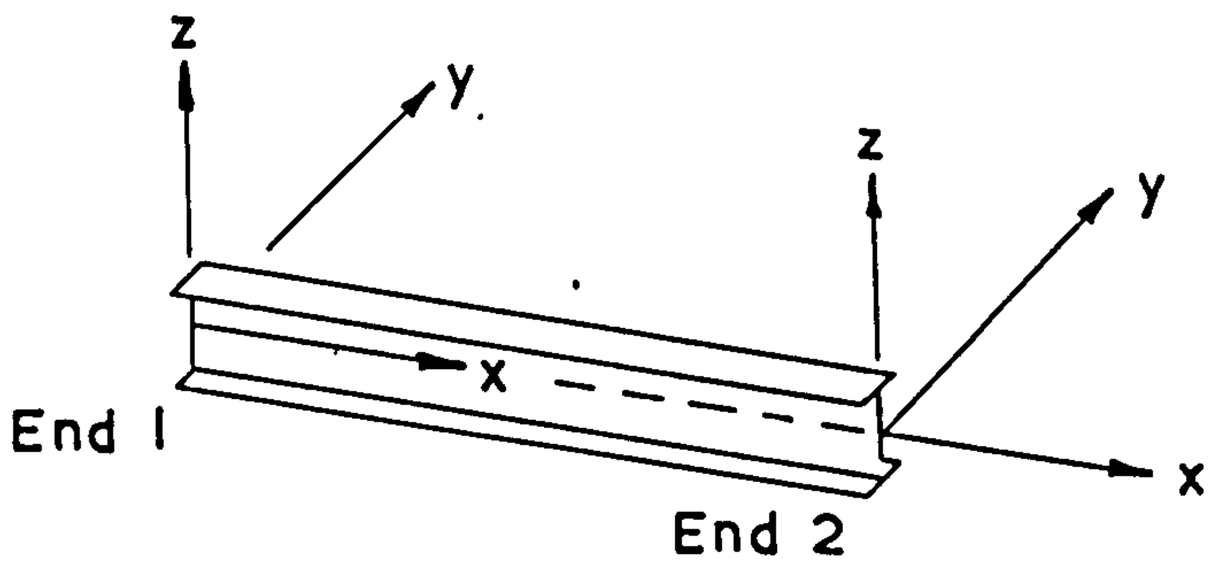

(b) Member Coordinate System

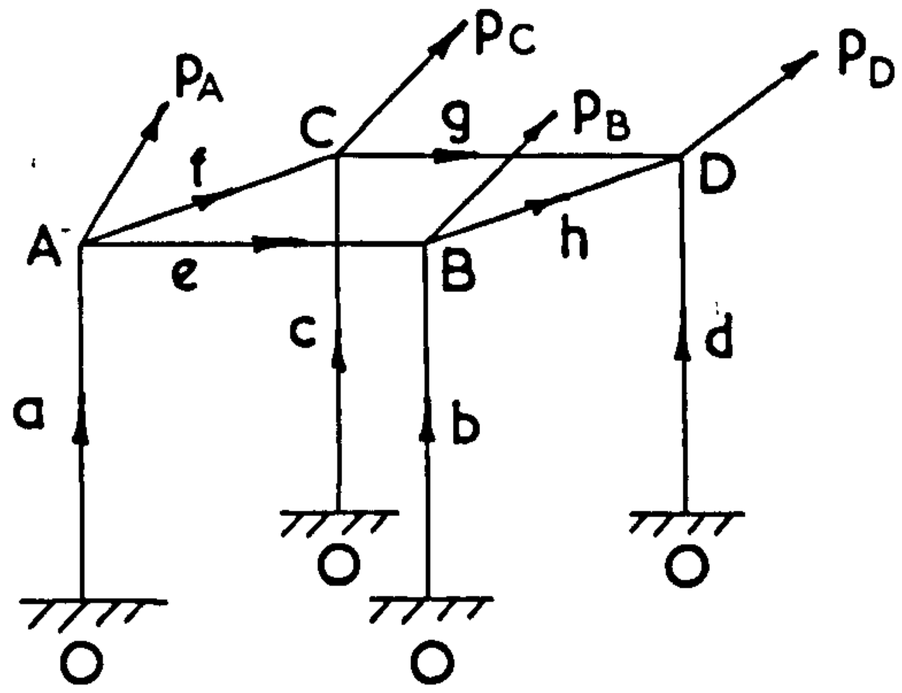

(c)

FIG. 26 MATRIX METHODS Sheet No. 1

F.A.A. Ph.D. Thesis
4th Dec., 1969

Structural Engineering Division
Department of Civil Engineering
University of Newcastle upon Tyne

Hence, normal structural analysis procedures consist of developing equations for the various types of structural element in their own appropriate coordinate systems and then transforming the equations into system coordinates.

The equations connecting the end-loads and the end-displacements of a structural member can be written, for the equilibrium method, in the following form:

$$\begin{aligned} p_1 &= K_{11}\, d_1 + K_{12}\, d_2 \\ p_2 &= K_{21} d_1 + K_{22} d_2 \end{aligned} \quad \ldots\ldots (6\cdot11)$$

In these expressions p_1, p_2 represent the end-loads and d_1, d_2 represent the end displacements. The members are also assumed to behave in a linear manner. The equilibrium method, as described earlier in this Art., employs the conditions of displacement compatibility and joint equilibrium to construct the set of load-displacement equations for a complete structure out of the load-displacement equations (6·11) of the individual members. This set of equations is written:

$$P = KD \quad \ldots\ldots (6\cdot12)$$

where P indicates the complete set of applied joint loads and D indicates the corresponding set of unknown joint displacements. K is referred to as the stiffness matrix of the structure and K_{11}, K_{12}, etc., in equations (6·11), are known as member stiffness matrices.

At first sight it might seem that equations (6·11) could also be written in an analogous form, the displacements d_1, d_2 being expressed in terms of the loads p_1, p_2. However, it is not possible. While the end-loads are defined for any pair of end-displacements, the converse is not true since the member may be given an arbitrary rigid-body displacement without affecting the forces acting on its ends. Mathematically this corresponds to saying that equations (6.11) are singular and cannot be written in inverse form.

Equations (6.11), although they are suitable for use with the

equilibrium method, are not necessarily so for other methods of analysis where it is often desirable to work in terms of member deformations rather than member end-displacements. This is due to the fact that the end-displacements of a member under given end-loads are indeterminate because of the possibility of rigid-body movement, whereas the deformation of the member is unique. The deformation vector of a member is defined as the displacement of end 2, relative to end 1, assuming end 1 to be rigidly fixed. This displacement is denoted by e so that the second of equations (6·11) can be written in the form:

$$p_2 = K_{22}.e \quad \ldots\ldots (6\cdot13)$$

and p_1 can be obtained from p_2 simply by considering the equilibrium of the member. Since e is defined uniquely for any given value of p_2, equation (6·13) can be inverted to obtain:

$$e = F_{22}.p_2 \quad \ldots\ldots (6\cdot14)$$

where F_{22} is the inverse of K_{22}. F_{22} is known as a flexibility matrix.

Although the equations (6·11) for a single member are singular and therefore cannot be inverted, the complete load-displacement equations (6·12) will always have a unique solution, provided that the members form a structure and not a mechanism. The matrix K, therefore, is non-singular and can be inverted as follows:

$$D = K^{-1}.P = F.P \quad \ldots\ldots (6\cdot15)$$

where F is the flexibility matrix of a structure. The matrices K and F represent alternative mathematical statements of the complete load-displacement characteristics of a structure and are both symmetric in form.

At this stage it is now possible to consider the equilibrium method of analysis in more detail and the stiffness matrices for a straight uniform member in a space structure can be evolved. Figure 26(b) shows the member coordinate system for a member of a three-dimensional frame. The y and z axes are assumed to be the principal

axes of the cross-section and the flexural rigidities of the beam in the xz and xy planes are denoted by EI_y and EI_z respectively. If the simple case is considered, in which warping effects are ignored, then GJ/L represents the torsional stiffness of the member about its centre-line. G is the shearing modulus and J is the polar second moment of area of the cross-section about an axis through the centre of the member. The load-displacement equations of the member may be written as follows:

$$\begin{aligned} p_1 &= K_{11}\, d_1 + K_{12}\, d_2 \\ p_2 &= K_{21} d_1 + K_{22}\, d_2 \end{aligned} \qquad \ldots\ldots (6\cdot11)$$

where

$$p = \begin{bmatrix} P_x \\ p_y \\ p_z \\ m_x \\ m_y \\ m_z \end{bmatrix} \qquad d = \begin{bmatrix} \delta_x \\ \delta_y \\ \delta_z \\ \theta_x \\ \theta_y \\ \theta_z \end{bmatrix}$$

and

$$K_{11} = \begin{bmatrix} EA/L & 0 & 0 & 0 & 0 & 0 \\ 0 & 12EI_z/L^3 & 0 & 0 & 0 & 6EI_z/L^2 \\ 0 & 0 & 12EI_y/L^3 & 0 & -6EI_y/L^2 & 0 \\ 0 & 0 & 0 & GJ/L & 0 & 0 \\ 0 & 0 & -6EI_y/L^2 & 0 & 4EI_y/L & 0 \\ 0 & 6EI_z/L^2 & 0 & 0 & 0 & 4EI_z/L \end{bmatrix}$$

$$K_{12} = K_{21}^t = \begin{bmatrix} -EA/L & 0 & 0 & 0 & 0 & 0 \\ 0 & -12EI_z/L^3 & 0 & 0 & 0 & 6EI_z/L^2 \\ 0 & 0 & -12EI_y/L^3 & 0 & -6EI_y/L^2 & 0 \\ 0 & 0 & 0 & -GJ/L & 0 & 0 \\ 0 & 0 & 6EI_y/L^2 & 0 & 2EI_y/L & 0 \\ 0 & -6EI_z/L^2 & 0 & 0 & 0 & 2EI_z/L \end{bmatrix}$$

and K_{22} is equal to K_{11} with the signs of the off-diagonal elements $-6EI_y/L^2$ and $6EI_z/L^2$ reversed. K_{21}^t is the transpose of K_{21}. The load-displacement equations, obtained above, are in member coordinates and have to be transformed into frame coordinates. By coordinate

geometry it can be shown that:

$$\begin{bmatrix} p'_x \\ p'_y \\ p'_z \\ m'_x \\ m'_y \\ m'_z \end{bmatrix} = \begin{bmatrix} \widehat{x'x} & \widehat{x'y} & \widehat{x'z} & 0 & 0 & 0 \\ \widehat{y'x} & \widehat{y'y} & \widehat{y'z} & 0 & 0 & 0 \\ \widehat{z'x} & \widehat{z'y} & \widehat{z'z} & 0 & 0 & 0 \\ 0 & 0 & 0 & \widehat{x'x} & \widehat{x'y} & \widehat{x'z} \\ 0 & 0 & 0 & \widehat{y'x} & \widehat{y'y} & \widehat{y'z} \\ 0 & 0 & 0 & \widehat{z'x} & \widehat{z'y} & \widehat{z'z} \end{bmatrix} \begin{bmatrix} p_x \\ p_y \\ p_z \\ m_x \\ m_y \\ m_z \end{bmatrix} \quad (6.16)$$

where $\widehat{x'x}$, $\widehat{x'y}$, etc., are the cosines of the angles between the appropriate member and system axes. This may be written as:

$$p' = T\,p \quad \ldots\ldots (6.17)$$

For any member in the system the stiffness matrix is then given by:

$$K'_{ij} = T\,K_{ij}\,T^t \quad \ldots\ldots (6.18)$$

Hence, the load-displacement equations of the member, as given in the member coordinate system and set out as equations (6.11), are transformed into the following frame coordinate equations:

$$\begin{aligned} p_1' &= K_{11}'\,d_1' + K_{12}'\,d_2' \\ p_2' &= K_{21}'\,d_1' + K_{22}'\,d_2' \end{aligned} \quad \ldots\ldots (6.17)$$

Equations (6.17) represent, in general terms, the stiffness matrix for a straight uniform member in a space structure.

The next stage in the analysis consists of applying the conditions of joint compatibility to the actual structure under consideration. For this it is best to consider an example and a suitable structure is illustrated in Figure 26(c). To satisfy the conditions of joint compatibility, the displacements of the ends of the members must be equal to the displacements of the appropriate joints. Hence, for the space frame in Figure 26(c), the following equations can be obtained:

$$\begin{aligned} &\text{Member a} \quad d_1' = 0 \quad d_2' = d_A \\ &\text{Member b} \quad d_1' = 0 \quad d_2' = d_B \\ &\text{Member c} \quad d_1' = 0 \quad d_2' = d_C \\ &\text{Member d} \quad d_1' = 0 \quad d_2' = d_D \end{aligned} \quad \ldots\ldots (6.18)$$

$$
\begin{aligned}
&\text{Member } e \quad d_1' = d_A \quad d_2' = d_B \\
&\text{Member } f \quad d_1' = d_A \quad d_2' = d_C \\
&\text{Member } g \quad d_1' = d_C \quad d_2' = d_D \\
&\text{Member } h \quad d_1' = d_B \quad d_2' = d_D
\end{aligned}
\qquad \ldots\ldots (6\cdot18)
$$

Substituting these expressions for the member end-displacements into equations (6·17) for each member gives:

$$
\begin{aligned}
&\text{Member } a \quad p'_{2a} = (K'_{22})_a d_A \\
&\text{Member } b \quad p'_{2b} = (K'_{22})_b d_B \\
&\text{Member } c \quad p'_{2c} = (K'_{22})_c d_C \\
&\text{Member } d \quad p'_{2d} = (K'_{22})_d d_D \\
&\text{Member } e \quad p'_{1e} = (K'_{11})_e d_A + (K'_{12})_e d_B \\
&\qquad\quad p'_{2e} = (K'_{21})_e d_A + (K'_{22})_e d_B \\
&\text{Member } f \quad p'_{1f} = (K'_{11})_f d_A + (K'_{12})_f d_C \\
&\qquad\quad p'_{2f} = (K'_{21})_f d_A + (K'_{22})_f d_C \\
&\text{Member } g \quad p'_{1g} = (K'_{11})_g d_C + (K'_{12})_g d_D \\
&\qquad\quad p'_{2g} = (K'_{21})_g d_C + (K'_{22})_g d_D \\
&\text{Member } h \quad p'_{1h} = (K'_{11})_h d_B + (K'_{12})_h d_D \\
&\qquad\quad p'_{2h} = (K'_{21})_h d_B + (K'_{22})_h d_D
\end{aligned}
\qquad \ldots\ldots (6\cdot19)
$$

The expressions for p'_{1a}, p'_{1b}, p'_{1c} and p'_{1d} have been omitted in the case of members a, b, c and d since they are foundation reactions and do not enter the joint equilibrium equations.

To obtain the stiffness matrix for the complete structure, the conditions of joint equilibrium must now be considered. For the structure being solved here these conditions are:

$$
\begin{aligned}
p_A &= p'_{2a} + p'_{1e} + p'_{1f} \\
p_B &= p'_{2b} + p'_{2e} + p'_{1h} \\
p_C &= p'_{2c} + p'_{2f} + p'_{1g} \\
p_D &= p'_{2d} + p'_{2g} + p'_{2h}
\end{aligned}
\qquad \ldots\ldots (6\cdot20)
$$

Substituting into these equations from (6·19) gives:

$$\begin{bmatrix} P_A \\ P_B \\ P_C \\ P_D \end{bmatrix} = \begin{bmatrix} (K'_{22})_a + (K'_{11})_e + (K'_{11})_f & (K'_{12})_e & (K'_{12})_f & 0 \\ (K'_{21})_e & (K'_{22})_b + (K'_{22})_e + (K'_{11})_h & 0 & (K'_{12})_h \\ (K'_{21})_f & 0 & (K'_{22})_c + (K'_{22})_f + (K'_{11})_g & (K'_{12})_g \\ 0 & (K'_{21})_h & (K'_{21})_g & (K'_{22})_d + (K'_{22})_g + (K'_{22})_h \end{bmatrix} \begin{bmatrix} d_A \\ d_B \\ d_C \\ d_D \end{bmatrix} \quad \ldots\ldots (6\cdot21)$$

These equations can be written in the form:

$$P = KD$$

where P indicates the complete set of applied joint loads, D indicates the corresponding set of unknown joint displacements and K is the stiffness matrix of the structure. By inverting K and solving for d_A, d_B, d_C and d_D a complete analysis is easily obtained as these values can be substituted in equations (6·19) to find the internal forces.

In describing the general features of the equilibrium method so far it has been necessary to choose an example involving relatively simple structural elements. By restricting the analysis to a structure formed from straight uniform members, the coefficients of the member stiffness matrices have been obtained direct from the known solutions of the differential equations of bending, torsion, etc., without actually having to consider the differential equations themselves. The problem of finding member stiffness matrices in the more general case, where the member may be both curved and non-uniform in cross-section, will now be considered.

Previously, in discussing the equilibrium method, the load-displacement equations for a single member have been written in the form:

$$p_1 = K_{11} d_1 + K_{12} d_2$$
$$p_2 = K_{21} d_1 + K_{22} d_2 \quad \ldots\ldots (6\cdot11)$$

and the matrices K_{11}, etc., have been referred to as the stiffness matrices of the member. Although this is the form most suited to the equilibrium method it is not the only way in which the relationships between end-forces and end-displacements may be written and it is not in fact the form in which they are most conveniently derived. An alternative formulation of these equations, in terms of the deformation vector e, will now be developed. The advantage of this formulation is that it provides a convenient way of obtaining the member stiffness matrices used in the equilibrium approach as the four matrices K_{11}, K_{12}, etc., can all be derived from a single flexibility matrix F and an equilibrium matrix H. Matrix H is of a very simple form and is independent of the elastic properties of the member.

The equilibrium equations connecting p_1 and p_2, as given by equations (6·11), may be written in matrix form as:

$$p_1 + Hp_2 = 0 \quad \ldots\ldots (6\cdot22)$$

or alternatively as:

$$H^{-1}p_1 + p_2 = 0 \quad \ldots\ldots (6\cdot23)$$

H is the equilibrium matrix associated with the member.

Considering a general three-dimensional member in which end 2 has coordinates L_x, L_y, L_z with respect to end 1, as shown in Figure 27(a), the equations of equilibrium for the member are:

$$p'_{x1} + p'_{x2} = 0 \qquad m'_{x1} + m'_{x2} + L_y p'_{z2} - L_z p'_{y2} = 0$$
$$p'_{y1} + p'_{y2} = 0 \qquad m'_{y1} + m'_{y2} + L_z p'_{x2} - L_x p'_{z2} = 0$$
$$p'_{z1} + p'_{z2} = 0 \qquad m'_{z1} + m'_{z2} + L_x p'_{y2} - L_y p'_{x2} = 0$$

which may be written:

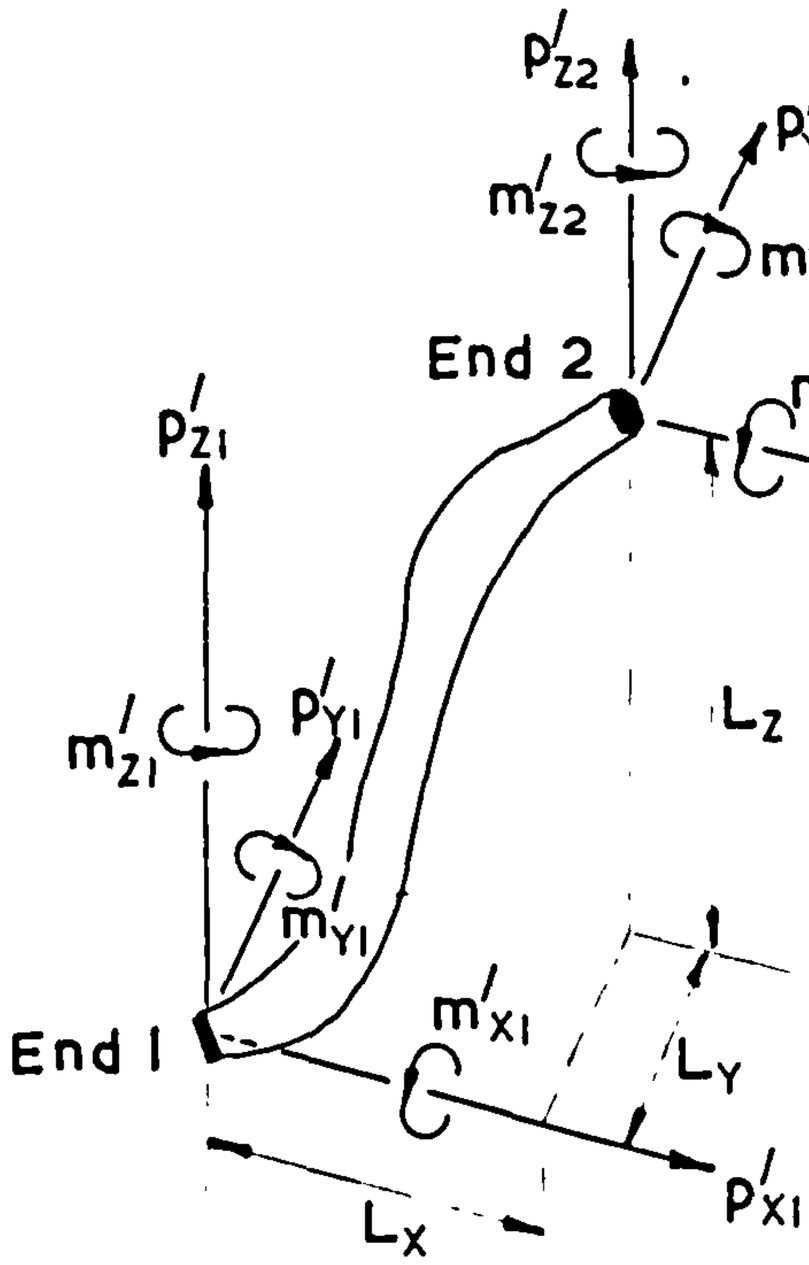

(a)

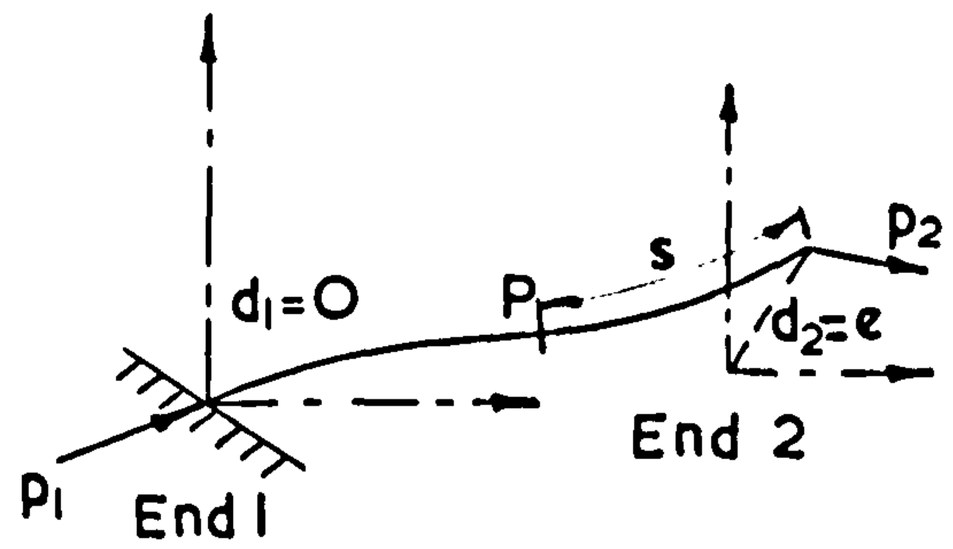

(b)

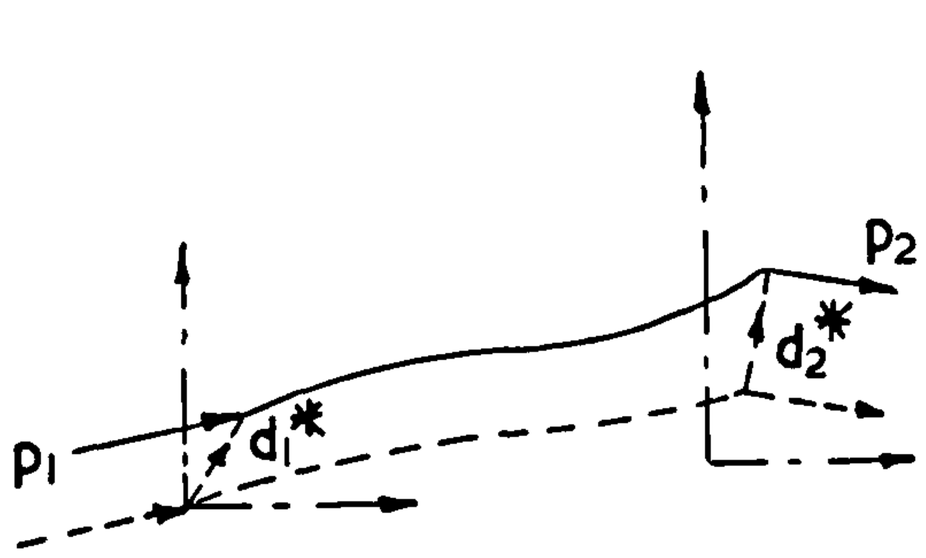

(c)

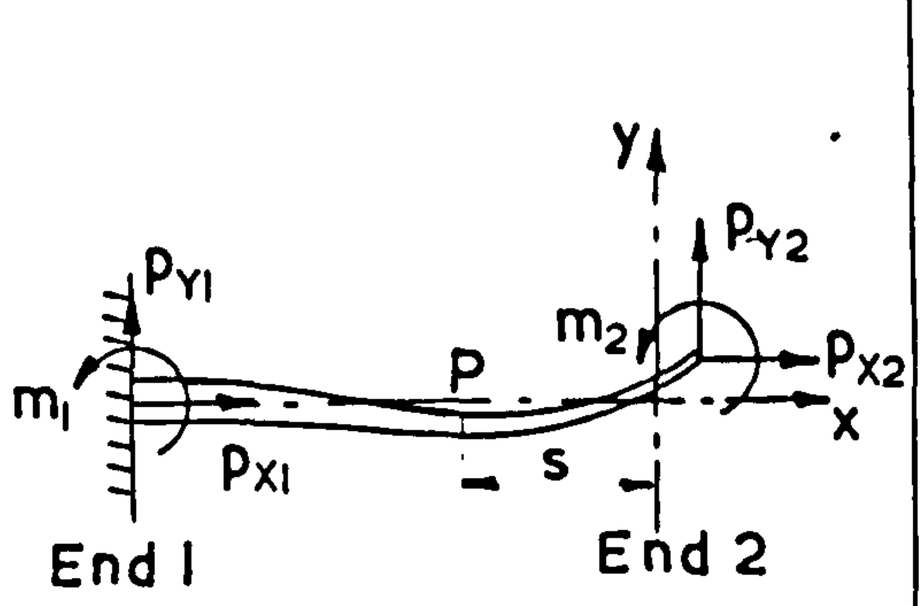

(d)

FIG. 27 MATRIX METHODS Sheet No. 2

F.A.A. Ph.D. Thesis
8th Dec., 1969

Structural Engineering Division
Department of Civil Engineering
University of Newcastle upon Tyne

$$\begin{bmatrix} p'_{x1} \\ p'_{y1} \\ p'_{z1} \\ m'_{x1} \\ m'_{y1} \\ m'_{z1} \end{bmatrix} + \begin{bmatrix} 1 & 0 & 0 & 0 & 0 & 0 \\ 0 & 1 & 0 & 0 & 0 & 0 \\ 0 & 0 & 1 & 0 & 0 & 0 \\ 0 & -L_z & L_y & 1 & 0 & 0 \\ L_z & 0 & -L_x & 0 & 1 & 0 \\ -L_y & L_x & 0 & 0 & 0 & 1 \end{bmatrix} \begin{bmatrix} p'_{x2} \\ p'_{y2} \\ p'_{z2} \\ m'_{x2} \\ m'_{y2} \\ m'_{z2} \end{bmatrix} = 0$$

..... (6·24)

Equation (6·24) defines the matrix H' in the most general case, the primes being attached because the axes resemble system coordinates.

To obtain the flexibility and stiffness matrices for a general linear member, the idea of a deformation vector, introduced earlier in this Art., must be developed further. The end-displacements d_1, d_2 of a structural element are considered to be the sum of two separate sets of displacements, one due to the elastic strains and the other due to rigid-body movement. Expressions for the general load-displacement characteristics of a linear element can be deduced by considering the two sets of displacements separately and then combining the results.

Considering the general member shown in Figures 27(b) and (c), the first case to be dealt with requires end 1 of the member to be completely restrained against displacement. The displacement at end 2, due to the load p_2, under these conditions is equal to the deformation e, the load and deformation vectors being measured in member coordinates. Strain energy can be used to determine e. Using simple statics, the moment and force components at any point P of the member can be expressed in terms of the coordinate s and the components of p_2. By integrating along the member the strain energy may be expressed in terms of these components and since the member is assumed to behave in a linear manner, Castigliano's Theorem, Part II, may be applied. Differentiating the strain energy U with respect to each

component of p_2 in turn gives, for a general member of a space structure the six components of e in the form:

$$\delta_{x2} = \delta U/\delta p_{x2} \quad \delta_{y2} = \delta U/\delta p_{y2} \quad \delta_{z2} = \delta U/\delta p_{z2} \quad .. (6\cdot25$$
$$\theta_{x2} = \delta U/\delta m_{x2} \quad \theta_{y2} = \delta U/\delta m_{y2} \quad \theta_{z2} = \delta U/\delta m_{z2}$$

These differential coefficients are linear functions of the components of p_2, so that the expressions for the displacement components can be written in the form:

$$e = \bar{F} p_2 \quad ..... (6\cdot26)$$

where $\bar{F}$ is the flexibility matrix of the member. $\bar{F}$ is non-singular and symmetric. It can be inverted and equation (6·26) can be written as:

$$p_2 = \bar{K} e \quad ..... (6\cdot27)$$

where $\bar{K}$ is the stiffness matrix of the member. $\bar{K}$ is also symmetric. $\bar{K}$ is equal to the matrix K_{22}, previously defined, and $\bar{F}$ is equivalent to F_{22} but the omission of the suffixes makes the analysis simpler to follow. Equation (6·22) now gives the corresponding load at end 1 as follows:

$$P_1 = -Hp_2 = -H\bar{K}e \quad ..... (6\cdot23)$$

Considering now the effect of superposing a rigid-body displacement of the member on the displacements $d_1 = 0$, $d_2 = e$. Let these rigid-body displacements be denoted by d_1^* and d_2^*, Figure 27($\overset{c}{f}$), where:

$$d_2^* = H^t d_1^* \quad ..... (6\cdot29)$$

Adding the two sets of displacements gives:

$$\begin{aligned} d_1 &= d_1^* \\ d_2 &= d_2^* + c \end{aligned} \quad .....(6\cdot30)$$

Eliminating the rigid-body displacements d_1^* and d_2^* from equations (6·29) and (6·30) produces:

$$e = d_2 - H^t d_1 \quad ..... (6\cdot31)$$

Combining equations (6·26) and (6·31) gives the equation:

$$d_2 = H^t d_1 + Fp_2 \quad ..... (6\cdot32)$$

Substituting the value for e, given in equation (6·31), into equations (6·27) and (6·28) produces the following expressions:

$$p_1 = (H\bar{K}H^t)d_1 - (H\bar{K})d_2$$
$$p_2 = -(\bar{K}H^t)d_1 + \bar{K}d_2 \qquad \ldots\ldots (6\cdot33)$$

Comparing equations (6·33) and (6·11), the important general expressions for the member stiffness matrices can be obtained thus:

$$K_{11} = H\bar{K}H^t \;;\; K_{12} = -H\bar{K} \;;\; K_{21} = -\bar{K}H^t \;;\; K_{22} = \bar{K} \quad \ldots (6\cdot34)$$

Where $\bar{K} = \bar{F}^{-1}$.

As an example of the application of the preceding analysis, consider the derivation of the flexibility and stiffness matrices for a straight non-uniform beam of length L under the action of forces and moments in a plane, as shown in Figure 27(d). The x axis of the co-ordinate system is assumed to coincide with the unstrained axis of the beam.

Firstly, consider the displacement d_2 of end 2, due to the load p_2, while the displacement of end 1 is kept equal to zero. At the point P the direct force is equal to p_{x2} and the moment is $m_2 + p_{y2}s$. The strain energy U is given by:

$$U = \int_0^L (p^2_{x2}/2EA)ds + \int_0^L ((m_2 + p_{y2}s)^2/2EI)ds \ldots\ldots (6\cdot35)$$

and the displacement components at end 2 are given by the expressions:

$$\delta_{x2} = \delta U/\delta p_{x2} = \left[\int_0^L (1/EA)ds\right] p_{x2}$$
$$\delta_{y2} = \delta U/\delta p_{y2} = \left[\int_0^L (s^2/EI)ds\right] p_{y2} + \left[\int_0^L (S/EI)ds\right] m_2$$
$$\theta_2 = \delta U/\delta m_2 = \left[\int_0^L (s/EI)ds\right] p_{y2} + \left[\int_0^L (1/EI)ds\right] m_2$$
$$\ldots\ldots (6.36)$$

Writing f_1, f_2, f_3, f_4 for the four different integrals appearing in these equations produces the following expressions:

$$\delta_{x2} = f_1 p_{x2}$$
$$\delta_{y2} = f_2 p_{y2} + f_3 m_2 \qquad \ldots\ldots (6\cdot37)$$
$$\theta_2 = f_3 p_{y2} + f_4 m_2$$

or in matrix form:

$$\begin{bmatrix} \delta_{x2} \\ \delta_{y2} \\ \theta_2 \end{bmatrix} = \begin{bmatrix} f_1 & 0 & 0 \\ 0 & f_2 & f_3 \\ 0 & f_3 & f_4 \end{bmatrix} \begin{bmatrix} p_{x2} \\ p_{y2} \\ m_2 \end{bmatrix} \quad \ldots\ldots (6\cdot38)$$

i.e. $d_2 = e = \bar{F}\, p_2$

The inverse of $\bar{F}$ can now be computed to give the stiffness matrix $\bar{K}$.

By the rules, already discussed in this Art., for transforming matrices from member coordinates into system coordinates the following relationships are obtained:

$$\bar{F}' = T\,\bar{F}\,T^t \quad ; \quad \bar{K}' = T\,\bar{K}T^t$$

The equilibrium method of analysis, which has been described in this Art., completely ignores the question of whether the structure being analysed is statically determinate or not. By this means the method can be applied to many different types of structure. However, when it comes to analysing determinate structures, or structures with a few redundancies, the method is 'inefficient.

The analysis of determinate structures is important for two reasons. Firstly, a great many engineering structures are in fact analysed as determinate systems during design and, although the analysis of determinate structures is theoretically elementary, large space frameworks of this type are best solved with the aid of a computer. The second reason is that the analysis of a hyperstatic structure by the compatibility method involves a consideration of an auxiliary statically determinate structure.

Before dealing with determinate systems, the equilibrium method must be considered again from a slightly different standpoint. This requires the introduction of what is known as a connection matrix. Consider once more the analysis of the rigid-jointed space frame shown in Figure 26(c). The load-displacement equations for this structure can be written, as before, in the form:

$$
\begin{bmatrix} p_A \\ p_B \\ p_C \\ p_D \end{bmatrix} = \begin{bmatrix} (K'_{22})_a + (K'_{11})_e + (K'_{11})_f & (K'_{12})_e & (K'_{12})_f & 0 \\ (K'_{21})_e & (K'_{22})_b + (K'_{22})_e + (K'_{11})_h & 0 & (K'_{12})_h \\ (K'_{21})_f & 0 & (K'_{22})_c + (K'_{22})_f + (K'_{11})_g & (K'_{12})_g \\ 0 & (K'_{21})_h & (K'_{21})_g & (K'_{22})_d + (K'_{22})_g + (K'_{22})_h \end{bmatrix} \begin{bmatrix} d_A \\ d_B \\ d_C \\ d_D \end{bmatrix}
$$

..... (6·21)

Equations (6·21) can be constructed directly in a straightforward manner. However, they can also be derived by a rather different approach. First of all the load-displacement equations of the individual elements of the structure are written down in system co-ordinates and arranged as a large banded matrix in the following form:

$$
\begin{bmatrix} p'_{1a} \\ p'_{2a} \\ p'_{1b} \\ p'_{2b} \\ \cdot \\ \cdot \\ p'_{1h} \\ p'_{2h} \end{bmatrix} = \begin{bmatrix} (K'_{11})_a & (K'_{12})_a & 0 & 0 & \cdot & \cdot & \cdot & 0 \\ (K'_{21})_a & (K'_{22})_a & 0 & 0 & \cdot & \cdot & \cdot & 0 \\ 0 & 0 & (K'_{11})_b & (K'_{12})_b & 0 & \cdot & \cdot & 0 \\ 0 & 0 & (K'_{21})_b & (K'_{22})_b & 0 & \cdot & \cdot & 0 \\ \cdot & \cdot & \cdot & \cdot & \cdot & \cdot & \cdot & \cdot \\ \cdot & \cdot & \cdot & \cdot & \cdot & \cdot & \cdot & \cdot \\ 0 & \cdot & \cdot & \cdot & \cdot & 0 & (K'_{11})_h & (K'_{12})_h \\ 0 & \cdot & \cdot & \cdot & \cdot & 0 & (K'_{21})_h & (K'_{22})_h \end{bmatrix} \begin{bmatrix} d'_{1a} \\ d'_{2a} \\ d'_{1b} \\ d'_{2b} \\ \cdot \\ \cdot \\ d'_{1h} \\ d'_{2h} \end{bmatrix}
$$

..... (6·39)

This equation can be written as:

$$P'_m = K'_m D'_m \qquad \text{..... (6·40)}$$

the suffix m standing for "members". Equation (6·40) resembles

equation (6·12) but, in fact, it only describes the elastic properties of the separate components when they are correctly oriented with respect to the system axes but not connected to the joints. It does not describe the behaviour of the structure and the components must be connected up by a mathematical process. The member end-loads, which make up the vector P'_m in equation (6·40), must satisfy the equations of equilibrium given by equations (6.20) previously:

$$\begin{aligned} P_A &= p'_{2a} + p'_{1e} + p'_{1f} \\ P_B &= p'_{2b} + p'_{2e} + p'_{1h} \\ P_C &= p'_{2c} + p'_{2f} + p'_{1g} \\ P_D &= p'_{2d} + p'_{2g} + p'_{2h} \end{aligned} \qquad \ldots\ldots (6·20)$$

Equations (6·20) can be written in the form:

$$\begin{bmatrix} P_A \\ P_B \\ P_C \\ P_D \end{bmatrix} = \begin{bmatrix} 0 & I & 0 & 0 & 0 & 0 & 0 & 0 & I & 0 & I & 0 & 0 & 0 & 0 & 0 \\ 0 & 0 & 0 & I & 0 & 0 & 0 & 0 & 0 & I & 0 & 0 & 0 & 0 & I & 0 \\ 0 & 0 & 0 & 0 & 0 & I & 0 & 0 & 0 & 0 & 0 & I & I & 0 & 0 & 0 \\ 0 & 0 & 0 & 0 & 0 & 0 & 0 & I & 0 & 0 & 0 & 0 & 0 & I & 0 & I \end{bmatrix} \begin{bmatrix} p'_{1a} \\ p'_{2a} \\ p'_{1b} \\ p'_{2b} \\ p'_{1c} \\ p'_{2c} \\ p'_{1d} \\ p'_{2d} \\ p'_{1e} \\ p'_{2e} \\ p'_{1f} \\ p'_{2f} \\ p'_{1g} \\ p'_{2g} \\ p'_{1h} \\ p'_{2h} \end{bmatrix} \qquad \ldots\ldots (6·41)$$

where I is a unit matrix. This can be written as:

$$P = C_o P'_m \qquad \ldots\ldots (6·42)$$

the matrix C_o being termed a connection matrix. The components of the vector D'_m in equation (6·40) must also satisfy the compatibility conditions:

$$d'_{1a} = d'_{1b} = d'_{1c} = d'_{1d} = 0 \; ; \; d'_{2a} = d'_{1e} = d'_{1f} = d_A ;$$
$$d'_{2b} = d'_{2e} = d'_{1h} = d_B \; ; \; d'_{2c} = d'_{2f} = d'_{1g} = d_C \; ;$$
$$d'_{2d} = d'_{2g} = d'_{2h} = d_D \qquad \ldots\ldots (6.18)$$

which can be written as:

$$\begin{bmatrix} d'_{1a} \\ d'_{2a} \\ d'_{1b} \\ d'_{2b} \\ d'_{1c} \\ d'_{2c} \\ d'_{1d} \\ d'_{2d} \\ d'_{1e} \\ d'_{2e} \\ d'_{1f} \\ d'_{2f} \\ d'_{1g} \\ d'_{2g} \\ d'_{1h} \\ d'_{2h} \end{bmatrix} = \begin{bmatrix} 0 & 0 & 0 & 0 \\ I & 0 & 0 & 0 \\ 0 & 0 & 0 & 0 \\ 0 & I & 0 & 0 \\ 0 & 0 & 0 & 0 \\ 0 & 0 & I & 0 \\ 0 & 0 & 0 & 0 \\ 0 & 0 & 0 & I \\ I & 0 & 0 & 0 \\ 0 & I & 0 & 0 \\ I & 0 & 0 & 0 \\ 0 & 0 & I & 0 \\ 0 & 0 & I & 0 \\ 0 & 0 & 0 & I \\ 0 & I & 0 & 0 \\ 0 & 0 & 0 & I \end{bmatrix} \begin{bmatrix} d_A \\ d_B \\ d_C \\ d_D \end{bmatrix} \qquad \ldots\ldots (6.43)$$

or as:

$$D'_m = C_o^t \, D \qquad \ldots\ldots (6.44)$$

Equations (6.42) and (6.44), when combined give:

$$P = (C_o K'_m C_o^t) \, D \qquad \ldots\ldots (6.45)$$

Comparing equation (6.45) with equation (6.12), it can be seen that the stiffness matrix of the assembled structure, K, is equal to $C_o K'_m C_o^t$.

The matrix C_o, which has just been defined, is simply a matrix composed of 0's and 1's that describes how the various members are connected together. Information concerning the elastic characteristics of the members and their orientations with respect to the system axes is contained entirely in the matrix K'_m. An alternative formulation of these equations can be introduced whereby the orientation of the

members is included in the connection matrix and K'_m is replaced by a matrix which is non-singular.

For each member of a structure the load p_a and the deformation vector e can be related, as previously mentioned in this Art., by the following expression:

$$p_a = \bar{K}_e \quad \ldots\ldots (6\cdot27)$$

The space structure, shown in Figure 26(c), will produce a set of equations in member coordinates as follows:

$$\begin{bmatrix} p_{aa} \\ p_{ab} \\ p_{ac} \\ p_{ad} \\ p_{ae} \\ p_{af} \\ p_{ag} \\ p_{ah} \end{bmatrix} = \begin{bmatrix} \bar{K}_a & 0 & 0 & 0 & 0 & 0 & 0 & 0 \\ 0 & \bar{K}_b & 0 & 0 & 0 & 0 & 0 & 0 \\ 0 & 0 & \bar{K}_c & 0 & 0 & 0 & 0 & 0 \\ 0 & 0 & 0 & \bar{K}_d & 0 & 0 & 0 & 0 \\ 0 & 0 & 0 & 0 & \bar{K}_e & 0 & 0 & 0 \\ 0 & 0 & 0 & 0 & 0 & \bar{K}_f & 0 & 0 \\ 0 & 0 & 0 & 0 & 0 & 0 & \bar{K}_g & 0 \\ 0 & 0 & 0 & 0 & 0 & 0 & 0 & \bar{K}_h \end{bmatrix} \begin{bmatrix} e_a \\ e_b \\ e_c \\ e_d \\ e_e \\ e_f \\ e_g \\ e_h \end{bmatrix} \quad \ldots (6\cdot46)$$

or more briefly:

$$P_m = K_m E_m \quad \ldots\ldots (6\cdot47)$$

This equation differs from equation (6·40) in that the diagonal matrix K_m represents the elastic properties of the completely unconnected members, without containing any information about their orientation, and the vectors P_m, E_m have only half the number of components appearing in the vectors P'_m and D'_m. The matrix K_m is also always non-singular and, therefore, equation (6·47) can be inverted to give:

$$E_m = F_m P_m \quad \ldots\ldots (6\cdot48)$$

where F_m is a diagonal matrix formed from the member flexibility matrices as follows:

$$\begin{bmatrix} \bar{F}_a & 0 & 0 & 0 & 0 & 0 & 0 & 0 \\ 0 & \bar{F}_b & 0 & 0 & 0 & 0 & 0 & 0 \\ 0 & 0 & \bar{F}_c & 0 & 0 & 0 & 0 & 0 \\ 0 & 0 & 0 & \bar{F}_d & 0 & 0 & 0 & 0 \\ 0 & 0 & 0 & 0 & \bar{F}_e & 0 & 0 & 0 \end{bmatrix}$$

$$\begin{bmatrix} 0 & 0 & 0 & 0 & 0 & \bar{F}_f & 0 & 0 \\ 0 & 0 & 0 & 0 & 0 & 0 & \bar{F}_g & 0 \\ 0 & 0 & 0 & 0 & 0 & 0 & 0 & \bar{F}_h \end{bmatrix}$$

The assembly of the members into a connected structure can now be considered. As before, for the rigid-jointed space frame illustrated in Figure 26(c), the equations of joint equilibrium are:

$$\begin{aligned} p_A &= p'_{2a} + p'_{1e} + p'_{1f} \\ p_B &= p'_{2b} + p'_{2e} + p'_{1h} \\ p_C &= p'_{2c} + p'_{2f} + p'_{1g} \\ p_D &= p'_{2d} + p'_{2g} + p'_{2h} \end{aligned} \qquad \ldots\ldots (6{\cdot}20)$$

For each member the equations of equilibrium, (6.22) and (6.23), can be combined with the equations describing the change to system coordinates:

$$\begin{aligned} p'_2 &= -T p_2 \\ p'_1 &= T p_1 = -TH p_2 \end{aligned} \qquad \ldots\ldots (6{\cdot}49)$$

Substituting these expressions into equations (6·20), the following relationships are obtained:

$$\begin{aligned} p_A &= T_a p_{2a} - T_e H_e p_{2e} - T_f H_f p_{2f} \\ p_B &= T_b p_{2b} + T_e p_{2e} - T_h H_h p_{2h} \\ p_C &= T_c p_{2c} + T_f p_{2f} - T_g H_g p_{2g} \\ p_D &= T_d p_{2d} + T_g p_{2g} + T_h p_{2h} \end{aligned} \qquad \ldots\ldots (6{\cdot}50)$$

which can be written in the form:

$$\begin{bmatrix} p_A \\ p_B \\ p_C \\ p_D \end{bmatrix} = \begin{bmatrix} T_a & 0 & 0 & 0 & -T_e H_e & -T_f H_f & 0 & 0 \\ 0 & T_b & 0 & 0 & T_e & 0 & 0 & -T_h H_h \\ 0 & 0 & T_c & 0 & 0 & T_f & -T_g H_g & 0 \\ 0 & 0 & 0 & T_d & 0 & 0 & T_g & T_h \end{bmatrix} \begin{bmatrix} p_{2a} \\ p_{2b} \\ p_{2c} \\ p_{2d} \\ p_{2e} \\ p_{2f} \\ p_{2g} \\ p_{2h} \end{bmatrix} \qquad \ldots\ldots (6{\cdot}51)$$

or simply as:

$$P = C\,P_m \qquad \ldots\ldots (6\cdot52)$$

The deformation vector E_m is related to the joint displacement vector D by the equation:

$$E_m = C^t D \qquad \ldots\ldots (6\cdot53)$$

Combining equations (6·47), (6·52 and (6·53) gives:

$$P = (C\,K_m C^t)D \qquad \ldots\ldots (6\cdot54)$$

At this stage, it is now possible to consider space frameworks which are statically determinate. By definition a determinate structure is one in which the equations of equilibrium are sufficient to determine all the internal forces and moments. As discussed earlior in this Art., the individual conditions of member equilibrium will always give the load at one end of a member in terms of the load at tho other. This implies that if the conditions of joint equilibrium are sufficient to determine the vector P_m, then all the other forcos and moments in the structure can be found from the individual equations of member equilibrium. Therefore, the determinacy or otherwise of a space framework will depend upon whether equation (6·52) can be solved for the vector P_m. If the matrix C, in this equation, is rectangular it is impossible to obtain a unique solution and the structure is hyper-static. However, if the inverse matrix C^{-1} exists then the internal forces and moments in the structure can be obtained immediately by writing equation (6·52) in the form:

$$P_m = C^{-1} P \qquad \ldots\ldots (6\cdot55)$$

This simple expression gives the displacements of a determinate structure, since if C is non-singular equation (6·54) can be written as:

$$D = (C^{-1})^t K_m^{-1} C^{-1} P \qquad \ldots\ldots (6\cdot56)$$

From equations (6·47) and (6·48), $K_m^{-1} = F_m$ and hence:

$$D = (C^{-1})^t F_m C^{-1} P \qquad \ldots\ldots (6\cdot57)$$

It is now possible to describe the application of the compatibility

method to space frame analysis. In this Art. so far, it has been shown that the load-displacement equations can be written in the form:

$$P = (CK_m C^t)D \quad \ldots\ldots (6.54)$$

where K_m is the non-singular stiffness matrix of the individual disconnected elements and C is a matrix which relates the applied loads to the internal forces and moments. The matrix C is independent of the elasticity of the structure and is derived simply from the conditions of joint equilibrium. The normal process of analysing a structure by the equilibrium method involves the inversion of the matrix $CK_m C^t$ to give an expression for the joint displacements in terms of the known applied loads. Since the order of this matrix is equal to the total number of degrees of freedom of the structure the inversion process may be regarded as the central computational problem of the method.

For a determinate structure, however, the matrix C is non-singular, so that the inverse of the matrix $CK_m C^t$ may be written in the simpler form $(C^{-1})^t F_m C^{-1}$. The matrix C is usually of a simple form and easily inverted. If only the forces and moments in the structure are required then it is unnecessary to compute the displacements, since the member end-loads can be found immediately from the equilibrium equations:

$$P_m = C^{-1} P \quad \ldots\ldots (6.55)$$

The relative simplicity of the analysis in the case of determinate structures suggests the possibility of employing a method which retains at least some of this simplicity when applied to structures whose degree of indeterminacy is small. The determinate system procedure is, therefore, used as a basis for the compatibility method. A hyperstatic structure is first made statically determinate by relaxing the conditions of compatibility at sufficient points. This structure is then analysed by means of the procedures previously

described for determinate structures. Finally the forces and moments which must be applied at the points of discontinuity to produce displacement compatibility are calculated.

To illustrate the compatibility method, consider the simple space frame with rigid joints as shown in Figure 28(a). The loads at the joints A and B are assumed to include any fixed-end forces and moments which may arise from mid-span loading on the beam. As in earlier calculations, the method will be described in terms of the H, F and T matrices of the members. The first step in an analysis by the compatibility method is to obtain the equations of joint equilibrium. These equations can be written as:

$$\begin{bmatrix} P_A \\ P_B \end{bmatrix} = \begin{bmatrix} T_a & -T_bH_b & 0 \\ 0 & T_b & -T_cH_c \end{bmatrix} \begin{bmatrix} p_{2a} \\ p_{2b} \\ p_{2c} \end{bmatrix} \quad \ldots\ldots (6\cdot53)$$

$$\text{i.e.} \quad P = CP_m \quad \ldots\ldots (6\cdot52)$$

It can be seen from equation (6·58) that the matrix C is rectangular and therefore singular. To make it square, a study of the related structure in Figure 28(b) is necessary. In this frame the joint C is allowed to displace and the foundation reaction at C is thought of as an external load q. This load is regarded as a self-equilibrating pair of loads. The relaxation of the compatibility condition at C introduces six extra displacement and load components. Equation (6·58) now becomes:

$$\begin{bmatrix} P_A \\ P_B \\ q \end{bmatrix} = \begin{bmatrix} T_a & -T_bH_b & 0 \\ 0 & T_b & -T_cH_c \\ 0 & 0 & T_c \end{bmatrix} \begin{bmatrix} p_{2a} \\ p_{2b} \\ p_{2c} \end{bmatrix} \quad \ldots\ldots (6\cdot59)$$

the matrix C being augmented with an extra row for the load q. When inverted, equation (6·59) becomes:

$$\begin{bmatrix} p_{2a} \\ p_{2b} \\ p_{2c} \end{bmatrix} = \left[\begin{array}{ccc:c} T_a^{\,t} & T_a^{\,t}H'_{AB} & \vdots & T_a^{\,t}H'_{AC} \\ 0 & T_b^{\,t} & \vdots & T_b^{\,t}H'_{BC} \\ 0 & 0 & \vdots & T_c^{\,t} \end{array}\right] \begin{bmatrix} P_A \\ P_B \\ q \end{bmatrix} \quad \ldots\ldots (6\cdot60)$$

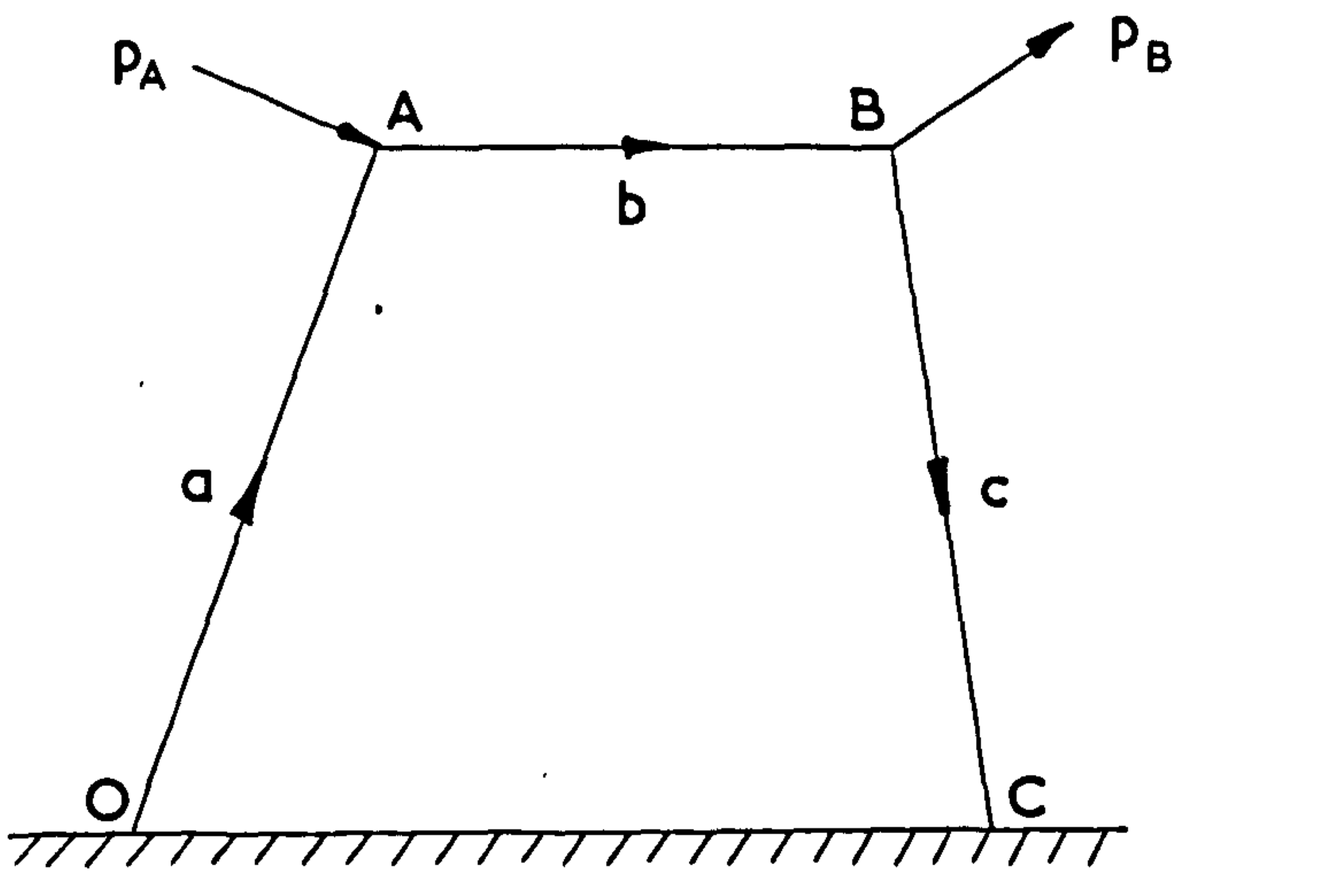

(a)

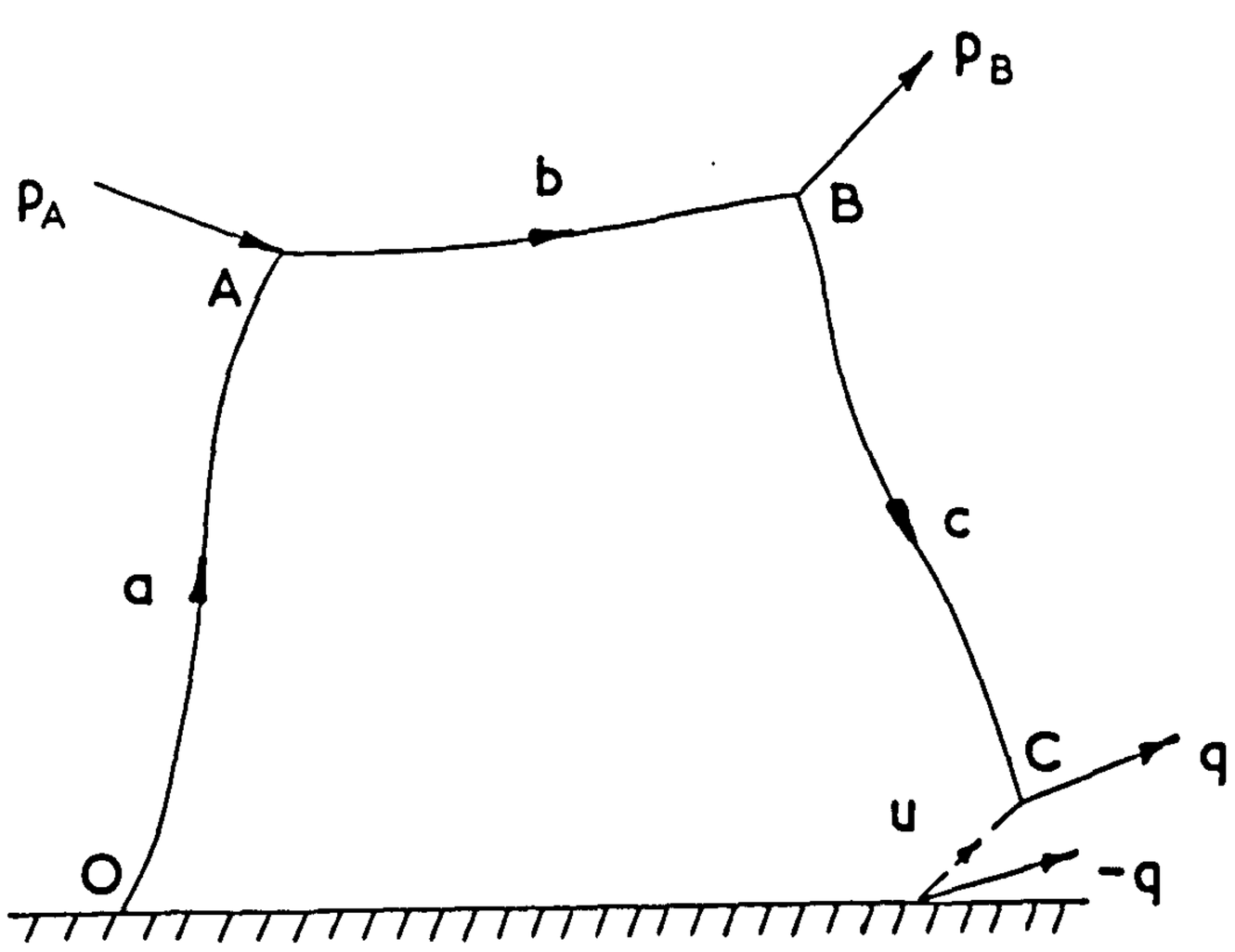

(b)

FIG. 28 MATRIX METHODS Sheet No. 3

F. A. A. Ph.D. Thesis
10th Dec., 1969

Structural Engineering Division
Department of Civil Engineering
University of Newcastle upon Tyne

The matrix appearing in equation (6·60) is written C_+^{-1} and is split up into two matrices B_o and B. Equation (6·60) is now written:

$$P_m = B_o P + B_q \quad \ldots\ldots (6\cdot61)$$

and the corresponding relation between the joint displacements and the member deformations is:

$$\begin{bmatrix} D \\ u \end{bmatrix} = \begin{bmatrix} B_o^t \\ B^t \end{bmatrix} E_m \quad \ldots\ldots (6\cdot62)$$

The member deformations may be expressed in terms of the membor end-loads in the usual way as:

$$E_m = F_m P_m \quad \ldots\ldots (6\cdot48)$$

where in this example:

$$F_m = \begin{bmatrix} F_a & 0 & 0 \\ 0 & F_b & 0 \\ 0 & 0 & F_c \end{bmatrix} \quad \ldots\ldots (6\cdot63)$$

and, eliminating P_m and E_m from equations (6·61), (6·62) and (6·48), the follcwing expressions are obtained:

$$\begin{aligned} D &= B_o^t F_m (B_o P + Bq) \\ u &= B^t F_m (B_o P + Bq) \end{aligned} \quad \ldots\ldots (6\cdot64)$$

Applying the vector equation $\ddot{u} = 0$ to the second of equations (6·64), the unknown load q is obtained from:

$$q = -(B^t F_m B)^{-1} B^t F_m B_o P \quad \ldots\ldots (6\cdot65)$$

The final expressions for the member end-loads P_m and the joint displacements D are then:

$$P_m = \left[1 - B (B^t F_m B)^{-1} B^t F_m\right] B_o \Gamma \quad \ldots\ldots (6\cdot66)$$

$$D = B_o^t F_m P_m \quad \ldots\ldots (6\cdot67)$$

In this example the position at which all six releases were introduced was at C. They could quite easily have been introduced at A or B and, in fact, three hinges, consisting of two releases each, could have been employed at A, B and C together. Although the values of the relevant matrices change with each system used, the final

values for the internal forces, the moments in the members and the joint displacements would be the same.

As it has been seen from the examples, both the equilibrium and compatibility methods use the equations of joint equilibrium which are written in the form:

$$P = C P_m \quad \ldots\ldots (6.52)$$

The equilibrium method merely uses the matrix C to transform the matrix K_m, and is not concerned with whether C is singular or not. On the other hand, the compatibility method transforms C into a non-singular matrix C_+ which it then inverts. This transformation is effected by introducing sufficient releases into the structure to make it determinate and by considering the self-equilibrating force systems, which act at these discontinuities, as external loads. The equilibrium and compatibility matrix methods of analysis both require a systematic approach to problem solving and, as such, are ideal for use in conjunction with automatic computers.

CHAPTER VII

THE STRESS ANALYSIS OF BRACED DOMES

7.1 THE SCHWEDLER DOME

A Schwedler dome is illustrated in Figure 10(a) and the main features of such structures are discussed in Art. 3.2. The primary members in a Schwedler dome are straight or curved bars called ribs lying, in general, on some surface of revolution. These ribs are connected together by means of polygonal rings which divide the surface into trapezoidal shaped bays. Each bay may contain either one or two diagonals which act as counter-bracing. Schwedler domes are assumed to be pin-jointed structures and without the diagonal bracing such systems would be unstable if loaded unsymmetrically.

As Schwedler domes are considered to be pin-jointed and statically determinate, some of the procedures discussed previously in Chapter IV can be employed in their analysis. In Art. 4.6, the analysis of a Schwedler type dome, Figure 21, was considered with regard to symmetry in complex trusses. The method of analysis was advanced by Johann W. A. Schwedler,[12] in 1863, when he first built a dome of this type named after him. Unfortunately Schwedler's solution only holds good for symmetrical loading.

Consider a single rib of a Schwedler dome as illustrated in Figures 29(a) and (b). At each joint, for vertical equilibrium, it can be shown that:

$$P_1 = S_1 \sin\alpha_1$$

$$P_1 + P_2 = S_2 \sin\alpha_2 \qquad \ldots\ldots (7{\cdot}1)$$

$$P_1 + \ldots\ldots + P_{m-1} + P_m = S_m \sin\alpha_m$$

where:

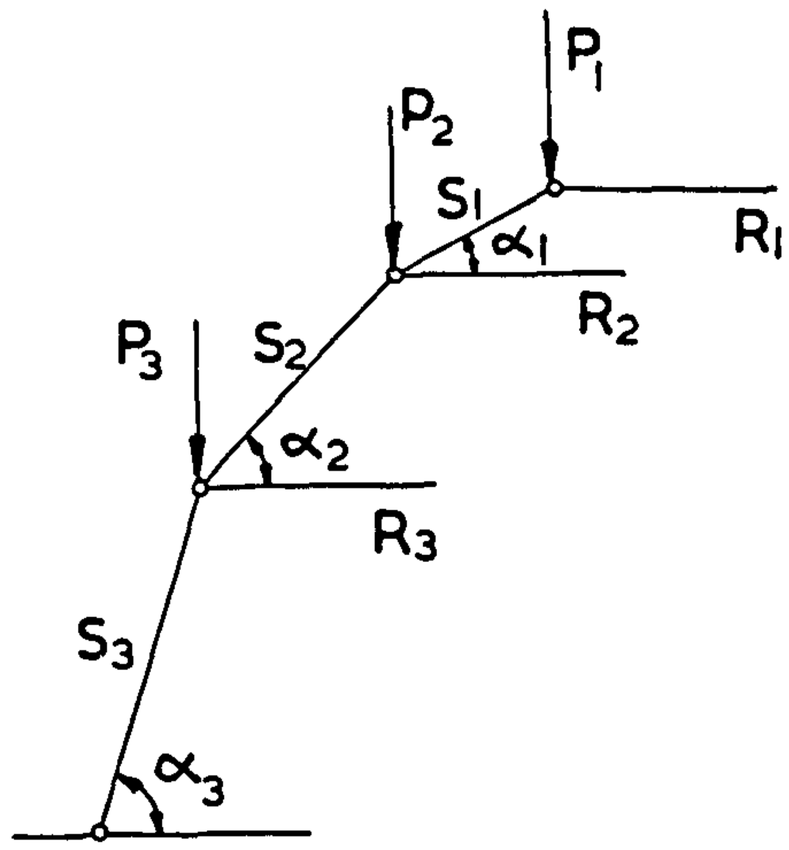

(a)

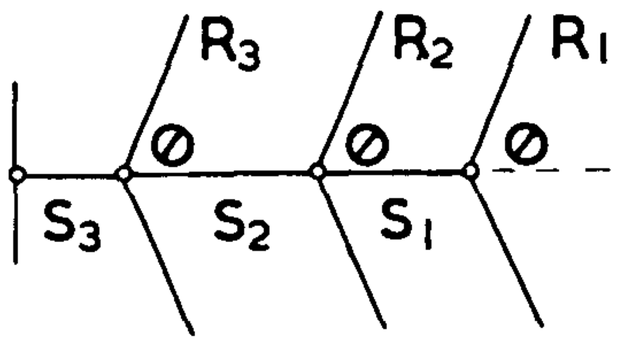

(b)

FIG 29 SCHWEDLER'S ANALYTICAL METHOD

F.A.A. Ph.D. Thesis
11th Dec., 1969

Structural Engineering Division
Department of Civil Engineering
University of Newcastle upon Tyne

S_1, S_2 = forces in the ribs;

R_1, R_2 = forces in the rings;

P_1, P_2 = loads at the joints;

α_1, α_2 = angles of rib inclinations;

n = number of meridian ribs;

m = number of horizontal rings.

To satisfy horizontal equilibrium, it can be shown that:

$$2R_1 \sin\frac{\pi}{n} = S_1 \cos\alpha_1$$

$$2R_2 \sin\frac{\pi}{n} = S_2 \cos\alpha_2 - S_1 \cos\alpha_1 \qquad \ldots\ldots (7\cdot2)$$

$$2R_m \sin\frac{\pi}{n} = S_m \cos\alpha_m - S_{m-1} \cos\alpha_{m-1}$$

Four general laws can easily be deduced for use in an analysis by Schwedler's method. These are:

(1) The ribs carry maximum stress when the whole dome is fully loaded.

(2) A ring is in maximum tension when the entire dome lying above the ring, but not the ring itself, is fully loaded.

(3) A ring is in maximum compression when all of the dome below the ring, and including the ring, is fully loaded.

(4) Under symmetrical loading the diagonals carry no stress. A diagonal carries maximum stress when the dome is fully loaded on one side of a meridian plane passing through the centre of the panel. For such a condition, Schwedler gave the following approximate formulae for stress in the diagonals:

$$D_1 = \frac{L_1}{2 \sin\alpha_1 \cos\beta_1} \qquad \ldots\ldots (7\cdot3)$$

$$D_2 = \frac{L_1 + L_2}{2 \sin\alpha_2 \cos\beta_2}$$

where:

L_1, L_2 = live loads at the joints;

D_1, D_2 = forces in the diagonals;

β_1, β_2 = angles made by the diagonals with the ribs.

Although Schwedler's formulae can be applied quickly and simply to give approximate results, they have one serious drawback. These formulae can only be used for symmetrical loading conditions and, as the rigidity of the joints is neglected, they lead in all cases to an over-estimation of the maximum stresses.

The Tension Coefficients Method, Art. 4.8, and the Method of Conjugate Forces, Art. 4.9, can both be employed in the analysis of Schwedler domes. For a structure which has a large number of members, the analytical procedure employing tension coefficients becomes tedious and errors are liable to occur when carrying over force values from one joint to the next. However the value of the graphical method, using the principle of conjugate forces, increases with the complexity of the system.

7.2 THE STIFF-JOINTED FRAMED DOME

(a) El-Sayed El-Schasly's Method[10],[12]

Stiff-jointed framed domes are identical in appearance to Schwedler domes. However, whereas the Schwedler dome is considered to be a pin-jointed structure, the joints in the first mentioned system are assumed to be rigid. The effect of rigid joints on the stress distribution in Schwedler domes was first investigated by El-Sayed El-Schasly. In order to simplify the calculations he assumed that the bending rigidities of only certain members in certain directions were important.

An analysis was carried out by considering the meridian ribs to be rigid in their bending plane, with torsional rigidity neglected. The rings and diagonals were regarded as being pin-connected to the ribs. El-Sayed El-Schasly assumed first that his primary structure was a completely pin-jointed system and then applied unknown moments $X_1, X_2 \ldots\ldots X_n$ at the nodes of the ribs. For any joint r this gives:

$$X_1 d_{r1} + X_2 d_{r2} + \ldots\ldots X_n d_{rn} + d_{ro} = 0 \qquad \ldots\ldots (7\cdot4)$$

where:

d_{r1} = change in the angle α_r due to $X_1 = 1$;

d_{r2} = change in the angle α_r due to $X_2 = 1$;

d_{ro} = change in the angle α_r due to the external load;

α_r = angle between the meridian bars at the node r.

For n rigid rib nodes there are n unknowns requiring the solution of n simultaneous equations to complete the analysis.

El-Sayed El-Schasly found that the flexural rigidity of the meridian ribs greatly influenced the stress distribution in the dome members. A more even stress distribution was produced and deflections were considerably reduced. He then considered the effect of ring rigidity, assuming bending to occur only in the horizontal plane. Two cases need to be investigated.

(1) Stiff Lantern Ring. The stiff connection of the continuous meridian rib and the lantern ring causes the moment at the node of interconnection to be distributed into three components M_{rb}, M_{r1} and M_{r2}, where:

M_{rb} = bending moment in the rib about an axis at right angles to the plane of the rib;

M_{r1} and M_{r2} = bending moments in the ring elements.

If w is the angle between the ring elements, then:

$$M_{rb} = (M_{r1} + M_{r2}) \sin \frac{w}{2} \qquad \ldots\ldots (7\cdot5)$$

As the ribs and the ring are rigidly connected, the angle of rotation of their ends at the node must be the same. If ϕ is the angle of rotation of a bar end due to unit moment, then:

$$\phi_{rb} M_{rb} = \frac{\phi_{r1} M_{r1}}{\sin \frac{w}{2}} = \frac{\phi_{r2} M_{r2}}{\sin \frac{w}{2}} \qquad \ldots\ldots (7\cdot6)$$

This leads to:

$$\frac{1}{\phi_{rb}} = \left(\frac{1}{\phi_{r1}} + \frac{1}{\phi_{r2}}\right) \sin^2 \frac{w}{2} \qquad \ldots\ldots (7\cdot7)$$

Owing to cyclic symmetry $\phi_{r_1} = \phi_{r_2} = \phi_r$.

Therefore:

$$\phi_{rb} = \frac{\phi_r}{2 \sin^2 \frac{w}{2}} \qquad \ldots\ldots (7\cdot8)$$

or:

$$\frac{M_{r_1}}{M_{rb}} = \frac{1}{2 \sin \frac{w}{2}} \qquad \ldots\ldots (7\cdot9)$$

This leads to the conclusion that the ratio of the bending moments in the ring and the rib is dependent only on the ring angle w.

(2) Stiff Intermediate Ring. A similar procedure to the one just discussed for the stiff lantern ring can be employed for the stiff intermediate rings. However, El-Sayed El-Schasly is of the opinion that such a connection need not be considered since the stress distribution is not greatly affected. This is especially so when the moment of inertia of the ribs is large compared with that of the rings.

The assumptions made in Art. 7.2(a) are valid only under certain conditions. Although the rigidities considered here are the most important ones for symmetrical loading cases, under asymmetrical loading this would not be so and a gross misrepresentation of the actual behaviour of a structure would be obtained. The labour required to solve a practical structure with a large number of ribs and rings would be enormous by this method and the redundancy of the system would prohibit its use.

(b) Kaufmann's Method[10],[12]

W. Kaufmann applied the simplifying properties of cyclically symmetrical systems to the analysis of stiff-jointed framed domes. A structure is said to be cyclically symmetrical to the nth degree when a rotation of $\frac{2\pi}{n}$ about its vertical axis causes it to reoccupy its original outline. Kaufmann considered a dome with a stiff ring girder. With the same notations as in Art. 7.2(a), the following expression is

obtained:

$$X_1 d_{r1} + X_2 d_{r2} + X_3 d_{r3} + \ldots\ldots + X_n d_{rn} = C_r \qquad \ldots\ldots (7.10)$$

where the left-hand side is the change in the angle at r produced by the redundant moments and the right-hand side is the change in the angle produced by the external load.

Due to cyclic symmetry:

$$d_{11} = d_{22} = d_{33} \ldots\ldots d_{nn} = \alpha_1$$

$$d_{21} = d_{32} = d_{43} \ldots\ldots d_{n,n-1} = \alpha_2 \qquad \ldots\ldots (7.11)$$

$$d_{31} = d_{42} = d_{53} \ldots\ldots d_{n,n-2} = \alpha_3$$

The general denominator of the elastic equation can hence be obtained in the form of a cyclic determinant of the nth order:

$$D = \begin{vmatrix} \alpha_1 & \alpha_2 & \alpha_3 & \alpha_4 & \ldots\ldots & \alpha_n \\ \alpha_n & \alpha_1 & \alpha_2 & \alpha_3 & \ldots\ldots & \alpha_{n-1} \\ \alpha_{n-1} & \alpha_n & \alpha_1 & \alpha_2 & \ldots\ldots & \alpha_{n-2} \\ \cdot & \cdot & \cdot & \cdot & \ldots\ldots & \cdot \\ \cdot & \cdot & \cdot & \cdot & \ldots\ldots & \cdot \\ \cdot & \cdot & \cdot & \cdot & \ldots\ldots & \cdot \\ \alpha_2 & \alpha_3 & \alpha_4 & \alpha_5 & \ldots\ldots & \alpha_1 \end{vmatrix} \qquad \ldots\ldots (7.12)$$

E. Pascal found that:

$$D = \Psi(\alpha Z_0)\Psi(\alpha Z_1) \ldots\ldots \Psi(\alpha Z_{n-1}) \qquad \ldots\ldots (7.13)$$

where:

$$\Psi(\alpha Z_k) = \alpha_1 + \alpha_2 Z_k + \alpha_3 Z_k^2 + \ldots\ldots \alpha_n Z_k^{n-1} \qquad \ldots\ldots (7.14)$$

Z_k are the roots of a special binomial.

$$Z^n - 1 = 0 \text{ where } k = 0, 1, \ldots\ldots n-1$$

$$Z_k = \cos k \frac{2\pi}{n} + i \sin k \frac{2\pi}{n} \qquad \ldots\ldots (7.15)$$

The unknowns are determined as follows:

For an even n:

$$X_1 = \frac{1}{D}\left[C_1 U_1 + (C_2 + C_n)U_2 + \ldots\ldots + C_{\frac{n}{2}+1} U_{\frac{n}{2}+1} \right]$$

$$X_2 = \frac{1}{D}\left[C_2 U_1 + (C_3 + C_1)U_2 + \ldots\ldots + C_{\frac{n}{2}+2} U_{\frac{n}{2}+1} \right] \qquad \ldots\ldots (7.16)$$

$$X_n = \frac{1}{D}\left[C_n U_1 + (C_1 + C_{n-1})U_2 + \ldots\ldots + C_{\frac{n}{2}} U_{\frac{n}{2}+1} \right]$$

For an odd n:

$$X_1 = \frac{1}{D}\left[C_1U_1 + (C_2 + C_n)U_2 + \cdots\cdots + \left(C_{\frac{n+1}{2}} + C_{\frac{n+3}{2}}\right)U_{\frac{n+1}{2}} \right]$$

$$X_2 = \frac{1}{D}\left[C_2U_1 + (C_3 + C_1)U_2 + \cdots\cdots + \left(C_{\frac{n+3}{2}} + C_{\frac{n+5}{2}}\right)U_{\frac{n+1}{2}} \right]$$

$$X_n = \frac{1}{D}\left[C_nU_1 + (C_1 + C_{n-1})U_2 + \cdots\cdots + \left(C_{\frac{n-1}{2}} + C_{\frac{n+1}{2}}\right)U_{\frac{n+1}{2}} \right]$$

$$\cdots\cdots (7\cdot17)$$

where for n even:

$$\frac{Ur}{D} = \frac{1}{n}\left[\frac{1}{\alpha_0} + \frac{(-1)^{\gamma-1}}{\alpha_\gamma} + 2\sum_{k=1}^{k=\gamma-1} \frac{\cos\,(\gamma-1)\,k\,\frac{2\pi}{n}}{\psi(\alpha Z_k)}\right] \quad \cdots\cdots(7\cdot18)$$

In this expression $\gamma = \frac{n}{2}$ (n = number of redundancies or thenumber of sides of the polygonal ring).

For n odd:

$$\frac{Ur}{D} = \frac{1}{n}\left[\frac{1}{\alpha_0} + 2\sum_{k=1}^{k=\frac{n-1}{2}} \frac{\cos\,(\gamma-1)\,k\,\frac{2\pi}{n}}{\psi(\alpha Z_k)}\right] \quad \cdots\cdots (7\cdot19)$$

Kaufmann's analysis is not a method which would be employed by design engineers. The expressions are extremely complicated even though only one stiff ring has been considered. If two stiff rings are considered the expressions become even more complicated. The general elastic equation is formed in the same way but the determinant is no longer cyclic. Stiff ribs can also be considered in a similar manner but it is unlikely that this method will be used in practice.

(c) <u>The Influence Coefficients Method</u>[12]

Influence coefficients can be employed to determine the stress distribution in stiff-jointed framed domes. Cuts or stress releases are introduced at appropriate points, keeping the system stable, to make the structure statically determinate. The redundancies are now introduced as external loads at these cuts and the relative displacements or rotations that would be caused between the different parts of the structure by each redundancy acting alone are determined. By equating to zero the sum of the deformations caused by the redundancies and the external loads at each cut, all the gaps in the structure

are closed and the structure returns to its original form.

Consider a structure which is statically indeterminate to the nth degree. Hence there are n redundancies $X_1, X_2, \ldots\ldots X_n$. Releases are introduced in the form of cuts with 6 releases, hinges with 3 releases, etc. The redundancies are now introduced separately as loads on the primary structure and the stress distribution determined over the entire frame. In order to obtain this stress distribution it is necessary to determine the influence coefficients d_{ik} for each redundancy.

d_{ik} is the displacement or rotation caused at the joint i due to unit redundancy $X_k = 1$ applied at the joint K. If X_i is a force then d_{ik} is a displacement and if X_i is a moment d_{ik} is a rotation. In both cases the deformation is in the direction of X_i. If continuity at i is to be restored, it follows that:

$$d_{i1}X_1 + d_{i2}X_2 + \ldots\ldots + d_{in}X_n + d_iR = 0 \qquad \ldots\ldots (7\cdot20)$$

where d_iR is the deformation at i and in the direction of X_i due to the external load.

All the equations for the structure can be grouped together as follows:

$$\begin{aligned}
&d_{11}X_1 + d_{12}X_2 + d_{13}X_3 + \ldots\ldots + d_{1n}X_n + d_1R = 0\\
&d_{21}X_1 + d_{22}X_2 + d_{23}X_3 + \ldots\ldots + d_{2n}X_n + d_2R = 0\\
&\vdots\quad\vdots\quad\vdots\qquad\vdots\quad\vdots\quad\vdots\qquad\qquad\vdots\quad\vdots\quad\vdots\quad\vdots\quad\vdots\\
&d_{n1}X_1 + d_{n2}X_2 + d_{n3}X_3 + \ldots\ldots + d_{nn}X_n + d_nR = 0
\end{aligned} \qquad \ldots\ldots (7\cdot21)$$

In matrix notation equations (7·21) become:

$$\begin{bmatrix} d_{11} & d_{12} & d_{13} & \ldots\ldots & d_{1n}\\ d_{21} & d_{22} & d_{23} & \ldots\ldots & d_{2n}\\ \vdots & \vdots & \vdots & & \vdots\\ d_{n1} & d_{n2} & d_{n3} & \ldots\ldots & d_{nn} \end{bmatrix} \begin{bmatrix} X_1\\ X_2\\ \vdots\\ X_n \end{bmatrix} = - \begin{bmatrix} d_1R\\ d_2R\\ \vdots\\ d_nR \end{bmatrix} \qquad \ldots\ldots (7\cdot22)$$

i.e. $FX = -U$ or $X = -F^{-1}U$

F is the flexibility matrix for the structure. It is unique and independent of the loading. By applying Clerk Maxwell's reciprocal theorem whereby:

$$d_{ik} = d_{ki}$$

the determination of the influence coefficients can be very much simplified. In an exact analysis, the values of the influence coefficients can be obtained from the following expression:

$$d_{ik} = \left[\int \frac{M_i^x M_k^x \, ds}{EI_x} + \int \frac{M_i^y M_k^y \, ds}{EI_y} + \int \frac{P_i P_k \, ds}{EA} + \int \frac{S_i^x S_k^x \, ds}{\alpha AN} + \int \frac{S_i^y S_k^y \, ds}{\alpha AN} + \int \frac{T_i T_k \, ds}{NC} \right] \quad \ldots\ldots (7.23)$$

where: M = bending moment;

P = axial force;

S = shear force;

T = torque;

E = modulus of elasticity;

N = modulus of rigidity;

α = a factor depending on the shape of the cross-section;

C = Polar second moment of area of the cross-section.

Although the expression for evaluating the influence coefficients appears to be complicated, in fact, it is a simple matter to integrate together regular diagrams.

Let the M_i and M_k diagrams for any bar be as shown in Figure 30(a), where:

$M_i = F_1(x)$ and $M_k = F_2(x)$

$F_1(x)$ can be any function of x, but $F_2(x)$ must in all cases be linear

i.e. $F_2(x) = ax + b$.

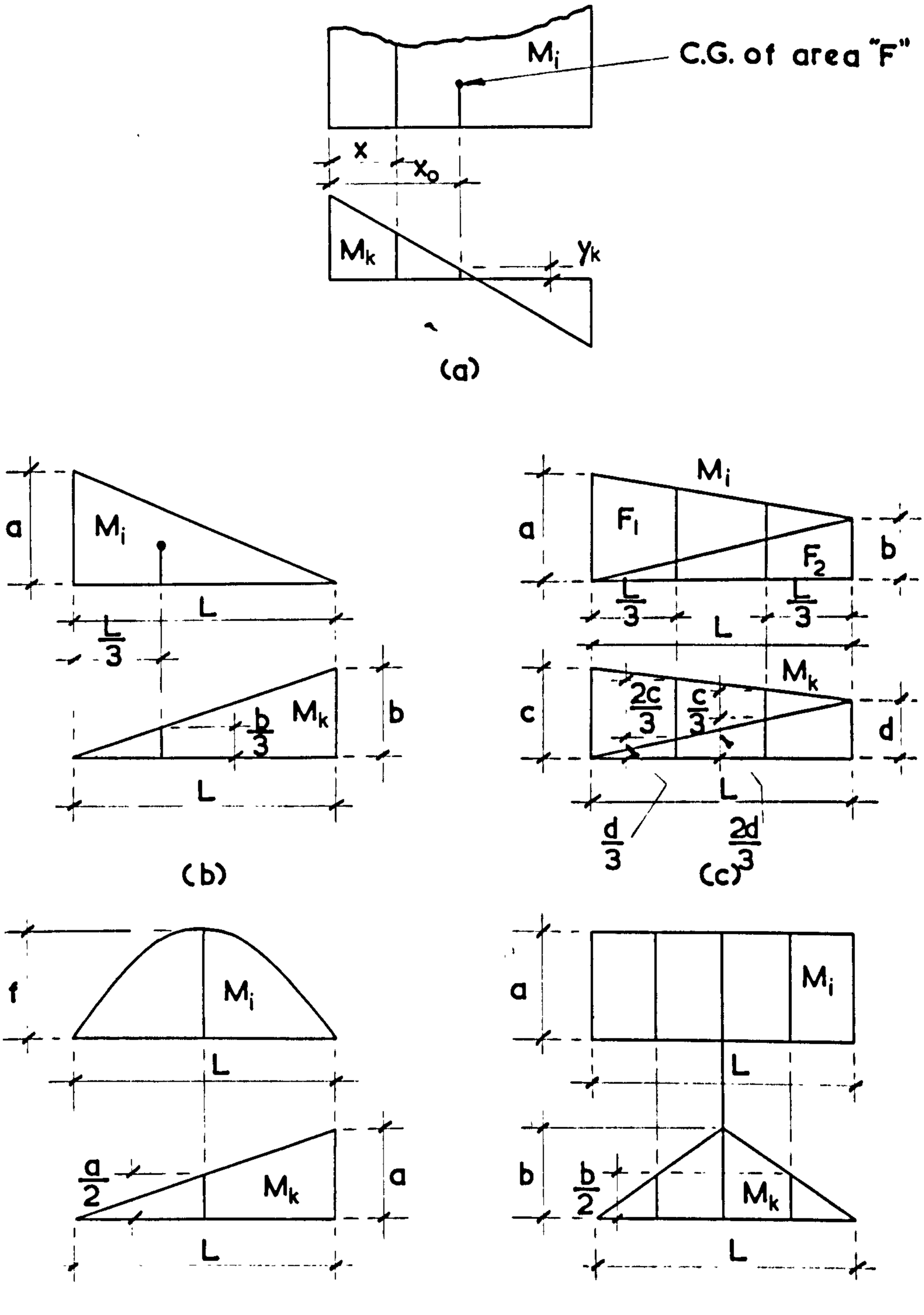

FIG. 30 THE INTEGRATION OF DIAGRAMS FOR THE DETERMINATION OF INFLUENCE COEFFICIENTS

F.A.A. Ph. D. Thesis
29th Dec., 1969

Structural Engineering Division
Department of Civil Engineering
University of Newcastle upon Tyne

$$d_{ik} = \int_0^L \frac{M_i M_k}{EI}\, ds = \frac{1}{EI}\int_0^L F_1(x)\, F_2(x)\, dx = \frac{1}{EI}\int_0^L F_1(x)(ax+b)dx$$

$$= \frac{1}{EI}\, a\int_0^L xF_1(x)dx + \frac{b}{EI}\int_0^L F_1(x)dx \qquad \ldots\ldots (7\cdot24)$$

If the total area of the $F_1(x)$ diagram is denoted by F and the ordinate of the $F_2(x)$ diagram at the centre of gravity of the area F is denoted by y_k, as shown in Figure 30(a), then:

$$\int_0^L F_1(\dot{x})\, dx = F$$

$$\int_0^L x\, F_1(x)dx = Fx_o$$

and:

$$y_k = ax_o + b$$

where x_o is the distance of the centre of gravity of the area F from the origin. Substituting in equation (7.24) above to obtain d_{ik} gives:

$$d_{ik} = \frac{1}{EI}\, aFx_o + \frac{b}{EI}\, F$$

$$= \frac{1}{EI}\, F\,(ax_o + b)$$

i.e $$d_{ik} = \frac{Fy_k}{EI} \qquad \ldots\ldots (7\cdot25)$$

It can be seen, therefore, that to integrate two diagrams together all that is necessary is to consider the area of the first and multiply it by the ordinate of the second at the centre of gravity of the first, assuming that the second diagram is linear.

Four simple cases, which can be integrated easily, are shown in Figures 30(b), (c), (d) and (e). To integrate together two triangular diagrams due to bending moments, as illustrated in Figure 30(b), values of $F = \frac{aL}{2}$ and $y_k = \frac{b}{3}$ give:

$$d_{ik} = \frac{Fy_k}{EI} = \frac{abL}{6EI} \qquad \ldots\ldots (7\cdot26)$$

The integration of two trapezoidal diagrams due to bending moments, as shown in Figure 30(c), produces:

$$d_{ik} = \frac{1}{EI}\left[\frac{aL}{2}\left(\frac{2c+d}{3}\right) + \frac{bL}{2}\left(\frac{c+2d}{3}\right)\right] \qquad \ldots\ldots (7\cdot27)$$

since:

$$F_1 = \frac{aL}{2}\ ;\ F_2 = \frac{bL}{2}\ ;\ y_{k1} = \frac{2c+d}{3}\ ;\ y_{k2} = \frac{c+2d}{3}$$

Bending moments in the form of a parabola and a triangle, Figure 30(d), when integrated together result in a value of:

$$d_{ik} = \frac{afL}{3EI} \quad \ldots\ldots (7.28)$$

where f is the maximum ordinate of the parabola and $F = \frac{2}{3}fL$, $y_k = \frac{a}{2}$. When the $F_2(x)$ diagram is linear but broken, as illustrated in Figure 30(e), a similar approach can be used but the integration must be carried out in parts. In this case $F_1 = \frac{aL}{2} = F_2$; $y_{k1} = \frac{b}{2} = y_{k2}$ and:

$$d_{ik} = \frac{1}{EI} \frac{abL}{4} \times 2 = \frac{abL}{2EI} \quad \ldots\ldots (7.29)$$

Many combinations of bending moment diagrams can occur in practice which can be worked out according to the principles outlined above. Professor Makowski[12] compiled a table of the more important cases and this has been reproduced in Figures 31, 32 and 33.

From equation (7.23) it can be seen that the total d_{ik} actually consists of a number of elements due to moment strains, axial strains, shear strains and torsional strains. Before the total d_{ik} can be evaluated, each element must be divided by the relevant value of EI, EA, $\propto$AN and NC respectively. Values for these rigidities must be assumed at the commencement of the dome analysis. The choice of these values materially affects the terms of the simultaneous equations and hence the final solution. It is possible for the final design of a dome to yield members whose rigidities have no relation to the assumed ones, hence invalidating all previous calculations. However, according to Benjamin,[12] the actual values of the rigidities themselves are not important in the analysis. It is only the relative values of the rigidities that are important since a common factor can be removed from all expressions leaving the solution unchanged. Benjamin also states that only the cross-sectional area A and the moment of inertia I_x are of importance in dome design.

In order to allow for the variation of cross-sectional area and moment of inertia across a dome, some simplifying assumptions must be

$\int_0^L M_i^2\,dx$	M_i – Diagram		M_k – Diagram
$\frac{L}{15}[2(a_i+2k_i+b_i)^2-6h_i(a_i+b_i)-5a_ib_i]$	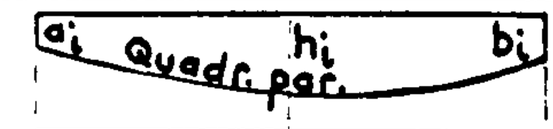	A	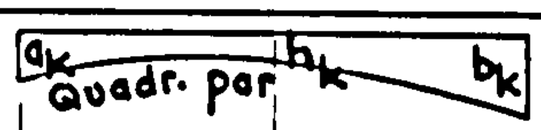
$\frac{8}{15}Lh_i^2$	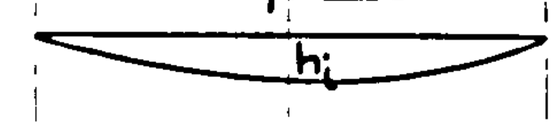	B	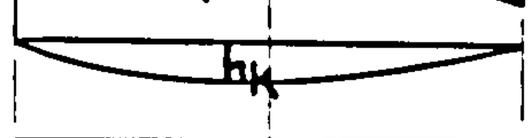
$\frac{8}{15}La_i^2$	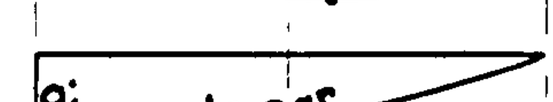	C	
$\frac{1}{5}La_i^2$	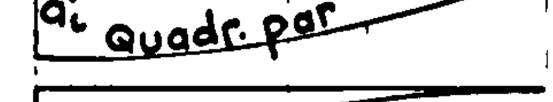	D	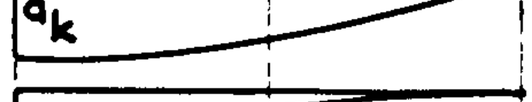
	NOTE All curves A to H are parabolas of second degree 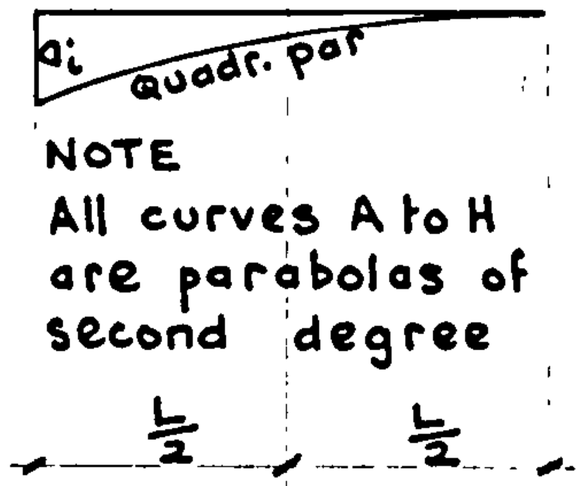	E	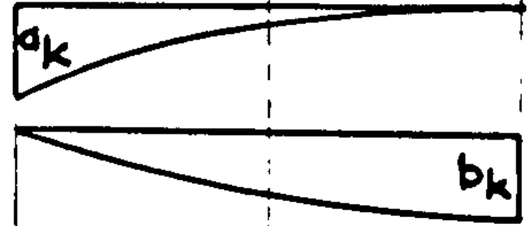
		F	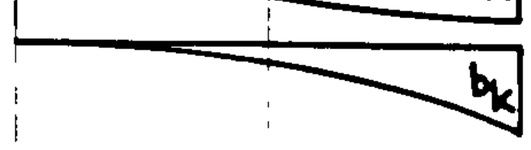
		G	
		H	
$\frac{L}{3}(a_i^2+a_ib_i+b_i^2)$	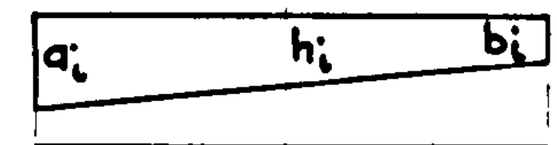	J	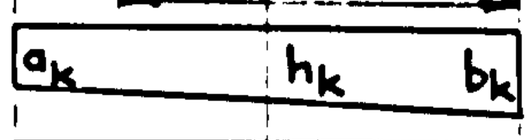
La_i^2	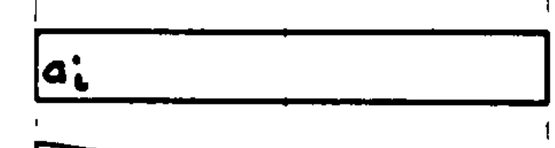	K	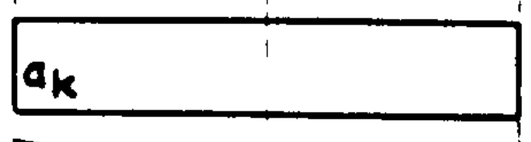
$\frac{La_i^2}{3}$	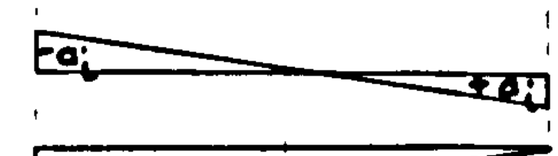	L	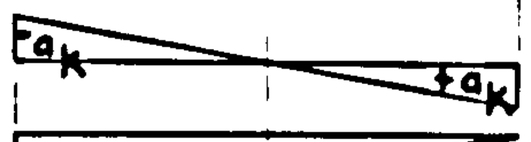
$\frac{La_i^2}{3}$	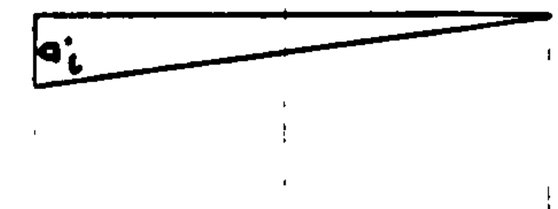	M	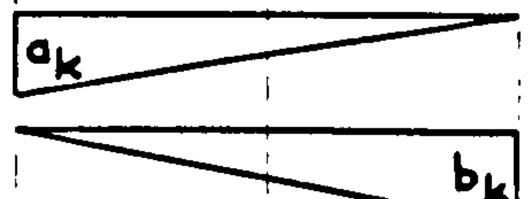
		N	
$\frac{L}{3}(a_i^2+a_ih_i+h_i^2)$	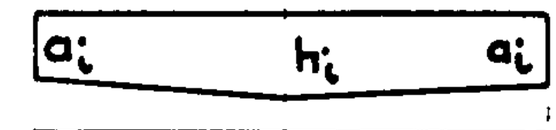	O	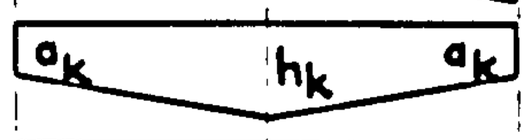
$\frac{Lf_i^2}{3}$	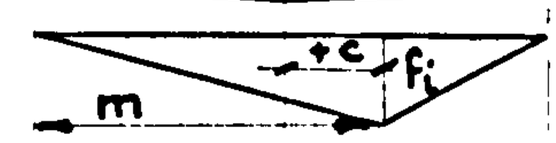	P	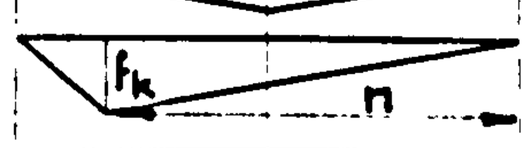
$\frac{Lh_i^2}{3}$	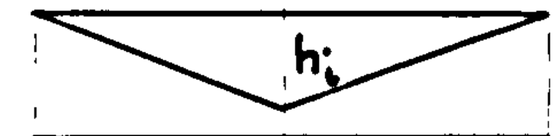	Q	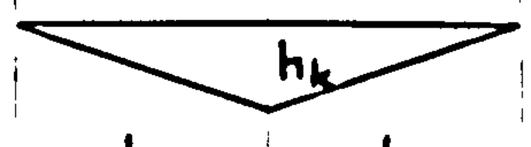
$\frac{(L+2c)a_i^2}{6}$	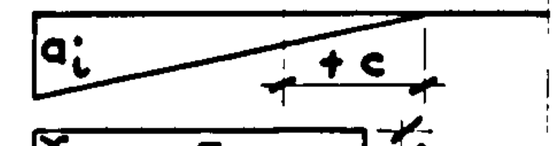	R	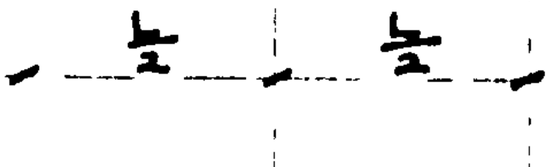
$\frac{f_i^2c(L-c)}{L}$	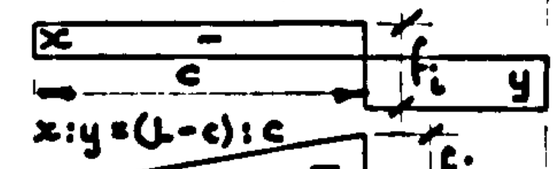	S	
$\frac{f_i^2}{3L}(L^2-3Lc+3c^2)$	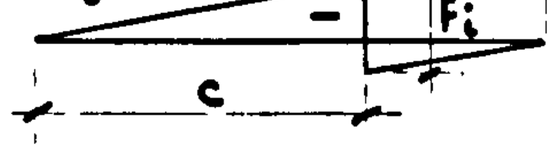	T	
		U	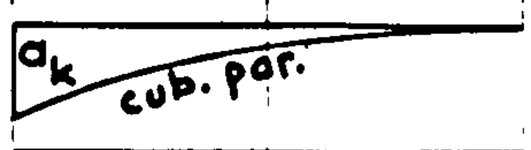
		V	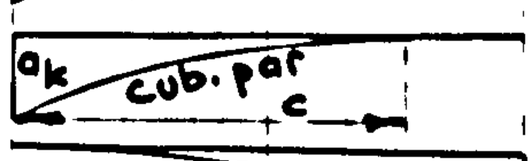
		W	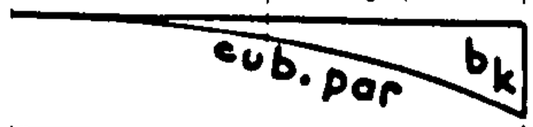
		X	

FIG. 31 EASY DETERMINATION OF INFLUENCE COEFFICIENTS (MAKOWSKI) Sheet No. 1

F.A.A. Ph.D. Thesis
30th Dec., 1969

Structural Engineering Division
Department of Civil Engineering
University of Newcastle upon Tyne

M_i	M_k	$\int_0^L M_i M_k \, dx$
A	A	$\frac{L}{30}[a_i(4a_k + 2h_k - b_k) + b_i(4b_k + 2h_k - a_k) + 2h_i(a_k + 8h_k + b_k)]$
	B	$\frac{Lh_k}{15}[a_i + 8h_i + b_i]$
	C	$\frac{La_k}{60}[11a_i + 28h_i + b_i]$
	D	$\frac{La_k}{60}[9a_i + 12h_i - b_i]$
	G	$\frac{ca_k}{60}[20a_i - 5\frac{c}{L}(3a_i - 4h_i + b_i) + 4(\frac{c}{L})^2(a_i - 2h_i + b_i)]$
	J	$\frac{L}{6}[a_i a_k + 4h_i h_k + b_i b_k]$
	K	$\frac{La_k}{6}[a_i + 4h_i + b_i]$
	L	$\frac{La_k}{6}(b_i - a_i)$
	M	$\frac{La_k}{6}(a_i + 2h_i)$
	O	$\frac{L}{24}[3a_k(a_i + 2h_i + b_i) + h_k(a_i + 10h_i + b_i)]$
	Q	$\frac{Lh_k}{24}[a_i + 10h_i + b_i]$
	U	$\frac{La_k}{60}[8a_i + 8h_i - b_i]$
	V	$\frac{ca_k}{60}[15a_i - 3(\frac{c}{L})(3a_i - 4h_i + b_i) + 2(\frac{c}{L})^2(a_i - 2h_i + b_i)]$
B	B	$\frac{8}{15}Lh_i h_k$
	C	$\frac{7}{15}Lh_i a_k$
	D	$\frac{1}{5}Lh_i a_k$
	G	$\frac{ca_k}{15}h_i \cdot \frac{c}{L}(5 - 2\frac{c}{L})$
	J	$\frac{2}{3}Lh_i h_k$
	K	$\frac{2}{3}Lh_i a_k$
	L	0
	M	$\frac{Lh_i a_k}{8}$
	O	$\frac{1}{12}Lh_i[3a_k + 5h_k]$
	Q	$\frac{5}{12}Lh_i h_k$
	U	$\frac{2}{15}Lh_i a_k$
	V	$\frac{ch_i a_k}{16} \cdot \frac{c}{L}(3 - \frac{c}{L})$
C	C	$\frac{8}{15}La_i a_k$
	D	$\frac{3}{10}La_i a_k$
	E	$\frac{11}{30}La_i b_k$
	F	$\frac{2}{15}La_i b_k$
	G	$\frac{ca_i a_k}{30}[10 - (\frac{c}{L})^2]$
	H	$\frac{ca_i b_k}{30} \cdot \frac{c}{L}(5 - \frac{c}{L})$
	J	$\frac{La_i}{12}(5a_k + 3b_k)$
	K	$\frac{2}{5}La_i a_k$
	L	$-\frac{1}{6}La_i a_k$
	M	$\frac{5}{12}La_i a_k$
	N	$\frac{1}{4}La_i b_k$
	O	$\frac{La_i}{48}[15a_k + 17h_k]$
	Q	$\frac{17}{48}La_i h_k$
	U	$\frac{7}{30}La_i a_k$
	V	$\frac{ca_i a_k}{60}[15 - (\frac{c}{L})^2]$
	W	$\frac{1}{12} \cdot La_i b_k$
	X	$\frac{ca_i b_k}{60} \cdot \frac{c}{L}(6 - \frac{c}{L})$
D	D	$\frac{1}{5}La_i a_k$
	F	$\frac{1}{30}La_i b_k$
	G	$\frac{ca_i a_k}{30}[10 - 5(\frac{c}{L}) + (\frac{c}{L})^2]$
	H	$\frac{ca_i b_k}{30}(\frac{c}{L})^2$
	J	$\frac{La_i}{12}(3a_k + b_k)$
	K	$\frac{La_i a_k}{3}$
	L	$-\frac{La_i a_k}{6}$
	M	$\frac{La_i a_k}{4}$
	N	$\frac{La_i b_k}{12}$
	O	$\frac{La_i}{48}[9a_k + 7h_k]$
	Q	$\frac{7}{48}La_i h_k$
	U	$\frac{1}{6}La_i a_k$
	V	$\frac{ca_i a_k}{60}[15 - 6(\frac{c}{L}) + (\frac{c}{L})^2]$
	W	$\frac{1}{60}La_i b_k$
	X	$\frac{1}{60}La_i b_k(\frac{c}{L})^2$
J	G	$\frac{1}{12}ca_k[4a_i - (\frac{c}{L})(a_i - b_i)]$
	J	$\frac{1}{6}L[a_i a_k + 4h_i h_k + b_i b_k]$
	K	$Lh_i a_k$
	L	$\frac{1}{6}La_k(b_i - a_i)$
	M	$\frac{La_k}{6}(2a_i + b_i)$
	O	$\frac{Lh_i}{2}(a_k + h_k)$
	Q	$\frac{Lh_i h_k}{2}$
	U	$\frac{1}{20}La_k(4a_i + b_i)$

FIG. 32 EASY DETERMINATION OF INFLUENCE COEFFICIENTS (MAKOWSKI) Sheet No. 2

F.A.A. Ph.D. Thesis
6th Jan., 1970

Structural Engineering Division
Department of Civil Engineering
University of Newcastle upon Tyne

M_i	M_k	$\int_0^L M_i M_k\,dx$
J	V	$\frac{1}{20} c a_k [5a_i - (\frac{c}{L})(a_i - b_i)]$
K	K	$L a_i a_k$
	L	0
	M	$\frac{L a_i a_k}{2}$
	O	$\frac{L}{2} a_i (a_k + h_k)$
	Q	$\frac{L a_i h_k}{2}$
	U	$\frac{L a_i a_k}{4}$
	V	$\frac{c a_i a_k}{4}$
L	G	$-\frac{1}{6} c a_i a_k [2 - (\frac{c}{L})]$
	L	$\frac{1}{3} L a_i a_k$
	M	$-\frac{1}{6} L a_i a_k$
	Q	0
	U	$-\frac{3}{20} L a_i a_k$
	V	$-\frac{1}{20} c a_i a_k [5 - 2(\frac{c}{L})^2]$
M	G	$\frac{1}{12} c a_i a_k [4 - \frac{c}{L}]$
	H	$\frac{1}{12} c a_i b_k \frac{c}{L}$
	M	$\frac{1}{3} L a_i a_k$
	N	$\frac{1}{6} L a_i b_k$
	O	$\frac{1}{4} L a_i (a_k + h_k)$
	Q	$\frac{1}{4} L a_i h_k$
	U	$\frac{1}{5} L a_i a_k$
	V	$\frac{1}{20} c a_i a_k [5 - \frac{c}{L}]$
	W	$\frac{1}{20} L a_i b_k$
	X	$\frac{1}{20} c a_i b_k \cdot \frac{c}{L}$
O	O	$\frac{L}{6} [a_i (2a_k + h_k) + h_i (a_k + 2h_k)]$
	Q	$\frac{L h_k}{6} (a_i + 2h_i)$
	U	$\frac{L a_k}{32} (5a_i + 3h_i)$
P	A	$\frac{L f_i}{24} [(a_k + 10h_k + b_k) - 4\frac{c}{L}(a_k - b_k) + 4(\frac{c}{L})^2 (a_k - 2h_k + b_k)]$
	B	$\frac{L f_i h_k}{12} [5 - 4(\frac{c}{L})^2]$
	J	$\frac{L f_i}{12} [3h_k - (\frac{c}{L})(a_k - b_k)]$
	K	$\frac{L f_i a_k}{2}$
	L	$\frac{c f_i a_k}{8}$
	M	$\frac{L f_i a_k}{12} [3 - 2\frac{c}{L}]$
	N	$\frac{L f_i b_k}{12} [3 + 2\frac{c}{L}]$

M_i	M_k	$\int_0^L M_i M_k\,dx$
P	P	$\frac{1}{6} L f_i f_k [m(2L-m) + n(2L-n) - L^2]$
	Q	$\frac{1}{3} L f_i f_k [1 - 2(\frac{c}{L})^2 / (1 + 2\frac{c}{L})]$
Q	Q	$\frac{1}{3} L h_i h_k$
	U	$\frac{3}{32} L h_i a_k$
R	K	$\frac{1}{2} a_i a_k (\frac{L}{2} + c)$
	L	$-\frac{1}{6} L a_i a_k [1 + \frac{c}{L} - 2(\frac{c}{L})^2]$
	M	$\frac{1}{24} L a_i a_k [5 + 8\frac{c}{L} - 4(\frac{c}{L})^2]$
	N	$\frac{1}{24} a_i b_k [1 + 4\frac{c}{L} + 4(\frac{c}{L})^2]$
S	A	$-\frac{f_i c(L-c)}{6L} [(5a_k - 4h_k - b_k) - 4\frac{c}{L}(a_k - 2h_k + b_k)]$
	B	$-\frac{2 f_i h_k c(L-c)}{3L} (2\frac{c}{L} - 1)$
	C	$-\frac{f_i a_k c(L-c)}{3L} (1 + \frac{c}{L})$
	D	$-\frac{f_i a_k c(L-c)}{3L} (2 - \frac{c}{L})$
	J	$-\frac{f_i c(L-c)}{3L} (a_k - b_k)$
	K	0
	L	$\frac{f_i a_k c(L-c)}{L}$
	M	$-\frac{f_i c(L-c) a_k}{2L}$
	N	$\frac{f_i c(L-c) b_k}{2L}$
	O	$\frac{f_i (h_k - a_k)(L-c)(L-2c)}{4L}$
	Q	$\frac{f_i h_k (L-c)(L-2c)}{4L}$
	U	$\frac{f_i a_k c(L-c)}{4L} [3 - 3\frac{c}{L} + (\frac{c}{L})^2]$
T	K	$\frac{1}{2} L f_i a_k (1 - 2\frac{c}{L})$
T $c=\frac{L}{2}$	A	$\frac{L f_i}{24} (b_k - a_k)$
	B	0
	C	$-\frac{L f_i a_k}{24}$
	D	$-\frac{L f_i a_k}{24}$
	J	$\frac{L f_i (b_k - a_k)}{24}$
	K	0
	L	$\frac{L f_i a_k}{12}$
	M	$-\frac{L f_i a_k}{24}$
	N	$\frac{L f_i b_k}{24}$
	O	0
	Q	0
	U	$-\frac{11}{320} L f_i a_k$

FIG. 33 EASY DETERMINATION OF INFLUENCE COEFFICIENTS (MAKOWSKI) Sheet No. 3

F.A.A. Ph.D. Thesis
6th Jan., 1970

Structural Engineering Division
Department of Civil Engineering
University of Newcastle upon Tyne

made. Two empirical laws which can be applied are discussed now. Firstly it may be assumed, as for arches, that:

$$I = \frac{Io}{\cos\phi} \quad ; \quad A = \frac{Ac}{\cos\phi}$$

where Io is the moment of inertia of the members at the crown and Ao is the cross-sectional area of the members at the crown. This applies to both rib and ring members, though an initial ratio of the values of the rib to the ring members has to be assumed.

Alternatively, it may be assumed that:

$$\frac{I}{A} = \text{constant}$$

and

$$\frac{A}{b} = \text{constant over the entire dome}$$

where b is the length of arc serving any particular bar at the centre of the bar as shown later in Figures 35(a) and (c). This latter assumption is best since both rib and ring members have their properties easily defined.

It is now possible to illustrate how the Influence Coefficients Method can be applied to stiff-jointed framed domes. Consider the stiff-jointed framed dome shown in Figure 34(a). It is fully rigid with 8 ribs and 3 rings. The top is open and no diagonals are provided. As the dome is assumed fixed at the base, 6 cuts are required to make the structure statically determinate and stable. The primary structure is now a cantilever and at each cut there are 6 unknowns as shown in Figure 34(b). Therefore, in the most general case, there are 36 unknowns. If the loading is symmetrical, however, the redundancies at the two cuts at each ring level are identical. In addition, as shear or torque would tend to make adjacent cantilevers unlike and as $M^y = 0$ there remain only six unknowns. These unknowns P_1, P_2, P_3, M_1^x, M_2^x and M_3^x are shown in Figure 34(c). Each one can be applied separately to the cantilevers as a unit value and the bending moments, axial forces and shear forces determined over the entire cantilever.

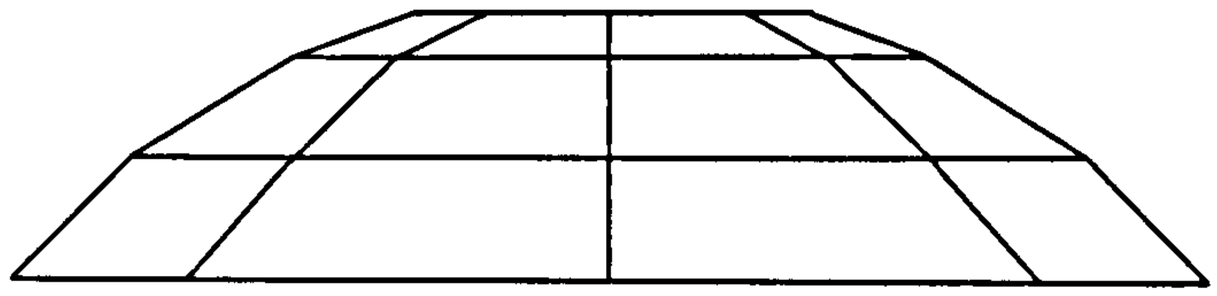

(a)

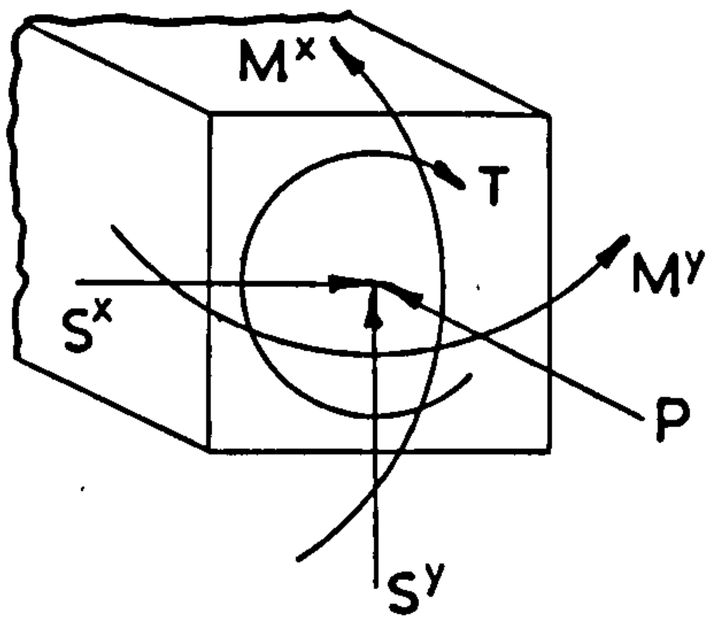

(b)

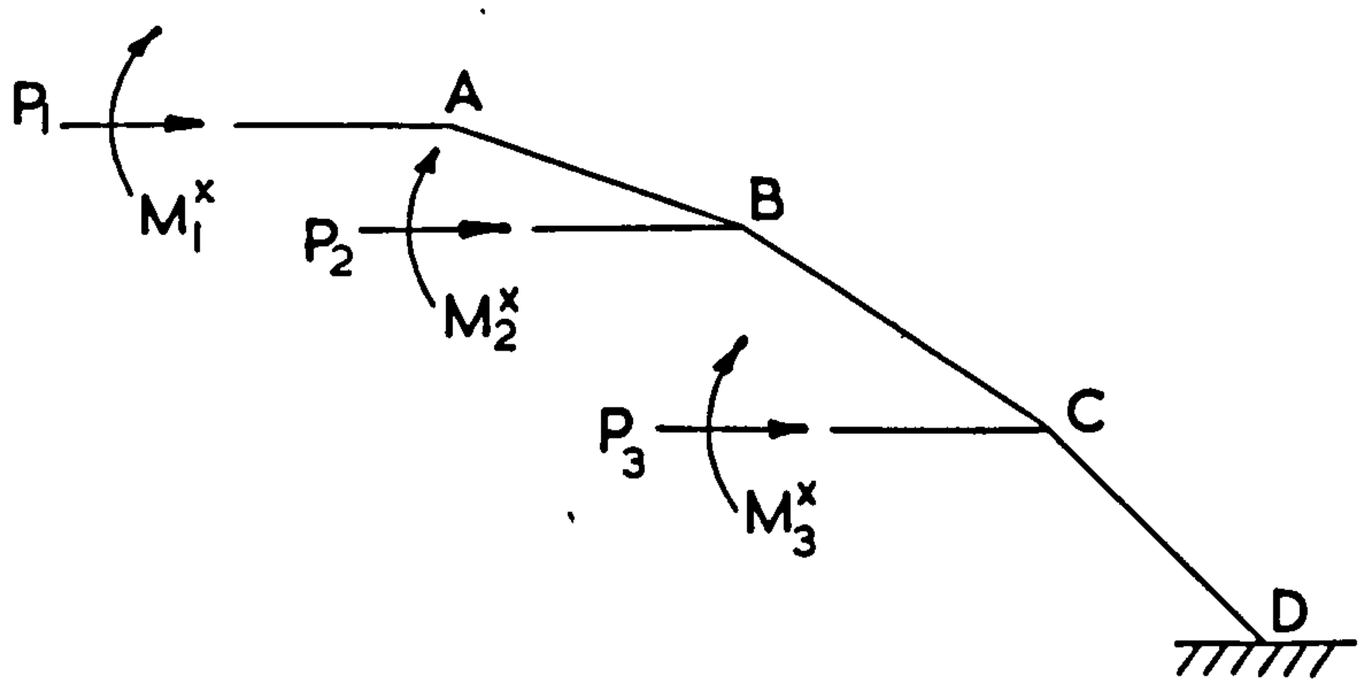

(c)

FIG. 34 STIFF-JOINTED FRAMED DOMES

F.A.A. Ph.D. Thesis
8th Jan., 1970

Structural Engineering Division
Department of Civil Engineering
University of Newcastle upon Tyne

A table of diagrams can be prepared for each redundancy and the integration of these diagrams is very much simplified by the fact that, for the redundancies considered, the M^y; S^x and T strains are zero over the entire structure. It is now a relatively easy task to determine the total d_{ik} from the formula:

$$d_{ik} = \int \frac{M_i^x M_k^x \, ds}{EI} + \int \frac{P_i P_k \, ds}{EA} + \int \frac{S_i^y S_k^y \, ds}{\alpha AN} \qquad \ldots\ldots (7\cdot30)$$

First of all, however, it is necessary to fix the values of EI, EA and αAN over the entire dome. On the assumption previously outlined that $\frac{I}{A}$ and $\frac{A}{b}$ are constant, it is possible to obtain the properties of all the members of the dome relative to a unit EI value of the bar CD, shown in Figure 34(c). The d_{ik} values can now be obtained by the determination of the separate terms in equation (7.30) and the total d_{ik} is obtained by summation. When all the d_{ik} terms have been evaluated for the structure, they can then be substituted in equation (7.22). Thus, so far in the analysis, the flexibility matrix for the dome has been obtained.

To complete the analysis it is necessary to obtain the $d_i R$ terms of equation (7.22). The external load is applied to the statically determinate structure and the process, outlined above, repeated identically to give these terms. On solving the simultaneous equations (7.21) by direct elimination or by inversion of matrices the X_i redundancies, i.e. P_1, P_2, P_3, M_1^x, M_2^x and M_3^x in the case under consideration, are obtained. It is now a simple matter to determine the axial forces, shearing forces and bending moments in the ribs and the rings.

Benjamin[12] has analysed the dome illustrated in Figure 34(a) and included axial and shear strains in his computations. Many investigators in the past, such as Schwedler, El-Sayed El-Schasly and Tsze-Sheng Shih,[24] neglected axial strains and shear strains on the

grounds of their unimportance. A detailed investigation carried out by Benjamin, for both open domes and domes closed in at the top, revealed that axial strains are of the utmost importance in determining the correct stress distribution over the structure. The shear strains, however, are not at all important. They do change the stresses slightly, but the change does not justify the amount of extra labour involved in their consideration.

Benjamin showed further that assuming the structure to be pin-connected leads to very heavy axial forces with complete absence of moments. The difference in the behaviour of the pin-connected dome and the rigidly-jointed dome is very great. Assuming the dome to be pin-connected also leads to excessive and unrealistic deflections. Benjamin's investigations were carried out with symmetrical loading at each ring level and therefore the difference between the pin-connected dome and the stiff-jointed one would be even more severe when considering wind loading, or loading of an unsymmetrical nature.

According to Benjamin it is necessary to provide diagonals in a stiff-jointed framed dome to take care of wind loading even though the structure is stable without them. Such a structure becomes very complex and under wind loading, for which the diagonals are inserted, the solution of any practical dome is very difficult. For the design of domes of this type Benjamin suggests the following procedure:

(1) Consider the dome as pin-connected and analyse the dome under self and snow load by the Tension Coefficients Method of Art. 4.8. Final results can be checked by the graphical method of Conjugate Forces, Art. 4.9.

(2) Analyse the pin-connected dome under wind loading by the Tension Coefficients Method using Reissner's formula $w = w_o \sin \phi \cos \theta$ (see Chapter IX, Loads on Domes), or any other suitable formula, for either diagonals capable of

taking both tension and compression or for only tension diagonals in each bay.

(3) By combining the stresses, obtained in (1) and (2) above, the preliminary design can be made.

(4) Remove the diagonals and, assuming the joints to be fully rigid, solve the dome under symmetrical unit loading at each ring level by the Influence Coefficients Method discussed earlier in this Art. Shear strains in the analysis may be safely neglected. The final stresses under dead or snow load can then be calculated by merely varying the loads at each ring level.

(5) Combine the stresses obtained in (4) with the stresses for the pin-connected dome under wind load obtained in (2).

(6) Design the dome members and joints for the final stresses obtained in (5) above.

(7) Determine the base horizontal reaction H and provide a base ring to take this force.

7.3 THE SHELL ANALOGY[12]

(a) Principles of the Shell Analogy Method

By reading the earlier chapters, and the previous articles in this chapter, it can be seen that the analysis of domes is very complicated. For large domes with many ribs and rings, as normally encountered in practice, the task is even more difficult. In some cases, however, the stresses in the members of a dome can be determined from the stresses in the equivalent shell. The stresses in the equivalent shell can be obtained by mathematical analysis and this approach can prove simpler than the "exact" methods discussed earlier.

A dome normally consists of individual members connected together to form a stable structure. If the separate members are replaced by a continuous medium, the structure becomes a shell. This shell is

called the "hypothetically equivalent shell" if the stresses in the members of the dome can be obtained from the stresses, mathematically determined, at various points on the shell. The principle applies to all domes and their equivalent shells of any shape, size and arrangement of members.

If a dome is imagined to consist of an infinite number of bars, such a dome approximates to a continuous shell. To transform the shell into a dome with an infinite number of bars, certain assumptions must be made. The loss of accuracy resulting from this set of assumptions is fundamentally basic and will always exist. It is impossible to obtain a dome with an infinite number of members and, therefore, a second set of assumptions must be made to reduce this dome to a structure with a finite number of bars. Inaccuracies resulting from this set of assumptions decrease with an increase in the number of members.

In the case of a shell, the stress pattern is frozen and the stress is static since the material is continuous. On converting the shell to a dome consisting of an infinite number of members, the material is no longer continuous and a stress flow occurs leaving the material between the bars unstressed. A condition of unique equilibrium establishes itself. The stress flow and final condition of equilibrium depend only on the bar configuration. Certain well-defined paths are followed by the stress flow and, in order to determine it, the concept of "bar field" must first be discussed.

Every bar has a field which comprises an area round it, the stress within which would, to some extent, flow to that bar. If the bars lie wholly along the stress axes of the equivalent shell, these fields do not overlap and stress at any point would flow in only one direction. However, if the bar configuration does not lie along the stress axes of the equivalent shell, the stress at any point may flow in various

directions depending on the relative positions of the point from the bars in the configuration and also on the relative physical sizes of the bars involved in the configuration. The properties of the equivalent shell, therefore, must first be defined in an effort to determine dome stresses. To accomplish this task requires the definition of three quantities:

(1) The linear dimensions of the shell;

(2) The thickness of the shell;

(3) The material of the shell.

For it to be unique for a specific dome of set dimensions, tho equivalent shell must have the same form and dimensions as the dome. This is especially true for domes in which no irregularities occur and is also true for the many cases where bar members of different areas are to be found in the structure. In the latter cases, a variation in the thickness of the equivalent shell is obtained but the linear dimensions are not affected. Where a large size edge ring beam occurs in a dome, it is sometimes necessary for the shell to overlap the dome in an effort to prevent discontinuity.

To define the thickness of the shell, the concept of bar field must again be considered. In addition to the stress flow already discussed, the bar field also determines the shell area over which a particular bar in a particular configuration exercises its influence. The thickness of the shell can be obtained immediately if the dimensions of the bar and the bar field are known. For pin-connected domes, it is only necessary to consider the areas of the bars when determining the shell thickness. In rigidly-jointed domes, the ratio of the flexural rigidity to the extensional rigidity must be considered before the thickness can be obtained.

The last quantity which needs defining is the material of the shell. An infinitely small area of the dome, with an infinite number

of bars, is considered and is subjected to stresses along the stress axes of the equivalent shell. Equations for the strains in the bars, in terms of these stresses, can now be set up. These equations are identically equated to similar equations for an infinitely small portion of the shell giving both the elastic modulus and the Poisson's ratio for the shell.

(b) <u>The Shell Analogy Applied to Schwedler and Stiff-Jointed Framed Domes</u>

Considering a Schwedler or a stiff-jointed framed dome with n ribs and m rings, let the rings 1, 2, ... r, ... m be placed at angles ϕ_1, ϕ_2, ... ϕ_r, ... ϕ_m, where ϕ is the meridional angle. The interior angle of a polygonal ring is $\frac{2n - 4}{n}$ right angles = θ, a constant. If D is the base diameter and a the radius, then the properties of the equivalent shell can now be determined.

The linear dimensions of the shell and the dome are the same. Hence the shell has a base diameter D and a radius.a. The shell also lies in such a way that all nodes of the dome pass through it.

The next property to be considered is the thickness of the equivalent shell. Schwedler and stiff-jointed framed domes consist of meridional ribs with horizontal rings. A spherical shell has a meridional stress axis and a hoop stress axis. Therefore, the bar configuration for the above mentioned domes lies along the stress axes of the equivalent shell and the bar fields do not overlap.

For a pin-connected dome, the bar field for the ribs is equal to bL, as shown in Figure 35(a), where b is the extent of bar field and depends on the spacing of the bars. Consider the rib at any angle ϕ_r, then as in Figure 35(b):

$$\sin \phi_r = \frac{x}{a} \qquad \ldots\ldots (7{\cdot}31)$$

Therefore:

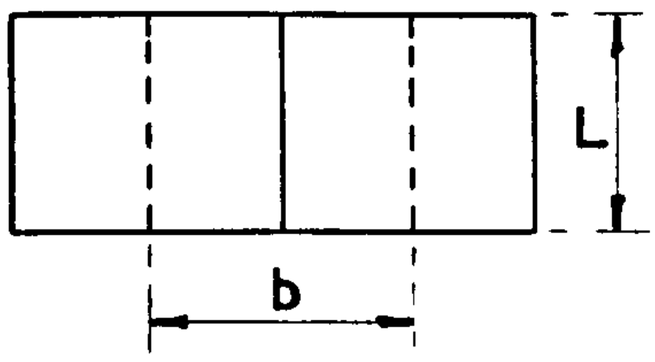

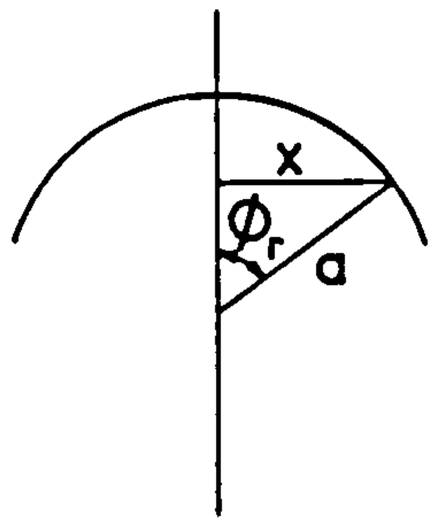

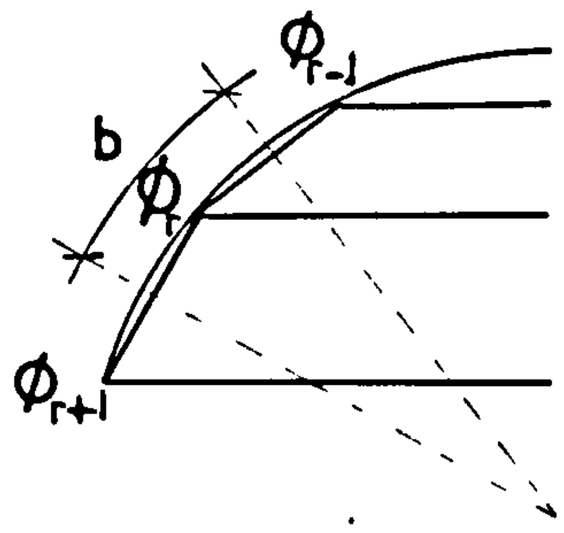

(a)

(b)

(c)

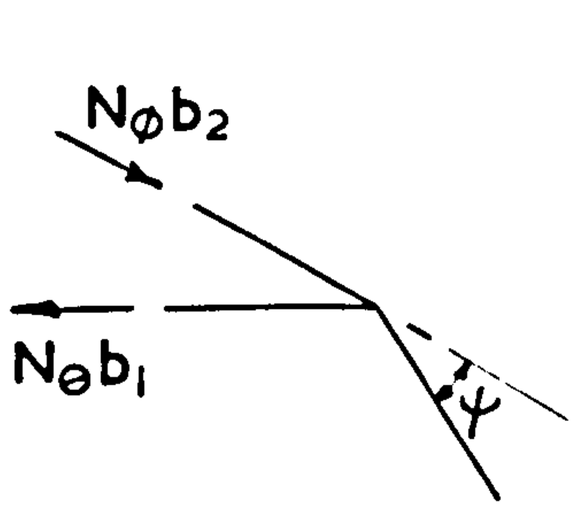

(d)

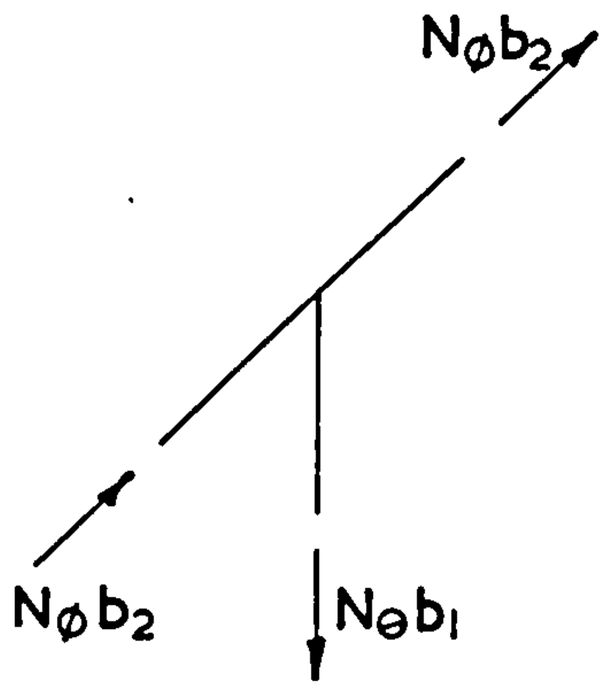

(e)

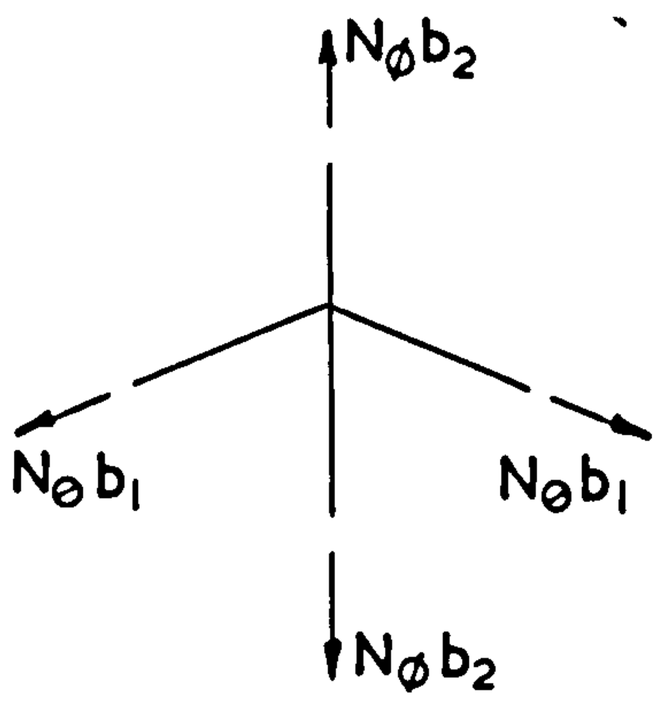

(f)

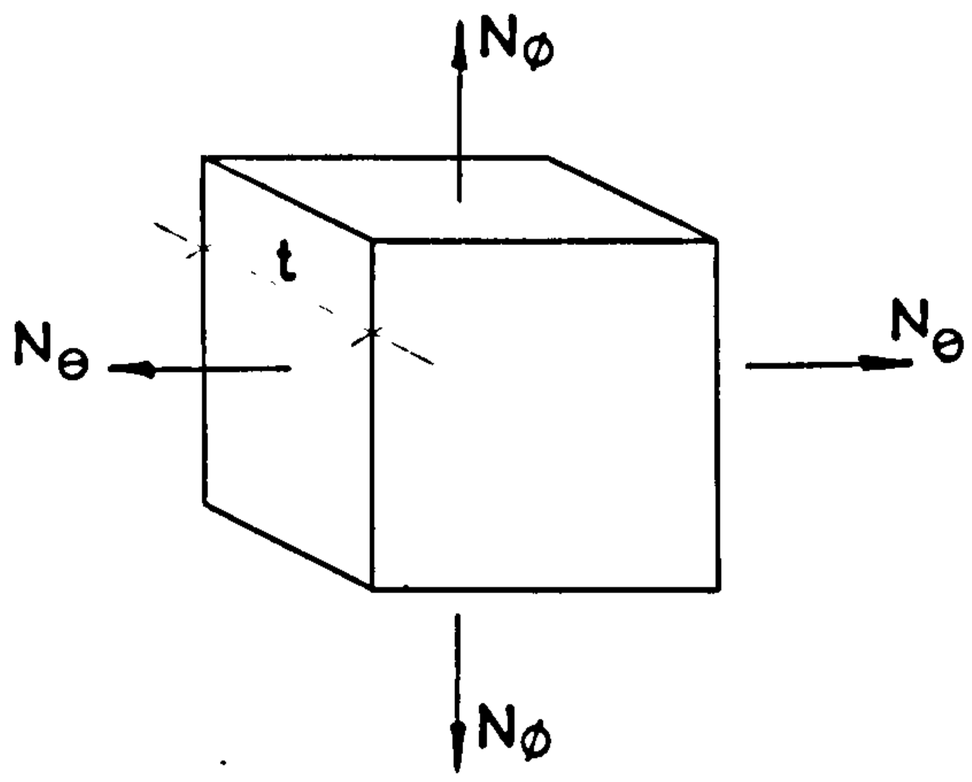

(g)

FIG. 35 THE SHELL ANALOGY Sheet No. 1

F.A.A. Ph.D. Thesis
12th Jan., 1970

Structural Engineering Division
Department of Civil Engineering
University of Newcastle upon Tyne

$$b = \frac{2\pi a \sin \phi r}{n}$$

and ..... (7·32)

$$A_{rb} = \frac{k\, 2\pi a \sin \phi_r t}{n}$$

where A_{rb} is the area of cross-section of the member and k is a constant equal to $\frac{E_o}{E}$. t is the thickness of the shell. Hence as ϕ_r varies along the bar length, $E_o t$ also varies along the length. For a large number of rings, however, the variation in ϕ_r is small and $E_o t$ is approximately constant for the shell. Referring now to Figure 35 (c), for the rings shown:

$$b = \frac{(\phi_{r+1} - \phi_{r-1})a}{2}$$

and ..... (7·33)

$$A_{rg} = \frac{(\phi_{r+1} - \phi_{r-1})kat}{2}$$

where A_{rg} is the area of cross-section of the ring member. To enable the dome to have a constant stiffness, the value of $E_o t$ obtained from the consideration of areas of rib and ring members must be the same. Therefore the bar areas have to be adjusted to maintain $E_o t$ constant.

For a stiff-jointed framed dome, let the moment of inertia of the bars and the cross-sectional area of the bars be represented by I and A respectively. By comparing the ratios of the flexural rigidity to the extensional rigidity of the rigid shell,[25] the following relationship is obtained:

$$\frac{EI}{EA} = \frac{E_o t^3 (1 - \nu^2)}{E_o t 12(1 - \nu^2)} = \frac{t^2}{12} \qquad \text{..... (7·34)}$$

where ν is Poisson's ratio. If, however, the flexural rigidity of the rigid shell is compared to the extensional rigidity of the basic pin-connected one, the relationship becomes:

$$\frac{EI}{EA} = \frac{E_o t^3}{E_o t 12(1 - \nu^2)} = \frac{t^2}{12(1 - \nu^2)} \qquad \text{..... (7·35)}$$

At this stage in the application of the Shell Analogy to Schwedler and stiff-jointed framed domes, only the material of the shell remains to be considered. Referring to the specimen area of such a dome which is illustrated in Figure 35(d). If the dome has an infinite number of rings and an infinitesimally small portion of it is considered, then $\Psi = 0$ and the condition shown in Figures 35(e) and (f) exists. For this case:

$$e_{\phi} = \left[\frac{N_{\phi} b_2}{EA_2} - \frac{2N_{\theta} \cos\left(\frac{\theta}{2}\right) \cos \phi \, b_1}{2EA_1} \right]$$

$$e_{\theta} = \left[\frac{N_{\theta} b_1}{EA_1} - \frac{2N_{\phi} \cos\left(\frac{\theta}{2}\right) \cos \phi \, b_2}{2EA_2} \right] \qquad \ldots\ldots (7.36)$$

where:

e_{ϕ} = strain in the meridional direction;

e_{θ} = strain in the hoop direction;

N_{ϕ} = force per unit length in the meridional direction;

N_{θ} = force per unit length in the hoop direction.

Considering an infinitesimally small portion of the shell it can be shown, as in Figure 35(g), that:

$$e_{\phi} = \frac{1}{E_o t} (N_{\phi} - \nu N_{\theta})$$

and $\ldots\ldots (7.37)$

$$e_{\theta} = \frac{1}{E_o t} (N_{\theta} - \nu N_{\phi})$$

Equations (7.37) are only valid for a shell of constant thickness. The members must, therefore, be varied in such a way that the cross-sectional areas of the members of the dome per unit extent of the bar field are constant over the entire dome. Thus:

$$\frac{A_1}{b_1} = \frac{A_2}{b_2} = \frac{A}{b} = \text{constant} \qquad \ldots\ldots (7.38)$$

The preceding equations for e_{ϕ} and e_{θ} for the dome members now reduce to:

$$e_{\phi} = \frac{b}{EA}\left[N_{\phi} - N_{\theta}\cos\frac{\theta}{2}\cos\phi\right]$$

$$e_{\theta} = \frac{b}{EA}\left[N_{\theta} - N_{\phi}\cos\frac{\theta}{2}\cos\phi\right] \qquad \ldots\ldots (7.39)$$

For exact equivalence between the dome and the shell the following relationships are necessary:

$$\frac{E\,t}{b} = \frac{EA}{b} \qquad \ldots\ldots (7.40)$$

and

$$\nu = \cos\frac{\theta}{2}\cos\phi = F(\phi)$$

From the foregoing considerations it can be seen that two equations are required to be satisfied in order that the equivalent shell may be one of constant thickness. The equations are:

$$\frac{A}{b} = \text{constant}$$
$$\frac{I}{A} = \text{constant} \qquad \ldots\ldots (7.41)$$

(c) Application to Pin-connected Domes

(1) Closed Dome Under Self Load. The equivalent shell can be obtained by the procedure outlined previously. Since $\nu = 0$, $\frac{EA}{b} = E_o t$. The stresses in both shell and dome, however, are independent of t.

The membrane stresses for such a shell per unit length are:

$$N_{\theta} = aq\left[\frac{1}{1+\cos\phi} - \cos\phi\right]$$
$$N_{\phi} = -aq\left[\frac{1}{1+\cos\phi}\right] \qquad \ldots\ldots (7.42)$$

where q is the self load per unit area of the middle surface. Consider a rib that lies between ϕ_r and ϕ_{r+1}, then:

Meridional stress at

$$\phi_r = -aq\left[\frac{1}{1+\cos\phi_r}\right]\frac{2\pi a \sin\phi r}{n}$$

Meridional stress at $\qquad \ldots\ldots (7.43)$

$$\phi_{r+1} = -aq\left[\frac{1}{1+\cos\phi_{r+1}}\right]\frac{2\pi a \sin\phi_{r+1}}{n}$$

Total stress in the bar rib r is then:

$$\int_{\phi_r}^{\phi_{r+1}} \frac{-aq\left[\frac{1}{1+\cos\phi}\right]\frac{2\pi a \sin\phi}{n}\, d\phi}{(\phi_{r+1}-\phi_r)}$$

Consider a ring lying at ϕ_r, then:

$$N_{er} = aq\left[\frac{1}{1+\cos\phi_r} - \cos\phi_r\right] \quad \ldots\ldots (7.44)$$

Since the ring bars are horizontal, the bar field extends from

$$b_2 = \frac{\phi_r + \phi_{r+1}}{2} \quad \text{to} \quad b_1 = \frac{\phi_r + \phi_{r-1}}{2}$$

Total stress in the ring bar =

$$\int_{b_1}^{b_2} aq\left[\frac{1}{1+\cos\phi} - \cos\phi\right] a\, d\phi$$

The stress in any bar can now be determined. In the meridional direction, the stress distribution approximates to a straight line but that in the hoop direction does not. The variation is small, however, and the application of Simpson's rule produces sufficiently accurate results.

Benjamin[12] analysed a dome, under self load, by the Shell Analogy outlined in this Art. and compared the results with a solution by the Tension Coefficients Method of Art. 4.8. The loads on the dome for the latter exact method of analysis were determined by considering the exact area of the equivalent shell transferring load to any node. A close correlation between the stresses obtained by the two methods was obtained.

In order to determine the deflections of the dome by the Shell Analogy it is necessary to determine the shell deflections from the equations:

$$v = \frac{a^2 q\,(1+\nu)}{Eot}\left[\frac{1}{1+\cos\alpha} - \frac{1}{1+\cos\phi} + \log\frac{1+\cos\phi}{1+\cos\alpha}\right]\sin\phi$$

$$w = v\cot\phi - \frac{a^2 q}{Eot}\left[\frac{1+\nu}{1+\cos\phi} - \cos\phi\right] \qquad ..(7.45)$$

where:

v = tangential deflection of the shell;

w = radial deflection of the shell.

(2) Open Dome Under Self Load. For a dome which has an opening at the top the membrane stresses are:

$$N_\phi = -aq\left[\frac{\cos\phi_o - \cos\phi}{\sin^2\phi}\right] - \frac{P\sin\phi_o}{\sin^2\phi}$$

$$N_\theta = aq\left[\frac{\cos\phi_o - \cos\phi}{\sin^2\phi} - \cos\phi\right] + \frac{P\sin\phi_o}{\sin^2\phi} \qquad ..... (7.46)$$

The rib bar stress is, therefore, given by:

$$\frac{1}{(\phi_{r+1} - \phi_r}\int_{\phi_r}^{\phi_{r+1}}\left[-aq\left(\frac{\cos\phi_o - \cos\phi}{\sin^2\phi}\right) - \frac{P\sin\phi_o}{\sin^2\phi}\right]\frac{2\pi a\sin\phi}{n}d\phi;$$

and the ring bar stress is:

$$\int_{\frac{\phi_r+\phi_{r-1}}{2}}^{\frac{\phi_r+\phi_{r+1}}{2}}\left[a^2 q\left(\frac{\cos\phi_o - \cos\phi}{\sin^2\phi} - \cos\phi\right) + \frac{aP\sin\phi_o}{\sin^2\phi}\right]d\phi$$

To determine the deflections, expressions for v and w are required. The method to be employed for finding these expressions has been indicated by Timoshenko[26] and is as follows:

$$\frac{dv}{d\phi} - v\cot\phi = \frac{1}{Eot}\left[N_\phi(r_1 + \nu r_2) - N_\theta(r_2 + \nu r_1)\right]$$

therefore:

$$\frac{dv}{d\phi} = f(\phi) + v\cot\phi$$

or:

$$v = \sin\phi\left[\int\frac{f(\phi)}{\sin\phi}\,d\phi + c\right] \qquad ..... (7.47)$$

Substituting expressions for N_ϕ and N_θ and since $r_1 = r_2 = a$, it can be shown that:

$$v = \left[- \frac{2a^2q(1+\nu)}{Eot} \cos\phi_o \left(- \frac{\text{cosec}\,\phi\,\cot\phi}{2} + \frac{\log\tan\left(\frac{\phi}{2}\right)}{2} \right) + \frac{2a^2q(1+\nu)}{Eot}\left(- \frac{1}{2\sin^2\phi} \right) + \frac{a^2q(1+\nu)\log\sin\phi}{Eot} - \frac{2aP(1+\nu)\sin\phi_o}{Eot} \times \left(- \frac{\text{cosec}\,\phi\,\cot\phi}{2} + \frac{\log\tan\left(\frac{\phi}{2}\right)}{2} \right) + C \right] \sin\phi$$

..... (7·48)

where C is a constant which can be determined from the boundary condition that at $\phi = \alpha$, $v = 0$

Therefore:

$$C = \left[- \frac{2a^2q\,(1+\nu)\cos\phi_o}{Eot} \left(- \frac{\text{cosec}\,\alpha\,\cot\alpha}{2} + \frac{\log\tan\left(\frac{\alpha}{2}\right)}{2} \right) + \frac{2a^2q\,(1+\nu)}{Eot}\left(- \frac{1}{2\sin^2\alpha} \right) + \frac{a^2q\,(1+\nu)}{Eot}\log\sin\alpha - \frac{2aP\,(1+\nu)\sin\phi_o}{Eot} \left(- \frac{\text{cosec}\,\alpha\,\cot\alpha}{2} + \frac{\log\tan\left(\frac{\alpha}{2}\right)}{2} \right) \right] \quad (7·49)$$

Knowing v, w can then be determined from the expression:

$$\frac{1}{Eot}\left[N_\theta - \nu N_\phi \right] = \frac{v}{a}\cot\phi - \frac{w}{a} \qquad \text{..... (7·50)}$$

At the support where v = 0,

$$w = \frac{a}{Eot}\left[\nu N_\phi - N_\theta \right] \qquad \text{..... (7·51)}$$

(3) Closed Dome Under Snow Load. Under snow loading it can be shown that:

$$N_\phi = - \frac{pa}{2}$$

and ..... (7·52)

$$N_\theta = - \frac{pa\cos 2\phi}{2}$$

where p is the snow load per unit area of the middle surface. The rib stress for a bar between ϕ_r and ϕ_{r+1} is hence:

$$\int_{\phi r}^{\phi_{r+1}} \frac{- \frac{pa}{2}\,\frac{2\pi a \sin\phi}{n}\,d\phi}{(\phi_{r+1} - \phi_r)}$$

The ring stress for the bar at ϕ_r is:

$$\int_{\frac{\phi_r + \phi_{r-1}}{2}}^{\frac{\phi_r + \phi_{r+1}}{2}} - \frac{pa \cos 2\phi}{2} a d\phi$$

For the deflections:

$$v = \frac{pa^2 \sin \phi}{Eot} \left[\cos \phi - \cos \alpha \right] \quad \ldots\ldots (7.53)$$

$$w = v \cot \phi + \frac{pa^2 \cos 2\phi}{2\, Eot}$$

(4) Open Dome Under Snow Load. The shell stresses are obtained by:

$$N_\phi = - p\frac{a}{2} \left[1 - \frac{\sin^2 \phi_o}{\sin^2 \phi} \right]$$

$$N_\theta = + p\frac{a}{2} \left[1 - \frac{\sin^2 \phi_o}{\sin^2 \phi} - 2 \cos^2 \phi \right] \quad \ldots\ldots (7.54)$$

The expressions for v and w can be obtained once more as follows:

$$f(\phi) = - (1 + \nu) \frac{pa^2}{Eot} \left[1 - \frac{\sin^2 \phi_o}{\sin^2 \phi} - \cos^2 \phi \right] \quad \ldots\ldots (7.55)$$

Therefore:

$$v = - \frac{pa^2 (1 + \nu) \sin \phi}{Eot} \int \left[\frac{1}{\sin \phi} - \frac{\sin^2 \phi_o}{\sin^3 \phi} - \frac{\cos^2 \phi}{\sin \phi} \right] d\phi + C$$

which results in:

$$v = \frac{pa^2 (1 + \nu) \sin \phi}{Eot} \left[\sin^2 \phi \left(- \frac{\operatorname{cosec} \phi \cot \phi}{2} + \frac{\log \tan \left(\frac{\phi}{2} \right)}{2} \right) + \cos \phi + C \right] \quad \ldots\ldots (7.56)$$

At $\phi = \alpha$, v = 0 so the value of C can be obtained. w can be obtained from equation (7.50).

(5) Wind Loading. The various formulae for wind pressure distribution, which are available in existing literature, are inadequate for the purpose of analysing dome structures (See Chapter IX, Loads on Domes). However, until improved wind pressure distribution formulae are developed and shell equations and their solutions based on these formulae are obtained, the Shell Analogy must employ the existing formulae. By applying the following formulae:

$$Z = p \sin \phi \cos \theta \quad ; \quad X = Y = 0$$

which assumes that the pressure is normal to the surface and that the tangential components are neglected, the stresses can then be found from:

$$N_\phi = - \frac{pa \cos \theta \cos \phi}{3 \sin^3 \phi} \left[2 - 3 \cos \phi + \cos^3 \phi \right]$$

$$N_\theta = \frac{pa \cos \theta}{3 \sin^3 \phi} \left[2 \cos \phi - 3 \sin^2 \phi - 2 \cos^4 \phi \right] \qquad \ldots\ldots (7.57)$$

$$N_{\theta\phi} = T = - \frac{pa \sin \theta}{3 \sin^3 \phi} \left[2 - 3 \cos \phi + \cos^3 \phi \right]$$

There are now three stress axes to be considered in the analysis. These are the meridonal, hoop and shear stress axes. The meridional and hoop stresses can be directed into the rib and ring bars as discussed previously. With regard to the shear stress, Dischinger[12] first suggested that shear would be taken by the diagonals. His assumption was that shear had no effect on the stresses in the ribs and rings. This assumption, however, is incorrect. If a normal domo bay is imagined to be frozen into its equivalent shell, then the shear stress distribution picture would be as shown in Figure 36(a). In the unfrozen condition, the material in between the bars is removed and a redistribution of stress occurs. All the shear stress in quadrant 1 will then have a tendency to move to node 1 in an attempt to enter the bars and establish equilibrium. Similarly the stresses in quadrants 2, 3 and 4 will move to nodes A, B and 2 respectively. Just before entry into the bars, therefore, the stress pattern readjusts itself into two sets of forces in the meridional and hoop directions as illustrated in Figure 36(b). It is a simple matter to calculate these forces as follows:

$$F_{1\phi} = \int_{\phi_r}^{\frac{\phi_r + \phi_{r+1}}{2}} \int_{\theta_r}^{\frac{\theta_r + \theta_{r+1}}{2}} \left[\frac{T a \sin \phi}{\frac{\phi_r + \phi_{r+1}}{2} - \phi_r} \right] d\theta \, d\phi \qquad \ldots\ldots (7.58)$$

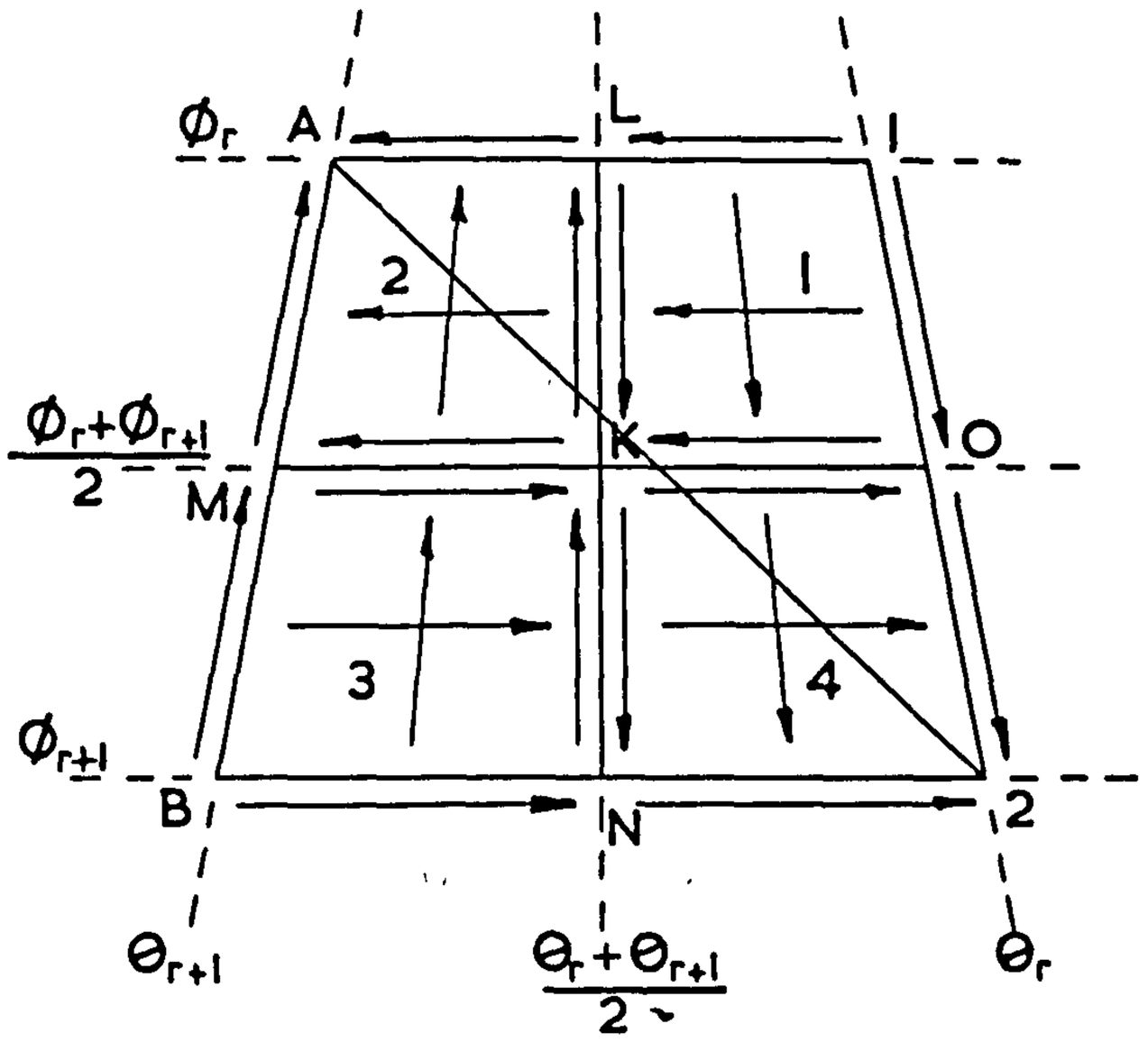

(a)

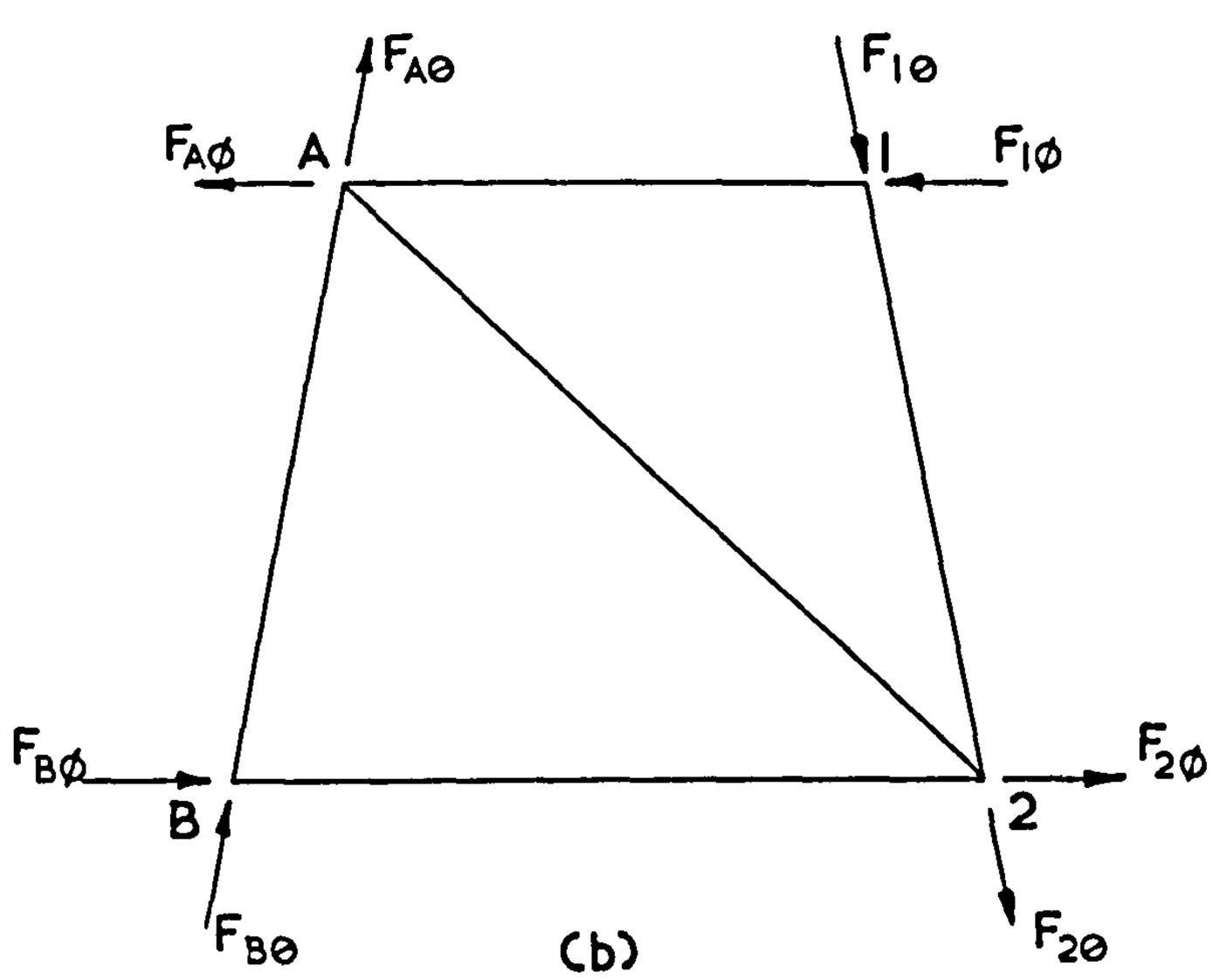

(b)

FIG. 36 THE SHELL ANALOGY Sheet No. 2

F.A.A. Ph.D. Thesis
13th Jan., 1970

Structural Engineering Division
Department of Civil Engineering
University of Newcastle upon Tyne

$$F_{1\theta} = \int_{\theta_r}^{\frac{\theta_r + \theta_{r+1}}{2}} \int_{\phi_r}^{\frac{\phi_r + \phi_{r+1}}{2}} \frac{Ta}{\left[\frac{\theta_r + \theta_{r+1}}{2} - \theta_r\right]} \, d\phi \, d\theta \qquad \ldots(7{\cdot}58)$$

The stress varies in both the meridional and hoop directions. If joints 1 and B have to be in equilibrium, it follows that:

$$1A = F_{1\phi}, \quad 2B = F_{B\phi}, \quad 12 = F_{1\theta}, \quad AB = F_{B\theta}$$

By solving joints A and 2 it is possible to obtain four values of the stress in A2, the mean of which gives the stress in the diagonal. The four values result from assuming a dome with a finite number of bars. If an infinite number of bars were present, and the entire phenomenon was being considered at the point K instead of round a trapezium, all the four values would merge to a common one. The meridian, hoop and shear stresses in the shell can now be summated to give the stresses in the bars. Two panels have to be considered for each rib and ring member in order to obtain the total effect of the shear stresses. To simplify calculations in the analysis, shear stresses at all node and intermediate points should be determined in each bay and a straight line distribution assumed between them.

(d) Application to Stiff-jointed Domes

The equivalent shell for the stiff-jointed framed dome can be obtained by the procedure discussed in Art. 7.3(b). In order to obtain all the stresses and moments over the dome, it is necessary to solve the equations for symmetrical bending of spherical shells. A shell with a fixed base requires an analysis based on the assumption that rollers are present and the solution is then corrected for bending. It is necessary to apply such forces and moments, which satisfy the boundary conditions, since the edges are not free. An approximate method for carrying out this procedure has been discussed by Timoshenko[26] and leads to the following solutions:

$$Q_{\phi} = \frac{C\, e^{-\lambda\psi} \sin(\lambda\psi + \gamma)}{\sqrt{\sin(\alpha - \psi)}}$$

$$V = \frac{-2\lambda^2 C e^{-\lambda\psi} \cos(\lambda\psi + \gamma)}{Et\sqrt{\sin(\alpha - \psi)}}$$

$$N_{\phi} = \frac{-\cot(\alpha - \psi)\, C e^{-\lambda\psi} \sin(\lambda\psi + \gamma)}{\sqrt{\sin(\alpha - \psi)}}$$

$$N_{\theta} = C\lambda e^{-\lambda\psi} \frac{2\cos(\lambda\psi + \gamma) - (k_1 + k_2)\sin(\lambda\psi + \gamma)}{2\sqrt{\sin(\alpha - \psi)}}$$

$$M_{\phi} = \frac{a\, C\, e^{-\lambda\psi}}{2\lambda}\left[\frac{k_1 \cos(\lambda\psi + \gamma) + \sin(\lambda\psi + \gamma)}{\sqrt{\sin(\alpha - \psi)}}\right]$$

$$\delta = \frac{a\, C\lambda e^{-\lambda\psi} \sin(\alpha - \psi)}{Et\sqrt{\sin(\alpha - \psi)}}\left[\cos(\lambda\psi + \gamma) - k_2 \sin(\lambda\psi + \gamma)\right]$$

$$M_{\theta} = \frac{a\, C\, e^{-\lambda\psi}}{4\nu\lambda\sqrt{\sin(\alpha - \psi)}}\Big[\left\{(1 + \nu^2)(k_1 + k_2) - 2k_2\right\}\cos(\lambda\psi + \gamma) + 2\nu^2 \sin(\lambda\psi + \gamma)\Big]$$

..... (7.59)

where:

$$k_1 = 1 - \frac{(1 - 2\nu)}{2\lambda}\cot(\alpha - \psi)$$

$$k_2 = 1 - \frac{(1 + 2\nu)}{2\lambda}\cot(\alpha - \psi)$$

..... (7.60)

$$\psi = \alpha - \phi$$

$$\lambda^4 = 3(1 - \nu^2)\left(\frac{a}{t}\right)^2$$

and C, γ = constants. Q_{ϕ} is the shearing force parallel to the Z axis per unit length of an axial section. M_{θ} and M_{ϕ} are the bending moments in a shell per unit length of meridional section and a section perpendicular to the meridian respectively. V is the rotation of a tangent to the meridian.

If M_{α} alone is applied, then

$$(M_{\phi})_{\phi = \alpha} = M_{\alpha}, \quad (N_{\phi})_{\phi = \alpha} = 0$$

which gives:

$$\gamma = 0 \quad \text{and} \quad C = \frac{M_{\alpha}\, 2\lambda\sqrt{\sin\alpha}}{ak_1}$$

Then:

$$(V)_{\psi=0} = \frac{-4\lambda^3 M_\alpha}{E\,a\,t\,k_1}$$

$$(\delta)_{\psi=0} = \frac{2\lambda^2 \sin\alpha M_\alpha}{E\,t\,k_1} \qquad \ldots\ldots (7.61)$$

If H, the horizontal reaction at the base, alone is applied, then:

$$(M_\phi)_{\phi=\alpha} = 0, \quad (N_\phi)_{\phi=\alpha} = H\cos\alpha$$

which gives the value of both γ and C. Therefore:

$$(V)_{\psi=0} = \frac{2\lambda^2 \sin\alpha H}{E\,t\,k_1}$$

$$(\delta)_{\psi=0} = \frac{-\lambda\, a \sin^2\alpha}{Et}\left(k_2 + \frac{1}{k_1}\right)H \qquad \ldots\ldots (7.62)$$

On applying both M_α and H simultaneously,

$$V_{total} = 0, \text{ and } \delta_{total} = \delta_m$$

where δ_m is the base expansion as obtained on the application of the membrane theory. Therefore:

$$\frac{-4\lambda^3 M_\alpha}{Eat\,k_1} + \frac{2\lambda^2 \sin\alpha H}{Etk_1} = 0 \qquad \ldots\ldots (7.63)$$

and

$$\frac{2\lambda^2 \sin\alpha M_\alpha}{Etk_1} - \frac{\lambda a \sin^2\alpha}{Et}\left(k_2 + \frac{1}{k_1}\right)H = \delta_m \qquad \ldots\ldots (7.64)$$

from which M_α and H can easily be determined. By applying M_α and H separately to the shell all the stresses can be evaluated.

The meridional and hoop stresses are again distributed into the ribs and rings. Dischinger[12] suggested that the shear would be taken by the ribs in the form of bending moments. If the shear is plotted along the meridian rib, then integration of the diagram up to any point determines the bending moment in the rib at that point due to shear.

Benjamin[12] found that an analysis by the Shell Analogy produced ring stresses which were underestimated by as much as 50 per cent when compared with a solution by the exact Influence Coefficients Method outlined in Art. 7.2(c). He recommends that, until such time as more research is done to give better correlation to the actual stresses in

a stiff-jointed framed dome, this approach should not be used by design engineers.

(e) The Shell Analogy as a Design Method

The analysis of Schwedler domes can be carried out very easily by the Shell Analogy. For a large structure, which has many ribs and rings, immense savings in solution time can be obtained. The Shell Analogy computations for both stresses and deflections for such a system are very similar to those obtained by an exact mathematical analysis.

In the analysis of an open dome, the Shell Analogy assumes that a stiff lantern girder is present which takes all the hoop compression arising from the load on the top ring. As a result of this assumption, a considerably reduced stress is obtained in the top ring members. If, however, the value of the hoop compression stress in the lantern girder is added to the member stress obtained by the Shell Analogy, then the stress in the top ring bar can be obtained accurately.

Small deflections at the base of the shell are experienced when applying the Shell Analogy to pin-connected domes. This is due to the difference in boundary conditions. The deflections correlate quite accurately over the rest of the structure.

Self loading and snow loading conditions on Schwedler domes can easily be solved by the Shell Analogy. Where wind loading is considered, this method of analysis is only limited by the availability of suitable shell formulae.

For domes with many ribs and rings, the Shell Analogy produces a more accurate result than if applied to a structure with less members. In the case of stiff-jointed framed domes, the method should not be used until much further research has been carried out.

7.4 MISCELLANEOUS DOMES

(a) The Grid Dome

Two-way and three-way grid domes are described in Art. 3.9

Figures 13(b) and 14(a) show their general arrangements respectively. They consist of an interconnecting grid of parabolic or circular arches, normally with a low rise-to-span ratio. The feet of a grid dome may be pinned or fixed, pinned feet generally being preferred in order to simplify the analysis.

Grid domes are analysed using the Influence Coefficients Method which is detailed in Art. 7.2(c). Consider the grid dome to be formed of two sets of interconnecting grids at right angles to each other. The two separate primary systems are illustrated in Figure 37(a). If the two systems are imagined to be connected at the original points of interconnection by short vertical links, pin-jointed at their ends, then these links can be assumed to transfer vertical forces without transferring moments. This assumption is valid where steel grids are employed since torsion can be neglected. Where torsion is important, however, it must be accounted for as shown in Figure 37(b).

Under the action of the known vertical loading, which may be applied to either the top system or to both systems, let the unknown vertical forces and moments in the links be X_1, X_2, X_3, ... X_r..... X_n. Each of these unknowns can now be applied separately to the two pinned arches and the bending moments, axial forces, shearing forces and torsional moments determined over the arches of both systems. The influence coefficients d_{ik} are evaluated from the following expression:

$$d_{ik} = \int \frac{M_i M_k ds}{EI} + \int \frac{P_i P_k ds}{EA} + \int \frac{S_i S_k ds}{\alpha AN} + \int \frac{T_i T_k ds}{NC} \qquad \text{..... (7.65)}$$

For steel grids, the only redundancies are the unknown vertical forces transferred by the links. The discussion on stiff-jointed framed domes in Art. 7.2(c) also showed that shear strains can be safely neglected in the analysis. Equation (7·65) therefore reduces to:

$$d_{ik} = \int \frac{M_i M_k ds}{EI} + \int \frac{P_i P_k ds}{EA} \qquad \text{..... (7.66)}$$

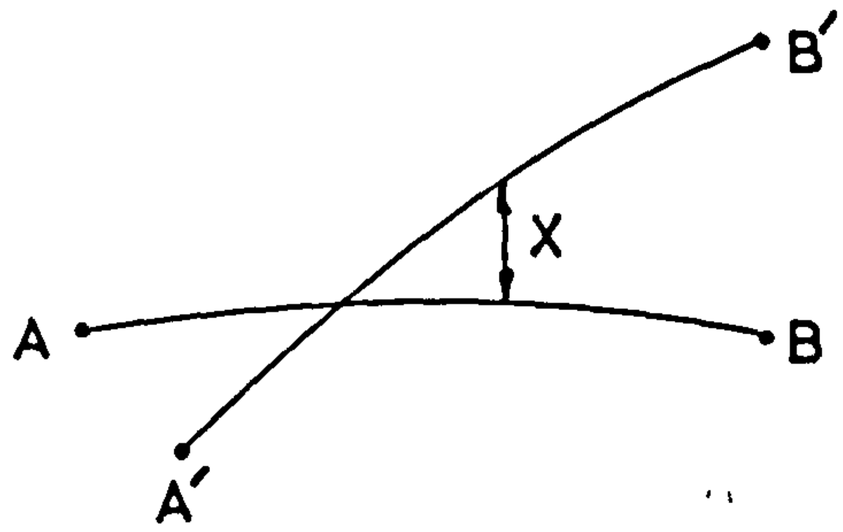

(a)

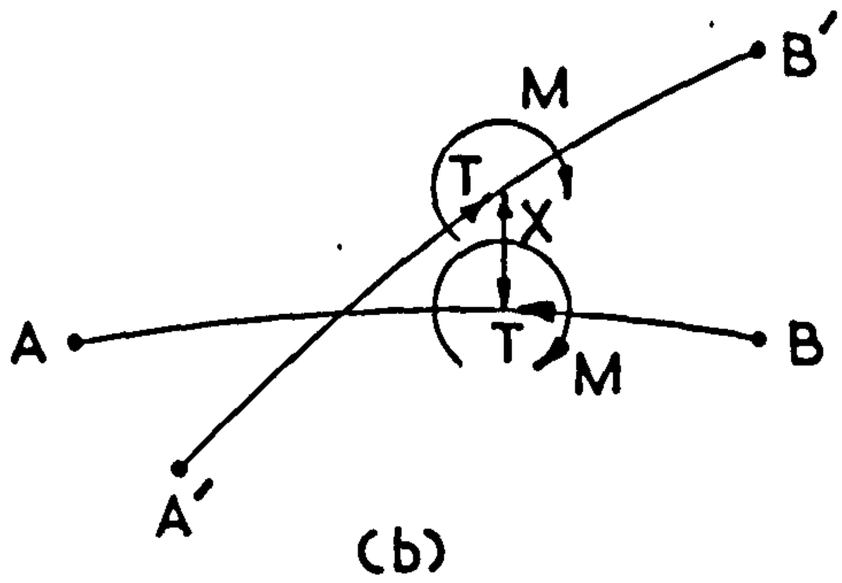

(b)

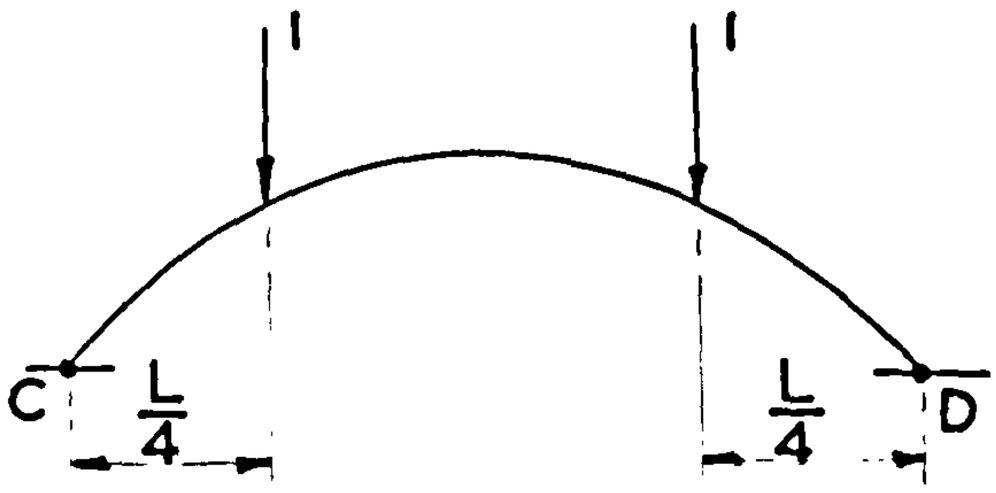

(c)

FIG. 37 GRID DOME ANALYSIS

F.A.A. Ph.D. Thesis
15th Jan., 1970

Structural Engineering Division
Department of Civil Engineering
University of Newcastle upon Tyne

The M_k diagram, however, is not linear and the integration of diagrams in this case is complicated. Values for d_{ik} have to be obtained by a mathematically performed integration.

For grid domes it is better to assume that the variation of the section is given by the formulae:

$$I = \frac{Io}{\cos\phi} \quad ; \quad A = \frac{Ao}{\cos\phi}$$

where:

Io = moment of inertia of the arch rib at the crown;

Ao = cross-sectional area of the arch rib at the crown.

If the variation in cross-section for the central arch rib is decided, the variation and properties of all the arch ribs is automatically fixed since at the points of interconnection two ribs would have the same cross-section and properties.

To illustrate how the influence coefficients may be determined for a grid dome, consider the parabolic arch rib CD which is illustrated in Figure 37(c). Unit loads are applied at the quarter points. The $d_{\parallel\ (M\ term)}$ is given by the following expression:

$$d_{\parallel\ (M\ term)} = \int_o^L \frac{M_1^2 ds}{EI} = 2\int_o^{\frac{L}{4}} \frac{M_1^2 ds}{EI} + 2\int_{\frac{L}{4}}^{\frac{L}{2}} \frac{M_1^2 ds}{EI}$$

$$= \frac{2}{EI}\int_o^{\frac{L}{4}} \left[\frac{H\ 4\ y_c\ x(L-x)}{L^2} - x\right] dx + \frac{2}{EI}\int_{\frac{L}{4}}^{\frac{L}{2}} \left[\frac{H4y_c x(L-x)}{L^2} - \frac{L}{4}\right] dx \quad ..(7.67)$$

where H is the horizontal thrust at the feet of the arch and hence is a constant for the loading system considered. For simplicity EI has been assumed constant in equation (7.67). The terms in the above expression are both functions which can easily be integrated and the value of the $d_{\parallel\ (M\ term)}$ can hence be obtained. By a similar process, the value of the $d_{\parallel\ (P\ term)}$ can also be determined.

The set of simultaneous equations for the system is:

$$
\begin{aligned}
d_{11}X_1 + d_{12}X_2 + \ldots\ldots d_{1n}X_n &= d_1R \\
d_{21}X_1 + d_{22}X_2 + \ldots\ldots d_{2n}X_n &= d_2R \\
\vdots \quad \vdots \quad \vdots \quad \vdots \quad \vdots \quad \vdots \quad \vdots & \\
d_{n1}X_1 + d_{n2}X_2 + \ldots\ldots d_{nn}X_n &= d_nR
\end{aligned}
\qquad \ldots\ldots (7\cdot63)
$$

Solving equations (7.68) gives the values of the unknown link forces or moments. The final axial forces, bending moments and shear forces for each individual arch can now be obtained.

(b) Network, Plate-type, Zimmermann and Geodesic Domes

These types of domes have been described in Arts. 3.3, 3.4, 3.5 and 3.10 respectively and Figures 10(b), 11(a), 11(b) and 14(b) respectively illustrate their layouts. Network domes are derived basically from Schwedler domes by a rotation at each ring level. All the members of network domes are stressed, due to the lack of diagonal members, under any point load. They are, therefore, theoretically more efficient than Schwedler domes but unfortunately they are only stable with an odd number of sides. Regular pin-connected network domes are statically determinate in the stable condition.

Plate-type domes can be solved in a similar way to Schwedler domes. The primary rib system of a plate-type dome is first analysed by this process and then the flat panels between the main members, which are further subdivided, can be analysed separately as plane frameworks. Plate-type domes are statically determinate if pin-jointed.

Zimmermann domes are an outdated form of construction, their one advantage being that they are easy to roof. Present day dome construction methods, which are more efficient, will always be preferred in place of this type.

Geodesic domes are mainly the work of Buckminster Fuller, the American architect and engineer. They are normally composed of units involving stressed skin construction and therefore need to be analysed as such.

CHAPTER VIII

THE STRESS ANALYSIS OF RADIAL RIBBED DOMES

8.1 DESIGN ASSUMPTIONS

A system of radial ribs in the form of circular, parabolic or elliptical arches, connected together at the crown, forms the simplest framework employed in the construction of domes. Each arch rib is erected as a single member from its base to the apex of the dome. This primary system of members is unstable under a general system of loading and horizontal purlin rings and diagonal bracing are normally provided to increase the stability of the complete structure.

However, the horizontal and diagonal stiffening members are usually considered to be pin-connected at the radial ribs and this simplifies the design of such a structure by reducing the analysis to a consideration of two separate simple member systems. The primary rib system is first designed to withstand bending moments and axial forces induced by dead and imposed loading conditions on the dome and then the complete structure is analysed as a pin-jointed system to determine the axial forces in the horizontal and diagonal bracing. In addition to the axial forces produced by symmetrical loading conditions over the dome, the horizontal purlins also carry bending moments set up by the transmission of load through the roof covering. The diagonal bracing members only carry axial load caused by unsymmetrical loading conditions over the dome. Analysis procedures for determining the forces in pin-jointed radial ribbed dome structures have already been discussed in this thesis and hence in this section only an analysis of the primary arch rib structure will be considered.

In small diameter ribbed domes, where only a few radial components

are employed, the members can be directly connected together at the crown. If the connections are made fully rigid then fixing moments occur at the apex and the stress analysis of such a structure becomes very complicated. However, according to Makowski and Gogate[27] the fixity of the apex joint, although it effects the stress distribution in small span domes, can be neglected for large span domes, especially those with slender ribs.

Normally, in large span ribbed domes, many radial members are employed and they are connected together at an apex ring. Although fixing moments occur at the rib-ring junctions, if the ring diameter is small, compared with the overall dimensions of the dome; then the assumption that the ribs meet at a common point is valid.[27] Domes which incorporate an apex ring are highly redundant structures and necessitate such assumptions to simplify their analysis.

The cross-sectional area and moment of inertia along the length of the arch ribs can also be assumed constant.[12] Since the maximum bending moment occurs towards the centre of the member and the maximum axial force is at the base, the tapering of the arch ribs towards their ends is not sufficiently severe to affect the stress distribution to a large extent.

To design radial ribbed domes with complete fixity at the base would be highly uneconomical and therefore, in the majority of cases, pinned footings are provided. If the ribs are pin-connected directly to heavy foundation blocks the dome is of the "unstiffened" type whereas if the ribs are connected to an elastic base ring the dome is then "stiffened".

8.2 THREE-PINNED UNSTIFFENED RADIAL RIBBED DOMES

Three-hinged and two-hinged arch design procedures can be employed to analyse the dome ribs in a two-dimensional form.[23] However, this method does not take into account any spread of load from one rib to

another, through the apex ring, under unsymmetrical loading conditions. A more economical design method has been put forward by Makowski and Gogate[27] whereby the structure is analysed as a space system.

The primary rib system of n arches pinned at the base and crown, Figure 38(a), is redundant to a degree of 2n-3. In practice many ribs are employed in the structure and this degree of redundancy is very large. Analysis by classical methods would be almost impossible. However, the analysis of such a system is simplified by expressing the unknown 2n-3 components in terms of the deflection of the apex joint which is the same for all ribs. This is the basis of the method of stress analysis employed by Makowski and Gogate[27] for three-pinned arch-ribbed domes and is reproduced, in part, in the following pages. The analysis given applies to three-pinned arch-ribbed domes with radial ribs semi-circular in shape and of constant moment of inertia, but the method can also be employed in the design of other domes. Ribs of any shape can be analysed and the effects of rigid connections can also be superimposed on the primary three-pinned system.

8.3 THE ANALYSIS OF THREE-PINNED UNSTIFFENED SEMI-CIRCULAR RADIAL RIBBED DOMES BY THE METHOD OF MAKOWSKI AND GOGATE[27]

(a) Notation

The notation used is shown in Figure 38(a); 1 - 0, 2 - 0, ... r - 0, ... n - 0, $1'$ - 0, $2'$ - 0, ... r' - 0, ... n' - 0 are 2n ribs forming the dome, numbered in a clockwise direction, n may be odd or even. Any load P acting on the structure can be resolved into horizontal and vertical components P_h and P_v. The point of application of the load is defined by the angle α. Because of the symmetry of the structure the effect of unit loads acting on one rib, say, rib 1 - 0, need only be studied. This rib 1 - 0 is called the directly loaded rib. The position of any rib r - 0, not directly loaded, is described by the angle θ_r, measured in a clockwise direction from the base line 1 - $1'$.

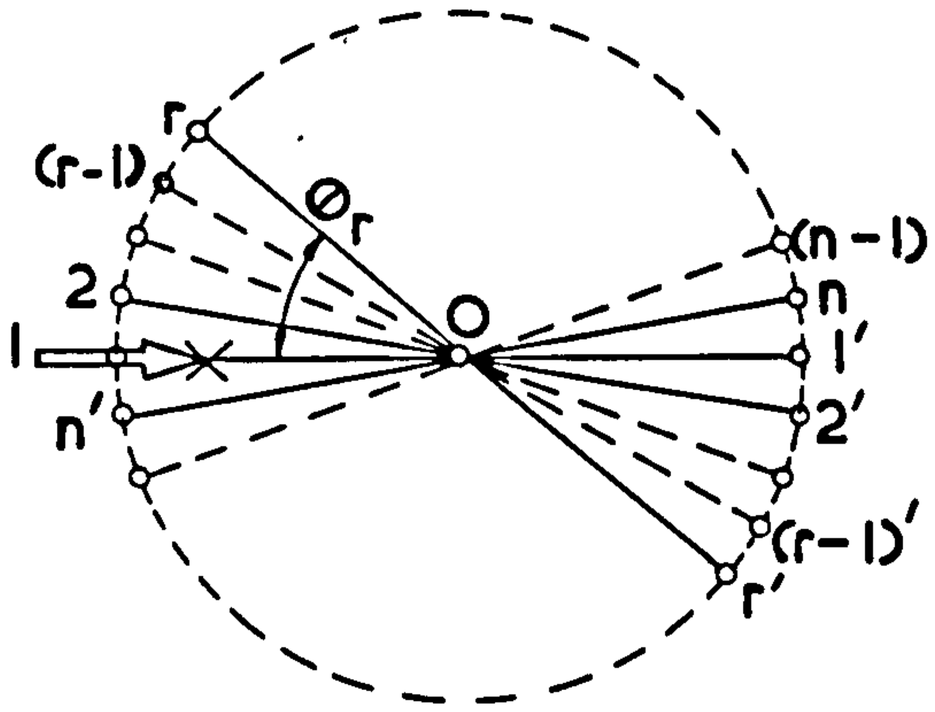

(a) NOTATION

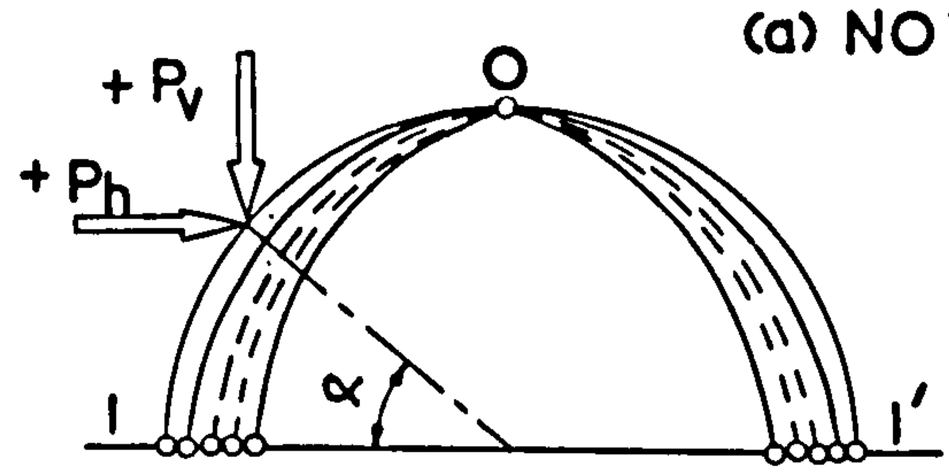

(b) LOAD CASE IA

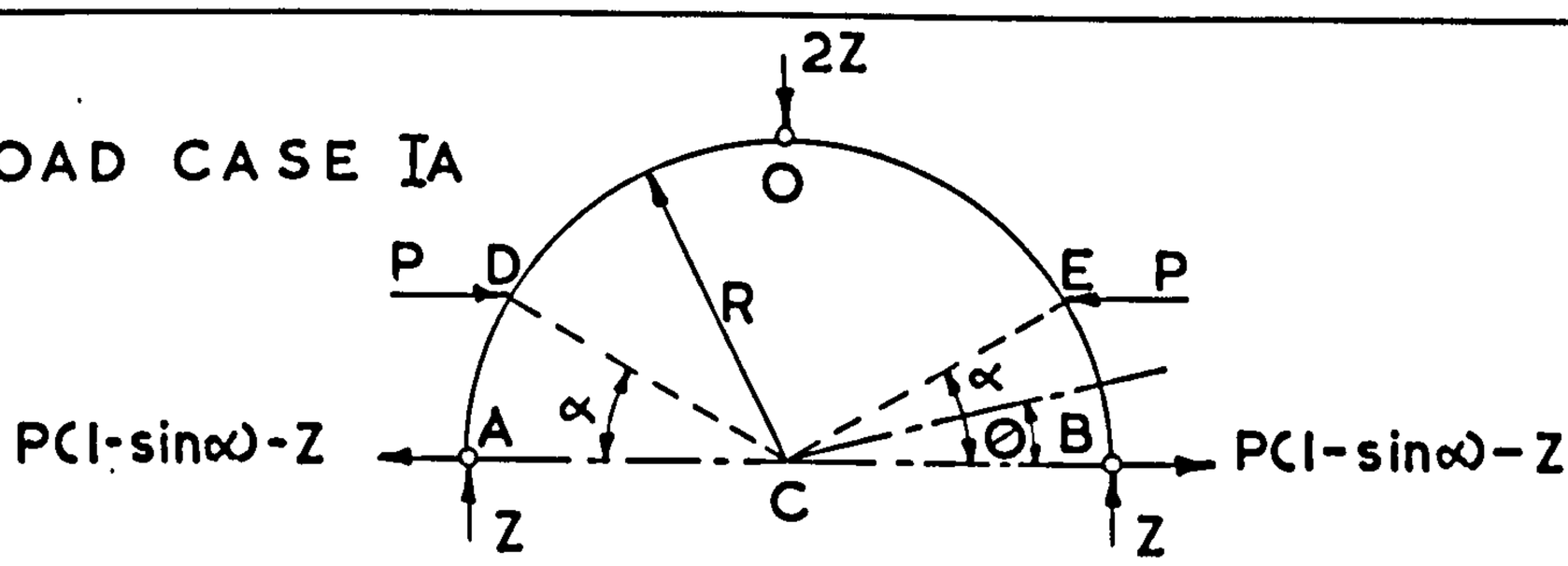

(c) SYMMETRICAL HORIZONTAL LOADS

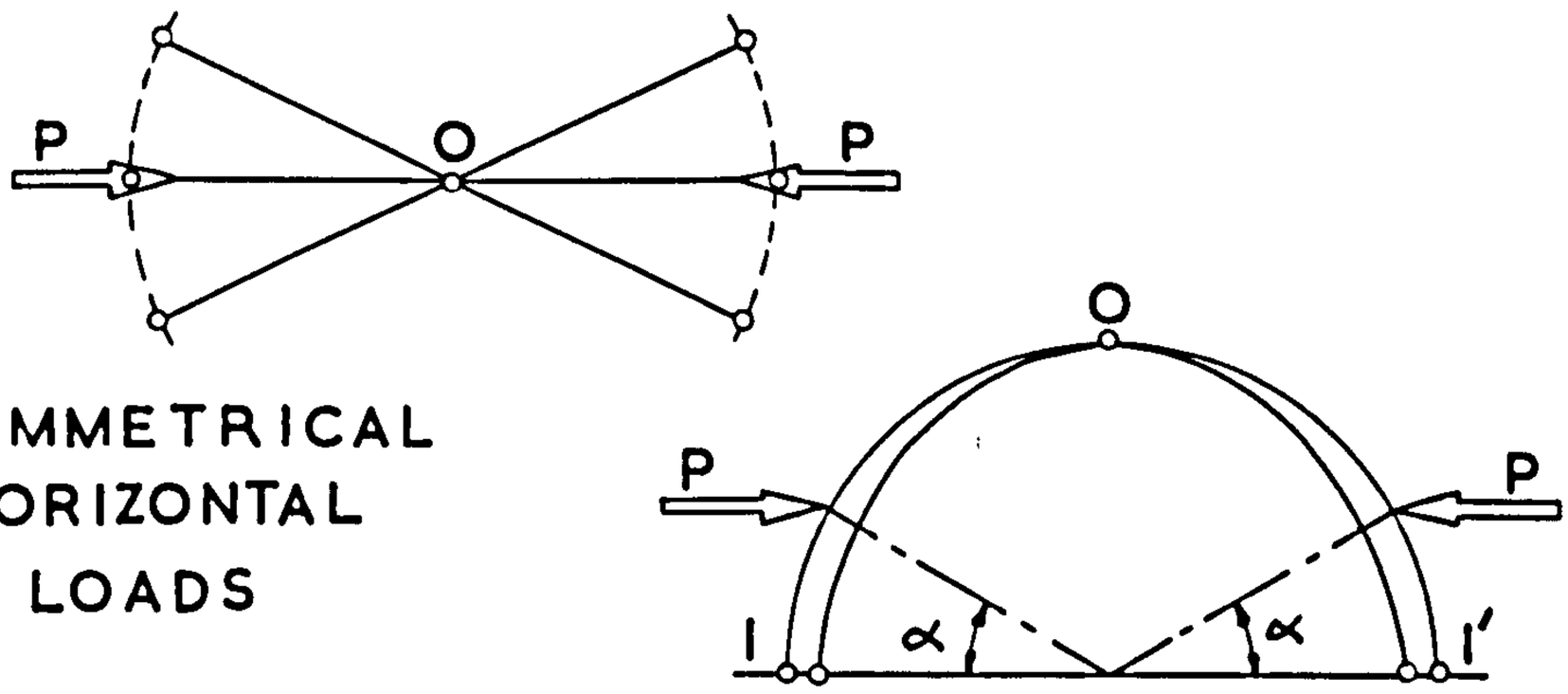

FIG. 38 STRESS ANALYSIS OF THREE-PINNED UNSTIFFENED SEMI-CIRCULAR ARCH-RIBBED DOMES (Makowski & Gogate) SHEET NO. 1

F.A.A. Ph.D. Thesis
29th Nov, 1968

Structural Engineering Division
Department of Civil Engineering
University of Newcastle upon Tyne

More complicated loading systems are dealt with using the principle of superposition. Downward vertical and inward horizontal forces are considered as positive; the deflection of the apex joint O is positive, if following the positive directions for forces acting on the rib 1 - O. Two cases of loading are considered separately:

Case I : a unit horizontal load in the plane of rib 1 - O;

Case II: a unit vertical load in the plane of rib 1 - O.

Each case is resolved into symmetrical and skew-symmetrical loading. (Cases IA and IB, IIA and IIB.)

The dome consists of n three-pinned arches r - O - r', interconnected by the common apex hinge. General formulae are first derived for the vertical and horizontal displacements δ_v° and δ_h° of the apex of a three-pinned arch, under unit vertical and horizontal loads.

(b) <u>General Expressions of the Apex Displacements</u>

Under horizontal symmetrical loads P (Case IA) acting on the three-pinned arch, the apex will deflect only vertically (see Figure 38(b)). This vertical displacement is obtained by the strain energy method using the first theorem of Castigliano.

Assuming a fictitious vertical force 2Z at O

$$\frac{\delta U}{\delta (2Z)_{Z=0}} = \delta_v^\circ \qquad \ldots\ldots (8.1)$$

If x is any point on the rib, at an angular distance θ from CB, the bending moment at x is:

for the part BE

$$M = ZR(1 - \cos\theta) + \left[P(1 - \sin\alpha) - Z \right] R \sin\theta \qquad \ldots\ldots (8.2)$$

$$\frac{\delta M}{R\,\delta Z} = 1 - \cos\theta - \sin\theta$$

therefore

$$\frac{\delta U}{\delta (2Z)_{z=0}} = \frac{PR^3}{2EI} (1 - \sin\alpha) \left(1 - \cos\alpha - \frac{\sin^2\alpha}{2} - \frac{\alpha}{2} + \frac{\sin\alpha\cos\alpha}{2}\right)$$

$$\ldots\ldots (8.3)$$

for the part EO

$$M = ZR(1 - \cos\theta) + \left[P(1 - \sin\alpha) - Z\right] R \sin\theta - PR(\sin\theta - \sin\alpha)$$

..... (8.4)

$$\frac{\delta M}{R\,\delta Z} = 1 - \cos\theta - \sin\theta$$

therefore

$$\frac{\delta U}{\delta(2Z)_{Z=0}} = \frac{PR^3}{2EI}(1 - \sin\alpha)\left(\frac{3\pi}{4} - \frac{1}{2} - \frac{3\alpha}{2} - 2\cos\alpha + \sin\alpha - \frac{\sin^2\alpha}{2} + \frac{\sin\alpha\cos\alpha}{2}\right) \quad \ldots\ldots (8.5)$$

and

$$\sum \frac{\delta U}{\delta(2Z)_{Z=0}} = \delta_v{}^{o} = \frac{PR^3}{EI}\left(1 - \frac{\alpha}{2}\alpha\sin\alpha + \frac{(3\pi - 6)}{4}\sin\alpha - \cos\alpha - \frac{1}{2}\sin\alpha\cos\alpha + \frac{1}{2}\sin^2\alpha\right) \quad \ldots\ldots (8.6)$$

Similar expressions can be obtained for other systems of loading. It is seen that the vertical and horizontal displacements of the apex can be expressed for any system of loading by the following general formula:

$$\delta = \frac{PR^3}{EI}\left(a + b\alpha + c\alpha\sin\alpha + d\alpha\cos\alpha + e\sin\alpha + f\cos\alpha + g\sin\alpha\cos\alpha + h\sin^2\alpha + i\cos^2\alpha\right) \quad \ldots\ldots (8.7)$$

The numerical values of the coefficients a, b, c, ... i, are given for each of the four loading cases IA, IB, IIA, IIB in Figure 39.

The displacement in each case is a function of the angle α which denotes the point of application of the load and it is convenient to use the following functions $f(\alpha)$ for each loading system:

$$f_1(\alpha) = 1 - \frac{1}{2}\alpha - \alpha\sin\alpha + \frac{(3\pi - 6)}{4}\sin\alpha - \cos\alpha - \frac{1}{2}\sin\alpha\cos\alpha + \frac{1}{2}\sin^2\alpha$$

$$f_2(\alpha) = -1 + \frac{1}{2}\alpha + \alpha\sin\alpha + \frac{(\pi - 6)}{4}\sin\alpha + \cos\alpha + \frac{1}{2}\sin\alpha\cos\alpha - \frac{1}{2}\sin^2\alpha$$

$$f_3(\alpha) = \frac{(3\pi - 8)}{4} + \frac{1}{2}\alpha + \alpha\cos\alpha - \sin\alpha + \frac{(6 - 3\pi)}{4}\cos\alpha - \frac{1}{2}\sin\alpha\cos\alpha + \frac{1}{2}\cos^2\alpha$$

$$f_4(\alpha) = \frac{(\pi - 4)}{4} - \frac{1}{2}\alpha - \alpha\cos\alpha + \sin\alpha + \frac{(6 - \pi)}{4}\cos\alpha + \frac{1}{2}\sin\alpha\cos\alpha - \frac{1}{2}\cos^2\alpha$$

..... (8.8)

Case	Loading System	1	α	$\alpha\sin\alpha$	$\alpha\cos\alpha$	$\sin\alpha$	$\cos\alpha$	$\sin\alpha\times\cos\alpha$	$\sin^2\alpha$	$\cos^2\alpha$
		multiply the above terms by the coefficients								
		a	b	c	d	e	f	g	h	i
IA	$\delta_V^I = \frac{PR^3}{EI}.f_1(\alpha)$ 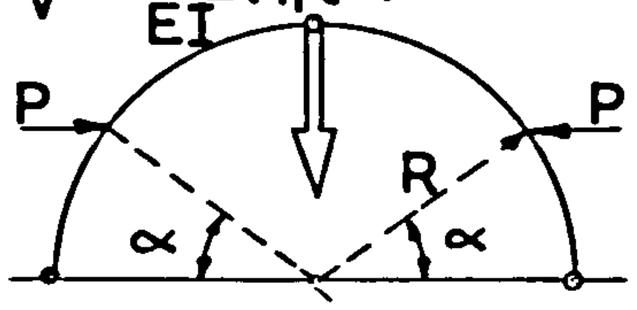	1	$-\frac{1}{2}$	−1	0	$\frac{3\pi-6}{4}$	−1	$-\frac{1}{2}$	$+\frac{1}{2}$	0
IB	$\delta_h^{II} = \frac{PR^3}{EI}.f_2(\alpha)$ 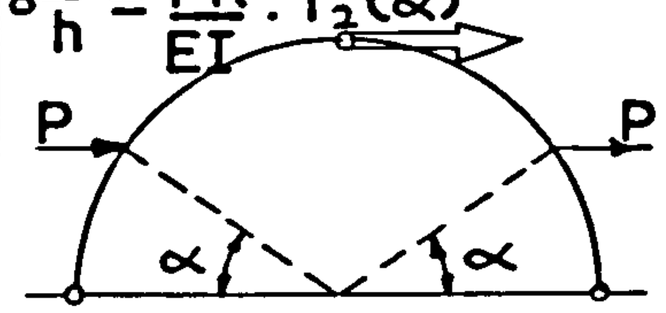	−1	$+\frac{1}{2}$	+1	0	$\frac{\pi-6}{4}$	+1	$+\frac{1}{2}$	$-\frac{1}{2}$	0
IIA	$\delta_V^{III} = \frac{PR^3}{EI}.f_3(\alpha)$ 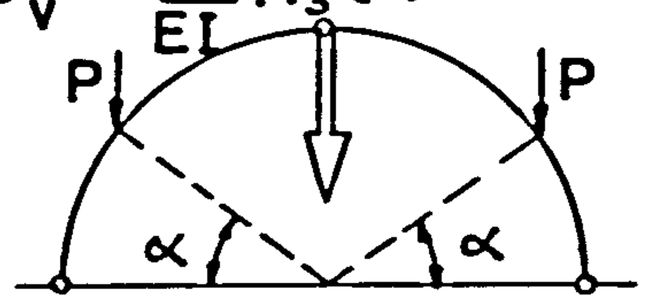	$\frac{3\pi-8}{4}$	$+\frac{1}{2}$	0	+1	−1	$\frac{6-3\pi}{4}$	$-\frac{1}{2}$	0	$+\frac{1}{2}$
II B	$\delta_h^{IV} = \frac{PR^3}{EI}.f_4(\alpha)$ 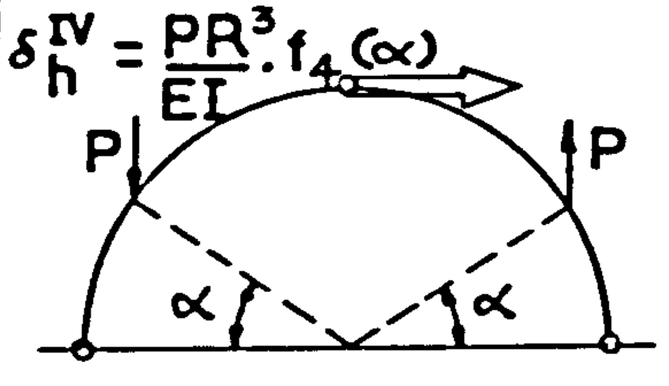	$\frac{\pi-4}{4}$	$-\frac{1}{2}$	0	−1	+1	$\frac{6-\pi}{4}$	$+\frac{1}{2}$	0	$-\frac{1}{2}$

FIG.39

DEFLEXIONS OF THE APEX OF A SEMI-CIRCULAR THREE-PINNED ARCH (Makowski & Gogate)

F.A.A. Ph.D. Thesis
2nd Dec., 1968

Structural Engineering Division
Department of Civil Engineering
University of Newcastle upon Tyne

The open arrow at the apex indicates the direction of the displacement

(c) General Expressions of the Reaction Components at Any Support of the Dome

Case IA: - Symmetrical horizontal loads acting on the arch 1-0-1′ (Figure 38(c)). All the ribs, forming the dome, are interconnected at the common hinge O and all undergo the same vertical displacement δ_v° of the apex joint. Owing to this interconnection, the external loading applied to the arch 1-0-1′ produces equal vertical reactions $2Y_1$ acting at the apex on all the other arches not directly loaded. From Case IIA, Figure 39, it may be seen that the vertical displacement of the crown point of any arch r-0-r′ caused by a unit vertical load at O equals

$$\frac{1}{2} \cdot \frac{R^3}{EI} \cdot f_3(90^\circ)$$

The directly loaded arch 1-0-1′ is under the action of two horizontal forces P and an upward force $2Y_1(n-1)$ representing the reaction from the remaining (n-1) arches. Under these forces the apex of the considered arch moves vertically by

$$\frac{PR^3}{EI} f_1(\alpha) - 2Y_1(n-1) \cdot \frac{1}{2} \frac{R^3}{EI} f_3(90^\circ) \qquad \ldots\ldots (8.9)$$

Owing to the interconnection, vertical displacements of the apex of the directly loaded arch 1-0-1′ and any arch r-0-r′ must be equal or:

$$\frac{1}{2} \cdot \frac{R^3}{EI} \cdot f_3(90^\circ) \cdot 2Y_1 = \frac{PR^3}{EI} \cdot f_1(\alpha) - 2Y_1(n-1) \cdot \frac{1}{2} \frac{R^3}{EI} \cdot f_3(90^\circ) \quad \ldots(8.10)$$

from which it follows that:

$$Y_1 = \frac{P \cdot f_1(\alpha)}{n \cdot f_3(90^\circ)} \qquad \ldots\ldots (8.11)$$

and the vertical displacement of the apex hinge in the dome

$$\delta_v^\circ = \frac{PR^3}{nEI} \cdot f_1(\alpha) \qquad \ldots\ldots (8.12)$$

Case IB: - Skew-symmetrical horizontal loads P acting on the arch 1-0-1′ (Figure 40). Under this loading the apex of the dome moves horizontally in the plane of the loaded arch 1-0-1′ by δ. The effect of the interconnection is that any arch rib r-0-r′, not directly loaded, has its apex horizontally displaced in its own plane by $\delta \cos \theta_r$ as in Figure 40(c). It should be noted that the displacement δ is very small, compared with other dimensions of the structure and does not

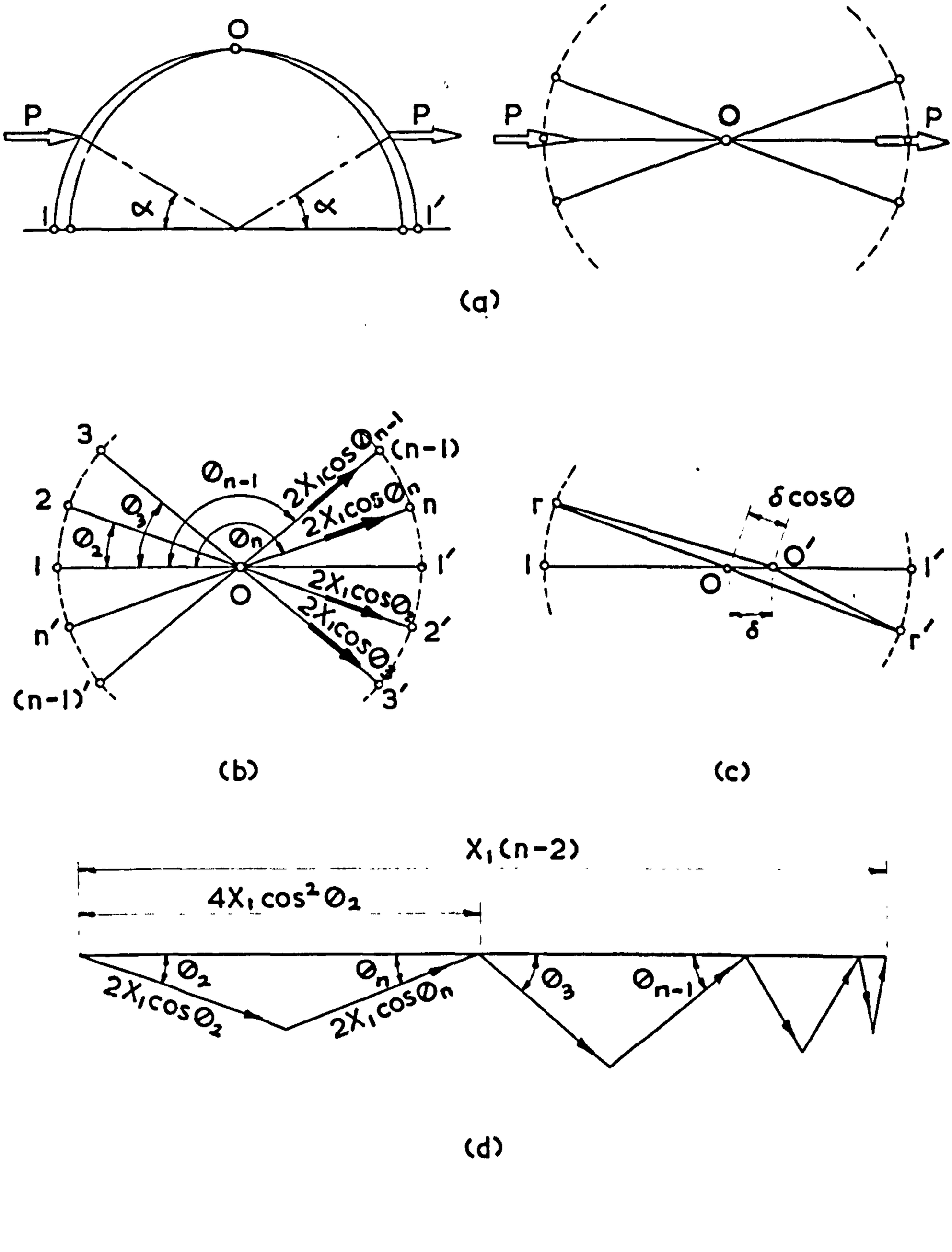

FIG. 40 STRESS ANALYSIS OF THREE-PINNED UNSTIFFENED SEMI-CIRCULAR ARCH-RIBBED DOMES (Makowski & Gogate) SHEET NO. 2

F.A.A. Ph.D. Thesis
17th July, 1969

Structural Engineering Division
Department of Civil Engineering
University of Newcastle upon Tyne

change the geometry of the dome, so that the value of the angle θ_r remains unaffected. Any arch r-O-r′ whose apex moves by $\delta \cos \theta_r$, is therefore pulled by a certain force, proportional to $\cos \theta_r$. This force is horizontal, acts in the plane of the arch, and is denoted in the subsequent analysis by $2X_1 \cos \theta_r$. By symmetry: $\theta_2 + \theta_n = \theta_3 + \theta_{n-1} = \ldots\ldots = \theta_r + \theta_{n-r+2} = \pi$; also $\theta_2 = \frac{\pi}{n}$, $\theta_3 = \frac{2\pi}{n}$ ..... or, generally, $\theta_r = \frac{(r-1)\pi}{n}$

Considering therefore two symmetrical arches, say, 2-O-2′ and n-O-n′ which are under the action of $2X_1 \cos \theta_2$ and $2X_1 \cos \theta_n$ respectively, it is clear that the resultant of these two forces is equal to a horizontal force $4X_1 \cos^2 \theta_2$, acting along the direction 1-O-1′ as in Figure 40(d). Such a resultant can be found for any pair of symmetrical arches and therefore the total horizontal force, representing the resultant of all these forces $2X_1 \cos \theta_r$ is given by the following equation:

$$\sum_{r=2}^{r=\frac{n}{2}} 4X_1 \cos^2 \theta_r = 4X_1 \left[\sum \cos^2 \theta_2 + \cos^2 \theta_3 + \ldots\ldots + \cos^2 \theta_{\frac{n}{2}} \right] \ldots\ldots (8.13)$$

$$= 4X_1 \left[\cos^2 \frac{\pi}{n} + \cos^2 \frac{2\pi}{n} + \ldots\ldots + \cos^2 \left(\frac{n}{2} - 1\right) \frac{\pi}{n} \right] \text{ for an}$$

even value of n and

$$= 4X_1 \left[\cos^2 \frac{\pi}{n} + \cos^2 \frac{2\pi}{n} + \ldots\ldots + \cos^2 \left(\frac{n-1}{2}\right) \frac{\pi}{n} \right] \text{for an odd value}$$

of n.

Putting $\beta = \frac{2\pi}{n}$ and using the relation $2 \cos^2 \theta = 1 + \cos 2\theta$ the resultant horizontal force given by equation (8.13) is expressed as:

$$\sum_{r=2}^{r=\frac{n}{2}} 4X_1 \cos^2 \theta_r = 2X_1 \left[\frac{(n-2)}{2} + \cos\beta + \cos 2\beta + \ldots\ldots + \cos \frac{(n-2)}{2}.\beta \right]$$

if n is even, or .... (8.14)

$$= 2X_1 \left[\frac{(n-1)}{2} + \cos\beta + \cos 2\beta + \ldots\ldots + \cos \frac{(n-1)}{2}.\beta \right]$$

if n is odd

It may be proved that equation (8.14) can be expressed by one very

simple formula, which is equally valid for even or odd values of n.

Observing that

$$\cos \phi + \cos 2\phi + \ldots\ldots \cos n\phi = \frac{\cos \frac{(n+1)}{2}\phi . \sin \frac{n}{2}\phi}{\sin \frac{\phi}{2}} \quad \ldots(8.15)$$

it is possible to simplify equation (8.14) as follows. If n is even:

$\cos\beta + \cos 2\beta + \ldots\ldots + \cos \frac{(n-2)}{2}\beta$ reduces to 0; since $\beta = \frac{2\pi}{n}$,

$\frac{n\beta}{4} = \frac{\pi}{2}$.

If n is odd: $\cos\beta + \cos 2\beta + \ldots\ldots + \cos \frac{(n-1)}{2}\beta$ reduces to

$\frac{\sin -\frac{\beta}{2}}{2 \sin \frac{\beta}{2}} = -\frac{1}{2}$; since $\frac{n\beta}{2} = \pi$ and $\sin \pi = 0$.

Adding these results to the corresponding constant terms contained in equation (8.15), for an even value of n

$$2X_1 \left[\frac{n-2}{2} + 0\right] = X_1(n-2)$$

and for an odd value of n

$$2X_1 \left[\frac{n-1}{2} \frac{1}{2}\right] = X_1(n-2)$$

It has been proved therefore that in each case, for n even or odd, the resultant horizontal force becomes

$$\sum_{r=2}^{r=\frac{n}{2}} 4X_1 \cos^2\theta_r = X_1(n-2) \ldots\ldots (8.16)$$

This force $X_1(n-2)$ representing the resultant of all forces $2X_1 \cos \theta_r$ acting on all r-0-r′ arches is directed towards support 1′.

An equal force, but acting in the opposite direction, applies at 0 on the directly loaded arch 1-0-1′. A unit horizontal load at the apex of a three-pinned arch would produce a horizontal deflection equal to

$$\frac{1}{2} \cdot \frac{R^3}{EI} \cdot f_2(90^\circ)$$

Therefore, the deflection of any arch r-0-r′ is

$$\delta \cos \theta_r = 2X_1 \cos \theta_r \frac{R^3}{2EI} f_2(90^\circ)$$

Similarly, by superposition the deflection of the arch 1-0-1′ is

$$\delta = f_2(\alpha).\frac{PR^3}{EI} - (n-2)\,X_1.\frac{R^3}{2EI}.\,f_2(90^\circ)$$

From these equations it follows that:

$$\delta = 2X_1.\frac{R^3}{2EI}.\,f_2(90^\circ)$$

and $$X_1 = \frac{2P\,f_2(\alpha)}{n\,f_2(90^\circ)} \qquad \ldots\ldots (8\cdot17)$$

Introducing now the known value of X_1 into the above expression of δ the final value of the displacement is

$$\delta = \frac{2P\,R^3\,f_2(\alpha)}{nEI} \qquad \ldots\ldots (8\cdot18)$$

The last two equations are valid for all values of $n \geq 2$. If $n = 2$, the arch 2-0-2′ will be unstressed under the considered system of loading.

8.4 THE ANALYSIS OF THREE-PINNED UNSTIFFENED CIRCULAR ARC RADIAL RIBBED DOMES

The Author's interest lies mainly in the field of low rise-to-span radial ribbed domes and the method of stress analysis employed by Makowski and Gogate,[27] for semi-circular ribbed domes, has been extended to include rib shapes which follow only part of the circumference of a circle. Vertical and horizontal displacements of the apex have been obtained in a similar manner to those given in Art 8.3 (b) and the numerical values of the coefficients a, b, c, ... i, which are included in equation (8·7), are given for the four loading cases IA, IB, IIA, IIB in Figure 41.

The $f(\alpha)$ functions, upon which the apex displacements depend, are as follows:

$$f_1(\alpha) = \frac{(1 + 2\sin\theta_o)}{(1 - \sin\theta_o)} + \cos\theta_o\frac{\left[\frac{\theta_o}{2} - \left(\frac{3\pi}{4} - \theta_o\right)\sin\theta_o\right]}{(1 - \sin\theta_o)^2} - \frac{\cos\theta_o.\alpha}{2(1-\sin\theta_o)}$$

$$- \frac{\cos\theta_o.\alpha\sin\alpha}{(1 - \sin\theta_o)} + \left[-\frac{3}{2}\frac{(1 + \sin\theta_o)}{(1 - \sin\theta_o)} + \cos\theta_o\left(\frac{\frac{3\pi}{4} - \frac{\theta_o}{2} - \theta_o\sin\theta_o}{(1 - \sin\theta_o)^2}\right)\right]\sin\alpha$$

Case	Loading System The open arrow at the apex indicates the direction of the displacement	1	α	$\alpha\sin\alpha$	$\alpha\cos\alpha$	$\sin\alpha$	$\cos\alpha$	$\sin\alpha\cos\alpha$	$\sin^2\alpha$	$\cos^2\alpha$
		multiply the above terms by the coefficients								
		a	b	c	d	e	f	g	h	i
IA	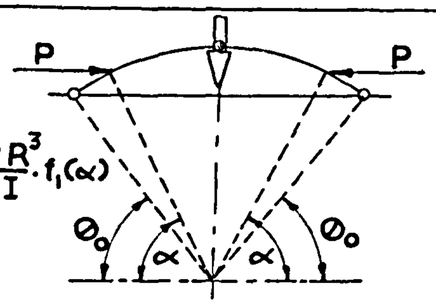 $\delta_v^I = \frac{PR^3}{EI}.f_1(\alpha)$	$\frac{(1+2\sin\phi_0)}{(1-\sin\phi_0)} + \frac{\cos\phi_0}{(1-\sin\phi_0)^2} \times \left[\frac{\phi_0}{2} - \left(\frac{3\pi}{4} - \phi_0\right)\sin\phi_0\right]$	$\frac{-\cos\phi_0}{2(1-\sin\phi_0)}$	$\frac{-\cos\phi_0}{(1-\sin\phi_0)}$	0	$-\frac{3(1+\sin\phi_0)}{2(1-\sin\phi_0)} + \frac{\cos\phi_0}{(1-\sin\phi_0)^2} \times \left[\frac{3\pi}{4} - \frac{\phi_0}{2} - \phi_0\sin\phi_0\right]$	$\frac{-\cos\phi_0}{(1-\sin\phi_0)}$	$\frac{-\cos\phi_0}{2(1-\sin\phi_0)}$	$+\frac{1}{2}$	0
IB	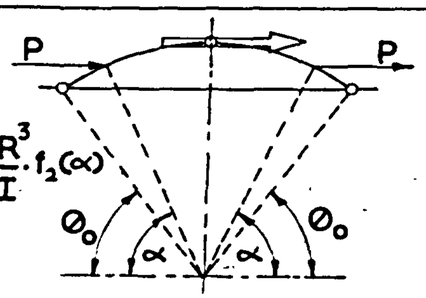 $\delta_h^{II} = \frac{PR^3}{EI}.f_2(\alpha)$	$-1 - \frac{1}{2\cos\phi_0} \times \left[\frac{\pi}{2}\sin\phi_0 + \phi_0\right]$	$\frac{(1+\sin\phi_0)}{2\cos\phi_0}$	$\frac{\cos\phi_0}{(1-\sin\phi_0)}$	0	$-\frac{3}{2} + \frac{1}{\cos\phi_0} \times \left[\frac{\pi}{4} - \frac{3\phi_0}{2} - \phi_0\sin\phi_0\right]$	$\frac{\cos\phi_0}{(1-\sin\phi_0)}$	$\frac{(1+\sin\phi_0)}{2\cos\phi_0}$	$-\frac{1}{2}$	0
IIA	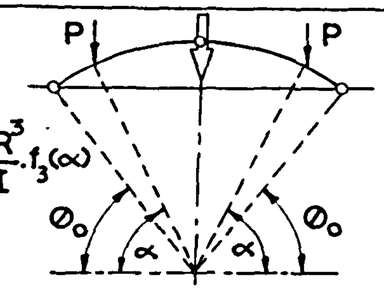 $\delta_v^{III} = \frac{PR^3}{EI}.f_3(\alpha)$	$\frac{1}{(1-\sin\phi_0)} \times \left[\frac{3\pi}{4} - 2\cos\phi_0 - 2\phi_0 + \sin\phi_0\left(\frac{3\pi}{4} - \phi_0\right)\right]$	$+\frac{1}{2}$	0	$\frac{\cos\phi_0}{(1-\sin\phi_0)}$	$\frac{-\cos\phi_0}{(1-\sin\phi_0)}$	$\frac{3(1+\sin\phi_0)}{2(1-\sin\phi_0)} + \frac{\cos\phi_0}{(1-\sin\phi_0)^2} \times \left[\frac{\phi_0}{2} - \frac{3\pi}{4} + \phi_0\sin\phi_0\right]$	$-\frac{1}{2}$	0	$\frac{\cos\phi_0}{2(1-\sin\phi_0)}$
IIB	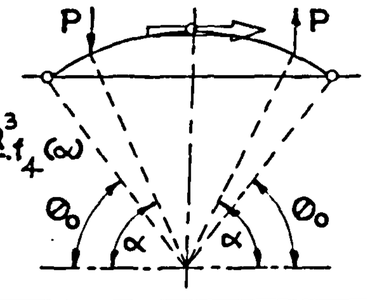 $\delta_h^{IV} = \frac{PR^3}{EI}.f_4(\alpha)$	$\frac{\pi}{4} - \frac{\cos\phi_0}{(1-\sin\phi_0)}$	$-\frac{1}{2}$	0	$\frac{-\cos\phi_0}{(1-\sin\phi_0)}$	$\frac{\cos\phi_0}{(1-\sin\phi_0)}$	$\frac{3}{2} + \frac{1}{\cos\phi_0} \times \left[\frac{3\phi_0}{2} - \frac{\pi}{4} + \phi_0\sin\phi_0\right]$	$+\frac{1}{2}$	0	$\frac{-\cos\phi_0}{2(1-\sin\phi_0)}$

FIG. 41 DEFLEXIONS OF THE APEX OF A CIRCULAR THREE-PINNED ARCH

F.A.A. Ph.D. Thesis
2nd Dec., 1968

Structural Engineering Division
Department of Civil Engineering
University of Newcastle upon Tyne

$$- \frac{\cos\theta_o}{(1-\sin\theta_o)} \cdot \cos\alpha - \frac{\cos\theta_o}{2(1-\sin\theta_o)} \cdot \sin\alpha\cos\alpha + \frac{\sin^2\alpha}{2}$$

$$f_2(\alpha) = -1 - \frac{(\frac{\pi}{2} \cdot \sin\theta_o + \theta_o)}{2\cos\theta_o} + \frac{(1+\sin\theta_o)}{2\cos\theta_o}\alpha$$

$$+ \frac{\cos\theta_o \cdot \alpha\sin\alpha}{(1-\sin\theta_o)} + \left[-\frac{3}{2} + \frac{(\frac{\pi}{4} - \frac{3}{2}\theta_o - \theta_o\sin\theta_o)}{\cos\theta_o}\right]\sin\alpha$$

$$+ \frac{\cos\theta_o\cos\alpha}{(1-\sin\theta_o)} + \frac{(1+\sin\theta_o)}{2\cos\theta_o}\sin\alpha\cos\alpha - \frac{\sin^2\alpha}{2}$$

$$f_3(\alpha) = \frac{\left[\frac{3\pi}{4} - 2\cos\theta_o - 2\theta_o + \sin\theta_o\,(\frac{3\pi}{4} - \theta_o)\right]}{1-\sin\theta_o} + \frac{\alpha}{2}$$

$$+ \frac{\cos\theta_o \cdot \alpha\cos\alpha}{(1-\sin\theta_o)} - \frac{\cos\theta_o \cdot \sin\alpha}{(1-\sin\theta_o)}$$

$$+ \left[\frac{3}{2}\frac{(1+\sin\theta_o)}{1-\sin\theta_o} + \cos\theta_o\,(\frac{\theta_o}{2} - \frac{3\pi}{4} + e_o\sin\theta_o)\right]\cos\alpha$$

$$- \frac{\sin\alpha\cos\alpha}{2} + \frac{\cos\theta_o\cos^2\alpha}{2(1-\sin\theta_o)}$$

$$f_4(\alpha) = \frac{\pi}{4} - \frac{\cos\theta_o}{(1-\sin\theta_o)} - \frac{\alpha}{2} - \frac{\cos\theta_o\,\alpha\cos\alpha}{(1-\sin\theta_o)} + \frac{\cos\theta_o\sin\alpha}{(1-\sin\theta_o)}$$

$$+ \left[\frac{3}{2} + \frac{(\frac{3\theta_o}{2} - \frac{\pi}{4} + \theta_o\sin\theta_o)}{\cos\theta_o}\right]\cos\alpha + \frac{\sin\alpha\cos\alpha}{2}$$

$$- \frac{\cos\theta_o \cdot \cos^2\alpha}{2(1-\sin\theta_o)} \qquad \ldots\ldots (8\cdot19)$$

In the above equations (8·19), θ_o denotes the angle of the rib base from the centre of the circle on which the rib lies.

Having determined the $f(\alpha)$ functions, the displacements of the apex, for the various load conditions, can be obtained from equations (8.12) and (8·18) while the forces at the apex are determined from equations (8·11) and (8·17). The reaction components at any support are easily evaluated once the forces acting on the ribs are known and are given in a general form in Figure 42. By superposition, the reactions caused by a unit horizontal load are given after adding

	Case I A	Case I B	Case II A	Case II B
Directly loaded arch 1-O-1′	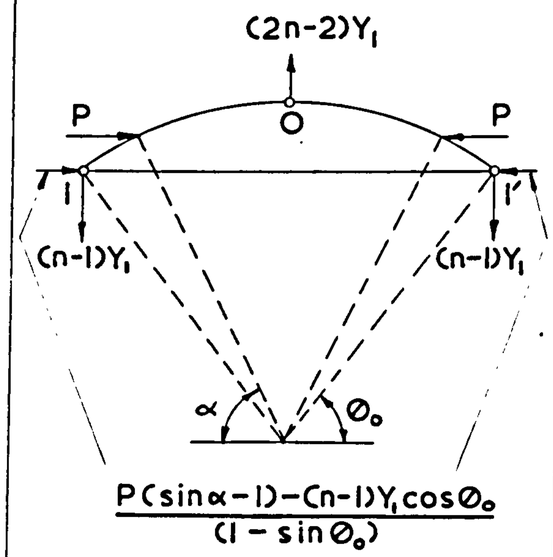	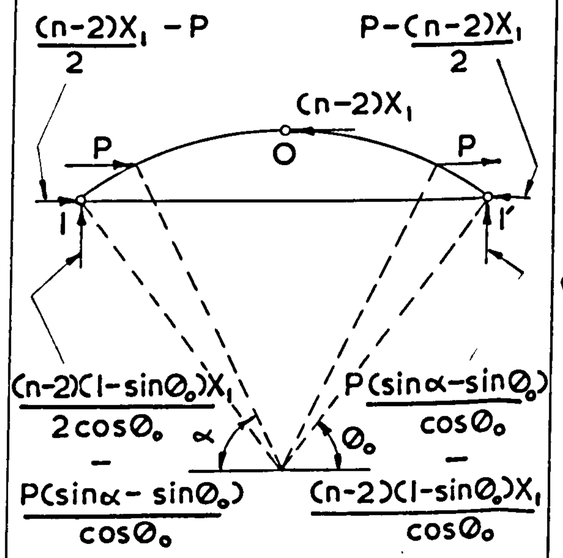	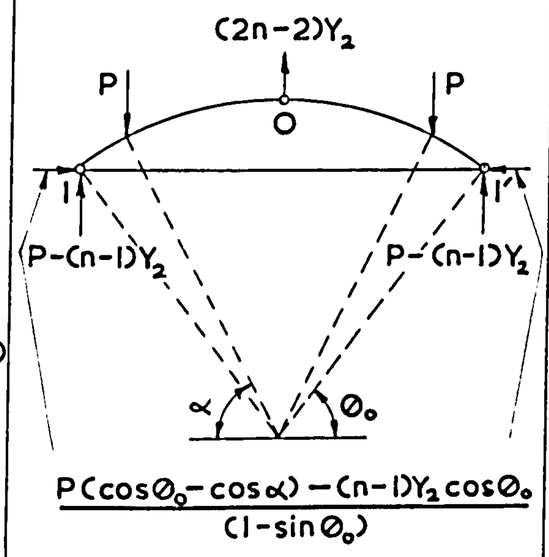	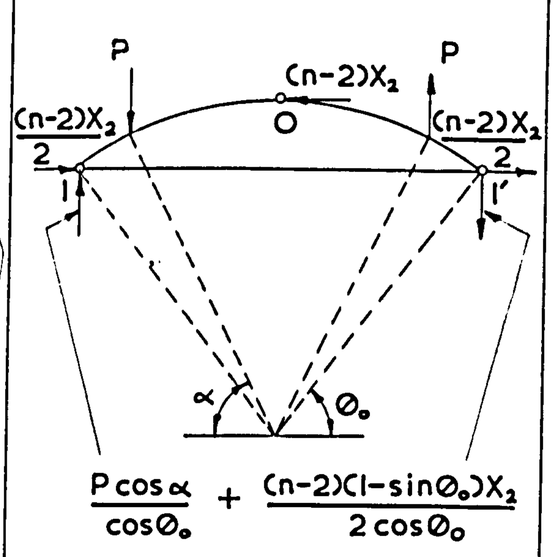
Any arch r-O-r′ not directly loaded	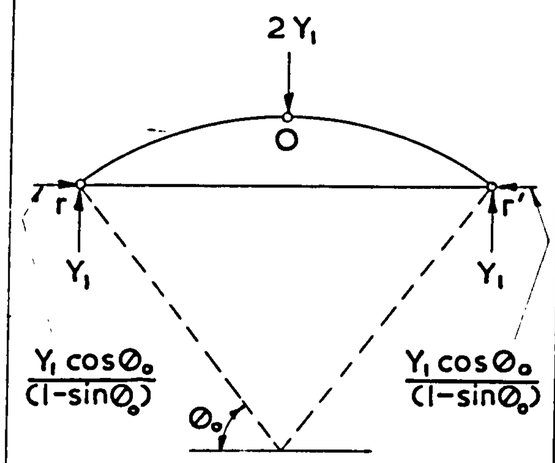	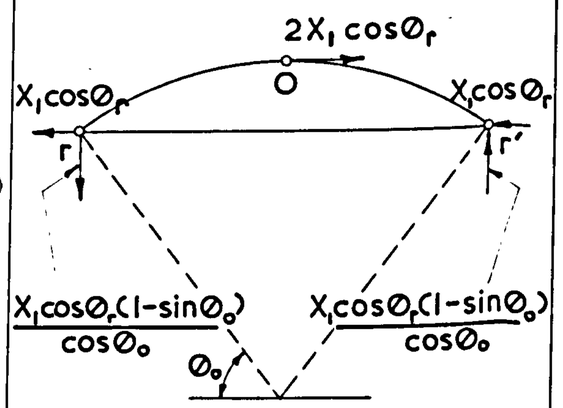	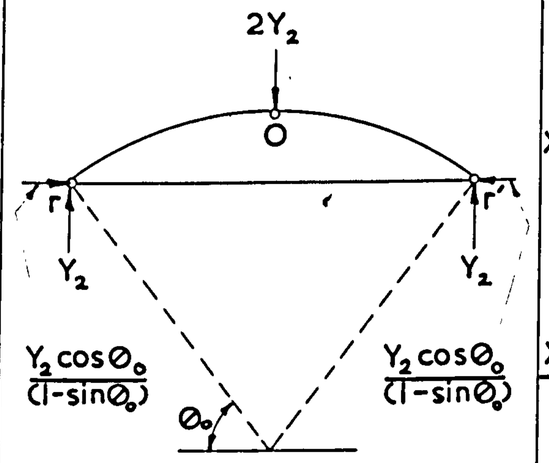	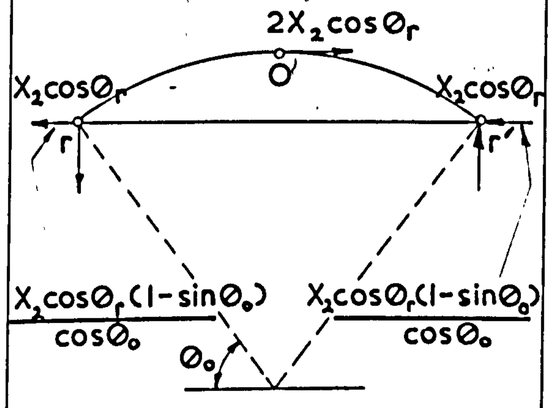
Crown displacement	where $Y_1 = \frac{P.f_1(\alpha)}{n.f_3(90°)}$ $\delta_V^{\circ}(\downarrow) = \frac{P.R^3.f_1(\alpha)}{nEI}$	where $X_1 = \frac{2P.f_2(\alpha)}{n.f_2(90°)}$ $\delta_{h\,(\rightarrow)}^{\circ} = \frac{2P.R^3.f_2(\alpha)}{nEI}$	where $Y_2 = \frac{P.f_3(\alpha)}{n.f_3(90°)}$ $\delta_V^{\circ}(\downarrow) = \frac{P.R^3.f_3(\alpha)}{nEI}$	where $X_2 = \frac{2P.f_4(\alpha)}{n.f_2(90°)}$ $\delta_{h\,(\rightarrow)}^{\circ} = \frac{2P.R^3.f_4(\alpha)}{nEI}$

FIG. 42 REACTIONS AND FORCES ACTING ON A CIRCULAR THREE-PINNED ARCH

F.A.A. Ph.D. Thesis
18th July, 1969

Structural Engineering Division
Department of Civil Engineering
University of Newcastle upon Tyne

together the results for Cases IA, IB and dividing by 2P. From Cases IIA, IIB the results for vertical load conditions have been obtained in a similar manner. The results are summarized in Figure 43, from which the reactions for any support of a dome consisting of any number of ribs can rapidly be determined. Bending moments, shearing forces and axial forces for any particular case may also be deduced once these reactions are known.

Having the general formulae, valid for any number of ribs, influence lines of reaction components at any support, or influence lines of bending moments, shearing forces and axial forces for any particular point in any of the ribs can be prepared very easily. Influence lines such as these are very useful when complicated loading cases are to be considered. Concentrated or distributed loads can be accounted for and the determination of the maximum stresses due to live loads, including wind forces, then becomes relatively simple.

In large diameter domes, the number of radial ribs and horizontal purlin rings is enormous. To carry out a unit load stress analysis of such a structure by hand would be almost impossible. However, in recent years electronic computers have eased the task of the engineer and the author has prepared a program which evaluates the theoretical reaction components and bending moments, induced in three-pinned circular arc radial ribbed domes, based on the method of analysis mentioned above. The program, notation diagram, explanation notes, input data and output data for domes with 6 and 36 ribs are included in Volume II of this thesis.

8.5 TWO-HINGED UNSTIFFENED RADIAL RIBBED DOMES

Two-hinged radial ribbed domes differ from the three-hinged type in that the ribs are rigidly fixed together at the apex. Pinned bases are employed in both types and heavy block footings are normally provided without an elastic base ring which is the requirement for an

Case	Type of loading	Reactions for directly loaded arch 1-1′	Reactions for any not directly loaded arch r-r′	Deflexions of the apex O
I	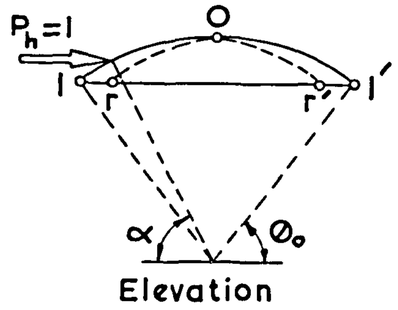 Elevation 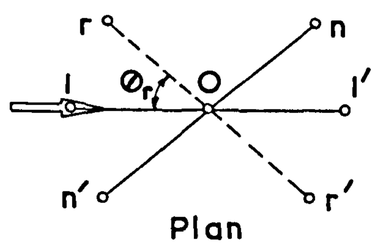 Plan	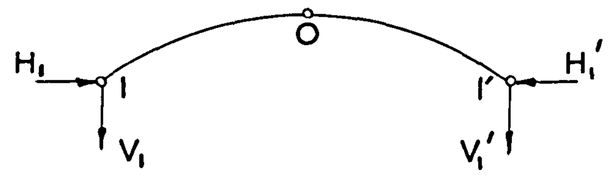 Vertical Reactions $V_1=\frac{(\sin\alpha-\sin\phi_o)}{2\cos\phi_o}+\frac{1}{2n}\left[\frac{(n-1)f_1(\alpha)}{f_3(90°)}-\frac{(n-2)(1-\sin\phi_o)f_2(\alpha)}{\cos\phi_o f_2(90°)}\right]$ $V_1'=-\frac{(\sin\alpha-\sin\phi_o)}{2\cos\phi_o}+\frac{1}{2n}\left[\frac{(n-1)f_1(\alpha)}{f_3(90°)}+\frac{(n-2)(1-\sin\phi_o)f_2(\alpha)}{\cos\phi_o f_2(90°)}\right]$ $\left[V_1'=-H_1'\frac{(1-\sin\phi_o)}{\cos\phi_o}\right]$ Horizontal Reactions $H_1=\frac{(\sin\alpha-1)}{2(1-\sin\phi_o)}-\frac{1}{2}+\frac{1}{2n}\left[\frac{-(n-1)f_1(\alpha)\cos\phi_o}{(1-\sin\phi_o)f_3(90°)}+\frac{(n-2)f_2(\alpha)}{f_2(90°)}\right]$ $H_1'=\frac{(\sin\alpha-1)}{2(1-\sin\phi_o)}+\frac{1}{2}+\frac{1}{2n}\left[\frac{-(n-1)f_1(\alpha)\cos\phi_o}{(1-\sin\phi_o)f_3(90°)}-\frac{(n-2)f_2(\alpha)}{f_2(90°)}\right]$	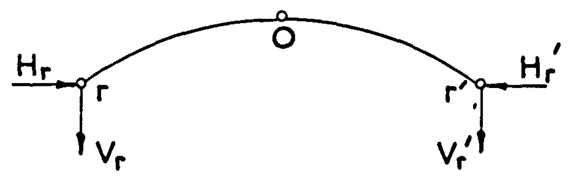 Vertical Reactions $V_r=\frac{1}{2n}\left[\frac{-f_1(\alpha)}{f_3(90°)}+\frac{2f_2(\alpha)\cos\phi_r(1-\sin\phi_o)}{f_2(90°)\cos\phi_o}\right]$ $V_r'=\frac{1}{2n}\left[\frac{-f_1(\alpha)}{f_3(90°)}-\frac{2f_2(\alpha)\cos\phi_r(1-\sin\phi_o)}{f_2(90°)\cos\phi_o}\right]$ $\left[V_r=-H_r\frac{(1-\sin\phi_o)}{\cos\phi_o};\ V_r'=-H_r'\frac{(1-\sin\phi_o)}{\cos\phi_o}\right]$ Horizontal Reactions $H_r=\frac{1}{2n}\left[\frac{f_1(\alpha)\cos\phi_o}{f_3(90°)(1-\sin\phi_o)}-\frac{2f_2(\alpha)\cos\phi_r}{f_2(90°)}\right]$ $H_r'=\frac{1}{2n}\left[\frac{f_1(\alpha)\cos\phi_o}{f_3(90°)(1-\sin\phi_o)}+\frac{2f_2(\alpha)\cos\phi_r}{f_2(90°)}\right]$	$\delta_{\text{vertical}}=\frac{R^3}{2EI}\cdot\frac{f_1(\alpha)}{n}$ $\delta_{\text{horizontal}}=\frac{R^3}{EI}\cdot\frac{f_2(\alpha)}{n}$ (in the plane 1-O-1′)
II	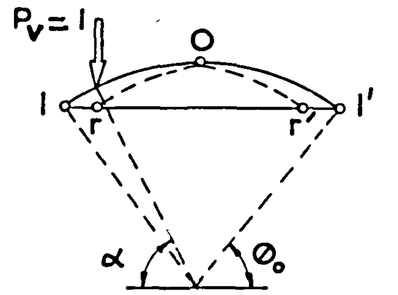 Elevation 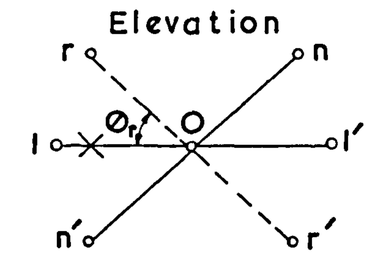 Plan	Vertical Reactions $V_1=-\frac{1}{2}-\frac{\cos\alpha}{2\cos\phi_o}+\frac{1}{2n}\left[\frac{(n-1)f_3(\alpha)}{f_3(90°)}-\frac{(n-2)(1-\sin\phi_o)f_4(\alpha)}{\cos\phi_o f_2(90°)}\right]$ $V_1'=-\frac{1}{2}+\frac{\cos\alpha}{2\cos\phi_o}+\frac{1}{2n}\left[\frac{(n-1)f_3(\alpha)}{f_3(90°)}+\frac{(n-2)(1-\sin\phi_o)f_4(\alpha)}{\cos\phi_o f_2(90°)}\right]$ $\left[V_1'=-H_1'\frac{(1-\sin\phi_o)}{\cos\phi_o}\right]$ Horizontal Reactions $H_1=\frac{(\cos\phi_o-\cos\alpha)}{2(1-\sin\phi_o)}+\frac{1}{2n}\left[\frac{-(n-1)\cos\phi_o f_3(\alpha)}{(1-\sin\phi_o)f_3(90°)}+\frac{(n-2)f_4(\alpha)}{f_2(90°)}\right]$ $H_1'=\frac{(\cos\phi_o-\cos\alpha)}{2(1-\sin\phi_o)}+\frac{1}{2n}\left[\frac{-(n-1)\cos\phi_o f_3(\alpha)}{(1-\sin\phi_o)f_3(90°)}-\frac{(n-2)f_4(\alpha)}{f_2(90°)}\right]$	Vertical Reactions $V_r=\frac{1}{2n}\left[\frac{-f_3(\alpha)}{f_3(90°)}+\frac{2f_4(\alpha)\cos\phi_r(1-\sin\phi_o)}{f_2(90°)\cos\phi_o}\right]$ $V_r'=\frac{1}{2n}\left[\frac{-f_3(\alpha)}{f_3(90°)}-\frac{2f_4(\alpha)\cos\phi_r(1-\sin\phi_o)}{f_2(90°)\cos\phi_o}\right]$ $\left[V_r=-H_r\frac{(1-\sin\phi_o)}{\cos\phi_o};\ V_r'=-H_r'\frac{(1-\sin\phi_o)}{\cos\phi_o}\right]$ Horizontal Reactions $H_r=\frac{1}{2n}\left[\frac{f_3(\alpha)\cos\phi_o}{f_3(90°)(1-\sin\phi_o)}-\frac{2f_4(\alpha)\cos\phi_r}{f_2(90°)}\right]$ $H_r'=\frac{1}{2n}\left[\frac{f_3(\alpha)\cos\phi_o}{f_3(90°)(1-\sin\phi_o)}+\frac{2f_4(\alpha)\cos\phi_r}{f_2(90°)}\right]$	$\delta_{\text{vertical}}=\frac{R^3}{2EI}\cdot\frac{f_3(\alpha)}{n}$ $\delta_{\text{horizontal}}=\frac{R^3}{EI}\cdot\frac{f_4(\alpha)}{n}$ (in the plane 1-O-1′)

FIG. 43 REACTION COMPONENTS FOR UNIT LOAD ON A CIRCULAR ARC RADIAL RIBBED DOME

F. A. A. Ph. D. Thesis
18th July, 1969

Structural Engineering Division
Department of Civil Engineering
University of Newcastle upon Tyne

"unstiffened" dome. A typical two-hinged radial ribbed dome is shown in Figures 44(a) and (b).

However, a rigid joint at the dome crown produces a different stress distribution in the system than if a spherical hinge is assumed to be present. A method of analysis which can be employed for this type of structure is given in the following pages and is attributed to Fichl.[10] The dome, which is considered in the analysis, is symmetrical about an axis lying along any rib shown in plan, Figure 44(b), and the load acts on one half of this rib, considered the main rib in Figure 44(a), without any load on the other or secondary ribs. Fichl's analysis requires two methods of approach to the problem:

(1) the vertex is assumed to be supported in such a way that rib rotations are allowed without any displacement of the vertex;

(2) the vertex translates while the rib rotations are prevented.

(a) Vertex Point Rotation Effect

Reactions are produced at the apex imaginary support due to external loads and the effect of these reactions on the complete structure constitutes the analysis procedure. The main rib, being acted upon by a load system, can be regarded as an elastic rib, pinned at the base and fixed elastically to the crown points. At the vertex a fixing moment occurs; this moment is considered to be the redundant value and has a magnitude which depends upon the degree of elastic fixity of the rib at the apex point. The loaded part of the main rib, therefore, can be considered as a two-hinged rib acted upon by external loads and a redundant moment, M. By introducing a hinge at the vertex point a statically determinate "primary" structure is obtained.

The degree of elastic fixity of the rib at the vertex is determined by the angle of rotation τ_o which occurs under a moment of M = 1, applied in the vertical plane at the top support as in Figure 44(c). A value for M, the fixed end moment, can be obtained from the elastic

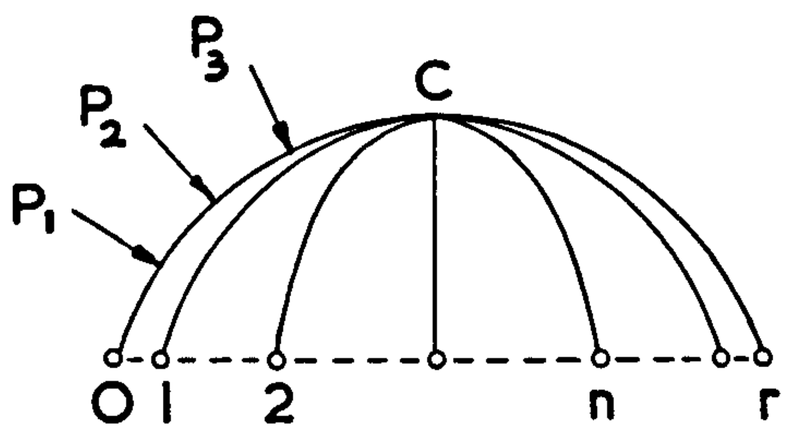

(a)

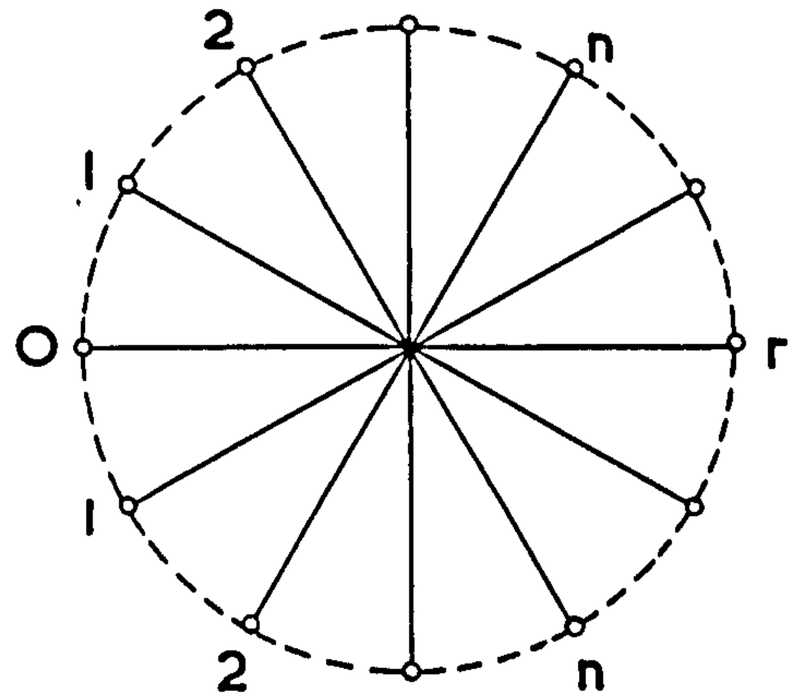

(b)

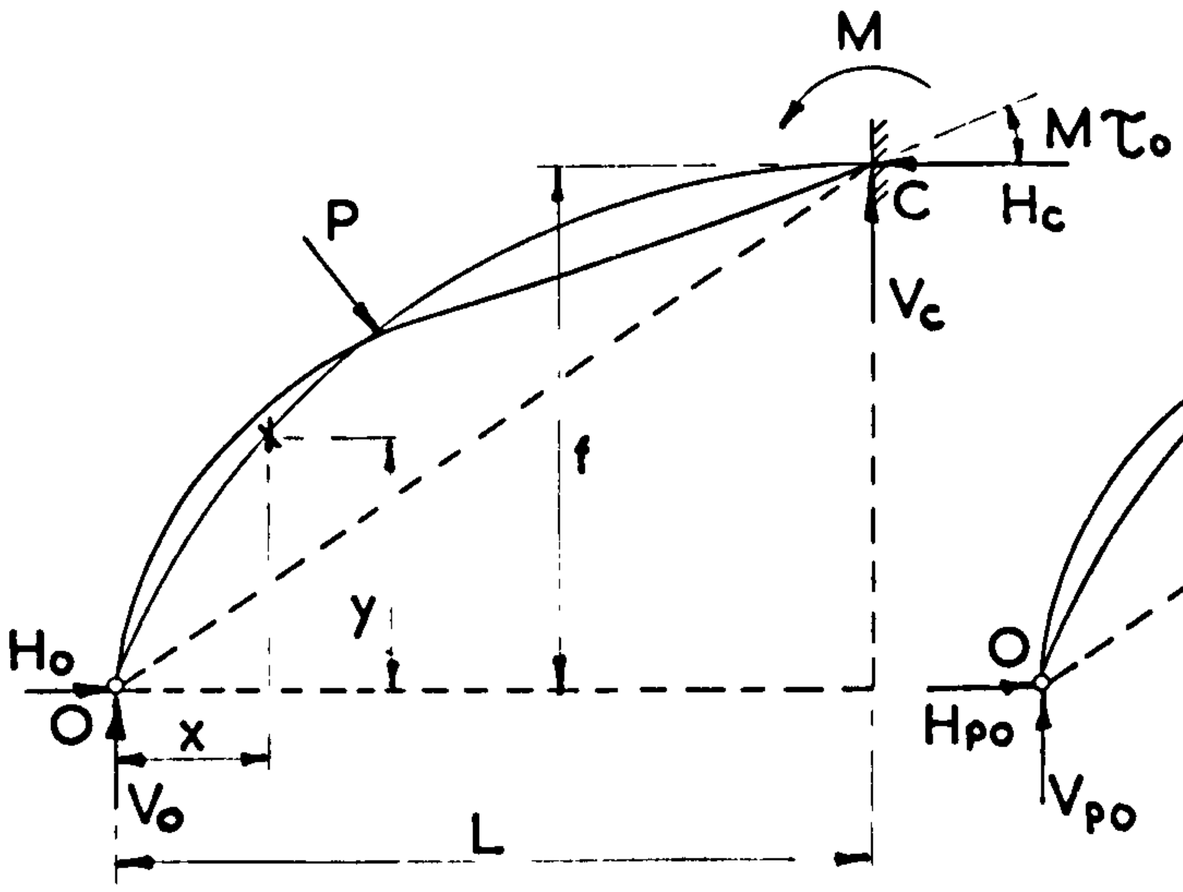

(c)

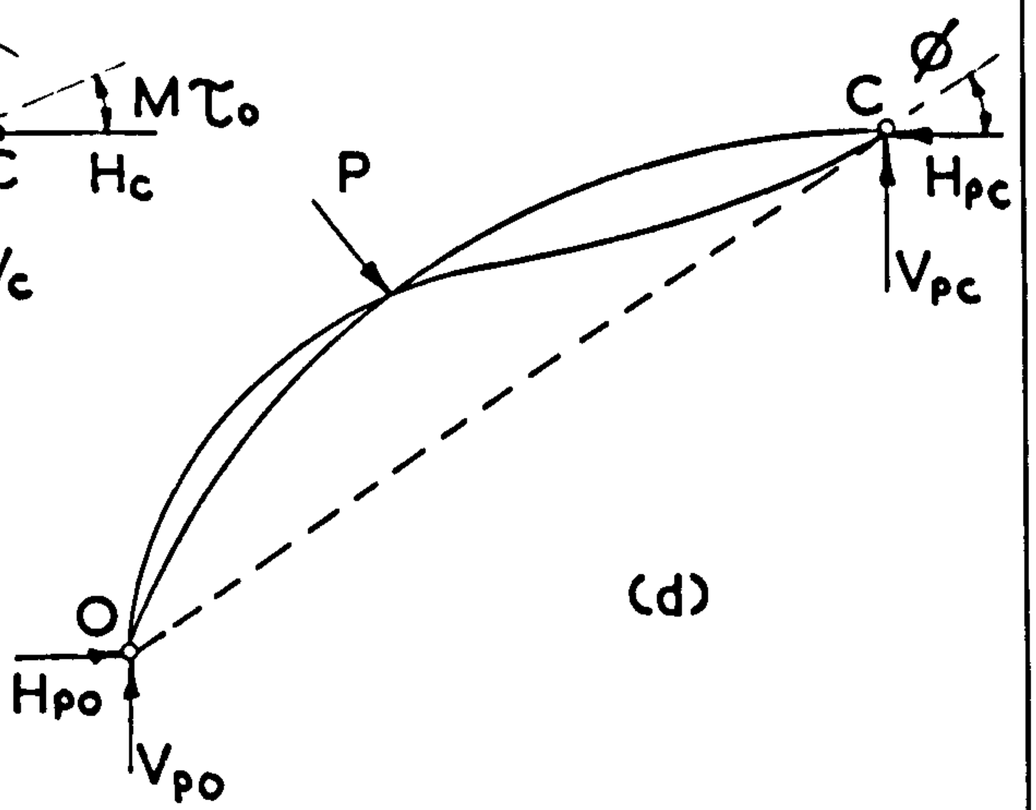

(d)

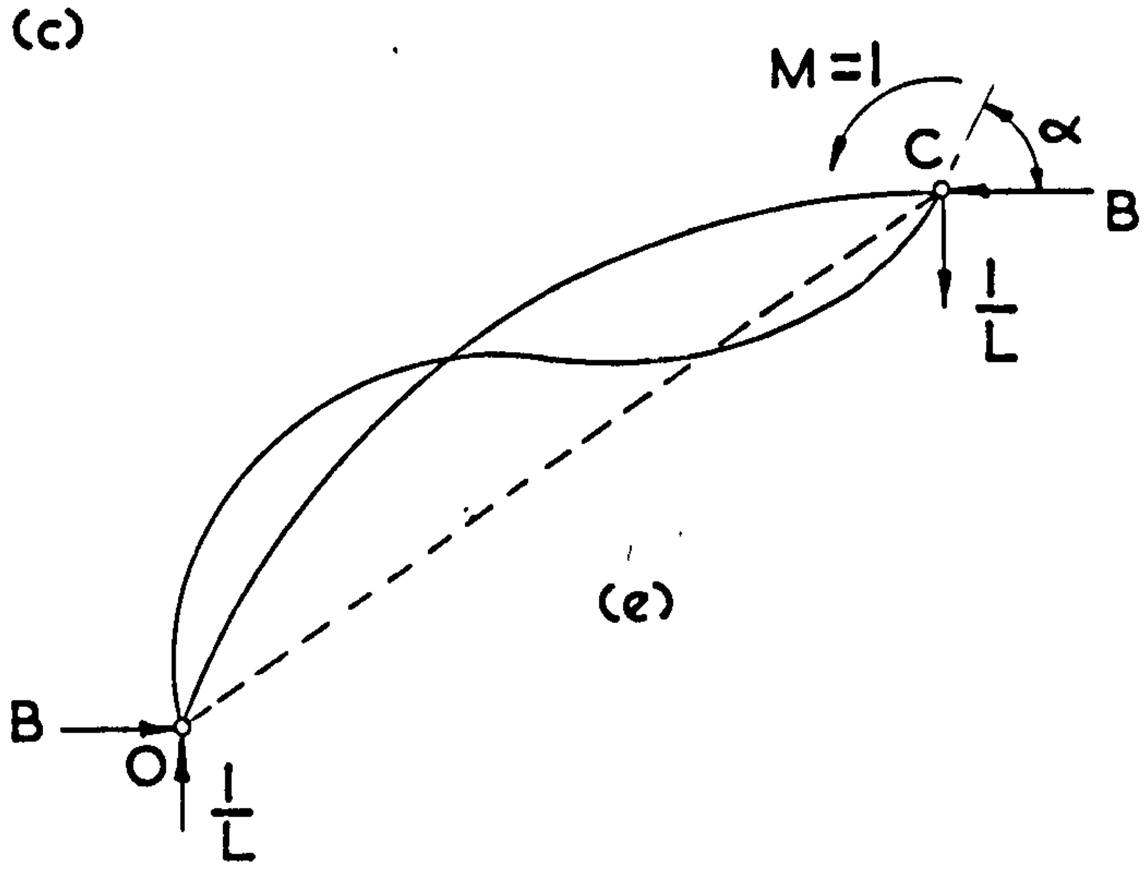

(e)

FIG. 44 TWO-HINGED UNSTIFFENED RADIAL RIBBED DOMES Sheet No.1

F.A.A. Ph.D. Thesis
24th July, 1969

Structural Engineering Division
Department of Civil Engineering
University of Newcastle upon Tyne

equation[10]:

$$M.\alpha + \phi = - M\tau_o$$

which gives

$$M = \frac{\phi}{\alpha + \tau_o} \qquad \ldots\ldots (8\cdot20)$$

where:

α = the angle of rotation of the vertex due to M = 1;

ϕ = the angle of rotation of the vertex due to the external load;

τ_o = the degree of elastic fixity of the vertex.

α and ϕ can be determined from a normal analysis of a two-hinged arch[10]:

$$\alpha = \frac{1}{E}\left(\frac{1}{L^2}\int_o^L x^2 . \frac{ds}{I} - B^2 \int_o^L y^2 . \frac{ds}{I}\right) \qquad \ldots\ldots (8\cdot21)$$

$$\phi = \frac{1}{E}\left(\frac{1}{L}\int_o^L Mo \cdot x \frac{ds}{I} - H_{PO}.B \int_o^L y^2 . \frac{ds}{I}\right) \qquad \ldots\ldots (8\cdot22)$$

where:

$H_{o_{M=1}} = B = \frac{1}{L}.\frac{\int_o^L xy \cdot \frac{ds}{I}}{\int_o^L y^2 . \frac{ds}{I}}$ = horizontal thrust due to M = 1 [Figure 44(c)];

$H_{PO} = \frac{\int_o^L Mo.y \frac{ds}{I}}{\int_o^L y^2 . \frac{ds}{I}}$ = horizontal thrust caused by the external loading [Figure 44(d)];

M_o = the bending moment in a simply supported beam of span L under the action of external loading;

$\frac{ds}{I}$ = "elastic weight".

The strain energy stored in the structure is assumed to be due only to bending when calculating the above values, i.e. the influence of axial forces is neglected.

Values of the reaction components are given by:

$H_C = H_{PC} + M.B$; $H_o = H_{PO} + M.B$;

$V_C = V_{PC} + \frac{1}{L}.M$; $V_o = V_{PO} + \frac{1}{L}.M.$

The bending moment at any cross-section is:

$$M_x = M_o - H.y - M.\frac{x}{L}$$

At the apex support the bending moment is distributed between all the ribs meeting there and may be expressed as

$$M = M_1 + M_2 + M_3 ..... + M_n$$

τ_o, the degree of elastic fixity of the main loaded rib, can be found from:

$$\tau_o = \frac{1}{\frac{1}{\epsilon_1} + \frac{1}{\epsilon_2} + \frac{1}{\epsilon_3} + ... + \frac{1}{\epsilon_n}} \qquad ..... (8.23)$$

ϵ_n is the rotation at the vertex of a system of two symmetrically placed secondary ribs n-c-n, Figure 45(a), caused by a unit moment applied in a vertical plane through the directly loaded rib OC.

The moment of M = 1 applied in the vertical plane of OC is distributed evenly between the symmetrically placed secondary ribs n-c-n, each of which carry a bending moment of $\frac{M}{2}$. Resolving this bending moment of $\frac{M}{2}$, as shown in Figure 45(a), the following values are obtained:

$M_1 = \frac{1}{2} \cos\rho$ in the plane of the secondary rib;

$M_2 = \frac{1}{2} \sin\rho$ in the vertical plane at right angles to the secondary rib plane.

Bending, torsion and rotation occur at the end of each rib due to these bending moment components. If the angles of rotation are as follows:

α = the angle of rotation due to M = 1 acting in the plane of the rib;

β = the angle of rotation due to a unit torsional moment M_d=1 acting perpendicular to the rib plane, Figure 45(b),

then

$$\epsilon = (\tfrac{1}{2}\alpha\cos\rho)\cos\rho + (\tfrac{1}{2}\beta\sin\rho)\sin\rho$$

$$= \tfrac{1}{2}(\alpha\cos^2\rho + \beta\sin^2\rho) \qquad ..... (8.24)$$

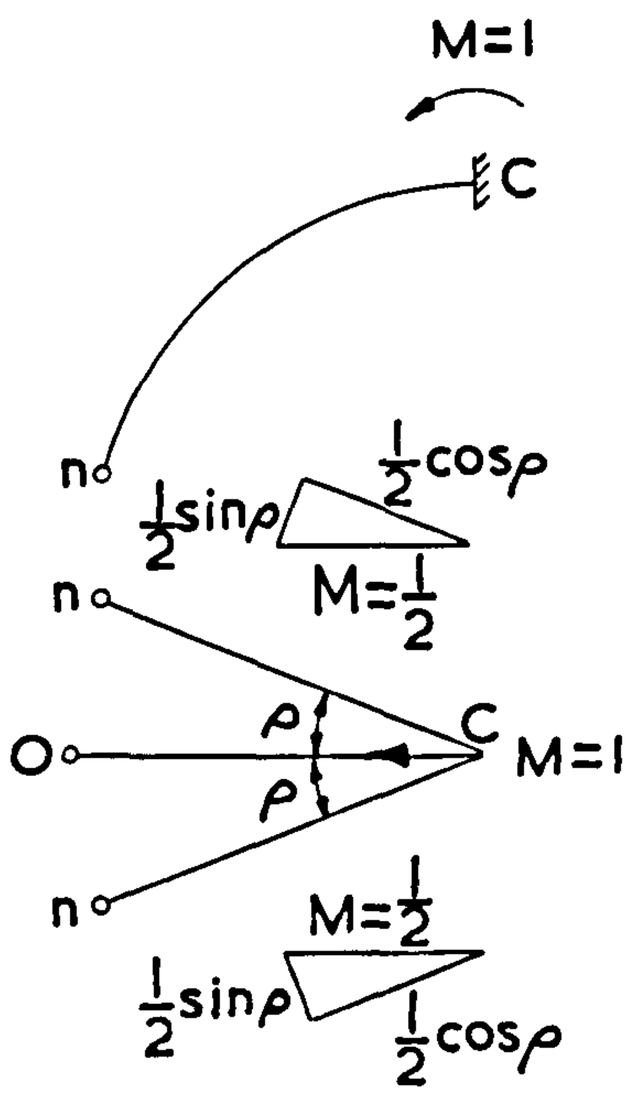

(a)

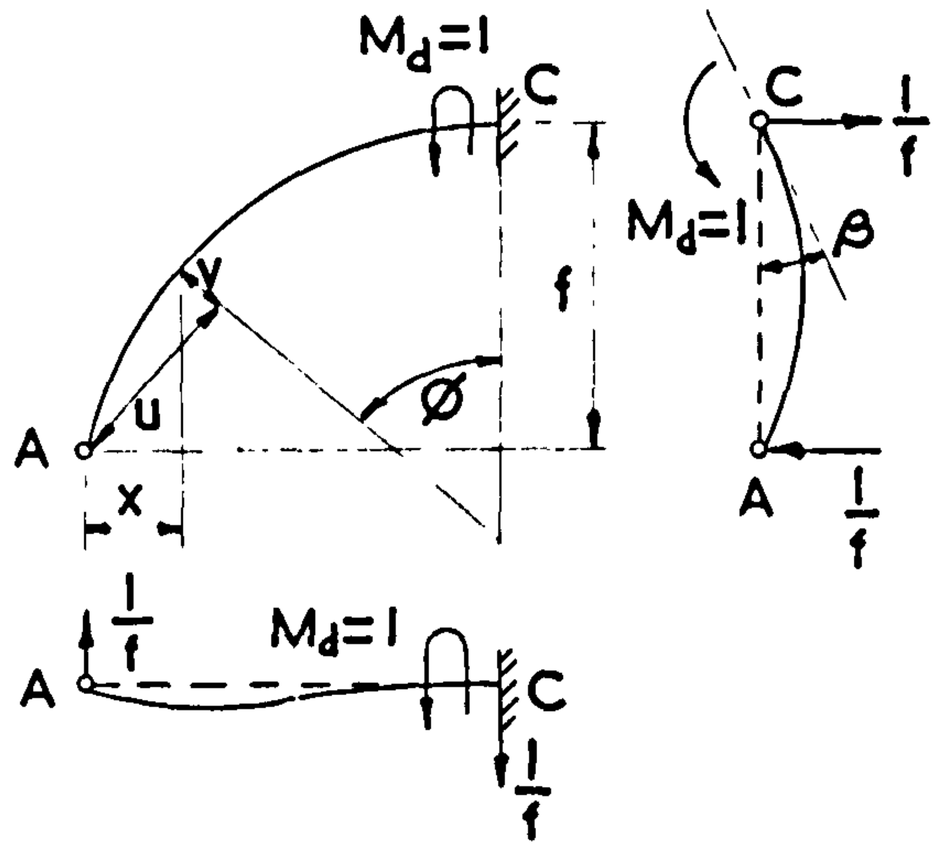

(b)

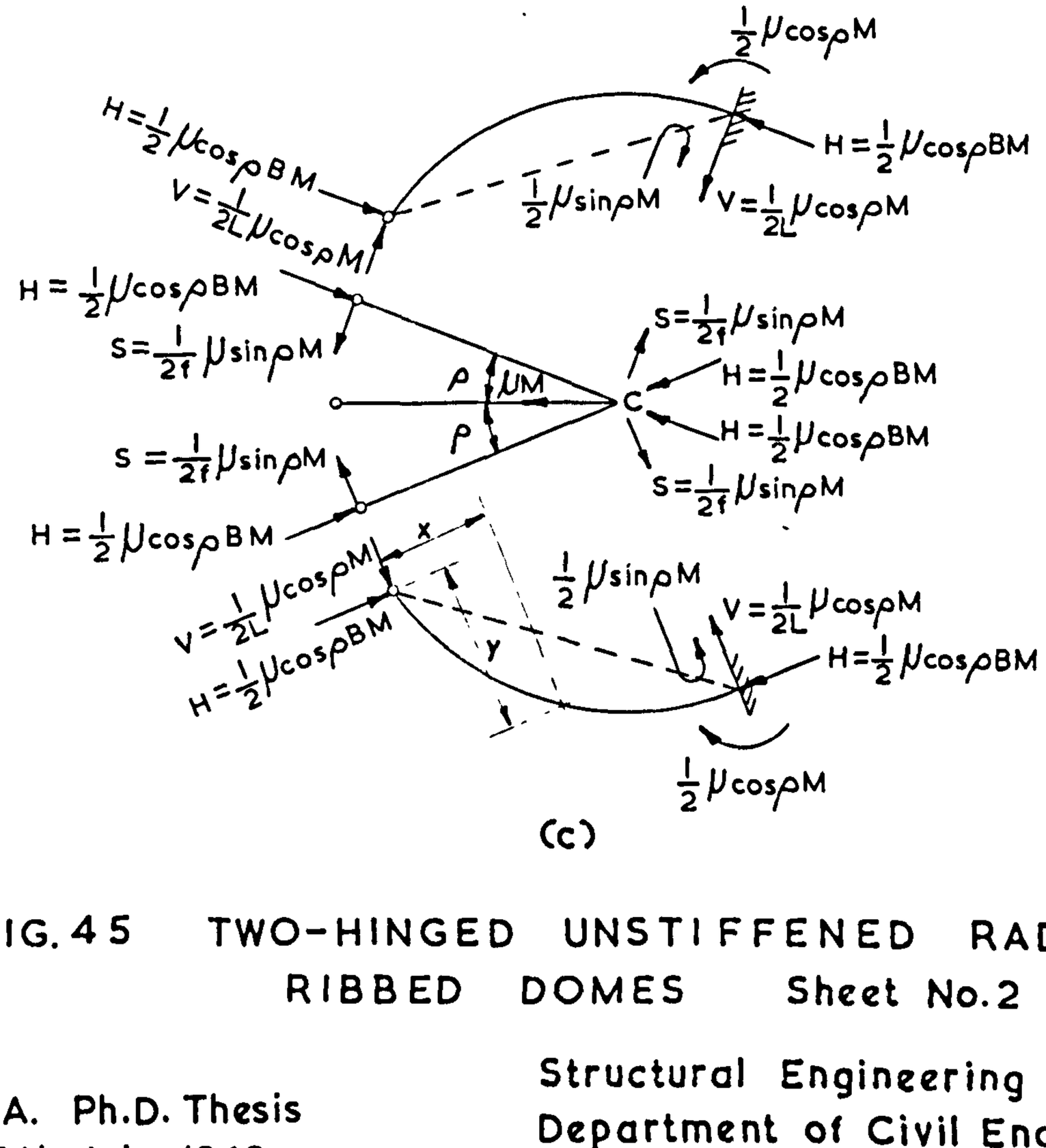

(c)

FIG. 45 TWO-HINGED UNSTIFFENED RADIAL RIBBED DOMES Sheet No. 2

F.A.A. Ph.D. Thesis
25 th July, 1969

Structural Engineering Division
Department of Civil Engineering
University of Newcastle upon Tyne

α can be determined from equation (8.21).

$$\beta = \int_0^L \frac{M_o}{EI} \cdot \frac{\delta M_o}{\delta M} \cdot ds + \int_0^L \frac{Md}{NJ} \cdot \frac{\delta Md}{\delta M} ds = \frac{1}{Ef^2}\left[\int_0^L u^2 dw' + 2(m+1)\int_0^L v^2 dw''\right]$$

..... (8.25)

where:

$dw' = \frac{ds}{Z}$, $dw'' = \frac{ds}{J}$ are the elastic weights;

m = Poisson's ratio

Z = the second moment of area for the lateral bending;

J = the polar moment of inertia;

N = the modulus of rigidity of the material.

Once ε has been established for each pair of ribs, symmetrically placed about the main loaded rib, and the fixed end moment M at the vertex has been evaluated, then the distribution of this moment among the secondary ribs can be deduced from the formula:

$$M_n = \frac{\tau_o}{\varepsilon_n} M = \mu_n \cdot M \quad \text{..... (8.26)}$$

where

$\mu_n = \frac{\tau_o}{\varepsilon_n}$ is the distribution factor for which $\sum_1^r \mu = 1$

Each separate secondary rib n-c carries $\frac{1}{2}\mu_n$.M which has components of:

$M' = \frac{1}{2} \mu \cos\rho \, M$;

$M'' = \frac{1}{2} \mu \sin\rho \, M$.

The resultant reactions in the ribs due to these components of the moment M are given in Figure 45(c). Each rib undergoes bending in two planes together with torsion as follows:

(1) Vertical plane bending moment, $M_x = \frac{1}{2} \mu \cos\rho \, M \, (\frac{x}{L} - D.y)$;

(2) Lateral bending moment, $M_{lx} = \frac{1}{2f} \mu \sin\rho . M . u$;

(3) Torque, $M_{tx} = \frac{1}{2f} . \mu \sin\rho . M . v$.

The secondary rib vertex reactions, together with the reactions caused by the external loads on the main rib, can be resolved into horizontal and vertical components:

$$H = H_C + B\sum_{1}^{r} \mu_{\cdot} \cos^2\rho\ M + \frac{1}{f}\sum_{1}^{r} \mu \sin^2\rho\ M \qquad \ldots\ldots (8\cdot25)$$

$$V = V_C + \frac{1}{L}\sum_{1}^{r} \mu \cos\rho\ M \qquad \ldots\ldots (8\cdot26)$$

(b) Vertex Point Translation Effect

In this part of the analysis the external loads are removed from the system and the reaction components, caused by the imaginary constraints at the vertex and given by equations (8·25) and (8·26), are applied in opposite directions as forces on the dome. The study of the influence of these forces on the system is carried out in two ways:

(1) a horizontal unit load is applied in the rib plane at the vertex;

(2) a vertical unit load is applied separately at the same point.

(1) Horizontal Unit Load at the Vertex. Instead of employing a unit horizontal load directly at the vertex, a unit displacement is assumed resulting in a horizontal force of H. By dividing all the effects of this displacement by H the horizontal unit load conditions can be obtained.

The dome with a horizontal displacement of Δ at the vertex, and no support movement, is equivalent to a system which has a fixed vertex point and a displacement of Δ at each support, Figure 46(a). This horizontal displacement of Δ, in a direction parallel to the main rib, is resolved into components $\Delta \cos\rho$ in the direction of the secondary rib under consideration and $\Delta \sin\rho$ normal to it. The effects of these two displacements are considered separately.

A horizontal displacement, Δ, of the rib AC, Figure 46(b), at its base produces reactions as follows:

$$H_\Delta = H_{o\Delta} + M'_{K\Delta} \cdot B \qquad \ldots\ldots (8\cdot27)$$

where

$H_{o\Delta}$ = the horizontal thrust due to displacement only in the two-hinged arch system = $\dfrac{\varepsilon\Delta}{\int y^2\, dw}$;

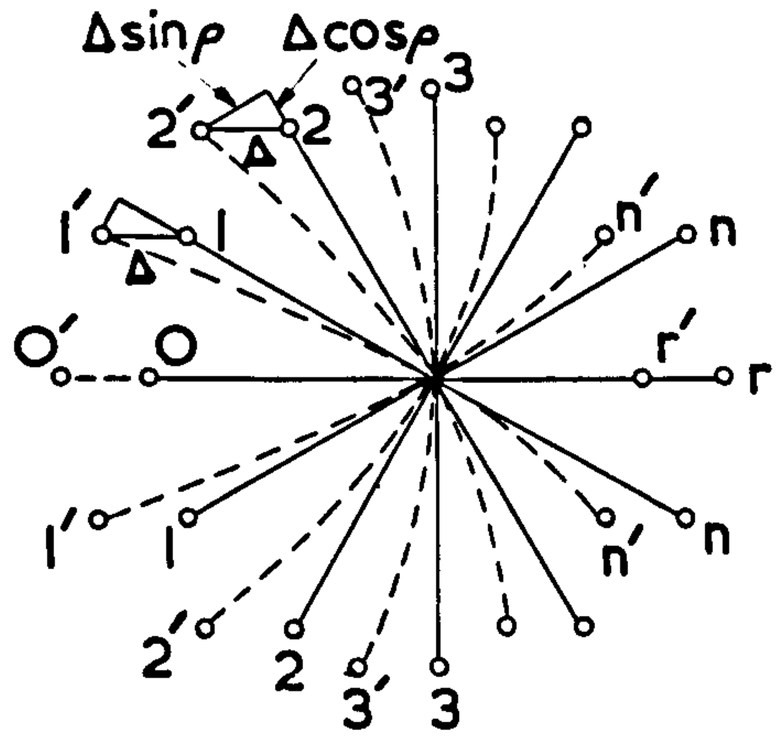

(a)

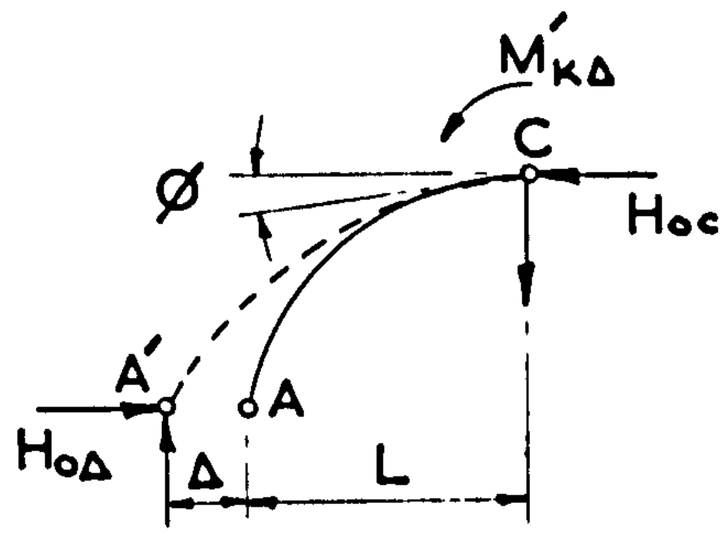

(b)

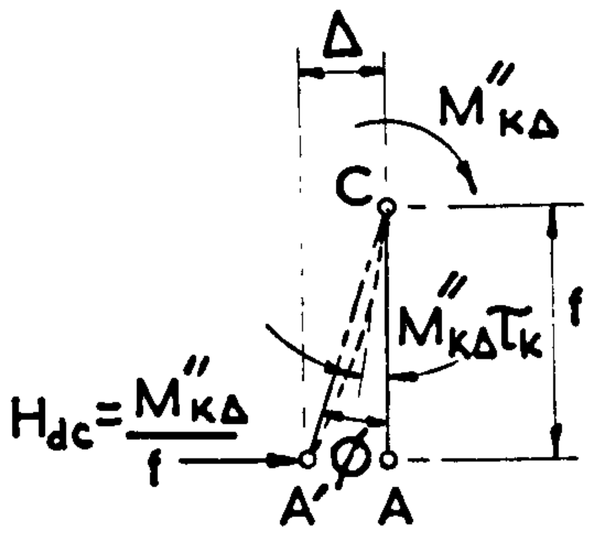

(c)

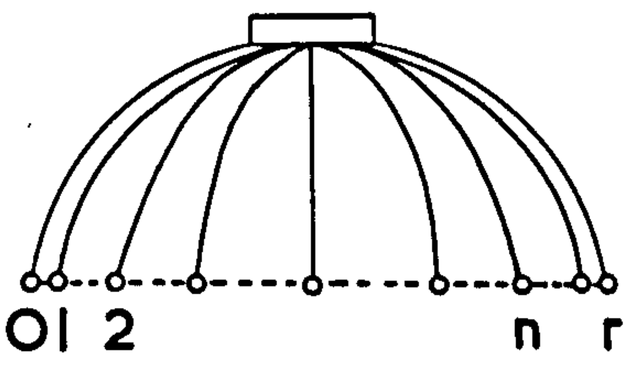

(d)

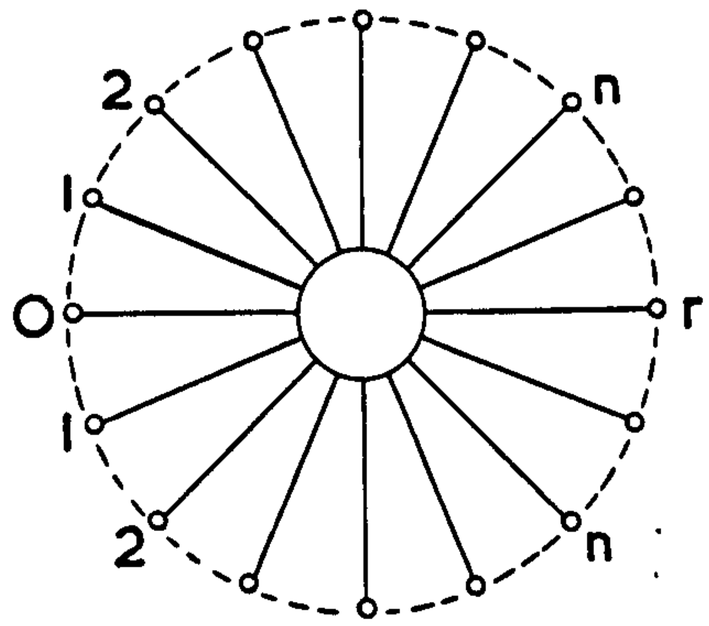

(e)

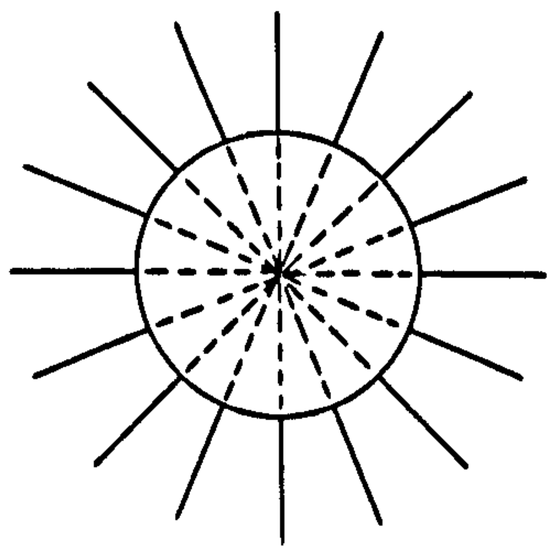

(f)

FIG. 46 TWO-HINGED UNSTIFFENED RADIAL RIBBED DOMES Sheet No. 3

F.A.A. Ph.D. Thesis
24th July, 1969

Structural Engineering Division
Department of Civil Engineering
University of Newcastle upon Tyne

$M'_{K\Delta}$ = the fixing moment in the vertex = $\frac{-B\Delta}{\alpha + \tau_{K\alpha}}$;

B = the horizontal thrust due to $M'_{K\Delta} = 1$ (see equation 8·22).

The vertical reaction is given by:

$$V = \frac{1}{L} \cdot M'_{K\Delta} \qquad \ldots\ldots (8\cdot28)$$

A displacement of Δ perpendicular to the rib AC, Figure 46(c), at the base produces an angle of twist of $\phi = \frac{\Delta}{f}$. The following reactions are also produced:

$$H_{dc} = \frac{1}{f} \cdot M''_{K\Delta} = S_\Delta \qquad \ldots\ldots (8\cdot29)$$

$$M''_{K\Delta} = \frac{\Delta \sin\rho}{f(\frac{1}{2}\beta \sin\rho + \tau_{K\beta})} \qquad \ldots\ldots (8\cdot30)$$

A lateral bending moment is also induced in the rib by the horizontal force H at the vertex:

$$M_{1\Delta} = S_\Delta \cdot u \qquad \ldots\ldots (8\cdot31)$$

and the torque is

$$M_{t\Delta} = S_\Delta \cdot v \qquad \ldots\ldots (8\cdot32)$$

The degree of elastic fixation of the vertex point of the secondary ribs can again be expressed in terms of rotation as previously:

$$\tau_K = \frac{1}{\frac{1}{\varepsilon_0} + \frac{1}{\varepsilon_1} + \ldots\ldots + \frac{1}{\varepsilon_{k-1}} + \frac{1}{\varepsilon_{k+1}} + \ldots\ldots \frac{1}{\varepsilon_r}} \qquad \ldots\ldots (8\cdot33)$$

This can be resolved into two components which represent the degree of fixation of this system:

$$\tau_{K\alpha} = \frac{\tau_K}{\varepsilon_K} \cdot \tfrac{1}{2}\alpha\cos\rho \qquad \text{(in the plane of the considered rib)} \quad \ldots\ldots (8\cdot34)$$

$$\tau_{K\beta} = \frac{\tau_K}{\varepsilon_K} \cdot \tfrac{1}{2}\beta\sin\rho \qquad \text{(in the vertical plane normal to the rib plane)} \quad \ldots\ldots (8\cdot35)$$

The moments at the vertex caused by the two components of the displacement $\Delta \sin\rho$ and $\Delta \cos\rho$ can therefore be expressed as a total bending moment acting in the plane of the main rib as follows:

$$M_{K\Delta} = M'_{K\Delta} \cdot \cos\rho + M''_{K\Delta} \sin\rho \qquad \ldots\ldots (8.36)$$

By multiplying with the corresponding distribution factor $\mu_{Kn} = \frac{\tau_K}{\epsilon_n}$, this moment can be distributed between all the remaining ribs. The distribution factor has to be calculated for each pair of symmetrically placed secondary ribs and each pair receives moments due to the displacements of all the other ribs as well as moments from its own displacements. Using the principle of superposition the influence of the total horizontal displacement can be deduced and a value for the corresponding total horizontal load obtained. The results for a horizontal unit load are obtained by dividing by the value obtained for the total horizontal load.

(2) Vertical Unit Load at the Vertex. When a vertical unit load is applied at the vertex of the dome, it is divided equally among all the ribs due to the symmetry of the system and only bending moments are produced in the plane of the ribs. If there are n ribs the reactions at the base of each rib are given as follows:

$$V = \frac{1}{n} \; ;$$

$$H = \frac{1}{n} \cdot \frac{\int_o^L xy.dw}{\int_o^L y^2.dw} \qquad \ldots\ldots (8.37)$$

The bending moments in the ribs are easily determined once H and V are known.

Having now considered the effects of rotation and translation of the vertex of a two-hinged unstiffened radial ribbed dome the final stresses in the system can be obtained by combining the rotation, without sway, from Art. 8.5(a), and the translation or sway effect from Art. 8.5(b). According to Makowski[10] this method of analysis can be employed for domes with apex rings as well as for the closed systems. However, the apex ring must be so stiff that its deflections are small compared with the rib displacements, Figures 46 (d),(e),(f).

In certain circumstances, in practice, this assumption is valid because the ring is often fixed to a lantern and needs to be relatively stiff.

8.6 TWO-HINGED UNSTIFFENED RADIAL RIBBED DOME WITH APEX RING

Another method which can be employed for the analysis of two-hinged radial ribbed domes was developed by H. Marcus.[10] For his solution Marcus considered the general case of an open radial ribbed dome, Figure 47, which has two main symmetry planes at right angles to each other. All the ribs lie in vertical planes intersecting a common main axis. The ribs are rigidly connected to a ring at the apex of the dome and pin-jointed at the base.

Marcus assumed that the external loading, employed in his method of analysis, was symmetrical in relation to one of the main ribs. He also assumed that the diameter of the apex ring was small and the analysis is, in fact, carried out as if the dome is of the closed type. Hence this procedure for analysing two-hinged radial ribbed domes is limited in its application.

After expressing, in general terms, the stresses in any secondary rib due to the reaction components and applied load, its influence upon the main ribs is determined. Two ribs, lying in the plane of symmetry of the loading and stiffly connected to the rigid top ring, form a two-hinged arch rib O-n. This main arch is under the action of its own external load applied in its plane and under the action of loads contributed by all secondary ribs connected with the main ribs by the stiff ring. Owing to symmetry, these loads can be resolved into three groups:

(1) the vertical load;

(2) the horizontal load applied at the vertex point;

(3) the bending moments at the vertex due to the interconnection of the considered arch with the secondary ribs.

All these loads act in the plane of the main arch rib. Using the

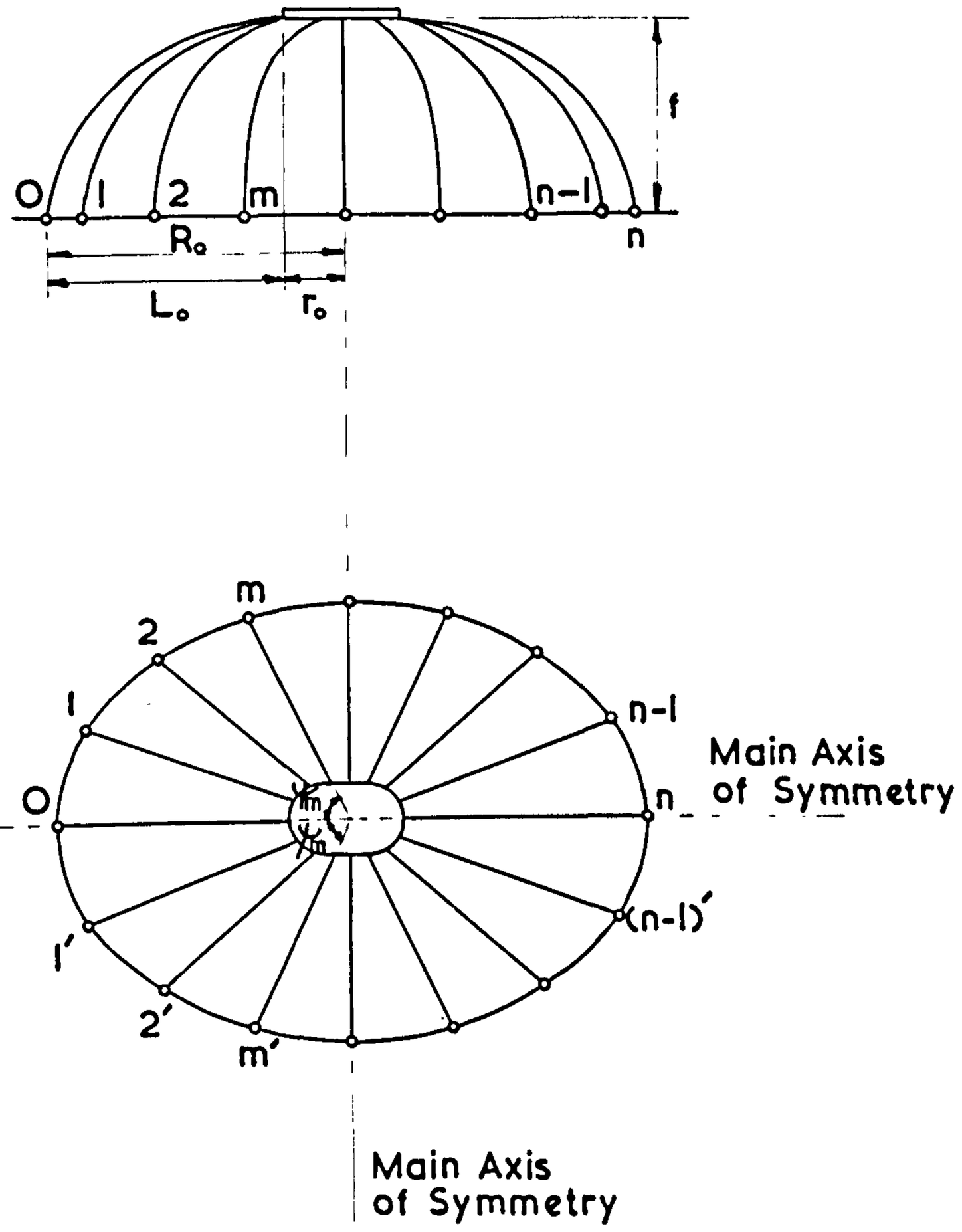

FIG. 47 TWO HINGED UNSTIFFENED RADIAL RIBBED DOME WITH APEX RING

F.A.A. Ph.D. Thesis
17th Jan., 1970

Structural Engineering Division
Department of Civil Engineering
University of Newcastle upon Tyne

Theorem of Castigliano, the analysis of this arch can now be carried out by the Method of Strain Energy as the translational displacements of all supports are equal to zero.

8.7 TWO-HINGED STIFFENED RADIAL RIBBED DOMES

In a "stiffened" radial ribbed dome the meridional members are connected, at their bases, to an elastic ring. The analysis of this type of structure can be carried out according to a method developed by Pohl.[10] For his solution, Pohl considered a dome of n identical two-hinged arch ribs supported by a regular polygonal ring. The lay-out of a dome of this type is shown in Figure 48(a).

Pohl assumed that the ribs do not resist lateral bending or torsion, being designed as thin and deep cross-sections. All ribs are assumed to be connected at the crown by means of a specially constructed vertical pin, which resists all horizontal loads and distributes bending moments in the vertical rib plane from any one rib to all others, but does not transmit any lateral moment or torque. The external loads are further assumed to act upon the ribs in their planes. Structures of the type being considered have a degree of redundancy equal to 4n-5.

Where the bearings are pin-connected to an elastic base ring, they are constructed so as to allow movement of the supports in a determined direction. An arrangement such as this produces, in the general case, a tangential reaction force perpendicular to the direction of the movement.

The reaction forces acting at the base ring supports are as follows:

Va, Vb, Vc ..... = the vertical reaction components;

Ha, Hb, Hc ..... = the horizontal reaction components;

Wa, Wb, Wc ..... = the reaction forces caused by the restriction of the direction of movement of the support joints;

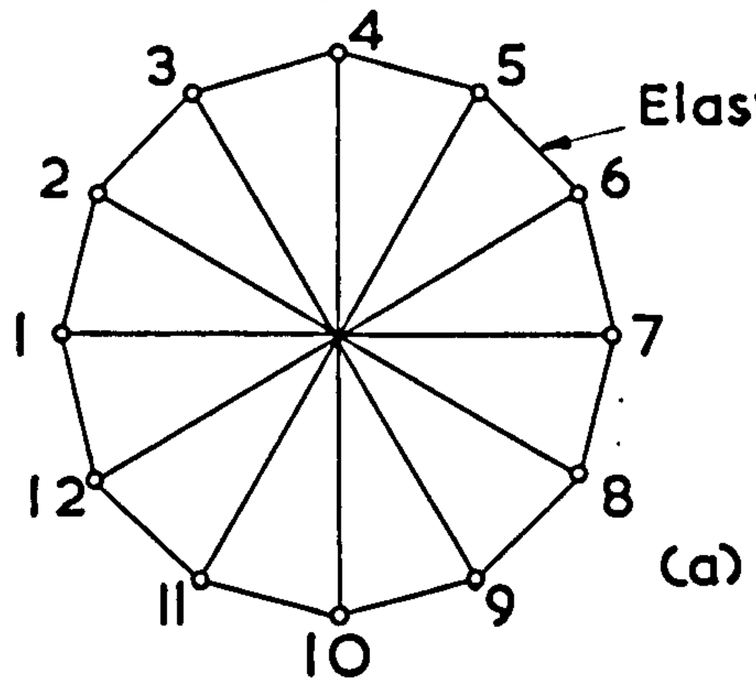

(a)

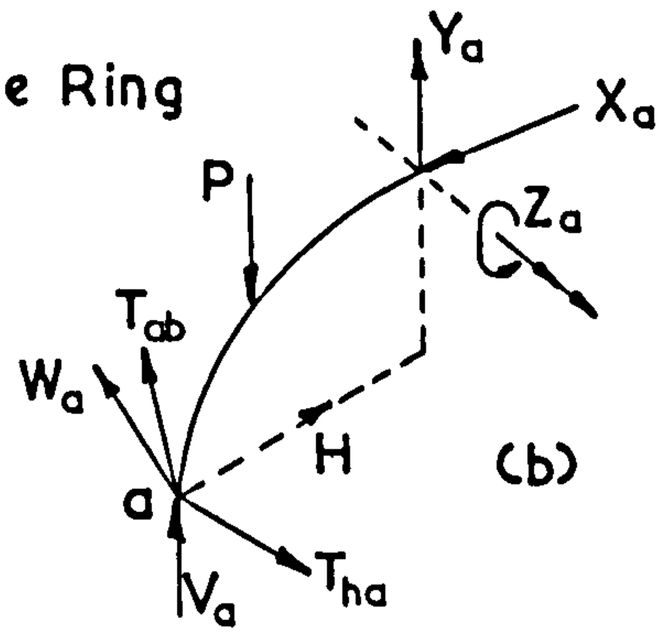

(b)

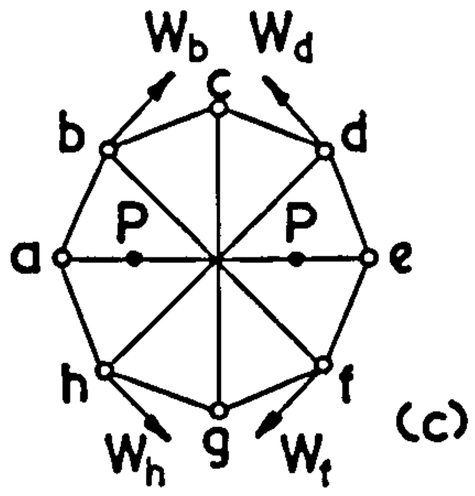

(c)

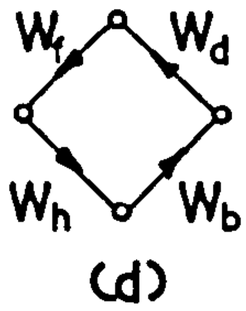

(d)

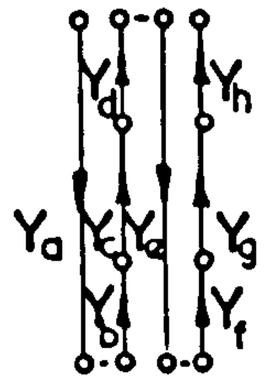

(e)

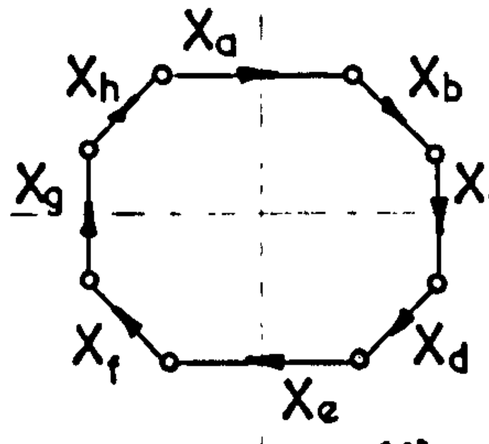

(f)

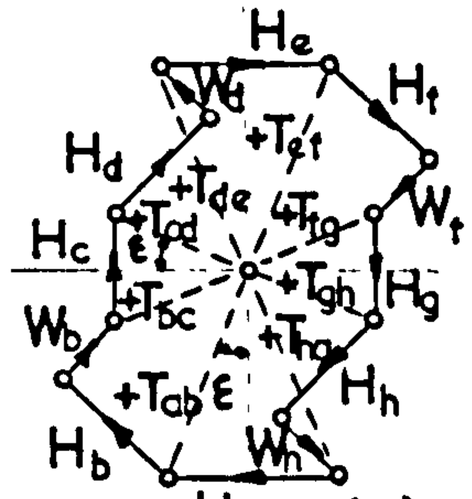

(g)

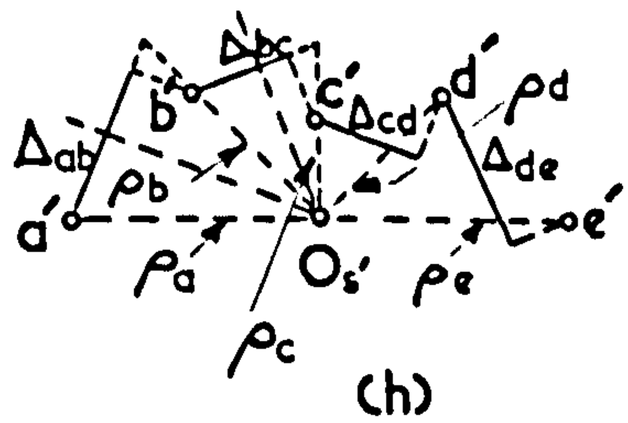

(h)

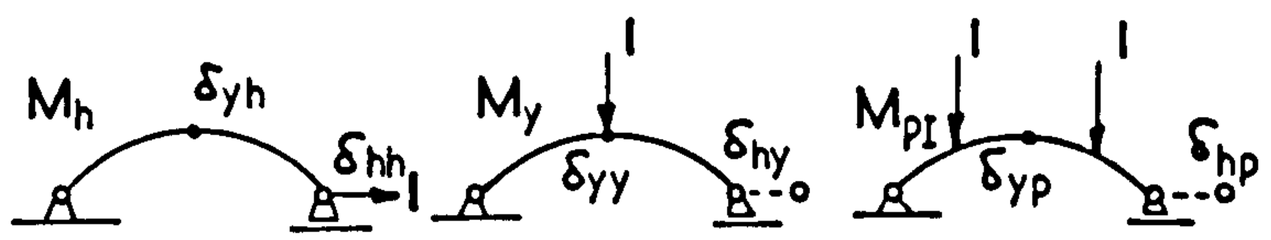

(i)

FIG. 48 TWO-HINGED STIFFENED RADIAL RIBBED DOMES Sheet No. 1

F.A.A. Ph.D. Thesis
17th Jan., 1970

Structural Engineering Division
Department of Civil Engineering
University of Newcastle upon Tyne

Tab, Tbc, Tcd ..... = the forces in the base ring bars.

Forces acting upon the ribs consist of the external loads, the support forces and the reactions X, Y and Z applied at the vertex due to the connection of the considered rib with all other arches, Figure 48(b). The vertex reactions are as follows:

Ya, Yb, Yc ..... = the shearing forces;

Xa, Xb, Xc ..... = the horizontal forces;

Za, Zb, Zc ..... = the bending moments in the rib planes.

The analysis is based on the conditions of equilibrium and on the fact that the translation and rotation components of the vertex joints are equal for all ribs due to their interconnection at this joint. In addition the displacements of all supporting points have to be compatible with the elongations of the elastic base ring. The analysis is limited to vertical forces applied at any point on the rib. Owing to the symmetry of the structure, the applied load is transformed into symmetrical and skew-symmetrical loads and each case is dealt with separately.

(a) Symmetrical Loading

Considering the structure shown in Figure 48(c), the following equations of equilibrium are obtained:

(1) the equilibrium of the external forces

$$Va = Ve \; ; \; Vb = Vd = Vf = Vh \; ; \; Vc = Vg \; ; \; \Sigma V = 2F ; \; Wa = We = Wc = Wg = 0 \; ; \; \Sigma Wbdfh = 0 \qquad \ldots\ldots (8.38)$$

(2) the equilibrium of the forces at the vertex

$$Yb = Yd = Yf = Yh \; ; \; Ya = Ye \; ; \; Yc = Yg \; ; \; \Sigma Y = 0 \qquad \ldots\ldots (8.39)$$

therefore

$$Yc = Ya - 2Yb \; ; \; Yae = 2Ya \; ; \qquad \text{Figures 48(e) and (f)}$$

$$Ybf = 2Yb \; ; \; Ycg = 2Ya - 4Yb \qquad \ldots\ldots (8.40)$$

(3) the equilibrium of the forces at the base ring

$$Ha = 2Tab \sin \varepsilon \; ; \; Hc = 2Tbc \sin \varepsilon \; ;$$

$$Tab - Tbc = \frac{Wb}{\cos \varepsilon} \quad ; \quad Hb + Wb\tan \varepsilon = 2Tab \sin \varepsilon \quad ; \text{ Figure 48(g)}$$

$$Hb = (Tab + Tbc) \sin \varepsilon \; ; \quad Wb = (Tab - Tbc) \cos \varepsilon \quad .....(8.41)$$

The bearings in the case considered are assumed to have freedom of radial displacement. These displacements can be expressed by the angles ε, formed by the adjacent ring bars, and their elastic elongations $\Delta = \frac{TL}{AE}$. The displacements are as follows:

$$\rho_b = \rho_a - \frac{Z_1}{\sin \varepsilon} \; ; \quad Z_1 = 2\rho_a \sin \varepsilon - \Delta_{ab};$$

$$\therefore \quad \rho_b = \frac{\Delta ab}{\sin \varepsilon} - \rho_a \quad ..... \; (8.42) \text{ (Figure 48h)}$$

$$\rho_c = \rho_b - \frac{Z_2}{\sin \varepsilon} \; ; \quad Z_2 = 2\rho_b \sin \varepsilon - \Delta_{bc} \; ;$$

$$\therefore \quad \rho_c = \frac{\Delta bc}{\sin \varepsilon} - \rho_b = \frac{\Delta bc - \Delta ab}{\sin \varepsilon} + \rho a \; ...(8.43) \text{(Figure 48h)}$$

These radial displacements constitute the spread of the arches. Their relationship with the external rib loads and horizontal thrusts is studied separately.

An arch rib of the same properties and dimensions, but simply supported is subjected to three different loading systems as shown in Figure 48 (i). In each case the horizontal spread of the movable bearing and the vertical drop of the arch crown is found from the bending moments M_h, M_y and M_{PI} as follows:

$$\delta_{hh} = \int_o^L M_h^2 \frac{ds}{EI} \; ; \quad \delta_{yy} = \int_o^L M^2 y \frac{ds}{EI} \; ; \quad \delta_{yh} = \delta_{hy} = \int_o^L M_h M_y \frac{ds}{EI} \; ;$$

$$\delta_{hp} = \int_o^L M_h M_{PI} \frac{ds}{EI} \quad ; \quad \delta_{yp} = \int_o^L M_y M_{PI} \frac{ds}{EI} \qquad ..... \; (8.44)$$

The influence of normal forces upon the deflections is neglected, except in the case of very flat arches.

The principle of superposition now gives the resultant crown deflections, D_{vs}, and the span increase of length ΔL. For the loaded arch a-e illustrated in Figure 49(a) these values are:

$$D_{vs} = P \delta_{yp} - Y_{ae} \delta_{yy} - H_a \delta_{yh} \qquad ..... \; (8.45)$$

$$\Delta L = 2\rho a = P\,\delta_{hp} - Y_{ae}\,\delta_{hy} - H_a\,\delta_{hh} \qquad \ldots\ldots (8.46)$$

Since the vertical deflection of the crown point is equal for all arches, a sufficient number of equations can be found relating P, Y and T to the calculated deflections for each arch. From these, the values of the support reactions can be found. If these relationships are expressed in general terms, some useful deductions can be made regarding the influence of the extensional rigidity of the base ring upon the stress distribution in the dome and its deflections. Assuming an inextensible, rigid base ring and modifying correspondingly the general expressions, the results obtained can be applied to the analysis of a two-hinged radial ribbed dome without a ring.

(b) Skew-symmetrical Loading. (Figures 49(b), (c), (d), (e), (f) and (g)).

In this case the general equilibrium equations supply the following relationships:

$$\begin{aligned}
&Vc = -Va \;;\; Vd = -Vb \;;\; Vc = 0 \;;\; \textstyle\sum V = 0 \;;\\
&Wc = Wb \times \sqrt{2} \;;\\
&Ye = -Ya \;;\; Yd = -Yb \;;\; Yc = 0 \;;\\
&Xc = -Xa \;;\; Xd = -Xb \;;\; Xc = 0 \;;\\
&Xb = -Xd + Xf = Hh = Xa\,\tfrac{1}{2}\sqrt{2} \;;\\
&Xbf = \textstyle\sum Xadeh = 2Xa\tfrac{1}{2}\sqrt{2} \text{ in the direction bf;}\\
&Xae = \textstyle\sum Xbdfh = 2Xa \text{ in the direction ae;}
\end{aligned} \qquad \ldots\ldots (8.47)$$

$$Zae = 2Za \;;\; Zbf = Za\sqrt{2} \;;$$

$$Tab = \frac{Ha}{2\sin\varepsilon} \;;\; Tbc = Tab\cot\varepsilon = \frac{Ha\cot\varepsilon}{2\sin\varepsilon} \;;$$

$$Hb = \frac{Ha}{2}\sqrt{2} \;;\; Wc = 2Tbc\cos\varepsilon = Ha\cot^2\varepsilon \;;$$

$$Wb = \tfrac{1}{2}\,Wc\sqrt{2} = \frac{Ha}{2}\cot^2\varepsilon\sqrt{2}$$

The displacements of the base ring joints can be expressed by the following equations:

$$\rho a = \frac{Ha}{2}K\,(1 + \cot\varepsilon) = \frac{Ha}{2}K\,(2 + \sqrt{2}) \qquad \ldots\ldots (8.48)$$

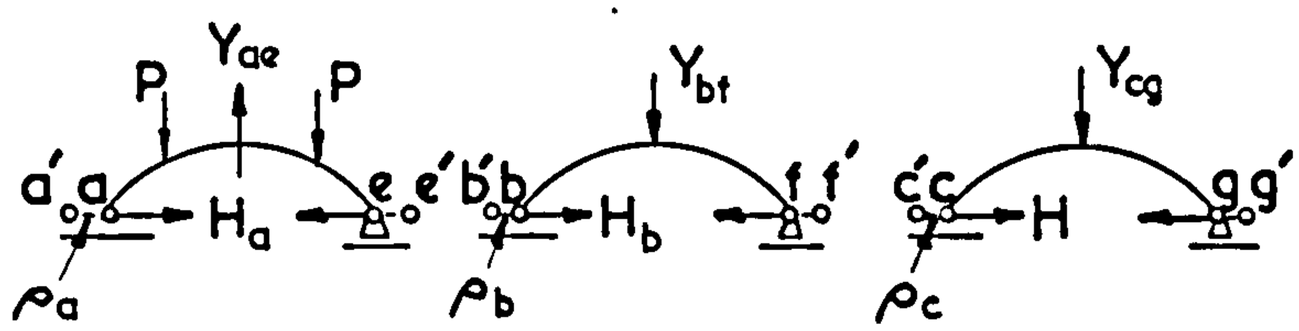

(a)

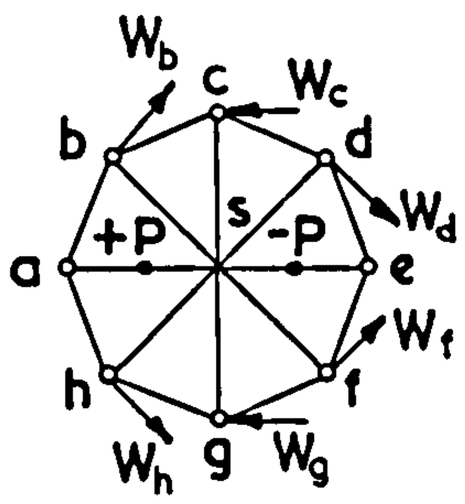

(b)

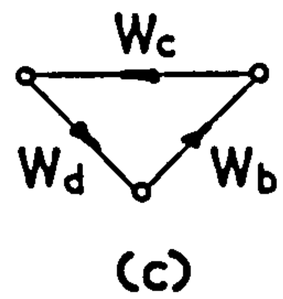

(c)

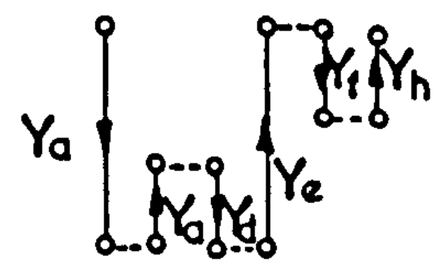

(d)

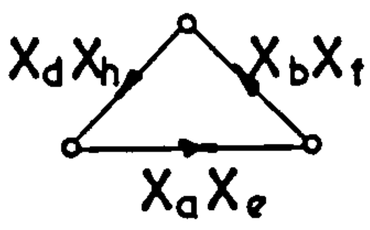

(e)

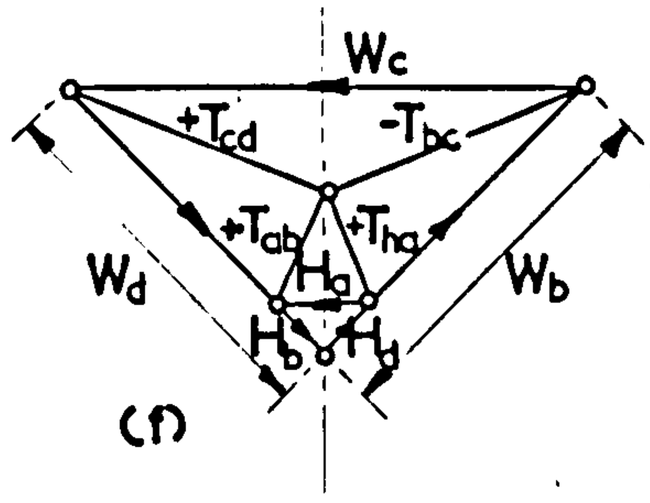

(f)

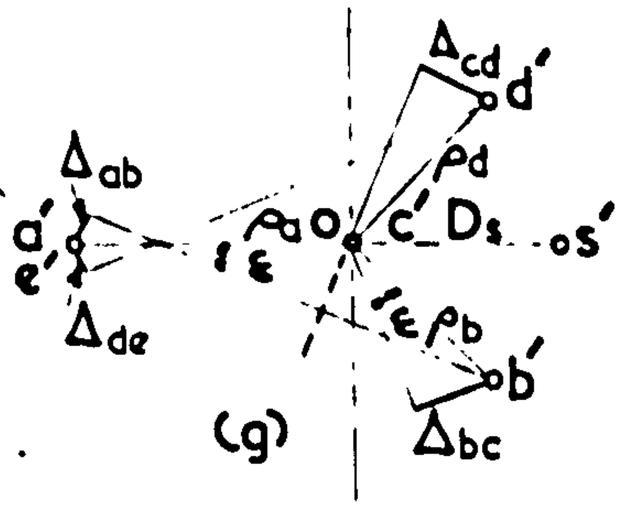

(g)

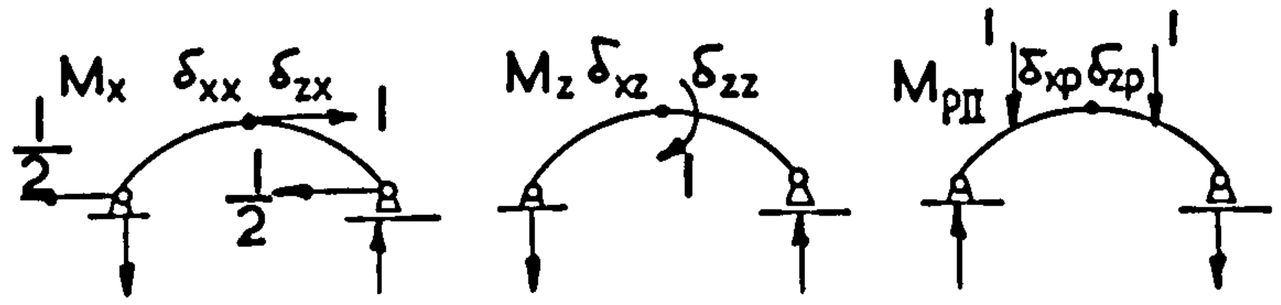

(h)

FIG. 49 TWO-HINGED STIFFENED RADIAL RIBBED DOMES Sheet No. 2

F.A.A. Ph.D. Thesis
17th Jan., 1970

Structural Engineering Division
Department of Civil Engineering
University of Newcastle upon Tyne

$$\rho b = \frac{Ha}{2} K \cot \varepsilon = \frac{Ha}{2} K (1 + \sqrt{2}) = \rho a \tfrac{1}{2} \sqrt{2} \quad \ldots(8.49)$$

as $\cot \varepsilon = 1 + \sqrt{2}$ in the case under consideration. In expressions (8.48) and (8.49), $K = \frac{L}{AE \sin \varepsilon}$.

Before the horizontal displacements and the rotation of the vertex point are found, the following unit loading cases have to be analysed and their effects upon the statically determinate arched beam found.

In each case, the bending moments Mx, Mz and M_{PII} have to be calculated and the deformations of the crown point found as shown in Figure 49(h). These deformations are found from the following expressions:

$EI\,\delta_{xx} = \int M_x^2 ds'$ = the horizontal displacement;

$EI\,\delta_{zz} = \int M_z^2 ds'$ = the rotation of the crown cross-section due to a unit bending moment;

$EI\,\delta_{xz} = \int M_x M_z ds'$ = the rotation of the crown cross-section due to a unit horizontal force X = 1, or the horizontal displacement due to a unit bending moment;

$EI\,\delta_{xp} = \int M_x M_{PII} ds'$ = the horizontal displacement under the skew-symmetrical unit loads;

$EI\,\delta_{zp} = \int M_z M_{PII} ds'$ = the rotation due to skew symmetrical unit loads. ..... (8.50)

Using the principle of superposition the general equations can be formed for each rib, expressing the horizontal displacement D_{HS}, and the rotation, R_s, of the crown point as a function of X and Z. For the loaded rib a-e in Figure 49(b), these values are given by:

$$D_s = P \delta_{zp} - X_{ae} \delta_{xz} + Z_{ae} \delta_{zz} \quad \ldots\ldots (8.51)$$

$$R_s = X_{ae} \delta_{xz} - Z_{ae} \delta_{zz} \quad \ldots\ldots (8.52)$$

Due to the interconnection of all ribs at the crown, all ribs are subjected to the same sinking and rotation of the crown point.

Corresponding equations can be found for all ribs and from the general equations of equilibrium of the structure and all joints of the base ring, unknowns can be gradually eliminated and the reaction components can be determined.

The assumption employed in the above analysis that the ribs do not resist lateral bending and torsional moments considerably simplifies the solution. With some modifications, as mentioned previously, the method can also be applied to radial ribbed domes without a base ring. However, the results obtained under such an assumption, when compared with corresponding values for a dome stiffened by a base ring, indicate that a considerable influence is exerted on the stress distribution in dome members by the displacements of the support points.

CHAPTER IX

LOADS ON DOMES

9.1 DEAD LOAD

Loading on domes consists of four types:

(1) dead load;

(2) live load;

(3) snow load;

(4) wind load.

The dead load of a dome is composed of the weight of the framing system and the weight of the dome itself. It is normally relatively easy to compute the weight of the framing system but it is more difficult to calculate the overall dead load. The latter value depends on several factors such as the type of dome adopted, the method of analysis employed, the dimensions of the dome and the type of roof framing. However, Benjamin[12] suggests that a rough value of 5 - 12lb per square foot of floor area can be assumed.

9.2 LIVE LOAD

Live loading consists of any additional weight which the dome may be subjected to throughout its use other than dead, snow and wind loads. British Standard Code of Practice CP3 : Chapter V : 1965[29] on loading recommends that for a roof-slope of 30° or less an imposed load of 15 lbf/ft^2, measured on plan, should be allowed since no access would normally be provided to the dome roof other than that necessary for cleaning and repair. For a roof-slope of 75° or more, no allowance is necessary. The imposed load to be allowed for roof-slopes between 30° and 75° can be obtained by linear interpolation between 15 lbf/ft^2 for a 30° roof-slope and nil for a 75° roof-slope. To provide for loads

incidental to maintenance, all roof coverings, other than glass, at a slope of less than 45° should be capable of carrying a load of 200 lbf concentrated on any area 5 in. square at normal stresses. The combined effect, as well as the separate effects, of imposed loads and wind pressure on roofs must also be accounted for. Wind pressure on dome roofs is discussed later in this chapter.

The American Standards Association[29] recommends, as a minimum, a design vertical live load of 20lbf/ft^2 of horizontal projection in addition to dead load and any special loads for all flat, pitched or curved roofs. This minimum roof live load should be applied as either full balanced or full unbalanced, whichever produces the greater stresses. A 25 per cent increase in allowable unit stresses is permissible since this minimum 20lbf/ft^2 load is for a seven-day duration of load.

9.3 SNOW LOAD

The shape of a roof controls the magnitude of forces and combinations of forces that come upon it. Many roof arrangements present special problems in designing for snow load; that is, some permit greater than usual slide-off of snow, whereas others tend to encourage snow accumulation at certain points. Unfortunately, there is very little known about snow load distribution on dome roof structures.

The imposed load value of 15lbf/ft^2, measured on plan, recommended for flat roofs in CP3 : Chapter V : 1965[29] includes an allowance for snow load. It is very unlikely that this loading will be exceeded in the British Isles. However, the distribution of this load over the dome surface is a matter for conjecture. According to the author's correspondence with N. Isyumov,[30] Research Engineer at the University of Western Ontario, Canadian building practices recommend that dome structures should be designed for an unbalanced snow load. The magnitude of the unbalanced load should be in the order of 1½ times

the basic design loads on the leeward portion of the roof and zero on the windward. Model investigations on curved roofs suggest that the degree of unbalance may be more severe for certain conditions of snow fall and wind. The more conservative value to choose would probably be twice the basic snow load on the leeward side. Snow loading on dome roofs is somewhat different in view of the more pronounced side effects.

In American practice, snow loads are as stipulated by the governing building code. Where no governing building code prevails, snow loading used in design is based on local investigation. The U.S. Weather Bureau possesses records which show the greatest snow pack on the ground encountered during the period 1871 - 1944.[28] If the snow load is larger than the 20lbf/ft^2 minimum roof live load, it is substituted for that minimum live load. Where the snow load is less than the minimum roof live load, snow load is not considered. Areas which require local investigations have snow load allowances of at least 45lbf/ft^2.

The snow loads experienced in America and Canada are far larger than those found in the British Isles. Different snow load duration times are also experienced. Snow load duration is the cumulative time during which the maximum design load is on the structure over its entire life. The American Standards Association mimumum roof live load allowance of 20lbf/ft^2 of horizontal projection is based on a 7-day duration of load. A 25 per cent increase in allowable unit stresses is then permissible. British Standard Code of Practice CP 112 : 1967, on the structural use of timber in buildings, also allows a 25 per cent increase in allowable unit stresses when designing timber members to carry the minimum imposed load of 15lbf/ft^2, measured on plan, as stipulated in CP3 : Chapter V : 1965. This imposed load includes an allowance for snow which, in the British Isles, has a short duration period.

However, in America, a 2 month duration is generally recognised as the proper design level for snow loads. Although some snow remains on roofs for periods exceeding 2 months in a single year, such snow loads seldom approach the design load, and the accumulation of periods of the full design load does not approach the 2 month duration for periods well in excess of 100 years. According to the American Standards Association, an increase of only 15 per cent is allowable on design stresses when employing a 2 month snow load duration.

Snow loads are based on the horizontal projection of roof areas. The snow loads for roofs having a rise of more than 1 in 4, and so designed as to have lesser snow retention values, may be progressively reduced in accordance with American Standards Association recommendations.(28)

Many dome structures have been built throughout the world but literature relating to the design loads employed is scarce. However, several papers are available. In the design of the Dome of Discovery(32) for the 1951 Festival of Britain, the maximum intensity of snow load was assumed to be 10lb per square foot. The distribution over the dome surface was a matter of doubt. Unevenness over the surface was an important possibility since unsymmetrical loads could have produced higher stresses in the dome structure than if the same intensity of load had been uniformly distributed. For the purposes of designing the Dome of Discovery, a snow load varying in intensity across a diameter of the dome was employed as illustrated in Figure 50(a). This distribution allowed for a drift of snow towards one side of the dome and discounted the likelihood of its lying on the steeper slope near the edge.

In the design of three Canadian reticulated steel domes,(33) various systems of snow loading were employed. The domes, all 225 ft in diameter, are the Agrodome in Vancouver and the two Altadomes in

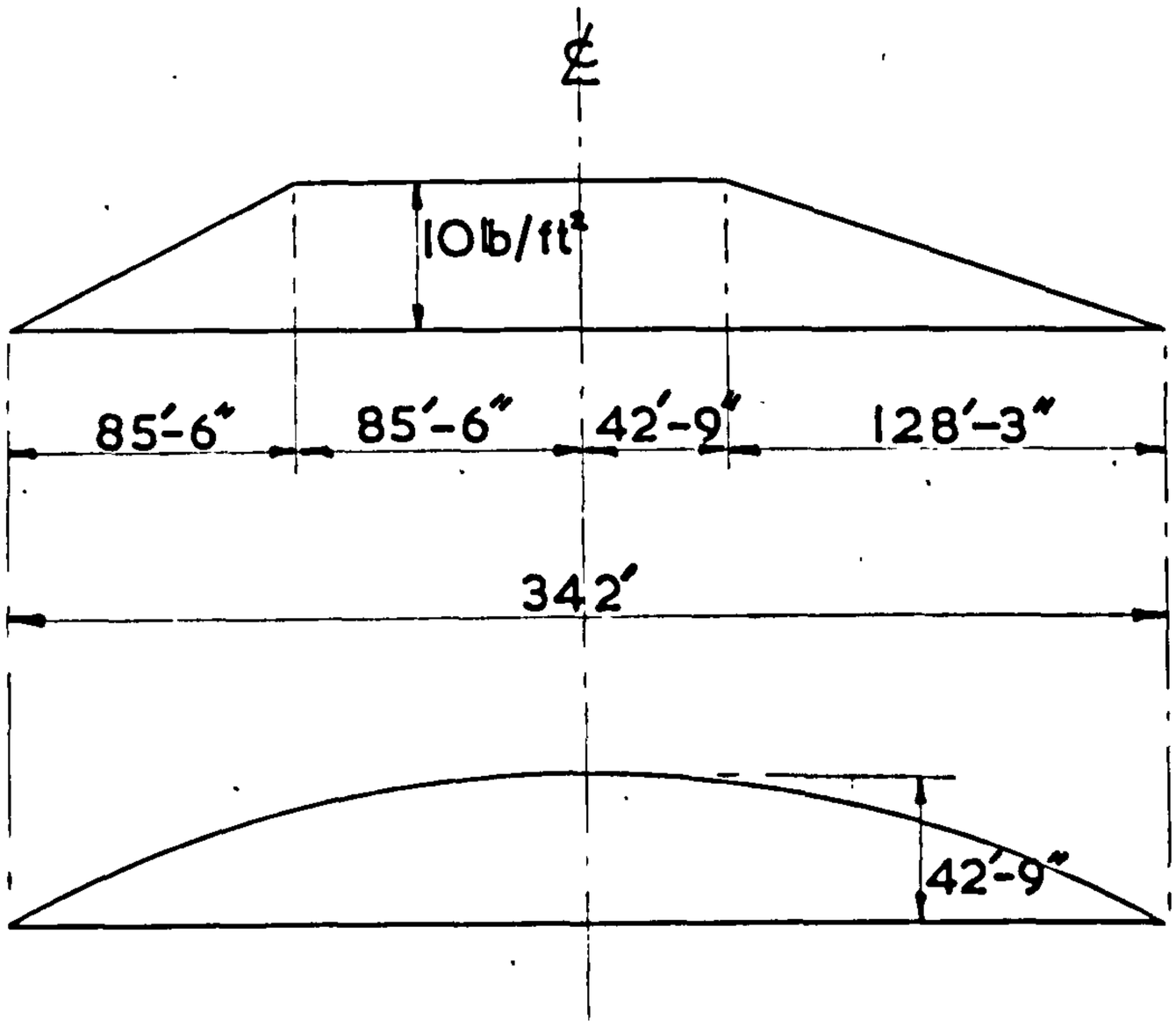

(a)

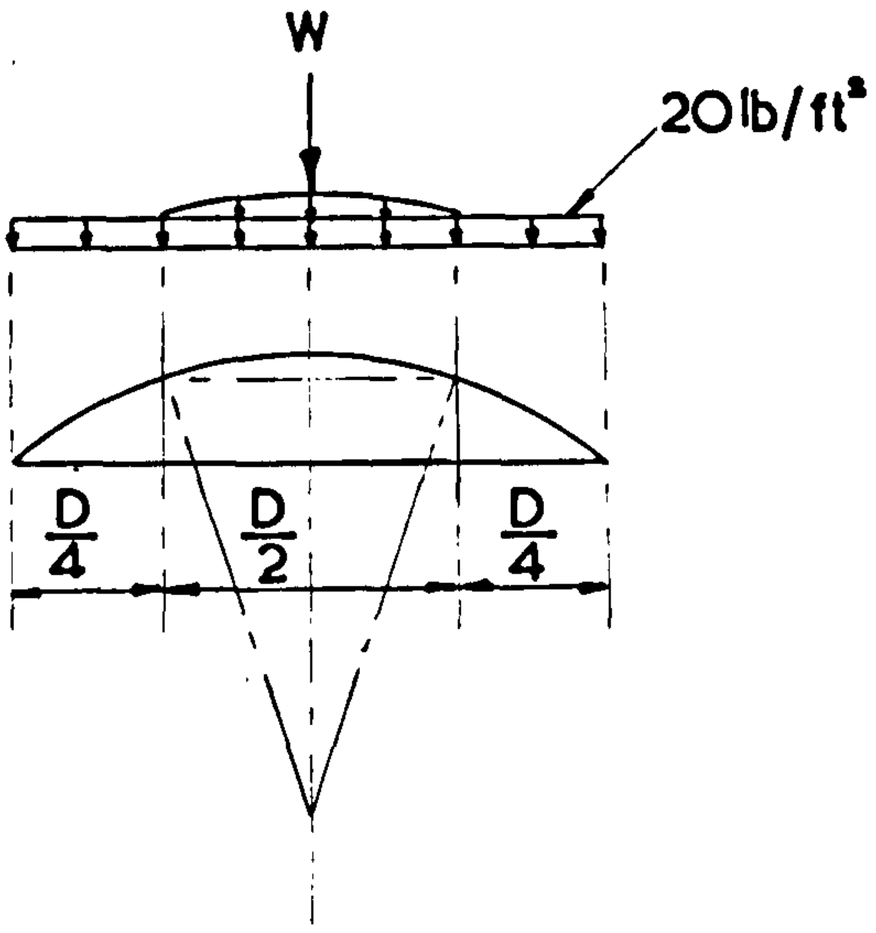

(b)

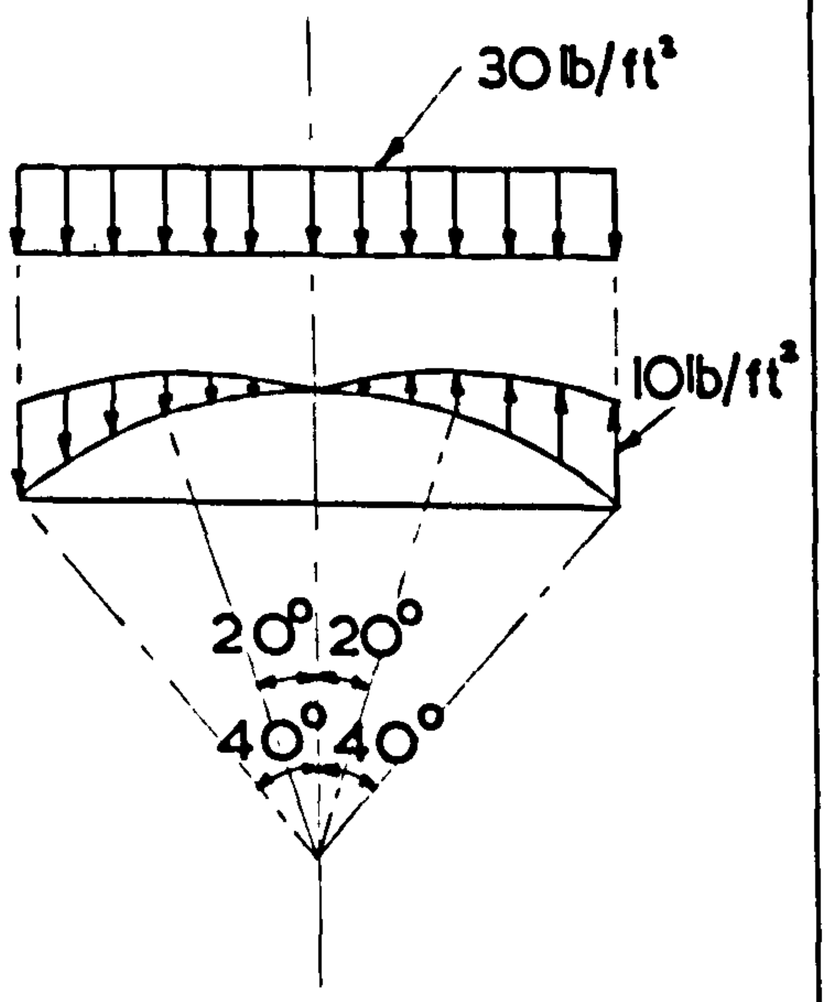

(c)

FIG. 50 SNOW LOADING ON DOMES

F.A.A. Ph.D. Thesis
28th Jan., 1970

Structural Engineering Division
Department of Civil Engineering
University of Newcastle upon Tyne

Fort Saskatchewan. A snow load of 40lbf/ft^2 was assumed for the Agrodome which is in an area of heavy precipitation. The Altadomes are in the interior with a drier climate where the snow load is 22 lbf/ft^2. Additional requirements for the Agrodome were an uneven snow load as follows:

(1) full snow load over top half and half snow load over bottom half of the dome;

(2) full and half snow load over opposite halves of the dome.

All three domes were designed for a uniform snow load and the additional requirements, just mentioned, were also considered in the design of the Agrodome. Case (1) above, for the Agrodome, is illustrated in Figure 50(b). Figure 50(c) shows Case (2) for which subsititute wind load, pressure and suction was employed.

9.4 WIND LOAD

(a) Basic Considerations

According to Scruton and Newberry,[34] interest in the study of the wind loading of structures has been stimulated by two major trends in recent years. Advances in structural theory are leading to refinement in design which can be effectively achieved only if there is adequate knowledge of the applied loads; at the same time there has been a considerable increase in the number of buildings where wind loads become important factors in the schedule of loadings. Two factors contribute especially to this latter circumstance:

(1) the remarkable growth of tall buildings;

(2) the increasing use of lightweight materials and claddings which may be specially susceptible to the influence of short duration local gusts.

It is the latter factor which is normally the most important when considering the design of domes.

The increased attention which is necessarily being given to wind

loading as a result of these conditions has emphasised the need for both a clarification and development of the techniques for deriving wind loads for use in design calculations. There are two basic issues to be considered in any assessment of the wind loading problem. These are:

(1) the maximum wind speed to which the structure is liable to be subjected in the course of its lifetime;

(2) the forces which are to be assumed to act on the structure for a given intensity of wind.

Although information is available about the factors which must be considered in arriving at a suitable value for the maximum wind speed appropriate to any part of a structure and data can be obtained to permit the calculations of wind loads on a wide variety of structural shapes, the values can never be complete enough to cover every possible structure. Further wind-tunnel tests are therefore necessary in some cases to determine the pressures or loads on structures in unusual surroundings.

The various national codes of practice adopt widely differing treatments for the determination of wind loads. In the American Standard Building Code,[23] the country is divided into zones for each of which a design pressure is tabulated, the values being stepped up for increasing height above the ground. The design pressures are based on the velocity of the fastest measured mile of wind multiplied by a factor of 1.3 to allow for gusts. Another factor equivalent to a shape or pressure coefficient, has then to be applied to allow for the combined effect of interior and exterior pressures on individual structures. According to this code, inward loads on roofs need only be considered if the roof slope is greater than 30° and then the design pressure is assumed to act on the windward slope only.

In the Swiss Code of Practice,[34] the dynamic pressure of the wind is defined for each of a number of height zones above the ground. The dynamic pressure of the wind, q, is a measure of the kinetic energy per unit volume of the air and is given by:

$$q = \tfrac{1}{2}\rho V^2 \quad \ldots\ldots (9.1)$$

where ρ is the density of the air and V is the wind speed. At sea level, the standard atmosphere gives $q = 0.00256\ V^2$ lbf/ft^2, where V is expressed in miles per hour. The Swiss Code of Practice sets out, in tabular form, the shape or pressure coefficient by which the dynamic pressure has to be multiplied to obtain the actual loading on the various surfaces comprising the structure in question. These coefficients have been derived from wind-tunnel tests for a considerable variety of shapes of building and for a range of wind directions. The Swiss method produces a more complete picture than the American system and is especially suited to the design of structures where wind loads are critical.

British Standard Code of Practice CP3 : Chapter V : 1965[29] gives values for the basic equivalent wind pressure plbf/ft^2, which is the equivalent static pressure in the windward direction, depending upon the height of the building above the general ground level and the degree of exposure to wind. Four exposure gradings are employed and the degree of exposure is governed by the wind velocity. Local Authorities usually decide the degree of exposure appropriate to the area within their jurisdiction, having regard to local meteorological records. The basic pressures are modified by various coefficients, either negative or positive which denote suction and pressure respectively, depending upon which part of the structure is being designed. Shape coefficients are also employed for buildings having different plan areas to a rectangle.

(b) Factors Influencing the Choice of a Design Wind Speed

Climatic conditions can vary considerably from one location to the next and, therefore, the estimation of the maximum winds which a structure will have to withstand during its lifetime will always be subject to a considerable degree of uncertainty. Despite the considerable quantity of meteorological data which has accumulated and the statistical studies of these data which have been made, a large specular element still remains. The following are the factors which need to be considered when choosing a design wind speed:

(1) Anticipated lifetime of the structure;

(2) Duration of gusts;

(3) Dimensions of gusts;

(4) Variation of gust speed with height;

(5) Gust spectrum;

(6) Local topography.

Maximum wind speeds recorded at a site tend to increase with the period of time over which wind records are taken. Hence a structure which has a long anticipated lifetime should be designed for a higher wind speed than one with a shorter life period.

The period of the gust required for the aerodynamic forces to develop and for the structure to react and become overstressed is an important factor about which little appears to be known. Only when the wake has become fully established does the aerodynamic force attain the final value reached in a steady wind. It is possible that the initial wind load will, for a very short period, considerably exceed the final load.

The dimensions of the volumes of air involved in a gust are significant. They vary widely both in the horizontal and vertical directions. The wind load may not develop simultaneously over the whole of a tall or wide structure and, because of this, it may be

permissible to assume a longer gust period than is given by considerations of the reactions of the structure to an impulsive force and it may be desirable to specify gust periods for structures of large dimensions longer than those for structures of small dimensions.

For tall structures, the increase of wind speed with height is very important. The reliability of the estimation of wind-loading depends to a large extent on a valid assessment of this wind-velocity profile.

Gusts occur in a random sequence of frequency and intensity. In certain circumstances it is possible that the dynamic response of a flexible structure to a gust sequence might be greater than that determined by the usual assumption of a steady wind load, even when the design wind speed is based on a maximum gust speed.

The local topography, in addition to its influence on the velocity profile, sometimes produces unusual wind conditions. Funnelling effects are obtained in valleys resulting in increased wind speeds and local accelerations of wind occur around and between bluff obstacles.

(c) Recommended Procedures for Determining the Design Wind Speed

The problem of determining design wind speeds has been considered by many investigators and various procedures have been outlined. Scruton and Newberry[34] have reviewed some of these procedures which involve allowances for the variation of speed with height and factors for determining mean hourly wind speeds and short duration gust speeds.

According to Scruton and Newberry, two procedures are to be recommended for determining the design wind speed at any height and locality in the British Isles. One is based on a surface wind at a height of 33ft and the other on the gradient wind as determined by the research of Davenport[35] and Nutt[34]. The advantage to be gained by employing the gradient wind is that its properties change only slightly from place to place and do not depend upon the type of terrain.

Wind is induced by the largo-scale pressure gradients which arise over the earth's surface. The wind moving freely under the influence of these pressure gradients and unaffected by the frictional stresses near the ground surface is known as the gradient wind and its velocity is termed the gradient velocity $\bar{V}g$. This velocity is first attained at the gradient height zg which is generally between 1,000 and 2,000 ft. Nearer the ground, however, the wind is retarded by the surface friction and some of its kinetic energy is dissipated in turbulence.

The wind gradient is expressed by the following power law using the gradient height for reference:

$$\frac{\bar{V}z}{\bar{V}g} = \left(\frac{z}{zg}\right)^{\frac{1}{\alpha}} \qquad \ldots\ldots (9.2)$$

where $\bar{V}z$ is the wind speed at a height of z ft. Davenport[35] gives values of zg and $\frac{1}{\alpha}$ for various terrain roughnesses as follows:

Category (1) $\frac{1}{\alpha} = \frac{1}{7.5}$, zg = 900ft, extreme exposure with large expanses of open water and grassland;

Category (2) $\frac{1}{\alpha} = \frac{1}{5.5}$, zg = 1100ft, open country with low obstructions such as trees, hedges and two-storey buildings;

Category (3) $\frac{1}{\alpha} = \frac{1}{4}$, zg = 1500ft, built-up areas and areas with high obstructions such as towns and cities.

Contours of maximum gradient winds have also been deduced, by Davenport, for the British Isles from which values of $\frac{1}{\alpha}$ and u, the mode of the data, can be read off according to the location considered.

By extreme value theory the maximum hourly-mean gradient speed is given by:

$$\bar{V}g = u - \frac{1}{\alpha}\left\{\log_e\left[-\log_e\left(1 - \frac{1}{r}\right)\right]\right\} \qquad \ldots\ldots (9.3)$$

where r is the required return period in years. For large values of r:

$$\bar{V}g = u + \frac{1}{\alpha}\log_e r \qquad \ldots\ldots (9.3a)$$

Davenport did propose gust factors to be applied but his work has

been modified by Nutt[34]. The effect of topography as well as the gust period on the gust factor was studied by Nutt. Different values of the gust factor exponent were obtained for the various terrain categories. The gust factor decreases with height and its variation is expressed by:

$$\frac{Fz}{Fg} = \left(\frac{z}{zg}\right)^{-\frac{1}{\beta}} \qquad \ldots\ldots (9{\cdot}4)$$

Nutt's recommended values for gust factor exponent $\frac{1}{\beta}$, for the three previously mentioned categories of terrain, are as follows:

Cateogry (1) $\frac{1}{\beta} = \frac{1}{16}$;

Category (2) $\frac{1}{\beta} = \frac{1}{11}$;

Category (3) $\frac{1}{\beta} = \frac{1}{8}$

Combining equations (9.2) and (9.4) the design wind speed Uz is given by:

$$Uz = Fg\ \bar{V}g\left(\frac{z}{zg}\right)\frac{1}{\gamma} \qquad \ldots\ldots (9{\cdot}5)$$

where $\frac{1}{\gamma} = \frac{1}{\alpha} - \frac{1}{\beta}$. The values of $\frac{1}{\gamma}$ for the different terrains are given by Scruton and Newberry as:

Category (1) $\frac{1}{\gamma} = \frac{1}{14}$

Category (2) $\frac{1}{\gamma} = \frac{1}{11}$

Category (3) $\frac{1}{\gamma} = \frac{1}{8}$

To determine, therefore, the design wind speed for a particular locality using gradient winds, the first step in the procedure is to estimate values of $\frac{1}{\alpha}$ and u from Davenport's contour map of the British Isles. The gradient speed $\bar{V}g$ is then calculated from equation (9.3). After classification of the type of terrain into one of the three categories previously mentioned, the gradient height and the exponent $\frac{1}{\gamma}$ are then known. The design speed is given by substituting these values in equation (9.5). A value of Fg is chosen according to the gust period. For extreme gusts, Fg = 1.25 and for 10-15 second gusts, Fg = unity. If the contour detail in Davenport's map is considered to be too coarse for the purpose and the area under consideration

contains a number of meteorological stations, analysis of the data from these stations may be made to obtain the gradient wind.

To determine the design wind speed using surface winds at the standard height of 33ft (10m), the highest probable mean hourly wind speed at this height, $\bar{V}_{33}$, can be computed from local meteorological records. Alternatively, it can be obtained from Shellard's[34] contoured diagram of highest mean hourly wind speeds at 33ft for the British Isles. In the latter case, the contours are based on wind speeds measured generally at open level sites approximating to Category (2) and should be adjusted for other categories by a factor K. Values for K of 1.1 and 0.8 respectively have been adopted for Categories (1) and (3). The design wind speed is now calculated from the following equation:

$$U_z = F_{33}\, K\bar{V}_{33}\left(\frac{z}{33}\right)^{\frac{1}{\gamma}} \qquad \ldots\ldots (9.6)$$

where the appropriate gust factor F_{33} has the values given below:

Category (1)	1.5	Extreme gust 3 seconds	1.3	10 second gust
Category (2)	1.7		1.4	
Category (3)	2.0		1.6	

In those cases where only the extreme gust is required as the basis for calculating the wind loading, the procedure may be simplified by turning direct to Shellard's[34] contoured map of the highest gust speeds at 33ft over the British Isles. Since maximum gust speeds are not affected very much by ground roughness, no correction factor for different categories of topography need be applied and the height adjustment is based on the exponent for Category 2, i.e. $\frac{1}{\gamma} = \frac{1}{11}$. Then

$$U_z = U_{33}\left(\frac{z}{33}\right)^{\frac{1}{11}} \qquad \ldots\ldots (9.7)$$

In the United Kingdom, as previously mentioned, maximum mean wind speeds over a period of one hour can be obtained from meteorological records together with the maximum peak gust speeds in some cases. For simplicity it was suggested by the Meteorological Office[34] that 10

miles per hour should be added to the maximum mean hourly wind speed to arrive at a value for the maximum mean minute speed. For considerations of the general stability of a building against wind, including gusts, CP3 : Chapter V : 1965[29] proposes that this maximum mean minute speed should be employed as a basis for deciding the exposure grading. The design speeds in this Code, therefore, are based on the velocity profile given by:

$$\frac{Vz}{V_{40}} = \left(\frac{z}{40}\right)^{0.13} \qquad \ldots\ldots (9{\cdot}8)$$

where z is the height above ground in feet and V_{40} is the mean wind speed at a height of 40ft, instead of 33ft, over a period of one minute. The basic wind pressures p of Table 3 in the Code do not accord with the dynamic pressures of the wind obtained from:

$$q_z = 0.00256V_z^2 \qquad \ldots\ldots(9{\cdot}9)$$

Tests on model buildings in a wind tunnel have shown that basic pressures exceed the dynamic pressures by a factor of 1.2 approximately.

(d) Pressure and Shape Coefficients

So far in this discussion of the wind loading on domes, only the basic considerations for determining wind speeds and wind loads for any type of structure have been considered. Although a general approach to the problem has been carried out, any investigation into wind pressures on full-scale dome structures would necessitate a study of these factors first. At this stage, it is now possible to study in more detail the wind pressures which are assumed to exist over dome structures.

A table of basic wind pressures, p lbf/ft^2, is given in CP3 : Chapter V : 1965[29]. The basic pressures or equivalent static pressures in the windward direction, are detailed according to four exposure gradings which are governed by the prevailing wind speed. The effective height above ground of a building is also accounted for, the effective height being measured to a point half-way between the eaves

and ridge levels of the roof. For wind velocities other than those for which data are tabulated, the pressure may be calculated from:

$$p = \frac{V^2}{5184} \times p_{72} \qquad \ldots\ldots (9.9)$$

where:

p = the pressure corresponding to a velocity of V miles per hour;

V = the velocity considered in miles per hour at an effective height of 40 ft;

p_{72} = the pressure corresponding to a velocity of 72 miles per hour.

The American Standards Association[28] also advocate the use of a table of basic wind pressures for various height zones above ground.

When considering wind pressures on a building as a whole, the design of such a structure should be carried out to resist the combined effects, as well as the separate effects, of imposed loads and wind loads having due regard to internal pressures. The effect of topography and adjacent buildings, present or future, must also be considered. In the case of sloping roofs, the basic wind pressures. as tabulated by the various codes of practice, are modified by pressure coefficients which are either positive or negative indicating pressure or suction respectively. The values of the pressure coefficients depend upon the angle of slope and upon which side, windward or leeward, the roof is positioned in relation to the direction of the wind.

Wind pressures on a curved roof, due to wind blowing at right angles to the axis of the roof, may be computed on the basis that the curved portion is divided into not less than four equal segments as shown in Figure 51(a). The pressures on each segment may be determined by multiplying the basic wind pressure values by the relevant pressure coefficients, given in the building codes of practice,[28],[29] appropriate to the slopes of the chords of the segments.

The pressures on curved surfaces, as obtained from CP3 : Chapter V:

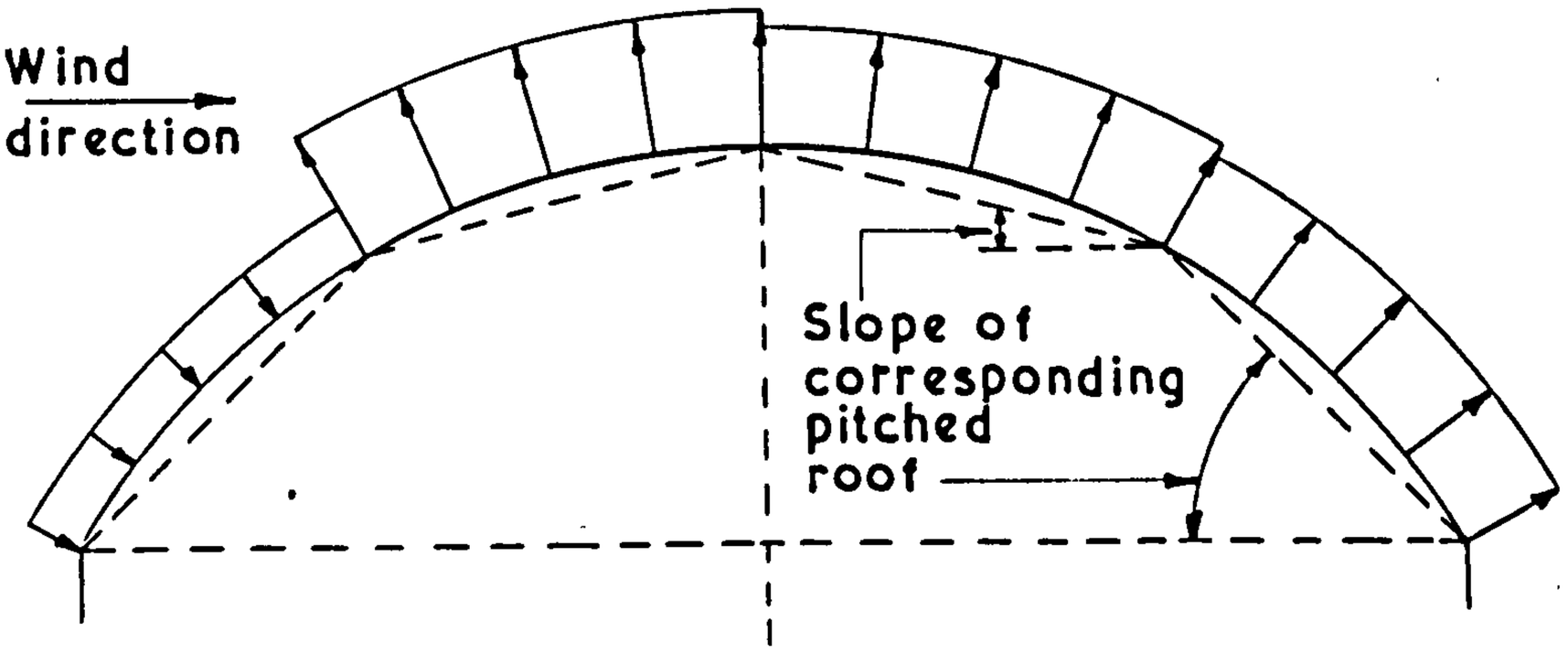

CP 3: Chapter V: 1965 Curved Roofs

(a)

Smooth Spherical Dome : Rise-to-Base Dia. Ratio = 1/5·9

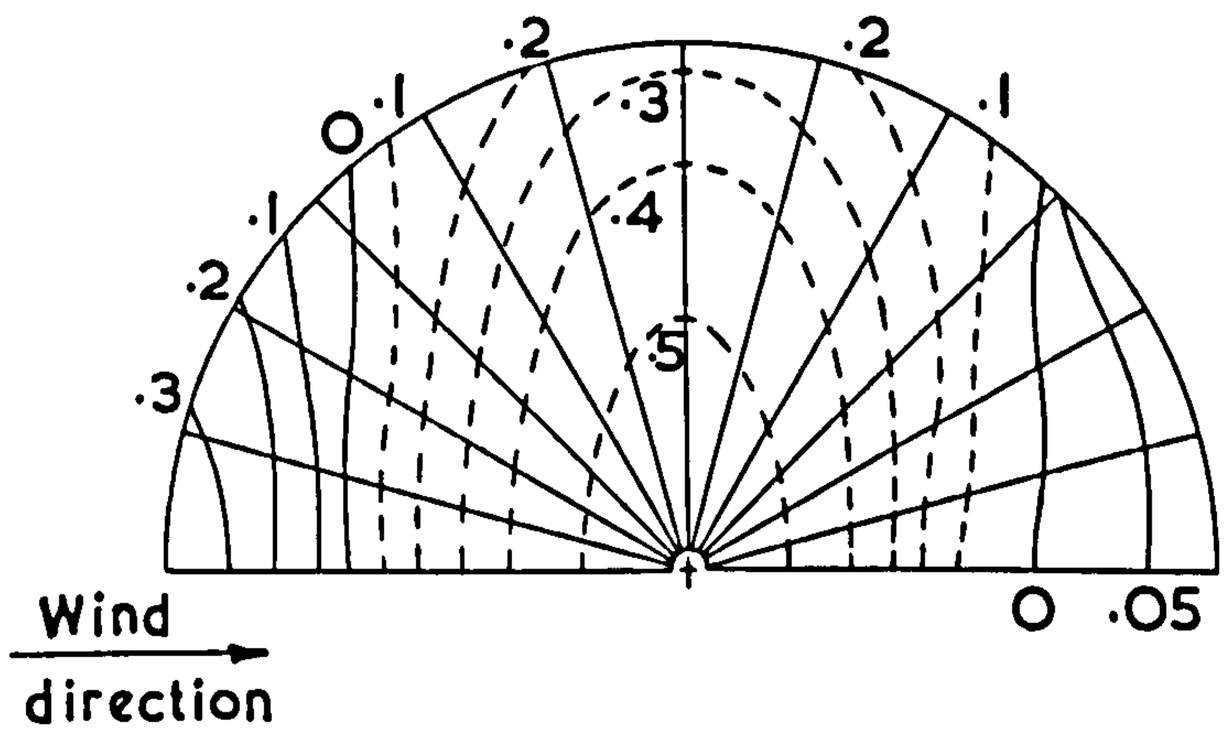

Half Plan

(b)

FIG. 51 WIND LOADS ON DOMES Sheet No. 1

F.A.A. Ph.D. Thesis
2nd Feb., 1970

Structural Engineering Division
Department of Civil Engineering
University of Newcastle upon Tyne

1965[29], are for buildings which have a rectangular plan area. For buildings which have circular plan areas, shape factors can be employed to modify the design pressures further. Depending on the ratio of height to base-width, shape factors of between 0.6 to 0.7 can be used for a structure with a circular plan area. The American Standards Association also employ shape factors depending, not only on the shape, but also on the surface roughness. Unfortunately, these shape factors do not account for the three-dimensional change in curvature which exists for domes and, therefore, a more accurate estimation of dome design pressures is still a matter for conjecture.

The overall wind loading on a dome, as determined by the procedures outlined so far, is only an average load over the structure. Pressures and suctions, specified by these methods, will be exceeded locally. The British Code of Practice[29] gives increased values for localized pressures and, indeed, the American Standards Association includes localized values over a hemispherical dome but these are not to be used for the overall dome roof loading.

(e) Wind Tunnel Test Values

The values of the pressure and shape coefficients, described in Art. 9.4(d), have largely been obtained by measurements on models in wind tunnels. Until recently there has been little effort to establish the correlation between model and full-scale results. However, for bluff, sharp-edged bodies in steady winds the aerodynamic scale effects are negligible and the model results can be extrapolated to full-scale. This is not so in the case of domes, since they have no sharp edges and possess a three-dimensional curvature. Despite the uncertainties of their application to full-scale conditions, engineers will, in general, continue to design with the aid of the static wind loading data as obtained from measurements on models in wind tunnels. Therefore, wind tunnel investigations into the pressure distribution over

buildings are very important.

The general conditions for similarity between the pressures on a model and on the prototype structure call for similarity in:

(1) the shape;

(2) the Reynolds number, R, where R = $\frac{\text{Wind speed x base diameter}}{\text{Kinematic wind viscosity}}$ for a dome;

(3) the kinetic properties of the incident flow.

Very few investigators attempted to reproduce a vertical wind speed gradient in their wind tunnel experiments as it was believed that the relative importance of the general conditions was in the order given. However, according to Jensen,[34],[35] the reverse may be true. In other words the careful simulation of the velocity profile and the turbulent character of the flow is more important than similarity of the Reynolds number. Since the wind is fully developed turbulent flow in the earth's boundary layer, disturbances produced in it are independent of the Reynolds number of the roughness elements or the obstacles placed in it. It is very important therefore, in wind tunnel testing, to maintain similarity of the approaching flows. This is governed by the roughness length of the surface and the correct model law requires that the roughness lengths in the model test be to the same scale as the model itself.

Although, in the majority of cases, wind tunnel test results have not been checked by measurements on actual structures, pressure values obtained by this means are still very valuable provided the correct model law is used. Whether or not it is possible to determine the fluctuating pressures due to gustiness by the same means is still not certain. This will depend on whether or not the structure of the turbulence in the wind tunnel is similar to that in the natural wind over the significant part of the spectrum.

Wind tunnel tests on dome, dome-cylinder and dome-cone shapes

have been carried out in the United States of America and the results are published in two papers by Maher.[36],[37] In the tests on dome shapes, several 2ft diameter models, including a hemisphere and various spherical domes with different rise-to-base diameter ratios, were placed on the floor of the wind tunnel in a boundary layer flow. This would be the actual condition which a full-scale building would experience. Pressure readings from the models were converted to pressure coefficients by dividing by the dynamic pressure in the uniform section of the flow.

A typical pressure contour diagram, as obtained by Maher for a smooth spherical dome with a rise-to-base diameter ratio of 1/5.9, is shown in Figure 51(b). The full lines indicate positive pressures and the broken lines show negative or suction values. Angular coordinates in the diagram correspond directly to angular coordinates in the base plane of the dome. Radial distances in the diagram correspond to distances measured along the arc from the top of the dome to the point in question. In order to make use of the information, it is necessary only to multiply the pressure coefficient by the design dynamic pressure to obtain true values in pounds per square foot.

The values, obtained by Maher, for the pressure coefficients over a hemisphere were different from those obtained for the shallow spherical domes. A maximum positive pressure coefficient of about 0.7 was obtained on the windward side of the hemisphere whereas the maximum negative or suction value at the apex was approximately 1.15. Negative coefficients were obtained everywhere over the leeward side of the hemisphere. Tests on a roughened hemisphere generated a slightly greater windward side positive pressure with a significantly lower negative pressure on the top section. Greater negative pressures were found in the wake.

The building codes of practice[28],[29] allow a step variation of wind pressure with height. In general, the assumption of a constant

velocity profile, typical of building code allowances, is over-conservative for a low structure. Maher found also that, particularly for the shallow domes, the pressure distributions are significantly different when some substructure is used as a support. For the 2ft diameter hemisphere on top of a 6in. high cylinder, maximum positive coefficients were about 20 per cent greater than for the hemisphere placed on the ground. The maximum negative pressure coefficients on top were 26 per cent greater. All the spherical domes had negative pressures over their surfaces when placed on top of cylinders.

The data obtained by Maher represents the effects of flow around basic shapes that are free of details. Entrances, surface conditions, vents, etc., all have some effect on the flow conditions and pressure distributions. Tests on shapes suitably modified would be necessary in these cases.

(f) Formulae for Use With the Shell Analogy

In 1912 H. Reissner[12] put forward his formula for the wind pressure distribution over a spherical dome. This formula is given as follows:

$$w = wo \sin \phi \cos \theta \quad \ldots\ldots (9{\cdot}10)$$

where w is the wind pressure normal to the surface, wo is the maximum intensity of pressure, i.e. at point A in Figure 52(b), θ is the horizontal angle from the axis of the wind direction to the point, X, being considered on the surface of the dome and ϕ is the angle from the central vertical axis of the dome to point X. This formula has been used ever since for the design of shell domes and is employed in standard texts by Flügge[38] and Pflüger.[39] Gondikas and Salvadori[40] also employ this formula in their paper on wind stresses in domes, published in 1960.

The main advantage of Reissner's formula is that it gives an antimetrical wind pressure distribution as shown in Figure 52(b).

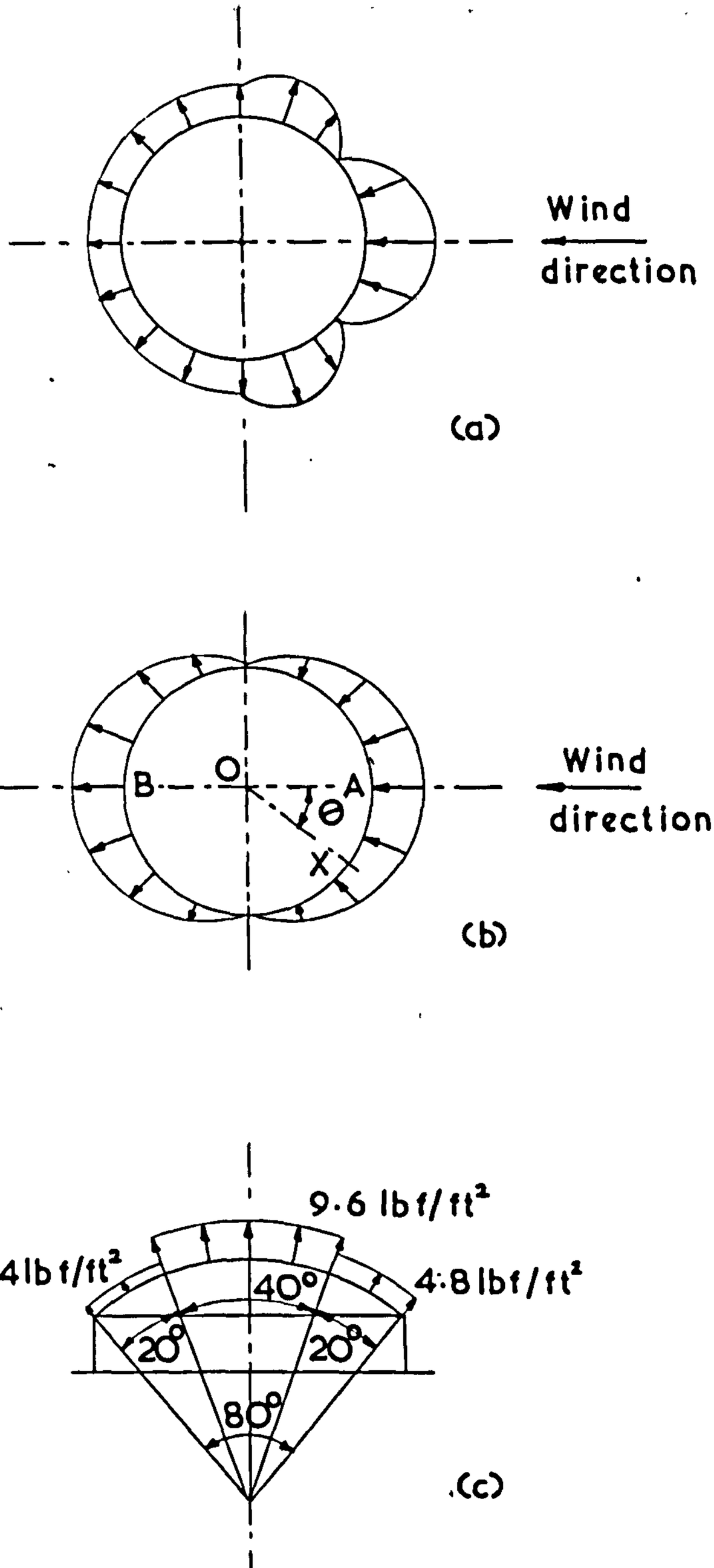

FIG. 52 WIND LOADS ON DOMES Sheet No. 2

F.A.A. Ph.D. Thesis
3rd Feb., 1970

Structural Engineering Division
Department of Civil Engineering
University of Newcastle upon Tyne

This enables the equations for stresses in shell domes to be solved very easily. Its main disadvantage is that it is not a true representation of the pressure distribution when wind acts on a dome. The tangential component of the wind pressure is neglected and only the component of the wind pressure normal to the dome is considered. Pflüger[39] also shows that the measured distribution of the wind pressure around the roughened surface of a circular cylinder is more like Figure 52(a) than the antimetrical system given in Figure 52(b).

F. Dischinger[12] found that the formula:

$$w = wo \sin^2 \phi \sin^2 \psi \quad \ldots\ldots (9.11)$$

where $\psi = 90^\circ - \theta$ was a better representation of the wind pressure distribution on a dome. He compared several cases using the two formulae and found that the latter gave a more critical stress distribution. Dischinger also found that experimental windtunnel tests gave results closer to those obtained by his own formula than to those given by Reissner's. The disadvantage of Dischinger's formula is that it does not give an antimetrical loading on the dome. This drawback was overcome by replacing $\sin^2\psi$ by $\sin\psi$ and $\sin^3\psi$ so that:

$$w = wo \sin^2 \phi \left[c \sin\psi + (1-c) \sin^3\psi \right] \quad \ldots\ldots (9.12)$$

This contains c as a constant which is determined from the consideration that the total horizontal load on the dome must, in both formulae, be the same. Dischinger obtained the value of c = 0.4. Substituting the value of:

$\sin^2\psi = 0.4 \sin\psi + 0.6 \sin^3\psi$ and the value of:

$\sin^3\psi = 0.75 \sin\psi - 0.25 \sin 3\psi$ it can be shown that:

$$w = wo \sin^2\phi \, (0.85 \sin\psi - 0.15 \sin 3\psi) \ldots\ldots (9.13)$$

In the design of the Agrodome in Vancouver, Canada, as mentioned previously in Art. 9.3 relating to snow loading on domes, the wind pressure distribution was assumed to vary according to equation (9.10). Membrane theory was employed in the analysis and the value of wo was

taken to be 0.26 times the basic wind pressure of 30lbf/ft^2 for the particular location. For the two Altadomes, in Fort Saskatchewan, the wind load distribution was assumed to be as shown in Figure 52(c) with suction prevailing over the entire area of the dome. The maximum intensity of suction, i.e. 9.6 lbf/ft^2, was arrived at by multiplying the basic wind pressure of 19.2 lbf/ft^2 by a coefficient of 0.5.

CHAPTER X

DESIGN, CONSTRUCTION AND TESTING OF THE MODEL RADIAL RIBBED DOME

10.1 DESIGN OF THE MODEL DOME

(a) General Considerations

The reasons for the research project considered in this thesis have been given in Art. 3.11. A model radial ribbed dome was needed for carrying out experimental work in connection with the project and such a model was designed and constructed in the Structural Engineering Division at Newcastle University. It was decided, by the author, that the best procedure for obtaining the sizes of the individual components in the dome was to design a prototype first, based on the available information relating to dead, live, snow and wind loading, and then construct a scale model having due regard for the principles of similarity employed in model analysis. In this way it was hoped that the deflections, forces and moments, obtained experimentally from the model, could be usefully employed in the design of full-scale structures. The principal dimensions of the prototype and model domes are shown in Drg. Ph.D. Thesis No. 1.

A diameter of 216 ft. was chosen for the prototype dome with a rise of 36 ft. The ribs were assumed to have a circular shape. These dimensions were chosen for three reasons:

(1) The dimensions are similar to those employed in the construction of the Lightfoot Sports Centre in Newcastle upon Tyne and are, hence, those which would be used for a practicable full-scale structure;

(2) At a scale of 1 in. to 1 ft. (i.e. $\frac{1}{12}$) the same

principal dimensions could be employed for both the prototype and the model dome, the only change being in the type of units (i.e. ft. to in.);

(3) Using these dimensions for the prototype dome resulted in, at $\frac{1}{12}$ scale, a model having a base diameter of 18 ft. and a rise of 3 ft. These dimensions were the maximum which could be employed in the available space set aside for the experimental work.

The author chose to carry out his experimental investigations on as large a scale model as possible in order to facilitate the application of loads to the system and to enable accurate measurements to be taken of the stresses incurred. With such a large scale model, it was hoped that, after testing in the laboratory, the model could be dismantled and re-erected in the field at some later date in order to investigate actual snow and wind loading conditions.

The number of radial ribs chosen for the prototype and model domes was 36. It was also decided to use 18 horizontal purlin rings and diagonal bracing as illustrated in Drg. Ph.D. Thesis No. 1. This system again represents one which would be found in practice and the author preferred to test a structure of this type rather than an idealized simple form.

European Redwood, of a first class grade suitable for joinery work, was employed in the manufacture of the laminated ribs for the dome. Timber was chosen for three reasons. Firstly, the Lightfoot Sports Centre was erected with laminated timber ribs and, hence, the use of such units was a feasible proposition. Secondly, the employment of a laminating process meant that the ribs could be manufactured easily by the author, himself, with the aid of a laboratory technician. The third reason for constructing the model dome with timber ribs was that the material was already available in the Structural Engineering

Division.

In order that the dome could be loaded easily and the stresses determined conveniently, the author decided to erect the model approximately 3 ft. above ground level on a rigid base ring. This gave a reasonable working height of 6 ft. at the crown and meant that any point could be reached, both inside and outside, on the dome. The Finnish Birch plywood and Dexion angle employed in the construction of the base ring were also readily available in the Structural Engineering Division.

In the design of the prototype dome the method employed in the American Institute of Timber Construction Manual[28] has been followed. This Manual states that design procedures for three-hinged and two-hinged arches can be used for the design of domes consisting of arches joined at the crown. In most cases, however, a ring is employed at the apex and a hinge action will occur which depends for its magnitude on the stiffness of the ring. The effect of the movement of such a ring on the stress distribution, and stability of, radial ribbed domes is one of the factors which has been investigated in this research project. Since the true pattern of behaviour of this criterion was not appreciated fully at the beginning of the testing process, it was necessary to employ some method of analysis to arrive at values for the radial rib section sizes. The author, therefore, designed his rib section sizes for both three-hinged and two-hinged arch conditions, remembering that the plane projection of the tributary area of load for each half of an arch in the dome was wedge-shaped.

Three principles are recommended, by the American Institute of Timber Construction Manual, for application to the design of radial ribbed domes:

(1) The ribs are in maximum stress when the entire dome is loaded.

(2) A ring member is in maximum tension when all of the dome above the ring is fully loaded, and in maximum compression when all of the dome below the ring, as well as the ring itself, is fully loaded.

(3) Diagonals are not stressed when the dome is symmetrically loaded. The diagonals in a panel are in maximum stress when the dome on one side of a vertical plane passing through the centre of that panel and through the crown is fully loaded and the other side unloaded.

Figure 53 shows the notation employed in the design of radial ribbed domes by the method stated in the American Institute of Timber Construction Manual and the general design proceduro is reproduced in the following Art.

(b) <u>American Institute of Timber Construction General Design Proceduro for Radial Ribbed Domes</u>

(1) Determine loads at rib-ring intersections. The loads W_1, W_2, etc., in Figure 53 (a) are the sums of the dead and applied loads acting on the area tributary to each rib-ring intersection. For example, the sum of the loads acting on the shaded area X in Figure 53(d) is equal to load W_3.

(2) Determine the required rib section. The axial compression load is greatest in that portion of the rib between rings 4 and 5 and may be determined from the formula:

$$P' = \frac{W_1 + W_2 + W_3 + W_4}{\sin \alpha_4} \quad \ldots\ldots (10.1)$$

where α_4 = angle between the horizontal and the straight line connecting rings 4 and 5, see Figures 53 (a) and (c). The cross-sectional area, A, required to resist the compression load P' can be determined from the formula:

$$A = \frac{P'}{F_c} \quad \ldots\ldots (10.2)$$

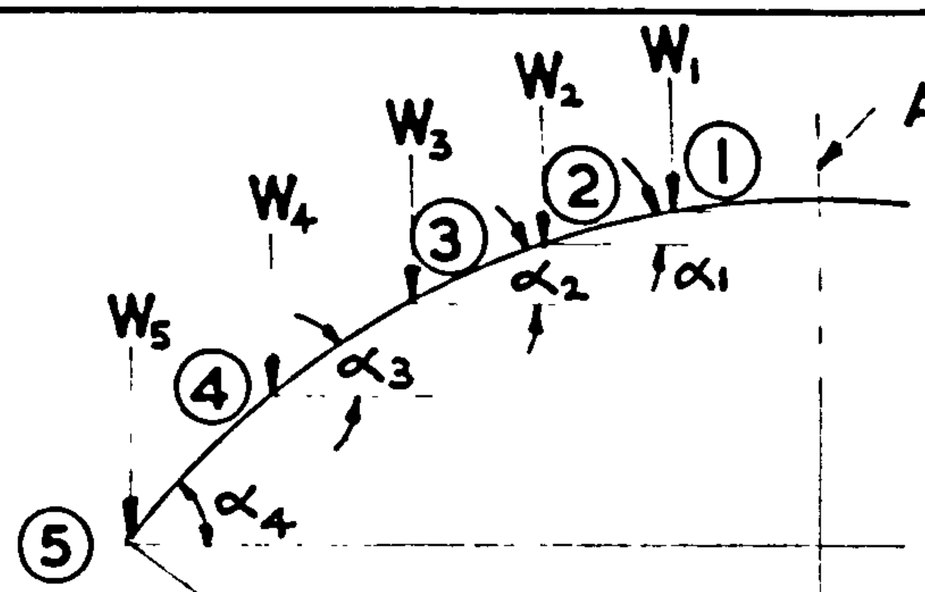

a. Section through rib

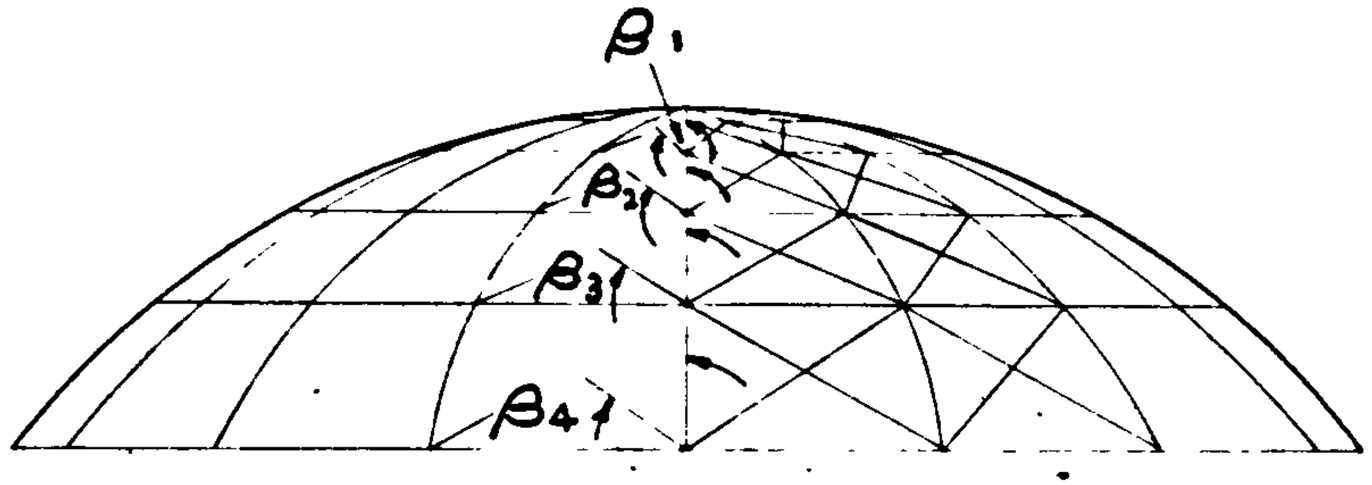

b. Partial elevation

AMERICAN INSTITUTE OF TIMBER CONSTRUCTION RADIAL RIBBED DOME NOTATION

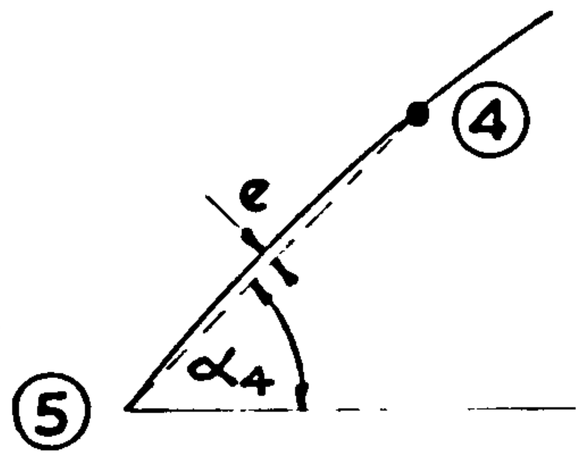

c. Section at base

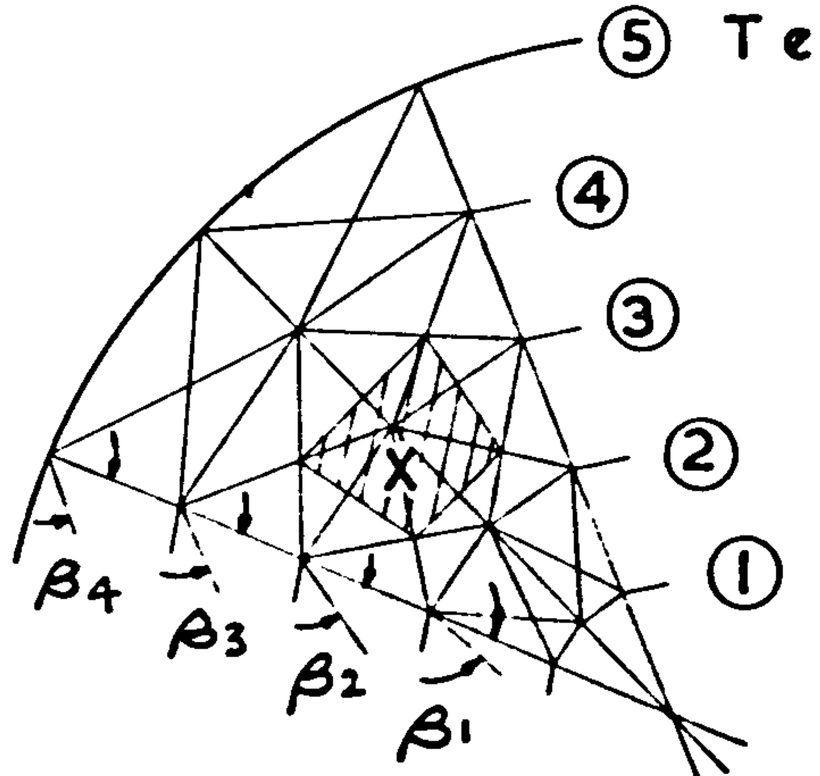

d. Partial plan

FIG. 53

Structural Engineering Division
Department of Civil Engineering
University of Newcastle upon Tyne
F.A.A. Ph.D. Thesis
28th Aug., 1969

where F_c = allowable unit stress in compression parallel to grain.

For ribs which are discontinuous at rib-ring intersections, the section modulus, S, required to resist the moment due to eccentricity is determined from the formula:

$$S = \frac{P'e}{F_b} \qquad \ldots\ldots (10.3)$$

where e = eccentricity;

F_b = allowable unit stress in extreme fibre in bending.

If the rib is continuous at a joint, carry-over moments will occur at that joint.

(3) Determine the required compression ring sections. The axial compression load carried by each ring will be different, and it can be determined by the formulae:

$$P_{R1} = \frac{W_1 \cot \alpha_1}{2 \sin (180°/N)} \qquad \text{for ring 1}$$

$$P_{R2} = \frac{W_1 \cot \alpha_1 - (W_1 + W_2) \cot \alpha_2}{2 \sin (180°/N)} \qquad \text{for ring 2}$$

$$P_{R3} = \frac{(W_1 + W_2) \cot \alpha_2 - (W_1 + W_2 + W_3) \cot \alpha_3}{2 \sin (180°/N)} \qquad \text{for ring 3} \qquad \ldots\ldots (10.4)$$

where P_{R1}, P_{R2}, P_{R3}, etc. = compression loads in rings 1, 2, 3, etc., respectively;

α_1, α_2, α_3, etc. = angle between the horizontal and the straight lines connecting rings 1 and 2, 2 and 3, 3 and 4, etc., respectively; see Figure 53(a)

N = number of ribs.

The cross-sectional area, A, required to resist the compression loads can be determined from the formula:

$$A = \frac{P_R}{F_c} \qquad \ldots\ldots (10.5)$$

Each ring member spanning between ribs acts as a beam; therefore, the section must also be adequate to resist bending moment, M, as determined by the formula:

$$M = \frac{wL_R^2}{8} \qquad \ldots\ldots (10{\cdot}6)$$

where w = load carried by each ring member span;

L_R = ring member span (varies between rings 1, 2, 3, etc.)

For appearance, it may be desirable to make all ring member sections equal.

(4) Determine the required tension ring section. The outward thrust, T, is contained by this ring and it may be determined by the formula:

$$T = \frac{(W_1 + W_2 + W_3 + W_4 + W_5)\cot\alpha_4}{2\sin(180^\circ/N)} \qquad \ldots\ldots (10{\cdot}7)$$

The cross-sectional area, A, required to resist the tension load can be determined from the formula:

$$A = \frac{T}{F_t} \qquad \ldots\ldots (10{\cdot}8)$$

where F_t = allowable unit stress in tension parallel to grain. If the tension ring spans between supports acting as a beam, the section must also be adequate to resist the moment due to the combined weights of the dome and the ring itself.

(5) Determine the required diagonal rod sizes. The diagonal rods carry only applied loads, and the load in each diagonal can be determined by the formulae:

$$P_{D1} = \frac{W_{A1}}{2\sin\alpha_1\cos\beta_1} \quad \text{for diagonals between rings 1 and 2}$$

$$P_{D2} = \frac{W_{A1} + W_{A2}}{2\sin\alpha_2\cos\beta_2} \quad \text{for diagonals between rings 2 and 3}$$

$\ldots\ldots(10{\cdot}9)$ cont/...

$$P_{D3} = \frac{W_{A1} + W_{A2} + W_{A3}}{2 \sin \alpha_3 \cos \beta_3} \quad \text{for diagonals between rings 3 and 4} \quad \ldots\ldots (10{\cdot}9)$$

where P_{D1}, P_{D2}, P_{D3}, etc. = loads in diagonals;

W_{A1}, W_{A2}, W_{A3}, etc. = total applied load at each rib-ring intersection in rings 1, 2, 3, etc., respectively;

β_1, β_2, β_3, etc. = angle between rib and diagonal between rings 1 and 2, rings 2 and 3, rings 3 and 4, etc., respectively; see Figures 53(b) and (d).

The cross-sectional rod area, A_s, required to resist these loads can be determined from the formula:

$$A_s = \frac{P_D}{F_s} \quad \ldots\ldots (10{\cdot}10)$$

where F_s = allowable unit stress in steel.

(6) Design the rib-ring joints, considering the loads carried by each member intersecting at that joint. When possible, it is best to use the same type and size of connection at each joint in the dome. Spacing, end distance and edge distance requirements must be met for the type and size of fastenings used.

(c) Prototype Dome Design

The general design procedure for radial ribbed domes, as issued by the American Institute of Timber Construction in the above form, follows the method employed in 1863 by Johann W. A. Schwedler when he constructed his first dome, of the type named after him, over a gas tank in Berlin (See Art. 7.1). This method of analysis is only suitable for symmetrical loading and, as the rigidity of the joints is neglected, leads in all cases to an over-estimation of the maximum stresses.

The method is, however, simple and can be quickly employed to give

approximate results. For this reason and because the size of each individual component in a structure must be known before a more accurate stress analysis can be carried out, the American Institute of Timber Construction recommendations were employed as a design basis for the prototype dome. The ribs of the dome were designed to carry bending moments which would be experienced by plane, two-dimensional three-hinged and two-hinged arches and the sizes of the remaining components were determined from the general design procedure detailed above.

Drgs. Ph.D. Thesis Nos. 2 - 8 contain the bending moments, shear forces and axial forces for the prototype dome designed according to three-pinned and two-pinned arch principles. Four load cases were considered:

(1) Uniformly distributed dead load of 5lb/ft^2 on surface area (see Art. 9.1);

(2) Uniformly distributed balanced live load of 15lb/ft^2 on plan area (see Arts. 9.2 and 9.3);

(3) Uniformly distributed unbalanced live load of 15lb/ft^2 on half plan area (see Arts 9.2 and 9.3);

(4) Wind load (see Art. 9.4 and Drg. Ph.D. Thesis No. 5 for distribution).

Drg. Ph.D. Thesis No. 2 shows the bending moment, shear force and axial force diagrams for Load Case (1) above, under three-pinned arch conditions. A graphical method, which is outlined in the Steel Designers' Manual,[41] has been employed to obtain these diagrams. The loading on each arch was first divided into point loads and the base reactions evaluated. A ray diagram was then drawn to allow the equilibrium polygon to be superimposed on the arch profile. The difference between the equilibrium polygon and the line representing the arch axis is the bending moment diagram for the dome rib. Actual

values of the bending moments at each load point are obtained by multiplying the vertical ordinates on this bending moment diagram by the horizontal reaction. The shear and axial forces were obtained from the ray diagram by resolving perpendicularly and parallel to the central axis of the rib. Drgs. Ph.D. Thesis Nos. 3 - 5 contain similar diagrams for Load Cases (2), (3) and (4).

The bending moments, shear forces and axial forces, obtained by assuming two-pinned arch conditions, are contained in Dwgs. Ph.D. Thesis Nos. 6 - 8. In Dwg. Ph.D. Thesis No. 6, the load cases are illustrated similar to those for the three-pinned arch conditions. To evaluate the horizontal reactions for a two-pinned arch, it is first necessary to compose a table containing the coordinates of the load points along with the bending moments obtained from considering the same load system applied to a simply supported straight beam. Such a table is included in Dwg. Ph.D. Thesis No. 6. By summating the simply supported bending moments at each load point multiplied by the vertical coordinates and multiplying by the arc length, then dividing by the summation of the squares of the vertical coordinates, which is also multiplied by the arc length, the horizontal reactions were obtained for each load system. The bending moments, shear forces and axial forces could then be easily determined and are tabulated in Dwg. Ph.D. Thesis No. 7.

In Calculation Sheet Nos. 1 - 23, section sizes are determined for the prototype dome laminated timber radial ribs, the horizontal timber purlin rings and the mild steel diagonal bracing rods. Permissible stresses for the timber components were obtained from C.P. 112 : 1967 - The Structural Use of Timber.[31] The thickness of the radial rib laminates was assumed to be $1\frac{1}{2}$ in., according to the Forest Products Research Laboratories Special Report No. 15.[42]

The bending moments, shear forces and axial forces, as determined

in Dwgs. Ph.D. Thesis Nos. 2 - 8, were extracted and reproduced in Calculation Sheet Nos. 4 - 11 in order to facilitate the perception of the largest rib stresses at each load point. Once the point of maximum stress had been obtained for the prototype dome rib, it was checked for combined bending and axial compression before arriving at a true section size. Section sizes were also determined along the length of the rib in a similar fashion and these values are tabulated in Calculation Sheet No. 14.

Since, in the prototype dome under consideration, the radial ribs are continuous from base to crown, the procedures adopted for arriving at the bending moments, shear forces and axial forces in these members were those of three-pinned and two-pinned arches. This approach replaces the pin-jointed framework system of axial forces employed in stages (1) and (2) of the American Institute of Timber Construction general design procedure outlined in Art. 10.1(b). However, stages (3) and (5) of this general method were employed to find the section sizes for the horizontal timber purlin rings and the mild steel diagonal bracing rods respectively. The purlins were checked for both bending and axial compression while the diagonal rods were checked for tension only. Calculation Sheet Nos. 17 - 22 give the prototype dome component sizes resulting from these determinations and they are also included, along with the radial rib sizes, in Drg. Ph.D. Thesis No. 9.

In Calculation Sheet No. 23, the slenderness ratios for the ribs are worked out as if no horizontal bracing rings were to be provided. These values are high and if the rib design had been carried out for such results, then larger sections would have been necessary. Since, in actual practice, full loading would not be applied without the bracing being in position, the slenderness ratios for the unbraced condition are not critical for the overall design. However, when erecting such a system, care must be taken to prevent overloading of

the individual ribs until the complete framework is in position. Some of the experimental work on the model dome was carried out without the horizontal bracing in position and, therefore, only small loads and deflections could be applied.

The design of the prototype dome apex ring is contained in Calculation Sheet Nos. 24 and 25. A section size has been obtained on the basis of single point loads being applied at diametrically opposite sides of the ring. To withstand the maximum bending moment induced by the design load, a rectangular solid steel section of $4\frac{1}{4}$ in. by $17\frac{1}{2}$ in. would be required and the deflection of such a ring under the single point loads would also be excessive. A reduction in both weight and deflection would be obtained by providing an apex ring with a box section. Although the decrease in diameter of the box section ring under the two point design load system would still be 12.6 in., this deflection would not occur in practice due to the restraining action of the other 34 ribs.

(d) Model Dome Component Sizes

As mentioned previously in Art. 10.1(a), the layout dimensions of the model were chosen to be 1/12 times those of the prototype. The cross-sectional dimensions of the model dome ribs were taken as 1/14 times those of the prototype, resulting in a maximum size of $\frac{1}{2}$ in. x 2 in. Thus, for the prototype structure without bracing, the deflections, forces, moments and stresses would be given by:(43)

$$\text{Deflection} \quad y = 12y_m \qquad \ldots\ldots (10\cdot11)$$

$$\text{Force} \quad F = \frac{14^4}{12^2} \cdot \frac{E}{E_m} \cdot F_m = 266\frac{7}{9} \cdot \frac{E}{E_m} \cdot F_m \qquad \ldots\ldots (10\cdot12)$$

$$\text{Moment} \quad M = \frac{14^4}{12} \cdot \frac{E}{E_m} \cdot M_m = 3201\frac{1}{3} \cdot \frac{E}{E_m} \cdot M_m \qquad \ldots\ldots (10\cdot13)$$

$$\text{Stress} \quad f = \frac{14^2}{12^2} \cdot \frac{E}{E_m} \cdot f_m = 1\frac{13}{36} \cdot \frac{E}{E_m} \cdot f_m \qquad \ldots\ldots (10\cdot14)$$

The suffix "m" denotes model values. Since the same material has been used for the model that was employed for the prototype, the ratio $\frac{E}{E_m}$ equals unity.

Unfortunately, for practical reasons, the cross-sectional dimensions of the horizontal timber purlin rings could not be taken as $\frac{1}{14}$ times those of the prototype. Ramin purlins, $\frac{1}{2}$ in. x $\frac{1}{2}$ in. in section, were employed in the model, this size being the minimum needed for attachment to the radial ribs. For simplicity in erection, one size was used for the purlins throughout the model. Wire was to be utilized to represent the mild steel diagonal bracing rods in the model.

The apex ring employed in the model dome had a solid section size of 1 in. by $\frac{1}{8}$ in. and the outside diameter was 24 in. This diameter was correctly scaled at 1/12. However, to scale the section size of the prototype apex ring by 1/14 would have required a model ring section of $1\frac{1}{4}$ in. by .304 in. (approximately 5/16 in.). Since one of the principal aims of the research project was to study the hinge action which was expected to occur at the apex ring, the author felt that a ring of slightly smaller depth and greater flexibility would be advantageous.

10.2 CONSTRUCTION OF THE MODEL DOME

(a) Base Ring Erection

The base ring for the model radial ribbed dome was constructed from 13 ply sanded Finnish Birch plywood and Dexion angle. Plate 4 is a photograph of the completed base ring and Dwg. Ph.D. Thesis No. 10 gives the structural details. Two thicknesses of plywood were provided at the base of the dome itself and one thickness of plywood was employed as a working base at floor level.

Eighteen similar sized segments, cut from two 10 ft. by 5 ft. sheets, were incorporated in the three plywood layers used in the base ring. Marking out of the segments was carried out on the floor of the

PLATE 4 - THE MODEL RADIAL RIBBED DOME BASE RING



laboratory according to the method illustrated in Dwg. Ph.D. Thesis No. 10. A 6 in. by 2 in. by $\frac{1}{8}$ in. thick aluminium plate was attached to a 1 in. by $\frac{1}{2}$ in. oak strip which could be rotated around a fixed $\frac{3}{8}$ in. diameter bolt as centre. The aluminium plate was drilled with two holes to allow pencil lines to be drawn at the correct radii for the outside and inside faces of the plywood rings. A third hole was employed for marking out the dome base centre line on the segments. Cutting was carried out by means of a jig saw and all segments were given two coats of polyurethane resin for protection and to improve the finish.

The first step in the erection of the base ring consisted of laying out six plywood segments to form the working base at floor level. These segments were not joined together but were held in position, around a fixed central point, by small blocks of wood nailed into the wooden laboratory floor.

Once the single layer of segments had been correctly positioned, it was employed as a guide for the assembly of the double layer plywood ring which formed the actual base to the dome, approximately 3 ft. above floor level. The six segments in the top layer of the double layer system were arranged so that they half overlapped the bottom layer pieces. Where the plywood segments butted together, 4 no. 1"/12 screws, with countersunk heads, were used to fasten the segments to the ring below or above depending upon which layer contained the joint. Details of the jointing method are given in Dwg. Ph.D. Thesis No. 10. By this method, a complete and relatively rigid plywood ring was made for screwing the dome rib bases into.

The next stage in the construction of the complete base ring involved the cutting and assembly of the steel Dexion angle for the supporting frames. 32 frames, approximately 3 ft. by 1 ft.6$\frac{3}{4}$ in., were made along with 2 access frames 3 ft. by 3 ft.2in. The access

frames were provided so that entry could be made into the centre of the dome. Two lengths of 225/80 steel Dexion angle, back to back, were employed in the top and bottom members of the access frames with single side members of 300/100S Dexion angle. All the other 32 frames had single members of 300/100S Dexion angle.

In order to obtain a uniform size for the 32 frames, a jig was made by screwing down spare pieces of Dexion angle onto a wooden base. The lengths of Dexion angle, in the frames, were fastened together by means of $\frac{3}{8}$ in. diameter by 1 in. long bolts having hexagon shaped heads and nuts. Two bolts were employed at each corner of the frames for stability. Additional bolts were used in the top and bottom members of the access frames.

After the frames had been assembled, they were screwed to the plywood working base and bolted together at the sides. The double layer plywood ring was then lifted on top of the steel frames and held rigidly in place by bolting to the Dexion angle. To ensure that the top of the base ring was at a constant height all round, it was levelled to within $\pm$. 020 in. using a Hilger and Watts Autoset level together with a 3ft. rule. The level of the ring was checked in the radial direction by a builders level. Adjustments were made to the Dexion angle frames to achieve this accuracy.

The dome base centre line, which had been marked out on the plywood ring segments at the same time as their outlines, was checked at the 3ft. level using the same oak strip and aluminium marking guide. A steel plate was positioned over the fixed central point of the base ring and a vertical steel rod was used to raise this centre level with the top of the double layer plywood ring. The oak strip was rotated about the steel rod and the pencil centre line of the dome rib bases correctly positioned. A Wild TIA theodolite was then used to mark off the positions of the dome ribs at 10° intervals.

(b) Rib Manufacture

The model dome radial ribs were constructed from European Redwood of a 1st Class joinery grade. Two 9 in. by 3 in. beams of this material and one 3 in. by 3 in. beam were cut into ¼ in. laminates approximately 9 ft. long. To produce ribs for the model which were shaped to a given radius, a jig was required to clamp the laminates in after they had been glued. Details of this jig are given in Figure 54. Plates 5, 6, 7 and 8 show the various stages in the laminating process.

Plate 5 is a photograph of the laminates lying alongside the jig before any glue had been applied. Blocks of 8 No. ¼ in. laminates, approximately 2½ in. wide, were produced at each casting. This allowed 4 model dome ribs to be cut from each block.

Plate 6 shows the glue being applied to the laminates. The method of application was by hand, using a paint brush, and the laminates were coated on both sides. Aerodux 185 resorcinol-formaldehyde resin mixed with Hardener HRP.155 was the adhesive employed for the laminating process. This glue had cold-setting and gap-filling properties. It was also weather-proof and boil proof conforming to B.S. 1204 : 1964, part I,[45] and, therefore, was a suitable adhesive to use for the model should it be required for site testing. The glue-to-hardener ratio employed was 100 : 20 parts by weight, the mixing being carried out by hand.

Plate 7 illustrates the clamping technique employed in the laminating process. Clamps were applied at approximately 12 in. centres and, in order to ensure that a uniform pressure was applied along the length of the block, a tensioning device was also incorporated in the jig. By tightening the bolts attached to the outer steel plate, see Figure 54, a uniform thickness of glue line could be obtained. The blocks of laminates were kept clamped for 24 hours, at a temperature of approximately 60 F, and then removed from the jig.

$2\frac{1}{2}"\times 2"\times 1"$ M.S. block drilled and tapped for $\frac{1}{2}"$ and $\frac{5}{16}"$ diameter bolts

2 No. $1"\times\frac{5}{16}"$ M.S. Whit. bolts

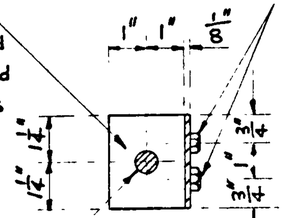

SECTION A-A

$\frac{1}{8}"$ thick black iron washer

$2"\times 2"\times\frac{1}{4}"$ M.S. angle

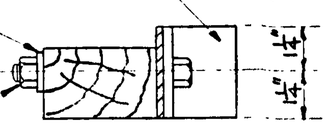

$4\frac{3}{4}"\times\frac{1}{2}"$ M.S. Whit. bolt

SECTION B-B

$1\frac{1}{2}"\times 1\frac{1}{2}"\times$ 12mm Finnish Birch plywood block nailed over rubber joint (3 No. $1\frac{1}{4}"$-10 nails)

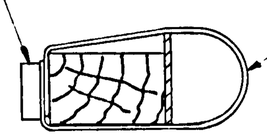

14"×1" rubber strip cut from car inner tube

SECTION C-C

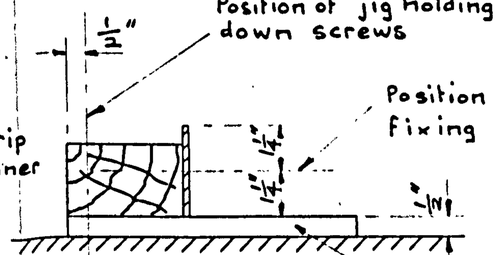

Position of jig holding down screws

Position of plate fixing screws

SECTION D-D

$7\frac{1}{2}"\times\frac{3}{4}"\times\frac{1}{2}"$ oak raising strip wrapped in polythene

$4\frac{3}{4}"\times\frac{1}{2}"$ M.S. Whit. bolt

$\frac{7}{16}"$ Whit. spanner required for tightening

12'-0"

10'-8"×2½"×⅛" M.S. outer plate

10'-0"×2½"×⅛" M.S. inner plate

10'-8"

9 No. plate fixing screws (2"-12) at 12" crs.

3"

3"

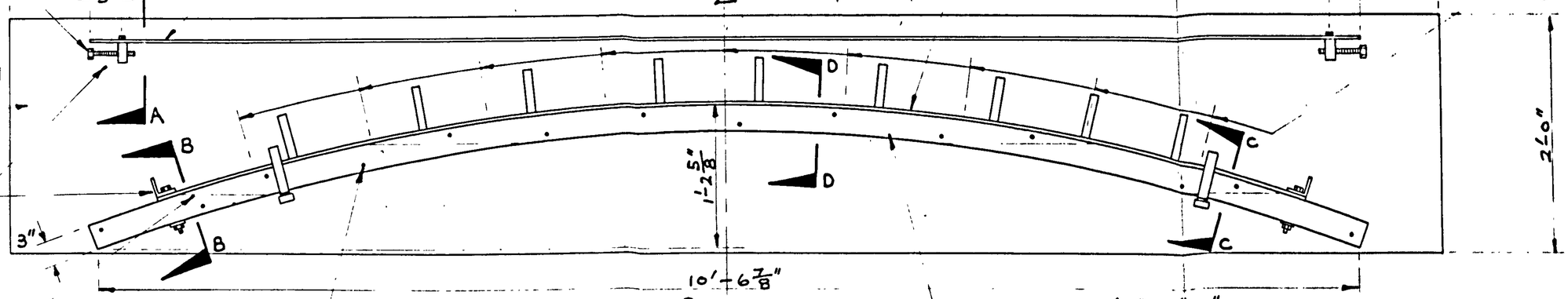

Table top of $\frac{3}{4}"$ thick Columbian Pine plywood (2 No. 8'×4' sheets) covered with polythene

Tensioning device

Aerolite 300 glued joint

10'-6⅞"

PLAN

14 No. jig holding down screws (3"-12) at random centres

Jig profile cut from 10'-0"×8"×2" dressed Sitka Spruce timber

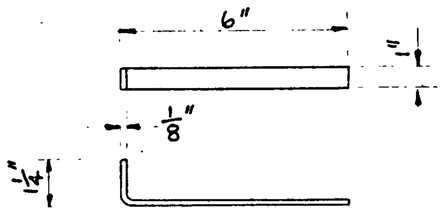

Detail of M.S. hook used for stretching rubber strips

FIG. 54 DETAILS OF JIG USED IN LAMINATING PROCESS FOR TIMBER DOME RIBS (MODEL)

SCALE:- Plan 1 in. to 1 ft.
Sections $\frac{1}{4}$ in. to 1 in.

F.A.A. Ph.D. Thesis
10th Feb., 1970

Structural Engineering Division
Department of Civil Engineering
University of Newcastle upon Tyne

PLATE 5 - MODEL DOME RIB LAMINATING PROCESS -
LAMINATES READY FOR GLUE APPLICATION

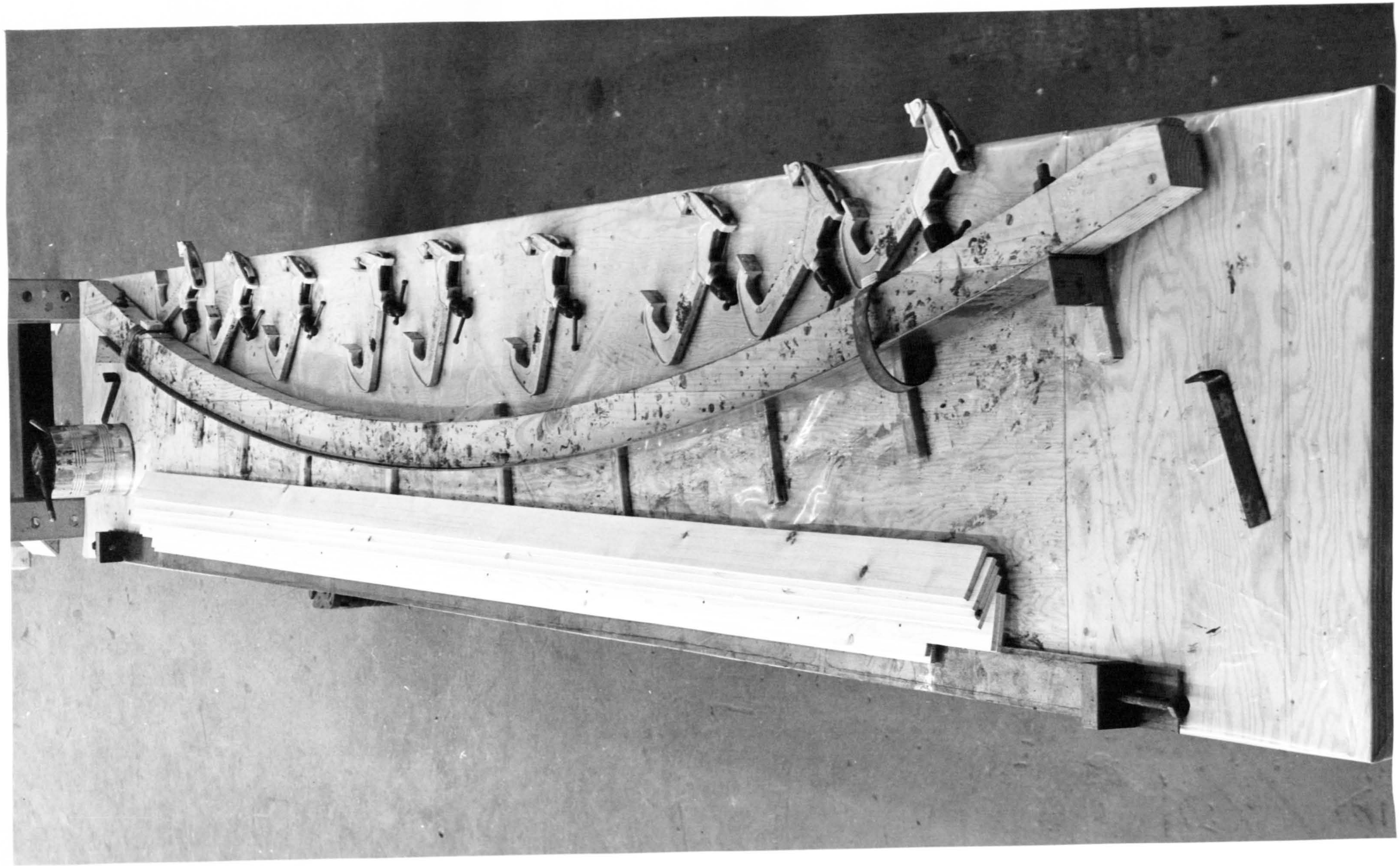

PLATE 6 - MODEL DOME RIB LAMINATING PROCESS -

GLUE BEING APPLIED TO LAMINATES



PLATE 7 - MODEL DOME RIB LAMINATING PROCESS - LAMINATES GLUED AND CLAMPED IN JIG

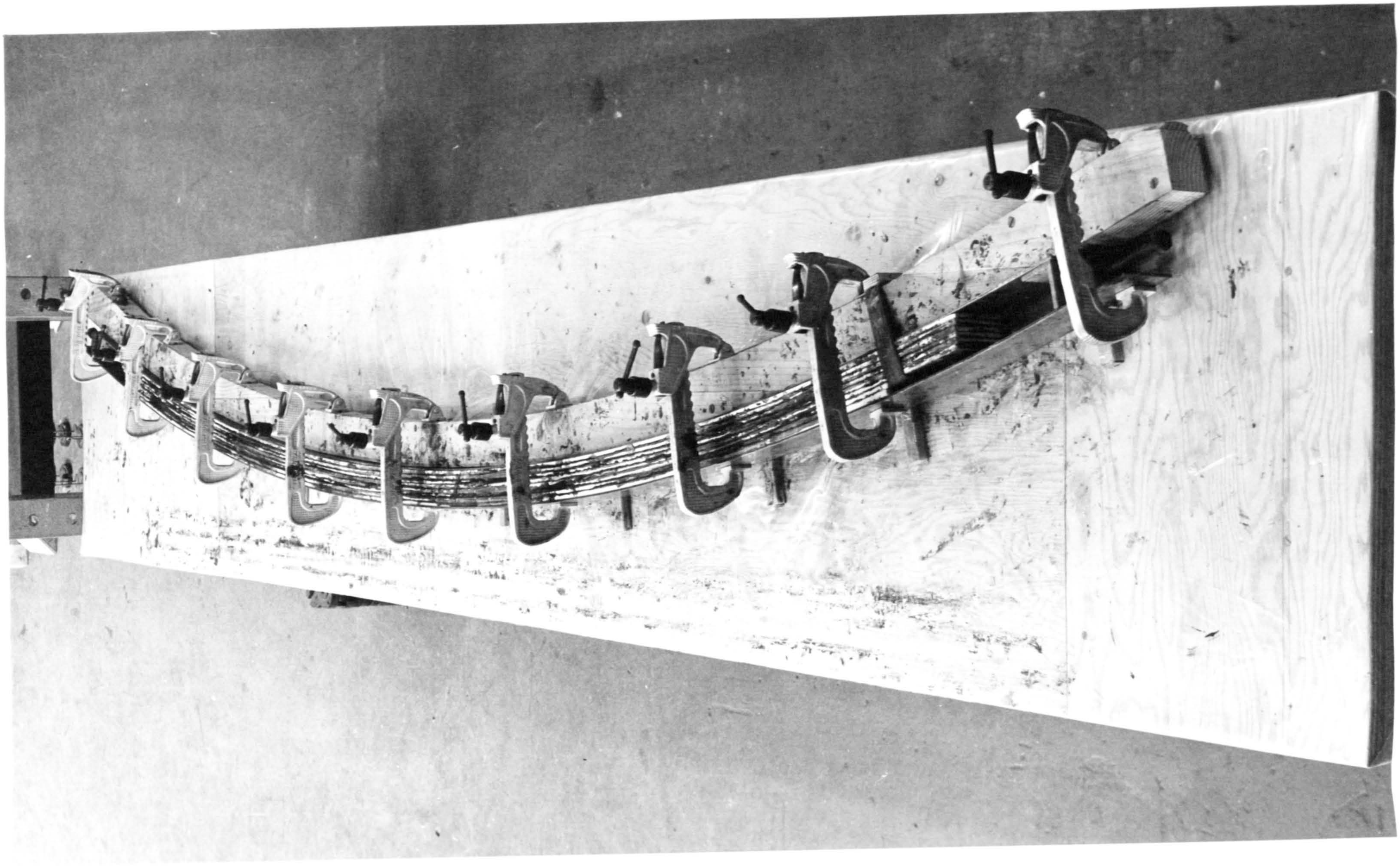

PLATE 8 - MODEL DOME RIB LAMINATING PROCESS - CURVED RIB BLOCKS REMOVED FROM JIG

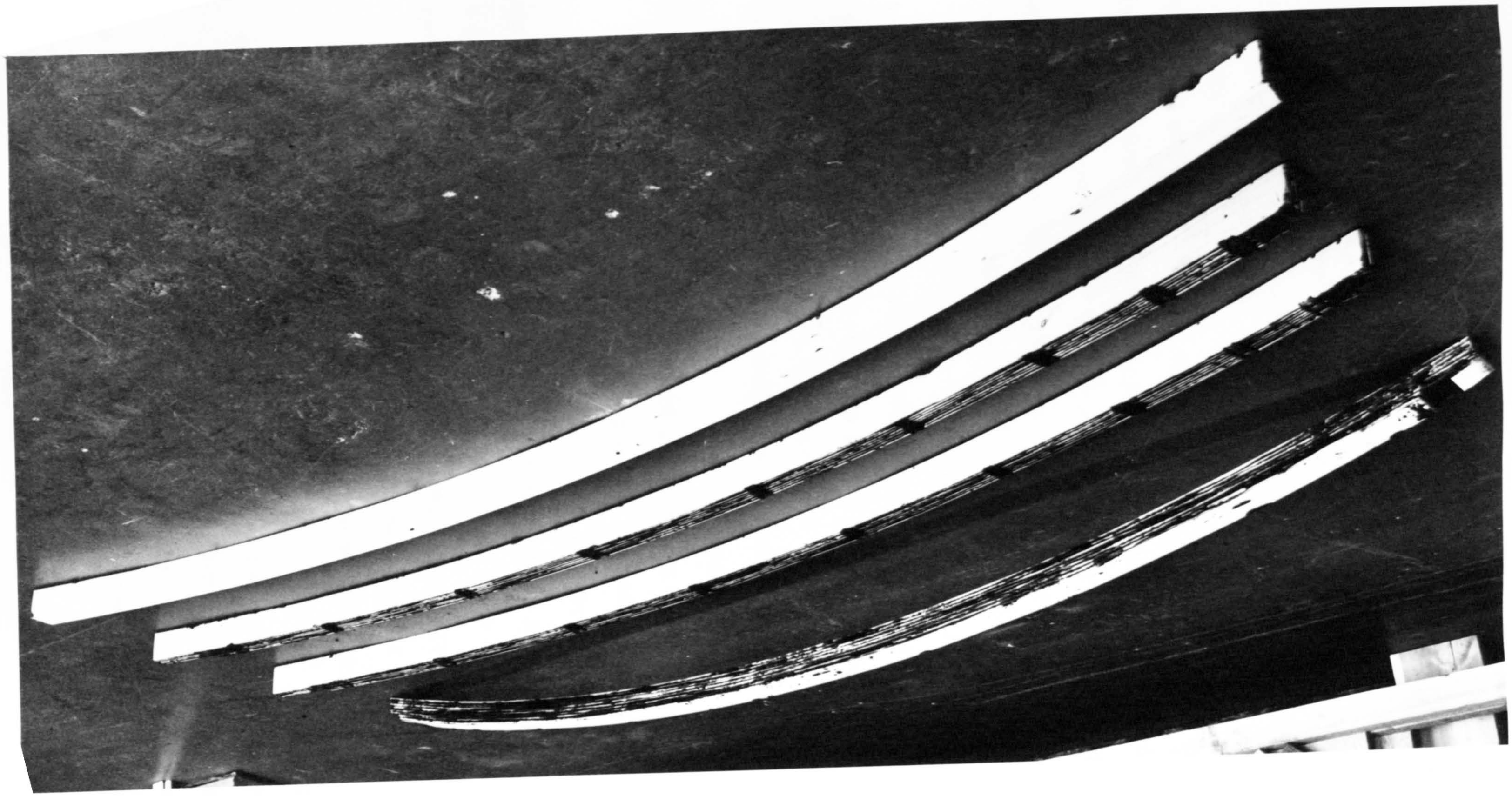

For each block formed, a sample of glue was retained and recordings of loss in weight with time were made at regular intervals. Since the adhesive was gap-filling, it was thought necessary to make this observation to see what changes, if any, took place in the glue line thickness.

The finished blocks of laminates can be seen in Plate 8 after they had been removed from the jig. Each block was cut into four sections slightly thicker than $\frac{1}{2}$ in. These sections were then cleaned up, planed both sides and cut to length to give ribs $\frac{1}{2}$ in. wide with a constant depth of approximately 2 in. along their length. Some of the ribs were tested in this condition before tapering to the finished shape. Plate 9 shows the finished tapered ribs erected on the base ring and Dwg. Ph.D. Thesis No. 11 gives the complete details of the model radial ribbed dome.

To obtain the correct tapered shape for all the 36 ribs employed in the dome, a template was needed. It was cut from 13 ply sanded Finnish Birch plywood and marked out according to the dimensions and radii shown in Dwg. Ph.D. Thesis No. 11. The marking was carried out on the floor of the laboratory using two 10 ft. lengths of Dexion angle, joined together, for a radius arm. Three radius centres were employed and these were set out, at the correct dimensions, on a $7\frac{1}{4}$ in. by 16 in. by 2 in. block of timber which was bolted to the laboratory floor. Holes were drilled in the timber block in the positions of the radii centres to allow a $\frac{3}{8}$ in. diameter bolt to be used as the central pivot.

After the template had been cut, sanded and all centre lines marked on, it was used as a profile for the actual laminated ribs. The correct shape was drawn on each laminated rib along with the centre lines and purlin positions. Each rib was then cut out by a jig saw and then sanded to give the final finish. Two coats of polyurethane

PLATE 9 - MODEL DOME - FINISHED RIBS ERECTED ON BASE RING


TEST IN PROG
PLEASE

resin were applied to all the ribs for protection, to maintain a constant moisture content and to improve the finish.

To facilitate the connection of purlins to the ribs, the template was first drilled at the correct positions for the fixing bolts. Drill guides, made from $\frac{1}{2}$ in. by 1 in. by $\frac{1}{8}$ in. case-hardened steel, were then screwed to the template over the holes and all the laminated ribs were drilled from the template. A drill guide is shown in Plate 13, E, and the drilling layout is illustrated in Plate 10.

(c) Fabrication of Base and Crown Connectors

The details of the bases and crown connectors provided for the model dome radial ribs are contained in Dwg. Ph.D. Thesis No. 11. In Plate 11, some of the connections can be seen together with the jigs which were employed in the machining and drilling of these components.

Two blocks of aluminium were employed as a foundation for each radial rib. One block was simply a rectangle $1\frac{1}{2}$ in. by 2 in. by $\frac{1}{2}$ in. thick which raised the level of the dome by $\frac{1}{2}$ in. all round to enable the displacement testing apparatus, discussed in Arts. 10.4 (a) and (b), to be incorporated in the system. The actual base block for the rib was cut from a bar of 1 in. by 1 in. aluminium and required shaping, machining and drilling. Jig 1, Plate 11, shows two shaped base blocks in position for drilling. The holes were $\frac{1}{4}$ in. diameter and the one drilled at an angle to the base was tapped to take $\frac{1}{4}$ in. Whitworth threads. Holes, $\frac{1}{4}$ in. in diameter, were also drilled in the larger $\frac{1}{2}$ in. thick pieces of aluminium so that these blocks and the shaped blocks could be fastened together by screwing into the plywood supporting ring. Jig 2 in Plate 11, was employed to hold the aluminium blocks for shaping and machining.

Aluminium U-shaped pieces were fastened to the shaped base blocks by means of $\frac{1}{4}$ in. Whitworth bolts with countersunk heads, Plate 11,

PLATE 10 - DRILLING OF MODEL DOME RIB PURLIN CONNECTION BOLT HOLES FROM PLYWOOD TEMPLATE



PLATE 11 - MODEL DOME BASES AND CROWN CONNECTOR WITH FABRICATION JIGS

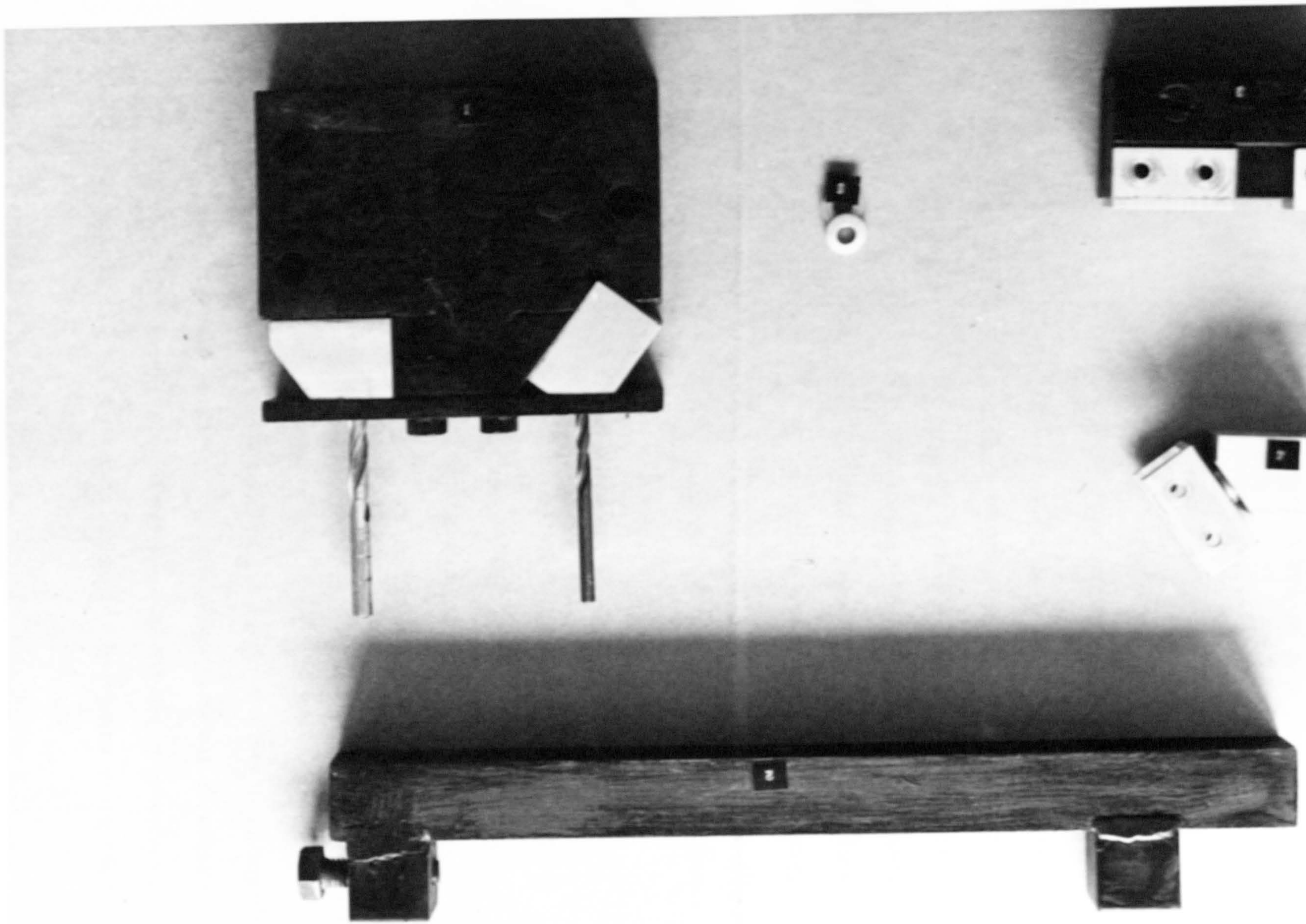

item 4. A chamfered aluminium washer, Plate 11, item 5, was placed between each U-piece and the shaped base block to provide a hinged action at the dome supports. The U-pieces were all drilled so that the ribs could be fastened in position by means of 2BA bolts.

Similar end pieces to those used at each base were provided at the apices of the radial ribs. The U-pieces were again cut from aluminium preformed strip and drilled for 2BA rib connection bolts. Attachment to the steel apex ring was made by $\frac{1}{4}$ in. Whitworth bolts with countersunk heads. Plate 11, jig 3, has base and crown connection U-pieces in position ready for drilling.

(d) Apex Ring Fabrication

To form the apex ring for the model dome, a strip of steel 1 in. wide by $\frac{1}{8}$ in. thick was shaped into a circle with an outside diameter of 24 in. In order to obtain a true circular form, a plywood disc was first cut to the correct radius and then employed as a template in the shaping process. The ends of the ring were scarf joined and brazed together. Holes were then drilled, at intervals of 10°, around the circumference of the ring to allow the radial ribs to be connected by means of $\frac{1}{4}$ in. Whitworth bolts. A photograph of the model dome steel apex ring is included in this thesis as Plate 12.

(e) Horizontal Purlin Ring Construction

The purlins for the model dome were cut from $\frac{1}{2}$ in. by $\frac{1}{2}$ in. strips of Ramin. For the cutting, trimming and drilling of the purlins, three jigs were employed and these are shown in Plate 13.

Since the span of the purlins, between adjacent radial ribs, varied for each horizontal ring, an adjustable jig was required for cutting the correct lengths. This is the large jig, A, at the bottom of Plate 13. The ends of each purlin needed cutting at an angle of 5° and therefore two tenon-saw guides of aluminium angle were mounted on a rectangular piece of plywood. By means of a stop, which could be

PLATE 12 - MODEL DOME APEX RING

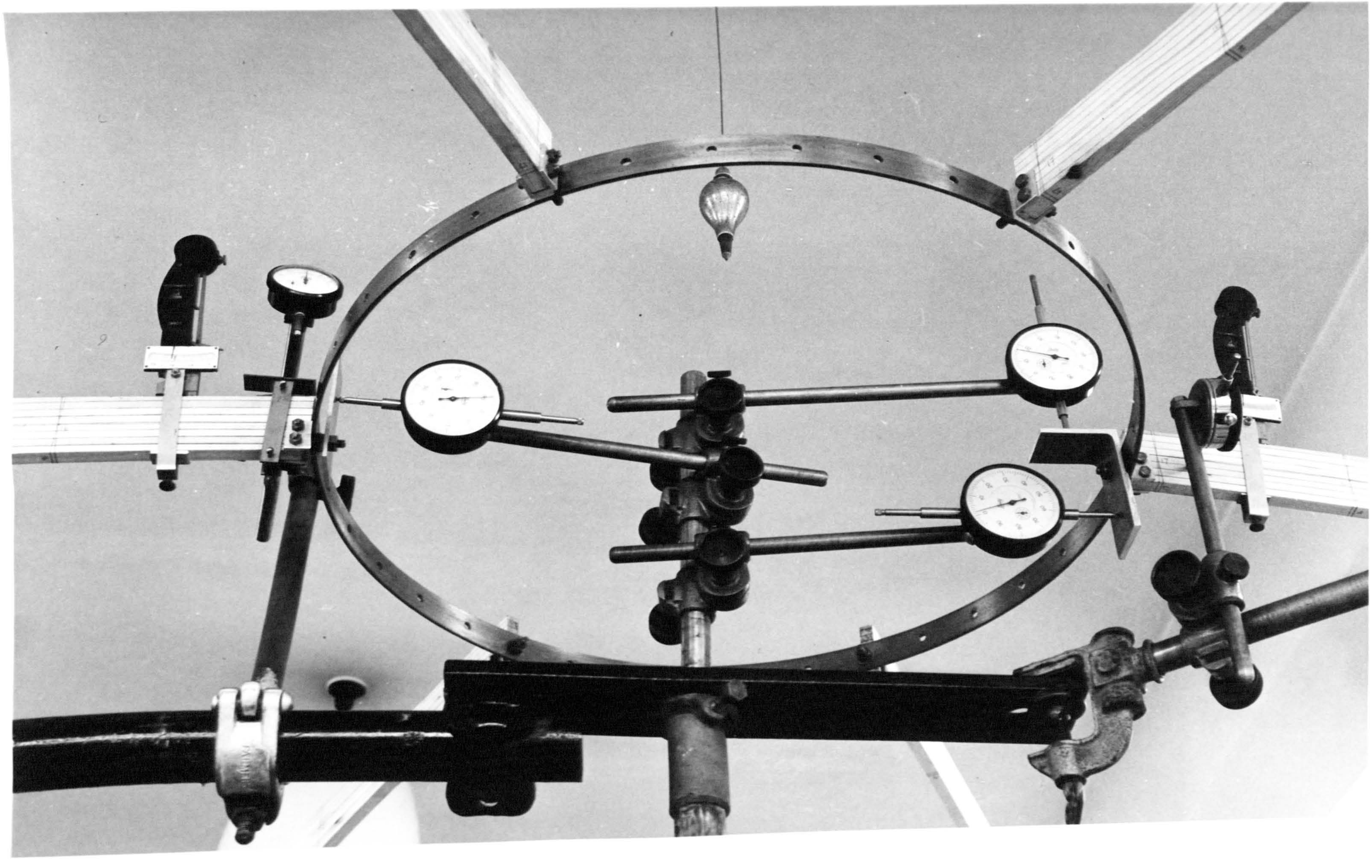

PLATE 13 - MODEL DOME PURLIN JIGS A, B AND C, LOAD HANGERS D AND PLYWOOD RIB TEMPLATE DRILL GUIDE E

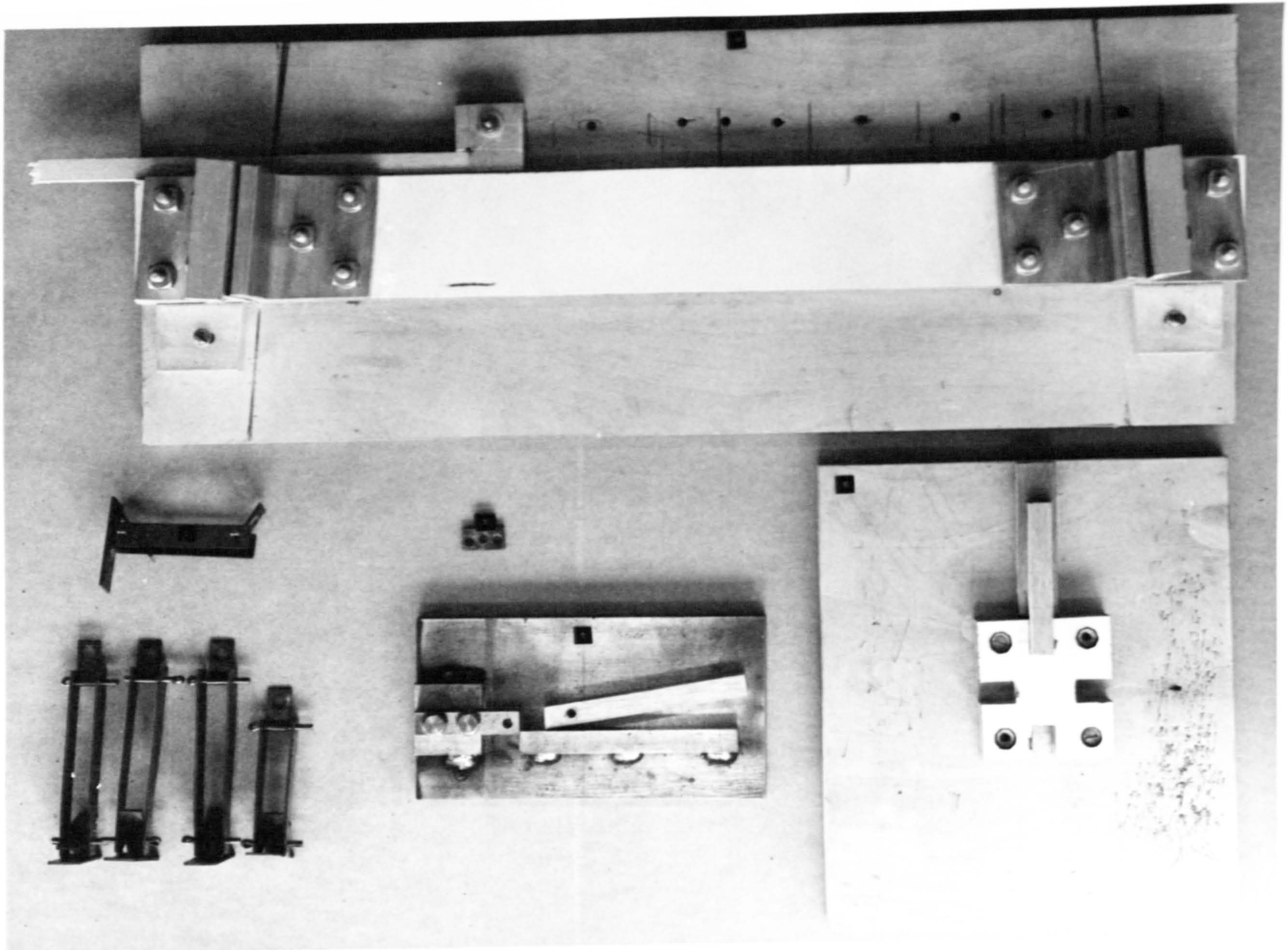

adjusted to various positions between the two saw guides, the purlins could be cut off with the right end shape and correct length in one operation.

The purlins were not only cut at an angle of 5° at each end, they were also rebated to allow adjacent purlins to butt together at the rib joint. Details of the purlin connections are given in Dwg. Ph.D. Thesis No. 11. To form the rebates, additional pieces of aluminium could be added to the saw guides of jig A, Plate 13, to allow controlled depth cuts to be made in the purlins, at right angles to their lengths, close to the ends. The necessary short length cuts, parallel to the purlin lengths, were made by a chisel with jig B, in the top left hand corner of Plate 13, for guidance.

For the connection of the purlins to the radial ribs, 2BA bolts were employed together with Meccano angle brackets. Drilling of the purlins for the bolts was carried out in jig C, top centre in Plate 13.

The fitting of the complete horizontal purlin rings to the primary radial rib system posed a special problem. Even though the purlins were all cut in the same jigs, very small errors in longitudinal dimensions were liable to build up around the rings as the purlins were systematically added. Two techniques were employed to help eradicate this problem. The first consisted of employing a ring, at mid-span of the ribs approximately, comprising of stiff wire purlins which could be slotted into the bolt holes of the Meccano brackets. In this way the ribs were correctly spaced and held in position to allow the timber purlins to be fitted. The other technique consisted of using the Meccano angle brackets in such a way that the elongated bolt hole legs were adjacent to the purlins. All the purlins could then be fitted without tightening the nuts on the bolts and small adjustments could be made, due to the elongated bolt holes, before final tightening took place. A photograph of the model dome with all

36 ribs erected on the base ring, together with alternate horizontal purlin rings, can be seen in Plate 14.

(f) Diagonal Bracing Attachment

The mild steel diagonal bracing rods, required in a normal radial ribbed dome, were to be represented in the model by lengths of wire. Although the author's research project did not advance to the diagonal bracing stage, provision was made for the addition of the wire bracing at a later date.

The sizes of the prototype dome mild steel rods are given in Dwg. Ph.D. Thesis No. 9. At 1/14 scale for the cross-section, wire bracing of approximately 1/16 in. in diameter would be required. Attachment to the radial ribs can be made at the purlin joints where the fixing bolts have been allowed to protrude in order to facilitate this arrangement. The bolts, to which the diagonal wire bracing can be attached, can be seen protruding from each end of the purlins in Plate 14.

10.3 TESTING OF THE MODEL DOME CONSTRUCTION MATERIALS

(a) Radial Rib Timber

The radial ribs in the model dome were constructed from laminates of European Redwood. In normal design procedures for prototype structures of this type, working stress values and moduli of elasticity are obtained from CP 112 : 1967[31] and the necessary strength and deformation calculations are made using these. However the working stresses and elasticity moduli are obtained from basic stress values which are representative of a species of timber in general and the author was of the opinion that such values would not be sufficiently accurate for estimating the stress distribution in, and deformation of, his model dome under load. A series of tests were therefore carried out, according to B.S. 373 : 1957,[46] on small clear specimens of the timber which was employed in the manufacture of the model dome ribs.

Figure Nos. 1 - 43, in Appendix I, contain the results of the rib

PLATE 14 - MODEL DOME - RIBS AND PURLINS

IN POSITION

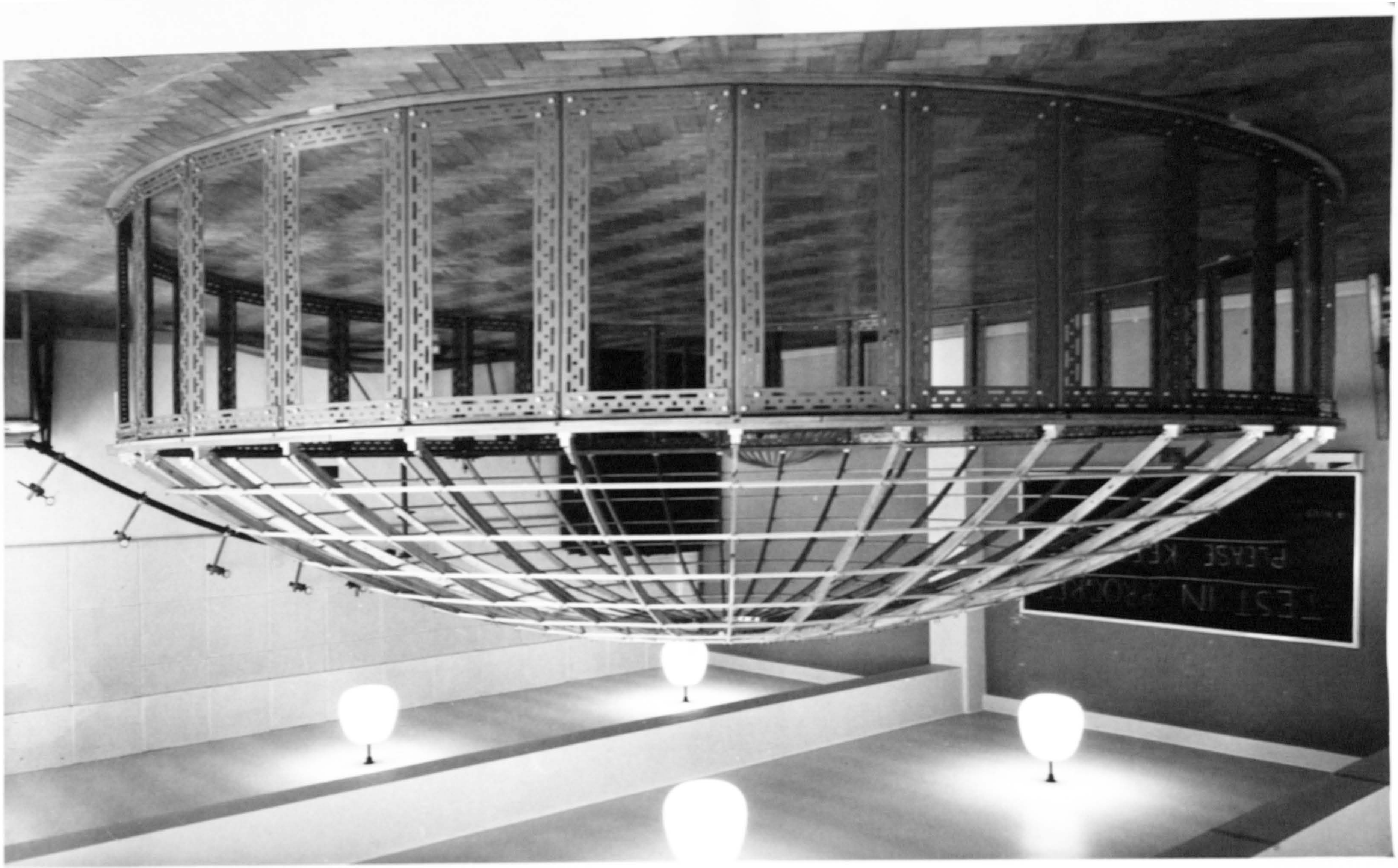

timber tests. Apart from the moisture content and specific gravity determinations, which only required a balance for weighing and an oven for drying, three sets of load testing apparatus were required. Those are shown in Plates 15, 16 and 17.

Plate 15 is a photograph of the Tensometer testing apparatus which was employed in the rib timber testing. Static bending tests, Plate 18, shear parallel to grain tests, Plate 19, tension parallel to grain tests, Plate 20, and compression perpendicular to grain tests, Plate 21, were carried out using this apparatus. Four 2 in. standard specimens were employed in the compression perpendicular to grain tests. In all the other tests carried out on the Tensometer apparatus, 2 cm standard specimens were employed and a total of six specimens were used in each type of test. The broken 2 cm standard static bending test specimens can be seen in Plate 22, the values of the rupture loads being marked on them. Plate 23 is a photograph of the shear parallel to grain and tension parallel to grain test specimens after failure had occurred. Again the failure loads are clearly visible. The compression perpendicular to grain test specimens are shown, along with their load carrying capacities, in Plate 24.

Static bending tests were also carried out on 2 in. standard beams in the load testing apparatus illustrated in Plate 16. Tests were performed on a total of four beams, two out of the four being of a laminated form. The 2 in. standard laminated beams were of a similar depth to the maximum depth employed in the model radial ribbed dome ribs and were composed of the same number of $\frac{1}{4}$ in. thick laminates. They therefore provided a comparison between the rib material and the non-laminated timber. Plate 22 shows the laminated and non-laminated beams with their rupture loads.

Compression parallel to grain tests were carried out on four 2 in. standard specimens using the Avery testing apparatus shown in Plate 17.

PLATE 15 - TENSOMETER TESTING APPARATUS

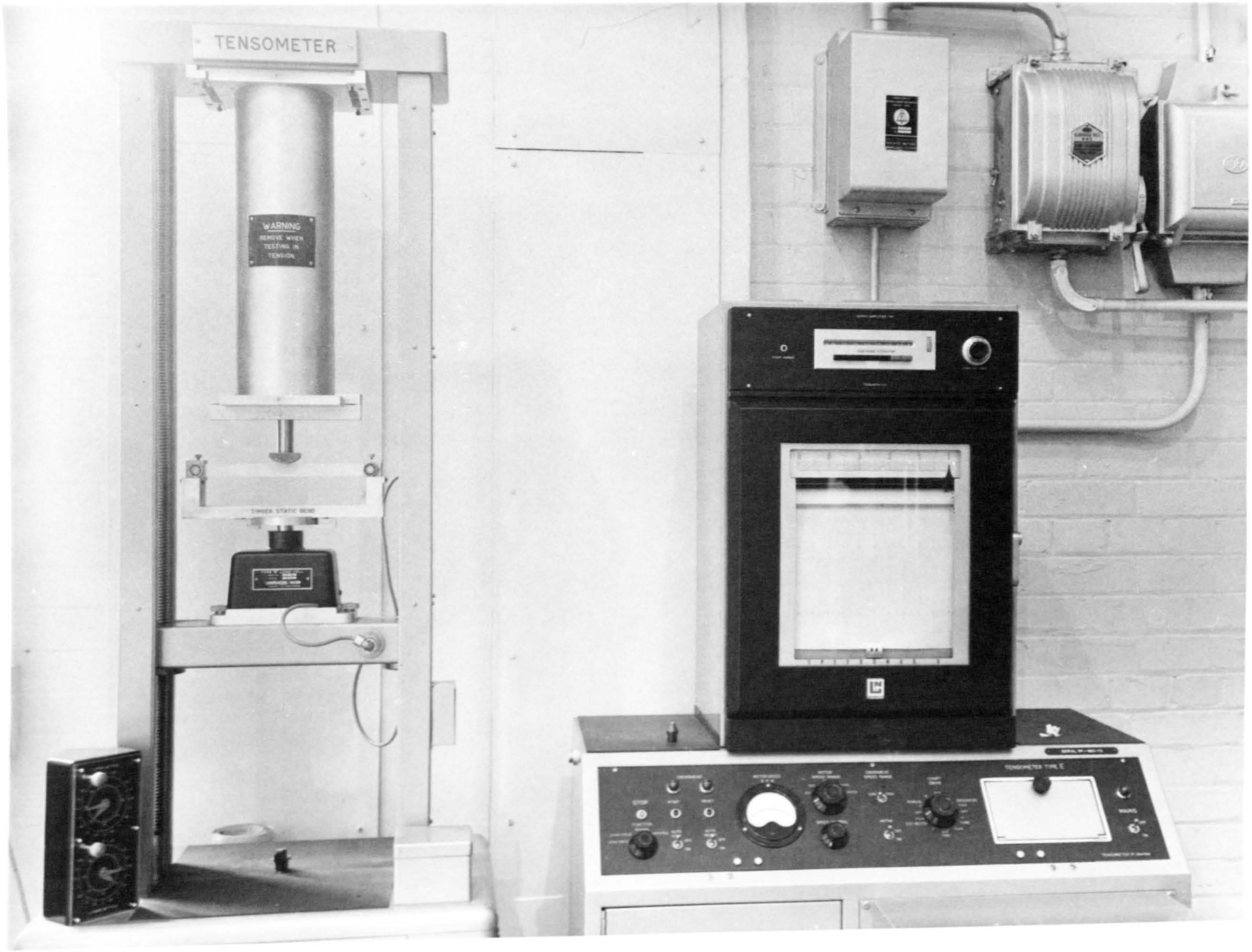
TENSOMETER
WARNING
REMOVE WHEN
TESTING IN
TENSION

PLATE 16 - 2 in. STANDARD BEAM TESTING APPARATUS

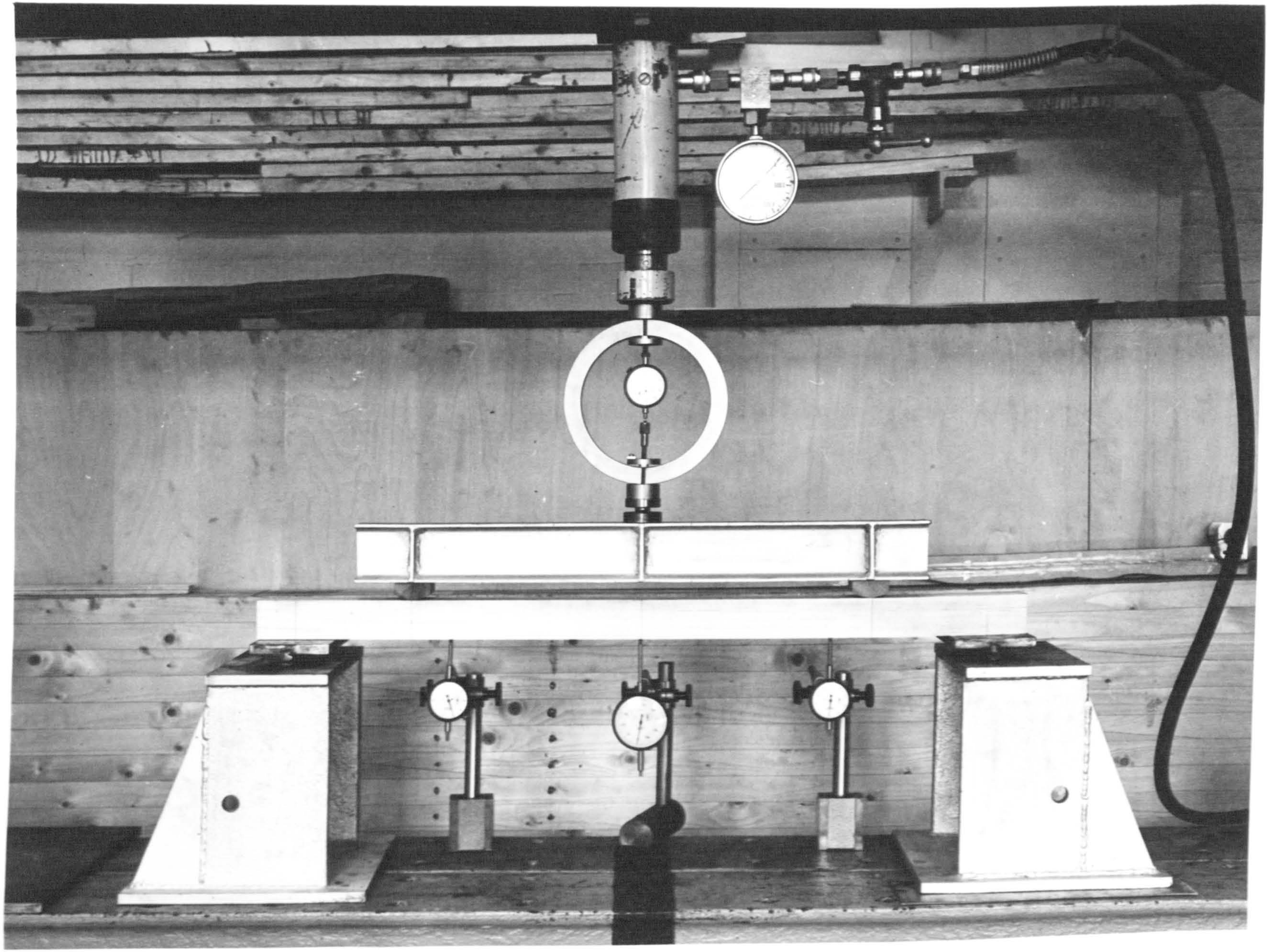

PLATE 17 - AVERY COMPRESSION TESTING APPARATUS WITH 2 in. STANDARD COMPRESSION PARALLEL TO GRAIN TEST SPECIMEN

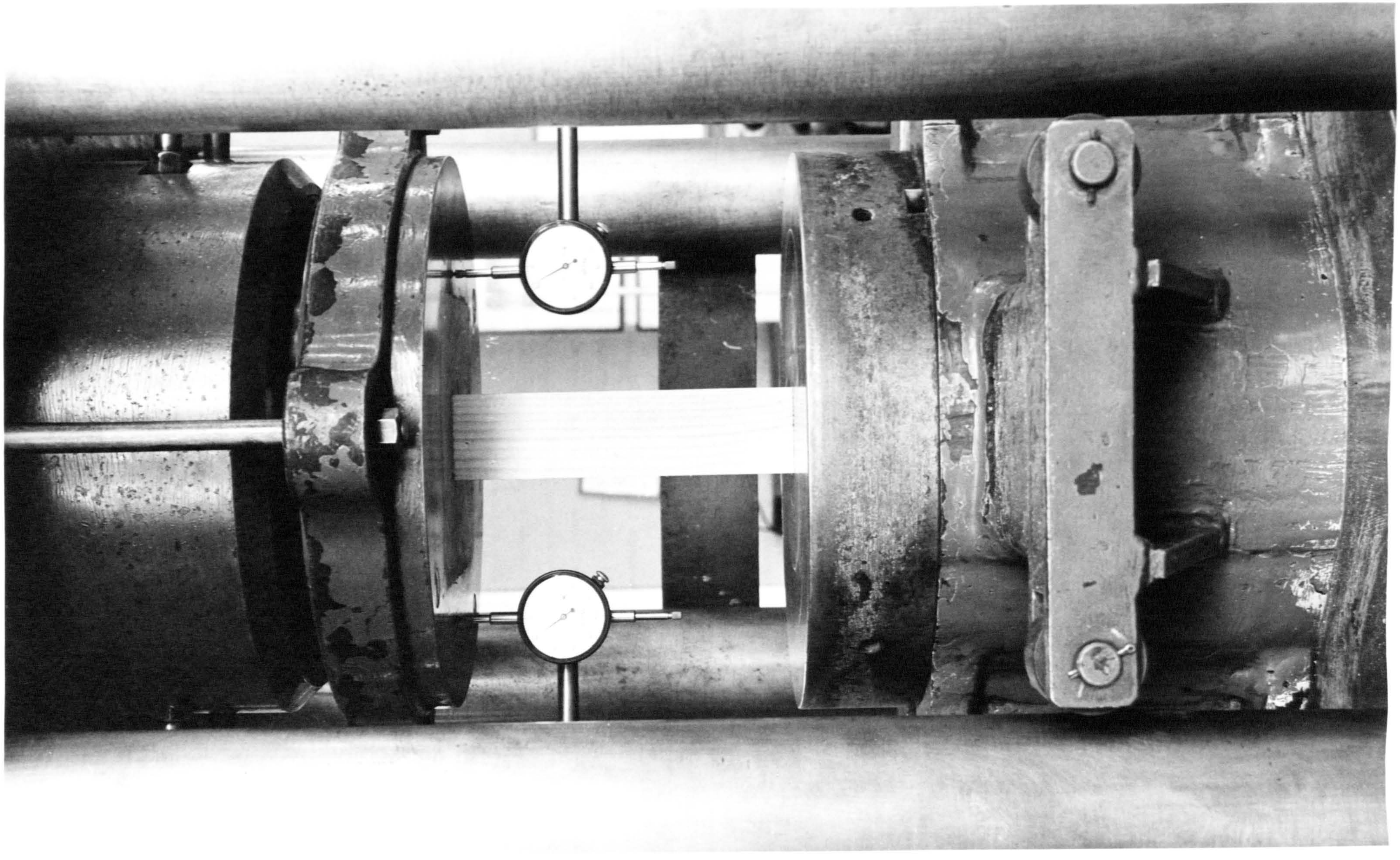

PLATE 18 - 2 cm STANDARD STATIC BENDING TEST TO B.S. 373 : 1957 IN TENSOMETER APPARATUS

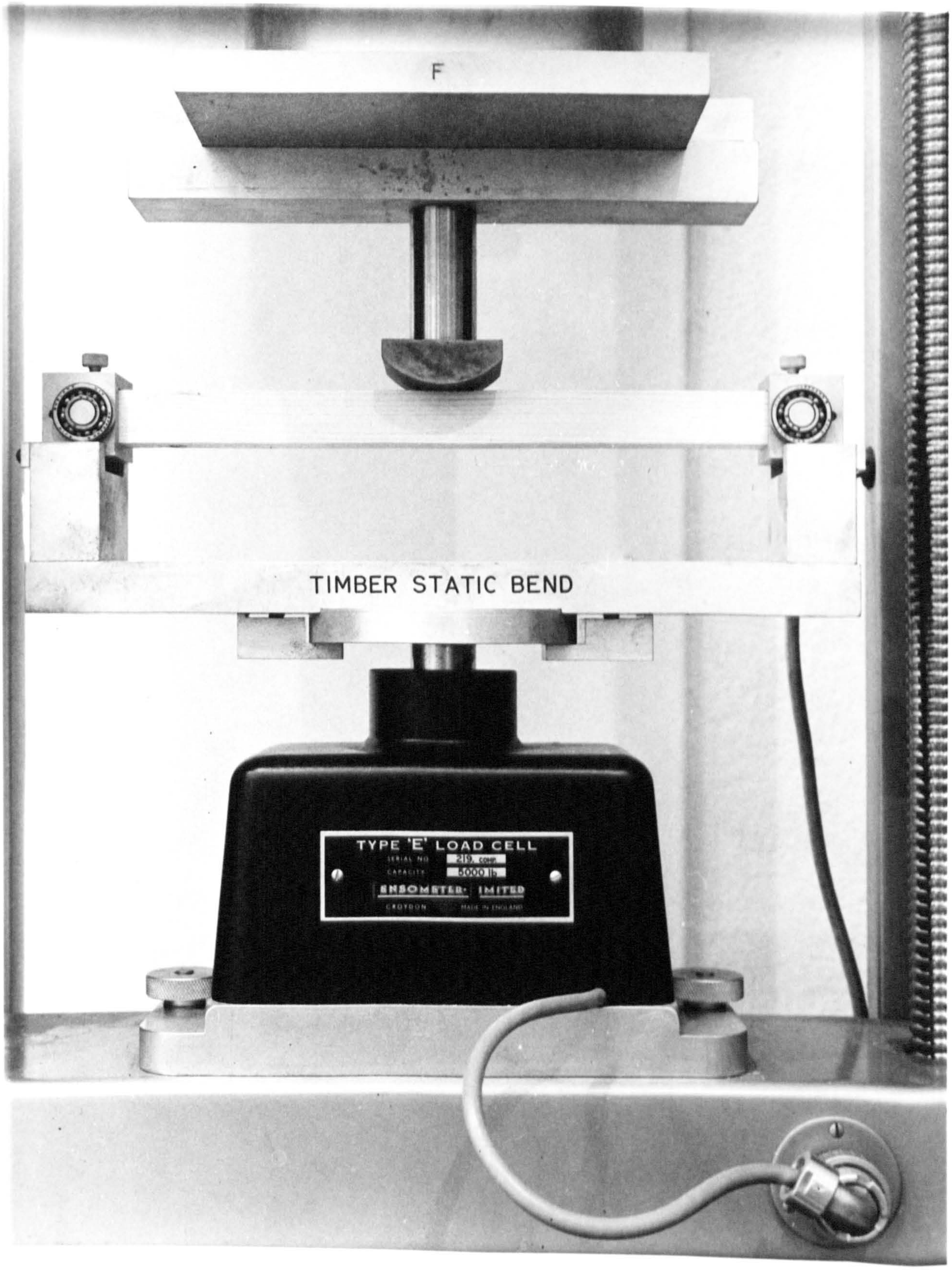
F
TIMBER STATIC BEND
TYPE 'E' LOAD CELL
SERIAL NO 219 comp
CAPACITY 5000 lb
ENSOMETER LIMITED
CROYDON MADE IN ENGLAND

PLATE 19 - 2 cm STANDARD SHEAR PARALLEL TO GRAIN TEST TO B.S. 373 : 1957 IN TENSOMETER APPARATUS


F
TYPE 'E' LOAD CELL
SERIAL NO 219. COMP.
CAPACITY 5000 lb
ENSOMETER· LIMITED
CROYDON
MADE IN ENGLAND

PLATE 20 - TENSION PARALLEL TO GRAIN TEST TO B.S. 373 : 1957 IN TENSOMETER APPARATUS

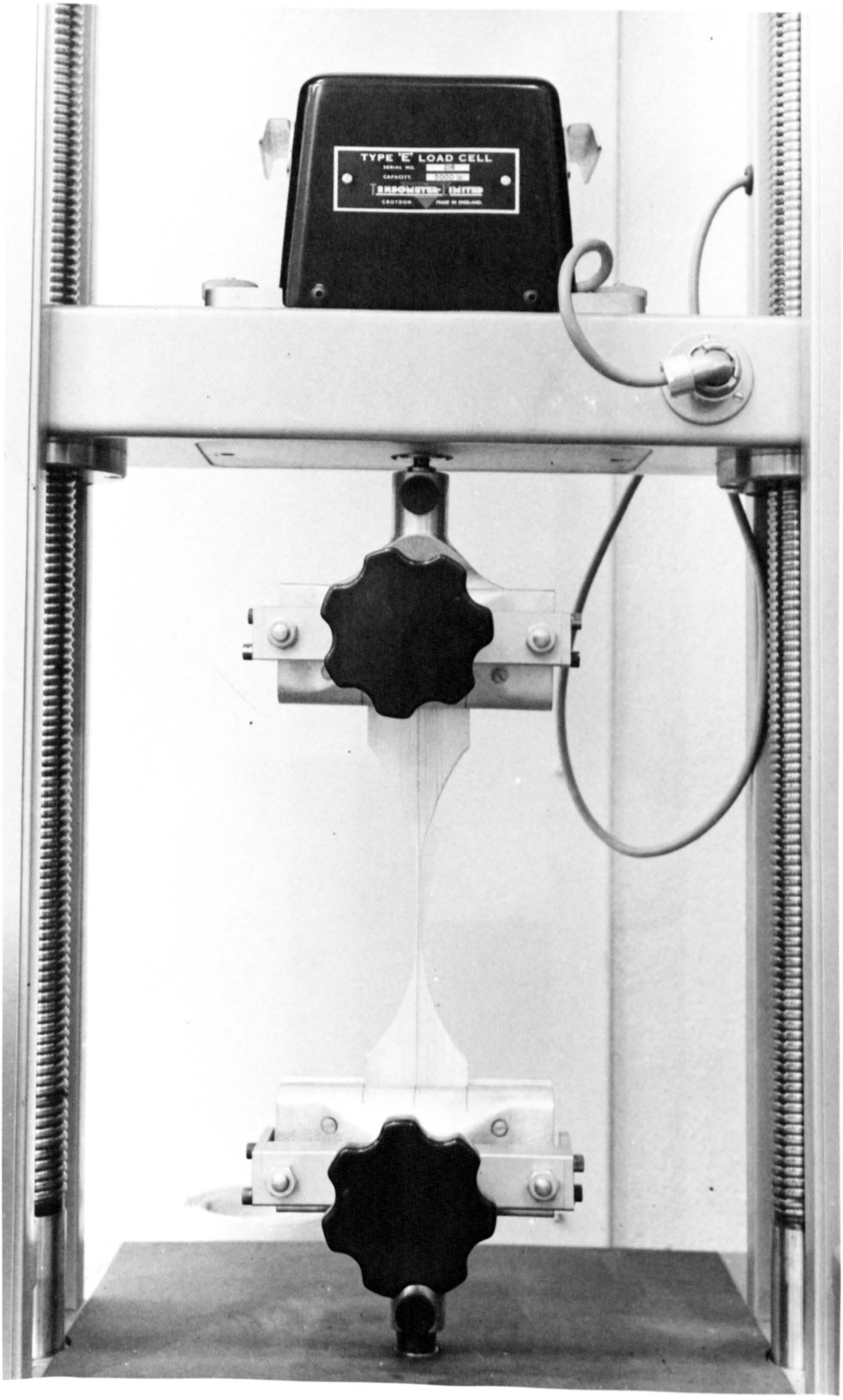
TYPE 'E' LOAD CELL
SERIAL NO.
CAPACITY
CROYDON

PLATE 21 - 2 in. STANDARD COMPRESSION PERPENDICULAR TO GRAIN TEST TO B.S. 373 : 1957 IN TENSOMETER APPARATUS


F
TYPE 'E' LOAD CELL
SERIAL NO 219 COMP
CAPACITY 5000 lb
ENSOMETER LIMITED
CROYDON
MADE IN ENGLAND

PLATE 22 - 2 cm AND 2 in. STANDARD STATIC BENDING TEST SPECIMENS (EUROPEAN REDWOOD)

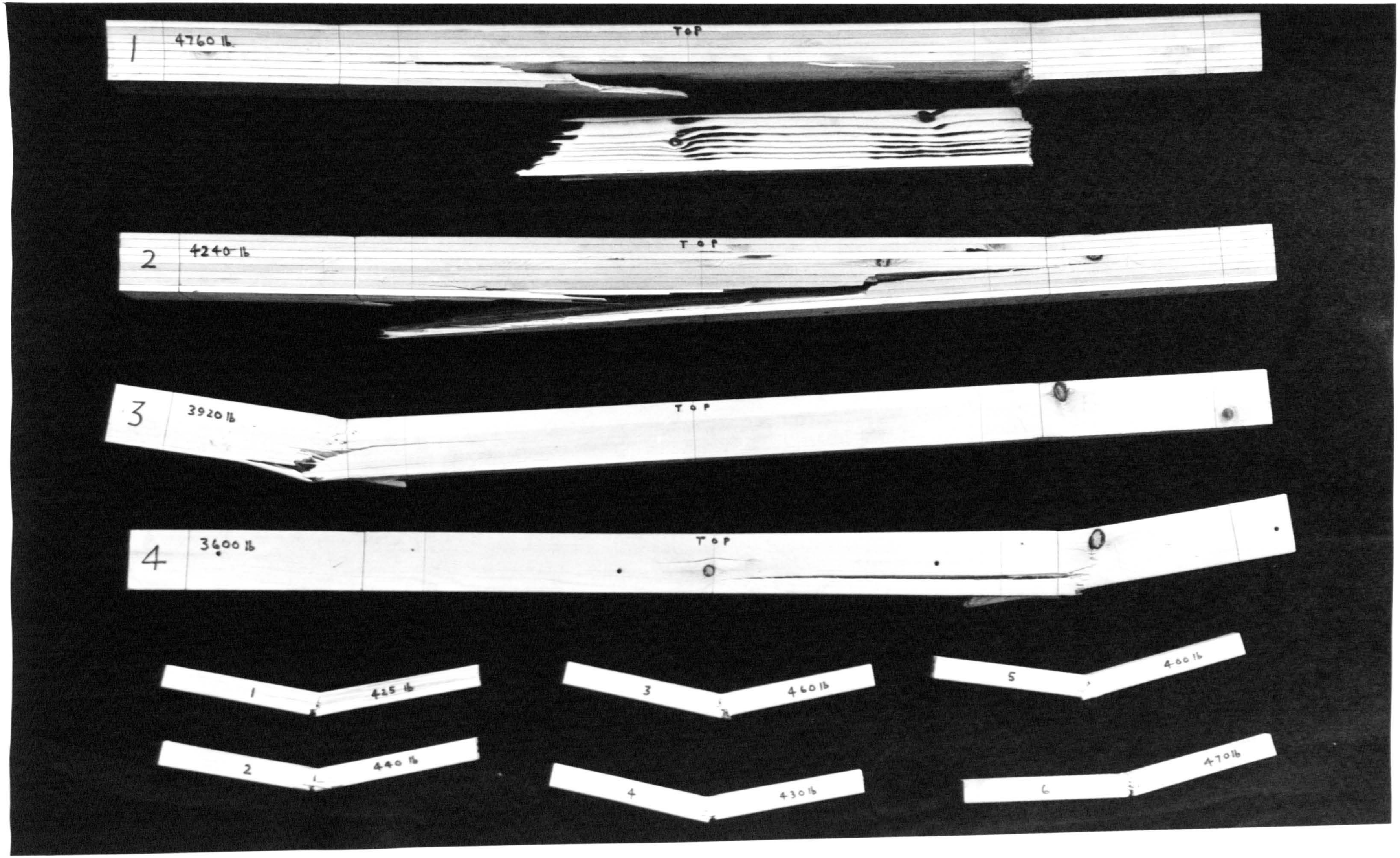
1
4760 lb
TOP
2
4240 lb
TOP
3
3920 lb
TOP
4
3600 lb
TOP
1
425 lb
2
440 lb
3
460 lb
4
430 lb
5
400 lb
6
470 lb

PLATE 23 - 2 cm STANDARD SHEAR PARALLEL TO GRAIN AND TENSION PARALLEL TO GRAIN SPECIMENS (EUROPEAN REDWOOD)

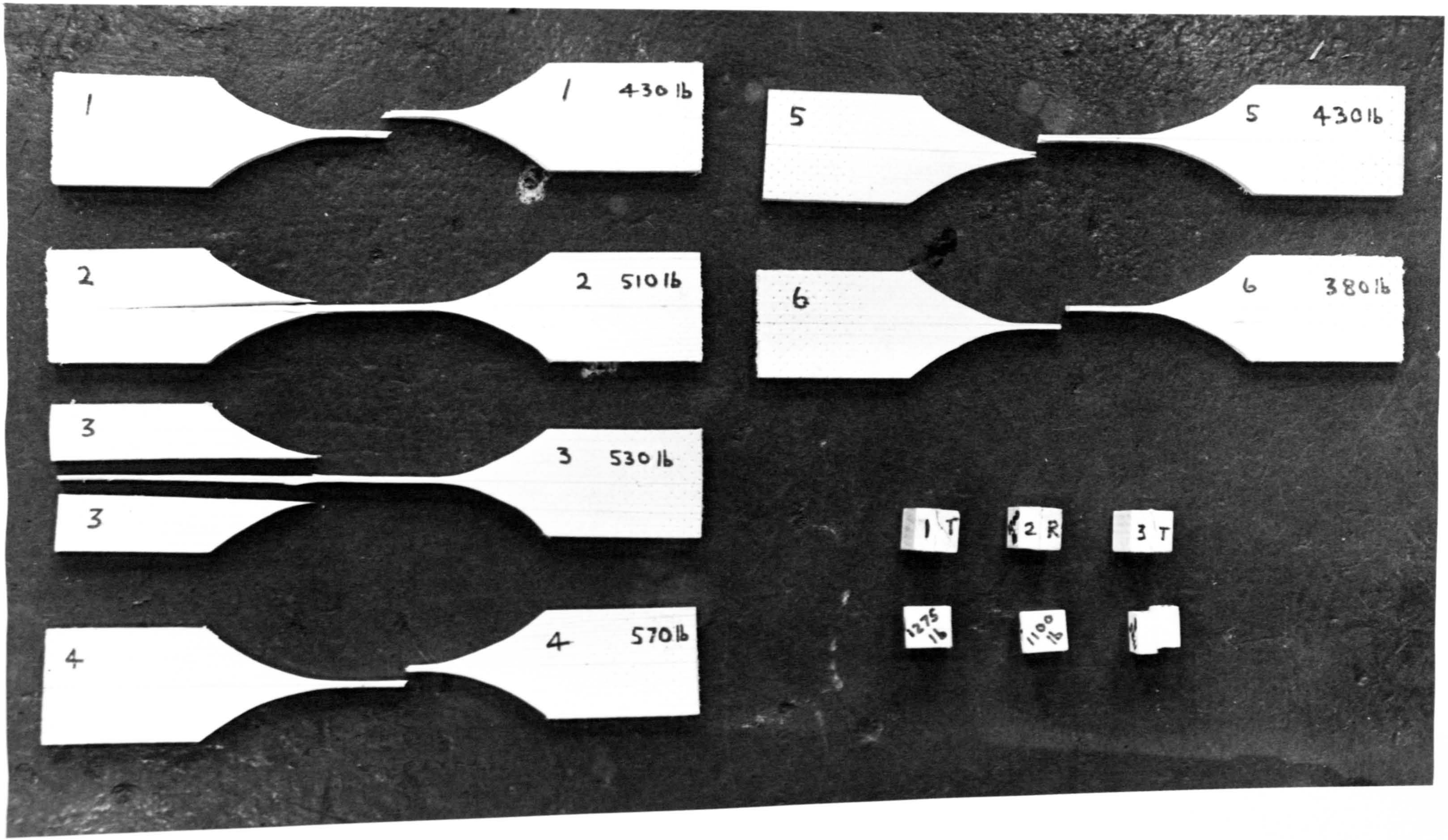
1
1 4301b
2
2 5101b
3
3 5301b
3
4
4 5701b
5
5 4301b
6
6 3801b
1 T
2 R
3 T
1275 lb
1100 lb

PLATE 24 - 2 in. STANDARD COMPRESSION PARALLEL TO GRAIN AND COMPRESSION PERPENDICULAR TO GRAIN SPECIMENS (EUROPEAN REDWOOD)

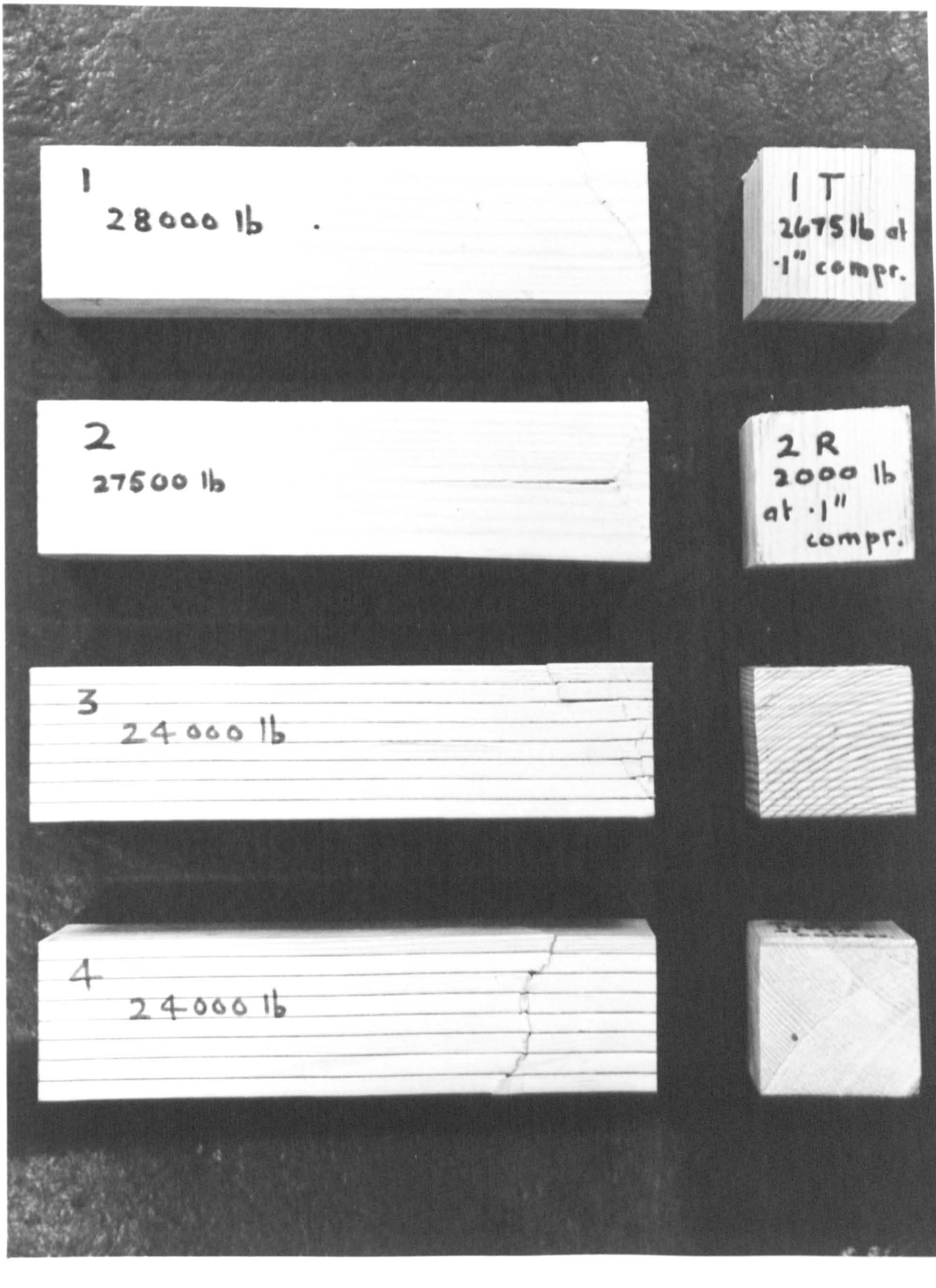
1
28000 lb
1 T
26751b at
·1" compr.
2
27500 lb
2 R
2000 lb
at ·1"
compr.
3
24000 lb
4
24000 lb

Again two specimens employed in these tests were of the laminated form and all four specimens can be seen in Plate 24 along with the loads obtained at failure.

(b) Adhesive Employed in Radial Rib Laminating Process

For each block of radial ribs formed, see Plate 8, a sample of the Aerodux 185 adhesive, mixed with HRP. 155 hardener, was retained. The samples were weighed in the liquid form and subsequent weighings were carried out over a period of 21 months. These readings are tabulated in Figure Nos. 44(a) and (b) in Appendix I. Graphs have been drawn of loss in weight with time of the adhesive and are contained in Figure No. 45 of Appendix I.

10.4 TESTING OF THE MODEL DOME

(a) Direct and Indirect Test Methods

Having constructed a model dome, from a prototype, with due regard to the principles of similarity employed in model analysis, two main experimental approaches can be used:[10],[27],[47]

(1) Loads can be applied directly to the model and the resulting strains in the members can be measured by suitable mechanical, optical or electrical strain-measuring devices.

(2) Loads need not be applied directly to the model. Instead, displacements of known magnitude can be introduced and the corresponding deflections of the nodes can be measured.

The first method, the direct method, is very expensive in labour and material. A large amount of time is also required for reducing the strain measurements.

The second method, the indirect method based on Clerk Maxwell's reciprocal theorem, is a much simpler approach. Suppose that one support I, say, of a space structure is released and an arbitrary displacement Δ is imposed in the direction X so that no component displacements occur in the directions of the other mutually perpendicular

axes Y and Z. Then if node A of the structure is thereby displaced δ in a specified direction "n", it follows from Clerk-Maxwell's reciprocal theorem that a load W applied in the direction "n" at joint A will produce a reaction $-\frac{W\delta}{\Delta}$ in the X- direction at the support I. If, therefore, an elastically similar flexible model of the structure is made and if displacements are successively applied in three mutually perpendicular directions to a released support point, the resulting displacements of the nodes can be measured and influence coefficients of reactions can be calculated, from which, in simple structures, all the stresses can be determined. In more complex structures this will not be possible and loads in certain individual members must also be found experimentally.

(b) Application of Direct and Indirect Test Methods to Model Dome

The indirect method of testing was employed in the majority of the experimental work on the model radial ribbed dome. To displace the rib bases by known amounts in given directions, two pieces of apparatus were employed.

The first piece of apparatus was a horizontal deformeter, Figure 55 and Plate 25, which allowed the base to be displaced in a radial direction only. By turning the screw device, incorporated in this deformeter, the given displacement was applied in a series of small and equal amounts. At the same time, the vertical deflection of a node point on the radial rib was observed and graphs were plotted of horizontal base displacement against vertical node displacement. The slope of these straight line graphs gave the influence coefficients of horizontal force at the support for the various rib node points.

The second piece of apparatus, used in the indirect testing procedure of displacing the rib bases, was a vertical deformeter, Figure 56 and Plate 26. This piece of apparatus allowed the bases to be displaced vertically in a series of known amounts. By plotting the

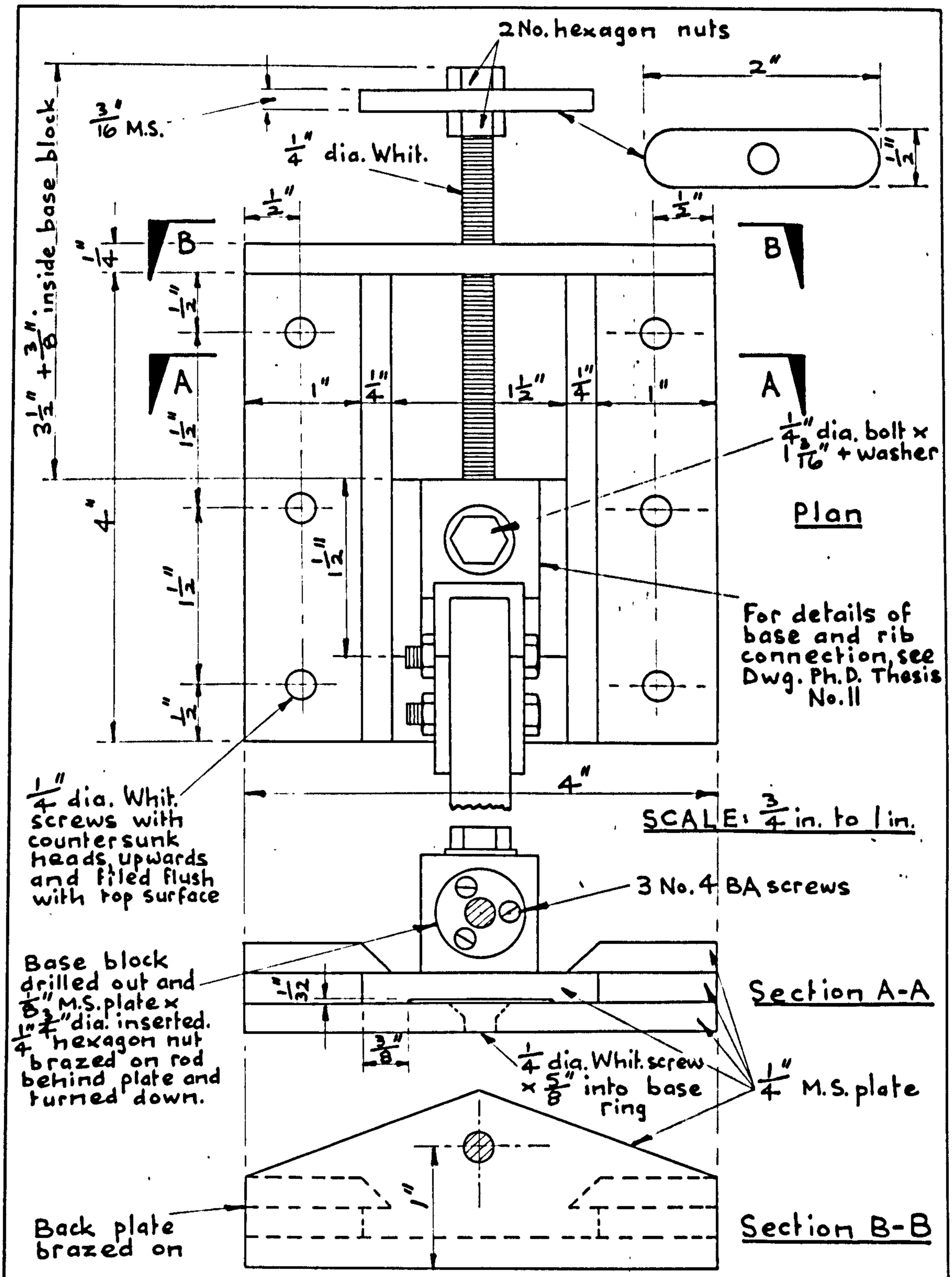

FIG. 55 BASE HORIZONTAL DEFORMETER

F. A. A. Ph.D. Thesis
3rd March, 1970

Structural Engineering Division
Department of Civil Engineering
University of Newcastle upon Tyne

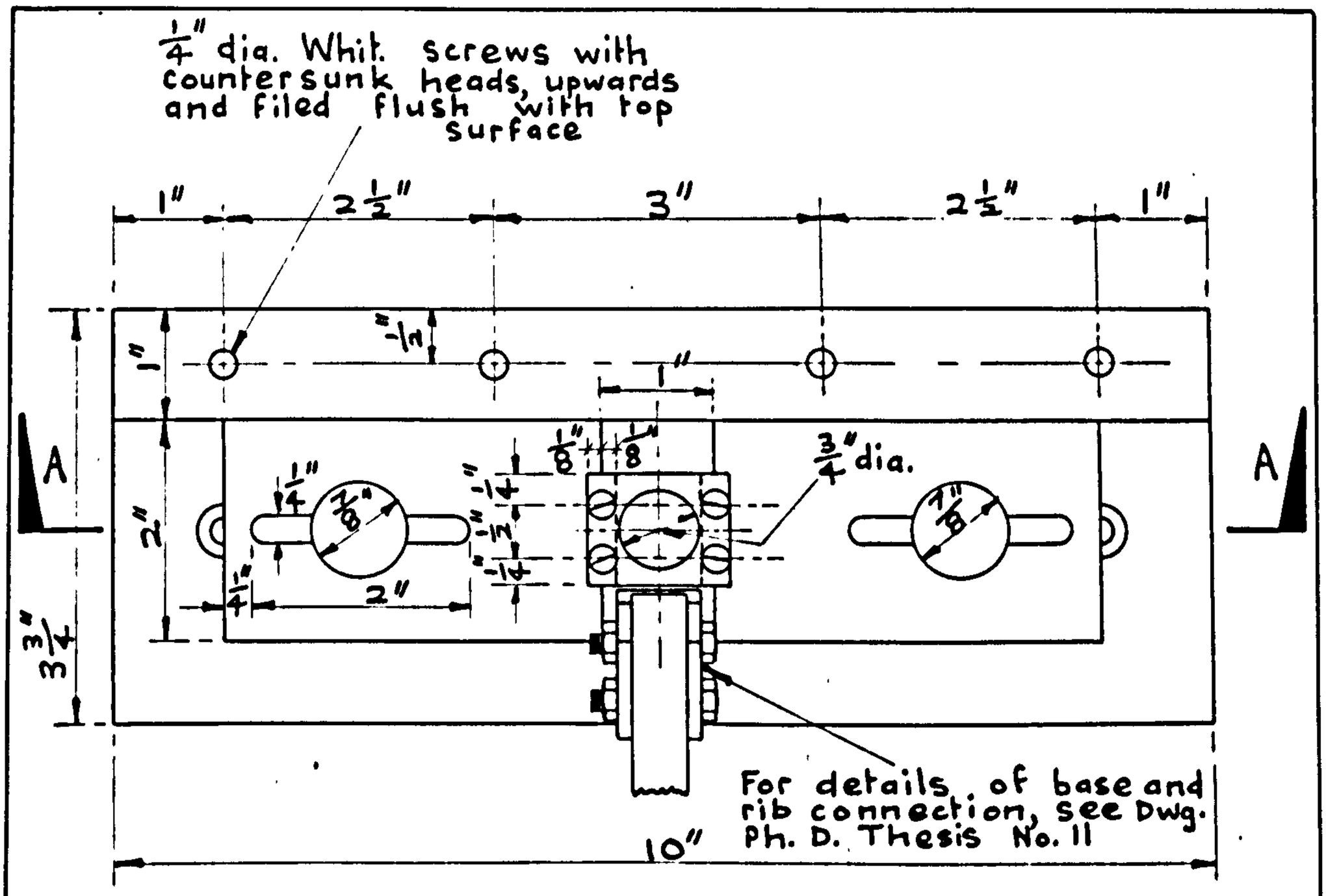

Plan

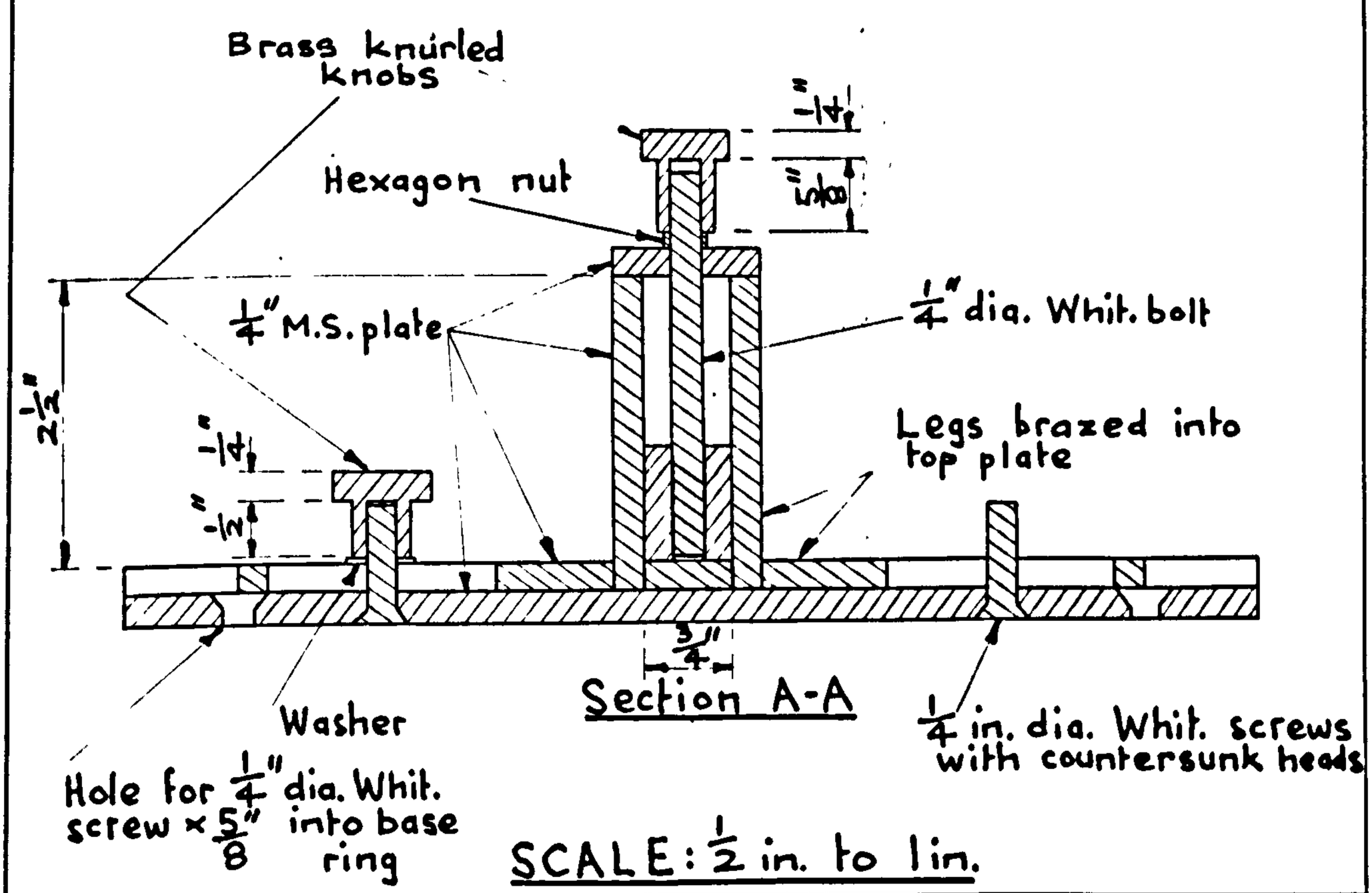

Section A-A

SCALE: 1/2 in. to 1in.

FIG. 56 BASE VERTICAL DEFORMETER

F.A.A. Ph.D. Thesis
4th March, 1970

Structural Engineering Division
Department of Civil Engineering
University of Newcastle upon Tyne

PLATE 25 - BASE HORIZONTAL DEFORMETER AND NODE POINT LOADING

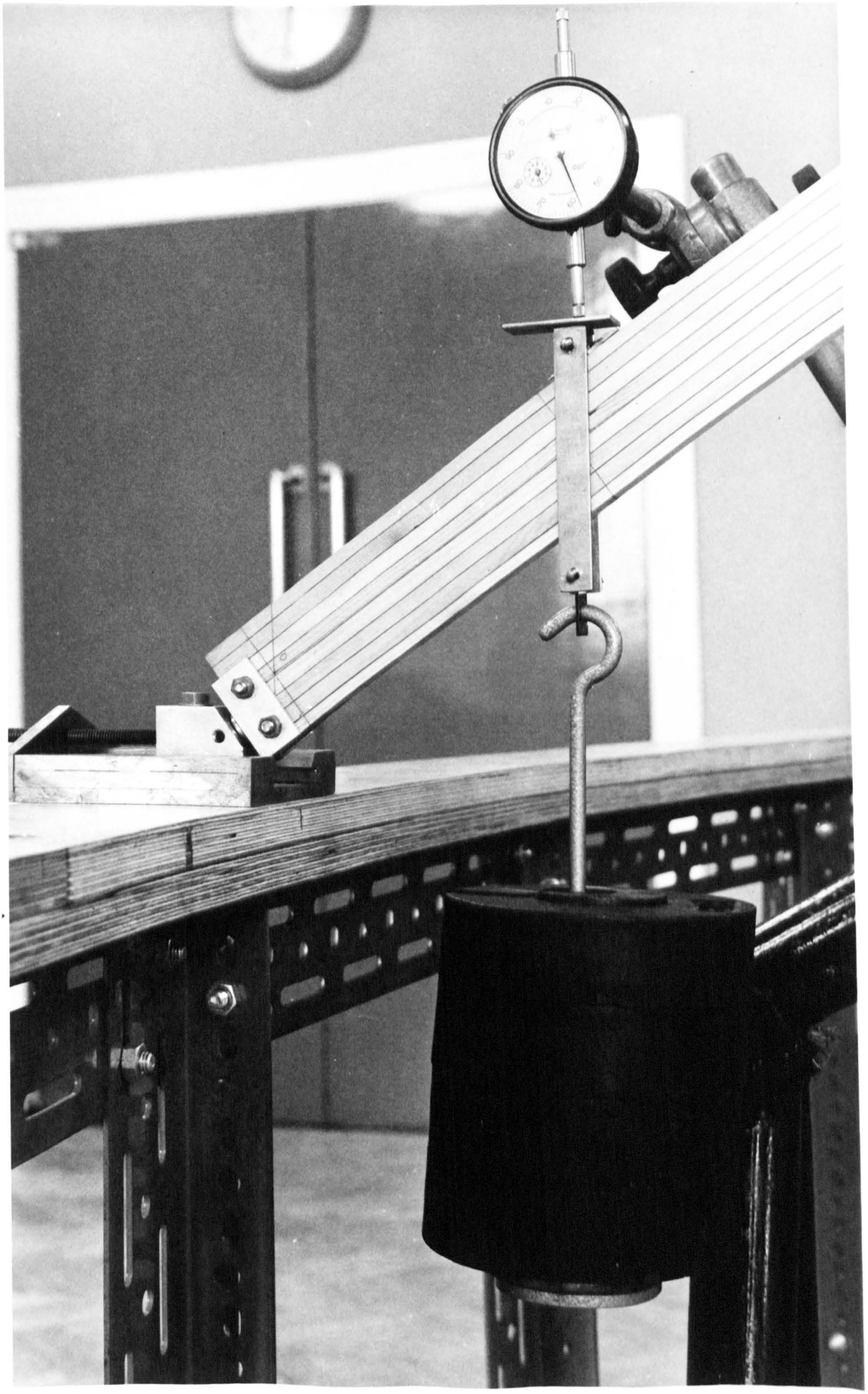

PLATE 26 - BASE VERTICAL DEFORMETER

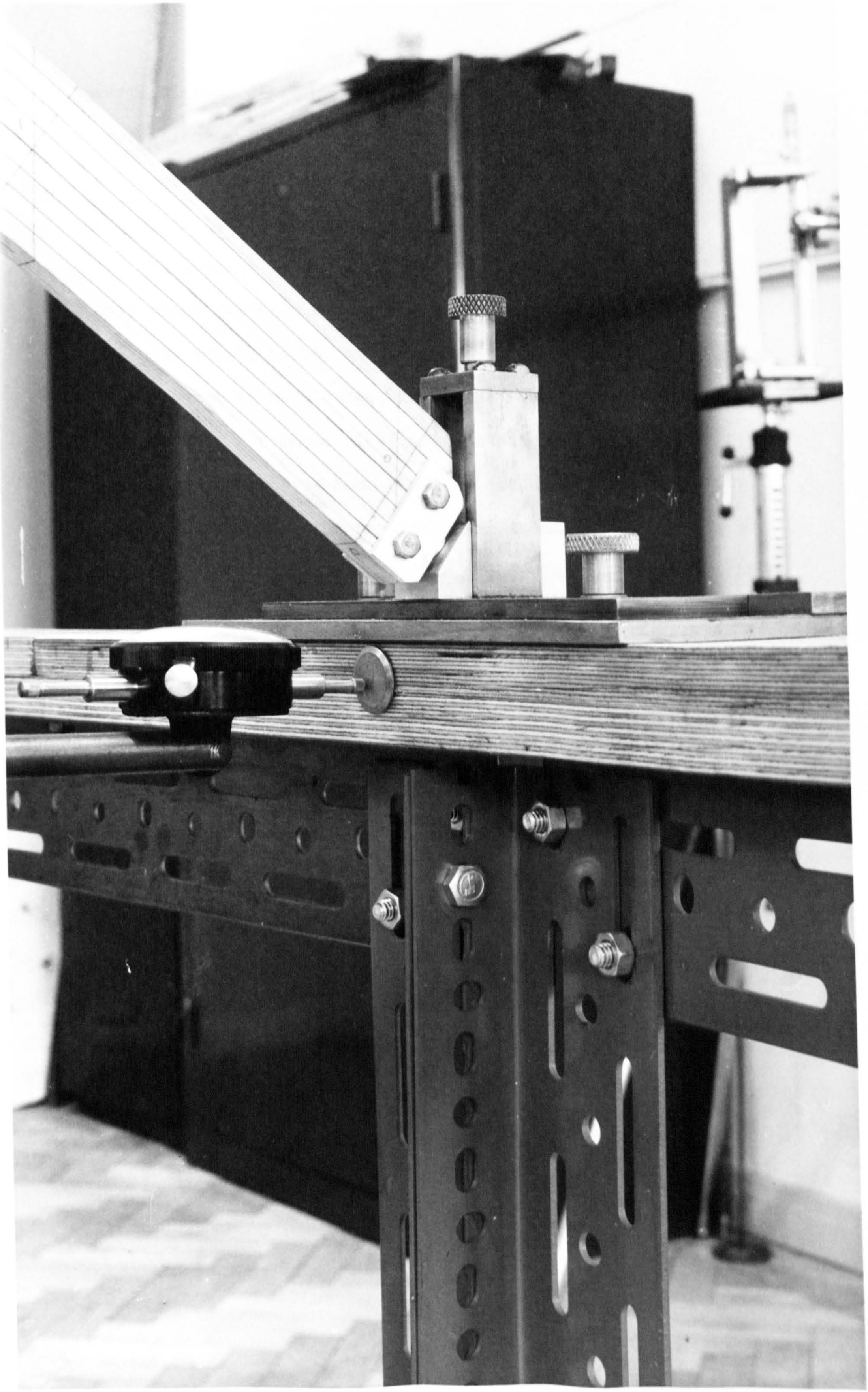

vertical base displacement against vertical node displacement, influence coefficients were obtained for the base vertical reactions. The vertical deformeter could also be employed for displacing the bases tangentially if required.

Node point displacements were measured in a vertical direction only since the required base reactions could be obtained by this means. The node points could, in fact, be displaced in three directions, at right angles to each other, if so desired and the various reaction coefficients for these directions obtained. In this way any load system on a prototype dome could be accounted for in design.

When measuring the vertical displacements of the node points, it was not necessary for loads to be applied at these points. Base displacements could have been coordinated with the node displacements of the structure in a straightforward manner. However, to facilitate the measurement of the vertical node deflections, loads were applied to maintain the weight hangers, illustrated in Plates 13 and 25, vertical and hence the true vertical deformation was obtained. In addition, as the loads were applied to the dome, some idea of the creep characteristics of the model were obtained.

Vertical deflections of the node points were measured using dial gauges which could be read to .001 in., Plate 25. Five observation node points were employed along each radial rib and five gauges, on adjustable clamps, were mounted on a moveable framework consisting of scaffold poles, see Plate 28, to facilitate measurements. Using the indirect method of testing, it was only necessary to displace one rib base, due to the symmetry of the system, and by moving the scaffold frame containing the dial gauges, node point deflections could be obtained for any rib.

The indirect method was also employed for determining the forces in the model dome apex ring. Figure 57 gives details of the apparatus

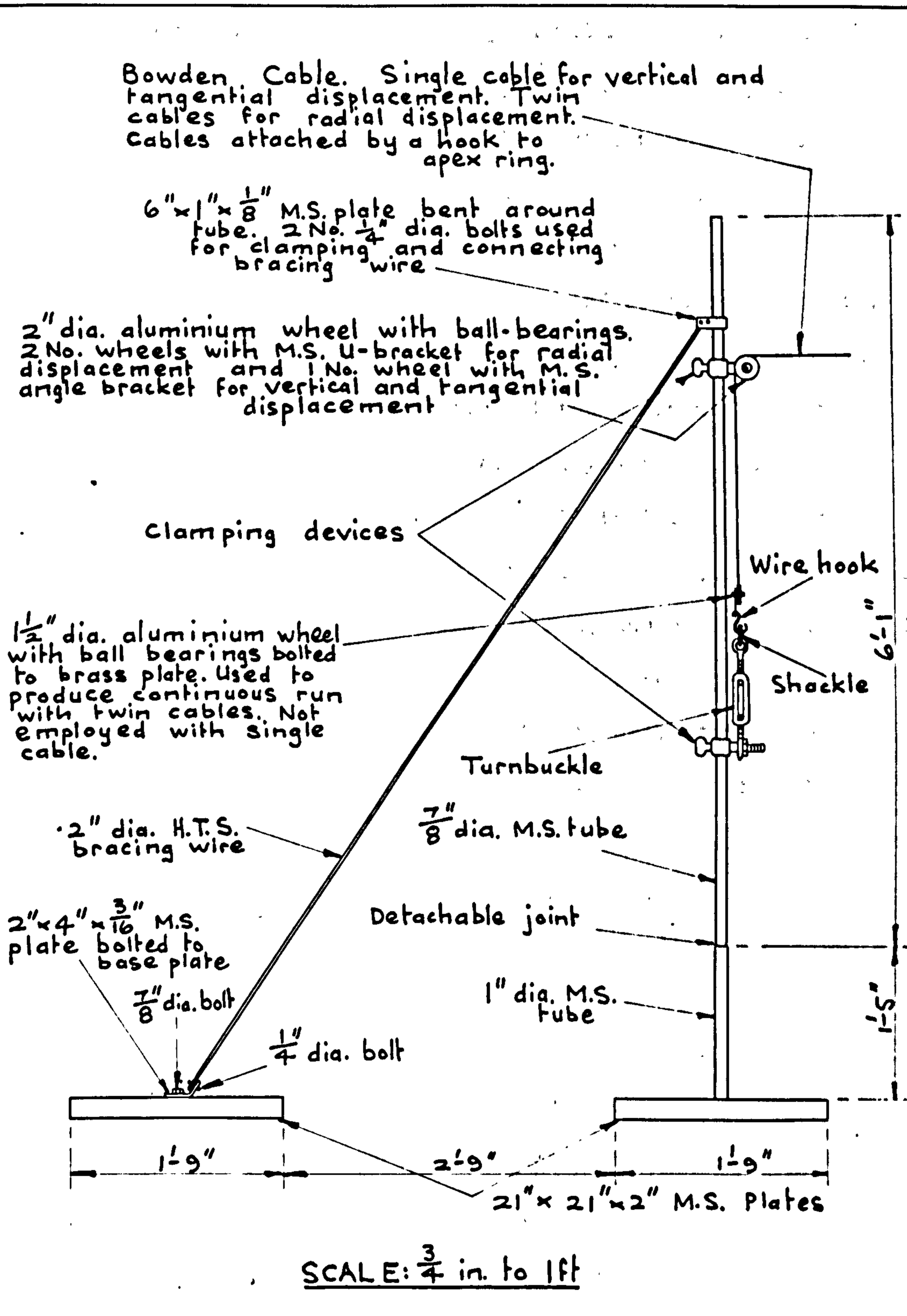

SCALE: 3/4 in. to 1ft

FIG. 57 . APEX RING DISPLACEMENT APPARATUS

F.A.A. Ph.D Thesis
5th March, 1970

Structural Engineering Division
Department of Civil Engineering
University of Newcastle upon Tyne

employed in the procedure adopted and Plates 27 and 28 illustrate the actual principle applied. Displacement of the apex ring was carried out in three directions at right angles to each other and graphs of vertical, radial and tangential apex ring displacement against node displacement were obtained in a similar manner to those employed in the determination of the base reaction influence coefficients.

Table Nos. 1 - 3, Test No. 1 in Appendix II, contain results for the experimental determination of the horizontal reaction influence coefficients. The rib set up, employed in this test, consisted of 6 ribs at 60° intervals as shown in Plate 28. This test was carried out with the ribs having a constant section size, along their length, of ½ in. by 2 in., before being tapered, and no horizontal or diagonal bracing was provided. Loads of 20 lb were applied to each node point when observations were made as to its deflection. Horizontal displacement intervals of .1 in. up to 1 in. were used for the rib base. The six rib set up, with ribs of constant section, was employed to determine what effect the actual tapering of the ribs had on the stress distribution. A similar set up, with tapered ribs, was employed in Test Nos. 6 - 11.

Sheet Nos. 1 - 4, Test No. 1 in Appendix II, contain the graphs of horizontal base displacement against vertical node displacement for the six untapered rib set up. The slope of the graphs give the influence coefficient values for the horizontal base reactions. These influence coefficients for the horizontal reactions, i.e. the values of the horizontal reactions when unit loads are applied at the node points, are plotted on a plan of the rib layout in Sheet No. 5 of Test No. 1. A diagram of this type is called an influence line diagram.

Similar test procedures to those detailed above were carried out to obtain influence line diagrams for the rib base vertical reactions and the apex ring vertical, radial and tangential forces. The results

PLATE 27 - APEX RING VERTICAL DISPLACEMENT


CIVIL ENG
DEPT
STRUCTURES
LAB
1839

PLATE 28 - APEX RING TANGENTIAL DISPLACEMENT

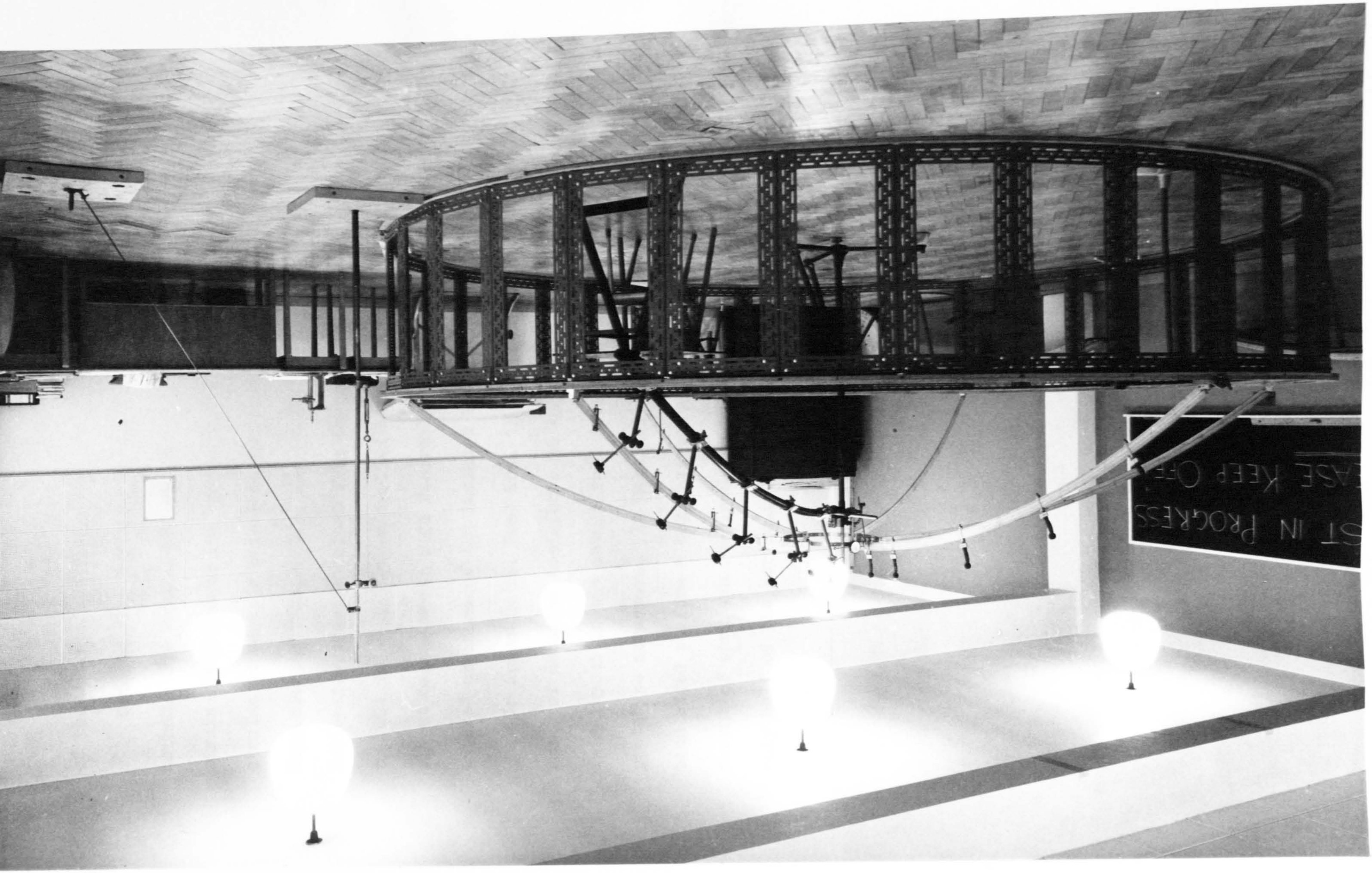
ST IN PROGRESS

of these tests are given in Appendix II under Test Nos. 2 - 5.

Some testing was also carried out on the model by the direct method. The results in Appendix II, under Test No. 1, include rib strain measurements and apex ring displacements. Values of the rib strains at various points on the radial ribs were measured using Huggenberger Tensometers, see Plates 12 and 28. The apex ring deflections were obtained from observations on dial gauges measuring to .001 in. Loads were applied at the various rib node points and direct measurements were recorded. Similar results for the six rib tapered arrangement are included in Test No. 11.

In Appendix II, Test Nos. 12 - 17 contain results of the complete range of detailed testsfor a 36 tapered rib layout without bracing. This layout is the actual radial rib arrangement required by the prototype structure. In Test Nos. 18 - 22, horizontal purlins have been added to form a complete braced dome structure. Since a large amount of work was required for the completion of such an arrangement, only half of the horizontal purlins have been added.

CHAPTER XI

ANALYSIS OF TEST RESULTS AND CONCLUSIONS

11.1 ASSESSMENT OF ANALYSIS METHODS

(a) Statically Determinate Pin-jointed Space Frames

Many space frames are designed under the assumption of statically determinate pin-jointed conditions, even though in practice joints are made rigid. The primary action of these structures is assumed to be unaltered to a large extent by the introduction of secondary bending and sufficiently accurate values of the axial forces are obtained, for design purposes, by considering a pin-jointed system. Secondary bending can be considered, if required, after a pin-jointed analysis has been carried out.

A review of the various methods which can be employed for solving the stress distribution in statically determinate pin-jointed space frames is contained in Chapter IV. The Method of Joints (Art. 4.2) and the Method of Sections (Art. 4.4) can be applied to simple and compound space trusses respectively in a straightforward manner. For complex trusses, the Method of Joints can be employed to obtain a set of simultaneous equations for subsequent solution, the number of equations being equal to the number of joints multiplied by three. Henneberg's Method (Art. 4.7) and the Tension Coefficients Method (Art. 4.8) can also be utilized for complex space trusses. Although some of these methods are elegant mathematically, they can result in a solution which is very tedious to obtain depending upon how many members are contained in the structure. Therefore, these methods are only to be recommended for space frames with a small number of components. The Method of Conjugate Forces (Art. 4.9), which is a

graphical method, can be employed for space frames of a more complex type but is not to be recommended for structures containing a large number of members.

(b) Statically Indeterminate Pin-jointed Space Frames

The application of the Theorem of Least Work (Art. 5.3) and the Maxwell-Mohr Method (Art. 5.4) to the stress analysis of statically indeterminate pin-jointed space frames is limited to systems which contain only a few members and are of low redundancy. In the analysis of these space frames a consideration of all the individual members is necessary and, therefore, a large number of components would complicate the calculations extensively.

The Gap Reduction Method (Art. 5.6) depends largely for its solution on the degree of redundancy of the frame and can be employed for more complex indeterminate pin-jointed space frames. However, such a method would still not be feasible for producing a pin-jointed analysis of radial ribbed domes with many members.

By using the Influence Coefficients Method (Art. 5.7), the labour involved in determining the stress distribution in a pin-jointed statically indeterminate space framework would depend upon the number of joints present and not upon the number of members. Although redundancy would not be so important, a structure with a large number of joints would again result in a laborious solution.

For domes of the size and type being studied by the author, which contain radial ribs, horizontal purlin rings and diagonal bracing, it would be almost impossible to produce a pin-jointed analysis even under the assumption of a statically determinate system. In addition, the radial ribs are continuous from base to crown and therefore bending moments also need to be considered.

(c) Statically Indeterminate Space Frames Without Pin-joints

Rigidly jointed space frameworks of low redundancy can be solved

by the classical methods of analysis such as strain energy, slope deflection or moment distribution. For high redundancies, relaxation methods may be employed and such a method using influence coefficients is described in Art. 6.1. With this method, influence coefficient values must first be determined for all members of a structure. Hence the work involved depends, to some extent, on the number of components present. However, the relaxation process of moving the joints, which is employed after the influence coefficients have been evaluated, mainly governs the amount of labour required to produce a solution and redundancy is of little importance.

Relaxation techniques require speed of convergence in the liquidation of residual forces. Block and group relaxation can be employed to achieve this end resulting in a reduction of time required to obtain a solution. For complicated rigidly jointed space frames the amount of calculation needed for a relaxation analysis would be enormous. and, therefore, an approach of this type was considered impracticable for the solution of radial ribbed domes as studied by the author.

The use of matrix algebra provides possibly the best means of obtaining the stresses in statically indeterminate space frames without pin-joints. To make full use of this technique an electronic computer is needed. Computers can be employed in two ways:

(1) they can be used only as a tool for solving standard matrix routines in which case a large amount of time is needed for preparing the input data;

(2) they can be programmed to solve a particular problem and programming requires laborious development and testing.

For the size and type of structure considered by the author it would have been virtually impossible to employ matrix routines or develop a separate program, based on matrix algebra, in the time available.

(d) Braced Domes

The stress analysis methods which are particularly suited to braced domes are contained in Chapter VII. In Art. 11.1(a) it was stated that the Method of Joints is only to be recommended for pin-jointed space frames with a small number of components. However, this method can be employed in the analysis of Schwedler domes, as discussed in Arts. 4.6 and 7.1, by making use of the symmetry of the structure. Using the analysis procedure advanced by Schwedler, values for the radial rib axial forces, the horizontal purlin ring axial forces and the forces in the diagonal bracing can be arrived at under the assumption of symmetrical loading. This, in fact, is the procedure adopted by the American Institute of Timber Construction in their Design Manual, as discussed in Arts. 10.1(a) and (b), and which was employed in the design of the author's prototype and model domes. Although this is a practical method which can be employed in designing radial ribbed domes under symmetrical loading conditions, it does not allow for unsymmetrical loads. The rigidity of the joints is also neglected and an overestimation of the maximum stresses is obtained. Since Schwedler's approach requires symmetrical loading conditions, it is not possible to obtain theoretical influence line diagrams for the base reactions and apex ring forces in a radial ribbed dome by this method.

An analysis of a stiff-jointed framed dome by El-Sayed El-Schasly's Method (Art. 7.2(a)) would not be considered in the case of a structure with a large number of ribs and rings. The redundancy of the system would prohibit the use of this method. Similarly, the mathematics involved in Kaufmann's Method (Art. 7.2(b)) would prevent it from being used by design engineers.

It is possible to analyse stiff-jointed radial ribbed domes using the Influence Coefficients Method, as detailed in Art. 7.2(c), provided the number of members is small. Although in Art. 7.2(c) a design

procedure has been mentioned, which is recommended by Benjamin[12] for radial ribbed domes and contains a combination of pin-jointed and fully-rigid procedures, it would be toilsome to analyse the author's dome by this method. The radial ribs, horizontal purlins and diagonal bracing form such a complex structure that a correct solution would be difficult to obtain.

Schwedler domes can be designed very easily using the Shell Analogy which is discussed in Art. 7.3. However, the method is limited to uniformly distributed loading over the equivalent shell, either in a symmetrical form or asymmetric condition. Therefore, it is again impossible to produce influence line diagrams for the base and apex ring forces by this method.

For stiff-jointed framed domes, according to Benjamin[12] as mentioned in Arts. 7.3(d) and (e), the Shell Analogy should not be used until much further research has been carried out. Despite this fact, it was employed in the design of three steel domes in Canada and good correlation between experimental and design stresses was reported.[33]

(e) Continuous Radial Ribbed Domes

In this Chapter so far, the assessment of the methods of analysis available for the design of space frames have shown that difficulties would be encountered in applying them to large dome structures consisting of continuous radial ribs, horizontal purlin rings and diagonal bracing. Such structures are too complex to be considered as a whole. Therefore, it appears that the only possible approach to the analysis of such structures is to consider two separate simple member systems. The primary system of radial ribs is first designed to withstand bending moments and axial forces induced by dead and imposed loading conditions on the dome and then the complete structure is analysed as a pin-jointed system under symmetrical loading conditions. Although axial force values can be obtained easily for the horizontal

purlins and diagonal bracing under symmetrical loads, to obtain similar results analytically for a general system of loads would be extremely difficult.

In designing the primary radial rib system, the procedures for three-hinged and two-hinged arches can be applied easily in a two-dimensional form. However, an approach of this kind does not take into account any spread of load from one rib to another, through the apex ring, under unsymmetrical loading conditions. It was for this reason that the author chose to modify the method put forward by Makowski and Gogate,[27] as detailed in Art. 8.3, so that a space frame approach could be applied to domes with circular-shaped radial ribs, of any span-to-height ratio, under three-hinged arch conditions. The values of the reactions and bending moments obtained theoretically by the modified Makowski and Gogate method are compared with the experimental results later in this Chapter.

In the analysis of radial ribbed domes, the assumption that three-hinged arch conditions can be employed for systems which contain apex rings leaves much to be desired. However, in such structures, the stability and stress distribution is governed by the stiffness of the apex ring. When loads of an unsymmetrical nature are applied to these structures the apex ring, originally lying horizontal in the unloaded condition, tilts producing in a sense a central hinge. Thus, the three-pinned arch approach is to be preferred to the two-hinged method of Pichl, as detailed in Art. 8.5, in which the ribs are considered to be rigidly fixed at the apex.

Pichl's two-hinged approach to the analysis of the radial rib primary structure in domes is complicated. With the three-hinged arch Makowski and Gogate method of analysis, reactions and bending moments can be obtained easily by expressing the unknown redundancies in terms of the deflection of the apex joint which is the same for all ribs.

In the two-hinged method, a study of the elastic fixity of the ribs at the vertex is necessary and leads to complicated calculations. The vertex point rotation effect, as detailed in Art. 8.5(a) for two-hinged unstiffened radial ribbed domes, can be determined with some effort but the vertex point translation effect is not so easy to perceive. The displacement of each rib produces moments in itself and on all the other ribs and these must be added together. For domes which contain large numbers of radial ribs, this process is very tedious. Makowski[10] recommends that Pichl's method be applied only to domes containing apex rings which are so stiff that their deflections are small compared with the rib displacements. It can be seen that, if desired, a designer can determine the performance of the dome ribs simply by varying the ring stiffness.

The method of analysis for two-hinged unstiffened radial ribbed domes containing apex rings, which was developed by H. Marcus[10] and is discussed in Art. 8.6, is again limited in its application. A symmetrical loading system is required and the apex ring diameter is assumed to be small. The analysis is carried out by considering the dome to be of the closed type. For large numbers of ribs, therefore, the method would prove difficult to apply.

Radial ribbed domes which are "stiffened" by an elastic base ring require different methods of analysis to account for the base ring forces. A method which can be used for such domes has been detailed in Art. 8.7.

11.2 COMMENTS ON DOME LOADING

The dead load, consisting of the weight of the covering and the framing system, is relatively easy to calculate in the design of domes. Allowances can also be made for loads imposed in the erection, repairing and cleaning of such structures which are all classified as live load. The main problems which are encountered in the design of domes are due

to the inadequacy of information relating to the distribution of snow loading and wind pressures over these systems.

The imposed snow load value for flat roofs recommended by CP3 : Chapter V : 1965,[29] as detailed in Art. 9.3, appears to be adequate for the British Isles but this figure does not take into account any build up of snow, due to drifting, over large domes which are curved in three-dimensions. Where this occurs, critical stresses may result from the unbalanced loading conditions.

A most important factor to be considered in the design of domes is the effect of short duration local wind gusts. More information is required about this aspect of wind loading as, in certain circumstances, it is possible that the dynamic response of a flexible structure to a gust sequence is greater than that determined by assuming a steady wind load.

With regard to the wind pressure distribution over curved surfaces, the values obtained by employing the data available in CP3 : Chapter V: 1965 are at variance with the wind tunnel test values obtained by Maher[36],[37] when applied to a dome which has a rise-to-base ratio of that used by the author. The Code of Practice results in suction pressure values over all the dome whereas Maher's wind tunnel test values, Figure 51(b), indicate positive pressures over parts of the windward and leeward slopes. Higher suction values near the dome apex were also observed in the experimental work. It is quite obvious, therefore, that more research is needed into wind pressure distributions over dome roofs and, in particular, measurements are needed from completed structures.

11.3 BASE REACTIONS

(a) 6 Ribs in Dome

The first series of tests on the model radial ribbed dome were concerned with a study of the effect of changes in cross-sectional area

and moment of inertia on the stress distribution in the primary rib system. For this investigation only six ribs were connected to the apex ring, without any bracing, and tests were carried out with members of constant cross-sectional area and again with areas which varied along the length of the ribs. The horizontal reaction influence lines for the uniform section ribs are shown in Sheet No. 5 of the Test No.1 results. Sheet No. 5, of Test No. 2, contains the vertical reaction influence lines. Influence lines for the tapered rib arrangement are plotted in Sheet No. 5 of Test No. 6 and Sheet No. 5 of Test No. 7 for horizontal and vertical reactions respectively. In addition to the influence line diagrams for the base reactions, the influence coefficients are set out in Table Nos. 3 and 6 of Appendix IV, along with summations of these values, to indicate the maximum outward horizontal or downward vertical reactions, the maximum inward horizontal or upward vertical reactions and also the horizontal or vertical reactions for a symmetrical loading system.

A study of the influence line diagrams, referred to above, along with Table Nos. 3 and 6 of Appendix IV indicates that a variation of cross-sectional area and moment of inertia along the length of the ribs in a radial ribbed dome produces little change on the values of the base reactions as obtained by using a constant section area. This verifies that the assumption to this effect, which was mentioned in Art. 8.1, is valid.

In all tests to obtain the horizontal and vertical reactions for the tapered and untapered ribs, it was also noticed that negative influence coefficient values occurred along the lower parts of the ribs adjacent to the directly loaded rib. After observing the apex ring radial force influence line diagrams shown in Sheet No. 5 of Test No. 4 and Sheet No. 5 of Test No. 9, which are discussed more fully in Art. 11.4 and which indicate positive radial force values for all

positions along the adjacent ribs, it must be concluded that the negative horizontal and vertical reaction coefficients are obtained due to the translation and rotation of the particular rib profile. The extent and manner in which the apex ring is displaced also governs the amount of displacement and rotation of the secondary ribs and, therefore, determines the size of the base reactions.

A comparison between the experimental results for the six rib primary member systems, given in Tables 3 and 6 of Appendix IV, and the theoretical values can now be considered. Calculated values for the base reactions are given in Table No. 1 of Appendix IV under the assumption of symmetrical unit loads on three-pinned and two-pinned arches. These values are easy to obtain on the basis of a plane frame method of analysis, but for unsymmetrical loads the space frame approach of Makowski and Gogate,[27] as modified by the author and programmed for an electronic computer, gives the theoretical values shown in Table No. 2 of Appendix IV.

Observing first the values for symmetrical unit vertical loads on the dome, it can be seen that the experimental values compare favourably with those obtained theoretically. It should also be mentioned at this stage that the space frame results computed by the author for symmetrical loading on a dome are the same as those obtained from the three-pinned arch plane frame method as this was used as a basis for the space frame analysis. The experimental values for the horizontal reactions are nearest to those of the three-pinned arch theoretical results except for positions close to the apex ring where the two-hinged arch values are nearest. This suggests that the fixity of the ribs at the apex ring does play some part in modifying the stress distribution throughout the system.

The accuracy of correlation between experimental and theoretical horizontal reactions is to within about 15 per cent. It is rather a

large difference but if the three-pinned arch approach is applied, then the size of the reactions will all be over-estimated by this amount and the result will be on the safe side. In fact, when comparing the vertical reactions, the results for symmetrical loading should all add up to unity. This does not happen with the experimental values suggesting lower results than those which should be obtained. The cause of this was put down to creep of the node points at which vertical deflections were measured as loads were used to maintain the node point weight hangers vertical so that only true displacements were observed. Creep was later taken into account in the tests on the complete rib arrangement.

Looking at the distribution of the forces throughout the dome for a unit load at any point, it can be seen from Table Nos. 2 and 6 of Appendix IV that the actual distribution is different from the theoretical. The theoretical three-pinned approach of Makowski and Gogato relies on the angle of the secondary ribs for distributing reactions in the system. However, the deformation in practice is governed by the movement of the apex ring and therefore, as mentioned previously, the stiffness of the apex ring dictates the values of the base reactions for unsymmetrical loading. It can be seen that the movement of the apex ring results in a more even stress distribution throughout the system.

One point to be noticed about the theoretical results in Table No. 2 of Appendix IV is that negative values for the coefficients are again present in the ribs adjacent to the directly loaded rib. This is due to the shape of the arch profile. Loads nearer the base of the adjacent ribs produce an upward displacement of the apex ring, instead of the normally expected downward movement, resulting in a direction change of the directly loaded rib reactions.

The last observations to make are concerned with the distribution

of loading to give the maximum reactions. By adding the influence coefficients of reaction for a unit load at any point, as illustrated in Tables 2 and 6 of Appendix IV, the maximum values can be obtained. Maximum inward horizontal or upward vertical reactions are obtained when all the ribs are loaded except for the lower regions of the ribs adjacent to that rib considered to be the directly loaded rib. Reactions of a maximum value in the reverse direction are only obtained when the lower regions of the adjacent ribs are loaded.

(b) 36 Ribs in Dome

The tests on the six rib primary member systems were employed to investigate the effect of tapering the cross-sections. They also served to improve the testing technique which was applied next to a primary system of thirty-six members. The thirty-six rib arrangement was that required by a prototype structure of the size represented by the scale model.

Horizontal reaction influence lines for thirty-six ribs are contained in Sheet No. 8 of Test No. 12 and the vertical reaction influence lines are drawn out in Sheet No. 6 of Test No. 13. The influence coefficient values are also tabulated and summated in Table Nos. 11 and 12 of Appendix IV.

Looking first at the influence line diagrams for the vertical and horizontal reactions, it is obvious that the major changes in reaction values occur when a unit point load is moved along the rib for which the forces at the base are being determined. A unit point load moving along the adjacent ribs results in reaction changes of a smaller size until, at approximately the fifth adjacent rib, a uniformity exists over the remainder of the structure. The four ribs at either side cause negative base reactions to occur in the directly loaded rib through the displacement of the apex ring. However, beyond the four ribs uniform positive reactions are produced.

A comparison between the theoretical horizontal reactions for unit symmetrical loads, given in Table No. 9 of Appendix IV, and the experimental values of Table No. 11, in the same Appendix, shows that in the thirty-six rib system the experimental values exceed the theoretical by about 10 per cent near the apex ring. This is the reverse of the condition which occurred for the six rib system and may be due to the lateral restraint of the larger number of ribs which limits the apex ring distortion. It could also be due to the accumulation of small errors in the influence coefficients when summated over such a large number of ribs and, therefore, the theoretical values provide a reasonably accurate estimate of the correct values.

The symmetrical loading experimental vertical reactions, given in Table No. 12 of Appendix IV, are approximately equal to unity, which is only to be expected, and are similar to the theoretical values of Table No. 10. Both the horizontal and vertical sets of experimental reaction coefficients have been adjusted to allow for the creep which occurred when measuring the vertical node point deflections.

The stress distribution in the thirty-six rib primary member arrangement for a unit load at any point on the dome is again radically different from the theoretical distribution. This was also shown by the six rib tests. Whereas the theoretical distributions in Table Nos. 9 and 10 of Appendix IV show negative reaction values for almost half the dome, the actual negative values are experienced only over a small area, i.e. in the four ribs either side of the directly loaded rib, as mentioned earlier in this Art. For loads over the greater part of the dome, small positive reactions are experienced by the directly loaded rib showing that the apex ring causes a more uniform stress distribution throughout the system.

From the theoretical coefficient values in Table No. 9 of Appendix IV it can be seen that a segment of the dome roof area with an angle

of 150°, symmetrically situated about the axis of the directly loaded rib and on the opposite side of the dome to it, would produce the maximum horizontal base reaction value. The experimental results in Table No. 11 show this angle to be 270°.

For the theoretical maximum vertical reaction to occur a segment of the dome area with an angle of 210°, symmetrically situated about the directly loaded rib, would need to be loaded as shown by Table No. 10 of Appendix IV. The experimental influence coefficients in Table 12 give the angle as 70°.

(c) 36 Ribs in Dome With Horizontal Purlin Rings

The time and effort required to add all the purlins to the dome and also to carry out a complete range of tests, similar to those completed for the primary systems, would be enormous. Therefore, only alternate rings were attached to the primary system of thirty-six ribs and influence coefficient values of reaction have been obtained just for the rib which is considered to be the directly loaded one. The experimental reaction coefficients for the braced rib arrangement are contained in Table No. 16 of Appendix IV.

From the results in Table No. 16 it is apparent immediately that the stress distribution is completely changed from that of the unbraced system. Unit point loads, near the apex ring, only transmit small reaction forces to the base and hence the resistance to applied forces must be spread throughout the space frame system.

Maximum values for the reactions are obtained in the directly loaded rib when a unit load is near the base of this rib. This indicates that the major effect of applied point loads is localized and disperses rapidly from member to member. Unfortunately results for symmetrical loading and maximum values of the reactions for a general load system cannot be deduced until further tests are carried out.

11.4 APEX RING FORCES

(a) 6 Ribs in Dome

The experimental apex ring vertical influence lines for the two primary member arrangements of six ribs are shown in Sheet No. 5 of Test No. 3 and Sheet No. 5 of Test No. 8. Values of the coefficients in Test No. 3 are for ribs of constant moment of inertia while those in Test No. 8 are for the tapered ribs. The coefficients have also been tabulated and summated in Table Nos. 4 and 7 of Appendix IV.

In general, from the influence line diagrams, it can be seen that the tapered ribs impose greater vertical forces on the apex ring. This is due to the larger displacements of the shaped ribs under load.

For the maximum downward apex ring vertical force to occur, the rib at which the force is being considered must be loaded together with the two adjacent ribs. A maximum upward apex ring vertical force is produced by loading the opposite three ribs. The change in direction of the vertical forces is brought about by the translation and rotation of the apex ring and therefore its stiffness governs the magnitude and direction of the vertical forces.

Considering now the apex ring radial force influence diagrams in Sheet No. 5 of Test No. 4 and Sheet No. 5 of Test No. 9, it is again apparent that the tapered ribs impose greater radial forces on the apex ring than the constant section members. Table Nos. 4 and 7 of Appendix IV show that the same distribution of loading over the primary rib arrangement as that for the maximum vertical forces in the apex ring also produces the maximum radial forces. A maximum inward radial force is obtained by loading the rib for which the force is being considered and also the two adjacent ribs. The outward force maximum value is produced by loading the opposite three ribs.

The apex ring tangential force influence lines for the six rib tests are contained in Sheet No. 4 of Test No. 5 and Sheet No. 4 of

Test No. 10. Table Nos. 5 and 8 of Appendix IV contain the influence coefficient values and their summation. At first sight the results appear to be strange. The distribution of the tangential force coefficients should be symmetrical about the rib at which the force is being considered. However, in the first series of tests, no account was taken of the creep experienced by the loaded node points and, therefore, small additional positive values have been added to the influence coefficients. This has resulted in larger positive coefficients, smaller negative coefficients and small positive coefficients on the ribs which should have zero values.

A maximum tangential force is produced in the apex ring when one half of the dome, lying to the right of the rib at which the force is being considered, is loaded. When the other half of the dome is loaded, a maximum apex ring tangential force is produced in the opposite direction.

Great difficulty was experienced in applying any theoretical analysis procedures to evaluate the forces imposed on the apex ring. The three-pinned arch method is not valid due to the movement of the apex ring. Pichl's method, described in Art. 8.5 and which considers a two-hinged arrangement of ribs, could be a possible approach but the exact degree of elastic fixity of the ribs at the apex is not easy to deduce and the effect of displacing the system results in even more complicated calculations. However, more research along this line may yield valuable information.

(b) 36 Ribs in Dome

It is now possible to study more closely the apex ring force influence coefficients for the full thirty-six rib primary member system. The experimental apex ring vertical force influence lines are plotted in Sheet No. 4 of Test No. 14 and the coefficient values are tabulated and added together in Table No. 13 of Appendix IV.

Looking at Table No. 13, the first point to be considered concerns the values of the vertical ring forces when all the dome is loaded. These values are given in the Total 3 line. For load points 1, 5 and 9 on the dome ribs, the results are negative and for points 13 and 17 they are positive with a particularly large value occurring at point 17. The change-over in direction is due to the mode in which the dome deforms under load. Symmetrical loading on the lower rib points tends to flatten the curvature of the radial members resulting in an upward movement of the apex ring. Loading of a symmetrical nature near the crown of the dome increases the curvature of the ribs and the apex ring is pushed downwards.

It is not so straightforward to define which areas of the dome need to be loaded to produce a maximum value of the apex ring vertical force in the primary member system. For the base reactions it was clearly divided at certain ribs. However, with the vertical apex ring forces, certain points along individual ribs should be included. This, of course, can be done if required by adding up the appropriate coefficients in a similar manner to the system adopted in Table No. 13 of Appendix IV.

One other point to be noticed from the influence lines for the apex ring vertical forces is that unit loads at the same level over a large part of the dome produce a similar size of vertical force at the apex ring. This indicates a uniform spread of stress throughout the system. Although a uniformity for the force pattern exists over most of the dome, the greatest changes in the influence coefficient values occur in the vicinity of the rib at which the vertical force is being considered. This effect is most noticeable in the five ribs at either side of the directly loaded rib.

Point loads on the five ribs at either side, and also on the rib at which the vertical force is being considered, cause downward vertical

forces to be exerted on the apex ring. A gradual change then takes place until a uniformity of upward vertical force coefficients is obtained around the remainder of the dome. Again the cause of this change can be attributed to the displacement and rotation of the apex ring.

Referring to the apex ring radial force influence lines which are drawn in Sheet No. 4 of Test No. 15 and the summation of the coefficient values in Table No. 14 of Appendix IV, it can be seen that, for all the dome loaded, the radial forces balance themselves. However if ten ribs and the rib at which the radial force is being considered are loaded, then a maximum inward force is obtained. This is equivalent to a roof area segment, symmetrically situated about the considered rib, with an angle of 110°. If the remainder of the dome is loaded, a maximum outward force is the result.

The apex ring tangential force influence line diagrams in Sheet No. 7 of Test No. 16, and the coefficient values set out in Table No. 15 of Appendix IV, indicate that no tangential forces are obtained when all the dome is loaded. What is also clear from the test data is the fact that if loads are applied over half of the dome to the right of the rib at which the apex ring tangential force is being considered, a maximum anticlockwise force is obtained. A maximum force in a clockwise direction is obtained when the other half of the dome is loaded.

(c) <u>36 Ribs in Dome With Horizontal Purlin Rings</u>

Comparing now the results in Table Nos 13, 14 and 16 of Appendix IV, it can be seen that the apex ring vertical and radial forces in the directly loaded rib are either similar or larger for the braced ribs than those for the unbraced system. This also applies to the rib which is positioned directly opposite to the one for which the apex ring force is being considered. The values of the apex ring force influence coefficients for loads on other ribs in the braced rib arrangement can

only be obtained by further testing.

11.5 RIB BENDING MOMENTS

In order to study more closely the bending moments in radial ribbed dome primary member systems, Huggenberger Tensometers were employed for direct measurement of the strains in the ribs. Although the bending moments can be obtained from the base reaction values, it was originally hoped that this procedure could be superseded by direct measurement. From knowing also the rib section sizes and the modulus of elasticity of the rib material, values of the bending moments could be obtained by application of simple bending theory. Measured values would then be compared with theoretical values. Unfortunately, as mentioned in Art. 11.3(a), the distribution of forces in the primary member systems are completely different from the theoretical ones and, therefore, the direct measurement of the rib strains only serves as a check on the values of the bending moments as computed from the base reactions.

The rib strains, obtained from the six rib, constant section, primary member arrangement, are contained in Table Nos. 4 and 5 of the Test No. 1 results. Table Nos. 1 and 2 of Test No. 11 show the values for the six tapered ribs. A general comparison of the readings for similar ribs produces the conclusion that variations in moment of inertia, along the length of slender ribs, do not change the strains by a noticeable amount. This applies to most of the dome. However, although this conclusion was deduced in Art. 11.3(a), small differences in the base reactions were noticed, for the two different set-ups, when the rib at which the reactions were being considered was loaded near the apex ring. This feature is emphasized by comparing the Rib No. 36 values in Table No. 4 of Test No. 1 and Table No. 1 of Test No. 11.

The accuracy to which the Huggenberger Tensometers could be read was to .01 in. This represents a strain value of 10×10^{-6} in. per in.

Bearing this in mind the conclusion made in the previous paragraph, that changes in moment of inertia along the length of slender ribs can be neglected, is valid.

Some of the values for the rib strains in the thirty-six rib arrangement, without any bracing, are contained in Table No. 5 of Test No. 17. One drawback to the Huggenberger strain measuring devices, which were employed in the experimental work, was their insensitiveness to small strains. Loads on ribs further away than two either side of the rib which contained the gauges gave little or no strain readings.

The positions on the ribs at which the Huggenberger Tensometers were attached in the braced rib system are different from those in the unbraced arrangement. This was a necessary change due to the horizontal purlin ring positioning and, as a result, direct comparisons of strain cannot be made. However, following from this, the author decided to position his mechanical strain gauges between alternate horizontal purlin rings in order to investigate the effect of the purlins on the bending action in the ribs. From the values of the strains, given in Table No. 1 of Test No. 22 for Rib No. 36, it appears that the horizontal purlins, if pin-connected at their ends, cause the primary rib bending moments to be changed consistent with the change in base reaction values as discussed in Art. 11.3(c).

11.6 APEX RING DEFLECTIONS

The values of the apex ring deflections for the six ribs of constant moment of inertia are given in Table No. 6 of Test No. 1. For the tapered ribs, similar results are included in Table No. 3 of Test No. 11. A comparison of results for any particular rib shows that larger apex ring displacements result from the more slender ribs. This confirms the findings of Art. 11.4(a) which deduced that the tapered ribs produce greater apex ring forces.

From Table No. 6 and Table No. 3 it can be seen that the apex ring

tangential, radial and vertical displacements have positive and negative values depending upon where the load is imposed on the dome. This occurrence evolves from the behaviour of the apex ring in that it tilts in conjunction with lateral displacement. If one side of the dome is loaded, then adjacent points on the apex ring move upward or downward depending upon the position of the loads on the ribs. Points on the apex ring at the opposite side of the dome are then displaced in the reverse direction.

The amount of displacement of the apex ring dictates the distribution of stress in the rib primary member system, as has been mentioned earlier, and therefore the stiffness of the ring itself is critical. Fixing moments in the ribs at the apex ring joints would also tend to reduce deflections and modify the stress distribution.

Apex ring displacement results for the thirty-six rib primary member system are contained in Table Nos. 1, 2, 3, and 4 of Test No. 17. For the horizontally braced arrangement of ribs, the apex displacements are set out in Table No. 2 of Test No. 22. Comparing the values for Rib Nos. 36 and 18 it can be seen that, in general for the same loads, the displacements are similar. This indicates that the horizontal bracing does not change the forces imposed on the apex ring as already noted in Art. 11.4(c).

One last point to be noted in connection with the stiffness of the apex ring, in order to apply the displacements of the model dome to prototype structures the sectional dimensions of the model and prototype apex rings must be compatible according to the principles of similarity for model analysis. If this is not so, then a completely different stress distribution will be produced.

11.7 FURTHER RESEARCH

Although the author's research project has not been taken as far as first envisaged, a thorough and systematic approach has been applied

throughout. By working in this fashion, a solid foundation has been laid upon which to base further research in the field of radial ribbed dome frameworks.

The majority of the completed research work has been involved with the primary rib system in radial ribbed domes. To study further the effect of horizontal purlin rings on the primary system, it is necessary to carry out more tests. The full range of tests, which were applied to the primary rib system in this research project, should also be carried out for the horizontally braced system. For the complete dome framework, including radial ribs, horizontal purlin rings and diagonal bracing, the range of tests should be applied yet again.

In the time allowed for the research project it was not possible to determine the forces in the horizontal purlin rings and the diagonal bracing. Further research into this aspect can also be carried out using the same displacement technique that was applied to find the influence coefficients of force in the ribs and apex ring. Extensions or contractions in the length of a purlin or diagonal bracing, between adjacent ribs, will produce displacements at the rib node points and these can be equated to give the required influence coefficients of force for the purlins and diagonal bracing.

Throughout the research project, difficulty was experienced in finding any theoretical methods which could be employed to estimate the apex ring forces. The three-pinned arch method was ruled out because the ribs did not actually meet at the crown of the dome. A two-hinged arch approach was difficult to apply because of the complexity of the rib system. However, in order to determine more accurately the distribution of stress in the apex ring, this aspect of the problem warrants a closer look and further research could be carried out in relation to the elastic fixity of the ribs at the crown.

One of the major findings of the experimental work has been that

the stiffness of the apex ring controls the stress distribution in radial ribbed domes. In order to appreciate this fact to its full extent, further tests could be carried out on the model with various apex rings, of the same diameter, but having different cross-sectional areas.

The final aspect of the research into radial ribbed domes which needs to be investigated more fully is concerned with loading. Information relating to the snow load distribution over large surfaces, which are curved in three-dimensions, is scarce. More results are needed from investigations on full-scale structures. Similarly, the effects of wind gusting and variation of wind pressure over the surface of domes need to be studied and valuable results could be obtained by erecting the author's scale model dome in a suitably exposed position.

11.8 SUMMARY OF CONCLUSIONS

1. In the analysis of large span domes with complex systems of radial ribs, horizontal purlin rings and diagonal bracing, none of the conventional space frame methods can be employed.

2. The best existing approach to the design of complex radial ribbed domes consists of considering two separate simple member systems. A primary system of radial ribs should first be designed to withstand bending moments and axial forces induced by dead and imposed loading conditions on the dome and then the complete structure should be assumed as being pin-jointed so that Schwedler's formulae (Art. 7.1) can be applied to give the axial forces in the horizontal purlin rings and the diagonal bracing. In addition to the axial forces produced by symmetrical loading conditions over the dome, the horizontal purlins should be designed to carry bending moments set up by the transmission of load through the roof covering. The diagonal bracing members should only be designed to carry axial loads caused by unsymmetrical loading conditions over the dome.

3. More information is required about the distribution of snow loading over domes and also concerning the effects of wind gusts and the variation of wind pressure over such structures.

4. In a radial ribbed dome of large span with slender ribs, variations in cross-sectional area and moment of inertia along the length of the ribs do not appreciably change the values of the base reactions.

5. The displacement and rotation of the apex ring, in the primary member system of a radial ribbed dome, determines the amount of displacement and rotation of the ribs and hence the ring stiffness governs the size and distribution of the base reactions.

6. For the analysis of the stresses in the primary member system of a circular arc radial ribbed dome, the three-pinned arch space frame approach of Makowski and Gogate[27] gives favourable results for symmetrical loading. However, under this condition the values of the reactions are the same as those for the three-pinned arch plane frame method of analysis.

7. The distribution of forces throughout the primary member system of a radial ribbed dome for unsymmetrical loading is completely different to that computed by the space frame method of Makowski and Gogate.

8. To obtain the maximum horizontal base reaction for the primary member system, a segment of the dome roof area with an angle of 270°, symmetrically situated about the axis of the rib at which the reaction is being considered and on the opposite side of the dome to it, would have to be loaded.

9. For the maximum vertical reaction to be obtained in the primary member system, a segment of the radial ribbed dome with an angle of 70°, symmetrically situated about the rib at which the reaction is required, would need to be loaded.

10. Adding horizontal purlin rings to the primary member system of a radial ribbed dome completely changes the distribution of the base

reactions.

11. The main concentrations of stress due to applied point loads on a radial ribbed dome framework are localized and rapidly decrease until small uniform forces are produced throughout the remainder of the system.

12. In a radial ribbed dome of large span with slender ribs, variations in cross-sectional area and moment of inertia, along the length of the ribs, affect the distribution of the forces imposed on the apex ring.

13. The stiffness of the apex ring in the primary member system of a radial ribbed dome controls the magnitude and direction of the forces imposed on it.

14. Great difficulty was experienced in obtaining any theoretical values for the apex ring forces.

15. Large downward vertical forces are imposed on the apex ring in the primary member system of a radial ribbed dome when all the ribs are loaded.

16. A maximum inward radial force occurs in the apex ring of the primary rib arrangement when a roof area segment with an angle of 110°, symmetrically situated about the considered rib, is loaded. If the remaining area alone is loaded, a maximum outward radial force is produced.

17. Maximum tangential apex ring forces occur in a radial ribbed dome primary member system when half of the dome is loaded at either side of the rib at which the force is being considered.

18. For the directly loaded rib and the rib opposite in the braced frame system, larger apex ring vertical and radial force influence coefficient values are obtained than those for the primary arrangement.

19. Horizontal purlins, if pin-connected at their ends to the radial ribs, cause the primary rib bending moments to be changed consistent with the change in base reaction values.

20. Slender radial ribs, which vary in cross-sectional area along their length, produce greater apex ring deflections than ribs of constant area.

21. When unsymmetrical loads are imposed on a dome with many radial ribs, the apex ring to which the ribs are attached is displaced and tilts.

22. Fixing moments in the ribs at the apex ring joints reduce the displacement of the ring and hence modify the stress distribution.

REFERENCES

1. MAKOWSKI, Z.S. (1965) — Steel Space Structures. Michael Joseph (London).

2. (1960) — The Concise Oxford Dictionary. Fourth Edition. Clarendon Press (Oxford).

3. DAVEY, N. (1961) — Vaults and Domes. A History of Building Materials. Phoenix House (London). 140-148.

4. ALLSOPP, B. (1955) — A General History of Architecture. Pitman (London).

5. HORSTMANN, F.C. (1965) — History of Building. I. Pitman (London).

6. CASSIE, W.F. & NAPPER, J.H. (1952) — Structure in Building. Architectural Press (London). 27.

7. RIVOIRA, G.T. (1918) — Moslem Architecture. Its Origins and Development. Oxford University Press (London) 45 - 137.

8. HAVELL, E.B. (1913) — Indian Architecture. Its Psychology, Structure, and History from the First Muhammadan Invasion to the Present Day. John Murray (London) 79-115.

9. MAKOWSKI, Z.S. (1962) — Braced Domes, Their History, Modern Trends and Recent Developments. Arch. Science Rev. 5, No. 2, July. 62 - 79.

10. MAKOWSKI, Z.S. (1953) — Theoretical and Experimental Stress Analysis of Braced Domes, With Special Reference to the Dome of Discovery. Ph.D. Thesis. University of London.

11. BENJAMIN, B.S. (1959) — The Analysis of Schwedler Domes. M.Sc. (Eng.) Thesis. University of London.

12. BENJAMIN, B.S. (1963) — The Analysis of Braced Domes. Asia Publishing House (New York).

13. TIMOSHENKO, S.P. & YOUNG, D.H. (1965) — Theory of Structures. 2nd. Ed. McGraw-Hill (New York) 161-214, 244, 245, 325 - 330.

14. TIMOSHENKO, S.P. & YOUNG, D.H. (1956) — Engineering Mechanics. 4th Ed. McGraw-Hill (New York) 41.

15. PIPPARD, A.J.S. & BAKER, J.F. (1948) — Analysis of Engineering Structures. Edward Arnold and Co. (London). 13 - 19.

16. SOUTHWELL, R.V. (1920) — Primary Stress-determination in Space Frames. Engineering CIX, Feb. 6th, 165 - 8.

17. MAYOR, B. (1926) — Introduction à la Statique Graphique des Systèmes de l'Espace. Payot & Co. (Lausanne).

18. CONSTANT, F.H. (1934) Stresses in Space Structures. Proc. Am. Soc. C.E., 60, 633 - 639.

19. NEAL, B.G. (1964) Structural Theorems and Their Applications. Pergamon Press (Oxford) 102 - 103.

20. WRIGHT, W. (1956) The Solution of Redundant Frameworks by Successive Reduction of the Gaps in Cut Members. Proc. Instn. Civ. Engrs. 5, (3), Dec., 845 - 850.

21. BYRNE, J.G. (1960) Using the Gap Reduction Method for the Analysis of a Hyperstatic Space Frame. Civil Eng. & P.W. Rev., 55, July, 923-4.

22. SOUTHWELL, R.V. (1940) Relaxation Methods in Engineering Science. Oxford University Press (London) 1 - 99.

23. LIVESLEY, R.K. (1964) Matrix Methods of Structural Analysis. Pergamon Press.

24. TSZE, S.S. (1956) Analysis of Ribbed Domes with Polygonal Rings. Proc. Am. Soc. C.E., 82, Paper No. 1101, Journal of the Structural Division, Nov., 1-20.

25. MITCHELL, L.H. (1953) A Shell Analogy for Framed Domes. Note A.R.L./SM. 208, Research and Development Branch, Aeronautical Research Labs., Melbourne, Australia.

26. TIMOSHENKO, S. (1940) Theory of Plates and Shells. McGraw-Hill (New York).

27. MAKOWSKI, Z.S. & GOGATE, M.N. (1956) Stress Analysis of Three-pinned Arch-ribbed Domes. Proc. Instn. Civ. Engrs. 5, (3), Dec., 824 - 844.

28. AMERICAN INSTITUTE OF TIMBER CONSTRUCTION. (1966). Timber Construction Manual. 1st. Ed. John Wiley & Sons (New York).

29. BRITISH STANDARDS INSTITUTION. CP3 : Chapter V : 1965 - Loading. British Standard Code of Practice.

30. ISYUMOV, N. (1967) Correspondence, February, 24th. Research Engineer, Boundary Layer Wind Tunnel Laboratory, Faculty of Engineering Science, The University of Western Ontario, Canada.

31. BRITISH STANDARDS INSTITUTION. CP 112 : 1967 The Structural Use of Timber. British Standard Code of Practice.

32. ROBERTS, G. (1951) The Structural Design of the Dome of Discovery, Festival of Britain, 1951. Jnl. Instn. Civ. Engrs. 36, Oct., 377 - 417.

33. LOO, H. (1966) The Design and Construction of Three Reticulated Steel Domes. International Conference on Space Structures, Paper No. G1, University of Surrey.

34. SCRUTON, C. & NEWBERRY, C.W. (1963) On the Estimation of Wind Loads for Building and Structural Design. Proc. Instn. Civ. Engrs. 25, June, 97 - 126.

35. DAVENPORT, A.G. (1961) The Application of Statistical Concepts to the Wind Loading of Structures. Proc. Instn. Civ. Engrs. 19, Aug., 449 - 472.

36. MAHER, F.J. (1965) Wind Loads on Basic Dome Shapes. Proc. Am. Soc. C.E. 91, Paper No. 4383, Journal of the Structural Division, June, 219 - 228.

37. MAHER, F.J. (1966) Wind Loads on Dome-cylinder and Dome-cone Shapes. Proc. Am. Soc. C.E. 92, Paper No. 4933, Journal of the Structural Division, October, 79 - 96.

38. FLÜGGE, W. (1960) Stresses in Shells. Springer-Verlag (Berlin) 50 - 53.

39. PFLÜGER, A. (1961) Elementary Statics of Shells. F.W. Dodge Corporation (New York) 9 - 11.

40. GONDIKAS, P. & SALVADORI, M.G. (1960) Wind Stresses in Domes. Proc. Am. Soc. C.E., Paper No. 2616, Journal of the Engineering Mechanics Division, October, 13 - 29.

41. GRAY, C.S.: KENT, L.E.: MITCHELL, W.A.: GODFREY, G.B. (1962) Steel Designers' Manual. Crosby Lockwood & Son Ltd. (London) 106 - 109.

42. CURRY, W.T. (1961) Working Stresses for Structural Laminated Timber. F.P.R.L. Special Report No. 15 H.M.S.O. (London) 4, 5.

43. CHARLTON, T.M. (1966) Model Analysis of Plane Structures. Pergamon Press. 7 - 17.

44. BRITISH STANDARDS INSTITUTION. B.S. 449:1959. The Use of Structural Steel in Building. British Standard Code of Practice.

45. BRITISH STANDARDS INSTITUTION. B.S. 1204:1964. Synthetic Resin Adhesives (Phenolic and Aminoplastic) for Wood. Part 1 : Gap-Filling Adhesives. British Standard Code of Practice.

46. BRITISH STANDARDS INSTITUTION. B.S. 373:1957. Methods of Testing Small Clear Specimens of Timber. British Standard Code of Practice.

47. MAKOWSKI, Z.S. & FIPPARD, A.J.S. (1952) Experimental Analysis of Space Structures, With Particular Reference to Braced Domes; With a Note on Stresses in Supporting Ring-Girders. Proc. Instn. Civ. Engrs. Part III, Dec., 420 - 441.

ADDITIONAL REFERENCES

(a) INSTITUTION OF STRUCTURAL ENGINEERS. List of References on Space Frames.

(b) INSTITUTION OF STRUCTURAL ENGINEERS. List of References on Domes.

(c) UNIVERSITY OF SURREY (1966). International Conference on Space Structures. Papers published by the Department of Civil Engineering.

(d) KETCHUM, V. (1959) Timber Domes. Design and Construction. Wood, October, 400 - 403.

(e) KETCHUM, V. (1959) Timber Domes. Loading Considerations and Erection Procedure. Wood, November, 440 - 443.

(f) MASON, J. (1969) British Standard Code of Practice for Loading: Wind Loads. The Structural Engineer 47, No. 10, October, 393 - 402.

APPENDIX I

TESTS ON MODEL RADIAL RIBBED DOME MATERIALS

RESULTS

a) Moisture Content Determination of Rib Timber (European Redwood)

W_1 = Weight of sample before drying (gm)

W_o = Oven-dry weight of sample (gm)

Specimen No.	W_1	W_o	$W_1 - W_o$	$\frac{W_1 - W_o}{W_o} \times 100\ \%$
1	58.07	52.16	5.91	11.3
2	59.11	53.13	5.98	11.3
3	56.96	51.05	5.91	11.6
4	59.45	53.24	6.21	11.7
5	56.33	50.48	5.85	11.6
6	58.40	52.36	6.04	11.5
Average Moisture Content				11.5 %

b) Specific Gravity Determination of Rib Timber (European Redwood)

V_1 = Volume of sample at test (cc) = l x b x h

l = Length (in.) ; b = Breadth (in.) ; h = Height (in.)

2cm standard static bending test samples employed

l = $\frac{30}{2.54}$ in. ; b = $\frac{2}{2.54}$ in. ; h = $\frac{2}{2.54}$ in.

Specimen No.	W_1	W_o	Specific Gravity $S_1 = \frac{W_1}{V_1}$	Nominal Specific Gravity $S_o = \frac{W_o}{V_1}$	Density lb/ft^3	Nominal Density lb/ft^3
1	58.07	52.16	.48	.43	33.3	29.8
2	59.11	53.13	.49	.44	34.0	30.5
3	56.96	51.05	.47	.43	32.6	30.0
4	59.45	53.24	.49	.44	34.1	30.6
5	56.33	50.48	.47	.42	32.6	29.2
6	58.40	52.36	.49	.44	34.1	30.6
Average			.48	.43	33.4	30.1

Density at test and nominal density, oven-dry, in lb/ft^3 obtained from S_1 and S_o by multiplication with $62.35(x + 100)/100$ where x is the percentage moisture content.

F.A.A. Ph.D. Thesis
19th Aug., 1968.

Structural Engineering Division,
Department of Civil Engineering,
University of Newcastle upon Tyne.

TESTS ON MODEL RADIAL RIBBED DOME MATERIALS

FIG. No. 2

STATIC BENDING TEST To B.S. 373 : 1957 ON RIB TIMBER
SPECIMEN No. 1. EUROPEAN REDWOOD.
CENTRAL LOADING METHOD a. 2cm STANDARD.
16th AUG., 1968.

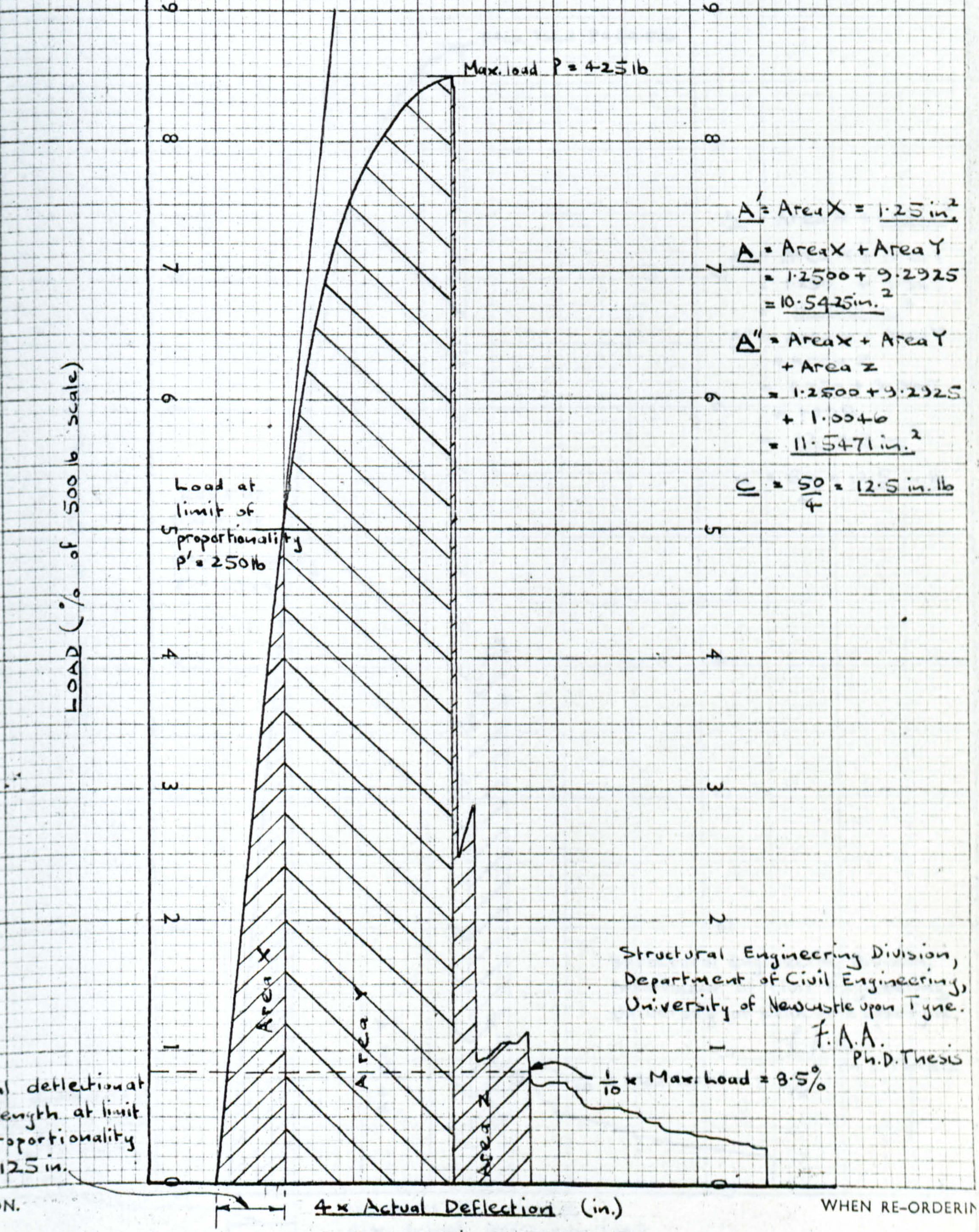

A' = Area X = 1·25 in.²

A = Area X + Area Y
= 1·2500 + 9·2925
= 10·5425 in.²

A'' = Area X + Area Y + Area Z
= 1·2500 + 9·2925 + 1·0046
= 11·5471 in.²

$C = \frac{50}{4} = 12·5$ in. lb

Structural Engineering Division,
Department of Civil Engineering,
University of Newcastle upon Tyne.
F. A. A.
Ph.D. Thesis

CROYDON.
WHEN RE-ORDERIN

TESTS ON MODEL RADIAL RIBBED DOME MATERIALS

FIG. No. 3

STATIC BENDING TEST to B.S. 373:1957 ON RIB TIMBER
SPECIMEN NO. 2. EUROPEAN REDWOOD.
CENTRAL LOADING METHOD a. 2cm STANDARD.
16th AUG., 1968

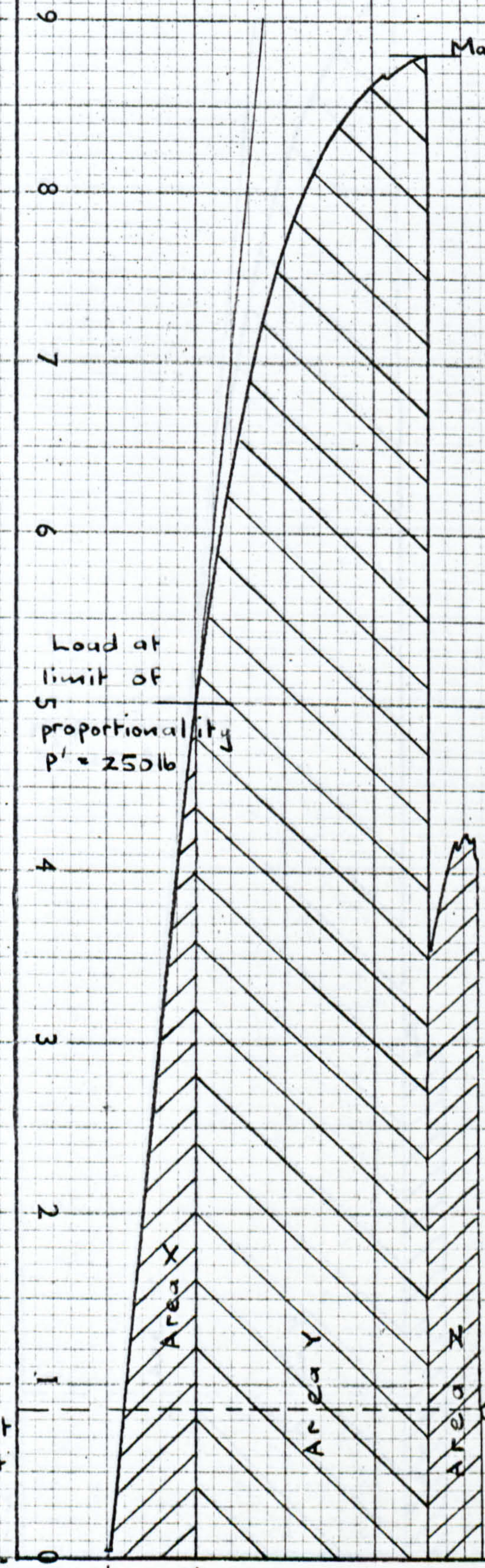

A' = Area X = 1.25 in.²

A = Area X + Area Y
= 1.250 + 9.965
= 11.215 in.²

A'' = Area X + Area Y + Area Z
= 1.250 + 9.965 + 1.198
= 12.413 in.²

C = 50/4 = 12.5 in.lb

Structural Engineering Division,
Department of Civil Engineering,
University of Newcastle upon Tyne.

f. A. A.
Ph.D. Thesis

TENSOMETER LTD. CROYDON.

TE E.1.

TESTS ON MODEL RADIAL RIBBED DOME MATERIALS

FIG. No. 4

STATIC BENDING TEST to B.S. 373: 1957 ON RIB TIMBER
SPECIMEN NO. 3. EUROPEAN REDWOOD.
CENTRAL LOADING METHOD a. 2cm STANDARD.
16th AUG., 1968.

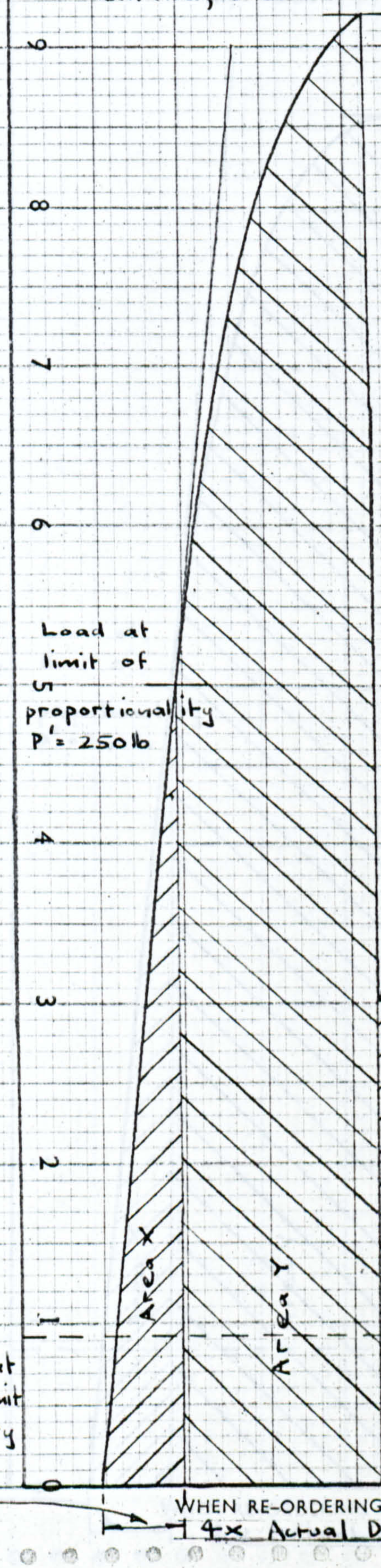

A' = Area X = 1·25 in.²

A = Area X + Area Y
= 1·2500 + 9·2035
= 10·4535 in.²

A'' = Area X + Area Y + Area Z
= 1·2500 + 9·2035 + 0·8460
= 11·2995 in.²

C = 50/4 = 12·5 in. lb

Structural Engineering Division,
Department of Civil Engineering,
University of Newcastle upon Tyne.

— F.A.A.
Ph.D. Thesis

WHEN RE-ORDERING QUOTE E.I.

TENSOMETE

TESTS ON MODEL RADIAL RIBBED DOME MATERIALS

FIG. No. 5

STATIC BENDING TEST To B.S. 373:1957 ON RIB TIMBER
SPECIMEN No. 4. EUROPEAN REDWOOD.
CENTRAL LOADING METHOD 4. 2cm STANDARD.
16th AUG., 1968.

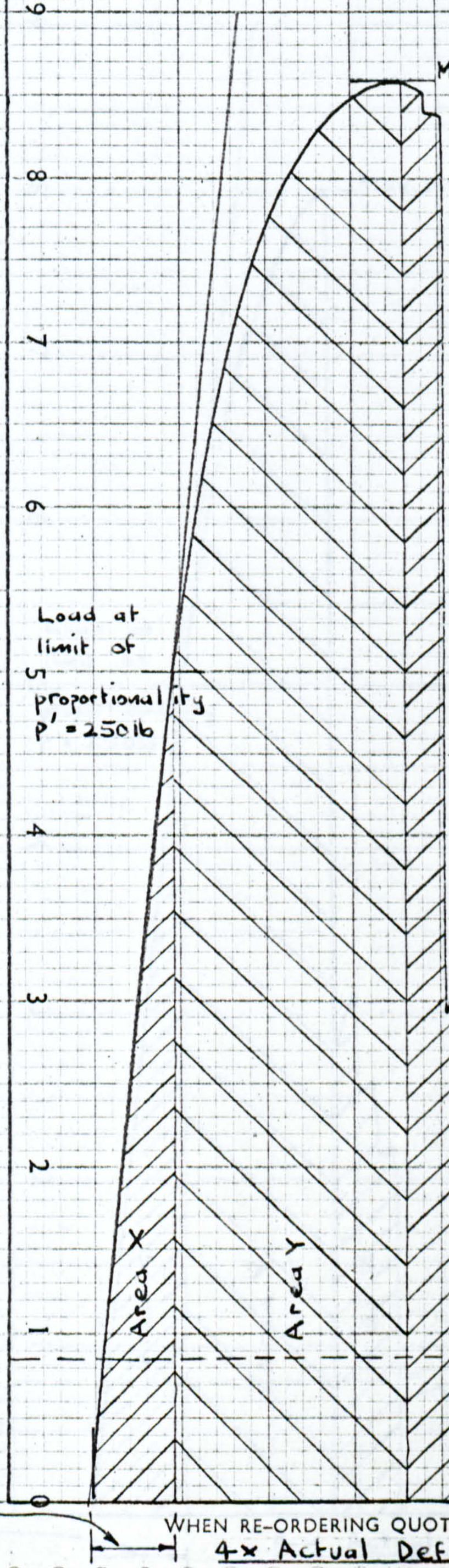

A' = Area X = 1·25 in.²

A = Area X + Area Y
= 1·25 + 10·17
= 11·42 in.²

A'' = Area X + Area Y + Area Z
= 1·2500 + 10·1700 + 3·0963
= 15·4163 in.²

C = 50/4 = 12·5 in.lb

Structural Engineering Division,
Department of Civil Engineering,
University of Newcastle upon Tyne.

F.A.A. Ph.D. Thesis

WHEN RE-ORDERING QUOTE E.1.

TENSOMET

TESTS ON MODEL RADIAL RIBBED DOME MATERIALS

FIG. No. 6

STATIC BENDING TEST to B.S. 373: 1957 ON RIB TIMBER
SPECIMEN No. 5. EUROPEAN REDWOOD.
CENTRAL LOADING METHOD a. 2cm STANDARD.
16th AUG., 1968.

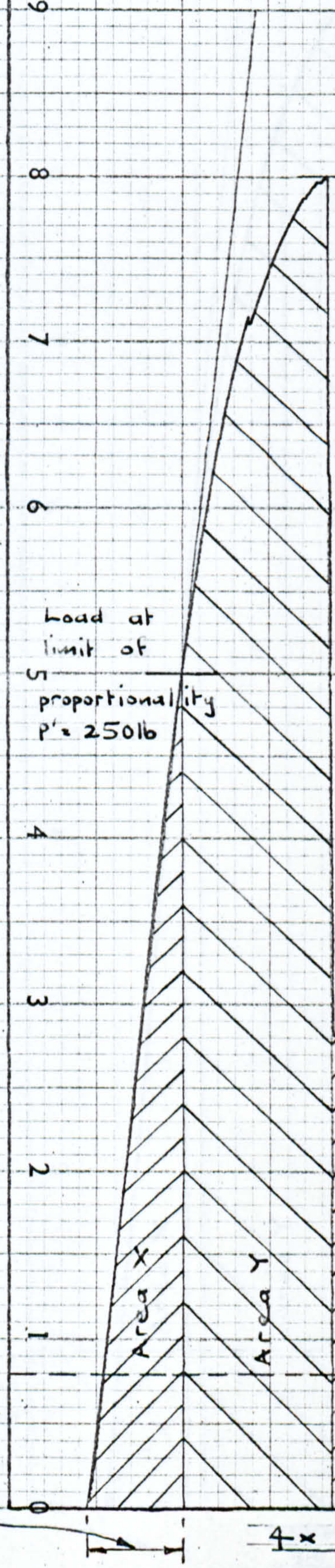

A' = Area X = 1·375 in.²

A = Area X + Area Y
= 1·375 + 5·920
= 7·295 in.²

A'' = Area X + Area Y + Area Z
= 1·375 + 5·920 + 0·895
= 8·18 in.²

C = 50/4 = 12·5 in.lb

Structural Engineering Division,
Department of Civil Engineering,
University of Newcastle upon Tyne.

F. A. A.
Ph. D. Thesis

CROYDON.

WHEN RE-ORDERI

TESTS ON MODEL RADIAL RIBBED DOME MATERIALS

FIG. No. 7

STATIC BENDING TEST To B.S. 373:1957 ON RIB TIMBER
SPECIMEN No. 6. EUROPEAN REDWOOD.
CENTRAL LOADING METHOD a. 2cm STANDARD.
16th AUG., 1968.

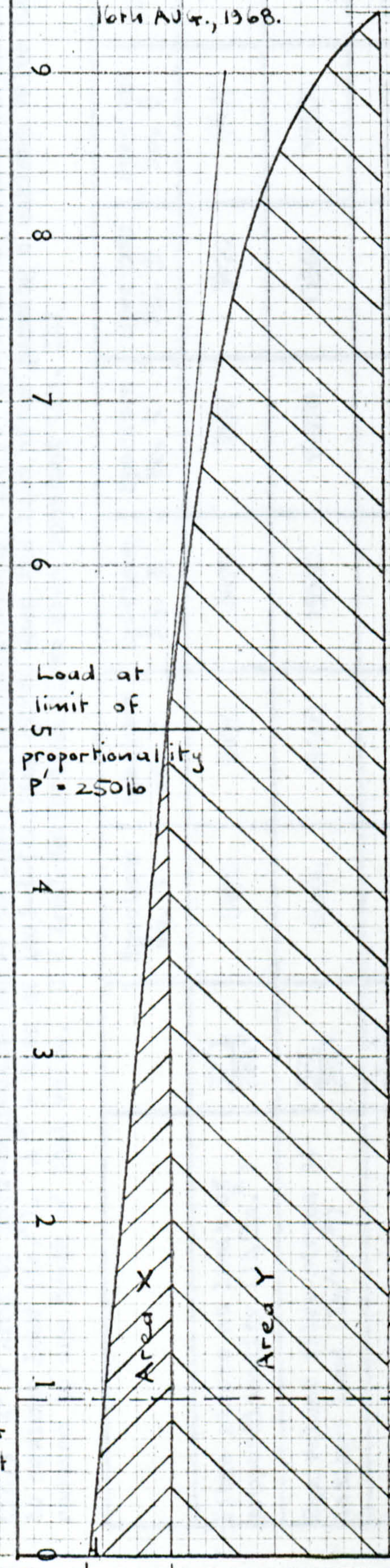

$\underline{A'}$ = Area X = $\underline{1{\cdot}25 in.^2}$

$\underline{A}$ = Area X + Area Y
= 1·2500 + 10·0971
= $\underline{11{\cdot}3471 in.^2}$

$\underline{A''}$ = Area X + Area Y + Area Z
= 1·2500 + 10·0971 + 0·2400
= $\underline{11{\cdot}5871 in.^2}$

$\underline{C} = \frac{50}{4} = \underline{12{\cdot}5 in.lb}$

Structural Engineering Division,
Department of Civil Engineering,
University of Newcastle upon Tyne.

— F.A.A.
Ph.D. Thesis

QUOTE E.1.

TENSOMETER LTD. CROYDON.

TESTS ON MODEL RADIAL RIBBED DOME MATERIALS

Fig. No. 8

Static Bending Tests to B.S. 373 : 1957 on Rib Timber

Specimen Nos. 1 - 6. European Redwood. Central loading method a. 2 cm. standard (specimen size :- b = breadth = $\frac{2}{2.54}$ in. h = depth = $\frac{2}{2.54}$ in., L = span = $\frac{28}{2.54}$ in.) For load-deflection curves, see Figs. 2 - 7. P = maximum load (lb). P' = Load at limit of proportionality (lb). Δ' = Deflection at mid length at limit of proportionality (in.) A' = Area of load-deflection curve to limit of proportionality ($in.^2$). A = Area of load-deflection curve to maximum load ($in.^2$). A''' = Area of load-deflection curve when the load after passing a maximum value has been reduced to one tenth of that value. C = load-deflection curve area constant (in. lb)

		Specimen No. 1	Specimen No. 2	Specimen No. 3	Specimen No. 4	Specimen No. 5	Specimen No. 6	Average
Fibre stress at limit of proportionality ($lb/in.^2$)	$\frac{3P'L}{2bh^2}$	8470	8470	8470	8470	8470	8470	8470
Equivalent fibre stress at maximum load ($lb/in.^2$)	$\frac{3PL}{2bh^2}$	14400	14900	15590	14570	13560	15930	14820
Modulus of Elasticity ($lb/in.^2$)	$\frac{P'L^3}{4\Delta' bh^3}$	1742000	1742000	1742000	1742000	1584000	1742000	1714000
Horizontal shear stress on neutral plane atlimit of proportionality ($lb/in.^2$)	$\frac{3P'}{4bh}$	302	302	302	302	302	302	302
Horizontal shear stress on neutral plane at maximum load ($lb/in.^2$)	$\frac{3P}{4bh}$	514	533	557	520	484	568	530
Work to limit of proportionality (in. $lb/in.^3$) ((Elastic resilience)	$\frac{CA'}{Lbh}$	2.3	2.3	2.3	2.3	2.5	2.3	2.3
Work to maximum load (in. $lb/in.^3$)	$\frac{CA}{Lbh}$	19.3	20.5	19.1	20.9	13.3	20.7	19.0
Total work (in.$lb/in.^3$)	$\frac{CA'''}{Lbh}$	21.1	22.7	20.7	28.2	15.0	21.1	21.5

TESTS ON MODEL RADIAL RIBBED DOME MATERIALS

FIG. No. 9

SHEAR PARALLEL TO GRAIN TEST TO B.S. 373 : 1957 ON RIB TIMBER

SPECIMEN NO. 1. EUROPEAN REDWOOD.

2cm STANDARD. SHEAR PLANE PARALLEL TO TANGENTIAL DIRECTION OF GRAIN.

19th AUG., 1968.

bh = Area in shear $(in.^2) = \frac{2}{2.54} \times \frac{2}{2.54}$

Apparent average shearing stress

$= \frac{P}{bh} = 1810 \ lb/in.^2$

Max. load P = 1125 lb

LOAD (% of 2500 lb scale)

Deflection (in.)

Structural Engineering Division,
Department of Civil Engineering,
University of Newcastle upon Tyne.

F.A.A.

Ph.D. Thesis

QUOTE E.1.

TENSOMETER LTD. CROYDON.

TESTS ON MODEL RADIAL RIBBED DOME MATERIALS

FIG. No. 10

SHEAR PARALLEL TO GRAIN TEST TO B.S. 373: 1957 ON RIB TIMBER

SPECIMEN NO. 2. EUROPEAN REDWOOD.

2-in STANDARD. SHEAR PLANE PARALLEL TO RADIAL DIRECTION OF GRAIN.

19TH AUG., 1968

bh = Area in shear = $\frac{2}{2.54} \times \frac{2}{2.54}$ in.^{2}

Apparent average shearing stress

$$= \frac{P}{bh} = 1930 \text{ lb/in.}^2$$

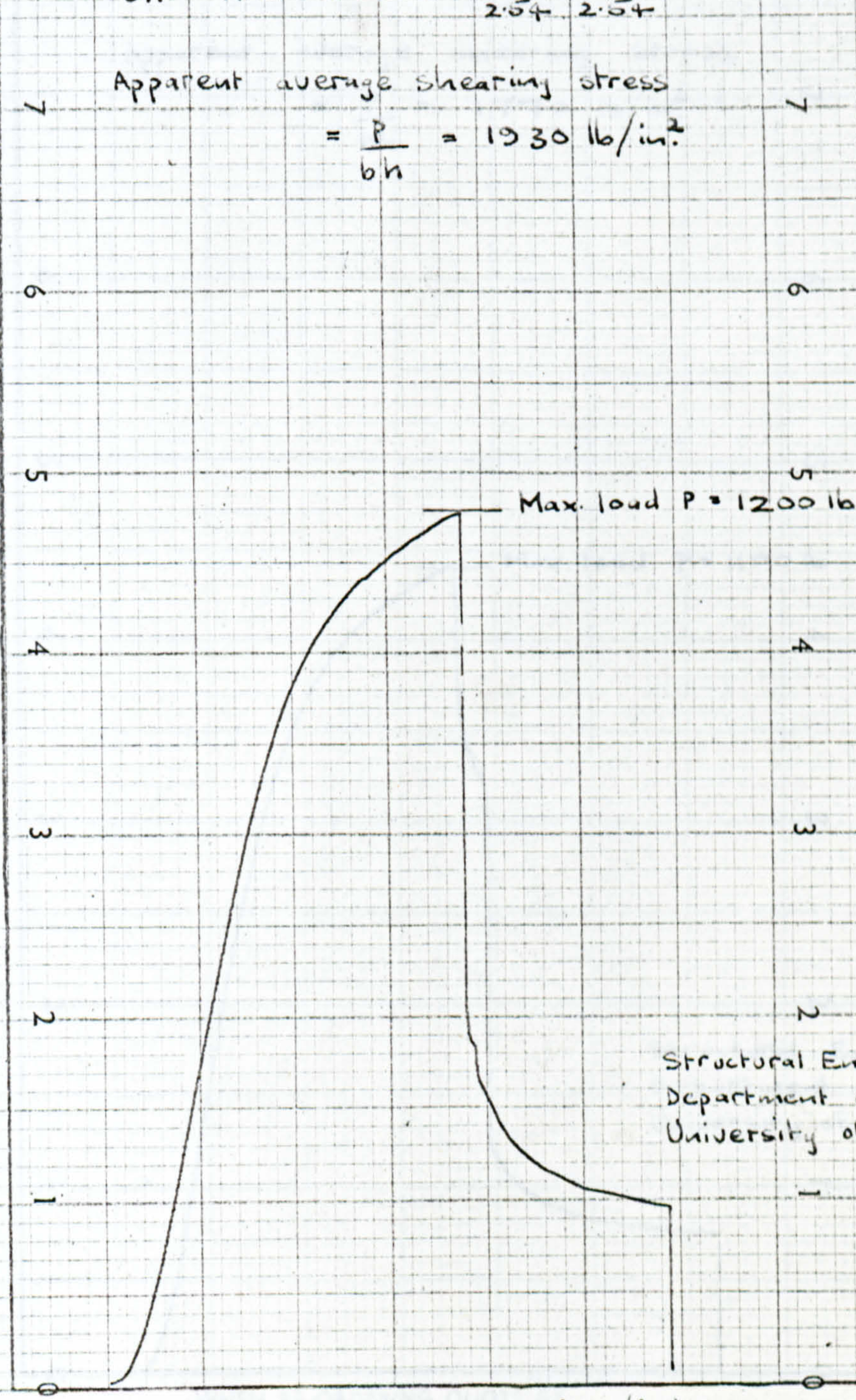

Structural Engineering Division,
Department of Civil Engineering,
University of Newcastle upon Tyne.

F.A.A.
Ph.D. Thesis

CROYDON.

WHEN RE-ORDERIN

TESTS ON MODEL RADIAL RIBBED DOME MATERIALS

FIG. No. 11

SHEAR PARALLEL TO GRAIN TEST TO B.S. 373: 1957 ON RIB TIMBER

SPECIMEN NO. 3. EUROPEAN REDWOOD.

2 cm STANDARD. SHEAR PLANE PARALLEL TO TANGENTIAL DIRECTION OF GRAIN.

19th AUG., 1968.

bh = Area in shear = $\frac{2}{2.54} \times \frac{2}{2.54}$ in.^{2}

Apparent average shearing stress

$= \frac{P}{bh} = 1770$ lb/in.^{2}

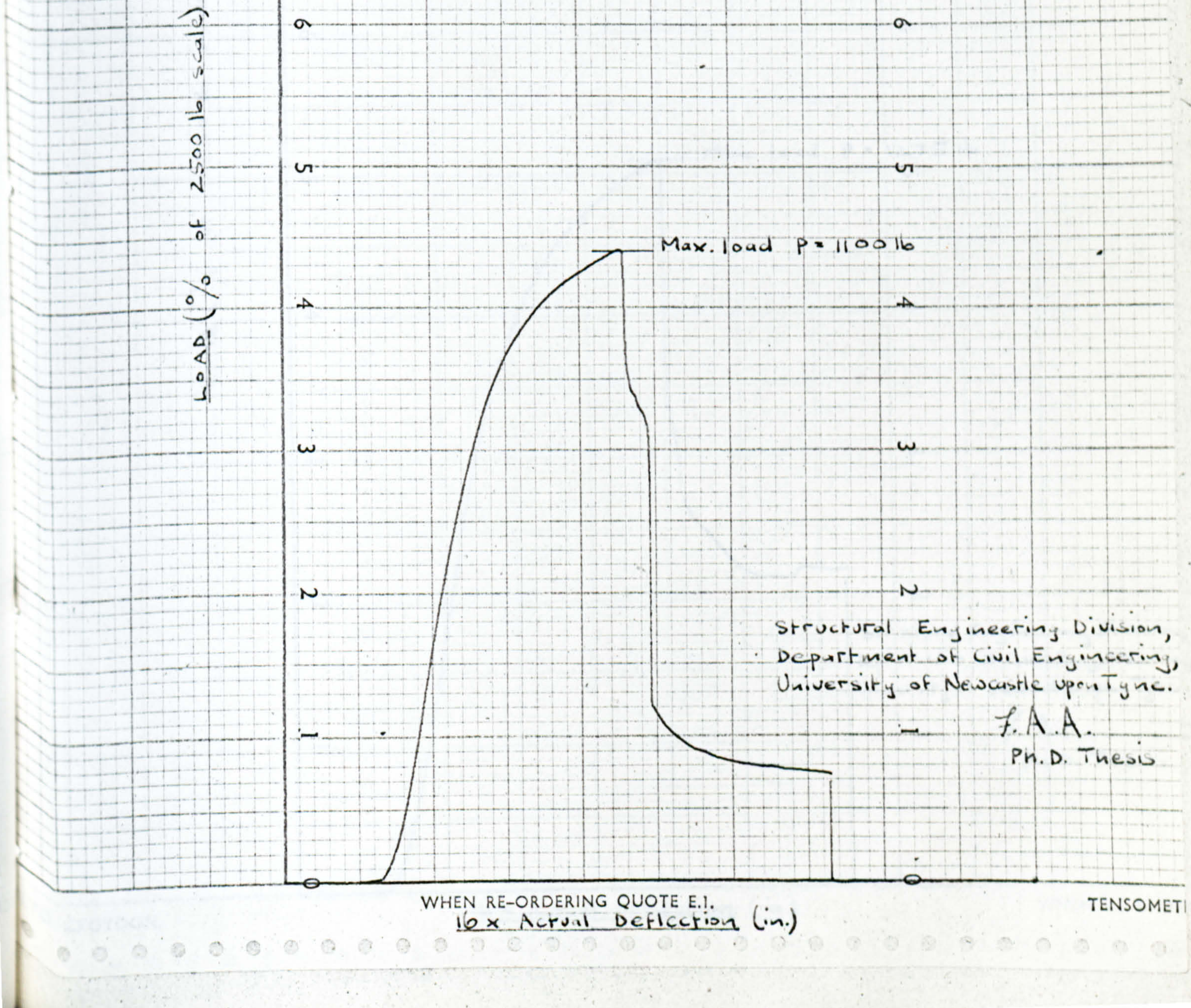

Structural Engineering Division,
Department of Civil Engineering,
University of Newcastle upon Tyne.

F.A.A.
Ph.D. Thesis

WHEN RE-ORDERING QUOTE E.I.

16 x Actual Deflection (in.)

TENSOMETI

TESTS ON MODEL RADIAL RIBBED DOME MATERIALS

FIG. No. 12

SHEAR PARALLEL TO GRAIN TEST TO B.S. 373: 1957 ON R.B TIMBER

SPECIMEN No. 4. EUROPEAN REDWOOD.

2 cm STANDARD. SHEAR PLANE PARALLEL TO RADIAL DIRECTION OF GRAIN.

19th AUG., 1968.

bh = Area in shear = $\frac{2}{2.54} \times \frac{2}{2.54}$ in.^{2}

Apparent average shearing stress

$= \frac{P}{bh} \times 2050$ lb/in.^{2}

Max. load P = 12.75 lb

LOAD ($\frac{1}{2}$ of 250 lb scale)

16 × Actual Deflection (in.)

Structural Engineering Division,
Department of Civil Engineering,
University of Newcastle upon Tyne.

F. A. A.

Ph. D. Thesis

LTD. CROYDON.

WHEN RE-ORDERI

TESTS ON MODEL RADIAL RIBBED DOME MATERIALS

FIG. No. 13

SHEAR PARALLEL TO GRAIN TEST TO B.S. 373: 1957 ON RIB TIMBER

SPECIMEN No. 5. EUROPEAN REDWOOD.

2 cm STANDARD. SHEAR PLANE PARALLEL TO TANGENTIAL DIRECTION OF GRAIN.

19th AUG., 1968.

bh = Area in shear = $\frac{2}{2{\cdot}54} \times \frac{2}{2{\cdot}54}$ in.^{2}

Apparent average shearing stress

$= \frac{P}{bh}$ = 1770 lb/in.^{2}

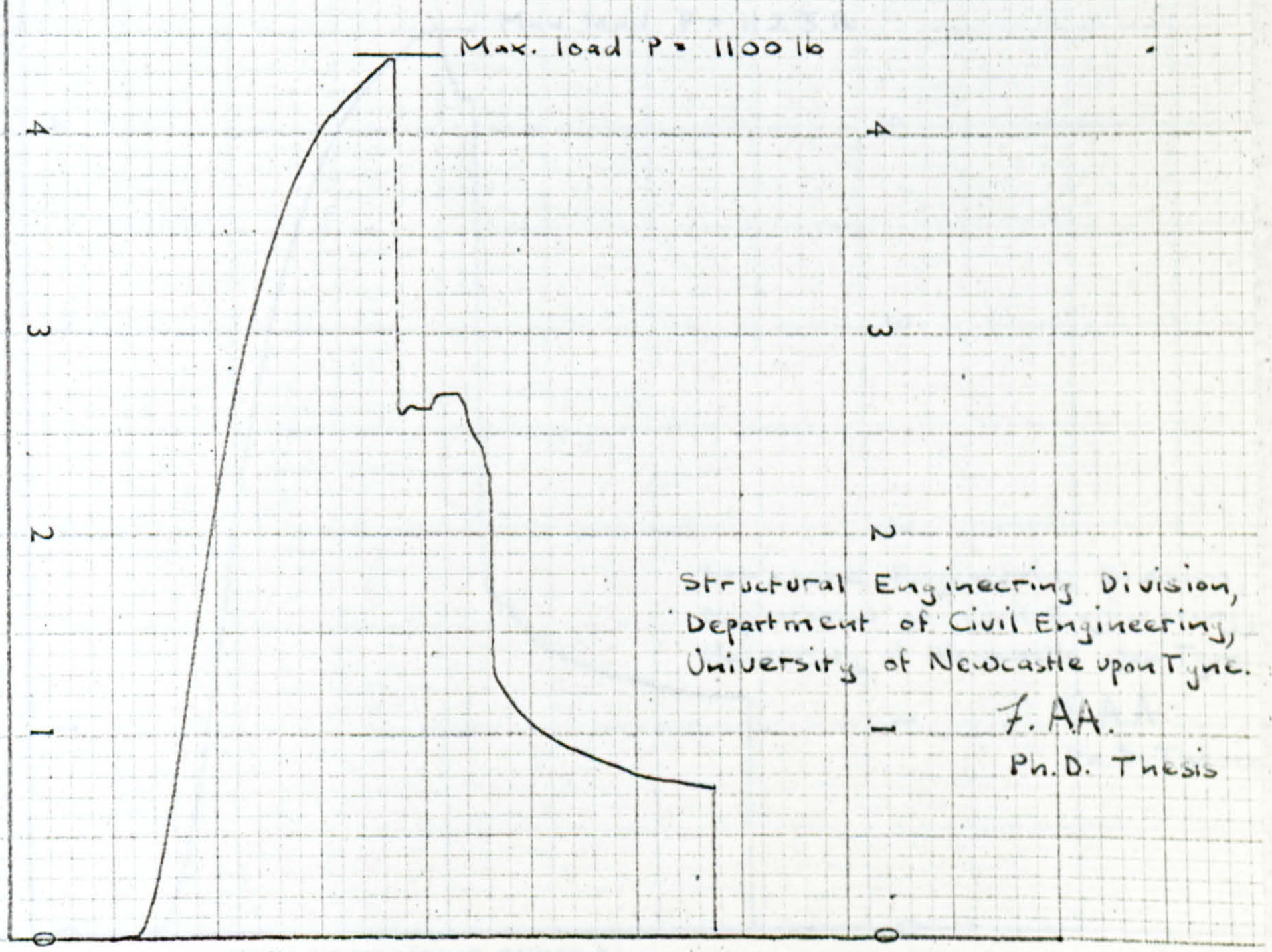

Structural Engineering Division,
Department of Civil Engineering,
University of Newcastle upon Tyne.

F.A.A.
Ph.D. Thesis

NOTE E.1.

TESTS ON MODEL RADIAL RIBBED DOME MATERIALS

FIG. No. 14

SHEAR PARALLEL TO GRAIN TEST TO B.S. 373 : 1957 ON RIB TIMBER

SPECIMEN NO. 6., EUROPEAN REDWOOD.

2 cm STANDARD. SHEAR PLANE PARALLEL TO RADIAL DIRECTION OF GRAIN.

19TH AUG., 1968.

bh = Area in shear = $\frac{3}{2.54} \times \frac{3}{2.64}$ in.^{2}

Apparent average shearing stress

$= \frac{P}{bh} = 1810$ lb/in.^{2}

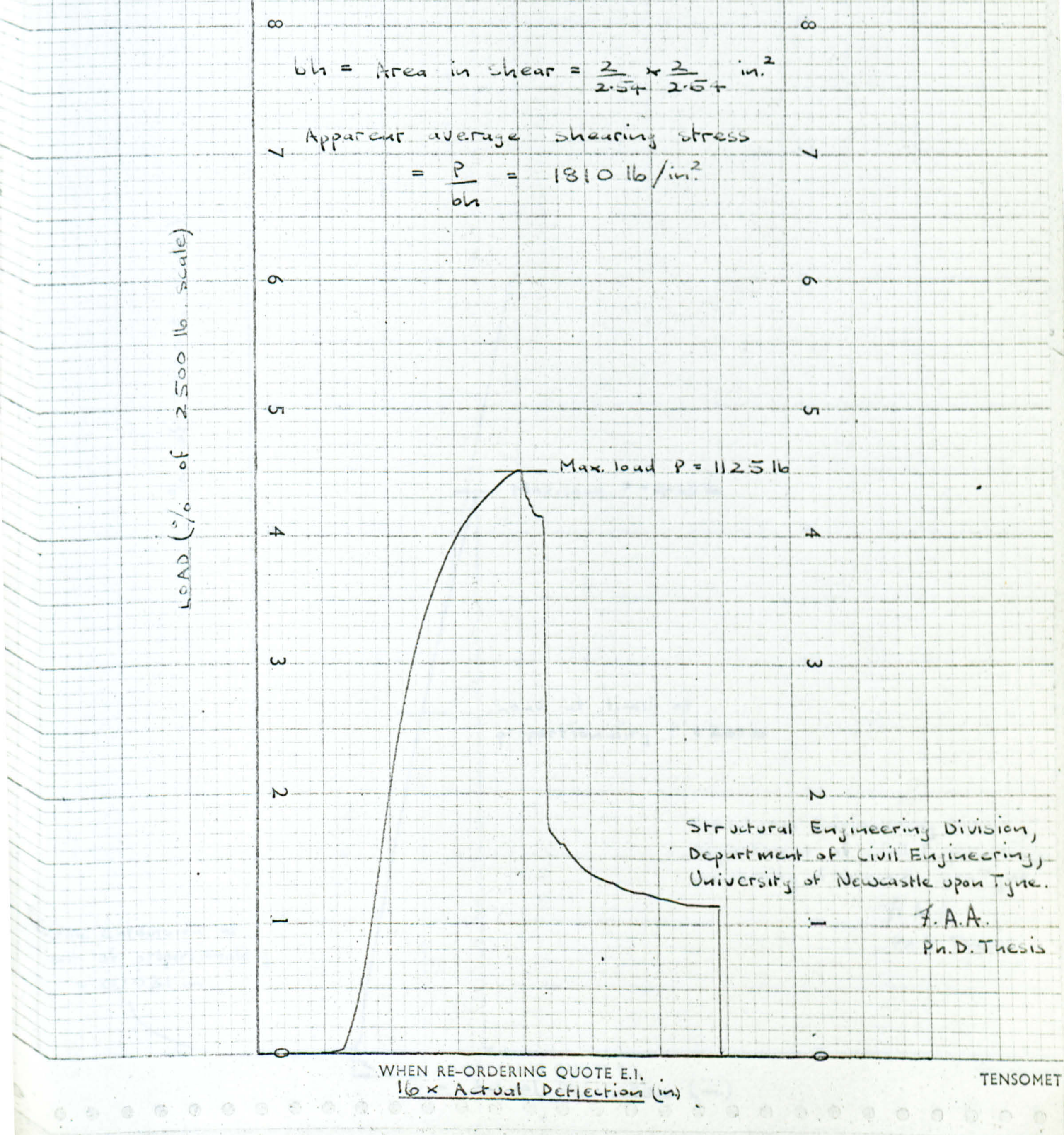

Structural Engineering Division,
Department of Civil Engineering,
University of Newcastle upon Tyne.

F.A.A.
Ph.D. Thesis

WHEN RE-ORDERING QUOTE E.1.

16 × Actual Deflection (in.)

TENSOMET

TESTS ON MODEL RADIAL RIBBED DOME MATERIALS

FIG. No. 15

TENSION PARALLEL TO GRAIN TEST
TO B.S. 373: 1957 ON RIB TIMBER
SPECIMEN NO. 1. EUROPEAN REDWOOD.
22nd AUG., 1968.

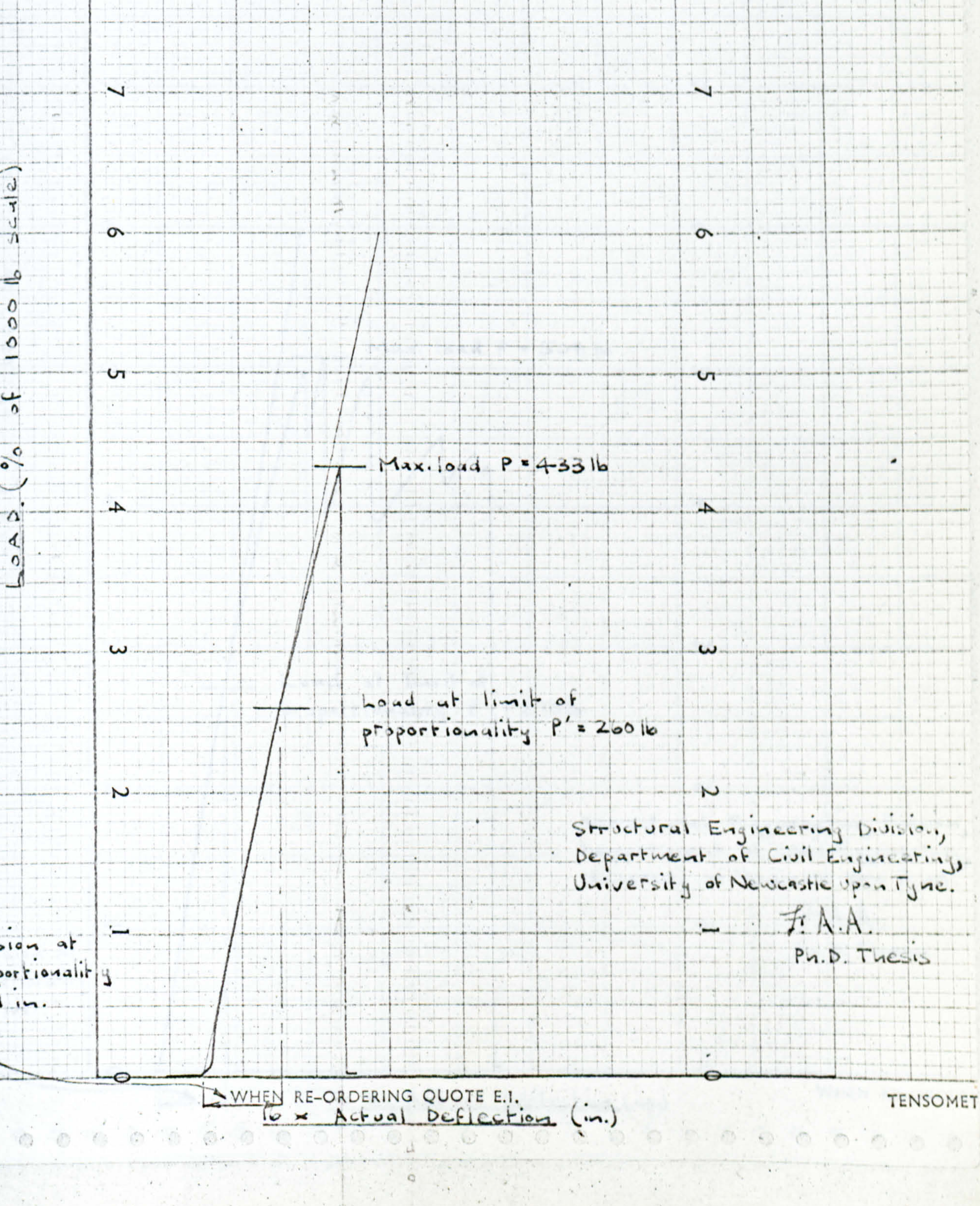

Structural Engineering Division,
Department of Civil Engineering,
University of Newcastle upon Tyne.

F. A. A.
Ph.D. Thesis

WHEN RE-ORDERING QUOTE E.I.

TENSOMET

TESTS ON MODEL RADIAL RIBBED DOME MATERIALS

FIG. No. 16

TENSION PARALLEL TO GRAIN TEST TO B.S. 373: 1957 ON RIB TIMBER

SPECIMEN No. 2. EUROPEAN REDWOOD.

22nd AUG., 1963.

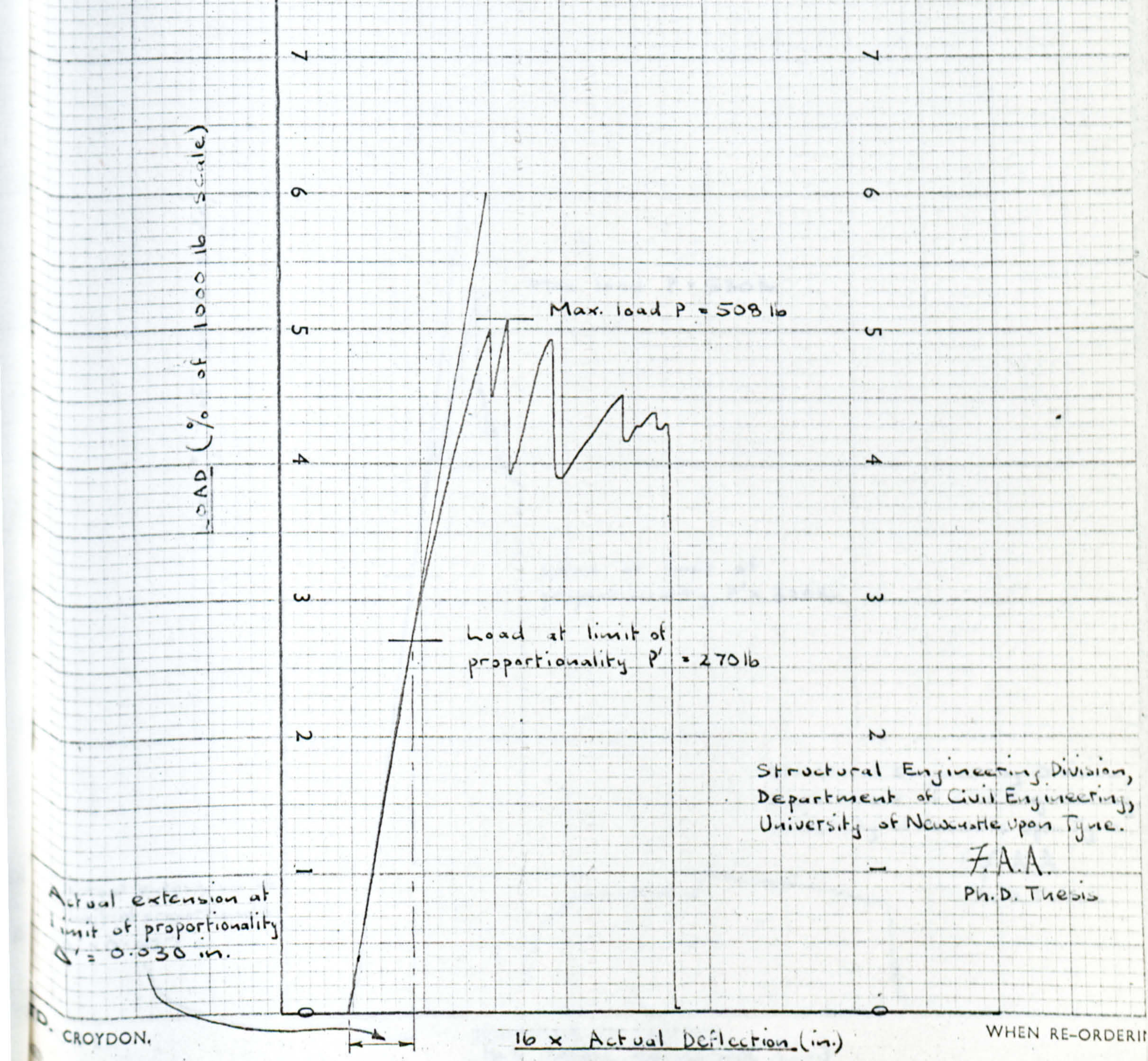

Structural Engineering Division,
Department of Civil Engineering,
University of Newcastle upon Tyne.

F.A.A.
Ph.D. Thesis

CROYDON.

WHEN RE-ORDERI

TESTS ON MODEL RADIAL RIBBED DOME MATERIALS

FIG. No. 17

TENSION PARALLEL TO GRAIN TEST TO B.S. 373: 1957 ON RIB TIMBER

SPECIMEN No. 3. EUROPEAN REDWOOD.

22nd AUG., 1968.

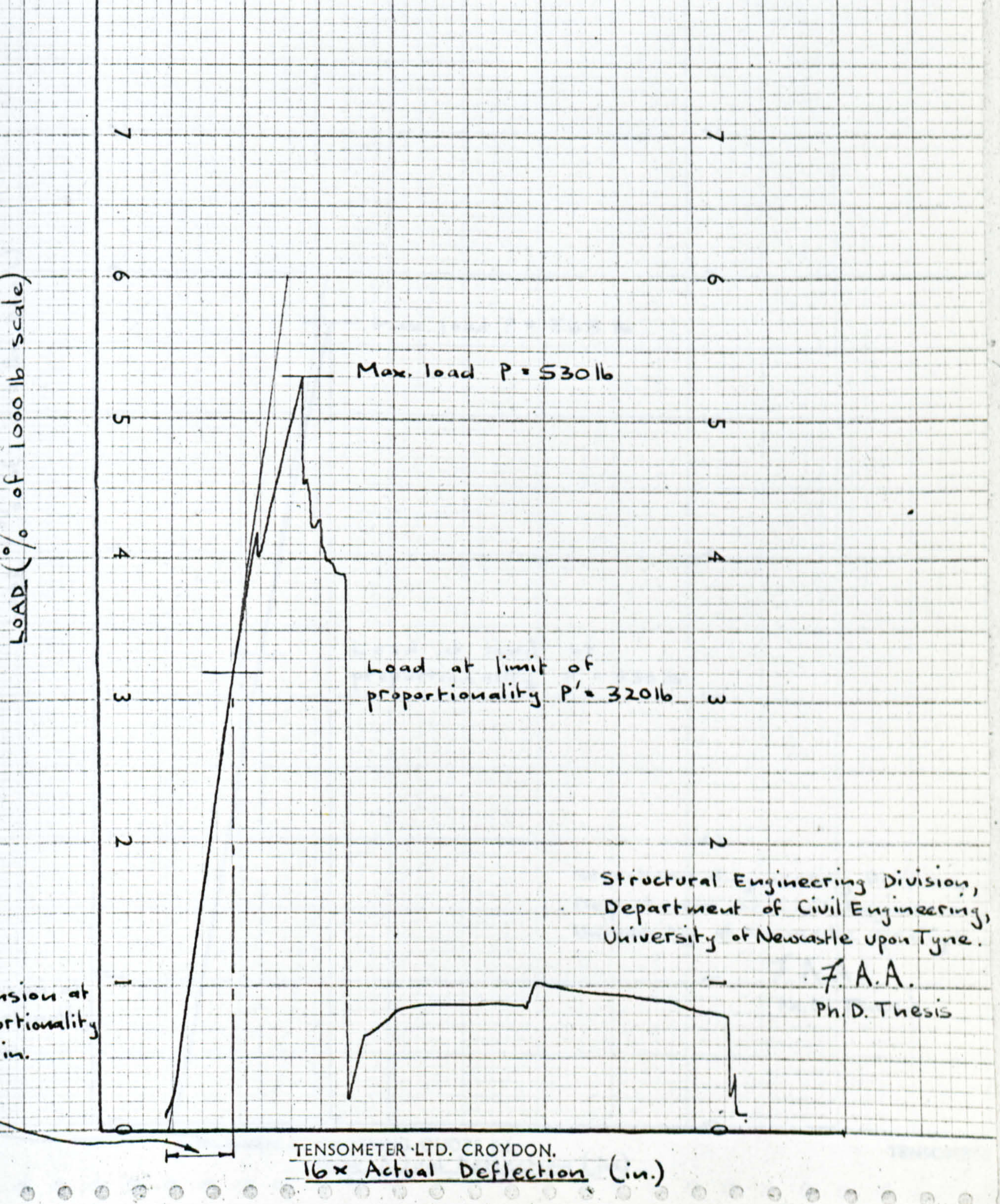

Structural Engineering Division, Department of Civil Engineering, University of Newcastle upon Tyne.

F. A. A.

Ph. D. Thesis

QUOTE E.1.

TENSOMETER LTD. CROYDON.

TESTS ON MODEL RADIAL RIBBED DOME MATERIALS

FIG. No. 18

TENSION PARALLEL TO GRAIN TEST TO B.S. 373 : 1957 ON RIB TIMBER

SPECIMEN NO. 4. EUROPEAN REDWOOD.

22nd AUG., 1968.

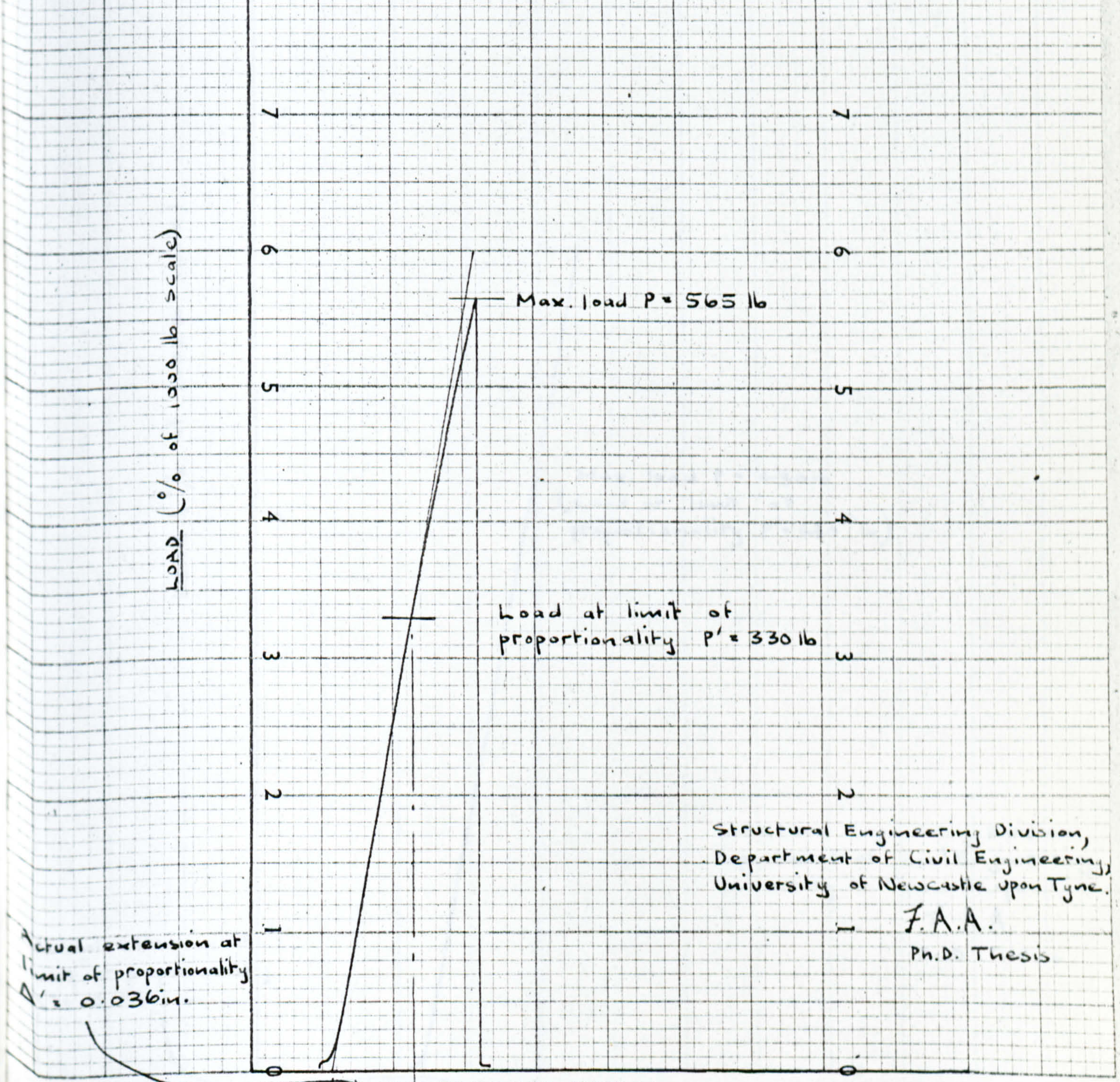

Structural Engineering Division,
Department of Civil Engineering,
University of Newcastle upon Tyne.

F.A.A.

Ph.D. Thesis

WHEN RE-ORDERING QUOTE E.I.

TENSOMETE

TESTS ON MODEL RADIAL RIBBED DOME MATERIALS

FIG. No. 19

TENSION PARALLEL TO GRAIN TEST TO B.S. 373: 1957 ON RIB TIMBER

SPECIMEN NO. 5. EUROPEAN REDWOOD.

22nd AUG., 1968.

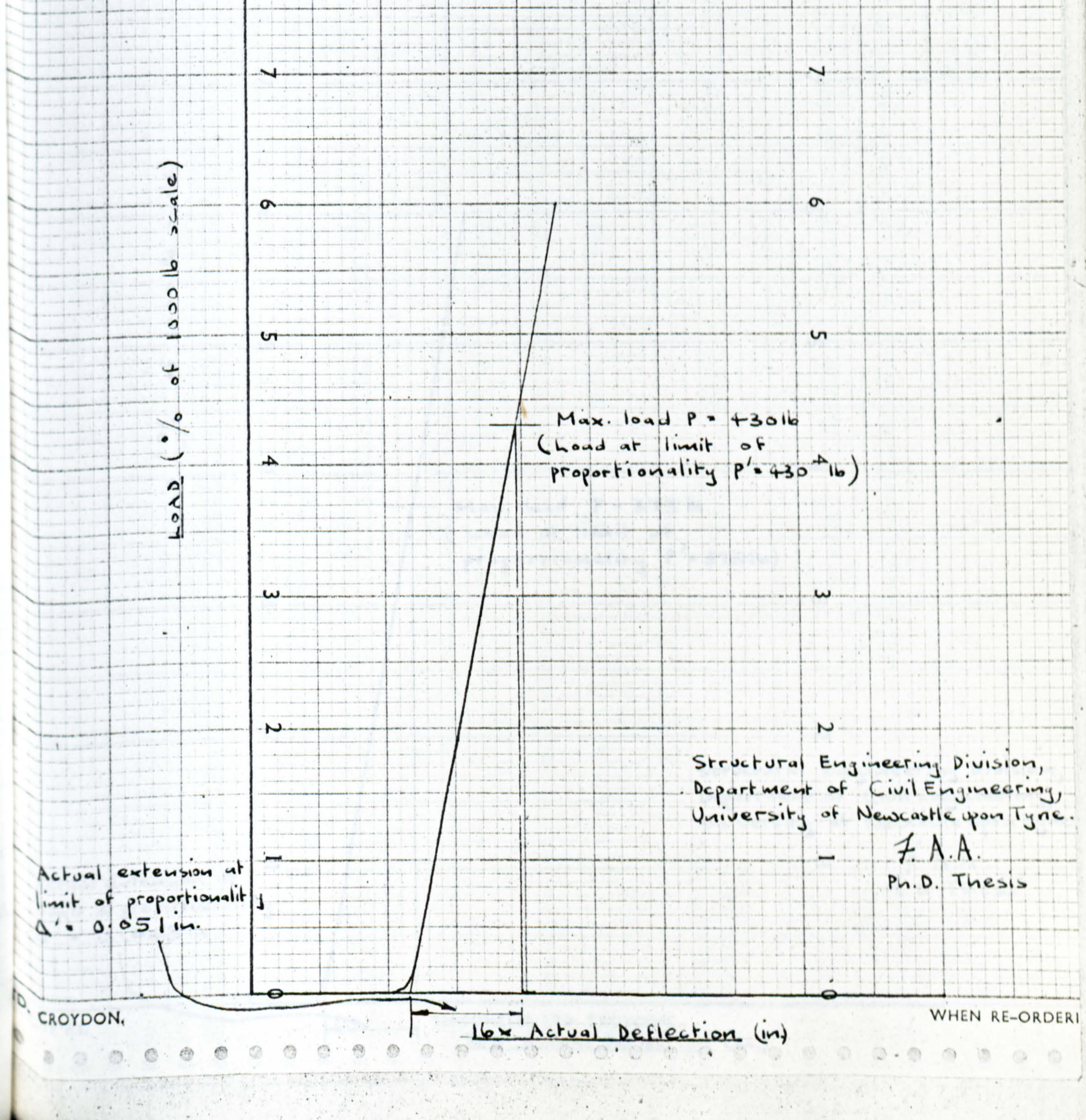

Structural Engineering Division,
Department of Civil Engineering,
University of Newcastle upon Tyne.

F. A. A.

Ph. D. Thesis

CROYDON.

WHEN RE-ORDERI

TESTS ON MODEL RADIAL RIBBED DOME MATERIALS

FIG. No. 20

TENSION PARALLEL TO GRAIN TEST TO B.S. 373: 1957 ON RIB TIMBER

SPECIMEN NO. 6. EUROPEAN REDWOOD.

22nd AUG., 1968.

LOAD (% of 1000 lb scale)

Max. load P = 375 lb
(load at limit of proportionality P' = 375 lb)

Actual extension at limit of proportionality Δ' = 0·043 in.

16× Actual Deflection (in.)

Structural Engineering Division,
Department of Civil Engineering,
University of Newcastle upon Tyne.

F. A. A.
Ph. D. Thesis

TENSOMETER LTD. CROYDON.

QUOTE E.1.

TESTS ON MODEL RADIAL RIBBED DOME MATERIALS

FIG. NO. 21

Tension Parallel to Grain Tests to B.S. 373 : 1957 on Rib Timber

Specimen Nos. 1 - 6. European Redwood. For load-deflection curves, see Figs. 15 - 20

A = Minimum area of cross-section of test length = $\frac{.3}{2.54} \times \frac{.6}{2.54}$ in.^{2} L = Gauge length between extensometer points = $\frac{21}{2.54}$ in.

		Specimen No. 1	Specimen No. 2	Specimen No. 3	Specimen No. 4	Specimen No. 5	Specimen No. 6	Average
Tensile stress at limit of proportionality lb/in.^{2}	$\frac{P'}{A}$	9330	9700	11480	11850	15450	13480	12250
Tensile stress at maximum load lb/in.^{2}	$\frac{P}{A}$	15530	18200	19000	20250	15450	13480	17000
Modulus of Elasticity E lb/in.^{2}	$\frac{P' L}{\Delta' A}$	2483000	2665000	3510000	2710000	2499000	2581000	2741300

F.A.A. Ph.D. Thesis
26th May, 1969.

Structural Engineering Division,
Department of Civil Engineering,
University of Newcastle upon Tyne.

TESTS ON MODEL RADIAL RIBBED DOME MATERIALS

FIG. No. 22

COMPRESSION PERPENDICULAR TO GRAIN

TEST TO B.S. 373: 1957 ON RIB TIMBER

SPECIMEN NO. 1. EUROPEAN REDWOOD.

CUBE OF 2 in. SIDE LOADED IN TANGENTIAL DIRECTION.

27th AUG., 1908.

A = Area of cross-section normal to direction of load
= 2×2 in.²

Compressive stress at limit of proportionality
$= \frac{P'}{A}$ = 400 lb/in.²

Compressive stress at compression of 0.1 in. (strain = 0.05)
$= \frac{P''}{A}$ = 675 lb/in.²

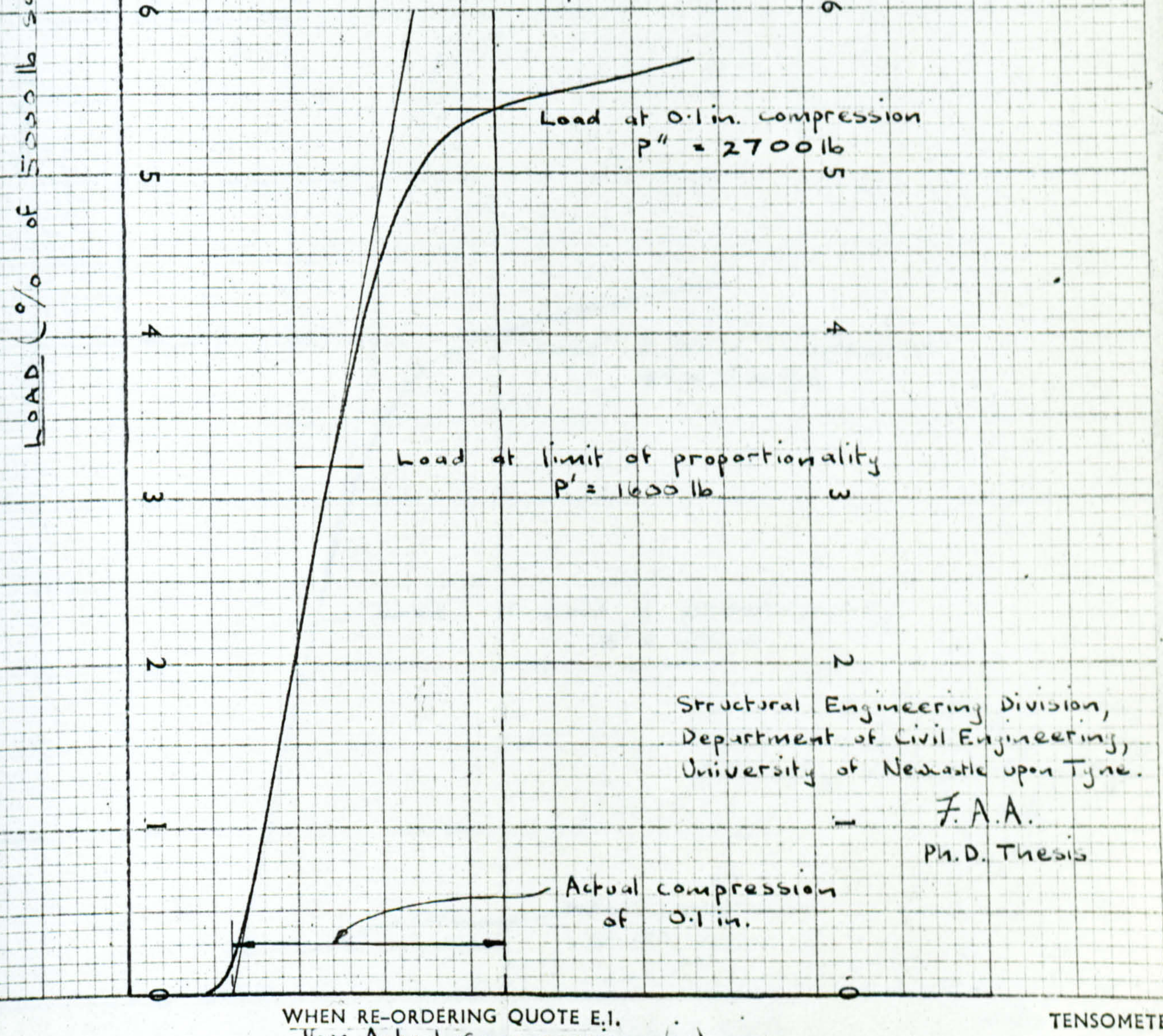

Structural Engineering Division,
Department of Civil Engineering,
University of Newcastle upon Tyne.

F.A.A.

Ph.D. Thesis

WHEN RE-ORDERING QUOTE E.1.

TENSOMETE

TESTS ON MODEL RADIAL RIBBED DOME MATERIALS

FIG. No 23

COMPRESSION PERPENDICULAR TO GRAIN

TEST TO B.S. 373:1957 ON RIB TIMBER SPECIMEN NO. 2. EUROPEAN REDWOOD. CUBE OF 2in. SIDE. LOADED IN RADIAL DIRECTION.

27th AUG., 1958.

A = Area of cross-section normal to direction of load
= 2×2 in.²

Compressive stress at limit of proportionality
$= \frac{P'}{A} = 288$ lb/in.²

Compressive stress at compression of 0.1 in. (strain = 0.05)
$= \frac{P''}{A} = 506$ lb/in.²

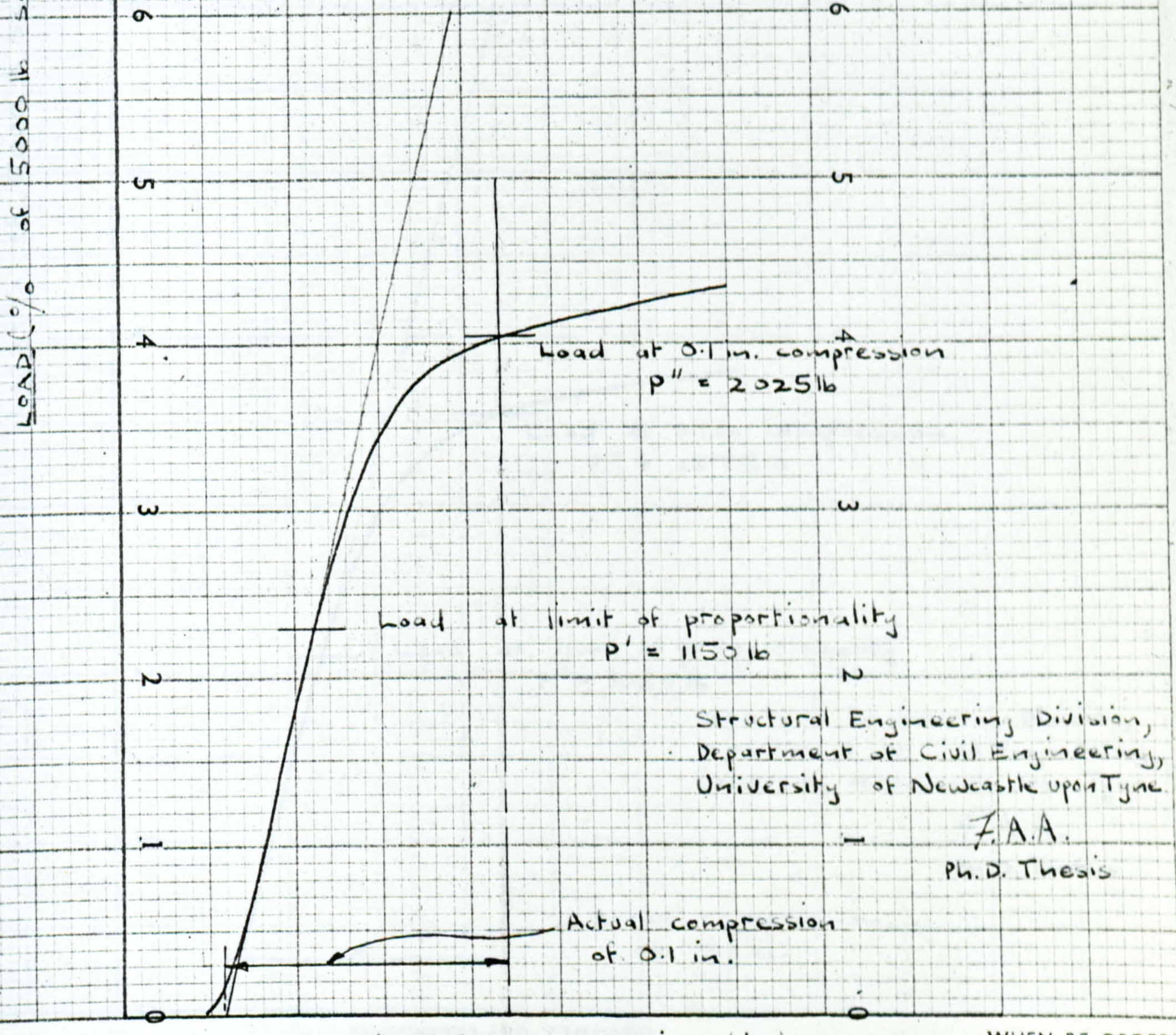

Structural Engineering Division,
Department of Civil Engineering,
University of Newcastle upon Tyne.

F.A.A.

Ph.D. Thesis

CROYDON.

WHEN RE-ORDERI

TESTS ON MODEL RADIAL RIBBED DOME MATERIALS

FIG. No. 24

COMPRESSION PERPENDICULAR TO GRAIN

TEST TO B.S. 373: 1957 ON RIB TIMBER SPECIMEN NO. 3. EUROPEAN REDWOOD. CUBE OF 2 in. SIDE. LOADED IN TANGENTIAL DIRECTION.

27th AUG., 1968.

A = Area of cross-section normal to direction of load
= 2 × 2 in.²

Compressive stress at limit of proportionality
$= \frac{P'}{A}$ = 263 lb/in.²

Compressive stress at compression of 0.1 in. (strain = 0.05)
$= \frac{P''}{A}$ = 444 lb/in.²

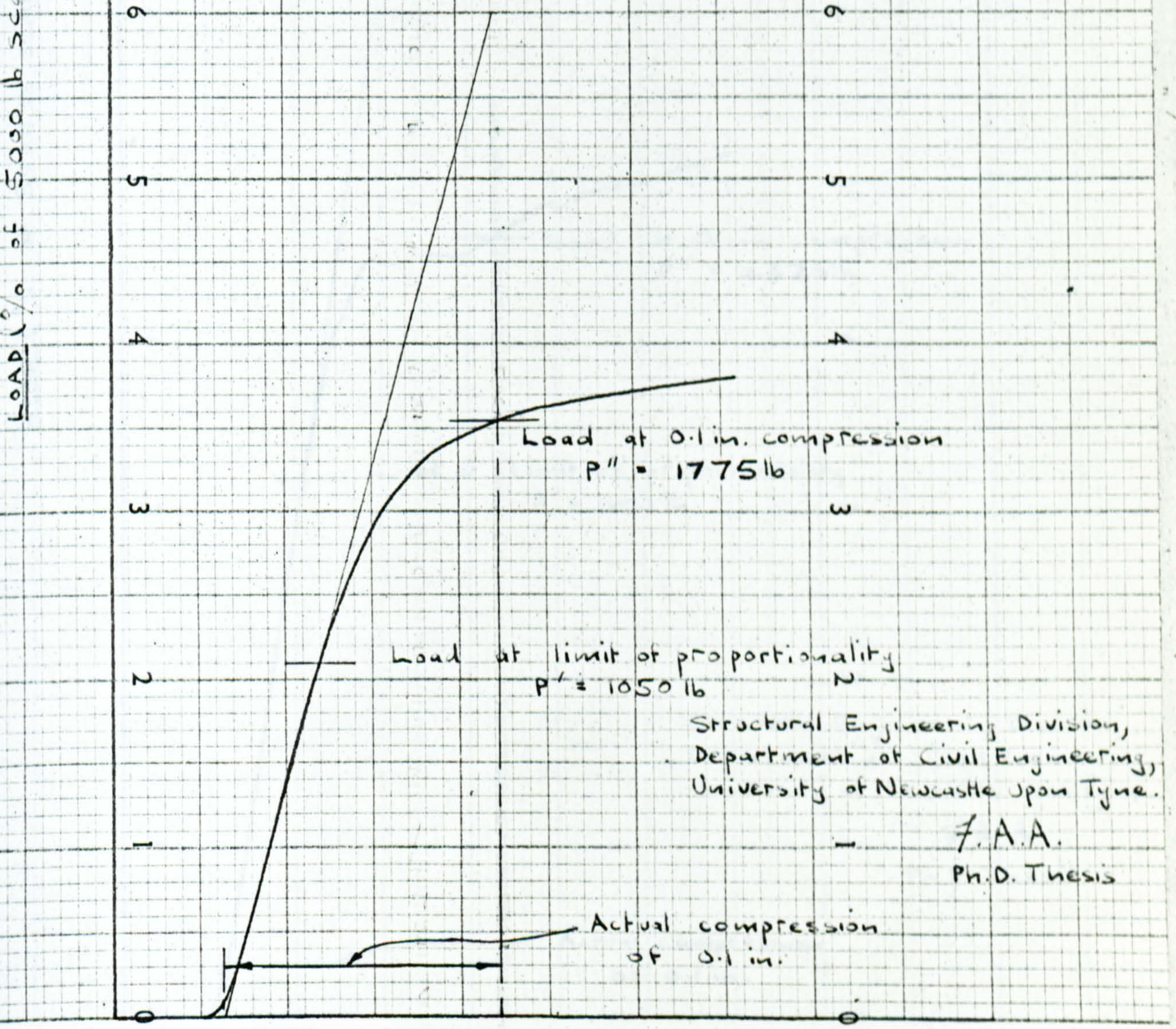

Structural Engineering Division,
Department of Civil Engineering,
University of Newcastle upon Tyne.

F.A.A.

Ph.D. Thesis

TENSOMETER LTD. CROYDON.

NOTE E.1.

TESTS ON MODEL RADIAL RIBBED DOME MATERIALS

FIG. No. 25

$\bar{O}$ COMPRESSION PERPENDICULAR TO GRAIN $\bar{O}$

TEST TO B.S. 373: 1957 ON RIB TIMBER

SPECIMEN NO. 4. EUROPEAN REDWOOD.

CUBE OF 2 in. SIDE. LOADED IN RADIAL DIRECTION.

27th AUG., 1962.

A = Area of cross-section normal to direction of load
$= 2 \times 2 \text{ in.}^2$

Compressive stress at limit of proportionality
$= \frac{P'}{A} = 400 \text{ lb/in.}^2$

Compressive stress at compression of 0.1 in. (strain = 0.05)
$= \frac{P''}{A} = 581 \text{ lb/in.}^2$

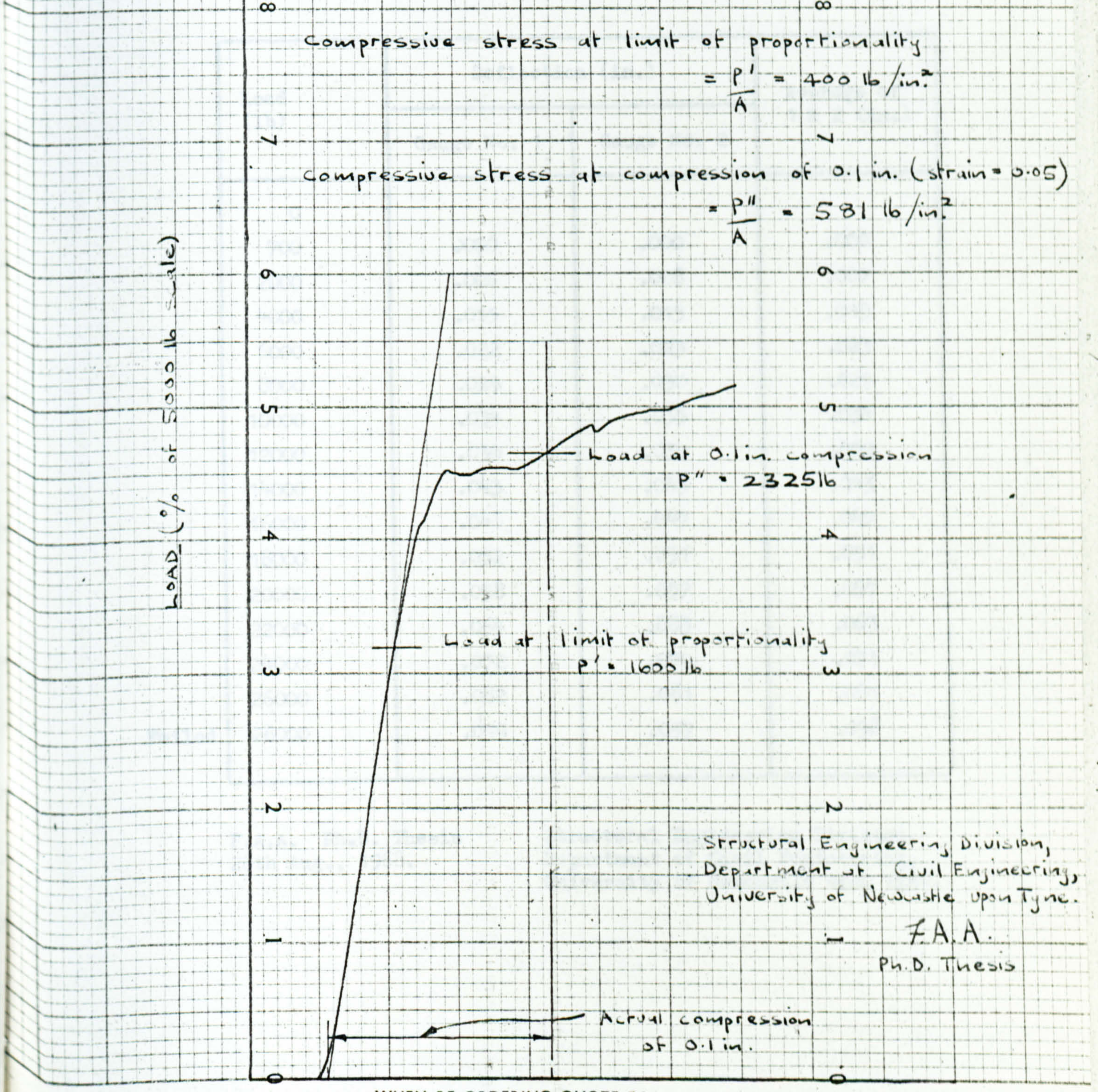

Structural Engineering Division,
Department of Civil Engineering,
University of Newcastle upon Tyne.

F.A.A.

Ph.D. Thesis

WHEN RE-ORDERING QUOTE E.I.

TENSOMET

TESTS ON MODEL RADIAL RIBBED DOME MATERIALS FIG. NO. 26

Compression Parallel to Grain Test to B.S. 373:1957 on Rib Timber

SPECIMEN NO. 1 EUROPEAN REDWOOD
2in. STANDARD (NON-LAMINATED)

Load (lb)	Deflection (in.)		Average of 1 & 2 (in.)
	Gauge No. 1	Gauge No. 2	
0			
700	.000	.000	.000
2000	.006	.008	.007
4000	.015	.015	.015
6000	.022	.023	.023
8000	.029	.030	.029
10000	.034	.035	.034
12000	.039	.039	.039
14000	.043	.043	.043
16000	.048	.047	.047
18000	.052	.051	.051
20000	.058	.057	.057
22000	.064	.063	.063
24000	.072	.070	.071
26000	.082	.081	.081
Failed 28000	.099	.097	.098

F.A.A. Ph.D. Thesis
26th Aug., 1968.

Structural Engineering Division,
Department of Civil Engineering,
University of Newcastle upon Tyne.-

TESTS ON MODEL RADIAL RIBBED DOME MATERIALS

FIG. No. 27

COMPRESSION PARALLEL TO GRAIN TEST TO B.S. 373: 1957 ON RIB TIMBER

SPECIMEN NO. 1. EUROPEAN REDWOOD.
2 in. STANDARD (NON-LAMINATED).
26th AUG., 1968.

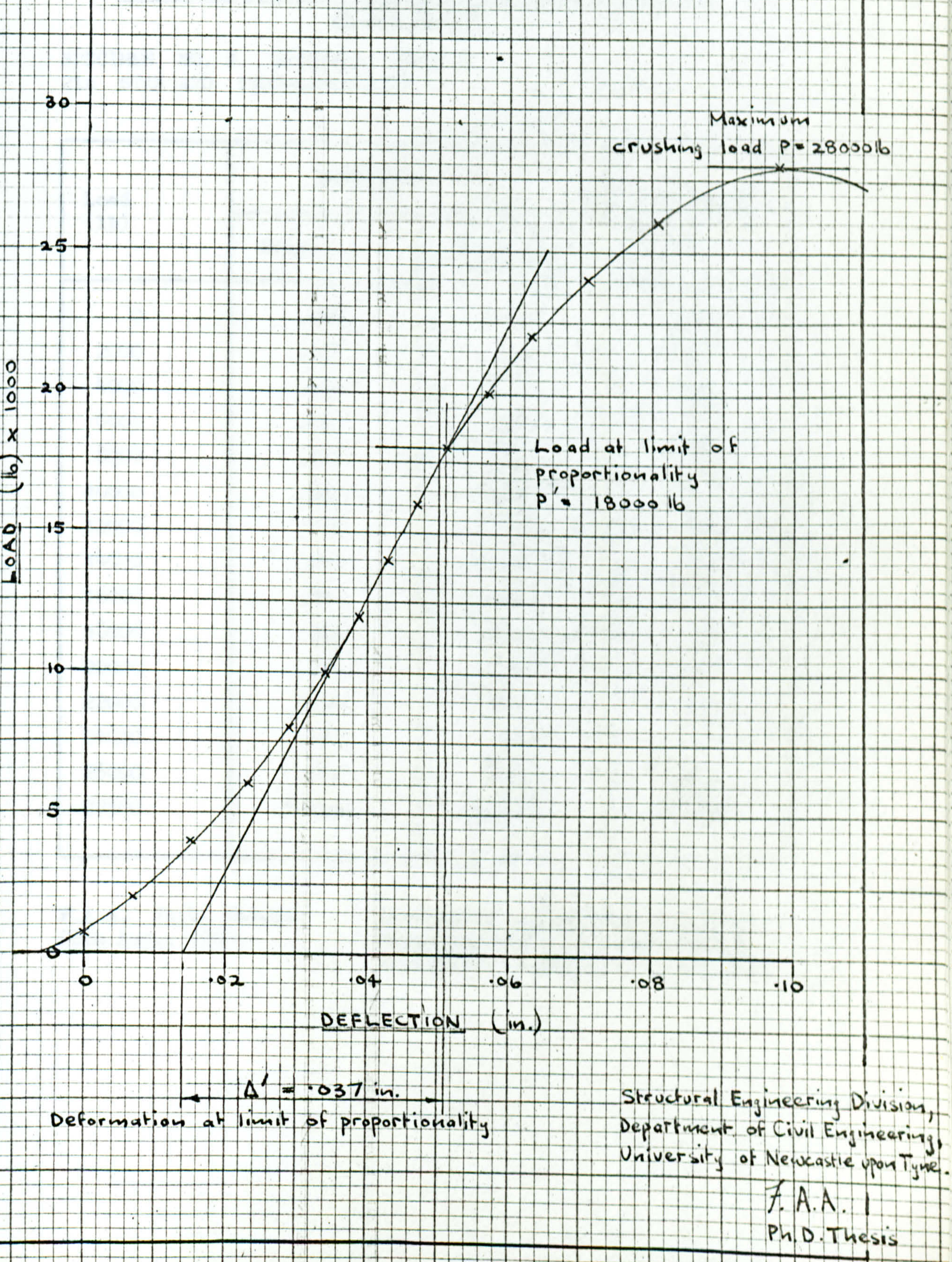

Structural Engineering Division,
Department of Civil Engineering,
University of Newcastle upon Tyne.

F. A. A.
Ph. D. Thesis

TESTS ON MODEL RADIAL RIBBED DOME MATERIALS FIG.NO. 28

Compression Parallel to Grain Test to B.S. 373:1957 on Rib Timber

SPECIMEN NO. 2 EUROPEAN REDWOOD
2in STANDARD (NON-LAMINATED)

Load (lb)	Deflection (in)		Average of 1 & 2 (in.)
	Gauge No. 1	Gauge No. 2	
0	.000	.000	.000
2000	.020	.017	.018
4000	.026	.023	.024
6000	.031	.027	.029
8000	.037	.033	.035
10000	.040	.036	.038
12000	.044	.040	.042
14000	.048	.043	.045
16000	.051	.047	.049
18000	.055	.050	.052
20000	.059	.054	.056
22000	.064	.059	.061
24000	.070	.065	.067
26000	.078	.073	.075
27500	Failed	Failed	Failed

F.A.A. Ph.D. Thesis
26th Aug., 1968.

Structural Engineering Division,
Department of Civil Engineering,
University of Newcastle upon Tyne.

TESTS ON MODEL RADIAL RIBBED DOME MATERIALS

FIG. No. 29

COMPRESSION PARALLEL TO GRAIN TEST TO B.S. 373:1957 ON RIB TIMBER

SPECIMEN No. 2. EUROPEAN REDWOOD.
2 in. STANDARD (NON-LAMINATED).
26 Th AUG., 1968.

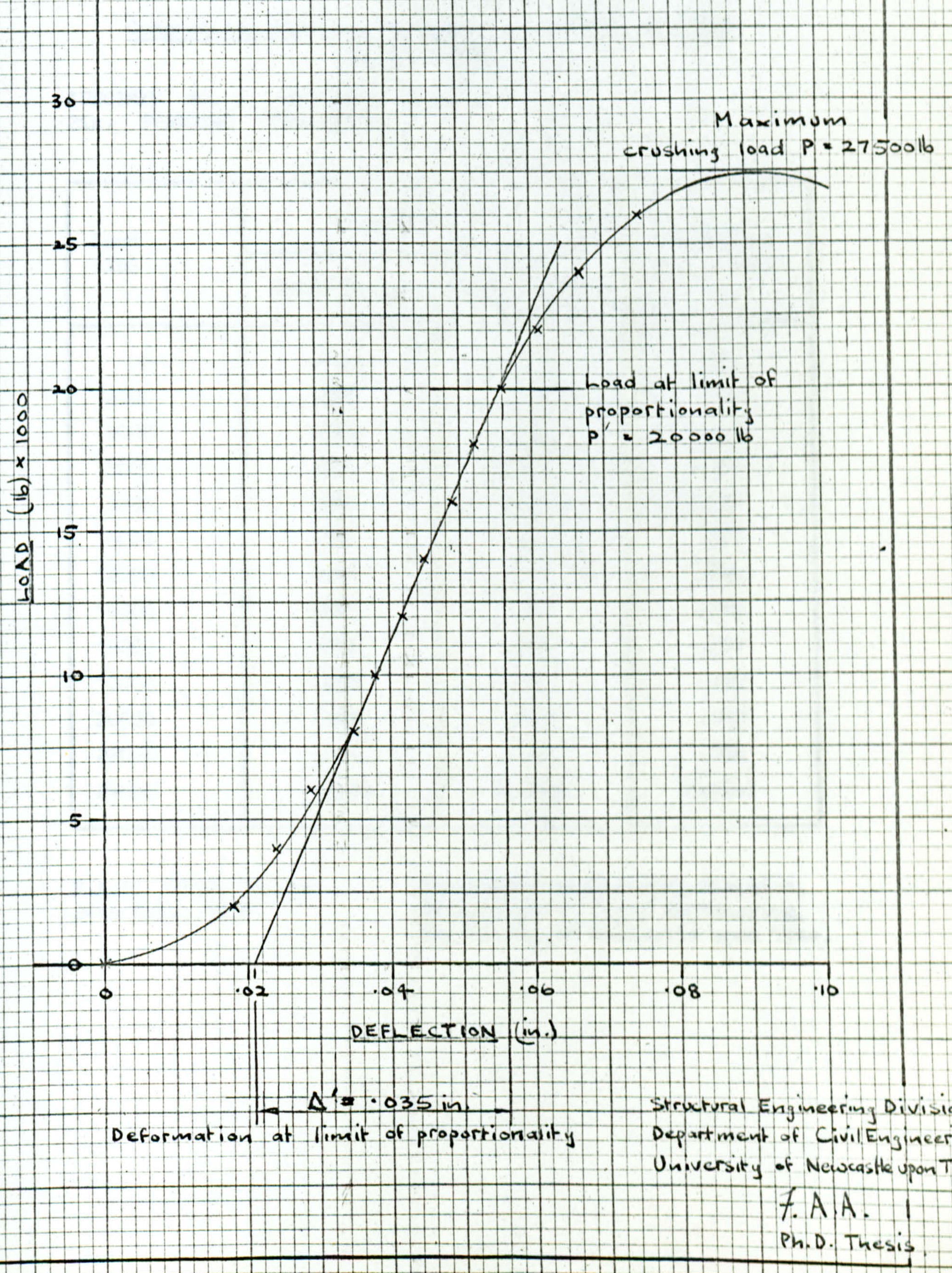

Structural Engineering Division,
Department of Civil Engineering,
University of Newcastle upon Tyne.

F. A. A.
Ph. D. Thesis

TESTS ON MODEL RADIAL RIBBED DOME MATERIALS FIG. NO.30

Compression Parallel to Grain Test to B.S. 373:1957 on Rib Timber

SPECIMEN NO. 3 EUROPEAN REDWOOD
2in. STANDARD (LAMINATED)

Load (lb)	Deflection (in.)		Average of 1 & 2 (in.)
	Gauge No. 1	Gauge No. 2	
0	.000	.000	.000
2000	.022	.016	.019
4000	.029	.023	.026
6000	.035	.029	.032
8000	.041	.034	.037
10000	.045	.038	.041
12000	.048	.041	.044
14000	.051	.044	.047
16000	.055	.048	.051
18000	.059	.052	.055
20000	.064	.057	.060
22000	.070	.062	.066
24000	Failed	Failed	Failed

F.A.A. Ph.D. Thesis
26th Aug., 1968.

Structural Engineering Division,
Department of Civil Engineering,
University of Newcastle upon Tyne.

TESTS ON MODEL RADIAL RIBBED DOME MATERIALS.

FIG. No. 31

COMPRESSION PARALLEL TO GRAIN TEST TO B.S. 373: 1957 ON RIB TIMBER

SPECIMEN No. 3. EUROPEAN REDWOOD.
2 in. STANDARD (LAMINATED).
26th AUG., 1968.

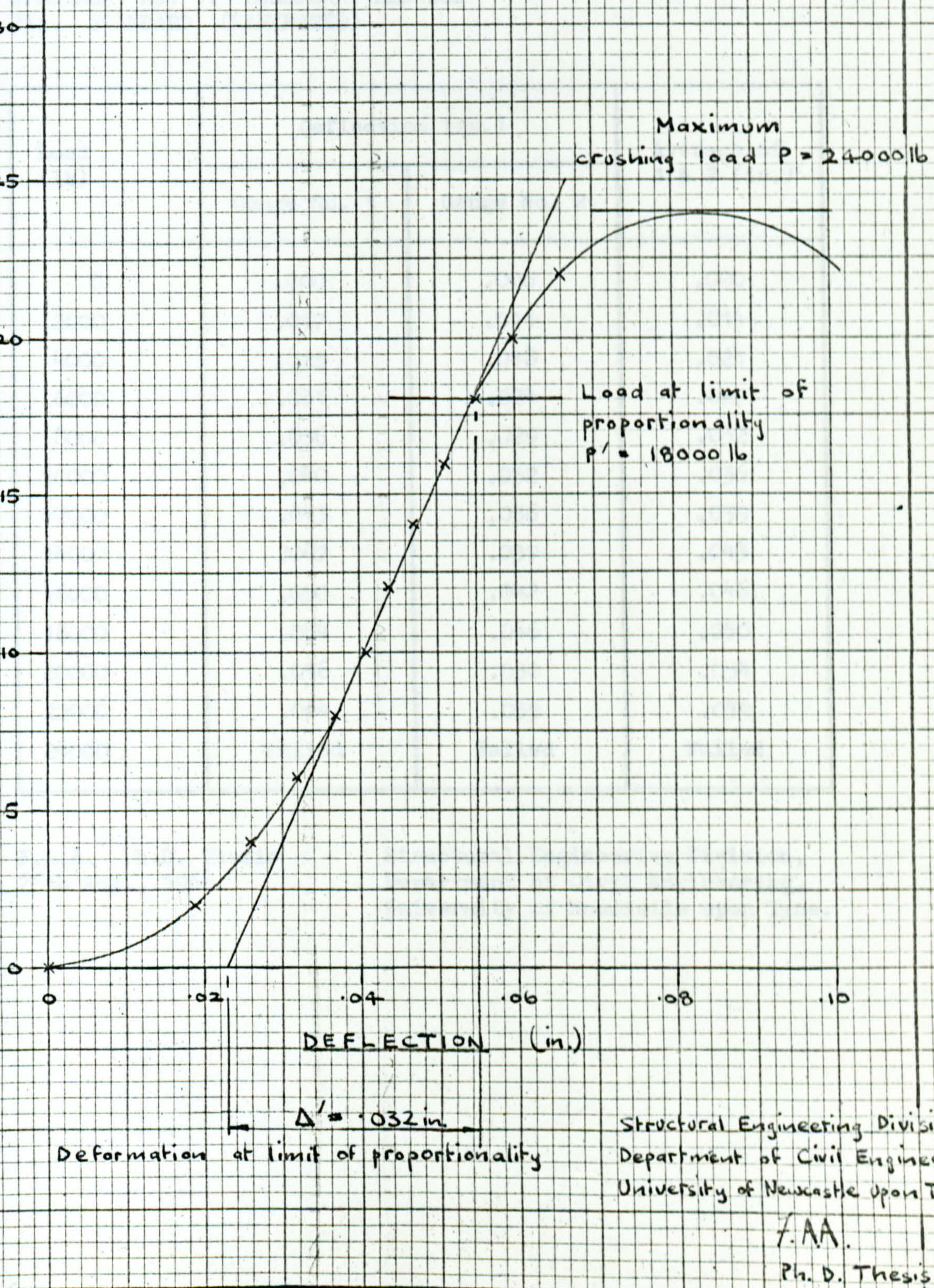

Structural Engineering Division,
Department of Civil Engineering,
University of Newcastle upon Tyne.

F.A.A.
Ph. D. Thesis

TESTS ON MODEL RADIAL RIBBED DOME MATERIALS FIG. NO.32

Compression Parallel to Grain Test to B.S. 373:1957
on Rib Timber

SPECIMEN NO. 4. EUROPEAN REDWOOD
2in. STANDARD (LAMINATED)

Load (lb)	Deflection (in.)		Average of 1 & 2 (in.)
	Gauge No. 1	Gauge No. 2	
0	.000	.000	.000
2000	.017	.011	.014
4000	.025	.018	.021
6000	.031	.024	.027
8000	.036	.029	.032
10000	.040	.032	.036
12000	.043	.036	.039
14000	.047	.039	.043
16000	.050	.042	.046
18000	.054	.046	.050
20000	.058	.050	.054
22000	.064	.055	.059
24000	Failed	Failed	Failed

F.A.A. Ph.D. Thesis
26th Aug., 1968.

Structural Engineering Division,
Department of Civil Engineering,
University of Newcastle upon Tyne.

TESTS ON MODEL RADIAL RIBBED DOME MATERIALS

FIG. No. 33

COMPRESSION PARALLEL TO GRAIN TEST TO B.S. 373: 1957 ON RIB TIMBER

SPECIMEN No. 4. EUROPEAN REDWOOD.

2 in. STANDARD (LAMINATED).

26th AUG., 1968.

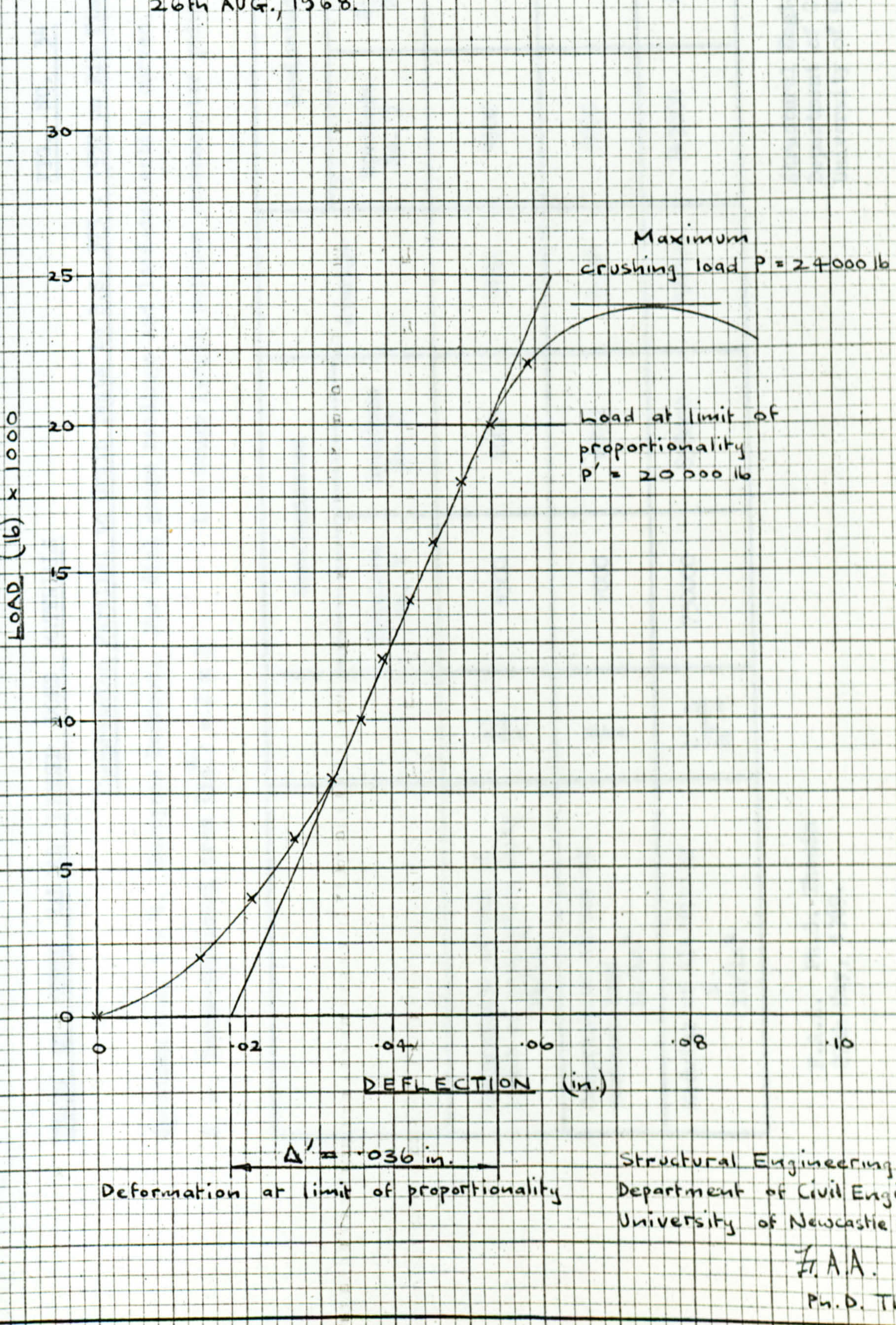

Structural Engineering Division,
Department of Civil Engineering,
University of Newcastle upon Tyne.

F. A. A.

Ph. D. Thesis

TESTS ON MODEL RADIAL RIBBED DOME MATERIALS FIG. NO. 34

Compression Parallel to Grain Tests to B.S. 373 : 1957 on Rib Timber

Specimen Nos. 1 - 4. European Redwood. For dial gauge readings and load-deflection curves, see Figs. 26 - 33.

A = Cross-sectional area ($in.^2$) = 2 x 2 L = Gauge length between extensometer points = 6 in.

		Non-laminated		Average	Laminated		Average
		Specimen No. 1	Specimen No. 2		Specimen No. 3	Specimen No. 4	
Compressive stress at limit of proportionality $lb/in.^2$	$\frac{P'}{A}$	4500	5000	4750	4500	5000	4750
Compressive stress at maximum load $lb/in.^2$	$\frac{P}{A}$	7000	6875	6938	6000	6000	6000
Modulus of Elasticity E $lb/in.^2$	$\frac{P' L}{\Delta' A}$	730000	858000	794000	843000	834000	839000

F.A.A. Ph.D. Thesis
27th May, 1969.

Structural Engineering Division,
Department of Civil Engineering,
University of Newcastle upon Tyne.

TESTS ON MODEL RADIAL RIBBED DOME MATERIALS

Fig. No. 35

STATIC BENDING TEST TO B.S. 373 : 1957 ON RIB TIMBER

SPECIMEN NO. 1. EUROPEAN REDWOOD

Four-Point Loading Method b.

2 in. STANDARD BEAM (LAMINATED).

Load (lb)	Proving Ring Reading (Divisions)	Deflection (in.)			Average of 1 & 3 (in).
		Gauge No. 1	Gauge No. 2	Gauge No. 3	
0	0	.000	.000	.000	.000
200	9.3	.034	.050	.035	.034
400	18.6	.061	.089	.063	.062
600	27.9	.087	.128	.089	.088
800	37.2	.117	.171	.118	.117
1000	46.6	.145	.213	.148	.146
1200	55.9	.174	.256	.177	.175
1400	65.2	.206	.302	.209	.207
1600	74.5	.237	.348	.241	.239
1800	83.8	.267	.391	.271	.269
2000	93.0	.294	.431	.298	.296
2200	102.3	.330	.483	.334	.332
2400	111.6	.359	.523	.363	.361
2600	120.9	.396	.574	.398	.397
2800	130.2	.421	.615	.424	.422
3000	139.4	.451	.658	.456	.453
3200	148.9	.488	.710	.494	.491
3400	158.4	.538	.777	.542	.540
3600	167.9	.588	.845	.590	.589
3800	177.4	.671	.951	.664	.667
4760	225	Failed	Failed	Failed	Failed

Proving Ring No. 2006 (6000 lb)

Weight of distribution beam = 12lb

F. A. A. Ph.D. Thesis
21st Aug., 1968.

Structural Engineering Division,
Department of Civil Engineering,
University of Newcastle upon Tyne.

TESTS ON MODEL RADIAL RIBBED DOME MATERIALS

FIG. No. 36

STATIC BENDING TEST TO B.S. 373 : 1957 ON RIB TIMBER
SPECIMEN No. 1. EUROPEAN REDWOOD.
FOUR-POINT LOADING METHOD b. 2in. STANDARD BEAM (LAMINATED)
21st AUG., 1968.

⊙ Load-deflection curve for ends of gauge length.

× Load-deflection curve for mid point.

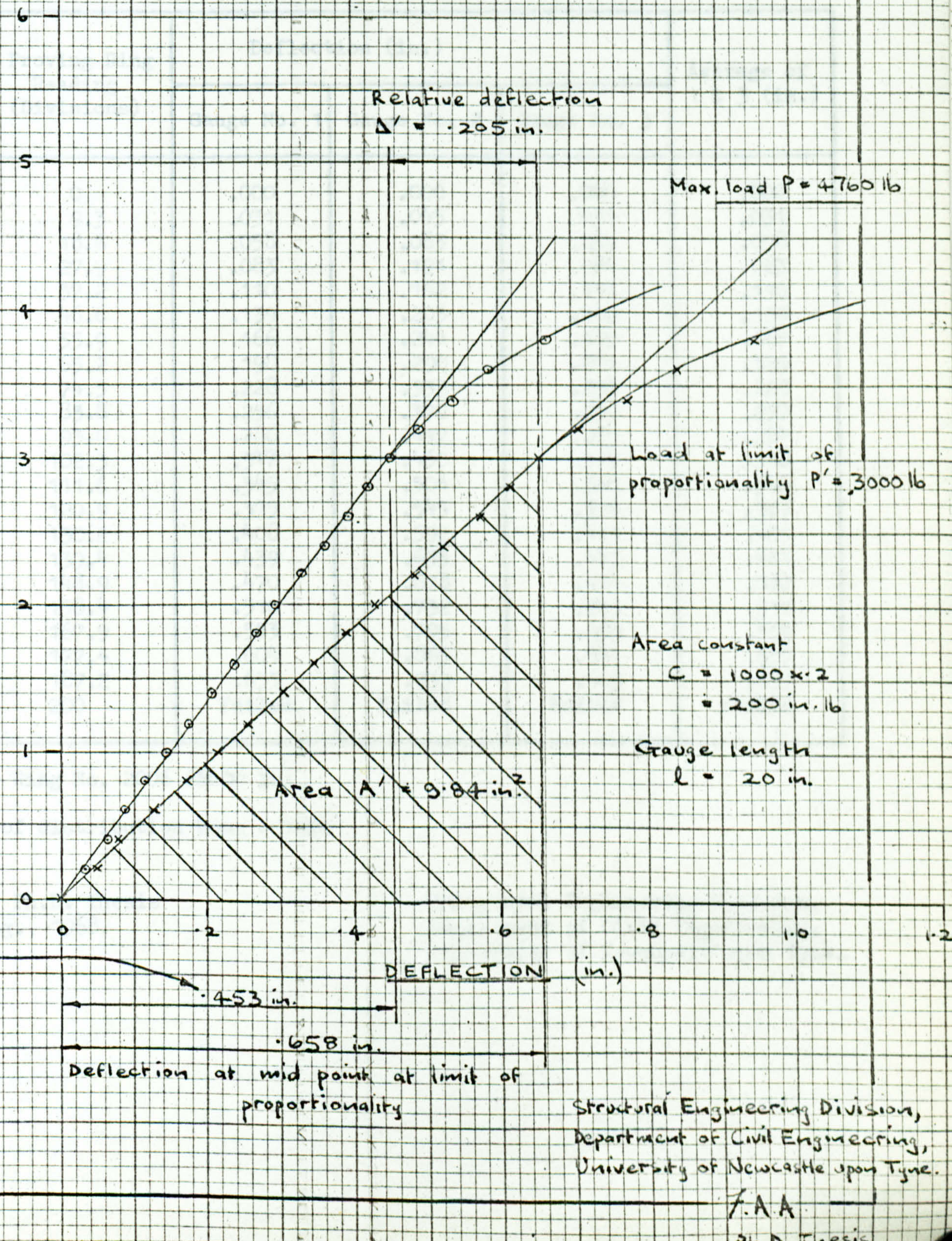

Structural Engineering Division,
Department of Civil Engineering,
University of Newcastle upon Tyne.

F.A.A
Ph.D. Thesis

TESTS ON MODEL RADIAL RIBBED DOME MATERIALS — Fig. No. 37

STATIC BENDING TEST TO B.S. 373 : 1957 ON RIB TIMBER

SPECIMEN NO. 2. EUROPEAN REDWOOD

FOUR-POINT LOADING METHOD b.

2in. STANDARD BEAM (LAMINATED)

Load (lb)	Proving Ring Reading (Divisions)	Deflection (in.)			Average of 1 & 3 (in.)
		Gauge No. 1	Gauge No. 2	Gauge No. 3	
0	0	.000	.000	.000	.000
200	9.3	.031	.045	.031	.031
400	18.6	.058	.083	.059	.058
600	27.9	.083	.121	.084	.083
800	37.2	.110	.162	.111	.110
1000	46.6	.139	.203	.140	.139
1200	55.9	.166	.244	.169	.167
1400	65.2	.198	.290	.201	.199
1600	74.5	.228	.333	.230	.229
1800	83.8	.256	.372	.259	.257
2000	93.0	.286	.417	.289	.287
2200	102.3	.317	.460	.319	.318
2400	111.6	.345	.501	.348	.346
2600	120.9	.375	.545	.379	.377
2800	130.2	.408	.592	.411	.409
3000	139.4	.439	.635	.443	.441
3200	148.9	.470	.678	.474	.472
3400	158.4	.510	.732	.513	.511
3600	167.9	.553	.795	.559	.556
3800	177.4	.604	.865	.611	.607
4000	187.2	.655	.933	.663	.659
4240	200	Failed	Failed	Failed	Failed

Proving Ring No. 2006 (6000 lb)

Weight of distribution beam = 12lb

F.A.A. Ph.D. Thesis
21st Aug., 1968.

Structural Engineering Division,
Department of Civil Engineering,
University of Newcastle upon Tyne.

TESTS ON MODEL RADIAL RIBBED DOME MATERIALS

FIG. No. 38

STATIC BENDING TEST TO B.S. 373 : 1957 ON RIB TIMBER
SPECIMEN NO. 2. EUROPEAN REDWOOD.
FOUR-POINT LOADING METHOD b. 2 in. STANDARD BEAM (LAMINATED)
21st AUG., 1968.

⊙ Load-deflection curve for ends of gauge length.

× Load-deflection curve for mid point.

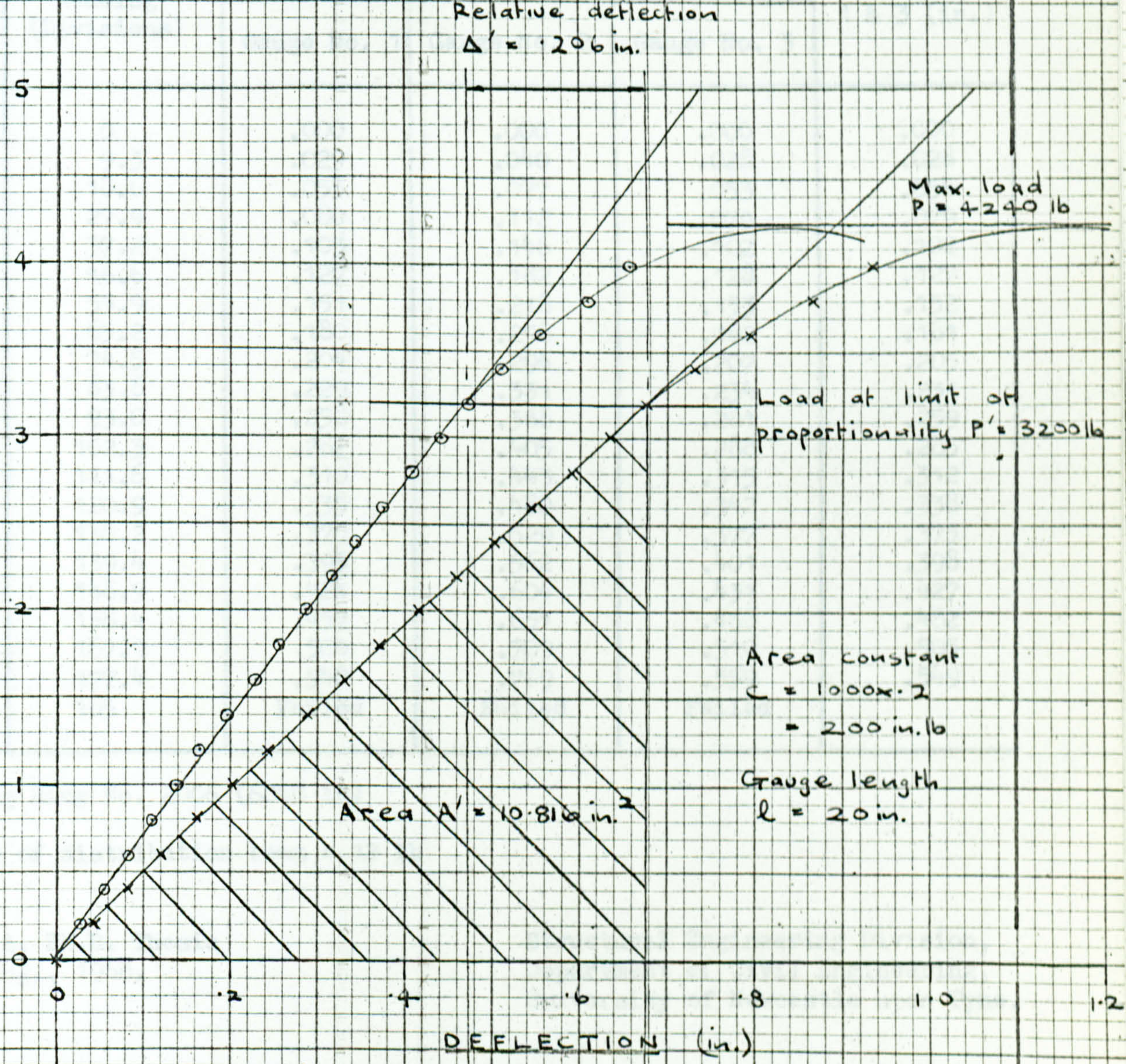

Structural Engineering Division,
Department of Civil Engineering,
University of Newcastle upon Tyne.

F.A.A.

Ph.D. Thesis

TESTS ON MODEL RADIAL RIBBED DOME MATERIALS — Fig. No. 39

STATIC BENDING TEST TO B.S. 373 : 1957 ON RIB TIMBER

SPECIMEN NO. 3 EUROPEAN REDWOOD

FOUR-POINT LOADING METHOD b.

2in. STANDARD BEAM (NON-LAMINATED).

Load (lb)	Proving Ring Reading (Divisions)	Deflection (in.)			Average of 1 & 3 (in.)
		Gauge No. 1	Gauge No. 2	Gauge No. 3	
0	0	.000	.000	.000	.000
200	9.3	.029	.040	.028	.028
400	18.6	.055	.077	.053	.054
600	27.9	.080	.112	.079	.079
800	37.2	.103	.146	.102	.102
1000	46.6	.127	.182	.128	.127
1200	55.9	.151	.218	.153	.152
1400	65.2	.180	.258	.182	.181
1600	74.5	.204	.294	.207	.205
1800	83.8	.229	.331	.234	.231
2000	93.0	.258	.368	.261	.259
2200	102.3	.282	.405	.288	.285
2400	111.6	.310	.443	.315	.312
2600	120.9	.335	.482	.342	.338
2800	130.2	.370	.529	.377	.373
3000	139.4	.395	.562	.401	.398
3200	148.9	.424	.604	.431	.427
3400	158.4	.457	.651	.468	.462
3600	167.9	.500	.709	.510	.505
3800	177.4	.540	.769	.559	.549
3920	185	Failed	Failed	Failed	

Proving Ring No. 2006 (6000 lb)

Weight of distribution beam = 12 lb

F. A. A. Ph.D. Thesis
21st Aug., 1968.

Structural Engineering Division,
Department of Civil Engineering,
University of Newcastle upon Tyne.

TESTS ON MODEL RADIAL RIBBED DOME MATERIALS

FIG. No. 40

STATIC BENDING TEST TO B.S. 373: 1957 ON RIB TIMBER SPECIMEN No. 3. EUROPEAN REDWOOD.
FOUR-POINT LOADING METHOD b. 2in. STANDARD BEAM (NON-LAMINATED)
21st AUG, 1968.

⊙ Load-deflection curve for ends of gauge length.

× Load-deflection curve for mid point.

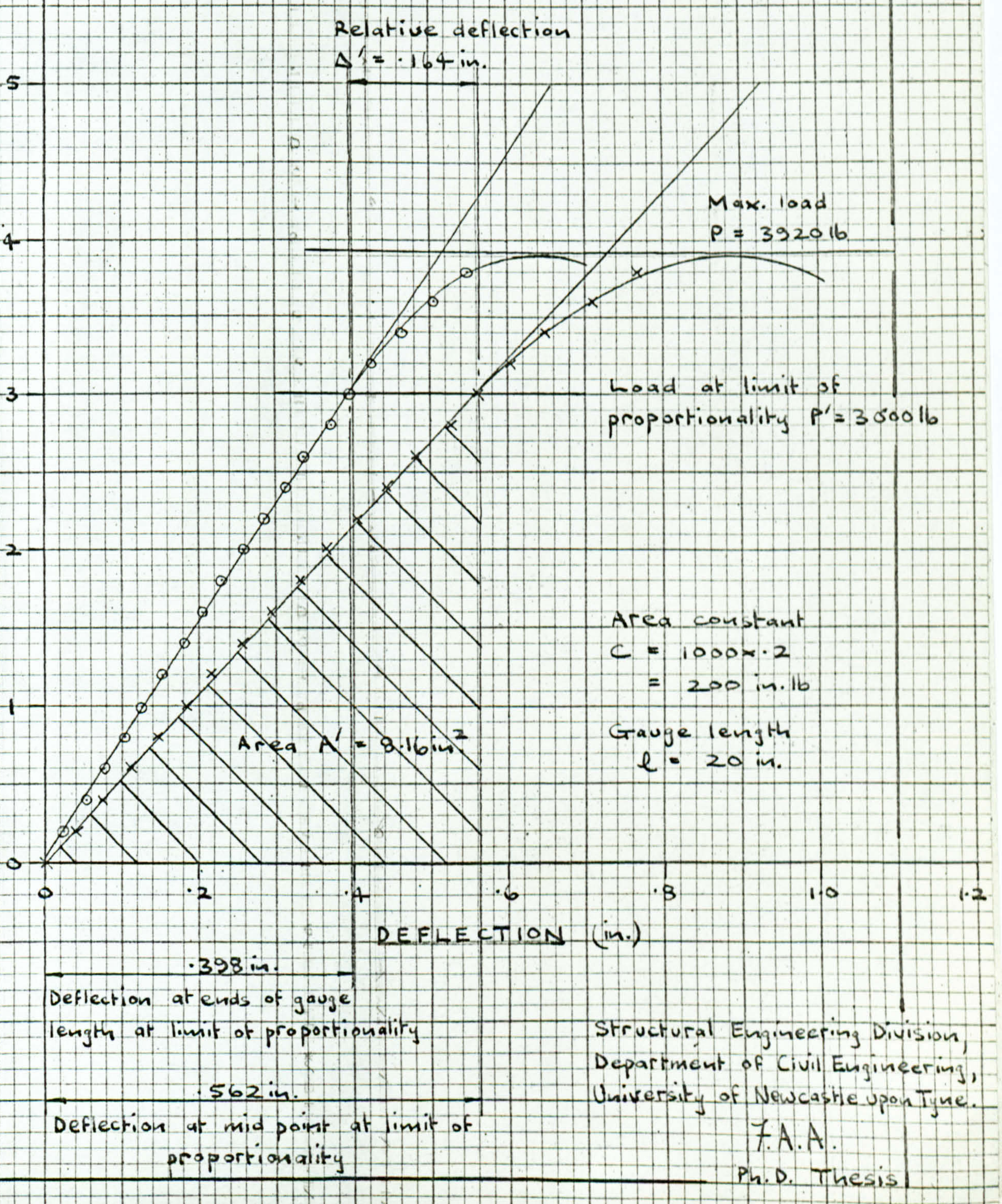

Structural Engineering Division,
Department of Civil Engineering,
University of Newcastle upon Tyne.

F.A.A.

Ph.D. Thesis

TESTS ON MODEL RADIAL RIBBED DOME MATERIALS

Fig. No. 41

STATIC BENDING TEST TO B.S. 373 : 1957 ON RIB TIMBER

SPECIMEN NO. 4 EUROPEAN REDWOOD

FOUR-POINT LOADING METHOD b

2in. STANDARD BEAM (NON-LAMINATED)

Load (lb)	Proving Ring Reading (Divisions)	Deflection (in.)			Average of 1 & 3 (in.)
		Gauge No. 1	Gauge No. 2	Gauge No. 3	
0	0	.000	.000	.000	.000
200	9.3	.032	.042	.029	.030
400	18.6	.060	.081	.056	.058
600	27.9	.086	.118	.082	.084
800	37.2	.115	.161	.110	.112
1000	46.6	.141	.200	.139	.140
1200	55.9	.171	.241	.166	.168
1400	65.2	.203	.285	.197	.200
1600	74.5	.230	.325	.224	.227
1800	83.8	.259	.365	.253	.256
2000	93.0	.290	.409	.285	.287
2200	102.3	.322	.452	.318	.320
2400	111.6	.353	.496	.348	.350
2600	120.9	.383	.539	.380	.381
2800	130.2	.418	.588	.417	.417
3000	139.4	.448	.626	.447	.447
3200	148.9	.481	.674	.484	.482
3400	158.4	.527	.739	.536	.531
3600	170	Failed	Failed	Failed	Failed

Proving Ring No. 2006 (6000 lb)

Weight of distribution beam = 12 lb

F. A. A. Ph.D. Thesis
21st Aug., 1968

Structural Engineering Division,
Department of Civil Engineering,
University of Newcastle upon Tyne.

TESTS ON MODEL RADIAL RIBBED DOME MATERIALS

FIG. No. 42

STATIC BENDING TEST TO B.S. 373: 1957 ON RIB TIMBER
SPECIMEN No. 4. EUROPEAN REDWOOD.
FOUR-POINT LOADING METHOD 6. 2in. STANDARD BEAM
21st AUG., 1968. (NON-LAMINATED)

⊙ Load-deflection curve for ends of gauge length.

× Load-deflection curve for mid point.

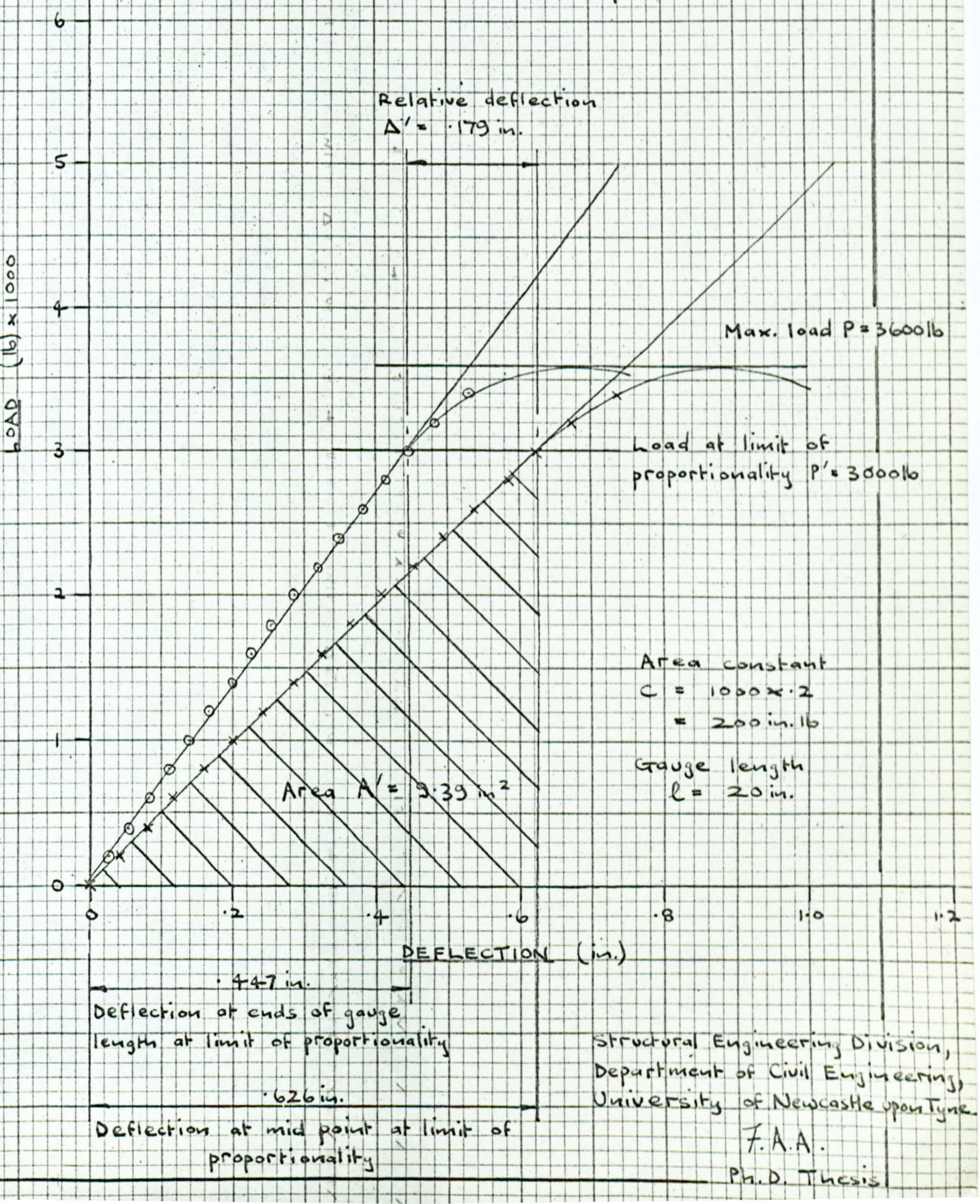

Structural Engineering Division,
Department of Civil Engineering,
University of Newcastle upon Tyne.

F. A. A.

Ph. D. Thesis

TESTS ON MODEL RADIAL RIBBED DOME MATERIALS

Fig. No. 43

Static Bending Tests to B.S. 373 : 1957 on Rib Timber

Specimen Nos. 1 - 4. European Redwood. Four-point loading method b. 2 in. standard beam (specimen dimensions :- b = breadth = 2 in. ; h = depth = 2in. ; l = gauge length = 20 in. ; a = distance between point of application of load and support = 6 in.) P = max. load (lb) ; P' = Load at limit of proportionality (lb) ; Δ' = Relative deflection at mid length at limit of proportionality (in.) ; C = load-deflection curve area constant (in. lb) ; A' = Area of load-deflection curve to limit of proportionality ($in.^2$). For dial gauge readings and load-deflection curves see Fig. 35 - 42.

		Laminated		Average	Non-laminated		Average
		Specimen No. 1	Specimen No. 2		Specimen No. 3	Specimen No. 4	
Fibre stress at limit of proportionality $lb/in.^2$	$\frac{3P'a}{bh^2}$	6750	7200	6975	6750	6750	6750
Equivalent fibre stress at maximum load $lb/in.^2$	$\frac{3Pa}{bh^2}$	10710	9540	10125	8820	8100	8460
Modulus of elasticity $lb/in.^2$	$\frac{3P'al^2}{4\Delta' bh^3}$	1646000	1746000	1696000	2059000	1885000	1972000
Horizontal shear stress on neutral plane at limit of proportionality $lb/in.^2$	At centre = 0 At ends = $\frac{3P'}{4bh}$	563	600	582	563	563	563
Horizontal shear stress on neutral plane at maximum load $lb/in.^2$	At centre = 0 At ends = $\frac{3P}{4bh}$	892	795	844	735	675	705
Work to limit of proportionality (Elastic resilience) $in.lb/in.^3$	$\frac{CA'}{lbh}$	24.6	27.0	25.8	20.4	23.5	22.0

F.A.A. Ph.D. Thesis
27th May, 1969.

Structural Engineering Division,
Department of Civil Engineering,
University of Newcastle upon Tyne.

TESTS ON MODEL RADIAL RIBBED DOME MATERIALS

Fig. No. 44a

Measurement of the Loss in Weight with Time of Adhesive Employed in the Construction of the Dome Ribs (Aerodux 185 ; HRP 155 Hardener 100 = 20 Parts by weight) A = Sample weight (gm) B = Loss in weight (gm) C = Percentage loss in Weight

Glue Sample No.		Date									
		18 Sept., 67	19 Sept., 67	20 Sept., 67	21 Sept., 67	22 Sept., 67	25 Sept., 67	26 Sept., 67	28 Sept., 67	2 Oct., 67	4 Oct., 67
1	A	39.25	37.21	35.92	34.05	33.46	32.03	31.63	30.93	30.11	29.67
	B	0	2.04	3.33	5.20	5.79	7.22	7.62	8.32	9.14	9.58
	C	0	5.2	8.5	13.3	14.8	18.4	19.4	21.2	23.3	24.4
2	A			45.78	43.33	41.70	38.94	38.29	37.22	35.90	35.28
	B			0	2.45	4.08	6.84	7.49	8.56	9.38	10.50
	C			0	5.4	8.9	15.0	16.4	18.7	21.6	22.9
3	A				45.77	43.63	39.98	39.13	38.03	36.49	35.80
	B				0	2.14	5.79	6.64	7.74	9.28	9.97
	C				0	4.7	12.7	14.5	16.9	20.3	21.8
4	A					45.79	42.11	40.39	38.70	36.66	35.89
	B					0	3.68	5.40	7.09	9.13	9.90
	C					0	8.0	11.8	15.5	20.0	21.6
5	A						45.70	43.81	40.23	37.17	36.12
	B						0	1.89	5.47	8.53	9.58
	C						0	4.1	12.0	18.7	21.0
6	A							45.79	42.56	38.77	37.27
	B							0	3.23	7.02	8.52
	C							0	7.1	15.3	18.6
7	A								45.74	40.70	38.30
	B								0	5.04	7.44
	C								0	11.0	16.3

F.A.A. Ph.D. Thesis
23rd May, 1969.

Structural Engineering Division,
Department of Civil Engineering,
University of Newcastle upon Tyne.

TESTS ON MODEL RADIAL RIBBED DOME MATERIALS

Fig. No. 44b

Measurement of the Loss in Weight with Time of Adhesive Employed in the Construction of the Dome Ribs (Aerodux 185 HRP 155 Hardener 100 = 20 Parts by weight) A = Sample weight (gm) B = Loss in weight (gm) C = Percentage Loss in Weight

Glue Sample No.		Date									
		6 Oct., 67	11 Oct., 67	20 Oct., 67	7 Nov., 67	27 Nov., 67	1 Dec., 67	11 Jan., 68	14 Mar., 68	17 July, 68	20 May, 69
1	A	29.17	28.63	27.98	27.64	27.40	27.34	26.67	26.94	27.13	26.76
	B	10.08	10.62	11.27	11.61	11.85	11.91	12.58	12.31	12.12	12.49
	C	25.7	27.1	28.7	29.6	30.2	30.4	32.0	31.4	30.9	31.8
2	A	34.64	33.90	33.03	32.54	32.20	32.12	31.35	31.56	31.70	31.28
	B	11.14	11.88	12.75	13.24	13.58	13.66	14.43	14.22	14.08	14.50
	C	24.4	26.0	27.9	29.0	29.7	29.9	31.6	31.1	30.8	31.7
3	A	35.06	34.20	33.26	32.71	32.36	32.27	31.50	31.70	31.86	31.43
	B	10.71	11.57	12.51	13.06	13.41	13.50	14.27	14.07	13.91	14.34
	C	23.4	25.3	27.4	28.6	29.3	29.5	31.2	30.8	30.4	31.4
4	A	35.06	34.14	33.17	32.61	31.25	32.17	31.40	31.61	31.76	31.33
	B	10.73	11.65	12.62	13.18	13.54	13.62	14.39	14.18	14.03	14.46
	C	23.4	25.5	27.6	28.8	29.6	29.8	31.4	31.0	30.7	31.6
5	A	35.17	34.14	33.12	32.50	32.13	32.04	31.26	31.46	31.56	31.17
	B	10.53	11.56	12.58	13.20	13.57	13.66	14.44	14.24	14.14	14.53
	C	23.1	25.3	27.5	28.9	29.7	29.9	31.6	31.2	31.0	31.8
6	A	36.03	34.74	33.56	32.85	32.44	32.35	31.54	31.73	31.83	31.42
	B	9.76	11.05	12.23	12.94	13.35	13.44	14.25	14.06	13.96	14.37
	C	21.4	24.2	26.7	28.3	29.2	29.4	31.2	30.7	30.5	31.4
7	A	36.58	34.95	33.58	32.80	32.38	32.29	31.47	31.67	31.79	31.36
	B	9.16	10.79	12.16	12.94	13.36	13.45	14.27	14.07	13.95	14.38
	C	20.1	23.6	26.6	28.3	29.2	29.4	31.2	30.8	30.5	31.4

F.A.A. Ph.D. Thesis
23rd May, 1969.

Structural Engineering Division,
Department of Civil Engineering,
University of Newcastle upon Tyne.

TESTS ON MODEL RADIAL RIBBED DOME MATERIALS

FIG. NO. 45

Graphs of loss in weight with time of adhesive employed in the construction of the dome ribs

Adhesive : Aerodux 185 ; HRP 155 Hardener.

Adhesive: Hardener proportions 100 : 20 by weight

Sample Nos. 1 – 7 all lie within envelope shown

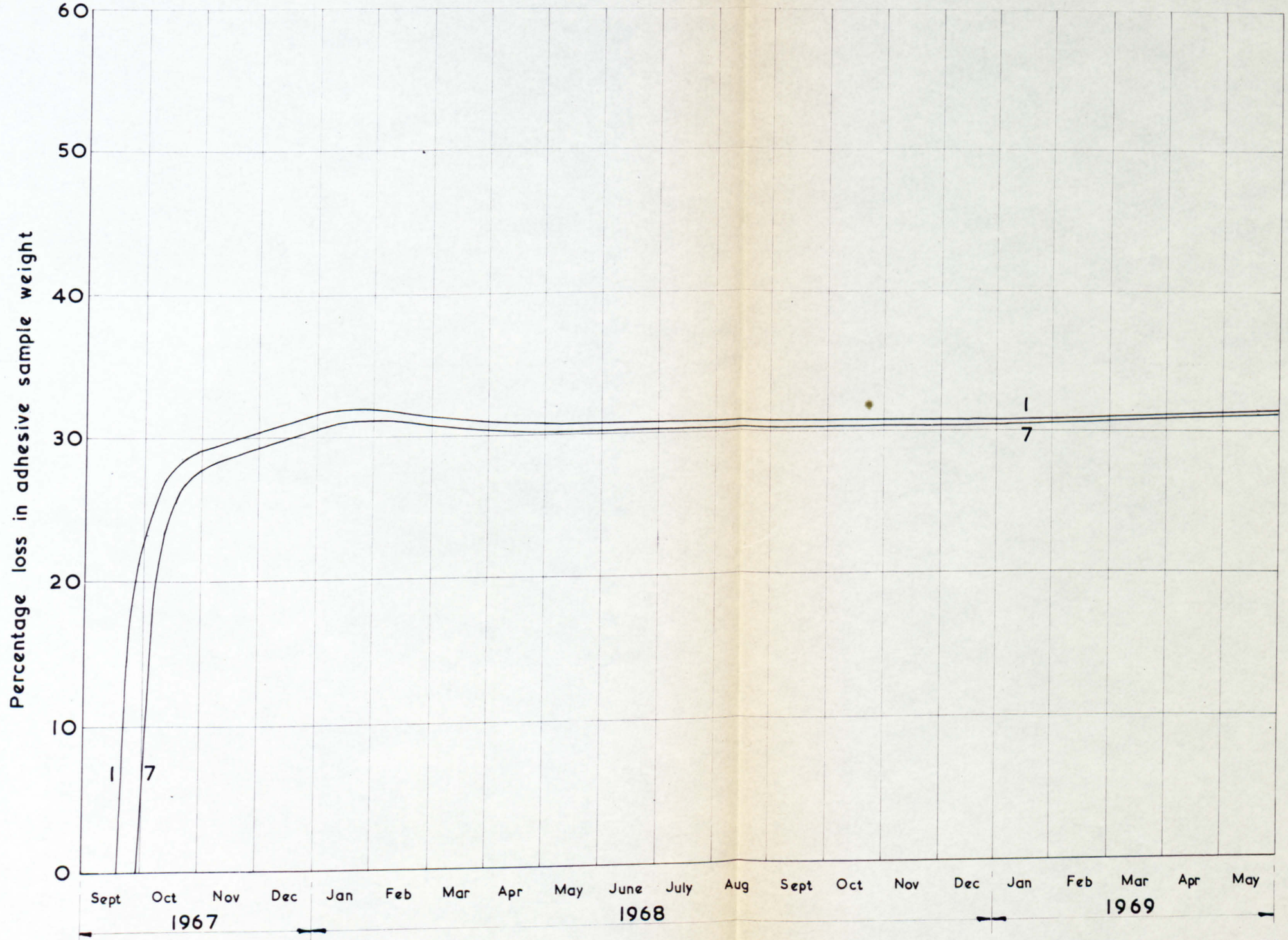

F.A.A. Ph.D. Thesis
23rd May, 1969

Structural Engineering Division
Department of Civil Engineering
University of Newcastle upon Tyne

APPENDIX II

TESTS ON MODEL RADIAL RIBBED DOME

TEST RESULTS

TESTS 1 - 22

TESTS ON MODEL RADIAL RIBBED DOME

TEST NO. 1. TABLE NO.1.

Experimental Determination of Horizontal Reaction Influence Coefficients

Load at point = 20 lb. For position of load points, rib layout, details of model dome and graphs of tabulated results, see Test No. 1. Sheet Nos. 1 & 2.

Horizontal Base displacement at Rib No. 36 (Toward centre of dome.)	Dial Gauge Readings (A) and Actual Vertical Displacement of Point Load (B; +ve upwards) in inches																			
	Rib No. 36										Rib No. 30									
	Point 1		Point 5		Point 9		Point 13		Point 17		Point 1		Point 5		Point 9		Point 13		Point 17	
	A	B	A	B	A	B	A	B	A	B	A	B	A	B	A	B	A	B	A	B
0 in.	.442	.000	.091	,000	.113	.000	.219	.000	.540	.000	.458	.000	.368	.000	.104	.000	.153	.000	.236	.000
.1 in.	.448	+.006	.118	+.027	.164	+.051	.256	+.037	.578	+.038	.455	-.003	.360	-.008	.105	+.001	.169	+.016	.274	+.038
.2 in.	.454	+.012	.148	+.057	.212	+.099	.309	+.090	.620	+.080	.454	-.004	.357	-.011	.106	+.002	.184	+.031	.312	+.076
.3 in.	.459	+.017	.174	+.083	.255	+.142	.352	+.133	.657	+.117	.453	-.005	.353	-.015	.107	+.003	.197	+.044	.343	+.107
.4 in.	.464	+.022	.200	+.109	.300	+.187	.399	+.180	.696	+.156	.452	-.006	.349	-.019	.107	+.003	.210	+.057	.377	+.141
.5 in.	.469	+.027	.227	+.136	.343	+.230	.445	+.226	.732	+.192	.450	-.008	.345	-.023	.108	+.004	.222	+.069	.410	+.174
.6 in.	.473	+.031	.255	+.164	.387	+.274	.493	+.274	.770	+.230	.449	-.009	.341	-.027	.108	+.004	.236	+.083	.443	+.207
.7 in.	.478	+.036	.280	+.189	.432	+.319	.536	+.317	.806	+.266	.448	-.010	.338	-.030	.108	+.004	.249	+.093	.475	+.239
.8 in.	.484	+.042	.311	+.220	.481	+.368	.586	+.367	.845	+.305	.447	-.011	.333	-.035	.108	+.004	.262	+.109	.511	+.275
.9 in.	.489	+.047	.341	+.250	.524	+.411	.637	+.418	.882	+.342	.445	-.013	.329	-.039	.108	+.004	.274	+.121	.545	+.309
1.0 in.	.495	+.053	.362	+.271	.562	+.449	.679	+.460	.917	+.377	.444	-.014	.325	-.043	.107	+.003	.285	+.132	.574	+.338

F.A.A. Ph.D. Thesis
3rd-7th Oct., 1968.

Structural Engineering Division,
Department of Civil Engineering,
University of Newcastle upon Tyne.

TESTS ON MODEL RADIAL RIBBED DOME

TEST NO. 1. TABLE NO. 2.

Experimental Determination of Horizontal Reaction Influence Coefficients

Load at Point = 20 lb. For position of load points, rib layout, details of model dome and graphs of tabulated results, see Test No. 1 Sheet Nos. 3 & 4.

Horizontal Base displacement at Rib No. 36 (Towards centre of dome.)	Dial Gauge Readings (A) and Actual Vertical Displacement of Point Load (B; +ve upwards) in inches																			
	Rib No. 24										Rib No. 18									
	Point 1		Point 5		Point 9		Point 13		Point 17		Point 1		Point 5		Point 9		Point 13		Point 17	
	A	B	A	B	A	B	A	B	A	B	A	B	A	B	A	B	A	B	A	B
0 in.	.452	.000	.393	.000	.223	.000	.146	.000	.204	.000	.456	.000	.369	.000	.087	.000	.167	.000	.383	.000
.1 in.	.456	+.004	.411	+.018	.250	+.027	.185	+.039	.248	+.044	.459	+.003	.382	+.013	.109	+.022	.200	+.033	.428	+.045
.2 in.	.460	+.008	.429	+.036	.278	+.055	.223	+.077	.290	+.086	.461	+.005	.393	+.024	.130	+.043	.231	+.064	.470	+.087
.3 in.	.464	+.012	.440	+.047	.302	+.079	.255	+.109	.326	+.122	.464	+.008	.404	+.035	.148	+.061	.260	+.093	.508	+.125
.4 in.	.467	+.015	.456	+.063	.326	+.103	.290	+.144	.364	+.160	.466	+.010	.414	+.045	.167	+.080	.289	+.122	.546	+.163
.5 in.	.471	+.019	.469	+.076	.351	+.128	.322	+.176	.401	+.197	.469	+.013	.425	+.056	.187	+.100	.317	+.150	.583	+.200
.6 in.	.475	+.023	.485	+.092	.377	+.154	.357	+.211	.440	+.236	.471	+.015	.436	+.067	.206	+.119	.346	+.179	.620	+.237
.7 in.	.478	+.026	.499	+.106	.402	+.179	.388	+.242	.476	+.272	.473	+.017	.446	+.077	.225	+.138	.374	+.207	.659	+.276
.8 in.	.482	+.030	.514	+.121	.429	+.206	.426	+.280	.518	+.314	.476	+.020	.458	+.089	.245	+.158	.406	+.239	.699	+.316
.9 in.	.486	+.034	.529	+.136	.455	+.232	.460	+.314	.555	+.351	.479	+.023	.469	+.100	.265	+.178	.436	+.269	.737	+.354
1.0 in.	.490	+.038	.543	+.150	.480	+.257	.492	+.346	.591	+.387	.481	+.025	.479	+.110	.284	+.197	.464	+.297	.774	+.391

F.A.A. Ph.D. Thesis
10th Oct., 1968.

Structural Engineering Division,
Department of Civil Engineering,
University of Newcastle upon Tyne.

TESTS ON MODEL RADIAL RIBBED DOME

TEST NO. 1. TABLE NO. 3.

Experimental Determination of Horizontal Reaction Influence Coefficients

Load at point = 20 lb. For position of load points, rib layout, details of model dome and graphs of tabulated results, see Test No. 1. Sheet Nos. 2 & 3.

Horizontal Base displacement at Rib No. 36 (Towards centre of dome.)	Dial Gauge Readings (A) and Actual Vertical Displacement of Point Load (B; +ve upwards) in inches																			
	Rib No. 12										Rib No. 6.									
	Point 1		Point 5		Point 9		Point 13		Point 17		Point 1		Point 5		Point 9		Point 13		Point 17	
	A	B	A	B	A	B	A	B	A	B	A	B	A	B	A	B	A	B	A	B
0 in.	.454	.000	.375	.000	.091	.000	.150	.000	.289	.000	.755	.000	.398	.000	.110	.000	.140	.000	.227	.000
.1 in.	.458	+.004	.393	+.018	.119	+.028	.187	+.037	.330	+.041	.754	-.001	.396	-.002	.113	+.003	.158	+.018	.263	+.036
.2 in.	.462	+.008	.411	+.036	.147	+.056	.224	+.074	.371	+.082	.753	-.002	.393	-.005	.114	+.004	.175	+.035	.301	+.074
.3 in.	.465	+.011	.426	+.051	.172	+.081	.256	+.106	.409	+.120	.752	-.003	.390	-.008	.115	+.005	.188	+.048	.335	+.108
.4 in.	.469	+.015	.443	+.068	.200	+.109	.291	+.141	.446	+.157	.751	-.004	.386	-.012	.117	+.007	.203	+.063	.369	+.142
.5 in.	.473	+.019	.459	+.084	.226	+.135	.323	+.173	.483	+.194	.750	-.005	.382	-.016	.118	+.008	.216	+.076	.403	+.176
.6 in.	.476	+.022	.476	+.101	.254	+.163	.357	+.207	.521	+.232	.749	-.006	.378	-.020	.119	+.009	.230	+.090	.437	+.210
.7 in.	.480	+.026	.493	+.118	.281	+.190	.391	+.241	.558	+.269	.747	-.008	.374	-.024	.120	+.010	.242	+.102	.470	+.243
.8 in.	.484	+.030	.512	+.137	.310	+.219	.425	+.275	.599	+.310	.746	-.009	.369	-.029	.122	+.012	.257	+.117	.505	+.278
.9 in.	.488	+.034	.528	+.153	.335	+.244	.458	+.308	.635	+.346	.745	-.010	.365	-.033	.123	+.013	.269	+.129	.538	+.311
1.0 in.	.491	+.037	.542	+.167	.360	+.269	.491	+.341	.671	+.382	.744	-.011	.361	-.037	.124	+.014	.281	+.141	.568	+.341

F.A.A. Ph.D. Thesis
11th Oct., 1968.

Structural Engineering Division,
Department of Civil Engineering,
University of Newcastle upon Tyne.

TESTS ON MODEL RADIAL RIBBED DOME

TEST NO. 1 TABLE NO. 4

Measurement of Rib Strains Using Huggenberger Tensometer Gauges

Load at point = 20lb L = Gauge Length = 1in. N = Lever multiplication A = Scale reading in inches Z = Scale movement in inches (+ve reading - tension) X = Strain (extension x 10^{-6} in inches per inch of gauge length) = $\frac{Z}{NxL}$ All scale zero readings 1.00 in. For position of load points, rib layout and details of model dome, see Test No. 1, Sheet No. 5. For position of gauge points, see Dwg. No. Ph.D. Thesis No.1. Principal Dimensions of Prototype and Model Domes.

	Load Point	Gauge No.1 (Actual No. 4904) On Rib No.36 at Pt. 3 ; N = 1210.6			Gauge No.2 (Actual No. 4903) On Rib No.36 at Pt. 7 ; N = 1196.3			Gauge No.3 (Actual No. 4902) On Rib No.36 at Pt. 11 ; N = 1198.9			Gauge No.4 (Actual No. 4901) On Rib No.36 at Pt. 15 ; N = 1193.8			Gauge No.5 (Actual No. 4905) On Rib No.36 mid 16, 17 ; N = 1202.3		
		A	Z	X	A	Z	X	A	Z	X	A	Z	X	A	Z	X
Rib No. 36	1	.82	-.18	-149	.89	-.11	- 92	.95	-.05	- 42	.98	-.02	- 17	1.00	.00	0
	5	.62	-.38	-314	.45	-.55	-459	.72	-.28	-236	.88	-.12	-101	.95	-.05	- 42
	9	.84	-.16	-132	.37	-.63	-527	.40	-.60	-506	.72	-.28	-235	.88	-.12	-100
	13	.98	-.02	- 17	.76	-.24	-201	.50	-.50	-422	.48	-.52	-436	.78	-.22	-183
	17	1.08	+.08	+ 66	1.07	+.07	+ 59	.99	-.01	- 8	.81	-.19	-159	.78	-.22	-183
Rib No. 30	1	1.00	.00	0	1.00	.00	0	1.00	.00	0	1.00	.00	0	1.00	.00	0
	5	.99	-.01	- 8	.99	-.01	- 8	.99	-.01	- 8	.98	-.02	- 17	.98	-.02	- 17
	9	1.00	.00	0	1.00	.00	0	.99	-.01	- 8	.96	-.04	- 33	.96	-.04	- 33
	13	1.02	+.02	+ 17	1.03	+.03	+ 25	1.02	+.02	+ 17	.96	-.04	- 33	.94	-.06	- 50
	17	1.07	+.07	+ 58	1.10	+.10	+ 84	1.06	+.06	+ 51	.97	-.03	- 25	.93	-.07	- 58
Rib No. 24	1	1.00	.00	0	1.02	+.02	+ 17	1.01	+.01	- 8	1.00	.00	0	1.00	.00	0
	5	1.03	+.03	+ 25	1.06	+.06	+ 50	1.06	+.06	+ 51	1.05	+.05	+ 42	1.03	+.03	+ 25
	9	1.05	+.05	+ 41	1.10	+.10	+ 84	1.10	+.10	+ 84	1.08	+.08	+ 67	1.07	+.07	+ 58
	13	1.07	+.07	+ 58	1.15	+.15	+125	1.14	+.14	+118	1.14	+.14	+117	1.09	+.09	+ 75
	17	1.08	+.08	+ 66	1.16	+.16	+134	1.15	+.15	+125	1.13	+.13	+109	1.08	+.08	+ 67

F.A.A. Ph.D. Thesis
3rd - 10th Oct., 1968.

Structural Engineering Division,
Department of Civil Engineering,
University of Newcastle upon Tyne.

TESTS ON MODEL RADIAL RIBBED DOME

TEST NO. 1 TABLE NO. 5

Measurement of Rib Strains Using Huggenberger Tensometer Gauges

Load at point = 20lb L = Gauge Length = 1in. N = Lever multiplication A = Scale reading in inches Z = Scale movement in inches (+ve reading - tension) X = Strain (extension x 10^{-6} in inches per inch of gauge length) = $\frac{Z}{NxL}$ All scale zero readings 1.00 in. For position of load points, rib layout and details of model dome, see Test No. 1, Sheet No. 5. For position of gauge points, see Dwg. No. Ph.D. Thesis No. 1. Principal Dimensions of Prototype and Model Domes.

	Load Point	Gauge No.1 (Actual No. 4904) On Rib No.36 at Pt. 3 ; N = 1210.6			Gauge No.2 (Actual No. 4903) On Rib No.36 at Pt. 7 ; N = 1196.3			Gauge No.3 (Actual No. 4902) On Rib No.36 at Pt. 11 ; N = 1198.9			Guage No.4 (Actual No. 4901) On Rib No.36 at Pt. 15 ; N = 1193.8			Gauge No.5 (Actual No. 4905) On Rib No.36 mid 16, 17 ; N = 1202.3		
		A	Z	X	A	Z	X	A	Z	X	A	Z	X	A	Z	X
Rib No. 18	1	1.00	.00	0	1.00	.00	0	1.00	.00	0	1.02	+.02	+ 17	1.01	+.01	+ 8
	5	1.02	+.02	+ 17	1.05	+.05	+ 42	1.05	+.05	+ 42	1.06	+.06	+ 50	1.05	+.05	+ 42
	9	1.03	+.03	+ 25	1.09	+.09	+ 75	1.10	+.10	+ 84	1.11	+.11	+ 92	1.08	+.08	+ 67
	13	1.05	+.05	+ 41	1.13	+.13	+109	1.16	+.16	+134	1.17	+.17	+143	1.12	+.12	+100
	17	1.07	+.07	+ 58	1.18	+.18	+151	1.18	+.18	+150	1.20	+.20	+168	1.13	+.13	+108
Rib No. 12	1	1.00	.00	0	1.01	+.01	+ 8	1.01	+.01	+ 8	1.00	.00	0	1.00	.00	0
	5	1.02	+.02	+ 17	1.06	+.06	+ 50	1.06	+.06	+ 51	1.06	+.06	+ 50	1.04	+.04	+ 33
	9	1.05	+.05	+ 41	1.11	+.11	+ 92	1.12	+.12	+100	1.11	+.11	+ 92	1.07	+.07	+ 58
	13	1.07	+.07	+ 58	1.14	+.14	+117	1.15	+.15	+125	1.15	+.15	+126	1.08	+.08	+ 67
	17	1.08	+.08	+ 66	1.15	+.15	+125	1.15	+.15	+125	1.14	+.14	+117	1.07	+.07	+ 58
Rib No. 6	1	1.00	.00	0	1.00	.00	0	1.00	.00	0	1.00	.00	0	1.00	.00	0
	5	1.00	.00	0	.99	-.01	- 8	.98	-.02	- 17	1.00	.00	0	.99	-.01	- 8
	9	1.01	+.01	+ 8	1.01	+.01	+ 8	1.01	+.01	+ 8	1.00	.00	0	.99	-.01	- 8
	13	1.04	+.04	+ 33	1.06	+.06	+ 50	1.04	+.04	+ 33	.99	-.01	- 8	.98	-.02	- 17
	17	1.08	+.08	+ 66	1.11	+.11	+ 92	1.08	+.08	+ 67	.99	-.01	- 8	.95	-.05	- 42

F.A.A. Ph.D. Thesis
10th, 11th Oct., 1969.

Structural Engineering Division,
Department of Civil Engineering,
University of Newcastle upon Tyne.

TESTS ON MODEL RADIAL RIBBED DOME

TEST NO. 1 TABLE NO. 6

Measurement of Apex Ring Displacements at Rib No. 36

Load at point = 20lb ; All dial gauge zeros 1.000 in. ; A = Tangential displacement in inches (+ve reading anti-clockwise viewed from above) ; B = Radial displacement in inches (+ve reading inwards) ; C = Vertical displacement in inches (+ve reading upwards) ; D = Dial Gauge Reading ; E = Actual Displacement.

	Load Point	Gauge No. 1 A		Gauge No. 2 B		Gauge No. 3 C			Load Point	Gauge No. 1 A		Gauge No.2 B		Gauge No. 3 C	
		D	E	D	E	D	E			D	E	D	E	D	E
Rib No. 36	1	1.003	+.003	1.054	+.054	.994	-.006	Rib No. 18	1	1.003	+.003	.980	-.020	1.031	+.031
	5	1.010	+.010	1.224	+.224	.947	-.053		5	.998	-.002	.913	-.087	1.135	+.135
	9	1.016	+.016	1.317	+.317	.845	-.155		9	.995	-.005	.854	-.146	1.196	+.196
	13	1.005	+.005	1.277	+.277	.728	-.272		13	.993	-.007	.782	-.218	1.231	+.231
	17	1.002	+.002	1.158	+.158	.540	-.460		17	.990	-.010	.846	-.154	1.045	+.045
Rib No. 30	1	.975	-.025	1.002	+.002	1.000	.000	Rib No. 12	1	1.017	+.017	.982	-.018	1.023	+.023
	5	.869	-.131	1.015	+.015	.982	-.018		5	1.088	+.088	.918	-.082	1.093	+.093
	9	.816	-.184	1.033	+.033	.918	-.082		9	1.124	+.124	.880	-.120	1.110	+.110
	13	.816	-.184	1.051	+.051	.794	-.206		13	1.139	+.139	.883	-.117	1.042	+.042
	17	.884	-.116	1.062	+.062	.660	-.340		17	1.108	+.108	.924	-.076	.925	-.075
Rib No. 24	1	.978	-.022	.984	-.016	1.020	+.020	Rib No. 6	1	1.020	+.020	1.003	+.003	1.003	+.003
	5	.894	-.106	.925	-.075	1.185	+.185		5	1.115	+.115	1.011	+.011	.999	-.001
	9	.815	-.185	.873	-.127	1.099	+.099		9	1.171	+.171	1.053	+.053	.900	-.100
	13	.796	-.204	.864	-.136	1.049	+.049		13	1.074	+.074	1.075	+.075	.776	-.224
	17	.853	-.147	.910	-.090	.916	-.084		17	1.118	+.118	1.072	+.072	.665	-.335

F.A.A. Ph.D. Thesis
3rd - 11th October, 1968.

Structural Engineering Division,
Department of Civil Engineering,
University of Newcastle upon Tyne.

TESTS ON MODEL RADIAL RIBBED DOME

Test No. 1.
Sheet No. 1.

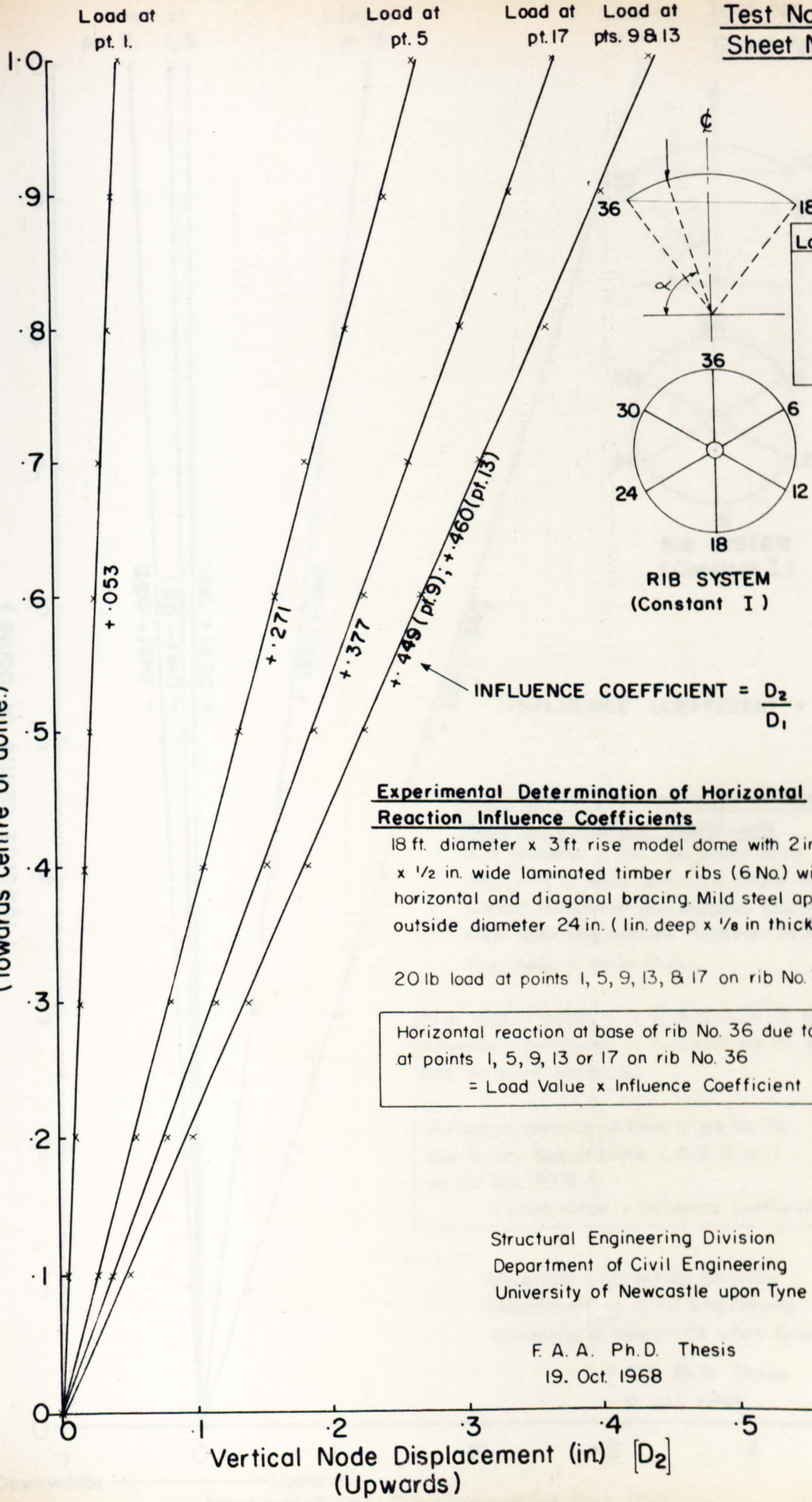

Load pt	∝ (rads)
1	·9657
5	1·0990
9	1·2324
13	1·3657
17	1·4990

RIB SYSTEM
(Constant I)

INFLUENCE COEFFICIENT = $\frac{D_2}{D_1}$

Experimental Determination of Horizontal Reaction Influence Coefficients

18 ft. diameter x 3 ft. rise model dome with 2 in. deep x ½ in. wide laminated timber ribs (6 No.) without horizontal and diagonal bracing. Mild steel apex ring outside diameter 24 in. (1in. deep x ⅛ in thick)

20 lb load at points 1, 5, 9, 13, & 17 on rib No. 36

Horizontal reaction at base of rib No. 36 due to any load at points 1, 5, 9, 13 or 17 on rib No. 36
= Load Value x Influence Coefficient

Structural Engineering Division
Department of Civil Engineering
University of Newcastle upon Tyne

F. A. A. Ph.D. Thesis
19. Oct. 1968

TESTS ON MODEL RADIAL RIBBED DOME

Test No. 1.

Sheet No. 2.

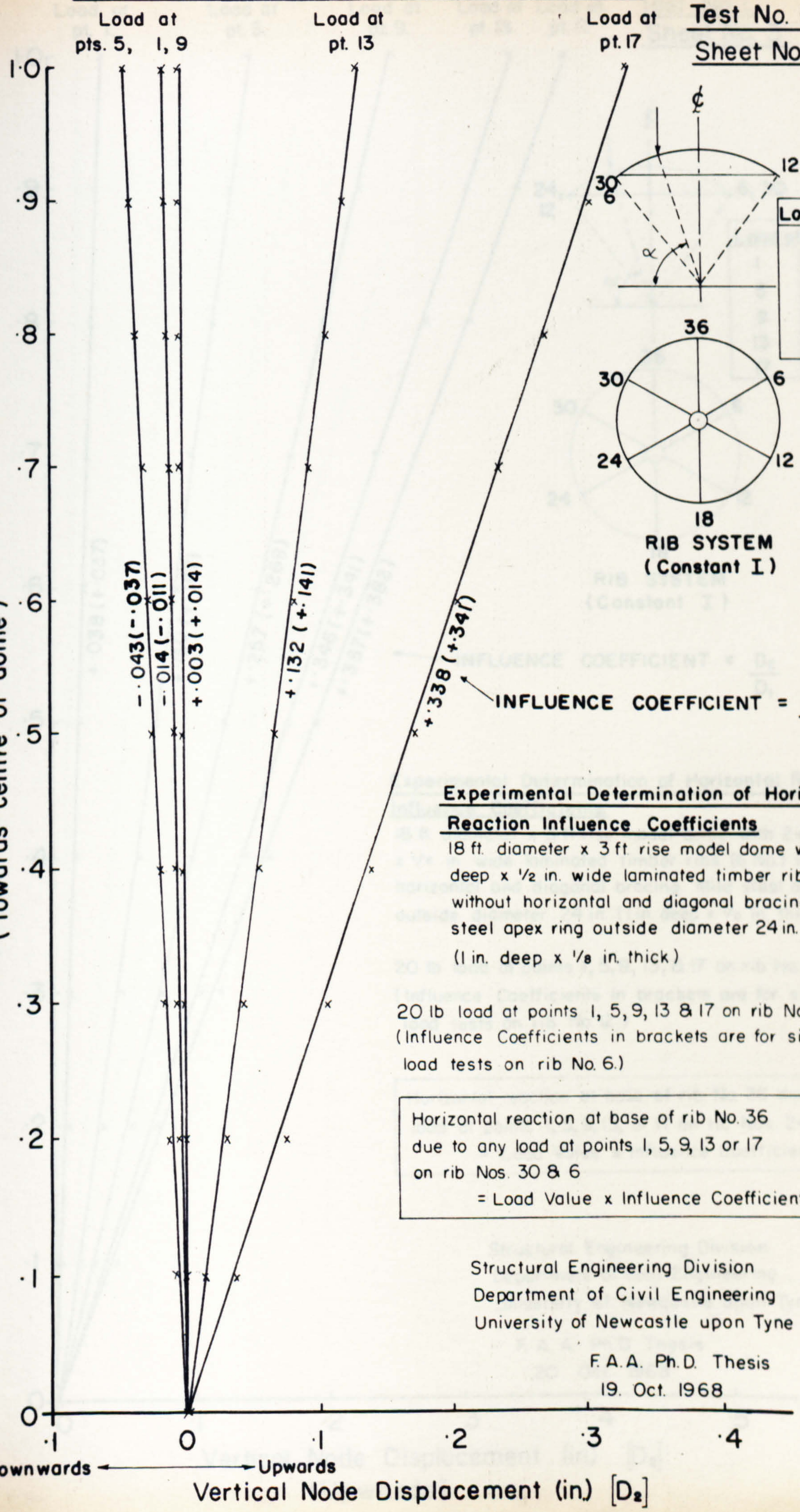

Load pt.	∝(rads.)
1	·9657
5	1·0990
9	1·2324
13	1·3657
17	1·4990

Experimental Determination of Horizontal Reaction Influence Coefficients

18 ft. diameter x 3 ft. rise model dome with 2 in. deep x ½ in. wide laminated timber ribs (6 No.) without horizontal and diagonal bracing. Mild steel apex ring outside diameter 24 in. (1 in. deep x ⅛ in. thick)

20 lb load at points 1, 5, 9, 13 & 17 on rib No. 30
(Influence Coefficients in brackets are for similar load tests on rib No. 6.)

Horizontal reaction at base of rib No. 36 due to any load at points 1, 5, 9, 13 or 17 on rib Nos. 30 & 6
= Load Value x Influence Coefficient

Structural Engineering Division
Department of Civil Engineering
University of Newcastle upon Tyne

F. A. A. Ph. D. Thesis
19. Oct. 1968

TESTS ON MODEL RADIAL RIBBED DOME

Test No. 1.
Sheet No. 3

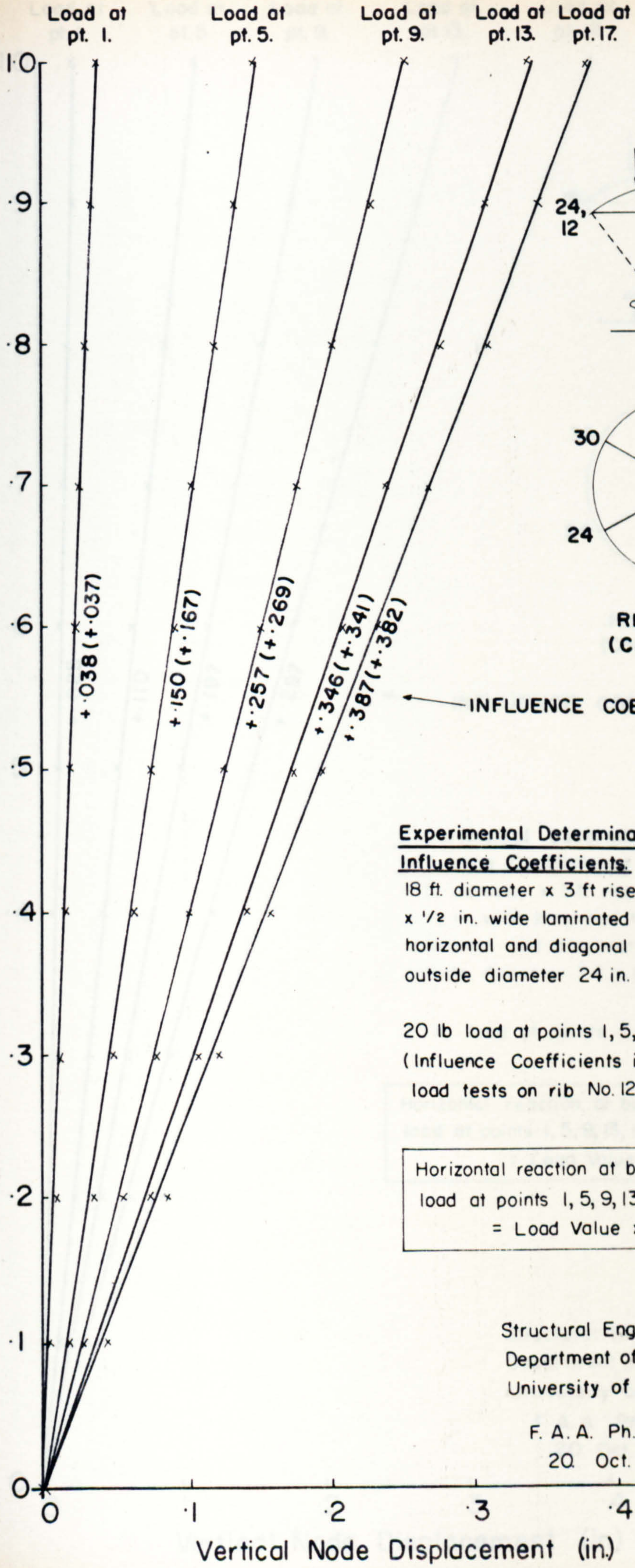

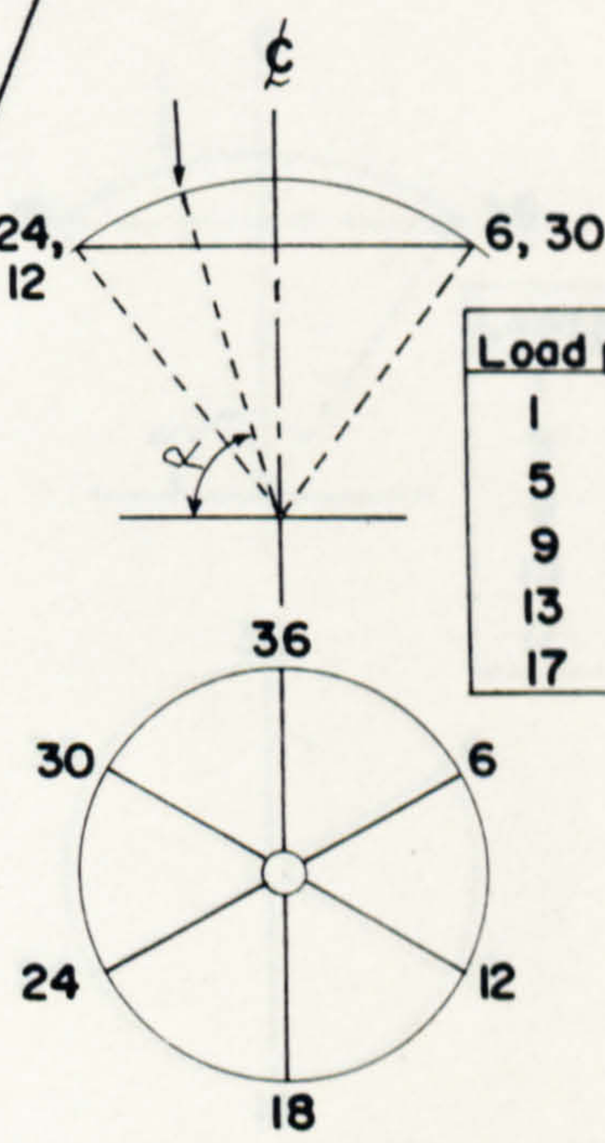

Load pt.	∝ (rads)
1	·9657
5	1·0990
9	1·2324
13	1·3657
17	1·4990

RIB SYSTEM
(Constant I)

← INFLUENCE COEFFICIENT = $\frac{D_2}{D_1}$

Experimental Determination of Horizontal Reaction Influence Coefficients.

18 ft. diameter x 3 ft rise model dome with 2in. deep x 1/2 in. wide laminated timber ribs (6 No.) without horizontal and diagonal bracing. Mild steel apex ring outside diameter 24 in. (1 in. deep x 1/8 in. thick)

20 lb load at points 1, 5, 9, 13, & 17 on rib No. 24
(Influence Coefficients in brackets are for similar load tests on rib No. 12.)

Horizontal reaction at base of rib No. 36 due to any load at points 1, 5, 9, 13, or 17 on rib Nos. 24 & 12
= Load Value x Influence Coefficient

Structural Engineering Division
Department of Civil Engineering
University of Newcastle upon Tyne

F. A. A. Ph.D Thesis
20 Oct. 1968.

TESTS ON MODEL RADIAL RIBBED DOME

Test No. 1.
Sheet No. 4.

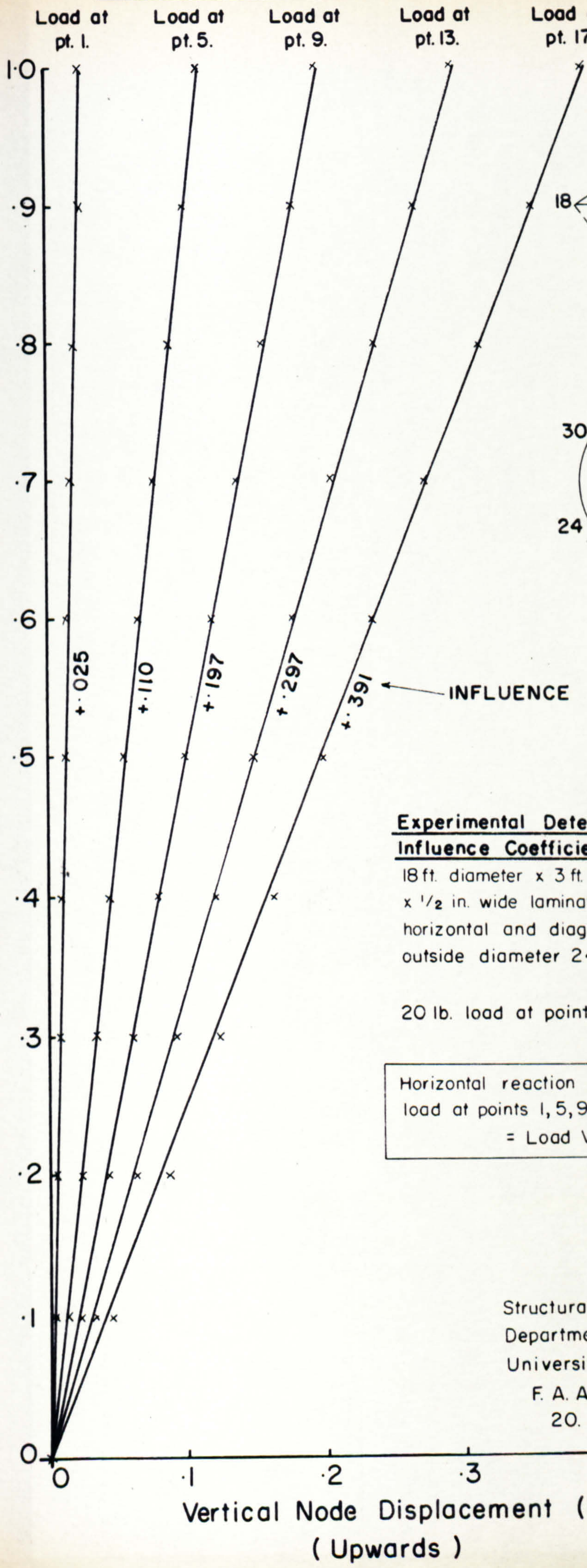

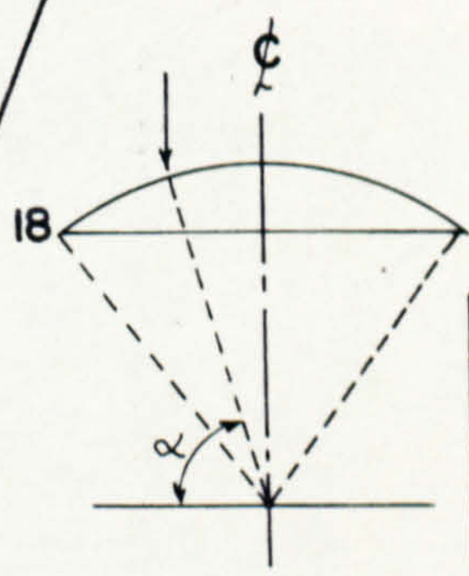

Load pt	α (rads)
1	·9657
5	1·0990
9	1·2324
13	1·3657
17	1·4990

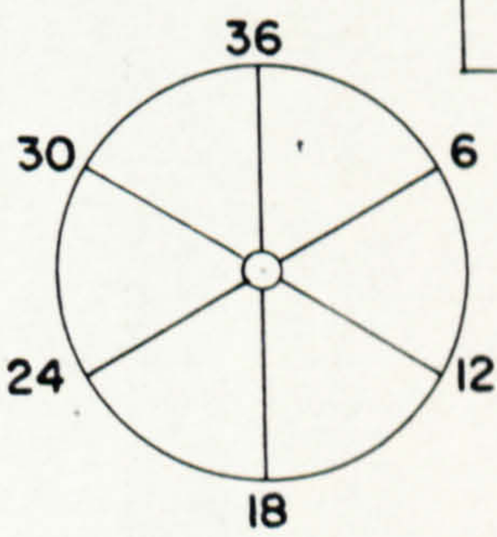

RIB SYSTEM
(Constant I)

INFLUENCE COEFFICIENT = $\frac{D_2}{D_1}$

Experimental Determination of Horizontal Reaction Influence Coefficients

18 ft. diameter x 3 ft. rise model dome with 2 in. deep x ½ in. wide laminated timber ribs (6 No.) without horizontal and diagonal bracing. Mild steel apex ring outside diameter 24 in. (1 in. deep x ⅛ in. thick.)

20 lb. load at points 1, 5, 9, 13, & 17 on rib No. 18

Horizontal reaction at base of rib No. 36 due to any load at points 1, 5, 9, 13, or 17 on rib No. 18
= Load Value x Influence Coefficient

Structural Engineering Division
Department of Civil Engineering
University of Newcastle upon Tyne
F. A. A. Ph. D. Thesis
20. Oct. 1968.

Structural Engineering Division
Department of Civil Engineering
University of Newcastle upon Tyne.

TESTS ON MODEL RADIAL RIBBED DOME

Test No. 1. Sheet No. 5.

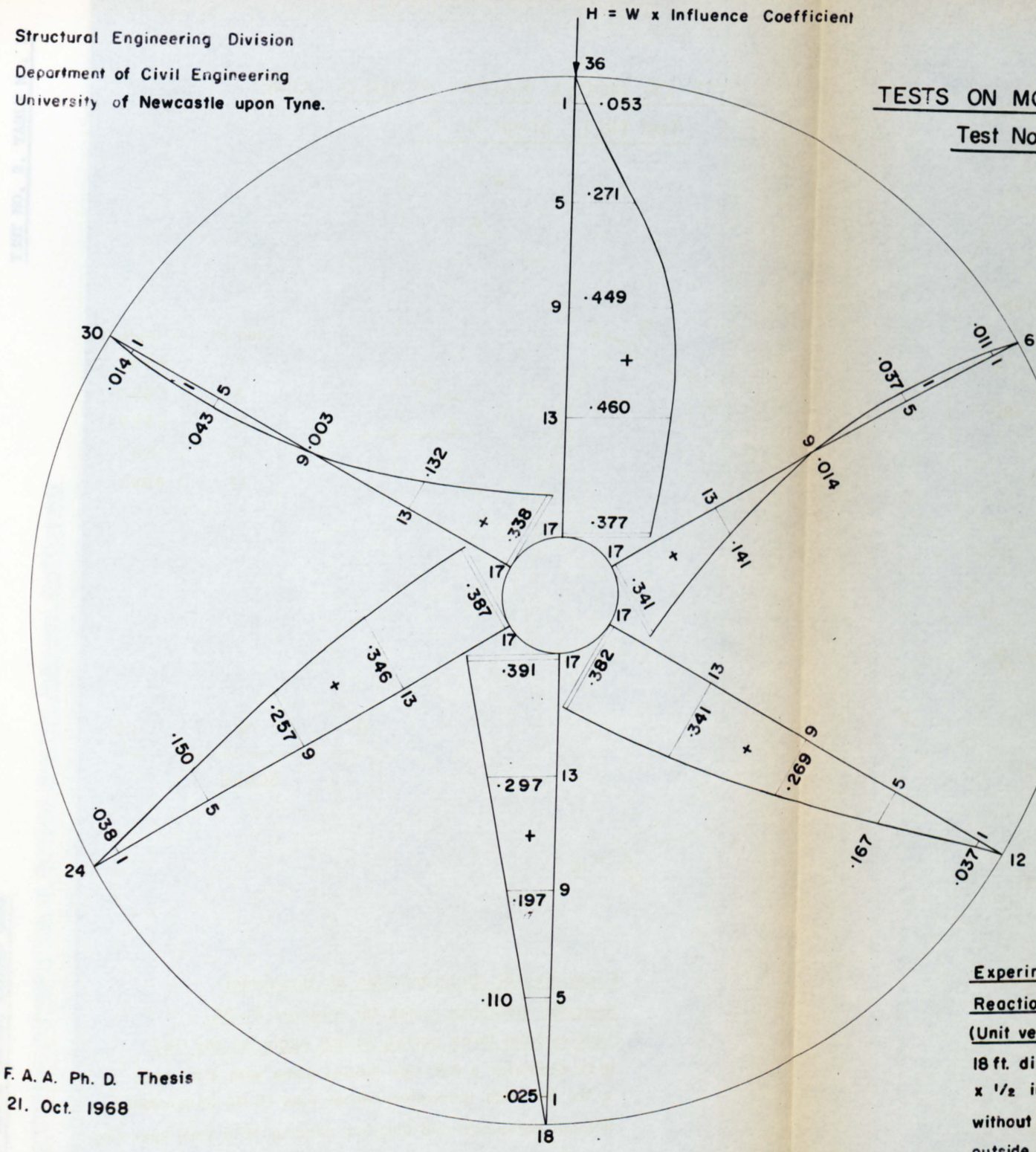

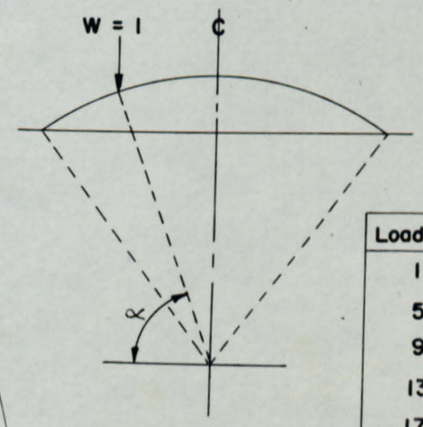

Load Pt.	∝ (rads.)
1	·9657
5	1·0990
9	1·2324
13	1·3657
17	1·4990

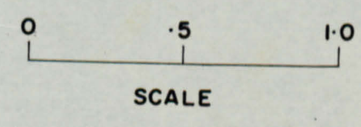

F. A. A. Ph. D. Thesis
21. Oct. 1968

Experimental Determination of Horizontal Reaction Influence Lines for Support No. 36.

(Unit vertical force acting at any angle on any rib)

18 ft. diameter x 3 ft. rise model dome with 2 in. deep x ½ in. wide laminated timber ribs (6 No. of constant I) without horizontal and diagonal bracing. Mild steel apex ring outside diameter 24 in. (1 in. deep x ⅛ in. thick)

TESTS ON MODEL RADIAL RIBBED DOME

TEST NO. 2. TABLE NO. 1.

Experimental Determination of Vertical Reaction Influence Coefficients

Load at point = 20 lb. For position of load points, rib layout, details of model dome and graphs of tabulated results, see Test No. 2 Sheet Nos. 1 & 2.

Vertical Base displacement at Rib. No. 18 (upwards)	Dial Gauge Readings (A) and Actual Vertical Displacement of Point load (B; +ve upwards) in inches																			
	Rib No. 18										Rib No. 12.									
	Point 1		Point 5		Point 9		Point 13		Point 17		Point 1		Point 5		Point 9		Point 13		Point 17	
	A	B	A	B	A	B	A	B	A	B	A	B	A	B	A	B	A	B	A	B
0 in.	.154	.000	1.075	.000	.070	.000	.154	.000	.316	.000	.455	.000	.350	.000	.052	.000	.127	.000	.303	.000
.1 in.	.236	+.082	1.139	+.064	.119	+.049	.185	+.031	.329	+.013	.454	-.001	.349	-.001	.052	.000	.131	+.004	.313	+.010
.2 in.	.333	+.179	1.226	+.151	.186	+.116	.232	+.078	.352	+.036	.453	-.002	.347	-.003	.052	.000	.136	+.009	.328	+.025
.3 in.	.432	+.278	1.311	+.236	.255	+.185	.278	+.124	.375	+.059	.453	-.002	.345	-.005	.052	.000	.142	+.015	.342	+.039
.4 in.	.528	+.374	1.394	+.319	.323	+.253	.325	+.171	.398	+.082	.452	-.003	.344	-.006	.052	.000	.148	+.021	.357	+.054
.5 in.	.624	+.470	1.482	+.407	.393	+.323	.373	+.219	.421	+.105	.452	-.003	.342	-.008	.052	.000	.154	+.027	.373	+.070
.6 in.	.723	+.569	1.569	+.494	.462	+.392	.421	+.267	.444	+.128	.451	-.004	.340	-.010	.052	.000	.160	+.033	.388	+.085
.7 in.	.821	+.667	1.655	+.580	.533	+.463	.469	+.315	.468	+.152	.451	-.004	.339	-.011	.052	.000	.166	+.039	.403	+.100
.8 in.	.917	+.763	1.742	+.667	.603	+.533	.517	+.363	.491	+.175	.450	-.005	.337	-.013	.053	+.001	.172	+.045	.418	+.115
.9 in.	1.016	+.862	1.829	+.754	.672	+.602	.565	+.411	.513	+.197	.450	-.005	.335	-.015	.053	+.001	.178	+.051	.433	+.130
1.0 in.	1.114	+.960	1.915	+.840	.741	+.671	.612	+.458	.536	+.220	.449	-.006	.334	-.016	.053	+.001	.184	+.057	.448	+.145

F.A.A. Ph.D. Thesis
17th-18th Oct., 1968.

Structural Engineering Division,
Department of Civil Engineering,
University of Newcastle upon Tyne.

TESTS ON MODEL RADIAL RIBBED DOME

TEST NO. 2. TABLE NO. 2.

Experimental Determination of Vertical Reaction Influence Coefficients

Load at point = 20 lb. For position of load points, rib layout, details of model dome and graphs of tabulated results, see Test No. 2. Sheet Nos. 3 & 4.

Vertical Base displacement at Rib. No. 18 (upwards)	Dial Gauge Readings (A) and Actual Vertical Displacement of Point Load (B; +ve upwards) in inches																			
	Rib No. 6										Rib No. 36									
	Point 1		Point 5		Point 9		Point 13		Point 17		Point 1		Point 5		Point 9		Point 13		Point 17	
	A	B	A	B	A	B	A	B	A	B	A	B	A	B	A	B	A	B	A	B
0 in.	.456	.000	.400	.000	.120	.000	.163	.000	.273	.000	.455	.000	.173	.000	.106	.000	.247	.000	.386	.000
.1 in.	.457	+.001	.403	+.003	.125	+.005	.171	+.008	.282	+.009	.455	.000	.174	+.001	.107	+.001	.252	+.005	.395	+.009
.2 in.	.458	+.002	.408	+.008	.132	+.012	.182	+.019	.295	+.022	.456	+.001	.176	+.003	.111	+.005	.260	+.013	.407	+.021
.3 in.	.459	+.003	.412	+.012	.139	+.019	.194	+.031	.308	+.035	.456	+.001	.178	+.005	.116	+.010	.269	+.022	.420	+.034
.4 in.	.460	+.004	.417	+.017	.146	+.026	.205	+.042	.321	+.048	.457	+.002	.181	+.008	.121	+.015	.278	+.031	.432	+.046
.5 in.	.461	+.005	.422	+.022	.154	+.034	.216	+.053	.334	+.061	.457	+.002	.184	+.011	.126	+.020	.286	+.039	.445	+.059
.6 in.	.462	+.006	.427	+.027	.161	+.041	.228	+.065	.348	+.075	.458	+.003	.186	+.013	.133	+.027	.295	+.048	.458	+.072
.7 in.	.464	+.008	.432	+.032	.169	+.049	.239	+.076	.360	+.087	.458	+.003	.189	+.016	.137	+.031	.303	+.056	.470	+.084
.8 in.	.465	+.009	.436	+.036	.177	+.057	.251	+.088	.373	+.100	.459	+.004	.192	+.019	.142	+.036	.312	+.065	.482	+.096
.9 in.	.466	+.010	.441	+.041	.185	+.065	.262	+.099	.387	+.114	.460	+.005	.195	+.022	.148	+.042	.320	+.073	.495	+.109
1.0 in.	.467	+.011	.446	+.046	.193	+.073	.274	+.111	.400	+.127	.460	+.005	.198	+.025	.153	+.047	.329	+.082	.507	+.121

F.A.A. Ph.D. Thesis
21st-22nd Oct., 1968.

Structural Engineering Division,
Department of Civil Engineering,
University of Newcastle upon Tyne.

TESTS ON MODEL RADIAL RIBBED DOME

TEST NO. 2. TABLE NO. 3.

Experimental Determination of Vertical Reaction Influence Coefficients

Load at point = 20 lb. For position of load points, rib layout, details of model dome and graphs of tabulated results, see Test No. 2 Sheet Nos. 2 & 3.

Vertical Base displacement at Rib No. 18 (upwards)	Dial Gauge Readings (A) and Actual Vertical Displacement of Point Load (B; +ve upwards) in inches																			
	Rib No. 30										Rib No. 24									
	Point 1		Point 5		Point 9		Point 13		Point 17		Point 1		Point 5		Point 9		Point 13		Point 17	
	A	B	A	B	A	B	A	B	A	B	A	B	A	B	A	B	A	B	A	B
0 in.	.554	.000	.064	.000	.029	.000	.172	.000	.280	.000	.658	.000	.387	.000	.117	.000	.152	.000	.237	.000
.1 in.	.555	+.001	.068	+.004	.034	+.005	.180	+.008	.289	+.009	.657	-.001	.385	-.002	.117	.000	.157	+.005	.249	+.012
.2 in.	.555	+.001	.072	+.008	.042	+.013	.190	+.018	.301	+.021	.657	-.001	.383	-.004	.118	+.001	.165	+.013	.264	+.027
.3 in.	.556	+.002	.077	+.013	.050	+.021	.200	+.028	.316	+.036	.656	-.002	.382	-.005	.119	+.002	.173	+.021	.279	+.042
.4 in.	.557	+.003	.082	+.018	.058	+.029	.211	+.039	.329	+.049	.656	-.002	.380	-.007	.121	+.004	.181	+.029	.295	+.058
.5 in.	.559	+.005	.087	+.023	.066	+.037	.222	+.050	.342	+.062	.655	-.003	.379	-.008	.122	+.005	.189	+.037	.310	+.073
.6 in.	.560	+.006	.092	+.028	.074	+.045	.233	+.061	.355	+.075	.655	-.003	.378	-.009	.124	+.007	.197	+.045	.326	+.089
.7 in.	.561	+.007	.098	+.034	.082	+.053	.244	+.072	.369	+.089	.655	-.003	.376	-.011	.126	+.009	.205	+.053	.341	+.104
.8 in.	.562	+.008	.102	+.038	.091	+.062	.256	+.084	.382	+.102	.654	-.004	.375	-.012	.127	+.010	.213	+.061	.356	+.119
.9 in.	.563	+.009	.108	+.044	.099	+.070	.266	+.094	.395	+.115	.654	-.004	.374	-.013	.129	+.012	.221	+.069	.371	+.134
1.0 in.	.564	+.010	.113	+.049	.108	+.079	.278	+.106	.408	+.128	.653	-.005	.373	-.014	.131	+.014	.228	+.076	.386	+.149

F.A.A. Ph.D. Thesis
21st-22nd Oct., 1968

Structural Engineering Division,
Department of Civil Engineering,
University of Newcastle upon Tyne.

TESTS ON MODEL RADIAL RIBBED DOME

Test No. 2.
Sheet No. 1.

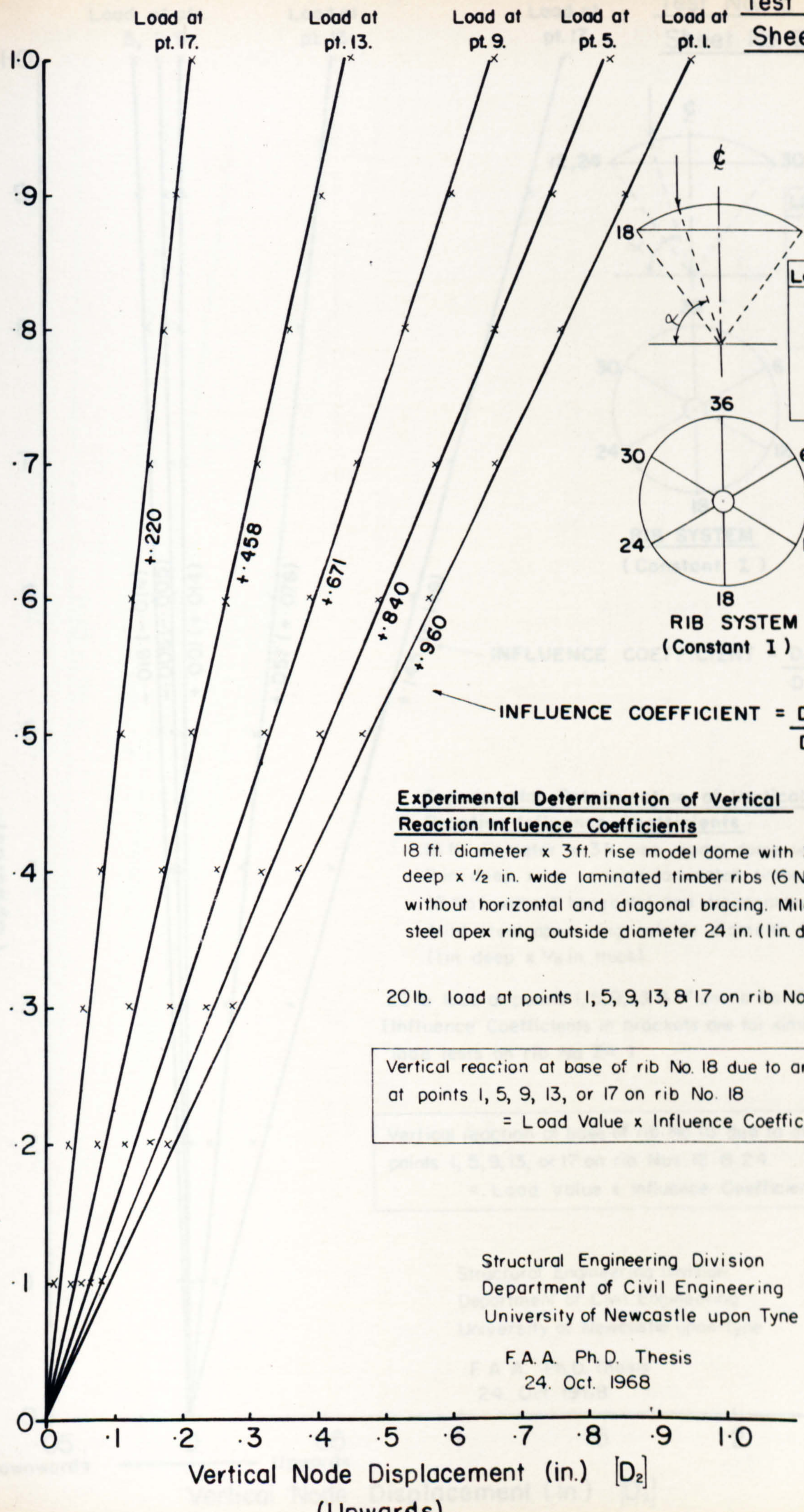

Load pt.	α (rads)
1	·9657
5	1·0990
9	1·2324
13	1·3657
17	1·4990

INFLUENCE COEFFICIENT = $\frac{D_2}{D_1}$

Experimental Determination of Vertical Reaction Influence Coefficients

18 ft. diameter x 3 ft. rise model dome with 2 in. deep x ½ in. wide laminated timber ribs (6 No.) without horizontal and diagonal bracing. Mild steel apex ring outside diameter 24 in. (1 in. deep x ⅛ in. thick)

20 lb. load at points 1, 5, 9, 13, & 17 on rib No. 18

Vertical reaction at base of rib No. 18 due to any load at points 1, 5, 9, 13, or 17 on rib No. 18
= Load Value x Influence Coefficient.

Structural Engineering Division
Department of Civil Engineering
University of Newcastle upon Tyne

F. A. A. Ph. D. Thesis
24. Oct. 1968

TESTS ON MODEL RADIAL RIBBED DOME

Test No. 2.

Sheet No. 2.

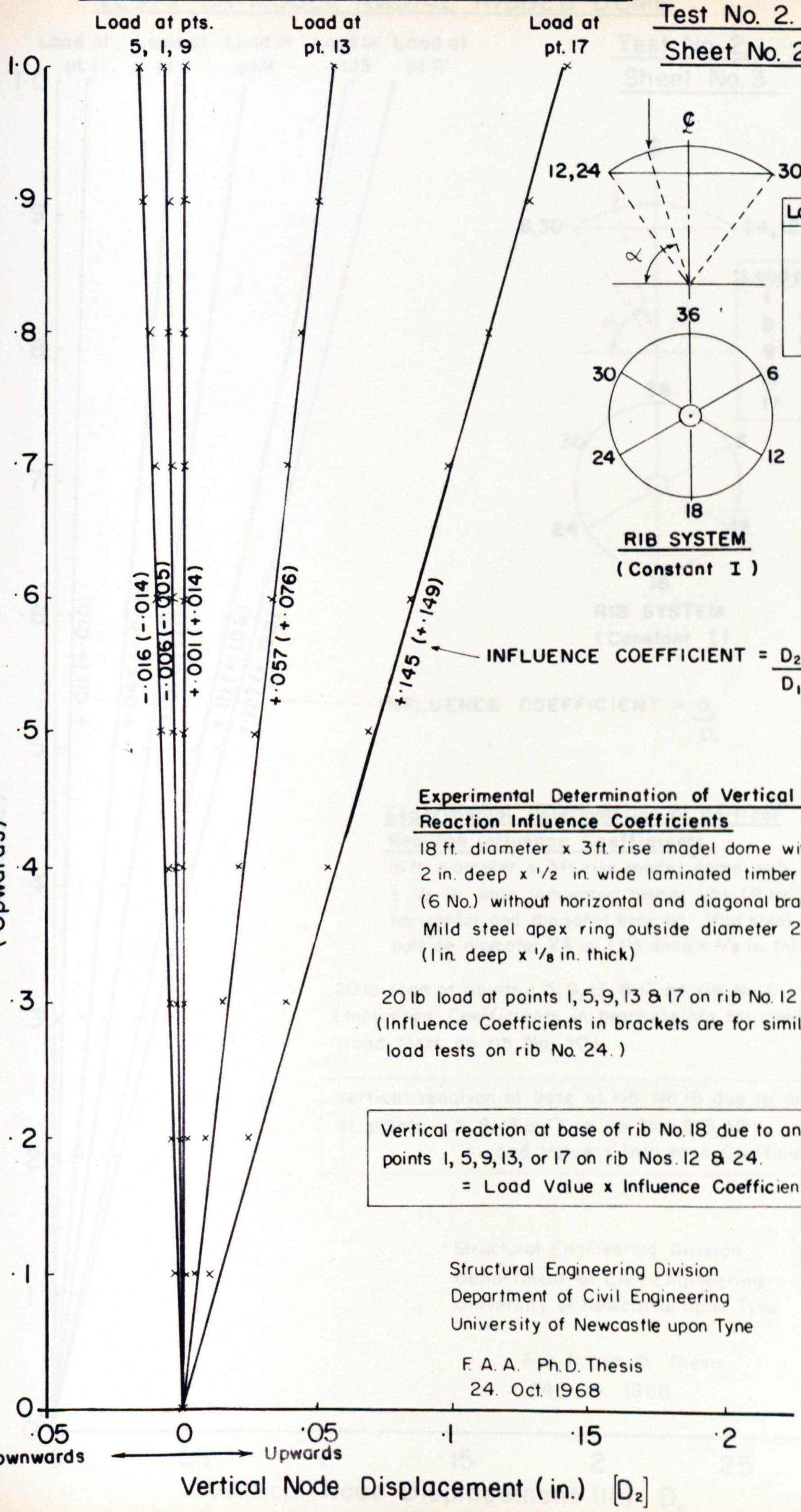

Load pt.	∝ rads
1	·9657
5	1·0990
9	1·2324
13	1·3657
17	1·4990

RIB SYSTEM

(Constant I)

Experimental Determination of Vertical Reaction Influence Coefficients

18 ft. diameter x 3 ft. rise model dome with 2 in. deep x 1/2 in. wide laminated timber ribs (6 No.) without horizontal and diagonal bracing. Mild steel apex ring outside diameter 24 in. (1 in. deep x 1/8 in. thick)

20 lb load at points 1, 5, 9, 13 & 17 on rib No. 12
(Influence Coefficients in brackets are for similar load tests on rib No. 24.)

Vertical reaction at base of rib No. 18 due to any load at points 1, 5, 9, 13, or 17 on rib Nos. 12 & 24.
= Load Value x Influence Coefficient

Structural Engineering Division
Department of Civil Engineering
University of Newcastle upon Tyne

F. A. A. Ph.D. Thesis
24. Oct. 1968

TESTS ON MODEL RADIAL RIBBED DOME

Test No. 2.
Sheet No. 3.

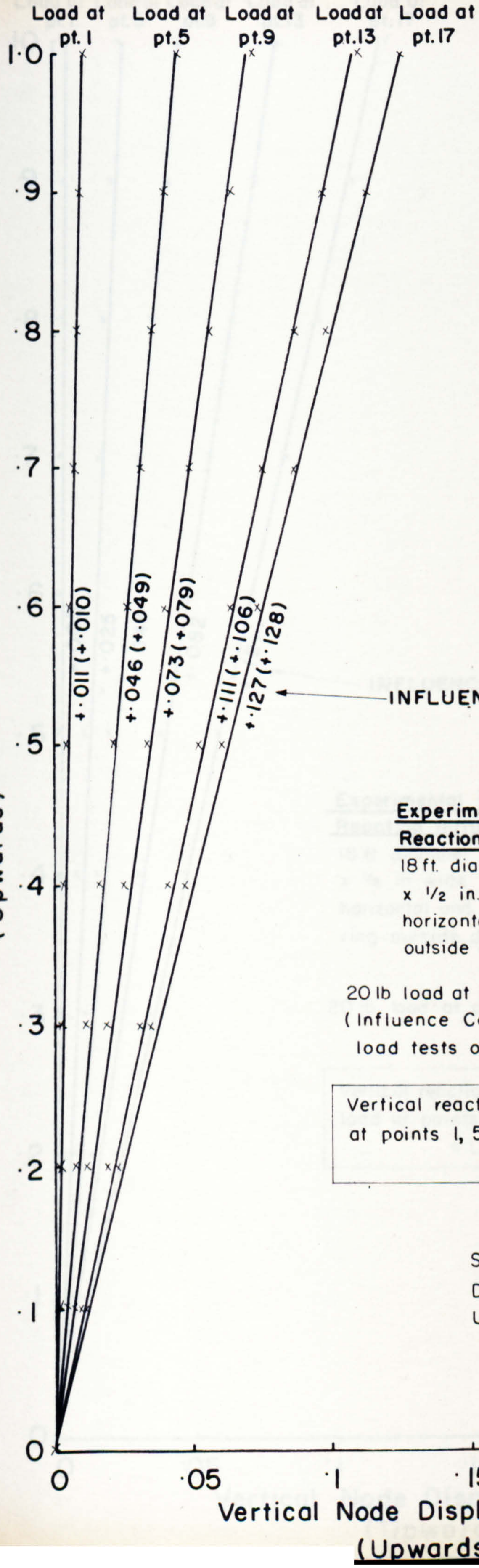

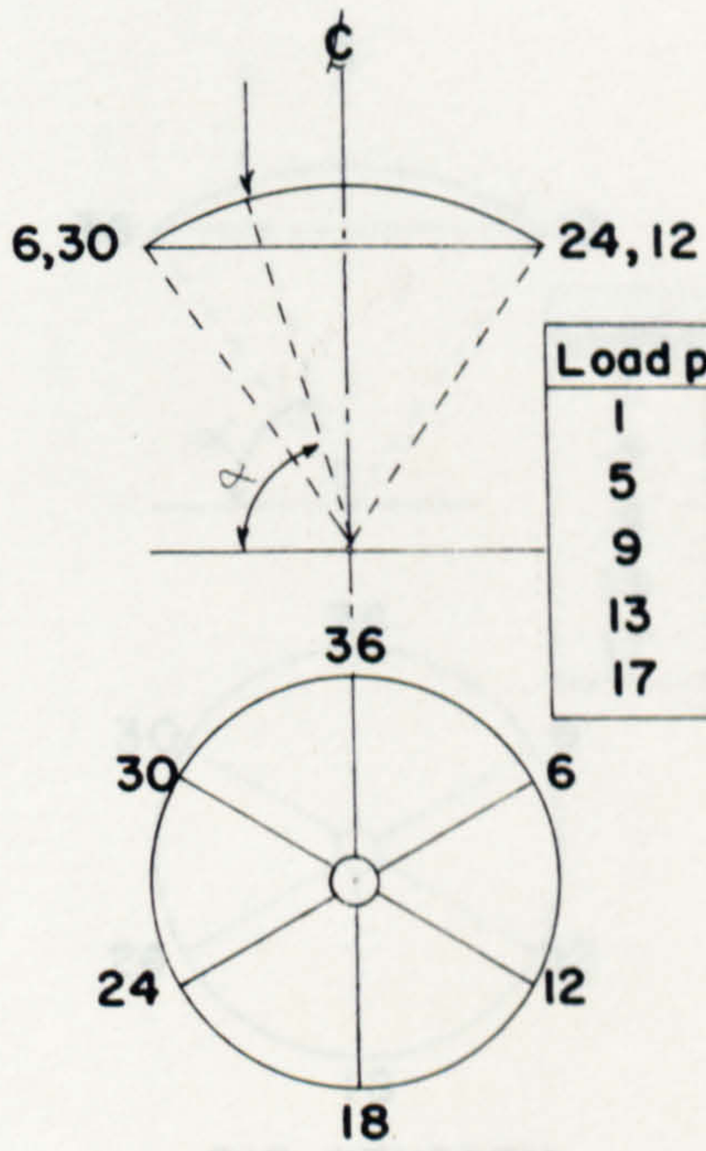

Load pt.	∝ (rads)
1	·9657
5	1·0990
9	1·2324
13	1·3657
17	1·4990

RIB SYSTEM
(Constant I)

INFLUENCE COEFFICIENT = $\frac{D_2}{D_1}$

Experimental Determination of Vertical Reaction Influence Coefficients

18 ft. diameter x 3 ft. rise model dome with 2 in. deep x ½ in. wide laminated timber ribs (6 No.) without horizontal and diagonal bracing. Mild steel apex ring outside diameter 24 in. (1 in. deep x ⅛ in. thick)

20 lb load at points 1, 5, 9, 13, & 17 on rib No. 6
(Influence Coefficients in brackets are for similar load tests on rib No. 30.)

Vertical reaction at base of rib No. 18 due to any load at points 1, 5, 9, 13 or 17 on rib Nos 6 & 30
= Load Value x Influence Coefficient

Structural Engineering Division
Department of Civil Engineering
University of Newcastle upon Tyne

F. A. A. Ph. D. Thesis
24 Oct. 1968

TESTS ON MODEL RADIAL RIBBED DOME

Test No. 2.
Sheet No. 4.

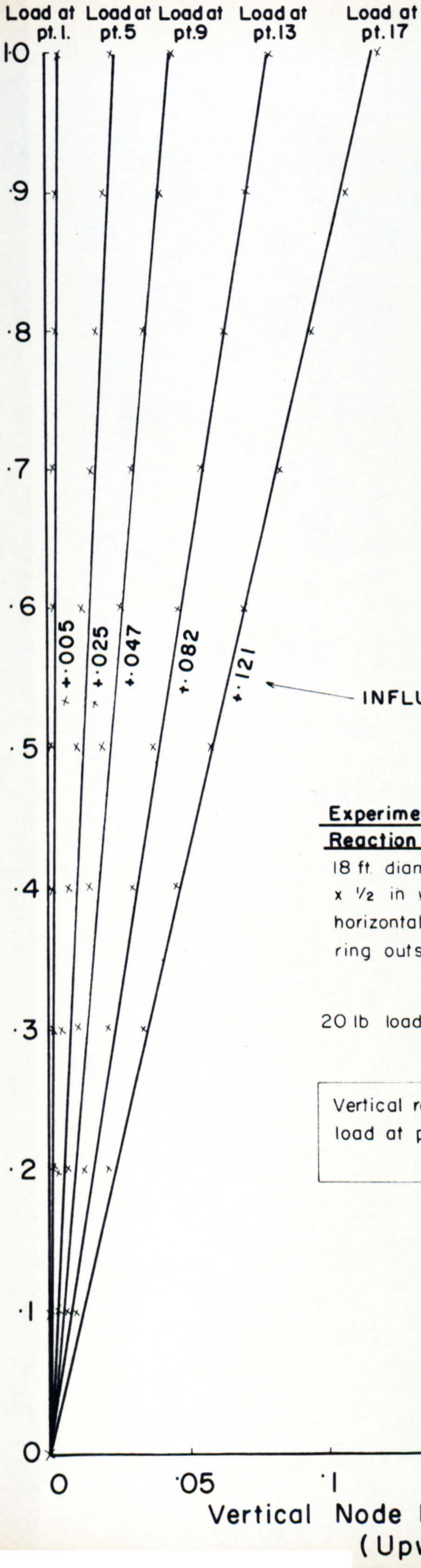

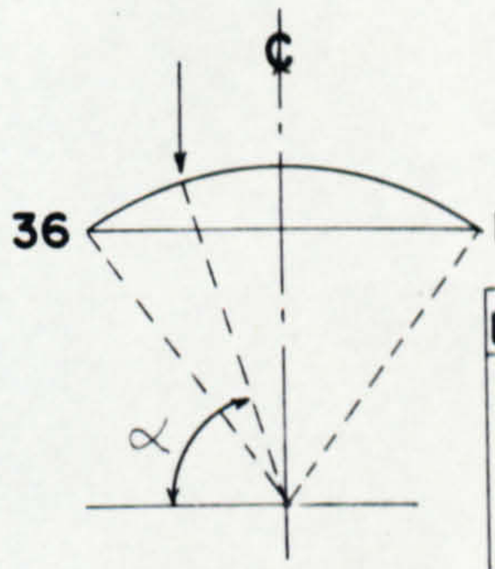

Load pt.	α (rads.)
1	·9657
5	1·0990
9	1·2324
13	1·3657
17	1·4990

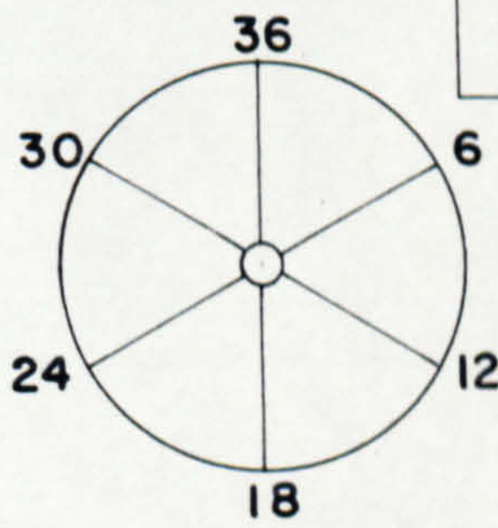

RIB STYSTEM
(Constant I)

INFLUENCE COEFFICIENT = $\frac{D_2}{D_1}$

Experimental Determination of Vertical Reaction Influence Coefficients

18 ft. diameter x 3ft. rise model dome with 2 in. deep x ½ in wide laminated timber ribs (6 No.) without horizontal and diagonal bracing. Mild steel apex ring outside diameter 24 in. (1in.deep x ⅛ in. thick)

20 lb load at points 1, 5, 9, 13, & 17 on rib No. 36

Vertical reaction at base of rib No. 18 due to any load at points 1, 5, 9, 13 or 17 on rib No. 36
= Load Value x Influence Coefficient

Structural Engineering Division
Department of Civil Engineering
University of Newcastle upon Tyne

F. A. A. Ph. D Thesis
24. Oct. 1968

Structural Engineering Division
Department of Civil Engineering
University of Newcastle upon Tyne

TESTS ON MODEL RADIAL RIBBED DOME

Test No. 2. Sheet No. 5

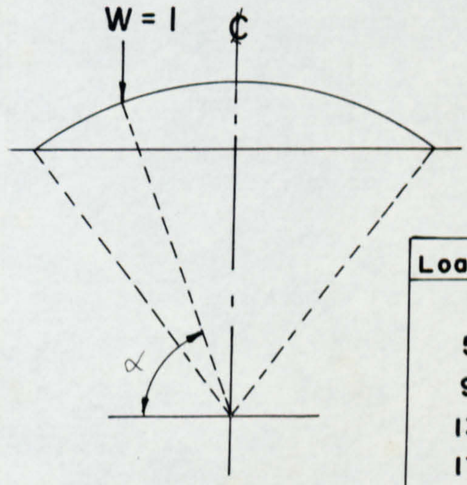

Load Pt.	∝ (rads)
1	·9657
5	1·0990
9	1·2324
13	1·3657
17	1·4990

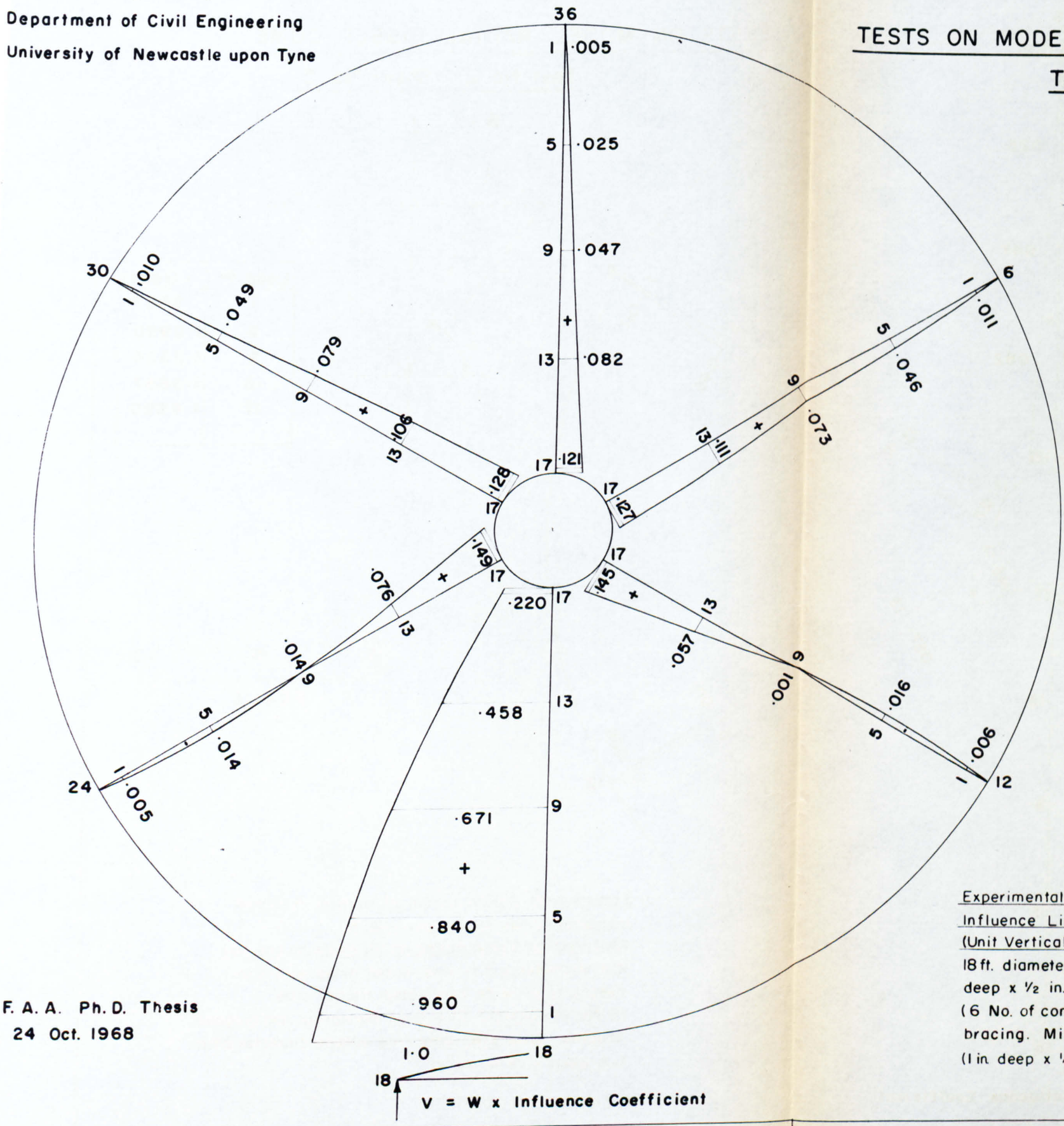

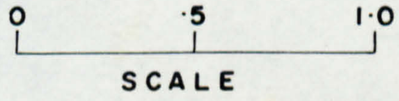

Experimental Determination of Vertical Reaction Influence Lines for Support No.18
(Unit Vertical Force acting at any angle on any rib)
18 ft. diameter x 3 ft. rise model dome with 2 in. deep x ½ in. wide laminated timber ribs (6 No. of constant I) without horizontal and diagonal bracing. Mild steel apex ring outside diameter 24 in. (1 in. deep x ⅛ in. thick)

F. A. A. Ph. D. Thesis
24 Oct. 1968

TESTS ON MODEL RADIAL RIBLED DOME

TEST No. 3 TABLE No. 1.

Experimental Determination of Apex Ring Vertical Force Influence Coefficients

Load at point = 20lb

For position of load points, rib layout, details of model dome and graphs of tabulated results, see Test No. 3 Sheet Nos. 1 & 2.

Vertical Displacement at Apex Ring on Rib No.36 (Upwards)	Dial gauge readings (A) and actual vertical displacement of point load (B; ve upwards) in inches																			
	Rib No. 36										Rib No. 6									
	Point 1		Point 5		Point 9		Point 13		Point 17		Point 1		Point 5		Point 9		Point 13		Point 17	
	A	B	A	B	A	B	A	B	A	B	A	B	A	B	A	B	A	B	A	B
0 in.	.454	.000	.087	.000	.112	.000	.175	.000	.515	.000	.463	.000	.095	.000	.118	.000	.139	.000	.214	.000
.01 in.	.455	+.001	.088	+.001	.115	+.003	.182	+.007	.525	+.010	.463	.000	.095	.000	.119	+.001	.142	+.003	.220	+.006
.02 in.	.455	+.001	.090	+.003	.119	+.007	.189	+.014	.535	+.020	.463	.000	.095	.000	.120	+.002	.145	+.006	.226	+.012
.03 in.	.455	+.001	.091	+.004	.123	+.011	.197	+.022	.545	+.030	.463	.000	.095	.000	.122	+.004	.149	+.010	.231	+.017
.04 in.	.455	+.001	.093	+.006	.127	+.015	.205	+.030	.555	+.040	.463	.000	.095	.000	.123	+.005	.152	+.013	.237	+.023
.05 in.	.456	+.002	.095	+.008	.131	+.019	.212	+.037	.565	+.050	.463	.000	.096	+.001	.124	+.006	.155	+.016	.243	+.029
.06 in.	.456	+.002	.096	+.009	.135	+.023	.220	+.045	.575	+.060	.463	.000	.096	+.001	.125	+.007	.159	+.020	.250	+.036
.07 in.	.456	+.002	.098	+.011	.139	+.027	.228	+.053	.585	+.070	.463	.000	.096	+.001	.126	+.008	.162	+.023	.256	+.042
.08 in.	.457	+.003	.099	+.012	.143	+.031	.235	+.060	.595	+.080	.463	.000	.097	+.002	.128	+.010	.166	+.027	.262	+.048
.09 in.	.457	+.003	.101	+.014	.147	+.035	.243	+.068	.605	+.090	.463	.000	.097	+.002	.129	+.011	.170	+.031	.268	+.054
.10 in.	.457	+.003	.102	+.015	.151	+.039	.250	+.075	.615	+.100	.463	.000	.098	+.003	.131	+.013	.173	+.034	.274	+.060

F.A.A. Ph.D. Thesis
11th Nov., 1968

Structural Engineering Division,
Department of Civil Engineering,
University of Newcastle upon Tyne.

Experimental Determination of Apex Ring Vertical Force Influence Coefficients

Load at point = 20lb

For position of load points, rib layout, details of model dome and graphs of tabulated results, see Test No. 3 Sheet Nos. 3 & 4.

Vertical Displacement at Apex Ring on Rib No.36 (Upwards)	Dial gauge readings (A) and actual vertical Displacement of point load (B; +ve upwards) in inches																			
	Rib No. 12										Rib No. 18									
	Point 1		Point 5		Point 9		Point 13		Point 17		Point 1		Point 5		Point 9		Point 13		Point 17	
	A	B	A	B	A	B	A	B	A	B	A	B	A	B	A	B	A	B	A	B
0 in.	.458	.000	.076	.000	.101	.000	.169	.000	.316	.000	.457	.000	.076	.000	.107	.000	.191	.000	.334	.000
.01 in.	.457	-.001	.073	-.003	.097	-.004	.166	-.003	.314	-.002	.456	-.001	.072	-.004	.100	-.007	.187	-.004	.331	-.003
.02 in.	.457	-.001	.070	-.006	.093	-.008	.164	-.005	.313	-.003	.455	-.002	.068	-.008	.095	-.012	.181	-.010	.329	-.005
.03 in.	.456	-.002	.068	-.008	.089	-.012	.161	-.008	.311	-.005	.454	-.003	.064	-.012	.090	-.017	.176	-.015	.327	-.007
.04 in.	.455	-.003	.065	-.011	.086	-.015	.159	-.010	.309	-.007	.454	-.003	.060	-.016	.084	-.023	.171	-.020	.325	-.009
.05 in.	.455	-.003	.063	-.013	.082	-.019	.157	-.012	.307	-.009	.453	-.004	.057	-.019	.079	-.028	.167	-.024	.322	-.012
.06 in.	.454	-.004	.060	-.016	.079	-.022	.155	-.014	.306	-.010	.452	-.005	.053	-.023	.074	-.033	.162	-.029	.319	-.015
.07 in.	.454	-.004	.058	-.018	.075	-.026	.153	-.016	.305	-.011	.451	-.006	.049	-.027	.068	-.039	.157	-.034	.317	-.017
.08 in.	.453	-.005	.055	-.021	.072	-.029	.150	-.019	.303	-.013	.450	-.007	.045	-.031	.063	-.044	.152	-.039	.315	-.019
.09 in.	.453	-.005	.053	-.023	.069	-.032	.148	-.021	.302	-.014	.449	-.008	.041	-.035	.057	-.050	.147	-.044	.312	-.022
.10 in.	.452	-.006	.051	-.025	.066	-.035	.146	-.023	.301	-.015	.448	-.009	.038	-.038	.052	-.055	.142	-.049	.310	-.024

F.A.A. Ph.D. Thesis
12th Nov., 1968

Structural Engineering Division,
Department of Civil Engineering,
University of Newcastle upon Tyne.

TESTS ON MODEL RADIAL RIBBED DOME

TEST No. 3 TABLE No. 3.

Experimental Determination of Apex Ring Vertical Force Influence Coefficients

Load at point = 20lb

For position of load points, rib layout, details of model dome and graphs of tabulated results, see Test No. 3 Sheet Nos. 2 & 3.

Vertical Displacement at Apex Ring on Rib No.36 (Upwards)	Dial gauge readings (A) and actual vertical displacement of point load (B; +ve upwards) in inches																			
	Rib No. 24										Rib No. 30									
	Point 1		Point 5		Point 9		Point 13		Point 17		Point 1		Point 5		Point 9		Point 13		Point 17	
	A	B	A	B	A	B	A	B	A	B	A	B	A	B	A	B	A	B	A	B
0 in.	.453	.000	.094	.000	.117	.000	.158	.000	.289	.000	.458	.000	.072	.000	.090	.000	.135	.000	.237	.000
.01 in.	.452	-.001	.091	-.003	.113	-.004	.155	-.003	.289	.000	.458	.000	.072	.000	.091	+.001	.139	+.004	.248	+.011
.02 in.	.452	-.001	.088	-.006	.109	-.008	.153	-.005	.289	.000	.458	.000	.072	.000	.093	+.003	.143	+.008	.255	+.018
.03 in.	.451	-.002	.085	-.009	.106	-.011	.151	-.007	.289	.000	.458	.000	.072	.000	.094	+.004	.147	+.012	.262	+.025
.04 in.	.451	-.002	.083	-.011	.102	-.015	.149	-.009	.289	.000	.458	.000	.072	.006	.096	+.006	.150	+.015	.268	+.031
.05 in.	.450	-.003	.080	-.014	.100	-.017	.147	-.011	.289	.000	.458	.000	.073	+.001	.098	+.008	.153	+.018	275	+.038
.06 in.	.450	-.003	.078	-.016	.096	-.021	.145	-.013	.289	.000	.458	.000	.073	+.001	.099	+.009	.158	+.023	.281	+.044
.07 in.	.449	-.004	.075	-.019	.093	-.024	.143	-.015	.288	-.001	.458	.000	.073	+.001	.101	+.011	.162	+.027	.287	+.050
.08 in.	.449	-.004	.073	-.021	.090	-.027	.141	-.017	.287	-.002	.458	.000	.074	+.002	.102	+.012	.165	+.030	.294	+.057
.09 in.	.448	-.005	.071	-.023	.087	-.030	.139	-.019	.287	-.002	.458	.000	.075	+.003	.104	+.014	.169	+.034	.301	+.064
.10 in	.448	-.005	.069	-.025	.084	-.033	.136	-.022	.287	-.002	.458	.000	.075	+.003	.105	+.015	.173	+.038	.308	+.071

F.A.A. Ph.D. Thesis
13th Nov., 1968

Structural Engineering Division,
Department of Civil Engineering,
University of Newcastle upon Tyne.

TESTS ON MODEL RADIAL RIBBED DOME

Test No. 3
Sheet No. 1.

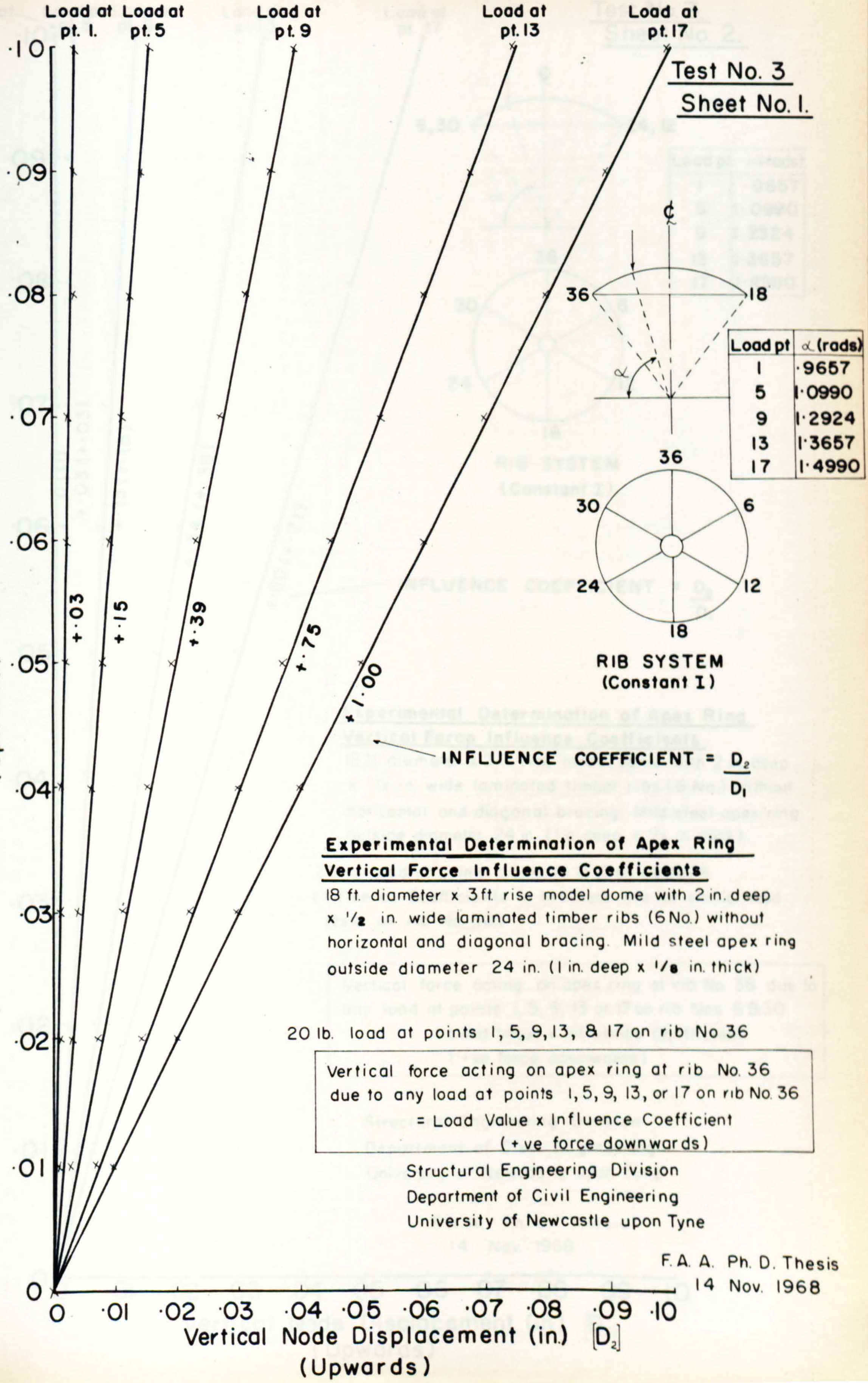

Load pt	α (rads)
1	·9657
5	1·0990
9	1·2924
13	1·3657
17	1·4990

INFLUENCE COEFFICIENT = $\frac{D_2}{D_1}$

Experimental Determination of Apex Ring
Vertical Force Influence Coefficients

18 ft. diameter x 3ft. rise model dome with 2 in. deep x 1/2 in. wide laminated timber ribs (6 No.) without horizontal and diagonal bracing. Mild steel apex ring outside diameter 24 in. (1 in. deep x 1/8 in. thick)

20 lb. load at points 1, 5, 9, 13, & 17 on rib No 36

Vertical force acting on apex ring at rib No. 36 due to any load at points 1, 5, 9, 13, or 17 on rib No. 36 = Load Value x Influence Coefficient (+ve force downwards)

Structural Engineering Division
Department of Civil Engineering
University of Newcastle upon Tyne

F. A. A. Ph. D. Thesis
14 Nov. 1968

TESTS ON MODEL RADIAL RIBBED DOME

Test No. 3.
Sheet No. 2.

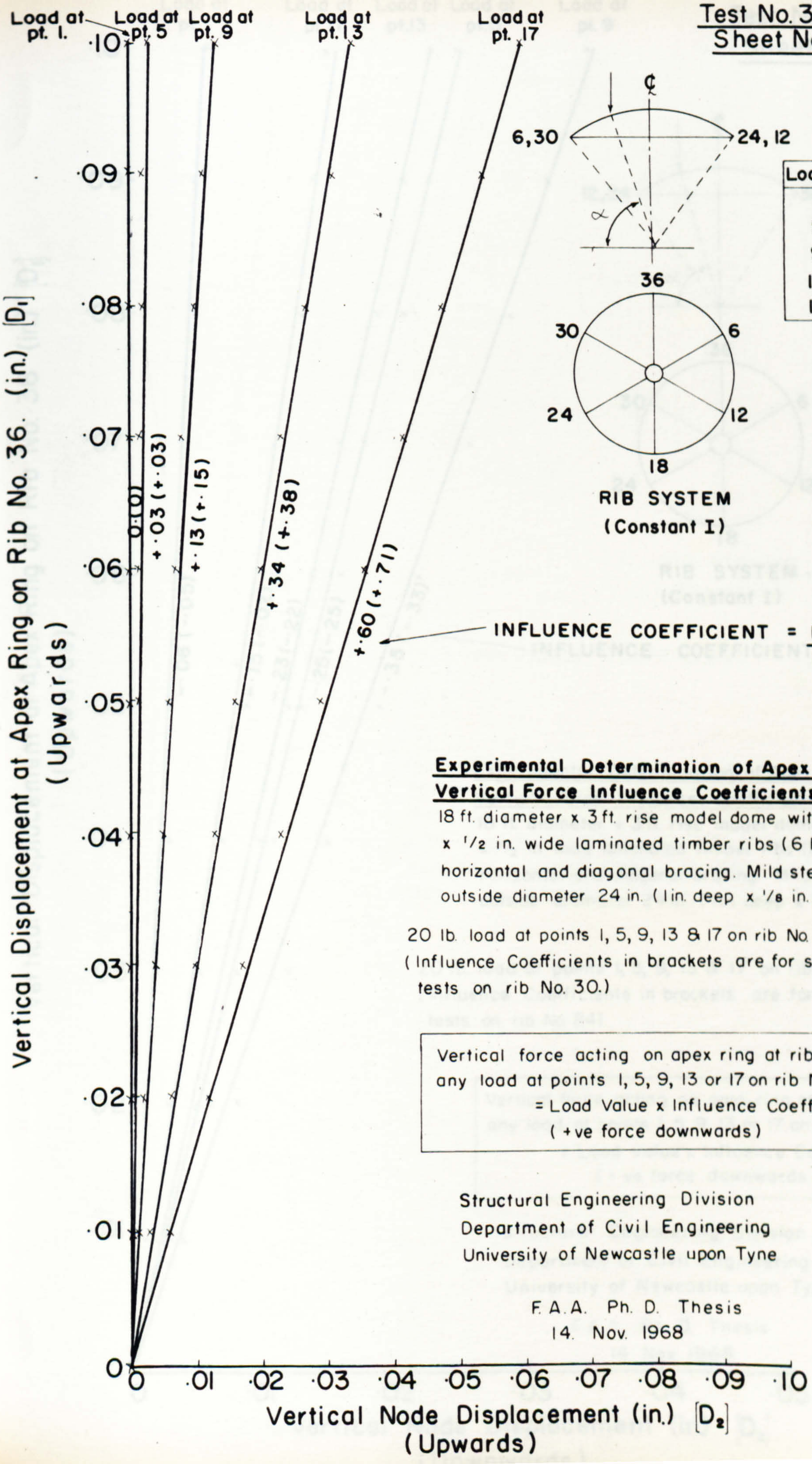

RIB SYSTEM
(Constant I)

Load pt.	α(rads)
1	·9657
5	1·0990
9	1·2324
13	1·3657
17	1·4990

INFLUENCE COEFFICIENT = $\frac{D_2}{D_1}$

Experimental Determination of Apex Ring Vertical Force Influence Coefficients

18 ft. diameter x 3 ft. rise model dome with 2 in. deep x 1/2 in. wide laminated timber ribs (6 No.) without horizontal and diagonal bracing. Mild steel apex ring outside diameter 24 in. (1 in. deep x 1/8 in. thick)

20 lb. load at points 1, 5, 9, 13 & 17 on rib No. 6.
(Influence Coefficients in brackets are for similar load tests on rib No. 30.)

Vertical force acting on apex ring at rib No. 36 due to any load at points 1, 5, 9, 13 or 17 on rib Nos. 6 & 30
= Load Value x Influence Coefficient
(+ve force downwards)

Structural Engineering Division
Department of Civil Engineering
University of Newcastle upon Tyne

F. A. A. Ph. D. Thesis
14. Nov. 1968

TESTS ON MODEL RADIAL RIBBED DOME

Test No. 3
Sheet No. 3.

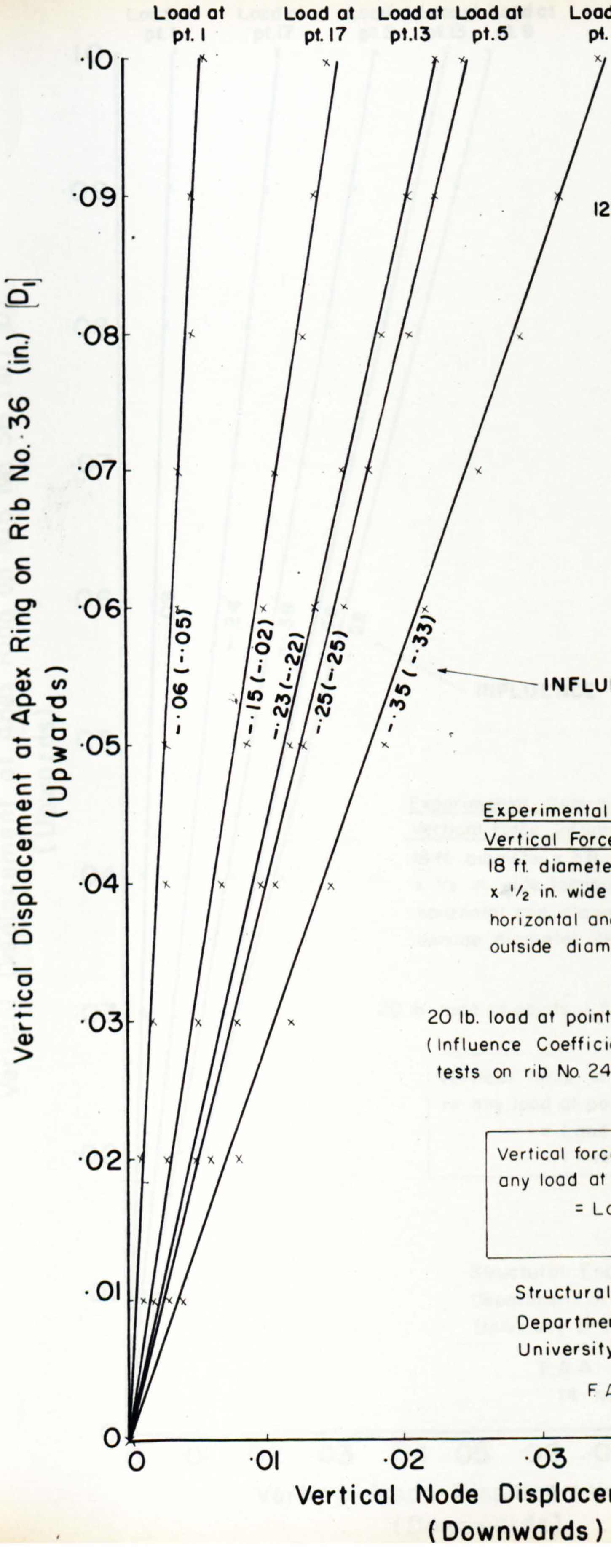

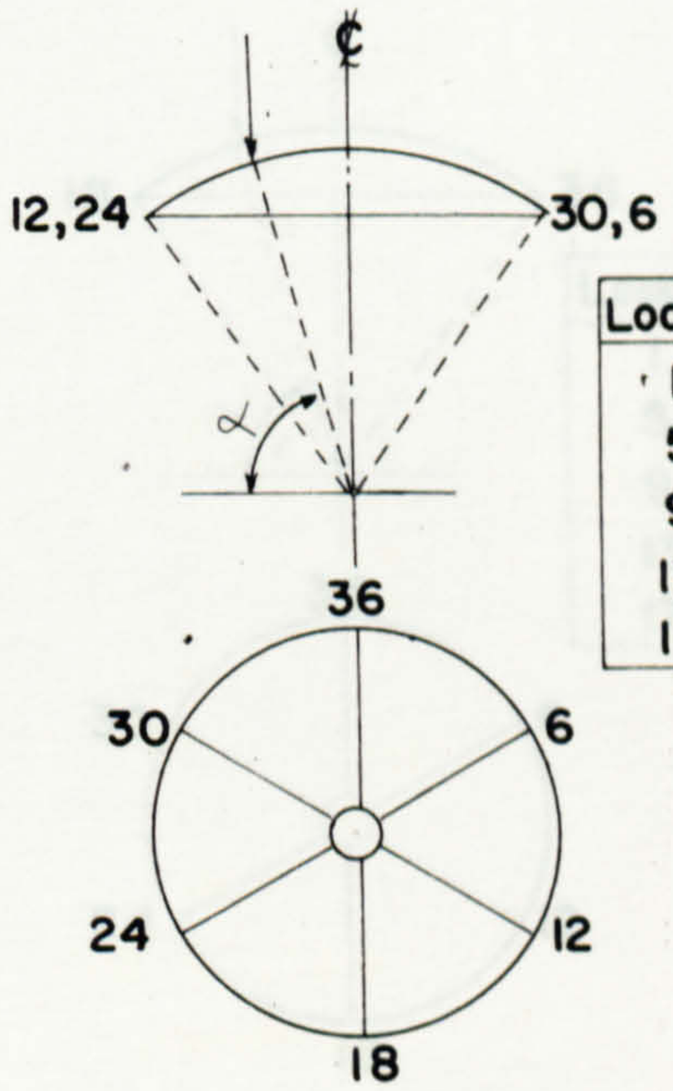

Load pt.	∝(rads)
1	·9657
5	1·0990
9	1·2324
13	1·3657
17	1·4990

RIB SYSTEM
(Constant I)

INFLUENCE COEFFICIENT = $\frac{D_2}{D_1}$

Experimental Determination of Apex Ring
Vertical Force Influence Coefficients

18 ft. diameter x 3 ft. rise model dome with 2 in. deep x ½ in. wide laminated timber ribs (6 No.) without horizontal and diagonal bracing. Mild steel apex ring outside diameter 24 in. (1 in. deep x ⅛ in. thick)

20 lb. load at points 1, 5, 9, 13 & 17 on rib No. 12
(Influence Coefficients in brackets are for similar load tests on rib No. 24)

Vertical force acting on apex ring at rib No. 36 due to any load at points 1, 5, 9, 13 or 17 on ribs Nos. 12 & 24
= Load Value x Influence Coefficient
(+ ve force downwards)

Structural Engineering Division
Department of Civil Engineering
University of Newcastle upon Tyne

F. A. A. Ph. D. Thesis
14 Nov. 1968

TESTS ON MODEL RADIAL RIBBED DOME

Test No. 3
Sheet No. 4

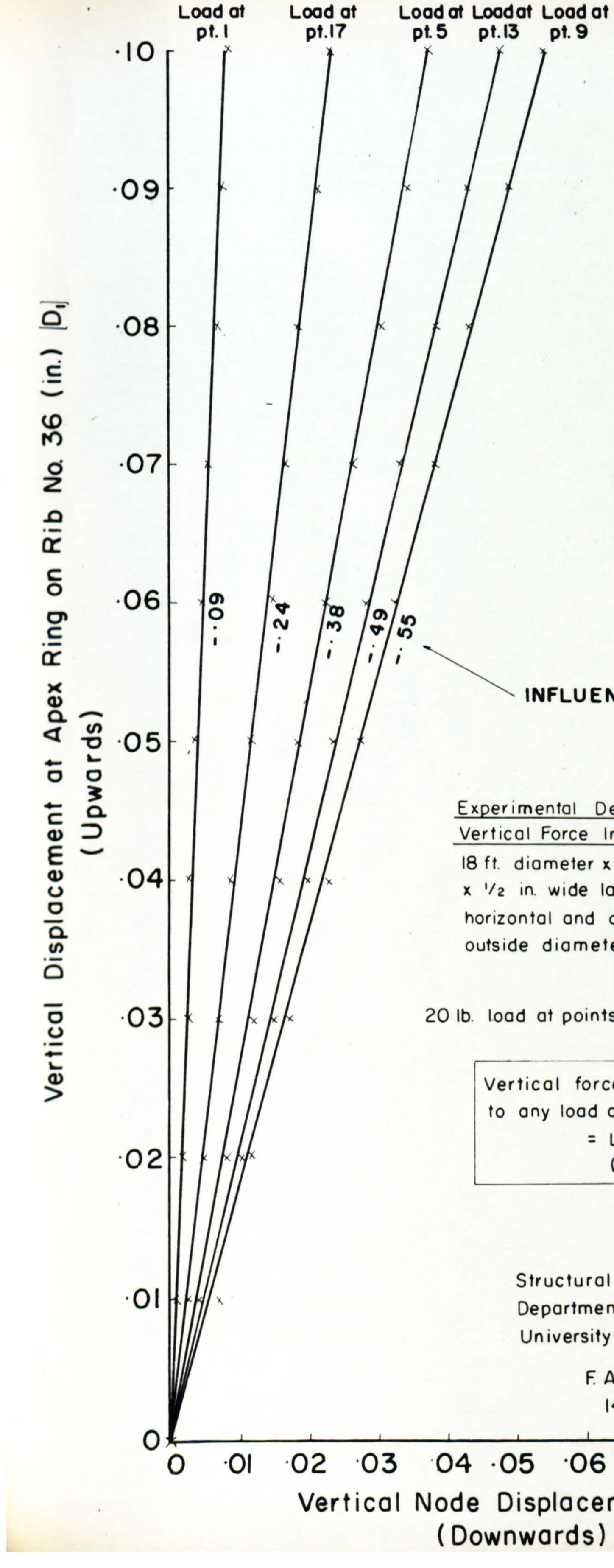

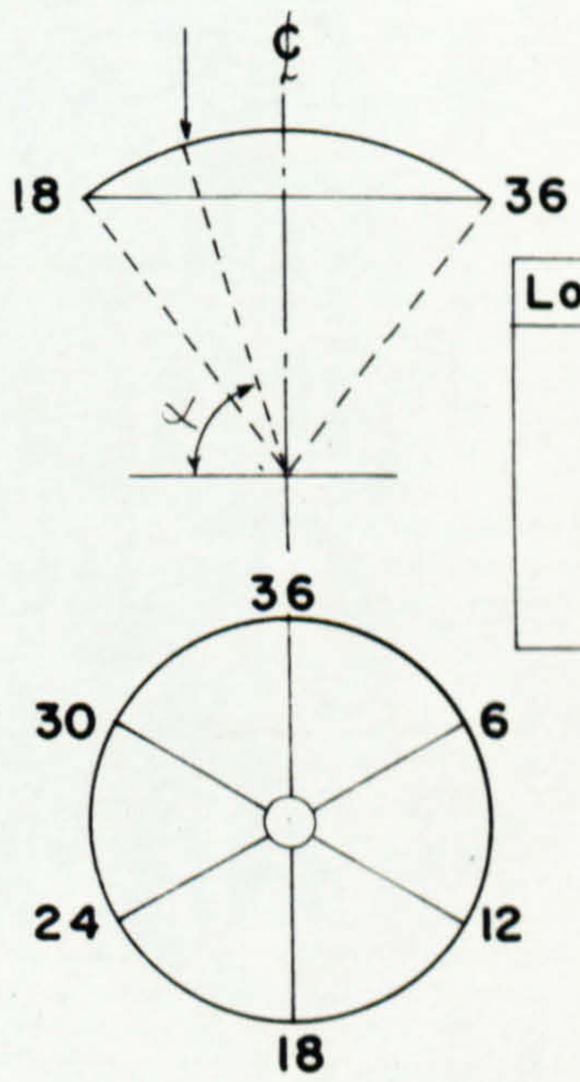

Load pt.	α (rads)
1	·9657
5	1·0990
9	1·2324
13	1·3657
17	1·4990

RIB SYSTEM
(Constant I)

INFLUENCE COEFFICIENT = $\frac{D_2}{D_1}$

Experimental Determination of Apex Ring
Vertical Force Influence Coefficients

18 ft. diameter x 3 ft. rise model dome with 2 in. deep x ½ in. wide laminated timber ribs (6 No.) without horizontal and diagonal bracing. Mild steel apex ring outside diameter 24 in. (1 in. deep x ⅛ in. thick)

20 lb. load at points 1, 5, 9, 13 & 17 on rib No. 18

Vertical force acting on apex ring at rib No. 36 due to any load at points 1, 5, 9, 13 or 17 on rib No. 18
= Load Value x Influence Coefficients
(+ ve force downward)

Structural Engineering Division
Department of Civil Engineering
University of Newcastle upon Tyne

F. A. A. Ph. D. Thesis
14 Nov. 1968

Structural Engineering Division
Department of Civil Engineering
University of Newcastle upon Tyne

TESTS ON MODEL RADIAL RIBBED DOME

Test No. 3. Sheet No. 5

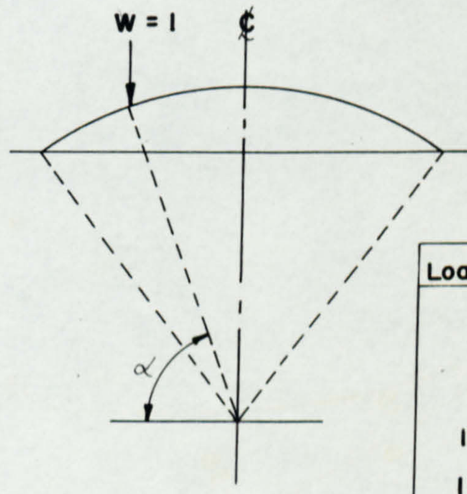

Load pt.	α (rads.)
1	·9657
5	1·0990
9	1·2324
13	1·3657
17	1·4990

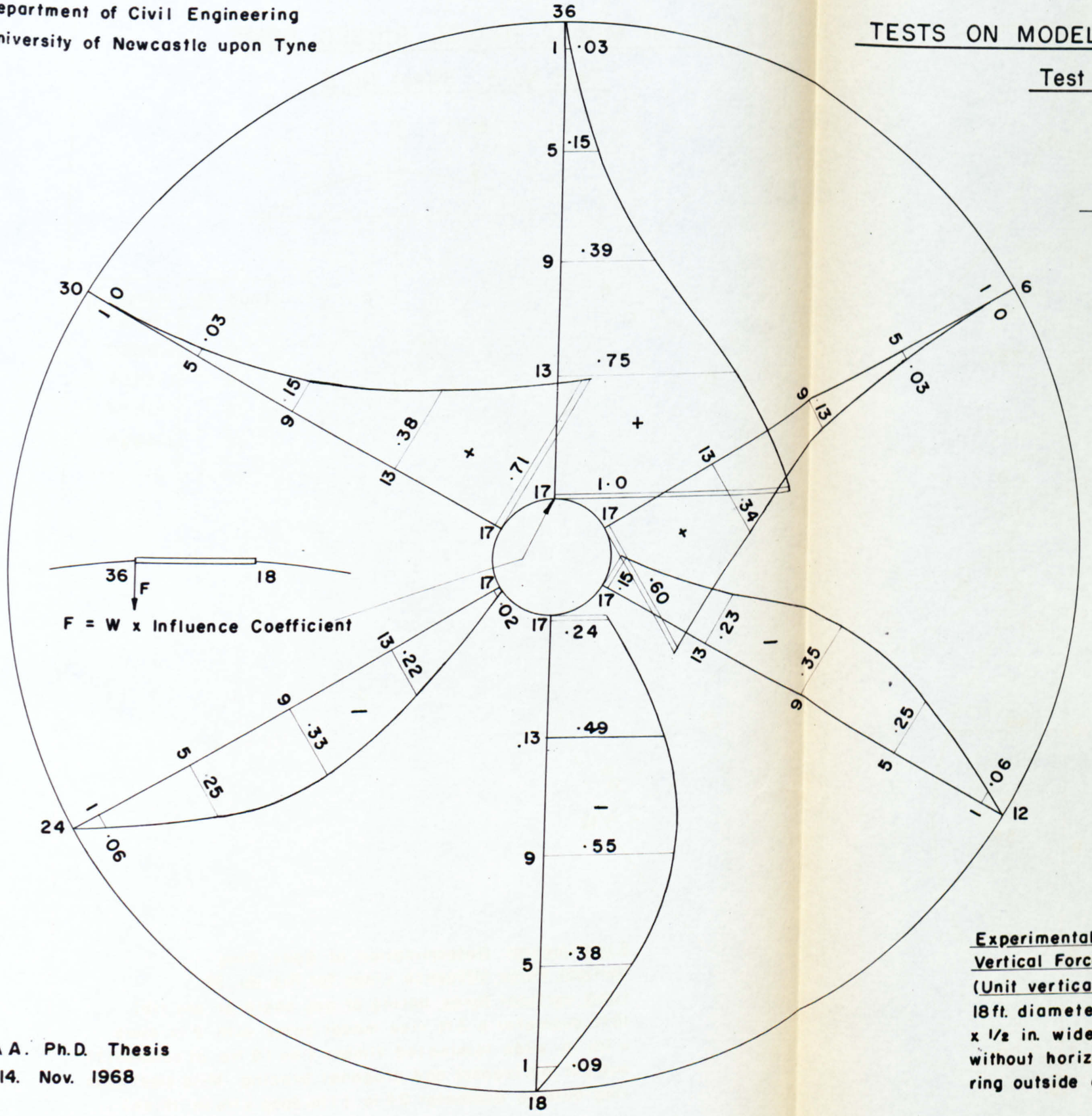

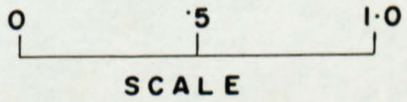

F. A. A. Ph.D. Thesis
14. Nov. 1968

Experimental Determination of Apex Ring Vertical Force Influence Lines for Rib No. 36
(Unit vertical force acting at any angle on any rib)
18 ft. diameter x 3 ft. rise model dome with 2 in. deep x 1/2 in. wide laminated timber ribs (6 No. of constant I) without horizontal and diagonal bracing. Mild steel apex ring outside diameter 24 in. (1 in. deep x 1/8 in. thick)

TESTS ON MODEL RADIAL RIBBED DOME

TEST No. 4 TABLE No. 1

Experimental Determination of Apex Ring Radial Force Influence Coefficients

Load at point = 20lb

For position of load points, rib layout, details of model dome and graphs of tabulated results, see Test No. 4 Sheet Nos. 1 & 2.

Radial Displacement of Apex Ring at Rib No. 36 (Outwards from centre of ring)	Dial gauge readings (A) and actual vertical displacement of point load (B; +ve upwards) in inches																			
	Rib No. 36										Rib.No. 6									
	Point 1		Point 5		Point 9		Point 13		Point 17		Point 1		Point 5		Point 9		Point 13		Point 17	
	A	B	A	B	A	B	A	B	A	B	A	B	A	B	A	B	A	B	A	B
0 in.	.453	.000	.086	.000	.109	.000	.174	.000	.285	.000	.457	.000	.099	.000	.123	.000	.140	.000	.172	.000
.01 in.	.456	+.003	.097	+.011	.126	+.017	.190	+.016	.290	+.005	.457	.000	.099	.000	.124	+.001	.141	+.001	.175	+.003
.02 in.	.458	+.005	.108	+.022	.142	+.033	.205	+.031	.298	+.013	.457	.000	.099	.000	.125	+.002	.143	+.003	.177	+.005
.03 in.	.461	+.008	.118	+.032	.158	+.049	.220	+.046	.306	+.021	.457	.000	.099	.000	.125	+.002	.144	+.004	.180	+.008
.04 in	.464	+.011	.130	+.044	.177	+.068	.237	+.063	.313	+.028	.457	.000	.100	+.001	.126	+.003	.146	+.006	.182	+.010
.05 in.	.466	+.013	.142	+.056	.193	+.084	.254	+.080	.320	+.035	.457	.000	.100	+.001	.127	+.004	.147	+.007	.184	+.012
.06 in.	.469	+.016	.154	+.068	.210	+.101	.269	+.095	.327	+.042	.457	.000	.100	+.001	.128	+.005	.149	+.009	.187	+.015
.07 in.	.472	+.019	.164	+.078	.229	+.120	.285	+.111	.336	+.051	.458	+.001	.101	+.002	.129	+.006	.151	+.011	.189	+.017
.08 in.	.475	+.022	.176	+.090	.245	+.136	.299	+.125	.343	+.058	.458	+.001	.101	+.002	.130	+.007	.153	+.013	.192	+.020
.09 in.	.477	+.024	.187	+.101	.260	+.151	.314	+.140	.350	+.065	.458	+.001	.102	+.003	.131	+.008	.155	+.015	.195	+.023
.10 in.	.480	+.027	.198	+.112	.277	+.168	.330	+.156	.359	+.074	.458	+.001	.102	+.003	.132	+.009	.157	+.017	.197	+.025

F.A.A. Ph.D. Thesis
4th - 5th Dec., 1963

Structural Engineering Division,
Department of Civil Engineering,
University of Newcastle upon Tyne.

TESTS ON MODEL RADIAL RIBBED DOME

TEST No. 4 TABLE No. 2

Experimental Determination of Apex Ring Radial Force Influence Coefficients

Load at point = 20lb

For position of load points, rib layout, details of model dome and graphs of tabulated results, see Test No. 4 Sheet Nos. 3 & 4.

Radial Displacement of Apex Ring at Rib No. 36 (Outwards from centre of ring)	Dial gauge readings (A) and actual vertical displacement of point load (B; +ve upwards) in inches																			
	Rib No. 12										Rib No. 18									
	Point 1		Point 5		Point 9		Point 13		Point 17		Point 1		Point 5		Point 9		Point 13		Point 17	
	A	B	A	B	A	B	A	B	A	B	A	B	A	B	A	B	A	B	A	B
0 in.	.456	.000	.062	.000	.082	.000	.152	.000	.273	.000	.454	.000	.069	.000	.102	.000	.187	.000	.305	.000
.01 in.	.455	-.001	.058	-.004	.076	-.006	.145	-.007	.270	-.003	.453	-.001	.065	-.004	.095	-.007	.179	-.008	.298	-.007
.02 in.	.454	-.002	.054	-.008	.070	-.012	.139	-.013	.265	-.008	.452	-.002	.060	-.009	.088	-.014	.172	-.015	.292	-.013
.03 in.	.453	-.003	.049	-.013	.064	-.018	.133	-.019	.261	-.012	.451	-.003	.056	-.013	.081	-.021	.165	-.022	.284	-.021
.04 in.	.452	-.004	.045	-.017	.058	-.024	.127	-.025	.256	-.017	.450	-.004	.052	-.017	.075	-.027	.157	-.030	.278	-.027
.05 in.	.451	-.005	.041	-.021	.052	-.030	.121	-.031	.251	-.022	.449	-.005	.048	-.021	.069	-.033	.150	-.037	.272	-.033
.06 in.	.450	-.006	.036	-.026	.045	-.037	.115	-.037	.247	-.026	.448	-.006	.043	-.026	.062	-.040	.142	-.045	.266	-.039
.07 in.	.449	-.007	.032	-.030	.040	-.042	.109	-.043	.242	-.031	.447	-.007	.039	-.030	.056	-.046	.134	-.053	.260	-.045
.08 in.	.449	-.007	.028	-.034	.034	-.048	.103	-.049	.238	-.035	.446	-.008	.034	-.035	.049	-.053	.127	-.060	.253	-.052
.09 in.	.448	-.008	.025	-.037	.028	-.054	.097	-.055	.234	-.039	.445	-.009	.030	-.039	.043	-.059	.119	-.068	.246	-.059
.10 in.	.447	-.009	.021	-.041	.023	-.059	.092	-.060	.229	-.044	.444	-.010	.026	-.043	.037	-.065	.112	-.075	.240	-.065

F.A.A. Ph.D. Thesis
4th - 5th Dec., 1963

Structural Engineering Division,
Department of Civil Engineering,
University of Newcastle upon Tyne.

TESTS ON MODEL RADIAL RIBBED DOME

TEST No. 4 TABLE No. 3

Experimental Determination of Apex Ring Radial Force Influence Coefficients

Load at point = 20lb

For position of load points, rib layout, details of model dome and graphs of tabulated results, see Test No. 4 Sheet Nos. 2 & 3.

Radial Displacement of Apex Ring at Rib No. 36 (Outwards from centre of ring)	Dial gauge readings (A) and actual vertical displacement of point load (B; +ve upwards) in inches																			
	Rib No. 24										Rib No. 30									
	Point 1		Point 5		Point 9		Point 13		Point 17		Point 1		Point 5		Point 9		Point 13		Point 17	
	A	B	A	B	A	B	A	B	A	B	A	B	A	B	A	B	A	B	A	B
0 in.	.460	.000	.091	.000	.104	.000	.133	.000	.260	.000	.455	.000	.068	.000	.082	.000	.115	.000	.215	.000
.01 in.	.459	-.001	.087	-.004	.098	-.006	.126	-.007	.256	-.004	.455	.000	.068	.000	.082	.000	.117	+.002	.217	+.002
.02 in.	.458	-.002	.083	-.008	.092	-.012	.120	-.013	.252	-.008	.455	.000	.069	+.001	.083	+.001	.119	+.004	.219	+.004
.03 in.	.457	-.003	.079	-.012	.086	-.018	.115	-.018	.248	-.012	.455	.000	.069	+.001	.084	+.002	.121	+.006	.222	+.007
.04 in.	.457	-.003	.075	-.016	.080	-.024	.110	-.023	.245	-.015	.456	+.001	.069	+.001	.085	+.003	.122	+.007	.224	+.009
.05 in.	.456	-.004	.071	-.020	.075	-.029	.105	-.028	.241	-.019	.456	+.001	.070	+.002	.086	+.004	.124	+.009	.226	+.011
.06 in.	.455	-.005	.067	-.024	.069	-.035	.098	-.035	.238	-.022	.456	+.001	.071	+.003	.087	+.005	.126	+.011	.228	+.013
.07 in.	.454	-.006	.064	-.027	.063	-.041	.093	-.040	.235	-.025	.456	+.001	.071	+.003	.089	+.007	.128	+.013	.231	+.016
.08 in.	.453	-.007	.059	-.032	.057	-.047	.088	-.045	.231	-.029	.456	+.001	.072	+.004	.090	+.008	.130	+.015	.233	+.018
.09 in.	.453	-.007	.056	-.035	.052	-.052	.082	-.051	.227	-.033	.457	+.002	.073	+.005	.091	+.009	.132	+.017	.236	+.021
.10 in.	.452	-.008	.052	-.039	.047	-.057	.076	-.057	.224	-.036	.457	+.002	.073	+.005	.092	+.010	.134	+.019	.239	+.024

F.A.A. Ph.D. Thesis
4th - 5th Dec., 1963

Structural Engineering Division,
Department of Civil Engineering,
University of Newcastle upon Tyne.

TESTS ON MODEL RADIAL RIBBED DOME

Test No. 4

Sheet No. 1.

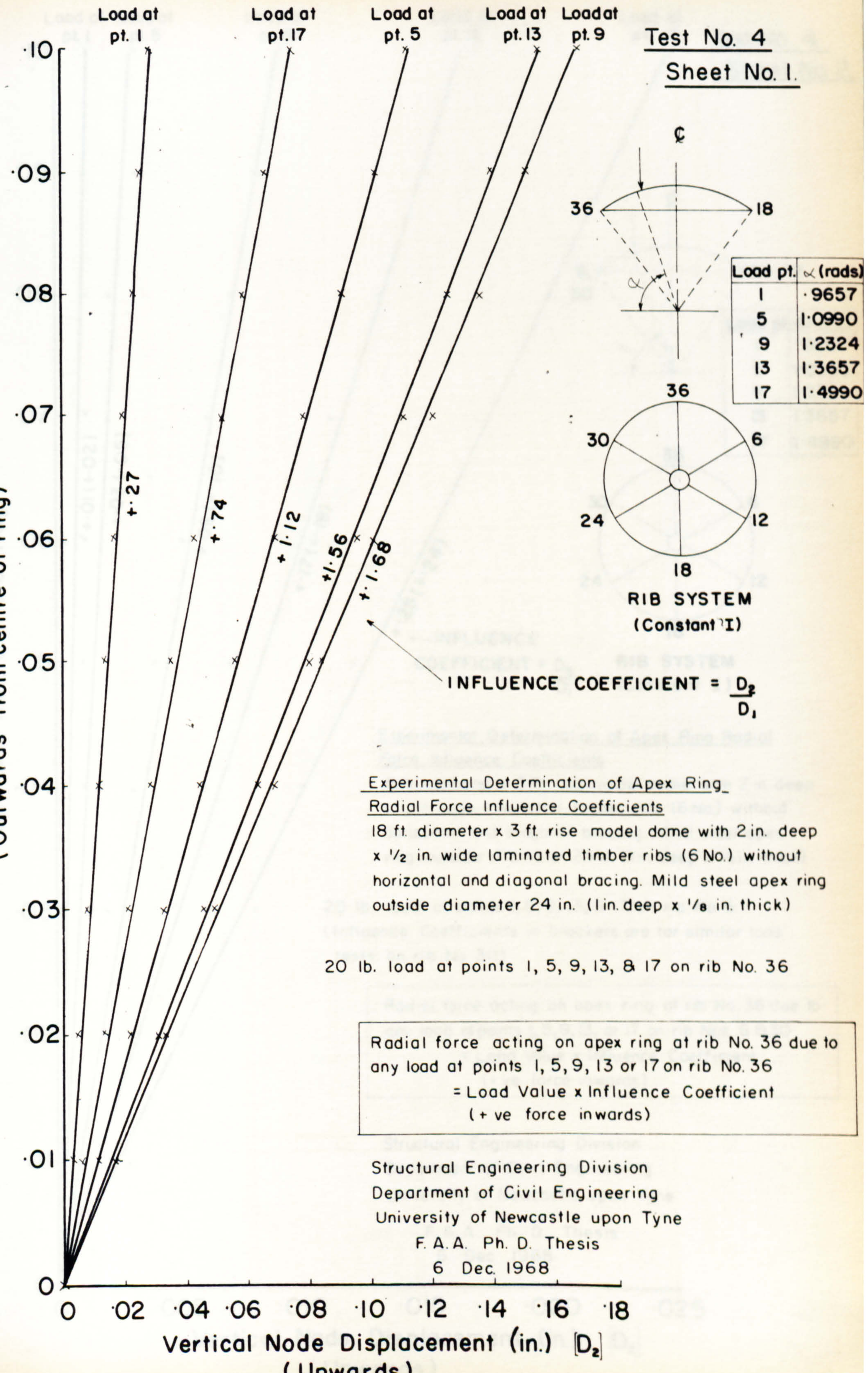

Load pt.	α (rads)
1	·9657
5	1·0990
9	1·2324
13	1·3657
17	1·4990

RIB SYSTEM
(Constant I)

INFLUENCE COEFFICIENT = $\frac{D_2}{D_1}$

Experimental Determination of Apex Ring Radial Force Influence Coefficients

18 ft. diameter x 3 ft. rise model dome with 2 in. deep x ½ in. wide laminated timber ribs (6 No.) without horizontal and diagonal bracing. Mild steel apex ring outside diameter 24 in. (1 in. deep x ⅛ in. thick)

20 lb. load at points 1, 5, 9, 13, & 17 on rib No. 36

Radial force acting on apex ring at rib No. 36 due to any load at points 1, 5, 9, 13 or 17 on rib No. 36
= Load Value x Influence Coefficient
(+ ve force inwards)

Structural Engineering Division
Department of Civil Engineering
University of Newcastle upon Tyne
F. A. A. Ph. D. Thesis
6 Dec. 1968

TESTS ON MODEL RADIAL RIBBED DOME

Test No. 4.
Sheet No. 2.

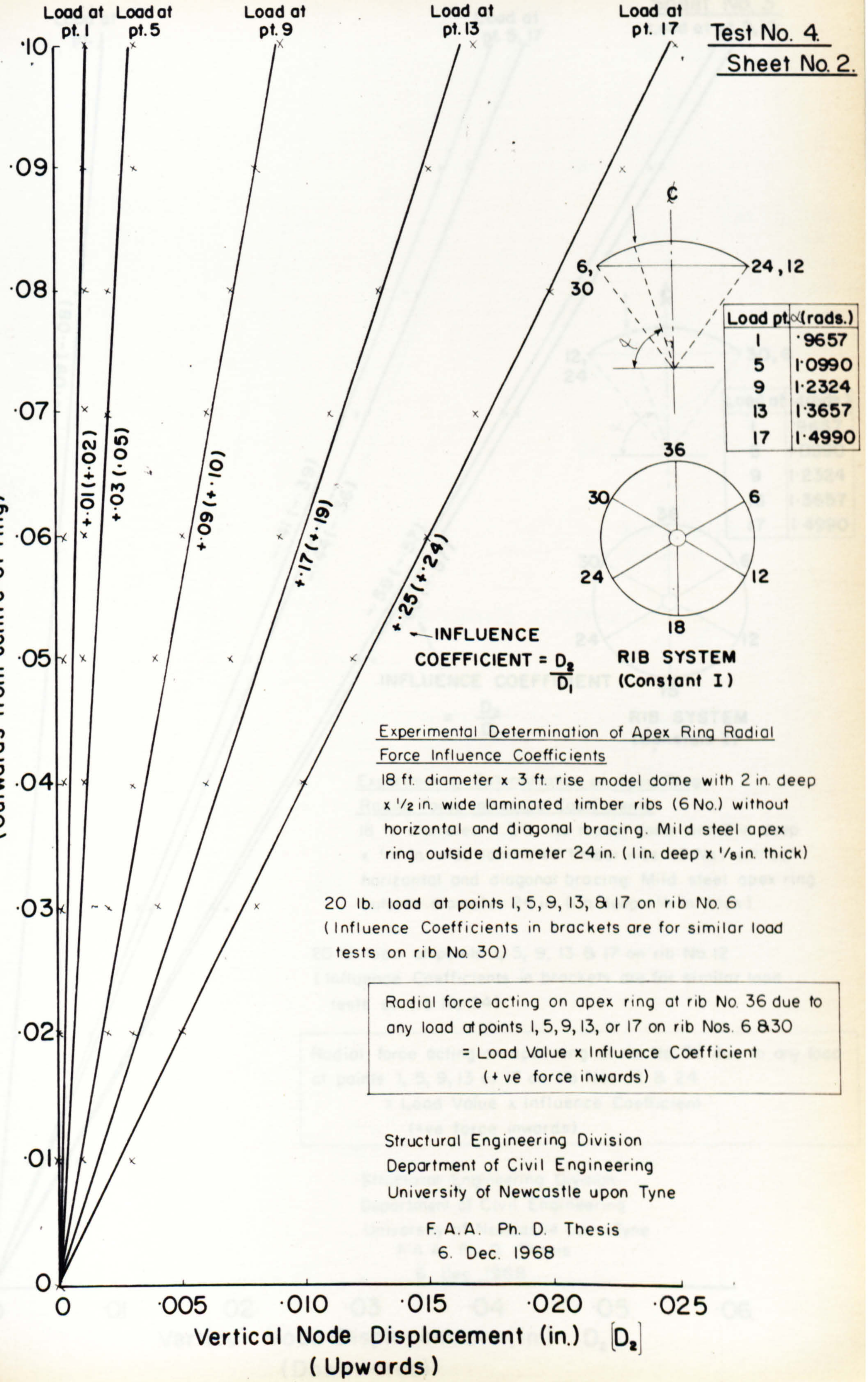

Load pt.	α (rads.)
1	·9657
5	1·0990
9	1·2324
13	1·3657
17	1·4990

RIB SYSTEM
(Constant I)

← INFLUENCE COEFFICIENT = $\frac{D_2}{D_1}$

Experimental Determination of Apex Ring Radial Force Influence Coefficients

18 ft. diameter x 3 ft. rise model dome with 2 in. deep x ½ in. wide laminated timber ribs (6 No.) without horizontal and diagonal bracing. Mild steel apex ring outside diameter 24 in. (1 in. deep x ⅛ in. thick)

20 lb. load at points 1, 5, 9, 13, & 17 on rib No. 6
(Influence Coefficients in brackets are for similar load tests on rib No. 30)

Radial force acting on apex ring at rib No. 36 due to any load at points 1, 5, 9, 13, or 17 on rib Nos. 6 & 30
= Load Value x Influence Coefficient
(+ ve force inwards)

Structural Engineering Division
Department of Civil Engineering
University of Newcastle upon Tyne

F. A. A. Ph. D. Thesis
6. Dec. 1968

TESTS ON MODEL RADIAL RIBBED DOME

Test No. 4
Sheet No. 3

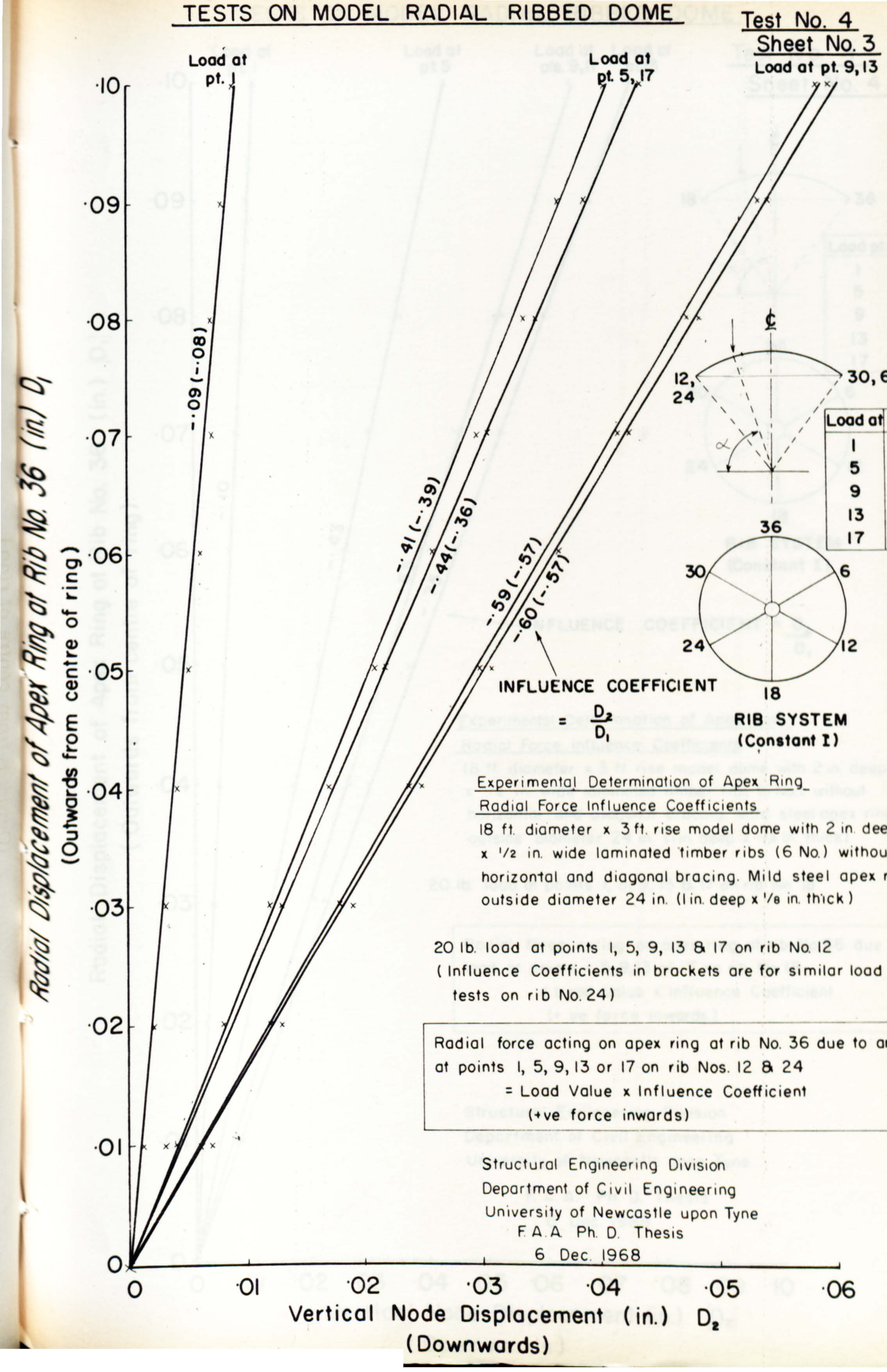

Load at	α (rads.)
1	·9657
5	1·0990
9	1·2324
13	1·3657
17	1·4990

Experimental Determination of Apex Ring Radial Force Influence Coefficients

18 ft. diameter x 3 ft. rise model dome with 2 in. deep x ½ in. wide laminated timber ribs (6 No.) without horizontal and diagonal bracing. Mild steel apex ring outside diameter 24 in. (1 in. deep x ⅛ in. thick)

20 lb. load at points 1, 5, 9, 13 & 17 on rib No. 12
(Influence Coefficients in brackets are for similar load tests on rib No. 24)

Radial force acting on apex ring at rib No. 36 due to any load at points 1, 5, 9, 13 or 17 on rib Nos. 12 & 24
= Load Value x Influence Coefficient
(+ve force inwards)

Structural Engineering Division
Department of Civil Engineering
University of Newcastle upon Tyne
F.A.A. Ph. D. Thesis
6 Dec. 1968

TESTS ON MODEL RADIAL RIBBED DOME

Test No. 4.

Sheet No. 4

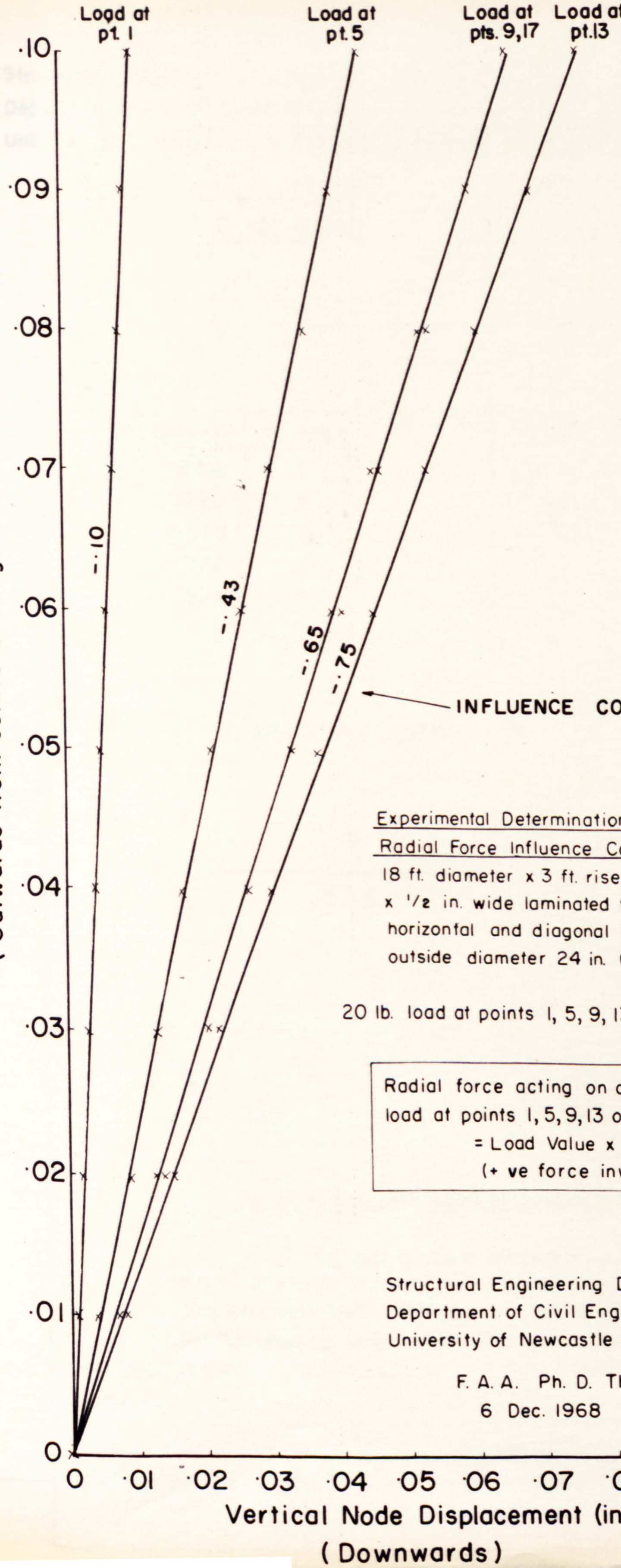

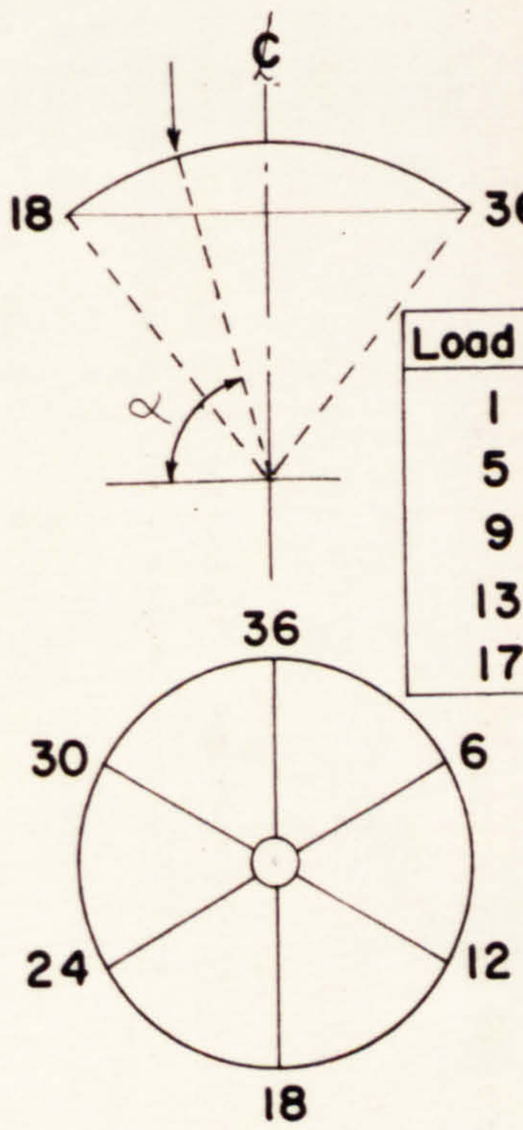

Load pt.	α (rads.)
1	·9657
5	1·0990
9	1·2324
13	1·3657
17	1·4990

RIB SYSTEM
(Constant I)

INFLUENCE COEFFICIENT = $\frac{D_2}{D_1}$

Experimental Determination of Apex Ring
Radial Force Influence Coefficients

18 ft. diameter x 3 ft. rise model dome with 2 in. deep x ½ in. wide laminated timber ribs (6 No.) without horizontal and diagonal bracing. Mild steel apex ring outside diameter 24 in. (1 in. deep x ⅛ in. thick)

20 lb. load at points 1, 5, 9, 13 & 17 on rib No. 18

Radial force acting on apex ring at rib No. 36 due to any load at points 1, 5, 9, 13 or 17 on rib No. 18
= Load Value x Influence Coefficient
(+ ve force inwards)

Structural Engineering Division
Department of Civil Engineering
University of Newcastle upon Tyne

F. A. A. Ph. D. Thesis
6 Dec. 1968

Structural Engineering Division
Department of Civil Engineering
University of Newcastle upon Tyne

TESTS ON MODEL RADIAL RIBBED DOME

Test No. 4

Sheet No. 5

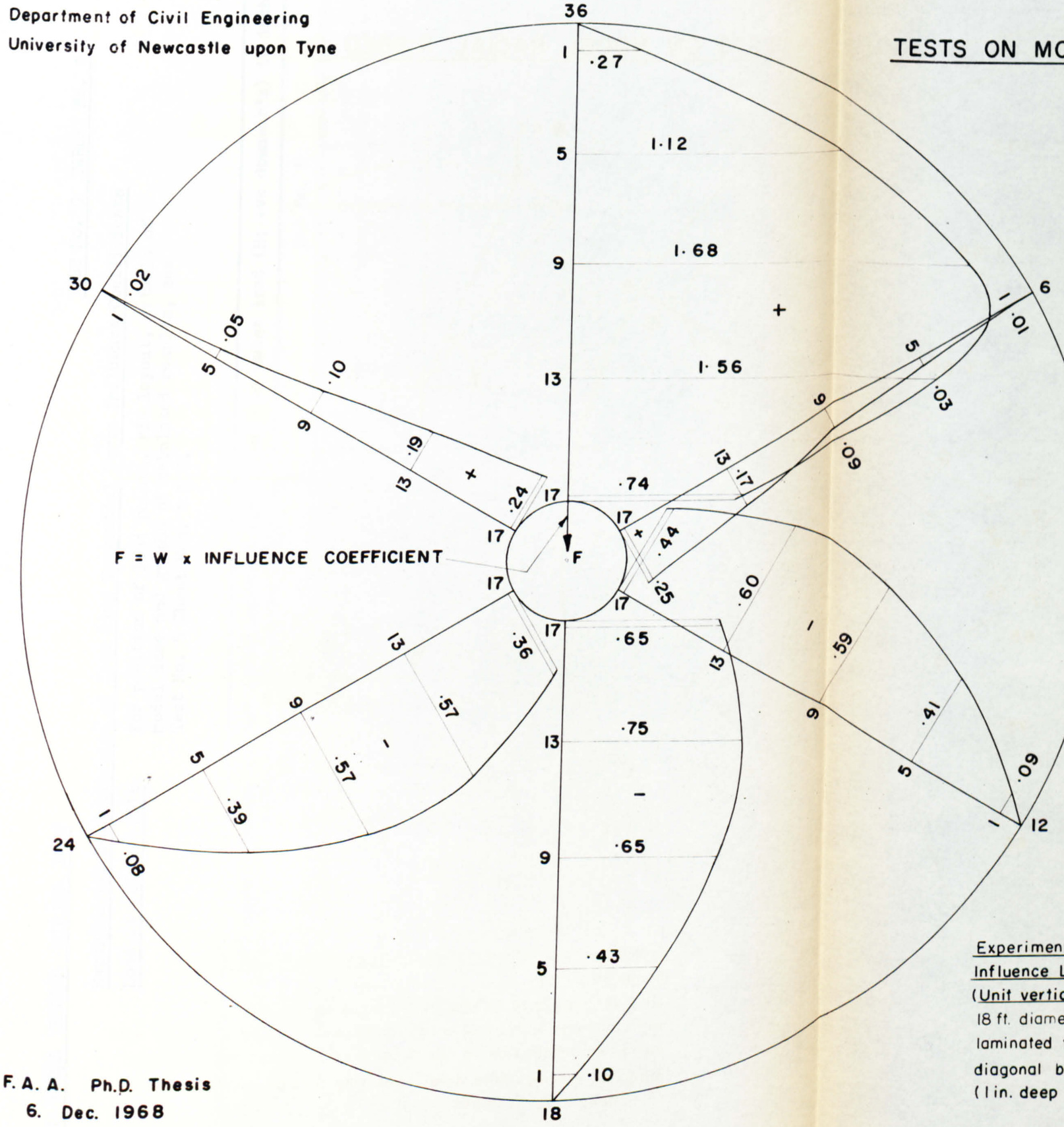

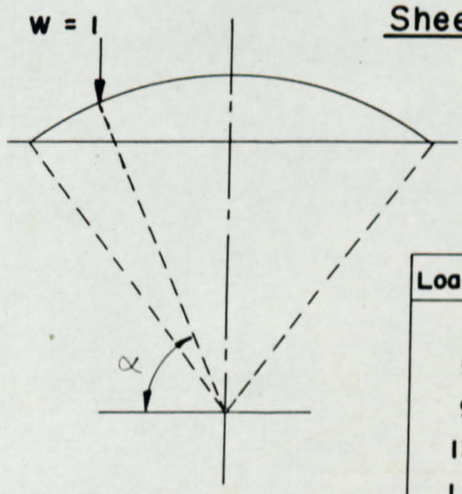

Load pt.	∝ (rads.)
1	·9657
5	1·0990
9	1·2324
13	1·3657
17	1·4990

0 ·5 1·0

SCALE

Experimental Determination of Apex Ring Radial Force Influence Lines.

(Unit vertical force acting at any angle on any rib)

18 ft. diameter x 3 ft. rise model dome with 2 in. deep x ½ in. wide laminated timber ribs (6 No. of constant I) without horizontal and diagonal bracing. Mild steel apex ring outside diameter 24 in. (1 in. deep x ⅛ in. thick)

F. A. A. Ph.D. Thesis
6. Dec. 1968

TESTS ON MODEL RADIAL RIBBED DOME

TEST No. 5 TABLE No. 1

Experimental Determination of Apex Ring Tangential Force Influence Coefficients

Load at point = 20lb

For position of load points, rib layout, details of model dome and graphs of tabulated results, see Test No. 5 Sheet Nos. 1 & 2.

Tangential Displacement of Apex Ring at Rib No.36 (Anti-clockwise viewed from above)	Dial gauge readings (A) and actual vertical displacement of point load (B; +ve downwards) in inches																			
	Rib No. 36										Rib No. 6									
	Point 1		Point 5		Point 9		Point 13		Point 17		Point 1		Point 5		Point 9		Point 13		Point 17	
	A	B	A	B	A	B	A	B	A	B	A	B	A	B	A	B	A	B	A	B
0 in.	.459	.000	.090	.000	.129	.000	.204	.000	.363	.000	.456	.000	.102	.000	.137	.000	.211	.000	.356	.000
.02 in.	.459	.000	.089	+.001	.127	+.002	.203	+.001	.362	+.001	.455	+.001	.097	+.005	.129	+.008	.206	+.005	.352	+.004
.04 in.	.459	.000	.089	+.001	.126	+.003	.201	+.003	.362	+.001	.454	+.002	.093	+.009	.123	+.014	.201	+.010	.349	+.007
.06 in.	.459	.000	.088	+.002	.125	+.004	.200	+.004	.361	+.002	.453	+.003	.088	+.014	.117	+.020	.195	+.016	.346	+.010
.08 in.	.459	.000	.088	+.002	.124	+.005	.199	+.005	.360	+.003	.452	+.004	.084	+.018	.112	+.025	.190	+.021	.342	+.014
.10 in.	.459	.000	.087	+.003	.123	+.006	.198	+.006	.360	+.003	.451	+.005	.080	+.022	.105	+.032	.186	+.025	.338	+.018
.12 in.	.459	.000	.087	+.003	.122	+.007	.196	+.008	.359	+.004	.450	+.006	.075	+.027	.100	+.037	.181	+.030	.334	+.022
.14 in.	.459	.000	.086	+.004	.121	+.008	.195	+.009	.358	+.005	.449	+.007	.070	+.032	.094	+.043	.176	+.035	.328	+.028
.16 in.	.459	.000	.086	+.004	.120	+.009	.193	+.011	.357	+.006	.448	+.008	.065	+.037	.088	+.049	.171	+.041	.324	+.032
.18 in.	.459	.000	.085	+.005	.119	+.010	.191	+.013	.356	+.007	.447	+.009	.061	+.041	.081	+.056	.165	+.046	.320	+.036
.20 in.	.459	.000	.085	+.005	.118	+.011	.190	+.014	.355	+.008	.446	+.010	.057	+.045	.075	+.062	.159	+.052	.314	+.042

F.A.A. Ph.D. Thesis
12th - 13th Dec., 1968

Structural Engineering Division,
Department of Civil Engineering,
University of Newcastle upon Tyne.

TESTS ON MODEL RADIAL RIBBED DOME

TEST No. 5 TABLE No. 2

Experimental Determination of Apex Ring Tangential Force Influence Coefficients

Load at point = 20lb

For position of load points, rib layout, details of model dome and graphs of tabulated results, see Test No. 5 Sheet Nos. 1 & 3.

Tangential Displacement of Apex Ring at Rib No.36 (Anti-clockwise viewed from above)	Dial gauge readings (A) and actual vertical displacement of point load (B; +ve downwards) in inches																			
	Rib No. 12										Rib No. 18									
	Point 1		Point 5		Point 9		Point 13		Point 17		Point 1		Point 5		Point 9		Point 13		Point 17	
	A	B	A	B	A	B	A	B	A	B	A	B	A	B	A	B	A	B	A	B
0 in.	.452	.000	.060	.000	.098	.000	.176	.000	.351	.000	.452	.000	.077	.000	.104	.000	.206	.000	.352	.000
.02 in.	.451	+.001	.056	+.004	.094	+.004	.171	+.005	.348	+.003	.452	.000	.077	.000	.104	.000	.205	+.001	.351	+.001
.04 in.	.451	+.001	.053	+.007	.090	+.008	.167	+.009	.345	+.006	.452	.000	.077	.000	.103	+.001	.204	+.002	.350	+.002
.06 in.	.450	+.002	.050	+.010	.085	+.013	.162	+.014	.341	+.010	.452	.000	.076	+.001	.103	+.001	.203	+.003	.348	+.004
.08 in.	.449	+.003	.046	+.014	.081	+.017	.157	+.019	.338	+.013	.452	.000	.076	+.001	.102	+.002	.202	+.004	.347	+.005
.10 in.	.449	+.003	.043	+.017	.076	+.022	.152	+.024	.335	+.016	.452	.000	.075	+.002	.102	+.002	.201	+.005	.345	+.007
.12 in.	.448	+.004	.040	+.020	.072	+.026	.147	+.029	.331	+.020	.452	.000	.075	+.002	.101	+.003	.200	+.006	.344	+.008
.14 in.	.447	+.005	.036	+.024	.068	+.030	.142	+.034	.327	+.024	.452	.000	.074	+.003	.100	+.004	.198	+.008	.342	+.010
.16 in.	.446	+.006	.033	+.027	.064	+.034	.137	+.039	.323	+.028	.452	.000	.074	+.003	.100	+.004	.196	+.010	.340	+.012
.18 in.	.446	+.006	.030	+.030	.059	+.039	.132	+.044	.319	+.032	.452	.000	.073	+.004	.099	+.005	.194	+.012	.338	+.014
.20 in.	.445	+.007	.026	+.034	.054	+.044	.127	+.049	.315	+.036	.452	.000	.073	+.004	.098	+.006	.192	+.014	.336	+.016

F.A.A. Ph.D. Thesis
12th -13th Dec., 1968

Structural Engineering Division,
Department of Civil Engineering,
University of Newcastle upon Tyne.

TESTS ON MODEL RADIAL RIBBED DOME

TEST No. 5 TABLE No. 3

Experimental Determination of Apex Ring Tangential Force Influence Coefficients

Load at point = 20lb

For position of load points, rib layout, details of model dome and graphs of tabulated results, see Test No. 5 Sheet Nos. 2 & 3

Tangential Displacement of Apex Ring at Rib No.36 (Anti-clockwise viewedfrom above)	Dial gauge readings (A) and actual vertical displacement of point load (B; +ve downwards) in inches																	
	Rib No. 24										Rib No. 30							
	Point 1		Point 5		Point 9		Point 13		Point 17		Point 1		Point 5		Point 9		Point 13		Point 17	
	A	B	A	B	A	B	A	B	A	B	A	B	A	B	A	B	A	B	A	B
0 in.	.454	.000	.098	.000	.132	.000	.190	.000	.279	.000	.453	.000	.076	.000	.113	.000	.180	.000	.219	.000
.02 in.	.455	-.001	.100	-.002	.135	-.003	.193	-.003	.281	-.002	.454	-.001	.080	-.004	.118	-.005	.185	-.005	.221	-.002
.04 in.	.456	-.002	.102	-.004	.138	-.006	.196	-.006	.282	-.003	.455	-.002	.083	-.007	.122	-.009	.189	-.009	.223	-.004
.06 in	.457	-.003	.104	-.006	.140	-.008	.199	-.009	.284	-.005	.456	-.003	.086	-.010	.126	-.013	.192	-.012	.224	-.005
.08 in.	.457	-.003	.106	-.008	.143	-.011	.202	-.012	.287	-.008	.457	-.004	.090	-.014	.130	-.017	.196	-.016	.226	-.007
.10 in.	.458	-.004	.108	-.010	.147	-.015	.205	-.015	.288	-.009	.458	-.005	.092	-.016	.134	-.021	.199	-.019	.228	-.009
.12 in.	.459	-.005	.110	-.012	.150	-.018	.207	-.017	.290	-.011	.459	-.006	.096	-.020	.138	-.025	.203	-.023	.229	-.010
.14 in.	.459	-.005	.112	-.014	.153	-.021	.210	-.020	.291	-.012	.460	-.007	.099	-.023	.141	-.028	.206	-.026	.231	-.012
.16 in.	.460	-.006	.114	-.016	.156	-.024	.212	-.022	.293	-.014	.461	-.008	.102	-.026	.145	-.032	.209	-.029	.232	-.013
.18 in.	.460	-.006	.116	-.018	.159	-.027	.215	-.025	.294	-.015	.462	-.009	.105	-.029	.148	-.035	.212	-.032	.233	-.014
.20 in.	.461	-.007	.118	-.020	.162	-.030	.217	-.027	.296	-.017	.463	-.010	.107	-.031	.152	-.039	.215	-.035	.235	-.016

F. A. A. Ph.D. Thesis
12th - 13th Dec., 1968

Structural Engineering Division,
Department of Civil Engineering,
University of Newcastle upon Tyne.

TESTS ON MODEL RADIAL RIBBED DOME

Test No. 5

Sheet No. 1.

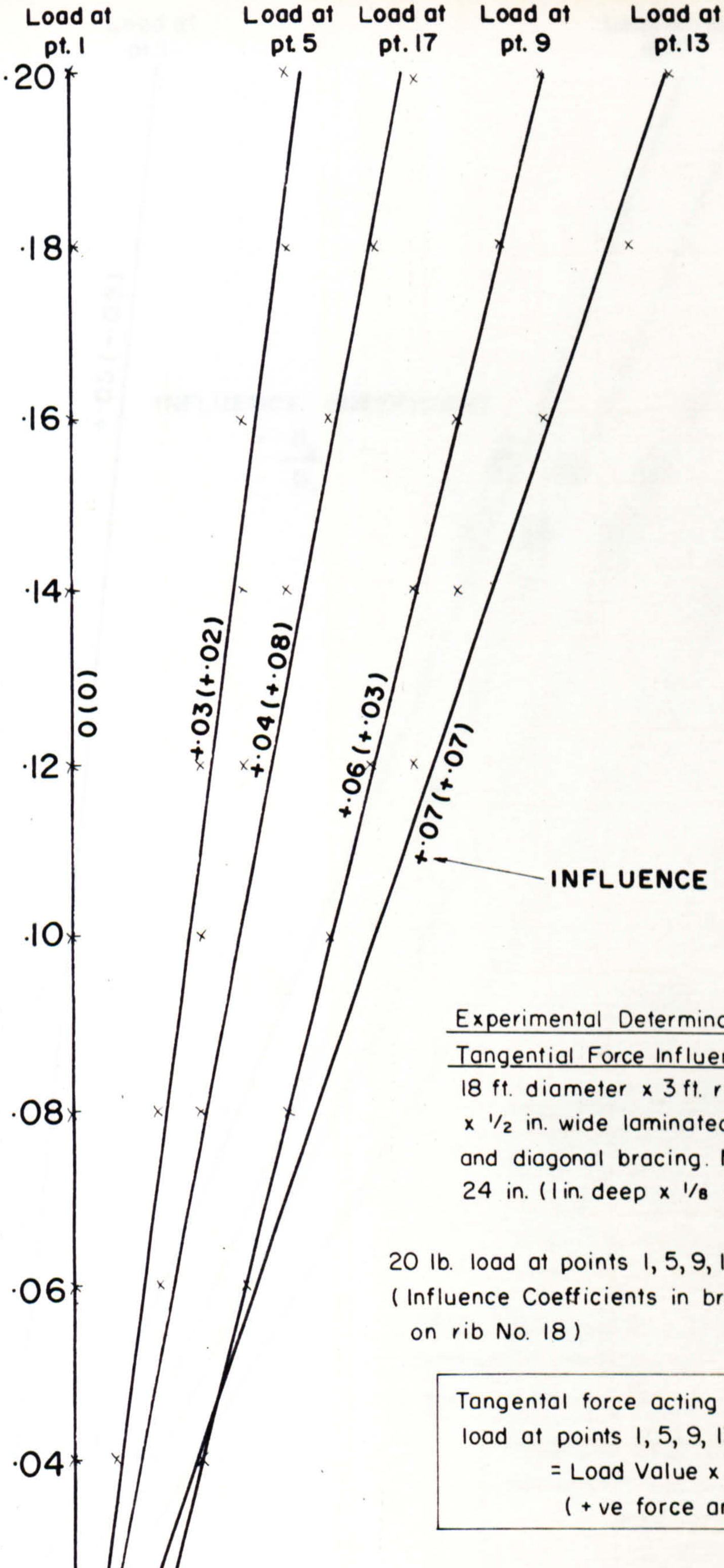

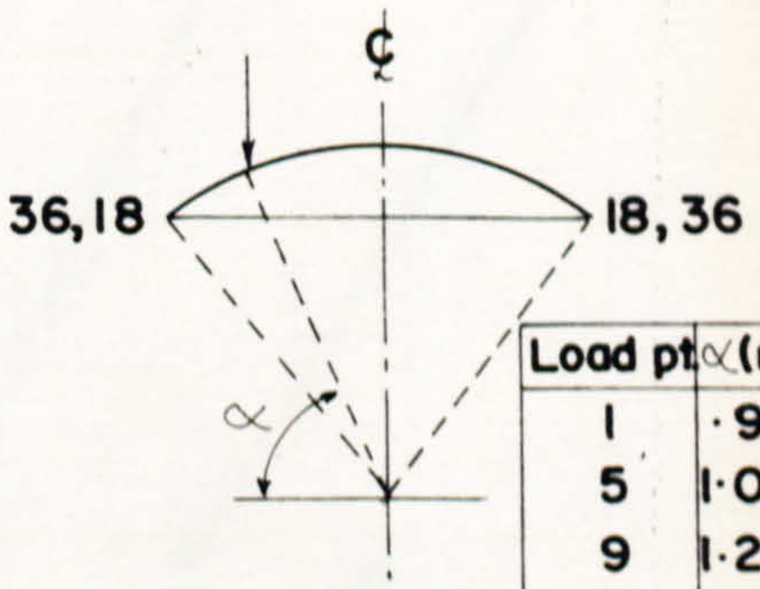

Load pt	α (rads.)
1	·9657
5	1·0990
9	1·2324
13	1·3657
17	1·4990

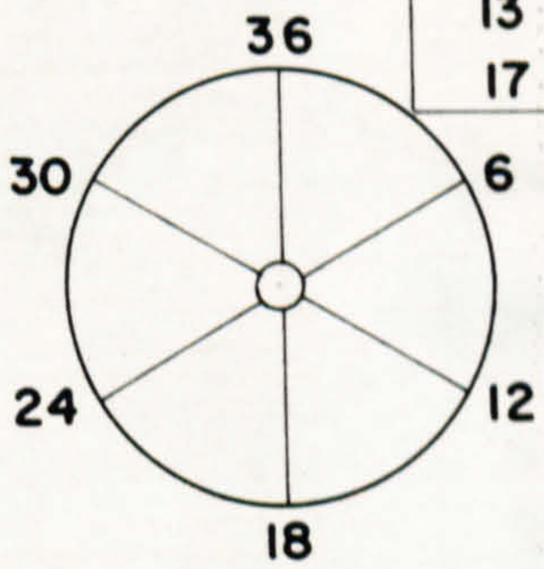

RIB SYSTEM
(Constant I)

INFLUENCE COEFFICIENT = $\frac{D_2}{D_1}$

Experimental Determination of Apex Ring
Tangential Force Influence Coefficients

18 ft. diameter x 3 ft. rise model dome with 2 in. deep x ½ in. wide laminated timber ribs (6 No.) without horizontal and diagonal bracing. Mild steel apex ring outside diameter 24 in. (1 in. deep x ⅛ in. thick)

20 lb. load at points 1, 5, 9, 13 & 17 on rib No. 36
(Influence Coefficients in brackets are for similar load tests on rib No. 18)

Tangental force acting on apex ring at rib No. 36 due to any load at points 1, 5, 9, 13 or 17 on rib Nos. 36 & 18
= Load Value x Influence Coefficient
(+ ve force anti-clockwise viewed from above)

Structural Engineering Division
Department of Civil Engineering
University of Newcastle upon Tyne

F. A. A. Ph. D. Thesis
16 Dec. 1968

TESTS ON MODEL RADIAL RIBBED DOME

Test No. 5
Sheet No. 2

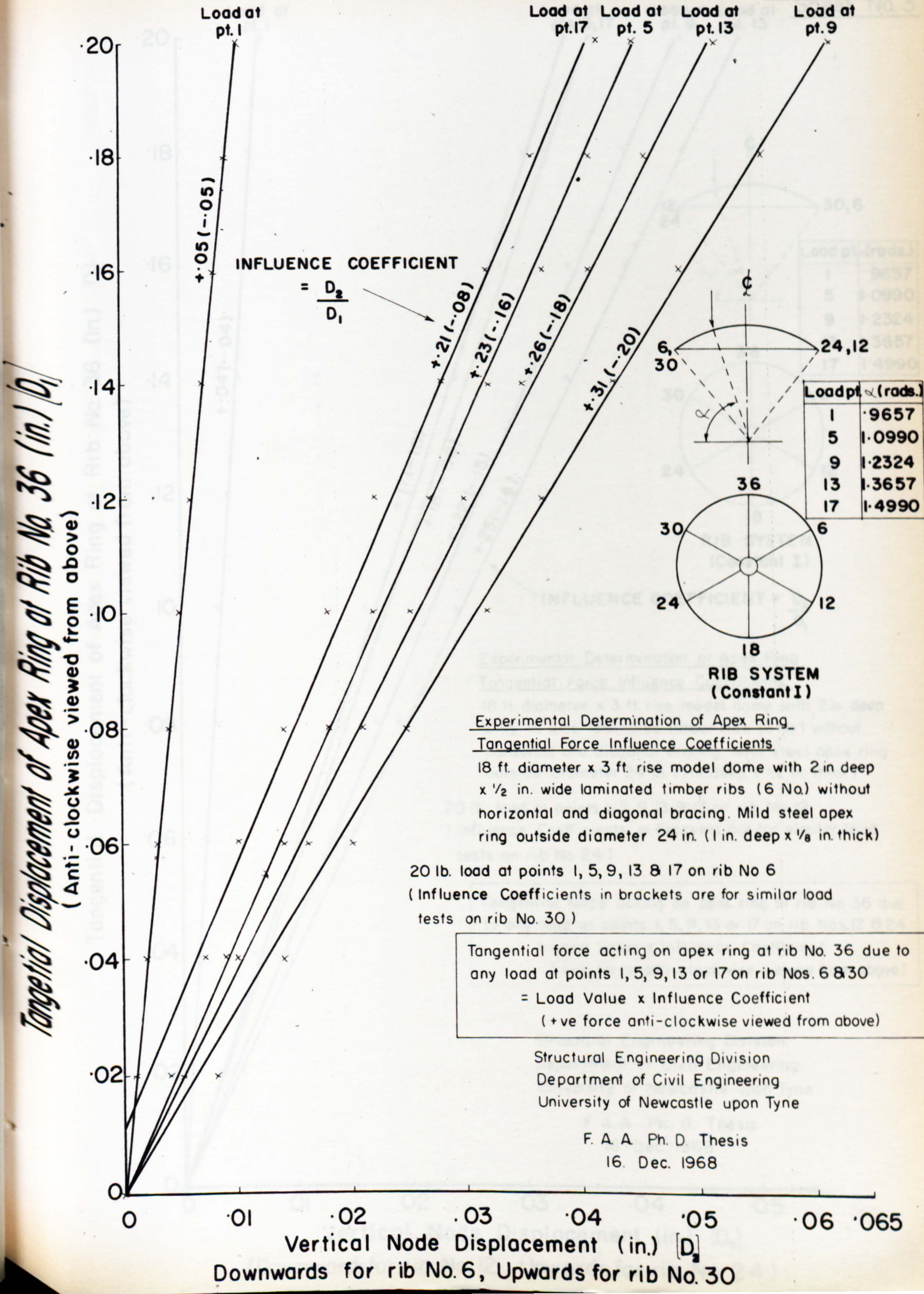

Load pt.	α (rads.)
1	·9657
5	1·0990
9	1·2324
13	1·3657
17	1·4990

Experimental Determination of Apex Ring Tangential Force Influence Coefficients

18 ft. diameter x 3 ft. rise model dome with 2 in deep x ½ in. wide laminated timber ribs (6 No.) without horizontal and diagonal bracing. Mild steel apex ring outside diameter 24 in. (1 in. deep x ⅛ in. thick)

20 lb. load at points 1, 5, 9, 13 & 17 on rib No 6
(Influence Coefficients in brackets are for similar load tests on rib No. 30)

Tangential force acting on apex ring at rib No. 36 due to any load at points 1, 5, 9, 13 or 17 on rib Nos. 6 & 30
= Load Value x Influence Coefficient
(+ve force anti-clockwise viewed from above)

Structural Engineering Division
Department of Civil Engineering
University of Newcastle upon Tyne

F. A. A. Ph. D. Thesis
16. Dec. 1968

TESTS ON MODEL RADIAL RIBBED DOME

Test No. 5
Sheet No. 3

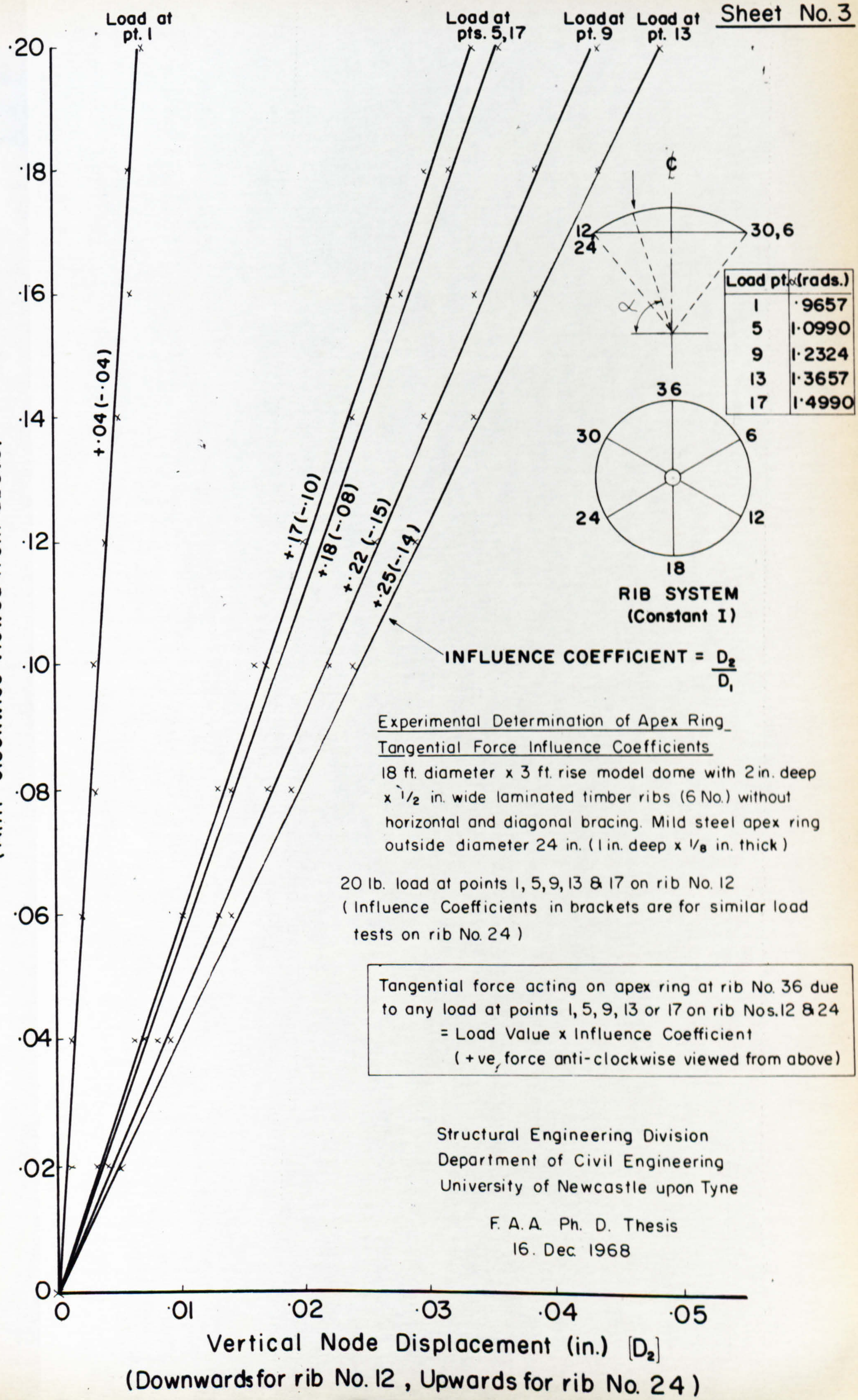

Load pt.	α (rads.)
1	·9657
5	1·0990
9	1·2324
13	1·3657
17	1·4990

RIB SYSTEM
(Constant I)

INFLUENCE COEFFICIENT = $\frac{D_2}{D_1}$

Experimental Determination of Apex Ring
Tangential Force Influence Coefficients

18 ft. diameter x 3 ft. rise model dome with 2 in. deep x 1/2 in. wide laminated timber ribs (6 No.) without horizontal and diagonal bracing. Mild steel apex ring outside diameter 24 in. (1 in. deep x 1/8 in. thick)

20 lb. load at points 1, 5, 9, 13 & 17 on rib No. 12
(Influence Coefficients in brackets are for similar load tests on rib No. 24)

Tangential force acting on apex ring at rib No. 36 due to any load at points 1, 5, 9, 13 or 17 on rib Nos. 12 & 24
= Load Value x Influence Coefficient
(+ve force anti-clockwise viewed from above)

Structural Engineering Division
Department of Civil Engineering
University of Newcastle upon Tyne

F. A. A. Ph. D. Thesis
16. Dec. 1968

Structural Engineering Division
Department of Civil Engineering
University of Newcastle upon Tyne

TESTS ON MODEL RADIAL RIBBED DOME

Test No. 5

Sheet No. 4

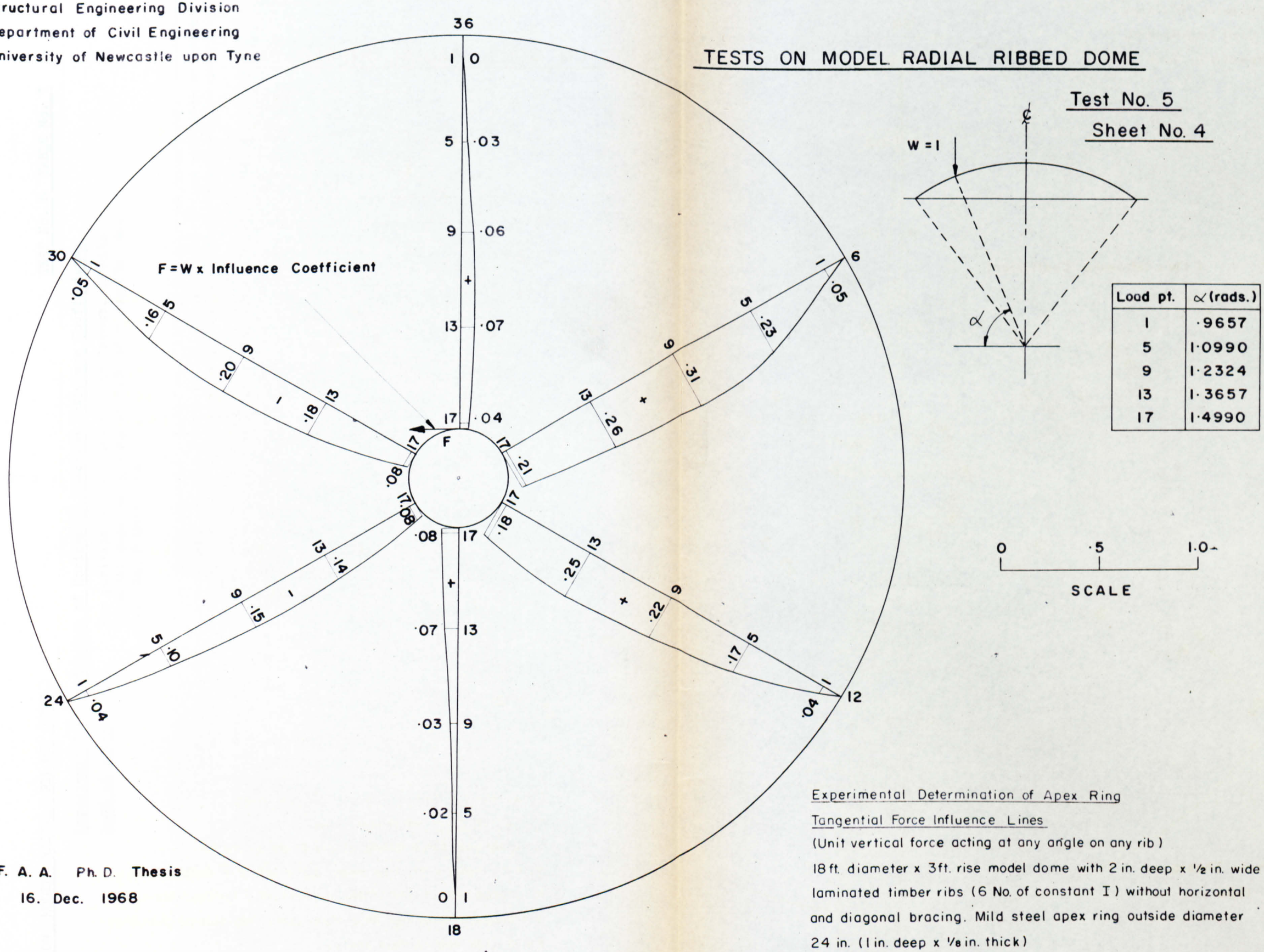

Load pt.	∝ (rads.)
1	·9657
5	1·0990
9	1·2324
13	1·3657
17	1·4990

0 ·5 1.0

SCALE

Experimental Determination of Apex Ring

Tangential Force Influence Lines

(Unit vertical force acting at any angle on any rib)

18 ft. diameter x 3ft. rise model dome with 2 in. deep x ½ in. wide laminated timber ribs (6 No. of constant I) without horizontal and diagonal bracing. Mild steel apex ring outside diameter 24 in. (1 in. deep x ⅛ in. thick)

F. A. A. Ph. D. Thesis

16. Dec. 1968

TESTS ON MODEL RADIAL RIBBED DOME

TEST No. 6 TABLE No. 1

Experimental Determination of Horizontal Reaction Influence Coefficients

Load at point = 20lb

For position of load points, rib layout, details of model dome and graphs of tabulated results, see Test No. 6 Sheet Nos. 1 & 2

Horizontal Base Displacement at Rib No. 36 (Towards centre of dome)	Dial gauge readings (A) and actual vertical displacement of point load (B; +ve upwards) in inches																			
	Rib No. 36										Rib No. 6									
	Point 1		Point 5		Point 9		Point 13		Point 17		Point 1		Point 5		Point 9		Point 13		Point 17	
	A	B	A	B	A	B	A	B	A	B	A	B	A	B	A	B	A	B	A	B
0 in.	.445	.000	.327	.000	.148	.000	.029	.000	.153	.000	.441	.000	.259	.000	.046	.000	.255	.000	.132	.000
.1 in.	.450	+.005	.357	+.030	.197	+.049	.086	+.057	.202	+.049	.439	-.002	.253	-.006	.046	.000	.266	+.011	.175	+.043
.2 in.	.455	+.010	.387	+.060	.246	+.098	.142	+.113	.250	+.097	.437	-.004	.246	-.013	.046	.000	.280	+.025	.214	+.082
.3 in.	.460	+.015	.412	+.085	.290	+.142	.192	+.163	.291	+.138	.434	-.007	.240	-.019	.045	-.001	.291	+.036	.251	+.119
.4 in.	.465	+.020	.439	+.112	.333	+.185	.243	+.214	.334	+.181	.432	-.009	.234	-.025	.045	-.001	.301	+.046	.288	+.156
.5 in.	.470	+.025	.466	+.139	.375	+.227	.293	+.264	.376	+.223	.430	-.011	.227	-.032	.044	-.002	.311	+.056	.322	+.190
.6 in.	.475	+.030	.493	+.166	.419	+.271	.343	+.314	.418	+.265	.428	-.013	.221	-.038	.043	-.003	.320	+.065	.357	+.225
.7 in.	.481	+.036	.519	+.192	.464	+.316	.393	+.364	.457	+.304	.426	-.015	.214	-.045	.042	-.004	.331	+.076	.391	+.259
.8 in.	.486	+.041	.547	+.220	.511	+.363	.446	+.417	.501	+.348	.424	-.017	.207	-.052	.040	-.006	.341	+.086	.428	+.296
.9 in.	.492	+.047	.574	+.247	.554	+.406	.496	+.467	.546	+.393	.422	-.019	.200	-.059	.039	-.007	.350	+.095	.461	+.329
1.0 in.	.497	+.052	.600	+.273	.595	+.447	.544	+.515	.583	+.430	.420	-.021	.194	-.065	.037	-.009	.358	+.103	.493	+.361

F. A. A. Ph.D. Thesis
30th Dec., 1968

Structural Engineering Division
Department of Civil Engineering,
University of Newcastle upon Tyne.

TESTS ON MODEL RADIAL RIBBED DOME

TEST No. 6 TABLE No. 2

Experimental Determination of Horizontal Reaction Influence Coefficients

Load at point = 20lb

For position of load points, rib layout, details of model dome and graphs of tabulated results, see Test No. 6 Sheet Nos. 3 & 4

Horizontal Base Displacement at Rib No. 36 (Towards centre of dome)	Dial gauge readings (A) and actual vertical displacement of point load (B; +ve upwards) in inches																			
	Rib No. 12										Rib No. 18									
	Point 1		Point 5		Point 9		Point 13		Point 17		Point 1		Point 5		Point 9		Point 13		Point 17	
	A	B	A	B	A	B	A	B	A	B	A	B	A	B	A	B	A	B	A	B
0 in.	.447	.000	.281	.000	.095	.000	.194	.000	.289	.000	.444	.000	.281	.000	.087	.000	.170	.000	.031	.000
.1 in.	.451	+.004	.299	+.018	.125	+.030	.230	+.036	.336	+.047	.447	+.003	.295	+.014	.112	+.025	.205	+.035	.081	+.050
.2 in.	.455	+.008	.315	+.034	.154	+.059	.269	+.075	.379	+.090	.450	+.006	.309	+.028	.135	+.048	.242	+.072	.125	+.094
.3 in.	.458	+.011	.330	+.049	.178	+.083	.300	+.106	.419	+.130	.452	+.008	.321	+.040	.158	+.071	.271	+.101	.166	+.135
.4 in.	.461	+.014	.345	+.064	.204	+.109	.334	+.140	.456	+.167	.455	+.011	.332	+.051	.178	+.091	.303	+.133	.206	+.175
.5 in.	.464	+.017	.360	+.079	.229	+.134	.365	+.171	.494	+.205	.457	+.013	.344	+.063	.200	+.113	.332	+.162	.248	+.217
.6 in.	.468	+.021	.376	+.095	.255	+.160	.398	+.204	.533	+.244	.460	+.016	.356	+.075	.221	+.134	.362	+.192	.288	+.257
.7 in.	.471	+.024	.391	+.110	.280	+.185	.430	+.236	.568	+.279	.462	+.018	.368	+.087	.242	+.155	.395	+.225	.328	+.297
.8 in.	.475	+.028	.407	+.126	.307	+.212	.463	+.269	.611	+.322	.465	+.021	.382	+.101	.267	+.180	.426	+.256	.372	+.341
.9 in.	.478	+.031	.422	+.142	.331	+.236	.495	+.301	.648	+.359	.468	+.024	.395	+.114	.288	+.201	.456	+.286	.412	+.381
1.0 in.	.481	+.034	.436	+.155	.355	+.260	.526	+.332	.682	+.393	.470	+.026	.405	+.124	.307	+.220	.485	+.315	.452	+.421

F. A. A. Ph.D. Thesis
30th Dec., 1968

Structural Engineering Division,
Department of Civil Engineering,
University of Newcastle upon Tyne.

TESTS ON MODEL RADIAL RIBBED DOME

Test No. 6
Sheet No. 1

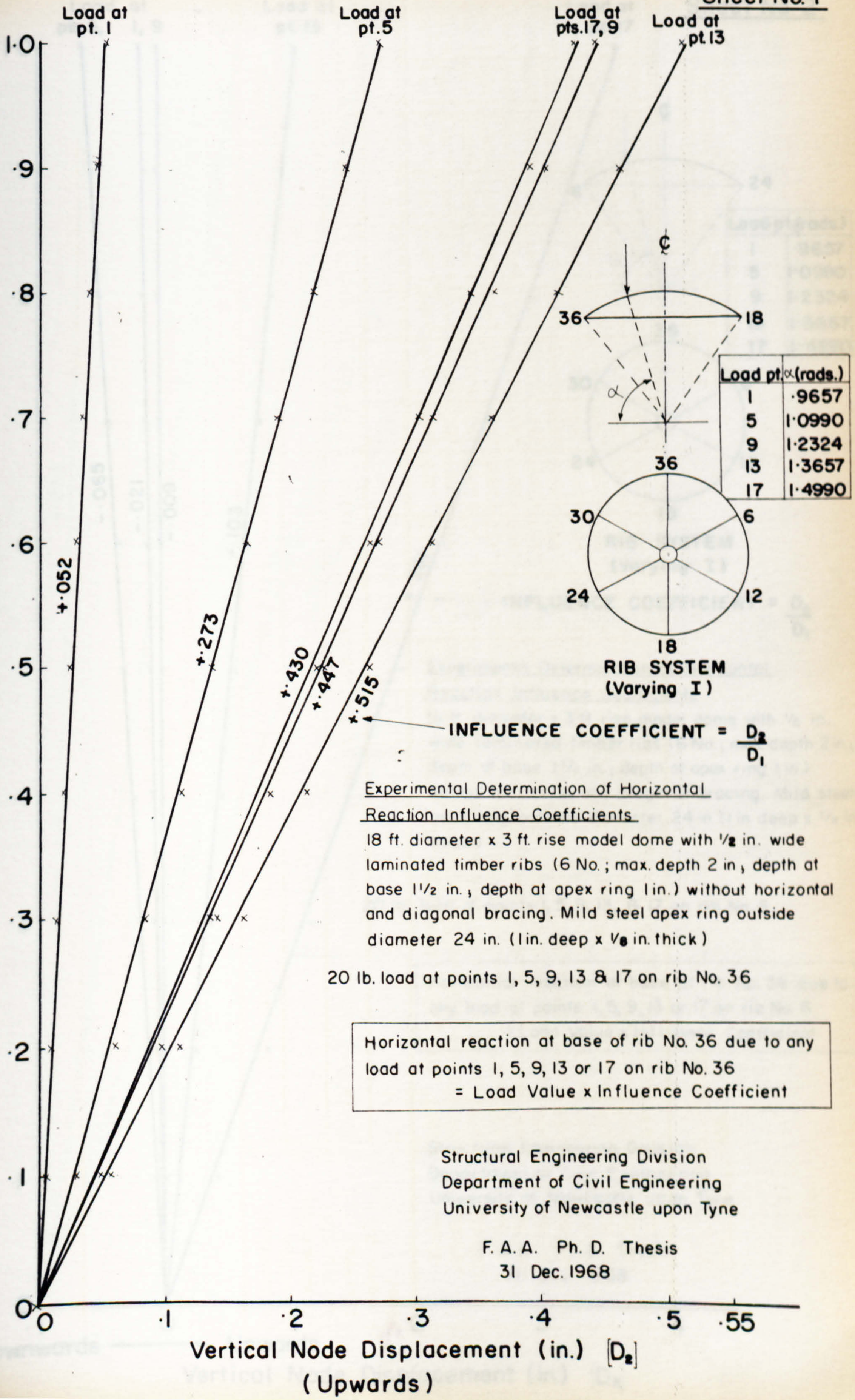

Load pt.	α (rads.)
1	·9657
5	1·0990
9	1·2324
13	1·3657
17	1·4990

RIB SYSTEM
(Varying I)

INFLUENCE COEFFICIENT = $\frac{D_2}{D_1}$

Experimental Determination of Horizontal Reaction Influence Coefficients

18 ft. diameter x 3 ft. rise model dome with ½ in. wide laminated timber ribs (6 No.; max. depth 2 in, depth at base 1½ in., depth at apex ring 1 in.) without horizontal and diagonal bracing. Mild steel apex ring outside diameter 24 in. (1 in. deep x ⅛ in. thick)

20 lb. load at points 1, 5, 9, 13 & 17 on rib No. 36

Horizontal reaction at base of rib No. 36 due to any load at points 1, 5, 9, 13 or 17 on rib No. 36
= Load Value x Influence Coefficient

Structural Engineering Division
Department of Civil Engineering
University of Newcastle upon Tyne

F. A. A. Ph. D. Thesis
31 Dec. 1968

TESTS ON MODEL RADIAL RIBBED DOME

Test No. 6
Sheet No. 2

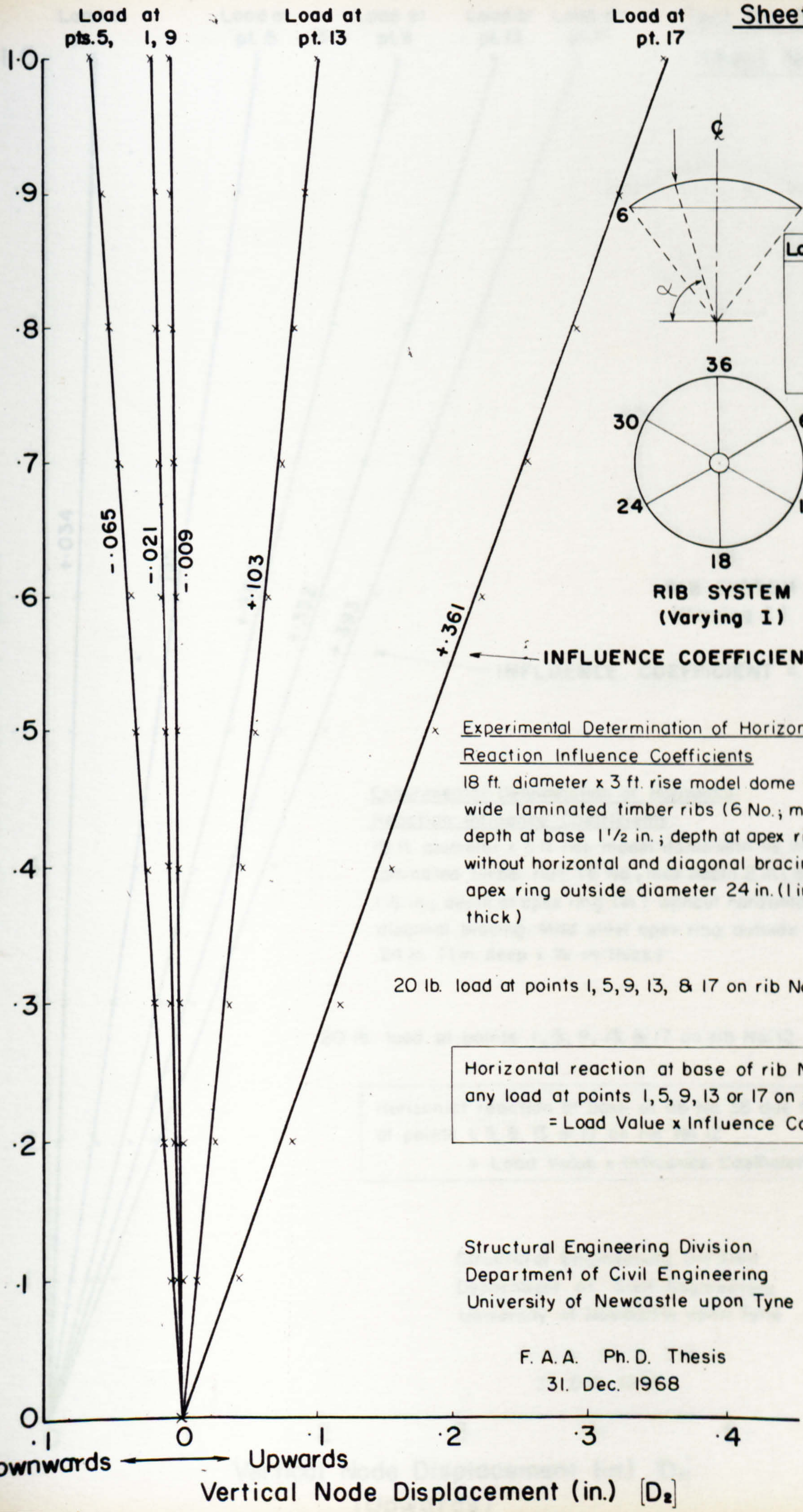

Load pt.	α (rads.)
1	·9657
5	1·0990
9	1·2324
13	1·3657
17	1·4990

RIB SYSTEM
(Varying I)

INFLUENCE COEFFICIENT = $\frac{D_2}{D_1}$

Experimental Determination of Horizontal Reaction Influence Coefficients

18 ft. diameter x 3 ft. rise model dome with ½ in. wide laminated timber ribs (6 No.; max depth 2 in.; depth at base 1½ in.; depth at apex ring 1 in.) without horizontal and diagonal bracing. Mild steel apex ring outside diameter 24 in. (1 in. deep x ⅛ in. thick)

20 lb. load at points 1, 5, 9, 13, & 17 on rib No. 6

Horizontal reaction at base of rib No. 36 due to any load at points 1, 5, 9, 13 or 17 on rib No. 6
= Load Value x Influence Coefficient

Structural Engineering Division
Department of Civil Engineering
University of Newcastle upon Tyne

F. A. A. Ph. D. Thesis
31. Dec. 1968

TESTS ON MODEL RADIAL RIBBED DOME

Test No. 6

Sheet No. 3

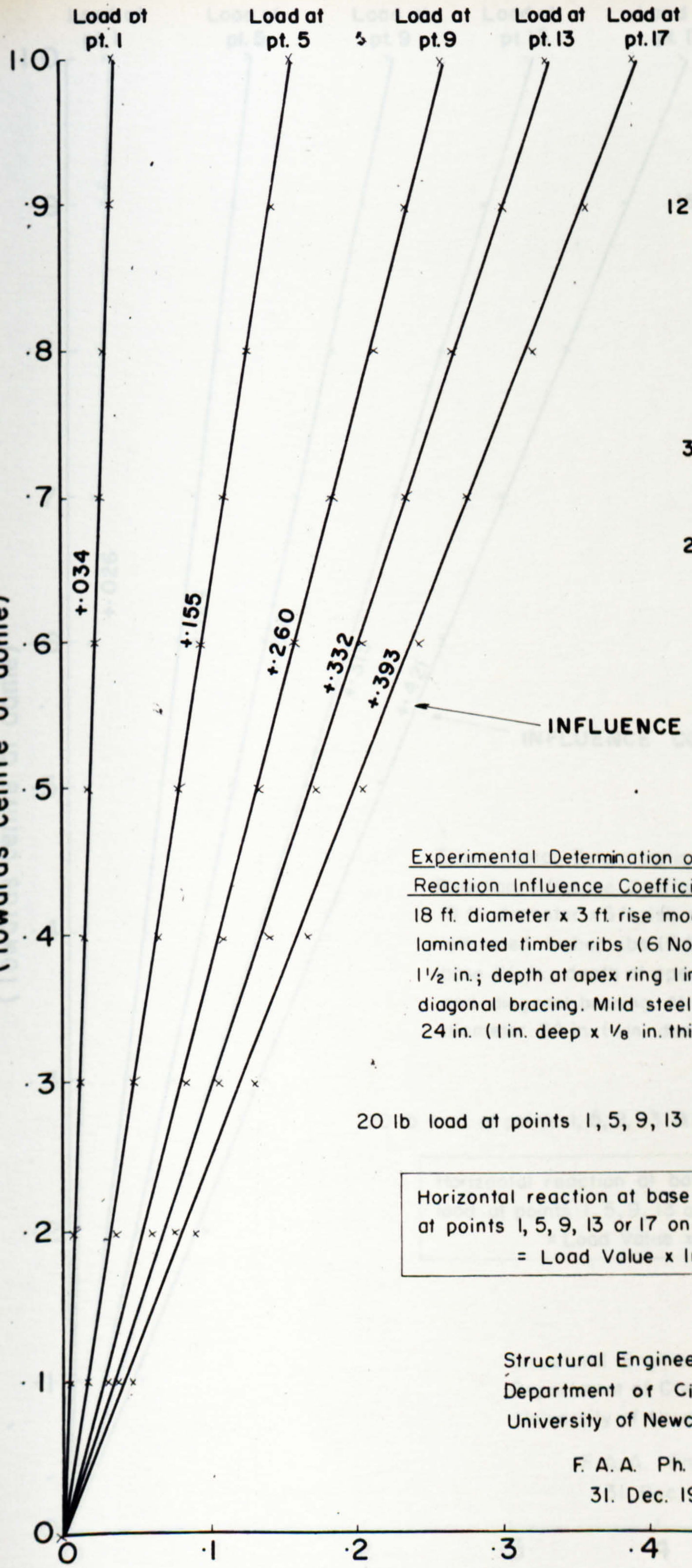

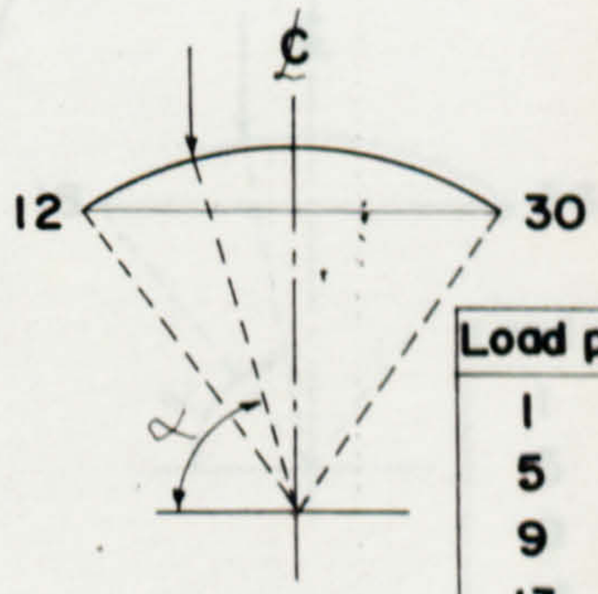

Load pt.	α (rads.)
1	·9657
5	1·0990
9	1·2324
13	1·3657
17	1·4990

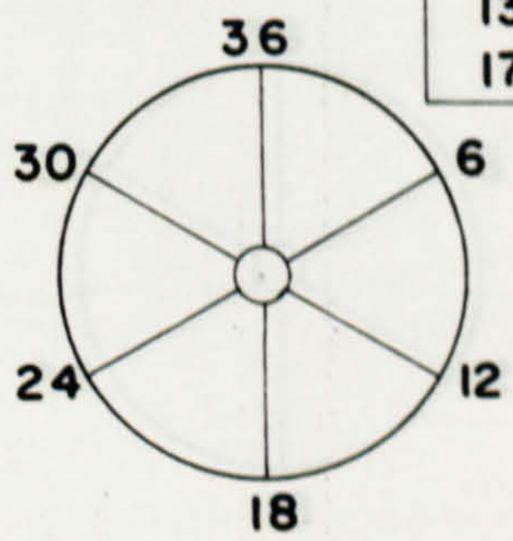

RIB SYSTEM
(Varying I)

INFLUENCE COEFFICIENT = $\frac{D_2}{D_1}$

Experimental Determination of Horizontal Reaction Influence Coefficients

18 ft. diameter x 3 ft. rise model dome with ½ in. wide laminated timber ribs (6 No.; max depth 2 in.; depth at base 1½ in.; depth at apex ring 1 in.) without horizontal and diagonal bracing. Mild steel apex ring outside diameter 24 in. (1 in. deep x ⅛ in. thick)

20 lb load at points 1, 5, 9, 13 & 17 on rib No. 12

Horizontal reaction at base of rib No. 36 due to any load at points 1, 5, 9, 13 or 17 on rib No. 12
= Load Value x Influence Coefficient

Structural Engineering Division
Department of Civil Engineering
University of Newcastle upon Tyne

F. A. A. Ph. D. Thesis
31. Dec. 1968

TESTS ON MODEL RADIAL RIBBED DOME

Test No. 6
Sheet No. 4

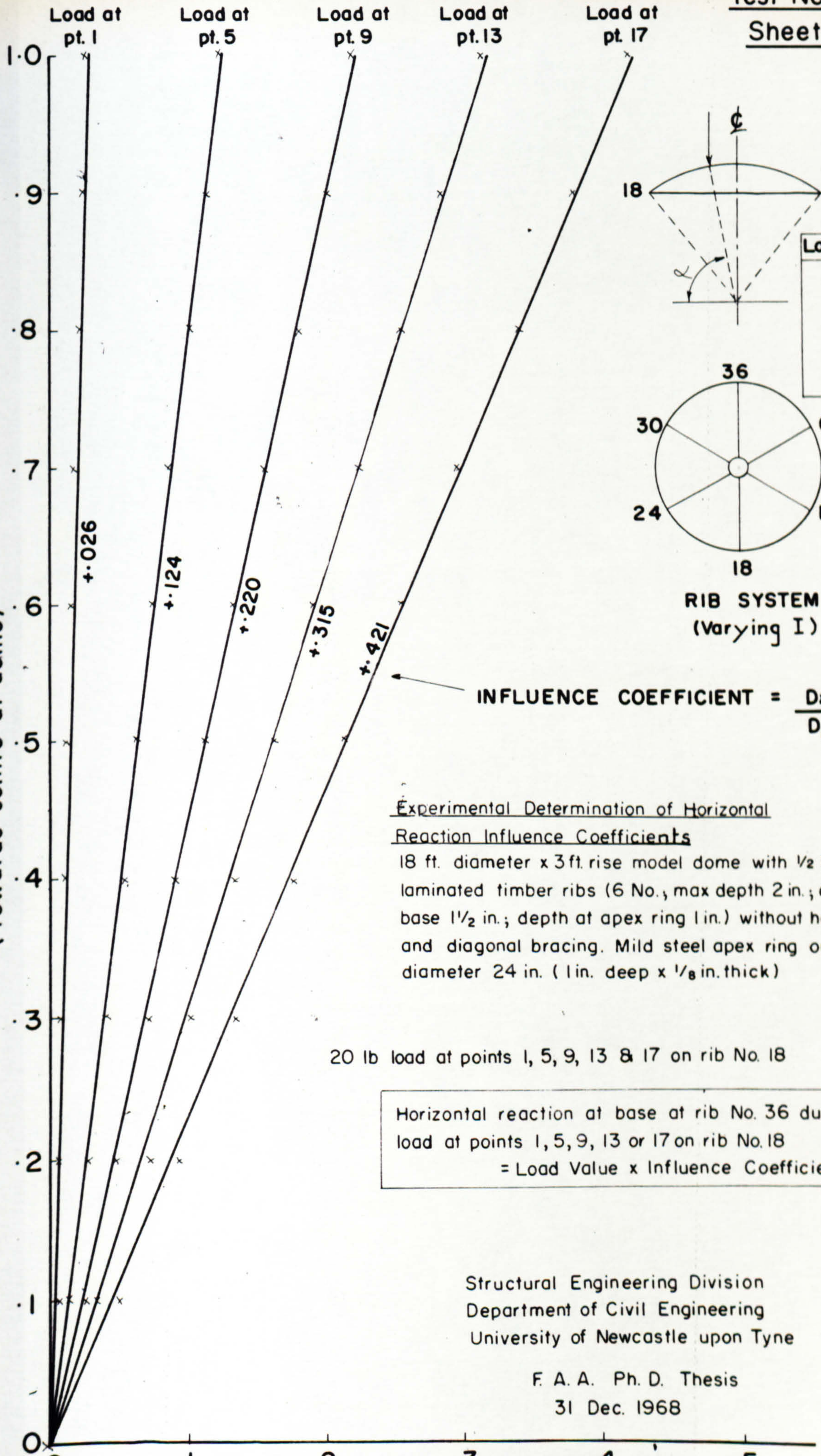

Load pt.	α (rads.)
1	·9657
5	1·0990
9	1·2324
13	1·3657
17	1·4990

RIB SYSTEM
(Varying I)

INFLUENCE COEFFICIENT = $\frac{D_2}{D_1}$

Experimental Determination of Horizontal Reaction Influence Coefficients

18 ft. diameter x 3 ft. rise model dome with ½ in. wide laminated timber ribs (6 No., max depth 2 in.; depth at base 1½ in.; depth at apex ring 1 in.) without horizontal and diagonal bracing. Mild steel apex ring outside diameter 24 in. (1 in. deep x ⅛ in. thick)

20 lb load at points 1, 5, 9, 13 & 17 on rib No. 18

Horizontal reaction at base at rib No. 36 due to any load at points 1, 5, 9, 13 or 17 on rib No. 18
= Load Value x Influence Coefficient

Structural Engineering Division
Department of Civil Engineering
University of Newcastle upon Tyne

F. A. A. Ph. D. Thesis
31 Dec. 1968

Structural Engineering Division
Department of Civil Engineering
University of Newcastle upon Tyne

TESTS ON MODEL RADIAL RIBBED DOME

Test No. 6
Sheet No. 5

H = W x Influence Coefficient

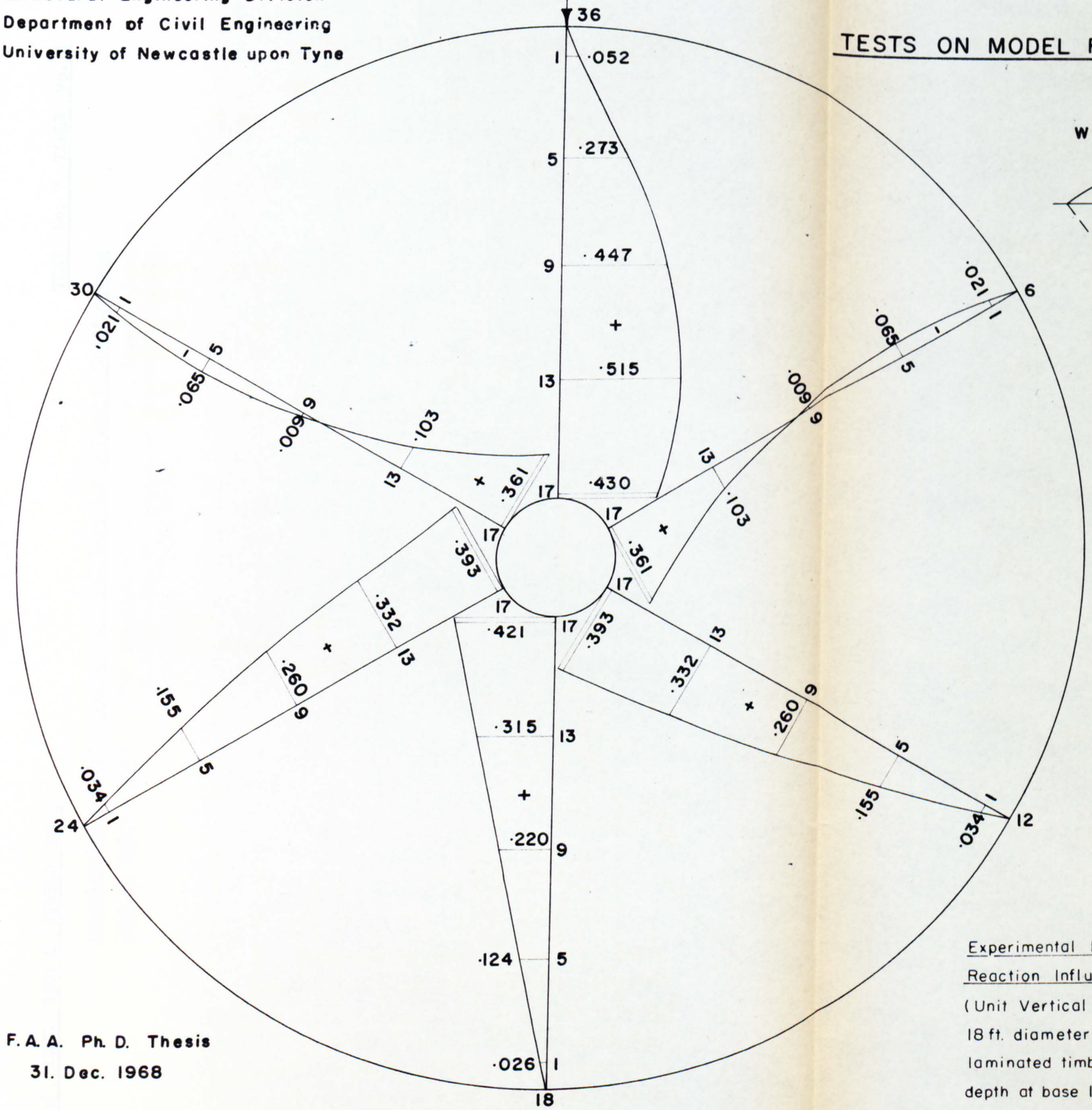

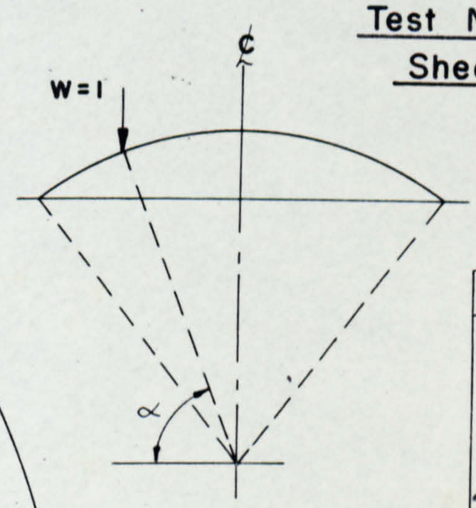

Load pt.	∝(rads.)
1	·9657
5	1·0990
9	1·2324
13	1·3657
17	1·4990

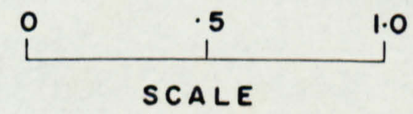

Experimental Determination of Horizontal Reaction Influence Lines for Support No. 36

(Unit Vertical force acting at any angle on any rib)

18 ft. diameter x 3 ft. rise model dome with ½ in. wide laminated timber ribs (6 No. of varying I; max. depth 2 in.; depth at base 1½ in; depth at apex ring 1 in.) without horizontal and diagonal bracing. Mild steel apex ring outside diameter 24 in. (1 in. deep x ⅛ in. thick)

F. A. A. Ph. D. Thesis
31. Dec. 1968

TESTS ON MODEL RADIAL RIBBED DOME

TEST No. 7 TABLE No. 1

Experimental Determination of Vertical Reaction Influence Coefficients

Load at point = 20lb

For position of load points, rib layout, details of model dome and graphs of tabulated results, see Test No. 7 Sheet Nos. 1 & 2

Vertical Base Displacement at Rib No.18 (Upwards)	Dial gauge readings (A) and actual vertical displacement of point load (B; +ve upwards) in inches																			
	Rib No. 18										Rib No. 24									
	Point 1		Point 5		Point 9		Point 13		Point 17		Point 1		Point 5		Point 9		Point 13		Point 17	
	A	B	A	B	A	B	A	B	A	B	A	B	A	B	A	B	A	B	A	B
0 in.	.149	.000	.195	.000	.095	.000	.195	.000	.045	.000	.440	.000	.232	.000	.023	.000	.191	.000	.217	.000
.1 in.	.225	+.076	.254	+.059	.140	+.045	.223	+.028	.061	+.016	.439	-.001	.228	-.004	.020	-.003	.193	+.002	.229	+.012
.2 in.	.319	+.170	.341	+.146	.212	+.117	.270	+.075	.085	+.040	.438	-.002	.225	-.007	.018	-.005	.197	+.006	.244	+.027
.3 in.	.420	+.271	.426	+.231	.282	+.187	.321	+.126	.108	+.063	.437	-.003	.222	-.010	.017	-.006	.202	+.011	.259	+.042
.4 in.	.521	+.372	.513	+.318	.350	+.255	.368	+.173	.131	+.086	.436	-.004	.219	-.013	.016	-.007	.206	+.015	.275	+.058
.5 in.	.615	+.466	.602	+.407	.421	+.326	.419	+.224	.155	+.110	.435	-.005	.215	-.017	.015	-.008	.210	+.019	.289	+.072
.6 in.	.714	+.565	.689	+.494	.492	+.397	.468	+.273	.178	+.133	.434	-.006	.212	-.020	.014	-.009	.213	+.022	.303	+.086
.7 in.	.818	+.669	.777	+.582	.564	+.469	.518	+.323	.201	+.156	.434	-.006	.209	-.023	.013	-.010	.217	+.026	.317	+.100
.8 in.	.919	+.770	.865	+.670	.634	+.539	.566	+.371	.223	+.178	.433	-.007	.205	-.027	.012	-.011	.221	+.030	.331	+.114
.9 in.	1.013	+.864	.955	+.760	.704	+.609	.616	+.421	.245	+.200	.432	-.008	.202	-.030	.011	-.012	.225	+.034	.346	+.129
1.0 in.	1.112	+.963	1.038	+.843	.774	+.679	.664	+.469	.267	+.222	.431	-.009	.199	-.033	.010	-.013	.228	+.037	.360	+.143

F. A. A. Ph.D. Thesis
2nd Jan., 1969

Structural Engineering Division,
Department of Civil Engineering,
University of Newcastle upon Tyne.

TESTS ON MODEL RADIAL RIBBED DOME

TEST No. 7 TABLE No. 2

Experimental Determination of Vertical Reaction Influence Coefficients

Load at point = 20lb

For position of load points, rib layout, details of model dome and graphs of tabulated results, see Test No. 7 Sheet Nos. 3 & 4

Vertical Base Displacement at Rib No.18 (Upwards)	Dial gauge readings (A) and actual vertical displacement of point load (B; +ve upwards) in inches																			
	Rib No. 30										Rib No. 36									
	Point 1		Point 5		Point 9		Point 13		Point 17		Point 1		Point 5		Point 9		Point 13		Point 17	
	A	B	A	B	A	B	A	B	A	B	A	B	A	B	A	B	A	B	A	B
0 in.	.443	.000	.283	.000	.114	.000	.284	.000	.243	.000	.447	.000	.307	.000	.128	.000	.302	.000	.340	.000
.1 in.	.444	+.001	.287	+.004	.121	+.007	.293	+.009	.253	+.010	.448	+.001	.309	+.002	.131	+.003	.306	+.004	.350	+.010
.2 in.	.445	+.002	.293	+.010	.130	+.016	.303	+.019	.266	+.023	.448	+.001	.312	+.005	.136	+.008	.315	+.013	.362	+.022
.3 in.	.446	+.003	.298	+.015	.138	+.024	.315	+.031	.280	+.037	.449	+.002	.315	+.008	.141	+.013	.323	+.021	.375	+.035
.4 in.	.447	+.004	.303	+.020	.146	+.032	.324	+.040	.292	+.049	.450	+.003	.318	+.011	.143	+.015	.332	+.030	.387	+.047
.5 in.	.448	+.005	.308	+.025	.155	+.041	.335	+.051	.306	+.063	.450	+.003	.321	+.014	.149	+.021	.340	+.038	.399	+.059
.6 in.	.450	+.007	.313	+.030	.163	+.049	.345	+.061	.319	+.076	.451	+.004	.324	+.017	.154	+.026	.350	+.048	.412	+.072
.7 in.	.451	+.008	.319	+.036	.172	+.058	.355	+.071	.332	+.089	.451	+.004	.327	+.020	.160	+.032	.360	+.058	.425	+.085
.8 in.	.452	+.009	.324	+.041	.179	+.065	.366	+.082	.345	+.102	.452	+.005	.330	+.023	.166	+.038	.368	+.066	.438	+.098
.9 in.	.453	+.010	.329	+.046	.187	+.073	.376	+.092	.358	+.115	.453	+.006	.333	+.026	.172	+.044	.377	+.075	.451	+.111
1.0 in.	.454	+.011	.334	+.051	.196	+.082	.386	+.102	.370	+.127	.453	+.006	.336	+.029	.176	+.048	.385	+.083	.464	+,124

F. A. A. Ph.D. Thesis
2nd Jan., 1969

Structural Engineering Division,
Department of Civil Engineering,
University of Newcastle upon Tyne.

TESTS ON MODEL RADIAL RIBBED DOME

Test No. 7

Sheet No. 1

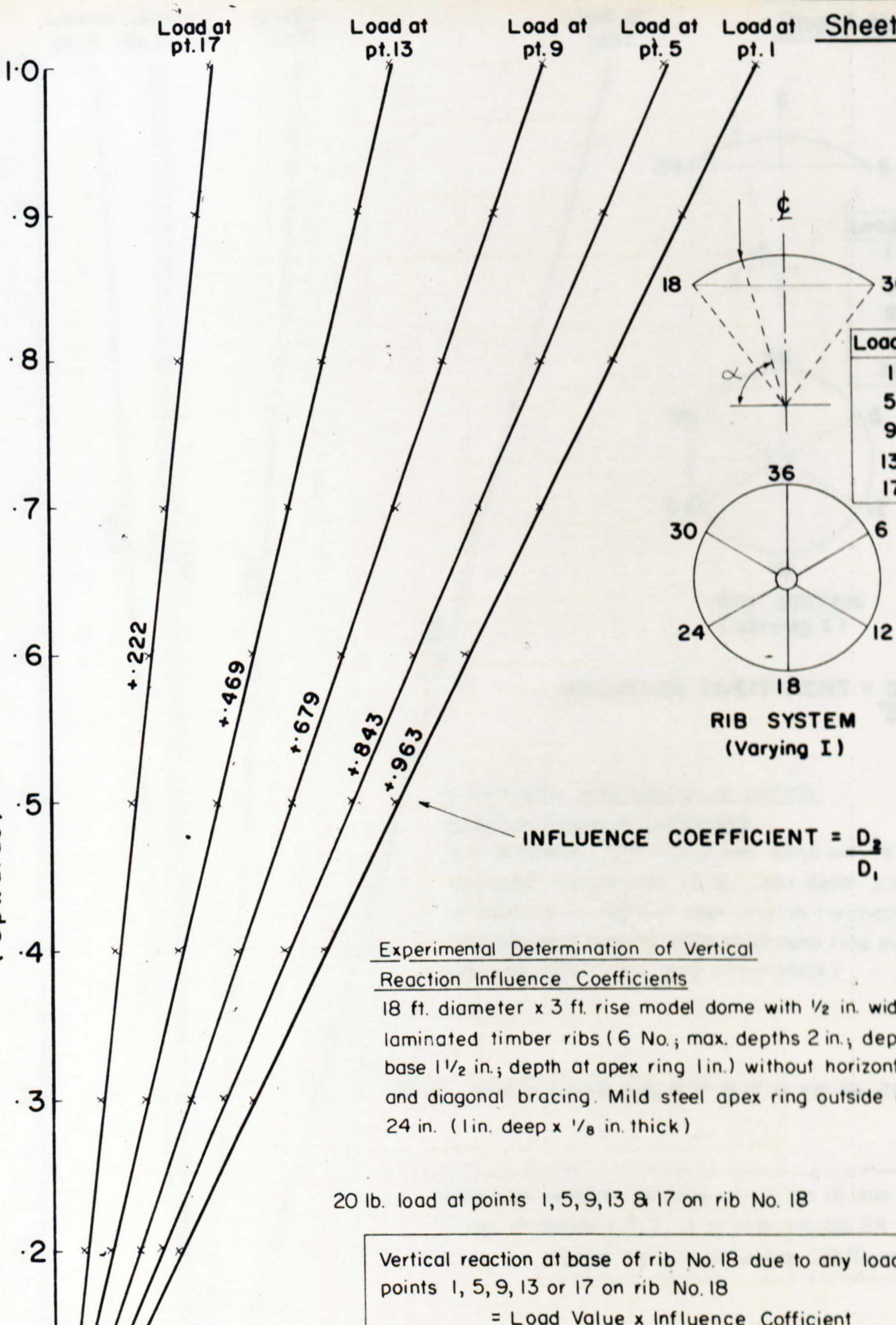

Load pt.	α (rads.)
1	·9657
5	1·0990
9	1·2324
13	1·3657
17	1·4990

RIB SYSTEM
(Varying I)

INFLUENCE COEFFICIENT = $\frac{D_2}{D_1}$

Experimental Determination of Vertical Reaction Influence Coefficients

18 ft. diameter x 3 ft. rise model dome with ½ in. wide laminated timber ribs (6 No.; max. depths 2 in.; depth at base 1½ in.; depth at apex ring 1 in.) without horizontal and diagonal bracing. Mild steel apex ring outside diameter 24 in. (1 in. deep x ⅛ in. thick)

20 lb. load at points 1, 5, 9, 13 & 17 on rib No. 18

Vertical reaction at base of rib No. 18 due to any load at points 1, 5, 9, 13 or 17 on rib No. 18
= Load Value x Influence Cofficient

Structural Engineering Division
Department of Civil Engineering
University of Newcastle upon Tyne

F. A. A. Ph. D. Thesis
2. Jan. 1969

TESTS ON MODEL RADIAL RIBBED DOME

Test No. 7

Sheet No. 2

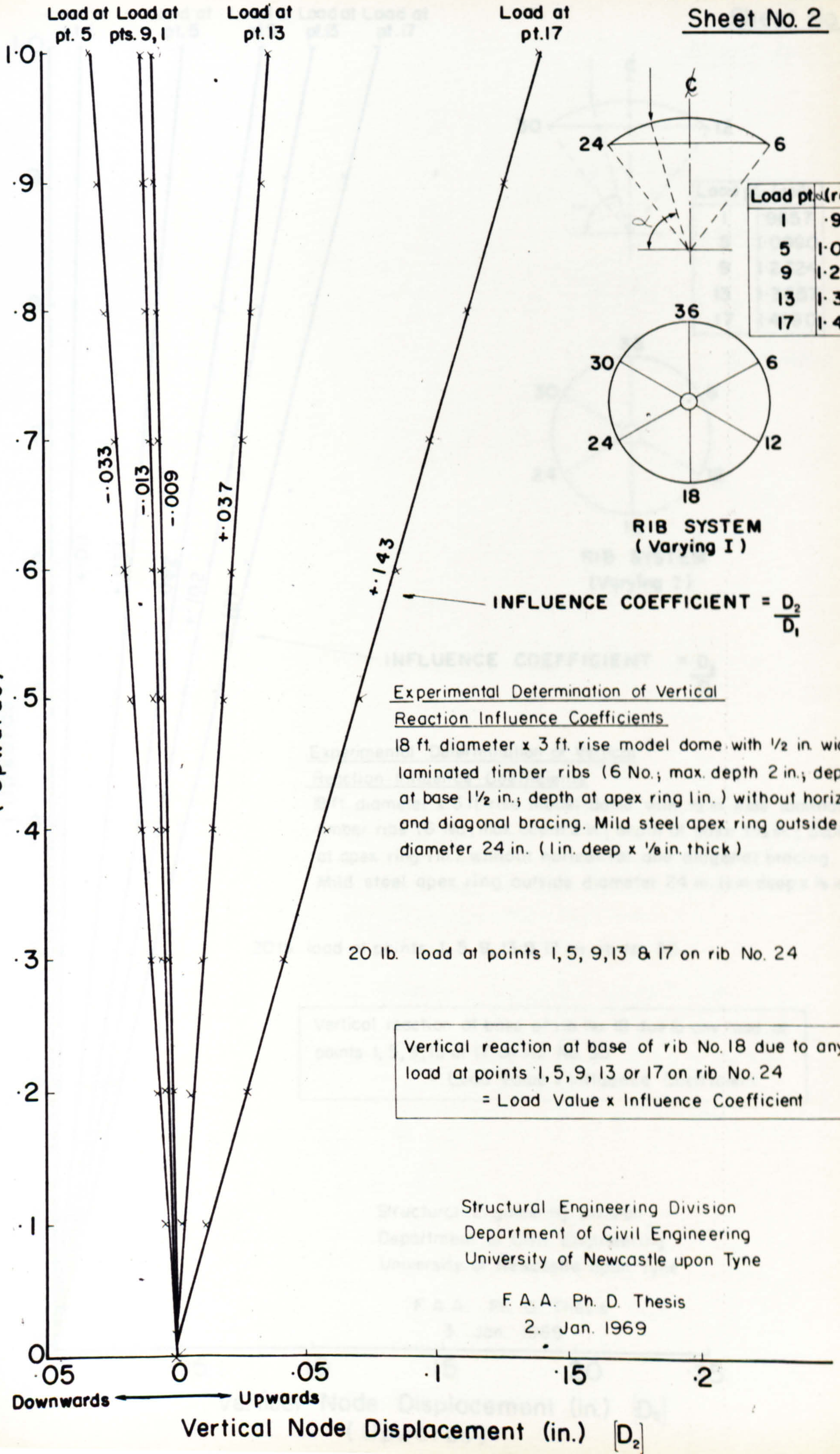

Load pt.	α (rads.)
1	·9657
5	1·0990
9	1·2324
13	1·3657
17	1·4990

RIB SYSTEM
(Varying I)

INFLUENCE COEFFICIENT = $\frac{D_2}{D_1}$

Experimental Determination of Vertical Reaction Influence Coefficients

18 ft. diameter x 3 ft. rise model dome with ½ in. wide laminated timber ribs (6 No.; max. depth 2 in.; depth at base 1½ in.; depth at apex ring 1 in.) without horizontal and diagonal bracing. Mild steel apex ring outside diameter 24 in. (1 in. deep x ⅛ in. thick)

20 lb. load at points 1, 5, 9, 13 & 17 on rib No. 24

Vertical reaction at base of rib No. 18 due to any load at points 1, 5, 9, 13 or 17 on rib No. 24
= Load Value x Influence Coefficient

Structural Engineering Division
Department of Civil Engineering
University of Newcastle upon Tyne

F. A. A. Ph. D. Thesis
2. Jan. 1969

TESTS ON MODEL RADIAL RIBBED DOME

Test No. 7

Sheet No. 3

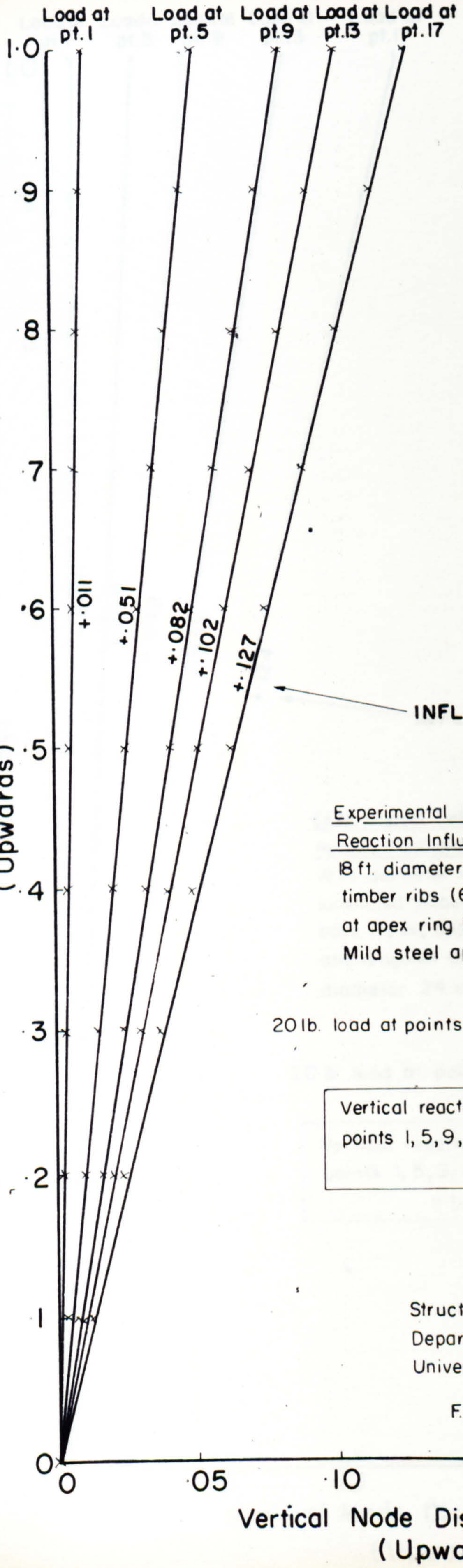

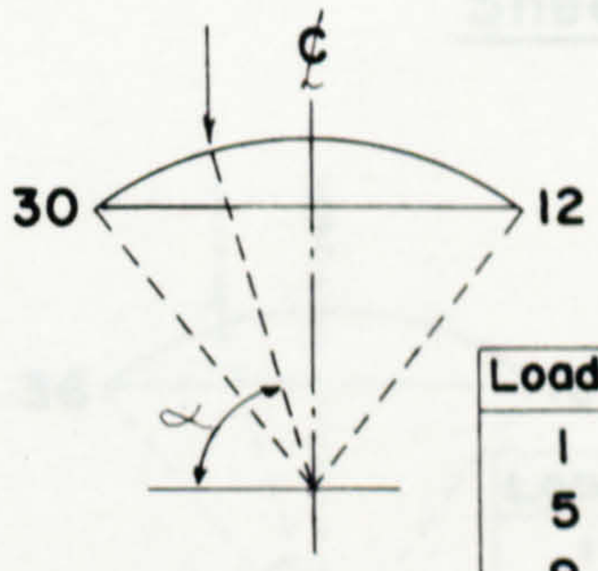

Load pt.	α (rads.)
1	·9657
5	1·0990
9	1·2324
13	1·3657
17	1·4990

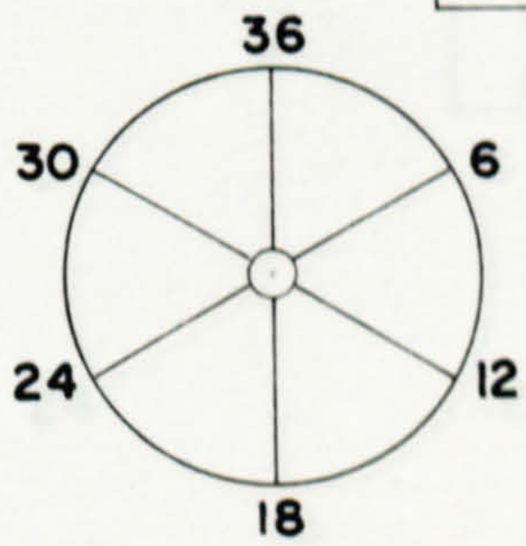

RIB SYSTEM
(Varying I)

INFLUENCE COEFFICIENT = $\frac{D_2}{D_1}$

Experimental Determination of Vertical Reaction Influence Coefficients

18 ft. diameter x 3 ft. rise model dome with ½ in. wide laminated timber ribs (6 No.; max. depth 2 in.; depth at base 1½ in.; depth at apex ring 1 in.) without horizontal and diagonal bracing. Mild steel apex ring outside diameter 24 in. (1 in. deep x ⅛ in. thick)

20 lb. load at points 1, 5, 9, 13 & 17 on rib No. 30

Vertical reaction at base of rib No. 18 due to any load at points 1, 5, 9, 13 or 17 on rib No. 30
= Load Value x Influence Coefficient

Structural Engineering Division
Department of Civil Engineering
University of Newcastle upon Tyne

F. A. A. Ph. D. Thesis
3. Jan. 1969

TESTS ON MODEL RADIAL RIBBED DOME

Test No. 7

Sheet No. 4

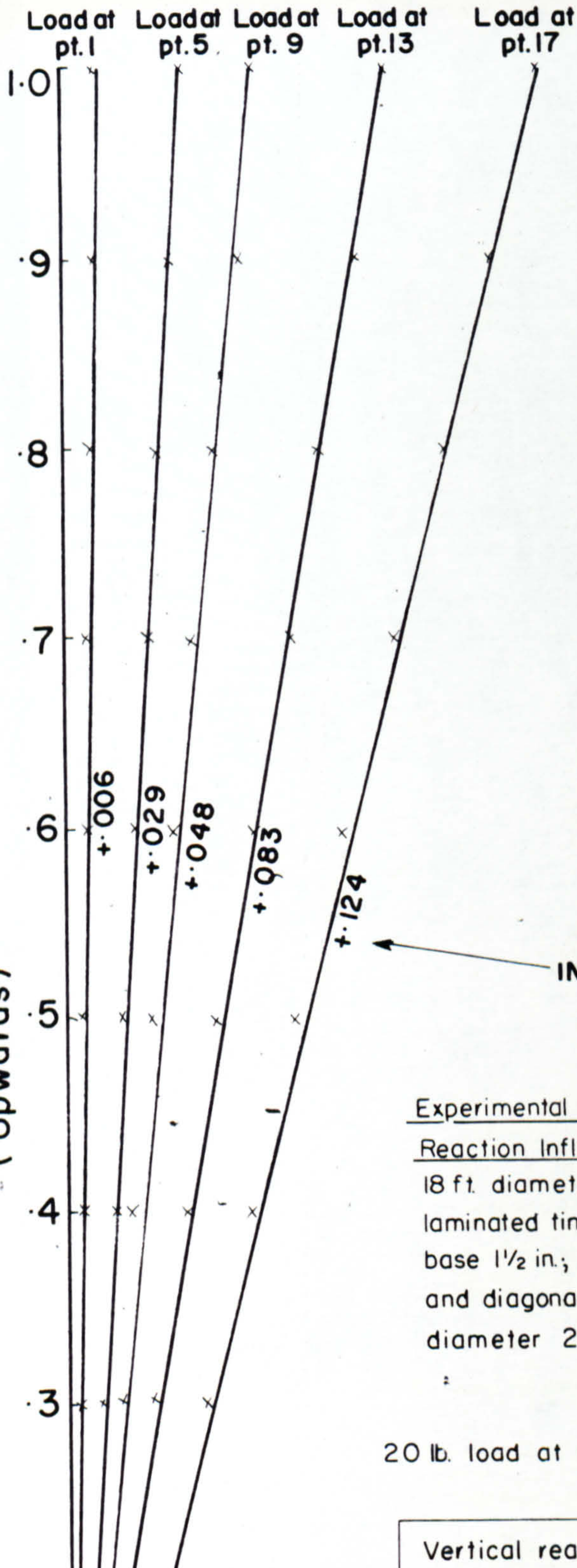

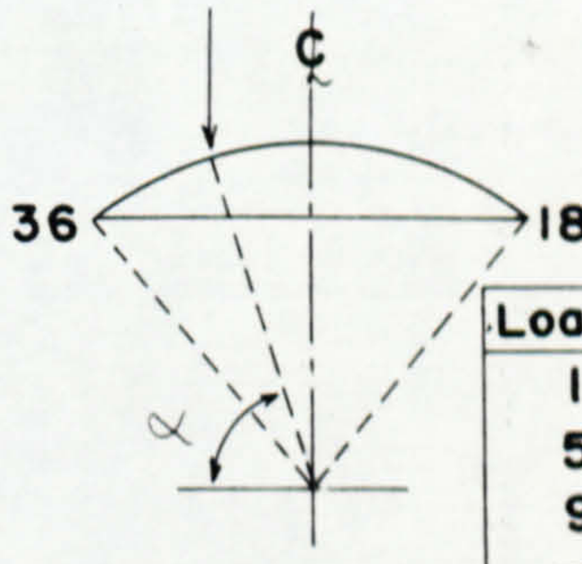

Load pt.	α (rads.)
1	·9657
5	1·0990
9	1·2324
13	1·3657
17	1·4990

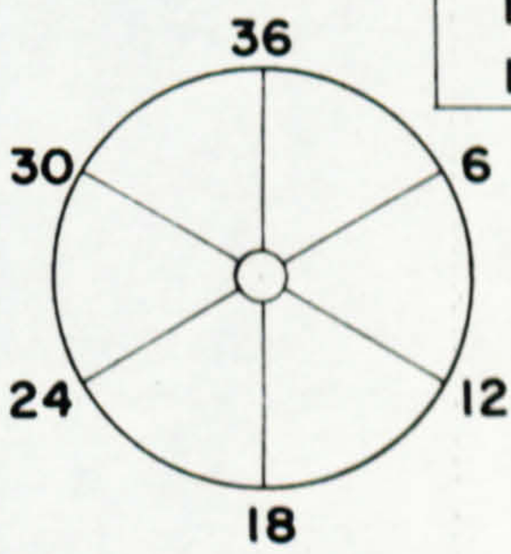

RIB SYSTEM
(Varying I)

INFLUENCE COEFFICIENT = $\frac{D_2}{D_1}$

Experimental Determination of Vertical Reaction Influence Coefficients

18 ft. diameter x 3 ft. rise model dome with ½ in. wide laminated timber ribs (6 No.; max. depth 2 in.; depth at base 1½ in.; depth at apex ring 1 in.) without horizontal and diagonal bracing. Mild steel apex ring outside diameter 24 in. (1 in. deep x ⅛ in. thick)

20 lb. load at points 1, 5, 9, 13 & 17 on rib No. 36

Vertical reaction at base of rib No. 18 due to any load at points 1, 5, 9, 13 or 17 on rib No. 36
= Load Value x Influence Coefficient

Structural Engineering Division
Department of Civil Engineering
University of Newcastle upon Tyne

F. A. A. Ph. D. Thesis
3. Jan. 1969

Structural Engineering Division
Department of Civil Engineering
University of Newcastle upon Tyne

TESTS ON MODEL RADIAL RIBBED DOME

Test No. 7
Sheet No. 5

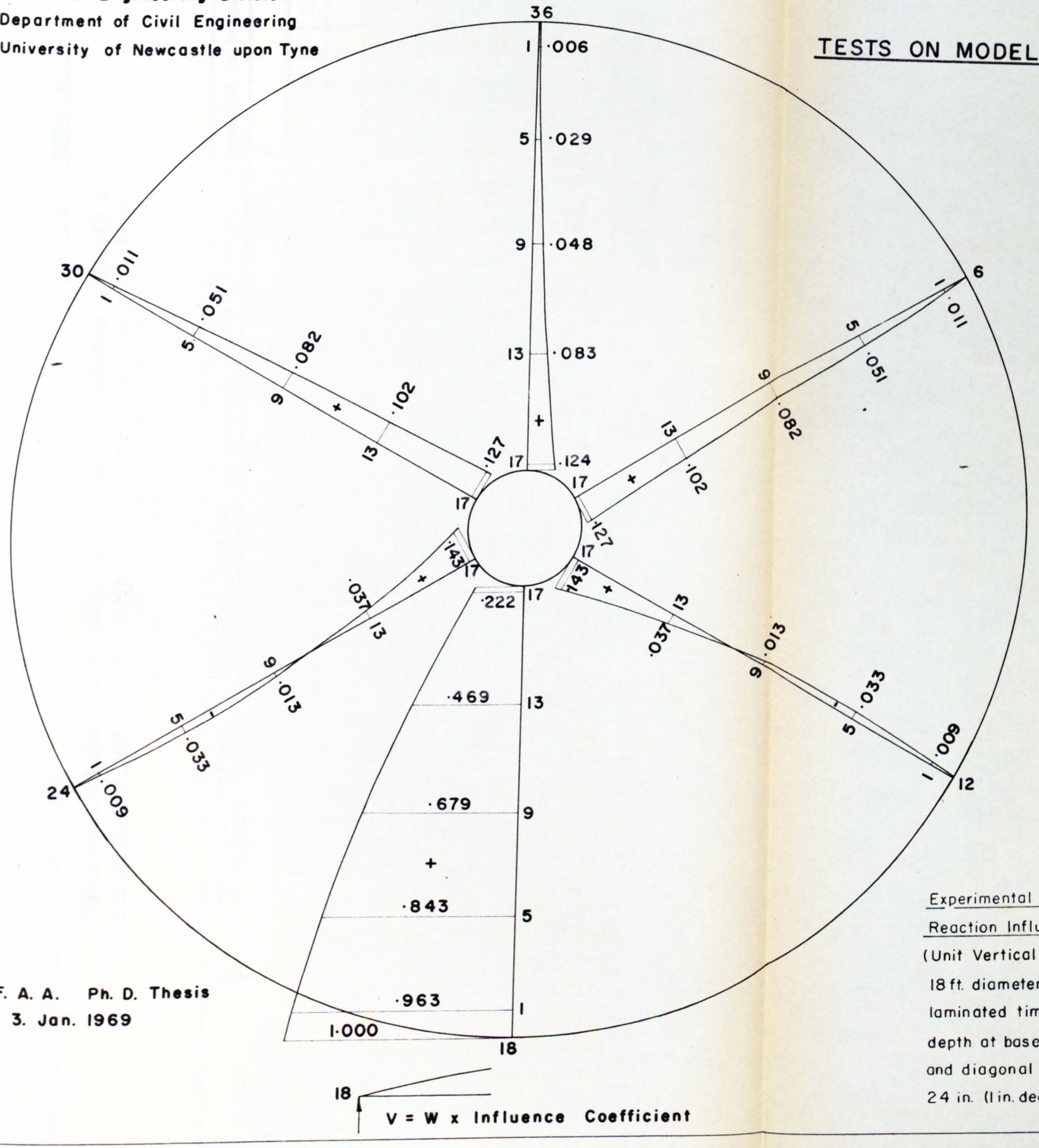

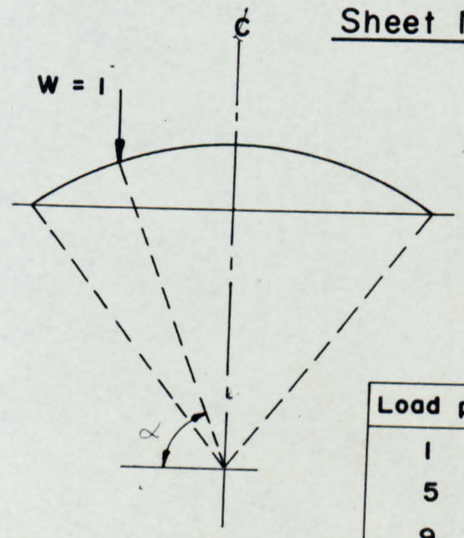

Load pt.	α (rads.)
1	·9657
5	1·0990
9	1·2324
13	1·3657
17	1·4990

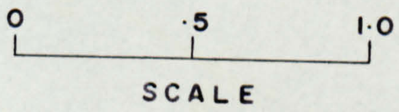

Experimental Determination of Vertical
Reaction Influence Lines for Support No. 18

(Unit Vertical force acting at any angle on any rib)

18 ft. diameter x 3 ft. rise model dome with ½ in. wide laminated timber ribs (6 No. of varying I; max. depth 2 in; depth at base 1½ in.; depth at apex ring 1 in.) without horizontal and diagonal bracing. Mild steel apex ring outside diameter 24 in. (1 in. deep x ⅛ in. thick)

F. A. A. Ph. D. Thesis
3. Jan. 1969

V = W x Influence Coefficient

TESTS ON MODEL RADIAL RIBBED DOME

TEST No. 8 TABLE No. 1

Experimental Determination of Apex Ring Vertical Force Influence Coefficients

Load at point = 20lb

For position of load points, rib layout, details of model dome and graphs of tabulated results, see Test No. 8 Sheet Nos. 1 & 2

Vertical Displacement at Apex Ring on Rib No.36 (Upwards)	Dial gauge readings (A) and actual vertical displacement of point load (B; +ve upwards) in inches																			
	Rib No. 36										Rib No. 6									
	Point 1		Point 5		Point 9		Point 13		Point 17		Point 1		Point 5		Point 9		Point 13		Point 17	
	A	B	A	B	A	B	A	B	A	B	A	B	A	B	A	B	A	B	A	B
0 in.	.449	.000	.313	.000	.126	.000	.278	.000	.380	.000	.441	.000	.254	.000	.041	.000	.236	.000	.334	.000
.01 in.	.449	.000	.314	+.001	.130	+.004	.289	+.011	.390	+.010	.441	.000	.254	.000	.042	+.001	.238	+.002	.343	+.009
.02 in.	.449	.000	.316	+.003	.135	+.009	.298	+.020	.400	+.020	.441	.000	.254	.000	.044	+.003	.242	+.006	.349	+.015
.03 in.	.449	.000	.318	+.005	.141	+.015	.308	+.030	.410	+.030	.441	.000	.254	.000	.045	+.004	.245	+.009	.357	+.023
.04 in.	.450	+.001	.321	+.008	.146	+.020	.317	+.039	.420	+.040	.441	.000	.254	.000	.046	+.005	.250	+.014	.364	+.030
.05 in.	.450	+.001	.323	+.010	.152	+.026	.326	+.048	.430	+.050	.441	.000	.254	.000	.047	+.006	.255	+.019	.371	+.037
.06 in.	.450	+.001	.325	+.012	.157	+.031	.335	+.057	.440	+.060	.441	.000	.254	.000	.049	+.008	.258	+.022	.377	+.043
.07 in.	.450	+.001	.327	+.014	.162	+.036	.344	+.066	.450	+.070	.441	.000	.254	.000	.050	+.009	.262	+.026	.384	+.050
.08 in.	.451	+.002	.330	+.017	.168	+.042	.351	+.073	.460	+.080	.441	.000	.254	.000	.052	+.011	.266	+.030	.392	+.058
.09 in.	.451	+.002	.332	+.019	.173	+.047	.360	+.082	.470	+.090	.441	.000	.254	.000	.053	+.012	.270	+.034	.398	+.064
.10 in.	.451	+.002	.334	+.021	.178	+.052	.368	+.090	.480	+.100	.441	.000	.254	.000	.055	+.014	.275	+.039	.405	+.071

F. A. A. Ph.D. Thesis
6th Jan., 1969

Structural Engineering Division,
Department of Civil Engineering,
University of Newcastle upon Tyne.

TESTS ON MODEL RADIAL RIBBED DOME

TEST No. 8 TABLE No. 2

Experimental Determination of Apex Ring Vertical Force Influence Coefficients

Load at point = 20lb

For positions of load points, rib layout, details of model dome and graphs of tabulated results, see Test No. 8 Sheet Nos. 3 & 4

Vertical Displacement at Apex Ring on Rib No.36 (Upwards)	Dial gauge readings (A) and actual vertical displacement of point load (B; +ve upwards) in inches																			
	Rib No. 12										Rib No. 18									
	Point 1		Point 5		Point 9		Point 13		Point 17		Point 1		Point 5		Point 9		Point 13		Point 17	
	A	B	A	B	A	B	A	B	A	B	A	B	A	B	A	B	A	B	A	B
0 in.	.444	.000	.293	.000	.082	.000	.212	.000	.087	.000	.446	.000	.290	.000	.085	.000	.146	.000	.038	.000
.01 in.	.443	-.001	.289	-.004	.077	-.005	.207	-.005	.085	-.002	.445	-.001	.284	-.006	.077	-.008	.139	-.007	.034	-.004
.02 in.	.443	-.001	.287	-.006	.073	-.009	.203	-.009	.084	-.003	.444	-.002	.280	-.010	.070	-.015	.131	-.015	.030	-.008
.03 in.	.442	-.002	.284	-.009	.069	-.013	.199	-.013	.083	-.004	.443	-.003	.275	-.015	.063	-.022	.123	-.023	.027	-.011
.04 in.	.441	-.003	.281	-.012	.065	-.017	.195	-.017	.082	-.005	.442	-.004	.271	-.019	.057	-.028	.116	-.030	.023	-.015
.05 in.	.441	-.003	.278	-.015	.061	-.021	.191	-.021	.081	-.006	.441	-.005	.267	-.023	.051	-.034	.108	-.038	.020	-.018
.06 in.	.440	-.004	.276	-.017	.057	-.025	.186	-.026	.080	-.007	.440	-.006	.263	-.027	.043	-.042	.101	-.045	.016	-.022
.07 in.	.439	-.005	.273	-.020	.053	-.029	.182	-.030	.078	-.009	.439	-.007	.258	-.032	.037	-.048	.093	-.053	.012	-.026
.08 in.	.439	-.005	.271	-.022	.049	-.033	.178	-.034	.077	-.010	.438	-.008	.254	-.036	.031	-.054	.086	-.060	.008	-.030
.09 in.	.438	-.006	.268	-.025	.044	-.038	.174	-.038	.075	-.012	.437	-.009	.250	-.040	.024	-.061	.079	-.067	.004	-.034
.10 in.	.438	-.006	.265	-.028	.040	-.042	.170	-.042	.073	-.014	.436	-.010	.245	-.045	.017	-.068	.071	-.075	.000	-.038

F. A. A. Ph.D. Thesis
6th Jan., 1969

Structural Engineering Division,
Department of Civil Engineering,
University of Newcastle upon Tyne.

TESTS ON MODEL RADIAL RIBBED DOME

Test No. 8

Sheet No. 1

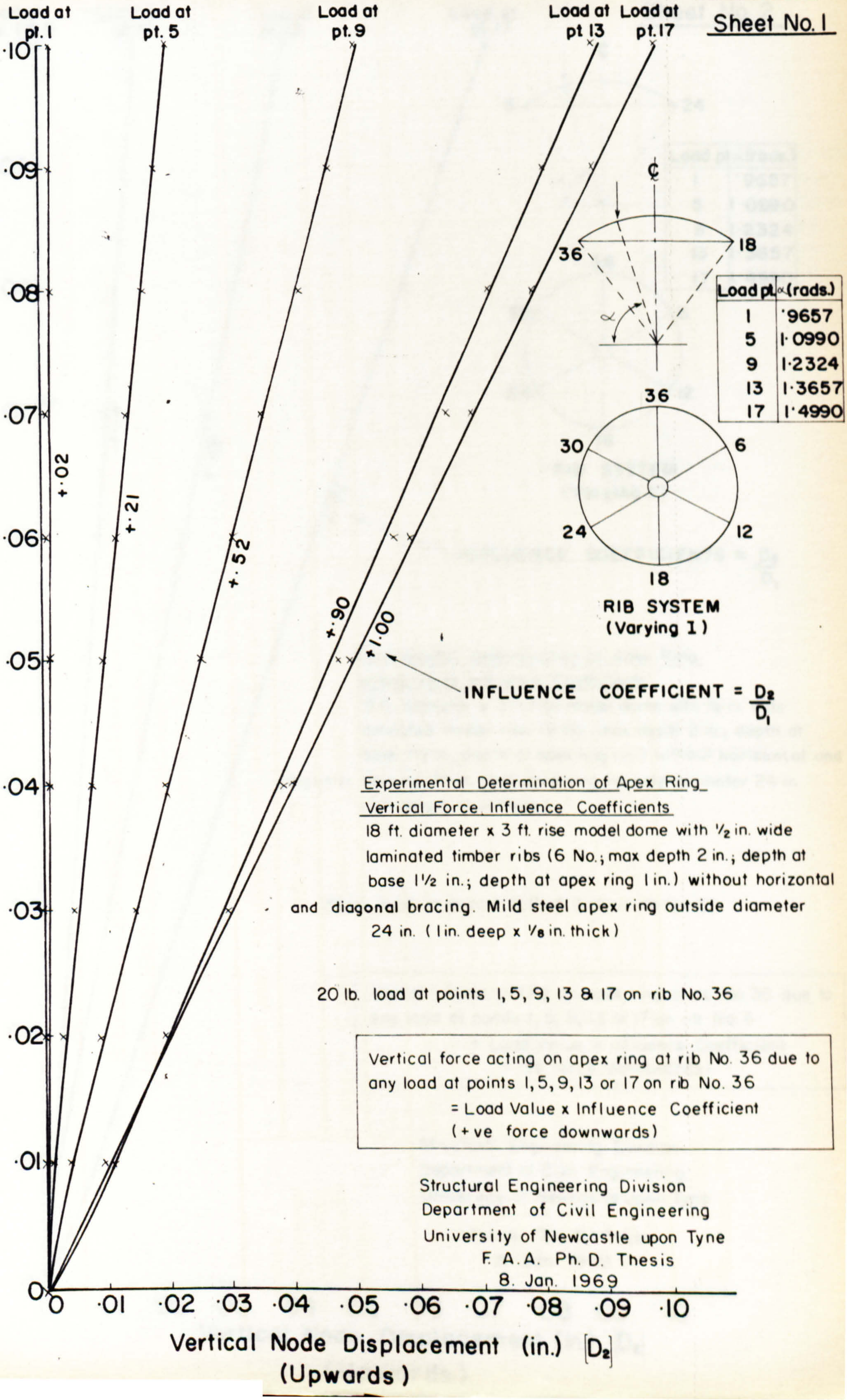

Load pt	α (rads.)
1	·9657
5	1·0990
9	1·2324
13	1·3657
17	1·4990

RIB SYSTEM
(Varying 1)

INFLUENCE COEFFICIENT = $\frac{D_2}{D_1}$

Experimental Determination of Apex Ring
Vertical Force Influence Coefficients

18 ft. diameter x 3 ft. rise model dome with ½ in. wide laminated timber ribs (6 No.; max depth 2 in.; depth at base 1½ in.; depth at apex ring 1 in.) without horizontal and diagonal bracing. Mild steel apex ring outside diameter 24 in. (1 in. deep x ⅛ in. thick)

20 lb. load at points 1, 5, 9, 13 & 17 on rib No. 36

Vertical force acting on apex ring at rib No. 36 due to any load at points 1, 5, 9, 13 or 17 on rib No. 36
= Load Value x Influence Coefficient
(+ve force downwards)

Structural Engineering Division
Department of Civil Engineering
University of Newcastle upon Tyne
F. A. A. Ph. D. Thesis
8. Jan. 1969

TESTS ON MODEL RADIAL RIBBED DOME

Test No. 8
Sheet No. 2

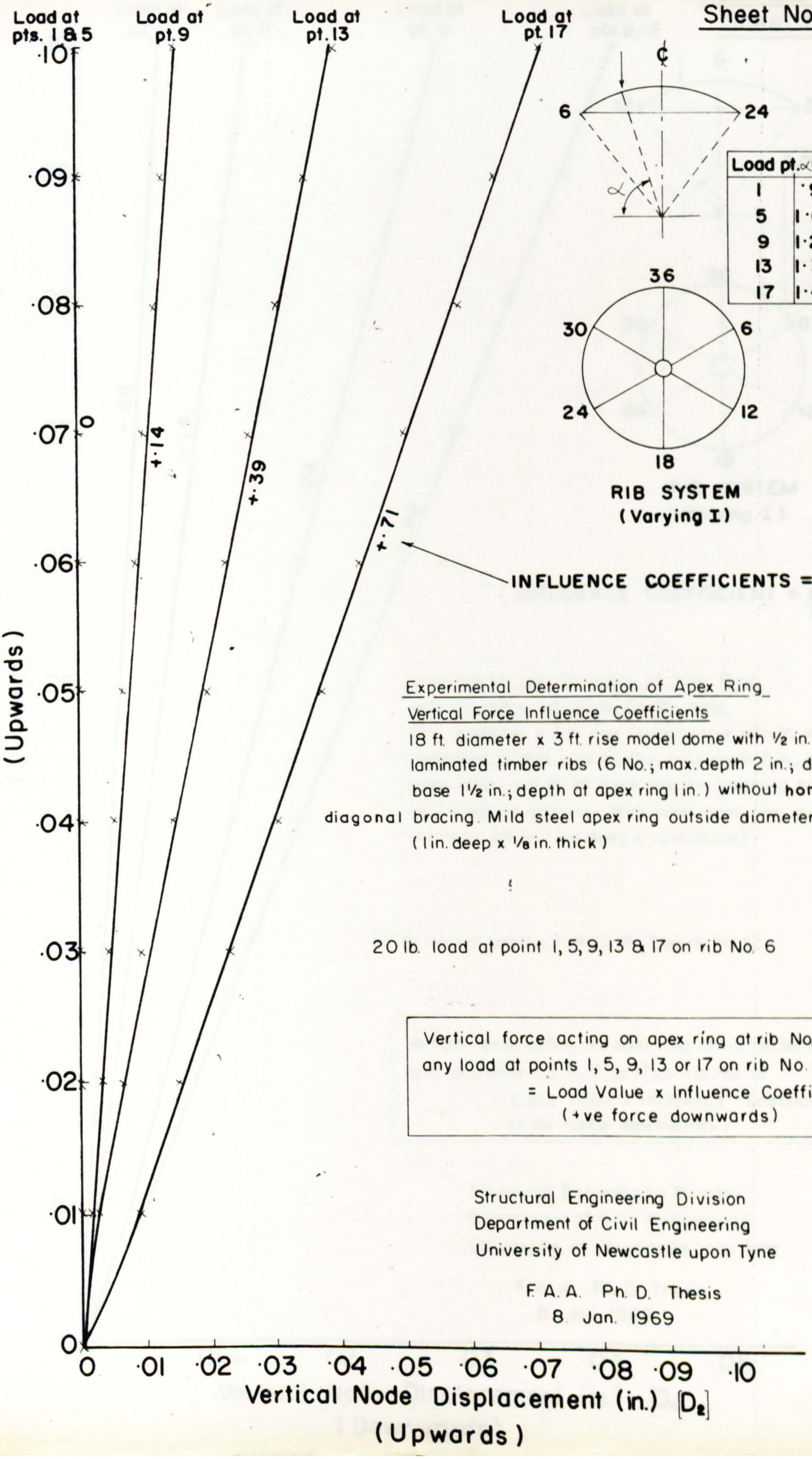

Load pt.	α (rads.)
1	·9657
5	1·0990
9	1·2324
13	1·3657
17	1·4990

RIB SYSTEM
(Varying I)

INFLUENCE COEFFICIENTS = $\frac{D_2}{D_1}$

Experimental Determination of Apex Ring
Vertical Force Influence Coefficients

18 ft. diameter x 3 ft. rise model dome with ½ in. wide laminated timber ribs (6 No.; max. depth 2 in.; depth at base 1½ in.; depth at apex ring 1 in.) without horizontal and diagonal bracing. Mild steel apex ring outside diameter 24 in. (1 in. deep x ⅛ in. thick)

20 lb. load at point 1, 5, 9, 13 & 17 on rib No. 6

Vertical force acting on apex ring at rib No. 36 due to any load at points 1, 5, 9, 13 or 17 on rib No. 6
= Load Value x Influence Coefficient
(+ve force downwards)

Structural Engineering Division
Department of Civil Engineering
University of Newcastle upon Tyne

F. A. A. Ph. D. Thesis
8 Jan. 1969

TESTS ON MODEL RADIAL RIBBED DOME

Test No. 8
Sheet No. 3

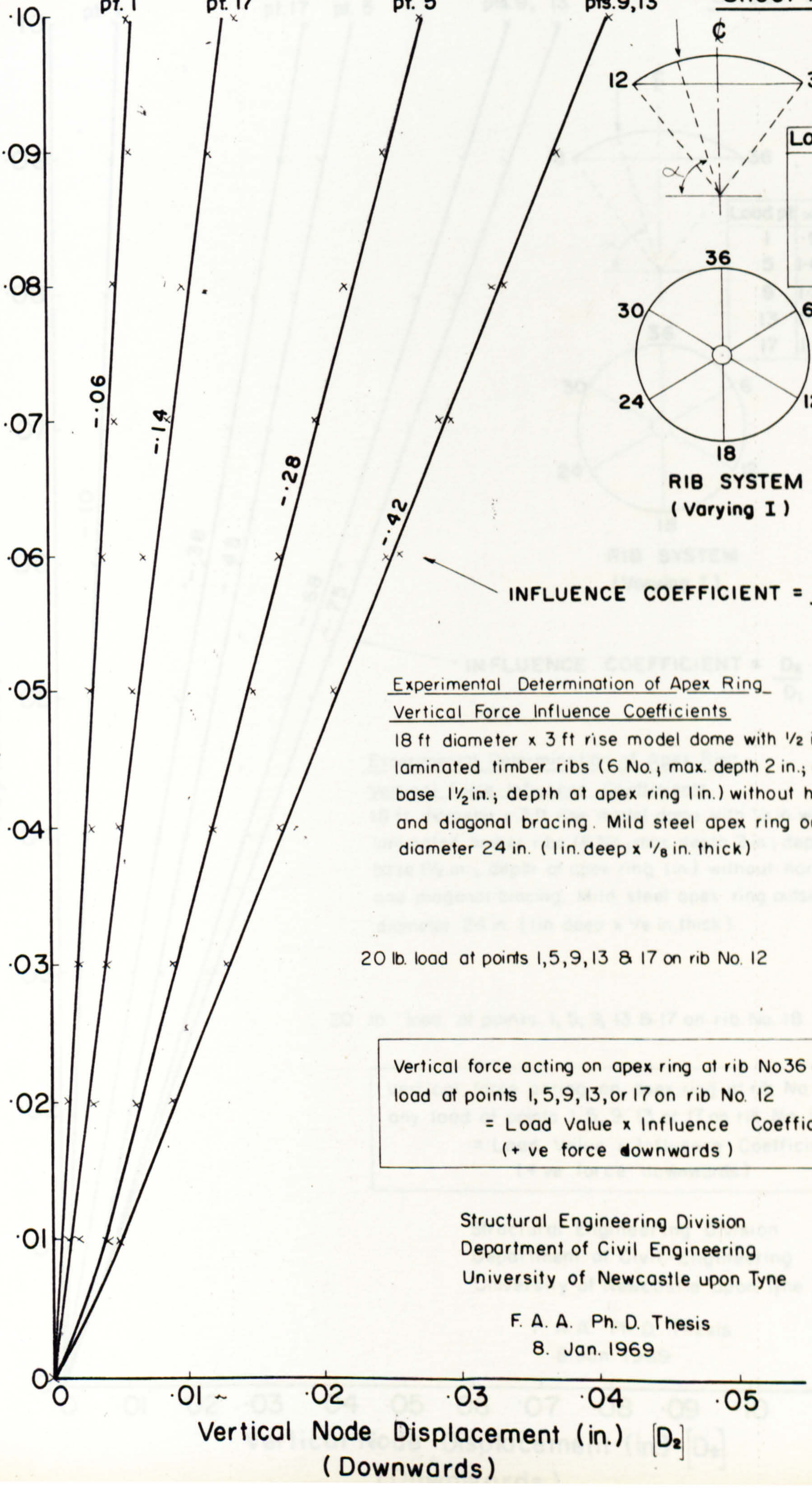

Load pt.	α (rads.)
1	·9657
5	1·0990
9	1·2324
13	1·3657
17	1·4990

RIB SYSTEM
(Varying I)

INFLUENCE COEFFICIENT = $\frac{D_2}{D_1}$

Experimental Determination of Apex Ring
Vertical Force Influence Coefficients

18 ft diameter x 3 ft rise model dome with ½ in. wide laminated timber ribs (6 No.; max. depth 2 in.; depth at base 1½ in.; depth at apex ring 1 in.) without horizontal and diagonal bracing. Mild steel apex ring outside diameter 24 in. (1 in. deep x ⅛ in. thick)

20 lb. load at points 1, 5, 9, 13 & 17 on rib No. 12

Vertical force acting on apex ring at rib No 36 due to any load at points 1, 5, 9, 13, or 17 on rib No. 12
= Load Value x Influence Coefficient
(+ ve force downwards)

Structural Engineering Division
Department of Civil Engineering
University of Newcastle upon Tyne

F. A. A. Ph. D. Thesis
8. Jan. 1969

TESTS ON MODEL RADIAL RIBBED DOME

Test No. 8

Sheet No. 4

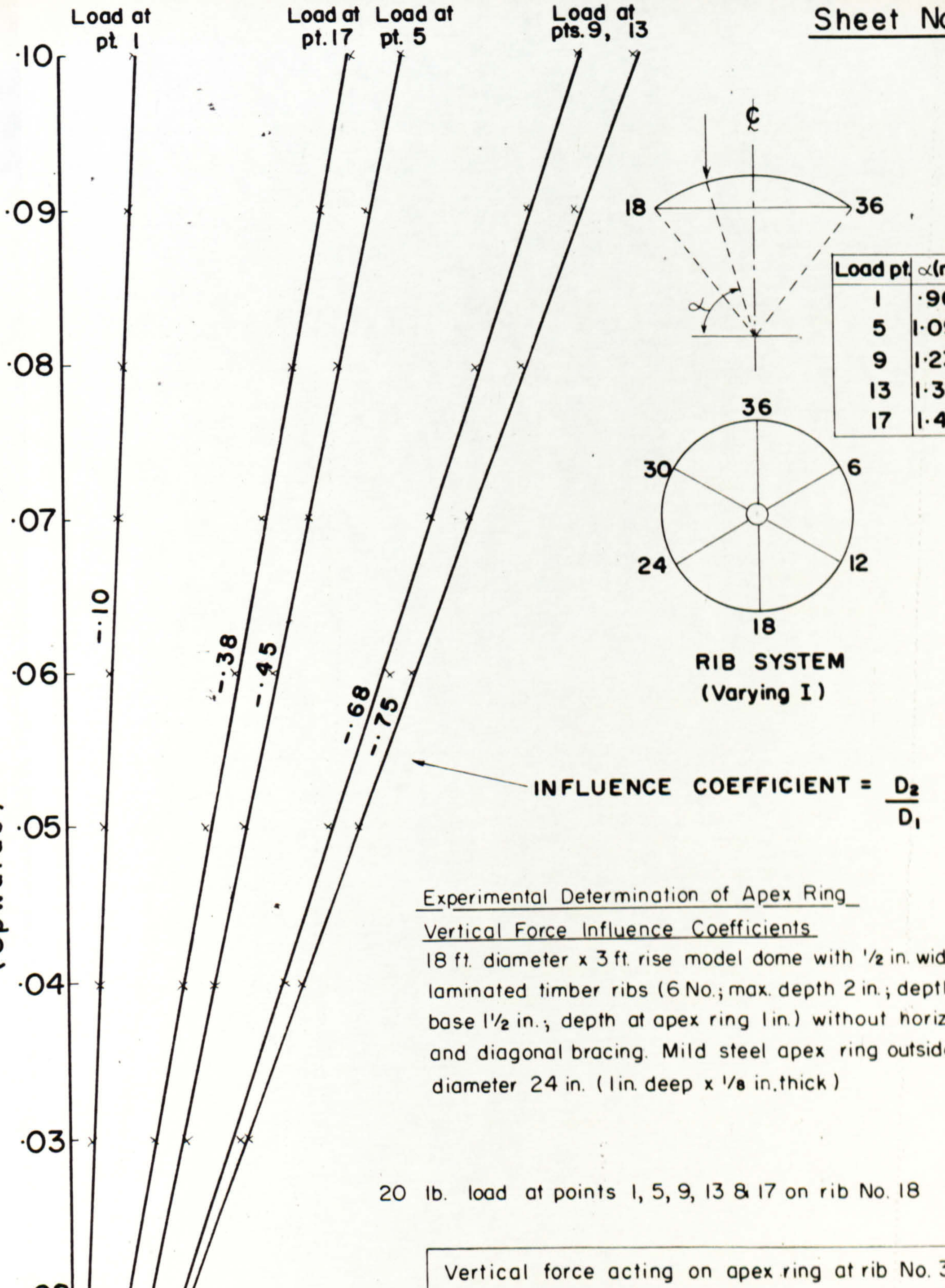

Load pt.	α (rads.)
1	·9657
5	1·0990
9	1·2324
13	1·3657
17	1·4990

RIB SYSTEM
(Varying I)

INFLUENCE COEFFICIENT = $\frac{D_2}{D_1}$

Experimental Determination of Apex Ring
Vertical Force Influence Coefficients

18 ft. diameter x 3 ft. rise model dome with ½ in. wide laminated timber ribs (6 No.; max. depth 2 in.; depth at base 1½ in.; depth at apex ring 1 in.) without horizontal and diagonal bracing. Mild steel apex ring outside diameter 24 in. (1 in. deep x ⅛ in. thick)

20 lb. load at points 1, 5, 9, 13 & 17 on rib No. 18

Vertical force acting on apex ring at rib No. 36 due to any load at points 1, 5, 9, 13 or 17 on rib No. 18
= Load Value x Influence Coefficient
(+ ve force downwards)

Structural Engineering Division
Department of Civil Engineering
University of Newcastle upon Tyne

F. A. A. Ph. D. Thesis
8. Jan. 1969

Structural Engineering Division
Department of Civil Engineering
University of Newcastle upon Tyne

TESTS ON MODEL RADIAL RIBBED DOME

Test No. 8
Sheet No. 5

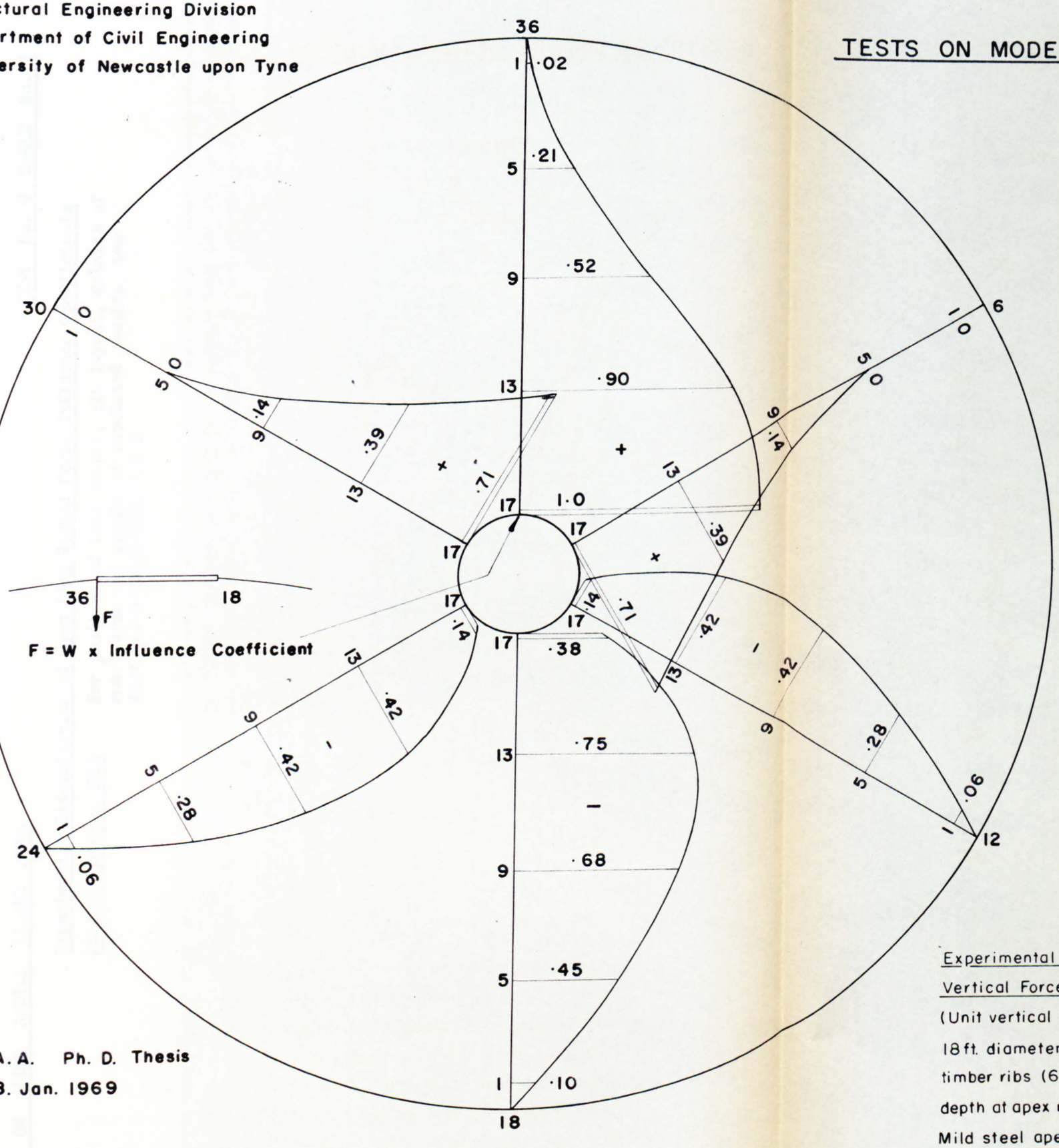

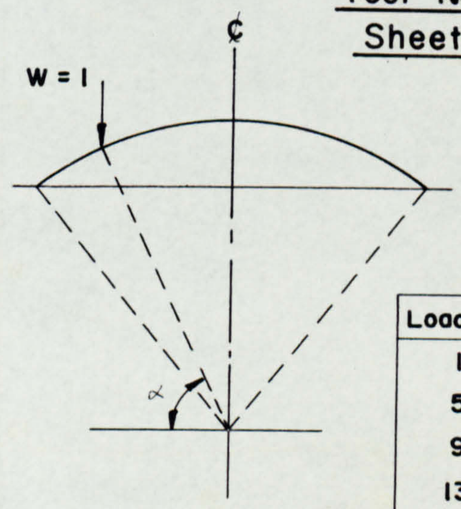

Load pt.	∝ (rads.)
1	·9657
5	1·0990
9	1·2324
13	1·3657
17	1·4990

0 ·5 1·0
SCALE

F. A. A. Ph. D. Thesis
8. Jan. 1969

Experimental Determination of Apex Ring
Vertical Force Influence Lines for Rib No. 36
(Unit vertical force acting at any angle on any rib)
18 ft. diameter x 3 ft. rise model dome with ½ in. wide laminated timber ribs (6 No. of varying I; max. depth 2 in.; depth at base 1½ in.; depth at apex ring 1 in.) without horizontal and diagonal bracing.
Mild steel apex ring outside diameter 24 in. (1 in. deep x ⅛ in. thick)

TESTS ON MODEL RADIAL RIBBED DOME

TEST No. 9 TABLE No. 1

Experimental Determination of Apex Ring Radial Force Influence Coefficients

Load at point = 20lb

For position of load points, rib layout, details of model dome and graphs of tabulated results, see Test No. 9 Sheet Nos. 1 & 2

Radial Displacement of Apex Ring at Rib No. 36 (outwards from centre of ring)	Dial gauge readings (A) and actual vertical displacement of point load (B; +ve upwards) in inches																			
	Rib No. 36										Rib No. 30									
	Point 1		Point 5		Point 9		Point 13		Point 17		Point 1		Point 5		Point 9		Point 13		Point 17	
	A	B	A	B	A	B	A	B	A	B	A	B	A	B	A	B	A	B	A	B
0 in.	.446	.000	.306	.000	.103	.000	.251	.000	.259	.000	.441	.000	.282	.000	.097	.000	.239	.000	.229	.000
.01 in.	.449	+.003	.316	+.010	.118	+.015	.267	+.016	.267	+.008	.441	.000	.282	.000	.098	+.001	.241	+.002	.231	+.002
.02 in.	.451	+.005	.327	+.021	.136	+.033	.287	+.036	.276	+.017	.441	.000	.283	+.001	.100	+.003	.243	+.004	.235	+.006
.03 in.	.454	+.008	.338	+.032	.154	+.051	.307	+.056	.286	+.027	.441	.000	.283	+.001	.101	+.004	.246	+.007	.239	+.010
.04 in.	.456	+.010	.349	+.043	.171	+.068	.325	+.074	.295	+.036	.441	.000	.284	+.002	.103	+.006	.249	+.010	.243	+.014
.05 in.	.459	+.013	.361	+.055	.188	+.085	.343	+.092	.305	+.046	.441	.000	.285	+.003	.105	+.008	.252	+.013	.246	+.017
.06 in.	.461	+.015	.371	+.065	.204	+.101	.361	+.110	.315	+.056	.442	+.001	.285	+.003	.107	+.010	.255	+.016	.250	+.021
.07 in.	.463	+.017	.383	+.077	.221	+.118	.379	+.128	.324	+.065	.442	+.001	.286	+.004	.108	+.011	.258	+.019	.254	+.025
.08 in.	.466	+.020	.395	+.089	.238	+.135	.398	+.147	.333	+.074	.442	+.001	.287	+.005	.110	+.013	.262	+.023	.258	+.029
.09 in.	.468	+.022	.406	+.100	.255	+.152	.417	+.166	.343	+.084	.442	+.001	.288	+.006	.112	+.015	.265	+.026	.263	+.034
.10 in.	.470	+.024	.417	+.111	.273	+.170	.434	+.183	.352	+.093	.443	+.002	.289	+.007	.114	+.017	.268	+.029	.266	+.037

F. A. A. Ph.D. Thesis
9th Jan., 1969

Structural Engineering Division,
Department of Civil Engineering,
Newcastle upon Tyne University.

TESTS ON MODEL RADIAL RIBBED DOME

TEST No. 9 TABLE No. 2

Experimental Determination of Apex Ring Radial Force Influence Coefficients

Load at point = 20lb

For position of load points, rib layout, details of model dome and graphs of tabulated results, see Test No. 9 Sheet Nos. 3 & 4

Radial Displacement of Apex Ring at Rib No. 36 (Outwards from centre of ring)	Dial gauge readings (A) and actual vertical displacement of point load (B; +ve upwards) in inches																			
	Rib No. 24										Rib No. 18									
	Point 1		Point 5		Point 9		Point 13		Point 17		Point 1		Point 5		Point 9		Point 13		Point 17	
	A	B	A	B	A	B	A	B	A	B	A	B	A	B	A	B	A	B	A	B
0 in.	.441	.000	.233	.000	.200	.000	.152	.000	.193	.000	.447	.000	.288	.000	.079	.000	.140	.000	.137	.000
.01 in.	.439	-.002	.227	-.006	.193	-.007	.143	-.009	.187	-.006	.445	-.002	.283	-.005	.070	-.009	.130	-.010	.129	-.008
.02 in.	.438	-.003	.222	-.011	.186	-.014	.135	-.017	.181	-.012	.444	-.003	.278	-.010	.062	-.017	.121	-.019	.121	-.016
.03 in.	.437	-.004	.218	-.015	.180	-.020	.127	-.025	.176	-.017	.443	-.004	.273	-.015	.054	-.025	.111	-.029	.113	-.024
.04 in.	.436	-.005	.213	-.020	.173	-.027	.118	-.034	.170	-.023	.442	-.005	.268	-.020	.046	-.033	.102	-.038	.106	-.031
.05 in.	.435	-.006	.208	-.025	.166	-.034	.110	-.042	.164	-.029	.441	-.006	.263	-.025	.039	-.040	.092	-.048	.098	-.039
.06 in.	.434	-.007	.204	-.029	.159	-.041	.101	-.051	.158	-.035	.440	-.007	.259	-.029	.031	-.048	.082	-.058	.089	-.048
.07 in.	.433	-.008	.199	-.034	.153	-.047	.093	-.059	.152	-.041	.439	-.008	.254	-.034	.023	-.056	.072	-.068	.080	-.057
.08 in.	.432	-.009	.195	-.038	.146	-.054	.085	-.067	.146	-.047	.438	-.009	.249	-.039	.015	-.064	.062	-.078	.072	-.065
.09 in.	.431	-.010	.190	-.043	.139	-.061	.077	-.075	.141	-.052	.437	-.010	.244	-.044	.008	-.071	.052	-.088	.063	-.074
.10 in.	.431	-.010	.186	-.047	.133	-.067	.069	-.083	.135	-.058	.436	-.011	.240	-.048	.000	-.079	.043	-.097	.054	-.083

F. A. A. Ph.D. Thesis
9th Jan., 1969

Structural Engineering Division,
Department of Civil Engineering,
University of Newcastle upon Tyne.

TESTS ON MODEL RADIAL RIBBED DOME

Test No. 9

Sheet No. 1

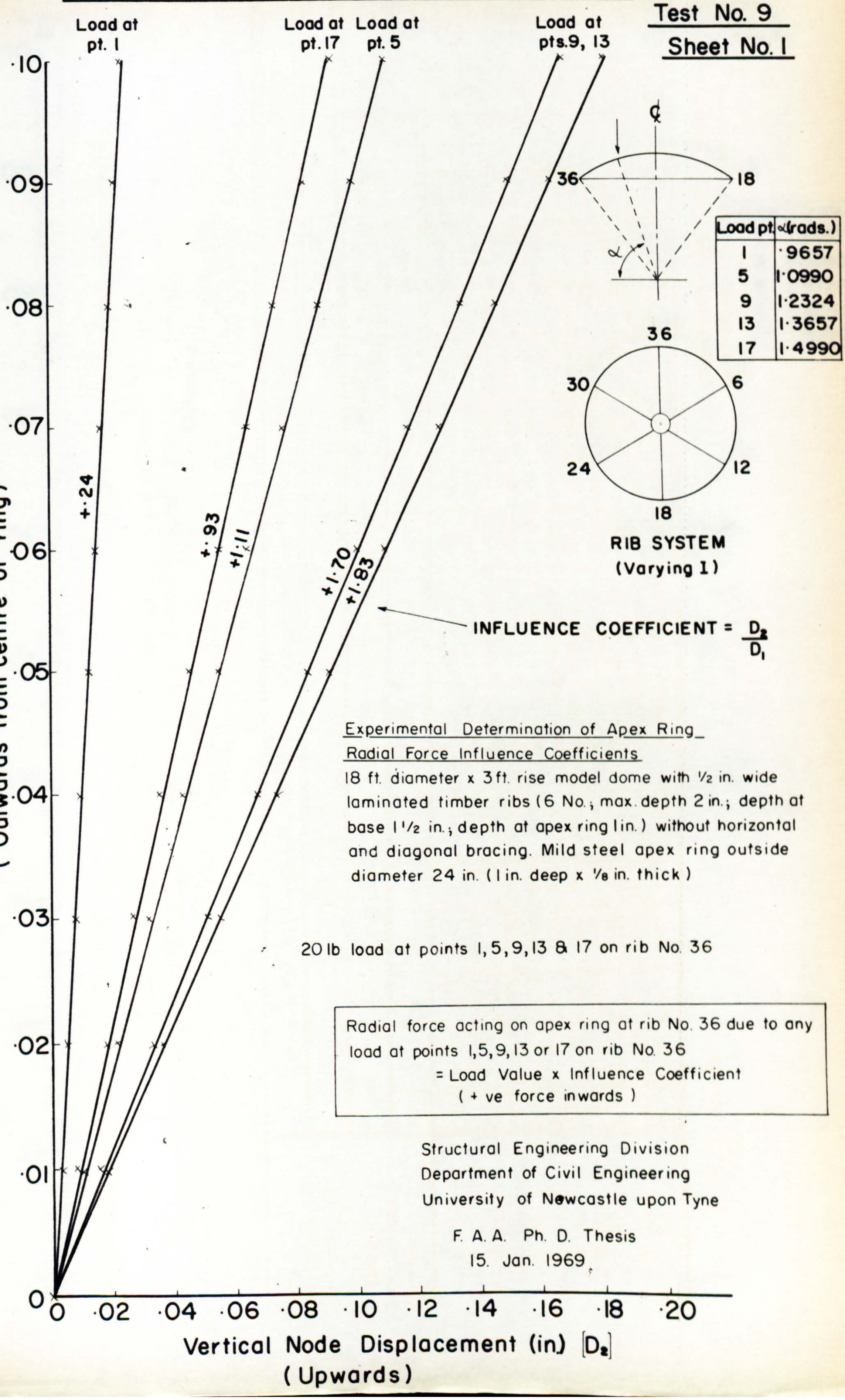

Experimental Determination of Apex Ring Radial Force Influence Coefficients

18 ft. diameter x 3 ft. rise model dome with ½ in. wide laminated timber ribs (6 No.; max. depth 2 in.; depth at base 1½ in.; depth at apex ring 1 in.) without horizontal and diagonal bracing. Mild steel apex ring outside diameter 24 in. (1 in. deep x ⅛ in. thick)

20 lb load at points 1, 5, 9, 13 & 17 on rib No. 36

Radial force acting on apex ring at rib No. 36 due to any load at points 1, 5, 9, 13 or 17 on rib No. 36
= Load Value x Influence Coefficient
(+ ve force inwards)

Structural Engineering Division
Department of Civil Engineering
University of Newcastle upon Tyne

F. A. A. Ph. D. Thesis
15. Jan. 1969

TESTS ON MODEL RADIAL RIBBED DOME

Test No. 9

Sheet No. 2

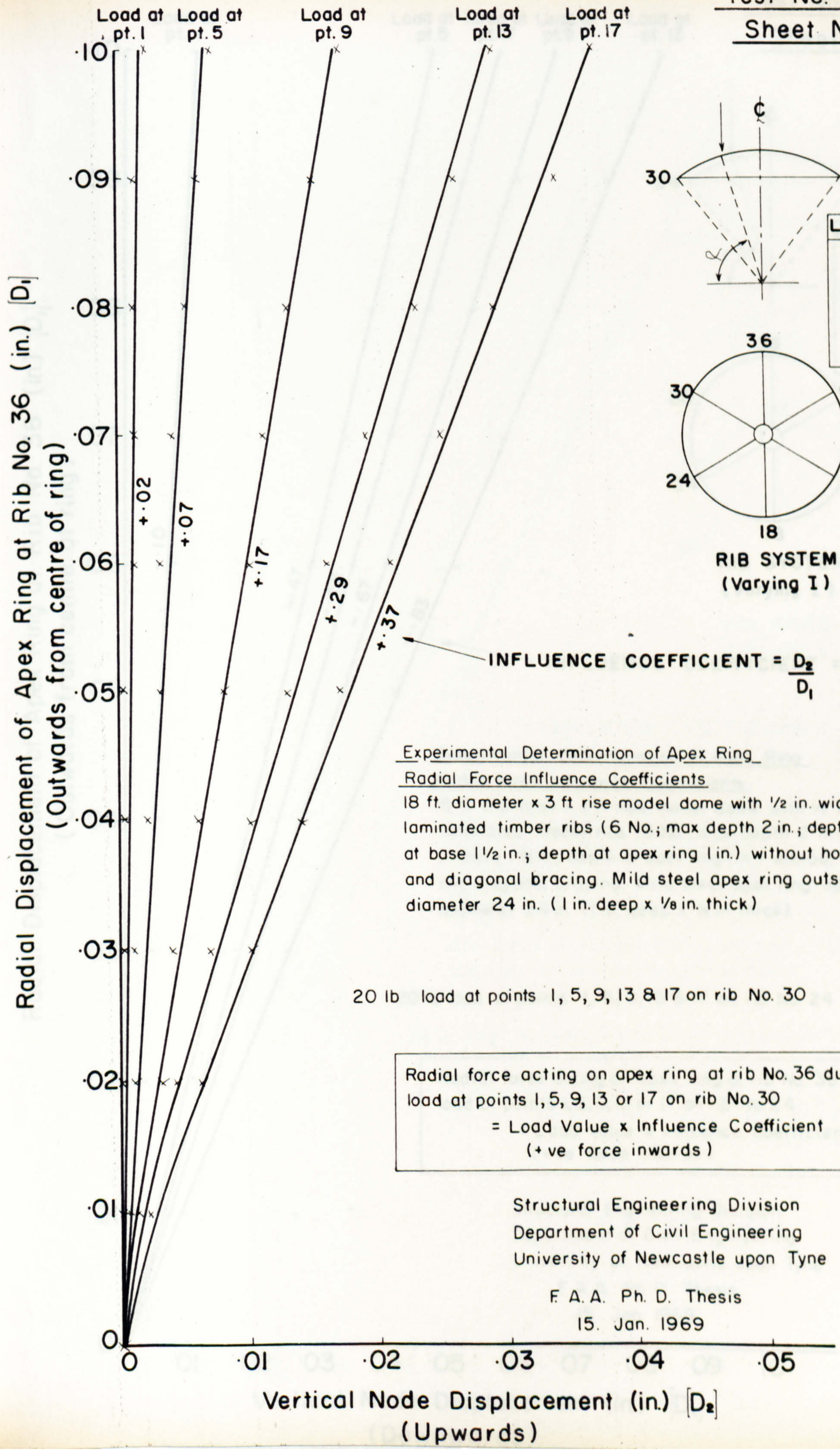

Load pt.	α (rads.)
1	·9657
5	1·0990
9	1·2324
13	1·3657
17	1·4990

RIB SYSTEM
(Varying I)

INFLUENCE COEFFICIENT = $\frac{D_2}{D_1}$

Experimental Determination of Apex Ring
Radial Force Influence Coefficients

18 ft. diameter x 3 ft rise model dome with ½ in. wide laminated timber ribs (6 No.; max depth 2 in.; depth at base 1½ in.; depth at apex ring 1 in.) without horizontal and diagonal bracing. Mild steel apex ring outside diameter 24 in. (1 in. deep x ⅛ in. thick)

20 lb load at points 1, 5, 9, 13 & 17 on rib No. 30

Radial force acting on apex ring at rib No. 36 due to any load at points 1, 5, 9, 13 or 17 on rib No. 30
= Load Value x Influence Coefficient
(+ ve force inwards)

Structural Engineering Division
Department of Civil Engineering
University of Newcastle upon Tyne

F. A. A. Ph. D. Thesis
15. Jan. 1969

TESTS ON MODEL RADIAL RIBBED DOME

Test No. 9

Sheet No. 3

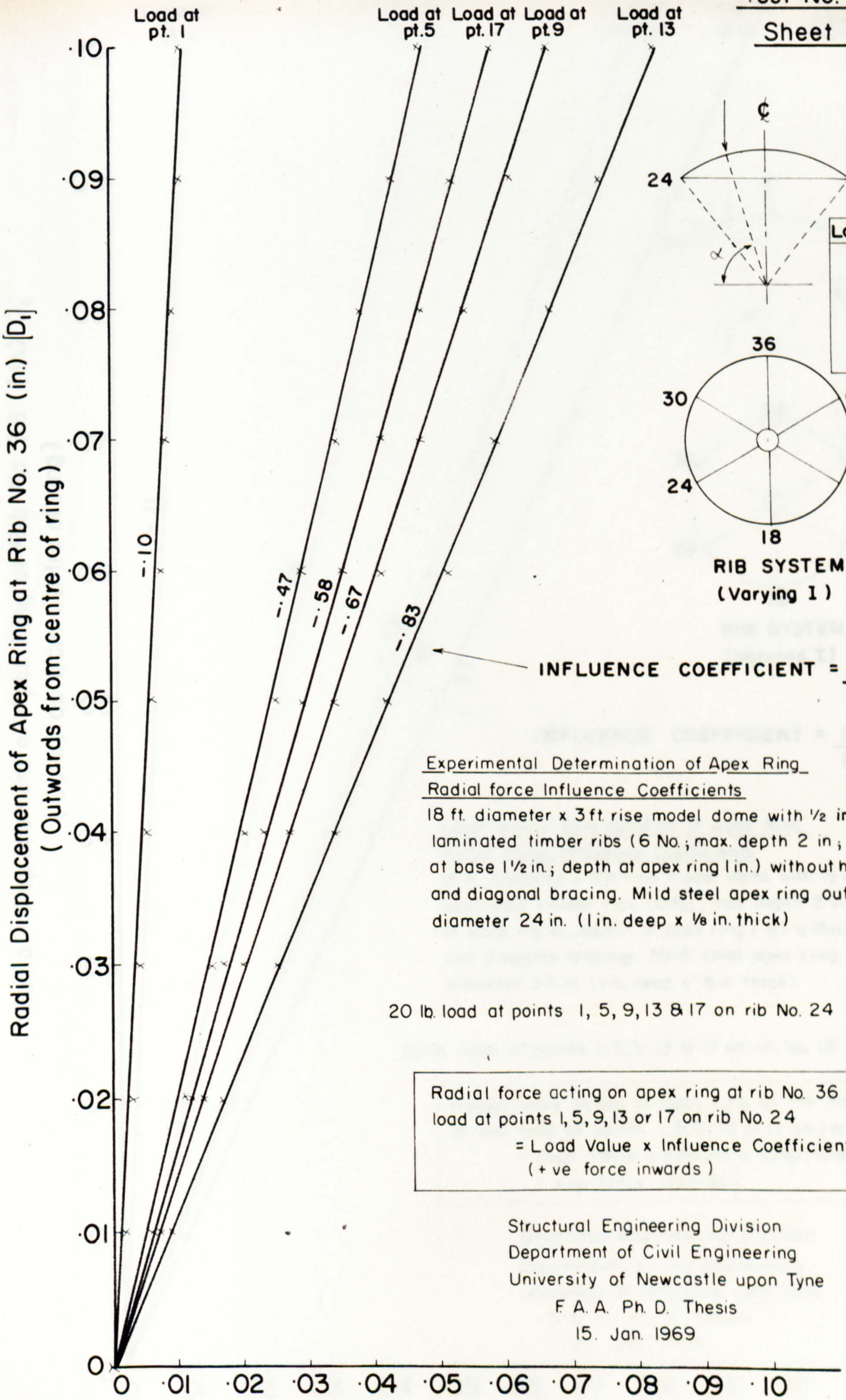

Load pt.	α (rads.)
1	·9657
5	1·0990
9	1·2324
13	1·3657
17	1·4990

RIB SYSTEM
(Varying 1)

INFLUENCE COEFFICIENT = $\frac{D_2}{D_1}$

Experimental Determination of Apex Ring
Radial force Influence Coefficients

18 ft. diameter x 3 ft. rise model dome with ½ in. wide laminated timber ribs (6 No.; max. depth 2 in; depth at base 1½ in.; depth at apex ring 1 in.) without horizontal and diagonal bracing. Mild steel apex ring outside diameter 24 in. (1 in. deep x ⅛ in. thick)

20 lb. load at points 1, 5, 9, 13 & 17 on rib No. 24

Radial force acting on apex ring at rib No. 36 due to any load at points 1, 5, 9, 13 or 17 on rib No. 24
= Load Value x Influence Coefficient
(+ ve force inwards)

Structural Engineering Division
Department of Civil Engineering
University of Newcastle upon Tyne
F. A. A. Ph. D. Thesis
15. Jan. 1969

TESTS ON MODEL RADIAL RIBBED DOME

Test No. 9

Sheet No. 4

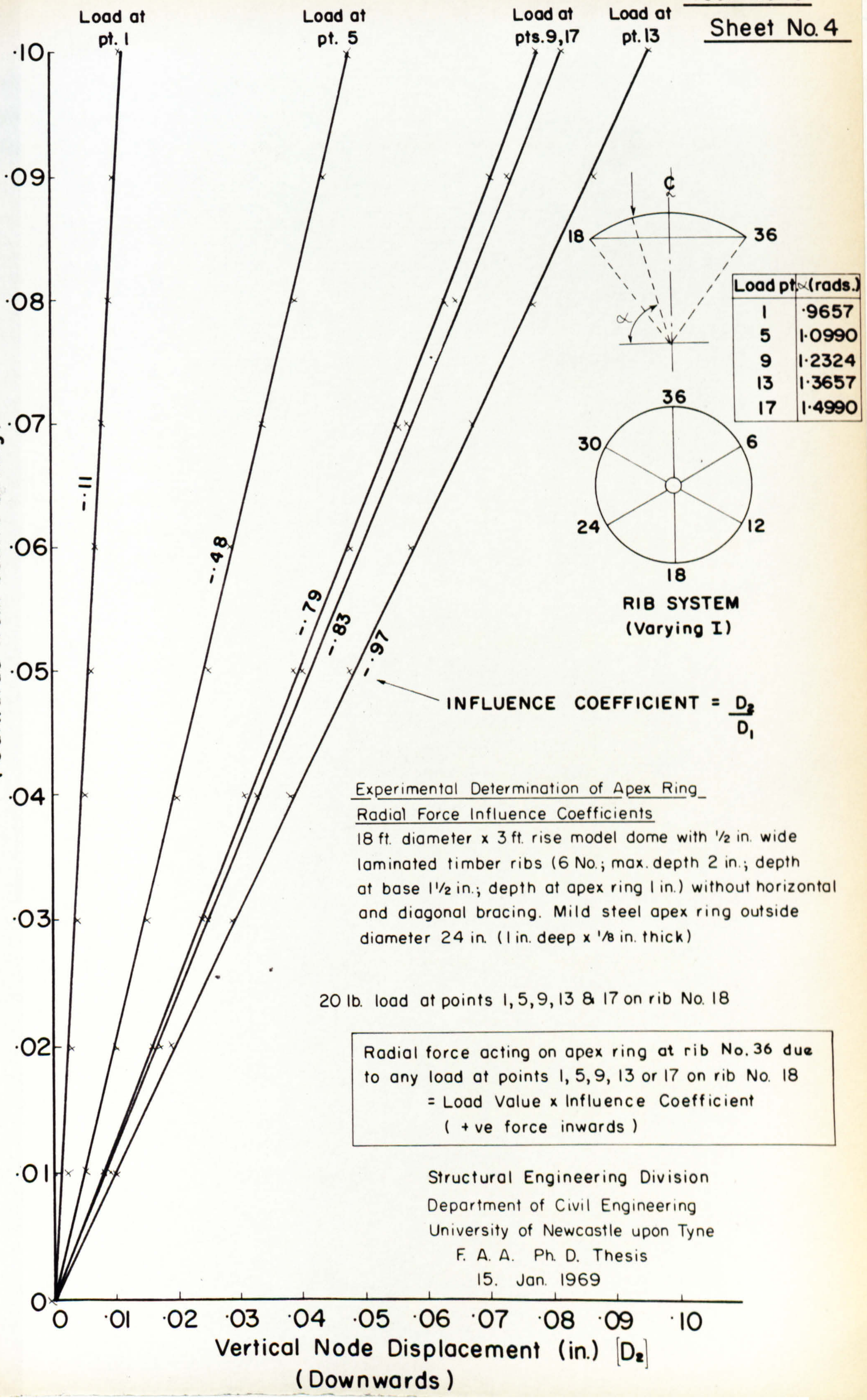

Load pt.	α (rads.)
1	·9657
5	1·0990
9	1·2324
13	1·3657
17	1·4990

RIB SYSTEM
(Varying I)

INFLUENCE COEFFICIENT = $\frac{D_2}{D_1}$

Experimental Determination of Apex Ring Radial Force Influence Coefficients

18 ft. diameter x 3 ft. rise model dome with ½ in. wide laminated timber ribs (6 No.; max. depth 2 in.; depth at base 1½ in.; depth at apex ring 1 in.) without horizontal and diagonal bracing. Mild steel apex ring outside diameter 24 in. (1 in. deep x ⅛ in. thick)

20 lb. load at points 1, 5, 9, 13 & 17 on rib No. 18

Radial force acting on apex ring at rib No. 36 due to any load at points 1, 5, 9, 13 or 17 on rib No. 18
= Load Value x Influence Coefficient
(+ ve force inwards)

Structural Engineering Division
Department of Civil Engineering
University of Newcastle upon Tyne

F. A. A. Ph. D. Thesis
15. Jan. 1969

Structural Engineering Division
Department of Civil Engineering
University of Newcastle upon Tyne

TESTS ON MODEL RADIAL RIBBED DOME

Test No. 9
Sheet No. 5

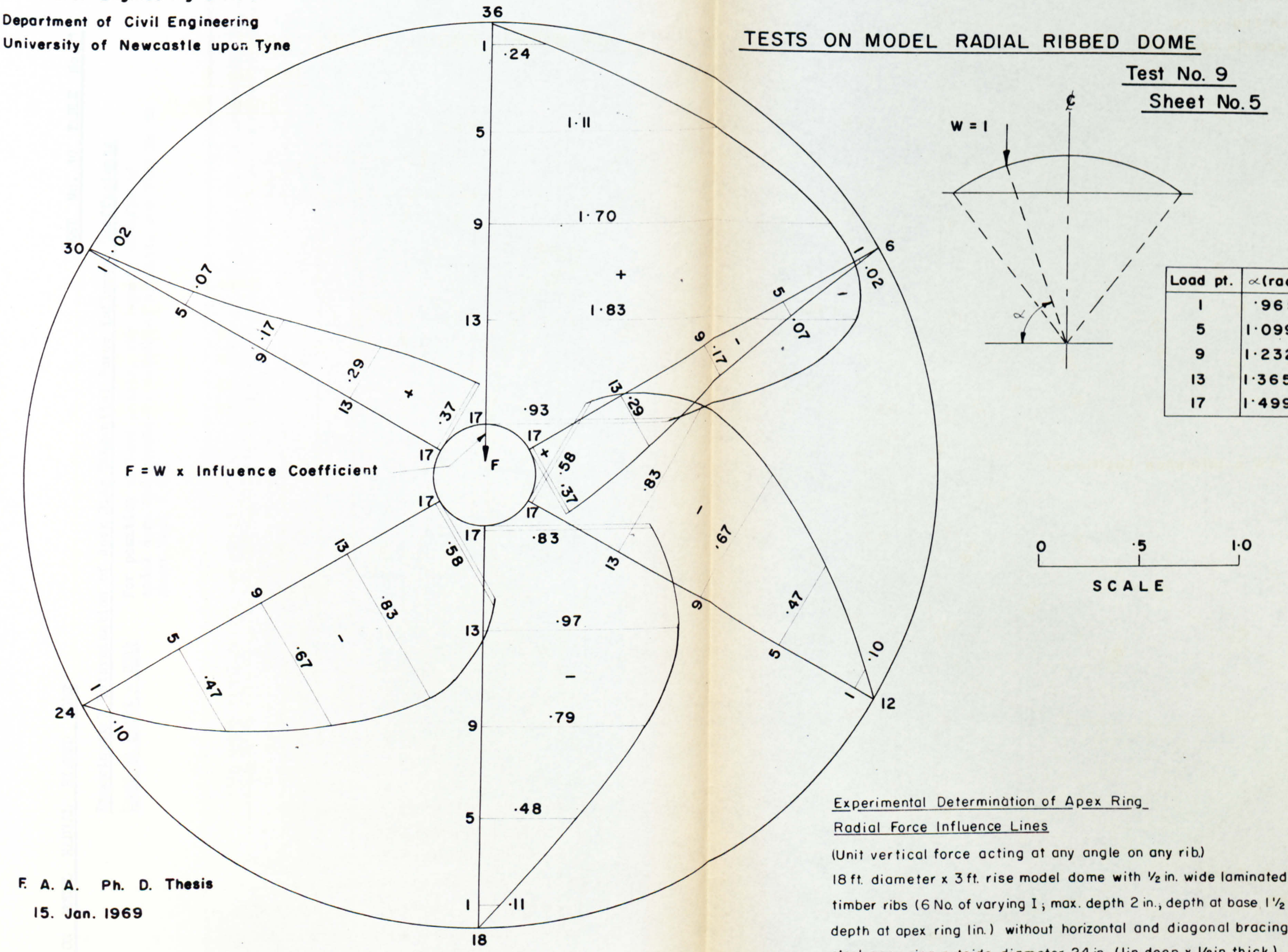

Load pt.	∝(rads.)
1	·9657
5	1·0990
9	1·2324
13	1·3657
17	1·4990

Experimental Determination of Apex Ring Radial Force Influence Lines

(Unit vertical force acting at any angle on any rib.)

18 ft. diameter x 3 ft. rise model dome with ½ in. wide laminated timber ribs (6 No. of varying I; max. depth 2 in., depth at base 1½ in., depth at apex ring 1in.) without horizontal and diagonal bracing. Mild steel apex ring outside diameter 24 in. (1in. deep x ⅛in. thick.)

F. A. A. Ph. D. Thesis
15. Jan. 1969

TESTS ON MODEL RADIAL RIBBED DOME

TEST No. 10 TABLE No. 1

Experimental Determination of Apex Ring Tangential Force Influence Coefficients

Load at point = 20lb

For position of load points, rib layout, details of model dome and graphs of tabulated results, see Test No 10 Sheet Nos. 1 & 2

Tangential Displacement of Apex Ring at Rib No.36 (Anti-clockwise viewed from above	Dial gauge readings (A) and actual vertical displacement of point load (B; +ve downwards) in inches																			
	Rib No. 36										Rib No. 6									
	Point 1		Point 5		Point 9		Point 13		Point 17		Point 1		Point 5		Point 9		Point 13		Point 17	
	A	B	A	B	A	B	A	B	A	B	A	B	A	B	A	B	A	B	A	B
0 in.	.448	.000	.312	.000	.129	.000	.242	.000	.293	.000	.439	.000	.249	.000	.127	.000	.220	.000	.330	.000
.02 in.	.448	.000	.312	.000	.128	+.001	.240	+.002	.291	+.002	.437	+.002	.244	+.005	.120	+.007	.213	+.007	.326	+.004
.04 in.	.448	.000	.311	+.001	.127	+.002	.239	+.003	.289	+.004	.436	+.003	.240	+.009	.114	+.013	.208	+.012	.320	+.010
.06 in.	.448	.000	.310	+.002	.126	+.003	.238	+.004	.288	+.005	.435	+.004	.236	+.013	.108	+.019	.202	+.018	.315	+.015
.08 in.	.448	.000	.310	+.002	.125	+.004	.237	+.005	.286	+.007	.434	+.005	.231	+.018	.102	+.025	.197	+.023	.309	+.021
.10 in.	.448	.000	.310	+.002	.124	+.005	.235	+.007	.284	+.009	.433	+.006	.226	+.023	.096	+.031	.192	+.028	.303	+.027
.12 in.	.447	+.001	.309	+.003	.123	+.006	.233	+.009	.282	+.011	.432	+.007	.222	+.027	.090	+.037	.186	+.034	.296	+.034
.14 in.	.447	+.001	.308	+.004	.123	+.006	.232	+.010	.280	+.013	.431	+.008	.217	+.032	.084	+.043	.180	+.040	.290	+.040
.16 in.	.447	+.001	.308	+.004	.122	+.007	.230	+.012	.278	+.015	.429	+.010	.213	+.036	.079	+.048	.175	+.045	.284	+.046
.18 in.	.447	+.001	.307	+.005	.121	+.008	.228	+.014	.275	+.018	.428	+.011	.208	+.041	.073	+.054	.169	+.051	.278	+.052
.20 in.	.447	+.001	.307	+.005	.119	+.010	.226	+.016	.273	+.020	.427	+.012	.203	+.046	.068	+.059	.164	+.056	.271	+.059

F. A. A. Ph.D. Thesis
13th - 14th Jan, 1969

Structural Engineering Division,
Department of Civil Engineering,
University of Newcastle upon Tyne.

TESTS ON MODEL RADIAL RIBBED DOME

TEST No. 10 TABLE No. 2

Experimental Determination of Apex Ring Tangential Force Influence Coefficients

Load at point = 20lb

For position of load points, rib layout, details of model dome and graphs of tabulated results, see Test No. 10 Sheet Nos. 3 & 1

Tangential Displacement of Apex Ring at Rib No.36 (Anti-clockwise viewed from above)	Dial gauge readings (A) and actual vertical displacement of point load (B; +ve downwards) in inches																			
	Rib No. 12										Rib No. 18									
	Point 1		Point 5		Point 9		Point 13		Point 17		Point 1		Point 5		Point 9		Point 13		Point 17	
	A	B	A	B	A	B	A	B	A	B	A	B	A	B	A	B	A	B	A	B
0 in.	.447	.000	.295	.000	.067	.000	.185	.000	.133	.000	.438	.000	.281	.000	.067	.000	.113	.000	.110	.000
.02 in.	.446	+.001	.292	+.003	.061	+.006	.178	+.007	.126	+.007	.438	.000	.280	+.001	.066	+.001	.112	+.001	.108	+.002
.04 in.	.445	+.002	.289	+.006	.056	+.011	.172	+.013	.120	+.013	.438	.000	.279	+.002	.064	+.003	.111	+.002	.105	+.005
.06 in.	.445	+.002	.286	+.009	.051	+.016	.166	+.019	.115	+.018	.437	+.001	.279	+.002	.063	+.004	.109	+.004	.101	+.009
.08 in.	.444	+.003	.283	+.012	.046	+.021	.160	+.025	.109	+.024	.437	+.001	.278	+.003	.061	+.006	.107	+.006	.096	+.014
.10 in.	.443	+.004	.280	+.015	.041	+.026	.154	+.031	.102	+.031	.437	+.001	.277	+.004	.060	+.007	.105	+.008	.091	+.019
.12 in.	.442	+.005	.277	+.018	.037	+.030	.149	+.036	.096	+.037	.437	+.001	.277	+.004	.058	+.009	.103	+.010	.087	+.023
.14 in.	.442	+.005	.274	+.021	.032	+.035	.143	+.042	.091	+.042	.437	+.001	.276	+.005	.057	+.010	.101	+.012	.083	+.027
.16 in.	.441	+.006	.271	+.024	.027	+.040	.136	+.049	.085	+.048	.437	+.001	.275	+.006	.056	+.011	.100	+.013	.079	+.031
.18 in.	.441	+.006	.268	+.027	.022	+.045	.130	+.055	.080	+.053	.437	+.001	.274	+.007	.055	+.012	.099	+.014	.075	+.035
.20 in.	.440	+.007	.265	+.030	.017	+.050	.124	+.061	.074	+.059	.437	+.001	.273	+.008	.053	+.014	.098	+.015	.070	+.040

F. A. A. Ph.D. Thesis
13th - 14th Jan., 1969

Structural Engineering Division,
Department of Civil Engineering,
University of Newcastle upon Tyne.

TESTS ON MODEL RADIAL RIBBED DOME

TEST No. 10 TABLE No. 3

Experimental Determination of Apex Ring Tangential Force Influence Coefficients

Load at point = 20lb

For position of load points, rib layout, details of model dome and graphs of tabulated results, see Test No. 10 Sheet Nos. 3 & 2

Tangential Displacement of Apex Ring at Rib No.36 (Anti-clockwise viewed from above)	Dial gauge readings (A) and actual vertical displacement of point load (B; +ve downwards) in inches																			
	Rib No. 24										Rib No. 30									
	Point 1		Point 5		Point 9		Point 13		Point 17		Point 1		Point 5		Point 9		Point 13		Point 17	
	A	B	A	B	A	B	A	B	A	B	A	B	A	B	A	B	A	B	A	B
0 in.	.439	.000	.231	.000	.103	.000	.153	.000	.200	.000	.440	.000	.328	.000	.090	.000	.214	.000	.210	.000
.02 in.	.439	.000	.232	-.001	.105	-.002	.154	-.001	.201	-.001	.441	-.001	.331	-.003	.093	-.003	.216	-.002	.212	-.002
.04 in.	.440	-.001	.234	-.003	.107	-.004	.156	-.003	.202	-.002	.442	-.002	.334	-.006	.095	-.005	.219	-.005	.213	-.003
.06 in.	.440	-.001	.236	-.005	.110	-.007	.158	-.005	.202	-.002	.442	-.002	.337	-.009	.098	-.008	.221	-.007	.214	-.004
.08 in.	.441	-.002	.238	-.007	.112	-.009	.160	-.007	.202	-.002	.443	-.003	.340	-.012	.101	-.011	.224	-.010	.214	-.004
.10 in.	.441	-.002	.240	-.009	.114	-.011	.162	-.009	.203	-.003	.444	-.004	.343	-.015	.104	-.014	.227	-.013	.215	-.005
.12 in.	.442	-.003	.242	-.011	.116	-.013	.164	-.011	.203	-.003	.445	-.005	.346	-.018	.106	-.016	.230	-.016	.215	-.005
.14 in.	.443	-.004	.244	-.013	.118	-.015	.165	-.012	.204	-.004	.446	-.006	.349	-.021	.109	-.019	.233	-.019	.215	-.005
.16 in.	.443	-.004	.246	-.015	.120	-.017	.167	-.014	.204	-.004	.446	-.006	.352	-.024	.111	-.021	.236	-.022	.216	-.006
.18 in.	.444	-.005	.247	-.016	.121	-.018	.168	-.015	.205	-.005	.447	-.007	.355	-.027	.114	-.024	.238	-.024	.216	-.006
.20 in.	.444	-.005	.249	-.018	.122	-.019	.169	-.016	.205	-.005	.448	-.008	.358	-.030	.117	-.027	.241	-.027	.216	-.006

F. A. A. Ph.D. Thesis
13th - 14th Jan., 1969

Structural Engineering Division,
Department of Civil Engineering,
University of Newcastle upon Tyne.

TESTS ON MODEL RADIAL RIBBED DOME

Test No. 10.

Sheet No. 1.

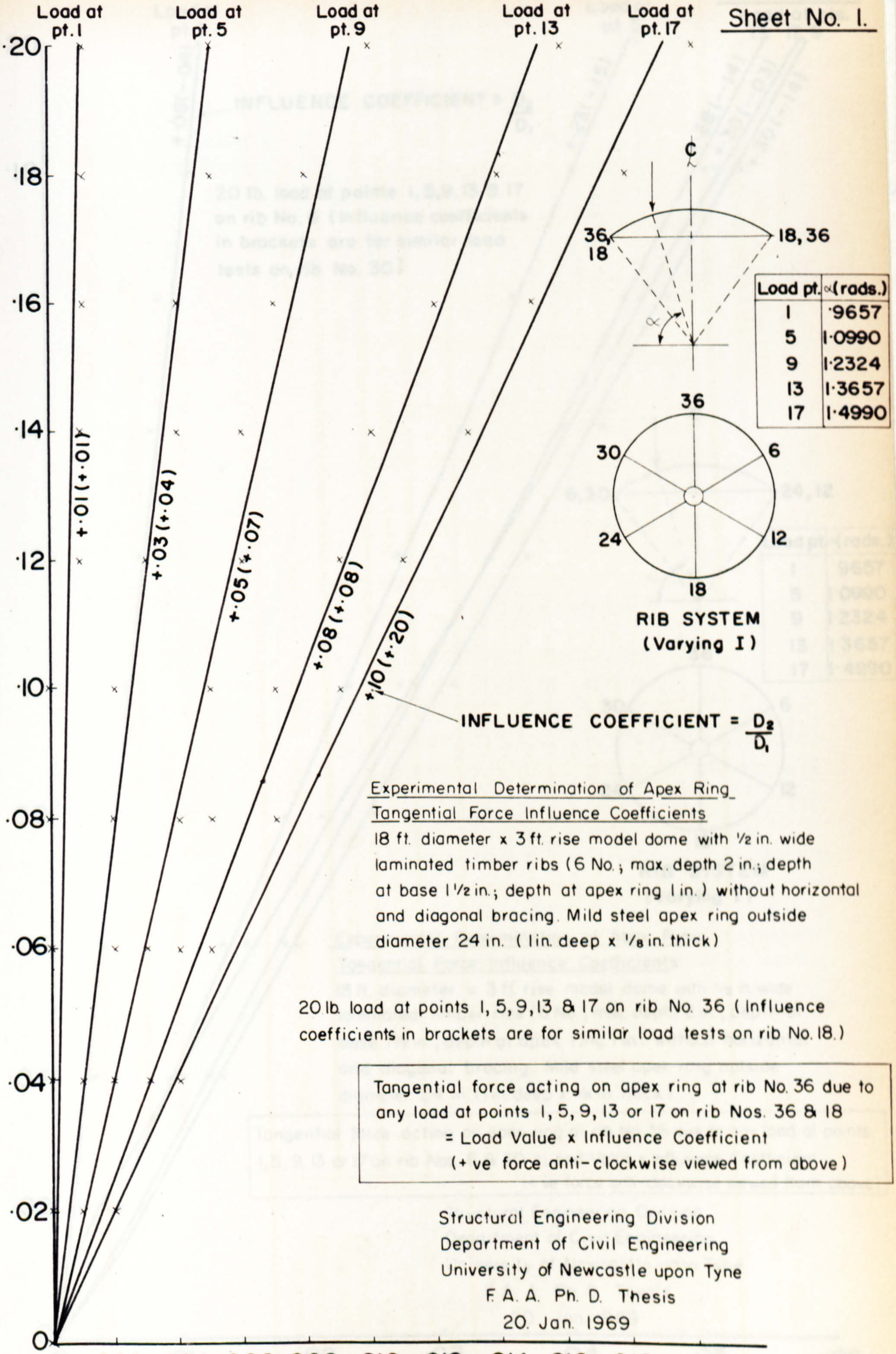

Load pt.	α (rads.)
1	·9657
5	1·0990
9	1·2324
13	1·3657
17	1·4990

RIB SYSTEM
(Varying I)

INFLUENCE COEFFICIENT = $\frac{D_2}{D_1}$

Experimental Determination of Apex Ring Tangential Force Influence Coefficients

18 ft. diameter x 3 ft. rise model dome with ½ in. wide laminated timber ribs (6 No.; max. depth 2 in.; depth at base 1½ in.; depth at apex ring 1 in.) without horizontal and diagonal bracing. Mild steel apex ring outside diameter 24 in. (1 in. deep x ⅛ in. thick)

20 lb. load at points 1, 5, 9, 13 & 17 on rib No. 36 (Influence coefficients in brackets are for similar load tests on rib No. 18.)

Tangential force acting on apex ring at rib No. 36 due to any load at points 1, 5, 9, 13 or 17 on rib Nos. 36 & 18
= Load Value x Influence Coefficient
(+ ve force anti-clockwise viewed from above)

Structural Engineering Division
Department of Civil Engineering
University of Newcastle upon Tyne
F. A. A. Ph. D. Thesis
20. Jan. 1969

TESTS ON MODEL RADIAL RIBBED DOME

Test No. 10

Sheet No. 2

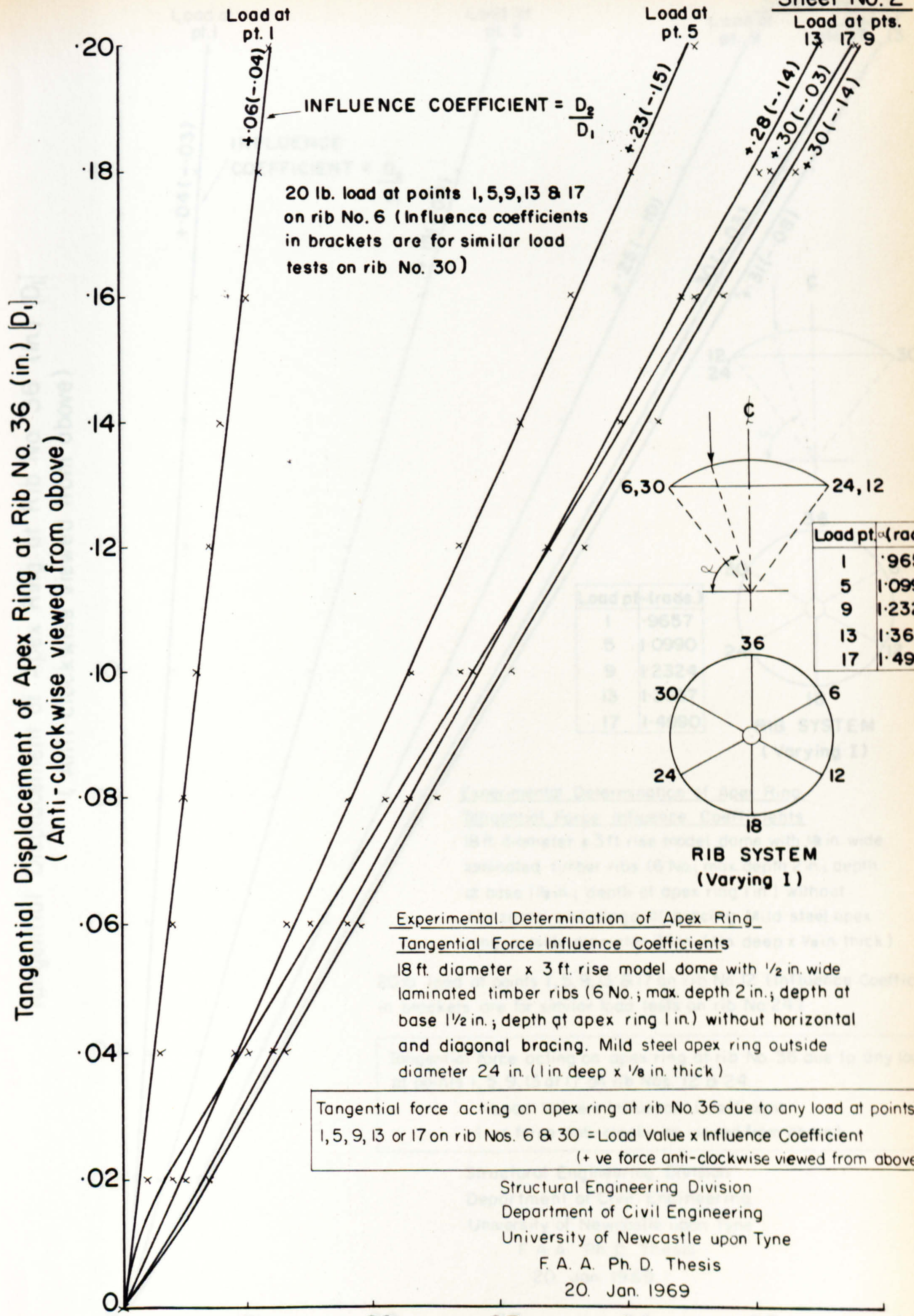

Load pt.	α (rads.)
1	·9657
5	1·0990
9	1·2324
13	1·3657
17	1·4990

Experimental Determination of Apex Ring Tangential Force Influence Coefficients

18 ft. diameter x 3 ft. rise model dome with ½ in. wide laminated timber ribs (6 No.; max. depth 2 in.; depth at base 1½ in.; depth at apex ring 1 in.) without horizontal and diagonal bracing. Mild steel apex ring outside diameter 24 in. (1 in. deep x ⅛ in. thick)

Tangential force acting on apex ring at rib No. 36 due to any load at points 1, 5, 9, 13 or 17 on rib Nos. 6 & 30 = Load Value x Influence Coefficient
(+ ve force anti-clockwise viewed from above)

Structural Engineering Division
Department of Civil Engineering
University of Newcastle upon Tyne

F. A. A. Ph. D. Thesis

20. Jan. 1969

TESTS ON MODEL RADIAL RIBBED DOME

Test No. 10

Sheet No. 3

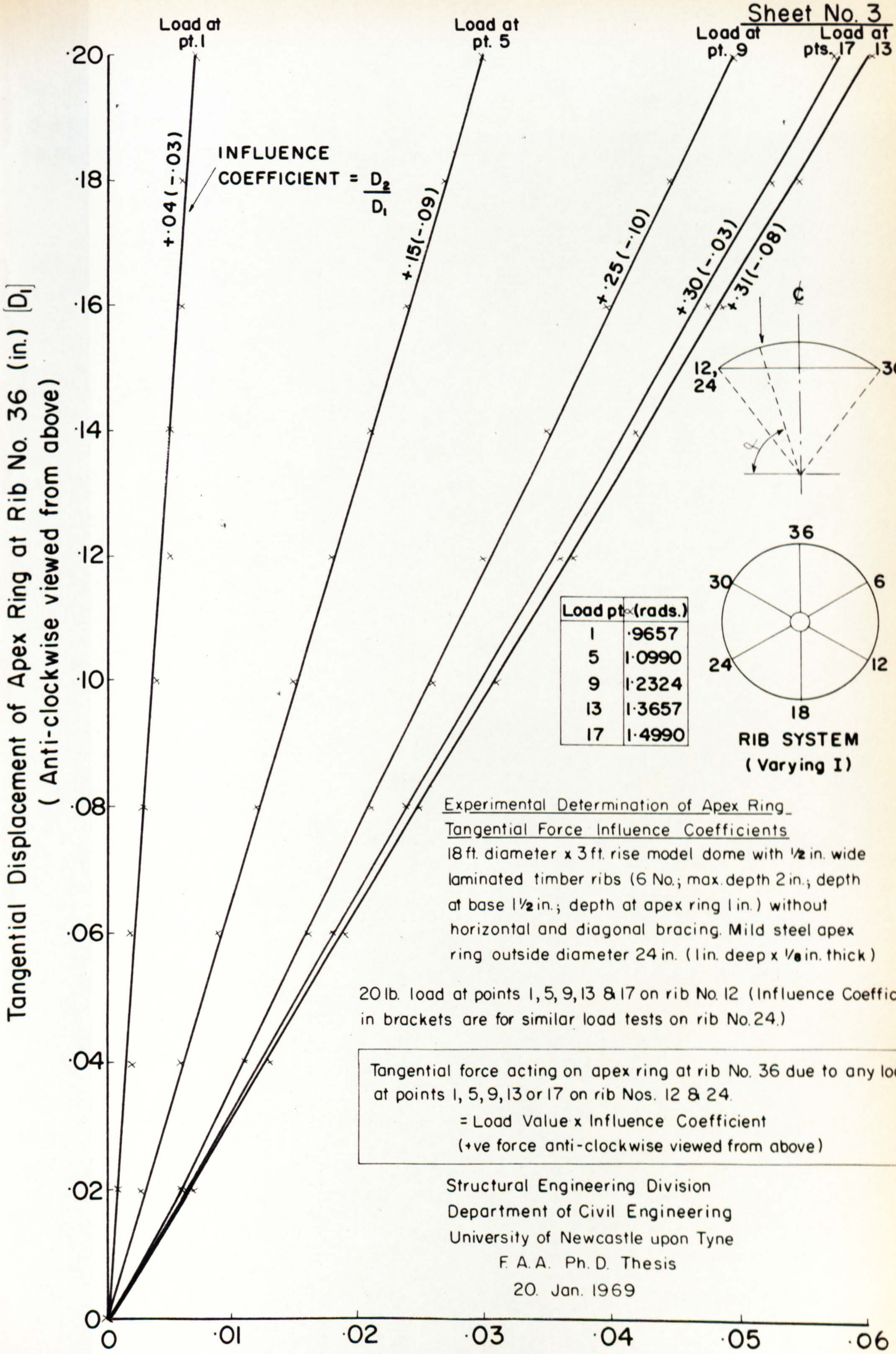

Load pt	∝ (rads.)
1	·9657
5	1·0990
9	1·2324
13	1·3657
17	1·4990

Experimental Determination of Apex Ring Tangential Force Influence Coefficients

18 ft. diameter x 3 ft. rise model dome with ½ in. wide laminated timber ribs (6 No.; max. depth 2 in.; depth at base 1½ in.; depth at apex ring 1 in.) without horizontal and diagonal bracing. Mild steel apex ring outside diameter 24 in. (1 in. deep x ⅛ in. thick)

20 lb. load at points 1, 5, 9, 13 & 17 on rib No. 12 (Influence Coefficients in brackets are for similar load tests on rib No. 24.)

Tangential force acting on apex ring at rib No. 36 due to any load at points 1, 5, 9, 13 or 17 on rib Nos. 12 & 24.

= Load Value x Influence Coefficient

(+ve force anti-clockwise viewed from above)

Structural Engineering Division
Department of Civil Engineering
University of Newcastle upon Tyne
F. A. A. Ph. D. Thesis

20. Jan. 1969

Structural Engineering Division
Department of Civil Engineering
University of Newcastle upon Tyne

TESTS ON MODEL RADIAL RIBBED DOME

Test No. 10
Sheet No. 4

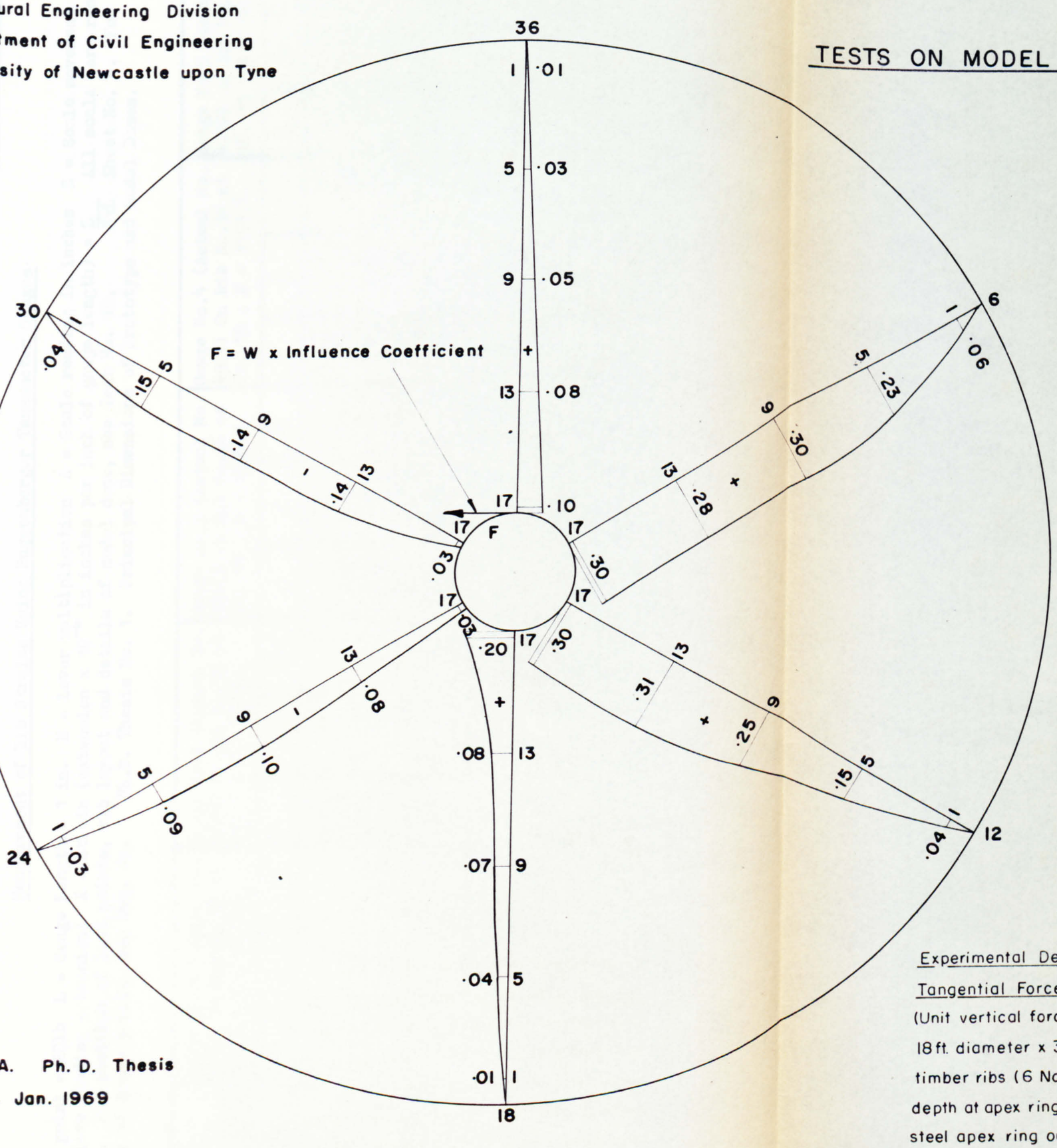

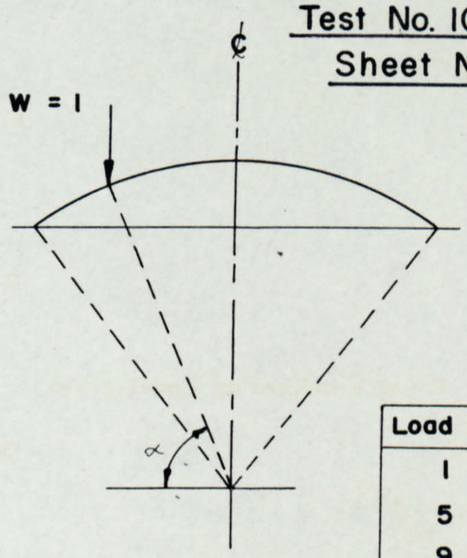

Load pt.	∝(rads.)
1	·9657
5	1·0990
9	1·2324
13	1·3657
17	1·4990

0 ·5 1·0
SCALE

Experimental Determination of Apex Ring
Tangential Force Influence Lines

(Unit vertical force acting at any angle on any rib.)

18 ft. diameter x 3 ft. rise model dome with ½ in. wide laminated timber ribs (6 No. of varying I; max. depth 2 in.; depth at base 1½ in.; depth at apex ring 1 in.) without horizontal and diagonal bracing. Mild steel apex ring outside diameter 24 in. (1 in. deep x ⅛ in. thick)

F. A. A. Ph. D. Thesis
28. Jan. 1969

TESTS ON MODEL RADIAL RIBBED DOME

TEST NO. 11 TABLE NO. 1

Measurement of Rib Strains Using Huggenberger Tensometer Gauges

Load at point = 20lb L = Gauge Length = 1 in. N = Lever multiplication A = Scale reading in inches Z = Scale movement in inches (+ve reading - tension) X = Strain (extension x 10^{-6} in inches per inch of gauge length) = $\frac{Z}{NxL}$ All scale zero readings 1.00 in. For position of load points, rib layout and details of model dome, see Test No. 10, Sheet No. 4. For position of gauge points, see Dwg. No. Ph.D. Thesis No. 1. Principal Dimensions of Prototype and Model Domes.

	Load Point	Gauge No.1 (Actual No. 4905) On Rib No.36 at Pt. 3 ; N = 1202.3			Gauge No.2 (Actual No. 4904) On Rib No.36 at Pt. 7 ; N = 1210.6			Gauge No.3 (Actual No. 4903) On Rib No.36 at Pt. 11 ; N = 1196.3			Gauge No.4 (Actual No. 4901) On Rib No.36 at Pt. 15 ; N = 1193.8			Gauge No.5 (Actual No. 4902) on Rib No.36 mid 16, 17 ; N = 1198.9		
		A	Z	X	A	Z	X	A	Z	X	A	Z	X	A	Z	X
Rib No. 30	1	1.00	.00	0	1.00	.00	0	1.00	.00	0	1.00	.00	0	.99	-.01	- 8
	5	1.00	.00	0	1.00	.00	0	.98	-.02	- 17	.97	-.03	- 25	.95	-.05	- 42
	9	1.02	+.02	+ 17	1.00	.00	0	.99	-.01	- 8	.93	-.07	- 59	.87	-.13	-108
	13	1.04	+.04	+ 33	1.03	+.03	+ 25	1.02	+.02	+ 17	.90	-.10	- 84	.79	-.21	-175
	17	1.10	+.10	+ 83	1.11	+.11	+ 91	1.08	+.08	+ 67	.92	-.08	- 67	.70	-.30	-250
Rib No. 36	1	.81	-.19	-158	.89	-.11	- 91	.95	-.05	- 42	.96	-.04	- 33	.98	-.02	- 17
	5	.57	-.43	-358	.40	-.60	-496	.65	-.35	-293	.77	-.23	-193	.83	-.17	-142
	9	.84	-.16	-133	.33	-.67	-553	.24	-.76	-636	.42	-.58	-486	.59	-.41	-342
	13	1.02	+.02	+ 17	.77	-.23	-190	.39	-.61	-510	.04	-.96	-803	.30	-.70	-584
	17	1.12	+.12	+100	1.10	+.10	+ 80	1.00	.00	0	.63	-.37	-310	.20	-.80	-668
Rib No. 6	1	1.00	.00	0	1.00	.00	0	1.00	.00	0	1.00	.00	0	.99	-.01	- 8
	5	1.00	.00	0	.98	-.02	- 17	.96	-.04	- 33	.95	-.05	- 42	.93	-.07	- 58
	9	1.00	.00	0	.99	-.01	- 8	.98	-.02	- 17	.92	-.08	- 67	.85	-.15	-125
	13	1.04	+.04	+ 33	1.02	+.02	+ 17	1.00	.00	0	.91	-.09	- 75	.75	-.25	-209
	17	1.09	+.09	+ 75	1.11	+.11	+ 91	1.07	+.07	+ 59	.91	-.09	- 75	.66	-.34	-284

F.A.A. Ph.D. Thesis.
16th Jan., 1969.

Structural Engineering Division,
Department of Civil Engineering,
University of Newcastle upon Tyne.

TESTS ON MODEL RADIAL RIBBED DOME

TEST NO. 11 TABLE NO. 2

Measurement of Rib Strains Using Huggenberger Tensometer Gauges

Load at point = 20lb L = Gauge length = 1 in. N = Lever multiplication A = Scale reading in inches Z = Scale movement in inches (+ve reading - tension) X = Strain (extension x 10^{-6} in inches per inch of gauge length) = $\frac{Z}{NxL}$ All scale zero readings 1.00 in. For position of load points, rib layout and details of model dome, see Test No. 10, Sheet No. 4. For position of gauge points, see Dwg. No. Ph.D. Thesis No. 1. Principal Dimensions of Prototype and Model Domes.

	Load Point	Gauge No.1 (Actual No. 4905) On Rib No.36 at Pt. 3 ; N = 1202.3			Gauge No.2 (Actual No. 4904) On Rib No.36 at Pt. 7 ; N = 1210.6			Gauge No.3 (Actual No. 4903) On Rib No.36 at Pt. 11 ; N = 1196.3			Gauge No.4 (Actual No. 4901) On Rib No.36 at Pt. 15 ; N = 1193.8			Gauge No.5 (Actual No. 4902) On Rib No.36 mid 16, 17 ; N = 1198.9		
		A	Z	X	A	Z	X	A	Z	X	A	Z	X	A	Z	X
Rib No. 12	1	1.01	+.01	+ 8	1.01	+.01	+ 8	1.01	+.01	+ 8	1.02	+.02	+ 17	1.02	+.02	+ 17
	5	1.03	+.03	+ 25	1.06	+.06	+ 50	1.08	+.08	+ 67	1.12	+.12	+100	1.11	+.11	+ 92
	9	1.06	+.06	+ 50	1.12	+.12	+ 99	1.15	+.15	+125	1.22	+.22	+184	1.23	+.23	+192
	13	1.08	+.08	+ 67	1.18	+.18	+149	1.21	+.21	+176	1.32	+.32	+268	1.33	+.33	+275
	17	1.10	+.10	+ 83	1.20	+.20	+165	1.24	+.24	+201	1.36	+.36	+302	1.39	+.39	+326
Rib No. 18	1	1.00	.00	0	1.00	.00	0	1.02	+.02	+ 17	1.02	+.02	+ 17	1.04	+.04	+ 33
	5	1.03	+.03	+ 25	1.05	+.05	+ 41	1.09	+.09	+ 75	1.15	+.15	+126	1.20	+.20	+167
	9	1.05	+.05	+ 42	1.11	+.11	+ 91	1.15	+.15	+125	1.28	+.28	+234	1.36	+.36	+301
	13	1.07	+.07	+ 58	1.18	+.18	+149	1.24	+.24	+201	1.43	+.43	+360	1.54	+.54	+451
	17	1.10	+.10	+ 83	1.23	+.23	+190	1.29	+.29	+243	1.48	+.48	+402	1.56	+.56	+467
Rib No. 24	1	1.00	.00	0	1.01	+.01	+ 8	1.02	+.02	+ 17	1.03	+.03	+ 25	1.02	+.02	+ 17
	5	1.04	+.04	+ 33	1.07	+.07	+ 58	1.09	+.09	+ 75	1.13	+.13	+109	1.15	+.15	+125
	9	1.06	+.06	+ 50	1.13	+.13	+107	1.16	+.16	+134	1.24	+.24	+201	1.28	+.28	+234
	13	1.09	+.09	+ 75	1.18	+.18	+149	1.22	+.22	+184	1.33	+.33	+276	1.35	+.35	+292
	17	1.10	+.10	+ 83	1.20	+.20	+165	1.23	+.23	+192	1.31	+.31	+259	1.33	+.33	+275

F.A.A. Ph.D. Thesis
16th Jan., 1969.

Structural Engineering Division,
Department of Civil Engineering,
University of Newcastle upon Tyne.

TESTS ON MODEL RADIAL RIBBED DOME — TEST NO. 11 TABLE NO. 3

Measurement of Apex Ring Displacements at Rib No. 36

Load at point = 2 lb ; All dial gauge zeros 1.000 in. ; A = Tangential displacement in inches (+ve reading anti-clockwise viewed from above) ; B = Radial displacement in inches (+ve reading inwards) ; C = Vertical displacement in inches (+ve reading upwards) ; D = Dial Gauge Reading ; E = Actual Displacement.

	Load Point	Gauge No. 1 A		Gauge No. 2 B		Gauge No. 3 C			Load Point	Gauge No. 1 A		Gauge No. 2 B		Gauge No. 3 C	
		D	E	D	E	D	E			D	E	D	E	D	E
Rib No. 30	1	.964	-.036	1.005	+.005	.999	-.001	Rib No. 12	1	1.029	+.029	.977	-.023	1.025	+.025
	5	.852	-.148	1.031	+.031	.959	-.041		5	1.148	+.148	.890	-.110	1.095	+.095
	9	.781	-.219	1.064	+.064	.857	-.143		9	1.245	+.245	.815	-.185	1.126	+.126
	13	.759	-.241	1.101	+.101	.699	-.301		13	1.273	+.273	.775	-.225	1.093	+.093
	17	.850	-.150	1.115	+.115	.545	-.455		17	1.208	+.208	.805	-.195	.959	-.041
Rib No. 36	1	1.004	+.004	1.068	+.068	.986	-.014	Rib No. 18	1	1.000	.000	.972	-.028	1.040	+.040
	5	1.020	+.020	1.301	+.301	.891	-.109		5	1.007	+.007	.866	-.134	1.172	+.172
	9	1.052	+.052	1.459	+.459	.712	-.288		9	1.029	+.029	.765	-.235	1.260	+.260
	13	1.082	+.082	1.505	+.505	.427	-.573		13	1.055	+.055	.677	-.323	1.296	+.296
	17	1.037	+.037	1.275	+.275	.295	-.705		17	1.056	+.056	.705	-.295	1.135	+.135
Rib No. 6	1	1.040	+.040	1.007	+.007	1.002	+.002	Rib No. 24	1	.973	-.027	.973	-.027	1.032	+.032
	5	1.179	+.179	1.036	+.036	.969	-.031		5	.875	-.125	.879	-.121	1.127	+.127
	9	1.252	+.252	1.069	+.069	.875	-.125		9	.849	-.151	.812	-.188	1.161	+.161
	13	1.285	+.285	1.099	+.099	.715	-.285		13	.813	-.187	.788	-.212	1.103	+.103
	17	1.185	+.185	1.095	+.095	.575	-.425		17	.875	-.125	.853	-.147	.930	-.070

F.A.A. Ph.D. Thesis
16th Jan., 1969.

Structural Engineering Division,
Department of Civil Engineering,
University of Newcastle upon Tyne.

TESTS ON MODEL RADIAL RIBBED DOME

TEST No. 12 TABLE No. 1

Experimental Determination of Horizontal Reaction Influence Coefficients

Load at point 101b

For position of load points, rib layout, details of model dome and graphs of tabulated results, see Test No. 12 Sheet Nos. 1 & 2

Horizontal Base Displacement at Rib No. 36 (Towards centre of dome)	Dial gauge readings (A) and actual vertical displacement of point load (B; +ve upwards) in inches																			
	Rib No. 36										Rib No. 6									
	Point 1		Point 5		Point 9		Point 13		Point 17		Point 1		Point 5		Point 9		Point 13		Point 17	
	A	B	A	B	A	B	A	B	A	B	A	B	A	B	A	B	A	B	A	B
0 in.	.478	.000	.393	.000	.648	.000	.332	.000	.434	.000	.476	.000	.391	.000	.343	.000	.325	.000	.440	.000
.02 in.	.483	+.005	.419	+.026	.681	+.033	.358	+.026	.437	+.003	.476	.000	.391	.000	.343	.000	.326	+.001	.442	+.002
.04 in.	.489	+.011	.444	+.051	.714	+.066	.384	+.052	.440	+.006	.476	.000	.391	.000	.344	+.001	.327	+.002	.444	+.004
.06 in.	.495	+.017	.470	+.077	.745	+.097	.410	+.078	.443	+.009	.477	+.001	.391	.000	.345	+.002	.328	+.003	.445	+.005
.08 in.	.502	+.024	.497	+.104	.781	+.133	.437	+.105	.446	+.012	.477	+.001	.391	.000	.345	+.002	.329	+.004	.447	+.007
.10 in.	.508	+.030	.523	+.130	.815	+.167	.464	+.132	.449	+.015	.477	+.001	.391	.000	.346	+.003	.330	+.005	.448	+.008
.12 in.	.514	+.036	.548	+.155	.850	+.202	.491	+.159	.452	+.018	.477	+.001	.392	+.001	.347	+.004	.331	+.006	.450	+.010
.14 in.	.520	+.042	.575	+.182	.884	+.236	.518	+.186	.455	+.021	.477	+.001	.392	+.001	.347	+.004	.332	+.007	.451	+.011
.16 in.	.526	+.048	.600	+.207	.919	+.271	.545	+.213	.458	+.024	.477	+.001	.392	+.001	.348	+.005	.333	+.008	.453	+.013
.18 in.	.532	+.054	.626	+.233	.954	+.306	.573	+.241	.460	+.026	.477	+.001	.393	+.002	.349	+.006	.334	+.009	.454	+.014
.20 in.	.537	+.059	.651	+.258	.988	+.340	.598	+.266	.463	+.029	.477	+.001	.393	+.002	.349	+.006	.335	+.010	.455	+.015

F. A. A. Ph.D. Thesis
24th Jan., 1969

Structural Engineering Division,
Department of Civil Engineering,
University of Newcastle upon Tyne.

TESTS ON MODEL RADIAL RIBBED DOME

TEST No. 12 TABLE No. 2

Experimental Determination of Horizontal Reaction Influence Coefficients

Load at point = 10lb

For position of load points, rib layout, details of model dome and graphs of tabulated results, see Test No 12 Sheet Nos. 3 & 4

Horizontal Base Displacement at Rib No. 36 (Towards centre of dome)	Dial gauge readings (A) and actual vertical displacement of point load (B; +ve upwards) in inches																			
	Rib No. 12										Rib No. 18									
	Point 1		Point 5		Point 9		Point 13		Point 17		Point 1		Point 5		Point 9		Point 13		Point 17	
	A	B	A	B	A	B	A	B	A	B	A	B	A	B	A	B	A	B	A	B
0 in.	.481	.000	.393	.000	.353	.000	.335	.000	.450	.000	.480	.000	.404	.000	.370	.000	.342	.000	.447	.000
.02 in.	.481	.000	.394	+.001	.354	+.001	.336	+.001	.452	+.002	.480	.000	.404	.000	.371	+.001	.343	+.001	.449	+.002
.04 in.	.481	.000	.394	+.001	.355	+.002	.337	+.002	.453	+.003	.480	.000	.404	.000	.372	+.002	.344	+.002	.450	+.003
.06 in.	.481	.000	.395	+.002	.356	+.003	.338	+.003	.455	+.005	.480	.000	.404	.000	.372	+.002	.345	+.003	.452	+.005
.08 in.	.482	+.001	.395	+.002	.357	+.004	.340	+.005	.456	+.006	.480	.000	.404	.000	.373	+.003	.345	+.003	.453	+.006
.10 in.	.482	+.001	.395	+.002	.357	+.004	.341	+.006	.458	+.008	.480	.000	.405	+.001	.374	+.004	.346	+.004	.454	+.007
.12 in.	.482	+.001	.396	+.003	.358	+.005	.342	+.007	.459	+.009	.480	.000	.405	+.001	.374	+.004	.347	+.005	.456	+.009
.14 in.	.482	+.001	.396	+.003	.359	+.006	.343	+.008	.461	+.011	.480	.000	.405	+.001	.375	+.005	.348	+.006	.457	+.010
.16 in.	.482	+.001	.397	+.004	.360	+.007	.344	+.009	.462	+.012	.480	.000	.406	+.002	.376	+.006	.349	+.007	.459	+.012
.18 in.	.482	+.001	.397	+.004	.361	+.008	.345	+.010	.464	+.014	.480	.000	.406	+.002	.376	+.006	.350	+.008	.460	+.013
.20 in.	.482	+.001	.398	+.005	.362	+.009	.347	+.012	.465	+.015	.480	.000	.406	+.002	.377	+.007	.351	+.009	.462	+.015

F. A. A. Ph.D. Thesis
24th Jan., 1969

Structural Engineering Division,
Department of Civil Engineering,
Newcastle upon Tyne University.

TESTS ON MODEL RADIAL RIBBED DOME

TEST No. 12 TABLE No. 3

Experimental Determination of Horizontal Reaction Influence Coefficients

Load at point = 10lb

For position of load points, rib layout, details of model dome and graphs of tabulated results, see Test No. 12 Sheet No. 5

Horizontal Base Displacement of Rib No. 36 (Towards centre of dome)	Dial gauge readings (A) and actual vertical displacement of point load (B; +ve upwards) in inches																			
	Rib No. 1										Rib No. 2									
	Point 1		Point 5		Point 9		Point 13		Point 17		Point 1		Point 5		Point 9		Point 13		Point 17	
	A	B	A	B	A	B	A	B	A	B	A	B	A	B	A	B	A	B	A	B
0 in.	.477	.000	.391	.000	.357	.000	.334	.000	.438	.000	.482	.000	.396	.000	.357	.000	.333	.000	.443	.000
.02 in.	.475	-.002	.383	-.008	.347	-.010	.328	-.006	.440	+.002	.481	-.001	.392	-.004	.352	-.005	.330	-.003	.444	+.001
.04 in.	.474	-.003	.374	-.017	.338	-.019	.323	-.011	.442	+.004	.480	-.002	.388	-.008	.348	-.009	.327	-.006	.446	+.003
.06 in.	.472	-.005	.366	-.025	.329	-.028	.318	-.016	.444	+.006	.479	-.003	.384	-.012	.343	-.014	.324	-.009	.447	+.004
.08 in.	.470	-.007	.358	-.033	.320	-.037	.312	-.022	.445	+.007	.478	-.004	.381	-.015	.339	-.018	.321	-.012	.449	+.006
.10 in.	.468	-.009	.350	-.041	.311	-.046	.307	-.027	.447	+.009	.478	-.004	.377	-.019	.334	-.023	.318	-.015	.450	+.007
.12 in.	.467	-.010	.343	-.048	.303	-.054	.302	-.032	.449	+.011	.477	-.005	.373	-.023	.330	-.027	.315	-.018	.451	+.008
.14 in.	.465	-.012	.335	-.056	.294	-.063	.296	-.038	.450	+.012	.476	-.006	.369	-.027	.326	-.031	.312	-.021	.452	+.009
.16 in.	.463	-.014	.328	-.063	.286	-.071	.290	-.044	.452	+.014	.475	-.007	.366	-.030	.321	-.036	.309	-.024	.453	+.010
.18 in.	.462	-.015	.320	-.071	.278	-.079	.284	-.050	.453	+.015	.474	-.008	.363	-.033	.317	-.040	.306	-.027	.453	+.010
.20 in.	.460	-.017	.313	-.078	.270	-.087	.278	-.056	.453	+.015	.473	-.009	.359	-.037	.312	-.045	.302	-.031	.454	+.011

F. A. A. Ph.D. Thesis
6th Feb., 1969

Structural Engineering Division,
Department of Civil Engineering,
University of Newcastle upon Tyne.

TESTS ON MODEL RADIAL RIBBED DOME

TEST No. 12 TABLE No. 4

Experimental Determination of Horizontal Reaction Influence Coefficients

Load at point = 10lb

For position of load points, rib layout, details of model dome and graphs of tabulated results, see Test No. 12 Sheet No. 5

Horizontal Base Displacement of Rib No. 36 (Towards centre of dome)	Dial Gauge readings (A) and actual vertical displacement of point load (B; +ve upwards) in inches																			
	Rib No. 3										Rib No. 4									
	Point 1		Point 5		Point 9		Point 13		Point 17		Point 1		Point 5		Point 9		Point 13		Point 17	
	A	B	A	B	A	B	A	B	A	B	A	B	A	B	A	B	A	B	A	B
0 in.	.482	.000	.399	.000	.363	.000	.336	.000	.443	.000	.478	.000	.399	.000	.354	.000	.327	.000	.440	.000
.02 in.	.482	.000	.398	-.001	.361	-.002	.335	-.001	.444	+.001	.478	.000	.398	-.001	.354	.000	.327	.000	.441	+.001
.04 in.	.481	-.001	.396	-.003	.359	-.004	.334	-.002	.446	+.003	.478	.000	.398	-.001	.354	.000	.327	.000	.443	+.003
.06 in.	.481	-.001	.394	-.005	.358	-.005	.333	-.003	.447	+.004	.478	.000	.397	-.002	.354	.000	.327	.000	.444	+.004
.08 in.	.480	-.002	.393	-.006	.356	-.007	.332	-.004	.449	+.006	.478	.000	.397	-.002	.354	.000	.328	+.001	.446	+.006
.10 in.	.480	-.002	.391	-.008	.354	-.009	.331	-.005	.450	+.007	.478	.000	.396	-.003	.353	-.001	.328	+.001	.447	+.007
.12 in.	.479	-.003	.390	-.009	.353	-.010	.330	-.006	.451	+.008	.478	.000	.396	-.003	.353	-.001	.328	+.001	.449	+.009
.14 in.	.479	-.003	.388	-.011	.351	-.012	.329	-.007	.452	+.009	.478	.000	.396	-.003	.353	-.001	.328	+.001	.450	+.010
.16 in.	.479	-.003	.387	-.012	.349	-.014	.328	-.008	.453	+.010	.478	.000	.395	-.004	.352	-.002	.329	+.002	.451	+.011
.18 in.	.478	-.004	.385	-.014	.347	-.016	.326	-.010	.454	+.011	.478	.000	.395	-.004	.352	-.002	.329	+.002	.452	+.012
.20 in.	.478	-.004	.383	-.016	.345	-.018	.325	-.011	.454	+.011	.478	.000	.395	-.004	.351	-.003	.329	+.002	.452	+.012

F. A. A. Ph.D. Thesis
6th Feb., 1969

Structural Engineering Division,
Department of Civil Engineering,
University of Newcastle upon Tyne.

TESTS ON MODEL RADIAL RIBBED DOME

TEST No. 12 TABLE No. 5

Experimental Determination of Horizontal Reaction Influence Coefficients

Load at point = 10lb

For position of load points, rib layout, details of model dome and graphs of tabulated results, see Test No.12 Sheet Nos. 5 & 6

Horizontal Base Displacement at Rib No. 36 (Towards centre of dome)	Dial gauge readings (A) and actual vertical displacement of point load (B; +ve upwards) in inches																			
	Rib No. 5										Rib No. 7									
	Point 1		Point 5		Point 9		Point 13		Point 17		Point 1		Point 5		Point 9		Point 13		Point 17	
	A	B	A	B	A	B	A	B	A	B	A	B	A	B	A	B	A	B	A	B
0 in.	.480	.000	.398	.000	.360	.000	.343	.000	.443	.000	.479	.000	.393	.000	.362	.000	.331	.000	.442	.000
.02 in.	.480	.000	.398	.000	.360	.000	.343	.000	.445	+.002	.479	.000	.394	+.001	.363	+.001	.332	+.001	.444	+.002
.04 in.	.480	.000	.398	.000	.361	+.001	.344	+.001	.447	+.004	.479	.000	.394	+.001	.363	+.001	.333	+.002	.445	+.003
.06 in.	.480	.000	.398	.000	.361	+.001	.345	+.002	.448	+.005	.479	.000	.394	+.001	.364	+.002	.334	+.003	.447	+.005
.08 in.	.480	.000	.399	+.001	.361	+.001	.346	+.003	.450	+.007	.479	.000	.395	+.002	.365	+.003	.335	+.004	.448	+.006
.10 in.	.480	.000	.399	+.001	.362	+.002	.347	+.004	.451	+.008	.480	+.001	.395	+.002	.365	+.003	.336	+.005	.450	+.008
.12 in.	.480	.000	.399	+.001	.362	+.002	.347	+.004	.453	+.010	.480	+.001	.395	+.002	.366	+.004	.337	+.006	.451	+.009
.14 in.	.480	.000	.399	+.001	.363	+.003	.348	+.005	.454	+.011	.480	+.001	.396	+.003	.367	+.005	.338	+.007	.453	+.011
.16 in.	.480	.000	.399	+.001	.363	+.003	.349	+.006	.455	+.012	.480	+.001	.396	+.003	.367	+.005	.339	+.008	.454	+.012
.18 in.	.480	.000	.400	+.002	.364	+.004	.350	+.007	.456	+.013	.480	+.001	.397	+.004	.368	+.006	.340	+.009	.455	+.013
.20 in.	.480	.000	.400	+.002	.364	+.004	.351	+.008	.457	+.014	.480	+.001	.397	+.004	.369	+.007	.341	+.010	.456	+.014

F. A. A. Ph.D. Thesis
6th, 10th Feb., 1969

Structural Engineering Division,
Department of Civil Engineering,
University of Newcastle upon Tyne.

TESTS ON MODEL RADIAL RIBBED DOME

TEST No. 12 TABLE No. 6

Experimental Determination of Horizontal Reaction Influence Coefficients

Load at point = 10lb

For position of load points, rib layout, details of model dome and graphs of tabulated results, see Test No. 12 Sheet No. 6

Horizontal Base Displacement at Rib No. 36 (Towards centre of dome)	Dial gauge readings (A) and actual vertical displacement of point load (B; +ve upwards) in inches																			
	Rib No. 8										Rib No. 9									
	Point 1		Point 5		Point 9		Point 13		Point 17		Point 1		Point 5		Point 9		Point 13		Point 17	
	A	B	A	B	A	B	A	B	A	B	A	B	A	B	A	B	A	B	A	B
0 in.	.474	.000	.388	.000	.358	.000	.329	.000	.442	.000	.480	.000	.395	.000	.367	.000	.342	.000	.439	.000
.02 in.	.474	.000	.389	+.001	.359	+.001	.330	+.001	.444	+.002	.480	.000	.395	.000	.367	.000	.343	+.001	.440	+.001
.04 in.	.474	.000	.389	+.001	.360	+.002	.331	+.002	.445	+.003	.480	.000	.396	+.001	.368	+.001	.344	+.002	.442	+.003
.06 in.	.474	.000	.390	+.002	.360	+.002	.332	+.003	.447	+.005	.480	.000	.396	+.001	.369	+.002	.346	+.004	.443	+.004
.08 in.	.474	.000	.390	+.002	.361	+.003	.333	+.004	.448	+.006	.480	.000	.397	+.002	.370	+.003	.347	+.005	.445	+.006
.10 in.	.474	.000	.390	+.002	.362	+.004	.334	+.005	.450	+.008	.480	.000	.397	+.002	.370	+.003	.348	+.006	.446	+.007
.12 in.	.474	.000	.391	+.003	.363	+.005	.335	+.006	.451	+.009	.480	.000	.397	+.002	.371	+.004	.349	+.007	.448	+.009
.14 in.	.474	.000	.391	+.003	.363	+.005	.337	+.008	.453	+.011	.480	.000	.398	+.003	.372	+.005	.350	+.008	.449	+.010
.16 in.	.474	.000	.391	+.003	.364	+.006	.338	+.009	.454	+.012	.480	.000	.398	+.003	.373	+.006	.351	+.009	.451	+.012
.18 in.	.474	.000	.392	+.004	.365	+.007	.339	+.010	.455	+.013	.480	.000	.399	+.004	.373	+.006	.352	+.010	.452	+.013
.20 in.	.474	.000	.392	+.004	.366	+.008	.340	+.011	.456	+.014	.480	.000	.399	+.004	.374	+.007	.354	+.012	.454	+.015

F. A. A. Ph.D. Thesis
10th, 11th Feb., 1969

Structural Engineering Division,
Department of Civil Engineering,
University of Newcastle upon Tyne.

TESTS ON MODEL RADIAL RIBBED DOME

TEST No. 12 TABLE No. 7

Experimental Determination of Horizontal Reaction Influence Coefficients

Load at point = 10lb

For position of load points, rib layout, details of model dome and graphs of tabulated results, see Test No. 12 Sheet No. 6

Horizontal Base Displacement at Rib No. 36 (Towards centre of dome)	Dial gauge readings (A) and actual vertical displacement of point load (B; +ve upwards) in inches																			
	Rib No. 10										Rib No. 11									
	Point 1		Point 5		Point 9		Point 13		Point 17		Point 1		Point 5		Point 9		Point 13		Point 17	
	A	B	A	B	A	B	A	B	A	B	A	B	A	B	A	B	A	B	A	B
0 in.	.481	.000	.394	.000	.354	.000	.341	.000	.444	.000	.482	.000	.392	.000	.367	.000	.339	.000	.444	.000
.02 in.	.481	.000	.395	+.001	.355	+.001	.342	+.001	.445	+.001	.482	.000	.393	+.001	.368	+.001	.340	+.001	.446	+.002
.04 in.	.481	.000	.395	+.001	.356	+.002	.343	+.002	.447	+.003	.482	.000	.393	+.001	.369	+.002	.341	+.002	.448	+.004
.06 in.	.481	.000	.396	+.002	.356	+.002	.345	+.004	.449	+.005	.482	.000	.394	+.002	.370	+.003	.343	+.004	.449	+.005
.08 in.	.481	.000	.396	+.002	.357	+.003	.346	+.005	.450	+.006	.482	.000	.394	+.002	.371	+.004	.344	+.005	.451	+.007
.10 in.	.481	.000	.396	+.002	.358	+.004	.347	+.006	.452	+.008	.482	.000	.395	+.003	.372	+.005	.345	+.006	.452	+.008
.12 in.	.481	.000	.397	+.003	.358	+.004	.348	+.007	.453	+.009	.482	.000	.395	+.003	.372	+.005	.346	+.007	.454	+.010
.14 in.	.481	.000	.397	+.003	.359	+.005	.349	+.008	.455	+.011	.482	.000	.395	+.003	.373	+.006	.347	+.008	.455	+.011
.16 in.	.481	.000	.398	+.004	.360	+.006	.350	+.009	.456	+.012	.482	.000	.396	+.004	.374	+.007	.348	+.009	.457	+.013
.18 in.	.481	.000	.398	+.004	.360	+.006	.352	+.011	.457	+.013	.482	.000	.396	+.004	.375	+.008	.350	+.011	.458	+.014
.20 in.	.481	.000	.399	+.005	.361	+.007	.353	+.012	.459	+.015	.482	.000	.397	+.005	.376	+.009	.351	+.012	.460	+.016

F. A. A. Ph.D. Thesis
12th Feb., 1969

Structural Engineering Division,
Department of Civil Engineering,
Newcastle upon Tyne University.

TESTS ON MODEL RADIAL RIBBED DOME

TEST No. 12 TABLE No. 8

Experimental Determination of Horizontal Reaction Influence Coefficients

Load at poirt - 10lb

For position of load points, rib layout, details of model dome and graphs of tabulated results, see Test No. 12 Sheet No. 7

Horizontal Base Displacement at Rib No. 36 (Towards centre of dome)	Dial gauge readings (A) and actual vertical displacement of point load (B; +ve upwards) in inches																			
	Rib No. 13										Rib No. 14									
	Point 1		Point 5		Point 9		Point 13		Point 17		Point 1		Point 5		Point 9		Point 13		Point 17	
	A	B	A	B	A	B	A	B	A	B	A	B	A	B	A	B	A	B	A	B
0 in.	.481	.000	.390	.000	.358	.000	.334	.000	.448	.000	.476	.000	.396	.000	.363	.000	.338	.000	.446	.000
.02 in.	.481	.000	.391	+.001	.359	+.001	.335	+.001	.450	+.002	.476	.000	.396	.000	.364	+.001	.339	+.001	.448	+.002
.04 in.	.481	.000	.391	+.001	.360	+.002	.336	+.002	.451	+.003	.476	.000	.397	+.001	.365	+.002	.340	+.002	.449	+.003
.06 in.	.481	.000	.392	+.002	.361	+.003	.338	+.004	.453	+.005	.476	.000	.397	+.001	.366	+.003	.341	+.003	.451	+.005
.08 in.	.482	+.001	.392	+.002	.361	+.003	.339	+.005	.454	+.006	.476	.000	.398	+.002	.367	+.004	.343	+.005	.452	+.006
.10 in.	.482	+.001	.393	+.003	.362	+.004	.340	+.006	.456	+.008	.476	.000	.398	+.002	.367	+.004	.344	+.006	.454	+.008
.12 in.	.482	+.001	.393	+.003	.363	+.005	.341	+.007	.457	+.009	.476	.000	.398	+.002	.368	+.005	.345	+.007	.455	+.009
.14 in.	.482	+.001	.394	+.004	.364	+.006	.342	+.008	.459	+.011	.476	.000	.399	+.003	.369	+.006	.346	+.008	.456	+.010
.16 in.	.482	+.001	.394	+.004	.365	+.007	.343	+.009	.460	+.012	.476	.000	.399	+.003	.370	+.007	.347	+.009	.458	+.012
.18 in.	.482	+.001	.395	+.005	.366	+.008	.345	+.011	.462	+.014	.476	.000	.399	+.003	.370	+.007	.348	+.010	.460	+.014
.20 in.	.482	+.001	.395	+.005	.367	+.009	.346	+.012	.463	+.015	.476	.000	.400	+.004	.371	+.008	.350	+.012	.461	+.015

F. A. A. Ph.D. Thesis
12th Feb., 1969

Structural Engineering Division,
Department of Civil Engineering,
University of Newcastle upon Tyne.

TESTS ON MODEL RADIAL RIBBED DOME

TEST No. 12 TABLE No. 9

Experimental Determination of Horizontal Reaction Influence Coefficients

Load at point = 10lb

For position of load points, rib layout, details of model dome and graphs of tabulated results, see Test No.12 Sheet No. 7

Horizontal Base Displacement at Rib No. 36 (Towards centre of dome)	Dial gauge readings (A) and actual vertical displacement of point load (B; +veupwards) in inches																			
	Rib No. 15										Rib No. 16									
	Point 1		Point 5		Point 9		Point 13		Point 17		Point 1		Point 5		Point 9		Point 13		Point 17	
	A	B	A	B	A	B	A	B	A	B	A	B	A	B	A	B	A	B	A	B
0 in.	.481	.000	.392	.000	.369	.000	.337	.000	.447	.000	.481	.000	.391	.000	.363	.000	.339	.000	.448	.000
.02 in.	.481	.000	.393	+.001	.370	+.001	.339	+.002	.448	+.001	.481	.000	.392	+.001	.363	.000	.340	+.001	.450	+.002
.04 in.	.481	.000	.393	+.001	.370	+.001	.340	+.003	.450	+.003	.481	.000	.392	+.001	.364	+.001	.341	+.002	.451	+.003
.06 in.	.481	.000	.393	+.001	.371	+.002	.341	+.004	.451	+.004	.481	.000	.393	+.002	.365	+.002	.342	+.003	.453	+.005
.08 in.	.481	.000	.394	+.002	.372	+.003	.342	+.005	.453	+.006	.481	.000	.393	+.002	.365	+.002	.343	+.004	.455	+.007
.10 in.	.481	.000	.394	+.002	.372	+.003	.343	+.006	.454	+.007	.481	.000	.393	+.002	.366	+.003	.344	+.005	.456	+.008
.12 in.	.481	.000	.394	+.002	.373	+.004	.344	+.007	.456	+.009	.481	.000	.394	+.003	.366	+.003	.345	+.006	.457	+.009
.14 in.	.481	.000	.395	+.003	.374	+.005	.345	+.008	.457	+.010	.481	.000	.394	+.003	.367	+.004	.346	+.007	.459	+.011
.16 in.	.481	.000	.395	+.003	.374	+.005	.346	+.009	.459	+.012	.481	.000	.394	+.003	.368	+.005	.348	+.009	.460	+.012
.18 in.	.481	.000	.396	+.004	.375	+.006	.348	+.011	.460	+.013	.481	.000	.395	+.004	.369	+.006	.349	+.010	.462	+.014
.20 in.	.481	.000	.396	+.004	.376	+.007	.349	+.012	.462	+.015	.481	.000	.395	+.004	.370	+.007	.350	+.011	.463	+.015

F. A. A. Ph.D. Thesis
13th Feb., 1969

Structural Engineering Division,
Department of Civil Engineering,
University of Newcastle upon Tyne.

TESTS ON MODEL RADIAL RIBBED DOME — TEST NO. 12 TABLE NO. 10

Experimental Determination of Horizontal Reaction Influence Coefficients

Load at point = 10lb

For position of load points, rib layout, details of model dome and graphs of tabulated results, see Test No. 12, Sheet No. 7.

Horizontal Base Displacement at Rib No. 36 (Towards centre of dome)	Dial gauge readings (A) and actual vertical displacement of point load (B; +ve upwards) in inches									
	Rib No. 17									
	Point 1		Point 5		Point 9		Point 13		Point 17	
	A	B	A	B	A	B	A	B	A	B
0 in.	.481	.000	.404	.000	.368	.000	.339	.000	.447	.000
.02 in.	.481	.000	.405	+.001	.369	+.001	.340	+.001	.448	+.001
.04 in.	.481	.000	.405	+.001	.370	+.002	.341	+.002	.450	+.003
.06 in.	.481	.000	.405	+.001	.370	+.002	.342	+.003	.451	+.004
.08 in.	.481	.000	.406	+.002	.371	+.003	.342	+.003	.453	+.006
.10 in.	.481	.000	.406	+.002	.372	+.004	.343	+.004	.455	+.008
.12 in.	.482	+.001	.406	+.002	.372	+.004	.344	+.005	.456	+.009
.14 in.	.482	+.001	.407	+.003	.373	+.005	.345	+.006	.457	+.010
.16 in.	.482	+.001	.407	+.003	.374	+.006	.346	+.007	.459	+.012
.18 in.	.482	+.001	.407	+.003	.375	+.007	.348	+.009	.460	+.013
.20 in.	.482	+.001	.408	+.004	.375	+.007	.349	+.010	.462	+.015

F.A.A. Ph.D. Thesis
13th Feb., 1969.

Structural Engineering Division,
Department of Civil Engineering,
University of Newcastle upon Tyne.

TESTS ON MODEL RADIAL RIBBED DOME

Test No. 12.
Sheet No. 1

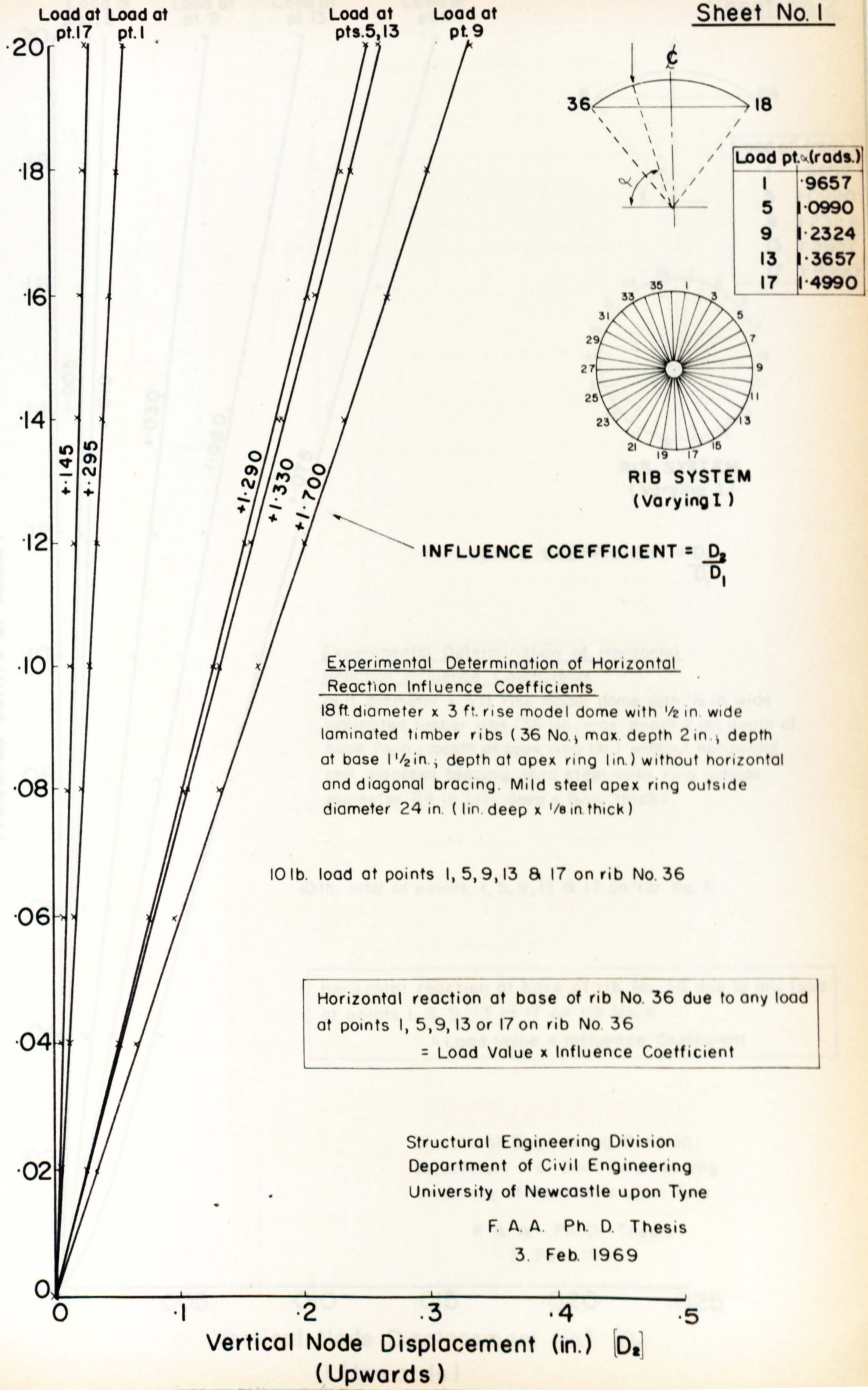

Load pt.	α (rads.)
1	·9657
5	1·0990
9	1·2324
13	1·3657
17	1·4990

RIB SYSTEM
(Varying I)

INFLUENCE COEFFICIENT = $\frac{D_2}{D_1}$

Experimental Determination of Horizontal Reaction Influence Coefficients

18 ft. diameter x 3 ft. rise model dome with ½ in. wide laminated timber ribs (36 No.; max. depth 2 in.; depth at base 1½ in.; depth at apex ring 1 in.) without horizontal and diagonal bracing. Mild steel apex ring outside diameter 24 in. (1 in. deep x ⅛ in. thick)

10 lb. load at points 1, 5, 9, 13 & 17 on rib No. 36

Horizontal reaction at base of rib No. 36 due to any load at points 1, 5, 9, 13 or 17 on rib No. 36
= Load Value x Influence Coefficient

Structural Engineering Division
Department of Civil Engineering
University of Newcastle upon Tyne

F. A. A. Ph. D. Thesis
3. Feb. 1969

TESTS ON MODEL RADIAL RIBBED DOME

Test No. 12

Sheet No. 2

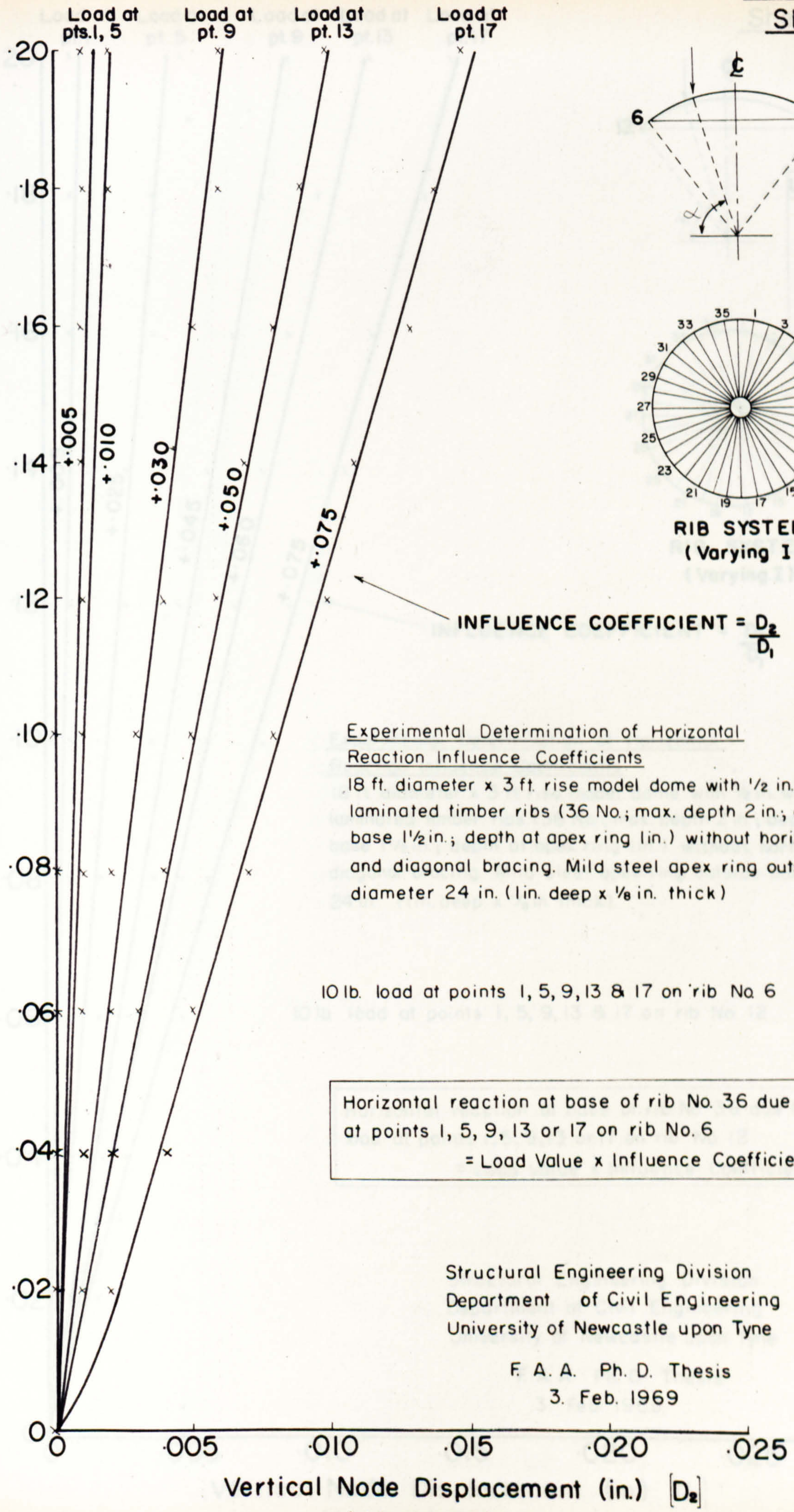

Load pt.	α (rads.)
1	·9657
5	1·0990
9	1·2324
13	1·3657
17	1·4990

RIB SYSTEM
(Varying I)

INFLUENCE COEFFICIENT = $\frac{D_2}{D_1}$

Experimental Determination of Horizontal Reaction Influence Coefficients

18 ft. diameter x 3 ft. rise model dome with ½ in. wide laminated timber ribs (36 No.; max. depth 2 in.; depth at base 1½ in.; depth at apex ring 1in.) without horizontal and diagonal bracing. Mild steel apex ring outside diameter 24 in. (1in. deep x ⅛ in. thick)

10 lb. load at points 1, 5, 9, 13 & 17 on rib No. 6

Horizontal reaction at base of rib No. 36 due to any load at points 1, 5, 9, 13 or 17 on rib No. 6
= Load Value x Influence Coefficient

Structural Engineering Division
Department of Civil Engineering
University of Newcastle upon Tyne

F. A. A. Ph. D. Thesis
3. Feb. 1969

TESTS ON MODEL RADIAL RIBBED DOME

Test No. 12

Sheet No. 3

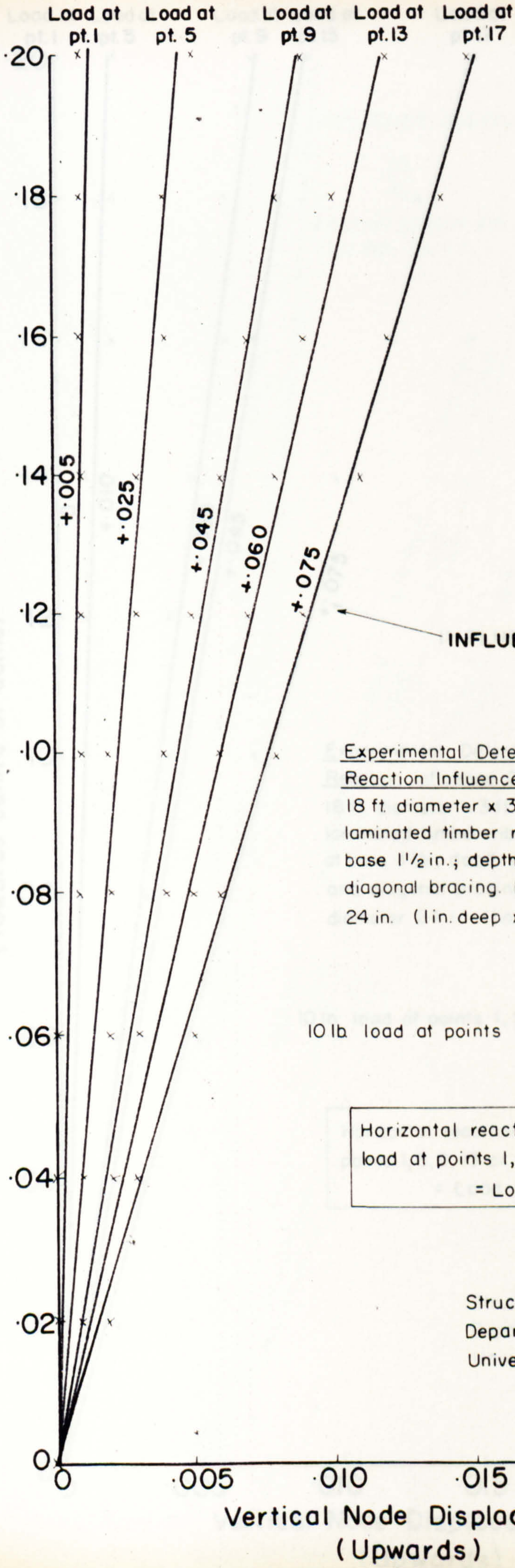

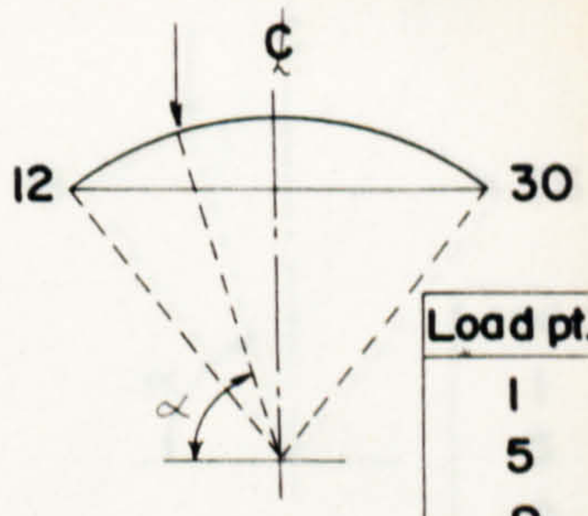

Load pt.	α (rads.)
1	·9657
5	1·0990
9	1·2324
13	1·3657
17	1·4990

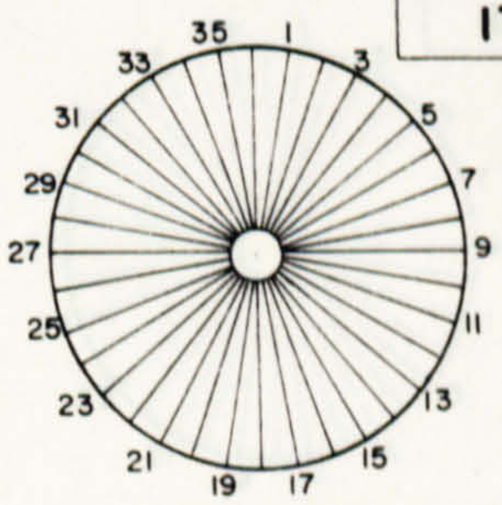

RIB SYSTEM
(Varying I)

INFLUENCE COEFFICIENT = $\frac{D_2}{D_1}$

Experimental Determination of Horizontal Reaction Influence Coefficients

18 ft. diameter x 3 ft. rise model dome with ½ in. wide laminated timber ribs (36 No.; max. depth 2 in.; depth at base 1½ in.; depth at apex ring 1 in.) **without horizontal and** diagonal bracing. Mild steel apex ring outside diameter 24 in. (1 in. deep x ⅛ in. thick)

10 lb. load at points 1, 5, 9, 13 & 17 on rib No. 12

Horizontal reaction at base of rib No. 36 due to any load at points 1, 5, 9, 13 or 17 on rib No. 12
= Load Value x Influence Coefficient

Structural Engineering Division
Department of Civil Engineering
University of Newcastle upon Tyne

F. A. A. Ph. D. Thesis
3. Feb. 1969

TESTS ON MODEL RADIAL RIBBED DOME

Test No. 12
Sheet No. 4

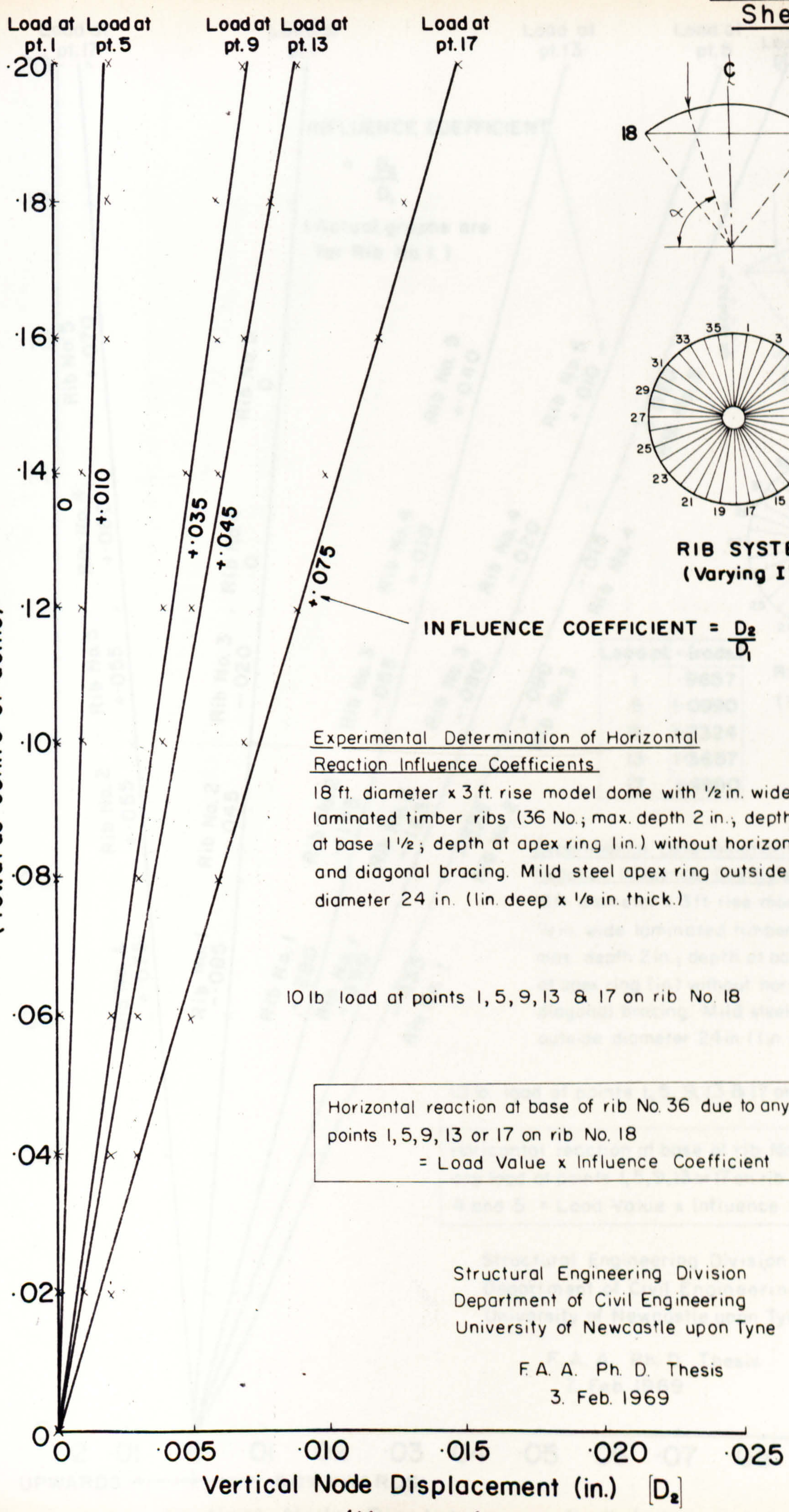

Load pt.	α (rads.)
1	·9657
5	1·0990
9	1·2324
13	1·3657
17	1·4990

RIB SYSTEM
(Varying I)

INFLUENCE COEFFICIENT = $\frac{D_2}{D_1}$

Experimental Determination of Horizontal Reaction Influence Coefficients

18 ft. diameter x 3 ft. rise model dome with ½ in. wide laminated timber ribs (36 No.; max. depth 2 in., depth at base 1½; depth at apex ring 1 in.) without horizontal and diagonal bracing. Mild steel apex ring outside diameter 24 in. (1 in. deep x ⅛ in. thick.)

10 lb load at points 1, 5, 9, 13 & 17 on rib No. 18

Horizontal reaction at base of rib No. 36 due to any load at points 1, 5, 9, 13 or 17 on rib No. 18
= Load Value x Influence Coefficient

Structural Engineering Division
Department of Civil Engineering
University of Newcastle upon Tyne

F. A. A. Ph. D. Thesis
3. Feb. 1969

TESTS ON MODEL RADIAL RIBBED DOME

Test No. 12

Sheet No. 5

Load at pt. 17 | Load at pt. 1 | Load at pt. 13 | Load at pt. 5 | Load at pt. 9

INFLUENCE COEFFICIENT

$= \frac{D_2}{D_1}$

(Actual graphs are for Rib No. 1.)

Rib No. 1. +·075 | Rib No. 2 +·055 | Rib No. 3 +·055 | Rib No. 4 +·060 | Rib No. 5 +·070

Rib No. 1 −·085 | Rib No. 2 −·045 | Rib No. 3 −·020 | Rib No. 4 0 | Rib No. 5 0

Rib No. 1 −·280 | Rib No. 2 −·155 | Rib No. 3 −·055 | Rib No. 4 +·010 | Rib No. 5 +·040

Rib No. 1 −·390 | Rib No. 2 −·185 | Rib No. 3 −·080 | Rib No. 4 −·020 | Rib No. 5 +·010

Rib No. 1 −·435 | Rib No. 2 −·225 | Rib No. 3 −·090 | Rib No. 4 −·015 | Rib No. 5 +·020

Horizontal Base Displacement at Rib No. 36 (in.) [D_1]
(Towards centre of dome)

·20 ·18 ·16 ·14 ·12 ·10 ·08 ·06 ·04 ·02 0

·02 ·01 0 ·01 ·02 ·03 ·04 ·05 ·06 ·07 ·08 ·09

UPWARDS ← → DOWNWARDS

Vertical Node Displacement (in.) [D_2]

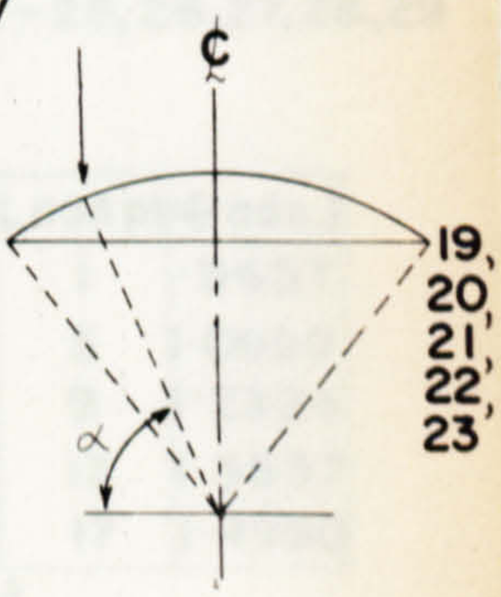

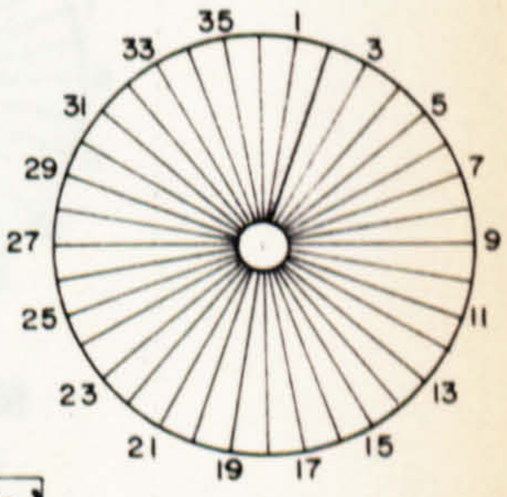

RIB SYSTEM
(Varying I)

Load pt.	∝(rads.)
1	·9657
5	1·0990
9	1·2324
13	1·3657
17	1·4990

Experimental Determination of Horizontal Reaction Influence Coefficients

18 ft. diameter x 3 ft. rise model dome with ½ in. wide laminated timber ribs (36 No.; max. depth 2 in.; depth at base 1½ in.; depth at apex ring 1 in.) without horizontal and diagonal bracing. Mild steel apex ring outside diameter 24 in. (1 in. deep x ⅛ in. thick)

10 lb. load at points 1, 5, 9, 13 & 17 on rib Nos. 1, 2, 3, 4, 5.

Horizontal reaction at base of rib No. 36 due to any load at points 1, 5, 9, 13 or 17 on rib Nos. 1, 2, 3, 4 and 5 = Load Value x Influence Coefficient

Structural Engineering Division
Department of Civil Engineering
University of Newcastle upon Tyne

F. A. A. Ph. D. Thesis
7. Feb. 1969

TESTS ON MODEL RADIAL RIBBED DOME

Test No. 12

Sheet No. 6

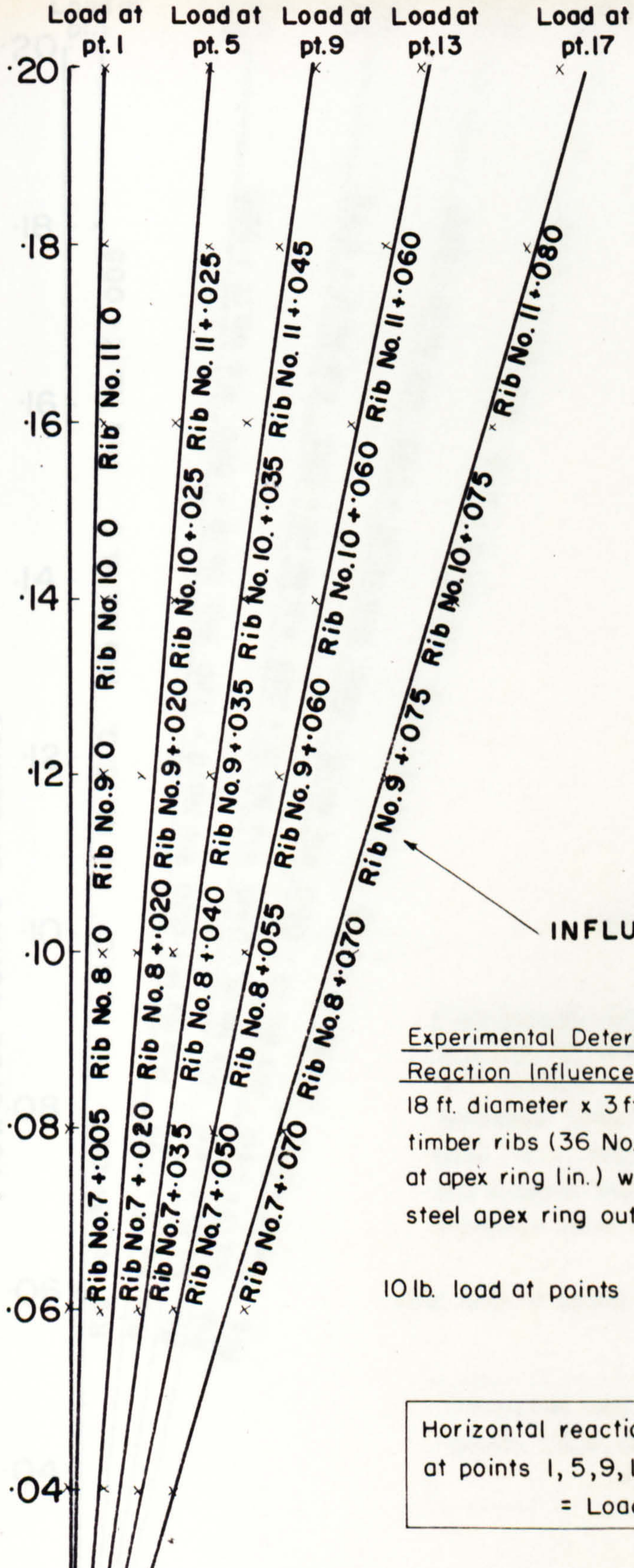

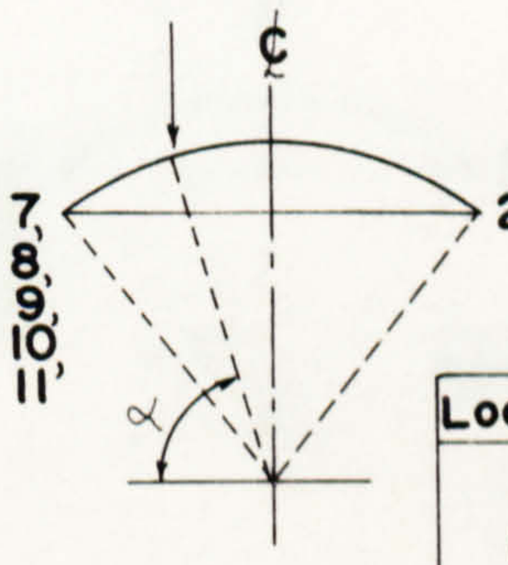

Load pt	α (rads.)
1	·9657
5	1·0990
9	1·2324
13	1·3657
17	1·4990

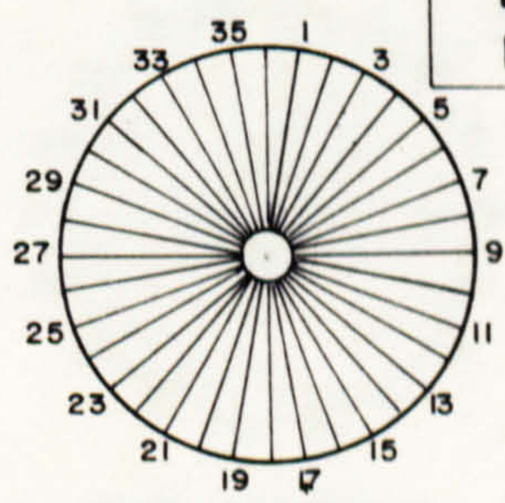

RIB SYSTEM
(Varying I)

INFLUENCE COEFFICIENT = $\frac{D_2}{D_1}$

Experimental Determination of Horizontal Reaction Influence Coefficients

18 ft. diameter x 3 ft. rise model dome with ½ in. wide laminated timber ribs (36 No.; max. depth 2 in.; depth at base 1½ in.; depth at apex ring 1 in.) without horizontal and diagonal bracing. Mild steel apex ring outside diameter 24 in. (1 in. deep x ⅛ in. thick)

10 lb. load at points 1, 5, 9, 13 & 17 on rib Nos. 7, 8, 9, 10, 11

Horizontal reaction at base of rib No. 36 due to any load at points 1, 5, 9, 13 or 17 on rib Nos. 7, 8, 9, 10 and 11
= Load Value x Influence Coefficient

Structural Engineering Division
Department of Civil Engineering
University of Newcastle upon Tyne

F. A. A. Ph. D. Thesis
11. Feb. 1969

TESTS ON MODEL RADIAL RIBBED DOME

Test No. 12
Sheet No. 7

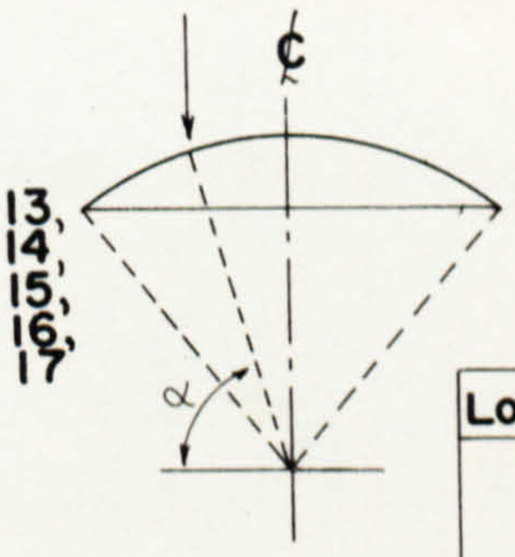

Load pt.	α (rads.)
1	·9657
5	1·0990
9	1·2324
13	1·3657
17	1·4990

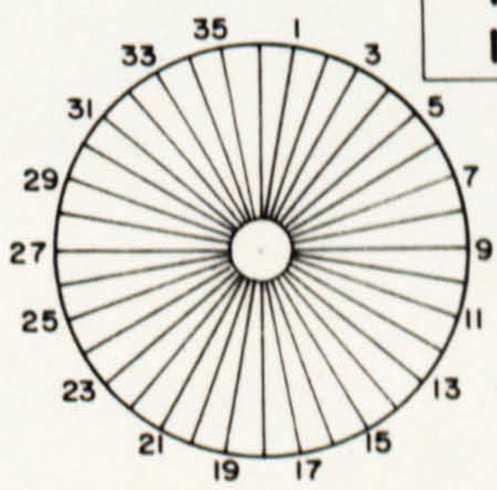

RIB SYSTEM
(Varying I)

Load at pt.1 · Load at pt. 5 · Load at pt.9 · Load at pt.13 · Load at pt.17

Rib No.17.+·005 · Rib No.17.+·020 · Rib No.17.+·035 · Rib No.17.+·050 · Rib No.17.+·075

Rib No. 13+·005 · Rib No.14.0 · Rib No. 15.0. · Rib No. 16. 0 · Rib No.14+·020 · Rib No 15.+·020 · Rib No.16.+·020 · Rib No.14.+·040 · Rib No. 15.+·035 · Rib No.16.+·035 · Rib No.14.+·060 · Rib No.15.+·060 · Rib No.16.+·055 · Rib No.14.+·075 · Rib No.15.+·075 · Rib No.16.+·075

Rib No. 13+·025 · Rib No. 13.+·045 · Rib No. 13+·060 · Rib No. 13+·075

Rib

·02 · ·04 · ·06 · ·08 · ·10 · ·12 · ·14 · ·16 · ·18 · ·20

0 · ·005 · ·010 · ·015 · ·020 · ·025

Horizontal Base Displacement at Rib No. 36 (in.) [D₁]
(Towards centre of dome)

Vertical Node Displacement (in.) [D₂]
(Upwards)

INFLUENCE COEFFICIENT = $\frac{D_2}{D_1}$

Experimental Determination of Horizontal Reaction Influence Coefficients

18 ft. diameter x 3 ft. rise model dome with ½ in. wide laminated timber ribs (36 No.; max. depth 2 in.; depth at base 1½ in.; depth at apex ring 1 in.) without horizontal and diagonal bracing. Mild steel apex ring outside diameter 24 in. (1 in. deep x ⅛ in. thick)

10 lb. load at points 1, 5, 9, 13 & 17 on rib Nos. 13, 14, 15, 16, 17

Horizontal reaction at base of rib No. 36 due to any load at points 1, 5, 9, 13 or 17 on rib Nos. 13, 14, 15, 16 and 17
= Load Value x Influence Coefficient

Structural Engineering Division
Department of Civil Engineering
University of Newcastle upon Tyne

F. A. A. Ph. D. Thesis
13. Feb. 1969

Structural Engineering Division
Department of Civil Engineering
University of Newcastle upon Tyne

H = W × Influence Coefficient

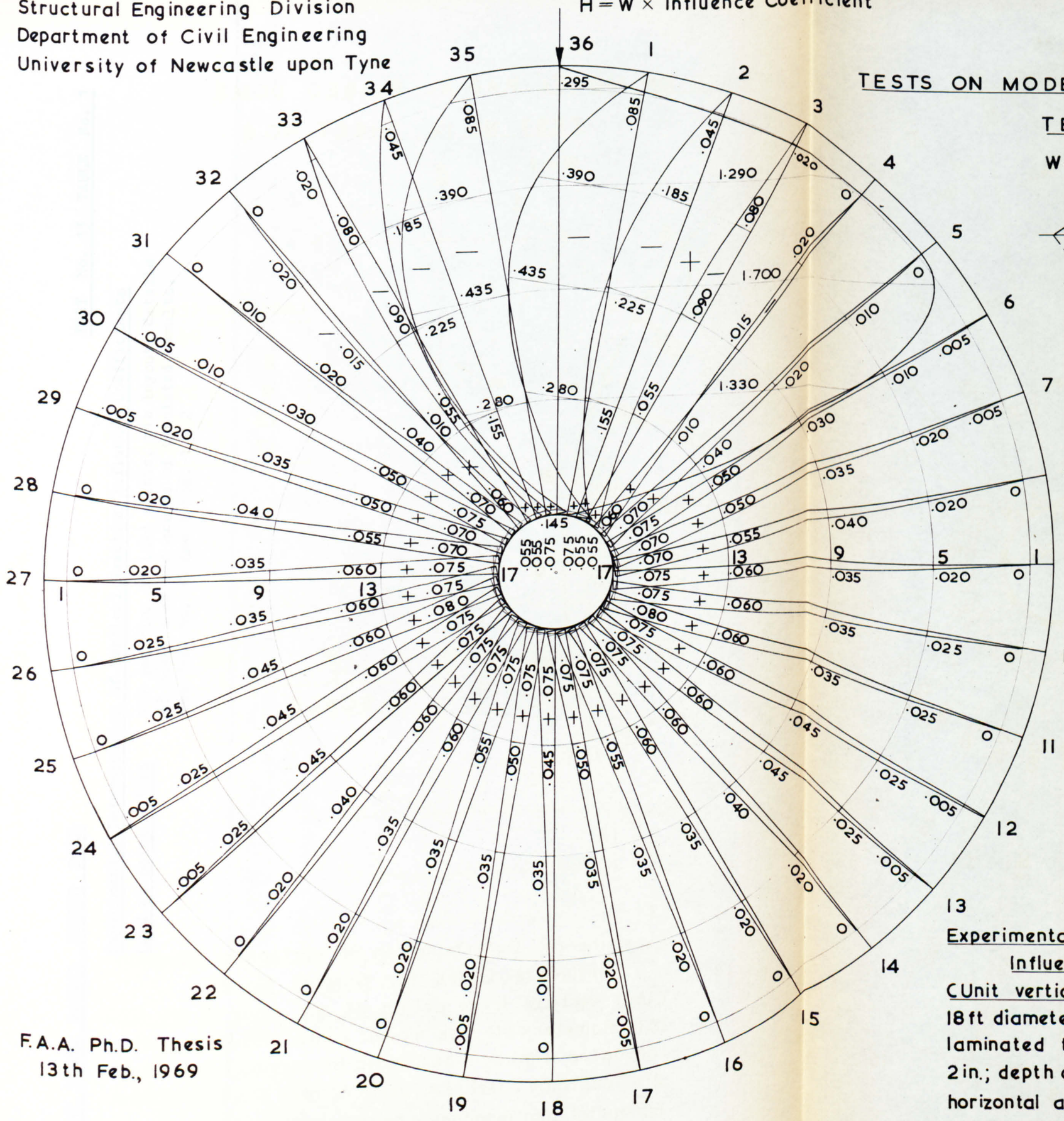

TESTS ON MODEL RADIAL RIBBED DOME

TEST NO. 12 SHEET NO. 8

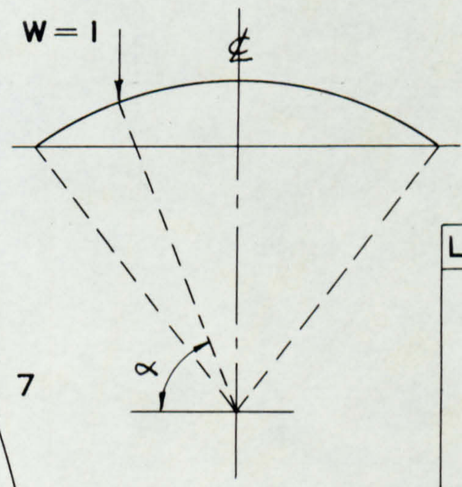

Load Pt.	∝ (rads.)
1	.9657
5	1.0990
9	1.2324
13	1.3657
17	1.4990

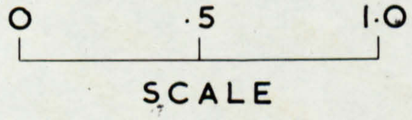

Experimental Determination of Horizontal Reaction Influence Lines for Support No. 36

(Unit vertical force acting at any angle on any rib)

18 ft diameter × 3 ft rise model dome with 1/2 in. wide laminated timber ribs (36 No. of varying I; max. depth 2 in.; depth at base 1 1/2 in.; depth at apex ring 1 in.) without horizontal and diagonal bracing. Mild steel apex ring outside diameter 24 in. (1 in. deep × 1/8 in. thick)

F.A.A. Ph.D. Thesis
13th Feb., 1969

TESTS ON MODEL RADIAL RIBBED DOME

TEST No. 13 TABLE No. 1

Experimental Determination of Vertical Reaction Influence Coefficients

Load at point = 10lb

For position of load points, rib layout, details of model dome and graphs of tabulated results, see Test No. 13 Sheet Nos. 1 & 2

Vertical Base Displacement at Rib No. 18 (Upwards)	Dial gauge readings (A) and actual vertical displacement of point load (B; +ve upwards) in inches																			
	Rib No. 18										Rib No. 19									
	Point 1		Point 5		Point 9		Point 13		Point 17		Point 1		Point 5		Point 9		Point 13		Point 17	
	A	B	A	B	A	B	A	B	A	B	A	B	A	B	A	B	A	B	A	B
0 in.	.482	.000	.401	.000	.371	.000	.341	.000	.439	.000	.478	.000	.397	.000	.359	.000	.338	.000	.445	.000
.02 in.	.500	+.018	.419	+.018	.391	+.020	.356	+.015	.440	+.001	.477	-.001	.394	-.003	.356	-.003	.336	-.002	.446	+.001
.04 in.	.520	+.038	.442	+.041	.414	+.043	.371	+.030	.441	+.002	.476	-.002	.392	-.005	.353	-.006	.335	-.003	.447	+.002
.06 in.	.542	+.060	.466	+.065	.436	+.065	.386	+.045	.443	+.004	.475	-.003	.389	-.008	.350	-.009	.334	-.004	.447	+.002
.08 in.	.565	+.083	.493	+.092	.461	+.090	.402	+.061	.445	+.006	.475	-.003	.387	-.010	.347	-.012	.332	-.006	.448	+.003
.10 in.	.585	+.103	.516	+.115	.482	+.111	.416	+.075	.446	+.007	.474	-.004	.384	-.013	.345	-.014	.331	-.007	.448	+.003
.12 in.	.608	+.126	.543	+.142	.505	+.134	.431	+.090	.447	+.008	.473	-.005	.382	-.015	.342	-.017	.330	-.008	.449	+.004
.14 in.	.628	+.146	.567	+.166	.527	+.156	.445	+.104	.449	+.010	.473	-.005	.379	-.018	.340	-.019	.329	-.009	.449	+.004
.16 in.	.650	+.168	.592	+.191	.550	+.179	.461	+.120	.450	+.011	.472	-.006	.377	-.020	.337	-.022	.327	-.011	.450	+.005
.18 in.	.673	+.191	.616	+.215	.574	+.203	.476	+.135	.452	+.013	.472	-.006	.375	-.022	.335	-.024	.326	-.012	.450	+.005
.20 in.	.692	+.210	.638	+.237	.595	+.224	.491	+.150	.453	+.014	.471	-.007	.373	-.024	.332	-.027	.324	-.014	.450	+.005

F. A. A. Ph.D. Thesis
20th Feb., 1969

Structural Engineering Division,
Department of Civil Engineering,
University of Newcastle upon Tyne.

TESTS ON MODEL RADIAL RIBBED DOME

TEST No. 13 TABLE No. 2

Experimental Determination of Vertical Reaction Influence Coefficients

Load at point = 10lb

For position of load points, rib layout, details of model dome and graphs of tabulated results, see Test No. 13 Sheet No. 2

Vertical Base Displacement at Rib No. 18 (Upwards)	Dial gauge readings (A) and actual vertical displacement of point load (B; +ve upwards) in inches																			
	Rib No. 20										Rib No. 21									
	Point 1		Point 5		Point 9		Point 13		Point 17		Point 1		Point 5		Point 9		Point 13		Point 17	
	A	B	A	B	A	B	A	B	A	B	A	B	A	B	A	B	A	B	A	B
0 in.	.480	.000	.400	.000	.360	.000	.342	.000	.441	.000	.481	.000	.398	.000	.363	.000	.331	.000	.444	.000
.02 in.	.480	.000	.399	-.001	.358	-.002	.341	-.001	.442	+.001	.480	-.001	.397	-.001	.363	.000	.331	.000	.445	+.001
.04 in.	.479	-.001	.397	-.003	.357	-.003	.340	-.002	.442	+.001	.480	-.001	.397	-.001	.362	-.001	.330	-.001	.445	+.001
.06 in.	.479	-.001	.396	-.004	.355	-.005	.339	-.003	.443	+.002	.480	-.001	.396	-.002	.362	-.001	.330	-.001	.446	+.002
.08 in.	.479	-.001	.395	-.005	.354	-.006	.338	-.004	.443	+.002	.480	-.001	.396	-.002	.362	-.001	.330	-.001	.447	+.003
.10 in.	.478	-.002	.394	-.006	.353	-.007	.338	-.004	.444	+.003	.480	-.001	.395	-.003	.361	-.002	.330	-.001	.447	+.003
.12 in.	.478	-.002	.393	-.007	.352	-.008	.337	-.005	.445	+.004	.480	-.001	.395	-.003	.361	-.002	.330	-.001	.448	+.004
.14 in.	.478	-.002	.391	-.009	.350	-.010	.336	-.006	.445	+.004	.480	-.001	.394	-.004	.360	-.003	.329	-.002	.448	+.004
.16 in.	.477	-.003	.390	-.010	.349	-.011	.335	-.007	.446	+.005	.480	-.001	.394	-.004	.360	-.003	.329	-.002	.449	+.005
.18 in.	.477	-.003	.389	-.011	.347	-.013	.335	-.007	.446	+.005	.479	-.002	.394	-.004	.360	-.003	.329	-.002	.449	+.005
.20 in.	.477	-.003	.388	-.012	.346	-.014	.334	-.008	.446	+.005	.479	-.002	.393	-.005	.359	-.004	.329	-.002	.450	+.006

F. A. A. Ph.D. Thesis
21st Feb., 1969

Structural Engineering Division,
Department of Civil Engineering,
University of Newcastle upon Tyne.

TESTS ON MODEL RADIAL RIBBED DOME

TEST No. 13 TABLE No. 3

Experimental Determination of Vertical Reaction Influence Coefficients

Load at point = 10lb

For position of load points, rib layout, details of model dome and graphs of tabulated results, see Test No. 13 Sheet Nos. 2 & 3

Vertical Base Displacement at Rib No. 18 (Upwards)	Dial gauge readings (A) and actual vertical displacement of point load (B; +ve upwards) in inches																			
	Rib No. 22										Rib No. 23									
	Point 1		Point 5		Point 9		Point 13		Point 17		Point 1		Point 5		Point 9		Point 13		Point 17	
	A	B	A	B	A	B	A	B	A	B	A	B	A	B	A	B	A	B	A	B
0 in.	.481	.000	.396	.000	.360	.000	.334	.000	.442	.000	.481	.000	.392	.000	.357	.000	.320	.000	.444	.000
.02 in.	.481	.000	.396	.000	.360	.000	.334	.000	.442	.000	.481	.000	.392	.000	.357	.000	.320	.000	.445	+.001
.04 in.	.481	.000	.396	.000	.360	.000	.334	.000	.443	+.001	.481	.000	.392	.000	.357	.000	.320	.000	.445	+.001
.06 in.	.481	.000	.396	.000	.360	.000	.335	+.001	.443	+.001	.481	.000	.392	.000	.357	.000	.320	.000	.446	+.002
.08 in.	.481	.000	.396	.000	.360	.000	.335	+.001	.444	+.002	.481	.000	.392	.000	.357	.000	.320	.000	.447	+.003
.10 in.	.480	-.001	.396	.000	.360	.000	.335	+.001	.445	+.003	.481	.000	.392	.000	.358	+.001	.321	+.001	.447	+.003
.12 in.	.480	-.001	.395	-.001	.360	.000	.335	+.001	.445	+.003	.481	.000	.392	.000	.358	+.001	.321	+.001	.448	+.004
.14 in.	.480	-.001	.395	-.001	.360	.000	.335	+.001	.446	+.004	.481	.000	.392	.000	.358	+.001	.321	+.001	.448	+.004
.16 in.	.480	-.001	.395	-.001	.360	.000	.335	+.001	.446	+.004	.481	.000	.392	.000	.358	+.001	.321	+.001	.449	+.005
.18 in.	.480	-.001	.395	-.001	.360	.000	.336	+.002	.447	+.005	.481	.000	.392	.000	.358	+.001	.322	+.002	.450	+.006
.20 in.	.480	-.001	.395	-.001	.360	.000	.336	+.002	.447	+.005	.481	.000	.392	.000	.358	+.001	.322	+.002	.450	+.006

F. A. A. Ph.D. Thesis
24th Feb., 1969

Structural Engineering Division,
Department of Civil Engineering,
University of Newcastle upon Tyne.

TESTS ON MODEL RADIAL RIBBED DOME

TEST No. 13 TABLE No. 4

Experimental Determination of Vertical Reaction Influence Coefficients

Load at point = 10lb

For position of load points, rib layout, details of model dome and graphs of tabulated results, see Test No. 13 Sheet No. 3

Vertical Base Displacement at Rib No. 18 (Upwards)	Dial gauge readings (A) and actual vertical displacement of point load (B; +ve upwards) in inches																			
	Rib No. 24										Rib No. 25									
	Point 1		Point 5		Point 9		Point 13		Point 17		Point 1		Point 5		Point 9		Point 13		Point 17	
	A	B	A	B	A	B	A	B	A	B	A	B	A	B	A	B	A	B	A	B
0 in.	.479	.000	.385	.000	.353	.000	.333	.000	.446	.000	.477	.000	.395	.000	.365	.000	.335	.000	.445	.000
.02 in.	.479	.000	.385	.000	.353	.000	.333	.000	.446	.000	.477	.000	.395	.000	.365	.000	.335	.000	.446	+.001
.04 in.	.479	.000	.385	.000	.353	.000	.334	+.001	.447	+.001	.477	.000	.395	.000	.365	.000	.335	.000	.446	+.001
.06 in.	.479	.000	.385	.000	.353	.000	.334	+.001	.447	+.001	.477	.000	.395	.000	.366	+.001	.335	.000	.447	+.002
.08 in.	.479	.000	.385	.000	.353	.000	.334	+.001	.448	+.002	.477	.000	.395	.000	.366	+.001	.336	+.001	.447	+.002
.10 in.	.479	.000	.385	.000	.353	.000	.335	+.002	.448	+.002	.477	.000	.395	.000	.366	+.001	.336	+.001	.448	+.003
.12 in.	.479	.000	.385	.000	.353	.000	.335	+.002	.449	+.003	.477	.000	.395	.000	.366	+.001	.336	+.001	.448	+.003
.14 in.	.479	.000	.385	.000	.353	.000	.335	+.002	.449	+.003	.477	.000	.395	.000	.366	+.001	.337	+.002	.449	+.004
.16 in.	.479	.000	.385	.000	.354	+.001	.336	+.003	.450	+.004	.477	.000	.395	.000	.366	+.001	.337	+.002	.449	+.004
.18 in.	.479	.000	.385	.000	.354	+.001	.336	+.003	.450	+.004	.477	.000	.395	.000	.366	+.001	.337	+.002	.450	+.005
.20 in.	.479	.000	.385	.000	.354	+.001	.336	+.003	.451	+.005	.477	.000	.395	.000	.367	+.002	.337	+.002	.450	+.005

F. A. A. Ph.D. Thesis
25th Feb., 1969

Structural Engineering Division,
Department of Civil Engineering,
University of Newcastle upon Tyne.

TESTS ON MODEL RADIAL RIBBED DOME

TEST No. 13 TABLE No. 5

Experimental Determination of Vertical Reaction Influence Coefficients

Load at point = 10lb

For position of load points, rib layout, details of model dome and graphs of tabulated results, see Test No. 13 Sheet No. 3

Vertical Base Displacement at Rib No. 18 (Upwards)	Dial gauge readings (A) and actual vertical displacement of point load (B; +ve upwards) in inches																			
	Rib No. 26										Rib No. 27									
	Point 1		Point 5		Point 9		Point 13		Point 17		Point 1		Point 5		Point 9		Point 13		Point 17	
	A	B	A	B	A	B	A	B	A	B	A	B	A	B	A	B	A	B	A	B
0 in.	.479	.000	.391	.000	.357	.000	.330	.000	.441	.000	.476	.000	.377	.000	.344	.000	.325	.000	.444	.000
.02 in.	.479	.000	.391	.000	.357	.000	.330	.000	.442	+.001	.476	.000	.377	.000	.344	.000	.325	.000	.444	.000
.04 in.	.479	.000	.391	.000	.357	.000	.330	.000	.442	+.001	.476	.000	.377	.000	.344	.000	.325	.000	.445	+.001
.06 in.	.479	.000	.391	.000	.357	.000	.331	+.001	.442	+.001	.476	.000	.377	.000	.344	.000	.325	.000	.445	+.001
.08 in.	.479	.000	.391	.000	.357	.000	.331	+.001	.443	+.002	.476	.000	.377	.000	.344	.000	.325	.000	.446	+.002
.10 in.	.479	.000	.391	.000	.357	.000	.331	+.001	.443	+.002	.476	.000	.377	.000	.344	.000	.326	+.001	.446	+.002
.12 in.	.479	.000	.391	.000	.357	.000	.331	+.001	.444	+.003	.476	.000	.377	.000	.344	.000	.326	+.001	.446	+.002
.14 in.	.479	.000	.391	.000	.358	+.001	.331	+.001	.444	+.003	.476	.000	.377	.000	.345	+.001	.326	+.001	.447	+.003
.16 in.	.479	.000	.391	.000	.358	+.001	.332	+.002	.445	+.004	.476	.000	.377	.000	.345	+.001	.326	+.001	.447	+.003
.18 in.	.479	.000	.391	.000	.358	+.001	.332	+.002	.445	+.004	.476	.000	.377	.000	.345	+.001	.327	+.002	.448	+.004
.20 in.	.479	.000	.391	.000	.358	+.001	.332	+.002	.446	+.005	.476	.000	.377	.000	.345	+.001	.327	+.002	.448	+.004

F. A. A. Ph.D. Thesis
27th Feb., 1969

Structural Engineering Division,
Department of Civil Engineering,
University of Newcastle upon Tyne.

TESTS ON MODEL RADIAL RIBBED DOME

TEST No. 13 TABLE No. 6

Experimental Determination of Vertical Reaction Influence Coefficients

Load at point = 10lb

For position of load points, rib layout, details of model dome and graphs of tabulated results, see Test No.13 Sheet No. 4

Vertical Base Displacement at Rib No. 18 (Upwards)	Dial gauge readings (A) and actual vertical displacement of point load (B; +ve upwards) in inches																			
	Rib No. 28										Rib No. 29									
	Point 1		Point 5		Point 9		Point 13		Point 17		Point 1		Point 5		Point 9		Point 13		Point 17	
	A	B	A	B	A	B	A	B	A	B	A	B	A	B	A	B	A	B	A	B
0 in.	.481	.000	.390	.000	.354	.000	.331	.000	.442	.000	.479	.000	.390	.000	.354	.000	.331	.000	.445	.000
.02 in.	.481	.000	.390	.000	.354	.000	.331	.000	.442	.000	.479	.000	.390	.000	.354	.000	.331	.000	.446	+.001
.04 in.	.481	.000	.390	.000	.354	.000	.331	.000	.443	+.001	.479	.000	.390	.000	.354	.000	.331	.000	.446	+.001
.06 in.	.481	.000	.390	.000	.354	.000	.331	.000	.443	+.001	.479	.000	.390	.000	.354	.000	.331	.000	.447	+.002
.08 in.	.481	.000	.390	.000	.354	.000	.332	+.001	.443	+.001	.479	.000	.390	.000	.354	.000	.332	+.001	.447	+.002
.10 in.	.481	.000	.390	.000	.355	+.001	.332	+.001	.444	+.002	.479	.000	.390	.000	.355	+.001	.332	+.001	.447	+.002
.12 in.	.481	.000	.390	.000	.355	+.001	.332	+.001	.444	+.002	.479	.000	.390	.000	.355	+.001	.332	+.001	.448	+.003
.14 in.	.481	.000	.390	.000	.355	+.001	.332	+.001	.445	+.003	.479	.000	.390	.000	.355	+.001	.332	+.001	.448	+.003
.16 in.	.481	.000	.390	.000	.355	+.001	.333	+.002	.445	+.003	.479	.000	.390	.000	.355	+.001	.333	+.002	.449	+.004
.18 in.	.481	.000	.390	.000	.355	+.001	.333	+.002	.445	+.003	.479	.000	.390	.000	.355	+.001	.333	+.002	.449	+.004
.20 in.	.481	.000	.390	.000	.355	+.001	.333	+.002	.446	+.004	.479	.000	.390	.000	.355	+.001	.333	+.002	.449	+.004

F. A. A. Ph.D. Thesis
27th Feb., 1969

Structural Engineering Division,
Department of Civil Engineering,
University of Newcastle upon Tyne.

TESTS ON MODEL RADIAL RIBBED DOME

TEST No. 13 TABLE No. 7

Experimental Determination of Vertical Reaction Influence Coefficients

Load at point = 10lb

For position of load points, rib layout, details of model dome and graphs of tabulated results, see Test No. 13 Sheet No. 4

Vertical Base Displacement at Rib No. 18 (Upwards)	Dial gauge readings (A) and actual vertical displacement of point load (B; +ve upwards) in inches																	
	Rib No. 30										Rib No. 31							
	Point 1		Point 5		Point 9		Point 13		Point 17		Point 1		Point 5		Point 9		Point 13		Point 17	
	A	B	A	B	A	B	A	B	A	B	A	B	A	B	A	B	A	B	A	B
0 in.	.480	.000	.392	.000	.359	.000	.343	.000	.445	.000	.479	.000	.397	.000	.362	.000	.340	.000	.444	.000
.02 in.	.480	.000	.392	.000	.359	.000	.343	.000	.446	+.001	.479	.000	.397	.000	.362	.000	.340	.000	.444	.000
.04 in.	.480	.000	.392	.000	.359	.000	.343	.000	.446	+.001	.479	.000	.397	.000	.362	.000	.340	.000	.445	+.001
.06 in.	.480	.000	.392	.000	.359	.000	.344	+.001	.446	+.001	.479	.000	.397	.000	.362	.000	.341	+.001	.445	+.001
.08 in.	.480	.000	.392	.000	.359	.000	.344	+.001	.447	+.002	.479	.000	.397	.000	.362	.000	.341	+.001	.445	+.001
.10 in.	.480	.000	.392	.000	.359	.000	.344	+.001	.447	+.002	.479	.000	.397	.000	.362	.000	.341	+.001	.446	+.002
.12 in.	.480	.000	.392	.000	.359	.000	.344	+.001	.447	+.002	.479	.000	.397	.000	.362	.000	.341	+.001	.446	+.002
.14 in.	.480	.000	.392	.000	.359	.000	.345	+.002	.448	+.003	.479	.000	.397	.000	.363	+.001	.342	+.002	.446	+.002
.16 in.	.480	.000	.392	.000	.360	+.001	.345	+.002	.448	+.003	.479	.000	.397	.000	.363	+.001	.342	+.002	.447	+.003
.18 in.	.480	.000	.392	.000	.360	+.001	.345	+.002	.449	+.004	.479	.000	.397	.000	.363	+.001	.342	+.002	.447	+.003
.20 in.	.480	.000	.392	.000	.360	+.001	.345	+.002	.449	+.004	.479	.000	.397	.000	.363	+.001	.342	+.002	.447	+.003

F. A. A. Ph.D. Thesis
27th, 28th Feb., 1969

Structural Engineering Division,
Department of Civil Engineering,
University of Newcastle upon Tyne.

TESTS ON MODEL RADIAL RIBBED DOME

TEST No. 13 TABLE No. 8

Experimental Determination of Vertical Reaction Influence Coefficients

Load at point = 10lb

For position of load points, rib layout, details of model dome and graphs of tabulated results, see Test No. 13 Sheet Nos. 4 & 5

Vertical Base Displacement at Rib No. 18 (Upwards)	Dial gauge readings (A) and actual vertical displacement of point load (B; +ve upwards) in inches																			
	Rib No. 32										Rib No. 33									
	Point 1		Point 5		Point 9		Point 13		Point 17		Point 1		Point 5		Point 9		Point 13		Point 17	
	A	B	A	B	A	B	A	B	A	B	A	B	A	B	A	B	A	B	A	B
0 in.	.482	.000	.401	.000	.365	.000	.343	.000	.444	.000	.479	.000	.397	.000	.357	.000	.324	.000	.442	.000
.02 in.	.482	.000	.401	.000	.365	.000	.343	.000	.444	.000	.479	.000	.397	.000	.357	.000	.324	.000	.443	+.001
.04 in.	.482	.000	.401	.000	.365	.000	.343	.000	.445	+.001	.479	.000	.397	.000	.357	.000	.324	.000	.443	+.001
.06 in.	.482	.000	.401	.000	.365	.000	.343	.000	.445	+.001	.479	.000	.397	.000	.357	.000	.324	.000	.444	+.002
.08 in.	.482	.000	.401	.000	.365	.000	.343	.000	.445	+.001	.479	.000	.397	.000	.357	.000	.324	.000	.444	+.002
.10 in.	.482	.000	.401	.000	.365	.000	.343	.000	.446	+.002	.479	.000	.397	.000	.357	.000	.324	.000	.444	+.002
.12 in.	.482	.000	.401	.000	.365	.000	.343	.000	.446	+.002	.479	.000	.397	.000	.357	.000	.325	+.001	.445	+.003
.14 in.	.482	.000	.401	.000	.366	+.001	.344	+.001	.446	+.002	.479	.000	.397	.000	.357	.000	.325	+.001	.445	+.003
.16 in.	.482	.000	.401	.000	.366	+.001	.344	+.001	.447	+.003	.479	.000	.397	.000	.357	.000	.325	+.001	.445	+.003
.18 in.	.482	.000	.401	.000	.366	+.001	.344	+.001	.447	+.003	.479	.000	.397	.000	.358	+.001	.325	+.001	.446	+.004
.20 in.	.482	.000	.401	.000	.366	+.001	.344	+.001	.447	+.003	.479	.000	.397	.000	.358	+.001	.325	+.001	.446	+.004

F. A. A. Ph.D. Thesis
28th Feb., 1969

Structural Engineering Division,
Department of Civil Engineering,
University of Newcastle upon Tyne.

TESTS ON MODEL RADIAL RIBBED DOME

TEST No. 13 TABLE No. 9

Experimental Determination of Vertical Reaction Influence Coefficients

Load at point = 10lb

For position of load points, rib layout, details of model dome and graphs of tabulated results, see Test No. 13 Sheet No. 5

Vertical Base Displacement at Rib No. 18 (Upwards)	Dial gauge readings (A) and actual vertical displacement of point load (B; +ve upwards) in inches																			
	Rib No. 34										Rib No. 35									
	Point 1		Point 5		Point 9		Point 13		Point 17		Point 1		Point 5		Point 9		Point 13		Point 17	
	A	B	A	B	A	B	A	B	A	B	A	B	A	B	A	B	A	B	A	B
0 in.	.481	.000	.384	.000	.349	.000	.323	.000	.445	.000	.479	.000	.398	.000	.365	.000	.342	.000	.445	.000
.02 in.	.481	.000	.384	.000	.349	.000	.323	.000	.445	.000	.479	.000	.398	.000	.365	.000	.342	.000	.445	.000
.04 in.	.481	.000	.384	.000	.349	.000	.323	.000	.446	+.001	.479	.000	.398	.000	.365	.000	.342	.000	.446	+.001
.06 in	.481	.000	.384	.000	.349	.000	.323	.000	.446	+.001	.479	.000	.398	.000	.365	.000	.342	.000	.446	+.001
.08 in.	.481	.000	.384	.000	.349	.000	.323	.000	.446	+.001	.479	.000	.398	.000	.365	.000	.342	.000	.446	+.001
.10 in.	.481	.000	.384	.000	.349	.000	.324	+.001	.446	+.001	.479	.000	.398	.000	.365	.000	.342	.000	.447	+.002
.12 in.	.481	.000	.384	.000	.349	.000	.324	+.001	.447	+.002	.479	.000	.398	.000	.366	+.001	.343	+.001	.447	+.002
.14 in.	.481	.000	.384	.000	.349	.000	.324	+.001	.447	+.002	.479	.000	.398	.000	.366	+.001	.343	+.001	.447	+.002
.16 in.	.481	.000	.384	.000	.349	.000	.324	+.001	.448	+.003	.479	.000	.398	.000	.366	+.001	.343	+.001	.448	+.003
.18 in.	.481	.000	.384	.000	.349	.000	.324	+.001	.448	+.003	.479	.000	.398	.000	.366	+.001	.343	+.001	.448	+.003
.20 in.	.481	.000	.384	.000	.349	.000	.324	+.001	.448	+.003	.479	.000	.398	.000	.366	+.001	.343	+.001	.448	+.003

F. A. A. Ph.D. Thesis
28th Feb., 1969

Structural Engineering Division,
Department of Civil Engineering,
University of Newcastle upon Tyne.

Experimental Determination of Vertical Reaction Influence Coefficients
Load at point = 10lb For position of load points, rib layout, details of model dome and graphs of tabulated results, see Test No. 13, Sheet No. 5.

Vertical Base Displacement at Rib No.18 (Upwards)	Dial gauge readings (A) and actual vertical displacement of point load (B; +ve upwards) in inches									
	Rib No. 36									
	Point 1		Point 5		Point 9		Point 13		Point 17	
	A	B	A	B	A	B	A	B	A	B
0 in.	.480	.000	.391	.000	.344	.000	.335	.000	.447	.000
.02 in.	.480	.000	.391	.000	.344	.000	.335	.000	.447	.000
.04 in.	.480	.000	.391	.000	.344	.000	.335	.000	.448	+.001
.06 in.	.480	.000	.391	.000	.344	.000	.335	.000	.448	+.001
.08 in.	.480	.000	.391	.000	.344	.000	.335	.000	.448	+.001
.10 in.	.480	.000	.391	.000	.344	.000	.336	+.001	.449	+.002
.12 in.	.480	.000	.391	.000	.344	.000	.336	+.001	.449	+.002
.14 in.	.480	.000	.391	.000	.344	.000	.336	+.001	.449	+.002
.16 in.	.480	.000	.391	.000	.344	.000	.336	+.001	.450	+.003
.18 in.	.480	.000	.391	.000	.344	.000	.336	+.001	.450	+.003
.20 in.	.480	.000	.391	.000	.344	.000	.336	+.001	.450	+.003

F.A.A. Ph.D. Thesis
28th Feb., 1969.

Structural Engineering Division,
Department of Civil Engineering,
University of Newcastle upon Tyne

TESTS ON MODEL RADIAL RIBBED DOME

Test No. 13

Sheet No. 1

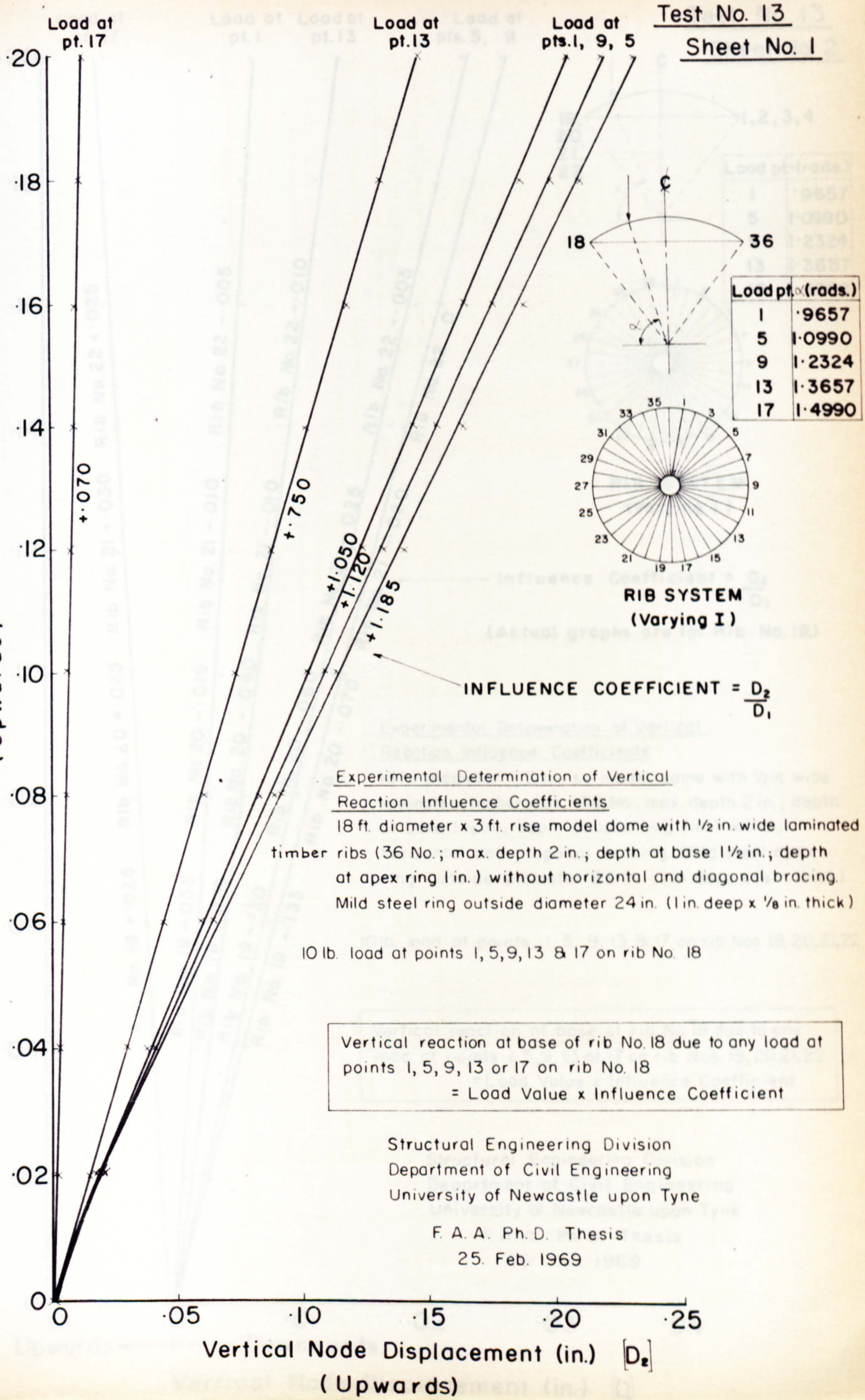

Load pt.	α (rads.)
1	·9657
5	1·0990
9	1·2324
13	1·3657
17	1·4990

RIB SYSTEM
(Varying I)

INFLUENCE COEFFICIENT = $\frac{D_2}{D_1}$

Experimental Determination of Vertical Reaction Influence Coefficients

18 ft. diameter x 3 ft. rise model dome with ½ in. wide laminated timber ribs (36 No.; max. depth 2 in.; depth at base 1½ in.; depth at apex ring 1 in.) without horizontal and diagonal bracing. Mild steel ring outside diameter 24 in. (1 in. deep x ⅛ in. thick)

10 lb. load at points 1, 5, 9, 13 & 17 on rib No. 18

Vertical reaction at base of rib No. 18 due to any load at points 1, 5, 9, 13 or 17 on rib No. 18
= Load Value x Influence Coefficient

Structural Engineering Division
Department of Civil Engineering
University of Newcastle upon Tyne

F. A. A. Ph. D. Thesis
25. Feb. 1969

TESTS ON MODEL RADIAL RIBBED DOME

Test No. 13

Sheet No. 2

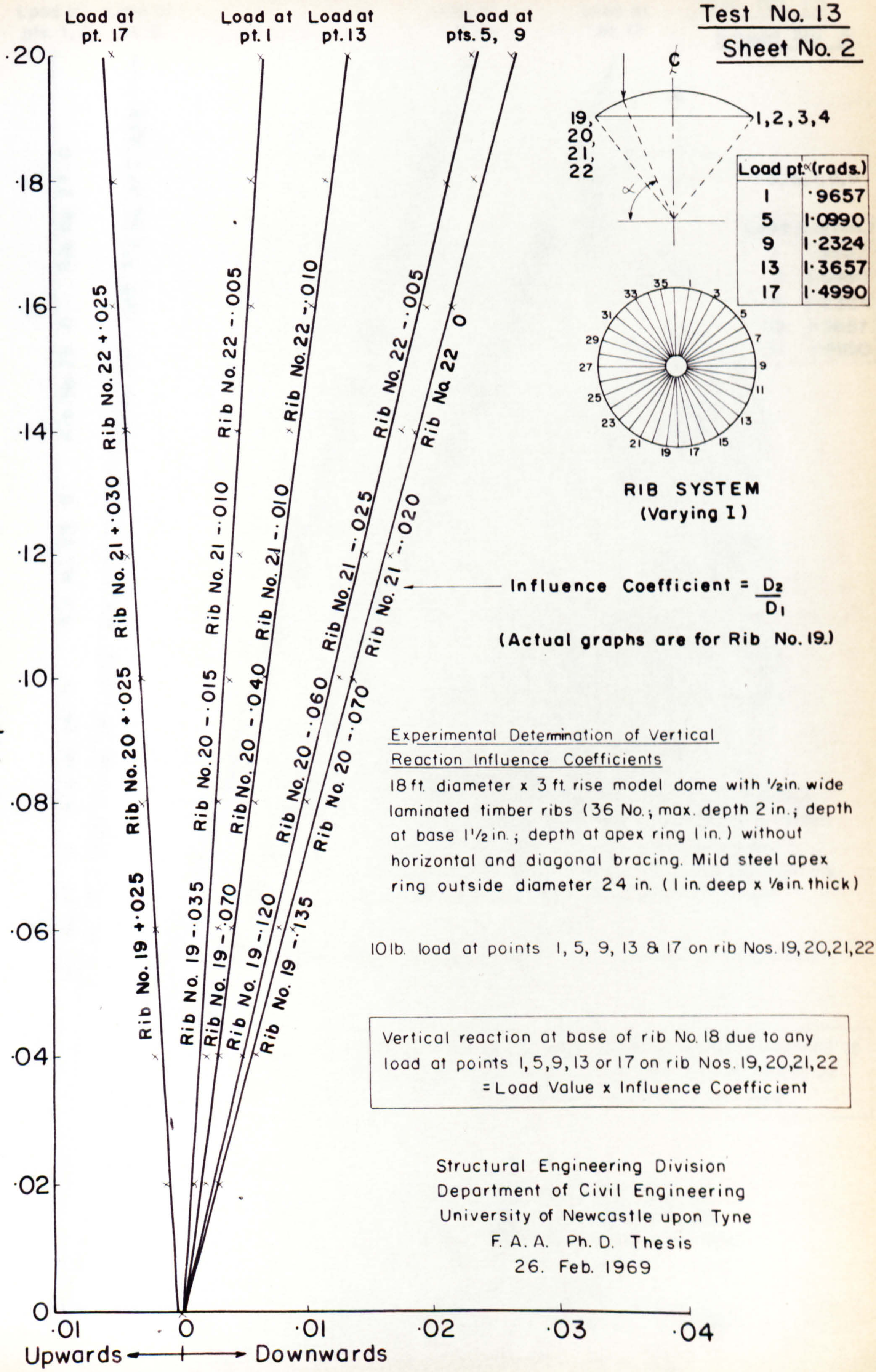

Load pt.	α (rads.)
1	·9657
5	1·0990
9	1·2324
13	1·3657
17	1·4990

RIB SYSTEM
(Varying I)

Influence Coefficient = $\frac{D_2}{D_1}$

(Actual graphs are for Rib No. 19.)

Experimental Determination of Vertical Reaction Influence Coefficients

18 ft. diameter x 3 ft. rise model dome with ½in. wide laminated timber ribs (36 No.; max. depth 2 in.; depth at base 1½ in.; depth at apex ring 1 in.) without horizontal and diagonal bracing. Mild steel apex ring outside diameter 24 in. (1 in. deep x ⅛in. thick)

10lb. load at points 1, 5, 9, 13 & 17 on rib Nos. 19, 20, 21, 22

Vertical reaction at base of rib No. 18 due to any load at points 1, 5, 9, 13 or 17 on rib Nos. 19, 20, 21, 22 = Load Value x Influence Coefficient

Structural Engineering Division
Department of Civil Engineering
University of Newcastle upon Tyne
F. A. A. Ph. D. Thesis
26. Feb. 1969

TESTS ON MODEL RADIAL RIBBED DOME

Test No. 13

Sheet No. 3

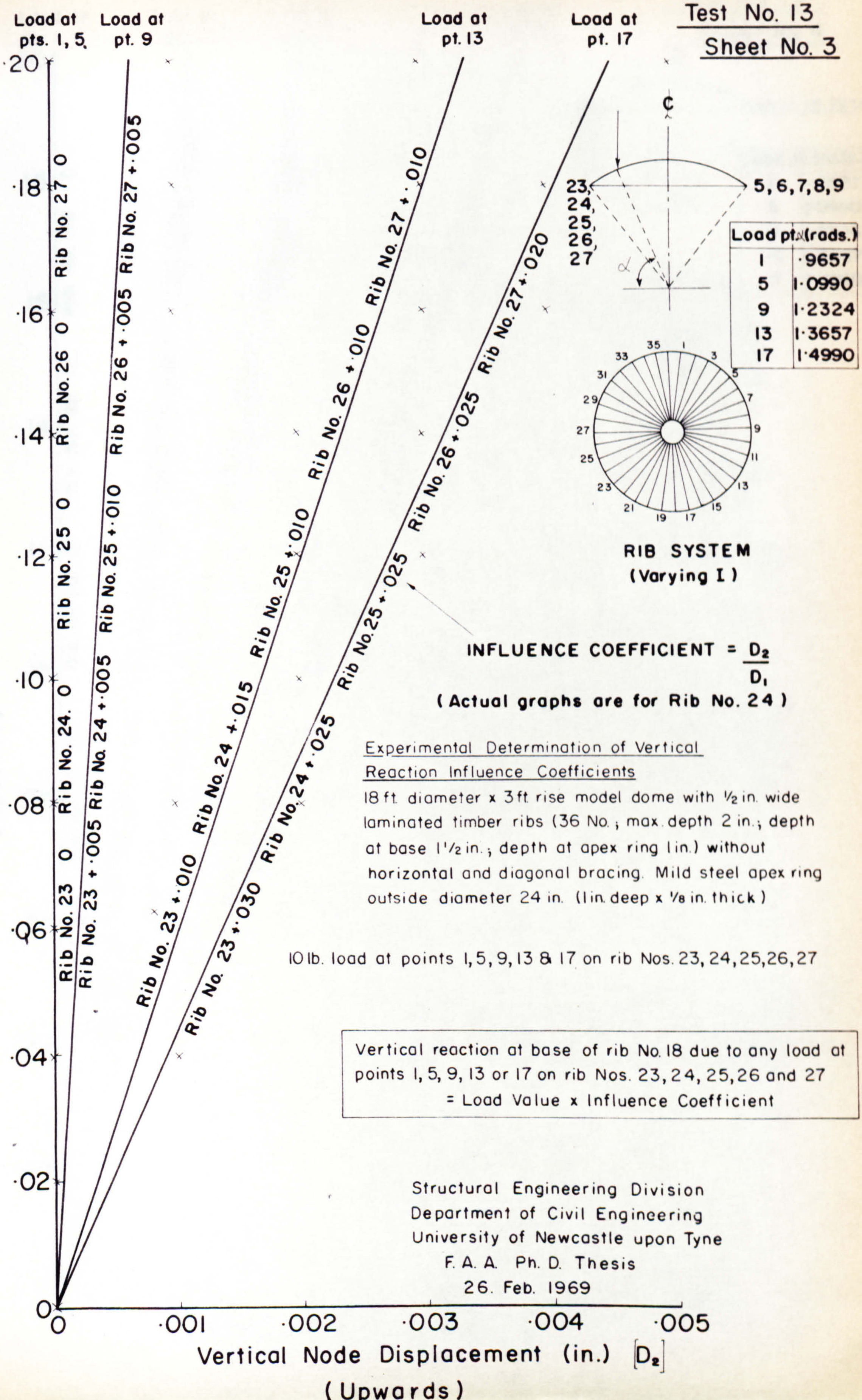

Load pt.	α (rads.)
1	·9657
5	1·0990
9	1·2324
13	1·3657
17	1·4990

RIB SYSTEM
(Varying I)

INFLUENCE COEFFICIENT = $\frac{D_2}{D_1}$

(Actual graphs are for Rib No. 24)

Experimental Determination of Vertical Reaction Influence Coefficients

18 ft. diameter x 3 ft. rise model dome with ½ in. wide laminated timber ribs (36 No.; max. depth 2 in.; depth at base 1½ in.; depth at apex ring 1 in.) without horizontal and diagonal bracing. Mild steel apex ring outside diameter 24 in. (1 in. deep x ⅛ in. thick)

10 lb. load at points 1, 5, 9, 13 & 17 on rib Nos. 23, 24, 25, 26, 27

Vertical reaction at base of rib No. 18 due to any load at points 1, 5, 9, 13 or 17 on rib Nos. 23, 24, 25, 26 and 27
= Load Value x Influence Coefficient

Structural Engineering Division
Department of Civil Engineering
University of Newcastle upon Tyne
F. A. A. Ph. D. Thesis
26. Feb. 1969

TESTS ON MODEL RADIAL RIBBED DOME

Test No. 13

Sheet No. 4

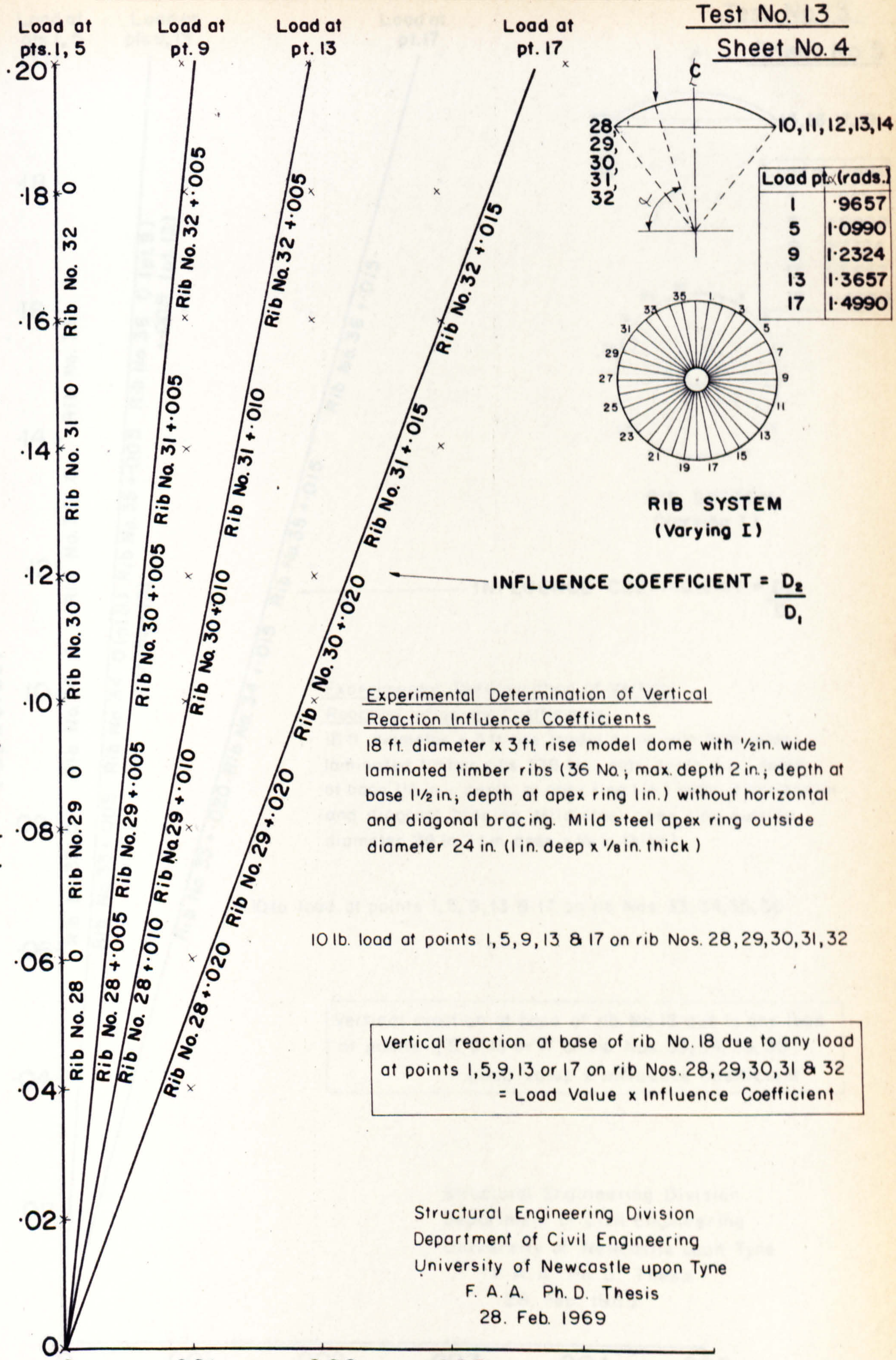

Load pt.	α (rads.)
1	·9657
5	1·0990
9	1·2324
13	1·3657
17	1·4990

RIB SYSTEM
(Varying I)

INFLUENCE COEFFICIENT = $\frac{D_2}{D_1}$

Experimental Determination of Vertical Reaction Influence Coefficients

18 ft. diameter x 3 ft. rise model dome with ½in. wide laminated timber ribs (36 No.; max. depth 2 in.; depth at base 1½ in.; depth at apex ring 1in.) without horizontal and diagonal bracing. Mild steel apex ring outside diameter 24 in. (1 in. deep x ⅛ in. thick)

10 lb. load at points 1, 5, 9, 13 & 17 on rib Nos. 28, 29, 30, 31, 32

Vertical reaction at base of rib No. 18 due to any load at points 1, 5, 9, 13 or 17 on rib Nos. 28, 29, 30, 31 & 32 = Load Value x Influence Coefficient

Structural Engineering Division
Department of Civil Engineering
University of Newcastle upon Tyne
F. A. A. Ph. D. Thesis
28. Feb. 1969

TESTS ON MODEL RADIAL RIBBED DOME

Test No. 13

Sheet No. 5

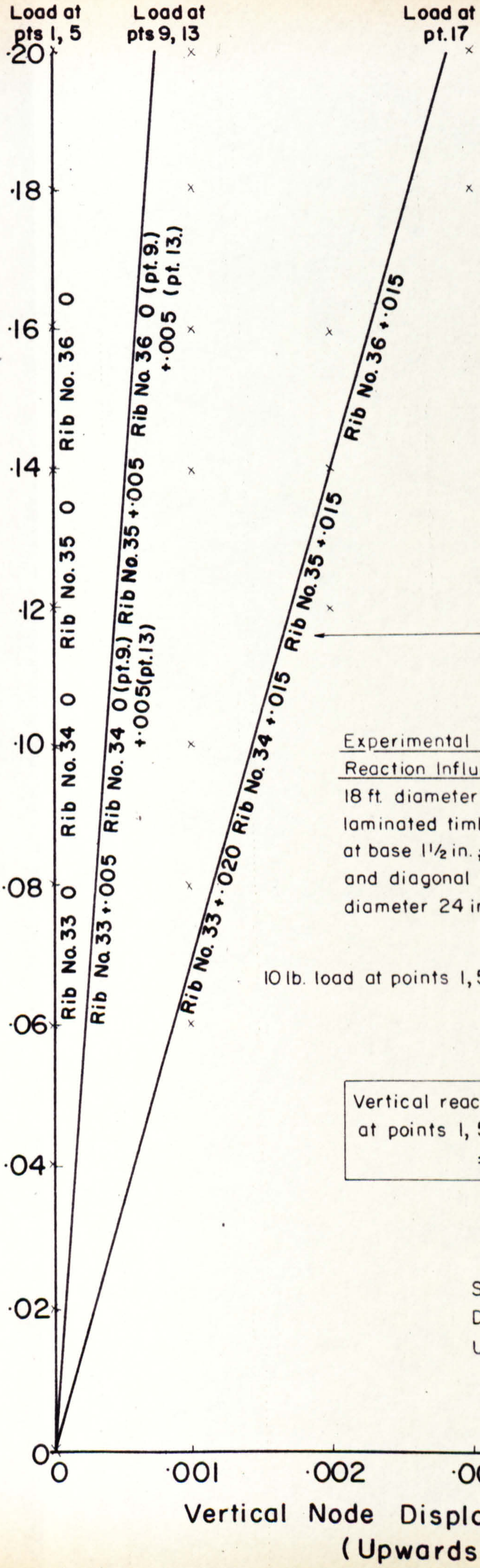

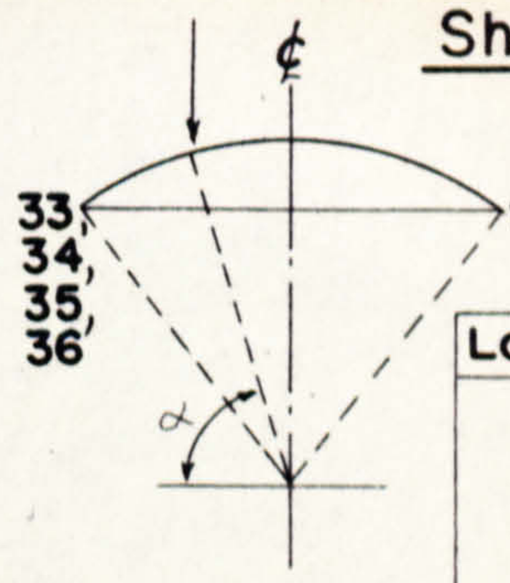

Load pt.	α (rads.)
1	·9657
5	1·0990
9	1·2324
13	1·3657
17	1·4990

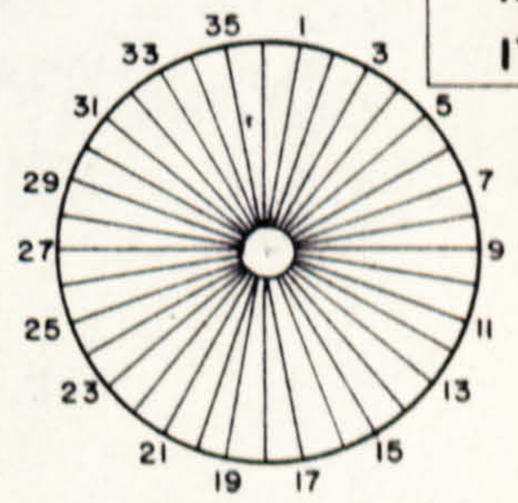

RIB SYSTEM
(Varying I)

INFLUENCE COEFFICIENT = $\frac{D_2}{D_1}$

Experimental Determination of Vertical Reaction Influence Coefficients

18 ft. diameter x 3 ft. rise model dome with ½ in. wide laminated timber ribs (36 No.; max. depth 2 in.; depth at base 1½ in.; depth at apex ring 1 in.) without horizontal and diagonal bracing. Mild steel apex ring outside diameter 24 in. (1 in. deep x ⅛ in. thick)

10 lb. load at points 1, 5, 9, 13 & 17 on rib Nos. 33, 34, 35, 36

Vertical reaction at base of rib No. 18 due to any load at points 1, 5, 9, 13 or 17 on rib Nos. 33, 34, 35, 36
= Load Value x Influence Coefficient

Structural Engineering Division
Department of Civil Engineering
University of Newcastle upon Tyne
F. A. A. Ph. D. Thesis
28. Feb. 1969

Structural Engineering Division
Department of Civil Engineering
University of Newcastle upon Tyne

TESTS ON MODEL RADIAL RIBBED DOME

TEST NO. 13 SHEET NO. 6

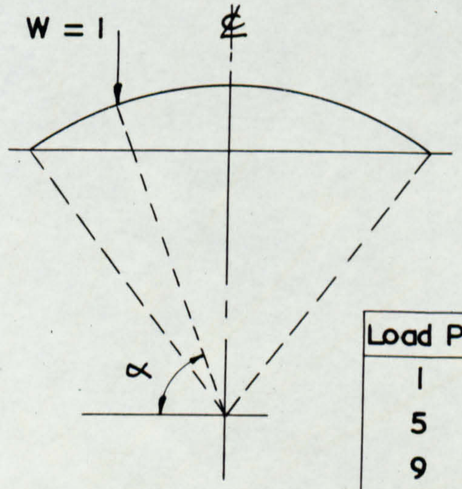

Load Pt.	α(rads.)
1	·9657
5	1·0990
9	1·2324
13	1·3657
17	1·4990

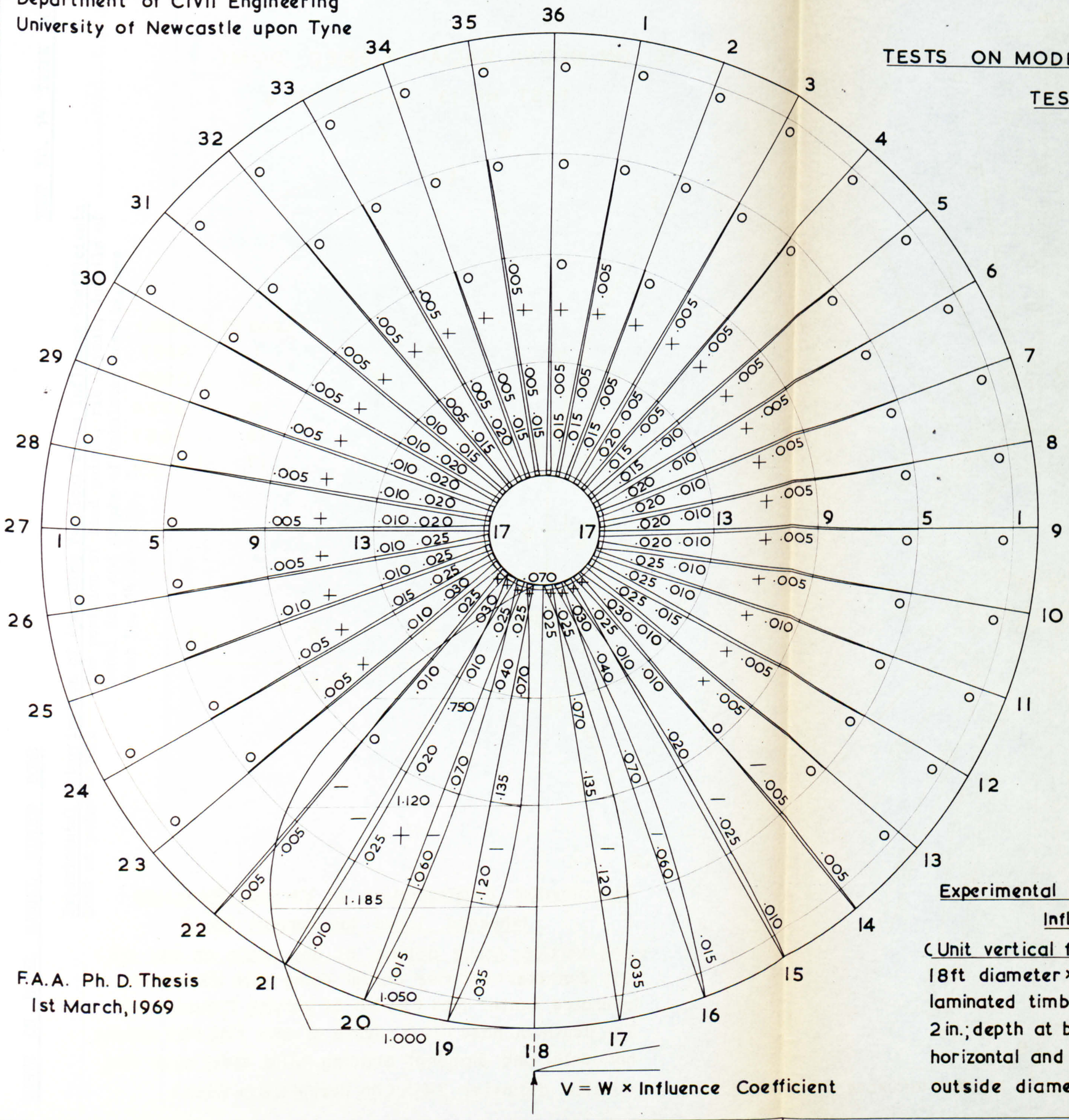

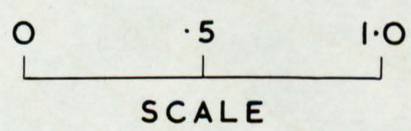

F.A.A. Ph. D. Thesis
1st March, 1969

Experimental Determination of Vertical Reaction Influence Lines for Support No. 18

(Unit vertical force acting at any angle on any rib)
18ft diameter × 3ft rise model dome with 1/2in. wide laminated timber ribs (36 No. of varying I; max. depth 2 in.; depth at base 1½ in.; depth at apex ring 1in.) without horizontal and diagonal bracing. Mild steel apex ring outside diameter 24in. (1in. deep × 1/8 in. thick)

Experimental Determination of Apex Ring Vertical Force Influence Coefficients

Load at point = 10lb

For position of load points, rib layout, details of model dome and graphs of tabulated results, see Test No. 14 Sheet No. 1.

Vertical Displacement At Apex Ring on Rib No. 36 (Upwards)	Dial gauge readings (A) and actual vertical displacement of point load (B; +ve upwards) in inches																			
	Rib No. 36										Rib No. 1									
	Point 1		Point 5		Point 9		Point 13		Point 17		Point 1		Point 5		Point 9		Point 13		Point 17	
	A	B	A	B	A	B	A	B	A	B	A	B	A	B	A	B	A	B	A	B
0 in.	.481	.000	.392	.000	.347	.000	.336	.000	.456	.000	.478	.000	.388	.000	.352	.000	.334	.000	.442	.000
.01 in.	.481	.000	.393	+.001	.352	+.005	.345	+.009	.466	+.010	.478	.000	.390	+.002	.357	+.005	.343	+.009	.453	+.011
.02 in.	.481	.000	.395	+.003	.358	+.011	.355	+.019	.476	+.020	.479	+.001	.392	+.004	.363	+.011	.352	+.018	.464	+.022
.03 in.	.482	+.001	.397	+.005	.362	+.015	.363	+.027	.486	+.030	.479	+.001	.394	+.006	.368	+.016	.360	+.026	.475	+.033
.04 in.	.482	+.001	.399	+.007	.368	+.021	.372	+.036	.496	+.040	.479	+.001	.396	+.008	.374	+.022	.369	+.035	.485	+.043
.05 in.	.482	+.001	.401	+.009	.373	+.026	.382	+.046	.506	+.050	.480	+.002	.399	+.011	.379	+.027	.379	+.045	.496	+.054
.06 in.	.483	+.002	.404	+.012	.379	+.032	.391	+.055	.516	+.060	.480	+.002	.401	+.013	.384	+.032	.388	+.054	.506	+.064
.07 in.	.483	+.002	.406	+.014	.384	+.037	.399	+.063	.526	+.070	.481	+.003	.404	+.016	.390	+.038	.396	+.062	.517	+.075
.08 in.	.484	+.003	.408	+.016	.389	+.042	.408	+.072	.536	+.080	.481	+.003	.406	+.018	.395	+.043	.406	+.072	.528	+.086
.09 in.	.484	+.003	.410	+.018	.394	+.047	.416	+.080	.546	+.090	.481	+.003	.409	+.021	.401	+.049	.415	+.081	.538	+.096
.10 in.	.485	+.004	.413	+.021	.400	+.053	.424	+.088	.556	+.100	.482	+.004	.411	+.023	.407	+.055	.424	+.090	.549	+.107

F. A. A. Ph.D. Thesis
3rd, 4th March, 1969

Structural Engineering Division,
Department of Civil Engineering,
University of Newcastle upon Tyne.

TESTS ON MODEL RADIAL RIBBED DOME

TEST NO. 14 TABLE NO. 2

Experimental Determination of Apex Ring Vertical Force Influence Coefficients

Load at point = 10lb

For position of load points, rib layout, details of model dome and graphs of tabulated results, see Test No. 14 Sheet No. 1.

Vertical Displacement at Apex Ring on Rib No. 36 (Upwards)	Dial gauge readings (A) and actual vertical displacement of point load (B; +ve upwards) in inches																			
	Rib No. 2										Rib No. 3									
	Point 1		Point 5		Point 9		Point 13		Point 17		Point 1		Point 5		Point 9		Point 13		Point 17	
	A	B	A	B	A	B	A	B	A	B	A	B	A	B	A	B	A	B	A	B
0 in.	.479	.000	.399	.000	.358	.000	.332	.000	.440	.000	.477	.000	.399	.000	.362	.000	.333	.000	.442	.000
.01 in.	.479	.000	.400	+.001	.363	+.005	.340	+.008	.451	+.011	.477	.000	.400	+.001	.366	+.004	.340	+.007	.452	+.010
.02 in.	.479	.000	.402	+.003	.368	+.010	.348	+.016	.461	+.021	.477	.000	.401	+.002	.370	+.008	.347	+.014	.461	+.019
.03 in.	.480	+.001	.404	+.005	.373	+.015	.356	+.024	.471	+.031	.477	.000	.402	+.003	.374	+.012	.354	+.021	.471	+.029
.04 in.	.480	+.001	.406	+.007	.378	+.020	.364	+.032	.481	+.041	.478	+.001	.404	+.005	.379	+.017	.360	+.027	.481	+.039
.05 in.	.480	+.001	.408	+.009	.383	+.025	.373	+.041	.492	+.052	.478	+.001	.405	+.006	.383	+.021	.367	+.034	.490	+.048
.06 in.	.480	+.001	.410	+.011	.388	+.030	.382	+.050	.502	+.062	.478	+.001	.407	+.008	.387	+.025	.374	+.041	.499	+.057
.07 in.	.481	+.002	.411	+.012	.393	+.035	.390	+.058	.512	+.072	.478	+.001	.409	+.010	.391	+.029	.381	+.048	.510	+.068
.08 in.	.481	+.002	.413	+.014	.398	+.040	.398	+.066	.522	+.082	.479	+.002	.411	+.012	.395	+.033	.387	+.054	.518	+.076
.09 in.	.481	+.002	.414	+.015	.403	+.045	.407	+.075	.532	+.092	.479	+.002	.412	+.013	.399	+.037	.394	+.061	.528	+.086
.10 in.	.482	+.003	.416	+.017	.407	+.049	.415	+.083	.542	+.102	.479	+.002	.414	+.015	.403	+.041	.401	+.068	.538	+.096

F. A. A. Ph.D. Thesis
4th, 5th March, 1969

Structural Engineering Division,
Department of Civil Engineering,
University of Newcastle upon Tyne.

TESTS ON MODEL RADIAL RIBBED DOME

TEST NO. 14 TABLE NO. 3

Experimental Determination of Apex Ring Vertical Force Influence Coefficients

Load at point = 10lb

For position of load points, rib layout, details of model dome and graphs of tabulated results, see Test No. 14, Sheet No. 1.

Vertical Displacement at Apex Ring on Rib No. 36 (Upwards)	Dial gauge readings (A) and actual vertical displacement of point load (B;+ve upwards) in inches																	
	Rib No. 4										Rib No. 5							
	Point 1		Point 5		Point 9		Point 13		Point 17		Point 1		Point 5		Point 9		Point 13		Point 17	
	A	B	A	B	A	B	A	B	A	B	A	B	A	B	A	B	A	B	A	B
0 in.	.479	.000	.395	.00	.352	.000	.328	.000	.443	.000	.478	.000	.398	.000	.357	.000	.342	.000	.436	.000
.01 in.	.479	.000	.396	+.001	.355	+.003	.334	+.006	.452	+.009	.478	.000	.398	.000	.359	+.002	.347	+.005	.444	+.008
.02 in.	.479	.000	.396	+.001	.359	+.007	.340	+.012	.460	+.017	.478	.000	.399	+.001	.361	+.004	.352	+.010	.451	+.015
.03 in.	.479	.000	.397	+.002	.362	+.010	.346	+.018	.468	+.025	.478	.000	.399	+.001	.363	+.006	.356	+.014	.459	+.023
.04 in.	.479	.000	.398	+.003	.365	+.013	.351	+.023	.477	+.034	.478	.000	.400	+.002	.365	+.008	.361	+.019	.466	+.030
.05 in.	.479	.000	.399	+.004	.368	+.016	.357	+.029	.486	+.043	.478	.000	.400	+.002	.367	+.010	.365	+.023	.475	+.039
.06 in.	.479	.000	.400	+.005	.371	+.019	.363	+.035	.495	+.052	.478	.000	.401	+.003	.369	+.012	.369	+.027	.481	+.045
.07 in.	.480	+.001	.401	+.006	.375	+.023	.368	+.040	.503	+.060	.478	.000	.401	+.003	.371	+.014	.374	+.032	.490	+.054
.08 in.	.480	+.001	.402	+.007	.378	+.026	.375	+.047	.511	+.068	.478	.000	.401	+.003	.373	+.016	.378	+.036	.497	+.061
.09 in.	.480	+.001	.403	+.008	.381	+.029	.380	+.052	.520	+.077	.478	.000	.402	+.004	.375	+.018	.383	+.041	.504	+.068
.10 in.	.480	+.001	.404	+.009	.384	+.032	.386	+.058	.529	+.086	.478	.000	.403	+.005	.377	+.020	.387	+.045	.512	+.076

F. A. A. Ph.D. Thesis
5th March, 1969.

Structural Engineering Division,
Department of Civil Engineering,
University of Newcastle upon Tyne.

TESTS ON MODEL RADIAL RIBBED DOME

TEST NO. 14 TABLE NO. 4

Experimental Determination of Apex Ring Vertical Force Influence Coefficients

Load at point = 10 lb

For position of load points, rib layout, details of model dome and graphs of tabulated results, see Test No. 14, Sheet No. 2.

Vertical Displacement At Apex Ring on Rib No. 36 (Upwards)	Dial Gauge Readings (A) and actual vertical displacement of point load (B;+ve upwards) in inches																	
	Rib No. 6										Rib No. 7							
	Point 1		Point 5		Point 9		Point 13		Point 17		Point 1		Point 5		Point 9		Point 13		Point 17	
	A	B	A	B	A	B	A	B	A	B	A	B	A	B	A	B	A	B	A	B
0 in.	.477	.000	.385	.000	.345	.000	.325	.000	.443	.000	.480	.000	.394	.000	.359	.000	.331	.000	.438	.000
.01 in.	.477	.000	.385	.000	.346	+.001	.329	+.004	.449	+.006	.480	.000	.393	-.001	.359	.000	.333	+.002	.444	+.006
.02 in.	.477	.000	.385	.000	.347	+.002	.332	+.007	.456	+.013	.480	.000	.392	-.002	.359	.000	.335	+.004	.450	+.012
.03 in.	.477	.000	.385	.000	.348	+.003	.335	+.010	.462	+.019	.480	.000	.392	-.002	.359	.000	.337	+.006	.455	+.017
.04 in.	.476	-.001	.384	-.001	.349	+.004	.339	+.014	.469	+.026	.479	-.001	.391	-.003	.359	.000	.339	+.008	.460	+.022
.05 in.	.476	-.001	.384	-.001	.350	+.005	.342	+.017	.476	+.033	.479	-.001	.390	-.004	.359	.000	.341	+.010	.465	+.027
.06 in.	.476	-.001	.384	-.001	.351	+.006	.346	+.021	.483	+.040	.479	-.001	.389	-.005	.359	.000	.343	+.012	.471	+.033
.07 in.	.476	-.001	.384	-.001	.352	+.007	.349	+.024	.490	+.047	.478	-.002	.388	-.006	.359	.000	.345	+.014	.476	+.038
.08 in.	.476	-.001	.384	-.001	.353	+.008	.353	+.028	.496	+.053	.478	-.002	.388	-.006	.359	.000	.347	+.016	.482	+.044
.09 in.	.475	-.002	.384	-.001	.354	+.009	.356	+.031	.503	+.060	.478	-.002	.387	-.007	.359	.000	.349	+.018	.487	+.049
.10 in.	.475	-.002	.384	-.001	.355	+.010	.360	+.035	.510	+.067	.478	-.002	.386	-.008	.359	.000	.351	+.020	.493	+.055

F. A. A. Ph.D. Thesis
5th March, 1969.

Structural Engineering Division,
Department of Civil Engineering,
University of Newcastle upon Tyne.

TESTS ON MODEL RADIAL RIBBED DOME

TEST NO. 14 TABLE NO. 5

Experimental Determination of Apex Ring Vertical Force Influence Coefficients

Load at point = 10lb

For position of load points, rib layout, details of model dome and graphs of tabulated results, see Test No. 14, Sheet No. 2.

Vertical Displacement at Apex Ring on Rib No. 36 (Upwards)	Dial gauge readings (A) and actual vertical displacement of point load (B; +ve upwards) in inches																	
	Rib No. 8										Rib No. 9							
	Point 1		Point 5		Point 9		Point 13		Point 17		Point 1		Point 5		Point 9		Point 13		Point 17	
	A	B	A	B	A	B	A	B	A	B	A	B	A	B	A	B	A	B	A	B
0 in.	.477	.000	.388	.000	.350	.000	.330	.000	.439	.000	.480	.000	.406	.000	.365	.000	.344	.000	.441	.000
.01 in.	.476	-.001	.387	-.001	.355	-.001	.331	+.001	.444	+.005	.480	.000	.405	-.001	.363	-.002	.344	.000	.444	+.003
.02 in.	.476	-.001	.385	-.003	.351	-.002	.332	+.002	.448	+.009	.480	.000	.403	-.003	.361	-.004	.343	-.001	.447	+.006
.03 in.	.476	-.001	.384	-.004	.353	-.003	.333	+.003	.453	+.014	.479	-.001	.401	-.005	.360	-.005	.343	-.001	.450	+.009
.04 in.	.475	-.002	.383	-.005	.353	-.003	.334	+.004	.457	+.018	.479	-.001	.399	-.007	.358	-.007	.343	-.001	.453	+.012
.05 in.	.475	-.002	.382	-.006	.352	-.004	.335	+.005	.461	+.022	.478	-.002	.398	-.008	.357	-.008	.343	-.001	.456	+.015
.06 in.	.474	-.003	.380	-.008	.351	-.005	.336	+.006	.465	+.026	.478	-.002	.396	-.010	.355	-.010	.342	-.002	.459	+.018
.07 in.	.474	-.003	.379	-.009	.350	-.006	.336	+.006	.469	+.030	.478	-.002	.395	-.011	.354	-.011	.342	-.002	.462	+.021
.08 in.	.474	-.003	.378	-.010	.350	-.006	.337	+.007	.474	+.035	.477	-.003	.393	-.013	.352	-.013	.342	-.002	.465	+.024
.09 in.	.473	-.004	.377	-.011	.349	-.007	.338	+.008	.478	+.039	.477	-.003	.391	-.015	.351	-.014	.342	-.002	.468	+.027
.10 in.	.473	-.004	.375	-.013	.348	-.008	.339	+.009	.483	+.044	.476	-.004	.390	-.016	.349	-.016	.342	-.002	.471	+.030

F. A. A. Ph.D. Thesis
6th March, 1969.

Structural Engineering Division,
Department of Civil Engineering,
University of Newcastle upon Tyne.

TESTS ON MODEL RADIAL RIBBED DOME

TEST NO. 14 TABLE NO. 6

Experimental Determination of Apex Ring Vertical Force Influence Coefficients
Load at point = 10lb

For position of load points, rib layout, details of model dome and graphs of tabulated results, see Test No. 14, Sheet No. 2.

Vertical Displacement at Apex Ring on Rib No. 36 (Upwards)	Dial gauge readings (A) and actual vertical displacement of point load (B; +ve upwards) in inches																			
	Rib No. 10										Rib No. 11									
	Point 1		Point 5		Point 9		Point 13		Point 17		Point 1		Point 5		Point 9		Point 13		Point 17	
	A	B	A	B	A	B	A	B	A	B	A	B	A	B	A	B	A	B	A	B
0 in.	.480	.000	.389	.000	.352	.000	.337	.000	.442	.000	.479	.000	.397	.000	.362	.000	.338	.000	.443	.000
.01 in.	.479	-.001	.387	-.002	.350	-.002	.335	-.002	.444	+.002	.479	.000	.395	-.002	.359	-.003	.335	-.003	.444	+.001
.02 in.	.479	-.001	.385	-.004	.347	-.005	.334	-.003	.446	+.004	.478	-.001	.392	-.005	.356	-.006	.333	-.005	.446	+.003
.03 in.	.478	-.002	.382	-.007	.345	-.007	.332	-.005	.448	+.006	.477	-.002	.390	-.007	.352	-.010	.330	-.008	.447	+.004
.04 in.	.477	-.003	.380	-.009	.342	-.010	.331	-.006	.450	+.008	.477	-.002	.387	-.010	.349	-.013	.328	-.010	.448	+.005
.05 in.	.477	-.003	.378	-.011	.340	-.012	.330	-.007	.452	+.010	.476	-.003	.384	-.013	.346	-.016	.326	-.012	.449	+.006
.06 in.	.476	-.004	.376	-.013	.338	-.014	.328	-.009	.454	+.012	.475	-.004	.382	-.015	.343	-.019	.323	-.015	.450	+.007
.07 in.	.476	-.004	.374	-.015	.335	-.017	.327	-.010	.456	+.014	.475	-.004	.379	-.018	.340	-.022	.321	-.017	.451	+.008
.08 in.	.475	-.005	.371	-.018	.333	-.019	.325	-.012	.458	+.016	.474	-.005	.377	-.020	.336	-.026	.318	-.020	.453	+.010
.09 in.	.474	-.006	.369	-.020	.330	-.022	.324	-.013	.460	+.018	.473	-.006	.374	-.023	.333	-.029	.316	-.022	.454	+.011
.10 in.	.474	-.006	.367	-.022	.328	-.024	.323	-.014	.462	+.020	.473	-.006	.372	-.025	.330	-.032	.314	-.024	.455	+.012

F. A. A. Ph.D. Thesis
6th, 7th March, 1969.

Structural Engineering Division,
Department of Civil Engineering,
University of Newcastle upon Tyne.

TESTS ON MODEL RADIAL RIBBED DOME

TEST NO. 14 TABLE NO. 7

Experimental Determination of Apex Ring Vertical Force Influence Coefficients
Load at point = 10 lb

For position of load points, rib layout, details of model dome and graphs of tabulated results, see Test No. 14, Sheet Nos. 2 & 3.

Vertical Displacement at Apex Ring on Rib No. 36 (Upwards)	Dial gauge readings (A) and actual vertical displacement of point load (B; +ve upwards) in inches																	
	Rib No. 12										Rib No. 13							
	Point 1		Point 5		Point 9		Point 13		Point 17		Point 1		Point 5		Point 9		Point 13		Point 17	
	A	B	A	B	A	B	A	B	A	B	A	B	A	B	A	B	A	B	A	B
0 in.	.479	.000	.392	.000	.354	.000	.334	.000	.448	.000	.475	.000	.393	.000	.357	.000	.332	.000	.445	.000
.01 in.	.479	.000	.389	-.003	.350	-.004	.331	-.003	.448	.000	.474	-.001	.390	-.003	.353	-.004	.328	-.004	.445	.000
.02 in.	.478	-.001	.386	-.006	.346	-.008	.328	-.006	.449	+.001	.473	-.002	.387	-.006	.349	-.008	.325	-.007	.444	-.001
.03 in.	.477	-.002	.383	-.009	.343	-.011	.325	-.009	.449	+.001	.472	-.003	.384	-.009	.345	-.012	.321	-.011	.444	-.001
.04 in.	.476	-.003	.380	-.012	.339	-.015	.322	-.012	.450	+.002	.472	-.003	.381	-.012	.340	-.017	.317	-.015	.443	-.002
.05 in.	.476	-.003	.377	-.015	.335	-.019	.318	-.016	.450	+.002	.471	-.004	.378	-.015	.336	-.021	.313	-.019	.443	-.002
.06 in.	.475	-.004	.374	-.018	.331	-.023	.315	-.019	.450	+.002	.470	-.005	.374	-.019	.332	-.025	.309	-.023	.442	-.003
.07 in.	.474	-.005	.371	-.021	.327	-.027	.312	-.022	.450	+.002	.469	-.006	.371	-.022	.328	-.029	.305	-.027	.442	-.003
.08 in.	.473	-.006	.368	-.024	.323	-.031	.308	-.026	.450	+.002	.469	-.006	.368	-.025	.323	-.034	.301	-.031	.441	-.004
.09 in.	.473	-.006	.365	-.027	.319	-.035	.305	-.029	.451	+.003	.468	-.007	.365	-.028	.319	-.038	.297	-.035	.440	-.005
.10 in.	.472	-.007	.362	-.030	.315	-.039	.301	-.033	.451	+.003	.467	-.008	.362	-.031	.315	-.042	.293	-.039	.439	-.006

F. A. A. Ph.D. Thesis
7th March, 1969.

Structural Engineering Division,
Department of Civil Engineering,
University of Newcastle upon Tyne.

TESTS ON MODEL RADIAL RIBBED DOME

TEST NO. 14 TABLE NO. 8

Experimental Determination of Apex Ring Vertical Force Influence Coefficients

Load at point = 10lb

For position of load points, rib layout, details of model dome and graphs of tabulated results, see Test No. 14, Sheet No. 3.

Vertical Displacement at Apex Ring on Rib No. 36 (Upwards)	Dial gauge readings (A) and actual vertical displacement of point load (B; +ve upwards) in inches																			
	Rib No. 14										Rib No. 15									
	Point 1		Point 5		Point 9		Point 13		Point 17		Point 1		Point 5		Point 9		Point 13		Point 17	
	A	B	A	B	A	B	A	B	A	B	A	B	A	B	A	B	A	B	A	B
0 in.	.481	.000	.402	.000	.359	.000	.340	.000	.445	.000	.480	.000	.392	.000	.367	.000	.337	.000	.446	.000
.01 in.	.480	-.001	.399	-.003	.354	-.005	.336	-.004	.444	-.001	.479	-.001	.389	-.003	.362	-.005	.333	-.004	.444	-.002
.02 in.	.479	-.002	.395	-.007	.350	-.009	.331	-.009	.443	-.002	.478	-.002	.385	-.007	.357	-.010	.328	-.009	.443	-.003
.03 in.	.478	-.003	.392	-.010	.345	-.014	.327	-.013	.442	-.003	.477	-.003	.381	-.011	.353	-.014	.323	-.014	.441	-.005
.04 in.	.478	-.003	.388	-.014	.341	-.018	.323	-.017	.441	-.004	.476	-.004	.378	-.014	.347	-.020	.318	-.019	.439	-.007
.05 in.	.477	-.004	.385	-.017	.336	-.023	.318	-.022	.440	-.005	.475	-.005	.374	-.018	.343	-.024	.313	-.024	.437	-.009
.06 in.	.476	-.005	.382	-.020	.331	-.028	.314	-.026	.438	-.007	.474	-.006	.370	-.022	.337	-.030	.308	-.029	.436	-.010
.07 in.	.475	-.006	.378	-.024	.326	-.033	.309	-.031	.437	-.008	.473	-.007	.367	-.025	.332	-.035	.303	-.034	.434	-.012
.08 in.	.474	-.007	.375	-.027	.321	-.038	.305	-.035	.436	-.009	.473	-.007	.363	-.029	.327	-.040	.298	-.039	.432	-.014
.09 in.	.473	-.008	.371	-.031	.316	-.043	.300	-.040	.435	-.010	.472	-.008	.360	-.032	.322	-.045	.293	-.044	.430	-.016
.10 in.	.473	-.008	.368	-.034	.311	-.048	.295	-.045	.433	-.012	.471	-.009	.356	-.036	.316	-.051	.288	-.049	.428	-.018

F. A. A. Ph.D. Thesis
10th March, 1969.

Structural Engineering Division,
Department of Civil Engineering,
University of Newcastle upon Tyne.

TESTS ON MODEL RADIAL RIBBED DOME

TEST NO. 14 TABLE NO. 9

Experimental Determination of Apex Ring Vertical Force Influence Coefficients
Load at point = 10lb

For position of load points, rib layout, details of model dome and graphs of tabulated results, see Test No. 14, Sheet No. 3.

Vertical Displacement at Apex Ring on Rib No. 36 (Upwards)	Dial gauge readings (A) and actual vertical displacement of point load (B; +ve upwards) in inches																	
	Rib No. 16										Rib No. 17							
	Point 1		Point 5		Point 9		Point 13		Point 17		Point 1		Point 5		Point 9		Point 13		Point 17	
	A	B	A	B	A	B	A	B	A	B	A	B	A	B	A	B	A	B	A	B
0 in.	.479	.000	.398	.000	.358	.000	.338	.000	.444	.000	.476	.000	.403	.000	.368	.000	.342	.000	.445	.000
.01 in.	.478	-.001	.394	-.004	.353	-.005	.333	-.005	.443	-.001	.475	-.001	.400	-.003	.362	-.006	.337	-.005	.443	-.002
.02 in.	.477	-.002	.391	-.007	.348	-.010	.328	-.010	.441	-.003	.475	-.001	.396	-.007	.357	-.011	.331	-.011	.441	-.004
.03 in.	.476	-.003	.387	-.011	.342	-.016	.322	-.016	.439	-.005	.474	-.002	.392	-.011	.352	-.016	.326	-.016	.438	-.007
.04 in.	.475	-.004	.383	-.015	.337	-.021	.317	-.021	.437	-.007	.473	-.003	.389	-.014	.347	-.021	.321	-.021	.436	-.009
.05 in.	.474	-.005	.379	-.019	.331	-.027	.311	-.027	.435	-.009	.472	-.004	.385	-.018	.341	-.027	.315	-.027	.434	-.011
.06 in.	.473	-.006	.376	-.022	.326	-.032	.306	-.032	.433	-.011	.471	-.005	.381	-.022	.336	-.032	.310	-.032	.432	-.013
.07 in.	.472	-.007	.372	-.026	.320	-.038	.301	-.037	.431	-.013	.470	-.006	.378	-.025	.330	-.038	.304	-.038	.430	-.015
.08 in.	.472	-.007	.368	-.030	.315	-.043	.295	-.043	.429	-.015	.469	-.007	.374	-.029	.325	-.043	.298	-.044	.427	-.018
.09 in.	.471	-.008	.365	-.033	.310	-.048	.290	-.048	.426	-.018	.468	-.008	.370	-.033	.319	-.049	.293	-.049	.424	-.021
.10 in.	.470	-.009	.361	-.037	.304	-.054	.284	-.054	.424	-.020	.467	-.009	.366	-.037	.314	-.054	.287	-.055	.422	-.023

F. A. A. Ph.D. Thesis,
10th March, 1969.

Structural Engineering Division,
Department of Civil Engineering,
University of Newcastle upon Tyne.

Experimental Determination of Apex Ring Vertical Force Influence Coefficients
Load at point = 10lb

For position of load points, rib layout, details of model dome and graphs of tabulated results, see Test No. 14, Sheet No. 3.

Vertical Displacement At Apex Ring on Rib No.36 (Upwards)	Dial gauge readings (A) and actual vertical displacement of point load (B; +ve upwards) in inches									
	Rib No. 18									
	Point 1		Point 5		Point 9		Point 13		Point 17	
	A	B	A	B	A	B	A	B	A	B
0 in.	.479	.000	.402	.000	.369	.000	.340	.000	.443	.000
.01 in.	.478	-.001	.399	-.003	.363	-.006	.335	-.005	.441	-.002
.02 in.	.477	-.002	.395	-.007	.358	-.011	.330	-.010	.439	-.004
.03 in.	.476	-.003	.391	-.011	.353	-.016	.324	-.016	.436	-.007
.04 in.	.476	-.003	.388	-.014	.348	-.021	.318	-.022	.434	-.009
.05 in.	.475	-.004	.384	-.018	.343	-.026	.313	-.027	.432	-.011
.06 in.	.474	-.005	.381	-.021	.337	-.032	.307	-.033	.429	-.014
.07 in.	.473	-.006	.377	-.025	.332	-.037	.301	-.039	.426	-.017
.08 in.	.472	-.007	.373	-.029	.326	-.043	.296	-.044	.424	-.019
.09 in.	.471	-.008	.369	-.033	.321	-.048	.290	-.050	.421	-.022
.10 in.	.470	-.009	.366	-.036	.316	-.053	.285	-.055	.418	-.025

F.A.A. Ph.D. Thesis
10th March, 1969.

Structural Engineering Division,
Department of Civil Engineering,
University of Newcastle upon Tyne.

TESTS ON MODEL RADIAL RIBBED DOME

Test No. 14

Sheet No. 1

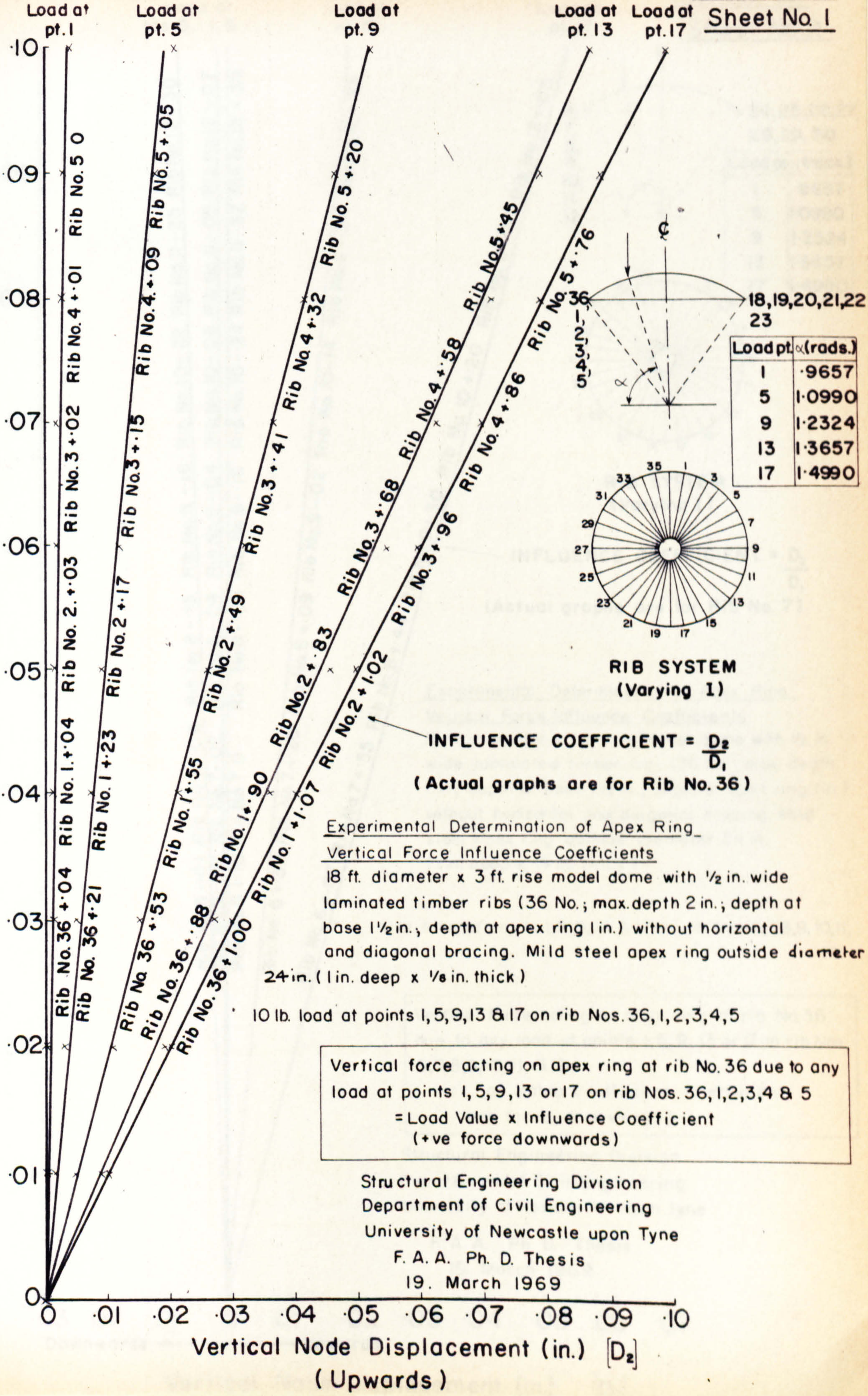

Load pt.	α (rads.)
1	·9657
5	1·0990
9	1·2324
13	1·3657
17	1·4990

RIB SYSTEM
(Varying 1)

INFLUENCE COEFFICIENT = $\frac{D_2}{D_1}$

(Actual graphs are for Rib No. 36)

Experimental Determination of Apex Ring
Vertical Force Influence Coefficients

18 ft. diameter x 3 ft. rise model dome with ½ in. wide laminated timber ribs (36 No.; max. depth 2 in.; depth at base 1½ in.; depth at apex ring 1 in.) without horizontal and diagonal bracing. Mild steel apex ring outside diameter 24 in. (1 in. deep x ⅛ in. thick)

10 lb. load at points 1, 5, 9, 13 & 17 on rib Nos. 36, 1, 2, 3, 4, 5

Vertical force acting on apex ring at rib No. 36 due to any load at points 1, 5, 9, 13 or 17 on rib Nos. 36, 1, 2, 3, 4 & 5
= Load Value x Influence Coefficient
(+ve force downwards)

Structural Engineering Division
Department of Civil Engineering
University of Newcastle upon Tyne

F. A. A. Ph. D. Thesis
19. March 1969

TESTS ON MODEL RADIAL RIBBED DOME

Test No. 14

Sheet No. 2

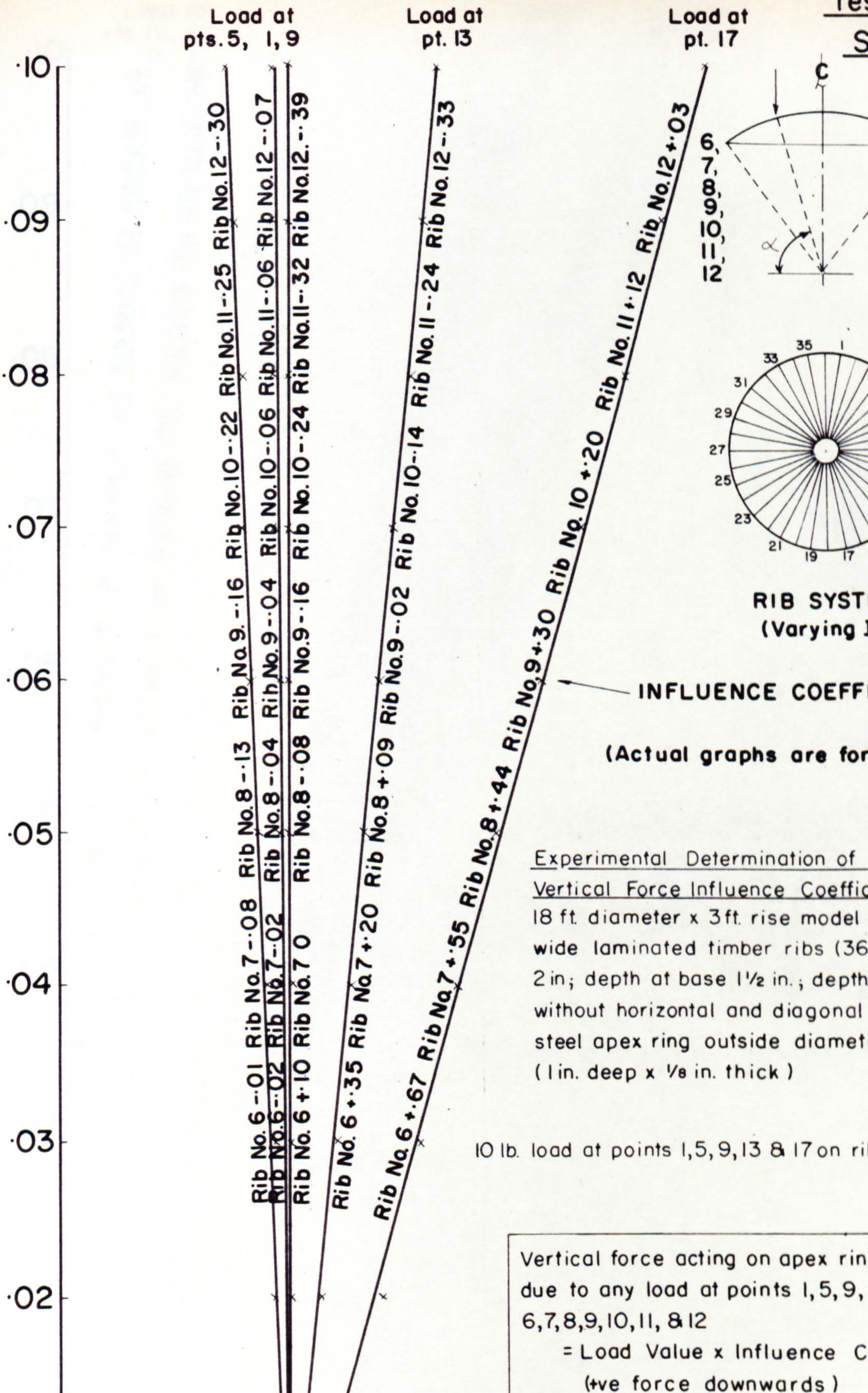

Load pt	α (rads.)
1	·9657
5	1·0990
9	1·2324
13	1·3657
17	1·4990

RIB SYSTEM
(Varying I)

INFLUENCE COEFFICIENT = $\frac{D_2}{D_1}$

(Actual graphs are for Rib No. 7)

Experimental Determination of Apex Ring Vertical Force Influence Coefficients

18 ft. diameter x 3 ft. rise model dome with ½ in. wide laminated timber ribs (36 No.; max. depth 2 in; depth at base 1½ in.; depth at apex ring 1 in.) without horizontal and diagonal bracing. Mild steel apex ring outside diameter 24 in. (1 in. deep x ⅛ in. thick)

10 lb. load at points 1, 5, 9, 13 & 17 on rib Nos. 6, 7, 8, 9, 10, 11, 12.

Vertical force acting on apex ring at rib No. 36 due to any load at points 1, 5, 9, 13 or 17 on rib Nos. 6, 7, 8, 9, 10, 11, & 12
= Load Value x Influence Coefficient
(+ve force downwards)

Structural Engineering Division
Department of Civil Engineering
University of Newcastle upon Tyne

F. A. A. Ph. D. Thesis
19. March 1969

TESTS ON MODEL RADIAL RIBBED DOME

Test No. 14
Sheet No. 3

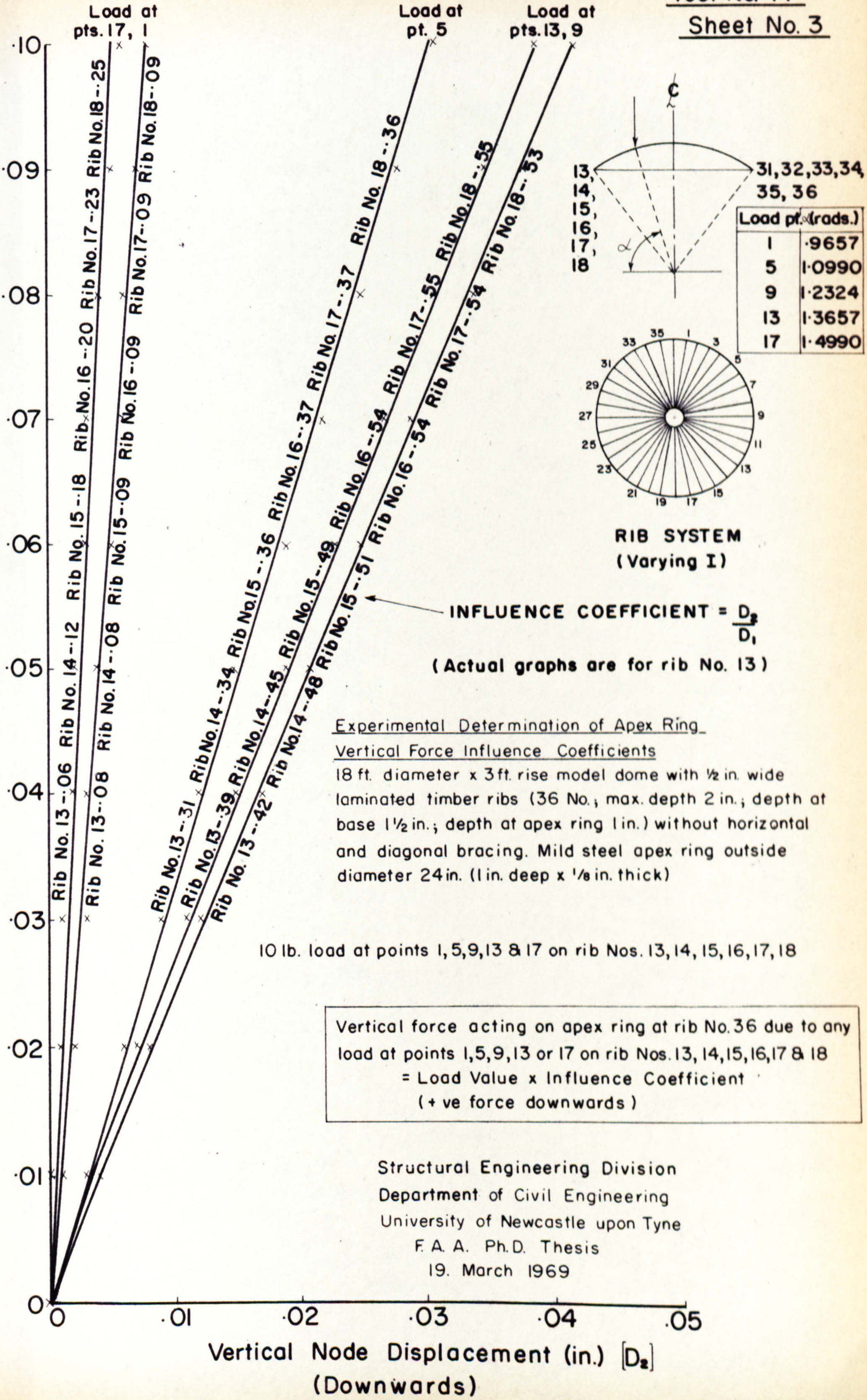

Load pt.	α (rads.)
1	·9657
5	1·0990
9	1·2324
13	1·3657
17	1·4990

RIB SYSTEM
(Varying I)

INFLUENCE COEFFICIENT = $\frac{D_2}{D_1}$

(Actual graphs are for rib No. 13)

Experimental Determination of Apex Ring
Vertical Force Influence Coefficients

18 ft. diameter x 3 ft. rise model dome with ½ in. wide laminated timber ribs (36 No.; max. depth 2 in.; depth at base 1½ in.; depth at apex ring 1 in.) without horizontal and diagonal bracing. Mild steel apex ring outside diameter 24 in. (1 in. deep x ⅛ in. thick)

10 lb. load at points 1, 5, 9, 13 & 17 on rib Nos. 13, 14, 15, 16, 17, 18

Vertical force acting on apex ring at rib No. 36 due to any load at points 1, 5, 9, 13 or 17 on rib Nos. 13, 14, 15, 16, 17 & 18
= Load Value x Influence Coefficient
(+ ve force downwards)

Structural Engineering Division
Department of Civil Engineering
University of Newcastle upon Tyne
F. A. A. Ph.D. Thesis
19. March 1969

Structural Engineering Division
Department of Civil Engineering
University of Newcastle upon Tyne

TESTS ON MODEL RADIAL RIBBED DOME

TEST NO. 14. SHEET NO. 4

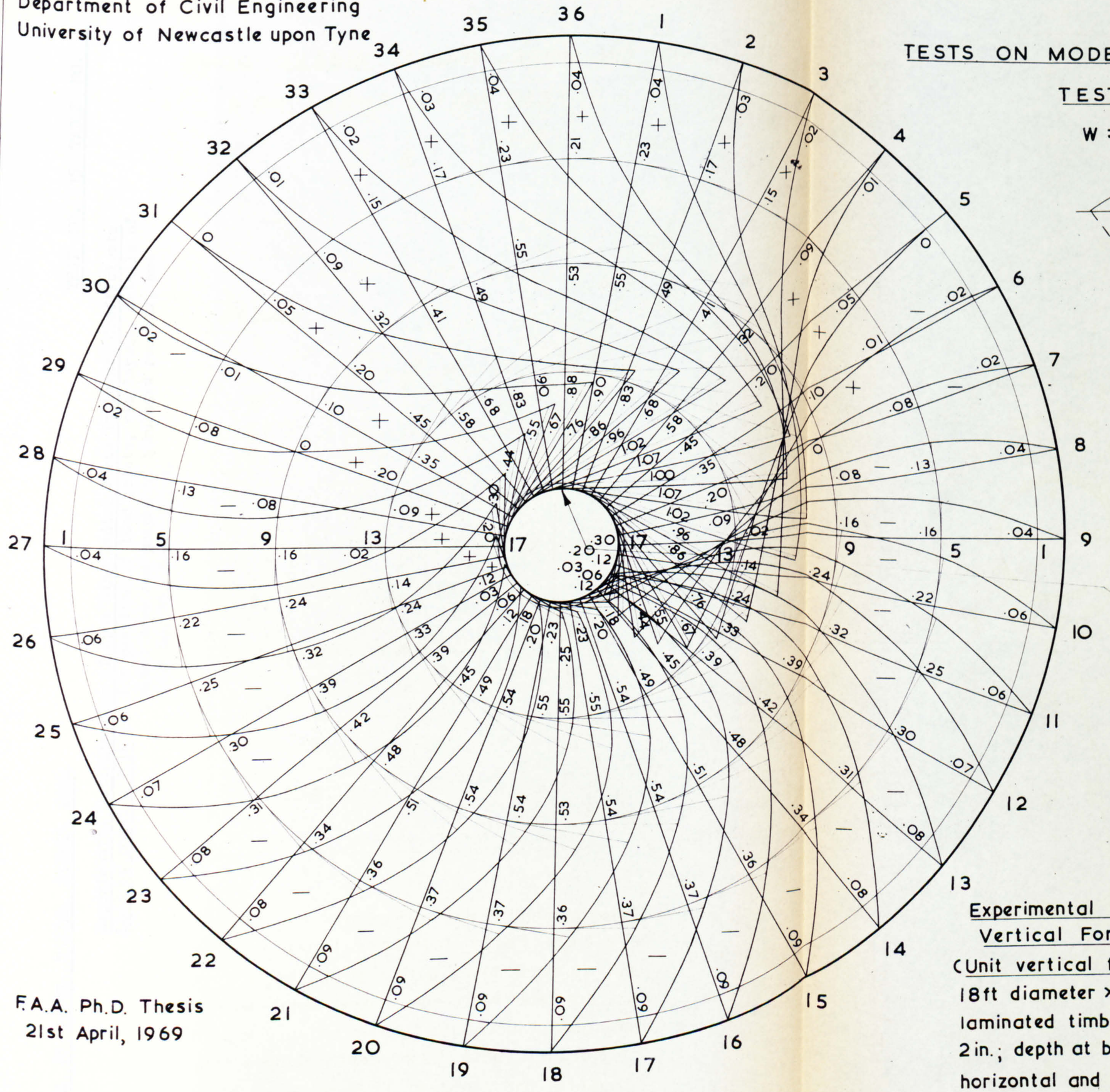

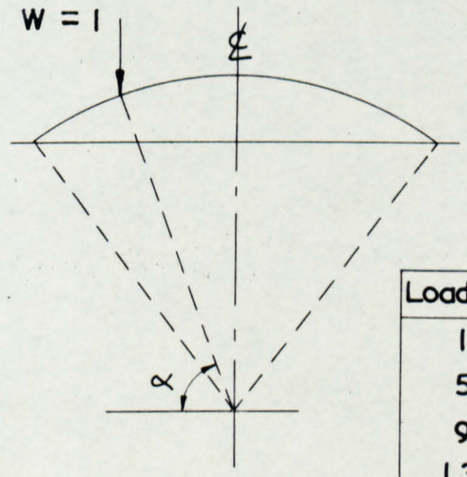

Load Pt.	∝ (rads.)
1	·9657
5	1·0990
9	1·2324
13	1·3657
17	1·4990

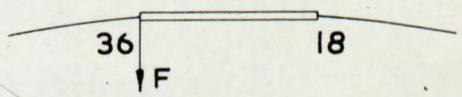

F = W × Influence Coefficient

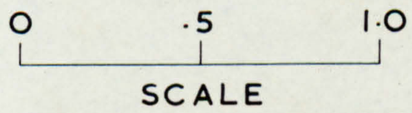

F.A.A. Ph.D. Thesis
21st April, 1969

Experimental Determination of Apex Ring Vertical Force Influence Lines for Rib No. 36

(Unit vertical force acting at any angle on any rib)

18ft diameter × 3ft rise model dome with 1/2 in. wide laminated timber ribs (36 No. of varying I; max. depth 2 in.; depth at base 1½ in.; depth at apex ring 1in.) without horizontal and diagonal bracing. Mild steel apex ring outside diameter 24 in. (1in. deep × 1/8 in. thick)

TESTS ON MODEL RADIAL RIBBED DOME

TEST NO. 15 TABLE NO. 1

Experimental Determination of Apex Ring Radial Force Influence Coefficients
Load at point = 1Olb

For position of load points, rib layout, details of model dome and graphs of tabulated results, see Test No. 15, Sheet No. 1.

Radial Displacement of Apex Ring at Rib No. 36 (Outwards from centre of ring)	Dial gauge readings (A) and actual vertical displacement of point load (B; +ve upwards) in inches																			
	Rib No. 18										Rib No. 19									
	Point 1		Point 5		Point 9		Point 13		Point 17		Point 1		Point 5		Point 9		Point 13		Point 17	
	A	B	A	B	A	B	A	B	A	B	A	B	A	B	A	B	A	B	A	B
0 in.	.480	.000	.404	.000	.369	.000	.342	.000	.442	.000	.479	.000	.399	.000	.359	.000	.344	.000	.445	.000
.01 in.	.480	.000	.401	-.003	.365	-.004	.336	-.006	.438	-.004	.478	-.001	.396	-.003	.355	-.004	.339	-.005	.441	-.004
.02 in.	.479	-.001	.398	-.006	.360	-.009	.331	-.011	.434	-.008	.477	-.002	.393	-.006	.350	-.009	.333	-.011	.436	-.009
.03 in.	.478	-.002	.395	-.009	.356	-.013	.326	-.016	.430	-.012	.476	-.003	.390	-.009	.346	-.013	.328	-.016	.432	-.013
.04 in.	.478	-.002	.392	-.012	.351	-.018	.320	-.022	.425	-.017	.476	-.003	.387	-.012	.342	-.017	.323	-.021	.427	-.018
.05 in.	.477	-.003	.389	-.015	.347	-.022	.315	-.027	.421	-.021	.475	-.004	.384	-.015	.337	-.022	.317	-.027	.423	-.022
.06 in.	.476	-.004	.386	-.018	.342	-.027	.310	-.032	.416	-.026	.474	-.005	.381	-.018	.332	-.027	.312	-.032	.419	-.026
.07 in.	.476	-.004	.383	-.021	.338	-.031	.304	-.038	.412	-.030	.474	-.005	.378	-.021	.328	-.031	.306	-.038	.414	-.031
.08 in.	.475	-.005	.381	-.023	.333	-.036	.299	-.043	.408	-.034	.473	-.006	.375	-.024	.324	-.035	.301	-.043	.410	-.035
.09 in.	.474	-.006	.378	-.026	.329	-.040	.293	-.049	.403	-.039	.472	-.007	.372	-.027	.319	-.040	.296	-.048	.405	-.040
.10 in.	.474	-.006	.375	-.029	.324	-.045	.288	-.054	.399	-.043	.472	-.007	.370	-.029	.315	-.044	.291	-.053	.401	-.044

F. A. A. Ph.D. Thesis
19th March, 1969.

Structural Engineering Division,
Department of Civil Engineering,
University of Newcastle upon Tyne.

TESTS ON MODEL RADIAL RIBBED DOME

TEST NO. 15 TABLE NO. 2

Experimental Determination of Apex Ring Radial Force Influence Coefficients

Load at point = 10lb

For position of load points, rib layout, details of model dome and graphs of tabulated results, see Test No. 15, Sheet No. 1.

Radial Displacement of Apex Ring at Rib No. 36 (Outwards from centre of ring)	Dial gauge readings (A) and actual vertical displacement of point load (B; +ve upwards) in inches																			
	Rib No. 20										Rib No. 21									
	Point 1		Point 5		Point 9		Point 13		Point 17		Point 1		Point 5		Point 9		Point 13		Point 17	
	A	B	A	B	A	B	A	B	A	B	A	B	A	B	A	B	A	B	A	B
0 in.	.478	.000	.400	.000	.358	.000	.340	.000	.445	.000	.481	.000	.402	.000	.361	.000	.333	.000	.445	.000
.01 in.	.477	-.001	.397	-.003	.353	-.005	.335	-.005	.441	-.004	.480	-.001	.400	-.002	.356	-.005	.328	-.005	.441	-.004
.02 in.	.477	-.001	.394	-.006	.348	-.010	.329	-.011	.436	-.009	.480	-.001	.397	-.005	.352	-.009	.322	-.011	.437	-.008
.03 in.	.476	-.002	.391	-.009	.344	-.014	.324	-.016	.432	-.013	.479	-.002	.394	-.008	.347	-.014	.317	-.016	.433	-.012
.04 in.	.475	-.003	.388	-.012	.340	-.018	.318	-.022	.428	-.017	.478	-.003	.391	-.011	.343	-.018	.311	-.022	.429	-.016
.05 in.	.475	-.003	.385	-.015	.335	-.023	.313	-.027	.424	-.021	.478	-.003	.388	-.014	.338	-.023	.306	-.027	.425	-.020
.06 in.	.474	-.004	.382	-.018	.330	-.028	.308	-.032	.419	-.026	.477	-.004	.385	-.017	.334	-.027	.301	-.032	.421	-.024
.07 in.	.473	-.005	.379	-.021	.326	-.032	.302	-.038	.415	-.030	.476	-.005	.382	-.020	.330	-.031	.295	-.038	.417	-.028
.08 in.	.472	-.006	.376	-.024	.321	-.037	.297	-.043	.411	-.034	.476	-.005	.379	-.023	.325	-.036	.289	-.044	.413	-.032
.09 in.	.472	-.006	.373	-.027	.317	-.041	.292	-.048	.406	-.039	.475	-.006	.376	-.026	.320	-.041	.284	-.049	.409	-.036
.10 in.	.471	-.007	.370	-.030	.313	-.045	.287	-.053	.402	-.043	.474	-.007	.374	-.028	.316	-.045	.278	-.055	.404	-.041

F. A. A. Ph.D. Thesis
19th, 20th March, 1969

Structural Engineering Division,
Department of Civil Engineering,
University of Newcastle upon Tyne.

TESTS ON MODEL RADIAL RIBBED DOME

TEST NO. 15 TABLE NO. 3

Experimental Determination of Apex Ring Radial Force Influence Coefficients
Load at point = 10lb

For position of load points, rib layout, details of model dome and graphs of tabulated results, see Test No. 15, Sheet No. 1.

Radial Displacement of Apex Ring at Rib No. 36 (Outwards from centre of ring)	Dial gauge readings (A) and actual vertical displacement of point load (B; +ve upwards) in inches																			
	Rib No. 22										Rib No. 23									
	Point 1		Point 5		Point 9		Point 13		Point 17		Point 1		Point 5		Point 9		Point 13		Point 17	
	A	B	A	B	A	B	A	B	A	B	A	B	A	B	A	B	A	B	A	B
0 in.	.480	.000	.398	.000	.363	.000	.334	.000	.444	.000	.480	.000	.395	.000	.357	.000	.324	.000	.443	.000
.01 in.	.479	-.001	.395	-.003	.358	-.005	.329	-.005	.441	-.003	.479	-.001	.392	-.003	.352	-.005	.318	-.006	.440	-.003
.02 in.	.478	-.002	.392	-.006	.354	-.009	.324	-.010	.437	-.007	.479	-.001	.389	-.006	.348	-.009	.313	-.011	.436	-.007
.03 in.	.478	-.002	.389	-.009	.349	-.014	.319	-.015	.433	-.011	.478	-.002	.386	-.009	.344	-.013	.308	-.016	.433	-.010
.04 in.	.477	-.003	.386	-.012	.345	-.018	.313	-.021	.429	-.015	.477	-.003	.383	-.012	.339	-.018	.303	-.021	.430	-.013
.05 in.	.476	-.004	.383	-.015	.340	-.023	.308	-.026	.425	-.019	.476	-.004	.380	-.015	.335	-.022	.298	-.026	.427	-.016
.06 in.	.476	-.004	.380	-.018	.336	-.027	.303	-.031	.421	-.023	.476	-.004	.377	-.018	.330	-.027	.293	-.031	.423	-.020
.07 in.	.475	-.005	.377	-.021	.331	-.032	.297	-.037	.418	-.026	.475	-.005	.374	-.021	.326	-.031	.288	-.036	.420	-.023
.08 in.	.474	-.006	.375	-.023	.327	-.036	.292	-.042	.414	-.030	.474	-.006	.371	-.024	.321	-.036	.283	-.041	.416	-.027
.09 in.	.474	-.006	.372	-.026	.322	-.041	.287	-.047	.410	-.034	.474	-.006	.368	-.027	.317	-.040	.278	-.046	.413	-.030
.10 in.	.473	-.007	.369	-.029	.318	-.045	.282	-.052	.407	-.037	.473	-.007	.366	-.029	.313	-.044	.273	-.051	.410	-.033

F.A.A. Ph. D. Thesis
20th March, 1969.

Structural Engineering Division,
Department of Civil Engineering,
University of Newcastle upon Tyne.

TESTS ON MODEL RADIAL RIBBED DOME

TEST NO. 15 TABLE NO. 4

Experimental Determination of Apex Ring Radial Force Influence Coefficients
Load at point = 10lb

For position of load points, rib layout, details of model dome and graphs of tabulated results, see Test No. 15, Sheet Nos. 1 & 2.

Radial Displacement of Apex Ring at Rib No. 36 (Outwards from centre of ring)	Dial Gauge readings (A) and actual vertical displacement of point load (B; +ve upwards) in inches																			
	Rib No. 24										Rib No. 25									
	Point 1		Point 5		Point 9		Point 13		Point 17		Point 1		Point 5		Point 9		Point 13		Point 17	
	A	B	A	B	A	B	A	B	A	B	A	B	A	B	A	B	A	B	A	B
0 in.	.480	.000	.384	.000	.352	.000	.333	.000	.444	.000	.474	.000	.396	.000	.362	.000	.336	.000	.444	.000
.01 in.	.479	-.001	.381	-.003	.347	-.005	.328	-.005	.441	-.003	.474	.000	.393	-.003	.358	-.004	.332	-.004	.442	-.002
.02 in.	.479	-.001	.378	-.006	.343	-.009	.323	-.010	.438	-.006	.473	-.001	.391	-.005	.355	-.007	.327	-.009	.440	-.004
.03 in.	.478	-.002	.375	-.009	.339	-.013	.319	-.014	.435	-.009	.472	-.002	.388	-.008	.351	-.011	.323	-.013	.438	-.006
.04 in.	.477	-.003	.372	-.012	.334	-.018	.314	-.019	.432	-.012	.472	-.002	.385	-.011	.347	-.015	.319	-.017	.435	-.009
.05 in.	.477	-.003	.369	-.015	.330	-.022	.310	-.023	.429	-.015	.471	-.003	.383	-.013	.343	-.019	.315	-.021	.433	-.011
.06 in.	.476	-.004	.367	-.017	.326	-.026	.305	-.028	.426	-.018	.470	-.004	.380	-.016	.339	-.023	.311	-.025	.431	-.013
.07 in.	.475	-.005	.364	-.020	.321	-.031	.301	-.032	.423	-.021	.470	-.004	.377	-.019	.335	-.027	.306	-.030	.429	-.015
.08 in.	.475	-.005	.361	-.023	.317	-.035	.296	-.037	.420	-.024	.469	-.005	.374	-.022	.331	-.031	.302	-.034	.427	-.017
.09 in.	.474	-.006	.358	-.026	.313	-.039	.291	-.042	.417	-.027	.468	-.006	.372	-.024	.327	-.035	.298	-.038	.424	-.020
.10 in.	.473	-.007	.355	-.029	.309	-.043	.286	-.047	.414	-.030	.468	-.006	.369	-.027	.323	-.039	.294	-.042	.422	-.022

F.A.A. Ph.D. Thesis
21st March, 1969.

Structural Engineering Division,
Department of Civil Engineering,
University of Newcastle upon Tyne.

TESTS ON MODEL RADIAL RIBBED DOME

TEST NO. 15 TABLE NO. 5

Experimental Determination of Apex Ring Radial Force Influence Coefficients

Load at point = 10lb

For position of load points, rib layout, details of model dome and graphs of tabulated results, see Test No. 15, Sheet No. 2.

Radial Displacement of Apex Ring at Rib No. 36 (Outwards from centre of ring)	Dial gauge readings (A) and actual vertical displacement of point load (B; +ve upwards) in inches																			
	Rib No. 26										Rib No. 27									
	Point 1		Point 5		Point 9		Point 13		Point 17		Point 1		Point 5		Point 9		Point 13		Point 17	
	A	B	A	B	A	B	A	B	A	B	A	B	A	B	A	B	A	B	A	B
0 in.	.481	.000	.389	.000	.353	.000	.330	.000	.440	.000	.477	.000	.369	.000	.335	.000	.320	.000	.444	.000
.01 in.	.480	-.001	.387	-.002	.349	-.004	.327	-.003	.438	-.002	.476	-.001	.367	-.002	.332	-.003	.316	-.004	.443	-.001
.02 in.	.479	-.002	.384	-.005	.345	-.008	.323	-.007	.436	-.004	.476	-.001	.364	-.005	.329	-.006	.313	-.007	.442	-.002
.03 in.	.479	-.002	.381	-.008	.341	-.012	.320	-.010	.435	-.005	.475	-.002	.362	-.007	.325	-.010	.310	-.010	.441	-.003
.04 in.	.478	-.003	.378	-.011	.337	-.016	.316	-.014	.433	-.007	.474	-.003	.360	-.009	.322	-.013	.307	-.013	.440	-.004
.05 in.	.477	-.004	.376	-.013	.334	-.019	.312	-.018	.431	-.009	.473	-.004	.357	-.012	.318	-.017	.304	-.016	.439	-.005
.06 in.	.477	-.004	.373	-.016	.330	-.023	.309	-.021	.430	-.010	.473	-.004	.355	-.014	.315	-.020	.301	-.019	.438	-.006
.07 in.	.476	-.005	.371	-.018	.326	-.027	.305	-.025	.428	-.012	.472	-.005	.352	-.017	.312	-.023	.298	-.022	.437	-.007
.08 in.	.476	-.005	.368	-.021	.322	-.031	.302	-.028	.426	-.014	.472	-.005	.350	-.019	.308	-.027	.295	-.025	.436	-.008
.09 in.	.475	-.006	.365	-.024	.318	-.035	.298	-.032	.425	-.015	.471	-.006	.347	-.022	.305	-.030	.292	-.028	.435	-.009
.10 in.	.474	-.007	.363	-.026	.315	-.038	.294	-.036	.423	-.017	.470	-.007	.345	-.024	.301	-.034	.289	-.031	.434	-.010

F.A.A. Ph.D. Thesis
21st, 24th March, 1969.

Structural Engineering Division,
Department of Civil Engineering,
University of Newcastle upon Tyne.

Experimental Determination of Apex Ring Radial Force Influence Coefficients
Load at point = 10lb

For position of load points, rib layout, details of model dome and graphs of tabulated results, see Test No. 15, Sheet No. 2.

Radial Displacement of Apex Ring at Rib No. 36 (Outwards from centre of ring)	Dial gauge readings (A) and actual vertical displacement of point load (B; +ve upwards) in inches																			
	Rib No. 28										Rib No. 29									
	Point 1		Point 5		Point 9		Point 13		Point 17		Point 1		Point 5		Point 9		Point 13		Point 17	
	A	B	A	B	A	B	A	B	A	B	A	B	A	B	A	B	A	B	A	B
0 in.	.474	.000	.397	.000	.354	.000	.327	.000	.441	.000	.475	.000	.400	.000	.352	.000	.330	.000	.443	.000
.01 in.	.473	-.001	.395	-.002	.351	-.003	.325	-.002	.441	.000	.475	.000	.399	-.001	.350	-.002	.329	-.001	.444	+.001
.02 in.	.473	-.001	.393	-.004	.349	-.005	.323	-.004	.440	-.001	.474	-.001	.398	-.002	.348	-.004	.328	-.002	.445	+.002
.03 in.	.473	-.001	.391	-.006	.346	-.008	.321	-.006	.440	-.001	.474	-.001	.396	-.004	.347	-.005	.327	-.003	.446	+.003
.04 in.	.472	-.002	.389	-.007	.344	-.010	.319	-.008	.440	-.001	.474	-.001	.395	-.005	.345	-.007	.326	-.004	.447	+.004
.05 in.	.472	-.002	.387	-.010	.342	-.012	.317	-.010	.440	-.001	.473	-.002	.394	-.006	.344	-.008	.325	-.005	.447	+.004
.06 in.	.471	-.003	.385	-.012	.339	-.015	.315	-.012	.440	-.001	.473	-.002	.393	-.007	.342	-.010	.324	-.006	.448	+.005
.07 in.	.471	-.003	.384	-.013	.337	-.017	.313	-.014	.440	-.001	.473	-.002	.391	-.009	.341	-.011	.323	-.007	.449	+.006
.08 in.	.470	-.004	.382	-.015	.334	-.020	.311	-.016	.440	-.001	.473	-.002	.390	-.010	.339	-.013	.322	-.008	.449	+.006
.09 in.	.470	-.004	.380	-.017	.332	-.022	.309	-.018	.440	-.001	.472	-.003	.389	-.011	.338	-.014	.321	-.009	.450	+.007
.10 in.	.469	-.005	.378	-.019	.329	-.025	.307	-.020	.439	-.002	.472	-.003	.387	-.013	.336	-.016	.320	-.010	.451	+.008

F.A.A. Ph.D. Thesis
24th March, 1969.

Structural Engineering Division,
Department of Civil Engineering,
University of Newcastle upon Tyne.

TESTS ON MODEL RADIAL RIBBED DOME

TEST NO. 15 TABLE NO. 7

Experimental Determination of Apex Ring Radial Force Influence Coefficients
Load at point = 10lb

For position of load points, rib layout, details of model dome and graphs of tabulated results, see Test No. 15, Sheet Nos. 2 & 3.

Radial Displacement of Apex Ring at Rib No. 36 (Outwards from centre of ring)	Dial gauge readings (A) and actual vertical displacement of point load (B; +ve upwards) in inches																			
	Rib No. 30										Rib No. 31									
	Point 1		Point 5		Point 9		Point 13		Point 17		Point 1		Point 5		Point 9		Point 13		Point 17	
	A	B	A	B	A	B	A	B	A	B	A	B	A	B	A	B	A	B	A	B
0 in.	.478	.000	.397	.000	.358	.000	.339	.000	.443	.000	.483	.000	.402	.000	.360	.000	.341	.000	.443	.000
.01 in.	.478	.000	.397	.000	.357	-.001	.340	+.001	.444	+.001	.483	.000	.403	+.001	.361	+.001	.343	+.002	.446	+.003
.02 in.	.478	.000	.396	-.001	.357	-.001	.340	+.001	.446	+.003	.483	.000	.404	+.002	.362	+.002	.345	+.004	.449	+.006
.03 in.	.478	.000	.396	-.001	.356	-.002	.341	+.002	.448	+.005	.483	.000	.404	+.002	.364	+.004	.347	+.006	.452	+.009
.04 in.	.477	-.001	.395	-.002	.356	-.002	.341	+.002	.449	+.006	.483	.000	.405	+.003	.365	+.005	.349	+.008	.454	+.011
.05 in.	.477	-.001	.394	-.003	.356	-.002	.342	+.003	.451	+.008	.483	.000	.406	+.004	.366	+.006	.351	+.010	.457	+.014
.06 in.	.477	-.001	.394	-.003	.355	-.003	.342	+.003	.453	+.010	.483	.000	.406	+.004	.368	+.008	.353	+.012	.460	+.017
.07 in.	.477	-.001	.393	-.004	.355	-.003	.343	+.004	.454	+.011	.484	+.001	.407	+.005	.369	+.009	.355	+.014	.462	+.019
.08 in.	.477	-.001	.393	-.004	.355	-.003	.343	+.004	.456	+.013	.484	+.001	.408	+.006	.370	+.010	.357	+.016	.465	+.022
.09 in.	.477	-.001	.392	-.005	.355	-.003	.344	+.005	.457	+.014	.484	+.001	.408	+.006	.372	+.012	.359	+.018	.468	+.025
.10 in.	.477	-.001	.392	-.005	.354	-.004	.344	+.005	.459	+.016	.484	+.001	.409	+.007	.373	+.013	.361	+.020	.470	+.027

F. A. A. Ph.D. Thesis
24th, 25th March, 1969.

Structural Engineering Division,
Department of Civil Engineering,
University of Newcastle upon Tyne.

Experimental Determination of Apex Ring Radial Force Influence Coefficients

Load at point = 10lb

For position of load points, rib layout, details of model dome and graphs of tabulated results, see Test No. 15, Sheet No. 3.

Radial Displacement of Apex Ring at Rib No. 36 (Outwards from centre of ring)	Dial gauge readings (A) and actual vertical displacement of point load (B; +ve upwards) in inches																			
	Rib No. 32										Rib No. 33									
	Point 1		Point 5		Point 9		Point 13		Point 17		Point 1		Point 5		Point 9		Point 13		Point 17	
	A	B	A	B	A	B	A	B	A	B	A	B	A	B	A	B	A	B	A	B
0 in.	.479	.000	.404	.000	.361	.000	.344	.000	.446	.000	.478	.000	.402	.000	.357	.000	.325	.000	.445	.000
.01 in.	.480	+.001	.406	+.002	.365	+.004	.348	+.004	.449	+.003	.479	+.001	.406	+.004	.363	+.006	.332	+.007	.450	+.005
.02 in.	.480	+.001	.409	+.005	.368	+.007	.353	+.009	.452	+.006	.479	+.001	.410	+.008	.369	+.012	.338	+.013	.454	+.009
.03 in.	.481	+.002	.411	+.007	.372	+.011	.357	+.013	.456	+.010	.480	+.002	.413	+.011	.375	+.018	.345	+.020	.459	+.014
.04 in.	.481	+.002	.413	+.009	.375	+.014	.362	+.018	.459	+.013	.481	+.003	.417	+.015	.380	+.023	.351	+.026	.463	+.018
.05 in.	.482	+.003	.416	+.012	.379	+.018	.366	+.022	.462	+.016	.482	+.004	.421	+.019	.386	+.029	.358	+.033	.467	+.022
.06 in.	.482	+.003	.418	+.014	.383	+.022	.370	+.026	.466	+.020	.483	+.005	.425	+.023	.392	+.035	.365	+.040	.472	+.027
.07 in.	.483	+.004	.420	+.016	.386	+.025	.374	+.030	.469	+.023	.484	+.006	.429	+.027	.398	+.041	.372	+.047	.476	+.031
.08 in.	.483	+.004	.422	+.018	.389	+.028	.379	+.035	.472	+.026	.485	+.007	.433	+.031	.404	+.047	.378	+.053	.480	+.035
.09 in.	.484	+.005	.424	+.020	.393	+.032	.383	+.039	.476	+.030	.486	+.008	.436	+.034	.409	+.052	.384	+.059	.485	+.040
.10 in.	.484	+.005	.426	+.022	.396	+.035	.387	+.043	.479	+.033	.487	+.009	.440	+.038	.415	+.058	.390	+.065	.489	+.044

F.A.A. Ph.D. Thesis
25th March, 1969.

Structural Engineering Division,
Department of Civil Engineering,
University of Newcastle upon Tyne.

TESTS ON MODEL RADIAL RIBBED DOME

TEST NO. 15 TABLE NO. 9

Experimental Determination of Apex Ring Radial Force Influence Coefficients

Load at point = 10lb

For position of load points, rib layout, details of model dome and graphs of tabulated results, see Test No. 15, Sheet No. 3.

Radial Displacement of Apex Ring at Rib No. 36 (Outwards from centre of ring)	Dial gauge readings (A) and actual vertical displacement of point load (B; +ve upwards) in inches																			
	Rib No. 34										Rib No. 35									
	Point 1		Point 5		Point 9		Point 13		Point 17		Point 1		Point 5		Point 9		Point 13		Point 17	
	A	B	A	B	A	B	A	B	A	B	A	B	A	B	A	B	A	B	A	B
0 in.	.480	.000	.388	.000	.348	.000	.329	.000	.442	.000	.477	.000	.399	.000	.365	.000	.343	.000	.446	.000
.01 in.	.482	+.002	.395	+.007	.357	+.009	.339	+.010	.447	+.005	.479	+.002	.408	+.009	.379	+.014	.356	+.013	.452	+.006
.02 in.	.483	+.003	.401	+.013	.366	+.018	.347	+.018	.452	+.010	.481	+.004	.418	+.019	.391	+.026	.368	+.025	.458	+.012
.03 in.	.485	+.005	.407	+.019	.376	+.028	.357	+.028	.458	+.016	.484	+.007	.427	+.028	.403	+.038	.381	+.038	.463	+.017
.04 in.	.487	+.007	.413	+.025	.384	+.036	.367	+.038	.463	+.021	.486	+.009	.436	+.037	.417	+.052	.393	+.050	.469	+.023
.05 in.	.488	+.008	.420	+.032	.394	+.046	.376	+.047	.469	+.027	.488	+.011	.446	+.047	.429	+.064	.406	+.063	.475	+.029
.06 in.	.490	+.010	.426	+.038	.403	+.055	.386	+.057	.474	+.032	.491	+.014	.456	+.057	.443	+.078	.418	+.075	.480	+.034
.07 in.	.491	+.011	.432	+.044	.413	+.065	.396	+.067	.479	+.037	.493	+.016	.465	+.066	.455	+.090	.431	+.088	.486	+.040
.08 in.	.493	+.013	.439	+.051	.423	+.075	.406	+.077	.483	+.041	.495	+.018	.474	+.075	.468	+.103	.444	+.101	.492	+.046
.09 in.	.494	+.014	.445	+.057	.432	+.084	.415	+.086	.488	+.046	.498	+.021	.482	+.083	.481	+.116	.456	+.113	.497	+.051
.10 in.	.496	+.016	.451	+.063	.441	+.093	.425	+.096	.493	+.051	.500	+.023	.491	+.092	.493	+.128	.468	+.125	.502	+.056

F.A.A. Ph.D. Thesis
25th March, 1969.

Structural Engineering Division,
Department of Civil Engineering,
University of Newcastle upon Tyne.

TESTS ON MODEL RADIAL RIBBED DOME — TEST NO. 15 TABLE NO. 10

Experimental Determination of Apex Ring Radial Force Influence Coefficients

Load at point = 10lb

For position of load points, rib layout, details of model dome and graphs of tabulated results, see Test No. 15, Sheet No. 3.

Radial Displacement of Apex Ring at Rib No. 36 (Outwards from centre of ring)	Dial gauge readings (A) and actual vertical displacement of point load (B; +ve upwards) in inches									
	Rib No. 36									
	Point 1		Point 5		Point 9		Point 13		Point 17	
	A	B	A	B	A	B	A	B	A	B
0 in.	.479	.000	.396	.000	.353	.000	.337	.000	.447	.000
.01 in.	.482	+.003	.406	+.010	.369	+.016	.352	+.015	.453	+.006
.02 in.	.484	+.005	.418	+.022	.386	+.033	.368	+.031	.458	+.011
.03 in.	.487	+.008	.429	+.033	.400	+.047	.382	+.045	.464	+.017
.04 in.	.490	+.011	.440	+.044	.417	+.064	.397	+.060	.470	+.023
.05 in.	.492	+.013	.451	+.055	.432	+.079	.412	+.075	.476	+.029
.06 in.	.495	+.016	.462	+.066	.447	+.094	.426	+.089	.482	+.035
.07 in.	.498	+.019	.472	+.076	.462	+.109	.440	+.103	.488	+.041
.08 in.	.500	+.021	.483	+.087	.477	+.124	.456	+.119	.494	+.047
.09 in.	.503	+.024	.494	+.098	.494	+.141	.470	+.133	.499	+.052
.10 in.	.505	+.026	.506	+.110	.509	+.156	.485	+.148	.505	+.058

F.A.A. Ph.D. Thesis
25th March, 1969.

Structural Engineering Division,
Department of Civil Engineering,
University of Newcastle upon Tyne.

TESTS ON MODEL RADIAL RIBBED DOME

Test No. 15

Sheet No. 1

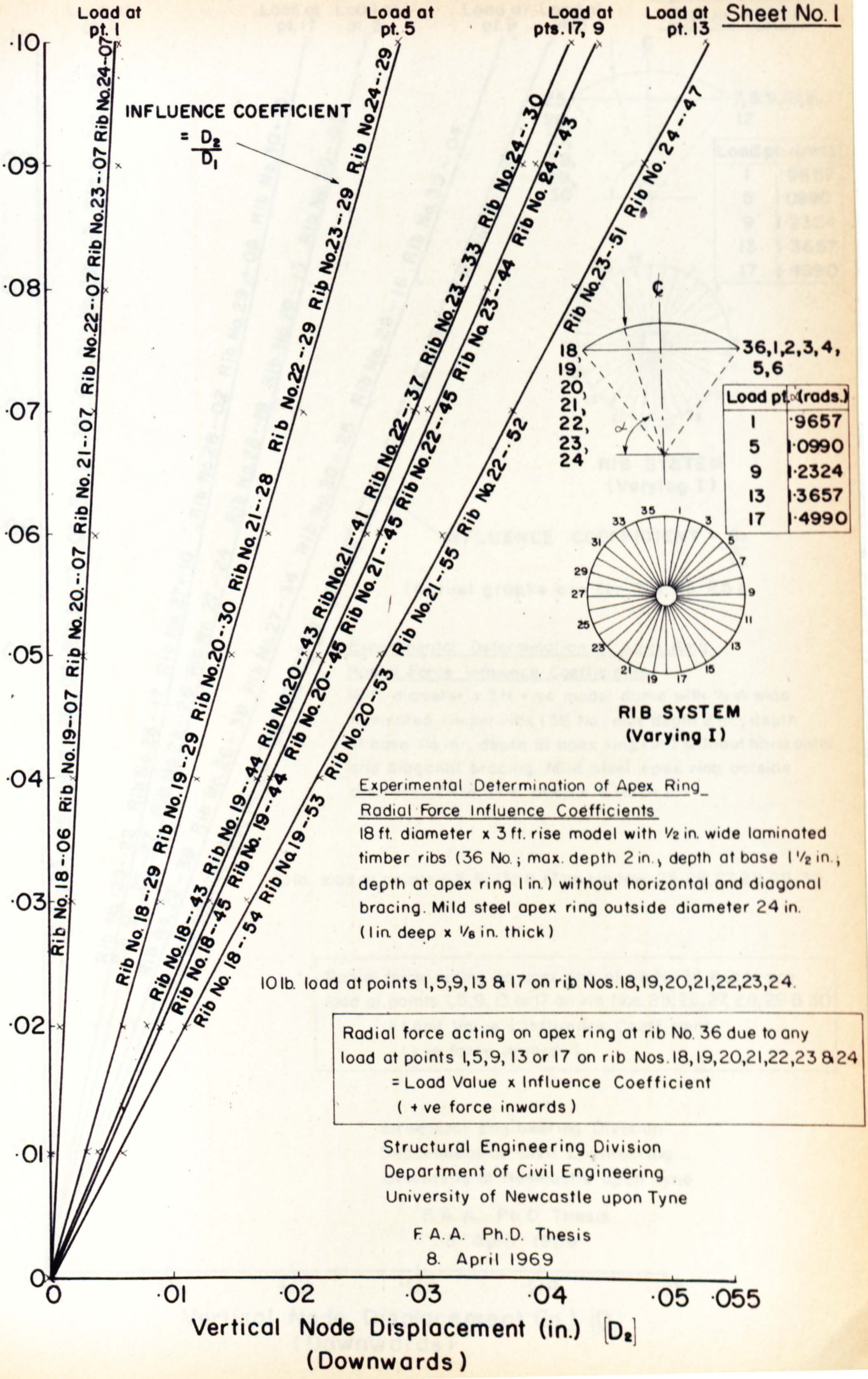

Experimental Determination of Apex Ring Radial Force Influence Coefficients

18 ft. diameter x 3 ft. rise model with ½ in. wide laminated timber ribs (36 No.; max. depth 2 in., depth at base 1½ in.; depth at apex ring 1 in.) without horizontal and diagonal bracing. Mild steel apex ring outside diameter 24 in. (1 in. deep x ⅛ in. thick)

10 lb. load at points 1, 5, 9, 13 & 17 on rib Nos. 18, 19, 20, 21, 22, 23, 24.

Radial force acting on apex ring at rib No. 36 due to any load at points 1, 5, 9, 13 or 17 on rib Nos. 18, 19, 20, 21, 22, 23 & 24
= Load Value x Influence Coefficient
(+ ve force inwards)

Structural Engineering Division
Department of Civil Engineering
University of Newcastle upon Tyne

F. A. A. Ph.D. Thesis
8. April 1969

TESTS ON MODEL RADIAL RIBBED DOME

Test No. 15
Sheet No. 2

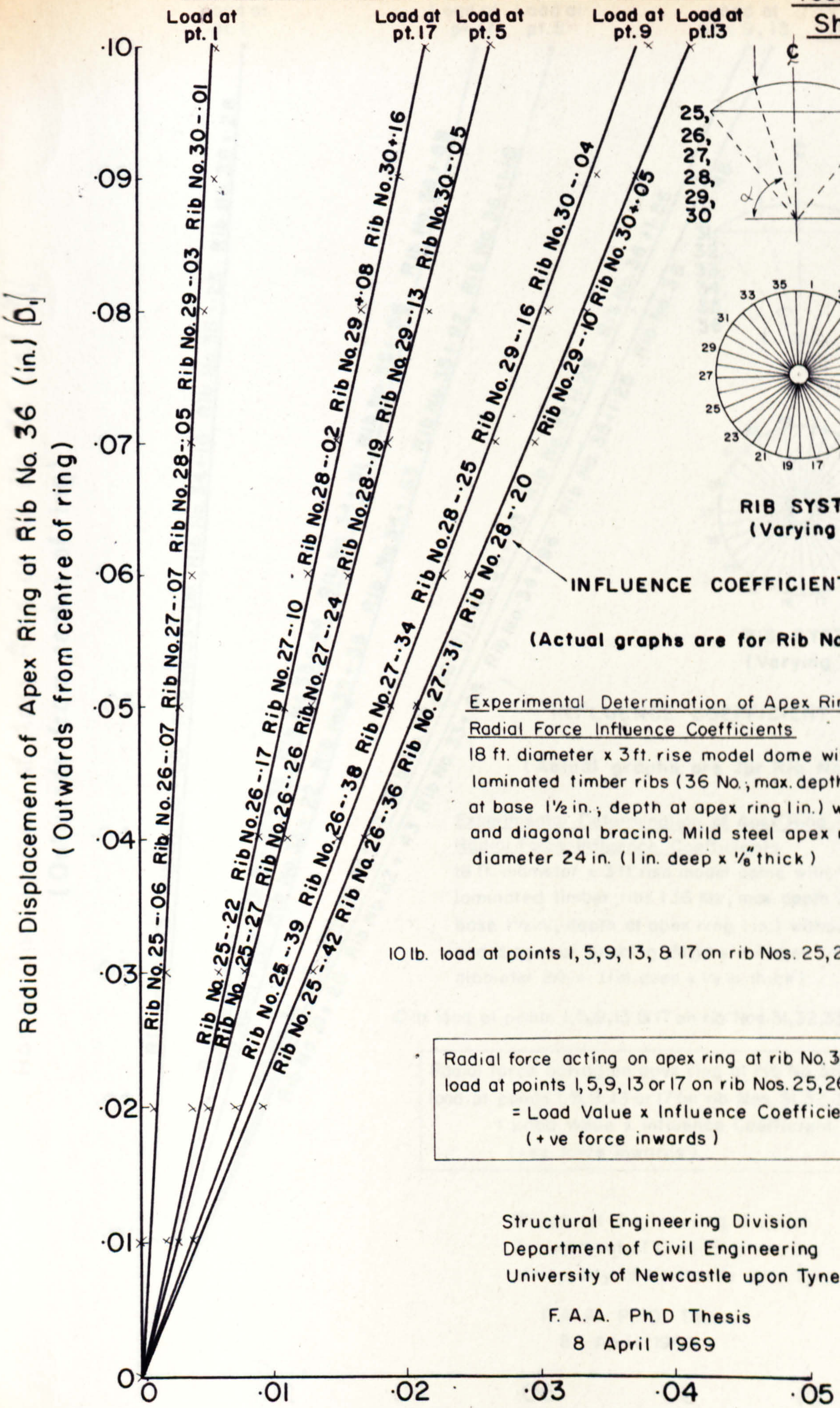

Load pt.	α (rads.)
1	·9657
5	1·0990
9	1·2324
13	1·3657
17	1·4990

RIB SYSTEM
(Varying I)

INFLUENCE COEFFICIENT = $\frac{D_2}{D_1}$

(Actual graphs are for Rib No. 25)

Experimental Determination of Apex Ring Radial Force Influence Coefficients

18 ft. diameter x 3 ft. rise model dome with ½ in. wide laminated timber ribs (36 No.; max. depth 2 in.; depth at base 1½ in.; depth at apex ring 1 in.) without horizontal and diagonal bracing. Mild steel apex ring outside diameter 24 in. (1 in. deep x ⅛" thick)

10 lb. load at points 1, 5, 9, 13, & 17 on rib Nos. 25, 26, 27, 28, 29, 30

Radial force acting on apex ring at rib No. 36 due to any load at points 1, 5, 9, 13 or 17 on rib Nos. 25, 26, 27, 28, 29 & 30
= Load Value x Influence Coefficient
(+ ve force inwards)

Structural Engineering Division
Department of Civil Engineering
University of Newcastle upon Tyne

F. A. A. Ph. D Thesis
8 April 1969

TESTS ON MODEL RADIAL RIBBED DOME

Test No. 15
Sheet No. 3

Load at pt. 1 | Load at pt. 17 | Load at pt. 5 | Load at pts. 9, 13

Rib No. 31 +·01 Rib No. 32 +·05 Rib No. 33 +·09 Rib No. 34 +·16 Rib No. 35 +·23 Rib No. 36 +·26
Rib No. 31 +·27 Rib No. 32 +·33 Rib No. 33 +·44 Rib No. 34 +·51 Rib No. 35 +·56 Rib No. 36 +·58
Rib No. 31 +·07 Rib No. 32 +·22 Rib No. 33 +·38 Rib No. 34 +·63 Rib No. 35 +·92 Rib No. 36 +1·10
Rib No. 31 +·13 Rib No. 32 +·35 Rib No. 33 +·58 Rib No. 34 +·93 Rib No. 35 +1·28 Rib No. 36 +1·56
Rib No. 31 +·20 Rib No. 32 +·43 Rib No. 33 +·65 Rib No. 34 +·96 Rib No. 35 +1·25 Rib No. 36 +1·48

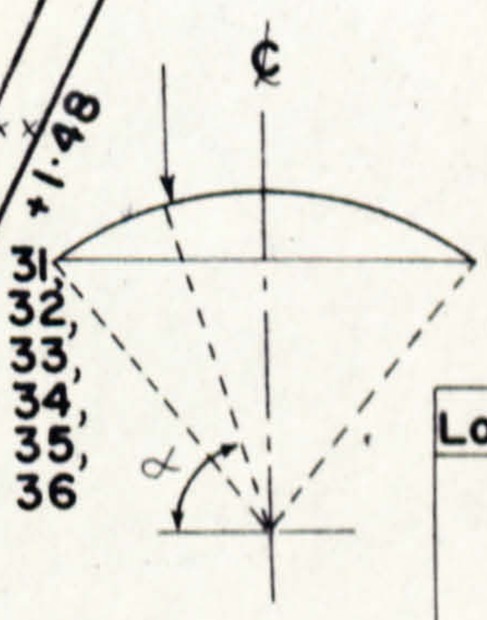

Load pt.	α (rads.)
1	·9657
5	1·0990
9	1·2324
13	1·3657
17	1·4990

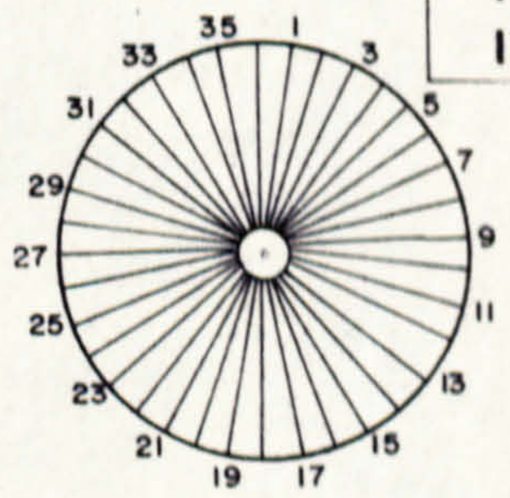

RIB SYSTEM
(Varying I)

INFLUENCE COEFFICIENT = $\frac{D_2}{D_1}$

(Actual graphs are for Rib No. 34)

Radial Displacement of Apex Ring at Rib No. 36 (in.) [D_1]
(Outwards from centre of ring)

0 | ·01 | ·02 | ·03 | ·04 | ·05 | ·06 | ·07 | ·08 | ·09 | ·10

Vertical Node Displacement (in.) [D_2]
(Upwards)

0 | ·02 | ·04 | ·06 | ·08 | ·10

Experimental Determination of Apex Ring Radial Force Influence Coefficients

18 ft. diameter x 3 ft. rise model dome with ½ in. wide laminated timber ribs (36 No.; max. depth 2 in.; depth at base 1½in.; depth at apex ring 1 in.) without horizontal and diagonal bracing. Mild steel apex ring outside diameter 24 in. (1 in. deep x ⅛ in. thick)

10 lb. load at points 1, 5, 9, 13 & 17 on rib Nos. 31, 32, 33, 34, 35, 36

Radial force acting on apex ring at rib No. 36 due to any load at points 1, 5, 9, 13 or 17 on rib Nos. 31, 32, 33, 34, 35 & 36
= Load Value x Influence Coefficient
(+ve force inwards)

Structural Engineering Division
Department of Civil Engineering
University of Newcastle upon Tyne

F. A. A. Ph. D. Thesis
8. April 1969

Structural Engineering Division
Department of Civil Engineering
University of Newcastle upon Tyne

TESTS ON MODEL RADIAL RIBBED DOME

TEST NO. 15 SHEET NO. 4

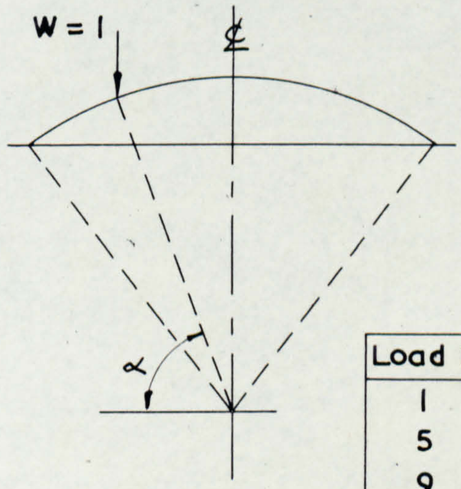

Load Pt.	α (rads.)
1	.9657
5	1.0990
9	1.2324
13	1.3657
17	1.4990

F = W × Influence Coefficient

SCALE 0 .5 1.0

Experimental Determination of Apex Ring Radial Force Influence Lines for Rib No. 36

(Unit vertical force acting at any angle on any rib)

18 ft diameter × 3 ft rise model dome with 1/2 in. wide laminated timber ribs (36 No. of varying I; max. depth 2 in.; depth at base 1½ in.; depth at apex ring 1in.) without horizontal and diagonal bracing. Mild steel apex ring outside diameter 24 in. (1 in. deep × 1/8 in. thick)

F.A.A. Ph.D. Thesis
24th April, 1969

TESTS ON MODEL RADIAL RIBBED DOME

TEST NO. 16 TABLE NO. 1

Experimental Determination of Apex Ring Tangential Force Influence Coefficients

Load at point = 10lb

For position of load points, rib layout, details of model dome and graphs of tabulated results, see Test No. 16, Sheet No. 1.

Tangential Diaplacement of Apex Ring at Rib No.36 (Anti-clockwise viewed from above)	Dial gauge readings (A) and actual vertical displacement of point load (B; +ve downwards) in inches																			
	Ril No. 36										Rib No. 1.									
	Point 1		Point 5		Point 9		Point 13		Point 17		Point 1		Point 5		Point 9		Point 13		Point 17	
	A	B	A	B	A	B	A	B	A	B	A	B	A	B	A	B	A	B	A	B
0 in.	.479	.000	.399	.000	.346	.000	.336	.000	.446	.000	.481	.000	.388	.000	.354	.000	.335	.000	.447	.000
.01 in.	.479	.000	.399	.000	.346	.000	.335	+.001	.446	.000	.481	.000	.386	+.002	.352	+.002	.334	+.001	.446	+.001
.02 in.	.479	.000	.399	.000	.346	.000	.335	+.001	.446	.000	.480	+.001	.385	+.003	.351	+.003	.332	+.003	.446	+.001
.03 in.	.479	.000	.399	.000	.346	.000	.335	+.001	.445	+.001	.480	+.001	.384	+.004	.349	+.005	.330	+.005	.445	+.002
.04 in.	.479	.000	.399	.000	.346	.000	.335	+.001	.445	+.001	.480	+.001	.382	+.006	.347	+.007	.328	+.007	.444	+.003
.05 in.	.479	.000	.398	+.001	.346	.000	.335	+.001	.445	+.001	.479	+.002	.381	+.007	.346	+.008	.326	+.009	.444	+.003
.06 in.	.479	.000	.398	+.001	.346	.000	.334	+.002	.444	+.002	.479	+.002	.379	+.009	.344	+.010	.324	+.011	.443	+.004
.07 in.	.479	.000	.398	+.001	.346	.000	.334	+.002	.444	+.002	.479	+.002	.378	+.010	.343	+.011	.322	+.013	.442	+.005
.08 in.	.479	.000	.398	+.001	.346	.000	.333	+.003	.443	+.003	.478	+.003	.377	+.011	.341	+.013	.320	+.015	.441	+.006
.09 in.	.479	.000	.398	+.001	.346	.000	.333	+.003	.443	+.003	.478	+.003	.375	+.013	.340	+.014	.318	+.017	.441	+.006
.10 in.	.479	.000	.398	+.001	.345	+.001	.332	+.004	.442	+.004	.478	+.003	.374	+.014	.338	+.016	.316	+.019	.440	+.007

F.A.A. Ph.D. Thesis
9th April, 1969.

Structural Engineering Division,
Department of Civil Engineering,
University of Newcastle upon Tyne.

TESTS ON MODEL RADIAL RIBBED DOME

TEST NO. 16 TABLE NO. 2

Experimental Determination of Apex Ring Tangential Force Influence Coefficients
Load at point = 10lb

For position of load points, rib layout, details of model dome and graphs of tabulated results, see Test No. 16, Sheet No. 1.

Tangential Displacement of Apex Ring at Rib No.36 (anti-clockwise viewed from above)	Dial gauge readings (A) and actual vertical displacement of point load (B; +ve downwards) in inches																			
	Rib No. 2										Rib No. 3									
	Point 1		Point 5		Point 9		Point 13		Point 17		Point 1		Point 5		Point 9		Point 13		Point 17	
	A	B	A	B	A	B	A	B	A	B	A	B	A	B	A	B	A	B	A	B
0 in.	.480	.000	.388	.000	.359	.000	.336	.000	.447	.000	.482	.000	.398	.000	.363	.000	.334	.000	.444	.000
.01 in.	.479	+.001	.386	+.002	.350	+.003	.333	+.003	.445	+.002	.481	+.001	.394	+.004	.359	+.004	.331	+.003	.442	+.002
.02 in.	.479	+.001	.384	+.004	.353	+.006	.330	+.006	.444	+.003	.480	+.002	.392	+.006	.356	+.007	.327	+.007	.440	+.004
.03 in.	.478	+.002	.382	+.006	.350	+.009	.327	+.009	.443	+.004	.480	+.002	.389	+.009	.352	+.011	.324	+.010	.439	+.005
.04 in.	.478	+.002	.380	+.008	.347	+.012	.324	+.012	.441	+.006	.479	+.003	.386	+.012	.348	+.015	.321	+.013	.437	+.007
.05 in.	.477	+.003	.378	+.010	.345	+.014	.321	+.015	.440	+.007	.478	+.004	.384	+.014	.345	+.018	.317	+.017	.435	+.009
.06 in.	.477	+.003	.376	+.012	.342	+.017	.318	+.018	.438	+.009	.478	+.004	.381	+.017	.341	+.022	.314	+.020	.434	+.010
.07 in.	.476	+.004	.374	+.014	.339	+.020	.315	+.021	.437	+.010	.477	+.005	.378	+.020	.338	+.025	.311	+.023	.432	+.012
.08 in.	.476	+.004	.372	+.016	.336	+.023	.312	+.024	.435	+.012	.476	+.006	.375	+.023	.334	+.029	.307	+.027	.430	+.014
.09 in.	.475	+.005	.370	+.018	.333	+.026	.309	+.027	.434	+.013	.476	+.006	.373	+.025	.330	+.033	.304	+.030	.428	+.016
.10 in.	.474	+.006	.368	+.020	.330	+.029	.306	+.030	.433	+.014	.475	+.007	.370	+.028	.326	+.037	.300	+.034	.426	+.018

F.A.A. Ph.D. Thesis
9th April, 1969.

Structural Engineering Division,
Department of Civil Engineering,
University of Newcastle upon Tyne.

TESTS ON MODEL RADIAL RIBBED DOME

TEST NO. 16 TABLE NO. 3

Experimental Determination of Apex Ring Tangential Force Influence Coefficients

Load at point = 10lb

For position of load points, rib layout, details of model dome and graphs of tabulated results, see Test No. 16, Sheet No. 1.

Tangential Displacement of Apex Ring at Rib No.36 (Anti-clockwise viewed from above)	Dial gauge readings (A) and actual vertical displacement of point load (B; +ve downwards) in inches																			
	Rib No. 4										Rib No. 5									
	Point 1		Point 5		Point 9		Point 13		Point 17		Point 1		Point 5		Point 9		Point 13		Point 17	
	A	B	A	B	A	B	A	B	A	B	A	B	A	B	A	B	A	B	A	B
0 in.	.475	.000	.395	.000	.353	.000	.329	.000	.444	.000	.480	.000	.396	.000	.356	.000	.342	.000	.439	.000
.01 in.	.474	+.001	.392	+.003	.349	+.004	.325	+.004	.442	+.002	.479	+.001	.393	+.003	.353	+.003	.338	+.004	.437	+.002
.02 in.	.473	+.002	.389	+.006	.345	+.008	.321	+.008	.440	+.004	.479	+.001	.390	+.006	.348	+.008	.334	+.008	.434	+.005
.03 in.	.473	+.002	.386	+.009	.340	+.013	.317	+.012	.438	+.006	.478	+.002	.388	+.008	.345	+.011	.331	+.011	.432	+.007
.04 in.	.472	+.003	.383	+.012	.336	+.017	.313	+.016	.436	+.008	.477	+.003	.385	+.011	.341	+.015	.326	+.016	.429	+.010
.05 in.	.471	+.004	.380	+.015	.331	+.022	.308	+.021	.434	+.010	.476	+.004	.382	+.014	.337	+.019	.322	+.020	.427	+.012
.06 in.	.471	+.004	.377	+.018	.326	+.027	.304	+.025	.432	+.012	.476	+.004	.379	+.017	.333	+.023	.318	+.024	.424	+.015
.07 in.	.470	+.005	.374	+.021	.322	+.031	.300	+.029	.429	+.015	.475	+.005	.377	+.019	.329	+.027	.314	+.028	.422	+.017
.08 in.	.469	+.006	.370	+.025	.316	+.037	.296	+.033	.427	+.017	.475	+.005	.374	+.022	.325	+.031	.310	+.032	.419	+.020
.09 in.	.468	+.007	.367	+.028	.312	+.041	.292	+.037	.425	+.019	.474	+.006	.371	+.025	.320	+.036	.306	+.036	.416	+.023
.10 in.	.467	+.008	.364	+.031	.307	+.046	.287	+.042	.422	+.022	.473	+.007	.368	+.028	.317	+.039	.302	+.040	.413	+.026

F.A.A. Ph.D. Thesis
9th April, 1969.

Structural Engineering Division,
Department of Civil Engineering,
University of Newcastle upon Tyne.

TESTS ON MODEL RADIAL RIBBED DOME

TEST NO. 16 TABLE NO. 4

Experimental Determination of Apex Ring Tangential Force Influence Coefficients

Load at point = 10lb

For position of load points, rib layout, details of model dome and graphs of tabulated results, see Test No. 16, Sheet Nos. 1 & 2.

Tangential Displacement of Apex Ring at Rib No.36 (Anti clockwise viewed from above)	Dial gauge readings (A) and actual vertical displacement of point load (B; +ve downwards) in inches																			
	Rib No. 6										Rib No. 7									
	Point 1		Point 5		Point 9		Point 13		Point 17		Point 1		Point 5		Point 9		Point 13		Point 17	
	A	B	A	B	A	B	A	B	A	B	A	B	A	B	A	B	A	B	A	B
0 in.	.477	.000	.390	.000	.345	.000	.326	.000	.442	.000	.480	.000	.390	.000	.358	.000	.331	.000	.438	.000
.01 in.	.476	+.001	.387	+.003	.341	+.004	.322	+.004	.439	+.003	.480	.000	.388	+.002	.354	+.004	.328	+.003	.436	+.002
.02 in.	.476	+.001	.385	+.005	.337	+.008	.318	+.008	.437	+.005	.479	+.001	.385	+.005	.350	+.008	.325	+.006	.433	+.005
.03 in.	.475	+.002	.382	+.008	.333	+.012	.314	+.012	.434	+.008	.478	+.002	.383	+.007	.347	+.011	.320	+.011	.431	+.007
.04 in.	.474	+.003	.380	+.010	.330	+.015	.310	+.016	.432	+.010	.478	+.002	.380	+.010	.343	+.015	.316	+.015	.428	+.010
.05 in.	.474	+.003	.377	+.013	.326	+.019	.306	+.020	.429	+.013	.477	+.003	.377	+.013	.340	+.018	.313	+.018	.425	+.013
.06 in.	.473	+.004	.375	+.015	.323	+.022	.302	+.024	.426	+.016	.477	+.003	.375	+.015	.336	+.022	.309	+.022	.422	+.016
.07 in.	.473	+.004	.372	+.018	.319	+.026	.298	+.028	.423	+.019	.476	+.004	.372	+.018	.333	+.025	.306	+.025	.419	+.019
.08 in.	.472	+.005	.370	+.020	.315	+.030	.294	+.032	.420	+.022	.475	+.005	.369	+.021	.329	+.029	.302	+.029	.416	+.022
.09 in.	.471	+.006	.367	+.023	.311	+.034	.290	+.036	.417	+.025	.475	+.005	.367	+.023	.326	+.032	.298	+.033	.413	+.025
.10 in.	.470	+.007	.364	+.026	.307	+.038	.286	+.040	.414	+.028	.474	+.006	.364	+.026	.322	+.036	.294	+.037	.410	+.028

F.A.A. Ph.D. Thesis
9th, 10th April, 1969.

Structural Engineering Division,
Department of Civil Engineering,
University of Newcastle upon Tyne.

TESTS ON MODEL RADIAL RIBBED DOME

TEST NO. 16 TABLE NO. 5

Experimental Determination of Apex Ring Tangential Force Influence Coefficients

Load at point = 10lb

For position of load points, rib layout, details of model dome and graphs of tabulated results, see Test No. 16, Sheet No. 2.

Tangential Displacement of Apex Ring at Rib No.36 (Anti-clockwise viewed from above)	Dial gauge readings (A) and actual vertical displacement of point load (B; +ve downwards) in inches																	
	Rib No. 8										Rib No. 9							
	Point 1		Point 5		Point 9		Point 13		Point 17		Point 1		Point 5		Point 9		Point 13		Point 17	
	A	B	A	B	A	B	A	B	A	B	A	B	A	B	A	B	A	B	A	B
0 in.	.476	.000	.384	.00	.35(	.000	.332	.000	.439	.000	.480	.000	.396	.000	.363	.000	.344	.000	.446	.000
.01 in.	.476	.000	.382	+.00	.353	+.003	.329	+.003	.437	+.002	.479	+.001	.393	+.003	.360	+.003	.341	+.003	.443	+.003
.02 in.	.475	+.001	.379	+.005	.34(	+.007	.325	+.007	.434	+.005	.478	+.002	.391	+.005	.357	+.006	.337	+.007	.441	+.005
.03 in.	.474	+.002	.377	+.007	.346	+.010	.321	+.011	.432	+.007	.477	+.003	.389	+.007	.354	+.009	.333	+.011	.438	+.008
.04 in.	.474	+.002	.374	+.010	.342	+.014	.318	+.014	.429	+.010	.477	+.003	.387	+.009	.350	+.013	.329	+.015	.435	+.011
.05 in.	.473	+.003	.371	+.013	.338	+.018	.315	+.017	.426	+.013	.476	+.004	.385	+.011	.347	+.016	.325	+.019	.432	+.014
.06 in.	.472	+.004	.369	+.015	.334	+.022	.311	+.021	.423	+.016	.476	+.004	.382	+.014	.344	+.019	.321	+.023	.429	+.017
.07 in.	.472	+.004	.366	+.018	.331	+.025	.307	+.025	.420	+.019	.475	+.005	.380	+.016	.341	+.022	.318	+.026	.426	+.020
.08 in.	.471	+.005	.363	+.021	.327	+.029	.303	+.029	.417	+.022	.475	+.005	.378	+.018	.338	+.025	.314	+.030	.423	+.023
.09 in.	.47(	+.006	.361	+.023	.323	+.033	.300	+.032	.414	+.025	.474	+.006	.376	+.020	.335	+.028	.310	+.034	.420	+.026
.10 in.	.470	+.006	.358	+.026	.32(	+.036	.296	+.036	.411	+.028	.474	+.006	.374	+.022	.332	+.031	.306	+.038	.417	+.029

F.A.A. Ph.D. Thesis
10th April, 1969.

Structural Engineering Division,
Department of Civil Engineering,
University of Newcastle upon Tyne.

TESTS ON MODEL RADIAL RIBBED DOME

TEST NO. 16 TABLE NO. 6

Experimental Determination of Apex Ring Tangential Force Influence Coefficients

Load at point = 10lb

For position of load points, rib layout, details of model dome and graphs of tabulated results, see Test No. 16, Sheet No. 2.

Tangential Displacement of Apex Ring at Rib No.36 (Anti-clockwise viewed from above)	Dial gauge readings (A) and actual vertical displacement of point load (B; +ve downwards) in inches																			
	Rib No. 10										Rib No. 11									
	Point 1		Point 5		Point 9		Point 13		Point 17		Point 1		Point 5		Point 9		Point 13		Point 17	
	A	B	A	B	A	B	A	B	A	B	A	B	A	B	A	B	A	B	A	B
0 in.	.471	.000	.394	.000	.354	.000	.339	.000	.444	.000	.468	.000	.396	.000	.362	.000	.341	.000	.442	.000
.01 in.	.470	+.001	.392	+.002	.351	+.003	.335	+.004	.442	+.002	.468	.000	.394	+.002	.359	+.003	.338	+.003	.440	+.002
.02 in.	.470	+.001	.389	+.005	.348	+.006	.331	+.008	.440	+.004	.467	+.001	.393	+.003	.356	+.006	.334	+.007	.438	+.004
.03 in.	.470	+.001	.387	+.007	.346	+.008	.328	+.011	.437	+.007	.467	+.001	.391	+.005	.353	+.009	.331	+.010	.436	+.006
.04 in.	.469	+.002	.385	+.009	.343	+.011	.324	+.015	.435	+.009	.466	+.002	.389	+.007	.350	+.012	.327	+.014	.434	+.008
.05 in.	.469	+.002	.384	+.010	.341	+.013	.321	+.018	.432	+.012	.466	+.002	.388	+.008	.347	+.015	.324	+.017	.431	+.011
.06 in.	.468	+.003	.382	+.012	.338	+.016	.317	+.022	.430	+.014	.466	+.002	.386	+.010	.344	+.018	.320	+.021	.429	+.013
.07 in.	.468	+.003	.380	+.014	.335	+.019	.314	+.025	.428	+.016	.465	+.003	.384	+.012	.341	+.021	.317	+.024	.426	+.016
.08 in.	.467	+.004	.378	+.016	.332	+.022	.310	+.029	.425	+.019	.465	+.003	.383	+.013	.338	+.024	.313	+.028	.424	+.018
.09 in.	.467	+.004	.376	+.018	.330	+.024	.306	+.033	.422	+.022	.464	+.004	.381	+.015	.335	+.027	.310	+.031	.421	+.021
.10 in.	.466	+.005	.374	+.020	.327	+.027	.302	+.037	.419	+.025	.464	+.004	.379	+.017	.332	+.030	.307	+.034	.419	+.023

F.A.A. Ph.D. Thesis
10th April, 1969.

Structural Engineering Division,
Department of Civil Engineering,
University of Newcastle upon Tyne.

TESTS ON MODEL RADIAL RIBBED DOME

TEST NO. 16 TABLE NO. 7

Experimental Determination of Apex Ring Tangential Force Influence Coefficients

Load at point = 10lb

For position of load points, rib layout, details of model dome and graphs of tabulated results, see Test No. 16, Sheet Nos. 2 & 3.

Tangential Displacement of Apex Ring at Rib No.36 (Anti-clockwise viewed from above)	Dial gauge readings (A) and actual vertical displacement of point load (B; +ve downwards) in inches																			
	Rib No. 12										Rib No. 13									
	Point 1		Point 5		Point 9		Point 13		Point 17		Point 1		Point 5		Point 9		Point 13		Point 17	
	A	B	A	B	A	B	A	B	A	B	A	B	A	B	A	B	A	B	A	B
0 in.	.474	.000	.396	.00	.354	.000	.336	.000	.445	.000	.476	.000	.397	.000	.360	.000	.335	.000	.446	.000
.01 in.	.474	.000	.394	+.002	.352	+.002	.333	+.003	.443	+.002	.476	.000	.396	+.001	.358	+.002	.332	+.003	.444	+.002
.02 in.	.473	+.001	.392	+.004	.349	+.005	.330	+.006	.440	+.005	.475	+.001	.394	+.003	.356	+.004	.330	+.005	.442	+.004
.03 in.	.473	+.001	.390	+.006	.347	+.007	.327	+.009	.438	+.007	.475	+.001	.393	+.004	.353	+.007	.327	+.008	.440	+.006
.04 in.	.473	+.001	.389	+.007	.34[illegible]	+.010	.324	+.012	.436	+.009	.475	+.001	.391	+.006	.351	+.009	.325	+.010	.438	+.008
.05 in.	.472	+.002	.387	+.009	.341	+.013	.321	+.015	.434	+.011	.474	+.002	.390	+.007	.349	+.011	.322	+.013	.436	+.010
.06 in.	.472	+.002	.385	+.011	.33[illegible]	+.015	.317	+.019	.432	+.013	.474	+.002	.389	+.008	.347	+.013	.319	+.016	.434	+.012
.07 in.	.471	+.003	.383	+.013	.33[illegible]	+.018	.314	+.022	.429	+.016	.474	+.002	.387	+.010	.345	+.015	.316	+.019	.432	+.014
.08 in.	.471	+.003	.381	+.015	.33[illegible]	+.021	.311	+.025	.427	+.018	.473	+.003	.386	+.011	.342	+.018	.314	+.021	.430	+.016
.09 in.	.470	+.004	.379	+.017	.33[illegible]	+.024	.308	+.028	.424	+.021	.473	+.003	.384	+.013	.340	+.020	.311	+.024	.428	+.018
.10 in.	.470	+.004	.378	+.018	.32[illegible]	+.026	.305	+.031	.422	+.023	.473	+.003	.382	+.015	.338	+.022	.308	+.027	.425	+.021

F.A.A. Ph.D. Thesis
10th, 11th April, 1969.

Structural Engineering Division,
Department of Civil Engineering,
University of Newcastle upon Tyne.

TESTS ON MODEL RADIAL RIBBED DOME

TEST NO. 16 TABLE NO. 8

Experimental Determination of Apex Ring Tangential Force Influence Coefficients

Load at point = 10lb

For position of load points, rib layout, details of model dome and graphs of tabulated results, see Test No. 16, Sheet No. 3.

Tangential Displacement of Apex Ring at Rib No.36 (Anti-clockwise viewed from above)	Dial gauge readings (A) and actual vertical displacement of point load (B; +ve downwards) in inches																			
	Rib No 14										Rib No. 15									
	Point 1		Point 5		Point 9		Point 13		Point 17		Point 1		Point 5		Point 9		Point 13		Point 17	
	A	B	A	B	A	B	A	B	A	B	A	B	A	B	A	B	A	B	A	B
0 in.	.479	.000	.402	.000	.356	.000	.340	.000	.445	.000	.477	.000	.397	.000	.360	.000	.345	.000	.440	.000
.01 in.	.479	.000	.400	+.002	.355	+.001	.338	+.002	.443	+.002	.477	.000	.396	+.001	.358	+.002	.342	+.001	.439	+.001
.02 in.	.478	+.001	.399	+.003	.353	+.003	.336	+.004	.442	+.003	.377	.000	.395	+.002	.357	+.003	.340	+.003	.437	+.003
.03 in.	.478	+.001	.398	+.004	.352	+.004	.334	+.006	.441	+.004	.477	.000	.394	+.003	.355	+.005	.339	+.004	.436	+.004
.04 in.	.478	+.001	.397	+.005	.350	+.006	.332	+.008	.440	+.005	.377	.000	.393	+.004	.354	+.006	.337	+.006	.435	+.005
.05 in.	.478	+.001	.396	+.006	.349	+.007	.330	+.010	.438	+.007	.377	.000	.392	+.005	.353	+.007	.336	+.007	.434	+.006
.06 in.	.477	+.002	.395	+.007	.347	+.009	.328	+.012	.437	+.008	.476	+.001	.391	+.006	.351	+.009	.334	+.009	.432	+.008
.07 in.	.477	+.002	.394	+.008	.345	+.011	.326	+.014	.435	+.010	.476	+.001	.390	+.007	.350	+.010	.333	+.010	.431	+.009
.08 in.	.477	+.002	.392	+.010	.344	+.012	.324	+.016	.434	+.011	.476	+.001	.389	+.008	.348	+.012	.331	+.012	.430	+.010
.09 in.	.477	+.002	.391	+.011	.342	+.014	.322	+.018	.433	+.012	.476	+.001	.388	+.009	.347	+.013	.330	+.013	.428	+.012
.10 in.	.476	+.003	.390	+.012	.341	+.015	.320	+.020	.431	+.014	.476	+.001	.386	+.011	.346	+.014	.328	+.015	.427	+.013

F.A.A. Ph.D. Thesis
11th April, 1969.

Structural Engineering Division,
Department of Civil Engineering,
University of Newcastle upon Tyne.

TESTS ON MODEL RADIAL RIBBED DOME

TEST NO. 16 TABLE NO. 9

Experimental Determination of Apex Ring Tangential Force Influence Coefficients

Load at point = 10lb

For position of load points, rib layout, details of model dome and graphs of tabulated results, see Test No. 16, Sheet No. 3.

Tangential Displacement of Apex Ring at Rib No.36 (Anti-clockwise viewed from above	Dial gauge readings (A) and actual vertical displacement of point load (B; +ve downwards) in inches																			
	Rib No. 16										Rib No. 17									
	Point 1		Point 5		Point 9		Point 13		Point 17		Point 1		Point 5		Point 9		Point 13		Point 17	
	A	B	A	B	A	B	A	B	A	B	A	B	A	B	A	B	A	B	A	B
0 in.	.479	.000	.401	.00	.35	.000	.338	.000	.447	.000	.481	.000	.403	.000	.362	.000	.342	.000	.446	.000
.01 in.	.479	.000	.400	+.00 1	.35	+.001	.337	+.001	.446	+.001	.481	.000	.402	+.001	.362	.000	.342	.000	.445	+.001
.02 in.	.479	.000	.400	+.001	.35	+.001	.336	+.002	.445	+.002	.481	.000	.402	+.001	.361	+.001	.341	+.001	.445	+.001
.03 in.	.478	+.001	.399	+.002	.35	+.002	.335	+.003	.444	+.003	.481	.000	.402	+.001	.360	+.002	.340	+.002	.445	+.001
.04 in.	.478	+.001	.398	+.003	.35	+.003	.334	+.004	.443	+.004	.480	+.001	.401	+.002	.360	+.002	.339	+.003	.444	+.002
.05 in.	.478	+.001	.398	+.003	.35	+.004	.333	+.005	.442	+.005	.480	+.001	.401	+.002	.359	+.003	.338	+.004	.444	+.002
.06 in.	.478	+.001	.397	+.004	.35	+.005	.332	+.006	.441	+.006	.480	+.001	.400	+.003	.358	+.004	.338	+.004	.443	+.003
.07 in.	.478	+.001	.396	+.005	.35	+.006	.331	+.007	.440	+.007	.480	+.001	.400	+.003	.358	+.004	.337	+.005	.443	+.003
.08 in.	.478	+.001	.396	+.005	.35	+.006	.330	+.008	.439	+.008	.480	+.001	.399	+.004	.357	+.005	.336	+.006	.442	+.004
.09 in.	.478	+.001	.395	+.006	.352	+.007	.329	+.009	.438	+.009	.480	+.001	.399	+.004	.356	+.006	.335	+.007	.441	+.005
.10 in.	.477	+.002	.394	+.007	.351	+.008	.328	+.010	.437	+.010	.480	+.001	.398	+.005	.355	+.007	.334	+.008	.441	+.005

F.A.A. Ph.D. Thesis
11th April, 1969.

Structural Engineering Division,
Department of Civil Engineering,
University of Newcastle upon Tyne.

Experimental Determination of Apex Ring Tangential Force Influence Coefficients

Load at point = 10lb

For position of load points, rib layout, details of model dome and graphs of tabulated results, see Test No. 16, Sheet Nos. 3. & 4.

Tangential Displacement of Apex Ring at Rib No.36 (Anti-clockwise viewed from above)	Dial gauge readings (A) and actual vertical displacement of point load (B; +ve downwards) in inches																	
	Rib No. 18										Rib No. 19							
	Point 1		Point 5		Point 9		Point 13		Point 17		Point 1		Point 5		Point 9		Point 13		Point 17	
	A	B	A	B	A	B	A	B	A	B	A	B	A	B	A	B	A	B	A	B
0 in.	.476	.000	.403	.000	.369	.000	.339	.000	.443	.000	.474	.000	.399	.000	.362	.000	.343	.000	.441	.000
.01 in.	.476	.000	.403	.000	.369	.000	.339	.000	.443	.000	.474	.000	.399	.000	.362	.000	.343	.000	.442	-.001
.02 in.	.476	.000	.402	+.001	.369	.000	.338	+.001	.443	.000	.474	.000	.399	.000	.362	.000	.343	.000	.442	-.001
.03 in.	.476	.000	.402	+.001	.368	+.001	.338	+.001	.443	.000	.474	.000	.399	.000	.362	.000	.343	.000	.442	-.001
.04 in.	.476	.000	.402	+.001	.368	+.001	.337	+.002	.443	.000	.474	.000	.399	.000	.362	.000	.343	.000	.442	-.001
.05 in.	.476	.000	.401	+.002	.368	+.001	.337	+.002	.443	.000	.474	.000	.399	.000	.362	.000	.343	.000	.443	-.002
.06 in.	.476	.000	.401	+.002	.368	+.001	.336	+.003	.443	.000	.474	.000	.399	.000	.362	.000	.343	.000	.443	-.002
.07 in.	.476	.000	.401	+.002	.367	+.002	.336	+.003	.443	.000	.474	.000	.399	.000	.362	.000	.343	.000	.443	-.002
.08 in.	.476	.000	.400	+.003	.367	+.002	.335	+.004	.443	.000	.474	.000	.399	.000	.362	.000	.343	.000	.443	-.002
.09 in.	.476	.000	.400	+.003	.367	+.002	.335	+.004	.442	+.001	.474	.000	.399	.000	.362	.000	.343	.000	.443	-.002
.10 in.	.476	.000	.400	+.003	.366	+.003	.334	+.005	.442	+.001	.474	.000	.399	.000	.362	.000	.343	.000	.443	-.002

F.A.A. Ph.D. Thesis.
11th April & 6th May, 1969.

Structural Engineering Division,
Department of Civil Engineering,
University of Newcastle upon Tyne.

TESTS ON MODEL RADIAL RIBBED DOME

TEST NO. 16 TABLE NO. 11

Experimental Determination of Apex Ring Tangential Force Influence Coefficients

Load at point = 10lb

For position of load points, rib layout, details of model dome and graphs of tabulated results, see Test No. 16, Sheet No. 4.

Tangential Displacement of Apex Ring at Rib No.36 (Anti-clockwise viewed from above	Dial gauge readings (A) and actual vertical displacement of point load (B; +ve downwards) in inches																			
	Rib No. 20										Rib No. 21									
	Point 1		Point 5		Point 9		Point 13		Point 17		Point 1		Point 5		Point 9		Point 13		Point 17	
	A	B	A	B	A	B	A	B	A	B	A	B	A	B	A	B	A	B	A	B
0 in.	.478	.000	.396	.000	.360	.000	.346	.000	.441	.000	.478	.000	.404	.000	.362	.000	.331	.000	.442	.000
.01 in.	.478	.000	.397	-.001	.361	-.001	.347	-.001	.441	.000	.478	.000	.405	-.001	.363	-.001	.332	-.001	.443	-.001
.02 in.	.478	.000	.397	-.001	.362	-.002	.347	-.001	.442	-.001	.478	.000	.405	-.001	.364	-.002	.334	-.003	.444	-.002
.03 in.	.478	.000	.398	-.002	.363	-.003	.348	-.002	.442	-.001	.478	.000	.406	-.002	.365	-.003	.335	-.004	.445	-.003
.04 in.	.478	.000	.398	-.002	.364	-.004	.349	-.003	.443	-.002	.478	.000	.407	-.003	.366	-.004	.336	-.005	.446	-.004
.05 in.	.478	.000	.399	-.003	.365	-.005	.350	-.004	.443	-.002	.478	.000	.407	-.003	.367	-.005	.338	-.007	.447	-.005
.06 in.	.479	-.001	.399	-.003	.365	-.005	.351	-.005	.444	-.003	.478	.000	.408	-.004	.367	-.005	.339	-.008	.448	-.006
.07 in.	.479	-.001	.400	-.004	.366	-.006	.352	-.006	.444	-.003	.478	.000	.409	-.005	.368	-.006	.340	-.009	.449	-.007
.08 in.	.479	-.001	.401	-.005	.367	-.007	.353	-.007	.445	-.004	.479	-.001	.409	-.005	.369	-.007	.342	-.011	.450	-.008
.09 in.	.479	-.001	.401	-.005	.368	-.008	.354	-.008	.445	-.004	.479	-.001	.410	-.006	.370	-.008	.343	-.012	.450	-.008
.10 in.	.479	-.001	.402	-.006	.368	-.008	.354	-.008	.445	-.004	.479	-.001	.410	-.006	.371	-.009	.344	-.013	.451	-.009

F.A.A. Ph.D. Thesis
6th May, 1969.

Structural Engineering Division,
Department of Civil Engineering,
University of Newcastle upon Tyne.

Experimental Determination of Apex Ring Tangential Force Influence Coefficients

Load at point = 10lb

For position of load points, rib layout, details of model dome and graphs of tabulated results, see Test No. 16, Sheet No. 4.

Tangential Displacement of Apex Ring at Rib No.36 (Anti-clockwise viewed from above)	Dial gauge readings (A) and actual vertical displacement of point load (B; +ve downwards) in inches																			
	Rib No. 22										Rib No. 23									
	Point 1		Point 5		Point 9		Point 13		Point 17		Point 1		Point 5		Point 9		Point 13		Point 17	
	A	B	A	B	A	B	A	B	A	B	A	B	A	B	A	B	A	B	A	B
0 in.	.481	.000	.406	.000	.359	.000	.337	.000	.442	.000	.480	.000	.400	.000	.359	.000	.330	.000	.445	.000
.01 in.	.481	.000	.407	-.001	.361	-.002	.339	-.002	.444	-.002	.481	-.001	.401	-.001	.361	-.002	.332	-.002	.447	-.002
.02 in.	.481	.000	.407	-.001	.363	-.004	.341	-.004	.445	-.003	.481	-.001	.402	-.002	.363	-.004	.334	-.004	.448	-.003
.03 in.	.481	.000	.408	-.002	.365	-.006	.342	-.005	.446	-.004	.481	-.001	.404	-.004	.365	-.006	.336	-.006	.450	-.005
.04 in.	.482	-.001	.409	-.003	.366	-.007	.344	-.007	.448	-.006	.481	-.001	.405	-.005	.367	-.008	.338	-.008	.451	-.006
.05 in.	.482	-.001	.410	-.004	.368	-.009	.346	-.009	.449	-.007	.482	-.002	.406	-.006	.369	-.010	.341	-.011	.453	-.008
.06 in.	.482	-.001	.411	-.005	.370	-.011	.348	-.011	.450	-.008	.482	-.002	.407	-.007	.371	-.012	.343	-.013	.455	-.010
.07 in.	.482	-.001	.412	-.006	.371	-.012	.349	-.012	.451	-.009	.482	-.002	.408	-.008	.373	-.014	.345	-.015	.456	-.011
.08 in.	.482	-.001	.413	-.007	.373	-.014	.351	-.014	.453	-.011	.482	-.002	.409	-.009	.374	-.015	.347	-.017	.458	-.013
.09 in.	.483	-.002	.414	-.008	.375	-.016	.353	-.016	.454	-.012	.483	-.003	.410	-.010	.376	-.017	.350	-.020	.459	-.014
.10 in.	.483	-.002	.415	-.009	.376	-.017	.355	-.018	.455	-.013	.483	-.003	.411	-.011	.378	-.019	.352	-.022	.461	-.016

F.A.A. Ph.D. Thesis
6th May, 1969.

Structural Engineering Division,
Department of Civil Engineering,
University of Newcastle upon Tyne.

Experimental Determination of Apex Ring Tangential Force Influence Coefficients

Load at point = 10lb

For position of load points, rib layout, details of model dome and graphs of tabulated results, see Test No. 16, Sheet Nos. 4 & 5.

Tangential Displacement of Apex Ring at Rib No.36 (Anti-clockwise viewed from above	Dial gauge readings (A) and actual vertical displacement of point load (B; +ve downwards) in inches																			
	Rib No. 24										Rib No. 25									
	Point 1		Point 5		Point 9		Point 13		Point 17		Point 1		Point 5		Point 9		Point 13		Point 17	
	A	B	A	B	A	B	A	B	A	B	A	B	A	B	A	B	A	B	A	B
0 in.	.480	.000	.389	.000	.352	.000	.334	.000	.446	.000	.478	.000	.403	.000	.365	.000	.342	.000	.444	.000
.01 in.	.480	.000	.391	-.002	.354	-.002	.337	-.003	.448	-.002	.478	.000	.405	-.002	.367	-.002	.345	-.003	.445	-.001
.02 in.	.480	.000	.392	-.003	.356	-.004	.340	-.006	.450	-.004	.478	.000	.406	-.003	.370	-.005	.348	-.006	.447	-.003
.03 in.	.480	.000	.394	-.005	.359	-.007	.342	-.008	.451	-.005	.479	-.001	.408	-.005	.372	-.007	.351	-.009	.449	-.005
.04 in.	.481	-.001	.395	-.006	.361	-.009	.344	-.010	.453	-.007	.479	-.001	.410	-.007	.375	-.010	.354	-.012	.451	-.007
.05 in.	.481	-.001	.397	-.008	.363	-.011	.347	-.013	.455	-.009	.479	-.001	.411	-.008	.377	-.012	.357	-.015	.452	-.008
.06 in.	.482	-.002	.398	-.009	.366	-.014	.349	-.015	.457	-.011	.480	-.002	.413	-.010	.380	-.015	.360	-.018	.454	-.010
.07 in.	.482	-.002	.400	-.011	.368	-.016	.352	-.018	.459	-.013	.480	-.002	.415	-.012	.382	-.017	.363	-.021	.456	-.012
.08 in.	.482	-.002	.401	-.012	.370	-.018	.354	-.020	.461	-.015	.480	-.002	.416	-.013	.384	-.019	.365	-.023	.457	-.013
.09 in.	.483	-.003	.403	-.014	.373	-.021	.357	-.023	.462	-.016	.481	-.003	.418	-.015	.387	-.022	.368	-.026	.459	-.015
.10 in.	.483	-.003	.404	-.015	.375	-.023	.359	-.025	.464	-.018	.481	-.003	.419	-.016	.389	-.024	.371	-.029	.461	-.017

F.A.A. Ph.D. Thesis
6th, 7th May, 1969.

Structural Engineering Division,
Department of Civil Engineering,
University of Newcastle upon Tyne.

TESTS ON MODEL RADIAL RIBBED DOME

TEST NO. 16 TABLE NO. 14

Experimental Determination of Apex Ring Tangential Force Influence Coefficients
Load at point = 10lb

For position of load points, rib layout, details of model dome and graphs of tabulated results, see Test No. 16, Sheet No. 5.

Tangential Displacement of Apex Ring at Rib No.36 (Anti-clockwise viewed from above)	Dial gauge readings (A) and actual vertical displacement of point load (B; +ve downwards) in inches																			
	Rib No. 26										Rib No. 27									
	Point 1		Point 5		Point 9		Point 13		Point 17		Point 1		Point 5		Point 9		Point 13		Point 17	
	A	B	A	B	A	B	A	B	A	B	A	B	A	B	A	B	A	B	A	B
0 in.	.478	.000	.400	.000	.356	.000	.330	.000	.442	.000	.471	.000	.385	.000	.346	.000	.331	.000	.444	.000
.01 in.	.479	-.001	.402	-.002	.359	-.003	.333	-.003	.444	-.002	.472	-.001	.387	-.002	.350	-.004	.335	-.004	.446	-.002
.02 in.	.479	-.001	.404	-.004	.362	-.006	.336	-.006	.446	-.004	.472	-.001	.389	-.004	.354	-.008	.338	-.007	.448	-.004
.03 in.	.480	-.002	.406	-.006	.365	-.009	.340	-.010	.448	-.006	.473	-.002	.392	-.007	.358	-.012	.342	-.011	.451	-.007
.04 in.	.480	-.002	.408	-.008	.368	-.012	.343	-.013	.450	-.008	.474	-.003	.394	-.009	.361	-.015	.345	-.014	.453	-.009
.05 in.	.481	-.003	.410	-.010	.371	-.015	.346	-.016	.452	-.010	.474	-.003	.396	-.011	.365	-.019	.349	-.018	.455	-.011
.06 in.	.481	-.003	.412	-.012	.374	-.018	.349	-.019	.455	-.013	.475	-.004	.399	-.014	.368	-.022	.353	-.022	.457	-.013
.07 in.	.482	-.004	.413	-.013	.377	-.021	.352	-.022	.457	-.015	.475	-.004	.401	-.016	.371	-.025	.356	-.025	.459	-.015
.08 in.	.482	-.004	.415	-.015	.380	-.024	.355	-.025	.459	-.017	.476	-.005	.403	-.018	.375	-.029	.360	-.029	.461	-.017
.09 in.	.482	-.004	.417	-.017	.383	-.027	.358	-.028	.461	-.019	.476	-.005	.405	-.020	.379	-.033	.363	-.032	.464	-.020
.10 in.	.483	-.005	.419	-.019	.386	-.030	.361	-.031	.463	-.021	.477	-.006	.407	-.022	.382	-.036	.367	-.036	.466	-.022

F.A.A. Ph.D. Thesis.
7th May, 1969.

Structural Engineering Division,
Department of Civil Engineering,
University of Newcastle upon Tyne.

TESTS ON MODEL RADIAL RIBBED DOME

TEST NO. 16 TABLE NO. 15

Experimental Determination of Apex Ring Tangential Force Influence Coefficients
Load at point = 10lb

For position of load points, rib layout, details of model dome and graphs of tabulated results, see Test No. 16, Sheet No. 5.

Tangential Displacement of Apex Ring at Rib No.36 (Anti-clockwise viewed from above)	Dial gauge readings (A) and actual vertical displacement of point load (B; +ve downwards) in inches																			
	Rib No. 28										Rib No. 29									
	Point 1		Point 5		Point 9		Point 13		Point 17		Point 1		Point 5		Point 9		Point 13		Point 17	
	A	B	A	B	A	B	A	B	A	B	A	B	A	B	A	B	A	B	A	B
0 in.	.479	.000	.393	.000	.350	.000	.330	.000	.438	.000	.479	.000	.390	.000	.356	.000	.332	.000	.440	.000
.01 in.	.479	.000	.396	-.003	.354	-.004	.333	-.003	.440	-.002	.480	-.001	.393	-.003	.360	-.004	.335	-.003	.442	-.002
.02 in.	.480	-.001	.398	-.005	.357	-.007	.337	-.007	.442	-.004	.480	-.001	.395	-.005	.364	-.008	.338	-.006	.445	-.005
.03 in.	.480	-.001	.400	-.007	.360	-.010	.340	-.010	.445	-.007	.481	-.002	.398	-.008	.367	-.011	.341	-.009	.447	-.007
.04 in.	.481	-.002	.403	-.010	.364	-.014	.344	-.014	.447	-.009	.482	-.003	.400	-.010	.371	-.015	.345	-.013	.449	-.009
.05 in.	.481	-.002	.405	-.012	.367	-.017	.348	-.018	.449	-.011	.482	-.003	.403	-.013	.374	-.018	.348	-.016	.451	-.011
.06 in.	.482	-.003	.407	-.014	.371	-.021	.351	-.021	.451	-.013	.483	-.004	.405	-.015	.378	-.022	.351	-.019	.453	-.013
.07 in.	.482	-.003	.409	-.016	.374	-.024	.354	-.024	.453	-.015	.484	-.005	.407	-.017	.381	-.025	.354	-.022	.455	-.015
.08 in.	.483	-.004	.411	-.018	.377	-.027	.357	-.027	.455	-.017	.484	-.005	.410	-.020	.385	-.029	.357	-.025	.457	-.017
.09 in.	.483	-.004	.413	-.020	.380	-.030	.360	-.030	.457	-.019	.485	-.006	.412	-.022	.389	-.033	.360	-.028	.459	-.019
.10 in.	.484	-.005	.415	-.022	.383	-.033	.363	-.033	.459	-.021	.485	-.006	.415	-.025	.392	-.036	.363	-.031	.461	-.021

F.A.A. Ph.D. Thesis
7th May, 1969.

Structural Engineering Division,
Department of Civil Engineering,
University of Newcastle upon Tyne.

Experimental Determination of Apex Ring Tangential Force Influence Coefficients
Load at point = 10lb

For position of load points, rib layout, details of model dome and graphs of tabulated results, see Test No. 16, Sheet Nos. 5 & 6.

Tangential Displacement of Apex Ring at Rib No.36 (Anti-clockwise viewed from above)	Dial gauge readings (A) and actual vertical displacement of point load (B; +ve downwards) in inches																			
	Rib No. 30										Rib No. 31									
	Point 1		Point 5		Point 9		Point 13		Point 17		Point 1		Point 5		Point 9		Point 13		Point 17	
	A	B	A	B	A	B	A	B	A	B	A	B	A	B	A	B	A	B	A	B
0 in.	.477	.000	.397	.000	.361	.000	.341	.000	.446	.000	.476	.000	.400	.000	.360	.000	.342	.000	.446	.000
.01 in.	.478	-.001	.399	-.002	.365	-.004	.344	-.003	.448	-.002	.476	.000	.403	-.003	.364	-.004	.346	-.004	.447	-.001
.02 in.	.478	-.001	.402	-.005	.369	-.008	.348	-.007	.450	-.004	.477	-.001	.405	-.005	.367	-.007	.350	-.008	.449	-.003
.03 in.	.479	-.002	.404	-.007	.372	-.011	.351	-.010	.452	-.006	.478	-.002	.407	-.007	.371	-.011	.353	-.011	.451	-.005
.04 in.	.479	-.002	.407	-.010	.376	-.015	.355	-.014	.454	-.008	.478	-.002	.410	-.010	.374	-.014	.357	-.015	.452	-.006
.05 in.	.480	-.003	.409	-.012	.380	-.019	.358	-.017	.456	-.010	.479	-.003	.412	-.012	.378	-.018	.360	-.018	.454	-.008
.06 in.	.481	-.004	.412	-.015	.383	-.022	.361	-.020	.458	-.012	.480	-.004	.415	-.015	.381	-.021	.364	-.022	.456	-.010
.07 in.	.482	-.005	.414	-.017	.387	-.026	.365	-.024	.460	-.014	.480	-.004	.417	-.017	.384	-.024	.367	-.025	.457	-.011
.08 in.	.482	-.005	.416	-.019	.390	-.029	.368	-.027	.461	-.015	.481	-.005	.419	-.019	.388	-.028	.371	-.029	.459	-.013
.09 in.	.483	-.006	.419	-.022	.394	-.033	.371	-.030	.463	-.017	.481	-.005	.422	-.022	.391	-.031	.374	-.032	.460	-.014
.10 in.	.483	-.006	.421	-.024	.397	-.036	.374	-.034	.465	-.019	.482	-.006	.424	-.024	.394	-.034	.377	-.035	.462	-.016

F.A.A. Ph.D. Thesis
7th, 8th May, 1969.

Structural Engineering Division,
Department of Civil Engineering,
University of Newcastle upon Tyne.

TESTS ON MODEL RADIAL RIBBED DOME

TEST NO. 16 TABLE NO. 17

Experimental Determination of Apex Ring Tangential Force Influence Coefficients

Load at point = 10lb

For position of load points, rib layout, details of model dome and graphs of tabulated results, see Test No. 16, Sheet No. 6.

Tangential Displacement of Apex Ring at Rib No.36 (Anti-clockwise viewed from above)	Dial gauge readings (A) and actual vertical displacement of point load (B; +ve downwards) in inches																			
	Rib No. 32										Rib No. 33									
	Point 1		Point 5		Point 9		Point 13		Point 17		Point 1		Point 5		Point 9		Point 13		Point 17	
	A	B	A	B	A	B	A	B	A	B	A	B	A	B	A	B	A	B	A	B
0 in.	.481	.000	.401	.00( )	.362	.000	.345	.000	.447	.000	.478	.000	.396	.000	.355	.000	.325	.000	.438	.000
.01 in.	.481	.000	.404	-.003	.366	-.004	.349	-.004	.449	-.002	.479	-.001	.399	-.003	.358	-.003	.327	-.002	.440	-.002
.02 in.	.482	-.001	.407	-.006	.370	-.008	.353	-.008	.451	-.004	.479	-.001	.401	-.005	.361	-.006	.330	-.005	.441	-.003
.03 in.	.483	-.002	.410	-.009	.373	-.011	.357	-.012	.453	-.006	.480	-.002	.403	-.007	.363	-.008	.333	-.008	.442	-.004
.04 in.	.483	-.002	.412	-.011	.377	-.015	.361	-.016	.455	-.008	.480	-.002	.405	-.009	.366	-.011	.336	-.011	.444	-.006
.05 in.	.484	-.003	.415	-.014	.380	-.018	.365	-.020	.457	-.010	.481	-.003	.407	-.011	.369	-.014	.339	-.014	.445	-.007
.06 in.	.485	-.004	.418	-.017	.384	-.022	.369	-.024	.459	-.012	.481	-.003	.409	-.013	.372	-.017	.342	-.017	.446	-.008
.07 in.	.485	-.004	.421	-.020	.388	-.026	.373	-.028	.461	-.014	.482	-.004	.411	-.015	.374	-.019	.344	-.019	.447	-.009
.08 in.	.486	-.005	.423	-.022	.391	-.029	.377	-.032	.463	-.016	.483	-.005	.413	-.017	.377	-.022	.347	-.022	.449	-.011
.09 in.	.487	-.006	.426	-.025	.395	-.033	.381	-.036	.465	-.018	.483	-.005	.415	-.019	.380	-.025	.350	-.025	.450	-.012
.10 in.	.487	-.006	.429	-.028	.399	-.037	.384	-.039	.467	-.020	.484	-.006	.417	-.021	.383	-.028	.353	-.028	.451	-.013

F.A.A. Ph.D. Thesis
8th May, 1969.

Structural Engineering Division,
Department of Civil Engineering,
University of Newcastle upon Tyne.

Experimental Determination of Apex Ring Tangential Force Influence Coefficients
Load at point = 10lb For position of load points, rib layout, details of model dome and graphs of tabulated results, see Test No. 16, Sheet No. 6.

Tangential Displacement of Apex Ring at Rib No. 36 (Anti-clockwise viewed from above)	Dial gauge readings (A) and actual vertical displacement of point load (B; +ve downwards) in inches																	
	Rib No. 34										Rib No. 35							
	Point 1		Point 5		Point 9		Point 13		Point 17		Point 1		Point 5		Point 9		Point 13		Point 17	
	A	B	A	B	A	B	A	B	A	B	A	B	A	B	A	B	A	B	A	B
0 in.	.481	.000	.390	.00	.34[illegible]	.000	.328	.000	.444	.000	.479	.000	.394	.000	.364	.000	.343	.000	.444	.000
.01 in.	.481	.000	.391	-.001	.35[illegible]	-.003	.330	-.002	.445	-.001	.479	.000	.396	-.002	.366	-.002	.344	-.001	.445	-.001
.02 in.	.482	-.001	.393	-.003	.35[illegible]	-.006	.333	-.005	.445	-.001	.479	.000	.397	-.003	.368	-.004	.346	-.003	.445	-.001
.03 in.	.482	-.001	.395	-.005	.35[illegible]	-.008	.335	-.007	.446	-.002	.479	.000	.398	-.004	.369	-.005	.347	-.004	.445	-.001
.04 in.	.483	-.002	.397	-.007	.35[illegible]	-.011	.337	-.009	.447	-.003	.480	-.001	.399	-.005	.371	-.007	.348	-.005	.446	-.002
.05 in.	.483	-.002	.399	-.009	.36[illegible]	-.014	.340	-.012	.447	-.003	.480	-.001	.400	-.006	.373	-.009	.350	-.007	.446	-.002
.06 in.	.483	-.002	.401	-.011	.36[illegible]	-.016	.342	-.014	.448	-.004	.480	-.001	.401	-.007	.374	-.010	.351	-.008	.446	-.002
.07 in.	.484	-.003	.402	-.012	.36[illegible]	-.019	.345	-.017	.449	-.005	.480	-.001	.402	-.008	.375	-.011	.353	-.010	.446	-.002
.08 in.	.484	-.003	.404	-.014	.37[illegible]	-.022	.347	-.019	.449	-.005	.481	-.002	.404	-.010	.377	-.013	.354	-.011	.447	-.003
.09 in.	.485	-.004	.406	-.016	.37[illegible]	-.024	.350	-.022	.450	-.006	.481	-.002	.405	-.011	.379	-.015	.355	-.012	.447	-.003
.10 in.	.485	-.004	.407	-.017	.37[illegible]	-.027	.352	-.024	.450	-.006	.481	-.002	.406	-.012	.380	-.016	.357	-.014	.447	-.003

F.A.A. Ph.D. Thesis
8th May, 1969.

Structural Engineering Division,
Department of Civil Engineering,
University of Newcastle upon Tyne.

TESTS ON MODEL RADIAL RIBBED DOME

Test No. 16

Sheet No. 1

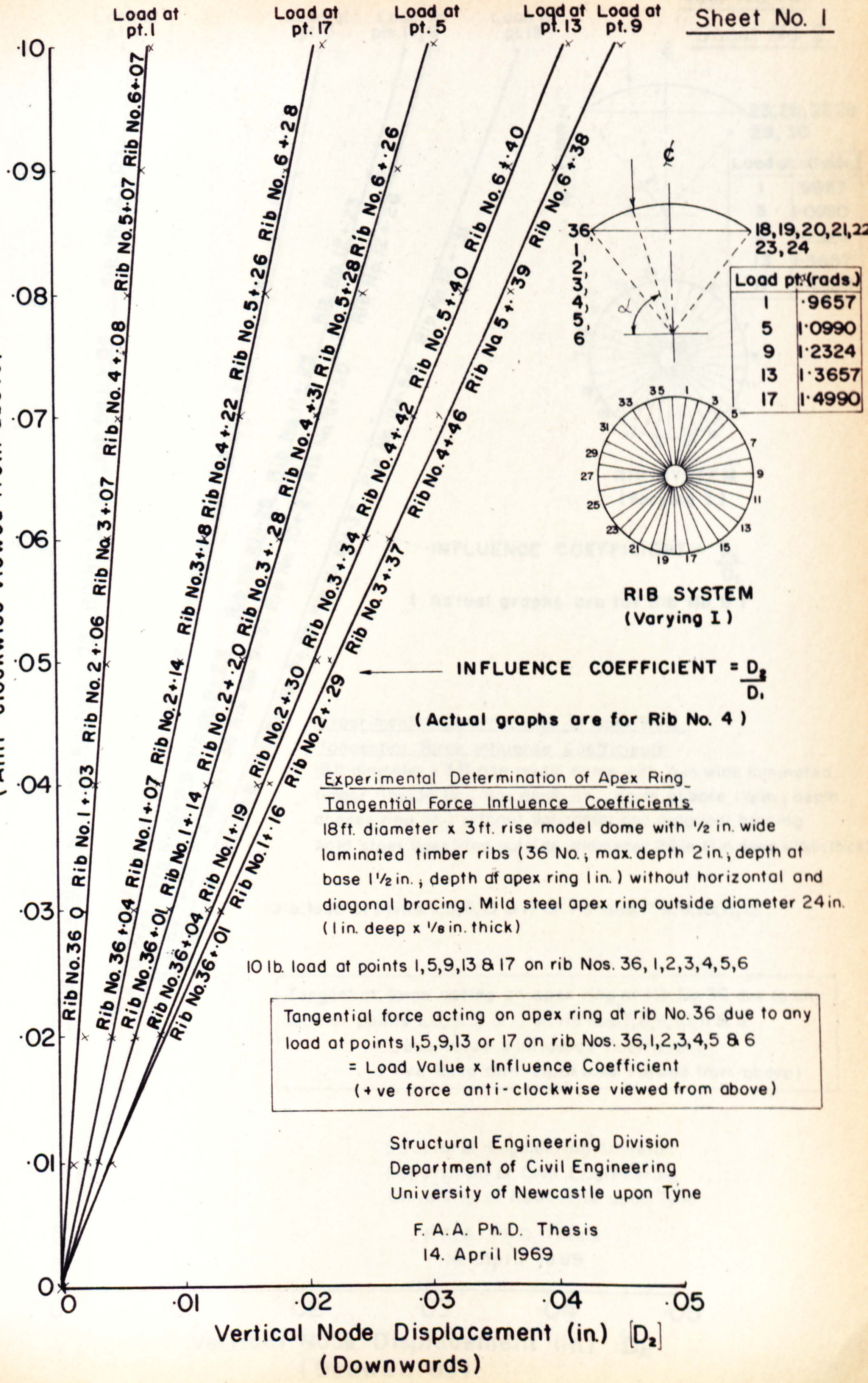

Load pt.	(rads.)
1	·9657
5	1·0990
9	1·2324
13	1·3657
17	1·4990

RIB SYSTEM
(Varying I)

← INFLUENCE COEFFICIENT = $\frac{D_2}{D_1}$

(Actual graphs are for Rib No. 4)

Experimental Determination of Apex Ring Tangential Force Influence Coefficients

18ft. diameter x 3ft. rise model dome with ½ in. wide laminated timber ribs (36 No.; max. depth 2 in.; depth at base 1½ in.; depth at apex ring 1 in.) without horizontal and diagonal bracing. Mild steel apex ring outside diameter 24 in. (1 in. deep x ⅛ in. thick)

10 lb. load at points 1, 5, 9, 13 & 17 on rib Nos. 36, 1, 2, 3, 4, 5, 6

Tangential force acting on apex ring at rib No. 36 due to any load at points 1, 5, 9, 13 or 17 on rib Nos. 36, 1, 2, 3, 4, 5 & 6
= Load Value x Influence Coefficient
(+ve force anti-clockwise viewed from above)

Structural Engineering Division
Department of Civil Engineering
University of Newcastle upon Tyne

F. A. A. Ph. D. Thesis
14. April 1969

TESTS ON MODEL RADIAL RIBBED DOME

Test No. 16

Sheet No. 2

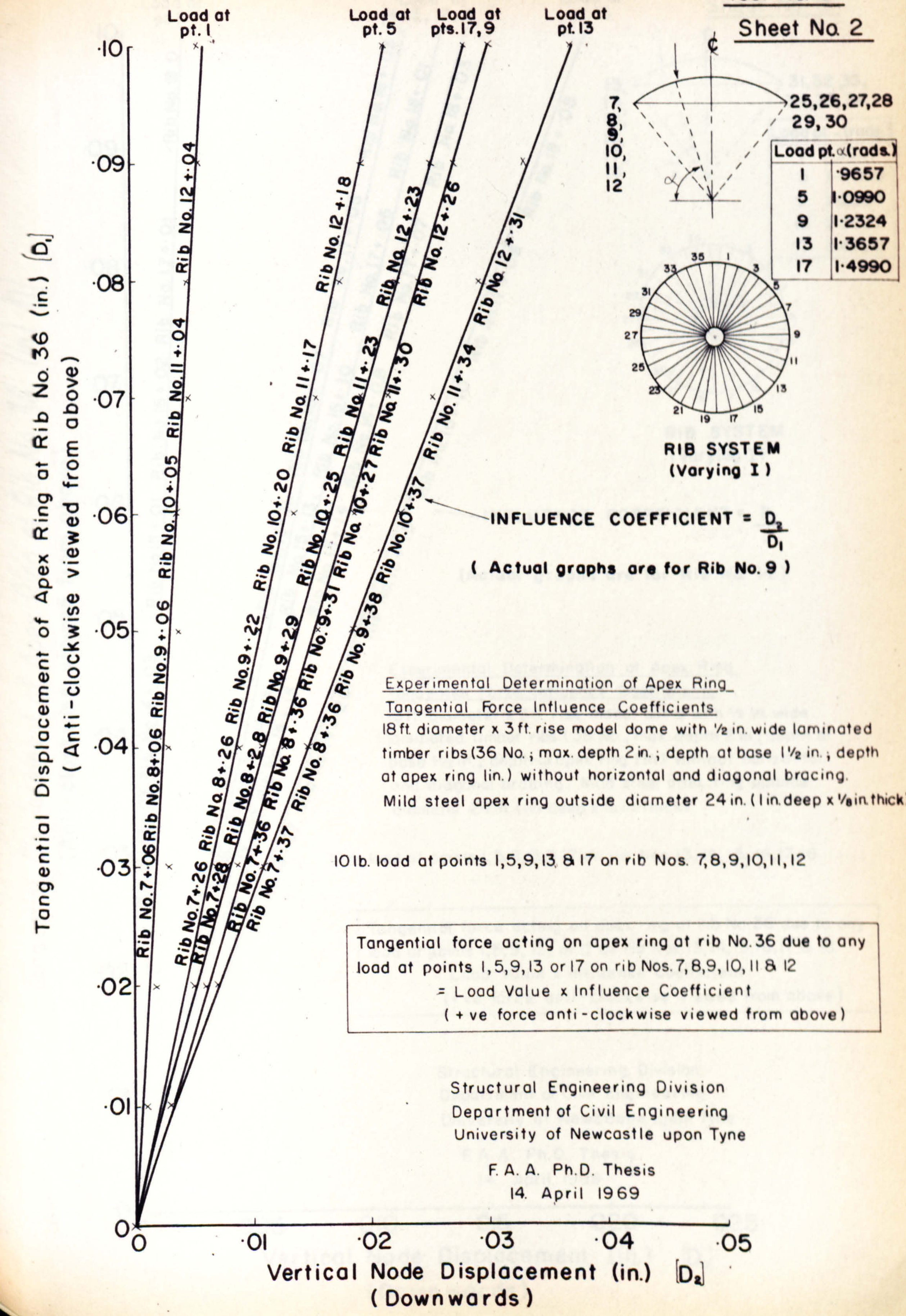

Load pt.	α (rads.)
1	·9657
5	1·0990
9	1·2324
13	1·3657
17	1·4990

RIB SYSTEM
(Varying I)

INFLUENCE COEFFICIENT = $\frac{D_2}{D_1}$

(Actual graphs are for Rib No. 9)

Experimental Determination of Apex Ring
Tangential Force Influence Coefficients

18 ft. diameter x 3 ft. rise model dome with ½ in. wide laminated timber ribs (36 No.; max. depth 2 in.; depth at base 1½ in.; depth at apex ring 1in.) without horizontal and diagonal bracing.
Mild steel apex ring outside diameter 24 in. (1 in. deep x ⅛ in. thick)

10 lb. load at points 1, 5, 9, 13 & 17 on rib Nos. 7, 8, 9, 10, 11, 12

Tangential force acting on apex ring at rib No. 36 due to any load at points 1, 5, 9, 13 or 17 on rib Nos. 7, 8, 9, 10, 11 & 12
= Load Value x Influence Coefficient
(+ ve force anti-clockwise viewed from above)

Structural Engineering Division
Department of Civil Engineering
University of Newcastle upon Tyne

F. A. A. Ph.D. Thesis
14. April 1969

TESTS ON MODEL RADIAL RIBBED DOME

Test No. 16
Sheet No. 3

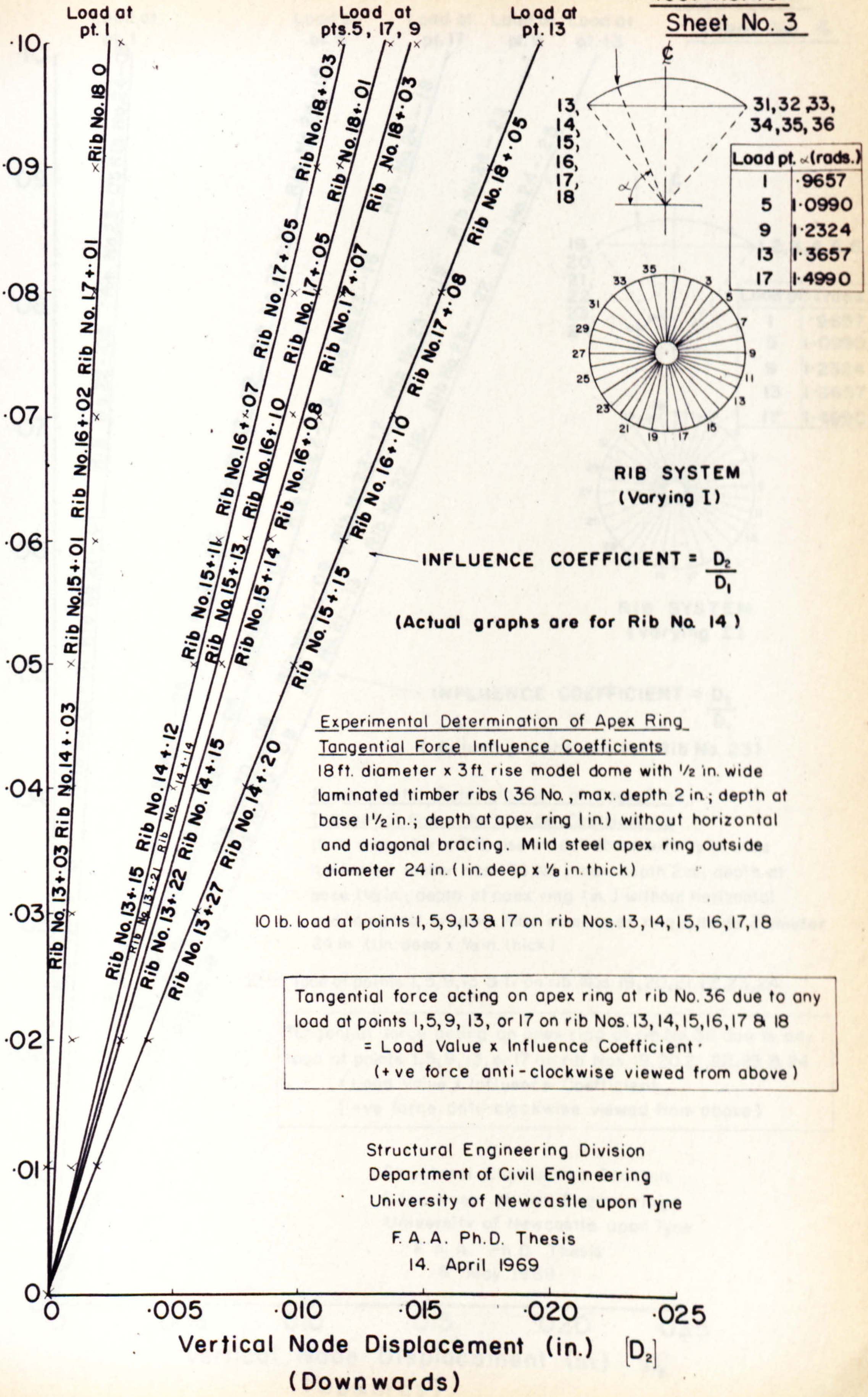

Load pt.	α (rads.)
1	·9657
5	1·0990
9	1·2324
13	1·3657
17	1·4990

RIB SYSTEM
(Varying I)

← INFLUENCE COEFFICIENT = $\frac{D_2}{D_1}$

(Actual graphs are for Rib No. 14)

Experimental Determination of Apex Ring Tangential Force Influence Coefficients

18 ft. diameter x 3 ft. rise model dome with ½ in. wide laminated timber ribs (36 No., max. depth 2 in.; depth at base 1½ in.; depth at apex ring 1 in.) without horizontal and diagonal bracing. Mild steel apex ring outside diameter 24 in. (1 in. deep x ⅛ in. thick)

10 lb. load at points 1, 5, 9, 13 & 17 on rib Nos. 13, 14, 15, 16, 17, 18

Tangential force acting on apex ring at rib No. 36 due to any load at points 1, 5, 9, 13, or 17 on rib Nos. 13, 14, 15, 16, 17 & 18
= Load Value x Influence Coefficient.
(+ve force anti-clockwise viewed from above)

Structural Engineering Division
Department of Civil Engineering
University of Newcastle upon Tyne

F. A. A. Ph.D. Thesis
14. April 1969

TESTS ON MODEL RADIAL RIBBED DOME

Test No. 16

Sheet No. 4

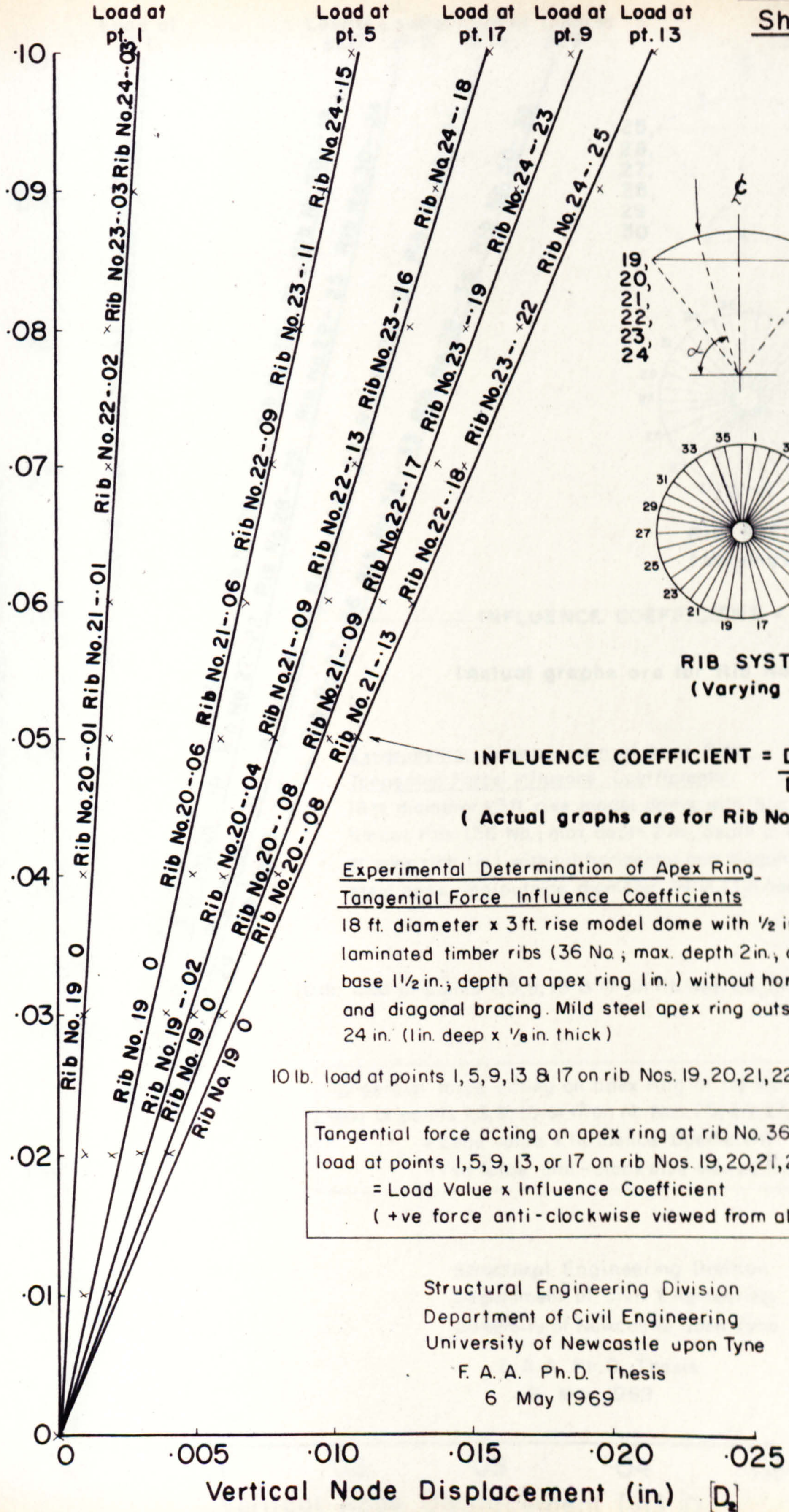

Load pt.	α (rads.)
1	·9657
5	1·0990
9	1·2324
13	1·3657
17	1·4990

RIB SYSTEM
(Varying I)

Experimental Determination of Apex Ring Tangential Force Influence Coefficients

18 ft. diameter x 3 ft. rise model dome with ½ in. wide laminated timber ribs (36 No.; max. depth 2 in., depth at base 1½ in.; depth at apex ring 1 in.) without horizontal and diagonal bracing. Mild steel apex ring outside diameter 24 in. (1 in. deep x ⅛ in. thick)

10 lb. load at points 1, 5, 9, 13 & 17 on rib Nos. 19, 20, 21, 22, 23, 24.

Tangential force acting on apex ring at rib No. 36 due to any load at points 1, 5, 9, 13, or 17 on rib Nos. 19, 20, 21, 22, 23 & 24
= Load Value x Influence Coefficient
(+ve force anti-clockwise viewed from above)

Structural Engineering Division
Department of Civil Engineering
University of Newcastle upon Tyne
F. A. A. Ph.D. Thesis
6 May 1969

TESTS ON MODEL RADIAL RIBBED DOME

Test No. 16

Sheet No. 5

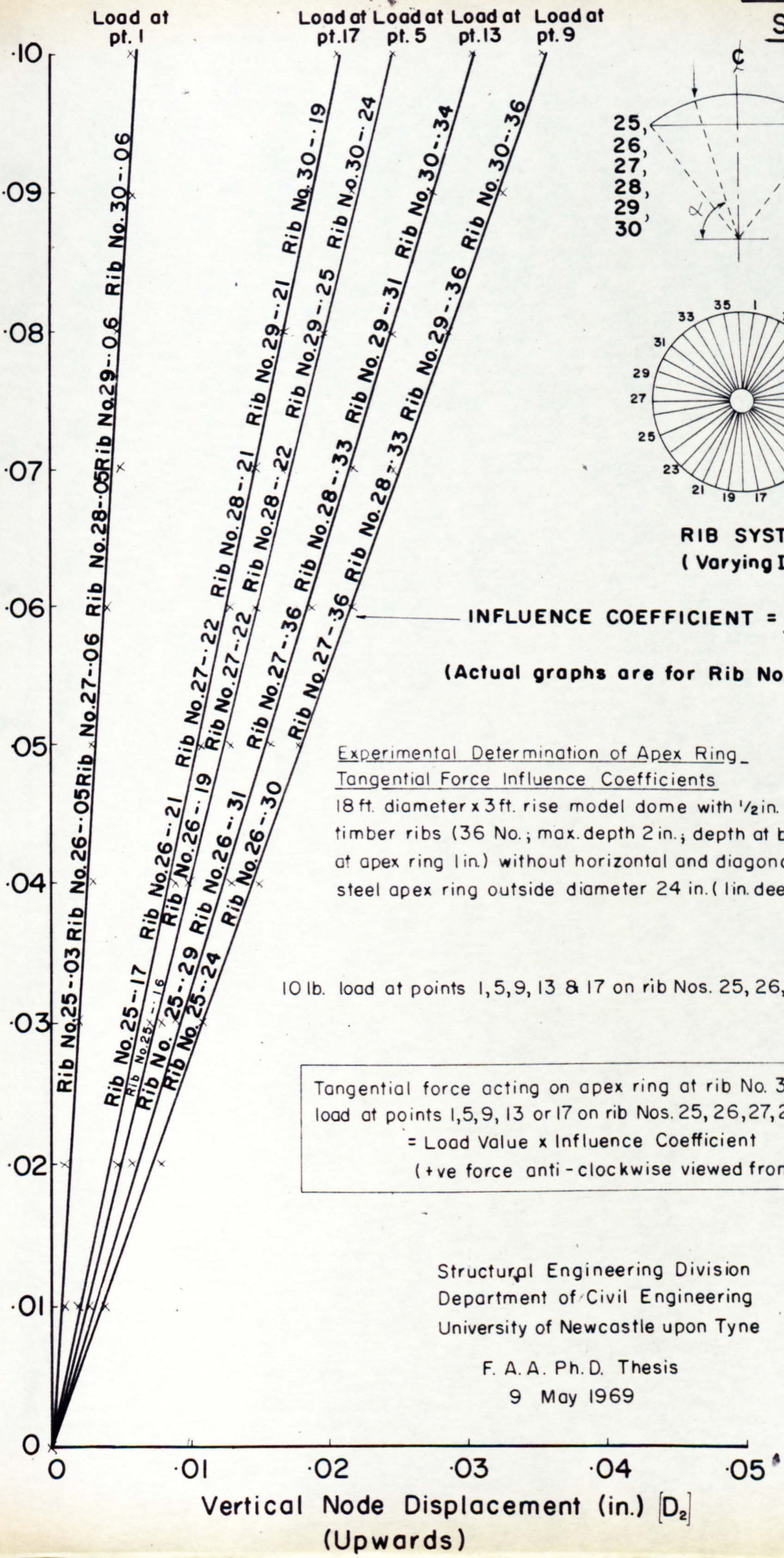

Load pt.	α (rads)
1	·9657
5	1·0990
9	1·2324
13	1·3657
17	1·4990

RIB SYSTEM
(Varying I)

INFLUENCE COEFFICIENT = $\frac{D_2}{D_1}$

(Actual graphs are for Rib No. 29)

Experimental Determination of Apex Ring
Tangential Force Influence Coefficients

18 ft. diameter x 3 ft. rise model dome with ½ in. wide laminated timber ribs (36 No.; max. depth 2 in.; depth at base 1½ in.; depth at apex ring 1 in.) without horizontal and diagonal bracing. Mild steel apex ring outside diameter 24 in. (1 in. deep x ⅛ in. thick)

10 lb. load at points 1, 5, 9, 13 & 17 on rib Nos. 25, 26, 27, 28, 29, 30

Tangential force acting on apex ring at rib No. 36 due to any load at points 1, 5, 9, 13 or 17 on rib Nos. 25, 26, 27, 28, 29 & 30
= Load Value x Influence Coefficient
(+ve force anti-clockwise viewed from above)

Structural Engineering Division
Department of Civil Engineering
University of Newcastle upon Tyne

F. A. A. Ph. D. Thesis
9 May 1969

TESTS ON MODEL RADIAL RIBBED DOME

Test No. 16
Sheet No. 6

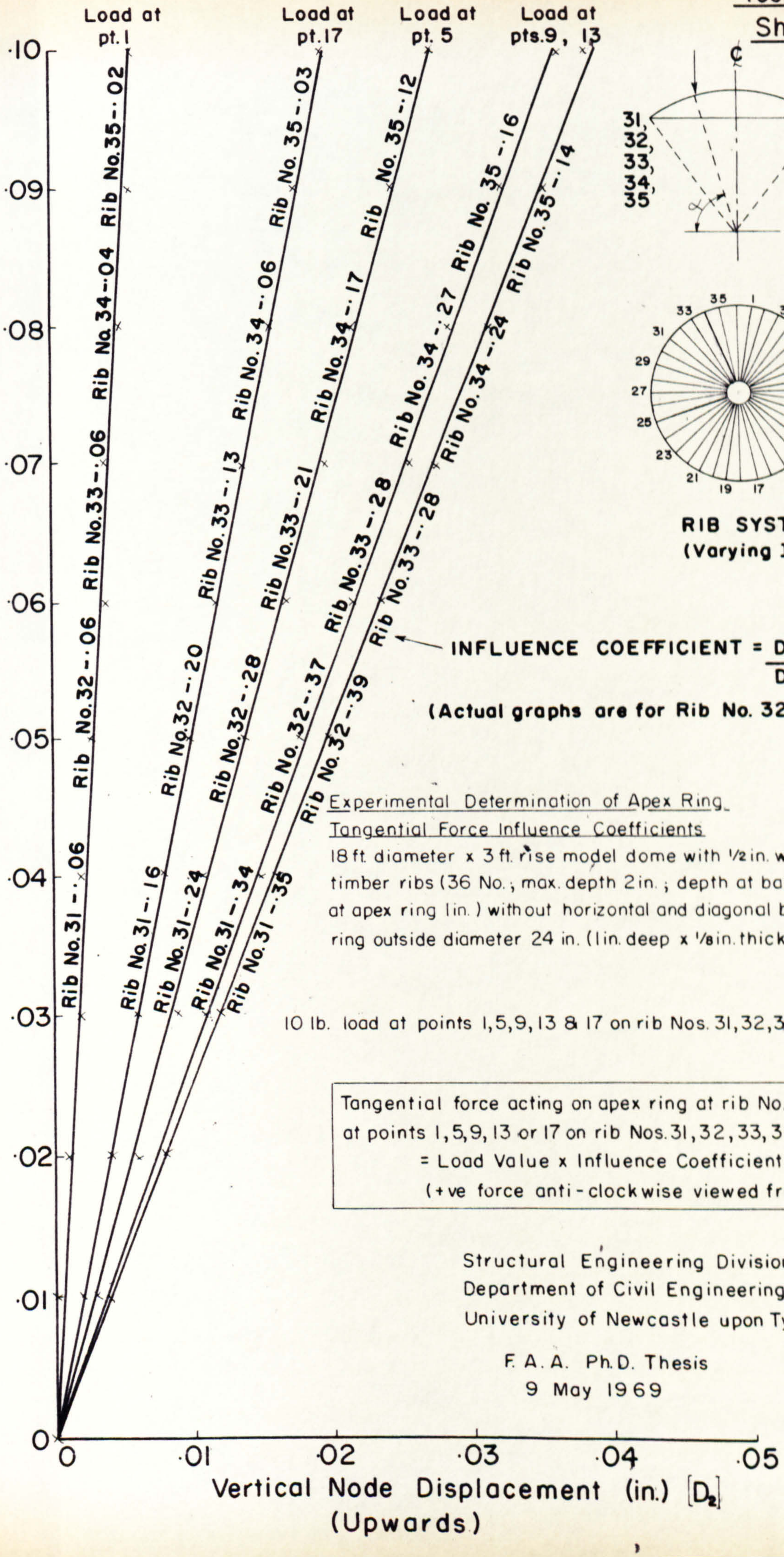

Load pt.	α (rads.)
1	·9657
5	1·0990
9	1·2324
13	1·3657
17	1·4990

RIB SYSTEM
(Varying I)

INFLUENCE COEFFICIENT = $\frac{D_2}{D_1}$

(Actual graphs are for Rib No. 32)

Experimental Determination of Apex Ring
Tangential Force Influence Coefficients

18 ft. diameter x 3 ft. rise model dome with ½ in. wide laminated timber ribs (36 No.; max. depth 2 in.; depth at base 1½ in.; depth at apex ring 1 in.) without horizontal and diagonal bracing. Mild steel apex ring outside diameter 24 in. (1 in. deep x ⅛ in. thick)

10 lb. load at points 1, 5, 9, 13 & 17 on rib Nos. 31, 32, 33, 34, 35

Tangential force acting on apex ring at rib No. 36 due to any load at points 1, 5, 9, 13 or 17 on rib Nos. 31, 32, 33, 34 & 35
= Load Value x Influence Coefficient
(+ve force anti-clockwise viewed from above)

Structural Engineering Division
Department of Civil Engineering
University of Newcastle upon Tyne

F. A. A. Ph.D. Thesis
9 May 1969

Structural Engineering Division
Department of Civil Engineering
University of Newcastle upon Tyne

TESTS ON MODEL RADIAL RIBBED DOME

TEST NO. 16 SHEET NO. 7

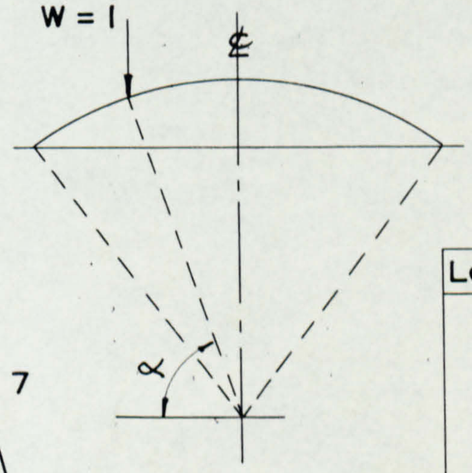

Load Pt.	∝(rads.)
1	.9657
5	1.0990
9	1.2324
13	1.3657
17	1.4990

F = W × Influence Coefficient

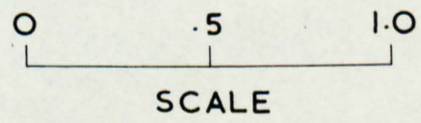

Experimental Determination of Apex Ring Tangential Force Influence Lines for Rib No.36

(Unit vertical force acting at any angle on any rib)

18ft diameter × 3ft rise model dome with 1/2 in. wide laminated timber ribs (36 No. of varying I; max. depth 2 in.; depth at base 1 1/2 in.; depth at apex ring 1in) without horizontal and diagonal bracing. Mild steel apex ring outside diameter 24 in. (1 in. deep × 1/8 in. thick)

F.A.A. Ph.D. Thesis
12th May, 1969

TESTS ON MODEL RADIAL RIBBED DOME

TEST NO. 17 TABLE NO. 1

Measurement of Apex Ring Displacements at Rib No. 36

Load at point = 10lb ; All dial gauge zeros .500 in. ; A = Tangential displacement in inches (+ve reading anti-clockwise viewed from above) ; B = Radial displacement in inches (+ve reading inwards) ; C = Vertical displacement in inches (+ve reading upwards) ; D = Dial gauge reading ; E = Actual Displacement.

	Load Point	Gauge No. 1 A		Gauge No. 2 B		Gauge No. 3 C			Load Point	Gauge No. 1 A		Gauge No. 2 B		Gauge No. 3 C	
		D	E	D	E	D	E			D	E	D	E	D	E
Rib No. 36	1	.500	.000	.509	+.009	.499	-.001	Rib No. 3	1	.502	+.002	.503	+.003	.500	.000
	5	.500	.000	.537	+.037	.493	-.007		5	.518	+.018	.517	+.017	.494	-.006
	9	.500	.000	.556	+.056	.484	-.016		9	.527	+.027	.525	+.025	.484	-.016
	13	.500	.000	.559	+.059	.471	-.029		13	.529	+.029	.527	+.027	.470	-.030
	17	.500	.000	.523	+.023	.457	-.043		17	.513	+.013	.516	+.016	.459	-.041
Rib No. 1	1	.501	+.001	.509	+.009	.499	-.001	Rib No. 4	1	.502	+.002	.501	+.001	.500	.000
	5	.510	+.010	.535	+.035	.493	-.007		5	.521	+.021	.509	+.009	.495	-.005
	9	.514	+.014	.550	+.050	.482	-.018		9	.531	+.031	.514	+.014	.487	-.013
	13	.514	+.014	.550	+.050	.468	-.032		13	.530	+.030	.516	+.016	.474	-.026
	17	.503	+.003	.521	+.021	.457	-.043		17	.516	+.016	.512	+.012	.463	-.037
Rib No. 2	1	.502	+.002	.506	+.006	.499	-.001	Rib No. 5	1	.502	+.002	.500	.000	.500	.000
	5	.515	+.015	.525	+.025	.494	-.006		5	.518	+.018	.503	+.003	.498	-.002
	9	.521	+.021	.537	+.037	.482	-.018		9	.528	+.028	.505	+.005	.491	-.009
	13	.522	+.022	.538	+.038	.467	-.033		13	.530	+.030	.508	+.008	.479	-.021
	17	.508	+.008	.518	+.018	.457	-.043		17	.518	+.018	.509	+.009	.466	-.034

F.A.A. Ph.D. Thesis
13th May, 1969.

Structural Engineering Division,
Department of Civil Engineering,
University of Newcastle upon Tyne.

TESTS ON MODEL RADIAL RIBBED DOME

TEST NO. 17 TABLE NO. 2

Measurement of Apex Ring Displacements at Rib No. 36

Load at point = 10lb ; All dial gauge zeros .500 in. ; A = Tangential displacement in inches (+ve reading anti-clockwise viewed from above) ; B = Radial displacement in inches (+ve reading inwards) ; C = Vertical displacement in inches (+ve reading upwards) ; D = Dial Gauge Reading ; E = Actual Displacement.

	Load Point	Gauge No. 1 A		Gauge No. 2 B		Gauge No. 3 C			Load Point	Gauge No. 1 A		Gauge No. 2 B		Gauge No. 3 C	
		D	E	I	E	D	E			D	E	D	E	D	E
Rib No. 6	1	.502	+.002	.500	.000	.500	.000	Rib No. 9	1	.501	+.001	.499	-.001	.501	+.001
	5	.516	+.016	.499	-.001	.500	.000		5	.513	+.013	.493	-.007	.506	+.006
	9	.525	+.025	.499	-.001	.494	-.006		9	.521	+.021	.491	-.009	.505	+.005
	13	.529	+.029	.502	+.002	.483	-.017		13	.524	+.024	.491	-.009	.499	-.001
	17	.519	+.019	.506	+.006	.471	-.029		17	.518	+.018	.498	-.002	.484	-.016
Rib No. 7	1	.502	+.002	.500	.000	.501	+.001	Rib No. 10	1	.502	+.002	.498	-.002	.502	+.002
	5	.516	+.016	.496	-.004	.502	+.002		5	.511	+.011	.493	-.007	.508	+.008
	9	.525	+.025	.495	-.005	.498	-.002		9	.518	+.018	.489	-.011	.509	+.009
	13	.529	+.029	.497	-.003	.490	-.010		13	.521	+.021	.489	-.011	.503	+.003
	17	.519	+.019	.503	+.003	.475	-.025		17	.517	+.017	.495	-.005	.489	-.011
Rib No. 8	1	.502	+.002	.499	-.001	.501	+.001	Rib No. 11	1	.501	+.001	.499	-.001	.503	+.003
	5	.516	+.016	.494	-.006	.505	+.005		5	.510	+.010	.491	-.009	.510	+.010
	9	.524	+.024	.492	-.008	.502	+.002		9	.517	+.017	.488	-.012	.512	+.012
	13	.527	+.027	.494	-.006	.494	-.006		13	.520	+.020	.487	-.013	.507	+.007
	17	.519	+.019	.500	.000	.480	-.020		17	.516	+.016	.493	-.007	.493	-.007

F.A.A. Ph.D. Thesis
13th May, 1969.

Structural Engineering Division,
Department of Civil Engineering,
University of Newcastle upon Tyne.

TESTS ON MODEL RADIAL RIBBED DOME

TEST NO. 17 TABLE NO. 3

Measurement of Apex Ring Displacements at Rib No. 36

Load at point = 10lb ; All dial gauge zeros .500 in. ; A = Tangential displacement in inches (+ve reading anti-clockwise viewed from above) ; B = Radial displacement in inches (+ve reading inwards) ; C = Vertical displacement in inches (+ve reading upwards) ; D = Dial gauge reading ; E = Actual Displacement.

	Load Point	Gauge No. 1 A		Gauge No. 2 B		Gauge No. 3 C			Load Point	Gauge No. 1 A		Gauge No. 2 B		Gauge No. 3 C	
		D	E	D	E	D	E			D	E	D	E	D	E
Rib No. 12	1	.502	+.002	.498	-.002	.503	+.003	Rib No. 15	1	.500	.000	.498	-.002	.503	+.003
	5	.510	+.010	.490	-.010	.512	+.012		5	.503	+.003	.492	-.008	.515	+.015
	9	.517	+.017	.485	-.015	.515	+.015		9	.505	+.005	.486	-.014	.520	+.020
	13	.519	+.019	.484	-.016	.512	+.012		13	.507	+.007	.482	-.018	.519	+.019
	17	.514	+.014	.491	-.009	.496	-.004		17	.506	+.006	.486	-.014	.504	+.004
Rib No. 13	1	.501	+.001	.499	-.001	.503	+.003	Rib No. 16	1	.500	.000	.498	-.002	.503	+.003
	5	.508	+.008	.491	-.009	.513	+.013		5	.502	+.002	.491	-.009	.515	+.015
	9	.513	+.013	.485	-.015	.517	+.017		9	.503	+.003	.485	-.015	.522	+.022
	13	.515	+.015	.483	-.017	.515	+.015		13	.503	+.003	.482	-.018	.521	+.021
	17	.512	+.012	.489	-.011	.500	.000		17	.503	+.003	.486	-.014	.506	+.006
Rib No. 14	1	.500	.000	.499	-.001	.504	+.004	Rib No. 17	1	.500	.000	.498	-.002	.504	+.004
	5	.506	+.006	.491	-.009	.514	+.014		5	.501	+.001	.491	-.009	.515	+.015
	9	.509	+.009	.486	-.014	.519	+.019		9	.502	+.002	.485	-.015	.522	+.022
	13	.511	+.011	.483	-.017	.517	+.017		13	.502	+.002	.482	-.018	.521	+.021
	17	.509	+.009	.488	-.012	.502	+.002		17	.501	+.001	.485	-.015	.507	+.007

F.A.A. Ph.D. Thesis
15th May, 1969.

Structural Engineering Division,
Department of Civil Engineering,
University of Newcastle upon Tyne.

Measurement of Apex Ring Displacements at Rib No. 36

Load at point = 10lb ; All dial gauge zeros .500 in. ; A = Tangential displacement in inches (+ve reading anti-clockwise viewed from above) ; B = Radial displacement in inches (+ve reading inwards) ; C = Vertical displacement in inches (+ve reading upwards) ; D = Dial Gauge Reading ; E = Actual Displacement.

	Load Point	Gauge No. 1 A		Gauge No. 2 B		Gauge No. 3 C	
		D	E	D	E	D	E
Rib No. 18	1	.500	.000	.499	-.001	.504	+.004
	5	.500	.000	.491	-.009	.515	+.015
	9	.500	.000	.484	-.016	.521	+.021
	13	.500	.000	.482	-.018	.522	+.022
	17	.500	.000	.485	-.015	.507	+.007

F.A.A. Ph.D. Thesis
13th May, 1969.

Structural Engineering Division,
Department of Civil Engineering,
University of Newcastle upon Tyne.

TESTS ON MODEL RADIAL RIBBED DOME

TEST NO. 17 TABLE NO. 5

Measurement of Rib Strains Using Huggenberger Tensometer Gauges

Load at point = 10lb L = Gauge Length = 1 in. N = Lever multiplication A = Scale reading in inches Z = Scale movement in inches (+ve reading - tension) X = Strain (extension x 10^{-6} in inches per inch of gauge length) = $\frac{Z}{NxL}$ All scale zero readings 1.00 in. For position of load points, rib layout and details of model dome, see Test No. 16, Sheet No. 7. For position of gauge points, see Dwg. No. Ph.D. Thesis No. 1. Principal Dimensions of Prototype and Model Domes.

	Load Point	Gauge No.1 (Actual No. 4901) On Rib No.36 at Pt. 3; N = 1193.8			Gauge No.2 (Actual No. 4902) On Rib No.36 at Pt. 7 ; N = 1198.9			Gauge No.3 (Actual No. 4903) On Rib No.36 at Pt. 11 ; N = 1196.3			Gauge No.4 (Actual No. 4904) on Rib No.36 at Pt. 15 ; N = 1210.6			Gauge No.5 (Actual No. 4905) On Rib No.36 mid 16, 17 ; N = 1202.3		
		A	Z	X	A	Z	X	A	Z	X	A	Z	X	A	Z	X
Rib No. 36	1	.94	-.06	- 50	.98	-.02	- 17	1.00	.00	0	1.01	+.01	+ 8	.99	-.01	- 8
	5	.88	-.12	-100	.86	-.14	-116	.98	-.02	- 17	1.01	+.01	+ 8	.97	-.03	- 25
	9	1.01	+.01	+ 8	.87	-.13	-108	.83	-.17	-142	.95	-.05	- 41	.98	-.02	- 17
	13	1.05	+.05	+ 42	1.02	+.02	+ 17	.86	-.14	-118	.80	-.20	-165	.96	-.04	- 33
	17	1.00	.00	0	1.01	+.01	+ 8	1.00	.00	0	.94	-.06	- 50	.88	-.12	-100
Rib No. 1	1	1.00	.00	0	.99	-.01	- 8	.99	-.01	- 8	1.00	.00	0	1.00	.00	0
	5	.98	-.02	- 17	.94	-.06	- 50	.95	-.05	- 42	.97	-.03	- 25	1.00	.00	0
	9	.98	-.02	- 17	.93	-.07	- 58	.93	-.07	- 59	.95	-.05	- 41	.96	-.04	- 33
	13	1.00	.00	0	.95	-.05	- 42	.95	-.05	- 42	.94	-.06	- 50	.91	-.09	- 75
	17	1.01	+.01	+ 8	1.00	.00	0	1.00	.00	0	.96	-.04	- 33	.92	-.08	- 67
Rib No. 2	1	1.00	.00	0	1.00	.00	0	1.00	.00	0	1.00	.00	0	1.00	.00	0
	5	1.00	.00	0	.97	-.03	- 25	.98	-.02	- 17	.98	-.02	- 17	.99	-.01	- 8
	9	1.00	.00	0	.97	-.03	- 25	.96	-.04	- 33	.97	-.03	- 25	.96	-.04	- 33
	13	1.00	.00	0	.98	-.02	- 17	.97	-.03	- 25	.96	-.04	- 33	.94	-.06	- 50
	17	1.01	+.01	+ 8	1.01	+.01	+ 8	1.00	.00	0	.98	-.02	- 17	.94	-.06	- 50

F.A.A. Ph.D. Thesis
13th May, 1969.

Structural Engineering Division,
Department of Civil Engineering,
University of Newcastle upon Tyne.

TESTS ON MODEL RADIAL RIBBED DOME

TEST NO. 18 TABLE NO. 1

Experimental Determination of Horizontal Reaction Influence Coefficients

Load at point = 20 lb For position of load points, rib layout and details of model dome, see Test No. 12 Sheet No. 8. Horizontal bracing at points 1, 3, 5, 7, 9, 11, 13, 15.

Horizontal Base Displacement at Rib No. 36 (Towards centre of dome)	Dial Gauge Readings (A) and Actual Vertical Displacement of point Load (B; +ve upwards) in inches																	
	Rib No. 36										Rib No. 18							
	Point 1		Point 5		Point 9		Point 13		Point 17		Point 1		Point 5		Point 9		Point 13		Point 17	
	A	B	A	B	A	B	A	B	A	B	A	B	A	B	A	B	A	B	A	B
0 in.	.500	.000	.500	.000	.500	.000	.500	.000	.500	.000	.500	.000	.500	.000	.500	.000	.500	.000	.500	.000
.01 in.	.503	+.003	.513	+.013	.512	+.012	.505	+.005	.501	+.001	.500	.000	.500	.000	.500	.000	.500	.000	.500	.000
.02 in.	.507	+.007	.527	+.027	.523	+.023	.510	+.010	.502	+.002	.500	.000	.500	.000	.501	+.001	.501	+.001	.500	.000
.03 in.	.510	+.010	.541	+.041	.535	+.035	.516	+.016	.502	+.002	.500	.000	.501	+.001	.501	+.001	.501	+.001	.500	.000
.04 in.	.513	+.013	.555	+.055	.547	+.047	.522	+.022	.504	+.004	.500	.000	.501	+.001	.501	+.001	.501	+.001	.500	.000
.05 in.	.517	+.017	.568	+.068	.561	+.061	.529	+.029	.505	+.005	.500	.000	.501	+.001	.502	+.002	.501	+.001	.499	-.001
.06 in.	.520	+.020	.581	+.081	.573	+.073	.536	+.036	.506	+.006	.500	.000	.501	+.001	.502	+.002	.501	+.001	.499	-.001
.07 in.	.523	+.023	.595	+.095	.588	+.088	.544	+.044	.507	+.007	.500	.000	.502	+.002	.502	+.002	.502	+.002	.499	-.001
.08 in.	.526	+.026	.609	+.109	.601	+.101	.552	+.052	.508	+.008	.501	+.001	.502	+.002	.503	+.003	.502	+.002	.499	-.001
.09 in.	.530	+.030	.621	+.121	.614	+.114	.559	+.059	.509	+.009	.501	+.001	.502	+.002	.503	+.003	.502	+.002	.499	-.001
.10 in.	.533	+.033	.635	+.135	.627	+.127	.567	+.067	.510	+.010	.501	+.001	.502	+.002	.503	+.003	.502	+.002	.499	-.001

F.A.A., Ph.D. Thesis,
22nd Dec., 1969.

Structural Engineering Division,
Department of Civil Engineering,
University of Newcastle upon Tyne.

TESTS ON MODEL RADIAL RIBBED DOME

TEST NO. 19 TABLE NO. 1

Experimental Determination of Vertical Reaction Influence Coefficients

Load at point = 20lb For position of load points, rib layout and details of model dome, see Test No. 13 Sheet No. 6. Horizontal bracing at points 1, 3, 5, 7, 9, 11, 13, 15.

Vertical Base Displacement at Rib No. 18 (Upwards)	Dial Gauge Readings (A) and Actual Vertical Displacement of point load (B; +ve upwards) in inches)																			
	Rib No. 18										Rib No. 36									
	Point 1		Point 5		Point 9		Point 13		Point 17		Point 1		Point 5		Point 9		Point 13		Point 17	
	A	B	A	B	A	B	A	B	A	B	A	B	A	B	A	B	A	B	A	B
0 in.	.500	.000	.500	.000	.500	.000	.500	.000	.500	.000	.500	.000	.500	.000	.500	.000	.500	.000	.500	.000
.01 in.	.510	+.010	.512	+.012	.507	+.007	.503	+.003	.500	.000	.500	.000	.500	.000	.499	-.001	.499	-.001	.500	.000
.02 in.	.522	+.022	.523	+.023	.514	+.014	.506	+.006	.501	+.001	.500	.000	.499	-.001	.499	-.001	.499	-.001	.500	.000
.03 in.	.531	+.031	.533	+.033	.521	+.021	.508	+.008	.501	+.001	.500	.000	.499	-.001	.499	-.001	.499	-.001	.500	.000
.04 in.	.542	+.042	.544	+.044	.528	+.028	.511	+.011	.502	+.002	.500	.000	.499	-.001	.499	-.001	.499	-.001	.501	+.001
.05 in.	.552	+.052	.555	+.055	.535	+.035	.513	+.013	.502	+.002	.499	-.001	.499	-.001	.499	-.001	.499	-.001	.501	+.001
.06 in.	.564	+.064	.566	+.066	.544	+.044	.516	+.016	.503	+.003	.499	-.001	.499	-.001	.498	-.002	.499	-.001	.502	+.002
.07 in.	.575	+.075	.578	+.078	.552	+.052	.520	+.020	.503	+.003	.499	-.001	.498	-.002	.498	-.002	.500	.000	.502	+.002
.08 in.	.585	+.085	.587	+.087	.559	+.059	.523	+.023	.504	+.004	.499	-.001	.498	-.002	.498	-.002	.500	.000	.502	+.002
.09 in.	.595	+.095	.598	+.098	.567	+.067	.525	+.025	.504	+.004	.499	-.001	.498	-.002	.498	-.002	.500	.000	.502	+.002
.10 in.	.605	+.105	.609	+.109	.574	+.074	.528	+.028	.504	+.004	.499	-.001	.498	-.002	.498	-.002	.500	.000	.503	+.003

F.A.A., Ph.D. Thesis,
22nd Dec., 1969.

Structural Engineering Division,
Department of Civil Engineering,
University of Newcastle upon Tyne.

TESTS ON MODEL RADIAL RIBBED DOME

TEST NO. 20 TABLE NO. 1

Experimental Determination of Apex Ring Vertical Force Influence Coefficients

Load at point = 20 lb For position of load points, rib layout and details of model dome, see Test No. 14 Sheet No. 4. Horizontal bracing at points 1, 3, 5, 7, 9, 11, 13, 15.

Vertical Displacement at Apex Ring on Rib No. 36 (Upwards)	Dial Gauge Readings (A) and Actual Vertical Displacement of point load (B; +ve upwards) in inches																			
	Rib No. 36										Rib No. 18									
	Point 1		Point 5		Point 9		Point 13		Point 17		Point 1		Point 5		Point 9		Point 13		Point 17	
	A	B	A	B	A	B	A	B	A	B	A	B	A	B	A	B	A	B	A	B
0 in.	.500	.000	.500	.000	.500	.000	.500	.000	.500	.000	.500	.000	.500	.000	.500	.000	.500	.000	.500	.000
.01 in.	.501	+.001	.504	+.004	.507	+.007	.510	+.010	.510	+.010	.499	-.001	.496	-.004	.494	-.006	.492	-.008	.493	-.007
.02 in.	.501	+.001	.507	+.007	.514	+.014	.520	+.020	.520	+.020	.499	-.001	.492	-.008	.487	-.013	.483	-.017	.486	-.014
.03 in.	.502	+.002	.511	+.011	.520	+.020	.531	+.031	.530	+.030	.498	-.002	.489	-.011	.481	-.019	.475	-.025	.478	-.022
.04 in.	.503	+.003	.514	+.014	.527	+.027	.541	+.041	.540	+.040	.497	-.003	.485	-.015	.474	-.026	.466	-.034	.469	-.031
.05 in.	.503	+.003	.518	+.018	.534	+.034	.550	+.050	.550	+.050	.497	-.003	.482	-.018	.468	-.032	.458	-.042	.462	-.038
.06 in.	.504	+.004	.522	+.022	.541	+.041	.561	+.061	.560	+.060	.496	-.004	.479	-.021	.462	-.038	.450	-.050	.454	-.046
.07 in.	.505	+.005	.525	+.025	.548	+.048	.571	+.071	.570	+.070	.495	-.005	.475	-.025	.455	-.045	.441	-.059	.446	-.054
.08 in.	.505	+.005	.528	+.028	.555	+.055	.581	+.081	.580	+.080	.495	-.005	.472	-.028	.449	-.051	.433	-.067	.439	-.061
.09 in.	.506	+.006	.532	+.032	.562	+.062	.592	+.092	.590	+.090	.494	-.006	.469	-.031	.443	-.057	.425	-.075	.431	-.069
.10 in.	.507	+.007	.535	+.035	.569	+.069	.602	+.102	.600	+.100	.493	-.007	.465	-.035	.437	-.063	.416	-.084	.423	-.077

F.A.A., Ph.D. Thesis,
22nd Dec., 1969.

Structural Engineering Division,
Department of Civil Engineering,
University of Newcastle upon Tyne.

TESTS ON MODEL RADIAL RIBBED DOME

TEST NO. 21 TABLE NO. 1

Experimental Determination of Apex Ring Radial Force Influence Coefficients

Load at point = 20 lb For position of load points, rib layout and details of model dome, see Test No. 15 Sheet No. 4. Horizontal bracing at points 1, 3, 5, 7, 9, 11, 13, 15.

Radial Displacement of Apex Ring at Rib No. 36 (Outwards from centre of ring)	Dial Gauge Readings (A) and Actual Vertical Displacement of point load (B; +ve upwards) in inches																	
	Rib No. 36										Rib No. 18							
	Point 1		Point 5		Point 9		Point 13		Point 17		Point 1		Point 5		Point 9		Point 13		Point 17	
	A	B	A	B	A	B	A	B	A	B	A	B	A	B	A	B	A	B	A	B
0 in.	.500	.000	.500	.000	.500	.000	.500	.000	.500	.000	.500	.000	.500	.000	.500	.000	.500	.000	.500	.000
.01 in.	.502	+.002	.510	+.010	.516	+.016	.516	+.016	.507	+.007	.499	-.001	.495	-.005	.493	-.007	.491	-.009	.493	-.007
.02 in.	.504	+.004	.521	+.021	.530	+.030	.531	+.031	.515	+.015	.498	-.002	.491	-.009	.486	-.014	.484	-.016	.487	-.013
.03 in.	.506	+.006	.530	+.030	.545	+.045	.545	+.045	.523	+.023	.497	-.003	.487	-.013	.479	-.021	.475	-.025	.481	-.019
.04 in.	.508	+.008	.541	+.041	.560	+.060	.558	+.058	.531	+.031	.496	-.004	.483	-.017	.472	-.028	.468	-.032	.474	-.026
.05 in.	.511	+.011	.551	+.051	.577	+.077	.574	+.074	.539	+.039	.496	-.004	.479	-.021	.465	-.035	.460	-.040	.468	-.032
.06 in.	.513	+.013	.561	+.061	.591	+.091	.589	+.089	.546	+.046	.495	-.005	.475	-.025	.459	-.041	.452	-.048	.462	-.038
.07 in.	.515	+.015	.573	+.073	.607	+.107	.604	+.104	.553	+.053	.494	-.006	.471	-.029	.453	-.047	.444	-.056	.455	-.045
.08 in.	.517	+.017	.583	+.083	.622	+.122	.618	+.118	.560	+.060	.493	-.007	.467	-.033	.446	-.054	.436	-.064	.449	-.051
.09 in.	.520	+.020	.593	+.093	.638	+.138	.635	+.135	.568	+.068	.493	-.007	.464	-.036	.440	-.060	.429	-.071	.443	-.057
.10 in.	.522	+.022	.603	+.103	.652	+.152	.648	+.148	.574	+.074	.492	-.008	.459	-.041	.433	-.067	.421	-.079	.437	-.063

F.A.A., Ph.D. Thesis,
22nd Dec., 1969.

Structural Engineering Division,
Department of Civil Engineering,
University of Newcastle upon Tyne.

TESTS ON MODEL RADIAL RIBBED DOME

TEST NO. 22 TABLE NO. 1

Measurement of Rib Strains Using Huggenberger Tensometer Gauges

Load at point = 20lb L = Gauge Length = 1 in. N = Lever multiplication A = Scale reading in inches Z = Scale movement in inches (+ve reading - tension) X = Strain (extension x 10^{-6} in inches per inch of gauge length) = $\frac{Z}{NxL}$ All scale zero readings 1.00 in. For position of load points, rib layout and details of model dome see Test No. 12 Sheet No. 8. For position of gauge points, see Dwg. No. Ph.D. Thesis No. 1. Principal Dimensions of Prototype and Model Domes. Horizontal bracing at points 1, 3, 5, 7, 9, 11, 13, 15.

	Load Point	Gauge No. 1(Actual No. 4901) On Rib No.36 at Pt. 4; N = 1193.8			Gauge No.2 (Actual No. 4902) On Rib No.36 at Pt. 6; N = 1198.9			Gauge No.3 (Actual No. 4903) On Rib No.36 at Pt. 8; N = 1196.3			Gauge No.4 (Actual No. 4904) On Rib No.36 at Pt. 10; N = 1210.6			Gauge No.5 (Actual No. 4905) On Rib No.36 at Pt. 12; N = 1202.3		
		A	Z	Y	A	Z	X	A	Z	X	A	Z	X	A	Z	X
Rib No. 36	1	.96	- .04	- 34	.98	- .02	- 17	1.00	- 0	0	1.00	0	0	1.00	0	0
	5	.71	- .29	- 242	.74	- .26	- 217	.89	- .11	- 93	.98	- .02	- 17	1.00	0	0
	9	.99	- .01	- 8	.89	- .11	- 93	.73	- .27	- 225	.75	- .25	- 210	.86	- .14	- 120
	13	1.04	+ .04	+ 34	1.03	+ .03	+ 25	.99	- .01	- 8	.93	- .07	- 58	.74	- .26	- 220
	17	1.00	0	0	1.00	0	0	1.00	0	0	1.00	0	0	.99	- .01	- 8
Rib No. 18	1	1.00	0	0	1.00	0	0	1.00	0	0	1.00	0	0	1.00	0	0
	5	1.00	0	0	1.00	0	0	1.00	0	0	1.00	0	0	1.00	0	0
	9	1.00	0	0	1.01	+ .01	+ 8	1.02	+ .02	+ 17	1.02	+ .02	+ 17	1.03	+ .03	+ 25
	13	1.00	0	0	1.01	+ .01	+ 8	1.01	+ .01	+ 8	1.01	+ .01	+ 8	1.03	+ .03	+ 25
	17	1.00	0	0	1.00	0	0	1.00	0	0	1.00	0	0	1.02	+ .02	+ 17

F.A.A., Ph.D. Thesis,
31st Dec., 1969.

Structural Engineering Division,
Department of Civil Engineering,
University of Newcastle upon Tyne.

TESTS ON MODEL RADIAL RIBBED DOME

TEST NO. 22 TABLE NO. 2

Measurement of Apex Ring Displacements at Rib No. 36

Load at point = 20lb; All dial gauge zeros .500 in.; A = Tangential displacement in inches (+ve reading anti-clockwise viewed from above); B = Radial displacement in inches (+ve reading inwards); C = Vertical displacement in inches (+ve reading upwards); D = Dial Gauge Reading; E = Actual Displacement. Horizontal bracing at points 1, 3, 5, 7, 9, 11, 13, 15.

	Load Point	Gauge No. 1 A		Gauge No. 2 B		Gauge No. 3 C	
		D	E	D	E	D	E
Rib No. 36	1	.500	.000	.508	+ .008	.497	- .003
	5	.500	.000	.546	+ .046	.482	- .018
	9	.500	.000	.569	+ .069	.465	- .035
	13	.500	.000	.573	+ .073	.450	- .050
	17	.500	.000	.540	+ .040	.438	- .062

	Load Point	Gauge No. 1 A		Gauge No. 2 B		Gauge No. 3 C	
		D	E	D	E	D	E
Rib No. 18	1	.500	.000	.497	- .003	.503	+ .003
	5	.500	.000	.484	- .016	.517	+ .017
	9	.500	.000	.472	- .028	.532	+ .032
	13	.500	.000	.467	- .033	.543	+ .043
	17	.500	.000	.474	- .026	.535	+ .035

F.A.A., Ph.D. Thesis,
31st Dec., 1969.

Structural Engineering Division,
Department of Civil Engineering,
University of Newcastle upon Tyne.

APPENDIX III

DESIGN OF PROTOTYPE LAMINATED TIMBER RADIAL RIBBED DOME

CALCULATION SHEET NOS. 1 - 25

CALCULATION SHEET NO. 1

DESIGN OF PROTOTYPE LAMINATED TIMBER RADIAL RIBBED DOME

1. RIB DESIGN

A. Design Data

NOTES

1. For general arrangement of dome, see drawing No. Ph.D. Thesis No.1.
2. Dome design carried out according to methods detailed in A.I.T.C. Timber Construction Manual. 1966. Sect. 2. P.40-42. Sect. 4. P.33-67.[28]
3. Loadings according to B.S.C.P. 3: Chpt. V. 1965 - Loading[29] and B.S. BENJAMIN. (1963). The Analysis of Braced Domes. P3.[12]
4. Permissible stresses according to B.S.C.P. 112 : 1967 - The Structural Use of Timber.[31]

Material :- European Redwood - dry conditions

Basic Stresses (B.S.C.P. 112. Table 4)

Bending and tension parallel to grain, f_{bpar} & t_{bpar} = 2100 lb/in.^{2}
Compression parallel to grain, c_{bpar} = 1600 lb/in.^{2}
Compression perpendicular to grain, c_{bperp} = 320 lb/in.^{2}
Shear parallel to grain = 220 lb/in.^{2}
Modulus of Elasticity, E_{mean} = $1{\cdot}2 \times 10^6$ lb/in.^{2}

Assuming ribs are constructed from 75 Grade material (i.e. LA) of more than 4 laminations then basic stresses are modified to give grade stresses as follows :-

Grade Stresses (B.S.C.P. 112 Table 5)

f_{gpar} and t_{gpar}	= 2100 × 1.00	= 2100 lb/in.^{2}
E_{mean}	= $1{\cdot}2 \times 10^6 \times 1{\cdot}00$	= $1{\cdot}2 \times 10^6$ lb/in.^{2}
c_{gpar}	= 1600 × 1.00	= 1600 lb/in.^{2}
Shear parallel to grain	= 220 × .90	= 198 lb/in.^{2}
c_{gperp}	= 320 × 1.00	= 320 lb/in.^{2}

CALCULATION SHEET NO. 2

Permissible Stresses

Modification factor K_{12} for duration of loading = 1·25

(Medium term) [dead + snow, dead + temporary loads) B.S.C.P. 112 Table 12.

f_{ppar} and t_{ppar}	= 2100 × 1·25	= 2625 lb/in.²
c_{ppar}	= 1600 × 1·25	= 2000 lb/in.²
c_{pperp}	= 320 × 1·25	= 400 lb/in.²
Shear parallel to grain	= 198 × 1·25	= 247 lb/in.²
Emean		= 1·2 × 10^6 lb/in.²

Radius of curvature of rib = R = 180 ft.

Thickness of laminations, t = 1½ in. (Forest Products Research. Special Report No. 15. Working Stresses for Structural Laminated Timber. (1961). P. 4, 5. (42) Max. lamination thickness of 1¾ in. for straight members and less for curved members)

$\frac{t}{R} = \frac{3}{2} \times \frac{1}{180 \times 12} = \frac{1}{1440}$ i.e. Curvature modification factor, K_{17} = 1·00

B. Loads

Load Case 1. Uniformly distributed load of 5 lb/ft² on surface area (Dead load) - B.S. BENJAMIN (1963). The Analysis of Braced Domes. P. 3.

Load Case 2. Uniformly distributed load of 15 lb/ft² on plan area (Balanced live load). B.S.C.P. 3 Chpt. V. 1965. P. 11.

Load Case 3. Uniformly distributed load of 15 lb/ft² on half plan area (Unbalanced live load). A.I.T.C. Timber Construction Manual. Sect. 3. P. 9.

Load Case 4. Wind Load. See drawing No. Ph. D. Thesis No. 5 for distribution of wind load.

Structural Engineering Division
Department of Civil Engineering
University of Newcastle upon Tyne

CALCULATION SHEET NO. 3

c. Bending Moments, Shear Forces and Axial Forces

Ribs designed as three-pinned and two-pinned arches. (A.I.T.C. Timber Construction Manual. Sect. 4. P.64)

For calculation of bending moments, shear forces and axial forces, see drawing Nos. Ph. D. Thesis Nos. 2-8.

For summation of bending moments, shear forces and axial forces, see Calculation Sheet Nos. 4 - 11.

F.A.A. Ph. D. Thesis
25th Aug., 1969.

Structural Engineering Division
Department of Civil Engineering
University of Newcastle upon Tyne

CALCULATION SHEET No. 4

Load Point (L.H.S.)	Three-pinned Arch - Dead Load			Three-pinned Arch - Balanced Live L.			Three-pinned Arch - Unbalanced L.L.			Three-pinned Arch - Wind Load		
	B.M. (ft lb)	S.F. (lb)	A.F. (lb)	B.M. (ft lb)	S.F. (lb)	A.F. (lb)	B.M. (ft lb)	S.F. (lb)	A.F. (lb)	B.M. (ft lb)	S.F. (lb)	A.F. (lb)
Base	0	+ 1250	+ 7730	0	+ 2960	+ 21400	0	+ 5560	+ 13720	0	+ 180	- 3815
0	+ 2704	+ 1160	+ 7480	+ 3817	+ 2880	+ 20800	+ 5115	+ 5260	+ 13050	+ 506	+ 160	- 3775
1	+ 9031	+ 1000	+ 7140	+ 13894	+ 2420	+ 19960	+ 35651	+ 4460	+ 12160	+ 1043	+ 105	- 3730
2	+ 14439	+ 930	+ 6820	+ 22902	+ 2280	+ 19 170	+ 63591	+ 4000	+ 11280	+ 1043	+ 65	- 3675
3	+ 18009	+ 620	+ 6570	+ 34353	+ 1700	+ 18 510	+ 86493	+ 3260	+ 10540	+ 1580	+ 15	- 3630
4	+ 21632	+ 420	+ 6340	+ 44430	+ 1160	+ 17890	+ 105578	+ 2440	+ 9900	+ 2118	- 20	- 3590
5	+ 24336	+ 210	+ 6140	+ 49621	+ 720	+ 17340	+ 119625	+ 1840	+ 9300	+ 1580	- 75	- 3555
6	+ 25255	+ 120	+ 5960	+ 53438	+ 260	+ 16890	+ 132307	+ 1020	+ 8800	+ 1043	- 120	- 3515
7	+ 25255	- 100	+ 5810	+ 55881	- 140	+ 16470	+ 137412	+ 380	+ 8360	+ 506	- 165	- 3480
8	+ 24336	- 240	+ 5700	+ 55881	- 440	+ 16 140	+ 139931	- 300	+ 8030	0	- 215	- 3445
9	+ 23417	- 260	+ 5600	+ 54659	- 680	+ 15870	+ 139931	- 790	+ 7740	- 1580	- 265	- 3425
10	+ 21632	- 450	+ 5520	+ 50842	- 1100	+ 15650	+ 134893	- 1300	+ 7540	- 3161	- 150	- 3340
11	+ 18928	- 450	+ 5470	+ 44430	- 1230	+ 15490	+ 127259	- 1760	+ 7380	- 4741	- 35	- 3280
12	+ 16224	- 450	+ 5440	+ 38170	- 1340	+ 15380	+ 117029	- 2170	+ 7290	- 5279	+ 55	- 3225
13	+ 13520	- 490	+ 5410	+ 32979	- 1180	+ 15330	+ 101761	- 2490	+ 7260	- 4741	+ 115	- 3195
14	+ 9951	- 480	+ 5405	+ 24123	- 1160	+ 15280	+ 86493	- 2690	+ 7270	- 4204	+ 165	- 3175
15	+ 8112	- 450	+ 5390	+ 19085	- 1100	+ 15260	+ 71225	- 2840	+ 7320	- 3667	+ 180	- 3165
16	+ 5408	- 370	+ 5400	+ 12672	- 860	+ 15270	+ 53438	- 2950	+ 7350	- 2118	+ 165	- 3155
17	+ 3623	- 300	+ 5390	+ 9161	- 840	+ 15240	+ 35651	- 3150	+ 7370	- 1580	+ 195	- 3150
Apex Ring	+ 2704	- 150	+ 5400	+ 7634	- 590	+ 15260	+ 33055	- 2780	+ 7520	- 1043	+ 95	- 3155
℄	0	0	+ 5408	0	0	+ 15268	0	- 2545	+ 7634	0	- 24	- 3161

F.A.A. Ph.D. Thesis
25th Aug., 1969.
Structural Engineering Division
Department of Civil Engineering
University of Newcastle upon Tyne

Load Point (L.H.S.)	Three-pinned Arch – D.L.+ Balanced L.L.			Three-pinned Arch – D.L.+ Unbalanced L.L.			Three-pinned Arch – D.L. + Wind		
	B.M. (ft lb)	S.F. (lb)	A.F. (lb)	B.M. (ft lb)	S.F. (lb)	A.F. (lb)	B.M. (ft lb)	S.F. (lb)	A.F. (lb)
Base	0	+ 4210	+ 29130	0	+ 6810	+ 21450	0	+ 1430	+ 3915
0	+ 6521	+ 4040	+ 28280	+ 7819	+ 6420	+ 20530	+ 3210	+ 1320	+ 3705
1	+ 22925	+ 3420	+ 27100	+ 44682	+ 5460	+ 19300	+ 10074	+ 1105	+ 3410
2	+ 37341	+ 3210	+ 25990	+ 78030	+ 4930	+ 18100	+ 15482	+ 995	+ 3145
3	+ 52362	+ 2320	+ 25080	+ 104502	+ 3880	+ 17110	+ 19589	+ 635	+ 2940
4	+ 66062	+ 1580	+ 24230	+ 127210	+ 2860	+ 16240	+ 23750	+ 400	+ 2750
5	+ 73957	+ 930	+ 23480	+ 143961	+ 2050	+ 15440	+ 25916	+ 135	+ 2585
6	+ 78693	+ 380	+ 22850	+ 157562	+ 1140	+ 14760	+ 26298	0	+ 2445
7	+ 81136	− 240	+ 22280	+ 162667	+ 280	+ 14170	+ 25761	− 265	+ 2330
8	+ 80217	− 680	+ 21840	+ 164267	− 540	+ 13730	+ 24336	− 455	+ 2255
9	+ 78076	− 940	+ 21470	+ 163348	− 1050	+ 13340	+ 21837	− 525	+ 2175
10	+ 72474	− 1550	+ 21170	+ 156525	− 1750	+ 13060	+ 18471	− 600	+ 2180
11	+ 63358	− 1680	+ 20960	+ 146187	− 2210	+ 12850	+ 14187	− 485	+ 2190
12	+ 54394	− 1790	+ 20820	+ 133253	− 2620	+ 12730	+ 10945	− 395	+ 2215
13	+ 46499	− 1670	+ 20740	+ 115281	− 2980	+ 12670	+ 8779	− 375	+ 2215
14	+ 34074	− 1640	+ 20685	+ 96444	− 3170	+ 12675	+ 5747	− 315	+ 2230
15	+ 27197	− 1550	+ 20650	+ 79337	− 3290	+ 12710	+ 4445	− 270	+ 2225
16	+ 18080	− 1230	+ 20670	+ 58846	− 3320	+ 12750	+ 3290	− 205	+ 2245
17	+ 12784	− 1140	+ 20630	+ 39274	− 3450	+ 12760	+ 2043	− 105	+ 2240
Apex Ring	+ 10338	− 740	+ 20660	+ 35759	− 2930	+ 12920	+ 1661	− 55	+ 2245
℄	0	0	+ 20676	0	− 2545	+ 13042	0	− 24	+ 2247

F.A.A. Ph.D. Thesis
25th Aug., 1969
Structural Engineering Division
Department of Civil Engineering
University of Newcastle upon Tyne

Load Point (R.H.S.)	Three-pinned Arch - Dead Load			Three-pinned Arch - Balanced Live L.			Three-pinned Arch - Unbalanced L.L.			Three-pinned Arch - Wind Load		
	B.M. (ft lb)	S.F. (lb)	A.F. (lb)	B.M. (ft lb)	S.F. (lb)	A.F. (lb)	B.M. (ft lb)	S.F. (lb)	A.F. (lb)	B.M. (ft lb)	S.F. (lb)	A.F. (lb)
Base	0	-1250	+7730	0	-2960	+21400	0	+2545	+7634	0	+575	-4375
0	+2704	-1160	+7480	+3817	-2880	+20800	-3817	+2140	+7750	-1580	+525	-4275
1	+9031	-1000	+7140	+13894	-2420	+19960	-15268	+2000	+7800	-5279	+455	-4110
2	+14439	-930	+6820	+22902	-2280	+19170	-28017	+1830	+7840	-7902	+380	-3960
3	+18009	-620	+6570	+34353	-1700	+18510	-39391	+1560	+7880	-9483	+300	-3820
4	+21632	-420	+6340	+44430	-1160	+17890	-49621	+1310	+7920	-11063	+225	-3700
5	+24336	-210	+6140	+49621	-720	+17340	-58553	+1020	+7960	-12138	+145	-3590
6	+25255	-120	+5960	+53438	-260	+16890	-63591	+860	+7990	-12644	+70	-3495
7	+25255	+100	+5810	+55881	+140	+16470	-68706	+570	+8030	-13150	0	-3420
8	+24336	+240	+5700	+55881	+440	+16140	-72523	+260	+8040	-13687	-50	-3350
9	+23417	+260	+5600	+54659	+680	+15870	-73821	+50	+8040	-13150	-110	-3295
10	+21632	+450	+5520	+50842	+1100	+15650	-73821	-340	+8010	-12138	-165	-3240
11	+18928	+450	+5470	+44430	+1230	+15490	-72523	-600	+8000	-11063	-225	-3205
12	+16224	+450	+5440	+38170	+1340	+15380	-68706	-770	+7980	-9989	-265	-3175
13	+13520	+490	+5410	+32979	+1180	+15330	-63591	-1040	+7950	-8440	-290	-3160
14	+9951	+480	+5405	+24123	+1160	+15280	-58553	-1360	+7900	-6828	-285	-3150
15	+8112	+450	+5390	+19085	+1100	+15260	-49621	-1600	+7850	-5279	-265	-3145
16	+5408	+370	+5400	+12672	+860	+15270	-39391	-1800	+7800	-3667	-220	-3150
17	+3623	+300	+5390	+9161	+840	+15240	-28017	-2130	+7720	-2655	-240	-3145
Apex Ring	+2704	+150	+5400	+7634	+590	+15260	-25421	-2160	+7690	-2118	-120	-3150
℄	0	0	+5408	0	0	+15268	0	-2545	+7634	0	-24	-3161

F.A.A. Ph.D. Thesis
25th Aug., 1969.
Structural Engineering Division
Department of Civil Engineering
University of Newcastle upon Tyne

CALCULATION SHEET NO. 7

Load-Point (R.H.S.)	Three-pinned Arch – D.L. + Balanced L.L.			Three-pinned Arch – D.L. + Unbalanced L.L.			Three-pinned Arch – D.L. + Wind		
	B.M. (ft lb)	S.F. (lb)	A.F. (lb)	B.M. (ft lb)	S.F. (lb)	A.F. (lb)	B.M. (ft lb)	S.F. (lb)	A.F. (lb)
Base	0	– 4210	+29 130	0	+ 1295	+ 15364	0	– 675	+ 3355
0	+ 6521	– 4040	+28280	– 1113	+ 980	+ 15230	+ 1124	– 635	+ 3205
1	+ 22925	– 3420	+27100	– 6237	+ 1000	+ 14940	+ 3752	– 545	+ 3030
2	+ 37341	– 3210	+25990	– 13578	+ 900	+ 14660	+ 6537	– 550	+ 2860
3	+ 52362	– 2320	+25080	– 21382	+ 940	+ 14450	+ 8526	– 320	+ 2750
4	+ 66062	– 1580	+24230	– 27989	+ 890	+ 14260	+10569	– 195	+ 2640
5	+ 73957	– 930	+23480	– 34217	+ 810	+ 14100	+12198	– 65	+ 2550
6	+ 78693	– 380	+22850	– 38336	+ 740	+ 13950	+12611	– 50	+ 2465
7	+ 81136	+ 240	+22280	– 43451	+ 670	+ 13840	+12105	+ 100	+ 2390
8	+ 80217	+ 680	+21840	– 48187	+ 500	+ 13740	+10649	+ 190	+ 2350
9	+ 78076	+ 940	+21470	– 50404	+ 310	+ 13640	+10267	+ 150	+ 2305
10	+ 72474	+ 1550	+21170	– 52189	+ 110	+ 13530	+ 9494	+ 285	+ 2280
11	+ 63358	+ 1680	+20960	– 53595	– 150	+ 13470	+ 7865	+ 225	+ 2265
12	+ 54394	+ 1790	+20820	– 52482	– 320	+ 13420	+ 6235	+ 185	+ 2265
13	+ 46499	+ 1670	+20740	– 50071	– 550	+ 13360	+ 5080	+ 200	+ 2250
14	+ 34074	+ 1640	+20685	– 48602	– 880	+ 13305	+ 3123	+ 195	+ 2255
15	+ 27197	+ 1550	+20650	– 41509	– 1150	+ 13240	+ 2833	+ 185	+ 2245
16	+ 18080	+ 1230	+20670	– 33983	– 1430	+ 13200	+ 1741	+ 150	+ 2250
17	+ 12784	+ 1140	+20630	– 24394	– 1830	+ 13110	+ 968	+ 60	+ 2245
Apex Ring	+ 10338	+ 740	+20660	– 22717	– 2010	+ 13090	+ 586	+ 30	+ 2250
℄	0	0	+20676	0	– 2545	+ 13042	0	– 24	+ 2247

F.A.A. Ph.D. Thesis
26th Aug., 1969.

Structural Engineering Division
Department of Civil Engineering
University of Newcastle upon Tyne

CALCULATION SHEET NO. 8

Load Point (L.H.S.)	Two-pinned Arch - Dead Load			Two-pinned Arch - Balanced L.L.			Two-pinned Arch - Unbalanced L.L.			Two-pinned Arch - Wind Load		
	B.M. (ft lb)	S.F. (lb)	A.F. (lb)	B.M. (ft lb)	S.F. (lb)	A.F. (lb)	B.M. (ft lb)	S.F. (lb)	A.F. (lb)	B.M. (ft lb)	S.F. (lb)	A.F. (lb)
Base	0	+1015	+8096	0	+2367	+22360	0	+5261	+14225	0	+260	-3953
0	+895	+878	+7866	+2080	+2078	+21799	+4703	+4817	+13609	+243	+235	-3921
1	+6189	+694	+7535	+14626	+1704	+20982	+33647	+4167	+12706	+1640	+185	-3873
2	+10422	+511	+7239	+25033	+1309	+20235	+58795	+3495	+11882	+2721	+136	-3827
3	+13437	+333	+6976	+32739	+903	+19560	+79676	+2810	+11138	+3563	+87	-3784
4	+15452	+162	+6747	+38212	+498	+18957	+96563	+2123	+10477	+4074	+39	-3744
5	+16346	+2	+6550	+40977	+106	+18429	+109178	+1447	+9899	+4349	-11	-3706
6	+16446	-144	+6382	+41857	-274	+17969	+117999	+782	+9399	+4235	-62	-3671
7	+15517	-276	+6243	+40038	-625	+17580	+122600	+146	+8979	+3901	-114	-3639
8	+13868	-388	+6129	+36316	-930	+17259	+123481	-448	+8638	+3213	-170	-3608
9	+11542	-480	+6040	+30747	-1195	+17001	+120804	-1000	+8368	+2186	-229	-3580
10	+8701	-549	+5972	+23880	-1405	+16800	+115054	-1498	+8166	+796	-106	-3499
11	+5393	-595	+5923	+15218	-1551	+16653	+105842	-1932	+8027	+161	-2	-3436
12	+1827	-614	+5891	+6915	-1628	+16553	+95264	-2296	+7944	+151	+80	-3389
13	-1825	-606	+5872	-3769	-1631	+16492	+80533	-2585	+7911	+616	+140	-3357
14	-5513	-568	+5865	-13708	-1549	+16464	+64925	-2789	+7919	+1487	+174	-3337
15	-8876	-502	+5864	-22868	-1382	+16460	+48269	-2907	+7961	+2506	+182	-3326
16	-11942	-404	+5869	-31319	-1126	+16471	+30742	-2933	+8028	+3631	+163	-3323
17	-14325	-407	+5868	-37957	-1142	+16466	+13203	-3110	+8059	+4583	+206	-3318
Apex Ring	-14749	-196	+5878	-39146	-550	+16496	+11489	-2818	+8165	+4801	+87	-3323
℄	-17078	0	+5882	-45682	0	+16506	-22320	-2545	+8255	+5829	-24	-3324

F.A.A. Ph.D. Thesis
26th Aug., 1969.
Structural Engineering Division
Department of Civil Engineering
University of Newcastle upon Tyne

CALCULATION SHEET No. 9

Load Point (L.H.S.)	Two-pinned Arch – D.L. + Balanced L.L.			Two-pinned Arch – D.L. + Unbalanced L.L.			Two-pinned Arch – D.L. + Wind		
	B.M. (ft lb)	S.F. (lb)	A.F. (lb)	B.M. (ft lb)	S.F. (lb)	A.F. (lb)	B.M. (ft lb)	S.F. (lb)	A.F. (lb)
Base	0	+3382	+30456	0	+6076	+22321	0	+1275	+4143
0	+2975	+2956	+29665	+5598	+5695	+21475	+1138	+1113	+3945
1	+20815	+2398	+28517	+39836	+4861	+20241	+7829	+879	+3662
2	+35455	+1820	+27474	+69217	+4006	+19121	+13143	+647	+3412
3	+46176	+1236	+26536	+93113	+3143	+18114	+17000	+420	+3192
4	+53664	+660	+25704	+112015	+2285	+17224	+19526	+201	+3003
5	+57323	+108	+24979	+125524	+1449	+16449	+20695	−9	+2844
6	+58303	−418	+24351	+134445	+638	+15781	+20681	−206	+2711
7	+55555	−901	+23823	+138117	−130	+15222	+19418	−390	+2604
8	+50184	−1318	+23388	+137349	−836	+14767	+17081	−558	+2521
9	+42289	−1675	+23041	+132346	−1480	+14408	+13728	−709	+2460
10	+32581	−1954	+22772	+123755	−2047	+14138	+9497	−655	+2473
11	+20611	−2146	+22576	+111235	−2527	+13950	+5554	−597	+2487
12	+8742	−2242	+22444	+97091	−2910	+13835	+1978	−534	+2502
13	−5594	−2237	+22364	+78708	−3191	+13782	−1209	−466	+2515
14	−19221	−2117	+22329	+59412	−3357	+13784	−4026	−394	+2528
15	−31744	−1884	+22324	+39393	−3409	+13825	−6370	−320	+2538
16	−43261	−1530	+22340	+18800	−3337	+13897	−8311	−241	+2546
17	−52282	−1549	+22334	−1122	−3517	+13927	−9742	−201	+2550
Apex Ring	−53895	−746	+22374	−3260	−3014	+14043	−9948	−109	+2555
℄	−62760	0	+22388	−39398	−2545	+14137	−11249	−24	+2558

F.A.A. Ph.D. Thesis
26th Aug., 1969.
Structural Engineering Division
Department of Civil Engineering
University of Newcastle upon Tyne

CALCULATION SHEET NO. 10

Load Point (R.H.S.)	Two-pinned Arch – Dead Load			Two-pinned Arch – Balanced L.L.			Two-pinned Arch – Unbalanced L.L.			Two-pinned Arch – Wind Load		
	B.M. (ft lb)	S.F. (lb)	A.F. (lb)	B.M. (ft lb)	S.F. (lb)	A.F. (lb)	B.M. (ft lb)	S.F. (lb)	A.F. (lb)	B.M. (ft lb)	S.F. (lb)	A.F. (lb)
Base	0	-1015	+8096	0	-2367	+22360	0	+2897	+8138	0	+486	-4510
0	+895	-878	+7866	+2080	-2078	+21799	-2626	+2741	+8192	-428	+435	-4402
1	+6189	-694	+7535	+14626	-1704	+20982	-19037	+2465	+8279	-3055	+367	-4241
2	+10422	-511	+7239	+25033	-1309	+20235	-33791	+2188	+8357	-5296	+294	-4094
3	+13437	-333	+6976	+32739	-903	+19560	-46979	+1909	+8425	-7032	+220	-3961
4	+15452	-162	+6747	+38212	-498	+18957	-58406	+1627	+8484	-8362	+145	-3841
5	+16346	-2	+6550	+40977	-106	+18429	-68266	+1343	+8533	-9188	+72	-3736
6	+16446	+144	+6382	+41857	+274	+17969	-76217	+1058	+8574	-9670	+3	-3645
7	+15517	+276	+6243	+40038	+625	+17580	-82648	+772	+8604	-9653	-61	-3567
8	+13868	+388	+6129	+36316	+930	+17259	-87261	+484	+8625	-9294	-117	-3502
9	+11542	+480	+6040	+30747	+1195	+17001	-90158	+196	+8636	-8596	-164	-3449
10	+8701	+549	+5972	+23880	+1405	+16800	-91284	-92	+8638	-7631	-224	-3401
11	+5393	+595	+5923	+15218	+1551	+16653	-90741	-380	+8630	-6279	-271	-3364
12	+1827	+614	+5891	+6915	+1628	+16553	-88472	-667	+8612	-4655	-301	-3340
13	-1825	+606	+5872	-3769	+1631	+16492	-84431	-954	+8586	-2868	-314	-3324
14	-5513	+568	+5865	-13708	+1549	+16464	-78767	-1240	+8549	-952	-309	-3316
15	-8876	+502	+5864	-22868	+1382	+16460	-71273	-1524	+8503	+873	-284	-3314
16	-11942	+404	+5869	-31319	+1126	+16471	-62203	-1807	+8447	+2611	-239	-3316
17	-14325	+407	+5868	-37957	+1142	+16466	-51303	-1968	+8411	+4024	-254	-3314
Apex Ring	-14749	+196	+5878	-39146	+550	+16496	-49591	-2269	+8335	+4285	-135	-3321
℄	-17078	0	+5882	-45682	0	+16506	-22320	-2545	+8255	+5829	-24	-3324

F.A.A. Ph.D. Thesis
27th Aug., 1969.

Structural Engineering Division
Department of Civil Engineering
University of Newcastle upon Tyne

CALCULATION SHEET NO. 11

Load Point (R.H.S.)	Two-pinned Arch – D.L.+ Balanced L.L.			Two-pinned Arch – D.L.+ Unbalanced L.L.			Two-pinned Arch – D.L. + Wind		
	B.M. (ft lb)	S.F. (lb)	A.F. (lb)	B.M. (ft lb)	S.F. (lb)	A.F. (lb)	B.M. (ft lb)	S.F. (lb)	A.F. (lb)
Base	0	– 3382	+ 30456	0	+ 1882	+ 16234	0	– 529	+ 3586
0	+ 2975	– 2956	+ 29665	– 1731	+ 1863	+ 16058	+ 467	– 443	+ 3464
1	+ 20815	– 2398	+ 28517	– 12848	+ 1771	+ 15814	+ 3134	– 327	+ 3294
2	+ 35455	– 1820	+ 27474	– 23369	+ 1677	+ 15596	+ 5126	– 217	+ 3145
3	+ 46176	– 1236	+ 26536	– 33542	+ 1576	+ 15401	+ 6405	– 113	+ 3015
4	+ 53664	– 660	+ 25704	– 42954	+ 1465	+ 15231	+ 7090	– 17	+ 2906
5	+ 57323	– 108	+ 24979	– 51920	+ 1341	+ 15083	+ 7158	+ 70	+ 2814
6	+ 58303	+ 418	+ 24351	– 59771	+ 1202	+ 14956	+ 6776	+ 147	+ 2737
7	+ 55555	+ 901	+ 23823	– 67131	+ 1048	+ 14847	+ 5864	+ 205	+ 2676
8	+ 50184	+ 1318	+ 23388	– 73393	+ 872	+ 14754	+ 4574	+ 271	+ 2627
9	+ 42289	+ 1675	+ 23041	– 78616	+ 676	+ 14676	+ 2946	+ 316	+ 2591
10	+ 32581	+ 1954	+ 22772	– 82583	+ 457	+ 14610	+ 1070	+ 325	+ 2571
11	+ 20611	+ 2146	+ 22576	– 85348	+ 215	+ 14553	– 886	+ 324	+ 2559
12	+ 8742	+ 2242	+ 22444	– 86645	– 53	+ 14503	– 2828	+ 313	+ 2551
13	– 5594	+ 2237	+ 22364	– 86256	– 348	+ 14458	– 4693	+ 292	+ 2548
14	– 19221	+ 2117	+ 22329	– 84280	– 672	+ 14414	– 6465	+ 259	+ 2549
15	– 31744	+ 1884	+ 22324	– 80149	– 1022	+ 14367	– 8003	+ 218	+ 2550
16	– 43261	+ 1530	+ 22340	– 74145	– 1403	+ 14316	– 9331	+ 165	+ 2553
17	– 52282	+ 1549	+ 22334	– 65628	– 1561	+ 14279	– 10301	+ 153	+ 2554
Apex Ring	– 53895	+ 746	+ 22374	– 64340	– 2073	+ 14213	– 10464	+ 61	+ 2557
℄	– 62760	0	+ 22388	– 39398	– 2545	+ 14137	– 11249	– 24	+ 2558

F.A.A. Ph.D. Thesis
27th Aug., 1969.

Structural Engineering Division
Department of Civil Engineering
University of Newcastle upon Tyne

CALCULATION SHEET NO. 12

D. Determination of Rib Section Sizes

1. Approx. Max. Section Size

Max. B.M. on rib = 164267 ft lb (Pt.8. Calc. sheet No.5)

for f_{ppar} = 2625 lb/in.^{2}

$$bd^2 = \frac{6 \times 164267 \times 12}{2625} = 4506 \text{ in.}^3$$

for d = 4b (B.S.C.P. 112 Table 17)

$$b^3 = \frac{4506}{16} = 282 \text{ in.}^3$$

$\therefore$ b = 6·56 in. and d = 26·24 in.

For an even no. of $1\frac{1}{2}$ in. thick laminates d = 27 in.

$\therefore$ Approx. max section size = 6·75 in. × 27·00 in.

2. Check section at point 8 for actual stress

Three-pinned Arch (D.L. + Unbalanced L.L.)

Lateral unbraced length = ℓ = 6ft = 72 in. (B.S.C.P. 112 Table 18)

Radius of gyration, r = 6·75 × ·289

Slenderness ratio $\frac{\ell}{r} = \frac{72}{6.75 \times .289} = 37$

For medium-term loads (B.S.C.P. 112 Table 16):

$$\sqrt{\frac{10 \times E_{min}}{c_{gpar}}} = \sqrt{\frac{10 \times 650000}{1600}} = 64 \quad \therefore \frac{\ell}{r} < \sqrt{\frac{10 \times E_{min}}{c_{gpar}}}$$

$\therefore$ Modification factor $K_{19} = 1.25 - \frac{0.0626 \times 1600 \times 37^2}{650\,000}$

$= 1.25 - 0.21 = 1.04$

$\therefore$ $c_{ppar} = 1600 \times 1.04 = 1665$ lb/in.^{2}

Depth factor, $K_{16} = .81 \times \left(\frac{d^2+143}{d^2+88}\right) = .81 \times \frac{872}{817} = .865$

$\therefore$ $f_{ppar} = 2625 \times K_{16} \times K_{17} = 2625 \times .865 \times 1.00 = 2270$ lb/in.^{2}

Section area, A = bd = 182 in.^{2}

Section modulus, $z = \frac{bd^2}{6} = 821$ in.^{3}

CALCULATION SHEET NO. 13

$f_{apar} = \frac{M}{Z} = \frac{164267 \times 12}{821} = 2400\ lb/in^2$

$c_{apar} = \frac{P}{A} = \frac{13730}{182} = 75\ lb/in^2$

$\therefore \frac{f_{apar}}{f_{ppar}} + \frac{c_{apar}}{c_{ppar}} = \frac{2400}{2270} + \frac{75}{1665} = 1.057 + .045$

$= 1.102 > 1$ (B.S.C.P. 112 Table 19)

∴ Section size is not suitable

3. Try section size 7.00 in. × 28.00 in.

$c_{ppar} = 1665\ lb/in^2$

$K_{16} = .81 \times \frac{927}{872} = .86$; $K_{17} = 1.00$

$f_{ppar} = 2625 \times .86 \times 1.00 = 2262\ lb/in^2$

$A = bd = 196\ in^2$; $Z = \frac{bd^2}{6} = 915\ in^3$

$f_{apar} = \frac{M}{Z} = \frac{164267 \times 12}{915} = 2154\ lb/in^2$

$c_{apar} = \frac{P}{A} = \frac{13730}{196} = 70\ lb/in^2$

$\therefore \frac{f_{apar}}{f_{ppar}} + \frac{c_{apar}}{c_{ppar}} = \frac{2154}{2262} + \frac{70}{1665} = .951 + .042$

$= .993 < 1$ O.K.

∴ Max. Section Size = 7.00 in. × 28.00 in. at point 8

4. Approx. Apex Ring Section Size (Also point 17)

Depth at Apex Ring = $\frac{5}{8}$ × Max. Depth = 17.50 in.

(A.I.T.C. Timber Construction Manual. Sect. 4. P.37 recommends minimum depth equal to arch width. Extra depth allowed to meet depth of purlins framing into arch)

∴ Approx. apex ring section size = 7.00 in. × 17.50 in.

F. A. A. Ph. D. Thesis
27th Aug., 1969.

Structural Engineering Division
Department of Civil Engineering
University of Newcastle upon Tyne

5. Check section at point 17 for actual stress

Two-pinned Arch (D.L. + Unbalanced L.L.)

$c_{ppar} = 1665\ lb/in^2$

$K_{16} = \cdot 81 \times \frac{449}{394} = \cdot 92$; $K_{17} = 1 \cdot 00$

$f_{ppar} = 2625 \times \cdot 92 \times 1 \cdot 00 = 2420\ lb/in^2$

$A = bd = 123\ in^2$; $z = \frac{bd^2}{6} = 357\ in^3$

$f_{apar} = \frac{65628 \times 12}{357} = 2206\ lb/in^2$; $c_{apar} = \frac{14279}{123} = 116\ lb/in^2$

$\therefore \frac{f_{apar}}{f_{ppar}} + \frac{c_{apar}}{c_{ppar}} = \frac{2206}{2420} + \frac{116}{1665} = \cdot 913 + \cdot 070$

$= \cdot 983 < 1$ O.K.

$\therefore$ Apex ring section size and point 17 section size

= 7·00 in. × 17·50 in.

6. Approx. Base Section Size

Depth at Base = ·75 × Max. Depth = ·75 × 28 = 21 in.

(A.I.T.C. Timber Construction Manual. Sect. 4. P.37 recommends $\frac{4}{5}$)

$\therefore$ Approx. base section size = 7·00 in. × 21·00 in.

7. Tabulation of Rib Section Sizes

Load Point	Base	0	1	2	3	4	5	6	7	8
Depth d (in.)	21·00	21·00	22·00	23·00	24·00	25·00	26·00	27·00	28·00	28·00

Load Point	9	10	11	12	13	14	15	16	17	Apex Ring
Depth d (in.)	28·00	28·00	26·50	25·00	23·50	22·00	20·50	19·00	17·50	17·50

CALCULATION SHEET NO. 15

8. Check intermediate points for actual stress

Point 4. Three-pinned Arch (D.L. + Unbalanced L.L.)

$c_{ppar} = 1665\ lb/in^2$

$K_{16} = \cdot 81 \times \frac{768}{713} = \cdot 87$; $K_{17} = 1 \cdot 00$

$f_{ppar} = 2625 \times \cdot 87 \times 1 \cdot 00 = 2285\ lb/in^2$

$A = bd = 175\ in^2$

$z = \frac{bd^2}{6} = 729\ in^3$

$f_{apar} = \frac{M}{z} = \frac{127210 \times 12}{729} = 2095\ lb/in^2$

$c_{apar} = \frac{16240}{175} = 93\ lb/in^2$

$\therefore \frac{f_{apar}}{f_{ppar}} + \frac{c_{apar}}{c_{ppar}} = \frac{2095}{2285} + \frac{93}{1665} = \cdot 917 + \cdot 056$

$= \cdot 973 < 1$ O.K.

Point 13 Three-pinned Arch (D.L. + Unbalanced L.L.)

$c_{ppar} = 1665\ lb/in^2$

$K_{16} = \cdot 81 \times \frac{695}{640} = \cdot 88$; $K_{17} = 1 \cdot 00$

$f_{ppar} = 2625 \times \cdot 88 \times 1 \cdot 00 = 2310\ lb/in^2$

$A = bd = 164\ in^2$

$z = \frac{bd^2}{6} = 644\ in^3$

$f_{apar} = \frac{M}{z} = \frac{115281 \times 12}{644} = 2150\ lb/in^2$

$c_{apar} = \frac{12670}{164} = 77\ lb/in^2$

$\therefore \frac{f_{apar}}{f_{ppar}} + \frac{c_{apar}}{c_{ppar}} = \frac{2150}{2310} + \frac{77}{1665} = \cdot 930 + \cdot 046$

$= \cdot 976 < 1$ O.K.

F. A. A. Ph. D. Thesis
27th Aug., 1969.

Structural Engineering Division
Department of Civil Engineering
University of Newcastle upon Tyne

9. Check radial stress

Max. B.M., M = 164267 ft lb (At pt. 8 - Calc. sheet No. 5)

Radius of curvature of rib centre line, R = 180 ft

b = 7 in. ; d = 28 in.

Radial stress perp. to grain, $f_r = \frac{3}{2} \times \frac{164267 \times 12}{180 \times 12 \times 7 \times 28} = 69.9$ lb/in².

Permissible shear stress parallel to grain = 247 lb/in². (Calc. sheet No. 2)

Permissible radial stress = $\frac{1}{3} \times 247 = 82$ lb/in². (B.S.C.P. 112 P. 41)

∴ Section is O.K.

---

10. Check axial and shear stresses at base

Max. shear force = 6,810 lb (Three-pinned Arch. D.L. + Unbalanced L.L. Calc. sheet No. 5)

Max. axial force = 30,456 lb (Two-pinned Arch. D.L. + Balanced L.L. Calc sheet Nos. 9, 11)

Shear stress = $\frac{3}{2} \times \frac{6810}{7 \times 21}$ = 63 lb/in². < 247 lb/in².

Axial stress = $\frac{30456}{7 \times 21}$ = 208 lb/in². < 2000 lb/in².

∴ Section is O.K.

---

2. HORIZONTAL PURLIN RING DESIGN

A. Axial Forces (P)

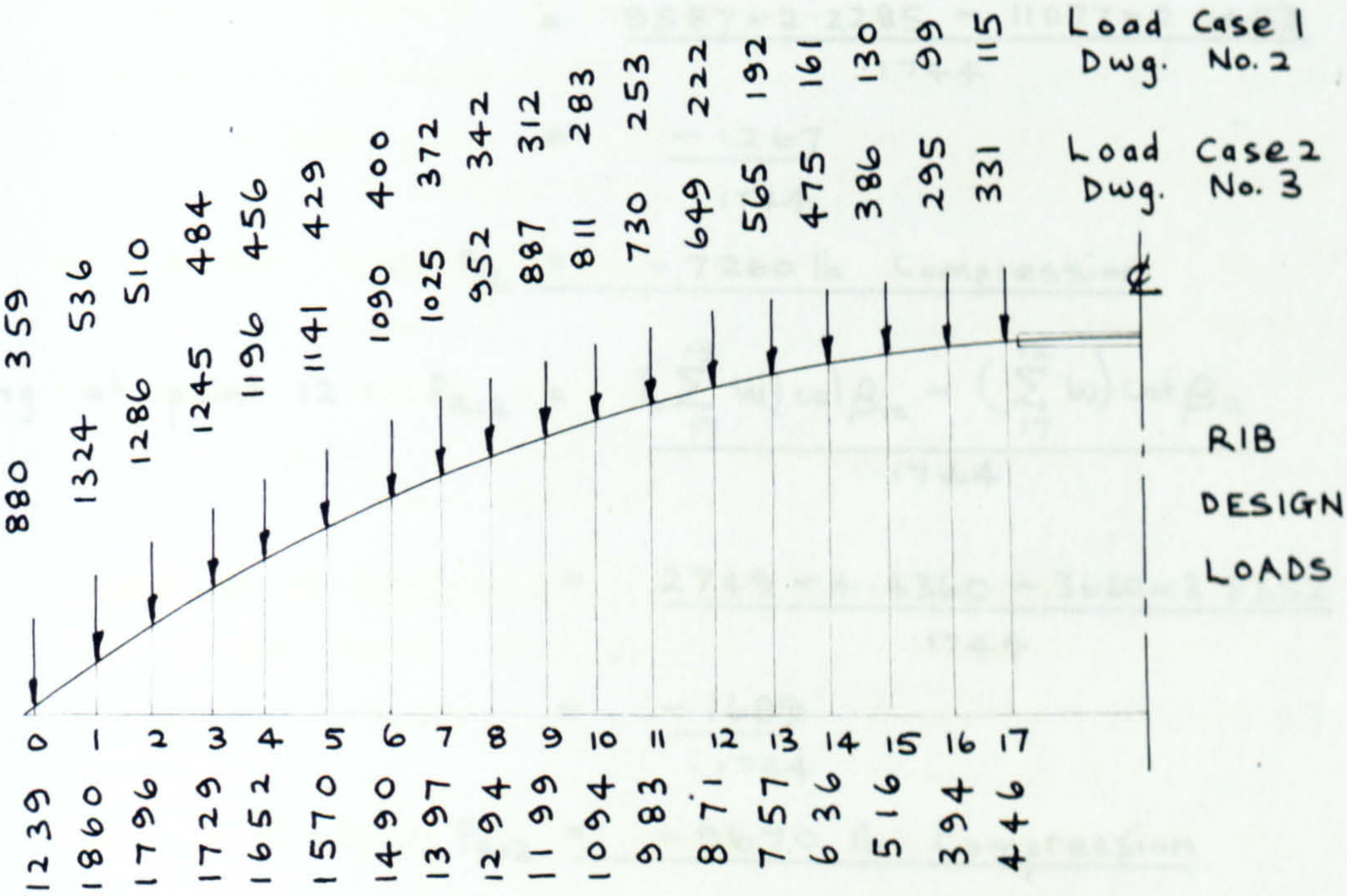

Ring at point 1 : $$P_{R1} = \frac{(\sum_{17}^{2} W)\cot\beta_1 - (\sum_{17}^{1} W)\cot\beta_0}{2\sin\left(\frac{180^\circ}{36}\right)}$$

(A.I.T.C. Timber Construction Manual. Sect. 4. P.66. For angle values, see drawing No. Ph. D. Thesis No. 1)

$$P_{R1} = \frac{17824 \times 1.4983 - 19684 \times 1.3952}{2 \times \sin 5^\circ}$$

$$= \frac{-757.4}{2 \times .0872}$$

$$= \frac{-757.4}{.1744}$$

$$\therefore P_{R1} = \underline{-4340 \text{ lb Compression}}$$

CALCULATION SHEET NO. 18

Ring at point 6 : $P_{R6} = \dfrac{(\sum_{17}^{7} W)\cot\beta_6 - (\sum_{17}^{6} W)\cot\beta_5}{\cdot 1744}$

$= \dfrac{9587 \times 2\cdot2285 - 11077 \times 2\cdot0433}{\cdot 1744}$

$= \dfrac{-1267}{\cdot 1744}$

$\therefore P_{R6} = -7260$ lb Compression

Ring at point 12 : $P_{R12} = \dfrac{(\sum_{17}^{13} W)\cot\beta_{12} - (\sum_{17}^{12} W)\cot\beta_{11}}{\cdot 1744}$

$= \dfrac{2749 \times 4\cdot4360 - 3620 \times 3\cdot8352}{\cdot 1744}$

$= \dfrac{-1689}{\cdot 1744}$

$\therefore P_{R12} = -9670$ lb Compression

B. Bending Moments (M)

Ring at point 1

Load on purlin = 1860 lb

$M = \dfrac{WL}{8} = \dfrac{1860 \times 17\cdot859 \times 12}{8}$ (For spans between adjacent ribs, see dwg. No. 1)

$= 49,800$ in.lb

Ring at point 6

Load on purlin = 1490 lb

$M = \dfrac{1490 \times 13\cdot326 \times 12}{8} = 29,800$ in.lb

Ring at point 12

Load on purlin = 871 lb

$M = \dfrac{871 \times 7\cdot415 \times 12}{8} = 9,690$ in.lb

CALCULATION SHEET NO. 19

C. Check sections for combined bending and compression
(B.S.C.P. 112 : 1967. Art. 314)

Ring at point 1 Assume 6"×6"; $A = bd = 36 in^2$; $z = \frac{bd^2}{6} = 36 in^3$

$$f_{apar} = \frac{M}{Z} = \frac{49800}{36} = 1380 \text{ lb/in}^2$$

$f_{ppar} = 2625 \text{ lb/in}^2$ (Calc. sheet No. 2)

$c_{apar} = \frac{4340}{36} = \frac{P}{A} = 121 \text{ lb/in}^2$

$c_{ppar} = 2000 \text{ lb/in}^2$ (Calc. sheet No. 2)

Slenderness Ratio, $\frac{\ell}{r} = \frac{17.859 \times 12}{.2887 \times 6} = 124 > 20$ (< 180)

$$\therefore \frac{f_{apar}}{f_{ppar}} + \frac{c_{apar}}{c_{ppar}} = \frac{1380}{2625} + \frac{121}{2000} = .525 + .061$$

$= .586 < .9$ O.K.

Ring at point 6 Assume 5"×5"; $A = 25 in^2$; $z = 21 in^3$

$f_{apar} = \frac{29800}{21} = 1420 \text{ lb/in}^2$; $f_{ppar} = 2625 \text{ lb/in}^2$

$c_{apar} = \frac{7260}{25} = .290 \text{ lb/in}^2$; $c_{ppar} = 2000 \text{ lb/in}^2$

Slenderness Ratio, $\frac{\ell}{r} = \frac{13.326 \times 12}{.2887 \times 5} = 111 > 20$ (< 180)

$$\therefore \frac{f_{apar}}{f_{ppar}} + \frac{c_{apar}}{c_{ppar}} = \frac{1420}{2625} + \frac{290}{2000} = .541 + .145$$

$= .686 < .9$

O.K.

CALCULATION SHEET NO. 20

Ring at point 12 Assume 5"×3" ; $A = 15 in^2$; $z = 12 in^3$.

$$f_{apar} = \frac{9690}{12} = 808 \ lb/in^2$$

$$f_{ppar} = 2625 \ lb/in^2$$

$$c_{apar} = \frac{9670}{15} = 645 \ lb/in^2$$

$$c_{ppar} = 2000 \ lb/in^2$$

Slenderness Ratio, $\frac{l}{r} = \frac{7.415 \times 12}{.2887 \times 3} = 103 > 20 \ (< 180)$

$$\therefore \frac{f_{apar}}{f_{ppar}} + \frac{c_{apar}}{c_{ppar}} = \frac{808}{2625} + \frac{645}{2000} = .308 + .323$$

$$= .631 < .9 \quad \text{O.K.}$$

F. A. A. Ph. D. Thesis
1st Sept., 1969.

Structural Engineering Division
Department of Civil Engineering
University of Newcastle upon Tyne

CALCULATION SHEET NO. 21

3. DIAGONAL ROD SIZES

Diagonals between rings at points 0 and 2

$$\text{Axial Force, } P_{D2} = \frac{\sum_{17}^{2} W_{LIVE}}{2\sin\left[\frac{(180^\circ - \alpha_2 + \alpha_0)}{2} - \alpha_0\right]\cos\gamma_0}$$

(A.I.T.C. Timber Construction Manual. Sect. 4. P.67.
For angle values, see drawing No. Ph.D. Thesis No.1.
For loads at rib-ring intersections, see drawing No. Ph. D. Thesis No. 3)

$$\therefore P_{D2} = \frac{13064}{\left\{2\sin\left[\frac{(180^\circ - 57^\circ 14' 08'' + 53^\circ 24' 52'')}{2} - 53^\circ 24' 52''\right] \times .5575\right\}}$$

$$= \frac{13064}{2\sin 34^\circ 40' 30'' \times .5575}$$

$$= \frac{13064}{2 \times .5689 \times .5575}$$

$$\therefore P_{D2} = \underline{20,600 \text{ lb}}$$

$$A_{st} = \frac{20,600}{20000} = 1.03 \text{ in}^2. \qquad 1 \text{ No. } 1\tfrac{1}{8} \text{ in. } \phi \text{ bar } (.994 \text{ in}^2.)$$

Diagonals between rings at points 6 and 8

$$\text{Axial Force, } P_{D8} = \frac{\sum_{17}^{8} W_{LIVE}}{2\sin\left[\frac{(180^\circ - \alpha_8 + \alpha_6)}{2} - \alpha_6\right]\cos\gamma_6}$$

$$= \frac{6081}{2\sin 23^\circ 12' 42'' \times .7266}$$

$$= \frac{6081}{2 \times .3942 \times .7266} = \underline{10,600 \text{ lb}}$$

$$A_{st} = \frac{10,600}{20,000} = .53 \text{ in}^2. \qquad 1 \text{ No. } \tfrac{7}{8} \text{ in. } \phi \text{ bar } (.601 \text{ in}^2.)$$

F. A. A. Ph. D. Thesis
2nd Sept., 1969.

Structural Engineering Division
Department of Civil Engineering
University of Newcastle upon Tyne

CALCULATION SHEET NO. 22

Diagonals between rings at points 12 and 14

$$\text{Axial Force, } P_{D14} = \frac{\sum_{17}^{14} W_{LIVE}}{2\sin\left[\frac{(180^\circ - \alpha_{14} + \alpha_{12}) - \alpha_{12}}{2}\right]\cos\gamma_{12}}$$

$$= \frac{1487}{2\sin 11^\circ 44' 54'' \times .9165}$$

$$= \frac{1487}{2 \times .2037 \times .9165}$$

$$= \frac{3980 \text{ lb}}{}$$

$$A_{st} = \frac{3980}{20000} = .199 \text{ in}^2 \qquad \text{1 No. } \tfrac{1}{2} \text{ in. } \phi \text{ bar } (.196 \text{ in}^2)$$

F. A.A. Ph. D. Thesis
2nd Sept., 1969.

Structural Engineering Division
Department of Civil Engineering
University of Newcastle upon Tyne

4. Slenderness Ratios of Ribs Without Bracing

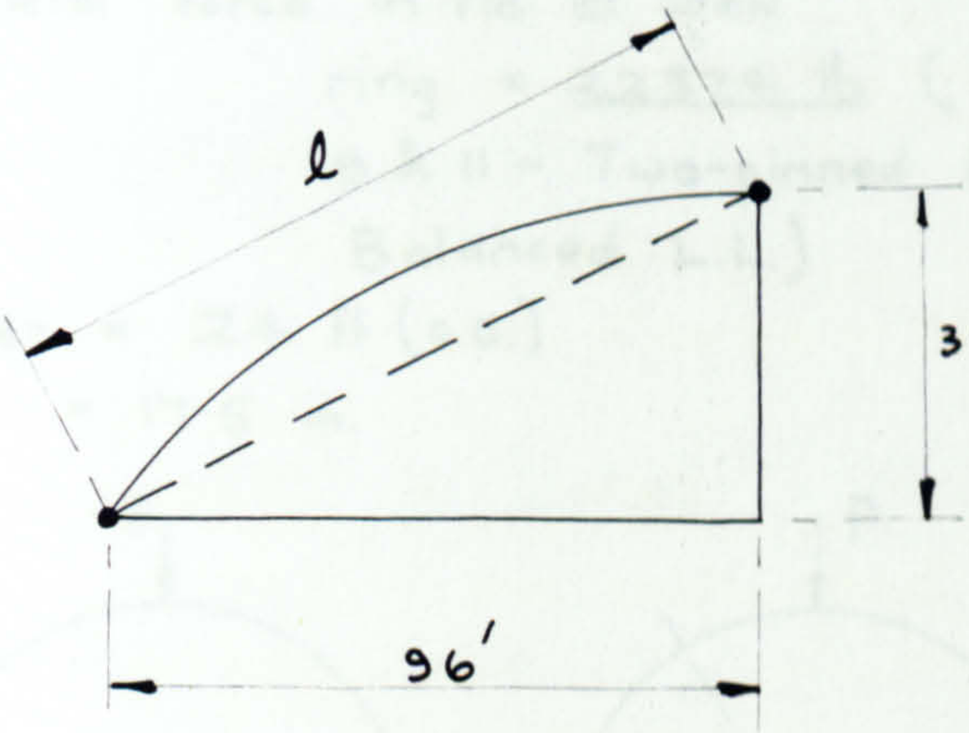

Max. section size = 7" × 28"

Eff. length, $l = \sqrt{96^2 + 35{\cdot}604^2} = 102{\cdot}5$ ft

Radii of gyration: $r_x = 28 \times {\cdot}289 = 8{\cdot}1$ in.

$r_y = 7 \times {\cdot}289 = 2{\cdot}02$ in.

Slenderness ratios: $\frac{l}{r_x} = \frac{102{\cdot}5 \times 12}{8{\cdot}1} = 152$

$\frac{l}{r_y} = \frac{102{\cdot}5 \times 12}{2{\cdot}02} = 608$

To reduce the slenderness ratios on this basis would require larger section sizes. The maximum depth to breadth ratio would also have to be 3 instead of 4 (CP 112 : 1967 Table 17 and A.I.T.C. Manual)

5. APEX RING DESIGN

Max. axial force in rib at apex ring = 22374 lb (Calc. Sheet Nos. 9 & 11 – Two-pinned Arch – D.L. + Balanced L.L.)

Ring Diameter = 24 ft (o.D.)

Ring Depth = 17·5 in.

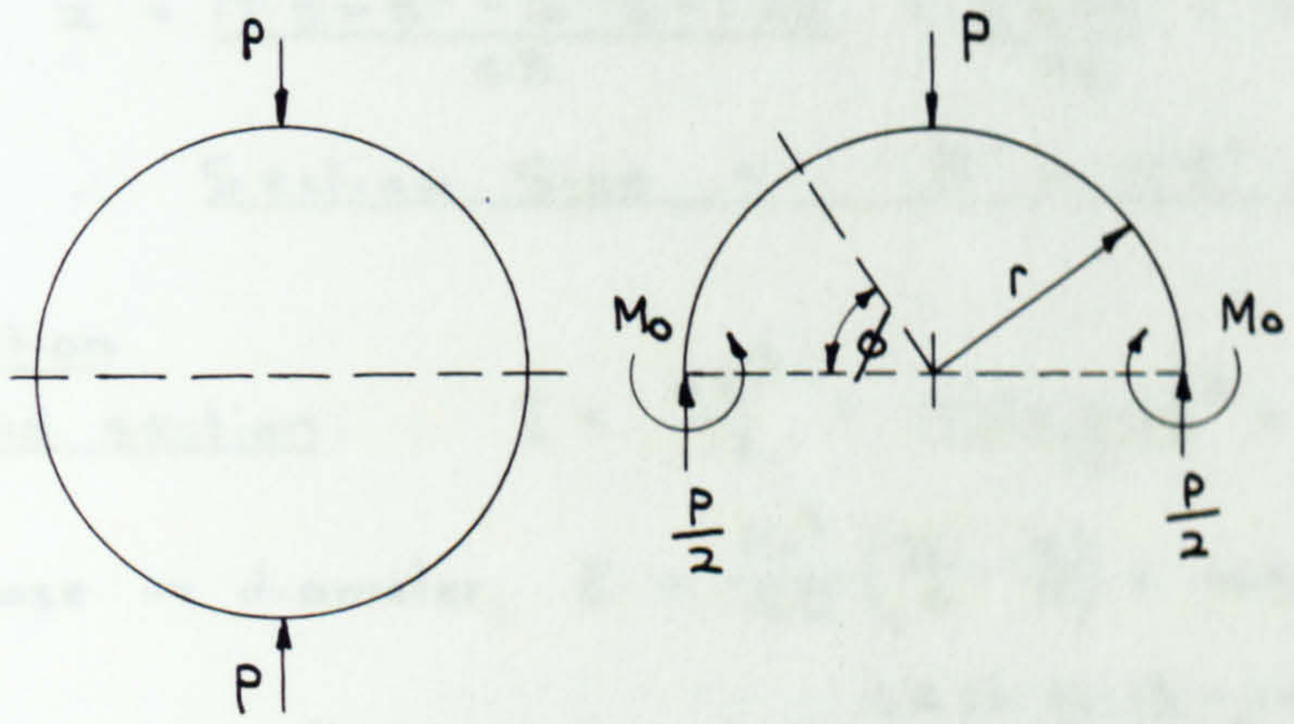

Max. B.M., $M_o = \frac{Pr}{2}\left(1 - \frac{2}{\pi}\right) = .182\,Pr$ (Ref. No. 13-244,245)

$M_o = .182 \times 22374 \times 24 \times 12 = 1,170,000$ lb in.

$f = 10.5 \times 2240 = 23,500$ lb/in.^{2} (B.S. 449: 1959$^{(44)}$ Table 2)

$$z = \frac{M_o}{f} = \frac{1,170,000}{23500} = 49.8 \text{ in.}^3$$

For solid rect. section:

$$z = \frac{db^2}{6} = \frac{17.5b^2}{6} = 49.8$$

$$\therefore\ b^2 = \frac{49.8 \times 6}{17.5} = 17.1$$

$$\therefore\ \underline{b = 4.14 \text{ in.}}\ \text{(Say 4.25 in.)}$$

CALCULATION SHEET NO. 25

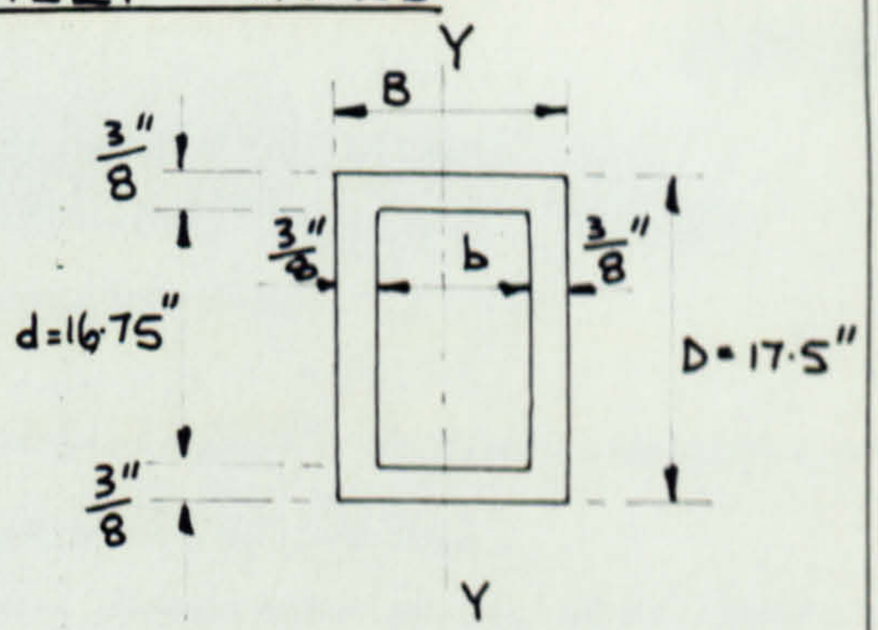

Box section:

$$z = \frac{DB^3 - db^3}{6B}$$

$$= \frac{17.5(b+\frac{3}{4})^3 - 16.75b^3}{6(b+\frac{3}{4})}$$

For $b = 7.25''$

$$z = \frac{17.5 \times 8^3 - 16.75 \times 7.25^3}{48} = \frac{2520}{48} = 52.5 \text{ in.}^3$$

$\therefore$ Section Size = 8" × 17.5" overall

Deflection

Solid section: $I = \frac{db^3}{12} = \frac{17.5 \times 4.25^3}{12} = 112 \text{ in.}^4$

Decrease in diameter, $\delta = \frac{P_r^3}{EI}\left(\frac{\pi}{4} - \frac{2}{\pi}\right) = .149 \frac{P_r^3}{EI}$

(Ref. No. 13 - 244, 245)

$$\therefore \delta = \frac{.149 \times 22374 \times 2 4^3 \times 1 2^3}{30 \times 10^6 \times 112}$$

$\therefore \delta = 23.6$ in.

Box section: $I = \frac{DB^3 - db^3}{12} = \frac{17.5 \times 8^3 - 16.75 \times 7.25^3}{12}$

$$= \frac{2520}{12} = 210 \text{ in.}^4$$

$$\therefore \delta = \frac{.149 \times 22374 \times 24^3 \times 12^3}{30 \times 10^6 \times 210}$$

$\therefore \delta = 12.6$ in.

These deflections are large and would not be obtained in practice due to the restraining action of the other 34 ribs.

F.A.A. Ph.D. Thesis
27th Feb., 1970

Structural Engineering Division
Department of Civil Engineering
University of Newcastle upon Tyne

APPENDIX IV

ANALYSIS OF TEST RESULTS

TABLES 1 - 16

ANALYSIS OF TEST RESULTS

TABLE NO. 1

Theoretical Force Influence Coefficients for Three-pinned and Two-pinned Arches (Plane Frames)

Symmetrical unit vertical loads on arch

Unit Loads at Points	Distance From Base	Vertical Base Reactions	Horizontal Base Reactions	Apex Ring Vertical Forces	Apex Ring Radial Forces
Three-pinned Arch (Plane Frame)					
Base	.000	+ 1	0	0	0
1	5.598	+ 1	+ .156	0	+ .156
5	26.190	+ 1	+ .728	0	+ .728
9	48.240	+ 1	+ 1.340	0	+ 1.340
13	71.334	+ 1	+ 1.980	0	+ 1.980
17	95.094	+ 1	+ 2.642	0	+ 2.642
Two-pinned Arch (Plane Frame)					
Base	.000	+ 1	0	0	0
1	5.598	+ 1	+ .188	0	+ .188
5	26.190	+ 1	+ .868	0	+ .868
9	48.240	+ 1	+ 1.510	0	+ 1.510
13	71.334	+ 1	+ 1.990	0	+ 1.990
17	95.094	+ 1	+ 2.254	0	+ 2.254

F.A.A. Ph.D. Thesis
18th March, 1970.

Structural Engineering Division,
Department of Civil Engineering,
University of Newcastle upon Tyne.

ANALYSIS OF TEST RESULTS — Table No. 2.

Theoretical Force Influence Coefficients for Radial Ribbed Dome (Space Frame - Makowski and Gogate Method Modified by Author). 6 No. Ribs. Total 1 = Max. outward horizontal or downward vertical reaction (except Pt. 17); Total 2 = Max. inward horizontal or upward vertical reaction (except Pt. 17); Total 3 = Horizontal or vertical reaction for symmetrical load. For determination of influence coefficients, see Ph.D. Thesis, Vol. 2, Computer Sheet Nos. 7 - 14.

Horizontal Reaction Influence Coefficients					
Rib Nos.	Pt. 1	Pt. 5	Pt. 9	Pt. 13	Pt. 17
30, 6	- .0986	- .3936	- .4878	- .2884	+ .1820
2 x (30, 6) = Total 1	- .1972	- .7872	- .9756	- .5768	+ .3640
24, 12	+ .0258	+ .1208	+ .2226	+ .3297	+ 4400
2 x(24, 12)	+ .0516	+ .2416	+ .4452	+ .6594	+ .8800
Directly Loaded Rib 36	+ .2128	+ .8939	+ 1.2904	+ 1.2586	+ .8277
18	+ .0884	+ .3795	+ .5799	+ .6405	+ .5698
Total 2	+ .3528	+ 1.5150	+ 2.3155	+ 2.5585	+ 2.2775
Total 3	+ .1556	+ .7278	+ 1.3399	+ 1.9817	+ 2.6415
Vertical Reaction Influence Coefficients					
24, 12	- .0329	- .1312	- .1626	- .0961	+ .0607
2 x(24, 12) = Total 1	- .0658	- .2624	- .3252	- .1922	+ .1214
30, 6	+ .0086	+ .0403	+ .0742	+ .1099	+ .1467
2 x (30, 6)	+ .0172	+ .0806	+ .1484	+ .2198	+ .2934
36	+ .0295	+ .1265	+ .1933	+ .2135	+ .1899
Directly Loaded Rib 18	+1.0190	+ 1.0554	+ .9835	+ .7590	+ .3954
Total 2	+1.0657	+ 1.2625	+ 1.3252	+ 1.1923	+ .8787
Total 3	+ .9999	+ 1.0001	+ 1.0000	+ 1.0001	+ 1.0001

F.A.A. Ph.D. Thesis
23rd March, 1970

Structural Engineering Division,
Department of Civil Engineering,
University of Newcastle upon Tyne.

Table No. 3.

Experimental Force Influence Coefficients for Model Radial Ribbed Dome

(6 No. Ribs of Constant I)

Total 1 = Max. outward horiz. or downward vert. reaction;
Total 2 = Max. inward horiz. or upward vert. reaction;
Total 3 = Horiz. or vert. reaction for symmetrical load.
For test results, see APPENDIX II, Test Nos. 1 and 2.

Rib No.	Pt. 1	Pt. 5	Pt. 9	Pt. 13	Pt. 17
Horizontal Reaction Influence Coefficients					
30	- .014	- .043	+ .003	+ .132	+ .338
6	- .011	- .037	+ .014	+ .141	+ .341
Total 1	- .025	- .080			
24	+ .038	+ .150	+ .257	+ .346	+ .387
12	+ .037	+ .167	+ .269	+ .341	+ .382
Directly Loaded Rib 36	+ .053	+ .271	+ .449	+ .460	+ .377
18	+ .025	+ .110	+ .197	+ .297	+ .391
Total 2	+ .153	+ .698	+ 1.189	+ 1.717	+ 2.216
Total 3	+ .128	+ .618	+ 1.189	+ 1.717	+ 2.216
Vertical Reaction Influence Coefficients					
24	- .005	- .014	+ .014	+ .076	+ .149
12	- .006	- .016	+ .001	+ .057	+ .145
Total 1	- .011	- .030			
30	+ .010	+ .049	+ .079	+ .106	+ .128
6	+ .011	+ .046	+ .073	+ .111	+ .127
36	+ .005	+ .025	+ .047	+ .082	+ .121
Directly Loaded Rib 18	+ .960	+ .840	+ .671	+ .458	+ .220
Total 2	+ .986	+ .960	+ .885	+ .890	+ .890
Total 3	+ .975	+ .930	+ .885	+ .890	+ .890

F.A.A., Ph.D. Thesis,
23rd March, 1970.

Structural Engineering Division,
Department of Civil Engineering,
University of Newcastle upon Tyne.

ANALYSIS OF TEST RESULTS — Table No. 4.

Experimental Force Influence Coefficients for Model Radial Ribbed Dome
(6 No. Ribs of Constant I)

Total 1 = Max. downward apex ring vert. or inward radial force;
Total 2 = Max. upward apex ring vert. or outward radial force;
Total 3 = Apex ring vert. or radial force for symmetrical load.
For Test Results, see APPENDIX II, Test Nos. 3 and 4.

Apex Ring Vertical Force Influence Coefficients					
Rib No.	Pt. 1	Pt. 5	Pt. 9	Pt. 13	Pt. 17
Directly Loaded Rib 36	+ .03	+ .15	+ .39	+ .75	+ 1.00
30	0	+ .03	+ .15	+ .38	+ .71
6	0	+ .03	+ .13	+ .34	+ .60
Total 1	+ .03	+ .21	+ .67	+ 1.47	+ 2.31
24	- .06	- .25	- .33	- .22	- .02
12	- .06	- .25	- .35	- .23	- .15
18	- .09	- .38	- .55	- .49	- .24
Total 2	- .21	- .88	- 1.23	- .94	- .41
Total 3	- .18	- .67	- .56	+ .53	+ 1.90
Apex Ring Radial Force Influence Coefficients					
Directly Loaded Rib 36	+ .27	+ 1.12	+ 1.68	+ 1.56	+ .74
30	+ .02	+ .05	+ .10	+ .19	+ .24
6	+ .01	+ .03	+ .09	+ .17	+ .25
Total 1	+ .30	+ 1.20	+ 1.87	+ 1.92	+ 1.23
24	- .08	- .39	- .57	- .57	- .36
12	- .09	- .41	- .59	- .60	- .44
18	- .10	- .43	- .65	- .75	- .65
Total 2	- .27	- 1.23	- 1.81	- 1.92	- 1.45
Total 3	+ .03	- .03	+ .06	0	- .22

F.A.A., Ph.D. Thesis,
23rd March, 1970.

Structural Engineering Division,
Department of Civil Engineering,
University of Newcastle upon Tyne.

ANALYSIS OF TEST RESULTS Table No. 5.

Experimental Force Influence Coefficients for Model Radial Ribbed Dome

(6 No. Ribs of Constant I)

Total 1 = Max. anticlockwise apex ring tang. force;

Total 2 = Max. clockwise apex ring tang. force;

Total 3 = Apex ring tang. force for symmetrical load.

For test results, see APPENDIX II, Test No. 5.

Apex Ring Tangential Force Influence Coefficients					
Rib No.	Pt. 1	Pt. 5	Pt. 9	Pt.13	Pt.17
Directly Loaded Rib 36	0	+ .03	+ .06	+ .07	+ .04
6	+ .05	+ .23	+ .31	+ .26	+ .21
12	+ .04	+ .17	+ .22	+ .25	+ .18
18	0	+ .02	+ .03	+ .07	+ .08
Total 1	+ .09	+ .45	+ .62	+ .65	+ .51
24	- .04	- .10	- .15	- .14	- .08
30	- .05	- .16	- .20	- .18	- .08
Total 2	- .09	- .26	- .35	- .32	- .16
Total 3	0	+ .19	+ .27	+ .33	+ .35

F.A.A., Ph.D. Thesis,
24th March, 1970.

Structural Engineering Division,
Department of Civil Engineering,
University of Newcastle upon Tyne.

ANALYSIS OF TEST RESULTS — Table No. 6.

Experimental Force Influence Coefficients for Model Radial Ribbed Dome
(6 No. Ribs of varying I)

Total 1 = Max. outward horiz. or downward vert. reaction;
Total 2 = Max. inward Horiz. or upward vert. reaction;
Total 3 = Horiz. or vert. reaction for symmetrical load.
For Test results, see APPENDIX II, Test Nos. 6 and 7.

Horizontal Reaction Influence Coefficients					
Rib No.	Pt. 1	Pt. 5	Pt. 9	Pt. 13	Pt. 17
30	- .021	- .065	- .009	+ .103	+ .361
6	- .021	- .065	- .009	+ .103	+ .361
Total 1	- .042	- .130	- .018		
24	+ .034	+ .155	+ .260	+ .332	+ .393
12	+ .034	+ .155	+ .260	+ .332	+ .393
Directly Loaded Rib 36	+ .052	+ .273	+ .447	+ .515	+ .430
18	+ .026	+ .124	+ .220	+ .315	+ .421
Total 2	+ .146	+ .707	+ 1.187	+ 1.700	+ 2.359
Total 3	+ .104	+ .577	+ 1.169	+ 1.700	+ 2.359
Vertical Reaction Influence Coefficients					
24	- .009	- .033	- .013	+ .037	+ .143
12	- .009	- .033	- .013	+ .037	+ .143
Total 1	- .018	- .066	- .026		
30	+ .011	+ .051	+ .082	+ .102	+ .127
6	+ .011	+ .051	+ .082	+ .102	+ .127
36	+ .006	+ .029	+ .048	+ .083	+ .124
Directly Loaded Rib 18	+ .963	+ .843	+ .679	+ .469	+ .222
Total 2	+ .991	+ .974	+ .891	+ .830	+ .886
Total 3	+ .973	+ .908	+ .865	+ .830	+ .886

F.A.A., Ph.D. Thesis,
24th March, 1970.

Structural Engineering Division,
Department of Civil Engineering,
University of Newcastle upon Tyne.

ANALYSIS OF TEST RESULTS — Table No. 7.

Experimental Force Influence Coefficients for Model Radial Ribbed Dome
(6 No. Ribs of varying I)

Total 1 = Max. downward apex ring vert. or inward radial force;
Total 2 = Max. upward apex ring vert. or outward radial force;
Total 3 = Apex ring vert. or radial force for symmetrical load.
For test results, see APPENDIX II, Test Nos. 8 and 9.

Apex Ring Vertical Force Influence Coefficients

Rib No.	Pt. 1	Pt. 5	Pt. 9	Pt. 13	Pt. 17
Directly Loaded Rib 36	+ .02	+ .21	+ .52	+ .90	+ 1.00
30	0	0	+ .14	+ .39	+ .71
6	0	0	+ .14	+ .39	+ .71
Total 1	+ .02	+ .21	+ .80	+ 1.68	+ 2.42
24	- .06	- .28	- .42	- .42	- .14
12	- .06	- .28	- .42	- .42	- .14
18	- .10	- .45	- .68	- .75	- .38
Total 2	- .22	- 1.01	- 1.52	- 1.59	- .66
Total 3	- .20	- .80	- .72	+ .09	+ 1.76

Apex Ring Radial Force Influence Coefficients

Directly Loaded Rib 36	+ .24	+ 1.11	+ 1.70	+ 1.83	+ .93
30	+ .02	+ .07	+ .17	+ .29	+ .37
6	+ .02	+ .07	+ .17	+ .29	+ .37
Total 1	+ .28	+ 1.25	+ 2.04	+ 2.41	+ 1.67
24	- .10	- .47	- .67	- .83	- .58
12	- .10	- .47	- .67	- .83	- .58
18	- .11	- .48	- .79	- .97	- .83
Total 2	- .31	- 1.42	- 2.13	- 2.63	- 1.99
Total 3	- .03	- .17	- .09	- .22	- .32

Structural Engineering Division,
Department of Civil Engineering,
University of Newcastle upon Tyne.

Experimental Force Influence Coefficients for Model Radial Ribbed Dome

(6 No. Ribs of varying I)

Total 1 = Max. anticlockwise apex ring tang. force;

Total 2 = Max. clockwise apex ring tang. force;

Total 3 = Apex ring tang. force for symmetrical load.

For test results, see APPENDIX II, Test No. 10.

Apex Ring Tangential Force Influence Coefficients					
Rib No.	Pt. 1	Pt. 5	Pt. 9	Pt.13	Pt.17
Directly Loaded Rib 36	+ .01	+ .03	+ .05	+ .08	+ .10
6	+ .06	+ .23	+ .30	+ .28	+ .30
12	+ .04	+ .15	+ .25	+ .31	+ .30
18	+ .01	+ .04	+ .07	+ .08	+ .20
Total 1	+ .12	+ .45	+ .67	+ .75	+ .90
24	- .03	- .09	- .10	- .08	- .03
30	- .04	- .15	- .14	- .14	- .03
Total 2	- .07	- .24	- .24	- .22	- .06
Total 3	+ .05	+ .21	+ .43	+ .53	+ .84

F.A.A., Ph.D. Thesis,
24th March, 1970.

Structural Engineering Division,
Department of Civil Engineering,
University of Newcastle upon Tyne.

ANALYSIS OF TEST RESULTS

Table No. 9.

Theoretical Horizontal Reaction Influence Coefficients for Radial Ribbed Dome (Space Frame - Makowski and Gogate Method Modified by Author). 36 No. Ribs. Total 1 = Max. outward horiz. reaction; Total 2 = Max. inward horiz. reaction; Total 3 = Horiz. reaction for symmetrical load. For determination of influence coefficients, see Ph.D. Thesis, Vol. 2, Computer Sheet Nos. 15 - 52.

Rib Nos.	Pt. 1	Pt. 5	Pt. 9	Pt. 13	Pt. 17
35, 1	- .0265	- .1072	- .1387	- .0980	+ .0095
34, 2	- .0255	- .1033	- .1334	- .0934	+ .0114
33, 3	- .0240	- .0970	- .1246	- .0858	+ .0146
32, 4	- .0219	- .0884	- .1128	- .0755	+ .0189
31, 5	- .0194	- .0778	- .0982	- .0628	+ .0242
30, 6	- .0164	- .0656	- .0813	- .0481	+ .0303
29, 7	- .0132	- .0521	- .0626	- .0318	+ .0371
28, 8	- .0097	- .0376	- .0427	- .0144	+ .0444
			Sum	- .5098	
			2 x Sum = Total 1	- 1.0196	
27, 9	- .0061	- .0227	- .0221	+ .0034	+ .0518
26, 10	- .0025	- .0079	- .0015	+ .0213	+ .0593
Sum	- .1652	- .6596	- .8179		
2 x sum = Total 1	- .3304	- 1.3192	- 1.6358		
25, 11	+ .0010	+ .0066	+ .0184	+ .0387	+ .0665
24, 12	+ .0043	+ .0201	+ .0371	+ .0549	+ .0733
23, 13	+ .0073	+ .0324	+ .0540	+ .0697	+ .0795
22, 14	+ .0098	+ .0429	+ .0686	+ .0823	+ .0848
21, 15	+ .0119	+ .0515	+ .0804	+ .0926	+ .0891
20, 16	+ .0134	+ .0578	+ .0892	+ .1002	+ .0922
19, 17	+ .0144	+ .0617	+ .0945	+ .1049	+ .0942
Sum	+ .0621	+ .2730	+ .4422	+ .5680	+ .8811
2 x Sum	+ .1242	+ .5460	+ .8844	+ 1.1360	+ 1.7622
18	+ .0150	+ .0645	+ .0984	+ .1083	+ .0957
Directly Loaded Rib 36	+ .3468	+ 1.4362	+ 1.9929	+ 1.7564	+ .7835
Total 2	+ .4860	+ 2.0467	+ 2.9757	+ 3.0007	+ 2.6414
Total 3	+ .1556	+ 0.7275	+ 1.3399	+ 1.9811	+ 2.6414

F.A.A., Ph.D. Thesis,
23rd March, 1970.

Structural Engineering Division,
Department of Civil Engineering,
University of Newcastle upon Tyne.

ANALYSIS OF TEST RESULTS — Table No. 10.

Theoretical Vertical Reaction Influence Coefficients for Radial Ribbed Dome (Space Frame - Makowski and Gogate Method Modified by Author). 36 No. Ribs. Total 1 = Max. downward vert. reaction; Total 2 = Max. upward vert. reaction; Total 3 = Vert. reaction for symmetrical load. For determination of influence coefficients, see Ph.D. Thesis, Vol. 2, Computer Sheet Nos. 15 - 52 (Signs reversed).

Rib Nos.	Pt. 1	Pt. 5	Pt. 9	Pt. 13	Pt. 17
17, 19	- .0088	- .0357	- .0462	- .0327	+ .0032
16, 20	- .0085	- .0344	- .0445	- .0311	+ .0038
15, 21	- .0080	- .0323	- .0415	- .0286	+ .0049
14, 22	- .0073	- .0295	- .0376	- .0252	+ .0063
13, 23	- .0065	- .0259	- .0327	- .0209	+ .0081
12, 24	- .0055	- .0219	- .0271	- .0160	+ .0101
11, 25	- .0044	- .0174	- .0209	- .0106	+ .0124
10, 26	- .0032	- .0125	- .0142	- .0048	+ .0148
			Sum	- .1699	
			2 x Sum = Total 1	- .3398	
9, 27	- .0020	- .0076	- .0074	+ .0011	+ .0173
8, 28	- .0008	- .0026	- .0005	+ .0071	+ .0198
Sum	- .0550	- .2198	- .2726		
2 x Sum = Total 1	- .1100	- .4396	- .5452		
7, 29	+ .0003	+ .0022	+ .0061	+ .0129	+ .0222
6, 30	+ .0014	+ .0067	+ .0124	+ .0183	+ .0244
5, 31	+ .0024	+ .0108	+ .0180	+ .0232	+ .0265
4, 32	+ .0033	+ .0143	+ .0229	+ .0274	+ .0283
3, 33	+ .0040	+ .0172	+ .0268	+ .0309	+ .0297
2, 34	+ .0045	+ .0193	+ .0297	+ .0334	+ .0307
1, 35	+ .0048	+ .0206	+ .0315	+ .0350	+ .0314
Sum	+ .0207	+ .0911	+ .1474	+ .1893	+ .2939
2 x Sum	+ .0414	+ .1822	+ .2948	+ .3786	+ .5878
36	+ .0050	+ .0215	+ .0328	+ .0361	+ .0319
Directly Loaded Rib 18	+ 1.0637	+ 1.2362	+ 1.2177	+ .9249	+ .3807
Total 2	+ 1.1101	+ 1.4399	+ 1.5453	+ 1.3396	+ 1.0004
Total 3	+ 1.0001	+ 1.0003	+ 1.0001	+ .9998	+ 1.0004

F.A.A., Ph.D. Thesis,
23rd March, 1970.

Structural Engineering Division,
Department of Civil Engineering,
University of Newcastle upon Tyne.

Table No. 11.

Experimental Horizontal Reaction Influence Coefficients for Model Radial Ribbed Dome (36 No. Ribs of varying I without bracing). Total 1 = Max. outward horiz. reaction; Total 2 = Max. inward horiz. reaction; Total 3 = Horiz. reaction for symmetrical load. N.B. All values in this table are modified for creep. For test results, see APPENDIX II, Test No. 12.

Rib Nos.	Pt. 1	Pt. 5	Pt. 9	Pt. 13	Pt. 17
35, 1	- .085	- .375	- .420	- .250	+ .075
34, 2	- .045	- .175	- .215	- .140	+ .070
33, 3	- .015	- .075	- .085	- .040	+ .065
			Sum	- .430	
			2 x Sum = Total 1	- .860	
32, 4	0	- .010	- .010	+ .015	+ .070
Sum	- .145	- .635	- .730		
2 x Sum = Total 1	- .290	- 1.270	- 1.460		
31, 5	0	+ .020	+ .030	+ .050	+ .070
30, 6	+ .005	+ .025	+ .040	+ .060	+ .075
29, 7	+ .005	+ .025	+ .040	+ .055	+ .075
28, 8	+ .005	+ .025	+ .045	+ .060	+ .075
27, 9	+ .005	+ .025	+ .045	+ .065	+ .080
26, 10	+ .005	+ .030	+ .045	+ .070	+ .080
25, 11	+ .005	+ .030	+ .050	+ .065	+ .080
24, 12	+ .005	+ .030	+ .050	+ .065	+ .075
23, 13	+ .005	+ .025	+ .050	+ .065	+ .075
22, 14	+ .005	+ .025	+ .045	+ .065	+ .080
21, 15	+ .005	+ .025	+ .045	+ .065	+ .080
20, 16	+ .005	+ .020	+ .045	+ .060	+ .075
19, 17	+ .005	+ .020	+ .040	+ .060	+ .075
Sum	+ .060	+ .325	+ .570	+ .820	+ 1.275
2 x Sum	+ .120	+ .650	+ 1.140	+ 1.640	+ 2.550
18	+ .005	+ .015	+ .040	+ .055	+ .080
Directly Loaded Rib 36	+ .295	+ 1.300	+ 1.720	+ 1.340	+ .145
Total 2	+ .420	+ 1.965	+ 2.900	+ 3.035	+ 2.775
Total 3	+ .130	+ .695	+ 1.440	+ 2.175	+ 2.775

Structural Engineering Division,
Department of Civil Engineering,
University of Newcastle upon Tyne.

ANALYSIS OF TEST RESULTS — Table No. 12.

Experimental Vertical Reaction Influence Coefficients for Model Radial Ribbed Dome (36 No. Ribs of varying I without bracing). Total 1 = Max. downward vert. reaction; Total 2 = Max. upward vert. reaction; Total 3 = Vert. reaction for symmetrical load. N.B. All values in this table are modified for creep. For test results, see APPENDIX II, Test No. 13.

Rib Nos.	Pt. 1	Pt. 5	Pt. 9	Pt. 13	Pt. 17
17, 19	- .030	- .115	- .125	- .065	+ .040
16, 20	- .010	- .055	- .060	- .030	+ .035
15, 21	- .005	- .020	- .020	0	+ .035
Sum	- .045	- .190	- .205	- .095	
2 x Sum = Total 1	- .090	- .380	- .410	- .190	
14, 22	0	0	+ .005	+ .015	+ .030
13, 23	0	+ .005	+ .010	+ .020	+ .030
12, 24	0	+ .005	+ .010	+ .020	+ .030
11, 25	+ .005	+ .005	+ .015	+ .015	+ .025
10, 26	+ .005	+ .005	+ .010	+ .015	+ .025
9, 27	0	0	+ .010	+ .015	+ .025
8, 28	0	+ .005	+ .010	+ .020	+ .025
7, 29	0	+ .005	+ .010	+ .015	+ .020
6, 30	0	+ .005	+ .010	+ .015	+ .020
5, 31	+ .005	+ .005	+ .010	+ .015	+ .020
4, 32	+ .005	+ .005	+ .010	+ .015	+ .020
3, 33	+ .005	+ .005	+ .010	+ .015	+ .020
2, 34	+ .005	+ .005	+ .005	+ .010	+ .020
1, 35	0	+ .005	+ .010	+ .010	+ .020
Sum	+ .030	+ .060	+ .135	+ .215	+ .440
2 x Sum	+ .060	+ .120	+ .270	+ .430	+ .880
36	0	0	+ .005	+ .010	+ .015
Directly Loaded Rib 18	+ 1.065	+ 1.210	+ 1.135	+ .760	+ .075
Total 2	+ 1.125	+ 1.330	+ 1.410	+ 1.200	+ .970
Total 3	+ 1.035	+ .950	+ 1.000	+ 1.010	+ .970

F.A.A., Ph.D. Thesis,
24th March, 1970.

Structural Engineering Division,
Department of Civil Engineering,
University of Newcastle upon Tyne.

Experimental Apex Ring Vertical Force Influence Coefficients for Model Radial Ribbed Dome (36 No. Ribs of varying I without bracing). Total 1 = Max. upward apex ring vert. force; Total 2 = Max. downward apex ring vert. force; Total 3 = Apex ring vert. force for symmetrical load. N.B. All values in this table are modified for creep. For test results, see APPENDIX II, Test No. 14.

Rib Nos.	Pt. 1	Pt. 5	Pt. 9	Pt. 13	Pt. 17
35, 1	+ .04	+ .25	+ .56	+ .92	+ 1.07
34, 2	+ .03	+ .21	+ .49	+ .84	+ 1.02
33, 3	+ .02	+ .17	+ .42	+ .71	+ .96
32, 4	+ .02	+ .13	+ .34	+ .61	+ .86
31, 5	0	+ .05	+ .22	+ .48	+ .76
Sum	+ .11	+ .81			
2 x Sum	+ .22	+ 1.62			
30, 6	- .02	0	+ .12	+ .36	+ .66
29, 7	- .02	- .06	+ .03	+ .22	+ .55
		Sum	+ 2.18		
		2 x Sum	+ 4.36		
28, 8	- .03	- .11	- .07	+ .10	+ .44
			Sum	+ 4.24	
			2 x Sum	+ 8.48	
27, 9	- .04	- .15	- .15	- .01	+ .31
26, 10	- .05	- .19	- .23	- .12	+ .21
25, 11	- .06	- .23	- .30	- .21	+ .12
24, 12	- .07	- .28	- .37	- .31	+ .04
				Sum	+ 7.00
				2 x Sum	+ 14.00
23, 13	- .08	- .29	- .41	- .37	- .05
22, 14	- .07	- .32	- .46	- .43	- .10
21, 15	- .08	- .34	- .49	- .47	- .15
20, 16	- .08	- .35	- .52	- .51	- .18
19, 17	- .08	- .36	- .52	- .52	- .21
Sum	- .68	- 2.68	- 3.52	- 2.95	- .69
2 x Sum	- 1.36	- 5.36	- 7.04	- 5.90	- 1.38
18	- .07	- .34	- .50	- .51	- .21
Total 1	- 1.43	- 5.70	- 7.54	- 6.41	- 1.59
Directly Loaded Rib 36	+ .04	+ .22	+ .54	+ .92	+ 1.00
Total 2	+ .26	+ 1.84	+ 4.90	+ 9.40	+ 15.00
Total 3	- 1.17	- 3.86	- 2.64	+ 2.99	+ 13.41

Experimental Apex Ring Radial Force Influence Coefficients for Model Radial Ribbed Dome (36 No. Ribs of varying I without bracing). Total 1 = Max. outward apex ring radial force; Total 2 = Max. inward apex ring radial force; Total 3 = Apex ring radial force for symmetrical load. N.B. All values in this table are modified for creep. For test results, see APPENDIX II, Test No. 15.

Rib Nos.	Pt. 1	Pt. 5	Pt. 9	Pt. 13	Pt. 17
35, 1	+ .23	+ .92	+ 1.30	+ 1.26	+ .56
34, 2	+ .16	+ .65	+ .95	+ .98	+ .51
33, 3	+ .10	+ .39	+ .60	+ .66	+ .44
32, 4	+ .05	+ .22	+ .36	+ .44	+ .34
31, 5	+ .02	+ .07	+ .14	+ .22	+ .27
Sum	+ .56	+ 2.25	+ 3.35		
2 x Sum	+ 1.12	+ 4.50	+ 6.70		
30, 6	- .01	- .03	- .02	+ .06	+ .17
			Sum	+ 3.62	
			2 x Sum	+ 7.24	
29, 7	- .03	- .12	- .14	- .07	+ .08
				Sum	+ 2.37
				2 x Sum	+ 4.74
28, 8	- .04	- .17	- .22	- .18	- .01
27, 9	- .06	- .23	- .32	- .28	- .08
26, 10	- .06	- .23	- .35	- .34	- .15
25, 11	- .05	- .25	- .37	- .40	- .21
24, 12	- .07	- .27	- .40	- .45	- .28
23, 13	- .06	- .27	- .42	- .48	- .31
22, 14	- .06	- .27	- .43	- .50	- .35
21, 15	- .06	- .26	- .43	- .52	- .39
20, 16	- .07	- .28	- .43	- .50	- .41
19, 17	- .06	- .27	- .42	- .50	- .41
Sum	- .63	- 2.65	- 3.95	- 4.22	- 2.60
2 x Sum	- 1.26	- 5.30	- 7.90	- 8.44	- 5.20
18	- .05	- .27	- .43	- .52	- .42
Total 1	- 1.31	- 5.57	- 8.33	- 8.96	- 5.62
Directly Loaded Rib 36	+ .26	+ 1.11	+ 1.58	+ 1.48	+ .58
Total 2	+ 1.38	+ 5.61	+ 8.28	+ 8.72	+ 5.32
Total 3	+ .07	+ .04	- .05	- .24	- .30

F.A.A., Ph.D. Thesis,
24th March, 1970.

Structural Engineering Division,
Department of Civil Engineering,
University of Newcastle upon Tyne.

Experimental Apex Ring Tangential Force Influence Coefficients for Model Radial Ribbed Dome (36 No. Ribs of varying I without bracing).

Total 1 = Max. anticlockwise apex ring tang. force; Total 2 = Max. clockwise apex ring tang. force; Total 3 = Apex ring tang. force for symmetrical load. N.B. All values in this table are modified for creep. For test results, see APPENDIX II, Test No. 16.

Rib No.	Pt. 1	Pt. 5	Pt. 9	Pt. 13	Pt. 17
36	0	0	0	+ .02	+ .04
1	+ .03	+ .13	+ .15	+ .18	+ .07
2	+ .05	+ .18	+ .27	+ .28	+ .13
3	+ .06	+ .25	+ .35	+ .31	+ .16
4	+ .08	+ .29	+ .43	+ .39	+ .20
5	+ .06	+ .25	+ .37	+ .38	+ .24
6	+ .07	+ .25	+ .36	+ .36	+ .26
7	+ .06	+ .24	+ .34	+ .35	+ .26
8	+ .06	+ .24	+ .35	+ .34	+ .26
9	+ .05	+ .19	+ .29	+ .36	+ .27
10	+ .05	+ .18	+ .26	+ .35	+ .24
11	+ .04	+ .14	+ .28	+ .32	+ .22
12	+ .04	+ .16	+ .25	+ .29	+ .22
13	+ .02	+ .13	+ .21	+ .25	+ .20
14	+ .03	+ .10	+ .15	+ .19	+ .13
15	+ .01	+ .08	+ .13	+ .14	+ .12
16	+ .02	+ .06	+ .07	+ .09	+ .09
17	+ .01	+ .04	+ ,06	+ .06	+ .04
18	0	+ .01	+ .02	+ .04	+ .01
Total 1	+ .74	+ 2.92	+ 4.34	+ 4.70	+ 3.16
19	- .01	- .01	- .02	- .01	- .02
20	- .01	- .06	- .08	- .09	- .05
21	- .02	- .06	- .10	- .14	- .09
22	- .03	- .10	- .18	- .19	- .13
23	- .03	- .12	- .20	- .23	- .16
24	- .04	- .16	- .24	- .26	- .18
25	- .04	- .17	- .26	- .31	- .18
26	- .05	- .19	- .31	- .32	- .21
27	- .06	- .24	- .36	- .37	- .23
28	- .06	- .23	- .34	- .36	- .21
29	- .06	- .26	- .37	- .33	- .21
30	- .06	- .25	- .38	- .34	- .20
31	- .06	- .24	- .35	- .35	- .17
32	- .06	- .28	- .37	- .40	- .21
33	- .06	- .22	- .29	- .29	- .13
34	- .05	- .19	- .29	- .25	- .07
35	- .03	- .12	- .17	- .15	- .03
Total 2	- .73	- 2.90	- 4.31	- 4.39	- 2.48
Total 3	+ .01	+ .02	+ .03	+ .31	+ .68

F.A.A., Ph.D. Thesis,
6th April, 1970.

Structural Engineering Division,
Department of Civil Engineering,
University of Newcastle upon Tyne.

ANALYSIS OF TEST RESULTS

Table No. 16

Experimental Force Influence Coefficients for Radial Ribbed Dome

18 ft. diameter x 3 ft. rise model dome with $\frac{1}{2}$ in. wide laminated timber ribs (36 No.; max. depth 2 in.; depth at base $1\frac{1}{2}$ in.; depth at apex ring 1 in.) without diagonal bracing. Mild steel apex ring outside diameter 24 in. (1 in. deep x $\frac{1}{8}$ in. thick). Horizontal bracing at points 1, 3, 5, 7, 9, 11, 13, 15. Directly loaded rib only.

	Unit Load at Point	x co-ord	L.H.S. Vertical Base Reaction	L.H.S. Horizontal Base Reaction	L.H.S. Apex Ring Vert. Force	L.H.S. Apex Ring Radial Force
L.H.S.	Base	.000	+ 1	0	0	0
	1	5.598	+ 1.05	+ .33	+ .07	+ .22
	5	26.190	+ 1.09	+ 1.35	+ .35	+ 1.03
	9	48.240	+ .74	+ 1.27	+ .69	+ 1.52
	13	71.334	+ .28	+ .67	+ 1.02	+ 1.48
	17	95.094	+ .04	+ .10	+ 1.00	+ .74
R.H.S.	17	120.906	+ .03	- .01	- .77	- .63
	13	144.666	0	+ .02	- .84	- .79
	9	167.760	- .02	+ .03	- .63	- .67
	5	189.810	- .02	+ .02	- .35	- .41
	1	210.402	- .01	+ .01	- .07	- .08
	Base	216.000	0	0	0	0

F.A.A., Ph.D. Thesis,
22nd Dec., 1969.

Structural Engineering Division,
Department of Civil Engineering,
University of Newcastle upon Tyne.